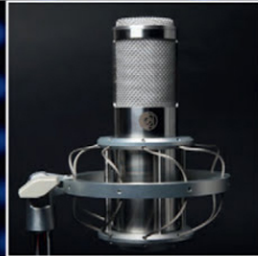
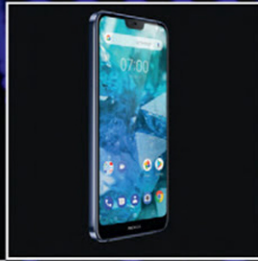


SECOND EDITION

ACOUSTICS

Sound Fields, Transducers and Vibration



Leo Beranek and Tim Mellow



Cover images, left - right, from top left

1. Horn tweeter in a sphere (transparent for illustration only) with tweeter model 27TFF (H0831), *courtesy of SEAS Fabrikker AS and prototyping courtesy of Object Envy Ltd*
2. Cell phone model Nokia 7.1, *courtesy of HMD Global OY*
3. Dynamic microphone model D230, *courtesy of AKG*
4. Condenser microphone model 4190, *courtesy of Brüel & Kjær Sound & Vibration Measurement A/S*
5. Aluminum-cone woofer model 100DW/8A, *courtesy of Bandor*
6. Transmission-line: Wave[®] music system, *courtesy of Bose Corporation*
7. Ribbon microphone model KSM313 *courtesy of Shure[®] microphones, which are copyrighted by Shure Incorporated and used with permission*
8. Electrostatic loudspeaker model FrontRo, *courtesy of Mellow Acoustics Ltd*



ACOUSTICS: SOUND FIELDS, TRANSDUCERS AND VIBRATION

Second Edition

LEO BERANEK
TIM MELLOW



ACADEMIC PRESS

An imprint of Elsevier

Academic Press is an imprint of Elsevier
125 London Wall, London EC2Y 5AS, United Kingdom
525 B Street, Suite 1650, San Diego, CA 92101, United States
50 Hampshire Street, 5th Floor, Cambridge, MA 02139, United States
The Boulevard, Langford Lane, Kidlington, Oxford OX5 1GB, United Kingdom

Copyright © 2019 Elsevier Inc. All rights reserved.

No part of this publication may be reproduced or transmitted in any form or by any means, electronic or mechanical, including photocopying, recording, or any information storage and retrieval system, without permission in writing from the publisher. Details on how to seek permission, further information about the Publisher's permissions policies and our arrangements with organizations such as the Copyright Clearance Center and the Copyright Licensing Agency, can be found at our website: www.elsevier.com/permissions.

This book and the individual contributions contained in it are protected under copyright by the Publisher (other than as may be noted herein).

Notices

Knowledge and best practice in this field are constantly changing. As new research and experience broaden our understanding, changes in research methods, professional practices, or medical treatment may become necessary.

Practitioners and researchers must always rely on their own experience and knowledge in evaluating and using any information, methods, compounds, or experiments described herein. In using such information or methods they should be mindful of their own safety and the safety of others, including parties for whom they have a professional responsibility.

To the fullest extent of the law, neither the Publisher nor the authors, contributors, or editors, assume any liability for any injury and/or damage to persons or property as a matter of products liability, negligence or otherwise, or from any use or operation of any methods, products, instructions, or ideas contained in the material herein.

Library of Congress Cataloging-in-Publication Data

A catalog record for this book is available from the Library of Congress

British Library Cataloguing-in-Publication Data

A catalogue record for this book is available from the British Library

ISBN: 978-0-12-815227-0

For information on all Academic Press publications visit our website at
<https://www.elsevier.com/books-and-journals>

Publisher: Mara Conner
Acquisition Editor: Tim Pitts
Editorial Project Manager: Emma Hayes
Production Project Manager: Prem Kumar Kaliamoorthi
Cover Designer: Alan Studholme

Typeset by TNQ Technologies



PREFACE TO THE SECOND EDITION

Since the first edition was published 7 years ago, my coauthor Leo Beranek has sadly passed away. Thankfully though, he lived long enough to not only contribute new material to the first edition but also to see its publication. His original 1954 book ‘Acoustics’, which still forms a substantial part of this edition, made an invaluable contribution to the field of electroacoustics and inspired many subsequent authors, including the current one. For example, it was the first book to show the electrical, mechanical and acoustic radiation impedances of a transducer on the same analogous circuit.

In this second edition, I have endeavored to stay faithful to his vision. For instance, he expressed surprise that I had not written anything about electrostatic loudspeakers, so this edition includes a new Chapter 15 devoted entirely to the subject. Preceding that is a new Chapter 14, which covers vibro-acoustics, including membranes, plates, and shells. Hence the new book title: ‘Acoustics: Sound Fields, Transducers, and *Vibration*.’ This replaces the old Chapter 14 on state variable analysis which, according to data from digital libraries, was the least viewed and so it has been removed to make space for the new one without the book becoming too unwieldy.

There are revisions throughout, many of which have been suggested to me by diligent readers whom I have listed in the acknowledgments section. There are too many changes to list here, but the following are particularly pertinent:

Chapter 3: This contains a new section on analogous circuits for 2-port networks.

Chapter 4: The mass and resistance end corrections for a perforated sheet have been updated according to a recent paper by Xianhui Li.

Chapter 7: The field inside a closed-box or bass-reflex loudspeaker enclosure is now described with circular apertures instead of square/rectangular ones, which simplifies the equations and is truer to most real-world applications.

Chapter 13: Equations for the radiation characteristics of a rigid disk in a circular baffle or free space and the resilient disk or rectangular piston in an infinite baffle are simplified as a result of recently published work. The mutual radiation impedance between pistons in an infinite baffle now allows for pistons of different radii.

I hope that, through this edition, Leo’s legacy continues to be relevant to readers into the 21st century.

Tim Mellow 2019

PREFACE TO THE FIRST EDITION

Acoustics is a most fascinating subject. Music reproduction, sound systems, telephone systems, measuring equipment, cell phones, underwater sound, hearing aids, and medical ultrasound all seek from acoustics answers pertinent to their fields. The annual meetings of the audio and acoustical societies are veritable five-ring shows, with papers and symposia on subjects in all the aforementioned fields.

This text is planned as a textbook for students of acoustics in engineering departments. It assumes knowledge of electrical circuit theory. It should be of particular value to experimenters, to acoustical consultants, and to those who anticipate being engineering designers of audio equipment. To practicing acoustical engineers, this is a basic reference book.

This text begins with the basics of sound fields in free space and simple enclosures.

The particular vocabulary of acoustics is treated early. Next follows the very basis for the subject, the laws governing sound generation, radiation, and propagation, which are expressed both mathematically and graphically. Then follow chapters dealing with microphones, loudspeakers, earphones, and horns. Following next is the performance of loudspeakers either in baffles or attached to waveguides. Directed toward the design of miniature systems, i-pods, and cell phones, for example, the next sections deal with squeezing the most sound out of tiny radiating surfaces. Then comes sound in enclosures of all sizes, including such spaces as school rooms, offices, auditoriums, and living rooms. Throughout the text, numerical examples and summary charts are given to facilitate application of the material to audio designer.

Fortunately, the behavior of most transducers can be analyzed with the aid of electromechanoacoustical circuits that are analogous to the circuits used in electronics. These analogous circuits, which were first introduced in the 1954 version of this book *Acoustics*, were cited by a large number of the leading writers on loudspeaker system design, including Villchur, Thiele, Small, Ashley, Broadhurst, Morita, Kyouno, Karminsky, Merhaut, Allison, Berkovitz, and others. Knowledge of these principles has led to the high quality of audio reproduction that we enjoy today.

When *Acoustics* was first published, the subject was already in the process of diversification, a trend that has continued unabated to this day. There are now over 300 subcategories of acoustics under the Physics and Astronomy Classification Scheme (PACS). Hence, it is no longer possible to produce such an all-encompassing book in any useful depth, so the current text has been limited to the subject of electroacoustics and can be considered as an updated and extended version of the first half of *Acoustics*. Chapter 11, part 24, through Chapter 13 of the original book have been largely

superseded by *Concert Halls and Opera Houses: Music, Acoustics, and Architecture* (Beranek, Springer 2004), *Noise and Vibration Control Engineering* (Ver and Beranek, John Wiley & Sons, Inc. 2006), and *Handbook of Noise and Vibration Control* (Crocker, John Wiley & Sons, 2007). Therefore, these sections have been omitted so that the remaining part of the book can be expanded to include more recent developments in the theory of electro-mechanoacoustic transducers and sound radiation and hence the new title.

In 1954, there were only a handful of electronic computers in the world, so it would not have made sense to include formulas for everything. Hence, *Acoustics* relied on graphical information for some of the more complicated concepts such as sound radiation from a loudspeaker diaphragm in free space. In this new text, we have provided formulas for everything so that interested readers can recreate the graphical results and use them in their simulations.

Leo L. Beranek and Tim J. Mellow 2012

ACKNOWLEDGMENTS

The authors wish to thank all those who contributed to the betterment of the 1954 edition of this book.

We are greatly indebted to those who have rendered assistance for this edition, in particular to Leo Kärkkäinen whose help has been especially pertinent, Noel Lobo for his invaluable guidance in numerical matters, Enrico Pascucci for his many helpful suggestions regarding Chapter 8 and for performing anechoic measurements, Philip Trevelyan for his support and assistance in acoustical measurements, and Rory Stoney for providing impedance tube measurements on absorbent materials in a very short time. We also stand indebted to our wives, Anne Mellow and Gabriella Beranek for their support and enduring patience.

Many improvements and corrections included in the second edition were kindly suggested by: Stephen Bolser, Huiqun Deng, Mads Dyrholm, Alan Feinerman, James Heddle, Mattias Johansson, Bjørn Kolbrek, Joe Ladish, Siegfried Linkwitz, Sidsel Marie Nørholm, Mark Thompson, Paolo La Torraca, Luigi Vigone, and Wojciech Rdzanek.

Introduction and terminology

PART I: INTRODUCTION

1.1 A LITTLE HISTORY

Acoustics has entered a new age—the era of precision engineering. In the 19th century, acoustics was an art. The primary measuring instruments used by engineers in the field were their ears. The only controlled noise sources available were whistles, gongs, sirens, and gunshots. Microphones consisted of either a diaphragm connected to a mechanical scratcher that recorded the shape of the wave on the smoked surface of a rotating drum or a flame whose height varied with the sound pressure. About that time the great names of Rayleigh, Stokes, Thomson, Lamb, Helmholtz, König, Tyndall, Kundt, and others appeared on important published papers. Their contributions to the physics of sound were followed by the publication of Lord Rayleigh's two-volume treatise *Theory of Sound* in 1877/1878 (revised in 1894/1896). In the late 19th century, Alexander Graham Bell invented the magnetic microphone and with it the telephone. Thomas Edison created the carbon microphone, which was the transmitter used in standard telephone handsets for almost 100 years. The next big advance was Edison's phonograph, which made it possible for the human voice and other sounds to be preserved for posterity.

In a series of papers published between 1900 and 1915, W. C. Sabine advanced architectural acoustics to the status of a science. He measured the duration of reverberation in rooms using organ pipes as the source of sound and a chronograph for the precision measurement of time. He showed that reverberation could be predicted for auditoria from knowledge of room volume, audience size, and the characteristics of the sound-reflecting surfaces—sidewalls and ceiling.

Although the contributions of these earlier workers were substantial, the greatest acceleration of research in acoustics followed the invention of the triode vacuum tube (1907) and the advent of radio broadcasting (1920). When vacuum tube amplifiers and loudspeakers became available, loud sounds of any desired frequency could be produced. With the invention of moving coil and condenser microphones, the intensity of very faint sounds could be measured. Above all, it became feasible to build acoustical measuring instruments that were compact, rugged, and insensitive to air drafts, temperature, and humidity.

The progress of communication acoustics was hastened through the efforts of the Bell Telephone Laboratories (1920*ff*), which were devoted to perfection of the telephone system in the United States. During the First World War, the biggest advances were in underwater sound. In the next two decades (1936*ff*) architectural acoustics strode forward through research at Harvard, the Massachusetts Institute of Technology, the University of California at Los Angeles, and several research centers in England and Europe, especially Germany. Sound decay in rectangular rooms was explained in detail, the impedance method of specifying acoustical materials was investigated, and the computation of sound attenuation in ducts was put on a precise basis. The advantages of skewed walls and use of acoustical materials in patches rather than on entire walls were demonstrated. Functional absorbers were introduced to the field, and a wider variety of acoustical materials came on the market. Morse, Stenzel, Mast, Rdzanek, and many others have helped to develop the mathematical theory of sound radiation and diffraction, not to mention the “Dutch school” of Zernike, Bouwkamp, Streng, Aarts, and Janssen, contributions from all of whom are found in the latter part of this book.

The science of psychoacoustics was rapidly developing. At the Bell Telephone Laboratories, under the leadership of Harvey Fletcher, the concepts of loudness and masking were quantified, and many of the factors governing successful speech communication were determined (1920–40). Acoustics, through the medium of ultrasonics, entered the fields of medicine and chemistry. For example, ultrasonic diathermy was being tried, and acoustically accelerated chemical reactions were reported.

Then came the Second World War with its demand for the successful detection of submerged submarines and for highly reliable speech communication in noisy environments such as in armored vehicles and high-flying nonpressurized aircraft. Government financing of improvements in these areas led to the formation of great laboratories in England, Germany, and France, as well as in the United States at Columbia University, Harvard, and the University of California. During this period, research in acoustics reached proportions undreamed of a few years before and has continued unabated since.

In the last 50 years, the greatest revolution has undoubtedly been the vast increase in computing power accompanied by a rapid rate of miniaturization, which has led to a previously unimaginable plethora of hand portable products, including cell phones, palmtop computers, and measuring devices. Size has presented new challenges for the acoustical designer as the pressure to reduce dimensions is ever increasing. Contrary to popular expectations, electroacoustic transducers do not obey Moore’s law [1], so it cannot be assumed that a reduction in size can be achieved without sacrificing performance, although new materials such as polysilicon membranes for microphones and neodymium magnets for loudspeakers have helped preserve performance to some extent. Reducing the size of loudspeakers usually compromises their maximum sound power

output, particularly at low frequencies, and in the case of microphones, the signal-to-noise ratio in their output deteriorates. Therefore, the ability of the acoustical engineer to optimize the design of transducers and electronics has never been more important.

In addition to the changes in products in which electroacoustic transducers are employed, computers have revolutionized the way in which the transducers themselves are modeled [2]. The first wave of tools came in the 1960s and early 1970s for simulating electrical circuits. Acoustical engineers were quick to adapt these for modeling loudspeakers and microphones using lumped mechanical and acoustical circuit elements analogous to electrical ones, as given in *Acoustics*. However, simulation by this method was largely a virtual form of trial-and-error experimentation, albeit much faster than actual prototyping, until Thiele and Small applied filter theory to the transfer function so that the designer could choose a target frequency response shape for a loudspeaker and engineer the electromechanoacoustic system accordingly. Finite element modeling (FEM) and boundary element modeling (BEM) both followed quickly. Unlike lumped element simulation, the range was no longer limited to that where the acoustical wavelength is much greater than the largest dimension of the device. With the wide availability of modern tools for acoustical simulation, it is perhaps tempting to neglect more traditional analytical methods, which are a focus of this text, especially in Chapters 12 and 13. However, analytical (mathematical) methods can offer some distinct benefits:

- According to Richard Hamming [3], “The purpose of computation is insight not just numbers.” By examining the mathematical relationships, we can gain a better understanding of the physical mechanisms than when the calculations are all “hidden” in a computer. This helps us to create improved systems, especially when we can manipulate the equations to arrive at formulas that enable us to design everything correctly first time such as those given in Chapter 7 for loudspeaker systems. By contrast, a simulation tool can only simulate the design we load into it. It cannot tell us directly how to design it, although it may be possible to tweak parameters randomly in a Monte Carlo optimization or “evolve” a design using a Darwinian genetic algorithm. Even then, a global optimum is not necessarily guaranteed.
- Although exact analytical formulas are generally limited to simple rectangular, cylindrical, or spherical geometries, many electroacoustic transducers have, or can be approximated by, these simple geometries. (Note this restriction does not apply to lumped elements that can have almost any shape.) It may sometimes take time and effort to derive a formula, but once it is done it can be used to generate as many plots as you like simply by varying the parameters. Furthermore, the right formula will give the fastest possible computation with the least amount of memory space. If a picture paints a 1000 words, it could be said that an equation paints a 1000 pictures. In the words of Albert Einstein, “Politics is for the moment, but an equation is for eternity.”

- Analytical solutions often yield simple asymptotic expressions for very low/high frequencies or the far field, which can form the basis for elements in circuit simulation programs.
- It is often useful to have an analytical benchmark against which to check FEM/BEM simulation results. This can tell us much about the required element size and what kind of meshing geometry to use. Of course, having two ways of solving a problem gives us increased confidence in both methods.
- Analytical formulas are universal and not restricted to a particular simulation tool. They can be written into a wide choice of programming languages.

Another area in which computers have contributed is that of symbolic computation. For example, if we did not know that the integral of $\cos x$ was $\sin x$, we would have to integrate $\cos x$ numerically, which is a relatively slow and error-prone process compared with evaluating $\sin x$ directly. Modern mathematical tools are capable of solving much more complicated integrals than this symbolically, which has led to new analytical solutions in sound radiation. For example, the previous formulas for radiation from a circular disk in free space were too lengthy to include in the original *Acoustics* but a more compact solution, with or without a circular baffle, is given in the new Chapter 13.

Not only have computers led to the advances mentioned above, but they have fallen dramatically in price so much that many devices such as cell phones, hearing aids, and sound level meters now contain a digital signal processor (DSP) as well as electroacoustical transducers. This enables an acoustical designer to design a complete system including DSP equalization. Although DSP algorithms are beyond the scope of this book, Chapter 14 has been written with the intention of aiding this part of the design process. It describes state-variable circuit simulation theory, which can be used to obtain a transfer function of the electroacoustical system. The inverse transfer function can then be used as a basis for DSP equalization. However, any form of equalization should come with a health warning because it cannot be used to compensate for a poor acoustical design. On the other hand, a DSP can be used in real time to monitor changes in the electromechanoacoustical parameters and to adjust the drive levels accordingly to extract the maximum possible performance, while avoiding burnout.

In 1962, Sessler and West invented a new kind of capacitor microphone, which contained a permanently stored charge on a metalized membrane as well as a preamplifier, which has become to be known as the foil electret microphone. This device has been followed by microelectromechanical systems (MEMS), now incorporated into microphones and vibration pickups (accelerometers) and gyroscopes, which have dimensions in the order of microns. One embodiment of MEMS is widely used in hearing aids and cell phones, where the trend is to incorporate more microphones for noise cancellation and beam forming. It consists of a freely vibrating diaphragm made from polysilicon, which is spaced from a perforated backplate that is coated with

vapor-deposited silicon nitride. When the device is moved, there is a change in capacitance in the order of femtofarads. The combination of low cost, small size, reliability, and near-studio quality has made the “crackly” carbon microphone obsolete. Hence, the electret and MEMS models are also described in this text. Other new additions include call loudspeakers for cell phones and an improved tube model for very small diameters.

Today, acoustics is no longer a tool of the telephone industry, a few enlightened architects, and the military. It is a concern in the daily life of nearly every person. International movements legislate and provide quiet housing. Labor and office personnel demand safe and comfortable acoustic environments in which to work. Architects in rapidly increasing numbers are hiring the services of acoustical engineers as a routine part of the design of buildings. Manufacturers are using acoustic instrumentation on their production lines. In addition, there has been great progress in the abatement of noise from jet engine propelled aircraft, in which efforts were instigated by the Port of New York Authority and its consultant Bolt Beranek and Newman in the late 1950s and have been carried on by succeeding developments in engine design. Acoustics is coming into its own in the living room, where high-fidelity reproduction of music has found a wide audience. Overall, we witness the rapid evolution of our understanding of electro-acoustics, architectural acoustics, structural acoustics, underwater sound, physiological and psychological acoustics, musical acoustics, and ultrasonics.

It is difficult to predict the future with any certainty, although nanotechnologies look as though they will play a steadily increasing role. One can truly say that although over 100 years have passed since the publication of Rayleigh’s *Theory of Sound*, there is still plenty to explore.

This book covers first the basic aspects of acoustics: wave propagation in the air, the theory of mechanical and acoustical circuits, the radiation of sound into free space, and the properties of acoustic components. It is then followed by chapters dealing with microphones, loudspeakers, enclosures for loudspeakers, and horns. The basic concepts of sound in enclosures are treated next, and methods for solving problems related to the radiation and scattering of sound are given. The final chapter describes a computer method for analyzing circuits. Throughout the text we shall speak to *you*—the student of this modern and exciting field.



1.2 WHAT IS SOUND?

In reading the material that follows, your goal should be to form and to keep in mind a picture of what transpires when the diaphragm on a loudspeaker, or any surface for that matter, is vibrating in contact with the air.

A sound is said to exist if a disturbance propagated through an elastic material causes an alteration in pressure or a displacement of the particles of the material which can be

detected by a person or by an instrument. Because this text deals primarily with devices for handling speech and music, the only types of elastic material with which we shall concern ourselves are gases (more particularly air). Because the physical properties of gases are relatively easy to express, it is not difficult to describe the way sound travels in such media.

Imagine that we could cut a tiny cubic “box” out of air and hold it in our hands as we would hold a block of wood. What physical properties would it exhibit? First, it would have weight and, hence, mass. In fact, a cubic meter of air has a mass of a little over 1 kg. If a force is applied to this box, it will accelerate according to Newton’s second law, which states that force equals mass times acceleration.

If we exert forces that compress two opposing sides of the little cube, the four other sides will bulge outward. The incremental pressure produced in the gas by this force will be the same throughout this small volume. This happens because pressure in a gas is a scalar, i.e., a nondirectional quantity.

Now imagine that the little box of air is held tightly between your hands. Move one hand toward the other so as to distort the cube into a parallelepiped. You find that no opposition to the distortion of the box is made by the air outside the two distorted sides. This indicates that air does not support a shearing force [4].

Furthermore, if we constrain five sides of the cube and push on the sixth one, we find that the gas is elastic; i.e., a force is required to compress the gas. The magnitude of the force is in direct proportion to the displacement of this unconstrained side of the container. A simple experiment proves this. Close off the hose of a bicycle tire pump so that the air is confined in the cylinder. Push down on the plunger. You will find that the confined air behaves like a simple spring.

What is air? The air that surrounds us consist of tiny molecules which are about 0.33 nm in diameter, but are 3.3 nm apart, so they only occupy 0.1% of the space! Even so, at room temperature, a cubic meter weighs 1.18 kg. Although the mean free path between collisions is 60 nm, air molecules travel at an average speed of 500 m/s at room temperature so that each one experiences 8.3×10^9 collisions per second! It is the force with which the molecules bombard the boundary of a confined space which explains the elastic (and viscous) properties of air.

The spring constant of the gas varies, however, with the speed of the compression. A displacement of the gas particles occurs when it is compressed. An incremental change in the volume of our box will cause an incremental increase in the pressure that is directly proportional to the displacement. If the compression takes place slowly, this relation obeys the formula:

$$\Delta P = -K \Delta V \text{ — slow process}$$

where K is a constant.

If, on the other hand, the incremental change in volume takes place rapidly, and if the gas is air, oxygen, hydrogen, or nitrogen, the incremental pressure that results is equal to $1.4K$ times the incremental change in volume:

$$\Delta P = -\gamma K \Delta V \text{—fast process, diatomic gas,}$$

where γ is the ratio of specific heats for a gas and is equal to 1.4 for air and other diatomic gases. Note that a positive increment (increase) in pressure produces a negative increment (decrease) in volume. Processes that take place at intermediate rates are more difficult to describe, even approximately, and fortunately need not be considered here.

What is the reason for the difference between these two occurrences? For slow variations in volume, the compressions are *isothermal*, which means that they take place at constant temperature throughout the volume. There is time for the heat generated in the gas during the compression to flow out through the walls of the container. Hence, the temperature of the gas remains constant. For rapid alternations in the volume, however, the temperature rises when the gas is compressed and falls when the gas is expanded. If the alternations are rapid enough, there is not enough time during a cycle of compression and expansion for the heat to flow away. Such rapid alternations in the compression of the gas are said to be *adiabatic*.

In either isothermal or adiabatic processes, the pressure in a gas is due to collisions of the gas molecules with the container walls. You will recall that pressure is force per unit area or, from Newton, time rate of change of momentum per unit area. Let us investigate the mechanism of this momentum change in a confined gas. The direction of motion of the molecules changes when they strike a wall so that the resulting change in momentum appears as pressure in the gas. The *rate* at which the change of momentum occurs, and so the magnitude of the pressure change, depends on two quantities. It increases either if the number of collisions per second between the gas particles and the walls increases or if the amount of momentum transferred per collision becomes greater, or both.

During an isothermal compression of a gas, an increase of pressure results because a given number of molecules are forced into a smaller volume and they necessarily collide with the container walls more frequently.

During an adiabatic compression of a gas, the pressure increase partly results from an increase in the number of wall collisions as described above, as well as from the greater momentum transfer per collision. Both of these increases are due to the temperature change which accompanies the adiabatic compression. From kinetic theory, we know that the velocity of gas molecules varies as the square root of the absolute temperature of the gas. As contrasted with the isothermal, in the adiabatic process the molecules get hotter, move faster, collide with the container walls more frequently, and, having greater momentum themselves, transfer more momentum to the walls during each individual collision. For a given volume change ΔV , the rate of momentum change, and therefore

the pressure increase, is seen to be greater in the adiabatic process. Hence, the gas is stiffer—it takes more force to expand or compress it. We shall see later in this chapter that sound waves are adiabatic alternations.



1.3 PROPAGATION OF SOUND THROUGH GAS

The propagation of sound through a gas can be fully predicted and described if we take into account the factors just discussed, viz., the mass and stiffness of the gas, and its conformance with basic physical laws. Such a mathematical description will be given in detail in later chapters. We are now concerned with a qualitative picture of sound propagation.

If we put a sinusoidally vibrating wall in a gas (see Fig. 1.1a), it will accelerate adjacent air particles and compress that part of the gas nearest to it as it moves forward from rest. This initial compression is shown in Fig. 1.1b as a crowding of dots in front of the wall. The dots represent air particles. These closely crowded air particles have, in addition to their random velocities, a forward momentum gained from the wall. They collide with their neighbors to the right and, during the collision, transfer forward momentum to these particles, which were at rest. These particles in turn move closer to their neighbors, with which they collide, and so on. Progressively more and more remote parts of the medium will be set into motion. In this way, through successive collisions, the force built up by the original compression may be transferred to distant parts of the gas.

When the wall reverses its motion, a rarefaction occurs immediately in front of it (see Fig. 1.1c and d). This rarefaction causes particles to be accelerated backward, and the above process is now repeated in the reverse direction, and so on, through successive cycles of the source.

It is important to an understanding of sound propagation that you keep in mind the relative variations in pressure, particle displacement, and particle velocity. Note that, at any one instant, the maximum particle displacement and the maximum pressure do not occur at the same point in the wave. To see this, consider Fig. 1.1c. The maximum pressure occurs where the particles are most tightly packed, i.e., at $D_2 = 1.7$ m. But at D_2 the particles have not yet moved from their original rest position, as we can see by comparison with Fig. 1.1a. At D_2 , then, the pressure is a maximum, and the particle displacement is zero. At this instant, the particles next to the wall are also at their zero-displacement position, for the wall has just returned to its zero position. Although the particles at both D_2 and d_0 have zero displacement, their environments are quite different. We found the pressure at D_2 to be a maximum, but the air particles around d_0 are far apart, and so the pressure there is a minimum. Halfway between d_0 and D_2 the pressure is found to be at the ambient value (zero incremental pressure) and the displacement of the particles at a maximum. At a point in the wave where pressure is a maximum, the particle displacement is zero. Where particle displacement is a maximum,

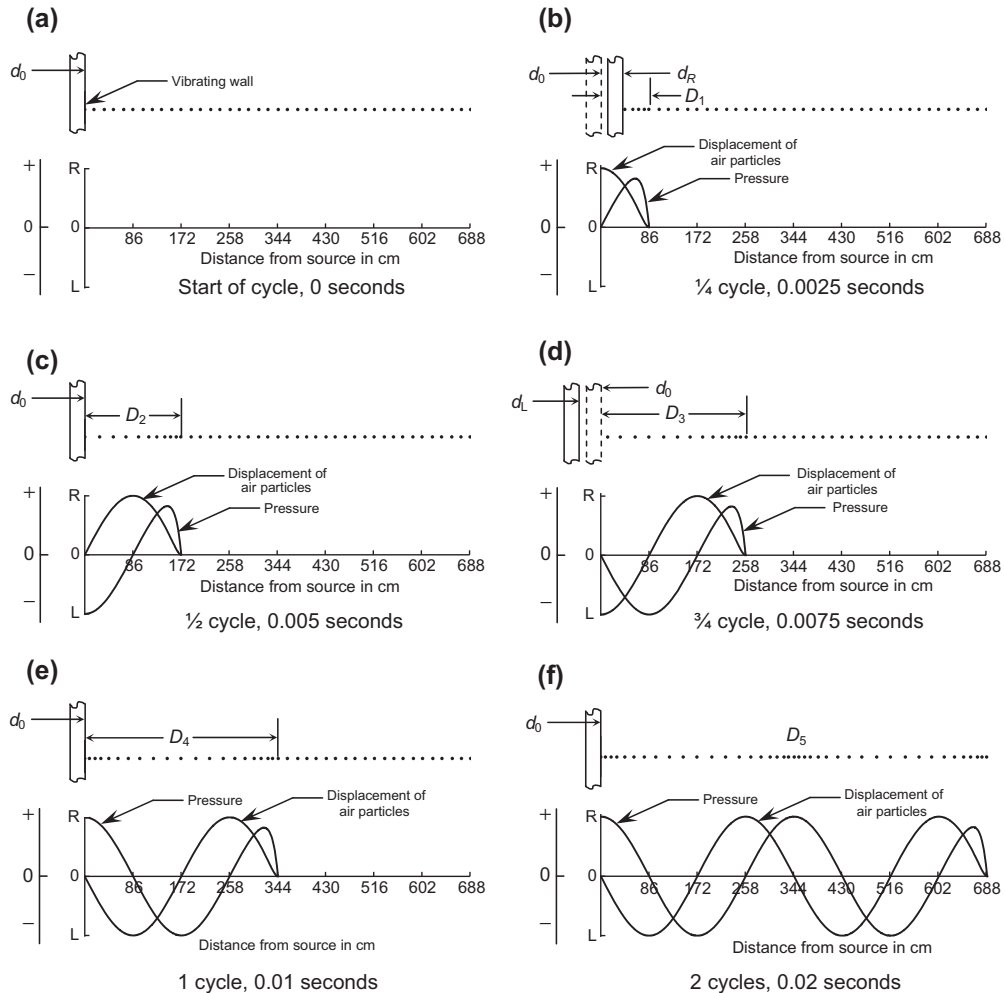


Figure 1.1 Pressure and displacement in a plane sound wave produced by a sinusoidally vibrating wall. D_1 = one-fourth wavelength; D_2 = one-half wavelength; D_3 = three-fourths wavelengths; D_4 = one wavelength; D_5 = two wavelengths. R means displacement of the air particles to the right, L means displacement to the left, and O means no displacement. *Crowded dots* mean positive excess pressure and *spread dots* mean negative excess pressure. The frequency of vibration of the piston is 100 Hz.

the incremental pressure is zero. Pressure and particle displacement are then 90 degrees out of phase with each other.

At any given point on the wave, the pressure and particle displacement are varying sinusoidally in time with the same frequency as the source. If the pressure is varying as $\cos 2\pi ft$, the particle displacement, 90 degrees out of phase, must be varying as $\sin 2\pi ft$. The velocity of the particles, however, is the time derivative of displacement and must be

varying as $\cos 2\pi ft$. At any one point on the wave, then, pressure and particle velocity are in phase.

We have determined the relative phases of the particle displacement, velocity, and pressure at a point in the wave. Now we ask, “What phase relationship exists between values of, say, particle displacement measured at two different points on the wave?” If the action originating from the wall were transmitted instantaneously throughout the medium, all particles would be moving in phase with the source and with each other. This is not the case, for the speed of propagation of sound is finite, and at points increasingly distant from the source there is an increasing delay in the arrival of the signal. Each particle in the medium is moved backward and forward with the same frequency as the wall, but not at the same time. This means that two points separated a finite distance from each other along the wave in general will not be moving in phase with each other. Any two points that are vibrating in exact phase will, in this example of a plane wave, be separated by an integral number of wavelengths. For example, in Fig. 1.1f, the 344.8- and 689.6-cm points are separated by exactly one wavelength. A disturbance at the 689.6-cm point occurs at about 0.01 s after it occurs at the 344.8-cm point. At room temperature, 22°C, this corresponds to a speed of propagation of 344.8 m/s. Mathematically stated, a wavelength is equal to the speed of propagation divided by the frequency of vibration.

$$\lambda = \frac{c}{f} \quad (1.1)$$

where λ is the wavelength in meters, c is the speed of propagation of the sound wave in m/s, and f is the frequency in hertz (or cycles/s).

What is a plane wave? In Fig. 1.1 it is assumed that the wall is infinite in size so that everywhere in front of it the air particles are moving as shown by the line at the center of the wall. Such a sound wave is called plane because it is behaving the same at every plane parallel to the surface of the oscillating wall.

Sound waves in air are longitudinal; i.e., the direction of the vibratory motion of air particles is the same as the direction in which the wave is traveling. This can be seen from Fig. 1.1. Light, heat, or radio waves in free space are transverse; i.e., the vibrations of the electric and magnetic fields are perpendicular to the direction in which the wave advances. By contrast, waves on the surface of water are circular. The vibratory motion of the water molecules is in a small circle or ellipse, but the wave travels horizontally.



1.4 MEASURABLE ASPECTS OF SOUND

Consider first what measurements might be made on the medium before a sound wave or a disturbance is initiated in it. The gas particles (molecules) are, on the average, at rest. They do have random motion, but there is no net movement of the gas in any direction. Hence, we say that the *particle displacement* is zero. It follows that the *particle*

velocity is zero. Also, when there is no disturbance in the medium, the *pressure* throughout is constant and is equal to the *ambient pressure*, so that the *incremental pressure* is zero. A value for the ambient pressure may be determined from the readings of a barometer. The *density*, another measurable quantity in the medium, is defined as usual as the mass per unit volume. It equals the *ambient density* when there is no disturbance in the medium.

When a sound wave is propagated in the medium, several measurable changes occur. The particles are accelerated and as a result are displaced from their rest positions. The particle velocity at any point is not zero except at certain instants during an alternation. The pressure at any point varies above and below the ambient pressure. Also, the temperature at a point fluctuates above and below its ambient value. The *incremental* variation of pressure is called the *sound pressure* or the *excess pressure*. An incremental pressure variation, in turn, causes a change in the density called the *incremental density*. An increase in sound pressure at a point causes an increase in the density of the medium at that point.

The speed with which an acoustical disturbance propagates outward through the medium is different for different gases. For any given gas, the speed of propagation is proportional to the square root of the absolute temperature of the gas (see Eq. 1.8). As is the case for all types of wave motion, the speed of propagation is given by Eq. (1.1).



PART II: TERMINOLOGY

You now have a general picture of the nature of a sound wave. To proceed further in acoustics, you must learn the particular “lingo” or accepted terminology. Many common words such as pressure, intensity, and level are used in a special manner. Become well acquainted with the special meanings of these words at the beginning as they will be in constant use throughout the text. The list of definitions below is not exhaustive, and some additional terminology will be presented as needed in later chapters [5]. If possible, your instructor should make you take measurements of sounds with a sound level meter and a sound analyzer so that the terminology becomes intimately associated with physical phenomena.



1.5 GENERAL

Acoustic

The word “acoustic,” an adjective, means intimately associated with sound waves or with the individual media, phenomena, apparatus, quantities, or units discussed in the science of sound waves. For example, “Through the acoustic medium came an acoustic radiation so intense as to produce acoustic trauma. The acoustic filter has an output acoustic impedance of 10-acoustic ohms.” Other examples are acoustic horn, transducer, energy, wave, admittance, refraction, mass, component, and propagation.

Acoustical

The word “acoustical,” an adjective, means associated in a general way with the science of sound or with the broader classes of media, phenomena, apparatus, quantities, or units discussed in the science of sound. For example, “Acoustical media exhibit acoustical phenomena whose well-defined acoustical quantities can be measured, with the aid of acoustical apparatus, in terms of an acceptable system of acoustical units.” Other examples are acoustical engineer, school, glossary, theorem, and circuit diagram.

Imaginary unit

The symbol $j = \sqrt{-1}$ is the imaginary unit. In the case of a complex quantity $z = x + jy$, we denote the real part by $\Re(z) = x$, where \Re is a capital R in the Fraktur typeface, and the imaginary part by $\Im(z) = y$, where \Im is a capital I in the Fraktur typeface. It is worth noting that $\sqrt{-1}$ can be positive or negative, as with the square root of any number, and many texts use the negative square root i , where $i = -j$. Mathematica also uses the positive square root but denotes it by a double-struck \mathbb{i} instead of j . A complex quantity $z = x + jy$ can also be represented in terms of magnitude $|z|$ and phase angle θ by

$$z = |z|e^{j\theta} = |z|(\cos \theta + j \sin \theta),$$

where the magnitude (aka modulus or absolute value) is given by

$$|z| = \sqrt{x^2 + y^2}$$

and the phase angle is given by

$$\theta = \arctan(y/x)$$

Harmonically varying quantity

In this text, a harmonically varying quantity will be denoted by a tilde. Hence, if ψ represents a generic quantity, we denote that it is harmonically varying by writing it as $\tilde{\psi}$. In the analyses that follow, the tilde will help us to distinguish time-dependent (or signal) variables from system parameters or constants. Although the wave is periodic, it may be of arbitrary shape. The simplest case is a sinusoidal wave, which means

$$\tilde{\psi} = \psi e^{j\omega t}, \quad (1.2)$$

where $\omega = 2\pi f$ is the angular frequency in rad/s and f is the frequency in Hz (hertz, formerly cycles/second). Note that if ψ is real, it represents the peak amplitude of $\tilde{\psi}$. However, it may be complex, containing phase information such as that relating to the

position in space, in which case the peak amplitude is the magnitude of ψ or $|\psi|$. Because most of the problems dealt with in this chapter relate to steady-state linear systems driven by sinusoidal sources, this simple shorthand saves us from having to carry the time dependency term, $e^{j\omega t}$, through the calculations. If we are deriving an expression for one harmonically varying quantity in terms of another, the exponent will cancel in the final transfer function.

Instantaneous value

In the steady state, the instantaneous value $\psi(t)$ is defined by

$$\psi(t) = \Re(\tilde{\psi}) = \Re(\psi e^{j\omega t}). \quad (1.3)$$

This is the actual value that would be observed at any instant in time t . However, the real part of a complex quantity should only be taken at the end of deriving an expression so that the correct phase relationships are maintained throughout. It is often the case that the product of two imaginary quantities yields a real one.

Root mean square value

The root mean square or rms value of a time-varying quantity is that which delivers the same amount of power on average as a constant quantity of the same value. For example, a direct electrical current passing through an electrical resistance produces the same amount of heat as an alternating current having the same rms value. The rms value ψ_{rms} is given by

$$\psi_{\text{rms}} = \sqrt{\frac{1}{T} \int_0^T (\psi(t))^2 dt}. \quad (1.4)$$

If the quantity $\psi(t)$ is a periodic function of time, then $T = 1/f$ is the period of repetition. It turns out that in the case of the simple sinusoidal function described by Eq. (1.3),

$$\psi_{\text{rms}} = \frac{|\tilde{\psi}|}{\sqrt{2}}, \quad (1.5)$$

where $|\tilde{\psi}|$ denotes the magnitude of $\tilde{\psi}$. However, the periodic function can have any arbitrary shape, which is expandable by a Fourier series of harmonics. The rms value is then given by the Euclidian norm (or root of the sum of the squares) of the peak amplitudes of the harmonics divided by $\sqrt{2}$. In the case of nonperiodic quantities, the interval T should be long enough to make the value obtained essentially independent of small changes in the length of the interval.



1.6 STANDARD INTERNATIONAL (SI) UNITS

The SI system of units is used throughout this book. Some of the fundamental units are listed in Table 1.1. However, this list is by no means exhaustive. Other units used in electroacoustics can be derived from them and will be introduced as and when needed.

In addition, for very large or very small quantities, it is useful to use the prefixes shown in Table 1.2.



1.7 PRESSURE AND DENSITY

The standard unit of pressure in the SI system is the pascal (Pa), where $1 \text{ Pa} = 1 \text{ N/m}^2$.

Static pressure (P_0)

The static pressure at a point in the medium is the pressure that would exist at that point with no sound waves present. At normal barometric pressure, P_0 equals approximately 10^5 Pa . Standard atmospheric pressure is usually taken to be 0.760 m Hg at 0°C . This is a pressure of $101,325 \text{ Pa}$. In this chapter, when solving problems we shall assume $P_0 = 10^5 \text{ Pa}$.

Table 1.1 List of SI units

Quantity	Unit	Symbol
Length	Meter	m
Mass	Kilogram	kg
Time	Second	s
Temperature	Kelvin	K
Magnetic flux density	Tesla	T
Force	Newton	N
Power	Watt	W

Table 1.2 Prefixes for large or small quantities

Multiples	Name	Deca	Hecto	Kilo	Mega	Giga	Tera	Peta	Exa	Zetta	Yotta
	Symbol	da	h	k	M	G	T	P	E	Z	Y
	Factor	10^1	10^2	10^3	10^6	10^9	10^{12}	10^{15}	10^{18}	10^{21}	10^{24}
Subdivisions	Name	Deci	Centi	Milli	Micro	Nano	Pico	Femto	Atto	Zepto	Yocto
	Symbol	d	c	m	μ	n	p	f	a	z	y
	Factor	10^{-1}	10^{-2}	10^{-3}	10^{-6}	10^{-9}	10^{-12}	10^{-15}	10^{-18}	10^{-21}	10^{-24}

Microbar (μbar)

Although not an SI unit, a microbar is a unit of pressure often used in acoustics. One microbar is equal to 0.1 Pa.

Instantaneous sound pressure [$p(t)$]

The instantaneous sound pressure at a point is the incremental change from the static pressure at a given instant caused by the presence of a sound wave. The unit is the pascal (Pa).

Effective sound pressure (p_{rms})

The effective sound pressure at a point is the root mean square (rms) value of the instantaneous sound pressure. The unit is the pascal (Pa).

Density of air (ρ_0)

The ambient density of air is given by the formula

$$\rho_0 = \frac{P_0}{287T} \text{ kg/m}^3, \quad (1.6)$$

where T is the absolute temperature and P_0 is the static pressure. At a normal room temperature of $T = 295^\circ\text{K}$ (22°C or 71.6°F) and for a static pressure $P_0 = 10^5$ Pa, the ambient density is

$$\rho_0 = 1.18 \text{ kg/m}^3.$$

This value of ρ_0 will be used in solving problems unless otherwise stated. Note that here the temperature in $^\circ\text{C}$ is obtained by subtracting 273 from the one in $^\circ\text{K}$.

**1.8 SPEED AND VELOCITY****Speed of sound (c)**

The speed of sound in air is given approximately by the formula

$$c = 331.4 + 0.607\theta \text{ m/s} \quad (1.7)$$

where θ is the ambient temperature in $^\circ\text{C}$. For temperatures above 30°C or below -30°C , the velocity of sound must be determined from the exact formula:

$$c = 331.4 \frac{\sqrt{T}}{273} = 331.4 \sqrt{1 + \frac{\theta}{273}} \text{ m/s}, \quad (1.8)$$

where T is the ambient temperature in °K. At a normal room temperature of $\theta = 22^\circ\text{C}$ ($=71.6^\circ\text{F}$),

$$c = 344.8 \text{ m/s, or } 1131.2 \text{ ft/s.}$$

These values of c will be used in solving problems unless otherwise stated.

Instantaneous particle velocity (particle velocity) [$u(t)$]

The instantaneous particle velocity at a point is the velocity, due to the sound wave only, of a given infinitesimal part of the medium at a given instant. It is measured over and above any motion of the medium as a whole. The unit is m/s.

Effective particle velocity (u_{rms})

The effective particle velocity at a point is the root mean square of the instantaneous particle velocity (see [Effective sound pressure](#) section for details). The unit is m/s.

Instantaneous volume velocity [$U(t)$]

The instantaneous volume velocity, due to the sound wave only, is the rate of flow of the medium perpendicularly through a specified area S . That is, $U(t) = Su(t)$, where $u(t)$ is the instantaneous particle velocity. The unit is m^3/s .



1.9 IMPEDANCE

Acoustic impedance (Z_A) (American standard acoustic impedance)

The acoustic impedance at a given surface is defined as the complex ratio [6] of effective sound pressure averaged over the surface to effective volume velocity through it. The surface may be either a hypothetical surface in an acoustic medium or the moving surface of a mechanical device. The unit is $\text{N}\cdot\text{s}/\text{m}^5$ or rayls/m^2 [7].

$$Z_A = \frac{\tilde{p}}{\tilde{U}} \text{ N}\cdot\text{s}/\text{m}^5 (\text{rayls}/\text{m}^2). \quad (1.9)$$

Specific acoustic impedance (Z_S)

The specific acoustic impedance is the complex ratio of the effective sound pressure at a point of an acoustic medium or mechanical device to the effective particle velocity at that point. The unit is $\text{N}\cdot\text{s}/\text{m}^3$ or rayls [8]. That is,

$$Z_S = \frac{\tilde{p}}{\tilde{u}} \text{ N}\cdot\text{s}/\text{m}^3 (\text{rayls}). \quad (1.10)$$

Mechanical impedance (Z_M)

The mechanical impedance is the complex ratio of the effective force acting on a specified area of an acoustic medium or mechanical device to the resulting effective linear velocity through or of that area, respectively. The unit is $\text{N}\cdot\text{s}/\text{m}$ or $\text{rayls}\cdot\text{m}^2$. That is,

$$Z_M = \frac{\tilde{f}}{\tilde{u}} \text{N}\cdot\text{s}/\text{m}(\text{rayls}\cdot\text{m}^2). \quad (1.11)$$

Characteristic impedance ($\rho_0 c$)

The characteristic impedance is the ratio of the effective sound pressure at a given point to the effective particle velocity at that point in a free, plane, progressive sound wave. It is equal to the product of the density of the medium times the speed of sound in the medium ($\rho_0 c$). It is analogous to the characteristic impedance of an infinitely long, dissipationless electric transmission line. The unit is $\text{N}\cdot\text{s}/\text{m}^3$ or rayls .

In the solution of problems in this book, we shall assume for air that

$$\rho_0 c = 407 \text{ rayls},$$

which is valid for a temperature of 22°C (71.6°F) and a static pressure of 10^5 Pa .



1.10 INTENSITY, ENERGY DENSITY, AND LEVELS

Sound intensity (I)

The sound intensity measured in a specified direction at a point is the average rate at which sound energy is transmitted through a unit area perpendicular to the specified direction at the point considered. The unit is W/m^2 . In a plane or spherical free-progressive sound wave, the intensity *in the direction of propagation* is

$$I = \frac{p_{\text{rms}}^2}{\rho_0 c} = \frac{|\tilde{p}|^2}{2\rho_0 c} \text{W}/\text{m}^2. \quad (1.12)$$

Sound energy density (D)

The sound energy density is the sound energy in a given infinitesimal part of the gas divided by the volume of that part of the gas. The unit is $\text{W}\cdot\text{s}/\text{m}^3$. In many acoustic environments, such as in a plane wave, the sound energy density at a point is

$$D = \frac{p_{\text{rms}}^2}{\rho_0 c^2} = \frac{p_{\text{rms}}^2}{\gamma P_0} \text{W}\cdot\text{s}/\text{m}^3. \quad (1.13)$$

where γ is the ratio of specific heats for a gas and is equal to 1.4 for air and other diatomic gases. The quantity γ is dimensionless.

Electric power level or acoustic intensity level

The electric power level, or the acoustic intensity level, is a quantity expressing the ratio of two electrical powers or of two sound intensities in logarithmic form. The unit is the decibel (dB). Definitions are

$$\text{Electric power level} = 10 \log_{10} \frac{W_1}{W_2} \text{ dB} \quad (1.14)$$

$$\text{Acoustic intensity level} = 10 \log_{10} \frac{I_1}{I_2} \text{ dB} \quad (1.15)$$

where W_1 and W_2 are two electrical powers and I_1 and I_2 are two sound intensities.

Extending this thought further, we see from Eq. (1.14) that

$$\begin{aligned} \text{Electric power level} &= 10 \log_{10} \frac{e_{1\text{rms}}^2}{R_1} \frac{R_2}{e_{2\text{rms}}^2} \text{ dB} \\ &= 20 \log_{10} \frac{e_{1\text{rms}}}{e_{2\text{rms}}} + 10 \log_{10} \frac{R_2}{R_1} \text{ dB} \end{aligned} \quad (1.16)$$

where $e_{1\text{rms}}$ is the voltage across the resistance R_1 in which a power W_1 is being dissipated and $e_{2\text{rms}}$ is the voltage across the resistance R_2 in which a power W_2 is being dissipated. Similarly,

$$\text{Acoustic intensity level} = 20 \log_{10} \frac{p_{1\text{rms}}}{p_{2\text{rms}}} + 10 \log_{10} \frac{R_{S2}}{R_{S1}} \text{ dB} \quad (1.17)$$

where $p_{1\text{rms}}$ is the pressure at a point where the specific acoustic resistance (i.e., the real part of the specific acoustic impedance) is R_{S1} and $p_{2\text{rms}}$ is the pressure at a point where the specific acoustic resistance is R_{S2} . We note that

$$10 \log_{10}(W_1/W_2) = 20 \log_{10}(E_1/E_2)$$

only if $R_1 = R_2$ and that

$$10 \log_{10}(I_1/I_2) = 20 \log_{10}(p_{1\text{rms}}/p_{2\text{rms}})$$

only if $R_{S2} = R_{S1}$.

The word “level” implies a position relative to another position, for example, “the water level is 2 m above its normal level.” This means that any quantity in acoustics designated as “level” is the magnitude of a quantity, expressed in logarithmic units,

which is so many units above the magnitude of another quantity, also expressed in logarithmic units. Hence, $10 \log A$ is not a level, but

$$10 \log A - 10 \log B = 10 \log(A/B)$$

is a level for A measured above a level for B . In electronics and acoustics, the level differences are measured in decibels. The quantity B is usually referred to as the “reference quantity.”

Levels involving voltage and pressure alone are sometimes spoken of with no regard to the equalities of the electric resistances or specific acoustic resistances. This practice leads to serious confusion. It is emphasized that the manner in which the terms are used should be clearly stated always by the user to avoid confusion.

Sound pressure level

The sound pressure level (SPL) of a sound, in decibels, is 20 times the logarithm to the base 10 of the ratio of the measured effective sound pressure of this sound to a reference effective sound pressure. That is,

$$\text{SPL} = 20 \log_{10} \frac{p_{\text{rms}}}{p_{\text{ref}}} \text{ dB.} \quad (1.18)$$

In the United States, p_{ref} is either

$p_{\text{ref}} = 20 \mu\text{Pa rms}$ (0.0002 $\mu\text{bar rms}$) or

$p_{\text{ref}} = 0.1 \text{ Pa rms}$ (1 $\mu\text{bar rms}$)

The reference pressure listed first above is in general use for measurements dealing with hearing and for sound level and noise measurements in air (e.g., in rooms and outdoors) and sometimes in liquids. The second reference pressure has gained widespread use for calibrations of transducers and some types of sound level measurements in liquids. The two reference levels are almost exactly 74 dB apart. The reference pressure must always be stated explicitly. Thus, in the case of Eq. (1.18), using the first reference pressure, the result of a measurement would be expressed. “The sound pressure level is X decibels *re* (0.0002 μbar).”

Intensity level (IL)

The intensity level of a sound, in decibels, is 10 times the logarithm to the base 10 of the ratio of the intensity of this sound to a reference intensity. That is,

$$\text{IL} = 10 \log_{10} \frac{I}{I_{\text{ref}}} \text{ dB} \quad (1.19)$$

In the United States the reference intensity is usually taken to be 10^{-12} W/m^2 . This reference at standard atmospheric conditions in a plane or spherical progressive wave was

originally selected as corresponding approximately to the reference pressure (0.0002 μbar).

The exact relation between intensity level and SPL in a plane or spherical progressive wave may be found by substituting Eq. (1.12) for intensity in Eq. (1.19):

$$\text{IL} = \text{SPL} + 10 \log_{10} \frac{p_{\text{ref}}^2}{\rho_0 c I_{\text{ref}}} \text{ dB.} \quad (1.20)$$

Substituting $p_{\text{ref}} = 20 \mu\text{Pa rms}$ and $I_{\text{ref}} = 10^{-12} \text{ W/m}^2$ yields

$$\text{IL} = \text{SPL} + 10 \log_{10} \frac{400}{\rho_0 c} \text{ dB.} \quad (1.21)$$

It is apparent that the intensity level IL will equal the SPL only if $\rho_0 c = 400$ rays. For certain combinations of temperature and static pressure, this will be true, although for $T = 22^\circ\text{C}$ and $P_0 = 10^5 \text{ Pa}$, $\rho_0 c = 407$ rays. For this common case then, the intensity level is smaller than the SPL by about 0.1 dB. The reference quantity must always be stated explicitly.

Acoustic power level (PWL)

The acoustic power level of a sound source, in decibels, is 10 times the logarithm to the base 10 of the ratio of the acoustic power radiated by the source to a reference acoustic power. That is,

$$\text{PWL} = 10 \log_{10} \frac{W}{W_{\text{ref}}} \text{ dB.} \quad (1.22)$$

In most countries, W_{ref} is 1 pW (i.e., 10^{-12} W). This means that a source radiating one acoustic watt has a power level of 120 dB.

If the temperature is 20°C (67°F) and the pressure is 101,325 Pa (0.76 m Hg), the SPL in a duct with an area of 1 m^2 cross section, or at a distance of 0.282 m from the center of a “point” source (at this distance, the spherical surface has an area of 1 m^2), is, from Eqs. (1.12) and (1.18),

$$\begin{aligned} \text{SPL}_{1\text{m}^2} &= 10 \log_{10} \frac{I \rho_0 c}{p_{\text{ref}}^2} = 10 \log_{10} \frac{W \rho_0 c}{S p_{\text{ref}}^2} \\ &= 10 \log_{10} \left(W \times 412.5 \times \frac{1}{(2 \times 10^{-5})^2} \right) \\ &= 10 \log_{10} \frac{W}{10^{-12}} + 0.1, \end{aligned}$$

where W is acoustic power in W, $\rho_0 c$ is characteristic impedance = 412.5 rays, $S = 1 \text{ m}^2$ of area, and p_{ref} is rms reference sound pressure = 20 μPa rms.

In words, the SPL equals the acoustic power level plus 0.1 dB under the special conditions that the power passes uniformly through an area of 1 m^2 , the temperature is 20°C (67°F), and the barometric pressure is 0.76 m (30 in.) Hg.

Sound level

The sound level at a point in a sound field is the reading in decibels (dB) of a sound level meter constructed and operated in accordance with the latest edition of “American National Standard Specification for Sound Level Meters [9].”

The meter reading (in decibels, dB) corresponds to a value of the sound pressure integrated over the audible frequency range with a specified frequency weighting and integration time. The standard sound level meter has three frequency weightings, A, B, and C, as shown in Fig. 1.2. The C scale treats all frequencies within the operating range approximately equally. The B scale is seldom used. The A scale discriminates against frequencies below 800 Hz. When reporting measurements, if the C scale has been used, the result is usually given in dB. If the A scale has been used, the result must be given in dBA.

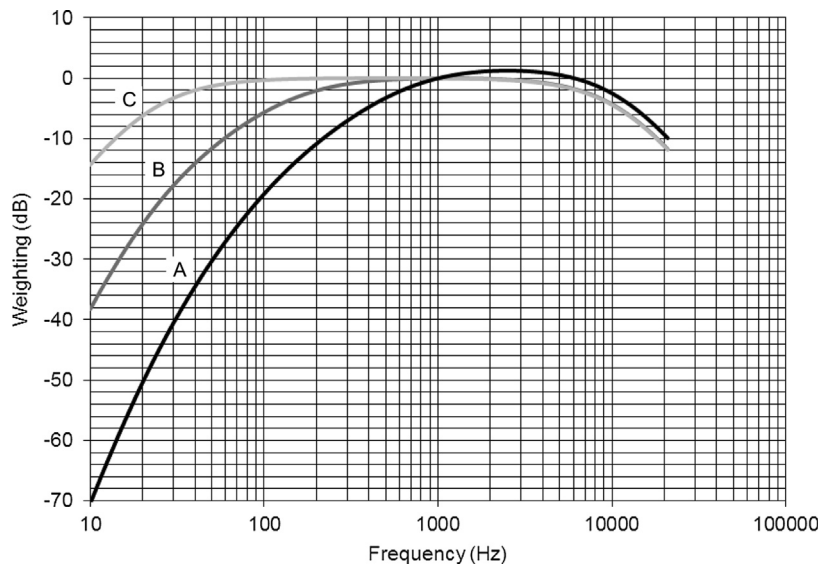


Figure 1.2 Weighting curves for sound level measurements. The A, B, and C curves can be regarded as very rough approximations to the contours of equal loudness [10] at 40, 70, and 100 phons, respectively, to compensate for the reduced sensitivity of the ear to very low and very high frequencies. Hence, the weighted sound level in phons at any frequency is the sound level in dB SPL (sound pressure level) at a frequency of 1 kHz that sounds as loud, and 0 phons is roughly the lower limit of perception, depending on the individual.

Band power level (PWL_{*n*})

The band power level for a specified frequency band is the acoustic power level for the acoustic power contained within the band. The width of the band and the reference power must be specified. The unit is the decibel. The letter *n* is the designation number for the band being considered.

Band pressure level (BPL_{*n*})

The band pressure level of a sound for a specified frequency band is the effective SPL for the sound energy contained within the band. The width of the band and the reference pressure must be specified. The unit is the decibel. The letter *n* is the designation number for the band being considered.

Power spectrum level

The power spectrum level of a sound at a specified frequency is the power level for the acoustic power contained in a band one cycle per second wide, centered at this specified frequency. The reference power must be specified. The unit is the decibel (see also the discussion under [Pressure spectrum level](#)).

Pressure spectrum level

The pressure spectrum level of a sound at a specified frequency is the effective SPL for the sound energy contained within a band one cycle per second wide, centered at this specified frequency. The reference pressure must be explicitly stated. The unit is the decibel.

Discussion. The concept of pressure spectrum level ordinarily has significance only for sound having a continuous distribution of energy within the frequency range under consideration.

The level of a band of uniform noise with a continuous spectrum exceeds the spectrum level by

$$C_n = 10 \log_{10}(f_b - f_a) \text{ dB}, \quad (1.23)$$

where f_b and f_a are the upper and lower frequencies of the band, respectively.

The level of a uniform noise with a continuous spectrum in a band of width $f_b - f_a$ Hz is therefore related to the spectrum level by the formula

$$L_n = C_n + S_n, \quad (1.24)$$

where L_n is SPL in dB of the noise in the band of width $f_b - f_a$, for C_n see [Eq. \(1.23\)](#), S_n is spectrum level of the noise, and *n* is designation number for the band being considered.

NOTES

- [1] Moore's law was originated by Gordon E. Moore, a co-founder of Intel, in 1965 and states that the number of transistors on an integrated circuit for minimum component cost doubles every 24 months.
- [2] For those who have wondered how those impedance and directivity plots were calculated for Acoustics in 1952, MIT hired a room of over 50 women, each were given a motorized mechanical computer of that era, and they did the computations for professors. They were efficient, accurate, and got large jobs done in short times by working long hours.
- [3] Hamming RW. Numerical methods for scientists and engineers. 2nd ed. Dover Publications; 1987 [Preface].
- [4] This is only approximately true, as the air does have viscosity, but the shearing forces are very small compared with those in solids.
- [5] A good manual of terminology is American national standard acoustical terminology. ANSI S1.1-1994 (R2004). New York (N.Y.): American National Standards Institute. <http://webstore.ansi.org/>.
- [6] Complex ratio has the same meaning as the complex ratio of voltage and current in electric-circuit theory.
- [7] This notation is taken from table 12.1 of American national standard acoustical terminology, ANSI S1.1-1994 (R2004).
- [8] Named in honor of Lord Rayleigh.
- [9] American National standard specification for sound level meters, ANSI S1.4-1983 (R2006)/ANSI S1.4A-1985 (R2006). New York (N.Y.): American National Standards Institute.
- [10] See ISO 226. Acoustics: Normal equal-loudness-level contours. Available from: 2003 <http://www.iso.org>.

The wave equation and solutions

PART III: THE WAVE EQUATION

2.1 INTRODUCTION

We have already outlined the nature of sound propagation in a gas in a qualitative way. In this chapter we shall put the physical principles described earlier into the language of mathematics. The approach is in two steps. First, we shall establish equations expressing Newton's second law of motion, the gas law, and the laws of conservation of mass. Second, we shall combine these equations to produce a wave equation.

The mathematical derivations are given in two ways: with and without use of vector algebra. Those who are familiar with vector notations will appreciate the generality of the three-dimensional vector approach. The two derivations are carried on in parallel; on the left sides of the pages, the one-dimensional wave equation is derived with the use of simple differential notations; on the right sides, the three-dimensional wave equation is derived with the use of vector notations. The simplicity of the vector operations is revealed in the side-by-side presentation of the two derivations.

2.2 DERIVATION OF THE WAVE EQUATION

2.2.1 The equation of motion

If we write Newton's second law for a small volume of gas located in a homogeneous medium, we obtain the equation of motion, or the force equation as it is sometimes called. Imagine the small volume of gas to be enclosed in a box with weightless flexible sides (Fig. 2.1).

One-dimensional derivation [1]

Let us suppose that the box is situated in a medium where the sound pressure p increases from left to right at a space rate of $\partial p/\partial x$ (see Fig. 2.1).

Three-dimensional derivation [2]

Let us suppose that the box is situated in a medium (see Fig. 2.1) where the sound pressure p changes in space at a space rate of

$$\mathbf{grad} p = \nabla p = \mathbf{i} \frac{\partial p}{\partial x} + \mathbf{j} \frac{\partial p}{\partial y} + \mathbf{k} \frac{\partial p}{\partial z},$$

where \mathbf{i} , \mathbf{j} , and \mathbf{k} are unit vectors in the x , y , and z directions, respectively, and p is the pressure at a point.

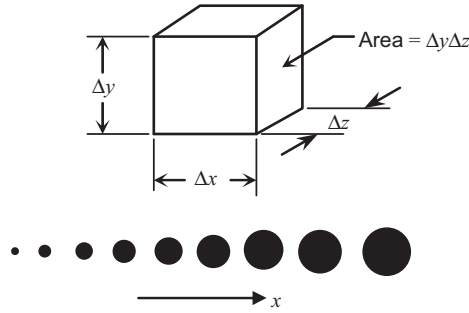


Figure 2.1 The very small “box” of air shown here is part of a gaseous medium in which the sound pressure increases from left to right at a space rate of $\partial p/\partial x$ (or, in vector notation, $\text{grad } p$). The sizes of the dots indicate the magnitude of the sound pressure at each point.

Assume that the sides of the box are completely frictionless, i.e., any viscous drag between gas particles inside the box and those outside is negligible. Thus the only forces acting on the enclosed gas are due to the pressures at the faces of the box.

The difference between the forces acting on the two sides of our tiny box of gas is equal to the rate at which the force changes with distance times the incremental length of the box:

Force acting to accelerate the box in the positive x direction

$$= -\left(\frac{\partial p}{\partial x}\Delta x\right)\Delta y\Delta z. \quad (2.1a)$$

Force acting to accelerate the box in the positive direction

$$= -\mathbf{i}\left[\left(\frac{\partial p}{\partial x}\Delta x\right)\Delta y\Delta z + \mathbf{j}\left(\frac{\partial p}{\partial y}\Delta y\right)\Delta x\Delta z + \mathbf{k}\left(\frac{\partial p}{\partial z}\Delta z\right)\Delta x\Delta y\right]. \quad (2.1b)$$

Note that the positive gradient causes an acceleration of the box in the negative direction of x .

Division of both sides of the above equation by $\Delta x \Delta y \Delta z = V$ gives the force per unit volume acting to accelerate the box:

$$\frac{f}{V} = -\frac{\partial p}{\partial x}. \quad (2.2a)$$

Division of both sides of the equation by $\Delta x \Delta y \Delta z = V$ gives the force per unit volume acting to accelerate the box:

$$\frac{f}{V} = -\nabla p. \quad (2.2b)$$

By Newton's Law, the force per unit volume (f/V) of Eq. (2.2) must be equal to the time rate of change of the momentum per unit volume of the box. We have already assumed that our box is a deformable packet so that the mass of the gas within it is always constant. That is,

$$\frac{f}{V} = -\frac{\partial p}{\partial x} = \frac{M}{V} \frac{\partial u}{\partial t} = \rho' \frac{\partial u}{\partial t}, \quad (2.3a)$$

$$\frac{f}{V} = -\nabla p = \frac{M}{V} \frac{D\mathbf{q}}{Dt} = \rho' \frac{D\mathbf{q}}{Dt}, \quad (2.3b)$$

Where u is the average velocity of the gas in the "box" in the x direction, ρ' is the space average of the instantaneous density of the gas in the box, and $M = \rho' V$ is the total mass of the gas in the box.

Where \mathbf{q} is the average vector velocity of the gas in the "box," ρ' is the average density of the gas in the box, and $M = \rho' V$ is the total mass of the gas in the box.

D/Dt is not a simple partial derivative but represents the total rate of the change of the velocity of the particular bit of gas in the box regardless of its position, i.e.,

$$\frac{D\mathbf{q}}{Dt} = \frac{\partial \mathbf{q}}{\partial t} + q_x \frac{\partial \mathbf{q}}{\partial x} + q_y \frac{\partial \mathbf{q}}{\partial y} + q_z \frac{\partial \mathbf{q}}{\partial z},$$

where q_x , q_y , and q_z are the components of the vector particle velocity \mathbf{q} .

If the vector particle velocity \mathbf{q} is small enough, the rate of change of momentum of the particles in the box can be approximated by the rate of change of momentum at a fixed point, $D\mathbf{q}/Dt \approx \partial \mathbf{q}/\partial t$, and the instantaneous density ρ' can be approximated by the average density ρ_0 . Then,

If the change in density of the gas due to the sound wave is small enough, then the instantaneous density ρ' is approximately equal to the average density ρ_0 .

Then,

$$-\frac{\partial p}{\partial x} = \rho_0 \frac{\partial u}{\partial t}. \quad (2.4a)$$

$$-\nabla p = \rho_0 \frac{\partial \mathbf{q}}{\partial t}. \quad (2.4b)$$

The approximations just given are generally acceptable provided the sound pressure levels being considered are below about 110 dB re 20 μPa . Levels above 110 dB are so large as to create hearing discomfort in many individuals.

2.2.2 The gas law

If we assume an ideal gas, the Charles–Boyle gas law applies to the box. It is

$$PV = RT \quad (2.5)$$

where P is the total pressure in the box, V is the volume equal to $\Delta x \Delta y \Delta z$, T is the absolute temperature in °K, and R is a constant for the gas whose magnitude is dependent on the mass of gas chosen [3]. Using this equation, we can find a relation between the sound pressure (excess pressure) and an incremental change in V for our box. Before we can establish this relation, however, we must know how the temperature T varies with changes in P and V and, in particular, whether the phenomenon is adiabatic or isothermal.

At audible frequencies the wavelength of a sound is long compared with the spacing between air molecules. For example, at 1000 Hz, the wavelength λ equals 0.34 m, as compared with an intermolecular spacing of 10^{-9} m. Now, whenever a portion of any gas is compressed rapidly, its temperature rises, and, conversely, when it is expanded rapidly, its temperature drops. At any one point in an alternating sound field, therefore, the temperature rises and falls relative to the ambient temperature. This variation occurs at the same frequency as that of the sound wave and is in phase with the sound pressure.

Let us assume, for the moment, that the sound wave has only one frequency. At points separated by one-half wavelength, the pressure and the temperature fluctuations will be 180° out of phase with each other. Now the question arises, is there sufficient time during one-half an alternation in the temperature for an exchange of heat to take place between these two points of maximally different temperatures?

It has been established [4] that under normal atmospheric conditions the speed of travel of a thermal diffusion wave at 1000 Hz is about 0.5 m/s, and at 10,000 Hz it is about 1.5 m/s. The time for one-half an alternation of 1000 Hz is 0.0005 s. In this time, the thermal wave travels a distance of only 0.00025 m. This number is very small compared with one-half wavelength (0.17 m) at 1000 Hz. At 10,000 Hz the heat travels 7.5×10^{-5} m, which is a small distance compared with a half wavelength (1.7×10^{-2} m). It appears safe for us to conclude, therefore, that there is negligible heat exchange in the wave in the audible frequency range. Gaseous compressions and expansions of this type are said to be adiabatic.

For adiabatic expansions, the relation between the total pressure and the volume is known to be [5].

$$PV^\gamma = \text{constant}, \quad (2.6)$$

where γ is the ratio of the specific heat of the gas at constant pressure to the specific heat at constant volume for the gas. This equation is obtained from the gas law in the form of

Eq. (2.5), assuming adiabatic conditions. For air, hydrogen, nitrogen, and oxygen, i.e., gases with diatomic molecules,

$$\gamma = 1.4.$$

Expressing Eq. (2.6) in differential form, we have

$$\frac{dP}{P} = -\frac{\gamma dV}{V}. \quad (2.7)$$

Let

$$P = P_0 + p, \quad V = V_0 + \tau, \quad (2.8)$$

where P_0 and V_0 are the undisturbed pressure and volume, respectively, and p and τ are the incremental pressure and volume, respectively, owing to the presence of the sound wave. Then, to the same approximation as that made preceding Eq. (2.4) and because $p \ll P_0$ and $\tau \ll V_0$,

$$\frac{p}{P_0} = -\frac{\gamma \tau}{V_0}. \quad (2.9)$$

The time derivative of this equation gives

$$\frac{1}{P_0} \frac{dp}{dt} = -\frac{\gamma}{V_0} \frac{d\tau}{dt}. \quad (2.10)$$

2.2.3 The continuity equation

The continuity equation is a mathematical expression stating that the total mass of gas in a deformable “box” must remain constant. Because of this law of conservation of mass, we are able to write a unique relation between the time rate of change of the incremental velocities at the surfaces of the box.

One-dimensional derivation

Refer to Fig. 2.2. If the mass of gas within the box remains constant, the change in volume τ depends only on the difference of displacement of the air particles on the opposite sides of the box. Another way of saying this is that, unless the air particles adjacent to any given side of the box move at the same velocity as the box itself, some will cross into or out of the box and the mass inside will change.

Three-dimensional derivation

If the mass of gas within the box remains constant, the change in incremental volume τ depends only on the divergence of the vector displacement. Another way of saying this is that, unless the air particles adjacent to any given side of the box move at the same velocity as the side of the box itself, some will cross into or out of the box and the mass inside will change; so

(Continued)

—cont'd

In a given interval of time the air particles on the left-hand side of the box will have been displaced ξ_x . In this same time, the air particles on the right-hand side will have been displaced

$$\xi_x + \frac{\partial \xi_x}{\partial x} \Delta x.$$

The difference of the two quantities above multiplied by the area $\Delta y \Delta z$ gives the increment in volume τ

$$\tau = \frac{\partial \xi_x}{\partial x} \Delta x \Delta y \Delta z \quad (2.11a)$$

$$\tau = V_0 \operatorname{div} \xi = V_0 \nabla \cdot \xi \quad (2.11b)$$

or

$$\tau = V_0 \frac{\partial \xi_x}{\partial x}. \quad (2.12)$$

Differentiating with respect to time yields,

$$\frac{\partial \tau}{\partial t} = V_0 \frac{\partial u}{\partial x}, \quad (2.13a)$$

Differentiating with respect to time yields,

$$\frac{\partial \tau}{\partial t} = V_0 \nabla \cdot q, \quad (2.13b)$$

where u is the instantaneous particle velocity.

where q is the instantaneous particle velocity.

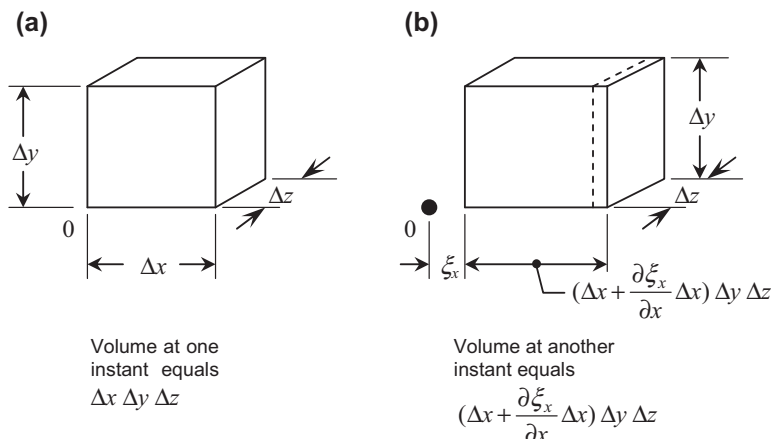


Figure 2.2 Change in volume of the box with change in position. From (a) and (b) it is seen that the incremental change in volume of the box is $\tau = (\partial \xi_x / \partial x) \Delta x \Delta y \Delta z$.

Example 2.1. In the steady state, that is,

$$\partial u / \partial t = j\omega \tilde{u} = \sqrt{2}u_{rms},$$

determine mathematically how the sound pressure in a plane progressive sound wave (one-dimensional case) could be determined from measurement of the particle velocity alone.

Solution. From Eq. (2.4a) we find in the steady state that

$$-\frac{\partial p_{rms}}{\partial x} = j\omega \rho_0 u_{rms}.$$

Written in differential form,

$$-\Delta p_{rms} = j\omega \rho_0 u_{rms} \Delta x.$$

If the particle velocity is 1 cm/s, ω is 1000 rad/s, and Δx is 0.5 cm, then

$$\begin{aligned} \Delta p_{rms} &= -j0.005 \times 1000 \times 1.18 \times 0.01 \\ &= -j0.059 \text{ Pa.} \end{aligned}$$

We shall have an opportunity in Chapter 5 of this text to see a practical application of these equations to the measurement of particle velocity by a velocity microphone.

2.2.4 The wave equation in rectangular coordinates

One-dimensional derivation

The one-dimensional wave equation is obtained by combining the equation of motion (2.4a), the gas law (2.10), and the continuity equation (2.13a). Combination of (2.10) and (2.3a) gives

$$\frac{\partial p}{\partial t} = -\gamma P_0 \frac{\partial u}{\partial x}. \quad (2.14a)$$

Differentiate (2.14a) with respect to t :

$$\frac{\partial^2 p}{\partial t^2} = -\gamma P_0 \frac{\partial^2 u}{\partial t \partial x}. \quad (2.15a)$$

Three-dimensional derivation

The three-dimensional wave equation is obtained by combining the equation of motion (2.4b), the gas law (2.10), and the continuity equation (2.13b). Combination of (2.10) and (2.13b) gives

$$\frac{\partial p}{\partial t} = -\gamma P_0 \nabla \cdot \mathbf{q}. \quad (2.14b)$$

Differentiate (2.14b) with respect to t :

$$\frac{\partial^2 p}{\partial t^2} = -\gamma P_0 \nabla \cdot \frac{\partial \mathbf{q}}{\partial t}. \quad (2.15b)$$

(Continued)

—cont'd

Differentiate (2.4a) with respect to x :

$$-\frac{\partial^2 p}{\partial x^2} = \rho_0 \frac{\partial^2 u}{\partial x \partial t}. \quad (2.16a)$$

Assuming interchangeability of the x and t derivatives, and combining (2.15a) and (2.16a), we get

$$\frac{\partial^2 p}{\partial x^2} = \frac{\rho_0}{\gamma P_0} \frac{\partial^2 p}{\partial t^2}. \quad (2.18a)$$

Take the divergence of each side of Eq. (2.4b):

$$-\nabla \cdot (\nabla p) = \rho_0 \nabla \cdot \frac{\partial \mathbf{q}}{\partial t}. \quad (2.16b)$$

Replacing the $\nabla \cdot (\nabla p)$ by $\nabla^2 p$, we get

$$-\nabla^2 p = \rho_0 \nabla \cdot \frac{\partial \mathbf{q}}{\partial t}, \quad (2.17)$$

where ∇^2 is the operator called the Laplace operator. Combining (2.15b) and (2.17), we get

$$\nabla^2 p = \frac{\rho_0}{\gamma P_0} \frac{\partial^2 p}{\partial t^2}. \quad (2.18b)$$

Let us, by definition, set

$$c^2 = \frac{\gamma P_0}{\rho_0}. \quad (2.19)$$

We shall see later that c is the speed of propagation of the sound wave in the medium. Also, the quantity γP_0 is the *bulk modulus* of the fluid medium.

We obtain the one-dimensional wave equation

$$\frac{\partial^2 p}{\partial x^2} = \frac{1}{c^2} \frac{\partial^2 p}{\partial t^2}. \quad (2.20a)$$

We obtain the three-dimensional wave equation

$$\nabla^2 p = \frac{1}{c^2} \frac{\partial^2 p}{\partial t^2}. \quad (2.20b)$$

In rectangular coordinates

$$\nabla^2 p \equiv \frac{\partial^2 p}{\partial x^2} + \frac{\partial^2 p}{\partial y^2} + \frac{\partial^2 p}{\partial z^2}. \quad (2.21)$$

(Continued)

—cont'd

We could also have eliminated p and retained u , in which case we would have

$$\frac{\partial^2 u}{\partial x^2} = \frac{1}{c^2} \frac{\partial^2 u}{\partial t^2}. \quad (2.22a)$$

We could also have eliminated p and retained \mathbf{q} , in which case we would have

$$\nabla^2 \mathbf{q} = \frac{1}{c^2} \frac{\partial^2 \mathbf{q}}{\partial t^2}, \quad (2.22b)$$

where $\nabla^2 \mathbf{q} = \nabla(\nabla \cdot \mathbf{q})$ when there is no rotation in the medium.

Eqs. (2.20) and (2.22) apply to sound waves of “small” magnitude propagating in a source-free, homogeneous, isotropic, frictionless gas at rest.

2.2.5 The wave equation in cylindrical coordinates

The one-dimensional wave equations derived above are for plane-wave propagation along one dimension of a rectangular coordinate system. In the case of a line source, such as a vertical stack of loudspeakers in an auditorium, the sound spreads out radially in all directions as a cylindrical wave. To apply the wave equation to cylindrical waves, we must replace the operators on the left side of Eqs. (2.20) and (2.22) by operators appropriate to cylindrical coordinates. Assuming equal radiation in all directions about the axis of symmetry, the wave equation in one-dimensional cylindrical coordinates is

$$\frac{\partial^2 p}{\partial w^2} + \frac{1}{w} \frac{\partial p}{\partial w} = \frac{1}{c^2} \frac{\partial^2 p}{\partial t^2}, \quad (2.23)$$

where w is the radial distance from the axis of symmetry or source if it is a line source.

2.2.6 The wave equation in spherical coordinates

In an anechoic (echo-free) chamber or in free space, we frequently wish to express mathematically the radiation of sound from a spherical (nondirectional) source of sound. In this case, the sound wave will expand as it travels away from the source, and the wave front always will be a spherical surface. To apply the wave equation to spherical waves, we must replace the operators on the left side of Eqs. (2.20) and (2.22) by operators appropriate to spherical coordinates.

Assuming equal radiation in all directions, the wave equation in one-dimensional spherical coordinates is

$$\frac{\partial^2 p}{\partial r^2} + \frac{2}{r} \frac{\partial p}{\partial r} = \frac{1}{c^2} \frac{\partial^2 p}{\partial t^2}, \quad (2.24)$$

where r is the distance from the origin of the spherical coordinate system or source if it is a point source. Simple differentiation will show that (2.24) can also be written

$$\frac{\partial^2(pr)}{\partial r^2} = \frac{1}{c^2} \frac{\partial^2(pr)}{\partial t^2}. \quad (2.25)$$

It is interesting to note that this equation has exactly the same form as Eq. (2.20a). Hence, the same formal solution will apply to either equation except that the dependent variable is $p(x,t)$ in one case and $p(r,t)r$ in the other case. The latter suggests that the solution for the spherical wave equation is of the same form as that to the plane wave equation, but divided by r as will be shown further in this text.

2.2.7 General one-dimensional wave equation (Webster's equation) [6]

A general one-dimensional equation that is often used to describe waves in flaring ducts or horns can be written as

$$\frac{1}{S(x)} \frac{\partial}{\partial x} \left(S(x) \frac{\partial p}{\partial x} \right) = \frac{1}{c^2} \frac{\partial^2 p}{\partial t^2}, \quad (2.26)$$

which in expanded form becomes

$$\frac{\partial^2 p}{\partial x^2} + \frac{1}{S(x)} \left(\frac{\partial S(x)}{\partial x} \right) \frac{\partial p}{\partial x} = \frac{1}{c^2} \frac{\partial^2 p}{\partial t^2}, \quad (2.27)$$

where $S(x)$ is a function that describes the variation of cross-sectional area with x . The first term is the Laplace operator and is present in all plane wave equations. It describes the curvature of the pressure distribution along the x ordinate. The second term describes the pressure gradient due to the variation of cross-sectional area with x . Naturally, this term is absent in the case of a plane wave, where the cross-sectional area is constant (and can be infinite in theoretical models). In the case of a cylindrical wave, the area is given by $S(w) = 2\pi w l$, where l is the width of the wave along the axis of symmetry (again this can be infinite). Note that x is replaced by the radial ordinate w . Substituting $S(w) = 2\pi w l$ in Eq. (2.27) yields Eq. (2.23), the wave equation for a cylindrical wave. Likewise, substituting $S(r) = 4\pi r^2$ in Eq. (2.27) and replacing x with r yields Eq. (2.24), the wave equation for a spherical wave.

PART IV: SOLUTIONS OF THE WAVE EQUATION IN ONE DIMENSION

2.3 GENERAL SOLUTIONS OF THE ONE-DIMENSIONAL WAVE EQUATION

The one-dimensional wave equation was derived with either sound pressure or particle velocity as the dependent variable. Particle displacement, or the variational density, may also be used as the dependent variable. This can be seen from Eqs. (2.4a) and (2.13a) and the conservation of mass, which requires that the product of the density and the volume of a small box of gas remain constant. That is,

$$\rho' V = \rho_0 V_0 = \text{constant} \quad (2.28)$$

and so

$$\rho' dV = -V d\rho'. \quad (2.29)$$

Let

$$\bar{\rho}' = \rho_0 + \rho, \quad (2.30)$$

where ρ is the incremental change in density. Then, approximately, from Eqs. (2.8) and (2.29),

$$\rho_0 \tau = -V_0 \rho. \quad (2.31)$$

Differentiating,

$$\frac{\partial \tau}{\partial t} = -\frac{V_0}{\rho_0} \frac{\partial \rho}{\partial t}$$

so that, from Eq. (2.13a),

$$\frac{\partial \rho}{\partial t} = -\rho_0 \frac{\partial u}{\partial x}. \quad (2.32)$$

Also, we know that the particle velocity is the time rate of change of the particle displacement:

$$u = \frac{\partial \xi_x}{\partial t}. \quad (2.33)$$

Inspection of Eqs. (2.4a), (2.13a), (2.32), and (2.33) shows that the pressure, particle velocity, particle displacement, and variational density are related to each other by derivatives and integrals in space and time. These operations performed on the wave equation do not change the form of the solution, as we shall see shortly. Because the form of the solution is not changed, the same wave equation may be used for determining density, displacement, or particle velocity as well as sound pressure by substituting p , or ξ_x , or u for p in Eq. (2.20a) or ρ , ξ , or \mathbf{q} for p in Eq. (2.20b), assuming, of course, that there is no rotation in the medium.

2.3.1 General solution

With pressure as the dependent variable, the wave equation is

$$\frac{\partial^2 p}{\partial x^2} = \frac{1}{c^2} \frac{\partial^2 p}{\partial t^2}. \quad (2.34)$$

The general solution to this equation is a sum of two terms,

$$p = f_1\left(t - \frac{x}{c}\right) + f_2\left(t + \frac{x}{c}\right), \quad (2.35)$$

where f_1 and f_2 are arbitrary functions. We assume only that they have continuous derivatives of the first and second order. Note that because t and x occur together, the first derivatives with respect to x and t are exactly the same except for a factor of $\pm c$.

The ratio x/c must have the dimensions of time, so that c is a speed. From

$$c^2 = \gamma P_0 / \rho_0 \quad [\text{Eq. (2.19)}]$$

we find that

$$c = \left(1.4 \times \frac{10^5}{1.18}\right)^{1/2} = 344.4 \text{ m/s}$$

in air at an ambient pressure of 10^5 Pa and at 22°C . This quantity is nearly the same as the experimentally determined value of the speed of sound, 344.8 see Eq. (1.8), so that we recognize c as the speed at which a sound wave is propagated through the air.

From the general solution to the wave equation given in Eq. (2.35) we observe two very important facts:

1. The sound pressure at any point x in space can be separated into two components: an outgoing wave, $f_1(t - x/c)$, and a backward-traveling wave, $f_2(t + x/c)$.
2. Regardless of the shape of the outward-going wave (or of the backward-traveling wave), it is propagated without change of shape. To show this, let us assume that, at $t = t_1$, the sound pressure at $x = 0$ is $f_1(t_1)$. At a time $t + t_1 + t_2$ the sound wave

will have traveled a distance x equal to t_2c m. At this new time the sound pressure is equal to

$$p = f_1(t_1 + t_2 - t_2c) = f_1(t_1).$$

In other words the sound pressure has propagated without change. The same argument can be made for the backward-traveling wave that goes in the $-x$ direction. It must be understood that inherent in Eqs. (2.34) and (2.35) are two assumptions. First, the wave is a plane wave, i.e., it does not expand laterally. Thus the sound pressure is not a function of the y and z ordinates but is a function of distance only along the x ordinate. Second, it is assumed that there are no losses or dispersion (scattering of the wave by turbulence or temperature gradients, etc.) in the air, so that the wave does not lose energy as it is propagated.

2.3.2 Steady-state solution

In nearly all the studies that we make in this text we are concerned with the steady state. Let us first consider the time-dependent part of the solution at a fixed point in space so that the pressure is only dependent on time. As is well known from the theory of Fourier series, a steady-state periodic wave of arbitrary shape can be represented by a linear summation of sine-wave functions, each of which is of the form

$$p(t) = \sum_{n=-\infty}^{\infty} p_n(t), \quad (2.36)$$

where

$$p_n(t) = c_n e^{j\omega_n t} = c_n (\cos \omega_n t + j \sin \omega_n t), \quad (2.37)$$

where $\omega_n = n\omega = 2\pi nf$ is the angular frequency and c_n is the peak amplitude of the n th component of the wave given by

$$c_n = \frac{1}{T} \int_0^T p(t) e^{-j\omega_n t} dt, \quad (2.38)$$

where $T = 1/f$ is the period of the wave. Taking the second time derivative of p_n yields

$$\frac{\partial^2}{\partial t^2} p_n(t) = \frac{\partial^2}{\partial t^2} c_n e^{j\omega_n t} = -\omega_n^2 c_n e^{j\omega_n t} = -\omega_n^2 p_n(t), \quad (2.39)$$

which gives the identities

$$\frac{\partial}{\partial t} = j\omega_n, \quad (2.40)$$

$$\frac{\partial^2}{\partial t^2} = -\omega_n^2. \quad (2.41)$$

Hence the steady-state plane-wave equation for any point in space can be written in the form

$$\left(\frac{\partial^2}{\partial x^2} + \frac{\omega_n^2}{c^2} \right) p_n(x, t) = 0, \quad (2.42)$$

which is generally known as the *Helmholtz wave equation*. Because the wave is propagated without change of shape, we need to consider, in the steady state, only those solutions to the wave equation for which the time dependence at each point in space is sinusoidal and which have the same angular frequencies $n\omega$ as the source. A general solution that satisfies this equation is given by

$$p_n(x, t) = \left(p_{n+} e^{-j\omega_n x/c} + p_{n-} e^{j\omega_n x/c} \right) e^{j\omega_n t}, \quad (2.43)$$

where the $+$ and $-$ subscripts indicate the forward and backward traveling waves respectively. In the steady state, therefore, we may replace f_1 and f_2 of Eq. (2.35) by a sum of functions each having a particular angular driving frequency ω_n so that

$$p(x, t) = \sum_{n=-\infty}^{\infty} p_n(x, t) = \sum_{n=-\infty}^{\infty} \Re \left(\left(p_{n+} e^{-j\omega_n x/c} + p_{n-} e^{j\omega_n x/c} \right) e^{j\omega_n t} \right). \quad (2.44)$$

Generally we omit writing \Re although it always must be remembered that the real part must be taken when using the final expression for the sound pressure that would actually be observed, for example, when making an animated plot of a sound field.

It is customary in texts on acoustics to define a wave-number k where

$$k = \frac{\omega}{c} = \frac{2\pi f}{c} = \frac{2\pi}{\lambda}, \quad (2.45)$$

which can be considered as the spatial angular frequency in rad/m. When k is multiplied by a characteristic dimension such as the length of a tube or the radius of a circular radiator, it forms a useful dimensionless parameter that is proportional to the frequency. Let us now drop \Re and the subscript n for convenience. Also, we will replace the factor $e^{j\omega t}$ with a tilde. Any one term of Eq. (2.44), with these changes, becomes

$$\tilde{p}(x) = \tilde{p}_+ e^{-jkx} + \tilde{p}_- e^{jkx}. \quad (2.46)$$

Eq. (2.46) represents two traveling waves: one with amplitude \tilde{p}_+ traveling in the positive x direction and the other with amplitude \tilde{p}_- traveling in the negative x direction, where the amplitudes are independent of position x . The appearance of these two solutions occurs because in solving the wave equation we have not specified the direction of travel or any boundary conditions and so the result simply tells us that these solutions can occur. The complex values of \tilde{p}_+ and \tilde{p}_- are determined from the boundary conditions. The real parts of the forward and reverse traveling solutions are represented in Fig. 2.3 (a) and (b) respectively, which shows the waveforms in space at a snapshot in time, whereas if the plots were animated, they would be moving in the directions of the arrows. At any fixed point, the pressure or velocity would oscillate as the wave passed through it, with the oscillations having the same shape versus time as versus distance. This is a property of plane waves where the waves propagate without changing shape. Similarly, the solution to Eq. (2.22a) for velocity, assuming steady-state conditions is

$$\tilde{u}(x) = \tilde{u}_+ e^{-jkx} + \tilde{u}_- e^{jkx}. \quad (2.47)$$

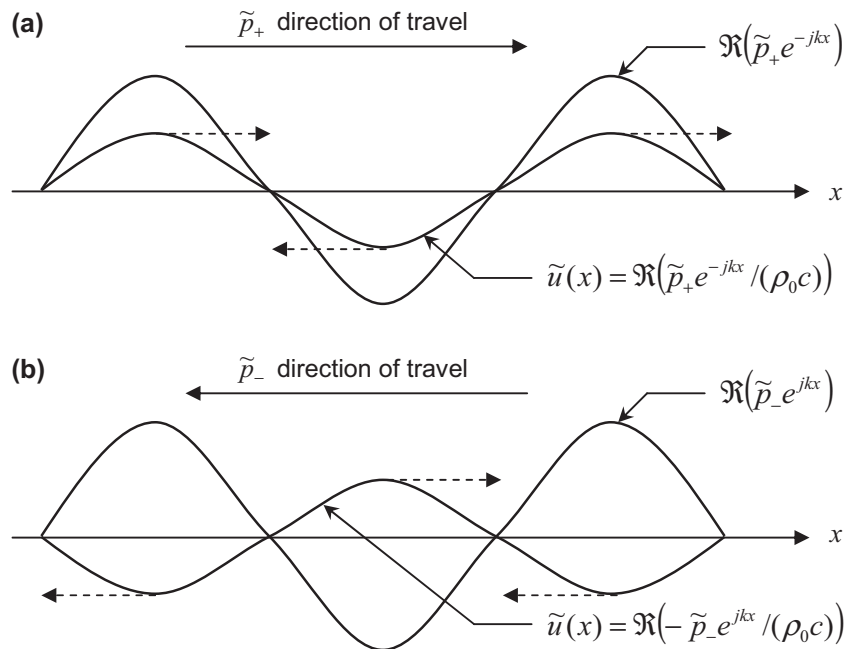


Figure 2.3 Solutions to the steady-state one-dimensional wave equation. (a) Forward and (b) reverse traveling waves.

A similar expression for the velocity can also be obtained from the expression for the pressure by applying Eq. (2.4a) to Eq. (2.46):

$$\begin{aligned}\tilde{u}(x) &= \frac{1}{-j\omega\rho_0} \frac{\partial}{\partial x} \tilde{p}(x) \\ &= \frac{1}{\rho_0 c} \left(\tilde{p}_+ e^{-jkx} - \tilde{p}_- e^{jkx} \right),\end{aligned}\tag{2.48}$$

the real part of which is also shown in Fig. 2.3. The wave Eq. (2.48) for velocity is similar to Eq. (2.46) for pressure except for one important difference, which is the minus sign preceding \tilde{p}_- . The reason for this is fairly simple. During a positive pressure half-cycle, the resulting velocity is always in the direction of travel. Therefore, in the case of the wave with amplitude \tilde{p}_+ traveling in the positive x direction, positive pressure produces positive velocity because it is in the positive x direction, as shown by the dashed arrows in Fig. 2.3a. However, in the case of the wave with amplitude \tilde{p}_- traveling in the negative x direction, positive pressure produces negative velocity because it is in the negative x direction, as shown by the dashed arrows in Fig. 2.3b. Of course, the converse applies during a negative pressure half cycle. The ratio of pressure to particle velocity is the specific acoustic impedance Z_s of the medium, which is obtained by dividing the pressure from Eq. (2.46) by the velocity from Eq. (2.48) to give

$$Z_s = \frac{\tilde{p}(x)}{\tilde{u}(x)} = \rho_0 c.\tag{2.49}$$

It is worth noting that in the case of freely traveling waves, which are also known as progressive waves, the pressure and particle velocity are in phase and hence the impedance has a real value. This is very much a characteristic of traveling longitudinal waves, a class that includes sound pressure waves because the particles oscillate in the direction of propagation as opposed to transverse waves whereby the medium oscillates in a direction at right angles to the direction of propagation. An example of the latter is the wave motion of a plucked string.

Example 2.2. Determine the power flow in a freely traveling wave at a fixed point as a function of time.

Answer:

$$p(t) = K \cos \omega t$$

$$u(t) = p(t)/\rho c$$

$$\text{Power flow} = p^* u = (K^2/\rho c) \cos^2 \omega t = (K^2/\rho c) (1 - \sin^2 \omega t)$$

Thus the power flows by a point in a freely traveling wave like a series of “sausages.” This is explained by referring back to Fig. 1.1. The vibrating surface sends power into the wave when it is moving either to the right or the left. At the instant whenever the surface changes direction, the power drops to zero.

Example 2.3. Assume that for the steady state, at a point $x = 0$, the sound pressure in a one-dimensional outward-traveling wave has the recurrent form shown by the dotted curve in Fig. Ex. 2.3a. This wave form is given by the real part of the equation

$$p(0, t) = 4e^{j628t} + 2e^{j1884t}.$$

(a) What are the particle velocity and the particle displacement as a function of time at $x = 5$ m? (b) What are the rms values of these two quantities? (c) Are the rms values dependent upon x ?

Solution

a. We have for the solution of the wave equation giving both x and t [see Eq. 2.46]

$$p(x, t) = 4e^{j628(t-x/c)} + 2e^{j1884(t-x/c)}.$$

From Eq. (2.4a) we see that

$$u(x, t) = -\frac{1}{j\omega\rho_0} \frac{\partial p(x, t)}{\partial x}$$

or

$$u(x, t) = \frac{1}{\rho_0 c} p(x, t).$$

And from Eq. (2.33) we have

$$\xi(x, t) = \frac{1}{j\rho_0 c} \left(\frac{4}{628} e^{j628(t-x/c)} + \frac{2}{1884} e^{j1884(t-x/c)} \right).$$

At $x = 5$ m, $x/c = 5/344.8 = 0.0145$ s,

$$u(5, t) = \frac{1}{407} \left(4e^{j628(t-0.0145)} + 2e^{j1884(t-0.0145)} \right)$$

and

$$\xi(5, t) = \frac{1}{407} \left(\frac{4}{628} e^{j[628(t-0.0145)-(\pi/2)]} + \frac{2}{1884} e^{j[1884(t-0.0145)-(\pi/2)]} \right).$$

Taking the real parts of the two preceding equations,

$$u(5, t) = \frac{1}{407} (4 \cos(628t - 9.1) + 2 \cos(1884t - 27.3))$$

$$\xi(5, t) = \frac{1}{407} \left(\frac{4}{628} \sin(628t - 9.1) + \frac{2}{1884} \sin(1884t - 27.3) \right).$$

Note that each term in the particle displacement is 90 degrees out of time phase with the velocity and that the wave shape is different. As might be expected, integration diminishes the higher frequencies. These equations are plotted in Fig. Ex. 2.3b.

- b.** The rms magnitude of a sine wave is equal to its peak amplitude divided by $\sqrt{2}$. This may be verified by squaring the sine wave and finding the average value over one cycle and then taking the square root of the result. If two sine waves of different frequencies are present at one time, the rms value of the combination is equal to the square root of the sums of the squares of the individual peak amplitudes divided by $\sqrt{2}$, so that

$$p = \frac{1}{\sqrt{2}} \sqrt{4^2 + 2^2} = 3.16 \text{ Pa,}$$

$$u = \frac{1}{407\sqrt{2}} \sqrt{4^2 + 2^2} = 7.77 \times 10^{-3} \text{ m/s,}$$

$$\xi_x = \frac{1}{407\sqrt{2}} \sqrt{\left(\frac{4}{628}\right)^2 + \left(\frac{2}{1884}\right)^2} = 1.12 \times 10^{-5} \text{ m.}$$

- c.** The rms values of u and ξ_x are independent of x for a plane progressive sound wave.

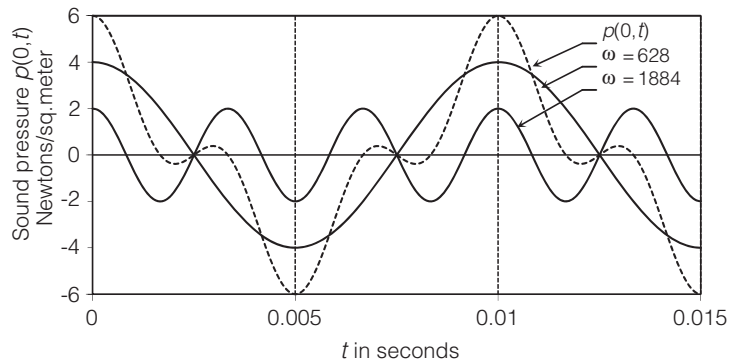


Figure Example 2.3A

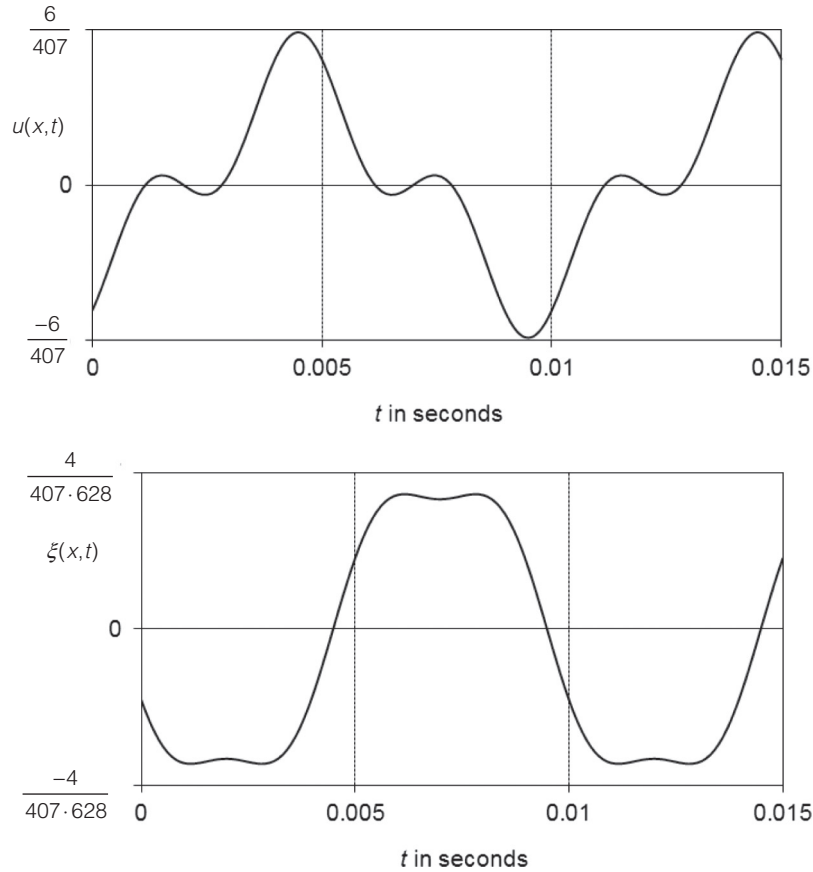


Figure Example 2.3B

2.4 SOLUTION OF WAVE EQUATION FOR AIR IN A TUBE TERMINATED BY AN IMPEDANCE

For this example of wave propagation, we shall consider a hollow cylindrical tube, terminated at one end ($x = 0$) by an impedance Z_T and at the other ($x = l$) end by a flat vibrating piston (see Fig. 2.4). Alternatively, we could have interchanged the positions of the piston and termination impedance, but the arrangement shown has been chosen because it simplifies the equations. For example, in the case of a rigid termination the particle velocity is shown to be proportional to $\sin x$ as opposed to $\sin(l - x)$. However, care needs to be taken when calculating the impedance where the velocity has to be taken as that in the negative x direction. The angular frequency of vibration of the piston

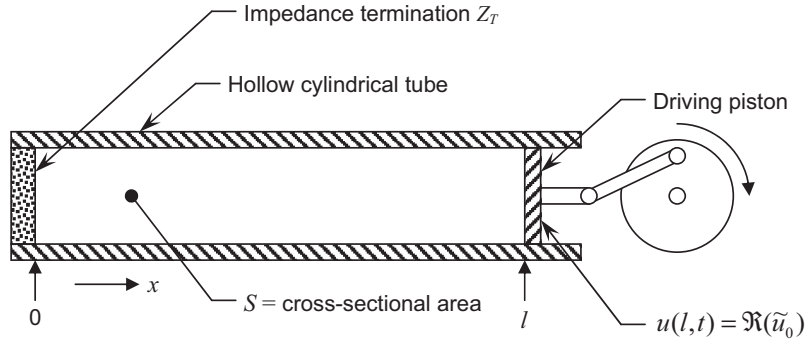


Figure 2.4 Tube with rigid side walls and termination impedance Z_T . The velocity at $x = 0$ has a value of $u_0 \cos \omega t$ m/s.

is ω , and its rms velocity is \tilde{u}_0 at $x = l$. We shall assume that the diameter of the tube is sufficiently small so that the waves travel down the tube with plane wave fronts. For this to be true, the ratio of the wavelength of the sound wave to the diameter of the tube must be greater than about 6.

Particle velocity

The form of solution we shall select is Eq. (2.48). If l is the length of the tube, then at $x = l$ the particle velocity must be equal to the velocity \tilde{u}_0 of the piston. The boundary conditions are:

$$\text{At } x = l, \tilde{u}(l) = \tilde{u}_0,$$

so that

$$\tilde{u}(l) = \frac{\tilde{p}_+ e^{-jkl} - \tilde{p}_- e^{jkl}}{\rho_0 c} = \tilde{u}_0. \quad (2.50)$$

At $x = 0$,

$$\tilde{p}(0)/(-\tilde{u}(0)) = Z_s(0) = Z_T,$$

where the pressure is taken from Eq. (2.46). Note that velocity is negative here because it is in the reverse x direction. Hence

$$\frac{\tilde{p}(0)}{-\tilde{u}(0)} = \frac{\tilde{p}_+ + \tilde{p}_-}{\tilde{p}_- - \tilde{p}_+} \rho_0 c = Z_T. \quad (2.51)$$

Transmitted and reflected pressures

Eliminating \tilde{p}_- between Eqs. (2.50) and (2.51) yields

$$\tilde{p}_+ = \frac{(\rho_0 c - Z_T)\rho_0 c \tilde{u}_0}{\rho_0 c(e^{jkl} + e^{-jkl}) + Z_T(e^{jkl} - e^{-jkl})}. \quad (2.52)$$

Similarly, eliminating \tilde{p}_+ between Eqs. (2.50) and (2.51) yields

$$\tilde{p}_- = \frac{-(\rho_0 c + Z_T)\rho_0 c \tilde{u}_0}{\rho_0 c(e^{jkl} + e^{-jkl}) + Z_T(e^{jkl} - e^{-jkl})}. \quad (2.53)$$

Remember that

$$\sin \gamma = (e^{j\gamma} - e^{-j\gamma})/(2j) \quad \text{and} \quad \cos \gamma = (e^{j\gamma} + e^{-j\gamma})/2.$$

Hence

$$\tilde{p}_+ = \frac{(\rho_0 c - Z_T)\rho_0 c \tilde{u}_0}{2(\rho_0 c \cos kl + jZ_s \sin kl)} \quad (2.54)$$

and

$$\tilde{p}_- = \frac{-(\rho_0 c + Z_T)\rho_0 c \tilde{u}_0}{2(\rho_0 c \cos kl + jZ_s \sin kl)}, \quad (2.55)$$

where \tilde{p}_- is the *transmitted* pressure magnitude and \tilde{p}_+ is *reflected* pressure magnitude. The amount of sound reflected depends on how the tube is terminated. The reflection coefficient Γ is given by

$$\Gamma = \frac{\tilde{p}_+}{\tilde{p}_-} = \frac{Z_T - \rho_0 c}{Z_T + \rho_0 c}. \quad (2.56)$$

In some places along the tube, the reflected wave will interfere *constructively* with the transmitted wave, thus producing a pressure *maximum*, and at others it will interfere *destructively* causing a pressure *minimum*. If the reflection is 100%, these maxima and minima become *antinodes* and *nodes* respectively. We shall examine these in greater detail in the next paragraph, which describes the case of a *rigid termination*. The ratio of maximum to minimum pressure along the tube is given by the *Standing Wave Ratio* or *SWR* where

$$SWR = \frac{1 + |\Gamma|}{1 - |\Gamma|}. \quad (2.57)$$

Table 2.1 Termination impedances, standing wave ratios, and reflection coefficients for three types of tube termination

Quantity	Resilient termination	Anechoic termination	Rigid termination
Termination impedance (Z_T)	0	$\rho_0 c$	∞
Standing wave ratio (SWR)	∞	1	∞
Reflection coefficient (Γ)	-1	0	1
Absorption coefficient (α)	0	1	0

Of particular interest are the cases where (1) the pressure is zero at the termination (resilient termination), (2) the termination impedance is equal to the characteristic impedance of the tube (anechoic termination), and (3) the velocity is zero at the termination (rigid termination). All three cases are summarized in [Table 2.1](#). The first case produces maximum negative reflection (that is, with reversed phase), the second zero reflection, and the third maximum positive reflection.

Sound-proofing materials are often defined by the *absorption coefficient* α , which is given by

$$\alpha = 1 - |\Gamma|^2.$$

Impedance

Inserting [Eqs. \(2.54\) and \(2.55\)](#) into [Eqs. \(2.46\) and \(2.48\)](#) gives us

$$\tilde{p}(x) = -\frac{Z_T \cos kx + j\rho_0 c \sin kx}{\rho_0 c \cos kl + jZ_T \sin kl} \rho_0 c \tilde{u}_0, \quad (2.58)$$

$$\tilde{u}(x) = \frac{\rho_0 c \cos kx + jZ_T \sin kx}{\rho_0 c \cos kl + jZ_T \sin kl} \tilde{u}_0. \quad (2.59)$$

The specific acoustic impedance Z_s along the tube is then given by the ratio of pressure to velocity:

$$Z_s(x) = \frac{\tilde{p}(x)}{-\tilde{u}(x)} = \frac{\frac{Z_T}{\rho_0 c} + j \tan kx}{1 + j \frac{Z_T}{\rho_0 c} \tan kx} \rho_0 c. \quad (2.60)$$

Let us now recast this equation into two series impedances, as seen at the piston:

$$Z_s(l) = \left(\frac{1}{Z_T} + j \frac{1}{\rho_0 c} \tan kl \right)^{-1} + \left(\frac{Z_T}{\rho_0^2 c^2} - j \frac{\cot kl}{\rho_0 c} \right)^{-1}, \quad (2.61)$$

the equivalent circuit for which is shown in [Fig. 2.5](#).

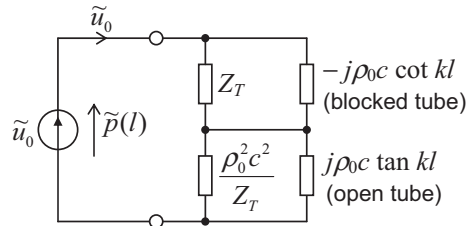


Figure 2.5 Equivalent electrical circuit for a tube with a termination impedance Z_T , in which the single tube is represented by two tube impedances, each in parallel with an external impedance. The piston is represented by a current generator. The reason for this will become clearer in the next chapter.

Amazingly, a tube with any termination impedance Z_T can be represented by the impedance of a blocked tube (with $Z_T = \infty$) in series with an open tube (with $Z_T = 0$) and two external impedances connected across them, which are related to the termination impedance Z_T and characteristic impedance $\rho_0 c$. However, this makes more sense when we consider that when the impedance of the open tube is zero, the impedance of the blocked tube is infinite and vice versa. Hence the impedance seen between the input terminals simply alternates between Z_T and $(\rho_0 c)^2 / Z_T$ as we sweep the piston generator frequency, which is entirely consistent with the standing wave ratio. When $Z_T = \rho_0 c$, the two series impedances are the complex conjugates of each other and we just see the characteristic impedance $\rho_0 c$ at the input terminals. We shall use equivalent circuits extensively in this text. Also, it will be shown in Figs. 10.6 and 10.7 how the impedances of a blocked tube and open tube respectively may be represented by arrays of electrical circuit elements.

Impedance measurement

If we place two probe microphones in the tube, with one at $x = l_1$ and the other at $x = l_2$, then the ratio of the pressures $\tilde{p}(l_1)$ and $\tilde{p}(l_2)$ is given by

$$\frac{\tilde{p}(l_1)}{\tilde{p}(l_2)} = \frac{Z_T \cos kl_1 + j\rho_0 c \sin kl_1}{Z_T \cos kl_2 + j\rho_0 c \sin kl_2}, \quad (2.62)$$

which is independent of \tilde{u}_0 . The termination impedance is then given by

$$\frac{Z_T}{\rho_0 c} = -j \frac{\sin kl_1 - (\sin kl_2) \tilde{p}(l_1) / \tilde{p}(l_2)}{\cos kl_1 - (\cos kl_2) \tilde{p}(l_1) / \tilde{p}(l_2)}, \quad (2.63)$$

which is the principle of an *impedance tube*, which is used for measuring samples of material for which the impedance is unknown. An elegant feature of the method is that the measurement is independent of the piston velocity or actual magnitudes of the

pressures. Only the relative pressure ratio is needed to calculate the impedance. However, when the impedance is a large multiple (or small fraction) of $\rho_0 c$, the calibration of the microphones becomes very critical, as does the accuracy of the distances l_1 and l_2 between them and the sample.

Rigid termination (infinite impedance)

If we let $Z_T = \infty$ in Eq. (2.59), the tube is terminated with a rigid wall, which gives us

$$\tilde{u}(x) = \tilde{u}_0 \frac{\sin kx}{\sin kl} \quad (2.64)$$

or

$$u(x, t) = u_0 e^{j\omega t} \frac{\sin kx}{\sin kl}. \quad (2.65)$$

Refer to Fig. 2.6. If the length l and the frequency are held constant, the particle velocity will vary from a value of zero at $x = 0$ to a maximum at $x = \lambda/4$, that is, at x equal to one-fourth wavelength. In the entire length of the tube the particle velocity varies according to a sine function.

Between the end of the tube and the $\lambda/4$ point, the oscillatory motions are *in phase*. In other words, there is no progressive phase shift with x . This type of wave is called a standing wave [5] because, in the equation, x and ct do not occur as a difference or a sum in the argument of the exponential function. Hence the wave is not propagated. In cases where there are absolutely no losses, the term stationary wave [5] is also used, although this can only be approximated in practice.

In the region between $x = \lambda/4$ and $x = \lambda/2$, the particle velocity still has the same phase except that its amplitude decreases sinusoidally. At $x = \lambda/2$, the particle velocity is zero. In the region between $x = \lambda/2$ and $x = \lambda$ the particle velocity varies with x

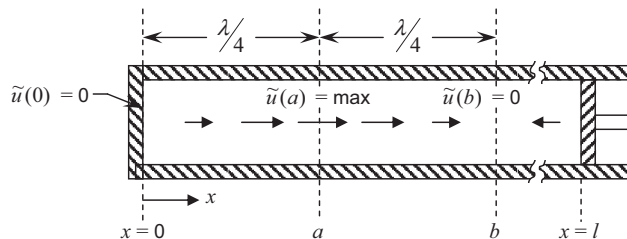


Figure 2.6 Portion of the tube with a rigid termination showing the direction and magnitude of movement of the air particles as a function of x . At position a , the particle velocity and displacement are a maximum. At position b , they are zero.

according to a sine function, but the particles move 180 degrees out of phase with those between 0 and $\lambda/2$. This is seen from Eq. (2.64), wherein the sines of arguments greater than π are negative.

If we fix our position at some particular value of x and assume constant l , then, as we vary frequency, both the numerator and denominator of Eq. (2.64) will vary. When kl is some multiple of π , the particle velocity will become very large, except at $x = l$ or at points where kx is a multiple of π , that is, at points where x equals multiples of $\lambda/2$. Then for $kl = n\pi$

$$l|_{u=\infty} \sim \frac{n\lambda}{2} \quad n = 1, 2, 3, \dots \quad (2.66)$$

Eq. (2.64) would indicate an infinite velocity under this condition. In reality, the presence of some dissipation in the tube, which was neglected in the derivation of the wave equation, will keep the particle velocity finite, though large.

The particle velocity $\tilde{u}(x)$ will be zero at those parts of the tube where $kx = n\pi$ and n is an integer or zero [7]. That is,

$$x|_{\tilde{u}=0} \sim \frac{\lambda}{2}n \quad n = 1, 2, 3, \dots \quad (2.67)$$

In other words, there will be planes of zero particle velocity at points along the length of the tube whenever l is greater than $\lambda/2$.

Some examples of the particle velocity for l slightly greater than various multiples of $\lambda/2$ are shown in Fig. 2.7. Two things in particular are apparent from inspection of these graphs. First, the quantity n determines the approximate number of half wavelengths that exist between the two ends of the tube. Secondly, for a fixed \tilde{u}_0 , the maximum velocity of the wave in the tube will depend on which part of the sine wave falls at $x = l$. For example, if $l - n\lambda/2 = \lambda/4$, the maximum amplitude in the tube will be the same as that at the piston. If $l - n\lambda/2$ is very near zero, the maximum velocity in the tube will become very large.

Let us choose a frequency such that $n = 2$ as shown. Two factors determine the amplitude of the sine function in the tube. First, at $x = l$ the sine curve must pass through the point u_0 . Second, at $x = 0$ the sine curve must pass through zero. It is obvious that one and only one sine wave meeting these conditions can be drawn so that the amplitude is determined. Similarly, we could have chosen a frequency such that $n = 2$, but where the length of the tube is slightly less than two half wavelengths. If this case had been asked for, the sine wave would have ended with a negative instead of a positive slope at $x = l$.

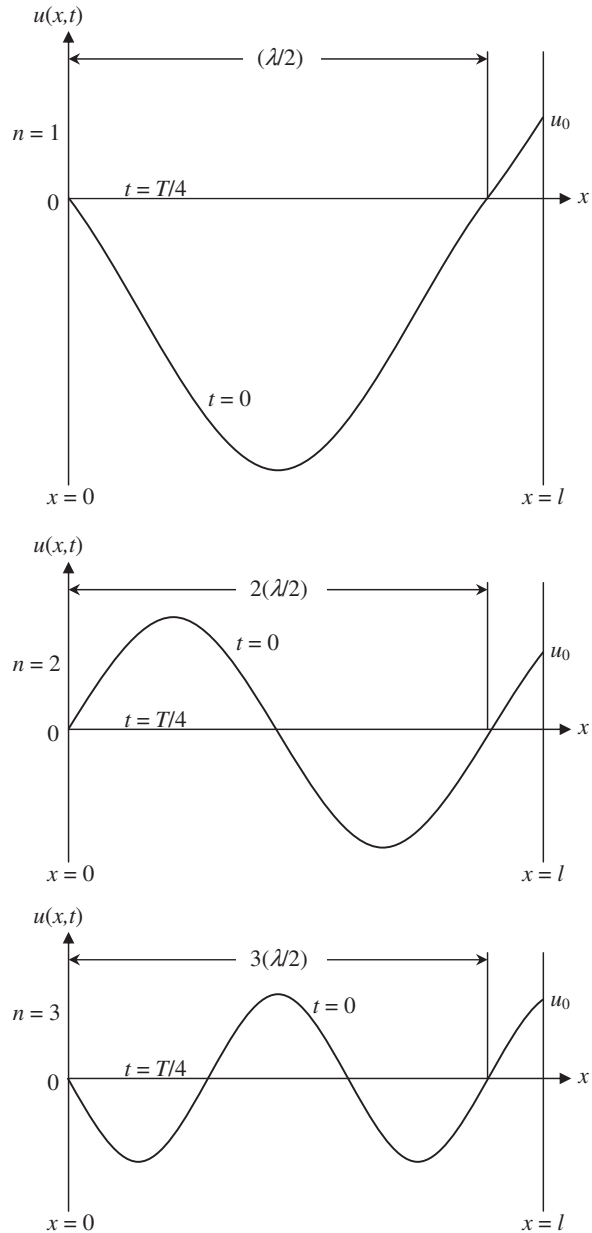


Figure 2.7 Variation of the particle velocity $u(x,t)$ for $t = 0$, as a function of the distance along the tube of Fig. 2.4 for three frequencies, i.e., for three wavelengths. At $x = l$, the rms particle velocity is u_0 , and at $x = 0$, the particle velocity is zero. The period $T = 1/f$.

Sound pressure

The sound pressure in the tube may be found from the velocity with the aid of the equation of motion Eq. (2.4a), which, in the steady state, becomes

$$\tilde{p}(x) = -j\omega\rho_0 \int \tilde{u}(x) dx. \quad (2.68)$$

The constant of integration in Eq. (2.68), resulting from the integration of Eq. (2.4a), must be independent of x because we integrated with respect to x . The constant then represents an increment to the ambient pressure of the entire medium through which the wave is passing. Such an increment does not exist in our tube, so that in Eq. (2.68) we have set the constant of integration equal to zero. Integration of Eq. (2.68), after we have replaced $\tilde{u}(x)$ by its value from Eq. (2.64), yields

$$\tilde{p}(x) = j\rho_0 c u_0 \frac{\cos kx}{\sin kl} \quad (2.69)$$

or

$$p(x, t) = j\rho_0 c u_0 e^{j\omega t} \frac{\cos kx}{\sin kl}. \quad (2.70)$$

This result could alternatively have been obtained by setting $Z_T = \infty$ in Eq. (2.58). The pressure \tilde{p} will be zero at those points of the tube where $kx = n\pi + \pi/2$ (where n is an integer or zero),

$$x|_{\tilde{p}=0} = \frac{\lambda}{2} \left(n + \frac{1}{2} \right). \quad (2.71)$$

The pressure will equal zero at one or more planes in the tube whenever l is greater than $\lambda/4$. Some examples are shown in Fig. 2.8. Here again, quantity n is equal to an approximate number of half wavelengths in the tube.

Refer once more to Fig. 2.7, which is drawn for $t = 0$. The instantaneous particle velocity is at its maximum (as a function of time). By comparison, in Fig. 2.8 at $t = 0$, the instantaneous sound pressure is zero. At a later time $t = T/4 = 1/(4f)$, the instantaneous particle velocity has become zero and the instantaneous sound pressure has reached its maximum. Eqs. (2.64) and (2.69) say that whenever kx is a small number, the sound pressure leads by one-fourth period behind the particle velocity. At some other places in the tube, for example when x lies between $\lambda/4$ and $\lambda/2$, the sound pressure lags the particle velocity by one-fourth period.

To see the relation between p and u more clearly, refer to Fig. 2.7 and Fig. 2.8, for the case of $n = 2$. In Fig. 2.7, the particle motion is to the right whenever u is positive and to

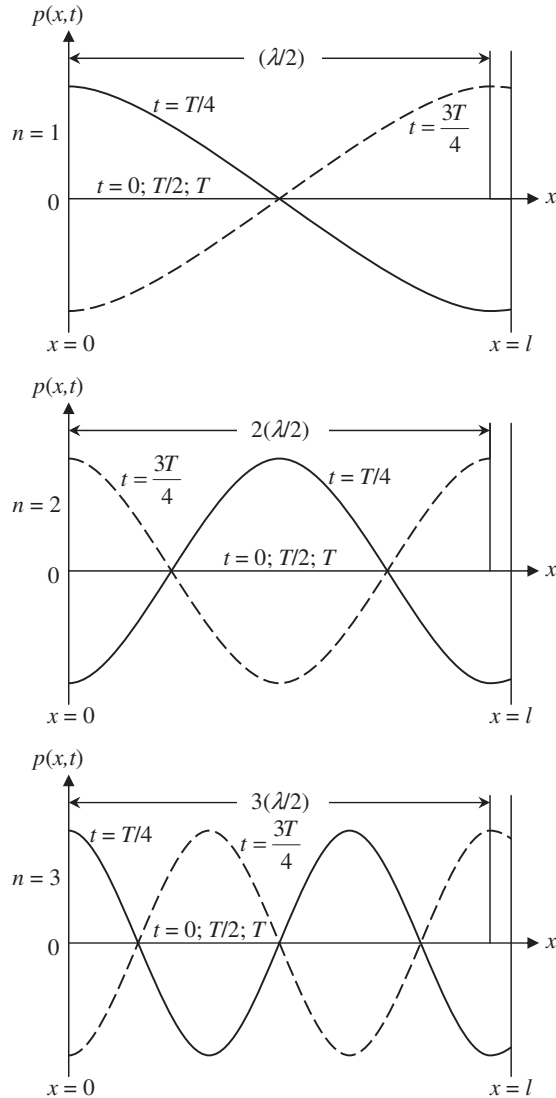


Figure 2.8 Variation of the sound pressure $p(x,t)$ as a function of the distance along the tube for three frequencies, i.e., for three wavelengths. At $x=l$, the rms particle velocity is u_0 , and at $x=0$, it is zero. The period T equals $1/f$.

the left when it is negative. Hence, at $x = \lambda/2$, the particles on either side are moving toward each other, so that one-fourth period later the sound pressure will have built up to a maximum, as can be seen from Fig. 2.8. At the $2\lambda/2$ point, the particles are moving apart, so that the pressure is dropping to below barometric as can be seen from Fig. 2.8.

Fig. 2.7 and Fig. 2.8 also reveal that, wherever along the tube the magnitude of the velocity is zero, the magnitude of the pressure is a maximum, and vice versa. Hence, for maximum pressure, Eq. (2.67) applies.

Specific acoustic impedance

It still remains for us to solve for the specific acoustic impedance Z_s , at any plane x , in the tube. Taking the ratio of Eq. (2.69) to Eq. (2.64) or setting $Z_T = \infty$ in Eq. (2.60) yields

$$Z_s = \frac{\tilde{p}(l')}{-\tilde{u}(l')} = -j\rho_0 c \cot kl' = jX_s, \quad (2.72)$$

where X_s is the reactance, and where we have set

$$x = l'. \quad (2.73)$$

That is, l' is the distance between any plane x in Fig. 2.4 and the rigid end of the tube at 0. The $-j$ indicates that at low frequencies where $\cot kl' \approx 1/kl'$, the particle velocity leads the pressure in time by 90 degrees and the reactance X_s is negative. At all frequencies the impedance is reactive and either leads or lags the pressure by exactly 90 degrees depending, respectively, on whether X_s is negative or positive. The reactance X_s varies as shown in Fig. 2.9. If the value of kl' is small, we may approximate the cotangent by the first two terms of a series

$$\cot kl' \approx \frac{1}{kl'} - \frac{kl'}{3}. \quad (2.74)$$

This approximation is valid whenever the product of frequency times the distance from the rigid end of the tube to the point of measurement is very small. If the second term is very small, then it may be neglected with respect to the first.

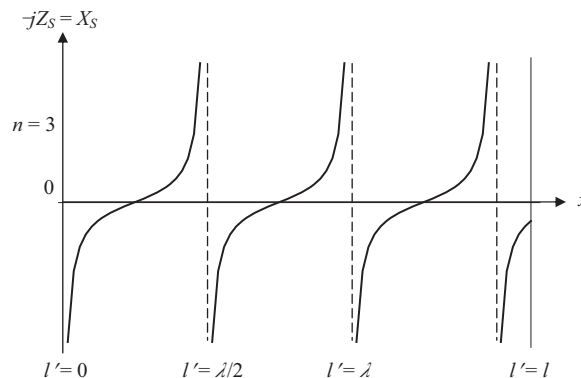


Figure 2.9 The specific acoustic reactance (p_{rms}/u_{rms}) along the tube of Fig. 2.4 for a particular frequency, i.e., a particular wavelength where $3(\lambda/2)$ is a little less than the tube length l . For this case, the number of zeros is three, and the number of poles is four.

Let us see how small the ratio of the distance l' to the wavelength λ must be if the second term of Eq. (2.74) is to be 3% or less than the first term. That is, let us solve for l'/λ from

$$\frac{2\pi l'}{3\lambda} \leq 0.03 \frac{\lambda}{2\pi l'}, \quad (2.75)$$

which gives us

$$\frac{l'}{\lambda} \leq 0.05. \quad (2.76)$$

In other words, if $\cot kl'$ is to be replaced within an accuracy of 3% by the first term of its series expansion, l' must be less than one-twentieth wavelength in magnitude.

Assuming $l' < \lambda/20$, Eq. (2.72) becomes

$$Z_s = jX_s = -j \frac{\rho_0 c}{kl'} = \frac{1}{j\omega(l'/\rho_0 c^2)} \equiv \frac{1}{j\omega C_s} \text{ rayls.} \quad (2.77)$$

Hence, the specific acoustic impedance of a short length of tube can be represented as a “capacitance” called specific acoustic compliance, of magnitude $C_s = l'/\rho_0 c^2$. Note also that $C_s = l'/\gamma P_0$, because of Eq. (2.19).

The acoustic impedance is of the same type, except that an area factor appears so that

$$Z_A = \frac{\tilde{p}}{S\tilde{u}} = \frac{1}{j\omega(V/\rho_0 c^2)} \equiv \frac{1}{j\omega C_A} \text{ N}\cdot\text{s/m}^5, \quad (2.78)$$

where $V = l'S$ is the volume and S is the area of cross section of the tube. C_A is called the *acoustic compliance* and equals $V/\rho_0 c^2$. Note also that $C_A = V/\gamma P_0$, from Eq. (2.19).

Example 2.3. A cylindrical tube is to be used in an acoustic device as an impedance element. (a) The impedance desired is that of a compliance. What length should it have to yield a reactance of 1.4×10^3 rayls at an angular frequency of 1000 rad/s? (b) What is the relative magnitude of the first and second terms of Eq. (2.74) for this case?

Solution: The reactance of such a tube is

$$(a) X_s = 1.4 \times 10^3 = \frac{\gamma P_0}{\omega l'} = \frac{1.4 \times 10^5}{10^3 l'}.$$

Hence, $l' = 0.1$ m.

$$(b) \frac{kl'}{3} \div \frac{1}{kl'} = \frac{k^2 l'^2}{3} = \frac{\omega^2 l'^2}{3c^2} = \frac{10^6 \times 10^{-2}}{(3)(344.8)^2} = 0.028.$$

Hence, the second term is about 3% of the first term.



2.5 IMPEDANCE OF A CLOSED TUBE USING THE INHOMOGENEOUS WAVE EQUATION

Boundary conditions

We have already found the impedance of a closed tube by taking the solution to the following Helmholtz wave equation

$$\left(\frac{\partial^2}{\partial x^2} + k^2\right)\tilde{p}(x) = 0 \quad (2.79)$$

and applying boundary conditions to the solution. It is known as a *homogeneous* wave equation because there are no sound sources explicit in the equation. These are included in the boundary conditions that are applied to the solution. Here we shall consider the *inhomogeneous* wave equation

$$\left(\frac{\partial^2}{\partial x^2} + k^2\right)\tilde{p}(x) = -\delta(x-l)\frac{\partial}{\partial x}\tilde{p}(x)|_{x=l}, \quad (2.80)$$

which includes the sound source at $x=l$ on the right-hand side, where δ is the Dirac delta function. This useful function describes a singularity when its argument is zero (in this case when $x=l$) but returns a zero value for all other arguments. In solving the equation using this alternative method, we shall introduce some useful techniques for approaching acoustical problems in general, which make use of orthogonality and the properties of the Dirac delta function. The solution itself will provide useful identities for trigonometrical functions with numerical advantages over more conventional ones. In Fig. 2.6, the piston at $x=l$ oscillates with velocity \tilde{u}_0 . Hence, using the relationship of Eq. (2.4a), gives

$$\left(\frac{\partial^2}{\partial x^2} + k^2\right)\tilde{p}(x) = jk\rho_0c\delta(x-l)\tilde{u}_0. \quad (2.81)$$

In other words, we are describing the piston as a point source at the end of the tube.

Solution of the inhomogeneous wave equation for a closed tube

Let the solution be in the form of an *eigenfunction* expansion

$$\tilde{p}(x) = \sum_{n=0}^{\infty} \tilde{A}_n \cos(n\pi x/l). \quad (2.82)$$

When the piston is stationary, this satisfies the boundary conditions

$$\frac{\partial}{\partial x}\tilde{p}(x)|_{x=0} = 0, \quad \frac{\partial}{\partial x}\tilde{p}(x)|_{x=l} = 0. \quad (2.83)$$

Inserting Eq. (2.82) in Eq. (2.81) and multiplying both sides by $\cos(m\pi x/l)$ while integrating over the length of the tube gives

$$\begin{aligned} \sum_{n=0}^{\infty} \left(k^2 - \frac{n^2 \pi^2}{l^2} \right) \tilde{A}_n \int_0^l \cos(m\pi x/l) \cos(n\pi x/l) dx \\ = jk\rho_0 \tilde{c}u_0 \int_0^l \cos(m\pi x/l) \delta(x-l) dx. \end{aligned} \quad (2.84)$$

The two integrals have the following identities

$$\int_0^l \cos(m\pi x/l) \cos(n\pi x/l) dx = \begin{cases} 0, & m \neq n \\ l, & m = n = 0 \\ l/2, & m = n \neq 0 \end{cases} \quad (2.85)$$

$$\int_0^l \cos(m\pi x/l) \delta(x-l) dx = \cos(m\pi) = (-1)^m. \quad (2.86)$$

The first is the property of *orthogonality* and the second is a property of the Dirac delta function

$$\int_{-\infty}^{\infty} F(x) \delta(x-l) dx = F(l). \quad (2.87)$$

Hence, $\cos(m\pi x/l)$ in this case is the *orthogonal* (or normalizing) function and we can eliminate the summation to yield

$$\tilde{A}_n = jkl\rho_0 \tilde{c}u_0 \frac{(2 - \delta_{0n})(-1)^n}{k^2 l^2 - n^2 \pi^2}, \quad (2.88)$$

so that the solution of Eqs. (2.80) and (2.81), given by Eq. (2.82), becomes

$$\tilde{p}(x) = jkl\rho_0 \tilde{c}u_0 \sum_{n=0}^{\infty} \frac{(2 - \delta_{0n})(-1)^n \cos(n\pi x/l)}{k^2 l^2 - n^2 \pi^2}, \quad (2.89)$$

where δ_{mm} is the Kronecker delta function

$$\delta_{0n} = \begin{cases} 0, & m \neq n \\ 1, & m = n. \end{cases} \quad (2.90)$$

Eq. (2.89) is equivalent to the solution of Eq. (2.79), given by Eq. (2.69)

$$\tilde{p}(x) = j\rho_0 c \tilde{u}_0 \frac{\cos kx}{\sin kl}. \quad (2.91)$$

Impedance of the closed tube

We saw previously that the impedance of a closed tube is given by

$$Z_s = \frac{\tilde{p}(l)}{-\tilde{u}_0} = -j\rho_0 c \cot kl, \quad (2.92)$$

which is equivalent to the following expression obtained using Eq. (2.89)

$$Z_s = \frac{\tilde{p}(l)}{-\tilde{u}_0} = -j\rho_0 c \sum_{n=0}^{\infty} \frac{(2 - \delta_{0n})kl}{k^2 l^2 - n^2 \pi^2}. \quad (2.93)$$

Because modes occur when $kl = n\pi$, the eigenfrequencies are given by

$$f = \frac{nc}{2l} \text{ or } l = \frac{n}{2}\lambda, \quad n = 1, 2, 3, \dots \quad (2.94)$$

Expansions for cot and csc

We have thus obtained a useful expansion for $\cot kl$, which converges when truncated to a finite number of terms and retains the singularities at $kl = n\pi$, unlike the more conventional formula $\cot kl = (\cos kl)/(\sin kl)$, where

$$\sin kl = \sum_{n=0}^{\infty} \frac{(-1)^n (kl)^{2n+1}}{(2n+1)!}, \quad (2.95)$$

$$\cos kl = \sum_{n=0}^{\infty} \frac{(-1)^n (kl)^{2n}}{(2n)!}. \quad (2.96)$$

Hence

$$\cot x = \sum_{n=0}^{\infty} \frac{(2 - \delta_{0n})x}{x^2 - n^2 \pi^2}. \quad (2.97)$$

Similarly, by comparing the pressures given by Eqs. (2.89) and (2.91) at $x = 0$, we obtain

$$\csc x = \sum_{n=0}^{\infty} \frac{(2 - \delta_{0n})(-1)^n x}{x^2 - n^2 \pi^2}. \quad (2.98)$$

It is also useful to have an expression for the difference between the above

$$\csc x - \cot x = \tan \frac{x}{2} = \sum_{n=0}^{\infty} \frac{4x}{(2n+1)^2 \pi^2 - x^2}. \quad (2.99)$$

Hence

$$\tan x = \sum_{n=0}^{\infty} \frac{2x}{(n+1/2)^2 \pi^2 - x^2}. \quad (2.100)$$



2.6 IMPEDANCE OF AN OPEN TUBE USING THE INHOMOGENEOUS WAVE EQUATION

Solution of the inhomogeneous wave equation for an open tube

If the tube of Fig. 2.6 is open at $x = 0$ instead of closed, let the solution be in the form of an *eigenfunction* expansion

$$\tilde{p}(x) = \sum_{n=0}^{\infty} \tilde{A}_n \sin((n+1/2)\pi x/l). \quad (2.101)$$

When the piston is stationary, this satisfies the boundary conditions

$$\tilde{p}(x)|_{x=0} = 0, \quad \frac{\partial}{\partial x} \tilde{p}(x)|_{x=l} = 0. \quad (2.102)$$

Inserting Eq. (2.101) in Eq. (2.81) and multiplying both sides by $\sin((m+1/2)\pi x/l)$ while integrating over the length of the tube gives

$$\begin{aligned} \sum_{n=0}^{\infty} \left(k^2 - \frac{(n+1/2)^2 \pi^2}{l^2} \right) \tilde{A}_n \int_0^l \sin((m+1/2)\pi x/l) \sin((n+1/2)\pi x/l) dx \\ = jk\rho_0 \tilde{c}u_0 \int_0^l \sin((m+1/2)\pi x/l) \delta(x-l) dx. \end{aligned} \quad (2.103)$$

The two integrals have the following identities

$$\int_0^l \sin((m+1/2)\pi x/l) \sin((n+1/2)\pi x/l) dx = \begin{cases} 0, & m \neq n \\ l/2, & m = n \end{cases} \quad (2.104)$$

$$\int_0^l \sin((m+1/2)\pi x/l) \delta(x-l) dx = \sin((m+1/2)\pi) = (-1)^m. \quad (2.105)$$

The first is the property of *orthogonality* and the second is a property of the Dirac delta function

$$\int_{-\infty}^{\infty} F(x)\delta(x-l)dx = F(l). \quad (2.106)$$

Hence, $\sin((n+1/2)\pi x/l)$ in this case is the *orthogonal* (or normalizing) function and we can eliminate the summation to yield

$$\tilde{A}_n = 2jkl\rho_0\tilde{c}\tilde{u}_0 \frac{(-1)^n}{k^2l^2 - (n+1/2)^2\pi^2}, \quad (2.107)$$

so that the solution of Eqs. (2.80) and (2.81), given by Eq. (2.101), becomes

$$\tilde{p}(x) = 2jkl\rho_0\tilde{c}\tilde{u}_0 \sum_{n=0}^{\infty} \frac{(-1)^n \sin((n+1/2)\pi x/l)}{k^2l^2 - (n+1/2)^2\pi^2}. \quad (2.108)$$

Eq. (2.108) is equivalent to the solution of Eq. (2.79), which would be obtained by applying the boundary conditions to the solution to the homogeneous wave equation, given by

$$\tilde{p}(x) = -j\rho_0\tilde{c}\tilde{u}_0 \frac{\sin kx}{\cos kl}. \quad (2.109)$$

Impedance of the open tube

We saw previously that the impedance of an open tube is given by

$$Z_s = \frac{\tilde{p}(l)}{-\tilde{u}_0} = j\rho_0c \tan kl, \quad (2.110)$$

which is equivalent to the following expression obtained using Eq. (2.108)

$$Z_s = \frac{\tilde{p}(l)}{-\tilde{u}_0} = j\rho_0c \sum_{n=0}^{\infty} \frac{2kl}{(n+1/2)^2\pi^2 - k^2l^2}. \quad (2.111)$$

Because modes occur when $kl = (n+1/2)\pi$, the eigenfrequencies are given by

$$f = \frac{(2n+1)c}{4l} \quad \text{or} \quad l = \frac{2n+1}{4}\lambda, \quad n = 0, 1, 2, 3, \dots \quad (2.112)$$

Expansion for tan

We have thus obtained a useful expansion for $\tan kl$, which converges when truncated to a finite number of terms and retains the singularities at $kl = (n+1/2)\pi$, unlike the more

conventional formula $\tan kl = (\sin kl)/(\cos kl)$, where the sine and cosine expansions are given by Eqs. (2.95) and (2.96) respectively. Hence

$$\tan x = \sum_{n=0}^{\infty} \frac{2x}{(n + 1/2)^2 \pi^2 - x^2}. \quad (2.113)$$



2.7 SOLUTION OF WAVE EQUATION FOR AIR IN A TUBE FILLED WITH ABSORBENT MATERIAL

Ducts and tubes are often filled with absorbent material in order to minimize standing waves, such as in transmission-line loudspeaker enclosures or exhaust-pipe mufflers, for example. Let us now modify the one-dimensional wave equation in rectangular coordinates, Eq. (2.34), taking into account the thermal and viscous losses in the material

$$\left(P_0 \frac{\partial}{\partial x^2} - j\omega R_f + \omega^2 \rho_0 \right) \tilde{p} = 0 \quad (2.114)$$

where in the steady state we have let $\partial^2/\partial t^2 = -\omega^2$ and R_f is the specific flow resistance *per unit length* of the absorptive material in rayls/m. For simplicity we are assuming that the resistance is constant for all frequencies. A more comprehensive treatment of sound in absorbent materials will be given in Section 7.6. Notice too that we have omitted the specific heat ratio γ because we are assuming that the heat conduction within the material is such that the pressure fluctuations are isothermal. We define a complex density by

$$\rho = \rho_0 + \frac{R_f}{j\omega}, \quad (2.115)$$

so that the wave equation simplifies to

$$\left(\frac{\partial^2}{\partial x^2} + \frac{\omega^2}{c^2} \right) \tilde{p} = 0, \quad (2.116)$$

where

$$c = \sqrt{\frac{P_0}{\rho}}. \quad (2.117)$$

Hence the solution is

$$\tilde{p}(x) = \tilde{p}_+ e^{-jkx} + p_- e^{jkx}, \quad (2.118)$$

where the complex wave number is given by

$$\mathbf{k} = \frac{\omega}{c} = \omega \sqrt{\frac{\rho}{P_0}}, \quad (2.119)$$

and the characteristic impedance of the tube is

$$Z_s = \sqrt{\rho P_0}. \quad (2.120)$$

In general, viscous or flow losses are dynamic and therefore associated with a change in the density of the medium whereas thermal conduction is static and therefore associated with a change in the bulk modulus. Viscous and thermal losses also occur in narrow unfilled tubes and these will be treated in some detail in [Sections 4.22 to 4.24](#).



2.8 FREELY TRAVELING PLANE WAVE

Sound pressure

If the rigid termination of [Fig. 2.4](#) is replaced by a perfectly absorbing termination, a backward-traveling wave will not occur. Hence, [Eq. \(2.46\)](#) becomes

$$\tilde{p}(x) = \tilde{p}_+ e^{-jkx}, \quad (2.121)$$

where \tilde{p}_+ is the complex amplitude of the wave. This equation also applies to a plane wave traveling in free space.

Particle velocity

From [Eq. \(2.4a\)](#) in the steady state, we have

$$\tilde{u}(x) = \frac{-1}{jk\rho_0 c} \frac{\partial}{\partial x} \tilde{p}(x). \quad (2.122)$$

Hence,

$$\tilde{u}(x) = \frac{\tilde{p}_+}{\rho_0 c} e^{-jkx} = \frac{\tilde{p}(x)}{\rho_0 c}. \quad (2.123)$$

The particle velocity and the sound pressure are in phase. This is mathematical proof of the statement made in connection with the qualitative discussion of the wave propagated from a vibrating wall in [Chapter 1](#) and [Fig. 1.1](#).

Specific acoustic impedance

The specific acoustic impedance is

$$Z_s = \frac{\tilde{p}(x)}{\tilde{u}(x)} = \rho_0 c \text{ rayls}. \quad (2.124)$$

This equation says that in a plane freely traveling wave the specific acoustic impedance is purely resistive and is equal to the product of the average density of the gas and the speed of sound. This particular quantity is generally called the *characteristic impedance of the gas* because its magnitude depends on the properties of the gas alone. It is a quantity that is analogous to the surge impedance of an infinite electrical line. For air at 22°C and a barometric pressure of 10^5 Pa, its magnitude is 407 rayls.



2.9 FREELY TRAVELING CYLINDRICAL WAVE

Sound pressure

A solution to the cylindrical wave equation (2.23) is

$$\tilde{p}(w) = \tilde{p}_+ H_0^{(2)}(kw) + \tilde{p}_- H_0^{(1)}(kw), \quad (2.125)$$

where \tilde{p}_+ is the amplitude of the sound pressure in the outgoing wave at unit distance from the axis of symmetry and \tilde{p}_- is the same for the reflected wave. $H_0^{(1)}(x)$ and $H_0^{(2)}(x)$ are Hankel functions defined by

$$H_0^{(1)}(x) = J_0(x) + jY_0(x), \quad (2.126)$$

$$H_0^{(2)}(x) = J_0(x) - jY_0(x), \quad (2.127)$$

where $J_0(x)$ and $Y_0(x)$ are Bessel functions of the first and second kind respectively, as plotted in Fig. 2.10. The “2” in parentheses denotes an outgoing cylindrical wave and the “1” denotes an incoming one. In the far field

$$\tilde{p}(w)|_{w \rightarrow \infty} = \sqrt{\frac{2}{\pi kw}} \left(\tilde{p}_+ e^{-j(kw - \pi/4)} + \tilde{p}_- e^{j(kw - \pi/4)} \right). \quad (2.128)$$

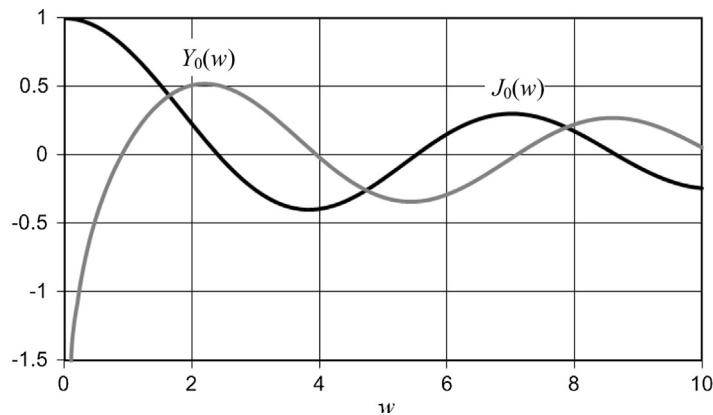


Figure 2.10 Bessel functions of the first (black curve) and second (gray curve) kind.

We can see from Fig. 2.10 that cylindrical waves, which are essentially two-dimensional because of the lack of axial dependency, differ from plane ones in two respects: firstly the radial wavelength is longer nearer the axis of symmetry than in the far field; secondly they decay in amplitude as they spread out, adopting an inverse square-root law in the far field. The latter makes sense when we consider that the area of the wave front is proportional to the radial distance w . The radiated power is the intensity multiplied by the area, where the intensity is given by Eq. (1.12). The intensity, in turn, is proportional to the square of the pressure and therefore inversely proportional to the radial distance. Hence the power remains constant. The same kind of wave deformation can be seen if you drop a pebble in a pond. Note the singularity in the $Y(x)$ function when $x = 0$. If there are no reflecting surfaces in the medium, only the first term of Eq. (2.125) is needed, i.e.,

$$\tilde{p}(w) = \tilde{p}_+ H_0^{(2)}(kw). \quad (2.129)$$

Particle velocity

With the aid of Eq. (2.4b), we solve for the particle velocity in the w direction:

$$\begin{aligned} \tilde{u}(w) &= -\frac{1}{jk\rho_0 c} \frac{\partial}{\partial w} \tilde{p}(w) \\ &= -j \frac{\tilde{p}_+}{\rho_0 c} H_1^{(2)}(kw). \end{aligned} \quad (2.130)$$

In the far field

$$\tilde{u}(w) = -j \frac{\tilde{p}_+}{\rho_0 c} \sqrt{\frac{2}{\pi kw}} e^{-j(kw-3\pi/4)} = \frac{\tilde{p}_+}{\rho_0 c} \sqrt{\frac{2}{\pi kw}} e^{-j(kw-\pi/4)}. \quad (2.131)$$

Specific acoustic impedance

The specific acoustic impedance is found from Eq. (2.129) divided by Eq. (2.130):

$$Z_s = \frac{\tilde{p}(w)}{\tilde{u}(w)} = j\rho_0 c \frac{H_0^{(2)}(kw)}{H_1^{(2)}(kw)} \text{ rayls.} \quad (2.132)$$

Plots of the magnitude and phase angle of the impedance as a function of kw are given in Fig. 2.11 and Fig. 2.12 respectively.

For large values of kw , that is, for large distances or for high frequencies, Eq. (2.132) becomes, approximately,

$$Z_s \approx \rho_0 c \text{ rayls.} \quad (2.133)$$

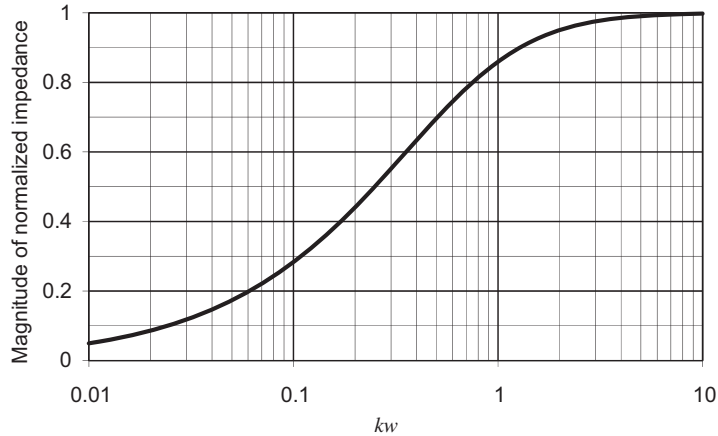


Figure 2.11 Plot of the magnitude of the specific acoustic-impedance ratio $|Z_s|/(\rho_0 c)$ in a cylindrical freely traveling wave as a function of kw , where k is the wave number equal to ω/c or $2\pi/\lambda$ and w is the distance from the axis of symmetry. $|Z_s|$ is the magnitude of the ratio of pressure to particle velocity in a cylindrical free-traveling wave, and $\rho_0 c$ is the characteristic impedance of air.

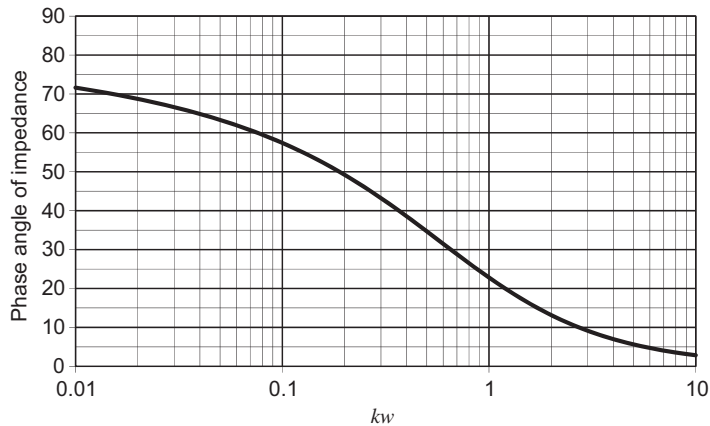


Figure 2.12 Plot of the phase angle, in degrees, of the specific acoustic-impedance ratio $|Z_s|/\rho_0 c$ in a cylindrical wave as a function of kw , where k is the wave number ω/c or $2\pi/\lambda$ and w is the distance from the axis of symmetry.

The impedance here is nearly purely resistive and approximately equal to the characteristic impedance for a plane freely traveling wave. In other words, the specific acoustic impedance for a large distance from a cylindrical source in free space is nearly equal to that in a tube in which no reflections occur from the end opposite the source.



2.10 FREELY TRAVELING SPHERICAL WAVE

Sound pressure

A solution to the spherical wave Eq. (2.25) is

$$\tilde{p}(r) = \tilde{A}_+ \frac{e^{-jkr}}{r} + \tilde{A}_- \frac{e^{jkr}}{r}, \quad (2.134)$$

where \tilde{A}_+ is the amplitude of the sound pressure in the outgoing wave at unit distance from the center of the sphere and \tilde{A}_- is the same for the reflected wave. This equation can also be written in terms of *spherical* Hankel functions $h_0^{(1)}(x)$ and $h_0^{(2)}(x)$

$$\tilde{p}(r) = -jk \left(\tilde{A}_+ h_0^{(2)}(kr) - \tilde{A}_- h_0^{(1)}(kr) \right), \quad (2.135)$$

which are also known as Hankel functions of fractional order, as defined by

$$h_0^{(1)}(x) = j_0(x) + jy_0(x), \quad (2.136)$$

$$h_0^{(2)}(x) = j_0(x) - jy_0(x), \quad (2.137)$$

$$j_0(x) = \frac{\sin x}{x}, \quad (2.138)$$

$$y_0(x) = -\frac{\cos x}{x}, \quad (2.139)$$

where $j_0(x)$ and $y_0(x)$ are spherical Bessel functions of the first and second kind respectively, as plotted in Fig. 2.13. The “2” in parentheses denotes an outgoing spherical wave and the “1” denotes an incoming one. These spherical Bessel functions are related to the cylindrical Bessel functions of half-integer order $J_{\frac{1}{2}}(x)$ and $Y_{\frac{1}{2}}(x)$ by

$$j_0(x) = \sqrt{\frac{\pi}{2x}} J_{\frac{1}{2}}(x), \quad (2.140)$$

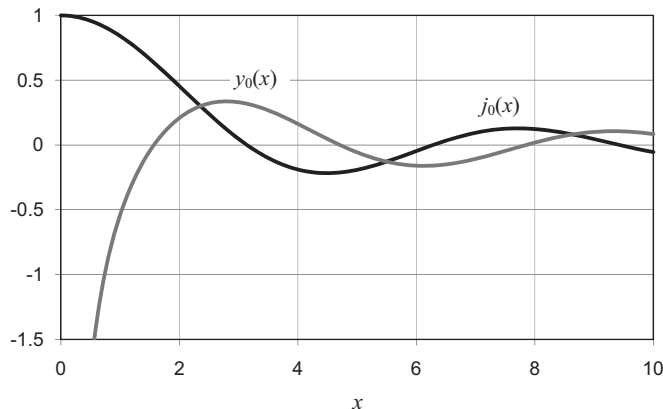


Figure 2.13 Spherical Bessel functions of the first (black curve) and second (gray curve) kind.

$$y_0(x) = \sqrt{\frac{\pi}{2x}} Y_{\frac{1}{2}}(x). \quad (2.141)$$

We can see that spherical waves differ from cylindrical ones in two respects: first, the radial wavelength remains constant as they progress, as is the case with plane waves; second, although they decay in amplitude as they spread out, they adopt a direct inverse law in the far field. The latter makes sense when we consider that the area of the wave front is proportional to the square of the radial distance r . The radiated power is the intensity multiplied by the area, where the intensity is given by Eq. (1.12). The intensity, in turn, is proportional to the square of the pressure and therefore inversely proportional to the square of the radial distance. Hence the power remains constant.

If there are no reflecting surfaces in the medium, only the first term of this equation is needed, i.e.,

$$\tilde{p}(r) = \tilde{A}_+ \frac{e^{-jkr}}{r}. \quad (2.142)$$

Particle velocity

With the aid of Eq. (2.4b), solve for the particle velocity in the r direction:

$$\begin{aligned} \tilde{u}(r) &= \frac{1}{-jk\rho_0 c} \frac{\partial}{\partial r} \tilde{p}(r) \\ &= \frac{\tilde{A}_+}{\rho_0 c} \left(1 + \frac{1}{jkr}\right) \frac{e^{-jkr}}{r}. \end{aligned} \quad (2.143)$$

Specific acoustic impedance

The specific acoustic impedance is found from Eq. (2.142) divided by Eq. (2.143),

$$Z_s = \frac{\tilde{p}(r)}{\tilde{u}(r)} = \rho_0 c \frac{jkr}{1 + jkr} = \frac{\rho_0 c kr}{\sqrt{1 + k^2 r^2}} / 90^\circ - \tan^{-1} kr \text{ rays}. \quad (2.144)$$

Plots of the magnitude and phase angle of the impedance as a function of kr are given in Figs. 2.14 and 2.15 respectively.

For large values of kr , that is, for large distances or for high frequencies, this equation becomes, approximately,

$$Z_s \approx \rho_0 c \text{ rays}. \quad (2.145)$$

The impedance here is nearly purely resistive and approximately equal to the characteristic impedance for a plane freely traveling wave. In other words, the specific

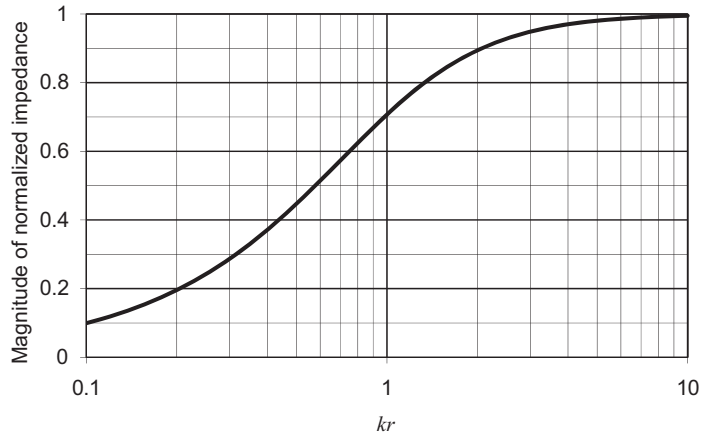


Figure 2.14 Plot of the magnitude of the specific acoustic-impedance ratio $|Z_s|/(\rho_0 c)$ in a spherical freely traveling wave as a function of kr , where k is the wave-number equal to ω/c or $2\pi/\lambda$ and r is the distance from the center of the spherical source. $|Z_s|$ is the magnitude of ratio of pressure to particle velocity in a spherical free-traveling wave, and $\rho_0 c$ is the characteristic impedance of air.

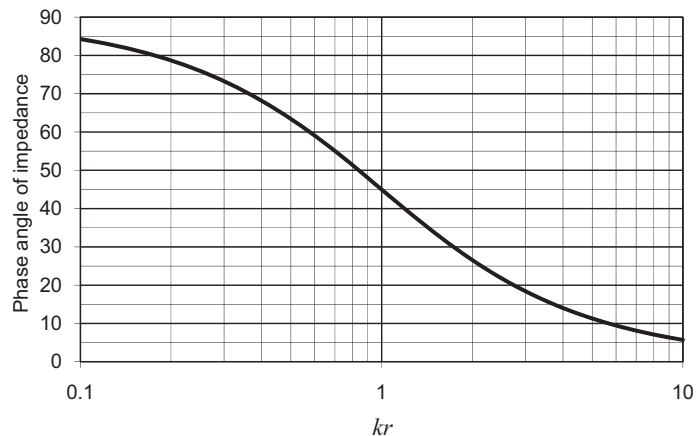


Figure 2.15 Plot of the phase angle, in degrees, of the specific acoustic-impedance ratio $|Z_s|/\rho_0 c$ in a spherical wave as a function of kr , where k is the wave number ω/c or $2\pi/\lambda$ and r is the distance from the center of the spherical source.

acoustic impedance for a large distance from a spherical source in free space is nearly equal to that in a tube in which no reflections occur from the end opposite the source.

The important steady-state relations derived in this chapter are summarized in [Table 2.2](#).

Table 2.2 General and steady-state relations for small-signal sound propagation in gases

Name	General equation	Steady-state equation
Wave equation in p or u	$\frac{\partial^2(\)}{\partial x^2} = \frac{1}{c^2} \frac{\partial^2(\)}{\partial t^2}$	$\frac{\partial^2(\)}{\partial x^2} = -\frac{\omega^2}{c^2}(\)$
	$\nabla^2(\) = \frac{1}{c^2} \frac{\partial^2(\)}{\partial t^2}$	$\nabla^2(\) = -\frac{\omega^2}{c^2}(\)$
	$\frac{\partial^2(pr)}{\partial r^2} = \frac{1}{c^2} \frac{\partial^2(pr)}{\partial t^2}$	$\nabla^2(pr) = -\frac{\omega^2}{c^2}(pr)$
Equation of motion	$\frac{\partial p}{\partial x} = -\rho_0 \frac{\partial u}{\partial t}$	$u = \frac{-1}{j\omega\rho_0} \frac{\partial p}{\partial x}$
	$\text{grad } p = -\rho_0 \frac{\partial \mathbf{q}}{\partial t}$	$p = -j\omega\rho_0 \int u \, dx$
		$\text{grad } p = -j\omega\rho_0 \mathbf{q}$
Displacement	$\xi = \int u \, dt$	$\xi = \frac{u}{j\omega}$
	$\xi = \int q \, dt$	$\xi = \frac{\mathbf{q}}{j\omega}$
Incremental density	$\rho = \frac{\rho_0}{\gamma P_0} p = \frac{p}{c^2}$	$\rho = \frac{\rho_0}{\gamma P_0} p = \frac{p}{c^2}$
	$\frac{\partial \rho}{\partial t} = -\rho_0 \frac{\partial u}{\partial x}$	$\rho = \frac{\rho_0}{j\omega} \frac{\partial u}{\partial x}$
Incremental temperature	$\Delta T = \frac{T_0}{P_0} \frac{\gamma - 1}{\gamma} p$	$\Delta T = \frac{T_0}{P_0} \frac{\gamma - 1}{\gamma} p$

PART V: SOLUTIONS OF THE HELMHOLTZ WAVE EQUATION IN THREE DIMENSIONS

2.11 RECTANGULAR COORDINATES

In the steady state, Eq. (2.20b) for the three-dimensional wave equation in rectangular coordinates can be written

$$(\nabla^2 + k^2)\tilde{p}(x, y, z) = 0, \quad (2.146)$$

where the Laplace operator is given by

$$\nabla^2 = \frac{\partial^2}{\partial x^2} + \frac{\partial^2}{\partial y^2} + \frac{\partial^2}{\partial z^2} \quad (2.147)$$

and $k = \omega/c = 2\pi/\lambda$. Let the solution to Eq. (2.146) be of the form

$$\tilde{p}(x, y, z) = \tilde{p}_0 X(x)Y(y)Z(z). \quad (2.148)$$

Substituting this in Eq. (2.146) and dividing through by $X(x)Y(y)Z(z)$ yields

$$\left(\frac{1}{X} \frac{\partial^2 X}{\partial x^2} + k_x^2\right) + \left(\frac{1}{Y} \frac{\partial^2 Y}{\partial y^2} + k_y^2\right) + \left(\frac{1}{Z} \frac{\partial^2 Z}{\partial z^2} + k_z^2\right) = 0, \quad (2.149)$$

where

$$k^2 = k_x^2 + k_y^2 + k_z^2. \quad (2.150)$$

For example, in the case of a plane wave with a direction of travel in the zx plane at an angle θ to the z axis, we have $k_z = k \cos \theta$, $k_x = k \sin \theta$, and $k_y = 0$. The first bracketed term of Eq. (2.149) depends on x only, whereas the second term depends on y only and the third term z only. However, they must all add up to zero, which means that either they all have constant values, the combination of which is zero, or they are all zero. We shall assume the latter, in which case Eq. (2.149) can be separated into three equations, one for each ordinate as follows.

The plane wave equation in x

$$\left(\frac{\partial^2}{\partial x^2} + k_x^2\right)X = 0. \quad (2.151)$$

The plane wave equation in y

$$\left(\frac{\partial^2}{\partial y^2} + k_y^2\right)Y = 0. \quad (2.152)$$

The plane wave equation in z

$$\left(\frac{\partial^2}{\partial z^2} + k_z^2\right)Z = 0. \quad (2.153)$$

The solutions to Eqs. (2.151), (2.152) and (2.153) are

$$\begin{aligned} X(x) &= X_+ e^{-jk_x x} + X_- e^{jk_x x}, \\ Y(y) &= Y_+ e^{-jk_y y} + Y_- e^{jk_y y}, \text{ and} \\ Z(z) &= Z_+ e^{-jk_z z} + Z_- e^{jk_z z} \end{aligned}$$

respectively, so that the solution to Eq. (2.146) is

$$\tilde{p}(x, y, z) = \tilde{p}_+ e^{-j(k_x x + k_y y + k_z z)} + \tilde{p}_- e^{j(k_x x + k_y y + k_z z)}. \quad (2.154)$$



2.12 CYLINDRICAL COORDINATES

In problems where there is axial symmetry, cylindrical coordinates are often useful, as shown in Fig. 2.16. We shall use these for planar circular radiators. In the xy plane of the rectangular coordinate system, the x and y ordinates are replaced by polar ordinates w and ϕ where the radial ordinate w is given by

$$w = \sqrt{x^2 + y^2} \quad (2.155)$$

and the azimuthal ordinate ϕ is given by

$$\phi = \arctan(y/x). \quad (2.156)$$

Conversely

$$x = w \cos \phi, \quad (2.157)$$

$$y = w \sin \phi. \quad (2.158)$$

The rectangular z ordinate simply becomes the axial cylindrical ordinate. The three-dimensional wave equation in cylindrical coordinates is

$$(\nabla^2 + k^2)\tilde{p}(w, \phi, z) = 0, \quad (2.159)$$

where the Laplace operator is given by

$$\nabla^2 = \frac{\partial^2}{\partial w^2} + \frac{1}{w} \frac{\partial}{\partial w} + \frac{1}{w^2} \frac{\partial^2}{\partial \phi^2} + \frac{\partial^2}{\partial z^2}, \quad (2.160)$$

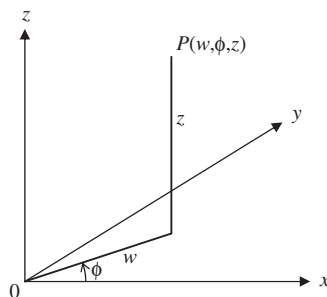


Figure 2.16 Cylindrical coordinates.

which is often written in the following short form:

$$\nabla^2 = \frac{1}{w} \frac{\partial}{\partial w} \left(w \frac{\partial}{\partial w} \right) + \frac{1}{w^2} \frac{\partial^2}{\partial \phi^2} + \frac{\partial^2}{\partial z^2}. \quad (2.161)$$

Let the solution to Eq. (2.159) be of the form

$$\tilde{p}(w, \phi, z) = \sum_{n=0}^{\infty} \tilde{p}_n W_n(w) \Phi_n(\phi) Z(z). \quad (2.162)$$

Substituting this in Eq. (2.159), multiplying through by w^2 , and dividing through by $W_n(w) \Phi_n(\phi) Z(z)$ yields

$$\frac{w^2}{W_n} \frac{\partial^2 W_n}{\partial w^2} + \frac{w}{W_n} \frac{\partial W_n}{\partial w} + k_w^2 w^2 = -\frac{1}{\Phi_n} \frac{\partial^2 \Phi_n}{\partial \phi^2} - \frac{w^2}{Z} \frac{\partial^2 Z}{\partial z^2} - k_z^2 w^2, \quad (2.163)$$

where

$$k^2 = k_w^2 + k_z^2. \quad (2.164)$$

If both sides of Eq. (2.163) are equated to a constant of separation n^2 , then Eq. (2.163) can then be separated into three equations for each ordinate as follows.

The radial equation in w

$$\left(\frac{\partial^2}{\partial w^2} + \frac{1}{w} \frac{\partial}{\partial w} + k_w^2 - \frac{n^2}{w^2} \right) W_n(w) = 0. \quad (2.165)$$

The solution to this equation is of the form

$$W_n(w) = W_{n+} H_n^{(2)}(k_w w) + W_{n-} H_n^{(1)}(k_w w), \quad (2.166)$$

where $H_n^{(1)}(x)$ and $H_n^{(2)}(x)$ are Hankel functions defined by

$$H_n^{(1)}(x) = J_n(x) + jY_n(x), \quad (2.167)$$

$$H_n^{(2)}(x) = J_n(x) - jY_n(x), \quad (2.168)$$

where $J_n(x)$ and $Y_n(x)$ are Bessel functions of the first and second kind respectively, as plotted in Figs. 2.17 and 2.18. The “2” in parentheses denotes an outgoing cylindrical wave and the “1” denotes an incoming one.

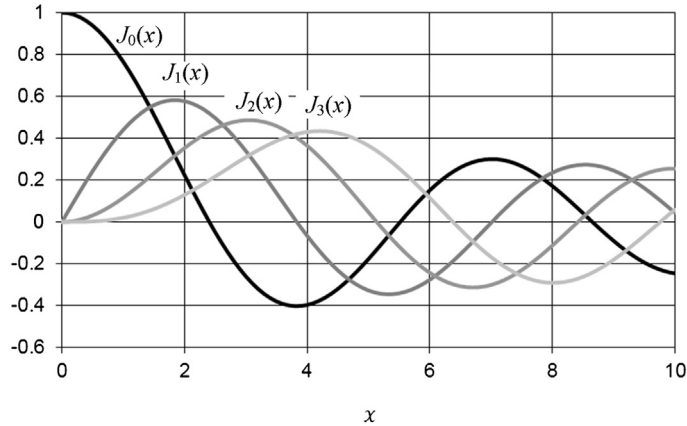


Figure 2.17 Bessel functions of the first kind.

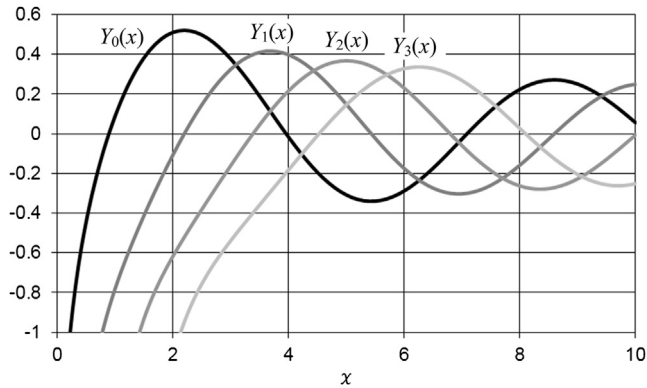


Figure 2.18 Bessel functions of the second kind.

The azimuthal equation in ϕ

$$\left(\frac{\partial^2}{\partial \phi^2} + n^2 \right) \Phi_n(\phi) = 0. \quad (2.169)$$

The solution to this equation is of the form

$$\Phi_n(\phi) = A_n \cos(n\phi) + B_n \sin(n\phi). \quad (2.170)$$

It can be seen that the integer n denotes the n th harmonic of the azimuthal modes of vibration where $\phi = 2\pi$ represents a full rotation about the z axis. The values of A_n and B_n depend on where the nodes and antinodes lie on the circumference. For example, setting $B_n = 0$ would place the nodes at $\phi = 0, \pi,$ and 2π .

The axial equation in z

$$\left(\frac{\partial^2}{\partial z^2} + k_z^2\right)Z(z) = 0. \quad (2.171)$$

The solution to this plane wave equation is of the form

$$Z(z) = Z_+e^{-jk_z z} + Z_-e^{jk_z z}, \quad (2.172)$$

where the $+$ sign denotes a forward traveling wave and the $-$ sign a reverse one. From Eq. (2.164) we observe that

$$k_z = \begin{cases} \sqrt{k^2 - k_w^2}, & k \geq k_w \\ -j\sqrt{k_w^2 - k^2}, & k < k_w \end{cases}, \quad (2.173)$$

Hence for $k < k_w$ the forward traveling term becomes an *evanescent* decaying one. Evanescent waves typically occur close to sound sources in the form of nonpropagating standing waves.



2.13 SPHERICAL COORDINATES

So far, we have only considered the one-dimensional spherical wave equation and its solution. In many problems where there are spherical surfaces but no axial or rotational symmetry, it is necessary to use spherical coordinates as shown in Fig. 2.19. The x , y , and z ordinates are replaced by spherical ordinates r , ϕ , and θ , where the radial ordinate r is given by

$$r = \sqrt{x^2 + y^2 + z^2}, \quad (2.174)$$

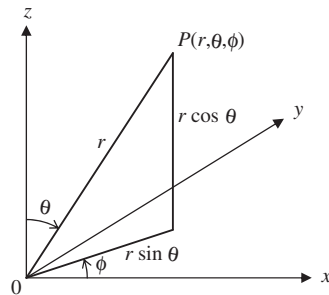


Figure 2.19 Spherical coordinates.

the inclination angle θ is given by

$$\theta = \operatorname{arccot} \left(z / \sqrt{x^2 + y^2} \right), \quad (2.175)$$

and the azimuth angle ϕ is given by

$$\phi = \arctan (y/x). \quad (2.176)$$

Conversely

$$x = r \sin \theta \cos \phi, \quad (2.177)$$

$$y = r \sin \theta \sin \phi, \quad (2.178)$$

$$z = r \cos \theta. \quad (2.179)$$

The three-dimensional wave equation in spherical coordinates is

$$(\nabla^2 + k^2)\tilde{p}(r, \theta, \phi) = 0, \quad (2.180)$$

where the Laplace operator is given by

$$\nabla^2 = \frac{\partial^2}{\partial r^2} + \frac{2}{r} \frac{\partial}{\partial r} + \frac{1}{r^2} \frac{\partial^2}{\partial \theta^2} + \frac{1}{r^2 \tan \theta} \frac{\partial}{\partial \theta} + \frac{1}{r^2 \sin^2 \theta} \frac{\partial^2}{\partial \phi^2}, \quad (2.181)$$

which is often written in the following short form:

$$\nabla^2 = \frac{1}{r^2} \frac{\partial}{\partial r} \left(r^2 \frac{\partial}{\partial r} \right) + \frac{1}{r^2 \sin \theta} \frac{\partial}{\partial \theta} \left(\sin \theta \frac{\partial}{\partial \theta} \right) + \frac{1}{r^2 \sin^2 \theta} \frac{\partial^2}{\partial \phi^2}. \quad (2.182)$$

Let the solution to Eq. (2.180) be of the form

$$\tilde{p}(r, \theta, \phi) = \sum_{n=0}^{\infty} \sum_{m=0}^n \tilde{p}_{mn} R_n(r) Z_{mn}(\theta) \Phi_m(\phi). \quad (2.183)$$

Substituting this in Eq. (2.180), multiplying through by r^2 , and dividing through by $R_n(r) Z_{mn}(\theta) \Phi_m(\phi)$ yields

$$\frac{r^2}{R_n} \frac{\partial^2 R_n}{\partial r^2} + \frac{2r}{R_n} \frac{\partial R_n}{\partial r} + k^2 r^2 = -\frac{1}{Z_{mn}} \frac{\partial^2 Z_{mn}}{\partial \theta^2} - \frac{1}{Z_{mn} \tan \theta} \frac{\partial Z_{mn}}{\partial \theta} - \frac{1}{\Phi_m \sin^2 \theta} \frac{\partial^2 \Phi_m}{\partial \phi^2}. \quad (2.184)$$

If both sides of Eq. (2.184) are equated to a constant of separation $n(n+1)$, then Eq. (2.184) can then be separated into three equations for each ordinate as follows.

The radial equation in r

After equating the left-hand side of Eq. (2.184) to $n(n+1)$, we have

$$\left(\frac{\partial^2}{\partial r^2} + \frac{2}{r} \frac{\partial}{\partial r} + k^2 - \frac{n(n+1)}{r^2}\right)R_n(r) = 0. \quad (2.185)$$

The solution to this equation is of the form

$$R_n(r) = R_{n+}h_n^{(2)}(kr) + R_{n-}h_n^{(1)}(kr), \quad (2.186)$$

where $h_n^{(1)}(x)$ and $h_n^{(2)}(x)$ are spherical Hankel functions, which are also known as Hankel functions of fractional order, as defined by

$$h_n^{(1)}(x) = j_n(x) + jy_n(x), \quad (2.187)$$

$$h_n^{(2)}(x) = j_n(x) - jy_n(x), \quad (2.188)$$

where $j_n(x)$ and $y_n(x)$ are spherical Bessel functions of the first and second kind respectively, as plotted in Figs. 2.20 and 2.21. The “2” in parentheses denotes an outgoing spherical wave and the “1” denotes an incoming one. These spherical Bessel functions are related to the cylindrical Bessel functions of integer order $J_{n+\frac{1}{2}}(x)$ and $Y_{n+\frac{1}{2}}(x)$ by

$$j_n(x) = \sqrt{\frac{\pi}{2x}}J_{n+\frac{1}{2}}(x), \quad (2.189)$$

$$y_n(x) = \sqrt{\frac{\pi}{2x}}Y_{n+\frac{1}{2}}(x). \quad (2.190)$$

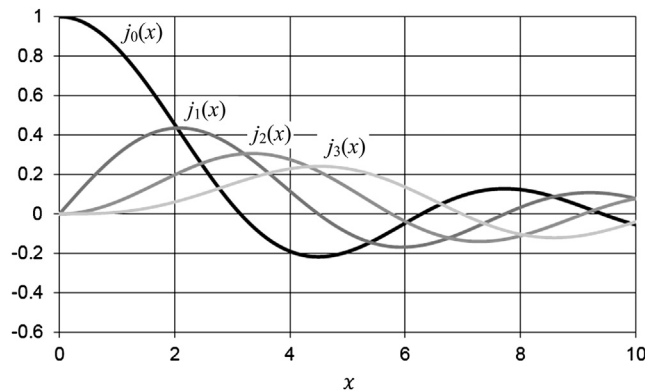


Figure 2.20 Spherical Bessel functions of the first kind.

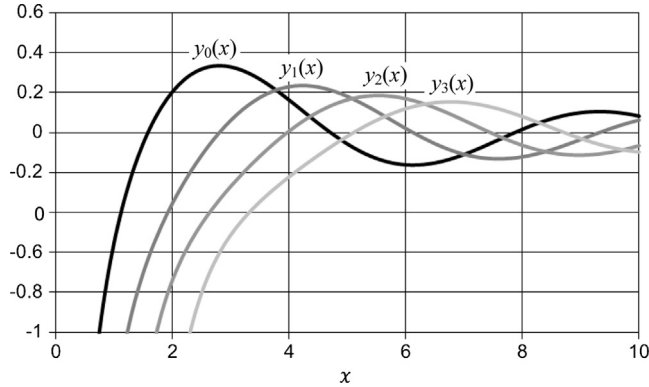


Figure 2.21 Spherical Bessel functions of the second kind.

The inclination equation in θ

After equating the right-hand side of Eq. (2.184) to $n(n+1)$, we have

$$\frac{1}{Z_{mn}} \frac{\partial^2 Z_{mn}}{\partial \theta^2} + \frac{1}{Z_{mn} \tan \theta} \frac{\partial Z_{mn}}{\partial \theta} + n + 1 = -\frac{1}{\Phi_m \sin^2 \theta} \frac{\partial^2 \Phi_m}{\partial \phi^2}. \quad (2.191)$$

Equating the left-hand side of Eq. (2.191) to another constant of separation $m^2/\sin^2 \theta$ yields

$$\left(\frac{\partial^2}{\partial \theta^2} + \frac{1}{\tan \theta} \frac{\partial}{\partial \theta} + n(n+1) - \frac{m^2}{\sin^2 \theta} \right) Z_{mn}(\theta) = 0. \quad (2.192)$$

After substituting $z = \cos \theta$, the inclination equation becomes

$$\left[(1-z^2) \frac{\partial^2}{\partial z^2} - 2z \frac{\partial}{\partial z} + n(n+1) - \frac{m^2}{1-z^2} \right] Z_{mn}(z) = 0. \quad (2.193)$$

The solution to this equation is of the form

$$Z_{mn}(z) = \Theta_{mn} P_n^m(z) \quad (2.194)$$

or

$$Z_{mn}(\theta) = \Theta_{mn} P_n^m(\cos \theta), \quad (2.195)$$

where $P_n^m(\cos \theta)$ is the *associated* Legendre function. In the case of axisymmetry, where $m = 0$, it reduces to the Legendre function (or Legendre polynomial) denoted by $P_n(\cos \theta)$, as plotted in Fig. 2.22.

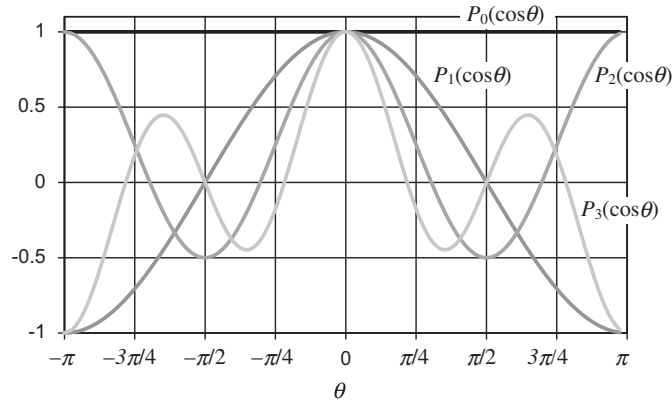


Figure 2.22 Legendre functions.

The azimuth equation in ϕ

Equating the right-hand side of Eq. (2.191) to the constant of separation $m^2/\sin^2 \theta$ yields

$$\left(\frac{\partial^2}{\partial \phi^2} + m^2\right)\Phi_m(\phi) = 0. \quad (2.196)$$

The solution to this equation is of the form

$$\Phi_m(\phi) = A_m \cos(m\phi) + B_m \sin(m\phi). \quad (2.197)$$

It can be seen that the integer m denotes the m th harmonic of the azimuthal modes of vibration where $\phi = 2\pi$ represents a full rotation about the z axis. The values of A_m and B_m depend on where the nodes and antinodes lie on the circumference. For example, setting $B_m = 0$ would place the nodes at $\phi = 0, \pi,$ and 2π . Now the complete solution to Eq. (2.180) may be written as

$$\begin{aligned} \tilde{p}(r, \theta, \phi) &= \sum_{n=0}^{\infty} \sum_{m=0}^n \tilde{p}_{mn} \left(R_{n+} h_n^{(2)}(kr) + R_{n-} h_n^{(1)}(kr) \right) \\ &\quad \times P_n^m(\cos \theta) (A_m \cos(m\phi) + B_m \sin(m\phi)). \end{aligned} \quad (2.198)$$

which in the case of axial symmetry ($m = 0$) simplifies to

$$\tilde{p}(r, \theta) = \sum_{n=0}^{\infty} \tilde{P}_n \left(R_{n+} h_n^{(2)}(kr) + R_{n-} h_n^{(1)}(kr) \right) P_n(\cos \theta). \quad (2.199)$$

Problem 2.1. A piccolo is a side-blown half-flute which is open at both ends (open-open pipe), whereas a pan flute is end blown and blocked at the opposite end (open-closed pipe). Assuming an effective air column length of 294 mm in both, including any end corrections, which instrument has the lowest fundamental resonance frequency? Which instrument does not produce even harmonics and thus has a “hollower” tone? Using Eq. (2.112), calculate the fundamental resonance frequency ($n = 0$) for the pan flute. Assuming the eigenfrequencies of an open-open pipe to be the same as those of a closed-closed one, use Eq. (2.94) to calculate the fundamental resonance frequency ($n = 1$) of the piccolo.

Problem 2.2. The wall of an infinitely long cylinder of radius a moves radially with velocity \tilde{u}_0 . Hence it may be considered to be “pulsating.” Derive the radial pressure distribution using both the homogeneous and inhomogeneous wave equations and thus verify the Bessel function identity used in Eq. (4.198).

Hint: Because of the infinite length and rotational symmetry of the cylinder, this reduces to a one-dimensional problem in the radial distance from the center w . The axial symmetry ensures that there is zero pressure gradient at the center, which behaves like a rigid termination to the waves transmitted from the wall. Hence, it is analogous to the closed tube of Section 2.7. In the steady state, the solution to the *homogenous* wave equation (2.23) in cylindrical coordinates is given by Eqs. (2.126) and (2.127). However, we omit the Y_0 function because of continuity at the center. Find the unknown coefficient by applying the velocity boundary condition at the wall ($w = a$) using the first line of Eq. (2.48) but replacing the axial ordinate x with the radial ordinate w and noting that $\partial/\partial w J_0(kw) = kJ_1(kw)$. To find the solution to the *inhomogeneous* wave equation, rewrite Eqs. (2.115) and (2.116) in cylindrical coordinates using the Laplace operator of Eq. (2.23) and replacing the length l with the radius a . Let the solution be in the form

$$\tilde{p}(w) = \sum_{n=0}^{\infty} \tilde{A}_n J_0(\beta_n w/a),$$

where β_n are the solutions to $J_1(\beta_n) = 0$. Insert this into the inhomogeneous wave equation and solve for \tilde{A}_n using the orthogonal integrals of Eqs. (A2.101a) and (A2.154) of Appendix II. Then equating the solutions to the *homogenous* and *inhomogeneous* wave equations gives the identity of Eq. (4.198).

NOTES

- [1] Nonvector derivations of the wave equation are given in Rayleigh, theory of sound, vol. 2, pp. 1–15, (Dover, 1945); P.M. Morse. Vibration and sound. 2nd ed. New York: Acoustical Society of America; 1981. p. 217–225; L.E. Kinsler, A. R. Frey, A. B. Coppens, and J. V. Sanders. Fundamentals of acoustics. 4th ed. New York: John Wiley & Sons, Inc.; 2000. p. 113–213; and other places.
- [2] A vector derivation of the wave equation is given in two papers that must be read together: W.J. Cunningham, application of vector analysis to the wave equation, J Acoust Soc Am 1950; 22:61 and R.V.L. Hartley. Note on Application of Vector Analysis to the Wave Equation. J Acoust Soc Am 1950;22:511.

- [3] If a mass of gas is chosen so that its weight in grams is equal to its molecular weight (known to chemists as the gram-molecular weight, or the mole), then the volume of this mass at 0°C and 0.76 m Hg is the same for all gases and equals 0.02242 m^3 . Then $R = 8.314$ watt-sec per degree centigrade per gram-molecular weight. If the mass of gas chosen is n times its molecular weight, Then $R = 8.314 n$.
- [4] Beranek See LL. Acoustic measurements. New York: Acoustical Society of America; 1988. p. 49.
- [5] Serway RA, Jewett JW. Principles of physics: a calculus - based text. 4th ed. Calif: Thomson Brooks/Cole, Belmont; 2006, ISBN 053449143X. p. 550.
- [6] Webster AG. Acoustical impedance, and the theory of horns and of the phonograph. Proc Natl Acad Sci USA 1919;5:275–82.
- [7] For the type of source we have assumed and no dissipation, this case breaks down for $kl = n\pi$.

Electromechanoacoustical circuits

PART VI: MECHANICAL CIRCUITS

3.1 INTRODUCTION

The subject of electromechanoacoustics (sometimes called dynamical analogies) is the application of electrical circuit theory to the solution of mechanical and acoustical problems. In classical mechanics, vibrational phenomena are represented entirely by differential equations. This situation existed early in the history of telephony and radio as well. As telephone and radio communication developed, it became obvious that a schematic representation of the elements and their interconnections was valuable. Unlike a mechanical drawing, a schematic representation simply shows how the individual circuit elements are connected, or their topology, rather than where they are physically located. One of the most celebrated examples outside the field of engineering is the map of the London Underground, which was designed by an electrical engineer [1] who realized that passengers simply wanted a clear diagram of how to get from one place to another without the geographical details of the route. Schematic diagrams made it possible for engineers to visualize the performance of a circuit without laboriously solving its equations. Such a study would have been hopelessly difficult if only the equations of the system were available.

There is another important advantage of a schematic diagram besides its usefulness in visualizing the system. Often one has a piece of equipment for which one desires the differential equations. The schematic diagram may then be drawn from visual inspection of the equipment. Following this, the differential equations may be formed directly from the schematic diagrams. Most engineers are trained to follow this procedure rather than to attempt to formulate the differential equations directly.

Schematic diagrams have their simplest applications in circuits that contain lumped elements, i.e., where the only independent variable is time. Such elements are valid when the wavelength greatly exceeds the dimensions of the component. In other words, lumped element models are models with zero space dimensions. In distributed systems, which are common in acoustics, there may be as many as three space variables and a time variable. Here, a schematic diagram becomes more complicated to visualize than the differential equations, and the classical theory comes into its own again. There are many

problems in acoustics, however, in which the elements are lumped and the schematic diagram may be used to good advantage.

Four principal requirements are fulfilled by the methods used in this text to establish schematic representations for acoustic and mechanical devices. They are as follows.

1. The methods must permit the formation of schematic diagrams from visual inspection of devices.
2. They must be capable of such manipulation as will make possible the combination of electrical, mechanical, and acoustical elements into one schematic diagram.
3. They must preserve the identity of each element in combined circuits so that one can recognize immediately a force, voltage, mass, inductance, and so on.
4. They must use the familiar symbols and the rules of manipulation for electrical circuits.

Several methods that have been devised fulfill one or two of the above four requirements, but not all four. A purpose of this chapter is to present a new method for handling combined electrical, mechanical, and acoustic systems. It incorporates the good features of previous theories and also fulfills the above four requirements. The symbols used conform with those of earlier texts wherever possible [2–6].

Note that a simple procedure for conversion of admittance-type circuits to impedance-type circuits is given in Part IX, [Section 3.8](#).



3.2 PHYSICAL AND MATHEMATICAL MEANINGS OF CIRCUIT ELEMENTS

The circuit elements we shall use in forming a schematic diagram are those of electrical circuit theory. These elements and their mathematical meaning are tabulated in [Table 3.1](#) and should be learned at this time. There are generators of two types. There are five types of circuit elements: resistance, capacitance, inductance, transformation, and gyration. There are three generic quantities: (1) the drop across the circuit element; (2) the flow through the circuit element; and (3) the magnitude of the circuit element [7].

Attention should be paid to the fact that the quantity \tilde{a} is neither restricted to voltage \tilde{e} nor \tilde{b} to electrical current \tilde{i} . In some problems \tilde{a} will represent force \tilde{f} or velocity \tilde{u} or pressure \tilde{p} or volume velocity \tilde{U} . In those cases \tilde{b} will represent, respectively, velocity \tilde{u} or force \tilde{f} or volume velocity \tilde{U} or pressure \tilde{p} . Similarly, the quantity c might be any appropriate quantity such as mass, compliance, inductance, resistance, etc. The physical meaning of the circuit elements c depends on the way in which the quantities \tilde{a} and \tilde{b} are chosen, with the restriction that $\frac{\tilde{a}^*}{\sqrt{2}} \cdot \frac{\tilde{b}}{\sqrt{2}}$ has the dimension of power in all cases. The complete array of alternatives is shown in [Table 3.2](#).

An important idea to fix in your mind is that the *mathematical operations associated with a given symbol are invariant*. If the element is of the inductance type, for example, the drop \tilde{a} across it is equal to the time derivative of the flow \tilde{b} through it multiplied by its size c .

Table 3.1 Mathematical and physical significance of symbols

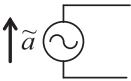
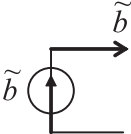
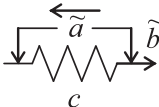
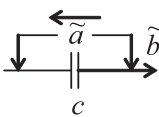
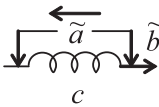
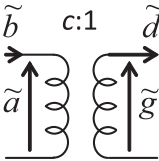
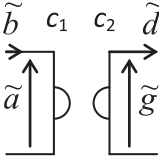
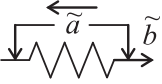
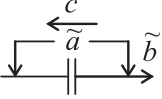
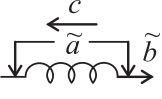
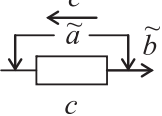
Symbol	Name	Meaning	
		Transient	Steady-state
	Constant drop generator	The drop \tilde{a} is independent of what is connected to the generator. Its internal impedance is zero so that if one of any number of generators in a circuit is switched off, it is replaced by a short circuit. The arrow points to the positive terminal of the generator.	
	Constant flow generator	The flow \tilde{b} is independent of what is connected to the generator. Its internal impedance is infinity so that if one of any number of generators in a circuit is switched off, it is replaced by an open circuit. The arrows point in the direction of positive flow.	
	Resistance-type element	$a = bc$	$\tilde{a} = \tilde{b}c$
	Capacitance-type element	$a = \frac{1}{c} \int b dt$	$\tilde{a} = \frac{\tilde{b}}{j\omega c}$
	Inductance-type element	$a = c \frac{db}{dt}$	$\tilde{a} = j\omega c \tilde{b}$
	Transformation-type element	$a = cg$ $b = \frac{d}{c}$ $\frac{a}{b} = c^2 \frac{g}{d}$	$\tilde{a} = c\tilde{g}$ $\tilde{b} = \frac{\tilde{d}}{c}$ $\frac{\tilde{a}}{\tilde{b}} = c^2 \frac{\tilde{g}}{\tilde{d}}$
	Gyration-type element	$c_1 a = d$ $b = c_2 g$ $\frac{a}{b} = \frac{1}{c_1 c_2} \frac{d}{g}$	$c_1 \tilde{a} = \tilde{d}$ $\tilde{b} = c_2 \tilde{g}$ $\frac{\tilde{a}}{\tilde{b}} = \frac{1}{c_1 c_2} \frac{\tilde{d}}{\tilde{g}}$

Table 3.2 Values for a , b , and c in electrical, mechanical, and acoustical circuits

Element	Electrical	Mechanical		Acoustical	
		Admittance analogy	Impedance analogy	Impedance analogy	Admittance analogy
\tilde{a}	\tilde{e}	\tilde{u}	\tilde{f}	\tilde{p}	\tilde{U}
\tilde{b}	\tilde{i}	\tilde{f}	\tilde{u}	\tilde{U}	\tilde{p}
	$c = R_E$	$c = \frac{1}{R_M} = Y_M$	$c = R_M$	$c = R_A$	$c = \frac{1}{R_A} = Y_A$
	$c = C_E$	$c = M_M$	$c = C_M$	$c = C_A$	$c = M_A$
	$c = L$	$c = C_M$	$c = M_M$	$c = M_A$	$c = C_A$
	$c = Z_E = \frac{\tilde{e}}{\tilde{i}}$	$c = Y_M = \frac{\tilde{u}}{\tilde{f}}$ $= \frac{1}{Z_M}$	$c = Z_M = \frac{\tilde{f}}{\tilde{u}}$ $= \frac{1}{Y_M}$	$c = Z_A = \frac{\tilde{p}}{\tilde{U}}$ $= \frac{1}{Y_A}$	$c = Y_M = \frac{\tilde{U}}{\tilde{p}}$ $= \frac{1}{Z_A}$

Note that this rule is not always followed in electrical circuit theory because conductance and resistance there are often indiscriminately written beside the symbol for a resistance-type element. The invariant operations to be associated with each symbol are shown in columns 3 and 4 of [Table 3.1](#).

An infinite impedance generator is a flow generator in the impedance analogy and a drop generator in the admittance analogy. Conversely, a zero impedance generator is a drop generator in the impedance analogy and a flow generator in the admittance analogy. A drop generator “hates” short circuits for obvious reasons. A flow generator “hates” open circuits because when the flow is blocked, the drop rises to infinity. In fact a flow generator can be approximated by a very large drop generator with a very large series resistance whose value is the drop divided by the desired flow.

The transformation element is ideal in that it neither creates nor dissipates power. Hence, the dot product $\tilde{a}^* \cdot \tilde{b}$ on the primary side is always equal to $\tilde{g}^* \cdot \tilde{d}$ on the secondary side. It is also reversible, unlike, for example, an amplifier. If the transformation ratio is $c:1$, as illustrated in [Table 3.1](#), then you divide the drop \tilde{a} on the primary side to obtain the drop \tilde{g} on the secondary side. Conversely, if the transformation ratio is $1:c$, then you multiply the drop \tilde{a} on the primary side to obtain the drop \tilde{g} on the secondary side. Of course, to conserve power, the opposite operation is performed on the flow so that it increases by the same ratio that the drop decreases or vice versa.

The gyration element is used to convert an admittance-type circuit to an impedance-type one or vice versa. This means that the flow \tilde{d} on the secondary side is equal to the drop \tilde{a} on the primary side multiplied by the forward mutual conductance c_1 . Likewise, the flow \tilde{b} on the primary side is equal to the drop \tilde{g} on the secondary side multiplied by reverse mutual conductance c_2 . The forward and reverse mutual conductances c_1 and c_2 , respectively, may have different values in which case energy is either consumed (as in an amplifier) or dissipated. In this chapter, it will be used exclusively as an energy conserving element in passive transducers, in which case $c_1 = c_2 = c$.



3.3 MECHANICAL ELEMENTS

Mechanical circuit elements need not always be represented by electrical symbols. Because one frequently draws a mechanical circuit directly from inspection of the mechanical device, more obvious forms of mechanical elements are sometimes useful, at least until the student is thoroughly familiar with the analogous circuit. We shall accordingly devise a set of “mechanical” elements to be used as an introduction to the elements of [Table 3.1](#).

In electrical circuits, a voltage measurement is made by attaching the leads from a voltmeter *across* the two terminals of the element. Voltage is a quantity that we can measure without breaking into the circuit. To measure electric current, however, we must break into the circuit because this quantity acts *through* the element. In mechanical devices, on the other hand, we can measure the velocity (or the displacement) without disturbing the machine by using a capacitive or inertially operated vibration pickup to determine the quantity at any point on the machine. It is not velocity but force that is analogous to electric current. Force cannot be measured unless one breaks into the device.

It becomes apparent then that if a mechanical element is strictly analogous to an electrical element, it must have a velocity difference appearing between (or across) its two terminals and a force acting through it. Analogously, also, the product of the rms force f in N and the in-phase component of the rms velocity u in m/s is the power in W. We shall call this type of analogy, in which a velocity corresponds to a voltage and a force to a current, the *admittance-type analogy*. It is also known as the “inverse” analogy.

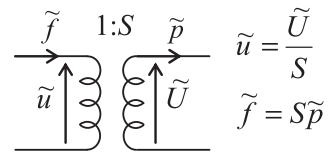
Many texts teach in addition a “direct” analogy. It is the opposite of the admittance analogy in that force is made to correspond to voltage and velocity to current. In this chapter, we shall call this kind of analogy an *impedance-type analogy*. To familiarize the student with both concepts, all examples will be given here both in admittance-type and impedance-type analogies. [Table 3.3](#) shows a comparison of the symbolic representation of elements in each analogy.

Table 3.3 Conversion from admittance-type analogy to impedance-type analogy, or vice versa

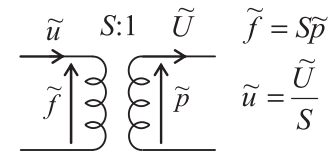
Element	Mechanical analogies		Acoustical analogies	
	Admittance type	Impedance type	Admittance type	Impedance type
Infinite impedance generator (impedance analogy) and zero admittance generator (admittance analogy)				
Zero impedance generator (impedance analogy) and infinite admittance generator (admittance analogy)				
Dissipative element – resistance (impedance analogy) and conductance (admittance analogy)				
Mass element				
Compliant element				
Impedance element (impedance analogy) and admittance element (admittance analogy)				

Transformation element If there are any drug dosages in this chapter, please verify them and indicate that you have done so by initialing this query. converts from one impedance to another and is useful for coupling between electrical, mechanical or acoustical domains

Mechanical to acoustic (admittance type)

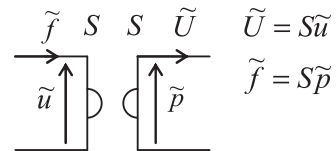


Mechanical to acoustic (impedance type)

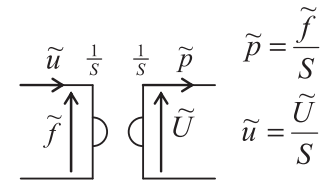


Gyrator element — converts an admittance circuit to an impedance one or vice versa and is useful for coupling between electrical, mechanical or acoustical domains

Mechanical (admittance) to acoustic (impedance)



Mechanical (impedance) to acoustic (admittance)



Mechanical impedance Z_M and mechanical admittance Y_M

The mechanical impedance is the complex ratio of force to velocity at a given point in a mechanical device. We commonly use the symbol Z_M for mechanical impedance, where the subscript M stands for “mechanical.” The unit is N s/m or mechanical ohm.

In the admittance analogy, the mechanical admittance is the inverse of the mechanical impedance. It may also be referred to as the mechanical mobility, but we shall use the more commonly used term admittance. It is the complex ratio of velocity to force at a given point in a mechanical device. We commonly use the symbol Y_M for mechanical admittance. The unit is m/ N·s or mechanical siemens (S).

Mass M_M

Mass is that physical quantity which when acted on by a force is accelerated in direct proportion to that force. The unit is kg. At first sight, mass appears to be a one-terminal quantity because only one connection is needed to set it in motion. However, the force acting on a mass and the resultant acceleration are reckoned with respect to the earth (inertial frame) so that in reality the second terminal of mass is the earth.

The mechanical symbol used to represent mass is shown in Fig. 3.1. The upper end of the mass moves with a velocity \tilde{u} with respect to the ground. The]-shaped configuration represents the “second” terminal of the mass and has zero velocity. The force can be measured by a suitable device inserted between the point 1 and the next element or generator connecting to it.

Mass M_M obeys Newton’s second law that

$$f(t) = M_M \frac{du(t)}{dt}, \quad (3.1)$$

where $f(t)$ is the instantaneous force in N, M_M is the mass in kg, and $u(t)$ is the instantaneous velocity in m/s.

In the steady state (see Eqs. (2.36–2.44)), with an angular frequency ω equal to 2π times the frequency of vibration, we have the special case of Newton’s second law,

$$\tilde{f} = j\omega M_M \tilde{u}, \quad (3.2)$$

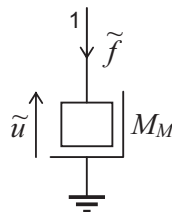


Figure 3.1 Mechanical symbol for a mass.

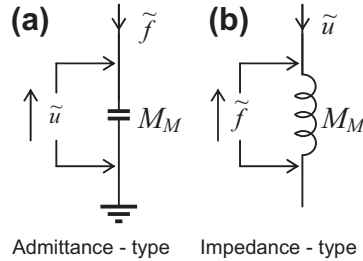


Figure 3.2 (a) Admittance-type and (b) impedance-type symbols for a mass.

where $j = \sqrt{-1}$ as usual.

The admittance-type analogous symbol that we use as a replacement for the mechanical symbol in our circuits is a capacitance type, which is shown in Fig. 3.2(a). The mathematical operation invariant for this symbol is found from Table 3.1. In the steady state, we have

$$\tilde{a} = \frac{\tilde{b}}{j\omega c} \quad \text{or} \quad \tilde{u} = \frac{\tilde{f}}{j\omega M_M}. \quad (3.3)$$

This equation is seen to satisfy the physical law given in Eq. (3.2). Note the similarity in appearance of the mechanical and analogous symbols in Figs. 3.1 and 3.2(a). In electrical circuits, the time integral of the current through a capacitor is charge. The analogous quantity here is the time integral of force, which is momentum.

The impedance-type analogous symbol for a mass is an inductance, which is shown in Fig. 3.2(b). The invariant operation for steady state is $\tilde{a} = j\omega c\tilde{b}$ or $\tilde{f} = j\omega M_M\tilde{u}$. It also satisfies Eq. (3.2). Note, however, that in this analogy, one side of the mass element is not necessarily grounded; this often leads to confusion. In electrical circuits, the time integral of the voltage across an inductance is flux turns. The analogous quantity here is momentum.

Mechanical compliance C_M

A physical structure is said to be a mechanical compliance C_M if, when it is acted on by a force, it is displaced in direct proportion to the force. The unit is m/N. Compliant elements usually have two apparent terminals.

The mechanical symbol used to represent a mechanical compliance is a spring. It is shown in Fig. 3.3. The upper end of the element moves with a velocity \tilde{u}_1 and the lower end with a velocity \tilde{u}_2 . The force required to produce the difference between the velocities \tilde{u}_1 and \tilde{u}_2 may be measured by breaking into the machine at either point 1 or point 2. Just as the same current would be measured at either end of an element in an



Figure 3.3 Mechanical symbol for a mechanical compliance.

electrical circuit, the same force will be found here at either end of the compliant element.

Mechanical compliance C_M obeys the following physical law:

$$a = \frac{1}{c} \int b \, dt \quad \text{or} \quad f(t) = \frac{1}{C_M} \int u(t) dt, \quad (3.4)$$

where C_M is the mechanical compliance in m/N, and $u(t)$ is the instantaneous velocity in m/s equal to $\tilde{u}_1 - \tilde{u}_2$, the difference in velocity of the two ends.

In the steady state, with an angular frequency ω , equal to 2π times the frequency of vibration, we have

$$\tilde{f} = \frac{\tilde{u}}{j\omega C_M}, \quad (3.5)$$

where \tilde{f} and \tilde{u} are taken to be complex quantities.

The admittance-type analogous symbol used as a replacement for the mechanical symbol in our circuits is an inductance, which is shown in Fig. 3.4(a). The invariant mathematical operation that this symbol represents is given in Table 3.1. In the steady state, we have

$$\tilde{u} = j\omega C_M \tilde{f}. \quad (3.6)$$

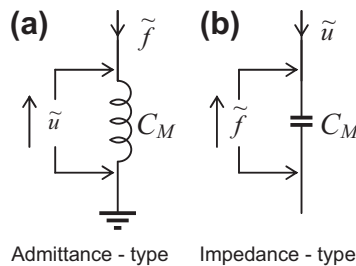


Figure 3.4 (a) Admittance-type and (b) impedance-type symbols for a mechanical compliance.

In electrical circuits, the time integral of the voltage across an inductance is flux turns. The analogous quantity here is the time integral of velocity, which is displacement.

This equation satisfies the physical law given in Eq. (3.5). Note the similarity in appearance of the mechanical and analogous symbols in Fig. 3.3 and 3.4(a).

The impedance-type analogous symbol for a mechanical compliance is a capacitance. It is shown in Fig. 3.4(b). The invariant operation for steady state is $\tilde{a} = \tilde{b}/j\omega c$ or $\tilde{f} = \tilde{u}/j\omega C_M$. It also satisfies Eq. (3.5). In electrical circuits, the time integral of the current through a capacitor is the charge. The analogous quantity here is the displacement.

Mechanical resistance R_M and mechanical conductance G_M

A physical structure is said to be a mechanical resistance R_M if, when it is acted on by a force, it moves with a velocity directly proportional to the force. The unit is $\text{N}\cdot\text{s}/\text{m}$ or rayls m^2 .

We also define here a quantity G_M , the mechanical conductance, which is the reciprocal of R_M . The unit of conductance is $\text{m}/\text{N}\cdot\text{s}$ or $1/\text{rayls m}^2$.

The above representation for mechanical resistance is usually limited to viscous resistance. Frictional resistance is excluded because, for it, the ratio of force to velocity is not a constant. Both terminals of resistive elements can usually be located by visual inspection.

The mechanical element used to represent viscous resistance is the fluid dashpot shown schematically in Fig. 3.5. The upper end of the element moves with a velocity \tilde{u}_1 and the lower with a velocity \tilde{u}_2 . The force required to produce the difference between the two velocities \tilde{u}_1 and \tilde{u}_2 may be measured by breaking into the machine at either point 1 or point 2.

Mechanical resistance R_M obeys the following physical law:

$$\tilde{f} = R_M \tilde{u} = \frac{1}{G_M} \tilde{u}, \quad (3.7)$$

where \tilde{f} is the force in N, \tilde{u} is the difference between the velocities \tilde{u}_1 and \tilde{u}_2 of the two ends, R_M is the mechanical resistance in $\text{N}\cdot\text{s}/\text{m}$, and G_M is the mechanical conductance in $\text{m}/\text{N s}$.

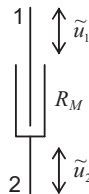


Figure 3.5 Mechanical symbol for mechanical (viscous) resistance.

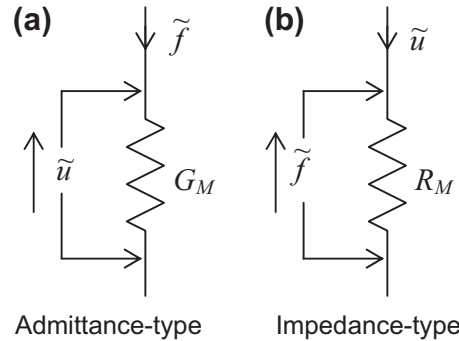


Figure 3.6 (a) Admittance-type and (b) impedance-type symbols for a mechanical resistance.

The admittance-type analogous symbol used to replace the mechanical symbol in our circuits is a resistance. It is shown in Fig. 3.6(a). The invariant mathematical operation that this symbol represents is given in Table 3.1. In either the steady or transient state, we have

$$\tilde{u} = G_M \tilde{f} = \frac{1}{R_M} \tilde{f}. \quad (3.8)$$

In the steady state, \tilde{u} and \tilde{f} are taken to be complex quantities. This equation satisfies the physical law given in Eq. (3.7).

The impedance-type analogous symbol for a mechanical resistance is shown in Fig. 3.6(b). It also satisfies Eq. (3.7).

Mechanical generators

The mechanical generators considered will be one of the two types: constant velocity or constant force. A *constant velocity generator* is represented as a very strong motor attached to a shuttle mechanism in the manner shown in Fig. 3.7. The opposite ends of the generator have velocities \tilde{u}_1 and \tilde{u}_2 . One of these velocities, either \tilde{u}_1 or \tilde{u}_2 , is determined by factors external to the generator. The difference between the velocities \tilde{u}_1 and \tilde{u}_2 , however, is a velocity \tilde{u} that is independent of the external load connected to the generator.

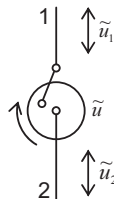


Figure 3.7 Mechanical symbol for a constant velocity generator.

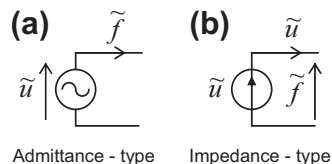


Figure 3.8 (a) Admittance-type and (b) impedance-type symbols for a constant velocity generator.

The symbols that we used in the two analogies to replace the mechanical symbol for a constant velocity generator are shown in Fig. 3.8. The invariant mathematical operations that these symbols represent are also given in Table 3.1. The tips of the arrows point to the “positive” terminals of the generators. The wave inside the circle in Fig. 3.8(a) indicates that the internal admittance of the generator is zero. The arrow inside the circle of Fig. 3.8(b) indicates that the internal impedance of the generator is infinite.

A *constant force generator* is represented here by an electromagnetic transducer (e.g., a moving-coil loudspeaker) in the primary of which an electric current of constant amplitude is maintained. Such a generator produces a force equal to the product of the current \tilde{i} , the flux density B , and the effective length of the wire l cutting the flux ($\tilde{f} = B\tilde{i}l$). This device is shown schematically in Fig. 3.9. The opposite ends of the generator have velocities \tilde{u}_1 and \tilde{u}_2 that are determined by factors external to the generator. The force that the generator produces and that may be measured by breaking into the device at either point 1 or point 2 is a constant force, independent of what is connected to the generator.

The symbols used in the two analogies to replace the mechanical symbol for a constant force generator are given in Fig. 3.10. The invariant mathematical operations that these symbols represent are also given in Table 3.1. The arrows point in the direction of positive flow. Here the arrow inside the circle indicates infinite admittance and the wave inside the circle zero impedance.

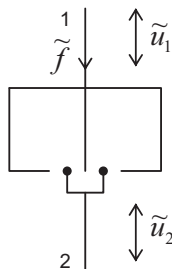


Figure 3.9 Mechanical symbol for a constant force generator.

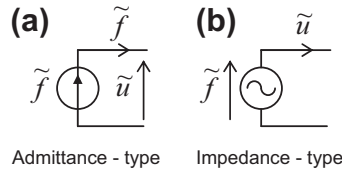


Figure 3.10 (a) Admittance-type and (b) impedance-type symbols for a constant force generator.

Lever

Simple lever

It is apparent that the lever is a device closely analogous to a transformer. The lever in its simplest form consists of a weightless bar resting on an immovable fulcrum, so arranged that a downward force on one end causes an upward force on the other end (see Fig. 3.11). From elementary physics, we may write the equation of balance of moments around the fulcrum

$$\tilde{f}_1 l_1 = \tilde{f}_2 l_2$$

or, if not balanced, assuming small displacements,

$$\tilde{u}_1 l_2 = \tilde{u}_2 l_1. \quad (3.9)$$

Also,

$$Y_{M1} = \frac{\tilde{u}_1}{\tilde{f}_1} = \left(\frac{l_1}{l_2}\right)^2 Y_{M2}, \quad (3.10)$$

$$Z_{M1} = \frac{\tilde{f}_1}{\tilde{u}_1} = \left(\frac{l_2}{l_1}\right)^2 Z_{M2}.$$

The above equations may be represented by the ideal transformers of Fig. 3.12, having a transformation ratio of $(l_1/l_2):1$ for the admittance type and $(l_2/l_1):1$ for the impedance type.

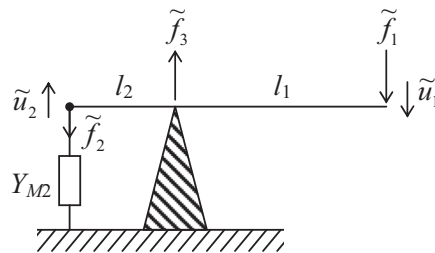


Figure 3.11 Simple lever.

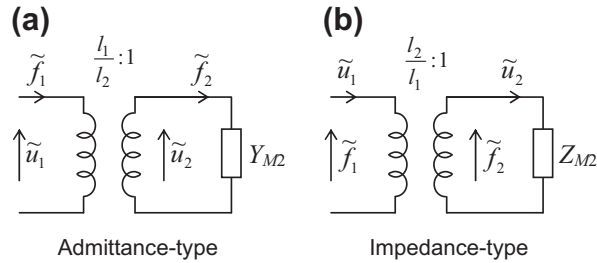


Figure 3.12 (a) Admittance-type and (b) impedance-type symbols for a simple lever.

Floating lever

As an example of a simple floating lever, consider a weightless bar resting on a fulcrum that yields under force. The bar is so arranged that a downward force on one end tends to produce an upward force on the other end. An example is shown in Fig. 3.13.

To solve this type of problem, we first write the equations of moments. Summing the moments about the center support gives

$$l_1 \tilde{f}_1 = l_2 \tilde{f}_2$$

and summing the moments about the end support gives

$$(l_1 + l_2) \tilde{f}_1 = l_2 \tilde{f}_3. \quad (3.11)$$

When the forces are not balanced and if we assume infinitesimal displacements, the velocities are related to the forces through the admittances so that

$$\begin{aligned} \tilde{u}_3 &= Y_{M3} \tilde{f}_3 = Y_{M3} \frac{l_1 + l_2}{l_2} \tilde{f}_1, \\ \tilde{u}_2 &= Y_{M2} \tilde{f}_2 = Y_{M2} \frac{l_1}{l_2} \tilde{f}_1. \end{aligned} \quad (3.12)$$

Also, by superposition, it is seen from simple geometry that

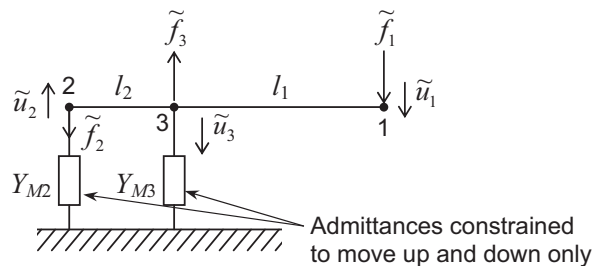


Figure 3.13 Floating lever.

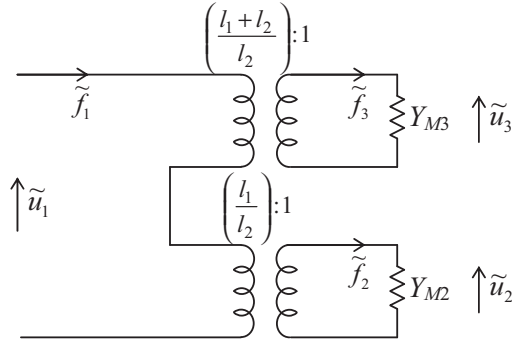


Figure 3.14 Admittance-type symbol for a floating lever.

$$\tilde{u}'_1 = \tilde{u}_3 \frac{l_1 + l_2}{l_2} \text{ for } \tilde{u}_2 = 0,$$

$$\tilde{u}''_1 = \tilde{u}_2 \frac{l_1}{l_2} \text{ for } \tilde{u}_3 = 0,$$

so that

$$\tilde{u}_1 = \tilde{u}'_1 + \tilde{u}''_1 = \frac{l_1 + l_2}{l_2} \tilde{u}_3 + \frac{l_1}{l_2} \tilde{u}_2 \quad (3.13)$$

and, finally,

$$\frac{\tilde{u}_1}{\tilde{f}_1} = Y_{M1} = Y_{M3} \left(\frac{l_1 + l_2}{l_2} \right)^2 + Y_{M2} \left(\frac{l_1}{l_2} \right)^2. \quad (3.14)$$

This equation may be represented by the analogous circuit of Fig. 3.14. The lever loads the generator with two admittances connected in series, each of which behaves as a simple lever when the other is equal to zero. It will be seen that this is a way of obtaining the equivalent of two series masses without a common zero-velocity (ground) point. This will be illustrated in Example 3.3.

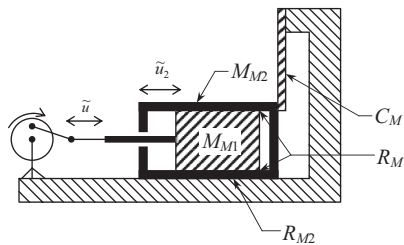


Figure 3.15 Six-element mechanical device.

Example 3.1. The mechanical device of Fig. 3.15 consists of a piston of mass M_{M1} sliding on an oil surface inside a cylinder of mass M_{M2} . This cylinder in turn slides in an oiled groove cut in a rigid body. The sliding (viscous) resistances are R_{M1} and R_{M2} , respectively. The cylinder is held by a spring of compliance C_M . The mechanical generator maintains a constant sinusoidal velocity of angular frequency ω , whose magnitude is \tilde{u} m/s. Solve for the force \tilde{f} produced by the generator.

Solution. Although the force will be determined ultimately from an analysis of the admittance-type analogous circuit for this mechanical device, it is frequently useful to draw a mechanical circuit diagram. This interim step to the desired circuit will be especially helpful to the student who is inexperienced in the use of analogies. Its use virtually eliminates errors from the final circuit.

To draw the mechanical circuit, note first the junction points of two or more elements. This locates all element terminals which move with the same velocity. There are in this example two velocities, \tilde{u} and \tilde{u}_2 , in addition to “ground” or zero velocity. These two velocities are represented in the mechanical circuit diagram by the velocities of two imaginary rigid bars, 1 and 2 of Fig. 3.16, which oscillate in a vertical direction. The circuit drawing is made by attaching all element terminals with velocity \tilde{u} to the first bar and all terminals with velocity \tilde{u}_2 to the second bar. All terminals with zero velocity are drawn to a ground bar. Note that a mass always has one terminal on ground [8]. Three elements of Fig. 3.15 have one terminal with the velocity \tilde{u} : the generator, the mass M_{M1} , and the viscous resistance R_{M1} . These are attached to bar 1. Four elements have one terminal with the velocity \tilde{u}_2 : the viscous resistances R_{M1} and R_{M2} , the mass M_{M2} , and the compliance C_M . These are attached to bar 2. Five elements have one terminal with zero velocity: the generator, both masses, the viscous resistance R_{M2} , and the compliance C_M .

We are now in a position to transform the mechanical circuit into an admittance-type analogous circuit. This is accomplished simply by replacing the mechanical elements with the analogous admittance-type elements. The circuit becomes such as that shown in Fig. 3.17. Remember that, in the admittance-type analogy, force “flows” through the elements and velocity is the drop across them. The resistors must have G_s written alongside them. As defined above, $G_M = 1/R_M$, and the unit is m/N·s or mechanical siemens.

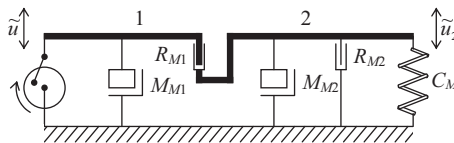


Figure 3.16 Mechanical circuit for the device of Fig. 3.15.

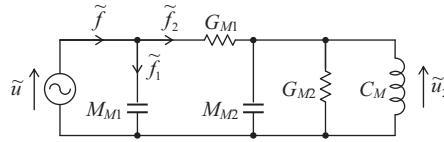


Figure 3.17 Admittance-type analogous circuit for the device of Fig. 3.15.

The equations for this circuit are found in the usual manner, using the rules of Table 3.1. Let us determine $Y_M = \tilde{u}/\tilde{f}$, the mechanical admittance presented to the generator. The mechanical admittance of the three elements in parallel on the right-hand side of the schematic diagram is

$$\begin{aligned} \frac{\tilde{u}_2}{\tilde{f}_2} &= \frac{1}{\frac{1}{1/j\omega M_{M2}} + \frac{1}{G_{M2}} + \frac{1}{j\omega C_M}} \\ &= \frac{1}{j\omega M_{M2} + R_{M2} + \frac{1}{j\omega C_M}}. \end{aligned}$$

Including the element G_{M1} , the mechanical admittance for that part of the circuit through which \tilde{f}_2 flows is, then,

$$\frac{\tilde{u}}{\tilde{f}_2} = G_{M1} + \frac{1}{j\omega M_{M2} + R_{M2} + \frac{1}{j\omega C_M}}.$$

Note that the input mechanical admittance Y_M is given by

$$Y_M = \frac{\tilde{u}}{\tilde{f}} = \frac{\tilde{u}}{\tilde{f}_1 + \tilde{f}_2}.$$

and

$$\tilde{f}_1 = \frac{\tilde{u}}{1/j\omega M_{M1}} = j\omega M_{M1}\tilde{u}.$$

Substituting \tilde{f}_1 and \tilde{f}_2 into the second equation preceding gives us the input admittance:

$$Y_M = \frac{\tilde{u}}{\tilde{f}} = \frac{1}{j\omega M_{M1} + \frac{1}{G_{M1} + \frac{1}{j\omega M_{M2} + R_{M2} + \frac{1}{j\omega C_M}}}}. \quad (3.15a)$$

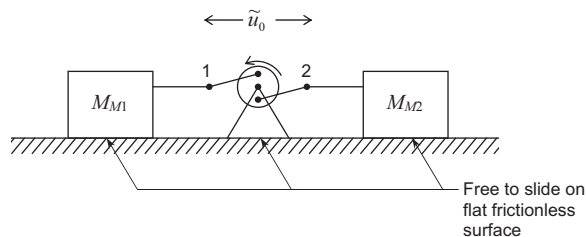


Figure 3.18 Three-element mechanical device.

The mechanical impedance is the reciprocal of Eq. (3.15a):

$$Z_M = \frac{\tilde{f}}{\tilde{u}} = j\omega M_{M1} + \frac{1}{G_{M1} + \frac{1}{j\omega M_{M2} + R_{M2} + \frac{1}{j\omega C_M}}}. \quad (3.15b)$$

The result is

$$\tilde{f} = Z_M \tilde{u} \text{ N}. \quad (3.16)$$

Example 3.2. As a further example of a mechanical circuit, let us consider the two masses of 2 and 4 kg shown in Fig. 3.18. They are assumed to rest on a frictionless plane surface and to be connected together through a generator of constant velocity that is also free to slide on the frictionless plane surface.

Let its velocity be

$$u_0(t) = 2 \cos 1000t \text{ cm/s}$$

so that

$$\tilde{u}_0 = 2e^{j1000t} \text{ cm/s}$$

or

$$|\tilde{u}_0| = 2 \text{ cm/s at } \omega = 1000 \text{ Hz.}$$

Draw the admittance-type analogous circuit and determine the force \tilde{f} produced by the generator. Also, determine the admittance presented to the generator.

Solution. The masses do not have the same velocity with respect to ground. The difference between the velocities of the two masses is \tilde{u}_0 . The element representing a mass is that shown in Fig. 3.2(a) with one end grounded and the other moving at the velocity of the mass.

The admittance-type circuit for this example is shown in Fig. 3.19. The velocity \tilde{u}_0 equals $\tilde{u}_1 + \tilde{u}_2$, where \tilde{u}_1 is the velocity *with respect to ground* of M_1 and \tilde{u}_2 is that for M_2 . The force \tilde{f} is

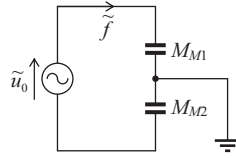


Figure 3.19 Admittance-type analogous circuit for the device of Fig. 3.18.

$$\begin{aligned}
 \tilde{f} &= \frac{1}{\frac{1}{j\omega M_{M1}} + \frac{1}{j\omega M_{M2}}} |\tilde{u}_0| e^{j1000t} \\
 &= \frac{j\omega M_{M1} M_{M2}}{M_{M1} + M_{M2}} |\tilde{u}_0| e^{j1000t} \\
 &= \frac{j1000 \times 2 \times 4 \times 0.02}{2 + 4} e^{j1000t} = j26.7 e^{j1000t} \text{ N.}
 \end{aligned} \tag{3.17}$$

The j indicates that the time phase of the force is 90 degrees leading with respect to that of the velocity of the generator. Hence, the rms force is

$$f_{\text{rms}} = \frac{|\tilde{f}|}{\sqrt{2}} \angle 90^\circ = 18.9 \text{ N} \angle 90^\circ \tag{3.18}$$

Obviously, when one mass is large compared with the other, the force is that necessary to move the smaller one alone. This example reveals the only type of case in which masses can be in series without the introduction of floating levers. At most, only two masses can be in series because a common ground is necessary.

The admittance presented to the generator is

$$\begin{aligned}
 Y_M &= \frac{\tilde{u}_0}{\tilde{f}} = \frac{M_{M1} + M_{M2}}{j\omega M_{M1} M_{M2}} \\
 &= \frac{6}{j1000 \times 8} = -j7.5 \times 10^{-4} \text{ m/N}\cdot\text{s}
 \end{aligned} \tag{3.19}$$

Example 3.3. An example of a mechanical device embodying a floating lever is shown in Fig. 3.20. The masses attached at points 2 and 3 may be assumed to be resting on very compliant springs. The driving force \tilde{f}_1 will be assumed to have a frequency well above the resonance frequencies of the masses and their spring supports so that

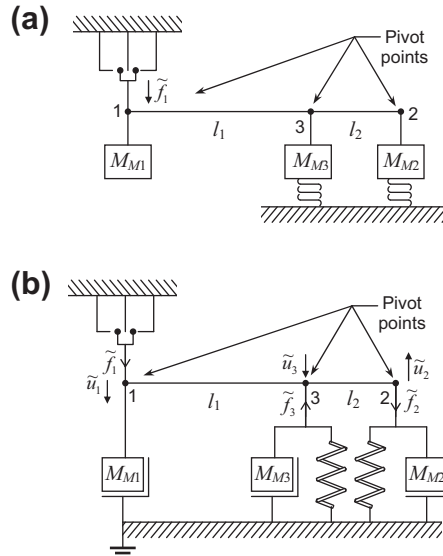


Figure 3.20 (a) Mechanical device embodying a floating lever. (b) Mechanical diagram of (a). The compliances of the springs are very large so that all of f_2 and f_3 go to move M_{M2} and M_{M3} .

$$Y_{M2} \approx \frac{1}{j\omega M_{M2}}$$

$$Y_{M3} \approx \frac{1}{j\omega M_{M3}}$$

Also, assume that a mass is attached to the weightless lever bar at point 1, with an admittance

$$Y_{M1} = \frac{1}{j\omega M_{M1}}.$$

Solve for the total admittance presented to the constant force generator \tilde{f}_1 .

Solution. By inspection, the admittance-type analogous circuit is drawn as shown in Fig. 3.21(a,b). Solving for $Y_M = \tilde{u}_1/\tilde{f}_1$, we get

$$Y_M = \frac{1}{j\omega \left[\frac{M_{M2}M_{M3}l_2^2}{M_{M3}l_1^2 + M_{M2}(l_1 + l_2)^2} + M_{M1} \right]} \quad (3.20)$$

Note that if $l_2 \rightarrow 0$, the admittance is simply that of the mass M_{M1} . Also, if $l_1 \rightarrow 0$, the admittance is that of M_{M1} and M_{M3} , that is,

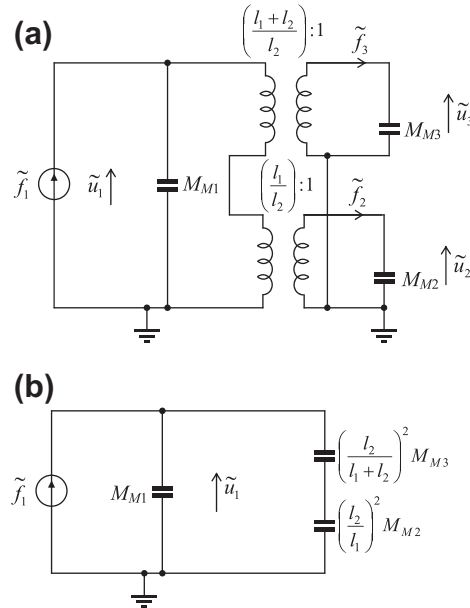


Figure 3.21 (a) Admittance-type analogous circuit for the device of Fig. 3.20. (b) Same as (a) but with transformers removed.

$$Y_M = \frac{1}{j\omega(M_{M3} + M_{M1})} \quad (3.21)$$

In an admittance-type circuit (with transformers eliminated), it is possible with one or more floating levers to have one or more M_M s with no ground terminal (s).

PART VII: ACOUSTICAL CIRCUITS

3.4 ACOUSTICAL ELEMENTS

Acoustical circuits are frequently more difficult to draw than mechanical ones because the elements are less easy to identify. As was the case for mechanical circuits, the more obvious forms of the elements will be useful as an intermediate step toward drawing the analogous circuit diagram. When the student is more familiar with acoustical circuits, he or she will be able to pass directly from the acoustic device to the final form of the equivalent circuit.

In acoustic devices, the quantity we are able to measure most easily without modification of the device is sound pressure. Such a measurement is made by inserting a small hollow probe tube into the sound field at the desired point. This probe tube leads to

one side of a microphone diaphragm. The other side of the diaphragm is exposed to atmospheric pressure. A movement of the diaphragm takes place when there is a difference in pressure across it. This difference between atmospheric pressure and the incremental pressure created by the sound field is the sound pressure \tilde{p} .

Because we can measure sound pressure by such a probe tube arrangement without disturbing the device, it seems that sound pressure is analogous to voltage in electrical circuits. Such a choice requires us to consider current as being analogous to some quantity which is proportional to velocity. As we shall show shortly, a good choice is to make current analogous to volume velocity, the volume of gas displaced per second.

A strong argument can be made for this choice of analogy when one considers the relations governing the flow of air inside such acoustic devices as loudspeakers, microphones, and noise filters. Inside a certain type of microphone, for example, there is an air cavity that connects to the outside air through a small tube (see Fig. 3.22). Assume, now, that the outer end of this tube is placed in a sound wave. The wave will cause a movement of the air particles in the tube. Obviously, there is a junction between the tube and the cavity at the inner end of the tube at point A . Let us ask ourselves the question “What physical quantities are continuous at this junction point?”.

First, the sound pressure just inside the tube at A is the same as that in the cavity just outside A . That is to say, we have continuity of sound pressure. Second, the quantity of air leaving the inner end of the small tube in a given interval of time is the quantity that enters the cavity in the same interval of time. That is, the mass per second of gas leaving the small tube equals the mass per second of gas entering the volume. Because the pressure is the same at both places, the density of the gas must also be the same, and it follows that there is continuity of volume velocity (cubic meters per second or m^3/s) at this junction. Analogously, in the case of electricity, there is continuity of electric current at a junction. Continuity of volume velocity must exist even if there are several tubes or cavities joining near one point. A violation of the law of conservation of mass otherwise would occur.

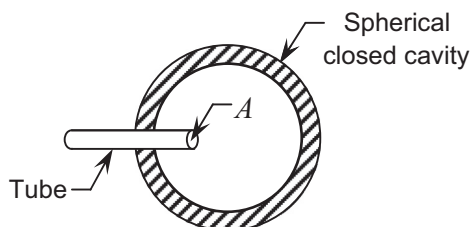


Figure 3.22 Closed cavity connecting to the outside air through a tube of cross-sectional area S . The junction plane between the tube and the cavity occurs at A .

We conclude that the quantity that flows *through* our acoustical elements must be the volume velocity U in m^3/s and the drop across our acoustical elements must be the pressure p in Pa. This conclusion indicates that the impedance type of analogy is the preferred analogy for acoustical circuits. The product of the effective sound pressure p times the in-phase component of the effective volume velocity U gives the acoustic power in W.

In this part, we shall discuss the more general aspects of acoustical circuits. In Chapter 4, we explain fully the approximations involved and the rules for using the concepts enunciated here in practical problems.

Acoustic mass M_A

Acoustic mass is a quantity proportional to mass but having the dimensions of kg/m^4 . It is associated with a mass of air accelerated by a net force which acts to displace the gas without appreciably compressing it. The concept of acceleration without compression is an important one to remember. It will assist you in distinguishing acoustic masses from other elements.

The acoustical element that is used to represent an acoustic mass is a tube filled with the gas as shown in Fig. 3.23.

The physical law governing the motion of a mass that is acted on by a force is Newton's second law, $f(t) = M_M du(t)/dt$. This law may be expressed in acoustical terms as follows:

$$\frac{f(t)}{S} = \frac{M_M}{S} \frac{d[u(t)S]}{dt S} = p(t) = \frac{M_M}{S^2} \frac{dU(t)}{dt}$$

$$p(t) = M_A \frac{dU(t)}{dt} \quad (3.22)$$

where

$p(t)$ is the instantaneous difference between pressures in Pa existing at each end of a mass of gas of M_M kg undergoing acceleration.

$M_A = M_M/S^2$ is the acoustic mass in kg/m^4 of the gas undergoing acceleration. This quantity is nearly equal to the mass of the gas inside the containing tube divided by the square of the cross-sectional area. To be more exact, we must note that the gas in the immediate vicinity of the ends of the tube also adds to the mass. Hence, there are

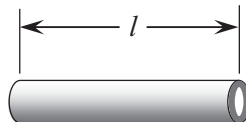


Figure 3.23 Tube of length l and cross-sectional area S .

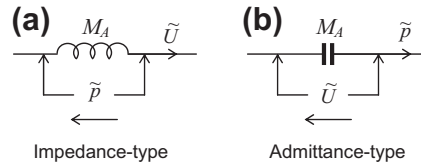


Figure 3.24 (a) Impedance-type and (b) admittance-type symbols for an acoustic mass.

“end corrections” that must be considered. These corrections are discussed in Chapter 4 (page 121).

$U(t)$ is the instantaneous volume velocity of the gas in m^3/s across any cross-sectional plane in the tube. The volume velocity $U(t)$ is equal to the linear velocity $u(t)$ multiplied by the cross-sectional area S .

In the steady state, with an angular frequency ω , we have

$$\tilde{p} = j\omega M_A \tilde{U} \quad (3.23)$$

where \tilde{p} and \tilde{U} are taken to be complex quantities.

The impedance-type analogous symbol for acoustic mass is shown in Fig. 3.24(a), and the admittance-type is given in Fig. 3.24(b). In the steady state, for either, we get Eq. (3.23). The arrows point in the direction of positive flow or positive drop.

Acoustic compliance C_A

Acoustic compliance is a constant quantity having the dimensions of m^5/N . It is associated with a volume of air that is compressed by a net force without an appreciable average displacement of the center of gravity of air in the volume. In other words, compression without acceleration identifies an acoustic compliance.

The acoustical element that is used to represent an acoustic compliance is a volume of air drawn as shown in Fig. 3.25.

The physical law governing the compression of a volume of air being acted on by a net force was given as

$$f(t) = (1/C_M) \int u(t) dt.$$

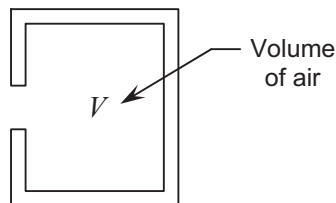


Figure 3.25 Enclosed volume of air V with opening for entrance of pressure variations.

Converting from mechanical to acoustical terms,

$$\frac{f(t)}{S} = \frac{1}{C_M S} \int u(t) \frac{S}{S} dt \quad \text{or} \quad p(t) = \frac{1}{C_M S^2} \int U(t) dt$$

or

$$p(t) = \frac{1}{C_A} \int U(t) dt. \quad (3.24)$$

where

$p(t)$ is instantaneous pressure in Pa acting to compress the volume V of the air.

$C_A = C_M S^2$ is acoustic compliance in m^5/N of the volume of the air undergoing compression. The acoustic compliance is nearly equal to the volume of air divided by γP_0 , as we shall see in Chapter 4 (page 121 to 125).

$U(t)$ is instantaneous volume velocity in m^3/s of the air flowing into the volume that is undergoing compression. The volume velocity $U(t)$ is equal to the linear velocity $u(t)$ multiplied by the cross-sectional area S .

In the steady state with an angular frequency ω , we have

$$\tilde{p} = \frac{\tilde{U}}{j\omega C_A}, \quad (3.25)$$

where \tilde{p} and \tilde{U} are taken to be complex quantities.

The impedance-type analogous element for acoustic compliance is shown in Fig. 3.26(a) and the admittance-type in Fig. 3.26(b). In the steady state for either, Eq. (3.25) applies.

Acoustic resistance R_A and acoustic conductance G_A

Acoustic resistance R_A is associated with the dissipative losses occurring when there is a viscous movement of a quantity of gas through a fine mesh screen or through a capillary tube. The unit is $\text{N}\cdot\text{s}/\text{m}^5$ or rays/m^2 .

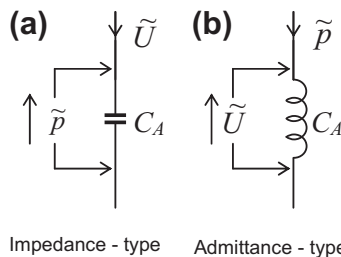


Figure 3.26 (a) Impedance-type and (b) admittance-type symbols for an acoustic compliance.



Figure 3.27 Fine mesh screen which serves as an acoustical symbol for acoustic resistance.

The acoustic element used to represent an acoustic resistance is a fine mesh screen drawn as shown in Fig. 3.27.

The reciprocal of acoustic resistance is the acoustic conductance G_A . The unit is $\text{m}^5/\text{N}\cdot\text{s}$ or acoustic siemens.

The physical law governing dissipative effects in a mechanical system was given by $f(t) = R_M u(t)$ or, in terms of acoustical quantities,

$$p(t) = R_A U(t) = \frac{1}{G_A} U(t), \quad (3.26)$$

where

$p(t)$ is the difference between instantaneous pressures in Pa across the dissipative element.

$R_A = R_M/S^2$ is acoustic resistance in $\text{N}\cdot\text{s}/\text{m}^5$.

$G_A = G_M S^2$ is acoustic conductance in $\text{m}^5/\text{N}\cdot\text{s}$.

$U(t)$ is instantaneous volume velocity in m^3/s of the gas through the cross-sectional area of resistance.

The impedance-type analogous symbol for acoustic resistance is shown in Fig. 3.28(a) and the admittance-type in Fig. 3.28(b).

Acoustic generators

Acoustic generators can be of either the constant volume velocity or the constant pressure type. The prime movers in our acoustical circuits will be exactly like those

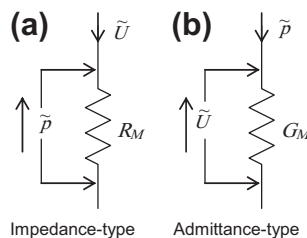


Figure 3.28 (a) Impedance-type symbol for acoustic resistance and (b) admittance-type symbol for acoustic conductance.

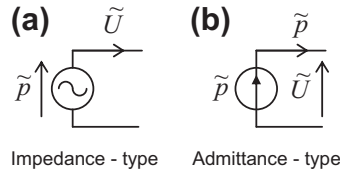


Figure 3.29 (a) Impedance-type and (b) admittance-type symbols for a constant pressure generator.

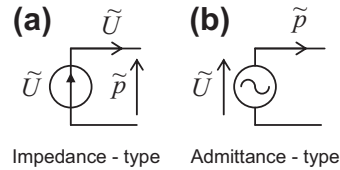


Figure 3.30 (a) Impedance-type and (b) admittance-type symbols for a constant volume velocity generator.

shown in Fig. 3.7 and 3.9 except that \tilde{u}_2 often will be zero and \tilde{u}_1 will be the velocity of a small piston of area S . Remembering that $\tilde{u} = \tilde{u}_1 - \tilde{u}_2$, we see that the generator of Fig. 3.7 has a constant volume velocity $\tilde{U} = \tilde{u}S$ and that of Fig. 3.9 a constant pressure of $\tilde{p} = \tilde{f}/S$.

The two types of analogous symbols for acoustic generators are given in Figs. 3.29 and 3.30. The arrows point in the direction of the positive terminal or the positive flow. As before, a wave inside the circle indicates zero impedance or admittance and an arrow inside the circle indicates infinite impedance or admittance.

Example 3.4. The acoustic device of Fig. 3.31 consists of three cavities V_1, V_2 , and V_3 , two fine mesh screens R_{A1} and R_{A2} , four short lengths of tube T_1, T_2, T_3 , and T_4 , and a constant pressure generator. Because the air in the tubes is not confined, it experiences negligible compression. Because the air in each of the cavities is confined, it experiences little average movement. Let the force of the generator be

$$f(t) = 10^{-5} \cos \omega t \text{ N}$$

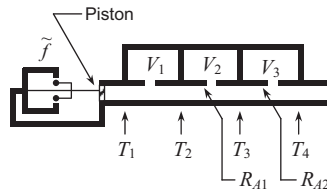


Figure 3.31 Acoustic device consisting of four tubes, three cavities, and two screens driven by a constant pressure generator.

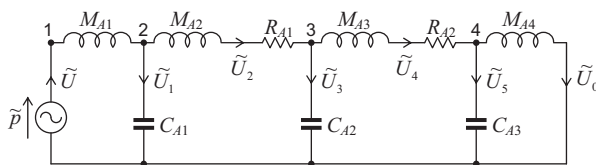


Figure 3.32 Impedance-type analogous circuit for the acoustic device of Fig. 3.31.

so that

$$\tilde{f} = 10^{-5} e^{j\omega t} \text{ N}$$

or

$$|\tilde{f}| = 10^{-5} \text{ N at } \omega = 1000 \text{ Hz.}$$

Also, let the radius of the tube $a = 0.5$ cm; the length of each of the four tubes $l = 5$ cm; the volume of each of the three cavities $V = 10 \text{ cm}^3$; and the magnitude of the two acoustic resistances $R_A = 10 \text{ N}\cdot\text{s}/\text{m}^5$. Neglecting end corrections, solve for the volume velocity \tilde{U}_0 at the end of the tube T_4 .

Solution. Remembering that there is continuity of volume velocity and pressure at the junctions, we can draw the impedance-type analogous circuit from inspection. It is shown in Fig. 3.32. The bottom line of the schematic diagram represents atmospheric pressure, which means that here the variational pressure \tilde{p} is equal to zero. At each of the junctions of the elements 1 to 4, a different variational pressure can be observed. The end of the fourth tube (T_4) opens to the atmosphere, which requires that M_{A4} be connected directly to the bottom line of Fig. 3.32.

Note that the volume velocity of the gas leaving the tube T_1 is equal to the sum of the volume velocities of the gas entering V_1 and T_2 . The volume velocity of the gas leaving T_2 is the same as that flowing through the screen R_{A1} and is equal to the sum of the volume velocities of the gas entering V_2 and T_3 .

One test of the validity of an analogous circuit is its behavior for direct current. If one removes the piston and blows into the end of the tube T_1 (Fig. 3.31), a steady flow of air from T_4 is observed. Some resistance to this flow will be offered by the two screens R_{A1} and R_{A2} . Similarly in the schematic diagram of Fig. 3.32, a steady pressure \tilde{p} will produce a steady flow \tilde{U} through M_{A4} , resisted only by R_{A1} and R_{A2} .

As an aside, let us note that an acoustic compliance can occur in a circuit without one of the terminals being at ground potential only if it is produced by an elastic diaphragm. For example, if the resistance in Fig. 3.31 were replaced by an impervious but elastic diaphragm, the element R_{A1} in Fig. 3.32 would be replaced by a compliance-type element with both terminals above ground potential. In this case, a steady flow of air

could not be maintained through the device of Fig. 3.31 as can also be seen from the circuit of Fig. 3.32, with R_{A1} replaced by a compliance.

Determine the element sizes of Fig. 3.32:

$$\tilde{p} = \frac{\tilde{f}}{S} = \frac{10^{-5}e^{j1000t}}{\pi(5 \times 10^{-3})^2} = 0.1273e^{j1000t} \text{ Pa,}$$

$$M_{A1} = M_{A2} = M_{A3} = M_{A4} = \frac{\rho_0 l}{S} = \frac{1.18 \times 0.05}{7.85 \times 10^{-5}} = 750 \text{ kg/m}^4,$$

$$C_{A1} = C_{A2} = C_{A3} = \frac{V}{\gamma P_0} = \frac{10^{-5}}{1.4 \times 10^5} = 7.15 \times 10^{-11} \text{ m}^5/\text{N},$$

$$R_{A1} = R_{A2} = 10 \text{ N}\cdot\text{s}/\text{m}^5.$$

We now determine the ratio \tilde{p}/\tilde{U}_0 .

$$\tilde{p}_4 = j\omega M_{A4}\tilde{U}_0 = j7.5 \times 10^5 \times \tilde{U}_0 \text{ Pa}$$

$$\tilde{U}_5 = j\omega C_{A3}\tilde{p}_4 = -5.36 \times 10^{-2} \times \tilde{U}_0 \text{ m}^3/\text{s}$$

$$\tilde{U}_4 = \tilde{U}_5 + \tilde{U}_0 = 0.946\tilde{U}_0$$

$$\tilde{p}_3 = (R_{A2} + j\omega M_{A3})\tilde{U}_4 + \tilde{p}_4 = (9.46 + j14.6 \times 10^5)\tilde{U}_0$$

$$\tilde{U}_3 = j\omega C_{A2}\tilde{p}_3 = (-0.1043 + j6.77 \times 10^{-7})\tilde{U}_0$$

$$\tilde{U}_2 = \tilde{U}_3 + \tilde{U}_4 = (0.842 + j6.77 \times 10^{-7})\tilde{U}_0$$

$$\tilde{p}_2 = (R_{A1} + j\omega M_{A2})\tilde{U}_2 + \tilde{p}_3 = (17.37 + j2.091 \times 10^6)\tilde{U}_0$$

$$\tilde{U}_1 = j\omega C_{A1}\tilde{p}_2 = (-0.1496 + j1.242 \times 10^{-6})\tilde{U}_0$$

$$\tilde{U} = \tilde{U}_2 + \tilde{U}_1 = (0.692 + j1.919 \times 10^{-6})\tilde{U}_0$$

$$\tilde{p} = j\omega M_{A1}\tilde{U} + \tilde{p}_2 = (15.93 + j2.61 \times 10^6)\tilde{U}_0.$$

The desired value of \tilde{U}_0 is

$$\tilde{U}_0 = \frac{0.1273e^{j1000t}}{15.93 + j2.61 \times 10^6}$$

or

$$\begin{aligned} U(t) &\approx 4.88 \times 10^{-8} \cos(1000t - 90^\circ) \\ &\approx 4.88 \times 10^{-8} \sin 1000t. \end{aligned}$$

In other words, the impedance is principally that of the four acoustic masses in series so that \tilde{U}_0 lags \tilde{p} by nearly 90 degrees.

Example 3.5. A Helmholtz resonator is frequently used as a means for eliminating an undesired frequency component from an acoustic system. An example is given in Fig. 3.33(a). A constant force generator G produces a series of tones, among which is one that is not wanted. These tones actuate a microphone M whose acoustic impedance is $500 \text{ N} \cdot \text{s}/\text{m}^5$. If the tube T has a cross-sectional area of 5 cm^2 , $l_1 = l_2 = 5 \text{ cm}$, $l_3 = 1 \text{ cm}$, $V = 1000 \text{ cm}^3$, and the cross-sectional area of l_3 is 2 cm^2 , what frequency is eliminated from the system?

Solution. By inspection we may draw the impedance-type analogous circuit of Fig. 3.33(b). The element sizes are

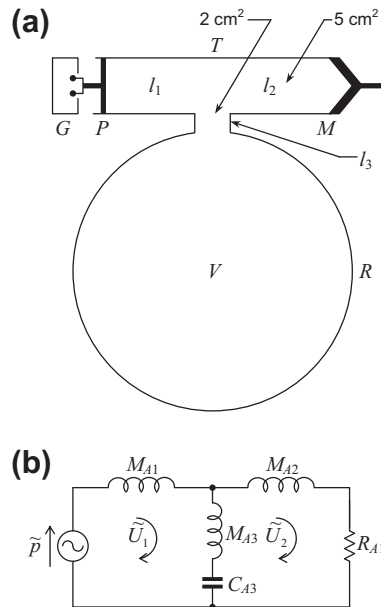


Figure 3.33 (a) Acoustic device consisting of a constant force generator G , piston P , tube T with length $l_1 + l_2$, microphone M , and Helmholtz resonator R with volume V and connecting tube as shown. (b) Impedance-type analogous circuit for the device of (a).

$$M_{A1} = M_{A2} = \frac{\rho_0 l_1}{S_T} = \frac{1.18 \times 0.05}{5 \times 10^{-4}} = 118 \text{ kg/m}^4,$$

$$M_{A3} = \frac{\rho_0 l_3}{S_R} = \frac{1.18 \times 0.01}{2 \times 10^{-4}} = 59 \text{ kg/m}^4,$$

$$C_{A3} = \frac{V}{\gamma P_0} = \frac{10^{-3}}{1.4 \times 10^5} = 7.15 \times 10^{-9} \text{ m}^5/\text{N},$$

$$R_{A1} = 500 \text{ N}\cdot\text{s/m}^5.$$

It is obvious that the volume velocity \tilde{U}_2 of the transducer M will be zero when the shunt branch is at resonance. Hence,

$$\omega = \frac{1}{\sqrt{M_{A3} C_{A3}}} = \frac{10^4}{\sqrt{42.2}} = 1540 \text{ rad/s},$$

$$f = 245 \text{ Hz}.$$

Mechanical rotational systems

Mechanical rotational systems are handled in the same manner as mechanical rectilinear systems. [Table 3.4](#) shows quantities analogous in the two systems.

Table 3.4 Analogous quantities in rectilinear and rotational systems

Rectilinear systems			Rotational systems		
Symbol	Quantity	Unit	Symbol	Quantity	Unit
\tilde{f}	Force	N	\tilde{T}	Torque	N·m
\tilde{u}	Velocity	m/s	$\tilde{\theta}$	Angular velocity	rad/s
$\tilde{\xi}$	Displacement	m	$\tilde{\phi}$	Angular displacement	rad
$Z_M = \tilde{f}/\tilde{u}$	Mechanical impedance	N·s/m	$Z_R = \tilde{T}/\tilde{\theta}$	Rotational impedance	N·m·s/rad
$Y_M = \tilde{u}/\tilde{f}$	Mechanical admittance	m/N ⁻¹ ·s ⁻¹	$Y_R = \tilde{\theta}/\tilde{T}$	Rotational admittance	rad/N·m·s
R_M	Mechanical resistance	N·s/m	R_R	Rotational resistance	N·m·s/rad
G_M	Mechanical conductance	m·N ⁻¹ /s ⁻¹	G_R	Rotational conductance	rad/N·m·s
M_M	Mass	kg	I_R	Moment of inertia	kg·m ²
C_M	Mechanical compliance	m/N	C_R	Rotational compliance	rad/N·m
W_M	Mechanical power	W	W_R	Rotational power	W



PART VIII: TRANSDUCERS

A transducer is defined as a device for converting energy from one form to another. Of importance in this text is the electromechanical transducer for converting electrical energy into mechanical energy, and vice versa. There are many types of such transducers. In acoustics, we are concerned with microphones, earphones, loudspeakers, and vibration pickups and vibration producers which are generally linear passive reversible networks.

The type of electromechanical transducer chosen for each of these instruments depends on such factors as the desired electrical and mechanical impedances, durability, and cost. It will not be possible here to discuss all means for electromechanical transduction. Instead we shall limit the discussion to electromagnetic and electrostatic types. Also, we shall deal with mechanoacoustic transducers for converting mechanical energy into acoustic energy.



3.5 ELECTROMECHANICAL TRANSDUCERS

Two types of electromechanical transducers, electromagnetic and electrostatic, are commonly employed in loudspeakers and microphones. Both may be represented by transformers with properties that permit the joining of mechanical and electrical circuits into one schematic diagram.

Electromagnetic-mechanical transducer

This type of transducer can be characterized by four terminals. Two have voltage and current associated with them. The other two have velocity and force as the measurable properties. Familiar examples are the moving-coil loudspeaker or microphone and the variable-reluctance earphone or microphone.

The simplest type of moving-coil transducer is a single length of wire in a uniform magnetic field as shown in Fig. 3.34. When a wire is moved upward with a velocity \tilde{u} as shown in Fig. 3.34(a), a potential difference \tilde{e} will be produced in the wire such that terminal 2 is positive. If, on the other hand, the wire is fixed in the magnetic field (Fig. 3.34(b)) and a current \tilde{i} is caused to flow into terminal 2 (therefore, 2 is positive), a force \tilde{f} will be produced that acts on the wire upward in the same direction as that indicated previously for the velocity.

The basic equations applicable to the moving-coil type of transducer are

$$\tilde{f} = Bl \tilde{i}, \quad (3.27a)$$

$$\tilde{e} = Bl \tilde{u}, \quad (3.27b)$$

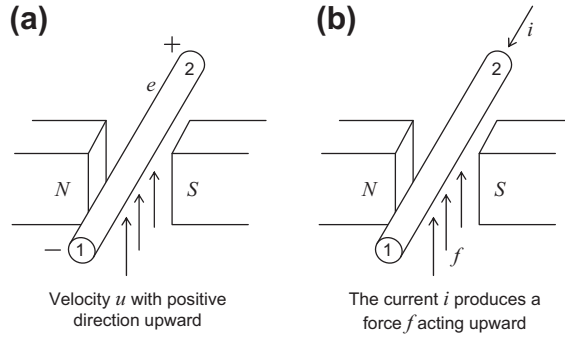


Figure 3.34 Simplified form of moving-coil transducer consisting of a single length of wire cutting a magnetic field of flux density B . (a) The conductor is moving vertically at constant velocity so as to generate an open-circuit voltage across terminals 1 and 2. (b) A constant current is entering terminal 2 to produce a force on the conductor in a vertical direction.

where

- \tilde{i} is electrical current in A,
- \tilde{f} is “open-circuit” force in N produced on the mechanical circuit by the current \tilde{i} ,
- B is magnetic flux density in T,
- l is effective length in m of the electrical conductor that moves at right angles across the lines of force of flux density B
- \tilde{u} is velocity in m/s
- \tilde{e} is “open-circuit” electrical voltage in V produced by a velocity \tilde{u} .

The right-hand sides of Eq. (3.27) have the same sign because when \tilde{u} and \tilde{f} are in the same direction, the electrical terminals have the same sign.

One analogous symbol for this type of transducer is the “ideal” transformer given in Fig. 3.35(a). The “windings” on this ideal transformer have infinite impedance, and the transformer obeys Eq. (3.27) at all frequencies, including steady flow. The mechanical

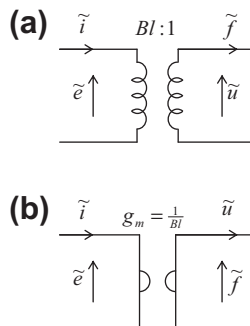


Figure 3.35 Analogous symbols for the electromagnetic transducer of Fig. 3.34. (a) The mechanical side is of the admittance type. (b) The mechanical side is of the impedance type.

side of this symbol necessarily is of the admittance type if current flows in the primary. The other analogous symbol is the “ideal” gyrator given in Fig. 3.35(b). It is customary to define the mutual conductance g_m of a gyrator, which is the same in both directions, as the ratio of the flow on one side to the drop on the other. The mechanical side of this symbol necessarily is of the impedance type if current flows in the primary. The invariant mathematical operations which these symbols represent are given in Table 3.1. They lead directly to Eq. (3.27). The arrows point in the directions of positive flow or positive potential.

Electrostatic-mechanical transducer

This type of transducer may also be characterized by four terminals. At two of them, voltages and currents can be measured. At the other two, forces and velocities can be measured.

An example is a piezoelectric crystal microphone such as is shown in Fig. 3.36. A force \tilde{f} applied uniformly over the face of the crystal causes an inward displacement of magnitude $\tilde{\xi}$ in meters. As a result of this displacement, a voltage \tilde{e} appears across the electrical terminals 1 and 2. Let us assume that a positive displacement (inward) of the crystal causes terminal 1 to become positive. For small displacements, the induced voltage is proportional to displacement. The inverse of this effect occurs when no external force acts on the crystal face but an electrical generator is connected to the terminals 1 and 2. If the external generator is connected so that terminal 1 is positive, an internal force \tilde{f} is produced which acts to expand the crystal. For small displacements, the developed force \tilde{f} is proportional to the electric charge \tilde{q} stored in the electrodes.

Using the above relationships, we can write

$$\tilde{q} = C_E \tilde{e} - d_{31} \tilde{f} \quad (3.28a)$$

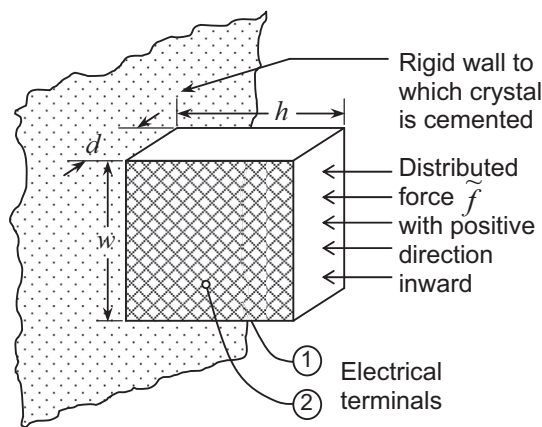


Figure 3.36 Piezoelectric crystal transducer mounted on a rigid wall.

$$\tilde{\xi} = d_{31}\tilde{e} - C_M\tilde{f} \quad (3.28b)$$

where

\tilde{q} is electrical charge in C stored in the electrodes of the piezoelectric device,

\tilde{e} is “open-circuit” electrical voltage in V produced by a displacement $\tilde{\xi}$,

\tilde{f} is “open-circuit” force in N produced by an electrical charge \tilde{q} ,

$\tilde{\xi}$ is displacement in m of a dimension of the piezoelectric device in m,

d_{31} is *piezoelectric strain coefficient* with dimensions of C/N or m/V. It is a real number when the network is linear, passive, and reversible. (The subscripts denote the relative directions of the applied field and resulting movement or vice versa. In this case, the two are at right angles. If they were in the same direction, for example, we would use d_{11} , d_{22} , or d_{33} , where 1, 2, and 3 can be regarded as denoting the x , y , or z directions.)

and the electrical capacitance C_E and mechanical compliance C_M are given by

$$C_E = \frac{\epsilon_0\epsilon_rhw}{d} \quad (3.29)$$

$$C_M = \frac{h}{Ydw} \quad (3.30)$$

where

ϵ_0 is permittivity of free space in F/m,

ϵ_r is relative permittivity of the free (nonblocked) piezoelectric dielectric (dimensionless),

Y is Young’s modulus of elasticity in N/m² with electrical short-circuited.

In reality, C_E and C_M vary with displacement $\tilde{\xi}$, but it is assumed that the displacement is very small, so these are *linearized* equations. If the material shows no piezoelectric effect, applying an external force \tilde{f} simply leads to a deflection $\tilde{\xi}$ according to Hooke’s law. Because of the piezoelectric effect, the displacement also leads to an induced charge \tilde{q} on the electrodes, which in turn leads to a voltage (electrical force) \tilde{e} . Conversely, applying an electrical voltage leads to a mechanical force. Solving Eqs. (3.28a) and (3.28b) for \tilde{e} and \tilde{f} gives

$$\tilde{e} = \frac{1}{1 - k_{31}^2} \left(\frac{1}{C_E}\tilde{q} - \frac{d_{31}}{C_EC_M}\tilde{\xi} \right) \quad (3.31a)$$

$$\tilde{f} = \frac{1}{1 - k_{31}^2} \left(\frac{d_{31}}{C_EC_M}\tilde{q} - \frac{1}{C_M}\tilde{\xi} \right) \quad (3.31b)$$

where k_{31} is the dimensionless *piezoelectric coupling coefficient* which is related to the piezoelectric strain coefficient d_{31} by

$$k_{31} = \frac{d_{31}}{\sqrt{C_E C_M}} = d_{31} \sqrt{\frac{Y}{\epsilon_0 \epsilon_r}}, \quad 0 < k_{31} < 1 \quad (3.32)$$

Another commonly used parameter is the *piezoelectric stress coefficient* g_{31} in Vm /N or m^2/C , which is defined by

$$g_{31} = \frac{d_{31}}{\epsilon_0 \epsilon_r} = \frac{k_{31}}{\sqrt{\epsilon_0 \epsilon_r Y}} \quad (3.33)$$

Eq. (3.31) is often inconvenient to use because they contain charge and displacement. One prefers to deal with current and velocity, which appear directly in the equation for power. Conversion to current and velocity may be made by the relations

$$\tilde{u} = \frac{d\xi}{dt} = j\omega \tilde{\xi}, \quad (3.34a)$$

$$\tilde{i} = \frac{dq}{dt} = j\omega \tilde{q}, \quad (3.34b)$$

so that Eq. (3.31) becomes, in z -parameter matrix form,

$$\begin{bmatrix} \tilde{e} \\ \tilde{f} \end{bmatrix} = \begin{bmatrix} \frac{1}{j\omega C'_E} & \frac{d_{31}}{j\omega C'_E C_M} \\ \frac{d_{31}}{j\omega C'_E C_M} & \frac{1}{j\omega C'_E} \end{bmatrix} \begin{bmatrix} \tilde{i} \\ -\tilde{u} \end{bmatrix}. \quad (3.35)$$

The elements of Eq. (3.35) are related by the equations

$$C'_E = (1 - k_{31}^2) C_E \quad (3.36)$$

$$C'_M = (1 - k_{31}^2) C_M \quad (3.37)$$

Note in particular that

C'_E is electrical capacitance measured with the mechanical “terminals” blocked so that no motion occurs ($\tilde{u} = 0$).

C_E is electrical capacitance measured with the mechanical “terminals” operating into zero mechanical impedance so that no force is built up ($\tilde{f} = 0$).

C'_E is mechanical compliance measured with the electrical terminals open-circuited ($\tilde{i} = 0$).

C_M is mechanical compliance measured with the electrical terminals short-circuited ($\tilde{e} = 0$).

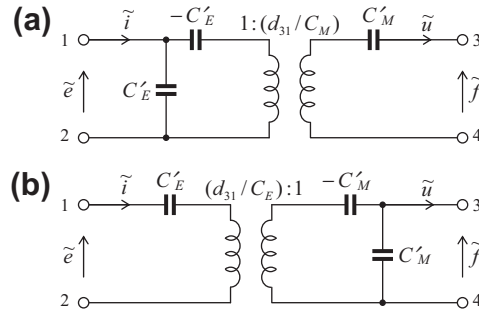


Figure 3.37 Two forms of analogous symbols for piezoelectric transducers. The mechanical sides are of the impedance type.

The equivalent circuit shown in Fig. 3.37(a) is essentially a two-port network defined by the z -parameters in the matrix of Eq. (3.35), although z -parameter matrices will be discussed in greater detail in Section. 3.10. Noting from Eqs. (3.36) and (3.37) that $C'_E C'_M = C_E C'_M$, Eq. (3.31) can alternatively be written as

$$\begin{bmatrix} \tilde{e} \\ \tilde{f} \end{bmatrix} = \begin{bmatrix} \frac{1}{j\omega C'_E} & \frac{d_{31}}{j\omega C_E C'_M} \\ \frac{d_{31}}{j\omega C_E C'_M} & \frac{1}{j\omega C'_M} \end{bmatrix} \begin{bmatrix} \tilde{i} \\ -\tilde{u} \end{bmatrix}. \quad (3.38)$$

which is represented by the equivalent circuit as shown in Fig. 3.37(b). The mechanical sides of Fig. 3.37(a,b) are of the impedance-type analogy. Let us discuss Fig. 3.37(a) first.

Looking into the electrical terminals 1 and 2, the element C'_E is the electrical capacitance of the transducer. To measure C'_E , a sinusoidal driving voltage \tilde{e} is applied to the transducer terminals 1 and 2, and the resulting sinusoidal current is measured. During this measurement, the mechanical terminals 3 and 4 are *open-circuited* (motion blocked, $\tilde{u} = 0$). A very low driving frequency is used so that the mass reactance and mechanical resistance can be neglected. The negative capacitance $-C'_E$ represents the force of attraction between the electrodes which varies with the displacement. Hence, it can be thought of as a negative stiffness which can be subtracted from the natural stiffness of the material.

Looking into the mechanical terminals 3 and 4 of Fig. 3.37(b), C'_M is the mechanical compliance of the transducer measured at low frequencies with the electrical terminals 1 and 2 *open-circuited* ($\tilde{i} = 0$). A sinusoidal driving force \tilde{f} is applied to terminals 3 and 4 of the transducer and the resulting sinusoidal displacement is measured. Again, the negative compliance $-C'_M$ is because of the force of attraction between the electrodes. Eliminating \tilde{q} and $\tilde{\xi}$ between Eq. (3.31) leads to the following simplified equations

$$\tilde{f} = \frac{d_{31}}{C_M} \tilde{e} - \frac{1}{C_M} \tilde{\xi} \quad (3.39a)$$

$$\tilde{e} = \frac{d_{31}}{C_E} \tilde{f} + \frac{1}{C_E} \tilde{q} \quad (3.39b)$$

In the steady state $\tilde{u} = j\omega\tilde{\xi}$ and $\tilde{i} = j\omega\tilde{q}$ so that

$$\tilde{f} = \frac{d_{31}}{C_M} \tilde{e} - \frac{1}{j\omega C_M} \tilde{u} \quad (3.40a)$$

$$\tilde{e} = \frac{d_{31}}{C_E} \tilde{f} + \frac{1}{j\omega C_E} \tilde{i} \quad (3.40b)$$

from which we obtain the two simplified equivalent electrical circuits as shown in Fig. 3.38.

Looking into the mechanical terminals 3 and 4 of Fig. 3.38(a), the element C_M is the mechanical compliance of the transducer but measured in a different way. A sinusoidal driving force \tilde{f} is applied to terminals 3 and 4 of the transducer at a very low frequency so that the mass reactance and mechanical resistance can be neglected, and the resulting sinusoidal displacement is measured. During this measurement, the electrical terminals 1 and 2 are short-circuited ($\tilde{e} = 0$). Looking into the electrical terminals 1 and 2 of Fig. 3.38(b), the element C_E is the electrical capacitance measured at low frequencies with the mechanical terminals 3 and 4 *short-circuited* ($\tilde{f} = 0$).

A sinusoidal driving voltage e applied to the terminals 1 and 2 of Fig. 3.38(a) produces an open-circuit force

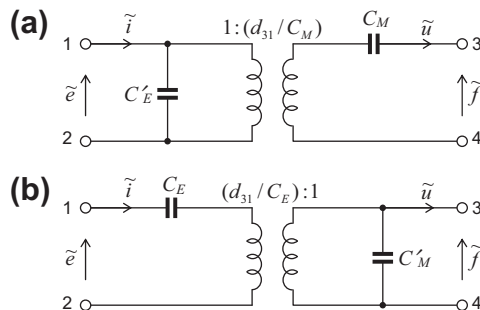


Figure 3.38 Two simplified forms of analogous symbols for piezoelectric transducers. The mechanical sides are of the impedance type.

$$\tilde{f} = \frac{d_{31}}{C_M} \tilde{e}. \quad (3.41)$$

A sinusoidal driving force \tilde{f} applied to the terminals 3 and 4 of Fig. 3.38(b) produces an open-circuit voltage

$$\tilde{e} = \frac{d_{31}}{C_E} \tilde{f}. \quad (3.42)$$

The choice between the alternative analogous symbols of Fig. 3.38 is usually made on the basis of the use to which the transducer will be put. If the electrostatic transducer is a microphone, it usually is operated into the gate of a field-effect transistor so that the electrical terminals are essentially open-circuited. In this case, the circuit of Fig. 3.38(b) is the better one to use because C_E can be neglected in the analysis when $\tilde{i} = 0$. On the other hand, if the transducer is a loudspeaker, it usually is operated from a low-impedance amplifier so that the electrical terminals are essentially short-circuited. In this case, the circuit of Fig. 3.38(a) is the one to use because $C'_E \omega$ is small in comparison with the output admittance of the amplifier.

The circuit of Fig. 3.38(a) corresponds more closely to the physical facts than does that of Fig. 3.38(b). If the device could be held motionless ($\tilde{u} = 0$) when a voltage was impressed across terminals 1 and 2, there would be no stored mechanical energy. All the stored energy would be electrical. This is the case for circuit (a), but not for (b). In other respects the two circuits are identical.

At higher frequencies, the mass M_M and the resistance R_M of the crystal must be considered in the circuit. These elements can be added in series with terminal 3 of Fig. 3.38.

These analogous symbols indicate an important difference between electromagnetic and electrostatic types of coupling. For the electromagnetic case, we ordinarily use an admittance-type analogy, but for the electrostatic case, we usually employ the impedance-type analogy.

In the next part we shall introduce a different method for handling electrostatic transducers. It involves the use of the admittance-type analog in place of the impedance-type analog. The simplification in analysis that results will be immediately apparent. By this new method, it will also be possible to use the impedance-type analog for the electromagnetic case.



3.6 MECHANOACOUSTIC TRANSDUCER

This type of transducer occurs at a junction point between the mechanical and acoustical parts of an analogous circuit. An example is the plane at which a loudspeaker diaphragm acts against the air. This transducer may also be characterized by four

terminals. At two of the terminals, forces and velocities can be measured. At the other two, pressures and volume velocities can be measured. The basic equations applicable to the mechanoacoustic transducer are

$$\tilde{f} = S\tilde{p}, \quad (3.43a)$$

$$\tilde{U} = S\tilde{u}, \quad (3.43b)$$

where

- \tilde{f} is force in N,
- \tilde{p} is pressure in Pa,
- \tilde{U} is volume velocity in m^3/s ,
- \tilde{u} is velocity in m/s,
- S is area in m^2 .

The analogous symbols for this type of transducer are given at the bottom of [Table 3.3](#) (page 70). They are seen to lead directly to [Eq. \(3.43\)](#).



3.7 EXAMPLES OF TRANSDUCER CALCULATIONS

Example 3.6. An ideal moving-coil loudspeaker produces 2 W of acoustic power into an acoustic load of $4 \times 10^4 \text{ N s/m}^5$ when driven from an amplifier with a constant voltage output of 1.0 V rms. The area of the diaphragm is 100 cm^2 . What open-circuit voltage will it produce when operated as a microphone with an rms diaphragm velocity of 10 cm/s?

Solution. From [Fig. 3.35](#) we see that, always,

$$\tilde{e} = Bl\tilde{u}.$$

The power dissipated W gives us the rms volume velocity of the diaphragm U_{rms} :

$$U_{\text{rms}} = \sqrt{\frac{W}{R_A}} = \sqrt{\frac{2}{4 \times 10^4}} = 7.07 \times 10^{-3} \text{ m}^3/\text{s}$$

or

$$u_{\text{rms}} = 0.707 \text{ m/s},$$

$$Bl = \frac{e_{\text{rms}}}{u_{\text{rms}}} = \frac{1}{0.707} = 1.414 \text{ T}\cdot\text{m}$$

Hence, the open-circuit voltage for an rms velocity of 0.1 m/s is

$$e_{\text{rms}} = 1.414 \times 0.1 = 0.1414 \text{ V}.$$

Example 3.7. A lead magnesium niobate–lead titanate (PMN–PT) crystal as shown in Fig. 3.36 with $w = 0.5$ mm, $d = 2$ mm, and $h = 2$ mm has the following mechanical and electrical properties:

$$d_{31} = 750 \times 10^{-12} \text{ C/N or m/V}$$

$$Y = 20 \times 10^9 \text{ N/m}^2$$

$$\rho = 8000 \text{ kg/m}^3$$

$$\epsilon_0 = 8.85 \times 10^{-12} \text{ F/m}$$

$$\epsilon_r = 6500$$

$$k_{31} = d_{31} \sqrt{\frac{Y}{\epsilon_0 \epsilon_r}} = 0.442$$

This crystal is to be used in a microphone with a circular (weightless) diaphragm. Determine the diameter of the diaphragm if the microphone is to yield an open-circuit voltage of -70 dB re 1 V rms for a sound pressure level of 74 dB re 20 μ Pa at 100 kHz.

Solution. The circuit for this transducer with the transformer removed is shown in Fig. 3.39, where the circuit elements are defined by

$$C'_M = (1 - k_{31}^2) \frac{h}{Ywd} = \frac{1 - 0.442^2}{20 \times 0.5 \times 10^6} = 8 \times 10^{-8} \text{ m/N},$$

$$M_M = \frac{4}{\pi^2} \rho w d h = \frac{4 \times 8 \times 0.5 \times 2 \times 2 \times 10^{-6}}{\pi^2} = 6.5 \times 10^{-6} \text{ kg/m}^3,$$

$$C_E = \frac{\epsilon_0 \epsilon_r w h}{d} = 8.85 \times 10^{-12} \times 6.5 \times 0.5 = 28.8 \times 10^{-12} \text{ F},$$

$$R_M = \text{negligibly small.}$$

Because only the open-circuit voltage is desired, C_E may be neglected in the calculations. f_{rms} is the total force applied to the crystal by the diaphragm. Solving for e_{rms} yields

$$e_{\text{rms}} = \frac{f_{\text{rms}}(d_{31}/C_E)}{1 - \omega^2 M_M C'_M}.$$

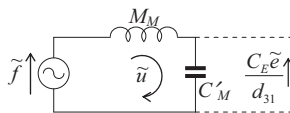


Figure 3.39 Analogous circuit of the impedance type for a crystal microphone.

The force f equals the area of the diaphragm S times the sound pressure p . Solving for p ,

$$\begin{aligned} p_{\text{rms}} &= 20 \times 10^{-6} \times 10^{74/20} \\ &= 0.1 \text{ N/m}^2 \end{aligned}$$

Solving for e ,

$$\frac{1}{e_{\text{rms}}} = 10^{70/20} = 3.16 \times 10^3,$$

or

$$e_{\text{rms}} = 3.16 \times 10^{-4} \text{ V}.$$

Hence,

$$\begin{aligned} S &= \frac{f_{\text{rms}}}{p_{\text{rms}}} = \frac{3.16 \times 10^{-4} (1 - 6.28^2 \times 10^{10} \times 6.5 \times 8 \times 10^{-14})}{0.1 \times (750/28.8)} \\ &= 9.65 \times 10^{-5} \text{ m}^2 \\ S &= 0.965 \text{ cm}^2. \end{aligned}$$

This corresponds to a diaphragm with a diameter of about 1.1 cm.

Example 3.8. A loudspeaker diaphragm couples to the throat of an exponential horn that has an acoustic impedance of $(300 + j300) \text{ N}\cdot\text{s/m}^5$. If the area of the loudspeaker diaphragm S_D is 0.08 m^2 , determine the mechanical impedance load on the diaphragm because of the horn.

Solution. The analogous circuit is shown in Fig. 3.40. The mechanical impedance at terminals 1 and 2 represent the load on the diaphragm:

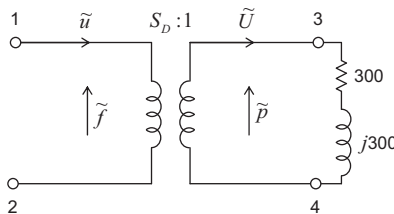


Figure 3.40 Example of a mechanoacoustic transducer. The acoustic impedance of a horn (at terminals 3 and 4) loads the diaphragm with a mechanical impedance $S_D^2(300 + j300) \text{ N s/m}$.

$$\begin{aligned}
 Z_M &= \frac{\tilde{f}}{\tilde{u}} = S_D^2(300 + j300) \\
 &= 6.4 \times 10^{-3}(300 + j300) \\
 &= 1.92 + j1.92 \text{ N}\cdot\text{s/m}.
 \end{aligned}$$

PART IX: CIRCUIT THEOREMS, ENERGY, AND POWER

In this part we discuss conversions from one type of analogy to the other, Thévenin's theorem, energy and power relations, transducer impedances, and combinations of transducers.

3.8 CONVERSION FROM ADMITTANCE-TYPE ANALOGIES TO IMPEDANCE-TYPE ANALOGIES

In the preceding parts, we showed that electromagnetic and electrostatic transducers require two different types of analogy if they are to be represented by the networks shown in Table 3.1. A further need for two types of analogy is apparent from the standpoint of ease of drawing an analogous circuit by inspection. The admittance type of analogy is better for mechanical systems and the impedance type for acoustic systems. The circuits we shall use, however, will frequently contain electrical, mechanical, and acoustical elements. Because analogies cannot be mixed in a given circuit, we must have a simple means for converting from one to the other.

We may readily derive one analogy from the other if we recognize that:

Elements in series in the circuit of one analogy correspond to elements in parallel in the other.

Resistance-type elements become conductance-type elements, capacitance-type elements become inductance-type elements, and inductance-type elements become capacitance-type elements.

The sum of the drops across the series elements in a mesh of one analogy corresponds to the sum of the currents at a branch point of the other analogy.

This is equivalent to saying that one analogy is the *dual* of the other. In electrical circuit theory one learns that the quantities that “flow” in one circuit are the same as the “drops” in the dual of that circuit. This is also true here.

To facilitate the conversion from one type of analogy to another, a method that we shall dub the “dot” method is used [9]. Assume that we have the admittance-type analog of Fig. 3.17 and that we wish to convert it to an impedance-type analog. The procedure is as follows (see Fig. 3.41):

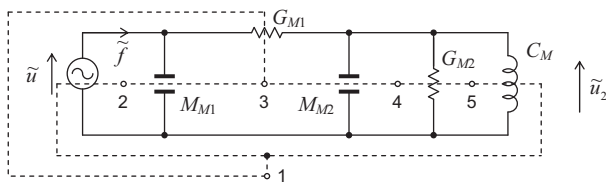


Figure 3.41 Preparation by the “dot” method for taking the dual of Fig. 3.17.

Place a dot at the center of each mesh of the circuit and one dot outside all meshes. Number these dots consecutively.

Connect the dots together with lines so that there is a line through each element and so that no line passes through more than one element.

Draw a new circuit such that each line connecting two dots now contains an element that is the inverse of that in the original circuit. The inverse of any given element may be seen by comparing corresponding columns for admittance-type analogies and impedance-type analogies of Table 3.3. The complete inversion (dual) of Fig. 3.41 is shown in Fig. 3.42.

Solving for the velocities or the forces in the two circuits using the rules of Table 3.1 will readily reveal that they give the same results.

After completing the formation of an analogous circuit, it is always profitable to ask concerning each element. If this element becomes very small or very large, does the circuit behave in the same way the device itself would behave? If the circuit behaves properly in the extremes, it is probably correct.

3.9 THÉVENIN'S THEOREM

It appears possible, from the foregoing discussions, to represent the operation of a transducer as a combination of electrical, mechanical, and acoustical elements. The connection between the electrical and mechanical circuit takes place through an electromechanical transducer. Similarly, the connection between the mechanical and acoustical circuit takes place through a mechanoacoustic transducer. A Thévenin's theorem may be written for the combined circuits, just as is written for electrical circuits only.

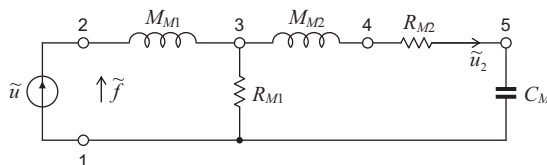


Figure 3.42 Dual of the circuit of Fig. 3.40. Solving for the forces or velocities in this circuit using the rules of Table 3.1 yields the same values as solving for the forces or velocities in Fig. 3.41.

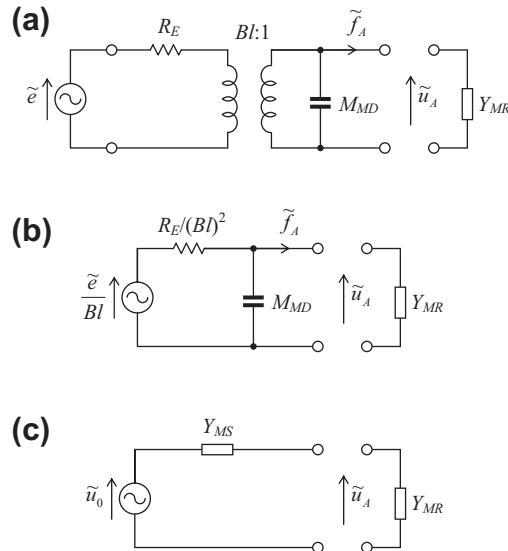


Figure 3.43 Analogous circuits for a simplified moving-coil loudspeaker radiating sound into air. (a) Analogous circuit. (b) Same with transformer removed. (c) Same, reduced to its Thévenin's equivalent.

The requirements which must be satisfied in the proper statement and use of Thévenin's theorem are that all the elements be linear and there be no hysteresis effects.

In the next few paragraphs, we shall demonstrate the application of Thévenin's theorem to a loudspeaker problem. The mechanical radiation impedance presented by the air to the vibrating diaphragm of a loudspeaker or microphone will be represented simply as Z_{MR} in the impedance-type analogy or $Y_{MR} = 1/Z_{MR}$ in the admittance-type analogy. The exact physical nature of Z_{MR} will be discussed in Chapters 4, 12, and 13.

Assume a simple electrodynamic (moving-coil) loudspeaker with a diaphragm that has only mass and a voice coil that has only electrical resistance (see Fig. 3.43(a)). Let this loudspeaker be driven by a constant voltage generator. By making use of Thévenin's theorem, we wish to find the equivalent mechanical generator \tilde{u}_0 and the equivalent mechanical admittance Y_{MS} of the loudspeaker, as seen in the interface between the diaphragm and the air. The circuit of Fig. 3.43(a) with the transformer removed is shown in Fig. 3.43(b). The Thévenin's equivalent circuit is shown in Fig. 3.43(c).

We arrive at the values of \tilde{u}_0 and Y_{MS} in two steps.

Step 1. Determine the open-circuit velocity \tilde{u}_0 by terminating the loudspeaker in an infinite admittance, $Y_{MA} = \infty$ (that is, $Z_{MA} = 0$), and then measuring the velocity of the diaphragm \tilde{u}_0 . As we discussed in Part II, $Z_{MA} = 0$ can be obtained by acoustically connecting the diaphragm to a tube whose length is equal to one-fourth wavelength. This is possible at low frequencies. Inspection of Fig. 3.43(b) shows that

$$\tilde{u}_0 = \frac{\tilde{e}Bl}{j\omega M_{MD}R_E + (Bl)^2}. \quad (3.44)$$

Step 2. Short-circuit the generator e without changing the mesh impedance in that part of the electrical circuit. Then determine the admittance Y_{MS} looking back into the output terminals of the loudspeaker. For example, Y_{MS} for the circuit of Fig. 3.43(b) is equal to the parallel combination of $1/j\omega M_{MD}$ and $R_E/(Bl)^2$, that is,

$$Y_{MS} = \frac{R_E}{j\omega M_{MD}R_E + (Bl)^2}. \quad (3.45)$$

The Thévenin's equivalent circuit for the loudspeaker (looking into the diaphragm) is shown schematically in Fig. 3.43(c), where \tilde{u}_0 and the admittance Y_{MS} are given by Eqs. (3.44) and (3.45), respectively.

The application of Thévenin's theorem as discussed above is an example of how general theorems originally applying to linear passive electrical networks can be applied to great advantage to the analogs of mechanical and acoustic systems, including transducers.



3.10 TRANSDUCER IMPEDANCES

Let us look a little closer at the impedances at the terminals of electromechanical transducers. It has become popular over the years for electrical circuit specialists to express the equations for their circuits in matrix form. The matrix notation is a condensed manner of writing systems of linear equations [10,11]. We shall express the properties of transducers in matrix form for those who are familiar with this concept. An explanation of the various mathematical operations to be performed with matrices is beyond the scope of this book. The student not familiar with matrix theory is advised to deal directly with the simultaneous equations from which the matrix is derived. A knowledge of matrix theory is not necessary, however, for an understanding of any material in this text.

Transmission matrix for an electrical two-port network

As we shall see, transmission matrices are particularly useful because an overall transmission matrix \mathbf{M} can be easily obtained by multiplying together the individual transmission matrices for each circuit element. The general two-port network shown in Fig. 3.44 can be represented by the following matrix equation:

$$\begin{bmatrix} \tilde{e}_{in} \\ \tilde{i}_{in} \end{bmatrix} = \mathbf{A} \cdot \begin{bmatrix} \tilde{e}_{out} \\ \tilde{i}_{out} \end{bmatrix} = \begin{bmatrix} a_{11} & a_{12} \\ a_{21} & a_{22} \end{bmatrix} \cdot \begin{bmatrix} \tilde{e}_{out} \\ \tilde{i}_{out} \end{bmatrix}, \quad (3.46)$$

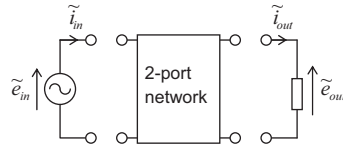


Figure 3.44 Electrical two-port network.

where the transmission parameters are given by

$$a_{11} = \frac{\tilde{e}_{in}}{\tilde{e}_{out}} \Big|_{\tilde{i}_{out} = 0}, \quad (3.47)$$

$$a_{12} = \frac{\tilde{e}_{in}}{\tilde{i}_{out}} \Big|_{\tilde{e}_{out} = 0}, \quad (3.48)$$

$$a_{21} = \frac{\tilde{i}_{in}}{\tilde{e}_{out}} \Big|_{\tilde{i}_{out} = 0}, \quad (3.49)$$

$$a_{22} = \frac{\tilde{i}_{in}}{\tilde{i}_{out}} \Big|_{\tilde{e}_{out} = 0}, \quad (3.50)$$

In other words:

a_{11} is ratio of applied input voltage to output voltage measured with the output terminals *open-circuited*.

a_{12} is ratio of applied input voltage to output current measured with the output terminals *short-circuited*.

a_{21} is ratio of applied input current to output voltage measured with the output terminals *open-circuited*.

a_{22} is ratio of applied input current to output current measured with the output terminals *short-circuited*.

Transmission matrix for an electromagnetic-mechanical transducer

Let us determine the transmission matrix for the electromagnetic-mechanical transducer of Fig. 3.45. In that circuit Z_E is the electrical impedance measured with the mechanical

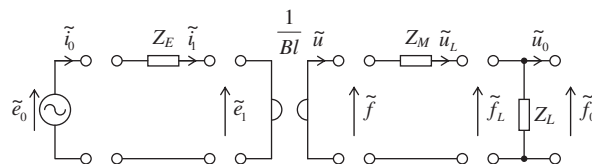


Figure 3.45 Analogous circuit for an electromagnetic-mechanical transducer. The mechanical side is of the impedance type.

terminals “blocked,” that is, $\tilde{u} = 0$; Z_M is the mechanical impedance of the mechanical elements in the transducer measured with the electrical circuit “open-circuited”; and Z_L is the mechanical impedance of the acoustic load on the diaphragm. The quantity Bl is the product of the flux density times the effective length of the wire cutting the lines of force perpendicularly. The individual transmission matrices for each element can be written from inspection

$$\begin{bmatrix} \tilde{e}_0 \\ \tilde{i}_0 \end{bmatrix} = \begin{bmatrix} 1 & Z_E \\ 0 & 1 \end{bmatrix} \cdot \begin{bmatrix} \tilde{e}_1 \\ \tilde{i}_1 \end{bmatrix} = \mathbf{M}_0 \cdot \begin{bmatrix} \tilde{e}_1 \\ \tilde{i}_1 \end{bmatrix}, \quad (3.51)$$

$$\begin{bmatrix} \tilde{e}_1 \\ \tilde{i}_1 \end{bmatrix} = \begin{bmatrix} 0 & Bl \\ 1/Bl & 0 \end{bmatrix} \cdot \begin{bmatrix} \tilde{f} \\ \tilde{u} \end{bmatrix} = \mathbf{M}_1 \cdot \begin{bmatrix} \tilde{f} \\ \tilde{u} \end{bmatrix}, \quad (3.52)$$

$$\begin{bmatrix} \tilde{f} \\ \tilde{u} \end{bmatrix} = \begin{bmatrix} 1 & Z_M \\ 0 & 1 \end{bmatrix} \cdot \begin{bmatrix} \tilde{f}_L \\ \tilde{u}_L \end{bmatrix} = \mathbf{M}_2 \cdot \begin{bmatrix} \tilde{f}_L \\ \tilde{u}_L \end{bmatrix}, \quad (3.53)$$

$$\begin{bmatrix} \tilde{f}_L \\ \tilde{u}_L \end{bmatrix} = \begin{bmatrix} 1 & 0 \\ 1/Z_L & 1 \end{bmatrix} \cdot \begin{bmatrix} \tilde{f}_0 \\ \tilde{u}_0 \end{bmatrix} = \mathbf{M}_3 \cdot \begin{bmatrix} \tilde{f}_0 \\ \tilde{u}_0 \end{bmatrix}. \quad (3.54)$$

The overall transmission matrix is then obtained as follows

$$\begin{aligned} \mathbf{M} &= \mathbf{M}_0 \cdot \mathbf{M}_1 \cdot \mathbf{M}_2 \cdot \mathbf{M}_3 \\ &= \begin{bmatrix} 1 & Z_E \\ 0 & 1 \end{bmatrix} \cdot \begin{bmatrix} 0 & Bl \\ 1/Bl & 0 \end{bmatrix} \cdot \begin{bmatrix} 1 & Z_M \\ 0 & 1 \end{bmatrix} \cdot \begin{bmatrix} 1 & 0 \\ 1/Z_L & 1 \end{bmatrix} \\ &= \begin{bmatrix} A_{11} & A_{12} \\ A_{21} & A_{22} \end{bmatrix}, \end{aligned} \quad (3.55)$$

where

$$A_{11} = \frac{Bl}{Z_L} + \frac{Z_E}{Bl} \left(1 + \frac{Z_M}{Z_L} \right), \quad (3.56)$$

$$A_{12} = Bl + \frac{Z_E Z_M}{Bl}, \quad (3.57)$$

$$A_{21} = \frac{1}{Bl} \left(1 + \frac{Z_M}{Z_L} \right), \quad (3.58)$$

$$A_{22} = \frac{Z_M}{Bl}. \quad (3.59)$$

We see from Fig. 3.45 that $\tilde{u}_o = 0$ so that

$$\begin{bmatrix} \tilde{e}_0 \\ \tilde{i}_0 \end{bmatrix} = \begin{bmatrix} A_{11} & A_{12} \\ A_{21} & A_{22} \end{bmatrix} \cdot \begin{bmatrix} \tilde{f}_0 \\ 0 \end{bmatrix} \quad (3.60)$$

From this matrix, we can gather everything we need to know about the transducer. For example, the parameters at the interfaces between the circuit elements (voltages, currents, forces and velocities, etc.) can be obtained through a combination of the overall transmission matrix and elemental matrices. Straightaway we obtain the force exerted on the load

$$\tilde{f}_L = \tilde{f}_0 = \frac{\tilde{e}_0}{A_{11}} = \frac{Z_L Bl \tilde{e}_0}{Z_E(Z_M + Z_L) + (Bl)^2} \quad (3.61)$$

and hence also the load velocity

$$\tilde{u}_L = \frac{\tilde{e}_0}{A_{11} Z_L} = \frac{Bl \tilde{e}_0}{Z_E(Z_M + Z_L) + (Bl)^2} \quad (3.62)$$

The latter is important for evaluating the radiated sound pressure, as will be explained in Chapters 4, 12, and 13. The total electrical impedance Z_{ET} as viewed from the voltage generator is found to be

$$Z_{ET} = \frac{\tilde{e}_0}{\tilde{i}_0} = \frac{A_{11} \tilde{f}_0}{A_{21} \tilde{f}_0} = Z_E + \frac{(Bl)^2}{Z_M + Z_L} \quad (3.63)$$

The second term on the right-hand side is usually called the *motional impedance* because if the mechanical side is blocked there is no movement (that is, $Z_L \rightarrow \infty$) and then $Z_{ET} = Z_E$, which is the *static impedance*. This equation illustrates a striking fact, viz., that the electromagnetic transducer is an *impedance inverter*. By an inverter we mean that a mass reactance on the mechanical side becomes a capacitance reactance when referred to the electrical side of the transformer, and vice versa. Similarly, an inductance on the electrical side reflects through the transformer as a mechanical compliance.

Impedance matrix for an electromagnetic-mechanical transducer

Refer to Fig. 3.44. Another type of matrix in common usage is the impedance matrix based on z -parameters:

$$\begin{bmatrix} \tilde{e}_{in} \\ \tilde{e}_{out} \end{bmatrix} = \mathbf{Z} \cdot \begin{bmatrix} \tilde{i}_{in} \\ -\tilde{i}_{out} \end{bmatrix} = \begin{bmatrix} z_{11} & z_{12} \\ z_{21} & z_{22} \end{bmatrix} \cdot \begin{bmatrix} \tilde{i}_{in} \\ -\tilde{i}_{out} \end{bmatrix}, \quad (3.64)$$

where the z -parameters are given by

$$z_{11} = \left. \frac{\tilde{e}_{in}}{\tilde{i}_{in}} \right|_{\tilde{i}_{out} = 0}, \quad (3.65)$$

$$z_{12} = \left. \frac{\tilde{e}_{in}}{-\tilde{i}_{out}} \right|_{\tilde{i}_{in} = 0}, \quad (3.66)$$

$$z_{21} = \left. \frac{\tilde{e}_{out}}{\tilde{i}_{in}} \right|_{\tilde{i}_{out} = 0}, \quad (3.67)$$

$$z_{22} = \left. \frac{\tilde{e}_{out}}{-\tilde{i}_{out}} \right|_{\tilde{i}_{in} = 0} \quad (3.68)$$

In other words,

z_{11} is ratio of input voltage to applied input current measured with the output terminals *open-circuited*.

z_{12} is ratio of input voltage to applied output current measured with the input terminals *open-circuited*.

z_{21} is ratio of output voltage to applied input current measured with the output terminals *open-circuited*.

z_{22} is ratio of output voltage to applied output current measured with the input terminals *open-circuited*.

Comparing Eq. (3.64) with Eq. (3.46), we can solve for the following transmission parameter to z -parameter transformation equations

$$z_{11} = a_{11}/a_{21}, \quad (3.69)$$

$$z_{12} = \det(\mathbf{A})/a_{21}, \quad (3.70)$$

$$z_{21} = 1/a_{21}, \quad (3.71)$$

$$z_{22} = a_{22}/a_{21}, \quad (3.72)$$

where

$$\det(\mathbf{A}) = a_{11}a_{22} - a_{12}a_{21}. \quad (3.73)$$

Many passive networks, especially ones in which no energy is created or lost, have a determinant whose magnitude is unity, in which case the z -parameter matrix is symmetrical about the diagonal. That is, $z_{12} = z_{21}$. However, we shall see that in the case of an electromagnetic-mechanical transducer, it turns out to be skew symmetrical, that is, with $z_{12} = -z_{21}$, because $\det(\mathbf{A}) = -1$, which in turn is because of the fact that the current flow in a wire resulting from movement through a magnetic field is in the opposite direction to that producing the same movement (Fleming's generator rule vs. motor rule). The reverse transformation equations are of the same form

$$a_{11} = z_{11}/z_{21}, \quad (3.74)$$

$$a_{12} = \det(\mathbf{Z})/z_{21}, \quad (3.75)$$

$$a_{21} = 1/z_{21}, \quad (3.76)$$

$$a_{22} = z_{22}/z_{21}, \quad (3.77)$$

where

$$\det(\mathbf{Z}) = z_{11}z_{22} - z_{12}z_{21}. \quad (3.78)$$

Applying the transformations of Eqs. (3.69–3.72) to the transmission parameters of Eq. (3.56–3.59), while noting that in this instance $\tilde{u}_0 = 0$ and $\tilde{f}_0 = \tilde{f}_L$, yields the following z -parameter impedance matrix:

$$\begin{bmatrix} \tilde{e}_0 \\ \tilde{f}_L \end{bmatrix} = \begin{bmatrix} Z_E + \frac{(Bl)^2}{Z_M + Z_L} & \frac{-BlZ_L}{Z_M + Z_L} \\ \frac{BlZ_L}{Z_M + Z_L} & \frac{Z_M Z_L}{Z_M + Z_L} \end{bmatrix} \cdot \begin{bmatrix} \tilde{i}_0 \\ 0 \end{bmatrix}, \quad (3.79)$$

Not surprisingly, $z_{11} = Z_{ET}$ as given by Eq. (3.63). If we remove the load impedance by letting $Z_L \rightarrow \infty$, we obtain the following simple z -parameter impedance matrix for just the transducer without any external load:

$$\begin{bmatrix} \tilde{e}_0 \\ \tilde{f}_L \end{bmatrix} = \begin{bmatrix} Z_E & -Bl \\ Bl & Z_M \end{bmatrix} \cdot \begin{bmatrix} \tilde{i}_0 \\ -\tilde{u}_L \end{bmatrix} \quad (3.80)$$

Transmission matrix for an electrostatic-mechanical transducer

For the electrostatic-mechanical transducer of the type shown in Fig. 3.46, Z_E is the electrical impedance with the mechanical motion free ($\tilde{f} = 0$),

$$Z'_E \equiv Z_E + \frac{1}{j\omega C'_E}$$

is the electrical impedance with the mechanical motion blocked ($\tilde{u} = 0$).

Z_L is the mechanical impedance of the acoustical load on the diaphragm.

$$Z_M \equiv R_M + j\omega M_M + \frac{1}{j\omega C_M}$$

is the mechanical impedance of the mechanical elements in the transducer measured with the electrical terminals short-circuited ($\tilde{e}_1 = 0$). Z'_M is the mechanical impedance of the mechanical elements measured with the electrical terminals open-circuited ($\tilde{i}_1 = 0$). It is defined by the same expression as that for Z_M above except that C_M is replaced by

$$C'_M = \left(1 - \frac{d_{31}^2}{C_E C_M}\right) C_M$$

which is the mechanical compliance in the transducer with $\tilde{i}_1 = 0$.

The individual transmission matrices for each element can be written from inspection:

$$\begin{bmatrix} \tilde{e}_0 \\ \tilde{i}_0 \end{bmatrix} = \begin{bmatrix} 1 & Z_E \\ 0 & 1 \end{bmatrix} \cdot \begin{bmatrix} \tilde{e}_1 \\ \tilde{i}_1 \end{bmatrix} = \mathbf{M}_0 \cdot \begin{bmatrix} \tilde{e}_1 \\ \tilde{i}_1 \end{bmatrix}, \quad (3.81)$$

$$\begin{bmatrix} \tilde{e}_1 \\ \tilde{i}_1 \end{bmatrix} = \begin{bmatrix} 1 & 0 \\ j\omega C'_M & 1 \end{bmatrix} \cdot \begin{bmatrix} \tilde{e}_2 \\ \tilde{i}_2 \end{bmatrix} = \mathbf{M}_1 \cdot \begin{bmatrix} \tilde{e}_2 \\ \tilde{i}_2 \end{bmatrix}, \quad (3.82)$$

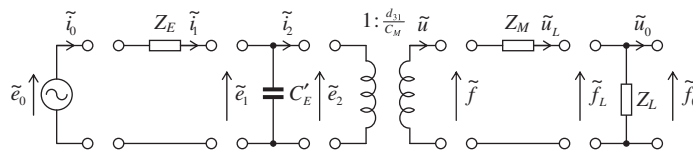


Figure 3.46 Analogous circuit for an electrostatic-mechanical transducer. The mechanical side is of the impedance type.

$$\begin{bmatrix} \tilde{e}_2 \\ \tilde{i}_2 \end{bmatrix} = \begin{bmatrix} C_M/d_{31} & 0 \\ 0 & d_{31}/C_M \end{bmatrix} \cdot \begin{bmatrix} \tilde{f} \\ \tilde{u} \end{bmatrix} = \mathbf{M}_2 \cdot \begin{bmatrix} \tilde{f} \\ \tilde{u} \end{bmatrix}, \quad (3.83)$$

$$\begin{bmatrix} \tilde{f} \\ \tilde{u} \end{bmatrix} = \begin{bmatrix} 1 & Z_M \\ 0 & 1 \end{bmatrix} \cdot \begin{bmatrix} \tilde{f}_L \\ \tilde{u}_L \end{bmatrix} = \mathbf{M}_3 \cdot \begin{bmatrix} \tilde{f}_L \\ \tilde{u}_L \end{bmatrix}, \quad (3.84)$$

$$\begin{bmatrix} \tilde{f}_L \\ \tilde{u}_L \end{bmatrix} = \begin{bmatrix} 1 & 0 \\ 1/Z_L & 1 \end{bmatrix} \cdot \begin{bmatrix} \tilde{f}_0 \\ \tilde{u}_0 \end{bmatrix} = \mathbf{M}_4 \cdot \begin{bmatrix} \tilde{f}_0 \\ \tilde{u}_0 \end{bmatrix}. \quad (3.85)$$

Using the relationship $C'_E C_M = C_E C'_M$ from Eqs. (3.36) and (3.37), the overall transmission matrix is then obtained as follows:

$$\begin{aligned} \mathbf{M} &= \mathbf{M}_0 \cdot \mathbf{M}_1 \cdot \mathbf{M}_2 \cdot \mathbf{M}_3 \cdot \mathbf{M}_4 \\ &= \begin{bmatrix} 1 & Z_E \\ 0 & 1 \end{bmatrix} \cdot \begin{bmatrix} 1 & 0 \\ j\omega C'_E & 1 \end{bmatrix} \cdot \begin{bmatrix} C_M/d_{31} & 0 \\ 0 & d_{31}/C_M \end{bmatrix} \cdot \begin{bmatrix} 1 & Z_M \\ 0 & 1 \end{bmatrix} \cdot \begin{bmatrix} 1 & 0 \\ 1/Z_L & 1 \end{bmatrix} \\ &= \begin{bmatrix} A_{11} & A_{12} \\ A_{21} & A_{22} \end{bmatrix}, \end{aligned} \quad (3.86)$$

where

$$A_{11} = \frac{j\omega C'_E C_M}{d_{31}} \left(1 + \frac{Z'_M}{Z_L} \right) \left(Z'_E + \frac{d_{31}^2}{\omega^2 C_E'^2 C_M^2 (Z'_M + Z_L)} \right), \quad (3.87)$$

$$A_{12} = \frac{j\omega C'_E C_M}{d_{31}} Z'_M \left(Z'_E + \frac{d_{31}^2}{\omega^2 C_E'^2 C_M^2 Z'_M} \right), \quad (3.88)$$

$$A_{21} = \frac{j\omega C'_E C_M}{d_{31}} \left(1 + \frac{Z'_M}{Z_L} \right), \quad (3.89)$$

$$A_{22} = \frac{j\omega C'_M C_M}{d_{31}} Z'_M. \quad (3.90)$$

Impedance matrix for an electrostatic-mechanical transducer

Applying the transformations of Eqs. (3.69–3.72) to the transmission parameters of Eqs. (3.87–3.90), while noting that in this instance $\tilde{u}_0 = 0$ and $\tilde{f}_0 = \tilde{f}_L$, yields the following z -parameter impedance matrix:

$$\begin{bmatrix} \tilde{e}_0 \\ \tilde{f}_L \end{bmatrix} = \begin{bmatrix} Z'_E + \left(\frac{d_{31}}{\omega C'_E C_M} \right)^2 \frac{1}{Z'_M + Z_L} & \frac{d_{31}}{j\omega C'_E C_M} \frac{Z_L}{Z'_M + Z_L} \\ \frac{d_{31}}{j\omega C'_E C_M} \frac{Z_L}{Z'_M + Z_L} & \frac{Z'_M Z_L}{Z'_M + Z_L} \end{bmatrix} \cdot \begin{bmatrix} \tilde{i}_0 \\ 0 \end{bmatrix}, \quad (3.91)$$

If we remove the load impedance by letting $Z_L \rightarrow \infty$, we obtain the following simple z -parameter impedance matrix for just the transducer without any external load:

$$\begin{bmatrix} \tilde{e}_0 \\ \tilde{f}_L \end{bmatrix} = \begin{bmatrix} Z'_E & \frac{d_{31}}{j\omega C'_E C_M} \\ \frac{d_{31}}{j\omega C'_E C_M} & Z'_M \end{bmatrix} \cdot \begin{bmatrix} \tilde{i}_0 \\ -\tilde{u}_L \end{bmatrix}. \quad (3.92)$$

This matrix is symmetrical about the main diagonal, as for any ordinary electrical passive network. By contrast matrix (3.80) is skew symmetrical because the off-diagonal elements have opposite signs. For transient problems, replace $j\omega$ by the operator $s = d/dt$ [9].

The impedance matrix for the electrostatic transducer is almost identical in form to that for the electromagnetic transducer, the difference being that the mutual terms have the same sign, as contrasted to opposite signs for the electromagnetic case. This means that while electrostatic transducers are *reciprocal*, electromagnetic transducers are *antireciprocal*. For the electrostatic transducer, the total impedance is given from Eq. (3.91) as

$$Z_{ET} = z_{11} = Z'_E + \left(\frac{d_{31}}{\omega C'_E C_M} \right)^2 \frac{1}{Z'_M + Z_L}. \quad (3.93)$$

The first and second terms on the right-hand side are called the static and motional impedances, respectively, as before.

Again we see that the transducer acts as a sort of *impedance inverter*. An added positive mechanical reactance ($+X_M$) comes through the transducer as a negative electrical reactance.

Some interesting facts can be illustrated by assuming that we have an electrostatic and an electromagnetic transducer, each stiffness controlled on the mechanical side so that

$$Z_M + Z_L = \frac{1}{j\omega C_{M1}}. \quad (3.94)$$

Substitution of Eqs. (3.94) into (3.63) yields

$$Z_{ET} = Z_E + j\omega(B^2 l^2 C_{M1}). \quad (3.95)$$

The mechanical compliance C_M appears from the electrical side to be an inductance with a magnitude $B^2 l^2 C_{M1}$. We now substitute Eqs. (3.94) into (3.63) to obtain

$$Z_{ET} = z_{11} = Z'_E + j\left(\frac{d_{31}}{C'_E C_M}\right)^2 \frac{C'_{M1}}{\omega}. \quad (3.96)$$

The mechanical compliance C'_M of this transducer appears from the electrical side to be a negative capacitance (see Fig. 3.37(b)), that is to say, C'_{M1} appears to be an inductance with a magnitude that varies inversely with ω^2 . The effect of this is simply to reduce the value of C'_M . Another way of looking at this is to note from Fig. 3.46 that with $R_M = M_M = 0$ and $Z_L = 1/j\omega C'_{ML}$, the total compliance is less than C'_M because of the added compliance C'_{ML} .

Analogous circuits for the two-port network using z-parameters [12]

The transmission matrix for a two-port network may be conveniently separated into three matrices

$$\begin{bmatrix} \tilde{e}_1 \\ \tilde{i}_1 \end{bmatrix} = \begin{bmatrix} 1 & z_{11} \\ 0 & 1 \end{bmatrix} \cdot \begin{bmatrix} 0 & -z_{12} \\ 1/z_{21} & 0 \end{bmatrix} \cdot \begin{bmatrix} 1 & z_{22} \\ 0 & 1 \end{bmatrix} \cdot \begin{bmatrix} \tilde{e}_2 \\ \tilde{i}_2 \end{bmatrix}. \quad (3.97)$$

These matrices multiply together to form a single transmission matrix containing the elements defined in Eqs. (3.74–3.77)

$$\begin{bmatrix} \tilde{e}_1 \\ \tilde{i}_1 \end{bmatrix} = \begin{bmatrix} a_{11} & a_{12} \\ a_{21} & a_{22} \end{bmatrix} \cdot \begin{bmatrix} \tilde{e}_2 \\ \tilde{i}_2 \end{bmatrix}. \quad (3.98)$$

The first matrix of Eq. (3.97) contains only the self-impedance z_{11} of the input port, which is shown as a series impedance in Fig. 3.47(a) and (b). Similarly, the third matrix contains only the self-impedance z_{22} of the output port, also shown as a series impedance in Fig. 3.47(a) and (b). The second matrix contains the mutual impedances z_{12} and z_{21} between the input and output, and vice versa

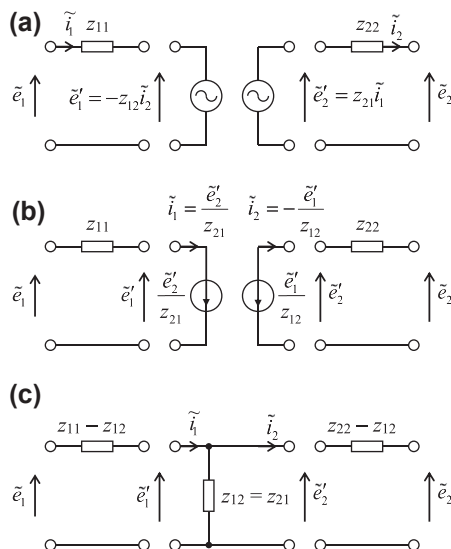


Figure 3.47 Analogous circuit of the two-port network using (a) current-controlled voltage sources (b) voltage-controlled current sources, and (c) all-passive elements for case where $z_{12} = z_{21}$.

$$\begin{bmatrix} \tilde{e}'_1 \\ \tilde{i}_1 \end{bmatrix} = \begin{bmatrix} 0 & -z_{12} \\ 1/z_{21} & 0 \end{bmatrix} \cdot \begin{bmatrix} \tilde{e}'_2 \\ \tilde{i}_2 \end{bmatrix}. \quad (3.99)$$

This may be considered as a gyrator in which the polarity of the forward transconductance is reversed. However, it is more intuitive to represent it as a pair of current-controlled voltage sources, as shown in Fig. 3.47(a). Then the relationships of Eq. (3.99) are shown explicitly. Alternatively, we may represent it as a pair of voltage-controlled current sources, as shown in Fig. 3.47(b). If the mutual impedances are equal, that is $z_{21} = z_{12}$, then we may use the purely passive scheme shown in Fig. 3.47(c). Here, the matrices divide up as follows

$$\begin{bmatrix} \tilde{e}_1 \\ \tilde{i}_1 \end{bmatrix} = \begin{bmatrix} 1 & z_{11} - z_{12} \\ 0 & 1 \end{bmatrix} \cdot \begin{bmatrix} 1 & 0 \\ 1/z_{12} & 1 \end{bmatrix} \cdot \begin{bmatrix} 1 & z_{22} - z_{12} \\ 0 & 1 \end{bmatrix} \cdot \begin{bmatrix} \tilde{e}_2 \\ \tilde{i}_2 \end{bmatrix}. \quad (3.100)$$

We will use this for modeling a lossy tube in Section. 4.23.

Example 3.9. A moving-coil earphone, which is driven at frequencies above its first resonance frequency, may be represented by the circuit of Fig. 3.43(a). Its mechanical and electrical characteristics are

$$R_E = 8 \Omega$$

$$B = 1 \text{ T } (10^4 \text{ G})$$

$$l = 3/4 \text{ m}$$

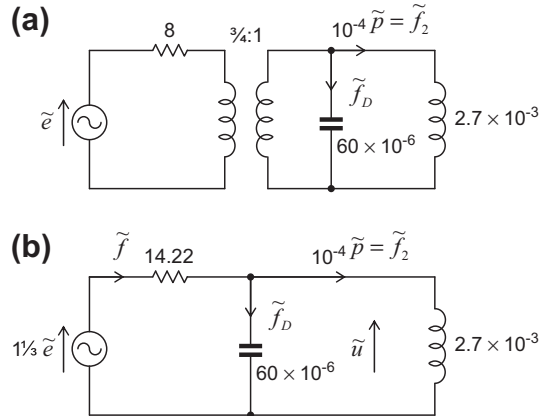


Figure 3.48 Analogous circuits for Example 3.9.

$$M_{MD} = 60 \text{ mg}$$

$$Y_{MR} = j\omega 2.7 \times 10^{-3} \text{ m/N}\cdot\text{s}$$

where Y_{MR} is the admittance that the diaphragm sees when the earphone is on the ear (because of the stiffness of the air trapped in the ear cavity), M_{MD} is the mass of the diaphragm, R_E and l are the resistance and the length of wire wound on the voice coil, and B is the flux density cut by the moving coil. Determine the sound pressure level produced at the ear at 1000 Hz when the earphone is operated from a very low impedance amplifier with an output voltage of $e_{\text{rms}} = 1$ V. Assume that the area of the diaphragm is 1 cm^2 .

Solution. The circuit diagram for the earphone with the element sizes given in SI units is shown in Fig. 3.48(a). Eliminating the transformer gives the circuit of Fig. 3.48(b). Solving, we get

$$\begin{aligned} \tilde{u} &= \tilde{f}_2 Y_{MR} = (10^{-4} \tilde{p}) j6280(2.7 \times 10^{-3}) \\ &= (j1.7 \times 10^{-3}) \tilde{p}, \end{aligned}$$

$$\tilde{f}_D = j\omega M_{MD} \tilde{u} = (-6.4 \times 10^{-4}) \tilde{p},$$

$$\tilde{f} = \tilde{f}_D + \tilde{f}_2 = (-5.4 \times 10^{-4}) \tilde{p},$$

$$\frac{1}{3} \tilde{e} = \tilde{u} + 14.22 \tilde{f} = (j1.7 \times 10^{-3} - 7.67 \times 10^{-3}) \tilde{p},$$

$$|p_{\text{rms}}| = \frac{1.33 \times 10^3}{\sqrt{1.7^2 + 7.67^2}} \approx 170 \text{ Pa},$$

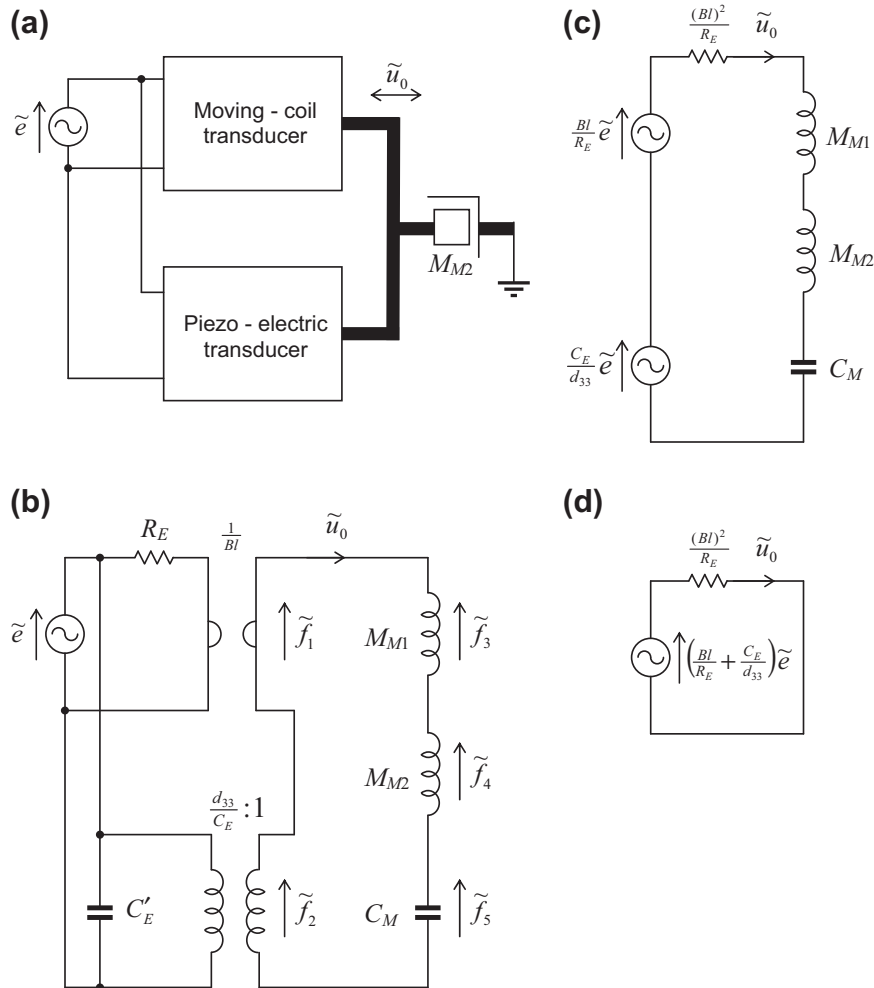


Figure 3.49 Combined electrostatic-electromagnetic transducers. (a) Block mechanical diagram of the device. (b) Analogous circuit with impedances on mechanical side. (c) Same as (b), except that the electrical elements are referred to the mechanical side. (d) Because the mechanical part of circuit (c) has zero impedance, (c) simplifies to this form.

$$\text{SPL} = 20 \log \frac{170}{2 \times 10^{-5}} = 138.6 \text{ dB re } 20 \mu \text{ Pa.}$$

Example 3.10. Two transducers, one a piezoelectric crystal and the other a moving coil in a magnetic field, are connected to a mass M_{M2} of 6.27 g as shown in Fig. 3.49(a). Determine the total stored mechanical energy in the masses M_{M1} and M_{M2} at 10 kHz for the following constants:

$$\begin{aligned}
e_{\text{rms}} &= 1 \text{ V} \\
R_E &= 10 \ \Omega \\
B &= 1 \text{ T} \\
l &= 20 \text{ m} \\
C_E &= 1.3 \times 10^{-9} \text{ F} \\
M_{M1} &= 6.4 \times 10^{-3} \text{ kg} \\
M_{M2} &= 6.27 \times 10^{-3} \text{ kg} \\
C_M &= 2 \times 10^{-8} \text{ m/N} \\
d_{33} &= 10^{-9} \text{ C/N} \\
\omega &= 62,800 \text{ rad/s}
\end{aligned}$$

Solution. The transducers are shown schematically in (b) of Fig. 3.49. A further simplification of this diagram is shown in (c). Let us determine the value of Z_M first.

$$\begin{aligned}
Z_{M1} &= j\omega(M_{M1} + M_{M2}) - j\frac{1}{C_M\omega} \\
&= j(402 + 394) - j796 = 0.
\end{aligned}$$

In other words, the impedance is zero at 10 kHz. Hence, circuit (c) simplifies to that shown in (d). Then the velocity \tilde{u}_0 of the two masses M_{M1} and M_{M2} is

$$\begin{aligned}
\tilde{u}_0 &= \left(\frac{Bl}{R_E} + \frac{C_E}{d_{33}} \right) \frac{R_E}{(Bl)^2} \tilde{e} \\
&= \left(\frac{1}{Bl} + \frac{R_E C_E}{(Bl)^2 d_{33}} \right) \tilde{e} \\
&= \left(\frac{1}{20} + \frac{10 \times 1.3}{20^2} \right) \tilde{e} = (82.5 \times 10^{-3}) \tilde{e}
\end{aligned}$$

so that $u_{0\text{rms}} = 82.5 \times 10^{-3} \text{ m/s}$. The total mechanical stored energy in the two masses M_{M1} and M_{M2} is

$$\frac{1}{2} (M_{M1} + M_{M2}) u_{0\text{rms}}^2 = 0.5 \times (6.4 + 6.27) \times 82.5^2 \times 10^{-9} = 4.31 \times 10^{-5} \text{ W}\cdot\text{s}.$$

NOTES

- [1] The London Underground map was designed by Harry Beck and introduced in 1933. He received only 5 guineas for his efforts.
- [2] Gehlshoj B. Electromechanical and electroacoustical analogies. Copenhagen: Academy of Technical Sciences; 1947.

- [3] Firestone FA. A new analogy between mechanical and electrical systems. *J Acoust Soc Am* 1933;4:249–67. The mobility method of computing the vibrations of linear mechanical and acoustical systems: Mechanical–electrical analogies. *J Appl Phys* 1938;9:373–478.
- [4] Olson HF. *Dynamical analogies*. New York: D. Van Nostrand Company, Inc.; 1943.
- [5] Mason WP. Electrical and mechanical analogies. *Bell System Tech J* 1941;20:405–14.
- [6] Bloch A. Electro–mechanical analogies and their use for the analysis of mechanical and electro–mechanical systems. *J Inst Elec Eng* 1945;92:157–69.
- [7] Among the four circuit elements, the first three are two–poles. This list is exhaustive. The transformation element is a four–pole. There are other lossless four–poles which one might have chosen in addition, e.g., the ideal gyrator.
- [8] An exception to this rule may occur when the mechanical device embodies one or more floating levers, as we just learned.
- [9] Gardner MF, Barnes JL. *Transients in linear systems*. New York: John Wiley & Sons, Inc.; 1942. p. 46–9.
- [10] Jeffrey A. *Mathematics for engineers and scientists*. 6th ed. London: Chapman & Hall; 2005. p. 463–548.
- [11] Attia JO. *Electronics and circuit analysis using MATLAB*. 2nd ed. Boca Raton, Florida: CRC; 2004. p. 151–81.
- [12] Lampton M. Transmission matrices in electroacoustics. *Acustica* 1978;39:239–51.



Acoustic components



4.1 INTRODUCTION

We have attempted to present the material in different parts of this text in three ways. The first way is in a form where acoustical phenomena can be visualized and thought of in terms, for example, of analogous electrical circuits. This form is found in the first three chapters. The second way is where straightforward mathematical analysis leads to results that are commonly encountered in engineering practice. This form is found in Chapter 7 where ready-made formulas and tables for loudspeaker systems are presented. The third way is where more advanced mathematical analysis or software is necessary to handle complex acoustical problems, such as when the wavelength is no longer much greater than the largest dimension of the physical structure. We will introduce the mathematical tools for tackling such problems in later chapters, starting with lossy tubes in [Section 4.22](#) and a model for an enclosure in [Section 7.18](#).

In this chapter, we will start with the acoustical and mechanical elements that are used to form electromechanoacoustic circuits that, in turn, are used to calculate the performance of loudspeakers, microphones, and acoustic filters. One obvious acoustical element is the air into which the sound is radiated. Others are air cavities, tubes, slots, and porous screens both behind and in front of actively vibrating diaphragms. These various elements have acoustic impedances associated with them, which can, in some frequency ranges, be represented as simple lumped elements. In other frequency ranges, where the length of the tube or cavity is greater than one-sixteenth of the wavelength such that we have to consider axial pressure fluctuations, distributed elements, analogous to electric lines, must be used in explaining the performance of the devices. For example, a two-port network for a tube of any length is given in [Section 4.23](#) together with analogous circuits. When the radius is greater than one-twenty fifth of the wavelength, we effectively have an enclosure and must consider lateral pressure fluctuations. Enclosures are treated in Chapters 7 and 10. This text does not pretend to advance the science of acoustic components to anything approaching a state of completion. Much research remains to be done. Nonlinearities that occur at higher sound levels, such as shock waves and turbulence, are not covered here. It does attempt to interpret the available theories in such a way that the reader can construct and understand the performance of common acoustic devices.

PART X: ACOUSTIC ELEMENTS

4.2 ACOUSTIC MASS (INERTANCE)

A tube open at both ends and with rigid walls behaves as an acoustic mass if it is short enough so that the air in it moves as a whole without appreciable compression. In setting up the boundary condition, the assumption is made that the sound pressure at the open end opposite the source is nearly zero. This assumption would be true if it were not for the radiation impedance of the open end, which acts very much like a piston radiating into open air. However, this radiation impedance is small for a tube of small diameter and acts only to increase the apparent length of the tube slightly. Therefore, the radiation impedance will be added as a correction factor later.

Tube of medium diameter

To be able to neglect viscous losses inside the tube, the radius of the tube a in meters must not be too small. Also, to be able to neglect transverse resonances in the tube, the radius must not be too large. The equations that follow are valid for a radius in meters greater than about $0.05/\sqrt{f}$ and less than about $10/f$, where f is the frequency in Hertz.

To demonstrate acoustic mass, take a tube of length ℓ' . Let us designate the boundary acoustic impedance at one end as $Z_A = 0$, i.e., $\tilde{p} = 0$. At the other end the acoustic impedance looking into the tube, using the solution of the one-dimensional wave Eq. (2.60), is

$$Z_A = j \frac{\rho_0 c}{\pi a^2} \tan k\ell' \quad (4.1)$$

where ρ_0 is density of the gas in kg/m^3 , c is speed of sound in m/s , a is radius of tube in m , k is wave number = ω/c in m^{-1} .

For small values of $k\ell'$,

$$\tan k\ell' = k\ell' + \frac{(k\ell')^3}{3} \quad (4.2)$$

If $\ell' < \lambda/16$, the second term will be less than 5% as large as the first, so

$$Z_A = j\omega \frac{\rho_0 \ell'}{\pi a^2} = j\omega M_A \text{N}\cdot\text{s}/\text{m}^5 \quad (4.3)$$

$$M_A = \frac{\rho_0 \ell'}{\pi a^2} \text{acoustic mass with units kg}/\text{m}^4 \quad (4.4)$$

End corrections. Most acoustic masses are tubes that terminate at one end or the other, or both, in open air or at the boundary of a large cavity. The air particles at the end

of a tube do not instantaneously disperse from their organized status inside the tube so that their behavior at the end is equivalent to a short extension of the tube, i.e., an *end correction*. In what follows, we will simply give the end corrections and later in the chapter will derive them.

End correction ℓ'' if the open end of the tube terminates in a wall is called an infinite baffle or flanged tube.

If $a < \lambda/25$, the end correction ℓ'' for this case is

$$\ell'' = \frac{M_{A1}\pi a^2}{\rho_0} = \frac{8a}{3\pi} \approx 0.85a \text{ m} \quad (4.5)$$

The total mass M_A of Eq. (4.4) now becomes

$$M_A = \frac{\rho_0(\ell' + \ell'')}{\pi a^2} = \frac{\rho_0 \ell}{\pi a^2} \text{ kg/m}^4 \quad (4.6)$$

If both ends terminate in a flange,

$$M_A = \frac{\rho_0(\ell' + 2\ell'')}{\pi a^2} = \frac{\rho_0 \ell}{\pi a^2} \text{ kg/m}^4 \quad (4.7)$$

End correction ℓ'' if the open end of the tube terminates in open air is called an unflanged tube.

If $a < \lambda/25$, the end correction in this case is again like a mass, but because the organized state of the gas particles drops off faster than in the flanged tube case, the size of M_{A1} is smaller. Hence,

$$\ell'' = \frac{M_{A1}\pi a^2}{\rho_0} = \frac{2a}{\pi} \approx 0.64a \text{ m} \quad (4.8)$$

Eqs. (4.6) and (4.7) are valid in either case, except ℓ'' must be properly chosen.



4.3 ACOUSTIC COMPLIANCES

In Eq. (2.72) we showed that a length of tube, rigidly closed on one end ($x = 0$), with a radius in meters greater than $0.05/\sqrt{f}$ (so that the sidewall friction can be neglected) and less than $10/f$ (so lateral standing waves are not present) has an input acoustic impedance at the open end equal to

$$Z_A = \frac{-j\rho_0 c}{\pi a^2} \cot k\ell' \quad (4.9)$$

where $Z_A = Z_s/(\pi a^2)$, ρ_0 is density of the gas in kg/m^3 , c is speed of sound in m/s , a is radius of tube in m , k is wave number $= \omega/c$ in m^{-1} , ℓ' is length of the tube in m .

For values of k that are not too large, the cotangent may be replaced by

$$\cot k\ell' = \frac{1}{k\ell'} - \frac{k\ell'}{3} \quad (4.10)$$

Thus

$$Z_A = -j \frac{1}{\omega(V/\rho_0 c^2)} + j\omega \frac{\ell' \rho_0}{3\pi a^2} + \dots \quad (4.11)$$

For $\ell' < \lambda/10$, Eq. (4.9) becomes

$$Z_A = -j \frac{1}{\omega C_A} \quad (4.12a)$$

The acoustic compliance obviously is

$$C_A = \frac{V}{\rho_0 c^2} = \frac{V}{\gamma P_0} \text{ with units } \text{m}^5/\text{N} \quad (4.13)$$

Limitations on an acoustic compliance

An acoustic compliance obtained by compressing air in a closed volume can be represented by a two-terminal device, but one *terminal must always be at “ground potential.”* That is to say, one terminal is outside of the enclosure V , which is at atmospheric pressure, i.e., a sound pressure of 0. *Therefore, it is never possible to insert an acoustic compliance between acoustic masses or acoustic resistances.*

Series acoustic compliance

To obtain a series acoustic compliance, a diaphragm or stretched membrane must be used. Of course, diaphragms and stretched membranes resonate at various frequencies. The range where they act as compliances is restricted to that region well below the lowest frequency of resonance. A combination of a series acoustic compliance, an acoustic mass, and an acoustic resistance is shown in Fig. 4.1.

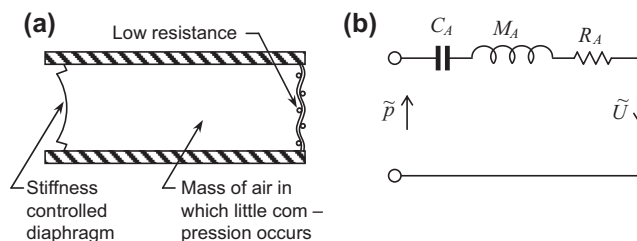


Figure 4.1 (a) Example of a series acoustic compliance obtained with a stiffness-controlled diaphragm. (b) Analogous circuit.

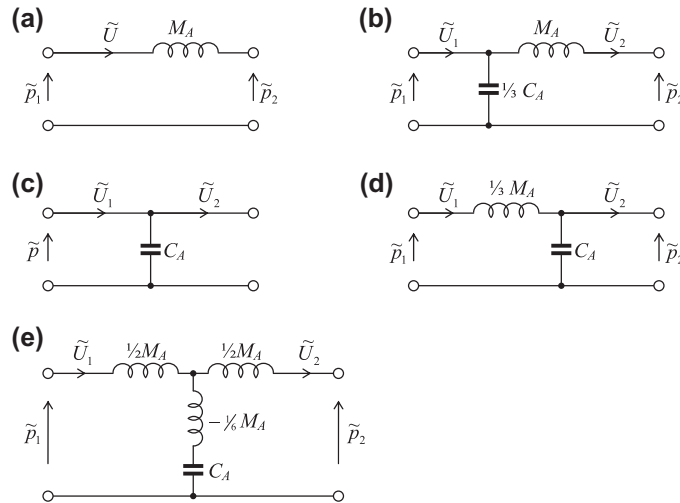


Figure 4.2 Approximate analogous circuits for a short tube of medium diameter. (a) and (b) Circuits used when \tilde{p}_2/\tilde{U}_2 is very small (open end). (c) and (d) Circuits used when \tilde{p}_2/\tilde{U}_2 is very large (closed end). (e) Circuit used for any value of \tilde{p}_2/\tilde{U}_2 . Circuits (a) and (c) yield the impedance within about 5% for a tube length l' that is less than $\lambda/16$. Circuits (b), (d), and (e) yield the impedance within about 5% for $l' < \lambda/8$.

Analogous circuits for acoustic masses and compliances are shown in Fig. 4.2. The circuits in (a) and (c) are for cases where $l' < \lambda/16$ and involve C_A and M_A alone. When $\lambda/16 > l' > \lambda/8$, the second terms in Eqs. (4.2) and (4.10) cannot be neglected and this leads to the added elements $C_A/3$ in (b), $M_A/3$ in (d), and the more complicated symmetric circuit of (e).

If the tube is not round, we may replace a by $\sqrt{S/\pi}$, where S is the cross-sectional area of the tube.

Example 4.1. The old-fashioned jug of Fig. 4.3 is used in a country dance band as a musical instrument. You are asked to analyze its performance acoustically. If the inside dimensions of the jug has diameter 20 cm and air cavity height 25 cm, give the analogous circuit, the element sizes, and the acoustic impedance for the air cavity portion of the jug at 50, 100, and 300 Hz. Assume $T = 22^\circ\text{C}$ and $P_0 = 10^5$ Pa. (Note: The neck portion will be discussed later in this part.)

Solution. The speed of sound at 22°C is about 345 m/s. Hence,

$$\lambda_{50} = 6.9 \text{ m}$$

$$\lambda_{100} = 3.45 \text{ m}$$

$$\lambda_{300} = 1.15 \text{ m}$$

The length l of the jug is 0.25 m. Hence,

$$l = \frac{\lambda_{50}}{27.6} = \frac{\lambda_{100}}{13.8} = \frac{\lambda_{300}}{4.6} = 0.25 \text{ m}$$

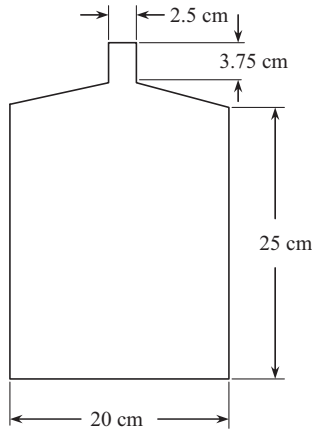


Figure 4.3 Sketch of a musical jug.

At 50 Hz, where $l/\lambda = 1/28$, the cavity portion of the jug may be represented by an acoustic compliance:

$$C_A = \frac{V}{\gamma P_0} = \frac{7.85 \times 10^{-3}}{1.4 \times 10^5} = 5.61 \times 10^{-8} \text{ m}^5/\text{N}$$

$$Z_A = -j \frac{10^8}{314 \times 5.61} = -j5.7 \times 10^4 \text{ N}\cdot\text{s}/\text{m}^5$$

At 100 Hz, where $l/\lambda = 1/14$, the cavity portion of the jug may be represented by a series acoustic mass and acoustic compliance:

$$M_A = \frac{l\rho_0}{3\pi a^2} = \frac{0.25 \times 1.19}{3\pi(0.1)^2} = 3.2 \text{ kg}/\text{m}^4$$

$$C_A = 5.61 \times 10^{-8} \text{ m}^5/\text{N}$$

$$Z_A = j \left(628 \times 3.2 - \frac{10^8}{628 \times 5.61} \right) = -j2.6 \times 10^4$$

At 300 Hz, where $l/\lambda = 1/5$, the acoustic impedance of the cavity portion of the jug must be solved directly from Eq. (4.9):

$$\begin{aligned} Z_A &= \frac{-j\rho_0 c}{\pi a^2} \cot kl \\ &= \frac{-j(1.19 \times 345)}{\pi(0.1)^2} \cot \frac{2\pi \times 300 \times 0.25}{345} \end{aligned}$$

$$Z_A = -j2.7 \times 10^3 \text{ N}\cdot\text{s}/\text{m}^5$$

Example 4.2. The jug of Example 4.1 has a neck with a diameter of 2.5 cm and a length of 3.75 cm (see Fig. 4.3). At what frequency will the jug resonate?

Solution. First, let us assume that the frequency of resonance is so low that the length of the neck l' is small compared with $\lambda/16$. Then, because the air in it is not constrained, it will be an acoustic mass:

$$\begin{aligned} M_A &= \frac{\rho_0(l' + 0.85a + 0.61a)}{\pi a^2} \\ &= 1.19 \left(\frac{0.0375 + 1.45 \times 0.0125}{\pi(0.0125)^2} \right) \\ &= 135 \text{ kg/m}^4 \end{aligned}$$

The volume velocity through the neck of the jug is the same as that entering the air cavity inside. Hence, the two elements are in series and will resonate at

$$\begin{aligned} f &= \frac{1}{2\pi\sqrt{M_A C_A}} = \frac{10^4}{2\pi\sqrt{135 \times 5.61}} \\ &= 58 \text{ Hz} \end{aligned}$$



4.4 ACOUSTIC RESISTANCES

Any device in which the flow of gas occurs in phase with and directly proportional to the applied pressure may be represented as a pure acoustic resistance. In other words, there is no stored (reactive) energy associated with the flow. Four principal forms of acoustic resistance are commonly employed in acoustic devices: fine-meshed screens made of metal or cloth, small-bore tubes, narrow slits, and porous acoustical materials.

Screens are often used in acoustic transducers because of their low cost, ease of selection and control in manufacture, satisfactory stability, and relative freedom from inductive reactance. Slits are often used where an adjustable resistance is desired. This is accomplished by changing the width of the slit. Tubes have the disadvantage that unless their diameter is very small, which in turn results in a high resistance, there is usually appreciable inductive reactance associated with them. However, if a combination of resistance and inductance is desired, they are useful. Such combinations will be treated later in this part. Fibrous or porous acoustic materials, porous ceramics, and sintered metals are often used in industrial applications and are mixtures of mass and resistance. In all four forms of acoustic resistance, the frictional effects producing the resistance occur in the same manner.

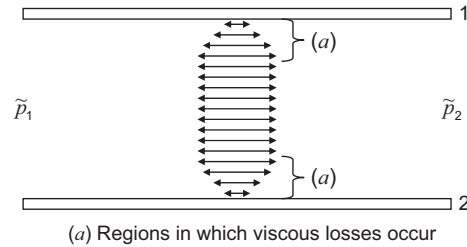


Figure 4.4 Sketch showing the diminution of the amplitude of vibration of air particles in a sound wave near a surface. The letters (a) show the regions in which viscous losses occur.

In Fig. 4.4, we see the opposite sides 1 and 2 of a slit, or tube, or of one mesh of screen. An alternating pressure difference ($\tilde{p}_1 - \tilde{p}_2$) causes a motion of the air molecules in the space between the sides 1 and 2. At 1 and 2, the air particles in contact with the sides must remain at rest. Halfway between the sides, the maximum amplitude of motion will occur. Frictional losses occur in a gas whenever adjacent layers of molecules move over each other with different velocities. Hence, frictional losses occur in the example of Fig. 4.4 near each of the walls as marked by the letter (a). In any tube, slit, mesh, or interstice, the losses become appreciable when the regions in which adjacent layers differ in velocity extend over the entire space.

Screens. The specific acoustic resistances of a variety of dust screen sizes are shown in Table 4.1. The acoustic resistance is obtained by dividing the values of R_s in this table by the area of screen being considered.

Care should be taken that a screen is tensioned before it is fitted. Otherwise it will not behave as a pure resistance but more like a membrane with compliance. If it is too slack, its motion will be nonlinear. The acoustic resistances of screens are generally determined by test and not by calculations.

Table 4.1 Specific acoustic resistances of dust screens

Type	R_s , raysl, $\text{N} \cdot \text{s}/\text{m}^3$	Mesh opening, μm	No. holes/ cm^2	Open area, %	Thickness, μm	Weight, g/m^2
Acoustex 003	3	285	529	43%	255	110
Acoustex 006	6	105	4761	52%	63	25
Acoustex 010	10	120	3025	44%	105	51
Acoustex 020	20	68	8100	38%	62	32
Acoustex 032	32	38	22,500	32%	48	25
Acoustex 047	47	38	19,600	28%	48	31
Acoustex 075	75	25	32,400	20%	52	33
Acoustex 090	90	41	8100	14%	125	86
Acoustex 145	145	27	19,600	14%	70	52
Acoustex 160	160	21	36,100	16%	58	45
Acoustex 260	260	18	40,000	13%	60	48

Courtesy of Saati Spa—data based on existing product range.

Tube of small diameter [$0.005 < \sqrt{l} < \text{radius } a \text{ (in meters)} < 0.002/\sqrt{f}$] [1]

As derived in Section 4.24, the acoustic impedance of a tube of very small diameter, neglecting the end corrections, is

$$Z_A = R_A + j\omega M_A \text{ N}\cdot\text{s}/\text{m}^5 \quad (4.14)$$

where

$$R_A = \frac{8\mu l}{(1 + 4B_u)\pi a^4} \text{ N}\cdot\text{s}/\text{m}^5 \quad (4.15)$$

$$M_A = \frac{4(1 + 3B_u)\rho_0 l}{3(1 + 4B_u)\pi a^2} \text{ kg}/\text{m}^4 \quad (4.16)$$

where μ is viscosity coefficient. For air $\mu = 1.86 \times 10^{-5} \text{ N}\cdot\text{s}/\text{m}^2$ at 20°C and 0.76 m Hg. This quantity varies with temperature, that is, $\mu \propto T^{0.7}$, where T is in $^\circ\text{K}$, l is length of tube in m, a is radius of tube in m, M_A is acoustic mass of air in tube in kg/m^4 , ρ is density of gas in kg/m^3 , and the boundary slip factor B_u is given by

$$B_u = (2\alpha_u^{-1} - 1)K_n (\approx 0 \text{ for } a > 6 \mu\text{m}), \quad (4.17)$$

where α_u is the accommodation coefficient, which is assumed to have a value of 0.9, and K_n is the (dimensionless) Knudsen number given by

$$K_n = \lambda_m/a, \quad (4.18)$$

where $\lambda_m = 60 \text{ nm}$ is the molecular mean free path length between collisions.

The mechanical impedance of a very small tube is found by multiplying Eq. (4.14) by $(\pi a^2)^2$, which yields

$$Z_M = 8\pi\mu l + j\frac{4}{3}M_M\omega \quad (4.19)$$

where $M_M = \rho_0\pi a^2 l$ = mass of air in the tube in kilograms.

Narrow slit [2] [$t \text{ (in meters)} < 0.003/\sqrt{f}$]

The acoustic impedance of a very narrow slit, neglecting end corrections, is

$$Z_A = \frac{12\mu l}{t^3 w} + j\frac{6\rho_0 l\omega}{5wt} \text{ N}\cdot\text{s}/\text{m}^5 \quad (4.20)$$

where l is length of slit in m in direction in which the sound wave is traveling (see Fig. 4.5), w is width of slit in m as viewed from the direction from which the wave is coming (see Fig. 4.5), t is thickness of slit in m (see Fig. 4.5).

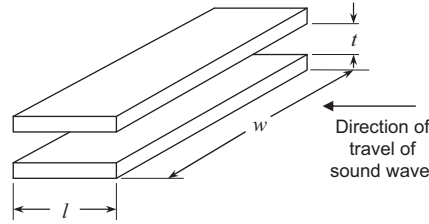


Figure 4.5 Dimension of a narrow slit.

The mechanical impedance of a very narrow slit is given by multiplying Eq. (4.20) by t^2w^2 :

$$Z_M = \frac{12\mu lw}{t} + j\frac{6}{5} M_M \omega \quad (4.21)$$

where $M_M = \rho_0 l w t =$ mass of air in the slit in kg.

Example 4.3. An acoustic resistance of $1 \text{ MN}\cdot\text{s}/\text{m}^5$ is desired as the damping element in an earphone. Select a screen and the diameter of hole necessary to achieve this resistance.

Solution. As the resistance is needed for an earphone, it should be quite small. If we select a 020 mesh screen (see Table 4.1), the *specific* acoustic resistance is 20 rayls. For an acoustic resistance of $10^6 \text{ N}\cdot\text{s}/\text{m}^5$, an area S is needed of

$$S = \frac{20}{10^6} = 20 \text{ mm}^2$$

The diameter d of the hole required for this area is

$$d = 2a = 2\sqrt{\frac{S}{\pi}} = 5.05 \text{ mm}$$



4.5 CAVITY WITH HOLES ON OPPOSITE SIDES—MIXED MASS-COMPLIANCE ELEMENT

A special case of an element that is frequently encountered in acoustical devices and that has often led to confusion in analysis is that shown in Fig. 4.6. Imagine this to be a doughnut-shaped element, each side of which has a hole of radius a bored in it. When a flow of air with a volume velocity \tilde{U}_1 enters opening 1, all the air particles in the vicinity of the opening will move with a volume velocity \tilde{U}_1 . Part of this velocity goes to compress the air in the cylindrical space 3, and part of it appears as a movement of air that is not appreciably compressed. It was pointed out earlier that a portion of a gas that compresses without appreciable motion of the particles is to be treated as an acoustic compliance.

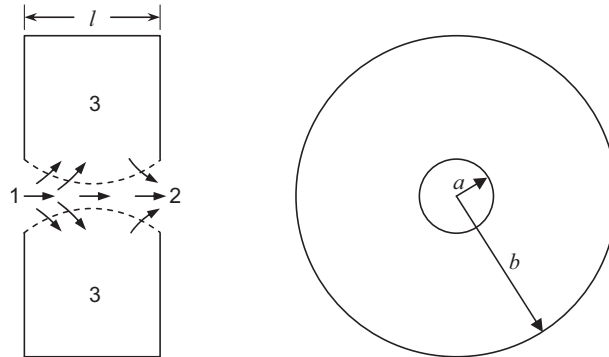


Figure 4.6 Example of a mixed mass-compliance element made from a cavity with holes on opposite sides.

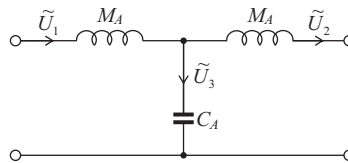


Figure 4.7 Analogous circuit for the device of Fig. 4.6.

By inspection of Fig. 4.6 we see that the portion enclosed approximately by the dotted lines moves without appreciable compression and, hence, is an acoustic mass and that lying outside the dotted lines is an acoustic compliance. The analogous circuit for this acoustic device is given in Fig. 4.7. The volume velocity \tilde{U}_1 entering opening 1 divides into two parts, one to compress the air (\tilde{U}_3) and the other (\tilde{U}_2) to leave opening 2. By judicious estimation, we arrive at values for M_A . If the length l of the cylinder is fairly long and the volume 3 is large, M_A is merely the end correction l'' of Eq. (4.5). If the volume 3 is small, then M_A becomes nearly the acoustic mass of a tube of radius a and length $l/2$. The acoustic compliance is determined by the volume of air lying outside of the estimated dotted lines of Fig. 4.6.



4.6 INTERMEDIATE-SIZED DUCTS—MIXED MASS-RESISTANCE ELEMENTS

Medium tube [a (in meters) $> 0.01/\sqrt{f}$ and $a < 10/f$] [3,4]

The acoustic impedance for a tube with a radius a (in meters) that is less than $0.002/\sqrt{f}$ was given by Eqs. (4.14) and (4.16). Here we shall give the acoustic impedance for a tube whose radius (in meters) is greater than $0.01/\sqrt{f}$ but still less than $10/f$. For a tube whose radius lies between $0.002/\sqrt{f}$ and $0.01/\sqrt{f}$ interpolation must be used. The acoustic impedance of the intermediate-sized tube is equal to

$$Z_A = R_A + j\omega M_A \quad (4.22)$$

where

$$R_A = \frac{\sqrt{2\omega\rho_0\mu}}{\pi a^2} \left(\frac{l'}{a} + (2) \times 0.7 \right) \text{N}\cdot\text{s}/\text{m}^5 \quad (4.23)$$

$$M_A = \frac{\rho_0(l' + (2)l'')}{\pi a^2} \text{kg}/\text{m}^4 \quad (4.24)$$

where a is radius of tube in m, ρ_0 is density of air in kg/m^3 , μ is viscosity coefficient. For air, $\mu = 1.86 \times 10^{-5} \text{N}\cdot\text{s}/\text{m}^2$ at 20°C and 0.76 m Hg. This quantity varies with temperature, that is, $\mu \propto T^{0.7}$, where T is in $^\circ\text{K}$, l' is actual length of the tube, l'' is end correction for the tube. It is given by Eq. (4.5) if the tube is flanged or by Eq. (4.8) if the tube is unflanged. The numbers (2) in parentheses in Eqs. (4.23) and (4.24) must be used if both ends of the tube are being considered. If only one end is being considered, replace the number (2) with the number 1, and ω is angular frequency in rad/s.

Medium slit [t (in meters) $> 0.02/\sqrt{f}$ and $t < 20/f$] [5]

The acoustic impedance of a medium slit, neglecting end corrections, is

$$Z_A = \frac{l\sqrt{2\omega\rho_0\mu}}{t^2w} + j\omega\frac{\rho_0l}{tw} \text{N}\cdot\text{s}/\text{m}^5$$



4.7 PERFORATED SHEET—MIXED MASS-RESISTANCE ELEMENT [a (IN METERS) $> 0.01/\sqrt{f}$ AND $a < 10/f$] [3,4]

Many times, in acoustics, perforated sheets are used as mixed acoustical elements. We shall assume a perforated sheet with the dimensions shown in Fig. 4.8 and holes whose centers are spaced more than one diameter apart. For this case, the acoustic impedance for each area b^2 , that is, each hole, is given by

$$Z_A = R_A + j\omega M_A$$

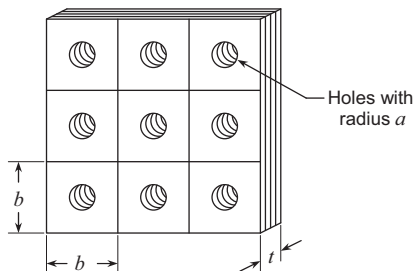


Figure 4.8 Thin perforated sheet with holes of radius a , and length l , spaced a distance b on centers.

where

$$R_A = \frac{\sqrt{2\omega\rho_0\mu}}{\pi a^2} \left\{ \frac{t}{a} + 1.4 \left(1 + 0.13 \sqrt{\frac{A_h}{A_b}} - \frac{A_h}{A_b} \right) \right\} \text{N}\cdot\text{s}/\text{m}^5 \quad (4.25)$$

$$M_A = \frac{\rho_0}{\pi a^2} \left\{ t + 1.7a \left(1 - 2.26 \frac{a}{b} \right) \right\} \text{kg}/\text{m}^4 \quad (4.26)$$

where $A_h = \pi a^2$ is area of hole in m^2 , $A_b = b^2$ is area of a square around each hole in m^2 , t is thickness of the sheet in m.

If there are n holes, the acoustic impedance is approximately equal to $1/n$ times that for one hole.

Definition of Q

If this mass–resistance element is used with a compliance to form a resonant circuit, we are often interested in the ratio of the angular frequency of resonance ω_0 to the angular bandwidth ω (rad/s) measured at the half–power points. This ratio is called the “ Q ” of the circuit and is a measure of the sharpness of the resonance curve.

The “ Q_A ” of a perforated sheet when used with a compliance of such size as to produce resonance at angular frequency ω_0 is

$$Q_A = \frac{\omega_0 M_A}{R_A} = \frac{\sqrt{\omega_0 \rho_0}}{2\mu} a \frac{t + 1.7a(1 - (a/b))}{t + 2a(1 - (\pi a^2/b^2))} \quad (4.27)$$

The Q_A is independent of the number of holes in the perforated sheet. We repeat that these formulas are limited to cases where the centers of the holes are spaced more than a diameter apart.



4.8 ACOUSTIC TRANSFORMERS

As for the other acoustical elements, there is no configuration of materials that will act as a “lumped” transformer over a wide frequency range. Also, what may appear to be an acoustic transformer when impedances are written as mechanical impedances may not appear to be one when written as acoustic impedances, and vice versa. As an example of this situation, let us investigate the case of a simple discontinuity in a pipe carrying an acoustic wave.

Junction of two pipes of different areas

A junction of two pipes of different areas is equivalent to a discontinuity in the area of a single pipe (see Fig. 4.9a).

If we assume that the diameter of the larger pipe is less than $\lambda/16$, then we may write the following two equations relating the pressure and volume velocities at the junction:

$$\tilde{p}_1 = \tilde{p}_2 \quad (4.28)$$

$$\tilde{U}_1 = \tilde{U}_2 \quad (4.29)$$

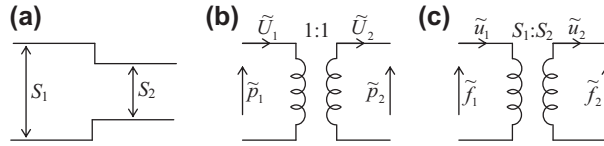


Figure 4.9 (a) Simple discontinuity between two pipes. (b) Acoustic-impedance transducer representation of (a); because the transformation ratio is unity, no transformer is required. (c) Mechanical impedance transducer representation of (a).

Eq. (4.28) says that the sound pressure on both sides of the junction is the same. Eq. (4.29) says that the volume of air leaving one pipe in an interval of time equals that entering the other pipe in the same interval of time. The transformation ratio for acoustic impedances is unity so that no transformer is needed.

For the case of a circuit using lumped *mechanical* elements, the discontinuity appears to be a transformer with a turns ratio of $S_1:S_2$ because, from Eq. (4.28),

$$\frac{\tilde{f}_1}{S_1} = \frac{\tilde{f}_2}{S_2} \quad (4.30)$$

and, from Eq. (4.29),

$$\tilde{u}_1 S_1 = \tilde{u}_2 S_2 \quad (4.31)$$

where \tilde{f}_1 and \tilde{f}_2 are the forces on the two sides of the junction, and \tilde{u}_1 and \tilde{u}_2 are the average particle velocities over the areas S_1 and S_2 . We have

$$\tilde{f}_1 = \frac{S_1}{S_2} \tilde{f}_2 \quad (4.32)$$

and

$$\tilde{u}_2 = \frac{S_1}{S_2} \tilde{u}_1 \quad (4.33)$$

so that

$$Z_{M1} = \frac{\tilde{f}_1}{\tilde{u}_1} = \left(\frac{S_1}{S_2}\right)^2 \frac{\tilde{f}_2}{\tilde{u}_2} = \left(\frac{S_1}{S_2}\right)^2 Z_{M2} \quad (4.34)$$

A transformer is needed in this case and is drawn as shown in Fig. 4.9c.

It must be noted that a reflected wave will be sent back toward the source by the simple discontinuity. We saw in Part IV that, in order that there be no reflected wave, the specific acoustic impedance in the second tube (\tilde{p}_2/\tilde{u}_2) must equal that in the first tube (\tilde{p}_1/\tilde{u}_1). This is possible only if $S_1 = S_2$, that is, if there is no discontinuity.

To find the magnitude and phase of the reflected wave in the first tube resulting from the discontinuity, we shall use material from Part IV. Assume that the discontinuity exists at $x = 0$. The specific acoustic impedance in the first tube is

$$Z_{S1} = \frac{\tilde{p}_1}{\tilde{u}_1} \quad (4.35)$$

If the second tube is infinitely long, the specific acoustic impedance for it at the junction will be

$$Z_{S2} = \frac{\tilde{p}_2}{\tilde{u}_2} = \rho_0 c \quad (4.36)$$

(see Eq. 2.124). The impedance Z_{S1} at the junction is, from Eqs. (4.28) and (4.33),

$$Z_{S1} = \frac{\tilde{p}_1}{\frac{S_2 \tilde{u}_2}{S_1}} = \frac{\tilde{p}_2}{\frac{S_2 \tilde{u}_2}{S_1}} \quad (4.37)$$

From Eqs. (4.36) and (4.37),

$$Z_{S1} = \frac{S_1}{S_2} \rho_0 c \quad (4.38)$$

Using Eqs. (2.46) and (2.122), setting $x = 0$, we may solve for the reflected wave \tilde{p}_- in terms of the incident wave \tilde{p}_+ .

$$\tilde{p}_1 = \tilde{p}_+ - \tilde{p}_- \quad (4.39)$$

$$\tilde{u}_1 = \frac{1}{\rho_0 c} (\tilde{p}_+ - \tilde{p}_-) \quad (4.40)$$

$$\frac{\tilde{p}_1}{\tilde{u}_1} = \frac{S_1}{S_2} \rho_0 c = \rho_0 c \frac{\tilde{p}_+ + \tilde{p}_-}{\tilde{p}_+ - \tilde{p}_-} \quad (4.41)$$

$$\tilde{p}_- = \frac{S_1 - S_2}{S_1 + S_2} \tilde{p}_+ \quad (4.42)$$

The sound pressure \tilde{p}_T of the transmitted wave in the second tube at the junction point must equal the sound pressure in the first tube at that point,

$$\tilde{p}_T = \tilde{p}_+ + \tilde{p}_- \quad (4.43)$$

so that

$$\tilde{p}_T = \frac{2S_1}{S_1 + S_2} \tilde{p}_+ \quad (4.44)$$

If S_1 equals S_2 , there is no reflected wave \tilde{p}_- and then $\tilde{p}_+ = \tilde{p}_T$.

Note also that if S_2 becomes vanishingly small, this case corresponds to the case of a rigid termination at the junction. For this case,

$$\tilde{p}_- = \tilde{p}_+ \quad (4.45)$$

and

$$\tilde{p}_+ + \tilde{p}_- = 2\tilde{p}_+ \quad (4.46)$$

This equation illustrates the often-mentioned case of *pressure doubling*. That is to say, when a plane sound wave reflects from a plane rigid surface, the sound pressure at the surface is double that of the incident wave.

Two pipes of different areas joined by an exponential connector [6]

An exponential connector may be used to join two pipes of different areas. Such a connector (see Fig. 4.10) acts as a simple discontinuity when its length is short compared with a wavelength and as a transformer for *acoustic* impedances when its length is greater than a half wavelength.

If the second tube is infinitely long, then at $x = l$ (see Fig. 4.10),

$$\frac{\tilde{p}_2}{\tilde{u}_2} = \rho_0 c \quad (4.47)$$

If the cross-sectional area of the exponential connector is given by

$$S(x) = S_1 e^{mx} \quad (4.48)$$

and the length of the connector is l , then the specific acoustic impedance at $x = 0$ is

$$Z_{S1} = \frac{\tilde{p}_1}{\tilde{u}_1} = \rho_0 c \frac{\cos(bl + \theta) + j \sin(bl)}{\cos(bl - \theta) + j \sin(bl)} \quad (4.49)$$

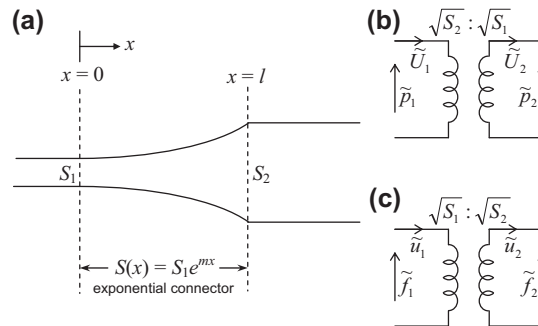


Figure 4.10 (a) Exponential connector between two pipes. (b) High-frequency representation of (a) using acoustic-impedance transducer. (c) High-frequency representation of (a) using mechanical-impedance transducer.

where

$$b = \frac{1}{2} \sqrt{(4\omega^2/c^2) - m^2} \text{ in m}^{-1}$$

where m is flare constant in m^{-1} (see Eq. 4.48), $\theta = \tan^{-1}(m/2b)$, c is speed of sound in m/s , l is length of the exponential connector in m , and ρ_0 is density of air in kg/m^3 .

At low frequencies (b imaginary and λ/l large),

$$\frac{\tilde{p}_1}{\tilde{U}_1} = \frac{\tilde{p}_2}{\tilde{U}_2} \quad \text{or} \quad Z_{A1} = Z_{A2} \quad (4.50)$$

At high frequencies (b real and $l/\lambda > 1$),

$$\frac{\tilde{p}_1}{\tilde{u}_1} = \frac{\tilde{p}_2}{\tilde{u}_2} \quad (4.51)$$

or

$$Z_{A1} = \frac{S_2}{S_1} Z_{A2} \quad (4.52)$$

At intermediate frequencies, the transformer introduces a phase shift, and the transformation ratio varies between the limits set by the two equations above.

The transformation ratio for acoustic impedance at high frequencies is seen from Eq. (4.52) to be $\sqrt{S_2/S_1}$ (see Fig. 4.10b). That is to say,

$$Z_{A1} = \left(\sqrt{\frac{S_2}{S_1}} \right)^2 Z_{A2} \quad (4.53)$$

For mechanical impedance at high frequencies, the transformation ratio is seen from Eq. (4.52) to be $\sqrt{S_2/S_1}$ (see Fig. 4.10c). That is to say,

$$Z_{M1} = \left(\sqrt{\frac{S_1}{S_2}} \right)^2 Z_{M2}$$

Example 4.4. It is desired to resonate the cavity in front of the diaphragm of a call loudspeaker, such as that found in a cellphone, to 3 kHz using an array of laser-drilled sound outlet holes. The cavity has a volume of 0.4 cm^3 and a wall thickness of 1 mm. Determine the size and number of holes needed, assuming $Q_A = 1.5$ and a ratio of hole diameter to on-center spacing of 0.5.

Solution. From Eq. (4.27) we see that, approximately,

$$Q_A \approx \frac{a\sqrt{1.18\omega_0}}{\sqrt{2 \times 1.86 \times 10^{-5}}}$$

$$a = \frac{1.5 \times 0.00397 \times \sqrt{2}}{\sqrt{6.28 \times 3000}} = 61.3 \text{ } \mu\text{m}$$

The diameter of the hole is 123 μm .

The reactance of the cavity at resonance equals

$$X_B = \frac{1}{\omega_0 C_A} = \frac{\gamma P_0}{18840 \times V} = \frac{1.4 \times 10^{11}}{18840 \times 0.4} = 18.6 \times 10^6 \text{ N}\cdot\text{s}/\text{m}^5$$

The desired acoustic mass of the holes is

$$M_A = \frac{X_B}{\omega_0} = \frac{18.6 \times 10^6}{18840} = 985 \text{ kg}/\text{m}^4$$

If there are n holes, the acoustic mass for each hole equals

$$nM_A = n(985) \text{ kg}/\text{m}^4$$

From Eq. (4.26),

$$n(985) = \frac{1.18}{\pi(61.3^2 \times 10^{12})} (0.001 + (1.7 \times 18.6 \times 10^{-6})(0.75))$$

$$n = \frac{(1.18)(1.024 \times 10^{-3})}{\pi(985)(3.76 \times 10^{-9})} \approx 104 \text{ holes}$$

Example 4.5. Design a single-section T low-pass wave filter, as shown in Figs. 4.6 and 4.7, with a cutoff frequency of 100 Hz and Q value of $1/\sqrt{2}$ for critical damping. The filter is driven by a piston at the entrance on the left and terminated with an impedance of $R_0 = 10^3 \text{ N}\cdot\text{s}/\text{m}^5$ at the exit on the right.

Solution. Because the filter is driven by a piston with a defined velocity, it can be regarded as having a source impedance that is very large in comparison with the acoustic mass on the left of Fig. 4.7. We can therefore ignore that element. The filter is thus reduced to a second-order type with a cutoff frequency of

$$f_0 = \frac{1}{2\pi\sqrt{M_A C_A}}$$

The design Q is equal to

$$Q = \frac{1}{R_0} \sqrt{\frac{M_A}{C_A}}$$

From these two equations, we can solve for C_A and M_A .

$$\begin{aligned} M_A &= \frac{1}{4\pi^2 f_0^2 C_A} \\ &= \frac{R_0 Q}{2\pi f_0} \end{aligned}$$

So

$$C_A = \frac{1}{2\pi f_0 R_0 Q}$$

$$= \frac{\sqrt{2}}{2\pi \times 100 \times 10^3} = 2.25 \times 10^{-6} \text{ m}^5/\text{N}$$

$$M_A = \frac{10^3}{2\pi \times 100 \times \sqrt{2}} = 1.125 \text{ kg/m}^4$$

From Section 4.6 and Eq. (4.24), with l' equal to zero, we get the size of the hole in the device of Fig. 4.6.

$$M_A = \frac{\rho_0(0.85a)}{\pi a^2}$$

$$\frac{(1.18)(0.85)}{\pi a} = 1.125$$

$$a = 28.4 \text{ cm}$$

The diameter of the hole is 0.57 m. The volume of the cavity is

$$V = C_A \gamma P_0 = 1.4 \times 2.25 \times 10^{-6} \times 10^5$$

$$= 0.315 \text{ m}^3$$

The elements for the T section are thereby determined.



PART XI: ELEMENTARY REFLECTION AND RADIATION OF SOUND

To fully specify a source of sound, we need to know, in addition to other properties, its directivity characteristics at all frequencies of interest. Some sources are nondirectional, that is to say, they radiate sound equally in all directions and as such are called spherical radiators. Others may be highly directional, either because their size is naturally large compared with a wavelength or because of special design. In particular, we shall examine how the shape of the radiator influences its directivity.

The most elementary radiator of sound is a spherical source whose radius is small compared with one-sixth of a wavelength. Such a radiator is called a *simple source* or a *point source*. Its properties are specified by the magnitude of the velocity of its surface and by its phase relative to some reference. More complicated sources such as plane or curved radiators may be treated analytically by applying boundary conditions or as a combination of simple sources, each with its own surface velocity and phase, and these will be covered in Chapters 12 and 13.

A particularly important consideration in the design of loudspeakers and horns is their directivity characteristics. This chapter serves as an important basis for later chapters dealing with loudspeakers, baffles, and horns.

The basic concepts governing radiation of sound must be grasped thoroughly at the outset. It is then possible to reason from those concepts in deducing the performance of any particular equipment or in planning new systems. Examples of measured radiation patterns for common loudspeakers are given here as evidence of the applicability of the basic concepts.

The *directivity pattern* of a transducer used for the emission or for reception of sound is a description, usually presented graphically, of the response of the transducer as a function of the direction of the transmitted or incident sound waves in a specified plane and at a specified frequency.

The *beam width* of a directivity pattern is used in this text as the angular distance between the two points on either side of the principal axis where the sound pressure level is down 6 dB from its value at $\theta = 0$.

Before considering specific sound sources, we will first study some fundamental properties of sound waves using the example of reflection from a plane.



4.9 REFLECTION OF A PLANE WAVE FROM A PLANE

Reflections from a plane are *specular*, meaning that they are well defined because of the regular geometry of the reflecting surface, as opposed to *diffuse*, as in the case of an irregular reflecting object. In the latter case, the sound waves are reflected in many different directions. However, although a sphere reflects sound over a wide angle, as we shall see in Sections 12.3 and 12.4, the reflection is specular because the reflecting surface is regular. Refer to Fig. 4.11. A plane wave with amplitude \tilde{p}_I is incident on a plane at $x = 0$, the surface of which has a specific acoustic impedance Z_s . Depending on the value of Z_s , a portion of the incident wave is reflected with amplitude \tilde{p}_R . The angle θ_I between the incident wave and the normal to the plane, formed by the x axis, is the *angle of incidence*. Similarly, the angle θ_R between the reflected wave and the normal to the

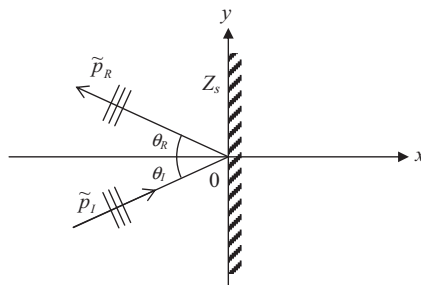


Figure 4.11 Reflection of a plane wave from a plane at $x = 0$.

plane is the *angle of reflection*. In this instance, we assume neither wave has any component in the z direction (away from the page).

Substituting $k_x = k \cos \theta$, $k_y = k \sin \theta$, and $k_z = 0$ in the wave equation solution of Eq. (2.154) (which satisfies $k^2 = k_x^2 + k_y^2 + k_z^2$), we obtain the following expression for the pressure field in the negative x region of Fig. 4.11:

$$\tilde{p}(x, y) = \tilde{p}_I e^{-jkx \cos \theta_I} e^{-jky \sin \theta_I} + \tilde{p}_R e^{jkx \cos \theta_R} e^{jky \sin \theta_R}. \quad (4.54)$$

where the particle velocity in the x direction is given by

$$\begin{aligned} \tilde{u}_x(x, y) &= \frac{1}{-jk\rho_0 c} \frac{\partial}{\partial x} \tilde{p}(x, y) \\ &= \frac{1}{\rho_0 c} \left(\tilde{p}_I e^{-jkx \cos \theta_I} e^{-jky \sin \theta_I} \cos \theta_I - \tilde{p}_R e^{jkx \cos \theta_R} e^{jky \sin \theta_R} \cos \theta_R \right). \end{aligned} \quad (4.55)$$

Let us now consider the boundary condition for two values of Z_S . When $Z_S = \infty$, the surface is totally rigid and the normal particle velocity at $x = 0$ is zero. This is often referred to as a *Neumann* boundary condition. Hence,

$$\tilde{u}_x(0, y) = \frac{1}{\rho_0 c} \left(\tilde{p}_I e^{-jky \sin \theta_I} \cos \theta_I - \tilde{p}_R e^{jky \sin \theta_R} \cos \theta_R \right) = 0, \quad (4.56)$$

which is satisfied if

$$\theta_R = -\theta_I \quad (4.57)$$

and

$$\tilde{p}_R = \tilde{p}_I. \quad (4.58)$$

The latter would appear to be a reasonable assumption considering that no losses occur during a reflection from a perfectly rigid boundary. When $Z_S = 0$, the surface is totally flexible or *resilient* and the surface pressure is zero. This is often referred to as a *Dirichlet* boundary condition and is somewhat akin to the boundary condition at the mouth of an open pipe if we assume that the radiation load is negligible. It is also often referred to as a “pressure release” boundary condition. In this case

$$\tilde{p}(0, y) = \tilde{p}_I e^{-jky \sin \theta_I} + \tilde{p}_R e^{jky \sin \theta_R} = 0, \quad (4.59)$$

which is satisfied if

$$\theta_R = -\theta_I \quad (4.60)$$

and

$$\tilde{p}_R = -\tilde{p}_I. \quad (4.61)$$

Again the latter would appear to be a reasonable assumption considering that no losses occur during a reflection from a perfectly resilient boundary. Eq. (4.60) is known as the *law of reflection*. Generally, the law of reflection can be shown to hold for all boundary impedance values. The impedance at the plane is simply the ratio of the pressure to particle velocity:

$$Z_s = \frac{\tilde{p}(0, \gamma)}{\tilde{u}_x(0, \gamma)} \Big|_{\theta_R = -\theta_I} = \frac{(\tilde{p}_I + \tilde{p}_R)\rho_0 c}{(\tilde{p}_I - \tilde{p}_R)\cos\theta_I}. \quad (4.62)$$

Rearranging for \tilde{p}_R gives

$$\Gamma = \frac{\tilde{p}_R}{\tilde{p}_I} = \frac{Z_s \cos\theta_I / (\rho_0 c) - 1}{Z_s \cos\theta_I / (\rho_0 c) + 1} \quad (4.63)$$

where Γ is the reflection coefficient.

The above equation tells us that if we let $Z_s = \rho_0 c$, only normal incident waves (i.e., $\theta_I = 0$) are totally absorbed. If $\theta_I \neq 0$, there will be a reflected wave. In other words, a $\rho_0 c$ boundary condition is not an open window. This has quite far reaching implications in acoustics. For example, when waves from a sound source in an anechoic chamber reach the walls, they are rarely perfectly normal. Hence, absorbent “wedges” are typically used to produce multiple or diffuse reflections so that after a certain number of reflections, the reverberant sound field is reduced to an acceptable level. Also, when modeling sound sources using the finite element method, it is usually necessary to create a virtual anechoic chamber filled with air elements. A sphere coated with $\rho_0 c$ elements should produce acceptable results provided that the sphere is large enough for the waves that reach its inner surface to be spherically diverging far-field ones. Otherwise, if the field immediately adjacent to the inner surface is the complex near-field, then reflections are guaranteed. We shall study the differences between the near-field and far-field pressure due to various sound sources further on in this text.



4.10 RADIATION FROM A PULSATING SPHERE

The pulsating sphere may be one of the most difficult sound sources to realize in practice, but it is the easiest three-dimensional source to analyze. Because of rotational symmetry, it can be treated as a one-dimensional problem with just a single radial ordinate r . Many practical sources behave in a similar way at low frequencies where they become virtually omnidirectional, as we shall see. Also, ultrasonic hydrosounders are often in the form of a sphere coated with a piezoelectric transducer. Essentially, the pulsating sphere is a sphere whose radius oscillates harmonically. In the limiting case, it will lead us to the point source, which forms a fundamental building block in acoustics.

Pressure field. Because the sphere is radiating into free space, where there are no reflections, we take the outward going part of the solution to the spherical wave

Eq. (2.25) given by Eq. (2.142), where \tilde{A}_+ is an unknown coefficient to be determined from the boundary conditions. Let us now impose a boundary condition at the surface of the sphere whereby the particle velocity normal to the surface, given by Eq. (2.143), is equal to the uniform surface velocity \tilde{u}_0 so that $\tilde{u}(R) = \tilde{u}_0$, where R is the radius, which gives

$$\tilde{A}_+ = \frac{jkR^2\rho_0ce^{jkR}}{1+jkR}\tilde{u}_0. \quad (4.64)$$

Inserting this into Eq. (2.142) and substituting $\tilde{U}_0 = 4\pi R^2\tilde{u}_0$, where \tilde{U}_0 is the total volume velocity, yields

$$\tilde{p}(r) = jk\rho_0c\tilde{U}_0\frac{e^{-jk(r-R)}}{4\pi r}D, \quad (4.65)$$

where D is called a directivity function, but here it has no angular dependency and is merely a frequency response function given by

$$D = \frac{1}{1+jkR}. \quad (4.66)$$

which is plotted in Fig. 4.12. Likewise from Eq. (2.143) for the velocity we have

$$\begin{aligned} \tilde{u}(r) &= \frac{1}{-jk\rho_0c}\frac{\partial}{\partial r}\tilde{p}(r) \\ &= (1+jkr)\tilde{U}_0\frac{e^{-jk(r-R)}}{4\pi r^2}D. \end{aligned} \quad (4.67)$$

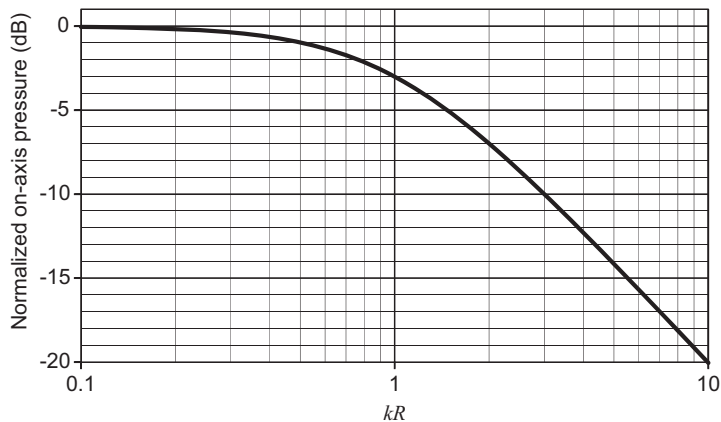


Figure 4.12 Plot of $20 \log_{10}(|D|)$ for a pulsating sphere with constant radial acceleration. Frequency is plotted on a normalized scale, where $kR = 2\pi R/\lambda = 2\pi fR/c$.

Radiation impedance

The specific radiation impedance is found by dividing the pressure at $r = R$ from Eq. (4.65) by the surface velocity \tilde{u}_0 as follows:

$$Z_s = \frac{\tilde{p}(R)}{\tilde{u}_0} = \frac{jkR}{1 + jkR} \rho_0 c, \quad (4.68)$$

or

$$Z_s = \mathbf{R}_s + jX_s = \frac{k^2 R^2 + jkR}{k^2 R^2 + 1} \rho_0 c. \quad (4.69)$$

It turns out that this is the same as the impedance from Eq. (2.144) for a freely propagating spherical wave at a distance R from the origin. It is also the first time derivative of D from Eq. (4.66), above, multiplied by $\rho_0 R$. The real and imaginary parts, \mathbf{R}_s and X_s , are plotted in Fig. 4.13.

It is seen from Fig. 4.13 that for $kR < 0.3$, that is, when the diameter is less than one-tenth of the wavelength, the radiation impedance is mainly that of a *mass* reactance because the resistive component is negligible compared with the reactance component. This mass loading may be thought of as a layer of air on the outside of the sphere, the thickness of which equals 0.587 of the radius of the sphere. At all frequencies, the loading shown in Fig. 4.13 may be represented by the equivalent circuit inset.

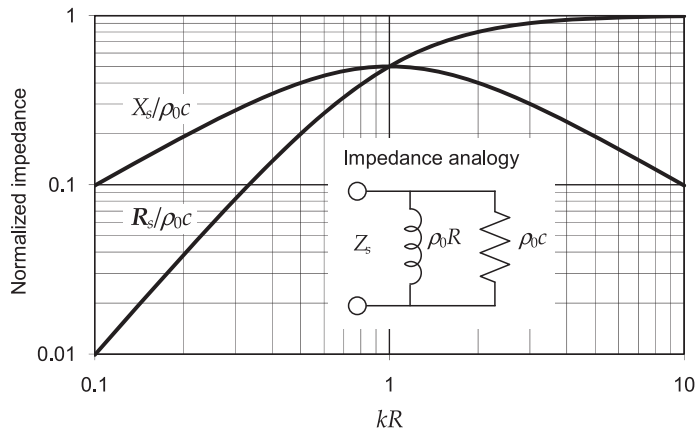


Figure 4.13 Real and imaginary parts of the normalized specific radiation impedance $Z_s/\rho_0 c$ of the air load on a pulsating sphere of radius R located in free space. Frequency is plotted on a normalized scale where $kR = 2\pi fR/c = 2\pi R/\lambda$. Note also that the ordinate is equal to $Z_M/\rho_0 cS$, where Z_M is the mechanical impedance; and to $Z_A S/\rho_0 c$, where Z_A is the acoustic impedance. The quantity S is the area for which the impedance is being determined, which in this case is $S = 4\pi R^2$ and $\rho_0 c$ is the characteristic impedance of the medium.

We also observe from Fig. 4.12 that for $kR < 0.3$, the radiated sound pressure is proportional to the volume *acceleration* ($j\omega\tilde{U}_0$) so that the radiated intensity, which is proportional to the square of the radiated pressure (see Eq. 1.12), is held constant. This is because of the fact that the decreasing velocity (which is the time integral of the acceleration) is compensated for by the rising radiation resistance, which is proportional to the square of the velocity:

$$I = \left| \frac{\tilde{p}(r)}{\sqrt{2}} \right|^2 \frac{1}{\rho_0 c} = \left| \frac{\tilde{u}_0}{\sqrt{2}} \right|^2 \frac{\mathbf{R}_M}{4\pi r^2} = \left| \frac{\tilde{u}_0}{\sqrt{2}} \right|^2 \frac{R^2}{r^2} \mathbf{R}_s, \quad (4.70)$$

where in this case the mechanical radiation resistance is given by $\mathbf{R}_M = 4\pi R^2 \mathbf{R}_s$.

The relationship between radiation impedance and far-field pressure forms the basis of a useful theorem developed in Section 13.13. For $kR > 3$, the pressure is proportional to the volume *velocity* \tilde{U}_0 because the radiation impedance is mainly resistive.

Eqs. (4.65) and (4.67) are significant because they reveal the difference between the responses of a microphone sensitive to pressure and a microphone sensitive to particle velocity as the microphones are brought close to a small spherical source of sound at low frequencies. As r is made smaller, the output of the pressure-responsive microphone will double for each halving of the distance between the microphone and the center of the spherical source. Expressed in decibels, the output increases 6 dB for each halving of distance. For the velocity-responsive microphone, the output variation is not so simple. Only at sufficiently large distances ($k^2 r^2 \gg 1$) does the output increase 6 dB for each halving of distance. For shorter distances, the second term inside the parentheses on the right-hand side of Eq. (4.67) becomes large, and the magnitude of \tilde{u} increases at a rate exceeding +6 dB for each halving of distance. For very short distances ($k^2 r^2 \ll 1$), the rate of increase of \tilde{u} approaches a limit of +12 dB for each halving of distance. It is for this reason that the voice of a vocalist sounds “bassy” when he or she sings very near to a velocity-sensitive microphone which was designed to have its best response when located a large distance from the source of sound. This is commonly known as the proximity effect.

Another significant thing is to be learned from Eq. (4.69). At low frequencies, it is very difficult to radiate sound energy from a small loudspeaker. A small loudspeaker may be likened to a pulsating balloon of some small radius R . The specific acoustic impedance Z_s of the air presented to each square centimeter of the balloon is given by Eq. (4.69) and Fig. 4.13. At low frequencies, the impedance becomes nearly purely reactive, and the resistance becomes very small. Hence, the power radiated by a small loudspeaker becomes very small. At high frequencies, $kR > 2$, the impedance Z_s becomes nearly purely resistive and has its maximum value of $\rho_0 c$ so that the power radiated for a given value of \tilde{U}_0 reaches its maximum.



4.11 RADIATION FROM A MONOPOLE POINT SOURCE (SIMPLE SOURCE)

Pressure and particle velocity

The pressure and particle velocity in the sound field of a monopole point source are obtained by setting $R \rightarrow 0$ in Eqs. (4.65) and (4.67), respectively:

$$\tilde{p}(r) = jk\rho_0c\tilde{U}_0\frac{e^{-jkr}}{4\pi r}, \quad (4.71)$$

$$\tilde{u}(r) = (1 + jkr)\tilde{U}_0\frac{e^{-jkr}}{4\pi r^2}, \quad (4.72)$$

where \tilde{U}_0 is volume velocity in m^3/s of the very small source and is equal to $(4\pi a^2)\tilde{u}_0$, \tilde{p} is sound pressure in Pa at a distance r from the simple source.

Strength of a point source [6]

The magnitude of the total air flow at the surface of a simple source in m^3/s is given by U_0 and is called the *strength of a point source*.

Intensity at distance r

At a distance r from the center of a simple source, the intensity is given by

$$I = \left| \frac{\tilde{p}(r)}{\sqrt{2}} \right|^2 \frac{1}{\rho_0c} = \left| \frac{\tilde{U}_0}{\sqrt{2}} \right|^2 \frac{f^2\rho_0}{4r^2c} \text{ W/m}^2. \quad (4.73)$$

When the dimensions of a source are *much smaller* than a wavelength, the radiation from it will be much the same no matter what shape the radiator has, as long as all parts of the radiator vibrate substantially in phase. The intensity at any distance is directly proportional to the square of the volume velocity and the frequency. We will show in Section 12.2 how the point source itself can form a very useful building block for solving problems in acoustics.



4.12 COMBINATION OF POINT SOURCES

The basic principles governing the directivity patterns from loudspeakers can be learned by studying combinations of simple sources. This approach is very similar to the consideration of Huygens wavelets in optics, which will be discussed more in Section 12.1. Basically, our problem is to add, vectorially, at the desired point in space, the sound pressures arriving at that point from all the simple sources. Let us see how this method of analysis is applied.

Two point sources

The geometric situation is shown in Fig. 4.14. It is assumed that the distance r from the two point sources to the point P at which the pressure p is being measured is large compared with the separation b between the two sources.

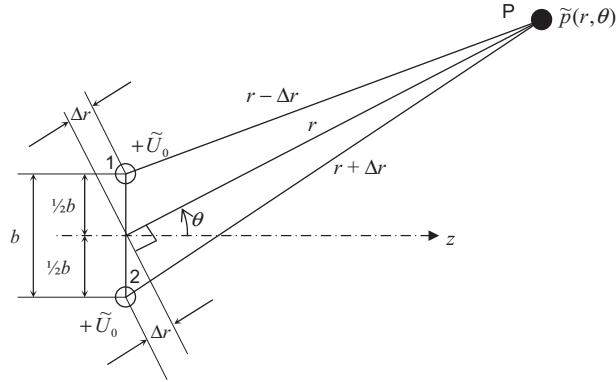


Figure 4.14 Two point (simple) sources vibrating in phase located a distance b apart and at distance r and angle θ with respect to the observation point P .

The spherical sound wave arriving at the point p from source 1 will have traveled a distance $r - \Delta r$ where

$$\Delta r = \frac{1}{2} b \sin \theta \quad (4.74)$$

and from Eq. (4.71) the sound pressure will be

$$\tilde{p}_1(r, \theta) = \frac{\tilde{A}_+}{r - \Delta r} e^{-jk(r - \Delta r)}, \quad (4.75)$$

where

$$\tilde{A}_+ = jk\rho_0 c \tilde{U}_0 / (4\pi).$$

The wave from source 2 will have traveled a distance $r + \Delta r$ so that

$$\tilde{p}_2(r, \theta) = \frac{\tilde{A}_+}{r + \Delta r} e^{-jk(r + \Delta r)}. \quad (4.76)$$

The sum of $p = p_1 + p_2$, assuming $r \gg b$, gives

$$\tilde{p}(r, \theta) = \frac{\tilde{A}_+}{r} e^{-jkr} (e^{jk\Delta r} + e^{-jk\Delta r}). \quad (4.77)$$

Noting that $e^{jx} = \cos x + j \sin x$ yields

$$\tilde{p}(r, \theta) = \frac{2\tilde{A}_+}{r} e^{-jkr} D(\theta), \quad (4.78)$$

where the directivity function $D(\theta)$ is given by $D(\theta) = \cos k\Delta r$. Substituting Eq. (4.74) and $k = 2\pi/\lambda$ in Eq. (4.78) gives

$$D(\theta)_{in-phase} = \cos((\pi b/\lambda) \sin \theta). \quad (4.79)$$

Note that if we reverse the polarity of one of the sources, we obtain

$$D(\theta)_{antiphase} = j \sin((\pi b/\lambda) \sin \theta), \quad (4.80)$$

which we will use together with Eq. (4.79) in Chapter 13 to derive the directivity pattern of two pistons in an infinite baffle.

Referring to Fig. 4.14, we see that if b is very small compared with a wavelength, the two sources essentially coalesce and the pressure at a distance r at any angle θ is double that for one source acting alone. The directivity pattern will be that of Fig. 4.25 for a pulsating sphere, i.e., omnidirectional.

As b gets larger, however, the pressures arriving from the two sources will be different in phase and the directivity pattern will not be a circle. In other words, the sources will radiate sound in some directions better than in others. Maxima will occur when

$$m\lambda = b \sin \theta, \quad m = 0, 1, \dots \quad (4.81)$$

and nulls will occur when

$$\left(m + \frac{1}{2}\right)\lambda = b \sin \theta, \quad m = 0, 1, \dots \quad (4.82)$$

As a specific example, let $b = \lambda/2$. For $\theta = 0$ or 180 degrees, it is clear that the pressure arriving at a point P will be double that from either source. However, for $\theta = \pm 90$ degrees, the time of travel between the two simple sources is just right so that the radiation from one source completely cancels the radiation from the other. Hence, the pressure at all points along the ± 90 degrees axis is zero. Remember, we have limited our discussion to $r \gg b$.

Directivity patterns, expressed in decibels relative to the pressure at $\theta = 0$, are given in Fig. 4.15 for the two in-phase sources with $b = \lambda/4$; $\lambda/2$; λ ; $3\lambda/2$; and 2λ .

A very important observation can be made from the directivity patterns for this simple type of radiator that applies to all types of radiation. The longer the extent of the radiator (i.e., here, the greater b is), the sharper will be the principal lobe along the $\theta = 0$ axis at any given frequency and the greater the number of side lobes. As we shall see in the next paragraph, it is possible to suppress the side lobes, that is to say, those other than the principal lobes at 0 and 180 degrees, by simply increasing the number of elements.

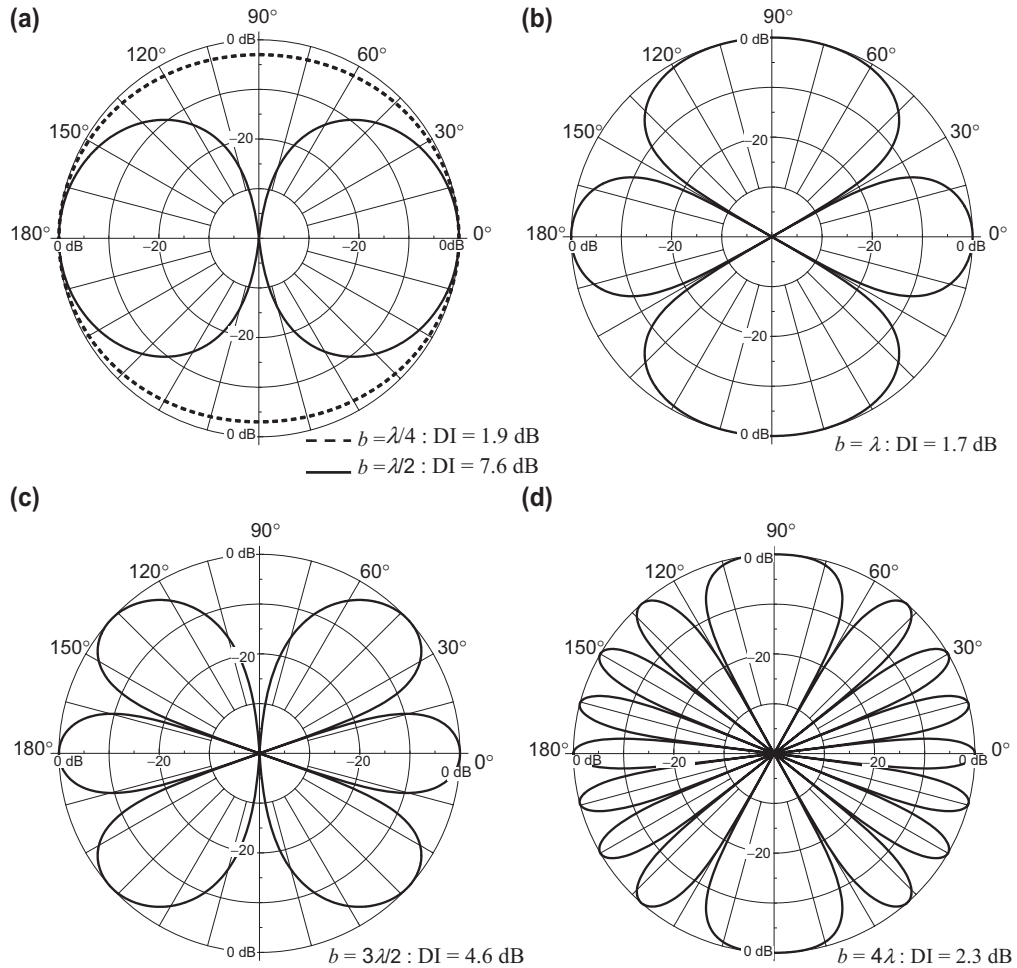


Figure 4.15 Far-field directivity patterns for the two in-phase point sources of Fig. 4.14. Symmetry of the directivity patterns occurs about the axis passing through the two sources. Hence, only a single plane is necessary to describe the directivity characteristics at any particular frequency. The directivity index (DI) is given at $\theta = 0^\circ$. (The directivity index is discussed in Section 4.16.)

Linear array of point sources

The geometric situation for this type of radiating array is shown in Fig. 4.16. The sound pressure produced at a point P by N identical in-phase point sources, lying in a straight line, the sources at distance b apart and with the extent $d = (N - 1)b$ small compared with the distance r , is

$$\tilde{p}(r, \theta) = N \frac{\tilde{A}_+}{r} e^{-jkr} D(\theta), \quad (4.83)$$

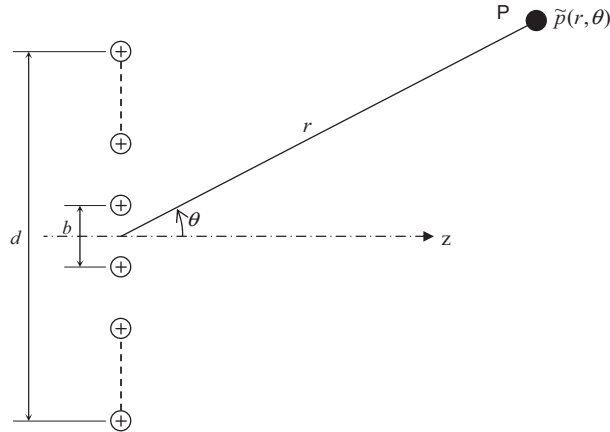


Figure 4.16 A linear array of N simple sources, vibrating in phase, located a distance b apart. The center of the array is at distance r and angle θ with respect to the observation point P .

where

$$D(\theta) = \frac{1}{N} \sum_{n=(1-N)/2}^{(N-1)/2} e^{-jnkb \sin \theta} = \frac{1}{N} \sum_{n=(1-N)/2}^{(N-1)/2} \cos(nkb \sin \theta). \quad (4.84)$$

Using the identity of Eq. (A2.51) from Appendix II, this simplifies to

$$D(\theta) = \frac{\sin((N\pi b/\lambda) \sin \theta)}{N \sin((\pi b/\lambda) \sin \theta)}. \quad (4.85)$$

Note that for $N = 2$ we can use the identity $\sin 2x = 2 \sin x \cos x$ (from Eq (A2.47) of Appendix II) to obtain Eq. (4.79).

From Fig. 4.17d, we see that when the wavelength is smaller than the pitch b of the point sources, we have global maxima with an amplitude of 0 dB and local maxima of smaller amplitude in between. The ratio between the amplitudes of the global maxima and the smallest local maxima approaches N as N increases. In this case, where $N = 4$, the ratio is 3.7 or 11.3 dB. Global maxima will occur when

$$m\lambda = b \sin \theta, \quad m = 0, 1, \dots \quad (4.86)$$

and nulls will occur when

$$m\lambda = Nb \sin \theta, \quad \begin{cases} m = 1, 2, \dots \\ m \neq 0, N, 2N, \dots \end{cases} \quad (4.87)$$

Hence, the global maxima are determined by the pitch of the individual point sources and the nulls are determined by the total length of the array. The global maxima correspond to the sampling wave number (or spatial sampling frequency) k_S of the array, which is the wave number at which the point sources are one wavelength apart, so that $k_S = 2\pi/b$. In this case, $d = 3b$ so that $\lambda_S = d/3$. Below this wavelength, the maxima of the directivity function no longer decay with increasing angle but begin to rise again after a specific angle given by $\lambda = 2b \sin \theta$. This phenomenon is known as *spatial aliasing* and is particularly important for microphone arrays.

As a special case, let us assume that the number of points becomes very large and that the separation b becomes very small. Then, as before,

$$d = (N - 1)b \approx Nb \quad (4.88)$$

which we insert into Eq. (4.85) and, noting that the denominator term $N \sin(\pi d/(N\lambda) \sin \theta) \rightarrow (\pi d/\lambda) \sin \theta$ as $N \rightarrow \infty$, we obtain the following directivity function for a linear line array

$$D(\theta) = \frac{\sin((\pi d/\lambda) \sin \theta)}{(\pi d/\lambda) \sin \theta}. \quad (4.89)$$

As before, it is assumed that the extent of the array d is small compared with the distance r . Nulls will occur when

$$m\lambda = d \sin \theta, \quad m = 1, 2, \dots \quad (4.90)$$

Now that there are no spaces between the point sources, which have coalesced into a line source, the global maxima have vanished and we are left with local maxima that decay with increasing angle θ .

Plots of Eq. (4.85) for $N = 4$ and $d = \lambda/4, \lambda/2, \lambda, 3\lambda/2,$ and 2λ are shown in Fig. 4.17. Similar plots for $N \rightarrow \infty$ and $b \rightarrow 0$, that is, Eq. (4.89), are given in Fig. 4.18.

The principal difference among Figs. 4.15, 4.17, and 4.18 for a given ratio of array length to wavelength is in the suppression of the “side lobes.” That is, sound is radiated well in the $\theta = 0$ degree and $\theta = 180$ degrees directions for all three arrays. However, as the array becomes longer and the number of elements becomes greater, the radiation becomes less in other directions than at $\theta = 0$ degree and $\theta = 180$ degrees.



4.13 STEERED BEAM-FORMING ARRAY OF POINT SOURCES

We saw in the previous paragraph that at high frequencies a linear array of point sources becomes highly directional. There are many applications in acoustics where we wish to concentrate sound in a particular direction or, in the case of microphones,

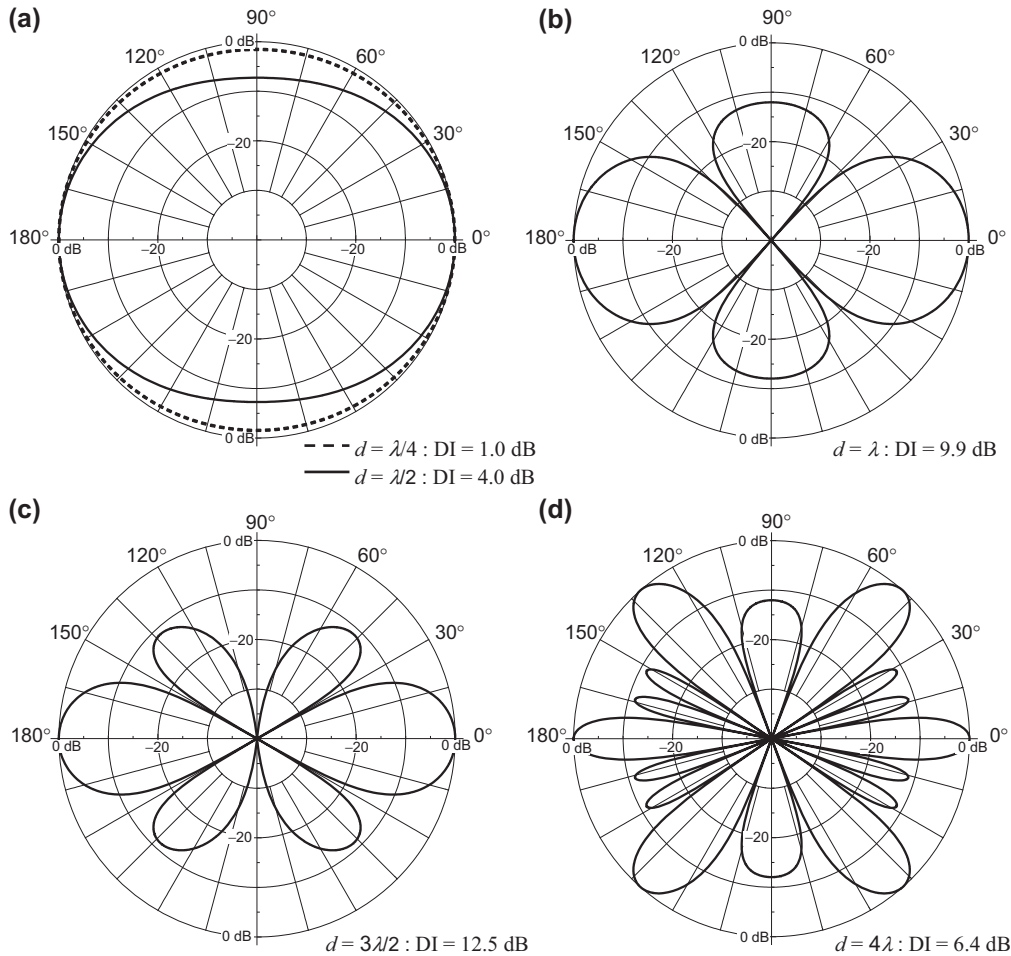


Figure 4.17 Far-field directivity patterns for a linear array of four simple in-phase sources evenly spaced over a length d . The directivity index (DI) is given at $\theta = 0^\circ$.

receive sound from a particular direction while blocking unwanted sounds from elsewhere. This can be achieved by applying appropriate time delays or advances to the point sources as shown in Fig. 4.19 to “steer” the beam in the desired direction at an angle α to the z axis. The other difference between Fig. 4.19 and the previous Fig. 4.16 is that we have rotated the reference z axis by 90 degrees so that it is now the axis of rotational symmetry. This is important when we come to optimize the array.

Although in this example delays *and* advances are applied to the sources in the positive and negative z positions, respectively, we would in practice only use delays so that the source with the largest advance would have zero delay and the delay would increase

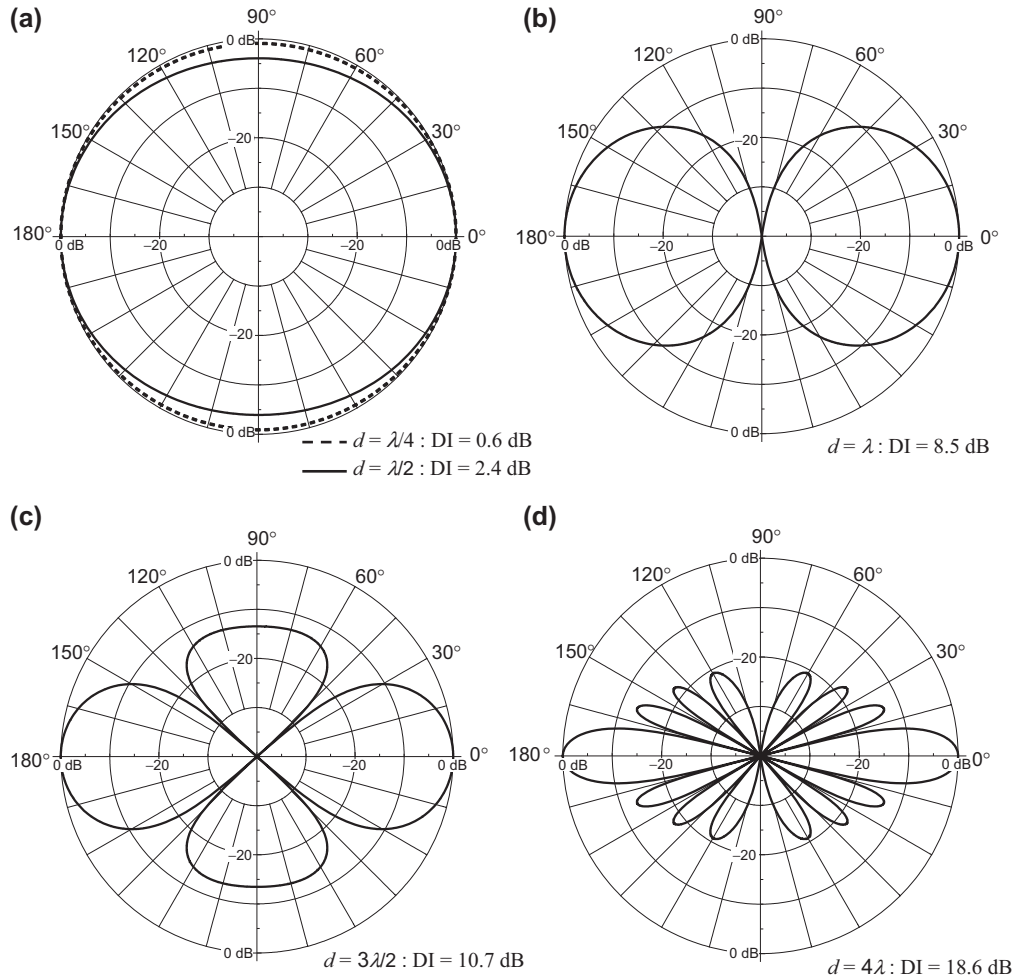


Figure 4.18 Far-field directivity patterns for a linear line array radiating uniformly along its length d . The directivity index (DI) is given at $\theta = 0^\circ$.

progressively toward the source with the largest delay, which would have its delay doubled. However, the symmetrical arrangement shown in Fig. 4.19 simplifies the analysis somewhat. In the first instance, let us assume that all the sources have equal strengths. Then, we can write

$$D(\theta) = \frac{1}{N} \sum_{n=(1-N)/2}^{(N-1)/2} e^{-jnkb(\cos \theta - \cos \alpha)}. \quad (4.91)$$

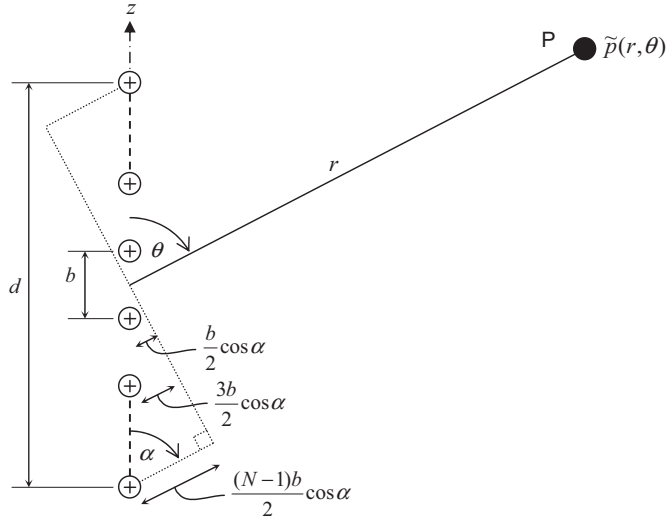


Figure 4.19 A steered beam-forming array of N simple sources, located a distance b apart and vibrating with different phases. The time advance applied to each source at a negative distance z from the center is given by the distance shown divided by the speed of sound c . Each source at a positive distance z from the center (not marked) has a time delay equal to the time advance of its opposite source the same negative z from the center. The center of the array is at distance r and angle θ with respect to the observation point P .

For simplicity, let us assume an even number of sources N so that the contribution from each side is equal and the sinusoidal parts of the exponents cancel each other

$$D(\theta) = \frac{2}{N} \sum_{n=1}^{N/2} \cos \left(\left(n - \frac{1}{2} \right) kb(\cos \theta - \cos \alpha) \right), \quad (4.92)$$

which leads to

$$D(\theta) = \frac{\sin((N\pi b/\lambda)(\cos \theta - \cos \alpha))}{N \sin((\pi b/\lambda)(\cos \theta - \cos \alpha))}. \quad (4.93)$$

which is plotted for $d = \lambda/2$ and $d = 5\lambda$ in Fig. 4.20a and b, respectively. We see that when the wavelength is greater than the length d of the array, the directivity degenerates to virtually omnidirectional. However, we can add different weightings A_n to the sources and optimize them using a technique known as the *least mean squares* method:

$$D(\theta) = \frac{2}{N} \sum_{n=1}^{N/2} A_n \cos \left(\left(n - \frac{1}{2} \right) kb(\cos \theta - \cos \alpha) \right). \quad (4.94)$$

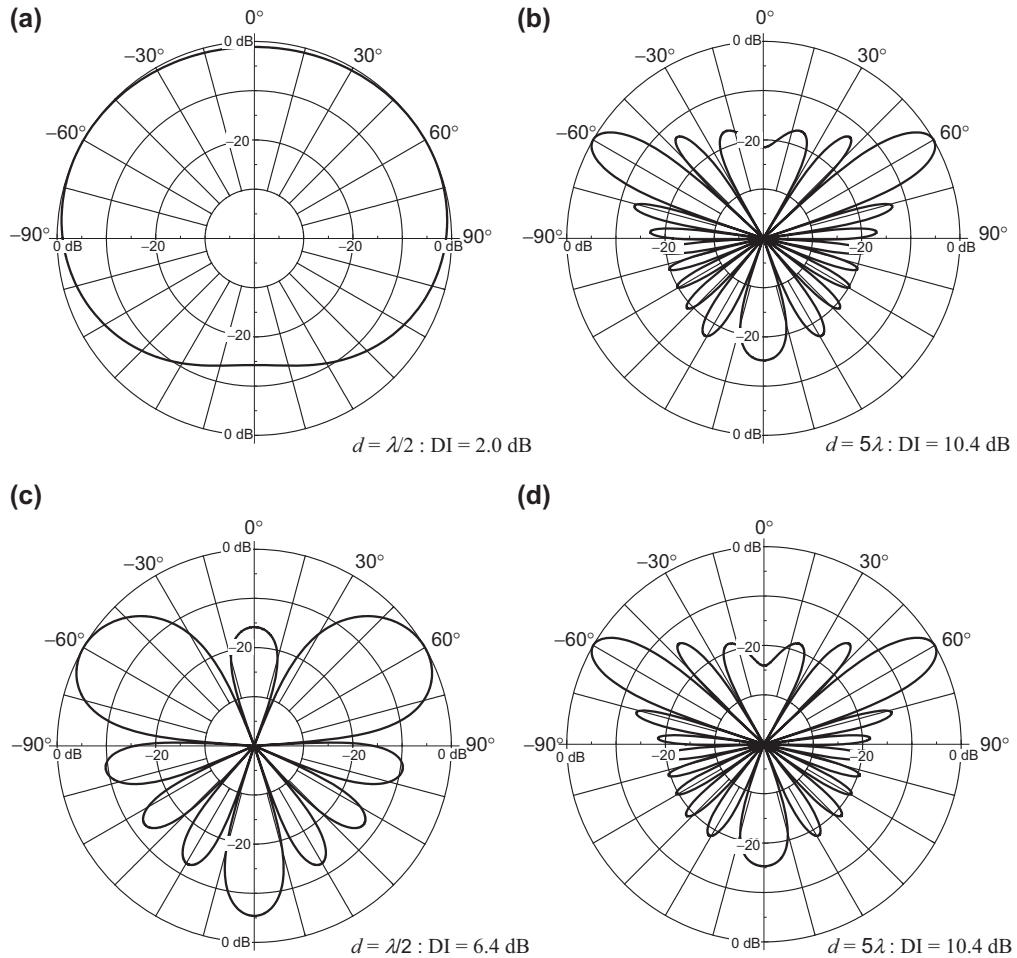


Figure 4.20 Far-field directivity patterns for a beam-forming array of 10 simple sources evenly spaced over a length d , where the steering angle $\alpha = 60$ degrees. The directivity index (DI) is given at $\theta = \alpha$. In (a) and (b) are shown directivity patterns for 10 sources of equal strength but with different time delays/advances according to Fig. 4.19. In (c) and (d) are shown directivity patterns for 10 sources with the same time delays/advances as (a) and (b) but with strengths optimized using the least-mean-squares method.

First of all, we define a target or reference directivity function $D_{ref}(\theta)$ to which we wish to find the best “fit.” The ideal directivity function is simply an infinite impulse at the angle α , which can be written using the Dirac delta function:

$$D_{ref}(\theta) = \delta(\theta - \alpha). \quad (4.95)$$

Of course, we may choose any function we like for $D_{ref}(\theta)$ depending on what directivity pattern we are aiming for. Let us define an error function $E(A_n)$ as

$$E(A_n) = \int_{-\pi}^{\pi} |D(\theta) - D_{ref}(\theta)|^2 \sin \theta d\theta. \quad (4.96)$$

To minimize the error, we differentiate it with respect to A_n and set the result to zero:

$$\begin{aligned} \frac{\partial}{\partial A_n} E(A_n) &= 2 \int_{-\pi}^{\pi} \cos((m - 1/2)kb(\cos \theta - \cos \alpha)) \\ &\times (D(\theta) - D_{ref}(\theta)) \sin \theta d\theta = 0, \quad m = 1, 2, \dots, N, \end{aligned} \quad (4.97)$$

which can be expressed in the following short form:

$$\sum_{n=1}^{N/2} A_n I_{mn} = J_m, \quad m = 1, 2, \dots, N, \quad (4.98)$$

where

$$I_{mn} = \frac{2}{N} \int_{-\pi}^{\pi} \cos((m - 1/2)kb(\cos \theta - \cos \alpha)) \cos((n - 1/2)kb(\cos \theta - \cos \alpha)) \sin \theta d\theta. \quad (4.99)$$

The evaluation of the integral I_{mn} has two parts

$$I_{mn} = K_{mn} + L_{mn}, \quad (4.100)$$

where

$$K_{mn} = \begin{cases} \frac{\sin((m - n)kb(1 + \cos \alpha)) + \sin((m - n)kb(1 - \cos \alpha))}{N(m - n)kb}, & m \neq n \\ \frac{2}{N}, & m = n, \end{cases} \quad (4.101)$$

$$L_{mn} = \frac{\sin((m + n - 1)kb(1 + \cos \alpha)) + \sin((m + n - 1)kb(1 - \cos \alpha))}{N(m + n - 1)kb}, \quad (4.102)$$

and

$$J_m = \int_{-\pi}^{\pi} D_{ref}(\theta) \cos((m - 1/2)kb(\cos \theta - \cos \alpha)) \sin \theta d\theta = \sin \alpha. \quad (4.103)$$

where we have used the property of the Dirac delta function from Eq. (A2.154) of Appendix II. Eq. (4.98) is a set of simultaneous equations which we now write in matrix form

$$\mathbf{M} \cdot \mathbf{a} = \mathbf{b} \Rightarrow \mathbf{a} = \mathbf{M}^{-1} \cdot \mathbf{b} \quad (4.104)$$

where

$$\mathbf{M}(m, n) = I_{mn} = K_{mn} + L_{mn} \quad (4.105)$$

$$\mathbf{a}(n) = A_n \quad (4.106)$$

$$\mathbf{b}(m) = J_m = \sin \alpha \quad (4.107)$$

Directivity patterns are plotted from Eq. (4.94) for $d = \lambda/2$ and $d = 5\lambda$ in Fig. 4.20c and d, respectively, using coefficients A_n calculated from Eqs. (4.101), (4.102), and (4.104). We see that for small wavelengths ($\lambda = d/5$), there is very little difference between the directivity pattern of the sources of equal strengths in (b) and that of the optimized sources in (d).

Here the optimized weightings are:

$$A_{\pm 1} = 4.72, A_{\pm 2} = 5.00, A_{\pm 3} = 4.90, A_{\pm 4} = 4.53, A_{\pm 5} = 4.64,$$

so there is no more $\pm 5\%$ variation between them.

However, there is a significant increase in directivity when the wavelength is larger than d ($\lambda = 2d$) as can be seen from (a) and (c).

But this comes at the expense of efficiency with optimized weightings of

$$A_{\pm 1} = 1,027,841, A_{\pm 2} = -2,097,341, A_{\pm 3} = 1,559,833,$$

$$A_{\pm 4} = -580,418, A_{\pm 5} = 90,094,$$

the sum of which is just 9. Hence, they virtually cancel each other!

Beam-forming arrays often have source strengths that progressively decrease toward the outer edges to reduce the side lobes. These are known as “shaded arrays” [7] and the technique is similar to windowing as used in Fourier transforms. Of course, delays can also be used in arrays to prevent high-frequency beaming so that the directivity pattern is as wide as possible regardless of wavelength [8].



4.14 DIPOLE POINT SOURCE (DOUBLET)

A dipole point source is a pair of monopole point sources separated by a very small distance and vibrating in opposing phase. The geometric situation is shown in Fig. 4.21. The average distance r to the observation point P is assumed to be large compared with the separation b between the two sources.

It can be clearly seen that the sound pressure at $\theta = 90$ degrees and $\theta = 270$ degrees will be zero because the contribution at those points will be equal from the two sources

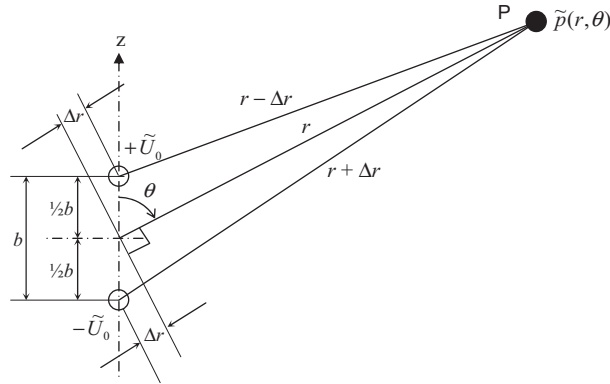


Figure 4.21 Geometry of dipole point source.

and 180 degrees out of phase. The pressures at $\theta = 0$ degree and $\theta = 180$ degrees will depend on the ratio of b to the wavelength λ . For example, if $b = \lambda$, we shall have zero sound pressure at those angles just as we did for $b = \lambda/2$ in the case of two in-phase sources. In the present case, we have a maximum pressure at $\theta = 0$ degree and $\theta = 180$ degrees for $b = \lambda/2$.

The usual case of interest, however, is the one for

$$b \ll \lambda \quad (4.108)$$

Obviously, the separation distance b can never be zero as this would result in complete cancellation of the two monopole outputs. As we shall see, their combined output is directly proportional to b . From Fig. 4.21, we have the following relationship

$$\Delta r = \frac{1}{2} b \cos \theta. \quad (4.109)$$

We can now write the pressure field as the sum of the two monopole point sources from Eq. (4.71) as follows:

$$\begin{aligned} \tilde{p}_d(r, \theta) &= \frac{jk\rho_0 c \tilde{U}_0}{4\pi} \left(\frac{e^{-jk(r-\Delta r)}}{r-\Delta r} - \frac{e^{-jk(r+\Delta r)}}{r+\Delta r} \right) \\ &= \frac{jk\rho_0 c \tilde{U}_0 e^{-jkr}}{4\pi} \left(\frac{(r+\Delta r)e^{jk\Delta r} - (r-\Delta r)e^{-jk\Delta r}}{r^2 - (\Delta r)^2} \right), \end{aligned} \quad (4.110)$$

where \tilde{U}_0 is the volume velocity of each source. Because $\Delta r < r$, we ignore the $(\Delta r)^2$ term in the denominator. This gives an error of $\leq 1\%$ for $r \geq 5b$, depending on θ . Also, we can expand the exponents within the parentheses in Eq. (4.110) as follows:

$$e^{\pm jk\Delta r} = \cos k\Delta r \pm j \sin k\Delta r. \quad (4.111)$$

Substituting Eq. (4.111) into Eq. (4.110) we obtain

$$\tilde{p}_d(r, \theta) = jk\rho_0c\tilde{U}_0 \left(2j \sin k\Delta r + 2 \frac{\Delta r}{r} \cos k\Delta r \right) \frac{e^{-jkr}}{4\pi r}. \quad (4.112)$$

We can make further approximations based on the assumption that the path difference Δr is very small in comparison with the wavelength λ as follows:

$$\sin k\Delta r \approx k\Delta r, \quad \cos k\Delta r \approx 1. \quad (4.113)$$

This gives an additional error of $<1.4\%$ for $kb \cos \theta < 0.5$. Substituting Eqs. (4.109) and (4.113) in Eq. (4.112) yields

$$\tilde{p}_d(r, \theta) = j(kb\rho_0c\tilde{U}_0) \left(\frac{1}{r} + jk \right) \frac{e^{-jkr}}{4\pi r} \cos \theta, \quad (4.114)$$

where $\tilde{U}_0 =$ strength in m^3/s of each point source and the first term in parentheses is a force known as the *dipole strength*.

The ratio of the complex sound pressure \tilde{p}_d produced by the dipole point source to the complex sound pressure \tilde{p}_m produced by a monopole point source is found by dividing Eq. (4.114) by Eq. (4.71). This division yields

$$\frac{\tilde{p}_d(r, \theta)}{\tilde{p}_m(r, \theta)} = -\frac{b}{r} (1 + jkr) \cos \theta. \quad (4.115)$$

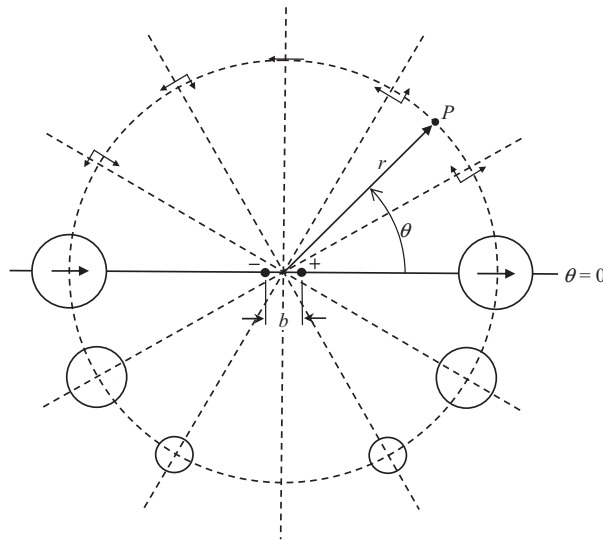


Figure 4.22 Dipole point source. This type of source consists of two monopole point sources vibrating 180 degrees out of phase. They are located a distance b apart and are at an angle θ and a distance r with respect to the observation point P . The lower half of the graph shows by the area of the circles the magnitude of the sound pressure as a function of angle θ . The upper half of the graph shows the variation of the radial and azimuthal components of the particle velocity as a function of angle θ .

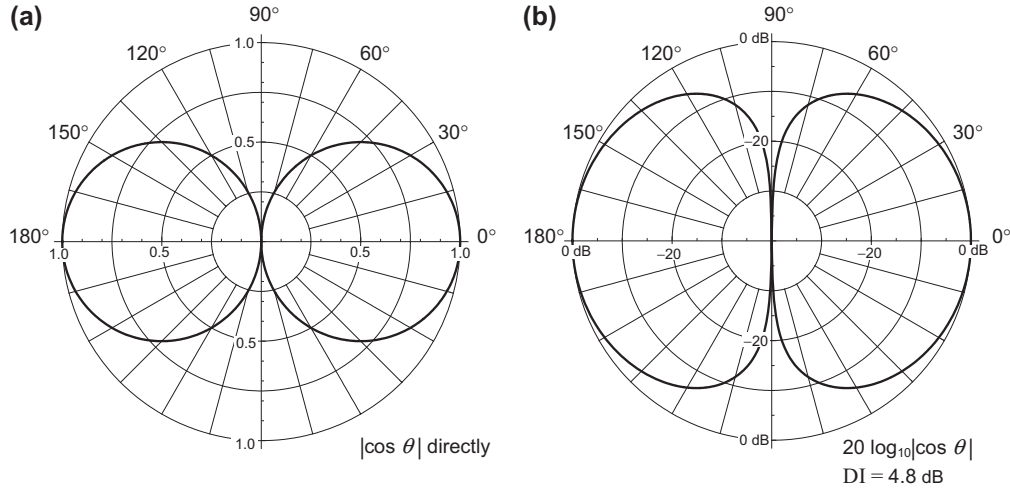


Figure 4.23 Far-field directivity pattern for a dipole point sound source (a) on a linear scale and (b) on a logarithmic scale. The directivity index (DI) is given at $\theta = 0^\circ$.

When the square of the distance r from the acoustic doublet is large compared with $\lambda^2/36$ ($k^2 r^2 \gg 1$), Eq. (4.114) reduces to

$$\tilde{p}_d(r, \theta) = -\frac{\omega^2 \rho_0 \tilde{U}_0 b}{c} \frac{e^{-jkr}}{4\pi r} \cos \theta. \quad (4.116)$$

For this case, the pressure varies with θ as shown in Figs. 4.22 and 4.23. It changes inversely with distance r in exactly the same manner as for the simple source.

Near the acoustic doublet, for $r^2 \ll \lambda^2/36$ (that is, $k^2 r^2 \ll 1$), Eq. (4.114) reduces to

$$\tilde{p}_d = \omega \rho_0 \tilde{U}_0 b \frac{e^{j(\pi/2 - kr)}}{4\pi r^2} \cos \theta. \quad (4.117)$$

For this case, the pressure also varies with $\cos \theta$ as shown in Fig. 4.23, but it changes inversely with the square of the distance r . We are still assuming that $r \gg b$. We can also derive the particle velocity $\tilde{u}(r, \theta)$ from Eq. (4.114) using Eq. (2.4a) as follows:

$$\begin{aligned} \tilde{u}(r, \theta) &= \frac{1}{-jk\rho_0 c} \frac{\partial}{\partial r} \tilde{p}(r, \theta) \\ &= \tilde{U}_0 b \left(\frac{2}{r^2} - k^2 + j \frac{2k}{r} \right) \frac{e^{-jkr}}{4\pi r} \cos \theta. \end{aligned} \quad (4.118)$$

Now we can derive the free-field specific acoustic impedance by dividing the pressure from Eq. (4.114) by the particle velocity from Eq. (4.118) as follows:

$$\begin{aligned} z_s &= \frac{\tilde{p}(r, \theta)}{\tilde{u}(r, \theta)} = \frac{jkr(1 + jkr)}{2 - k^2r^2 + 2jkr} \rho_0 c \\ &= \frac{k^4 r^4 + j(k^3 r^3 + 2kr)}{k^4 r^4 + 4} \rho_0 c. \end{aligned} \quad (4.119)$$

In the near field where $kr \ll 1$, the imaginary part of the impedance dominates and so the load is mass-like. This results from the fact that, at low frequencies in particular, we have a virtual acoustic short circuit between the two sources. Therefore, the dipole has to move a significant amount of air to radiate any sound. However, in the far field, the waves are spherically diverging and the impedance approaches the characteristic impedance of free space

$$z_s|_{kr \rightarrow \infty} = \rho_0 c. \quad (4.120)$$

Near-field and far-field

The difference between *near-field* and *far-field* behaviors of sources must always be borne in mind. When the directivity pattern of a loudspeaker or some other sound source is presented in a technical publication, it is always understood that the data were taken at a distance r sufficiently large so that the sound pressure was decreasing linearly with distance along a radial line connecting with the source, as was the case for Eq. (4.116). This is the *far-field* case. For this to be true, two conditions usually have to be met. First, the extent b of the radiating array must be small compared with r , and r^2 must be large compared with $\lambda^2/36$. In acoustics, the size factor indicated is usually taken to be larger than 3 to 10.

One more item is of interest in connection with the acoustic doublet. The particle velocity is composed of two components: one radially directed and the other perpendicular to that direction. At $\theta = 0$ and 180 degrees, the particle velocity is directed radially entirely (see Fig. 4.22). At $\theta = 90$ and 270 degrees, the particle velocity is entirely perpendicular to the radial line. In between, the radial component varies as the $\cos \theta$ and the perpendicular component as the $\sin \theta$.

An interesting fact is that at $\theta = 90$ and 270 degrees, a doublet sound source appears to propagate a transversely polarized sound wave. To demonstrate this, take two unbaffled small loudspeakers into an anechoic chamber. Unbaffled loudspeakers (transducers) are equivalent to doublets because the pressure increases on one side of the diaphragm whenever it decreases on the other. Hold the two transducers about 0.5 m apart with *both* diaphragms facing the floor (not facing each other). Let one transducer radiate a low-frequency sound and the other act as a microphone connected to the input of an audio amplifier. As we see from Fig. 4.22, no sound pressure will be produced at the

diaphragm of the microphone, but there will be transverse particle velocity. A particle velocity is always the result of a pressure gradient in the direction of the velocity. Therefore, the diaphragm of the microphone will be caused to move when the two transducers are held as described above. When one of the transducers is rotated through 90 degrees about the axis joining the units, the diaphragm of the microphone will not move because the pressure gradient will be in the plane of the diaphragm. Hence, the sound wave appears to be plane polarized.

You have now learned the elementary principles governing the directional characteristics of sound sources. We shall be able to use these principles in understanding the measured or calculated behavior of some of the more complicated sound sources found in acoustics.



4.15 RADIATION FROM AN OSCILLATING SPHERE

We saw that the monopole point source is effectively a pulsating sphere with an infinitesimally small radius. Similarly, the dipole point source can be considered as a rigid sphere with an infinitesimally small radius oscillating back and forth along its axis. This provides us with some useful insight into the operation of a loudspeaker without any baffle or enclosure whatsoever, but unlike the more accurate circular piston in free space (see Section 13.10), it yields simple closed-form solutions for the pressure field and radiation impedance. As in the case of the pulsating sphere, the impedance can be represented by a simple equivalent circuit. We shall now consider a sphere of radius R that oscillates back and forth along a dipole axis with velocity u_0 as shown in Fig. 4.24 so that the normal surface velocity in the radial direction is $u_0 \cos \theta$. A spherical coordinate system is used where r is the distance from the origin at the center of the sphere and θ is the angle subtended with the dipole axis. The area of each surface element is

$$\delta S = R^2 \sin \theta \delta \theta \delta \phi. \quad (4.121)$$

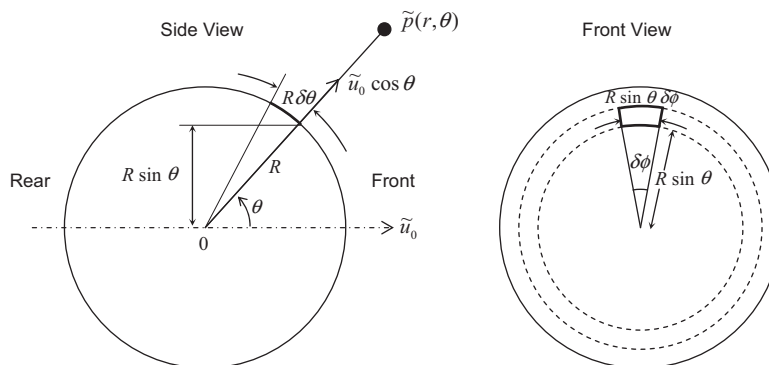


Figure 4.24 Geometry of oscillating sphere.

Near-field pressure

The volume velocity produced by each element is

$$\begin{aligned}\delta\tilde{U}_0 &= \tilde{u}_0 \cos \theta \delta S \\ &= \tilde{u}_0 \cos \theta (R^2 \sin \theta \delta\theta \delta\phi).\end{aligned}\quad (4.122)$$

If we now integrate this over the surface of the sphere, we obtain the volume velocity:

$$\tilde{U}_0 = 2R^2\tilde{u}_0 \int_0^{2\pi} \int_0^{\pi/2} \cos \theta \sin \theta d\theta d\phi = S\tilde{u}_0, \quad (4.123)$$

where S is the *effective* surface area of the sphere (including both front and rear surfaces) given by

$$S = 2\pi R^2. \quad (4.124)$$

We see from Eq. (4.114) that the dipole source produces a pressure field that is proportional to $\cos \theta$ as follows:

$$\tilde{p}(r, \theta) = jk\rho_0 c \tilde{A}_0 \left(\frac{1}{r} + jk \right) \frac{e^{-jkr}}{4\pi r} \cos \theta, \quad (4.125)$$

where the term $\tilde{U}_0 b$ has been replaced with the unknown coefficient $\tilde{A}_0 = \tilde{U}_0 b$. Likewise, from Eq. (4.118) we have the particle velocity

$$\tilde{u}(r, \theta) = \tilde{A}_0 \left(\frac{2}{r^2} - k^2 + j\frac{2k}{r} \right) \frac{e^{-jkr}}{4\pi r} \cos \theta. \quad (4.126)$$

Let us now impose a boundary condition at the surface of the sphere whereby the particle velocity normal to the surface is equal to the angle-dependent surface velocity $\tilde{u}_0 \cos \theta$. Hence, at $r = R$ we have

$$\begin{aligned}\tilde{u}(R, \theta) &= \tilde{A}_0 \left(\frac{2}{R^2} - k^2 + j\frac{2k}{R} \right) \frac{e^{-jkR}}{4\pi R} \cos \theta \\ &= \tilde{u}_0 e^{-jkR} \cos \theta.\end{aligned}\quad (4.127)$$

Solving this for \tilde{A}_0 yields

$$\tilde{A}_0 = \frac{4\pi R^3 \tilde{u}_0}{2 - k^2 R^2 + 2jkR}. \quad (4.128)$$

If we now substitute this in Eq. (4.125), together with $\tilde{U}_0 = 2\pi R^2 \tilde{u}_0$ from Eq. (4.123), we obtain the pressure

$$\tilde{p}(r, \theta) = j\rho_0 c \frac{kR\tilde{U}_0}{2 - k^2 R^2 + 2jkR} \left(\frac{1}{r} + jk \right) \frac{e^{-jkr}}{2\pi r} \cos \theta. \quad (4.129)$$

Far-field pressure

In the far field, where $r \rightarrow \infty$, Eq. (4.129) simplifies to

$$\tilde{p}(r, \theta)|_{r \rightarrow \infty} = jk\rho_0 c \tilde{U}_0 \frac{e^{-jkr}}{4\pi r} D(\theta), \quad (4.130)$$

where

$$D(\theta) = \frac{2jkR}{2 - k^2 R^2 + 2jkR} \cos \theta. \quad (4.131)$$

The directivity pattern $20 \log_{10}(D(\theta)/D(0))$ is plotted in Fig. 4.25 along with that of a pulsating sphere, and the on-axis response $D(0)$ is plotted in Fig. 4.26. It can be seen that when $kR = \sqrt{2}$, the pressure is proportional to *acceleration*:

$$\tilde{p}(r, \theta)|_{r \rightarrow \infty, kR = \sqrt{2}} = jk\rho_0 c \tilde{U}_0 \frac{e^{-jkr}}{4\pi r} \cos \theta. \quad (4.132)$$

At this frequency, we have a resonant peak with a Q factor of $1/\sqrt{2}$. Above this frequency, the pressure is proportional to *velocity* as in the case of the pulsating sphere:

$$\tilde{p}(r, \theta)|_{r \rightarrow \infty, kR \gg 1} = \rho_0 c \frac{\tilde{U}_0}{R} \cdot \frac{e^{-jkr}}{2\pi r} \cos \theta, \quad (4.133)$$

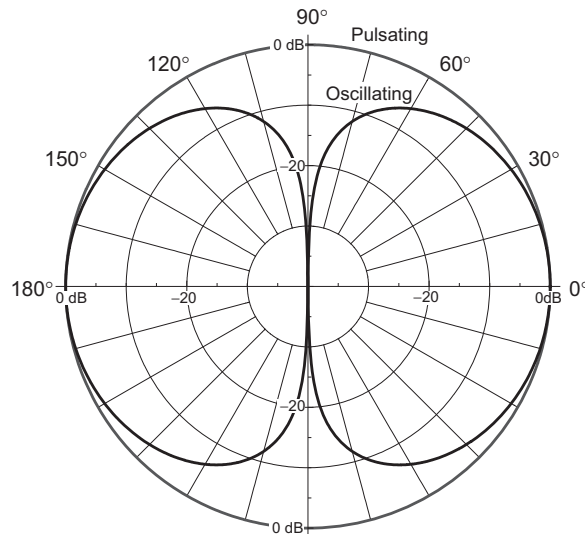


Figure 4.25 Far-field directivity patterns $20 \log_{10}(|D(\theta)|/|D(0)|)$ of the oscillating and pulsating spheres.

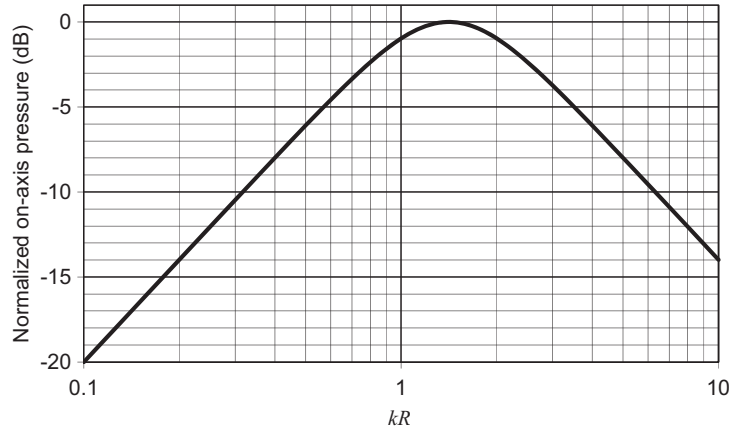


Figure 4.26 Plot of $20 \log_{10}(D(0))$ for an oscillating sphere of radius R with constant axial acceleration. Frequency is plotted on a normalized scale, where $kR = 2\pi R/\lambda = 2\pi fR/c$.

but below it the pressure is proportional to the *time derivative* of the acceleration:

$$\tilde{p}(r, \theta)|_{r \rightarrow \infty, kR \ll 1} = -k^2 R^2 \rho_0 c \frac{\tilde{U}_0}{R} \frac{e^{-jkr}}{4\pi r} \cos \theta. \quad (4.134)$$

When the sphere moves forward, it compresses the air in front of it causing an increase in pressure above static pressure. Similarly, it creates a partial vacuum behind it causing a net decrease in pressure. Hence, the radiated sound pressures in front of and behind it are in *opposite* phases. The antiphase sound from the rear partially cancels the sound from the front at low frequencies. However, complete cancellation never occurs because of the finite path length from the rear to the front of the sphere. Hence, the phase difference is

$$-(1 + 2\delta/\lambda)\pi \text{ radians}$$

where δ is the path length difference and λ is the wavelength. As the frequency decreases, the wavelength increases relative to the path difference and the phase difference asymptotically approaches $-\pi$. This results in a pressure response that falls at a rate of -6 dB per halving of frequency.

In Section 4.14 we derived the pressure field because of a *compact* dipole point source. However, from Eq. (4.112), we can write the equation for the on-axis pressure response of a dipole point source where the spacing Δz_0 between the two point sources is comparable to the wavelength λ of the sound being radiated:

$$\tilde{p}(r, 0) = -\rho_0 \omega \tilde{U}_0 \sin(\pi \Delta z_0 / \lambda) \frac{e^{-jkr}}{2\pi r}, \quad (4.135)$$

from which it can be seen that the pressure magnitude versus frequency, with constant acceleration, is just a series of half sinusoids like a comb filter. Nulls occur when $\Delta z_0 = n\lambda$ and peaks occur when $\Delta z_0 = (n + \frac{1}{2})\lambda$. This is in stark contrast with the oscillating sphere which has a continuous monotonic pressure response with just a single peak and no nulls. This is because the resulting sound field is due to an infinite number of point sources all over the surface according to the Huygens–Fresnel principle, which will be discussed in greater detail in Section 12.1. Hence, there are many path lengths between the rear and front and at no frequency do they all produce a cancellation. However, the peak at $kR = \sqrt{2}$ is because of an *average* path length difference of $\Delta z_0 = \pi R/\sqrt{2}$.

Radiation impedance

The total force \tilde{F} acting on the sphere is obtained by integrating the pressure from Eq. (4.129) over the surface as follows:

$$\begin{aligned} F &= 2R^2 \int_0^{2\pi} \int_0^{\pi/2} \tilde{p}(R, \theta) \cos \theta \sin \theta \, d\theta \, d\phi \\ &= \rho_0 c \tilde{U}_0 \frac{2}{3} \cdot \frac{jkR(1 + jkR)}{2 - k^2 R^2 + 2jkR} e^{-jkR}. \end{aligned} \quad (4.136)$$

The specific radiation impedance Z_s can be written as follows:

$$\begin{aligned} Z_s &= R_s + jX_s = \frac{\tilde{F}}{\tilde{U}_0 e^{-jkR}} \\ &= \frac{2}{3} \cdot \frac{jkR(1 + jkR)}{2 - k^2 R^2 + 2jkR} \rho_0 c \\ &= \frac{2}{3} \cdot \frac{k^4 R^4 + j(k^3 R^3 + 2kR)}{k^4 R^4 + 4} \rho_0 c. \end{aligned} \quad (4.137)$$

It turns out that this is the same as the impedance from Eq. (4.119) for a freely propagating wave due to a dipole point source at a distance R from the origin. The real and imaginary parts, R_s and X_s , are plotted in Fig. 4.27. The main difference between Fig. 4.27 and the impedance of a pulsating sphere shown in Fig. 4.13 is that the real part falls even more rapidly at low frequencies because of the rear wave cancellation. It is proportional to $(kR)^4$ as opposed to $(kR)^2$ in the case of the pulsating sphere. In both cases, the imaginary part is proportional to kR at low frequencies and $1/(kR)$ at high frequencies.

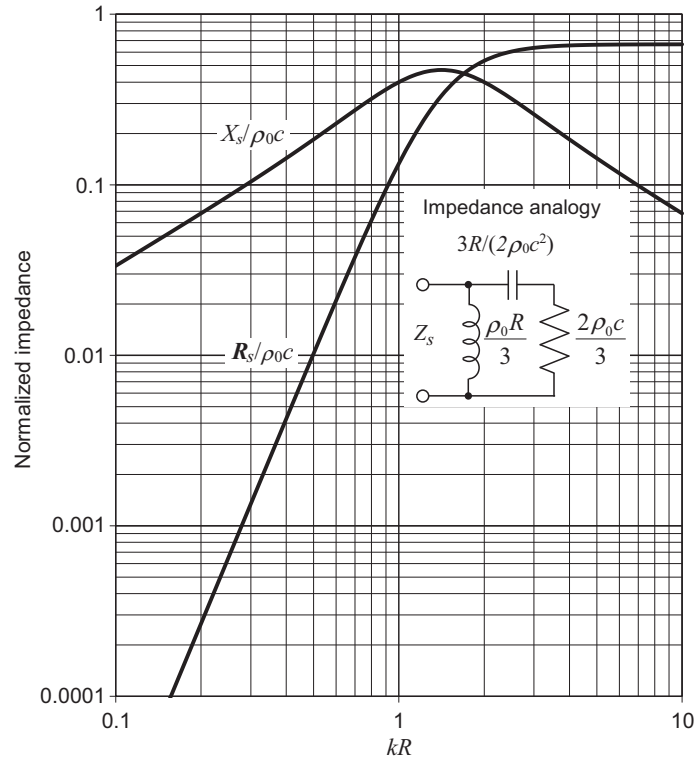


Figure 4.27 Real and imaginary parts of the normalized specific radiation impedance Z_s/ρ_0c of the air load on an oscillating sphere of radius R in free space. Frequency is plotted on a normalized scale, where $kR = 2\pi R/\lambda = 2\pi fR/c$.

PART XII: DIRECTIVITY INDEX

4.16 DIRECTIVITY INDEX AND DIRECTIVITY FACTOR

Charts of the directivity patterns of sound sources are sufficient in many cases, such as when the source is located outdoors at a distance from reflecting surfaces. Indoors, it is necessary in addition to know something about the total power radiated to calculate the reinforcing effect of the reverberation in the room on the output of the sound source. A number is calculated at each frequency that tells the degree of directivity without the necessity for showing the entire directivity pattern. This number is the directivity factor or, when expressed in decibels, the directivity index.

Directivity factor [Q(f)]

The directivity factor is the ratio of the intensity [9] on a designated axis of a sound radiator at a stated distance r to the intensity that would be produced at the same position by a point source if it were radiating the *same* total acoustic power as the radiator. Free space is assumed for the measurements. Usually, the designated axis is taken as the axis of maximum radiation, in which case $Q(f)$ always exceeds unity. In some cases, the directivity factor is desired for other axes where $Q(f)$ may assume any value equal to or greater than zero.

Directivity index [DI(f)]

The directivity index is 10 times the logarithm to the base 10 of the directivity factor:

$$DI(f) = 10 \log_{10} Q(f). \quad (4.138)$$

Calculation of Q(f) and DI(f)

The intensity I at a point removed a distance r from the acoustical center of a source of sound located in free space is determined by first measuring the effective sound pressure p_{rms} and letting $I = |p|_{rms}^2 / \rho_0 c$. If the source is a point source so that I is not a function of V and is located in free space, the total acoustic power radiated is

$$W_p = 4\pi r^2 I.$$

If the source is not a point source, the total acoustic power radiated is determined by summing the intensities over the surface of a sphere of radius r . That is, the total radiated power is

$$W = \frac{r^2}{\rho_0 c} \int_0^{2\pi} \int_0^\pi p_{rms}^2(\theta, \phi, r) \sin \theta \, d\theta \, d\phi, \quad (4.139)$$

where the coordinate of any point in space is given by the angles θ and ϕ and the radius r (see Fig. 4.28) and $P_{rms}^2(\theta, \phi, r)$ equals the mean square sound pressure at the point designated by θ , ϕ , and r .

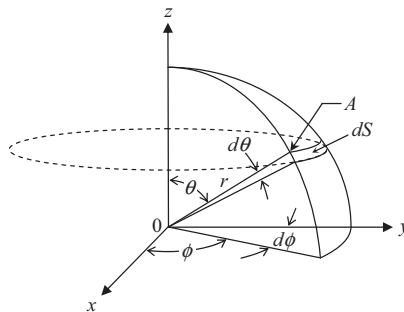


Figure 4.28 Coordinate system defining the angle θ and ϕ and the length r of a line connecting a point A to the center of a sphere. The area of the incremental surface $dS = r^2 \sin \theta \, d\theta \, d\phi$.

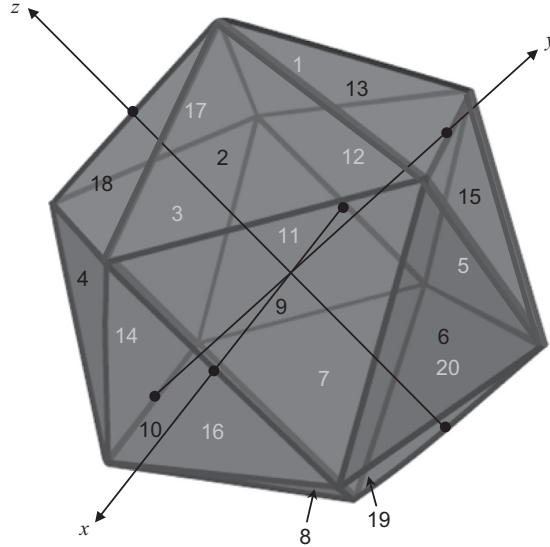


Figure 4.29 Division of a spherical surface into 20 planar surfaces bound by identical equilateral triangles. Black numbers denote surfaces on nearest side and white numbers denote ones on farthest side. Resulting polyhedron is a regular icosahedron, in which the 12 apexes are the corners of three intersecting golden rectangles (that is, having side ratios of $1:(1 + \sqrt{5})/2$) that lie in the xy , yz , and xz planes with their centers at the origin. The coordinates of the midpoints of the sectors are given in [Table 4.2](#).

Usually an analytical expression for $P_{rms}^2(\theta, \phi)$ does not exist. In practice, therefore, data are taken at the centers of a number of areas, approximately equal in magnitude, on the surface of a sphere of radius r surrounding the source. As an example, we show in [Fig. 4.29](#) a spherical surface divided into 20 equal parts of the same shape. The measured intensities on each of these parts may be called I_1, I_2, I_3 , etc. The total power radiated W is found from

$$W = I_1 S_1 + I_2 S_2 + \cdots + I_{20} S_{20}, \quad (4.140)$$

where S_1, S_2, \dots, S_{20} are the areas of the 20 parts of the spherical surface. If, as in [Fig. 4.29](#), the surface is divided into 20 equal parts, then $S_1 = S_2 = S_3 = \dots = S_{20}$.

By definition, the directivity factor $Q(f)$ is

$$Q(f) = \frac{|p_{ax}|^2}{\rho_0 c} \frac{4\pi r^2}{W} = \frac{4\pi |p_{rms}(\theta_{ax}, \phi_{ax})|^2}{\int_0^{2\pi} \int_0^\pi |p_{rms}(\theta, \phi)|^2 \sin \theta \, d\theta \, d\phi}, \quad (4.141)$$

where $|p_{ax}|^2$ is the magnitude of the mean square sound pressure on the designated axis of the sound source at a certain distance r (see [Fig. 4.31](#), 0° axis, as an example).

For the special case where, for any particular value of θ , the sound pressure produced by the sound source is independent of the value of ϕ , that is to say, there is an axis of symmetry, Eq. (4.141) simplifies to

$$Q(f) = \frac{4\pi p_{rms}^2(0)}{2\pi \int_0^\pi p_{rms}^2(\theta) \sin \theta d\theta}. \quad (4.142)$$

where the designated axis is the axis of symmetry. The magnitude signs are left off for convenience. Many sources, such as loudspeakers, are fairly symmetrical about the principal axes so that Eq. (4.142) is valid. We notice that the integral in the denominator has the same form as that of Eq. (13.271) used for the Bouwkamp impedance theorem and thus represents the total radiated power. Also, for pistons of area S , where $R_{AR} = R_s/S$, the on-axis pressure $p(0)$ is given by Eqs. (13.101) and (13.234) so that

$$Q(f) = \frac{k^2 a^2 \rho_0 c |D(0)|^2}{(2) \mathbf{R}_S} \quad (4.143)$$

which is a useful result because the on-axis directivity $D(0)$ and specific radiation resistance \mathbf{R}_S have relatively simple analytical solutions for pistons. Note that $a = \sqrt{S/\pi}$ for a noncircular piston and the number 2 in parentheses is only applicable to dipole pistons. Otherwise, for monopoles, it should be omitted. This is because dipole pistons radiate from both sides and therefore radiate twice as much power as monopoles. For pressure sources,

$$Q(f) = \frac{k^2 a^2 |D(0)|^2}{(2) \mathbf{G}_S \rho_0 c},$$

where \mathbf{G}_S is the specific radiation conductance.

If no analytical solution is available, the only choice is to take measurements at a number of points with the angles θ_n in a horizontal plane around the source so that

$$Q(f) = \frac{(4\pi p_{rms}^2(0))(180^\circ/\pi)}{2\pi \sum_{n=1}^{180^\circ/\Delta\theta} p_{rms}^2(\theta_n) \sin \theta_n \Delta\theta}, \quad (4.144)$$

where $\Delta\theta$ is separation in degrees of the successive points around the sound source at which measurement of $p_{rms}(\theta_n)$ was made (see Fig. 4.31 as an example), $180^\circ/\Delta\theta$ is the number of measurements that were made in passing from a point directly in front of the source to one directly behind the source (0–180 degrees). The sound source is assumed to be symmetrical so that the variation between 360 and 180 degrees is the same as that between 0 and 180 degrees.

If the source is mounted in an infinite baffle, measurement is possible only in a hemisphere. Hence, the value of n in Eq. (4.142) varies from 1 to 90 degrees/ $\Delta\theta$. If the source in an infinite baffle is nondirectional in the hemisphere, which is usually the case for $ka < 0.5$, then the directivity factor $Q = Q_h = 2$, that is, $DI = 3$ dB.

If the directivity pattern is not quite symmetrical, then the factor of 4 in the numerator of Eq. (4.142) becomes 8 and the value of n varies from 1 to 360 degrees/ $\Delta\theta$. This, in effect, averages the two sides of the directivity pattern.

For easy reference, the directivity indexes for (1) a piston in free space, (2) an oscillating sphere in free space, (3) a piston in an infinite plane baffle, (4) a hemispherical dome in an infinite baffle, and (5) a one-sided piston in free space are plotted as a function of ka in Fig. 4.30.

Detailed calculations are shown in Table 4.3 for a box-enclosed loudspeaker having the directivity pattern at a frequency of 3000 Hz shown in Fig. 4.31.

After a directivity factor has been calculated at each frequency, a plot of directivity index $DI(f)$ in decibels is made with the aid of Eq. (4.138). For the loudspeaker with the directivity patterns of Fig. 4.31, the directivity index as a function of frequency is shown in Fig. 4.32.

$$Q(f) = \frac{4\pi \times (180^\circ/\pi)}{2\pi \sum_1^{18} \frac{|p_{rms}(\theta_n)|^2}{|p_{rms}(0)|^2} \sin \theta_n \times 10^\circ} = \frac{11.5}{1.48} = 7.7,$$

$$DI(f) = 10 \log 7.7 = 8.9 \text{ dB}.$$

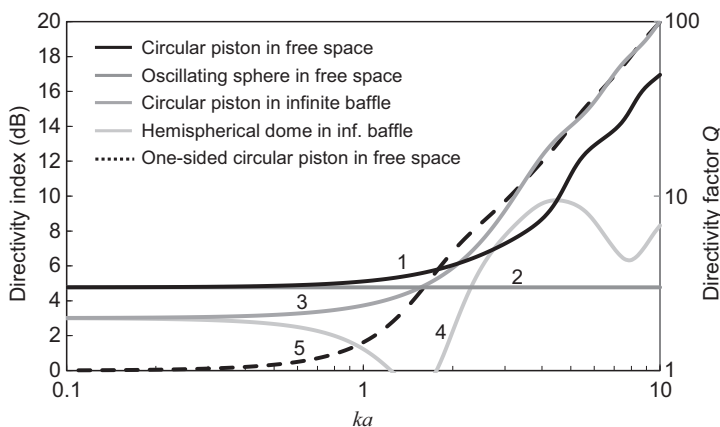


Figure 4.30 Directivity indexes for the radiation from (1) a circular piston in free space without any baffle; (2) an oscillating sphere in free space; (3) a circular piston in an infinite plane baffle; (4) a hemispherical dome in an infinite baffle; and (5) a one-sided circular piston in free space. These are plotted using Eq. (4.143), which is divided by two in the case of the piston and oscillating sphere in free space because they radiate from both sides and hence radiate twice the power. Frequency is plotted on a normalized scale, where $ka = 2\pi a/\lambda = 2\pi fa/c$.

Table 4.2 Coordinates of mid-points of sectors

Sector numbers	Coordinate		
	x	y	z
1–8	$\pm \frac{1}{\sqrt{3}} = \pm 0.577$	$\pm \frac{1}{\sqrt{3}} = \pm 0.577$	$\pm \frac{1}{\sqrt{3}} = \pm 0.577$
9–12	$\frac{\pm 2(\sqrt{5}+2)}{\sqrt{6(3\sqrt{5}+7)}} = \pm 0.934$	$\pm \frac{\sqrt{5}+1}{\sqrt{6(3\sqrt{5}+7)}} = \pm 0.357$	0
13–16	0	$\pm \frac{2(\sqrt{5}+2)}{\sqrt{6(3\sqrt{5}+7)}} = \pm 0.934$	$\pm \frac{\sqrt{5}+1}{\sqrt{6(3\sqrt{5}+7)}} = \pm 0.357$
17–20	$\pm \frac{\sqrt{5}+1}{\sqrt{6(3\sqrt{5}+7)}} = \pm 0.357$	0	$\pm \frac{2(\sqrt{5}+2)}{\sqrt{6(3\sqrt{5}+7)}} = \pm 0.934$

Table 4.3 Calculation of directivity index $DI(f)^a$

θ_n (degrees)	$\sin \theta_n$	Directivity (dB)	$\left \frac{p(\theta_n)}{p_{ax}} \right ^2$	$\left \frac{p(\theta_n)}{p_{ax}} \right ^2 \sin \theta_n$
5	0.087	0.1	1.02	0.09
15	0.259	-0.4	0.92	0.24
25	0.423	-1.5	0.71	0.30
35	0.574	-3.2	0.47	0.27
45	0.707	-5.3	0.30	0.21
55	0.819	-7.4	0.18	0.15
65	0.906	-10.4	0.09	0.08
75	0.966	-14.5	0.04	0.03
85	0.996	-16.9	0.02	0.02
95	0.996	-15.7	0.03	0.03
105	0.966	-16.5	0.02	0.02
115	0.906	-23.1	0.00	0.00
125	0.819	-22.7	0.01	0.00
135	0.707	-18.0	0.02	0.01
145	0.574	-22.3	0.01	0.00
155	0.423	-26.6	0.00	0.00
165	0.259	-16.6	0.02	0.01
175	0.087	-12.9	0.05	0.00
				1.48

^aAt $f = 3000$ Hz for a type 8030A loudspeaker having the directivity patterns shown in Fig. 4.31. The quantity $\Delta\theta = 10$ degrees = $\pi/18$ rad.

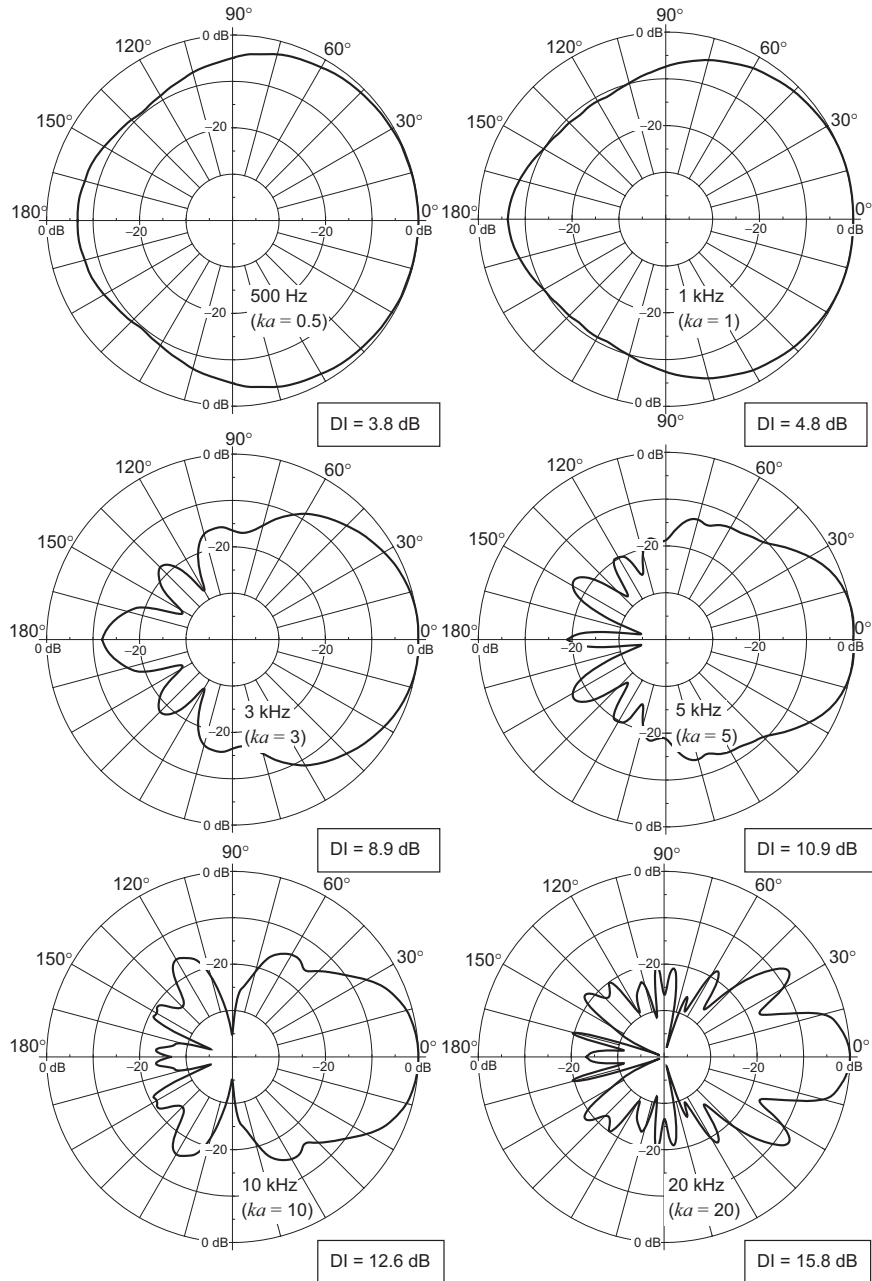


Figure 4.31 Measured directivity patterns for a type 8030A 5-in direct-radiator loudspeaker in a 285- by 189- by 178-mm aluminum box. The squares give the directivity index at $\theta = 0^\circ$. Courtesy of Genelec OY, Finland.

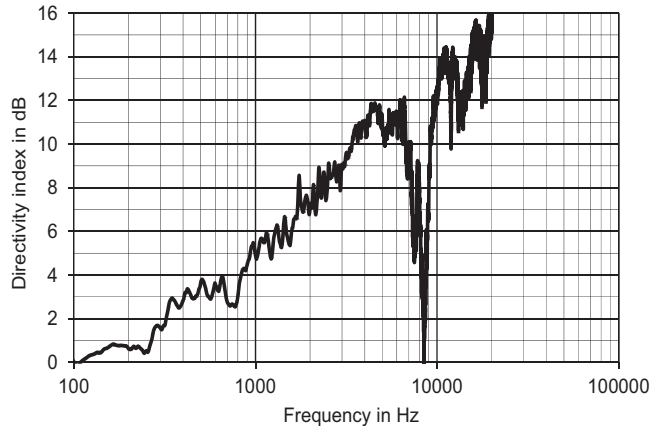


Figure 4.32 Directivity indexes for 0° axes of the directivity patterns of Fig. 4.31. The data apply to a type 8030A 5-in direct-radiator loudspeaker in a 285- by 189- by 178-mm aluminum box. Courtesy of Genelec OY, Finland.

PART XIII: RADIATION IMPEDANCES

4.17 PULSATING SPHERE

In Part XI, we derived the radiation impedance for a sphere with a uniformly pulsating surface. For the results, refer to Eq. (4.69) and Fig. 4.13.

It is seen from Fig. 4.13 that for $kR < 0.3$, that is, when the diameter is less than one-tenth the wavelength, the impedance load on the surface of the sphere is that of a mass reactance because the resistive component is negligible compared with the reactive component.

At all frequencies, the loading shown in Fig. 4.13 may be represented by the equivalent circuits of Fig. 4.33. The element sizes for the mechanical and acoustic admittances and impedances are given with the circuits.

4.18 OSCILLATING SPHERE

In Part XI we derived the radiation impedance for a rigid sphere that oscillates axially. For the results, refer to Eq. (4.137) and Fig. 4.27.

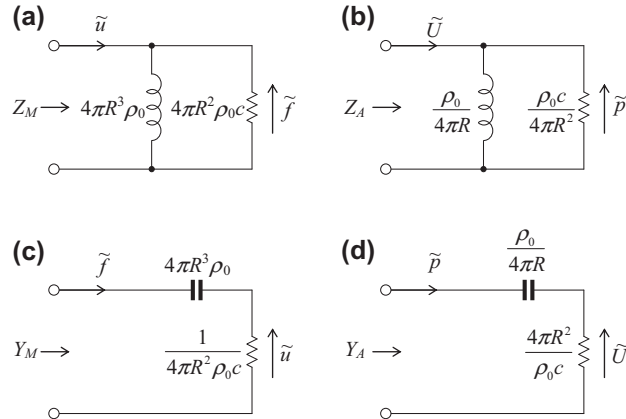


Figure 4.33 Exact radiation impedances and admittances for all values of kR for a sphere with a surface that vibrates radially. (a) Mechanical-impedance analogy; (b) acoustic-impedance analogy; (c) mechanical-admittance analogy; (d) acoustic-admittance analogy. The quantity R is the radius of the sphere.

It is seen from Fig. 4.27 that for $kR < 1$, that is, when the diameter is less than one-third the wavelength, the impedance load on the surface of the sphere is that of a mass reactance because the resistive component is negligible compared with the reactive component.

At all frequencies, the loading shown in Fig. 4.27 may be represented by the equivalent circuits of Fig. 4.34. The element sizes for the mechanical and acoustic admittances and impedances are given with the circuits.

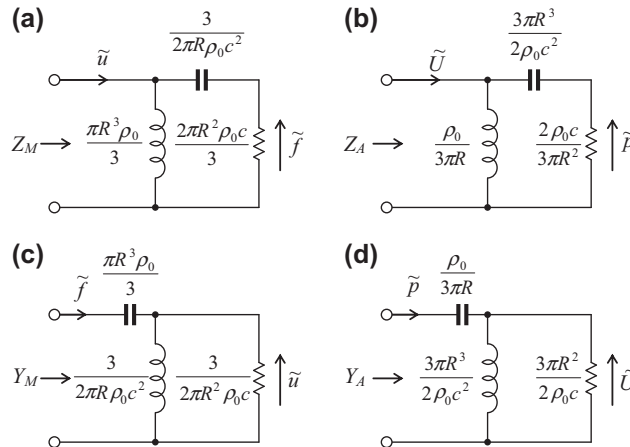


Figure 4.34 Exact radiation impedances and admittances for all values of kR for a rigid sphere that oscillates axially. (a) Mechanical-impedance analogy; (b) acoustic-impedance analogy; (c) mechanical-admittance analogy; (d) acoustic-admittance analogy. The quantity R is the radius of the sphere.



4.19 PLANE CIRCULAR PISTON IN INFINITE Baffle

The specific impedance in $\text{N}\cdot\text{s}/\text{m}^3$ of the air load on one side of a plane piston mounted in an infinite baffle (see Fig. 13.3) and vibrating sinusoidally is given by Eqs. (13.116)–(13.118). Plots of the real and imaginary parts of

$$\frac{Z_s}{\rho_0 c} = \frac{R_s + jX_s}{\rho_0 c} \quad (4.145)$$

are shown in Fig. 4.35 as a function of ka . Similar graphs of the real and imaginary parts of the specific admittance

$$Y_s \rho_0 c = \rho_0 c (\mathbf{G}_s + j\mathbf{B}_s) = \rho_0 c \left(\frac{R_s}{R_s^2 + X_s^2} - j \frac{X_s}{R_s^2 + X_s^2} \right) \quad (4.146)$$

are shown in Fig. 4.36. The specific admittance is in $\text{m}^3 \cdot \text{N}^{-1} \cdot \text{s}^{-1}$ (rays $^{-1}$).

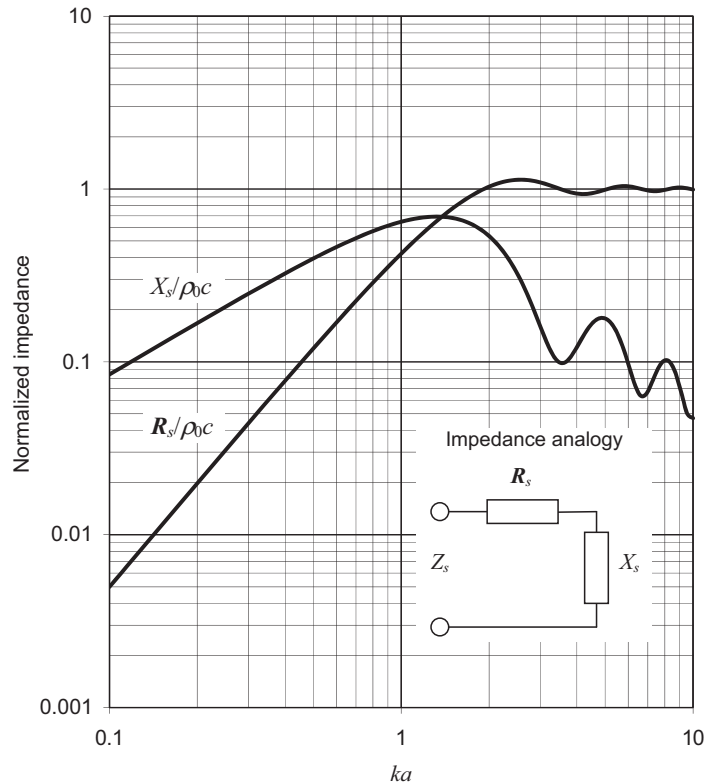


Figure 4.35 Real and imaginary parts of the normalized specific radiation impedance $Z_s/\rho_0 c$ of the air load on one side of a plane circular piston of radius a in an infinite flat baffle. Frequency is plotted on a normalized scale, where $ka = 2\pi a/\lambda = 2\pi fa/c$.

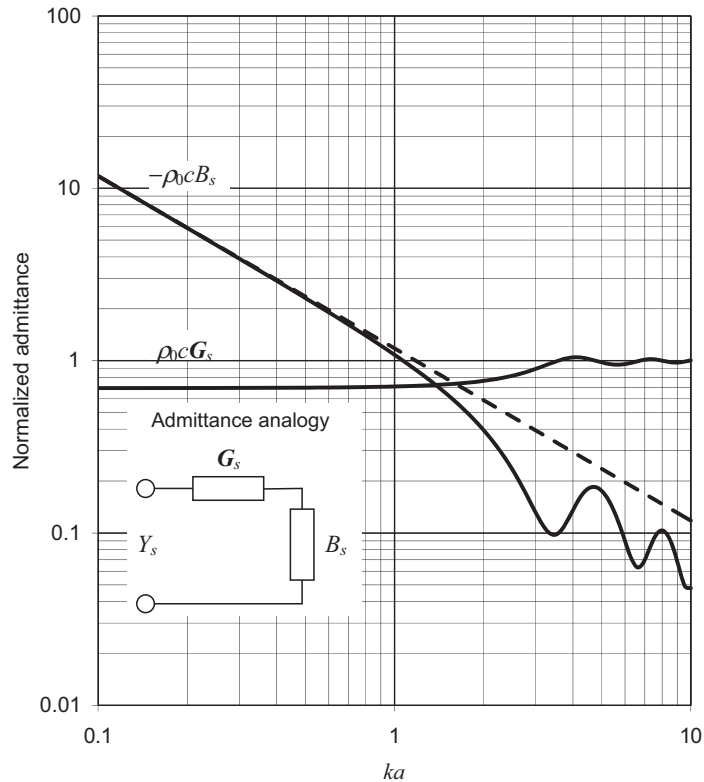


Figure 4.36 Real and imaginary parts of the normalized specific radiation admittance $\rho_0 c Y_s$ of the air load on one side of a plane circular piston of radius a in an infinite flat baffle. Frequency is plotted on a normalized scale, where $ka = 2\pi a/\lambda = 2\pi fa/c$.

The data of Fig. 4.35 are used in dealing with impedance analogies and the data of Fig. 4.36 in dealing with admittance analogies.

We see from Fig. 4.35 that, for $ka < 0.5$, the reactance varies as the first power of frequency while the resistance varies as the second power of frequency. At high frequencies, for $ka > 5$, the reactance becomes small compared with the resistance, and the resistance approaches a constant value.

The admittance, on the other hand, is better behaved. The conductance is constant for $ka < 0.5$, and it is also constant for $ka > 5$ although its value is larger.

Approximate analogous circuits

The behavior just noted suggests that, except for the ripples in the curves for ka between 1 and 5, the impedance and the admittance for a piston in an infinite baffle can be

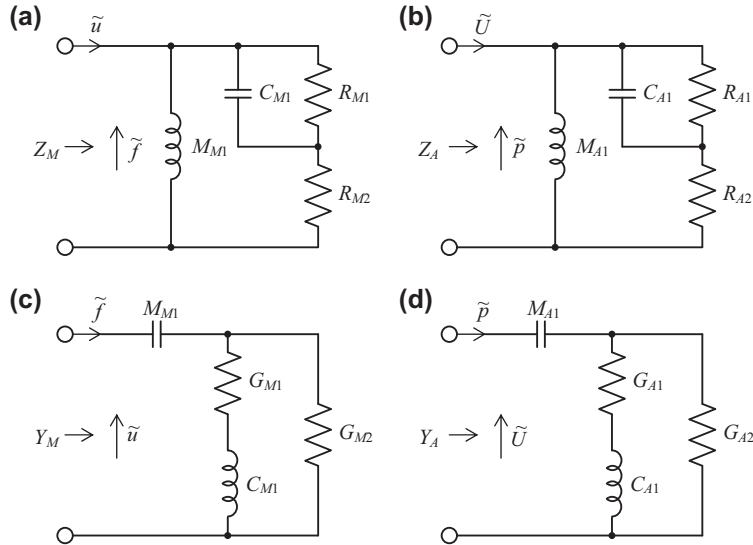


Figure 4.37 Approximate radiation impedances and admittances for a piston in an infinite baffle or for a closed-back piston for all values of ka . (a) Mechanical-impedance analogy; (b) acoustic-impedance analogy; (c) mechanical-admittance analogy; (d) acoustic-admittance analogy.

approximated over the whole frequency range by the analogous circuits of Fig. 4.37. Those circuits give the mechanical and acoustic impedances and admittances, where

$$R_{M2} = \pi a^2 \rho_0 c \text{ N}\cdot\text{s}/\text{m} \quad (4.147)$$

$$\begin{aligned} R_M &= R_{M2} + R_{M1} = 128a^2 \rho_0 c / (9\pi) \\ &= 4.53a^2 \rho_0 c \text{ N}\cdot\text{s}/\text{m} \end{aligned} \quad (4.148)$$

$$R_{M1} = 1.386a^2 \rho_0 c \text{ N}\cdot\text{s}/\text{m} \quad (4.149)$$

$$C_{M1} = 1.89 / (\pi a \rho_0 c^2) = 0.6 / (a \rho_0 c^2) \text{ m}/\text{N} \quad (4.150)$$

$$M_{M1} = 8a^3 \rho_0 / 3 = 2.67a^3 \rho_0 \text{ kg} \quad (4.151)$$

$$G_{M2} = 1 / (\pi a^2 \rho_0 c) = 0.318 / (a^2 \rho_0 c) \text{ m}\cdot\text{N}^{-1}\cdot\text{s}^{-1} \quad (4.152)$$

$$G_{M1} = 0.722 / (a^2 \rho_0 c) \text{ m}\cdot\text{N}^{-1}\cdot\text{s}^{-1} \quad (4.153)$$

$$R_{A2} = \rho_0 c / (\pi a^2) = 0.318 \rho_0 c / a^2 \text{ N}\cdot\text{s}/\text{m}^5 \quad (4.154)$$

$$\begin{aligned} R_A &= R_{A2} + R_{A1} = 128 \rho_0 c / (9 \pi^3 a^2) \\ &= 0.459 \rho_0 c / a^2 \text{ N}\cdot\text{s}/\text{m}^5 \end{aligned} \quad (4.155)$$

$$R_{A1} = 0.1404 \rho_0 c / a^2 \text{ N}\cdot\text{s}/\text{m}^5 \quad (4.156)$$

$$C_{A1} = 1.89 \pi a^3 / (\rho_0 c^2) = 5.94 a^3 / (\rho_0 c^2) \text{ m}^5/\text{N} \quad (4.157)$$

$$M_{A1} = 8 \rho_0 / (3 \pi^2 a) = 0.27 \rho_0 / a \text{ kg}/\text{m}^4 \quad (4.158)$$

$$G_{A2} = \pi a^2 / (\rho_0 c) \text{ m}^5 \cdot \text{N}^{-1} \cdot \text{s}^{-1} \quad (4.159)$$

$$G_{A1} = 7.12 a^2 / (\rho_0 c) \text{ m}^5 \cdot \text{N}^{-1} \cdot \text{s}^{-1} \quad (4.160)$$

All constants are dimensionless and were chosen to give the best average fit to the functions of Figs. 4.35 and 4.36.

Low- and high-frequency approximations

At low and high frequencies, these circuits may be approximated by the simpler circuits given in the last column of Table 4.4.

It is apparent that when $ka < 0.5$, that is, when the circumference of the piston $2\pi a$ is less than one-half wavelength $\lambda/2$, the impedance load presented by the air on the vibrating piston is that of a mass shunted by a very large resistance. In other words, $R^2 = (R_1 + R_2)^2$ is large compared with $\omega^2 M_1^2$. In fact, this loading mass may be imagined to be a layer of air equal in area to the area of the piston and equal in thickness to about 0.85 times the radius because

$$(\pi a^2)(0.85a)\rho_0 \approx 2.67 a^3 \rho_0 = M_{M1}$$

At high frequencies, $ka > 5$, the air load behaves exactly as though it were connected to one end of a tube of the same diameter as the piston, with the other end of the tube perfectly absorbing. As we saw in Eq. (2.124), the input mechanical resistance for such a tube is $\pi a^2 \rho_0 c$. Hence, intuitively one might expect that at high frequencies the vibrating rigid piston beams the sound outward in lines perpendicular to the face of the piston. This is actually the case for the immediate near field close to the piston. At a distance, however, the far-field radiation spreads, as we learned earlier in this chapter.

Table 4.4 Radiation impedance and admittance for one side of a plane circular piston in an infinite baffle^a

	Mechanical	Specific	Acoustic	Analogous circuits
Impedance	$f = \text{drop}$ $u = \text{flow}$	$p = \text{drop}$ $u = \text{flow}$	$p = \text{drop}$ $U = \text{flow}$	
$ka < 0.5$:				
Series resistance, R	$R_M = \frac{\pi a^4 \rho_0 \omega^2}{2c}$	$R_S = \frac{a^2 \rho_0 \omega^2}{2c}$	$R_A = \frac{\rho_0 \omega^2}{2\pi c}$	
Shunt resistance, R	$R_M = \frac{128 a^2 \rho_0 c}{9\pi}$	$R_S = \frac{128 \rho_0 c}{9\pi^2}$	$R_A = \frac{128 \rho_0 c}{9\pi^3 a^2}$	
Mass, M_1	$M_{M1} = \frac{8a^3 \rho_0}{3}$	$M_{S1} = \frac{8a\rho_0}{3\pi}$	$M_{A1} = \frac{8\rho_0}{3\pi^2 a}$	
$ka > 5$:				
Resistance, R_2	$R_{M2} = \pi a^2 \rho_0 c$	$R_{S2} = \rho_0 c$	$R_{A2} = \frac{\rho_0 c}{\pi a^2}$	
Admittance	$u = \text{drop}$ $f = \text{flow}$	$u = \text{drop}$ $p = \text{flow}$	$U = \text{drop}$ $p = \text{flow}$	
$ka < 0.5$:				
Series conductance, G	$G_M = \frac{9\pi}{128 a^2 \rho_0 c}$	$G_S = \frac{9\pi^2}{128 \rho_0 c}$	$G_A = \frac{9\pi^3 a^2}{128 \rho_0 c}$	
Mass, M_1	$M_{M1} = \frac{8a^3 \rho_0}{3}$	$M_{S1} = \frac{8a\rho_0}{3\pi}$	$M_{A1} = \frac{8\rho_0}{3\pi^2 a}$	
$ka > 5$:				
Conductance, G_2	$G_{M2} = \frac{1}{\pi a^2 \rho_0 c}$	$G_{S2} = \frac{1}{\rho_0 c}$	$G_{A2} = \frac{\pi a^2}{\rho_0 c}$	

^aThis table gives element sizes for analogous circuits in the region where $ka < 0.5$ and $ka > 5$. All constants are dimensionless. For the region between 0.5 and 5.0, the charts of Figs. 4.35 and 4.36 should be used.

4.20 PLANE CIRCULAR FREE DISK

A disk in free space without surrounding structure is a suitable model, at low frequencies, for a direct-radiator loudspeaker without a baffle of any sort. In other words, the loudspeaker radiates as a dipole. The radiation impedance is given by Eqs. (13.248)–(13.250).

Graphs of the real and imaginary parts of the normalized specific impedance load on one side of the diaphragm, $Z_s/\rho_0 c$, as a function of ka for the free disk, are shown in Fig. 4.38. The data of Fig. 4.38 are used in dealing with impedance analogies. For admittance analogies, the complex admittance can be obtained by taking the reciprocal of the complex impedance.

A simple equivalent circuit, approximately valid for all frequencies like those shown in Fig. 4.37, cannot be drawn for this case. At very low frequencies, however, it is

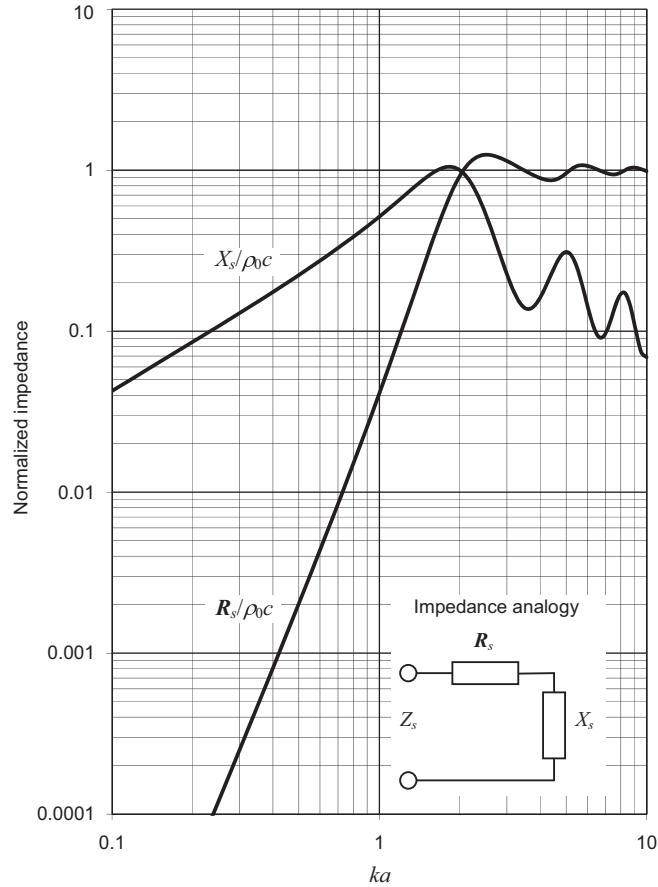


Figure 4.38 Real and imaginary parts of the normalized specific radiation impedance $Z_s/\rho_0 c$ of the air load on one side of a plane circular piston of radius a in free space. Frequency is plotted on a normalized scale, where $ka = 2\pi a/\lambda = 2\pi fa/c$.

possible to represent the impedance by an equivalent circuit, which is similar to that for an oscillating sphere. In the frequency ranges where $ka < 0.5$ and $ka > 5$, analogous circuits of the type shown in Table 4.5 may be used.



4.21 PLANE CIRCULAR PISTON RADIATING FROM ONE SIDE ONLY IN FREE SPACE

The specific impedance ($\text{N}\cdot\text{s}/\text{m}^3$) of the air load on a plane piston in free space, which has one surface vibrating sinusoidally while the other remains stationary, is given by Eqs. (13.254) and (13.255) and plotted in Fig. 4.39.

Table 4.5 Radiation impedance and admittance for one side of a plane circular piston in free space^a.

	<u>Mechanical</u>	<u>Specific</u>	<u>Acoustic</u>	
	<i>f</i> = drop <i>u</i> = flow	<i>p</i> = drop <i>u</i> = flow	<i>p</i> = drop <i>U</i> = flow	Analogous circuits
<i>ka</i> < 0.5:				
Series resistance, <i>R</i>	$R_M = \frac{8a^6 \rho_0 \omega^4}{27\pi c^3}$	$R_S = \frac{8a^4 \rho_0 \omega^4}{27\pi^2 c^3}$	$R_A = \frac{8a^2 \rho_0 \omega^4}{27\pi^3 c^3}$	
Series resistance, <i>R</i>	$M_{M1} = \frac{4a^3 \rho_0}{3}$	$M_{S1} = \frac{4a\rho_0}{3\pi}$	$M_{A1} = \frac{4\rho_0}{3\pi^2 a}$	
Mass, <i>M</i> ₁				
Compliance, <i>C</i> ₁	$C_{M1} = \frac{1}{\sqrt{6\pi a\rho_0 c^2}}$	$C_{S1} = \frac{a}{\sqrt{6\rho_0 c^2}}$	$C_{A1} = \frac{\pi a^3}{\sqrt{6\rho_0 c^2}}$	
<i>ka</i> > 5:				
Resistance, <i>R</i> ₂	$R_M = \pi a^2 \rho_0 c$	$R_S = \rho_0 c$	$R_A = \frac{\rho_0 c}{\pi a^2}$	

	<i>u</i> = drop <i>f</i> = flow	<i>u</i> = drop <i>p</i> = flow	<i>U</i> = drop <i>p</i> = flow	
<i>ka</i> < 0.5:				
Series conductance, <i>G</i>	$G_M = \frac{\omega^2}{6\pi\rho_0 c^3}$	$G_S = \frac{a^2 \omega^2}{6\rho_0 c^3}$	$G_A = \frac{\pi a^4 \omega^2}{6\rho_0 c^3}$	
Mass, <i>M</i> ₁	$M_{M1} = \frac{4a^3 \rho_0}{3}$	$M_{S1} = \frac{4a\rho_0}{3\pi}$	$M_{A1} = \frac{4\rho_0}{3\pi^2 a}$	
Compliance, <i>C</i> ₁	$C_{M1} = \frac{1}{\sqrt{6\pi a\rho_0 c^2}}$	$C_{M1} = \frac{\pi a^3}{\sqrt{6\rho_0 c^2}}$	$C_{A1} = \frac{\pi a^3}{\sqrt{6\rho_0 c^2}}$	
<i>ka</i> > 5:				
Conductance, <i>G</i> ₂	$G_M = \frac{1}{\pi a^2 \rho_0 c}$	$G_S = \frac{1}{\rho_0 c}$	$G_A = \frac{\pi a^2}{\rho_0 c}$	

^aThis table gives element sizes for analogous circuits in the region where *ka* < 0.5 and *ka* > 5. All constants are dimensionless. For the region between 0.5 and 5.0, the chart of Fig. 4.38 should be used.

Graphs of the real and imaginary parts of the normalized mechanical impedance $Z_M/\pi a^2 \rho_0 c$ as a function of *ka* for a piston so mounted are shown in Fig. 12.36. It is simply the mean of the impedances of a plane circular piston in an infinite baffle and the same in free space.

To a fair approximation, the radiation impedance for a one-sided piston in free space may be represented over the entire frequency range by the same analogous circuits used for the piston in an infinite baffle and shown in Fig. 4.37, where the elements now are

$$R_{M2} = \pi a^2 \rho_0 c \text{ N}\cdot\text{s/m} \tag{4.161}$$

$$\begin{aligned} R_M &= R_{M2} + R_{M1} = 16a^2 \rho_0 c / \pi \\ &= 5.09a^2 \rho_0 c \text{ N}\cdot\text{s/m} \end{aligned} \tag{4.162}$$

$$R_{M1} = 1.95a^2 \rho_0 c \text{ N}\cdot\text{s/m} \tag{4.163}$$

$$C_{M1} = 1/(\pi a \rho_0 c^2) = 0.318/(a \rho_0 c^2) \text{ m/N} \tag{4.164}$$

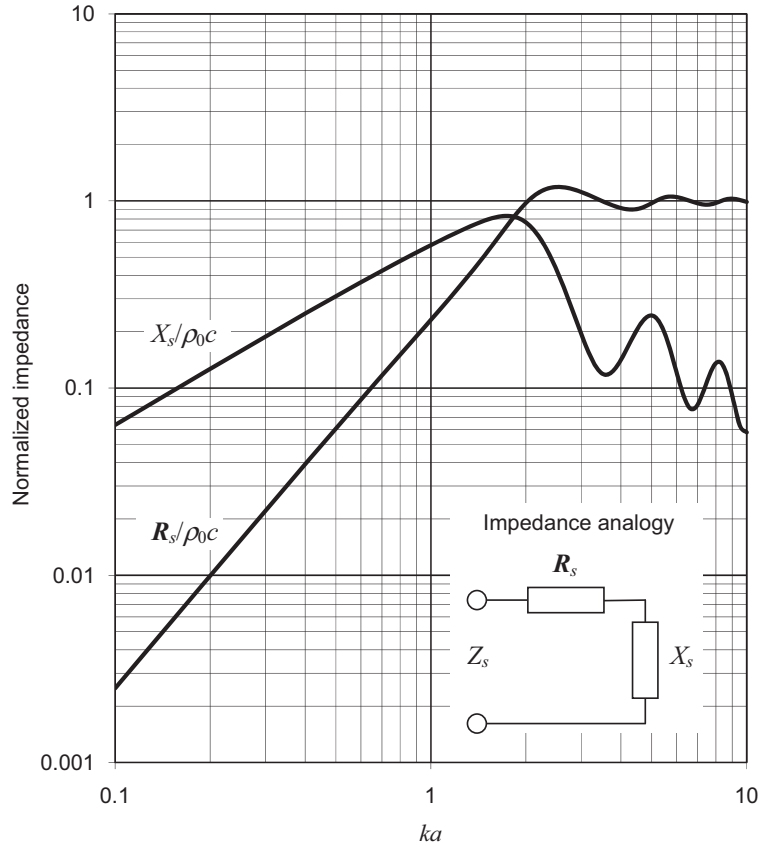


Figure 4.39 Real and imaginary parts of the normalized specific radiation impedance Z_s/ρ_0c of the air load on one side of a plane circular piston of radius a radiating from one side only into free space. Frequency is plotted on a normalized scale, where $ka = 2\pi a/\lambda = 2\pi fa/c$.

$$M_{M1} = 2a^3\rho_0 \text{ kg} \quad (4.165)$$

$$G_{M2} = 1/(\pi a^2\rho_0c) = 0.318/(a^2\rho_0c) \text{ m}\cdot\text{N}^{-1}\cdot\text{s}^{-1} \quad (4.166)$$

$$G_{M1} = 0.513/(a^2\rho_0c) \text{ m}\cdot\text{N}^{-1}\cdot\text{s}^{-1} \quad (4.167)$$

$$R_{A2} = \rho_0c/(\pi a^2) = 0.318\rho_0c/a^2 \text{ N}\cdot\text{s}/\text{m}^5 \quad (4.168)$$

$$\begin{aligned} R_A &= R_{A2} + R_{A1} = 16\rho_0c/(\pi^3 a^2) \\ &= 0.516\rho_0c/a^2 \text{ N}\cdot\text{s}/\text{m}^5 \end{aligned} \quad (4.169)$$

$$R_{A1} = 0.1977\rho_0c/a^2 \text{ N}\cdot\text{s}/\text{m}^5 \quad (4.170)$$

$$C_{A1} = \pi a^3/(\rho_0c^2) = 3.142a^3/(\rho_0c^2) \text{ m}^5/\text{N} \quad (4.171)$$

$$M_{A1} = 2\rho_0/(\pi^2a) = 0.2026\rho_0/a \text{ kg}/\text{m}^4 \quad (4.172)$$

$$G_{A2} = \pi a^2/(\rho_0c) \text{ m}^5\cdot\text{N}^{-1}\cdot\text{s}^{-1} \quad (4.173)$$

$$G_{A1} = 5.06a^2/(\rho_0c) \text{ m}^5\cdot\text{N}^{-1}\cdot\text{s}^{-1} \quad (4.174)$$

In the frequency ranges where $ka < 0.5$ and $ka > 5$, analogous circuits of the type shown in Table 4.6 may be used.

Table 4.6 Radiation impedance and admittance for a plane circular piston radiating from one side only in free space^a

Impedance	Mechanical	Specific	Acoustic	Analogous circuits
	$f = \text{drop}$ $u = \text{flow}$	$p = \text{drop}$ $u = \text{flow}$	$p = \text{drop}$ $U = \text{flow}$	
$ka < 0.5$:				
Series resistance, R	$R_M = \frac{\pi a^4 \rho_0 \omega^2}{4c}$	$R_S = \frac{a^2 \rho_0 \omega^2}{4c}$	$R_A = \frac{\rho_0 \omega^2}{4\pi c}$	
Series resistance, R	$R_M = \frac{16a^2 \rho_0 c}{\pi}$	$R_S = \frac{16\rho_0 c}{\pi^2}$	$R_A = \frac{16\rho_0 c}{\pi^3 a^2}$	
Mass, M_1	$M_{M1} = 2a^3 \rho_0$	$M_{S1} = \frac{2a\rho_0}{\pi}$	$M_{A1} = \frac{2\rho_0}{\pi^2 a}$	
Resistance, R_2	$R_{M2} = \pi a^2 \rho_0 c$	$R_{S2} = \rho_0 c$	$R_{A2} = \frac{\rho_0 c}{\pi a^2}$	
Admittance	$u = \text{drop}$ $f = \text{flow}$	$u = \text{drop}$ $p = \text{flow}$	$U = \text{drop}$ $p = \text{flow}$	
$ka < 0.5$:				
Series conductance, G	$G_M = \frac{\pi}{16a^2 \rho_0 c}$	$G_S = \frac{\pi^2}{16\rho_0 c}$	$G_A = \frac{\pi^3 a^2}{16\rho_0 c}$	
Mass, M_1	$M_{M1} = 2a^3 \rho_0$	$M_{S1} = \frac{2a\rho_0}{\pi}$	$M_{A1} = \frac{2\rho_0}{\pi^2 a}$	
$ka > 5$:				
Conductance, G_2	$G_{M2} = \frac{1}{\pi a^2 \rho_0 c}$	$G_{S2} = \frac{1}{\rho_0 c}$	$G_{A2} = \frac{\pi a^2}{\rho_0 c}$	

^aThis table gives element sizes for analogous circuits in the region where $ka < 0.5$ and $ka > 5$. All constants are dimensionless. For the region between 0.5 and 5.0, the chart of Fig. 4.39 should be used.



PART XIV: VISCOUS AND THERMAL LOSSES



4.22 SOUND IN LOSSY TUBES

In Section 2.4, we examined the propagation of one-dimensional waves in a loss-free tube. To be able to neglect viscous losses inside the tube, the radius of the tube must not be too small. Also, to be able to neglect transverse resonances in the tube, the radius must not be too large. Here we shall rederive the one-dimensional wave equation using a slightly different procedure than before, taking into account the viscous and thermal losses that take place at the boundary wall, using what are known as the Navier–Stokes equations. In accordance with the continuum theory of gases, traditional models have assumed that the axial velocity at the wall of the tube is zero and that the temperature there is ambient because of the sheer number of collisions occurring between air molecules and the wall. However, as the diameter of the tube is reduced relative to the mean free path of the molecules, fewer collisions occur so that the axial velocity and temperature both increase at the wall. This is generally known as a slip boundary condition. Formulation is now available [10] that models this slip, thus allowing us to model tubes of much smaller diameter than was previously possible. The resulting wave number is complex, and from this new wave number we shall derive two new parameters called the dynamic density and dynamic compressibility which replace the density and inverse bulk modulus, respectively, in the expressions for wave number and characteristic impedance. These result from the average flow over the cross section of the tube as if the losses were homogeneous throughout the bulk of the acoustic medium, although they are actually localized near the tube wall. We will also define a viscous boundary thickness to define the region within which most of the viscous losses occur. For those readers who are not interested in the full derivation but only wish to apply the results to practical uses, you may skip on to the results shown in Figs. 4.46–4.51.

Two-terminal electrical components generally obey Kirchhoff’s law. In other words, the current flowing out of one terminal is equal to that flowing into the other. However, the exact model of a tube does not obey this law because, due to losses, the volume velocity flowing out of one end is less than that flowing into the other. Therefore, we must model it as a four-terminal device or two-port model. We shall develop a discrete-element two-port model, which is a useful result as it allows us to apply electrical circuit theory. However, we shall see that under certain frequency or diameter ranges, we can make useful two-terminal approximations for an open or closed tube which form the basis of some of the acoustic components presented in Section 4.4.



4.23 WAVE EQUATION FOR AN INFINITE LOSSY TUBE

Assumptions

The circular tube of radius a shown in Fig. 4.40 has z as the axial ordinate and w as the radial ordinate. In the following discussion, it is assumed that the radial pressure distribution is uniform and that the pressure variations are purely axial. This has been shown to be valid provided that $a(\text{meters}) \leq 10^4/f^{3/2}$ [11]. Also, it is assumed that the radial velocity is zero, but the axial velocity is allowed to vary radially because of laminar flow resulting from viscous losses. Thermal conduction through the tube wall is also taken into consideration, where the wall is at ambient temperature T_0 . However, boundary slip is allowed for, whereby the axial particle velocity adjacent to the tube wall can be nonzero and the air temperature there can be nonambient. This is particularly relevant in the case of very narrow tubes, where the viscous and thermal losses are less than would be predicted if we were to assume “no slip”. By “no slip”, we mean if the axial velocity at the wall were zero and the temperature there were ambient. Furthermore, the degree of slip is proportional to the gradient of the radial distribution of the velocity or temperature at the tube wall. In this section, we shall introduce the concept of the *viscous boundary layer*, which is a region adjacent to the wall in which the axial velocity is less than it would be in a loss-free tube. Outside the boundary layer, the tube is considered to be loss-free such that the axial velocity is unaffected by the wall.

Categories

An open tube may be divided into five categories: wide, medium, narrow, very narrow, and ultra-narrow. In a wide tube, the viscous and thermal losses are negligible so that the tube can be treated as a pure mass. In a medium tube, the thickness of the viscous boundary layer increases with frequency. Although the resistance is smaller than the mass reactance, it increases with the square root of frequency.

In a narrow tube, the resistance is greater than the mass reactance and is relatively independent of frequency. The viscous boundary layer completely fills the tube so that the velocity distribution between the walls is parabolic. In a very narrow tube, the resistance remains independent of frequency, but the mass becomes negative. Finally, we have the ultra-narrow tube in which there is total absorption of the sound so that it appears infinite and the impedance seen at the entrance is the characteristic impedance of the tube.

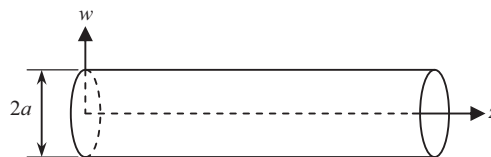


Figure 4.40 Geometry of tube.

The momentum conservation equation

In accordance with the conservation of momentum law, we can write the linearized Navier–Stokes equation [12].

$$\left(\rho_0 \frac{\partial}{\partial t} - \mu \nabla^2\right) u(w) = -\frac{\partial p}{\partial z}, \quad (4.175)$$

where

$$\nabla^2 = \partial^2 / (\partial w^2) + w^{-1} \partial / (\partial w)$$

and u is the axial velocity, p is the axial pressure, $\rho_0 = 1.18 \text{ kg/m}^3$ and $\mu = 18.6 \times 10^{-6} \text{ N}\cdot\text{s/m}^2$ are the density and viscosity of air, respectively, and z is the axial ordinate. Replacing the time derivative with $j\omega$ gives

$$(\nabla^2 + k_V^2) \tilde{u}(w) = -\frac{k_V^2}{j\omega\rho_0} \frac{\partial \tilde{p}}{\partial z}, \quad (4.176)$$

where k_V is the viscous (or shear) wave number given by

$$k_V = \sqrt{-j\omega\rho_0/\mu}. \quad (4.177)$$

Thermal conduction (entropy) and the gas law

Fourier's law for thermal conduction gives

$$\kappa \nabla^2 \tilde{\tau}(w) = j\omega T_0 (\rho_0 C_V \tilde{p}/P_0 - C_P \tilde{\delta}), \quad (4.178)$$

where \tilde{p} , $\tilde{\delta}$, and $\tilde{\tau}$ are the small pressure, density, and temperature fluctuations respectively. Also, $\kappa = 25.4 \times 10^{-3} \text{ N}\cdot\text{s}^{-1}\cdot\text{K}^{-1}$ is the thermal conductivity, $T_0 = 295^\circ\text{K}$ is the ambient temperature, C_V is the specific heat capacity under constant volume, and C_P is the specific heat capacity under constant pressure. For an ideal gas we can write the following linearized equation of state [12]

$$\frac{\tilde{p}}{P_0} = \frac{\tilde{\delta}}{\rho_0} + \frac{\tilde{\tau}(w)}{T_0}. \quad (4.179)$$

Eliminating $\tilde{\delta}$ from Eqs. (4.178) and (4.179) gives

$$\kappa \nabla^2 \tilde{\tau}(w) = j\omega\rho_0 T_0 \left((C_V - C_P) \frac{\tilde{p}}{P_0} + C_P \frac{\tilde{\tau}(w)}{T_0} \right). \quad (4.180)$$

We also note that $C_P - C_V = P_0/(\rho_0 T_0)$ [11] so that

$$(\nabla^2 + P_r k_V^2) \tilde{\tau}(w) = \frac{P_r k_V^2}{\rho_0 C_P} \tilde{p}, \quad (4.181)$$

where P_r is the (dimensionless) Prandtl number given by

$$P_r = \mu C_p / \kappa \quad (4.182)$$

which is the ratio of the viscous diffusion rate to the thermal diffusion rate.

Solution of the velocity and temperature radial equations

Eqs. (4.176) and (4.181) for the radial velocity and temperature distributions, respectively, are subject to the following slip boundary conditions:

$$\tilde{u}(a) = -aB_u \left. \frac{\partial \tilde{u}(w)}{\partial w} \right|_{w=a} \quad (4.183)$$

$$\tilde{\tau}(a) = -aB_e \left. \frac{\partial \tilde{\tau}(w)}{\partial w} \right|_{w=a} \quad (4.184)$$

where the boundary slip factors B_u and B_e are given by

$$B_u = (2\alpha_u^{-1} - 1)K_n, \quad (4.185)$$

$$B_e = \frac{2\gamma}{P_r(1 + \gamma)} \left(\frac{2}{\alpha_e} - 1 \right) K_n, \quad (4.186)$$

which are zero in the case of no slip, where $\tilde{u}(a) = \tilde{\tau}(a) = 0$.

We note that $\gamma = C_p/C_v$ is the specific heat ratio, α_u and α_e are the accommodation coefficients, both of which are assumed to have a value of 0.9, and K_n is the (dimensionless) Knudsen number given by

$$K_n = \lambda_m/a, \quad (4.187)$$

where $\lambda_m = 60$ nm is the molecular mean free path length between collisions [10]. We let

$$\tilde{u}(w) = -\frac{1}{j\omega\rho_0} \frac{\partial \tilde{p}}{\partial z} (1 - F(k_V, w, B_u)), \quad (4.188)$$

$$\tilde{\tau}(w) = \frac{\tilde{p}}{\rho_0 C_p} ((1 - F(k_T, w, B_e))), \quad (4.189)$$

which after substituting in Eqs. (4.176) and (4.181), respectively, leads to a new pair of equations:

$$(\nabla^2 + k_V^2)F(k_V, w, B_u) = 0, \quad (4.190)$$

$$(\nabla^2 + k_T^2)F(k_T, w, B_e) = 0, \quad (4.191)$$

where k_T is the thermal (or entropy) wave number given by

$$k_T = \sqrt{P_r} k_V. \quad (4.192)$$

Eqs. (4.190) and (4.191) are subject to the boundary conditions

$$F(k_V, a, B_u) + aB_u \frac{\partial}{\partial w} F(k_V, w, B_u) \Big|_{w=a} = 1, \quad (4.193)$$

$$F(k_T, a, B_e) + aB_e \frac{\partial}{\partial w} F(k_T, w, B_e) \Big|_{w=a} = 1 \quad (4.194)$$

Solutions to Eqs. (4.190) and (4.191) are given by

$$F(k_V, w, B_u) = AJ_0(k_V w), \quad (4.195)$$

$$F(k_T, w, B_e) = BJ_0(k_T w). \quad (4.196)$$

The unknown coefficients can be found by substituting Eqs. (4.195) and (4.196) in the boundary conditions of Eqs. (4.193) and (4.194), respectively, to give

$$A = (J_0(k_V a) - B_u k_V a J_1(k_V a))^{-1}$$

and

$$B = (J_0(k_T a) - B_e k_T a J_1(k_T a))^{-1}.$$

The average values across the tube cross section are defined by

$$\begin{aligned} \langle F(k_V, a, B_u) \rangle &= \frac{1}{\pi a^2} \int_0^{2\pi} \int_0^a F(k_V, w, B_u) w dw d\phi \\ &= \frac{Q(k_V a)}{1 - 0.5 B_u k_V^2 a^2 Q(k_V a)}, \end{aligned} \quad (4.197)$$

where

$$Q(x) = \frac{2J_1(x)}{xJ_0(x)} = \left(\sum_{n=0}^{\infty} \frac{x^2}{x^2 - \beta_n^2} \right)^{-1}, \quad (4.198)$$

where β_n are the zeros of $J_1(x)$, such that $J_1(\beta_n) = 0$, and for large n , we may use $\beta_n|_n \rightarrow \infty \approx (n + 1/4)\pi$. Unlike the conventional individual expansions for $J_0(x)$ and $J_1(x)$ given by Eq. (A2.71) of Appendix II, this expansion does not blow up for larger values of x when the expansion limit is truncated.

Similarly,

$$\langle F(k_T, a, B_e) \rangle = \frac{Q(k_T a)}{1 - 0.5 B_e k_T^2 a^2 Q(k_T a)}. \quad (4.199)$$

In Fig. 4.41, the axial velocity along the radius of a narrow tube is plotted at a frequency of 100 Hz using Eq. (4.188), where the radius of the tube is 1 μm . Also, the axial velocity along the radius of a wide tube is plotted in Fig. 4.42 at a frequency of 10 kHz, where the radius is 1 mm.

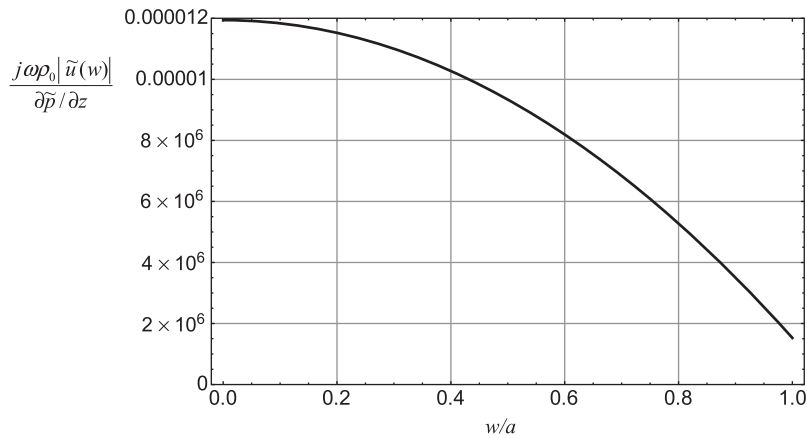


Figure 4.41 Variation of normalized velocity along radius of ultra-narrow tube of radius 1 μm at a frequency of 100 Hz. The effective boundary layer thickness is 224 μm .

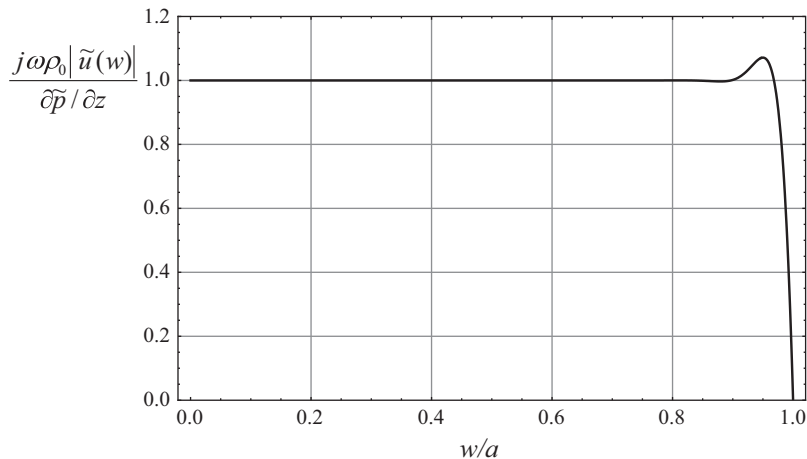


Figure 4.42 Variation of normalized velocity along radius of medium-sized tube of radius 1 mm at a frequency of 10 kHz. The effective boundary layer thickness is 22.4 μm .

The effective boundary layer thickness δ_{visc} can be calculated using the formula [12].

$$\delta_{visc} = \sqrt{\frac{2\mu}{\rho_0\omega}} \quad (4.200)$$

In Fig. 4.41, the effective boundary layer thickness of 224 μm is much greater than the radius of the tube, so the normalized velocity never reaches the theoretical maximum value of unity even at the center ($w = 0$). At the wall, the boundary slip condition is clearly visible as the velocity does not reach zero. By contrast, the effective boundary layer thickness in Fig. 4.42 of 22.4 μm is only 2.24% of the radius, which explains why the normalized velocity is unity over most of the radius and only falls rapidly close to the wall ($w = a$), albeit after a small peak. At the edge of the boundary layer, it is about 86% of the velocity at the center. At the wall, the velocity is virtually zero, so there is no appreciable slip.

Mass conservation and Helmholtz wave equation

Finally, we use the following mass conservation equation or equation of continuity [12].

$$j\omega\langle\tilde{\delta}\rangle + \rho_0\frac{\partial}{\partial z}\langle\tilde{u}\rangle = 0. \quad (4.201)$$

For the average velocity, we can write from Eq. (4.188)

$$\langle\tilde{u}\rangle = -\frac{1}{j\omega\rho_0}\frac{\partial\tilde{p}}{\partial z}(1 - \langle F(k_V, a, B_u)\rangle). \quad (4.202)$$

Differentiating Eq. (4.202) with respect to z and inserting it in Eq. (4.201) yields

$$\langle\tilde{\delta}\rangle = -\frac{1}{\omega^2}(1 - \langle F(k_V, a, B_u)\rangle)\frac{\partial^2\tilde{p}}{\partial z^2}. \quad (4.203)$$

Also, from the gas law of Eq. (4.178)

$$\frac{\tilde{p}}{P_0} = \frac{\langle\tilde{\delta}\rangle}{\rho_0} + \frac{\langle\tilde{\tau}\rangle}{T_0}, \quad (4.204)$$

where the average temperature is derived from Eq. (4.189) as follows

$$\langle\tilde{\tau}\rangle = \frac{\tilde{p}}{\rho_0 C_P}(1 - \langle F(k_T, a, B_e)\rangle). \quad (4.205)$$

Substituting Eq. (4.205) in Eq. (4.204) while noting that

$$C_P - C_V = P_0/(\rho_0 T_0) \quad \text{and} \quad \gamma = C_P/C_V$$

so that

$$C_P = \frac{\gamma P_0}{(\gamma - 1)\rho_0 T_0} \quad (4.206)$$

gives

$$\langle \tilde{\delta} \rangle = \frac{\rho_0}{\gamma P_0} (1 + (\gamma - 1)\langle F(k_T, a, B_e) \rangle) \tilde{p}. \quad (4.207)$$

Equating Eqs. (4.203) and (4.207) then leads to the following Helmholtz wave equation:

$$\frac{\partial^2 \tilde{p}}{\partial z^2} + k^2 \tilde{p} = 0, \quad (4.208)$$

where

$$k^2 = \frac{(1 + (\gamma - 1))\langle F(k_T, a, B_e) \rangle \omega^2 \rho_0}{(1 - \langle F(k_V, a, B_u) \rangle) \gamma P_0} \quad (4.209)$$

or, using Eqs. (4.197) and (4.199),

$$k^2 = \frac{\left(1 + (\gamma - 1) \frac{Q(k_T a)}{1 - 0.5 B_e k_T^2 a^2 Q(k_T a)}\right) \omega^2 \rho_0}{\left(1 - \frac{Q(k_V a)}{1 - 0.5 B_u k_V^2 a^2 Q(k_V a)}\right) \gamma P_0}. \quad (4.210)$$

Dynamic density

To simplify the expressions for the wave number k and characteristic impedance Z_0 , we can use the following shorthand known as the dynamic density where $\langle u \rangle$ is given by Eq. (4.202) so that

$$\begin{aligned} \rho &= -\frac{1}{j\omega \langle \tilde{u} \rangle} \frac{\partial \tilde{p}}{\partial z} = \frac{\rho_0}{1 - \langle F(k_V, a, B_u) \rangle} \\ &= \rho_0 \left(1 - \frac{Q(k_V a)}{1 - 0.5 B_u k_V^2 a^2 Q(k_V a)}\right)^{-1}. \end{aligned} \quad (4.211)$$

Dynamic compressibility

Also, the dynamic compressibility is defined by

$$C = \frac{\langle \tilde{\delta} \rangle}{\rho_0 \tilde{p}}. \quad (4.212)$$

From the ideal gas law of Eq. (4.207), we obtain

$$\frac{\langle \tilde{\delta} \rangle}{\rho_0 \tilde{p}} = \frac{1}{\gamma P_0} (1 + (\gamma - 1) \langle F(k_T, a, B_e) \rangle), \quad (4.213)$$

which is inserted in Eq. (4.212) to give

$$C = \frac{1}{\gamma P_0} \left(1 + \frac{(\gamma - 1) Q(k_T a)}{1 - 0.5 B_e k_T^2 a^2 Q(k_T a)} \right). \quad (4.214)$$

Wave number and characteristic impedance

Using the expressions for the dynamic density ρ and dynamic compressibility C from Eqs. (4.211) and (4.214), respectively, the wave number of Eq. (4.210) simply becomes

$$k = \omega \sqrt{\rho C} \quad (4.215)$$

By comparing this with the wave number for a loss-free plane wave (from Eqs. 2.19 to 2.45)

$$k = \omega \sqrt{\frac{\rho_0}{\gamma P_0}} \quad (4.216)$$

we see that when there are no viscous or thermal losses $\rho = \rho_0$ and $C = 1/(\gamma P_0)$. Hence, the compressibility is the inverse bulk modulus of the medium. Similarly, from Eq. (2.124), we see that the characteristic specific impedance of an infinite tube is

$$Z_s = \sqrt{\rho/C}. \quad (4.217)$$



4.24 FINITE LOSSY TUBES

A two-port network for a finite tube of any length [13]

We have already introduced two-port networks for transducers using z -parameters in Section 3.10. Here we shall apply the theory to a tube with viscous and thermal losses. A general equivalent circuit for passive two-port networks is shown in Fig. 4.43. Because of

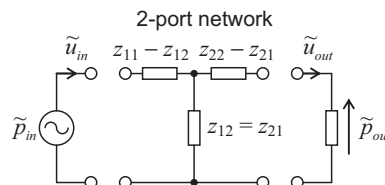


Figure 4.43 Equivalent electrical circuit for a general passive 2-port network.

the reciprocity of the tube, or in other words, the fact that it does not matter at which end there is a transmitter or receiver, we obtain $z_{22} = z_{11}$ and $z_{21} = z_{12}$.

From Eq. (3.64), we write

$$\begin{bmatrix} \tilde{p}_{in} \\ \tilde{p}_{out} \end{bmatrix} = \begin{bmatrix} z_{11} & z_{12} \\ z_{21} & z_{22} \end{bmatrix} \cdot \begin{bmatrix} \tilde{u}_{in} \\ -\tilde{u}_{out} \end{bmatrix}. \quad (4.218)$$

The equations for the tube with losses take on the same form as those without losses which we have already derived in Chapter 2. From Eqs. (2.58) to (2.59) for the pressure and velocity in a finite tube, the following z -parameters are obtained:

$$z_{11} = z_{22} = \left. \frac{\tilde{p}(l)}{-\tilde{u}(l)} \right|_{Z_T=\infty} = -jZ_s \cot kl, \quad (4.219)$$

$$z_{12} = z_{21} = \left. \frac{\tilde{p}(0)}{-\tilde{u}(l)} \right|_{Z_T=\infty} = -jZ_s \operatorname{cosec} kl, \quad (4.220)$$

$$z_{11} - z_{12} = z_{22} - z_{21} = jZ_s \tan(kl/2)$$

where we have replaced $\rho_0 c$ with Z_s for a tube with viscous and thermal losses. This is equivalent to using a piston to apply a velocity $u(l)$ at $z = l$ while the other end (at $z = 0$) is blocked (hence $z_T = \infty$) and using a probe microphone to measure the pressure at $z = l$ and $z = 0$. The pressures $\tilde{p}(l)$ and $\tilde{p}(0)$ are then divided by $\tilde{u}(l)$ to determine z_{11} and z_{12} , respectively. The wave number k and characteristic impedance Z_s with losses are given by Eqs. (4.215) and (4.217), respectively. The trigonometrical functions in Eqs. (4.219) and (4.220) can be conveniently calculated to within 1% using Eqs. (A2.42) and (A2.43) from Appendix II with the expansion limits set to $20(1 + |x|)/\arg x$. Using the relationships of Eqs. (3.74)–(3.77), we can write the following equations for the transmission parameters

$$\begin{bmatrix} \tilde{p}_{in} \\ \tilde{u}_{in} \end{bmatrix} = \begin{bmatrix} a_{11} & a_{12} \\ a_{21} & a_{22} \end{bmatrix} \cdot \begin{bmatrix} \tilde{p}_{out} \\ \tilde{u}_{out} \end{bmatrix}, \quad (4.221)$$

where

$$a_{11} = \left. \frac{\tilde{p}(l)}{\tilde{p}(0)} \right|_{Z_T=\infty} = \cos kl, \quad (4.222)$$

$$a_{12} = \left. \frac{\tilde{p}(l)}{-\tilde{u}(0)} \right|_{Z_T=0} = jZ_s \sin kl, \quad (4.223)$$

$$a_{21} = \left. \frac{-\tilde{u}(l)}{\tilde{p}(0)} \right|_{Z_T=\infty} = \frac{j \sin kl}{Z_s}, \quad (4.224)$$

$$a_{22} = \left. \frac{-\tilde{u}(l)}{-\tilde{u}(0)} \right|_{Z_T=0} = \cos kl. \quad (4.225)$$

If the tube is blocked at the far end, the impedance Z_{in} at the entrance is simply

$$Z_{in} = \left. \frac{\tilde{p}_{in}}{\tilde{u}_{in}} \right|_{\tilde{u}_{out}=0} = z_{11} = -jZ_s \cot kl. \quad (4.226)$$

If the far end is open, then

$$Z_{in} = \left. \frac{\tilde{p}_{in}}{\tilde{u}_{in}} \right|_{\tilde{p}_{out}=0} = z_{11} - z_{12} + \left(\frac{1}{z_{11} - z_{12}} + \frac{1}{z_{12}} \right)^{-1} = jZ_s \tan kl. \quad (4.227)$$

The tangent, cotangent, and cosecant functions may be conveniently calculated using Eqs. (A2.42), (A2.43), and (A2.43a), respectively, from Appendix II.

A two-port network for a short finite tube

When the wavelength is about six times greater than the length l of the tube or greater, we can take just the first two terms of the equivalent series forms for the cotangent and cosecant so that Eqs. (4.219) and (4.220) reduce to

$$z_{11} = z_{22} \approx -jZ_s \left(\frac{1}{kl} - \frac{kl}{3} \right) = \frac{1}{j\omega \mathbf{C}_s} + \frac{j\omega \mathbf{M}_s}{3}, \quad (4.228)$$

$$z_{12} = z_{21} \approx -jZ_s \left(\frac{1}{kl} + \frac{kl}{6} \right) = \frac{1}{j\omega \mathbf{C}_s} - \frac{j\omega \mathbf{M}_s}{6}. \quad (4.229)$$

where $\mathbf{C}_s = Cl$ is a lossy specific compliance and $\mathbf{M}_s = \rho l$ is a lossy specific mass. The bold typeface indicates that these are not pure reactances but also contain resistive components due to losses. The compliance \mathbf{C}_s contains thermal losses and \mathbf{M}_s contains viscous losses. The dynamic compressibility C and dynamic density ρ are given by Eqs. (4.214) and (4.211), respectively. The compliance and mass are shown in Fig. 4.44 as an equivalent electrical circuit. It is valid so long as the radius a is greater than the molecular mean free path length λ_m . When one end of the tube is open and the radiation load is negligible, the corresponding pair of terminals is effectively shorted and, at low frequencies, the two upper mass elements $\frac{1}{2}\mathbf{M}_s$ dominate so that the total mass is \mathbf{M}_s .

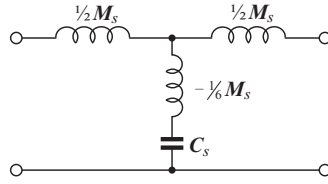


Figure 4.44 A 2-port network for a short tube of radius a , length l , which is valid for $a > \lambda_m$, the molecular mean free path.

When one end is closed, the corresponding pair of terminals is open-circuited and, at low frequencies, the compliance element C_s dominates. The mass is now due to one upper element and the negative middle element, which gives

$$\frac{1}{2}M_s - \frac{1}{6}M_s = \frac{1}{3}M_s.$$

The fact that the mass of a blocked tube is one-third of that of an open tube can be verified by expanding the tangent function of Eq. (4.227), as we did in Section 4.2.

A two-port network for a short finite tube using approximate discrete elements

Let us now shorten the equivalent series forms of the Bessel functions in the function $Q(x)$ of Eq. (4.198) to just their first two terms:

$$Q(x) = \frac{2J_1(x)}{xJ_0(x)} \approx \frac{8 - x^2}{8 - 2x^2} \quad (4.230)$$

We now apply this to the dynamic density from Eq. (4.211) to obtain

$$\rho = -\rho_0 \frac{8 - (2 + 4B_u)k_V^2 a^2 + 0.5B_u k_V^4 a^4}{(1 + 4B_u)k_V^2 a^2 + 0.5B_u k_V^4 a^4}. \quad (4.231)$$

For small values of $k_V a$, this simplifies to

$$\rho = \frac{-8\rho_0}{(1 + 4B_u)k_V^2 a^2}, \quad (4.232)$$

which after substituting k_V from Eq. (4.177) yields

$$\rho = \frac{8\mu}{j\omega(1 + 4B_u)a^2}. \quad (4.233)$$

We also apply Eq. (4.230) to the dynamic compressibility from Eq. (4.214) to obtain

$$C = \frac{1}{\gamma P_0} \left(\frac{8\gamma - (1 + \gamma + 4B_e)k_T^2 a^2 + 0.5B_e k_T^4 a^4}{8 - (2 + 4B_e)k_T^2 a^2 + 0.5B_e k_T^4 a^4} \right). \quad (4.234)$$

For small values of $k_T a$, this simplifies to

$$C = 1/P_0. \quad (4.235)$$

By substituting Eqs. (4.233) and (4.235) into Eqs. (4.215) and (4.217), we obtain the asymptotic wave number and characteristic impedance for a short very narrow tube

$$k|_{a \rightarrow 0} = \frac{2(1-j)}{a} \sqrt{\frac{\mu\omega}{(1+4B_u)P_0}}, \quad (4.236)$$

$$Z_s|_{a \rightarrow 0} = \frac{2(1-j)}{a} \sqrt{\frac{\mu P_0}{(1+4B_u)\omega}}. \quad (4.237)$$

To separate out the reactive and resistive elements of Fig. 4.44, we have to include the second-order terms of Eqs. (4.215) and (4.217). However, the approximation is not optimum because the singularity of the polynomial approximation of $Q(x)$ in Eq. (4.230) does not match that of the Bessel function expression. Hence, we will modify Eq. (4.230) to align the singularities

$$Q(x) = \frac{2J_1(x)}{xJ_0(x)} \approx \frac{\alpha^2 - (1 - \alpha^2/8)x^2}{\alpha^2 - x^2}, \quad (4.238)$$

where $\alpha = 2.4048$ is the first zero of $J_0(x)$. In other words, $J_0(\alpha) = 0$. The numerator part of this approximation has been determined to lead to the same asymptotic expressions for ρ , C , k , and Z_s as Eq. (4.230). We now apply this to the dynamic density from Eq. (4.211) to obtain

$$\rho = \rho_0 \frac{8 - \left(\frac{8}{\alpha^2} + 4B_u\right)k_V^2 a^2 + \frac{8 - \alpha^2}{2\alpha^2} B_u k_V^4 a^4}{-(1 + 4B_u)k_V^2 a^2 + \frac{8 - \alpha^2}{2\alpha^2} B_u k_V^4 a^4}. \quad (4.239)$$

Ignoring the fourth-order terms and substituting k_V from Eq. (4.177) yields

$$\rho = \frac{8\mu}{j\omega(1 + 4B_u)a^2} + \frac{(8/\alpha^2) + 4B_u}{1 + 4B_u} \rho_0. \quad (4.240)$$

The impedance because of the complex mass \mathbf{M}_s is then given by

$$Z_V = j\omega \mathbf{M}_s = j\omega \rho l = \frac{8\mu l}{(1 + 4B_u)a^2} + j\omega \rho_0 l \frac{(8/\alpha^2) + 4B_u}{1 + 4B_u}. \quad (4.241)$$

We see that the first term represents the resistance because of viscous flow losses while the second term represents the mass reactance. We also apply Eq. (4.238) to the dynamic compressibility from Eq. (4.214) to obtain

$$C = \frac{1}{\gamma P_0} \cdot \frac{8\gamma - \left(1 + \left(\frac{8}{\alpha^2} - 1\right)\gamma + 4B_e\right)k_T^2 a^2 + \frac{8 - \alpha^2}{2\alpha^2} B_e k_T^4 a^4}{8 - \left(\frac{8}{\alpha^2} + 4B_e\right)k_T^2 a^2 + \frac{8 - \alpha^2}{2\alpha^2} B_e k_T^4 a^4}. \quad (4.242)$$

Ignoring the fourth-order terms and substituting k_T from Eqs. (4.177), (4.182), (4.192), and (4.206) yields

$$C = \frac{1}{\gamma P_0} \cdot \frac{\gamma + j\omega \frac{(1 + ((8/\alpha^2) - 1)\gamma + 4B_e)\gamma P_0 a^2}{8(\gamma - 1)\kappa T_0}}{1 + j\omega \frac{((8/\alpha^2) + 4B_e)\gamma P_0 a^2}{8(\gamma - 1)\kappa T_0}}. \quad (4.243)$$

We will use the approximation that

$$1 + ((8/\alpha^2) - 1)\gamma \approx 8/\alpha^2.$$

The impedance because of the complex compliance C_s is then given by

$$\begin{aligned} Z_T &= \frac{1}{j\omega C_s} = \frac{1}{j\omega C_l} = \frac{1 + j\omega R_T C_T}{j\omega(C_0 + C_T + j\omega R_T C_0 C_T)} \\ &= \frac{1}{j\omega C_0 + \frac{1}{R_T + \frac{1}{j\omega C_T}}}, \end{aligned} \quad (4.244)$$

where

$$C_0 = \frac{l}{\gamma P_0}, \quad (4.245)$$

$$C_T = (\gamma - 1)C_0, \quad (4.246)$$

$$R_T = \frac{((8/\alpha^2) + 4B_e)\gamma P_0 a^2}{8(\gamma - 1)\kappa T_0 C_T}, \quad (4.247)$$

$$\approx \frac{(1 + 3B_e)\gamma P_0 a^2}{6(\gamma - 1)\kappa T_0 C_T}.$$

Similarly, we can separate Z_V from Eq. (4.241) into its constituent elements:

$$Z_V = R_V + j\omega M_0, \quad (4.248)$$

where

$$R_V = \frac{8\mu l}{(1 + 4B_u)a^2}, \quad (4.249)$$

$$M_0 = \frac{(8/\alpha^2) + 4B_u}{1 + 4B_u} \rho_0 l \approx \frac{1 + 3B_u}{1 + 4B_u} \cdot \frac{4}{3} \rho_0 l. \quad (4.250)$$

These elements are shown on the equivalent electrical circuit of Fig. 4.45 and are known as *lumped elements* as opposed to the *distributed* ones of Eqs. (4.219) and (4.220) because the mass, compliance, and resistance elements have been separated out into discrete elements, whereas in reality they are evenly distributed over the length of the tube. However, the distributed parameter model may be considered as an infinite number of lumped parameter sections coupled together, where each one is infinitesimally short. At low frequencies, the impedance because of C_T is larger than R_T so that the total compliance is effectively $C_0 + C_T = 1/P_0$. The low-frequency pressure fluctuations are isothermal because of heat transfer to and from the wall of the tube. At higher frequencies, R_T represents energy loss because of the time taken for the heat to flow back and forth. At even higher frequencies, R_T is greater than the impedance because of C_T , so very little heat is transferred, making the pressure fluctuations adiabatic in nature. The total compliance is then effectively $C_0 = 1/(\gamma P_0)$. Hence, the compliance at low frequencies is greater than that at high frequencies by a factor of γ (that is, around 40% greater).

Regimes for an open-ended tube

The real and imaginary impedances at the entrance of the tube with the far end open, that is, with one pair of terminals of the two-port network shorted, are shown in Figs. 4.46 and 4.47, respectively. In each case, a number of different curves are plotted. For the *exact* curves (black), Eq. (4.227) is used together with the exact wave number and

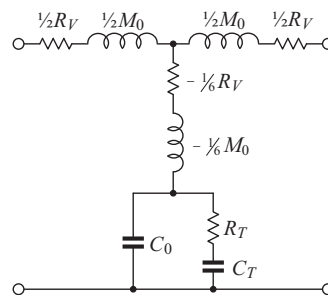


Figure 4.45 A 2-port network for a short narrow tube of radius a length l , which is valid for $a > \lambda_m$, the molecular mean free path.

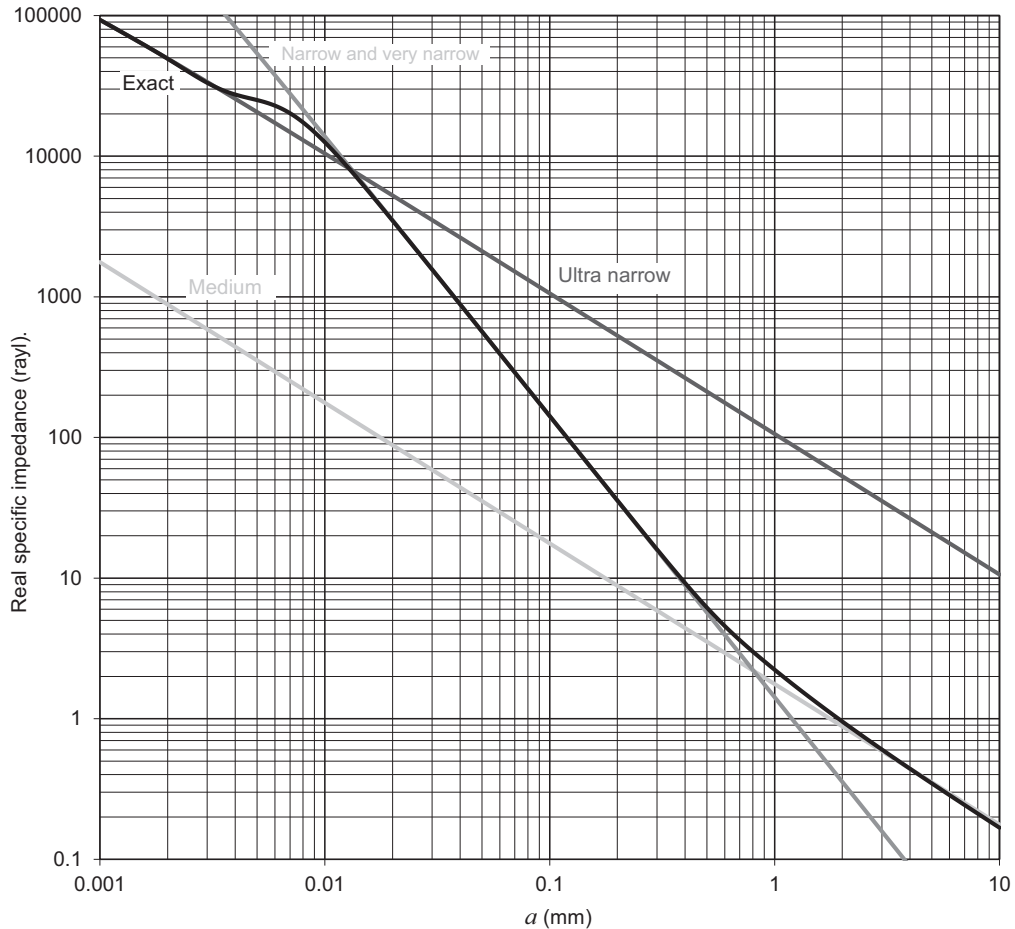


Figure 4.46 Real impedance at the entrance of an open-ended tube at a frequency of 100 Hz plotted against its radius a where the length l of the tube is 10 mm. The exact solution is given by Eq. (4.227) together with Eqs. (4.215) and (4.217). For medium, narrow and very narrow tubes, $Z_{in} = R_V + j\omega M_0$ where R_V and M_0 are given by Eqs. (4.251) and (4.252) for medium tubes, Eqs. (4.249) and (4.250) for narrow tubes, and Eqs. (4.249) and (4.250a) for very narrow tubes. The ultra narrow solution is given by Eq. (4.237).

characteristic impedance of Eqs. (4.215) and (4.217), respectively. These are valid for $a > \lambda_m$. Real and imaginary approximate curves are also shown for the three following regimes:

1. For the *very narrow* radius or asymptotic curves (medium gray dashed), Eq. (4.227) is also used but with the asymptotic wave number and characteristic impedance of Eqs. (4.236) and (4.237), respectively. The real curve is valid for $\lambda_m < a < 0.00008l\sqrt{f}$ and the imaginary curve for $\lambda_m < a < 0.0005\sqrt{l}$. We ignore the compliance elements of the analogous circuit of Fig. 4.45, which has the output terminals shorted in

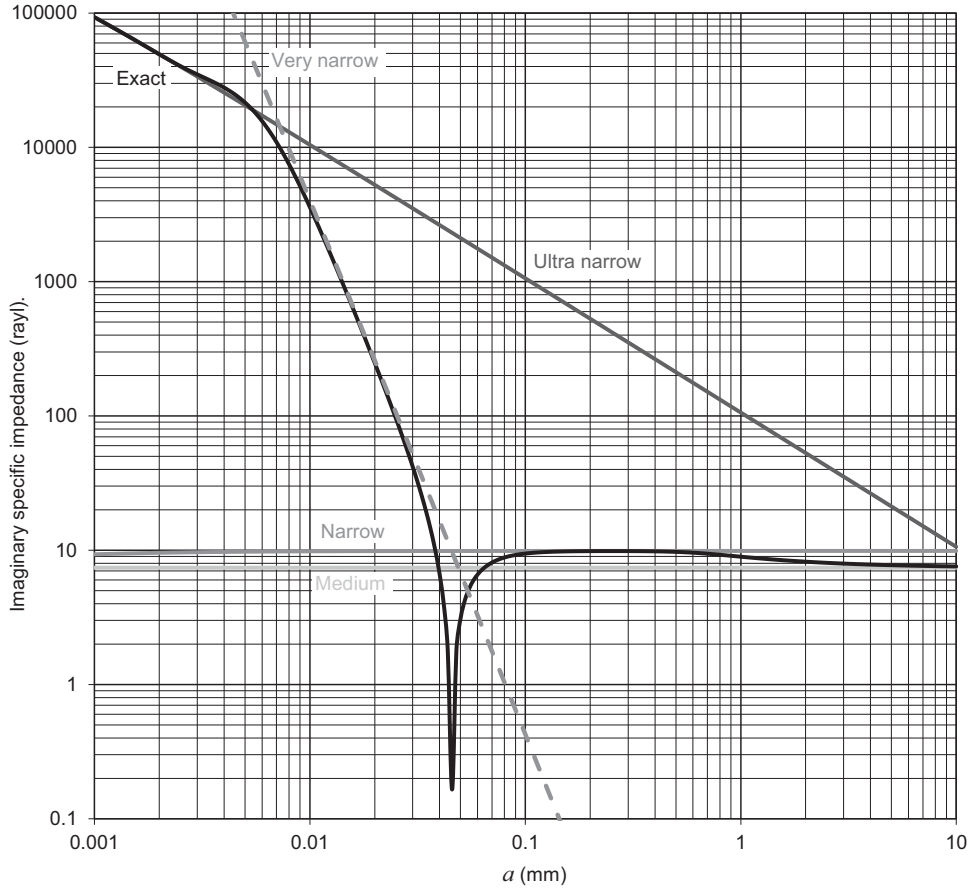


Figure 4.47 Imaginary impedance at the entrance of an open-ended tube at a frequency of 100 Hz plotted against its radius a where the length l of the tube is 10 mm. The exact solution is given by Eq. (4.227) together with Eqs. (4.215) and (4.217). For medium, narrow and very narrow tubes, $Z_{in} = R_V + j\omega M_0$ where R_V and M_0 are given by Eqs. (4.251) and (4.252) for medium tubes, Eqs. (4.249) and (4.250) for narrow tubes, and Eqs. (4.249) and (4.250a) for very narrow tubes. The ultra narrow solution is given by Eq. (4.237).

the case of an open tube, so that the input impedance reduces to $Z_{in} = R_V + j\omega M_0$, where R_V is given by Eq. (4.249) and M_0 becomes a negative mass given by

$$M_0 = -\frac{64\mu^2 l^3}{3(1 + 4B_u)^2 P_0 a^4}. \quad (4.250a)$$

Hence, there is a null in the black curve of Fig. 4.47 where the sign of the mass changes. The negative mass is derived from the property of the tangent function in Eq. (4.227) whereby $\Im(j(1-j)\tan((1-j)x)) \approx -4x^3/3$, $x \rightarrow 0$. Also, $\Re(j(1-j)\tan((1-j)x)) \approx 2x$, $x \rightarrow 0$.

2. At low frequencies, we can ignore the compliance elements of Fig. 4.45 for an open tube. Hence, the input impedance reduces to $Z_{in} = R_V + j\omega M_0$ where R_V and M_0 are given by Eqs. (4.249) and (4.250), respectively, and these are used for the *narrow* radius curves (medium gray), commonly known as the *Poiseuille flow*. The real curve is valid for $0.00008l\sqrt{f} < a < 0.002/\sqrt{f}$ and the imaginary curve for $0.0005\sqrt{l} < a < 0.002/\sqrt{f}$.
3. For *medium* radius tubes (light gray), that is for $a > 0.01/\sqrt{f}$, we again ignore the compliance elements of Fig. 4.45 and use the expression $Z_{in} = R_V + j\omega M_0$, but this time apply the expressions developed by Ingard for R_V and M_0 as follows:

$$R_V = \frac{l}{a} \sqrt{2\omega\rho_0\mu} \quad (4.251)$$

$$M_0 = \rho_0 l \quad (4.252)$$

The fact that the resistance in Eq. (4.251) varies with frequency does not really matter much in practice. In a resonant system, such as where the acoustic mass of the tube is combined with the acoustic compliance of a cavity, the resistance only dominates over a small range of frequencies either side of the resonant frequency, especially as the resistance of a medium tube is relatively small and so the Q value is likely to be high. Hence, we can simply use the value of the resistance at the resonant frequency for all frequency values.

Let us now examine the elements R_V and M_0 of Fig. 4.45. Using Eqs. (4.249) and (4.250) but with zero slip ($B_u = 0$), the frequency at which their impedances are equal is given by

$$\omega_V = \frac{R_V}{M_0} = \frac{6\mu}{a^2\rho_0} \quad \text{or} \quad a = \sqrt{\frac{6\mu}{\omega_V\rho_0}} \quad (4.253)$$

It turns out that an effective viscous boundary layer thickness δ_{visc} can be defined by

$$\delta_{visc} = \sqrt{\frac{2\mu}{\omega\rho_0}} \quad (4.254)$$

This can be obtained by letting $\tan kl \approx kl$ in Eq. (4.227) for a short tube, while letting $Q(x) \approx -2j/x$ in Eq. (4.211) for a medium radius as well as ignoring boundary slip and only keeping the higher powers of $(a\sqrt{\omega})$ in the resulting expression for Z_{in} .

In other words, at $\omega = \omega_V$ we have $a = \sqrt{3}\delta_{visc}$ so that the radius is about 1.73 times greater than the effective boundary layer thickness when the mass reactance and resistance are equal. Above this frequency, the mass reactance of the air in the tube

dominates and below it the viscous resistance dominates. If we insert the values $\mu = 1.86 \times 10^{-5} \text{ N}\cdot\text{s}/\text{m}^2$ and $\rho_0 = 1.18 \text{ kg}/\text{m}^3$ into Eq. (4.253) we also obtain $a = 0.004/\sqrt{f}$, which is the demarcation between narrow and medium radius tubes above. Hence, in a narrow tube, the frequency-invariant resistance dominates, and in a medium diameter one the mass reactance dominates and the resistance is proportional to the square root of frequency. This can be clearly seen from Figs. 4.46 and 4.47 where the mass reactance and resistance are both approximately 10 raysl at $a = 0.4 \text{ mm}$.

Ultra-narrow tube

At high frequencies in narrow tubes, we encounter a fourth regime which is distinct from those already discussed (very narrow, narrow, and medium) and where the lumped parameter model of Fig. 4.45 no longer applies. Let us now examine some properties of the tangent function in Eq. (4.227) for the impedance of an open tube. The argument kl and Z_s can be expressed in terms of lumped parameters using the wave number from Eq. (4.215) together with $j\omega pl = j\omega M_s = Z_V$ and $j\omega Cl = j\omega C_s = 1/Z_T$ so that

$$Z_{in} = j\sqrt{Z_V Z_T} \tan \sqrt{-Z_V/Z_T}. \quad (4.255)$$

We can see that for small arguments of the tangent function, where $\tan kl \approx kl$, the impedance of the open tube is just $Z_{in} = Z_V$. Using similar arguments with Eq. (4.226), where $\cot kl \approx 1/(kl)$, we find that the impedance of a blocked tube is $Z_{in} = Z_T$. From Eq. (4.248), $Z_V = R_V + j\omega M_0$. From Eq. (4.244), we will use the approximation $Z_T = 1/(j\omega C_0)$. Putting these into Eq. (4.255), we obtain

$$Z_{in} = j\sqrt{Z_V Z_T} \tan \sqrt{-(R_V + j\omega M_0)j\omega C_0}. \quad (4.256)$$

If $\omega \ll \omega_V$ then this simplifies to

$$Z_{in}|_{\omega \ll \omega_V} = j\sqrt{Z_V Z_T} \tan \sqrt{-j\omega R_V C_0} = j\sqrt{Z_V Z_T} \tan \left((1-j)\sqrt{\omega R_V C_0/2} \right). \quad (4.257)$$

From Eq. (A2.48) of Appendix II, one property of the tangent function is that $\tan(x - jy) \approx -j$ for virtually any value of x provided that y is greater than about 2. Hence, we can define a transition frequency ω_T by

$$\omega_T = \frac{8}{R_V C_0} = \frac{\gamma P_0 a^2}{\mu l^2}. \quad (4.258)$$

Below the transition frequency, the tube regimes are those for an open-ended tube above. Above it, the impedance is given by

$$Z_{in}|_{\omega \gg \omega_V} = \sqrt{Z_V Z_T} = Z_s. \quad (4.259)$$

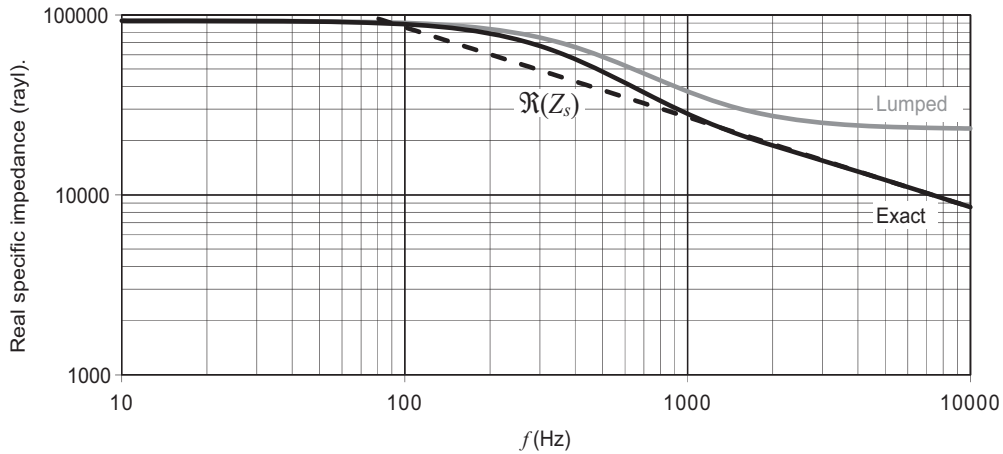


Figure 4.48 Real impedance at the entrance of an open-ended tube plotted against frequency f . The radius a of the tube is $1.1 \mu\text{m}$ and the length l is 1 mm . The exact solution is given by Eq. (4.227) and the characteristic impedance Z_s by Eq. (4.217). The lumped parameter model is as shown in Fig. 4.45, where the pair of terminals at the far end is short-circuited.

where the asymptotic expression for Z_s is given by Eq. (4.237). In this regime, the impedance is proportional to the inverse square root of frequency and the real and imaginary parts are equal, as can be seen in Figs. 4.48 and 4.49 where the transition frequency according to Eq. (4.258) is 1.45 kHz . Above this frequency, the dashed curves for Z_s from Eq. (4.237) match very closely with the black curves for the exact

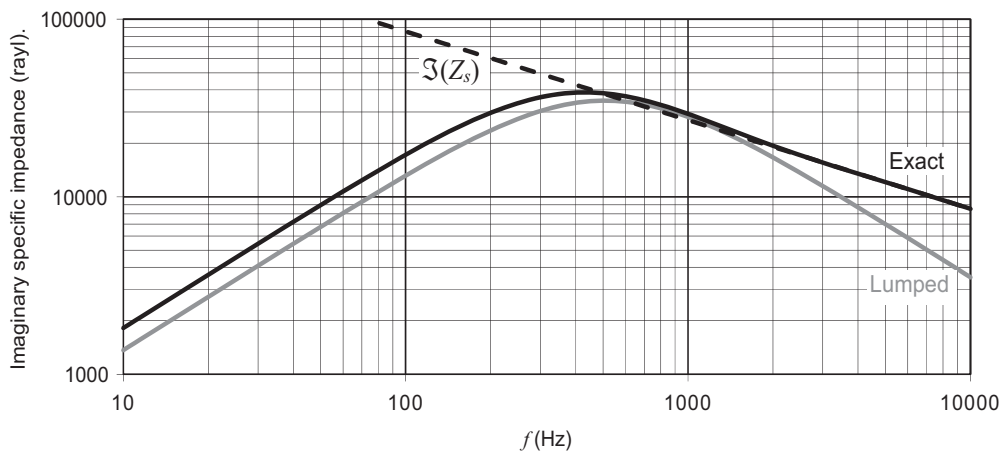


Figure 4.49 Imaginary impedance at the entrance of an open-ended tube plotted against frequency f . The radius a of the tube is $1.1 \mu\text{m}$ and the length l is 1 mm . The exact solution is given by Eq. (4.227) and the characteristic impedance Z_s by Eq. (4.217). The lumped parameter model is as shown in Fig. 4.45, where the pair of terminals at the far end is short-circuited.

expression of Eq. (4.227). At low frequencies, the dark gray curves representing the lumped parameter model of Fig. 4.45 with one pair of terminals shorted appear to be a good approximation for the black exact curves. Although there is up to 25% error in the imaginary lumped impedance at low frequencies, it is less than 10% of the total impedance, which is mainly resistive and so the impedance modulus is fairly accurate.

Interestingly, above the transition frequency of 1.45 kHz, the real and imaginary impedances of the closed tube shown in Figs. 4.50 and 4.51, respectively, are virtually identical to those of the open tube shown in Figs. 4.48 and 4.49, respectively. This is not so surprising considering that if the tangent function in Eq. (4.227) converges toward $-j$, then the cotangent function in Eq. (4.226) must converge toward j . Together with the fact that the input impedance is the characteristic impedance Z_s , this suggests that the tube under this regime behaves as an infinitely long one in which no sound is transmitted to the far end or reflected back from it because of full internal absorption. This can be confirmed if we take a look at the two-port model of Fig. 4.43.

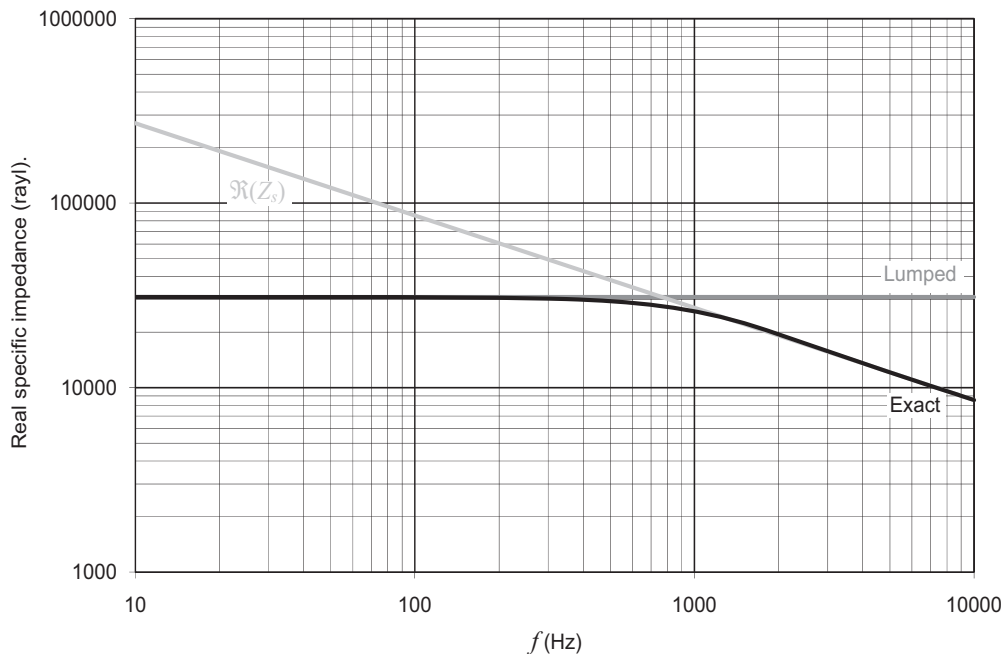


Fig. 4.50 Real impedance at the entrance of a closed tube plotted against frequency f . The radius a of the tube is $1.1 \mu\text{m}$ and the length l is 1 mm . The exact solution is given by Eq. (4.227) and the characteristic impedance Z_s by Eq. (4.217). The lumped parameter model is as shown in Fig. 4.45, where the pair of terminals at the far end is open-circuit.

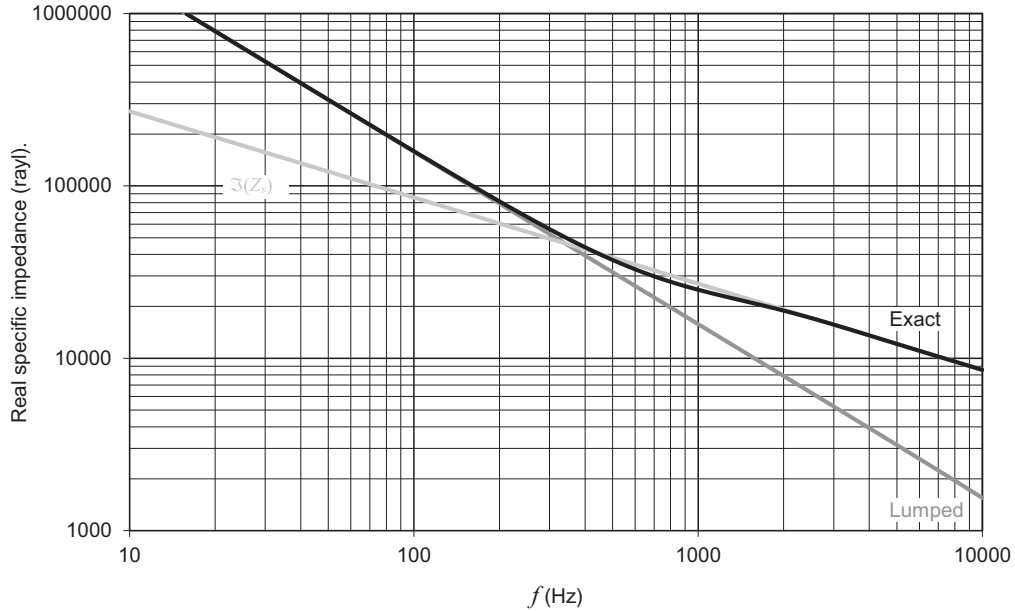


Figure 4.51 Imaginary impedance at the entrance of a closed tube plotted against frequency f . The radius a of the tube is $1.1 \mu\text{m}$ and the length l is 1 mm . The exact solution is given by Eq. (4.227) and the characteristic impedance Z_s by Eq. (4.217). The lumped parameter model is as shown in Fig. 4.45, where the pair of terminals at the far end is open-circuit.

The z -parameters are described by Eqs. (4.219) and (4.220), which under this regime reduce to

$$z_{11}|_{\omega > \omega_T} = z_{22}|_{\omega > \omega_T} \approx Z_s, \quad (4.260)$$

$$z_{12}|_{\omega > \omega_T} = z_{21}|_{\omega > \omega_T} \approx 0, \quad (4.261)$$

because $\cotan(x - jy) \rightarrow j$ and $\text{cosec}(x - jy) \rightarrow 0$ for $y > 2$ for any x . As stated above, the existence of this regime is conditional that $\omega_T \ll \omega_V$ where ω_V and ω_T are given by Eqs. (4.253) and (4.258), respectively. Hence,

$$\frac{8}{R_V C_0} \ll \frac{R_V}{M_0}. \quad (4.262)$$

Now let us define a Q value by

$$Q = \frac{1}{R_V} \sqrt{\frac{M_0}{C_0}} \ll \frac{1}{\sqrt{8}}. \quad (4.263)$$

In practice, the regime only exists for highly damped tubes where $Q < 0.05$ or $l > (6 \times 10^6)a^2$. According to Eq. (4.258), it describes the asymptotic curves in Fig. 4.46 and Fig. 4.47 for $a < 3 \mu\text{m}$ and hence can be regarded as an “ultra-narrow” tube regime.

REFERENCES

- [1] Rayleigh JWS. Theory of sound. 2nd ed., vol. 2. New York: Dover, Inc; 1945. p. 323–8.
- [2] Crandall IB. Vibrating systems and sound. New York: D. Van Nostrand Company, Inc; 1926.
- [3] Ingard U. Scattering and absorption by acoustic resonators, doctoral dissertation, Massachusetts Institute of Technology. J Acoust Soc Am 1953 1950;25:1044–5.
- [4] Li X. End correction model for the transfer impedance of microperforated panels using viscothermal wave theory. J Acoust Soc Am 2017;141(3):1426–36.
- [5] Borwick J, editor. Loudspeaker and headphone handbook. 3rd ed. Oxford: Focal; 2001. p. 588. Fig. 14.2.
- [6] Olson HF. Elements of acoustical engineering. 2nd ed. New York: D. Van Nostrand Company, Inc; 1947. p. 109–11.
- [7] Fincham L, Brown P. Line arrays with controllable directional characteristics - theory and practice. In: The 125th AES convention; 2008. paper no. 7535.
- [8] Walker PJ. New Developments in Electrostatic loudspeakers. J Audio Eng Soc 1980;28(11):795–9.
- [9] See the definition for intensity in Section 1.10. The intensity equals the sound pressure squared, divided by $\rho_0 c$ for a plane wave in free space or for a spherical wave.
- [10] Kozlov VF, Fedorov AV. Acoustic properties of rarefied gases inside pores of simple geometries. J Acoust Soc Am 2005;117(6):3402–12.
- [11] Stinson MR. The propagation of plane sound waves in narrow and wide circular tubes, and generalization to uniform tubes of arbitrary cross-sectional shape. J Acoust Soc Am 1991;89(2):550–8.
- [12] Morse PM, Ingard KU. Theoretical acoustics. New York: McGraw-Hill, Inc; 1968. p. 279. Eq. (6.4.17), p. 281; Eq. (6.4.21), p. 286; Eq. (6.4.31), p. 240; Eq. (6.1.13).
- [13] Veijola T. A two-port model for wave propagation along a long circular microchannel. Microfluid Nanofluidics 2007;3(3):359–68.



Microphones



PART XV: GENERAL CHARACTERISTICS OF MICROPHONES

Microphones are electroacoustic transducers for converting acoustic energy into electric energy. They serve two principal purposes. First, they are used for converting music or speech into electric signals that are transmitted or processed in some manner and then reproduced. Second, they serve as measuring instruments, converting acoustic signals into electric currents that are processed and displayed. In some applications such as telephony, high electrical output, low cost, and durability are greater considerations than fidelity of reproduction. In other applications, small size and high fidelity are of greater importance than high sensitivity and low cost. In measurement applications we may be interested in determining the sound pressure or the particle velocity. In some applications the microphone must operate without appreciable change in characteristics regardless of major changes in temperature and barometric pressure.

For these different applications, a variety of microphones have been developed. For the purposes of discussion in this part they are divided into three broad classes, in each of which there are a number of alternative constructions. The classes are:

- Pressure microphones.
- Pressure-gradient microphones.
- Combinations of (1) and (2).

In this part we shall describe the distinguishing characteristics of these three types. In the next two parts we shall discuss in detail several examples of each type involving electromagnetic and electrostatic types of transduction. A brief summary of their characteristics is given in [Table 5.1](#), which will be explained in greater detail in this chapter.

Table 5.1 Summary of different microphone types

Microphone type	Pressure	Pressure-gradient
Electrostatic: (condenser, electret, or piezoelectric)	Displacement sensitive Stiffness controlled High-frequency resonance	Velocity sensitive Resistance controlled Midfrequency resonance
Electromagnetic: (moving-coil or ribbon)	Velocity sensitive Resistance controlled Midfrequency resonance	Acceleration sensitive Mass controlled Low-frequency resonance



5.1 PRESSURE MICROPHONES

A pressure microphone is one that responds to changes in sound pressure. A common example of a pressure microphone is the one with a diaphragm, the back side of which is terminated in a closed cavity (see Fig. 5.1). A tiny hole through the wall of the cavity keeps the average pressure inside the cavity at atmospheric pressure. However, rapid changes in pressure, such as those produced by a sound wave, cause the diaphragm to move backward and forward.

If a pressure microphone is placed in a small cavity in which the pressure is varied, as shown in Fig. 5.2, the output voltage will be the same regardless of what position the microphone occupies in the cavity. On the other hand, if a pressure microphone is placed at successive points 1, 2, 3, and 4 of Fig. 5.3a, it will respond differently at each of these

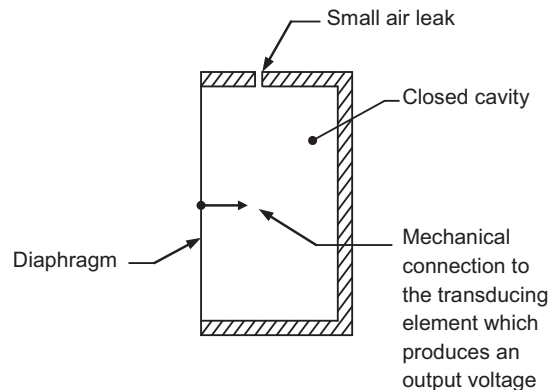


Figure 5.1 Sketch of a pressure-actuated microphone consisting of a rigid enclosure, in one side of which there is a flexible diaphragm connected to a transducing element.

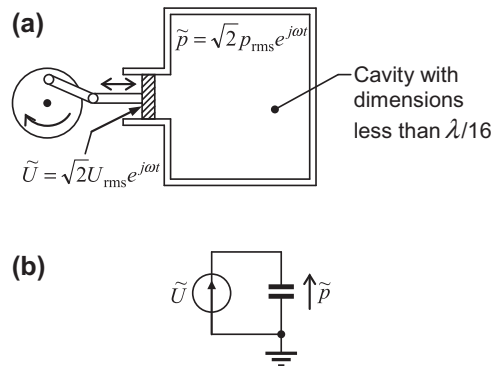


Figure 5.2 Sketch of a pressure chamber.

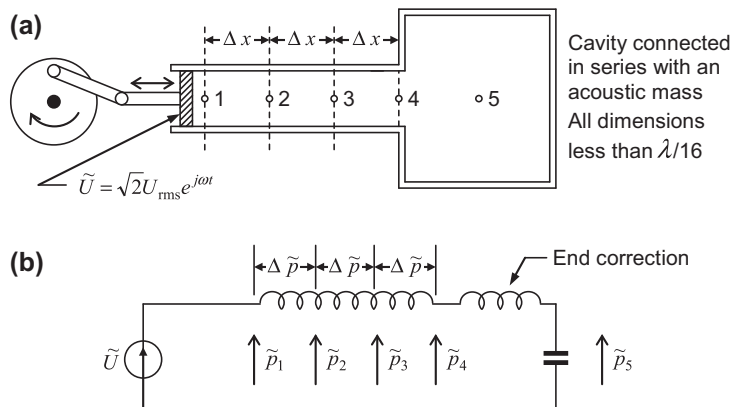


Figure 5.3 Sketch of an arrangement in which a pressure gradient is produced.

points for reasons that can be seen from Fig. 5.3b. The pressure drops p_1, p_2, p_3 , and p_4 are different from each other by an amount Δp , if the spacings Δx are alike.

If a pressure microphone is placed in a plane sound wave of constant intensity I (watts flowing through a unit area in the plane of the wave front), the force acting to move the diaphragm will be independent of frequency because $p_{rms} = \sqrt{I\rho_0 c}$ [see Eq. (1.12)].

5.2 PRESSURE-GRADIENT MICROPHONES

A pressure-gradient microphone is one that responds to a difference in pressure at two closely spaced points. A common example of this type of microphone has a diaphragm, both sides of which are exposed to the sound wave. Such a construction is shown in Fig. 5.4.

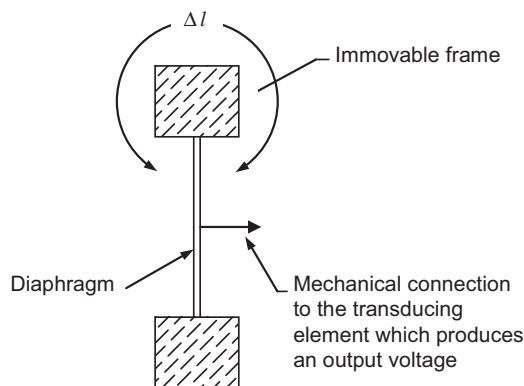


Figure 5.4 Sketch of a pressure-gradient microphone consisting of a movable diaphragm, both sides exposed, connected to a transducing element.

If a pressure-gradient microphone is placed in the cavity of Fig. 5.2a, there will be no net force acting on the diaphragm and its output will be zero. This happens because there is no pressure gradient in the cavity. In contrast, if a pressure-gradient microphone is placed at the successive positions 1–4 of Fig. 5.3a, it will produce an output voltage proportional to the pressure gradient $\Delta p/\Delta x$. In other words, if Δx is the same between successive points, the microphone output will be independent of whichever of the four positions it occupies in Fig. 5.3a.

If a very small pressure-gradient microphone is placed in a plane sound wave traveling in the x direction, the complex force \tilde{f}_D acting to move the diaphragm will be

$$\tilde{f}_D = -S \frac{\partial \tilde{p}}{\partial x} \Delta l \cos \theta \quad (5.1)$$

where

\tilde{p} is sound pressure

$\frac{\partial \tilde{p}}{\partial x} \cos \theta$ is the component of the x gradient of pressure acting across the faces of the diaphragm

θ is the angle the normal to the diaphragm makes with the direction of travel of the wave (see Fig. 5.5)

Δl is the effective distance between the two sides of the diaphragm (see Fig. 5.4)

S is area of diaphragm.

The equation for a plane traveling sound wave has already been given (Eq. (2.121)); It is

$$\tilde{p} = \tilde{p}_0 e^{-jkx} \quad (5.2)$$

where

$k = \omega/c$

\tilde{p}_0 is pressure at $x = 0$

If we assume that the introduction of the microphone into the sound field does not affect the pressure gradient, we may substitute Eq. (5.2) into Eq. (5.1) and get

$$\tilde{f}_D = \frac{j\tilde{p}_0 \omega S \Delta l \cos \theta}{c} e^{-jkx}. \quad (5.3)$$

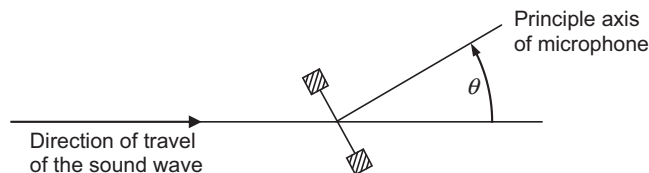


Figure 5.5 Pressure-gradient microphone with principal axis located at an angle θ with respect to the direction of travel of the sound wave.

The magnitude of the force at any point x is

$$|\tilde{f}_D| = \frac{|\tilde{p}|\omega S \Delta l \cos \theta}{c}. \quad (5.4)$$

It should be remembered (see Eq. (2.4)) that in the steady state the pressure gradient is proportional to $j\omega\rho_0$ times the component of particle velocity in the direction the gradient is being taken. The force f_D is therefore proportional to the particle velocity at any given frequency. A reference to Fig. 5.5 is sufficient to convince one that when $\theta = 90$ degrees, the force acting on the diaphragm will be zero because the conditions of symmetry require that the pressure be the same on both sides of the diaphragm. From Eq. (5.4) we also see that the effective force acting on the diaphragm is proportional to frequency and the sound pressure.

In spherical coordinates, for a microphone whose dimensions are small compared with r , Eq. (5.1) becomes

$$\tilde{f}_D = -S \frac{\partial \tilde{p}}{\partial r} \Delta l \cos \theta. \quad (5.5)$$

The equation for a spherical wave is found from Eq. (2.142)

$$\tilde{p}(r) = \tilde{A}_0 \frac{e^{-jkr}}{r} \quad (5.6)$$

Substituting (5.6) in (5.5) gives

$$\tilde{f}_D = \frac{\tilde{A}_0(1+jkr)}{r^2} e^{-jkr} S(\Delta l \cos \theta). \quad (5.7)$$

This yields

$$|\tilde{f}_D|_{\text{rms}} = \frac{|\tilde{p}|_{\text{rms}} \omega S \Delta l \cos \theta}{c} \cdot \frac{\sqrt{1+k^2 r^2}}{kr}. \quad (5.8)$$

However, we see from Eq. (2.124) that in a plane wave the rms velocity is related to the rms pressure by

$$|\tilde{u}|_{\text{rms}} = \frac{|\tilde{p}|_{\text{rms}}}{\rho_0 c} \quad (5.9)$$

and in a spherical wave (Eq. (2.144))

$$|\tilde{u}|_{\text{rms}} = \frac{|\tilde{p}|_{\text{rms}}}{\rho_0 c} \frac{\sqrt{1+k^2 r^2}}{kr} \quad (5.10)$$

where $|\tilde{u}|_{\text{rms}}$ is the rms particle velocity in the direction of travel of the sound wave. Hence, Eqs. (5.4) and (5.8) become

$$|\tilde{f}_D|_{\text{rms}} = |\tilde{u}|_{\text{rms}} \omega \rho_0 S \Delta l \cos \theta. \quad (5.11)$$

In other words, the effective (rms) force f_D acting on the diaphragm of a pressure-gradient microphone is directly proportional to the effective particle velocity in the direction of propagation of the wave, to the frequency, to the density of the air, to the size and area of the diaphragm, and to the angle it makes with the direction of propagation of the sound wave. This statement is true for any type of wave front—plane, spherical, cylindrical, or other—provided the microphone is so small that its presence does not appreciably disturb the sound wave.

At any given frequency, the response of the microphone is proportional to the $\cos \theta$, which yields the *directivity pattern* shown in Fig. 5.6a. This shape of plot is commonly referred to as a “figure of eight” pattern. The same pattern, plotted in decibels relative to the force at $\theta = 0$, is given in Fig. 5.6b. It is interesting to observe that the pattern is the same as that for an acoustic doublet or for an unflanged diaphragm at low frequencies (see Fig. 4.23 and Fig. 13.23).

The frequency response of a pressure-gradient (particle-velocity) microphone, when placed in a spherical wave, is a function of the curvature of the wave front. That is to say, from Eq. (5.10) we see that for values of $k^2 r^2$ (kr equals $\omega r/c$) large compared with 1 the particle velocity is linearly related to the sound pressure. A large value of kr means that either the frequency is high or the radius of curvature of the wave front

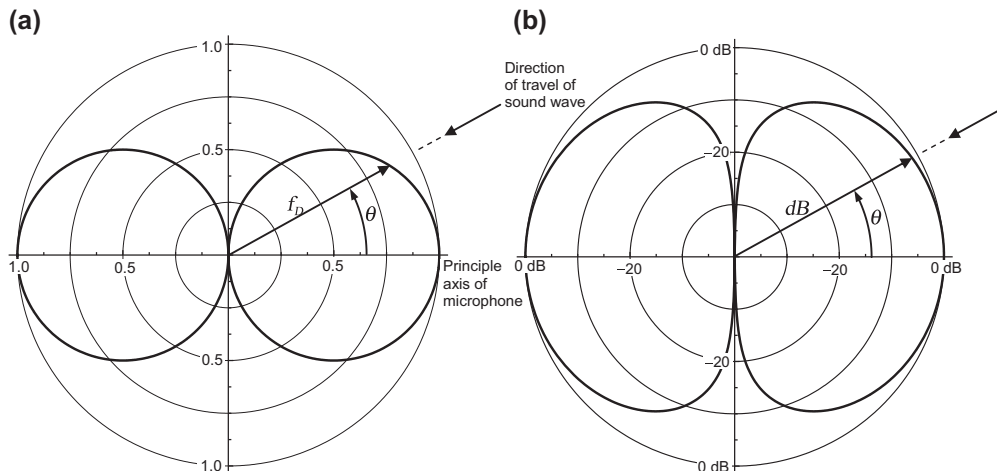


Figure 5.6 (a) Directivity characteristic of the pressure-gradient microphone of Fig. 5.4. (b) Same but with scale in dB.

is large. However, for values of $k^2 r^2$ small compared with 1, which means that the radius of curvature is small or the frequency is low, or both, the particle velocity is proportional to $|\tilde{p}|/(\omega r)$. As a result, when a person talking or singing moves near to a pressure-gradient microphone so that r is small, his voice seems to have become more “boomy” or “bassy” because the output of the microphone increases with decreasing frequency.

The path difference Δl depends on whether the diaphragm is a rigid piston or flexible. Because a microphone may be considered to be a sound source in reverse, we can use the radiation impedance of the equivalent rigid or flexible sound source to give us the relationship between the diaphragm pressure and velocity in Eqs. (5.1) and (5.11), which are rearranged as

$$Z_s = \frac{\tilde{f}_D}{S \tilde{u}} = j\omega\rho_0 \Delta l \cos \theta, \quad (5.12)$$

so that we can solve for Δl . We will assume that the incident sound waves are on-axis so that $\theta = 0$. In the case of a rigid circular piston of radius a with no baffle, the specific radiation impedance Z_s is given by

$$Z_s|_{\lambda \gg a} = \frac{\tilde{f}_D}{S \tilde{u}} = j\rho_0 c \frac{4ka}{3\pi}. \quad (5.13)$$

Equating Eqs. (5.12) and (5.13) yields

$$\Delta l = \frac{4a}{3\pi}. \quad (5.14)$$

Using the resilient disk in free space model to give the radiation impedance for a perfectly flexible diaphragm, where

$$Z_s|_{\lambda \gg a} = j\rho_0 c \pi k a / 4,$$

we find that

$$\Delta l = \frac{\pi a}{4}. \quad (5.15)$$



5.3 COMBINATION OF PRESSURE AND PRESSURE-GRADIENT MICROPHONES

A combination of pressure and pressure-gradient microphones is one that responds to both the pressure and the pressure gradient in a wave. A common example of such a microphone is the one having a cavity at the back side of the diaphragm that has an opening to the outside air containing an acoustic resistance (see Fig. 5.7a).

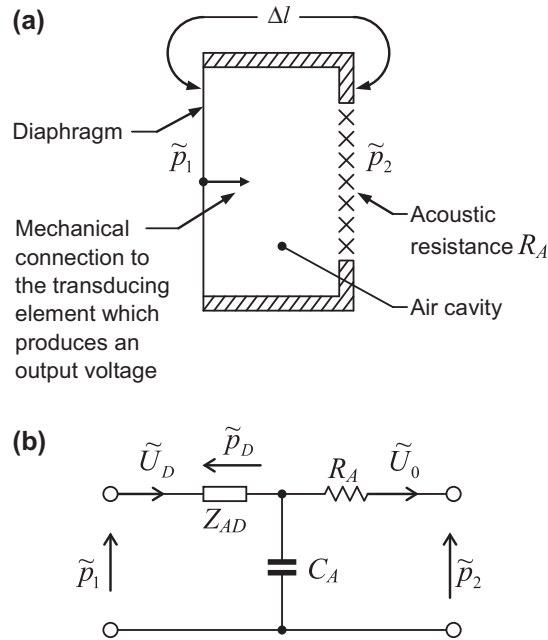


Figure 5.7 (a) Sketch of a combination pressure and pressure-gradient microphone consisting of a right enclosure in one side of which is a movable diaphragm connected to a transducing element and in another side of which is an opening with an acoustic resistance R_A . (b) Acoustic-impedance circuit for (a).

The analogous circuit for this device is shown in Fig. 5.7b. If we let

$$\tilde{p}_1 = \tilde{p}_0 e^{-jkx} \quad (5.16)$$

$$\begin{aligned} \tilde{p}_2 &= \tilde{p}_1 + \frac{\partial(\tilde{p}_0 e^{-jkx})}{\partial x} \Delta l \cos \theta \\ &= \tilde{p}_1 \left(1 - j \frac{\omega}{c} \Delta l \cos \theta \right). \end{aligned} \quad (5.17)$$

Let us say that \tilde{U}_D is the volume velocity of the diaphragm, \tilde{U}_0 is the volume velocity of the air passing through the resistance, \tilde{p}_D is the net pressure acting to move the diaphragm, and Z_{AD} is the diaphragm impedance. In the case of an electrostatic or ribbon microphone, the radiation mass will have a significant effect, so for the sake of simplicity let us lump this in with Z_D . The acoustic resistance R_A will also have a mass component,

but we assume that it is very small compared with the resistance. Then we can write the following equations from Fig. 5.7b:

$$\tilde{U}_D \left(Z_{AD} + \frac{1}{j\omega C_A} \right) - \frac{\tilde{U}_0}{j\omega C_A} = \tilde{p}_1 \quad (5.18)$$

$$\frac{-\tilde{U}_D}{j\omega C_A} + \tilde{U}_0 \left(R_A + \frac{1}{j\omega C_A} \right) = -\tilde{p}_2,$$

which are solved for \tilde{U}_D . The pressure difference across the diaphragm is

$$\tilde{p}_D = \tilde{U}_D Z_{AD} = \frac{Z_{AD} \left(\tilde{p}_1 R_A + \frac{\tilde{p}_1 - \tilde{p}_2}{j\omega C_A} \right)}{Z_{AD} R_A - j((R_A + Z_{AD})/\omega C_A)}. \quad (5.19)$$

Substitution of (5.17) in (5.19) yields

$$\tilde{p}_D = \tilde{p}_1 \frac{Z_{AD} \left(R_A + \frac{\Delta l \cos \theta}{c C_A} \right)}{Z_{AD} R_A - j((R_A + Z_{AD})/\omega C_A)}. \quad (5.20)$$

Let

$$\frac{\Delta l}{c C_A R_A} = B, \quad (5.21)$$

where B is an arbitrarily chosen dimensionless constant. Because $\tilde{f}_D = \tilde{p}_D S$, where S is the effective area of the diaphragm, we have

$$|\tilde{f}_D| = \tilde{p}_1 |A| S (1 + B \cos \theta), \quad (5.22)$$

where A is the ratio given by

$$A = \frac{Z_{AD} R_A}{Z_{AD} R_A - j((R_A + Z_{AD})/\omega C_A)}. \quad (5.23)$$

A plot of the force $|f_D|$ acting on the diaphragm as a function of θ for $B = 1$ is shown in Fig. 5.8a. The same pattern plotted in decibels is given in Fig. 5.8b. The *directivity pattern* for $B = 1$ is commonly called a *cardioid pattern*. Other directivity patterns are shown in Fig. 5.30 for $B = 0, \frac{1}{2}, 1, \sqrt{3}, 3,$ and ∞ .

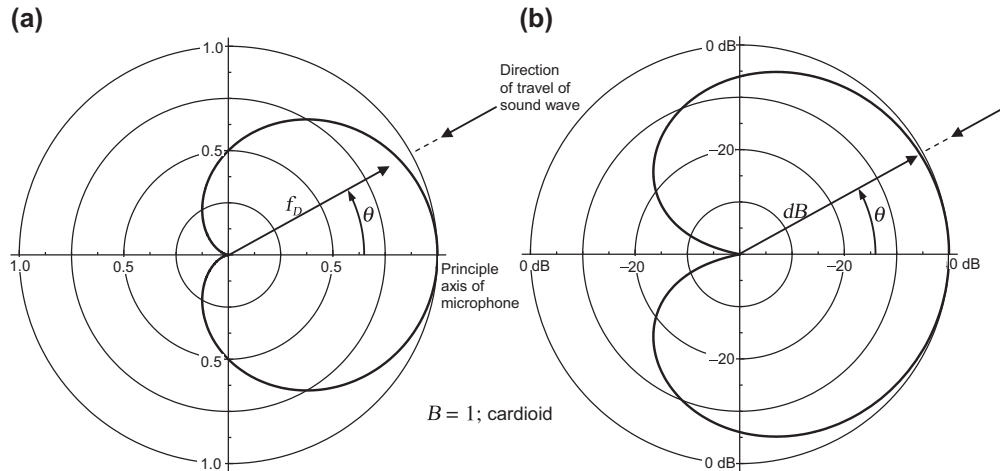


Figure 5.8 (a) Directivity characteristic of the combination pressure and pressure-gradient microphone of Fig. 5.7. (b) Same but with scale in dB.

PART XVI: PRESSURE MICROPHONES

Pressure microphones are the most widely used of the three basic types discussed in the preceding part. They are applicable to acoustic measuring systems and to the pickup of music and speech in broadcast studios, public-address installations, and hearing aids. Many engineers and artists believe that music reproduced from the output of a well-designed pressure microphone is superior to that from the more directional types of microphone because the quality of the reverberation in the auditorium or studio is fully preserved, because undesirable waveform distortion is minimized, and because the quality of the reproduced sound is not as strongly dependent as for other types on how close the talker or the musical instrument is to the microphone.

Two principal types of pressure microphones are commonly found in broadcast, public address, recording, and acoustical measurement. They are the electromagnetic and electrostatic types. We shall analyze one commercially available microphone of each of these two types in the next few sections of this part. Various other types of microphones are used in other applications, such as the piezoelectric hydrophone in underwater systems, the hot-wire microphone in aerodynamic measurements, and the Rayleigh disk in absolute particle velocity measurements. Lack of space precludes their inclusion here. However, electret (electrostatic with stored charge) and MEMS (micromechanical) types will be discussed in Chapter 8 in relation to cell phones.



5.4 ELECTROMAGNETIC MOVING-COIL MICROPHONE (DYNAMIC MICROPHONE)

General features

The moving-coil electromagnetic microphone is a medium-priced instrument of high sensitivity. It is principally used in broadcast work and in applications where long cables are required or where rapid fluctuations or extremes in temperature and humidity are expected.

The best designed moving-coil microphones have open-circuit voltage responses to sounds of random incidence that are within 5 dB of the average response over the frequency range between 40 and 16,000 Hz. Sound pressures as low as 16 dB SPL and as high as 140 dB SPL re 20 μ Pa can be measured. Changes of response with temperature, pressure, and humidity are believed to be, in the better instruments, of the order of 3–5 dB maximum below 1000 Hz for the temperature range of 10–100°F, pressure range of 0.65–0.78 m Hg, and humidity range of 0%–90% relative humidity.

The electrical impedance is that of a coil of wire. Below 1000 Hz, the resistive component predominates over the reactive component. Most moving-coil microphones have a nominal electrical impedance of about 300 Ω . The mechanical impedance is not high enough to permit use in a closed cavity without seriously changing the sound pressure therein.

To connect a dynamic microphone to an amplifier, a stepping-up transformer is required, which is usually contained within the microphone housing.

Construction

The electromagnetic moving-coil microphone consists of a diaphragm that has fastened to it a coil of wire situated in a magnetic field (see Fig. 5.9a). In addition, there are acoustical circuits behind and in front of the diaphragm to extend the response of the microphone over a greater frequency range. A cutaway view of a widely used type of moving-coil microphone is shown in Fig. 5.9b and a cross-sectional sketch is shown in Fig. 5.10.

Electro-mechano-acoustical relations

The sound passes through the dust screen and arrives at an array of sound holes in front of the diaphragm, which form a small acoustic mass and a small acoustic resistance, although most of the acoustic resistance is provided by the dust screen. The holes are so small that their radiation impedance, operating as a loudspeaker, is essentially reactive over the whole frequency range (see Fig. 4.39). The front cavity between the holes and diaphragm is a small acoustic compliance. Hence, the total acoustical circuit *in front of the diaphragm* is that of Fig. 5.11. The pressure \tilde{p}_B is that which the sound wave would

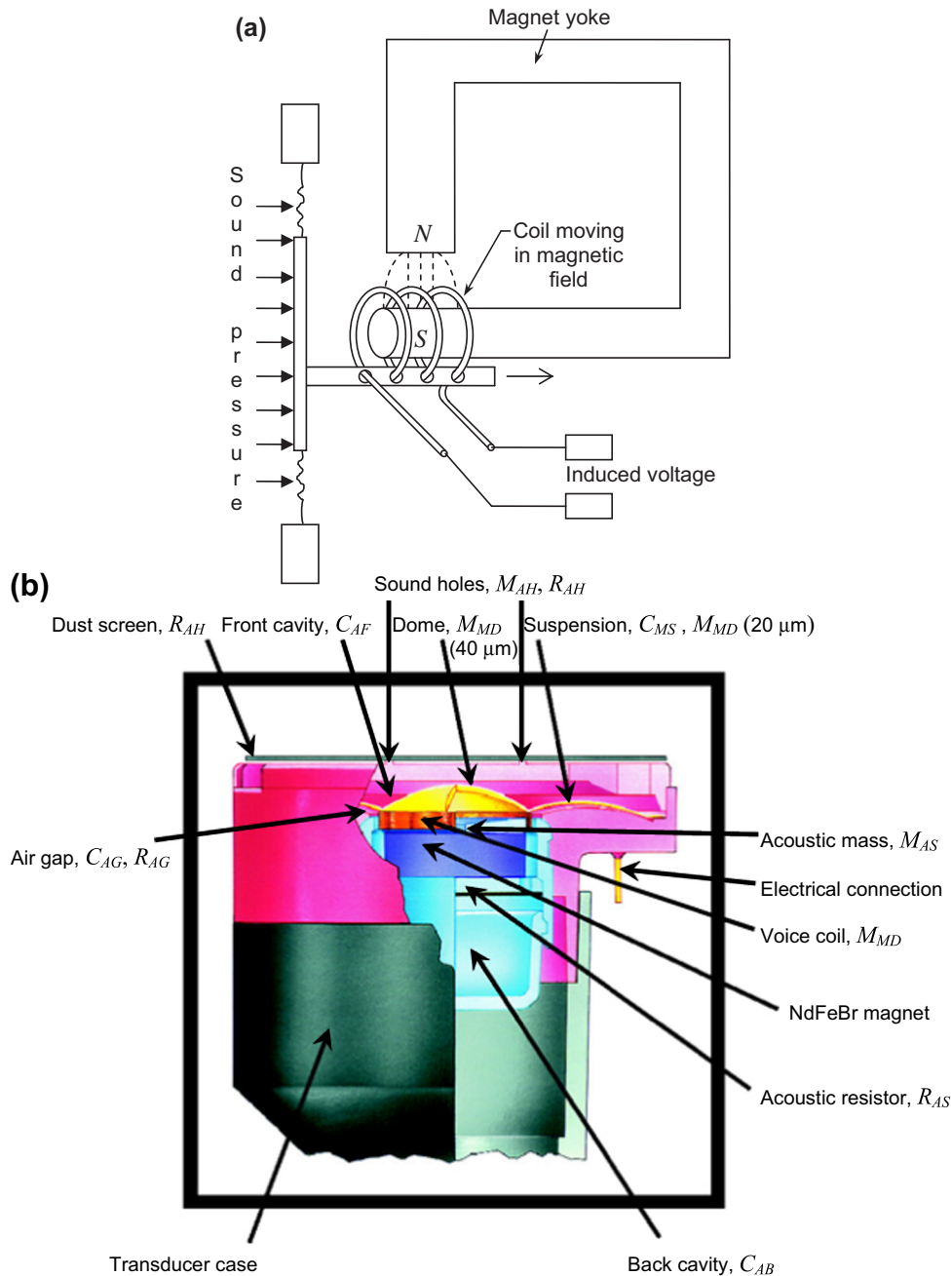


Figure 5.9 (a) Diagrammatic representation of the essential elements of a moving-coil (dynamic) microphone. (b) Cutaway view of a commercially available moving-coil microphone type D230. In this variation design, the thickness of the diaphragm varies radially to provide higher compliance in the suspension and greater stiffness at the center, which moves the dome break-up modes out of the operating frequency range. (a) From Beranek, *Acoustic Measurements*, John Wiley & Sons, Inc., New York, 1949. (b) Courtesy of AKG.

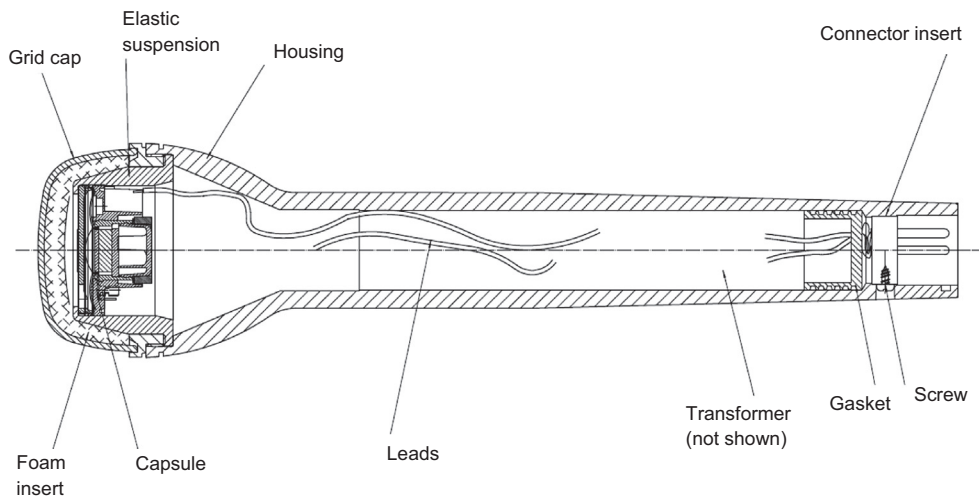


Figure 5.10 Cross-section of a commercially available moving-coil microphone type D230. *Courtesy of AKG.*

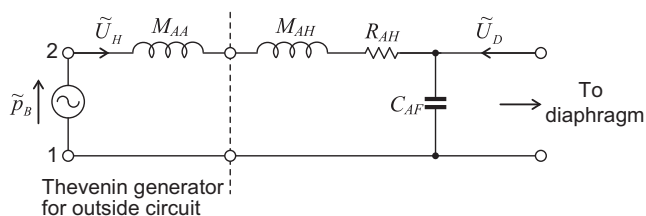


Figure 5.11 Acoustical circuit for the elements in front of the diaphragm of the microphone of Fig. 5.9 (acoustic-impedance analogy).

produce at the face of the grid if the holes of the grid were closed off. \tilde{U}_H is the volume velocity of the air that moves through the holes. \tilde{U}_D is the volume velocity of the diaphragm and is equal to the effective linear velocity \tilde{u}_D of the diaphragm times its effective area S_D . The radiation mass looking outward from the grid openings is M_{AA} . The acoustic mass and resistance of the holes and dust screen are M_{AH} and R_{AH} . The compliance of the air space in front of the diaphragm is C_{AF} . At all frequencies, except the very highest, the effect of the protective screen can be neglected.

Behind the diaphragm the acoustical circuit is more complicated. First there is an air gap between the diaphragm and the magnet that forms an acoustic compliance and resistance (see Fig. 5.9b). This air gap connects with a large back cavity that is also an acoustic compliance. In the connecting passages, there are screens that serve as acoustic resistances. Also, the interconnecting passages form an acoustic mass. The large air cavity connects to the outside of the microphone through a narrow pressure-equalizing tube, which prevents static displacements of the diaphragm due to variations in atmospheric

pressure. It also attenuates the output of the microphone at the very lowest frequencies because the sound arriving at the rear of the diaphragm via the tube cancels that at the front. However, for simplicity, we shall ignore this tube during our analysis because its effect is only evident well below the working frequency range of the microphone, although in some designs it is tuned to resonate with the back cavity and thus boost the low-frequency output rather like a bass-reflex port in a loudspeaker, a topic which is covered in more detail in Chapter 7.

The complete acoustical circuit behind the diaphragm is given in Fig. 5.12. The acoustic compliance and resistance directly behind the diaphragm are C_{AG} and R_{AG} respectively, the acoustic resistances of the screens are R_{AS} , the acoustic mass of the interconnecting passage is M_{AS} , and the acoustic compliance of the large back cavity is C_{AB} .

The electromechanical circuit (mechanical-admittance analogy) for the diaphragm and voice coil is given in Fig. 5.13. The force exerted on the diaphragm is \tilde{f}_D , and its resulting velocity is \tilde{u}_D . Here, M_{MD} is the mass of diaphragm and voice coil; C_{MS} is the compliance of the suspension; L is the inductance of voice coil; and R_E is the electric resistance of the voice coil. Z_{EL} is the electric impedance of the electric load to which the microphone is connected. The quantity $\tilde{e}_0 = Bl\tilde{u}_D$ is the open-circuit voltage produced by the microphone. There will also be some mechanical resistance due to the suspension, but this is generally very small compared with the acoustic resistance R_{AS} so we will ignore it.

To combine Figs. 5.11–5.13, the dual of Fig. 5.13 must first be taken; it is shown in Fig. 5.14. Now, to join Figs. 5.11, 5.12, and Fig. 5.14, all forces in Fig. 5.14 must be

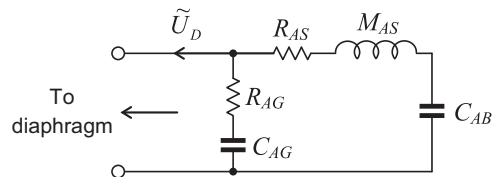


Figure 5.12 Acoustical circuit for the elements behind the diaphragm of the microphone of Fig. 5.9 (acoustic-impedance analogy).

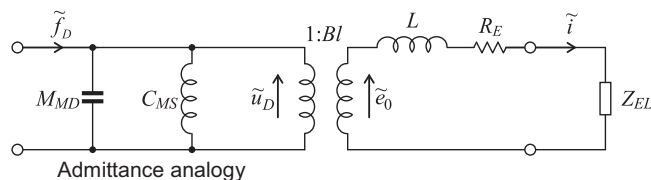


Figure 5.13 Mechano-electrical circuit of diaphragm, voice coil, and magnetic field of the microphone of Fig. 5.9 (mechanical-admittance analogy).

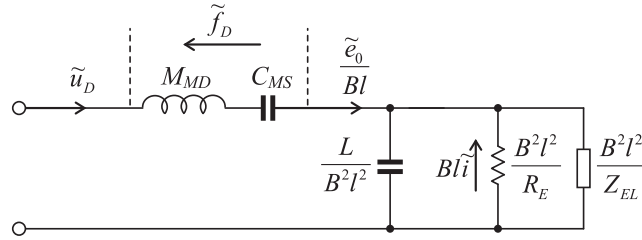


Figure 5.14 Mechano-electrical circuit of the diaphragm, voice coil, and magnetic field of the microphone of Fig. 5.9 (mechanical-impedance analogy). Note that u_D is also equal to e_0/Bl .

divided by the area of the diaphragm S_D and all velocities multiplied by S_D . This can be done by inserting an area transformer into the circuit. Recognizing that \tilde{U}_D must be the same for all three component circuits, we get the circuit of Fig. 5.15 for the moving-coil microphone.

Performance

The performance of the circuit of Fig. 5.15 can best be understood by reference to Fig. 5.16, which is derived from Fig. 5.15. Let us assume from now on that $Z_{EL} \rightarrow \infty$. This means that the electrical terminals are open circuited so that the voltage appearing across them is the open-circuit voltage \tilde{e}_0 (see Fig. 5.13). In the circuit of Fig. 5.15, the “short-circuit” velocity is equal to \tilde{e}_0/Bl .

At very low frequencies, Fig. 5.15 reduces to Fig. 5.16a. The generator \tilde{p}_B is effectively open circuited by the three acoustic compliances C_{AF} , C_{AG} , and C_{AB} , and the mechanical compliance C_{MS} of which only C_{AB} and C_{MS} have appreciable size. Also, all of the resistances and reactances of the masses are small compared with the reactances of C_{AB} and $C_{MS}S_D^2$. Hence, \tilde{e}_0 is very small. This region is marked (a) in Fig. 5.17, where we see the voltage response in decibels as a function of frequency. In region (a), the response increases at the rate of 6 dB per octave increase in frequency.

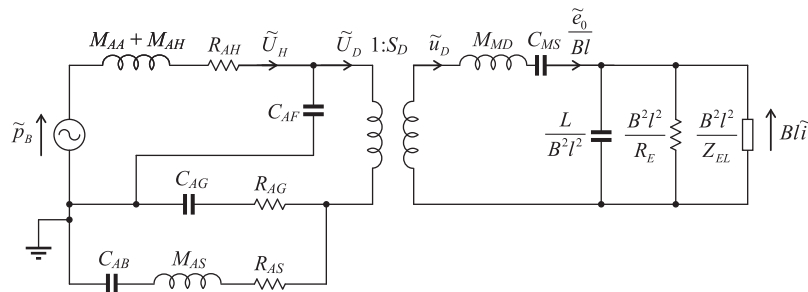


Figure 5.15 Complete electro-mechano-acoustical circuit of the moving-coil microphone of Fig. 5.9 (impedance analogy). The electromechanical transformer has been cleared from the circuit.

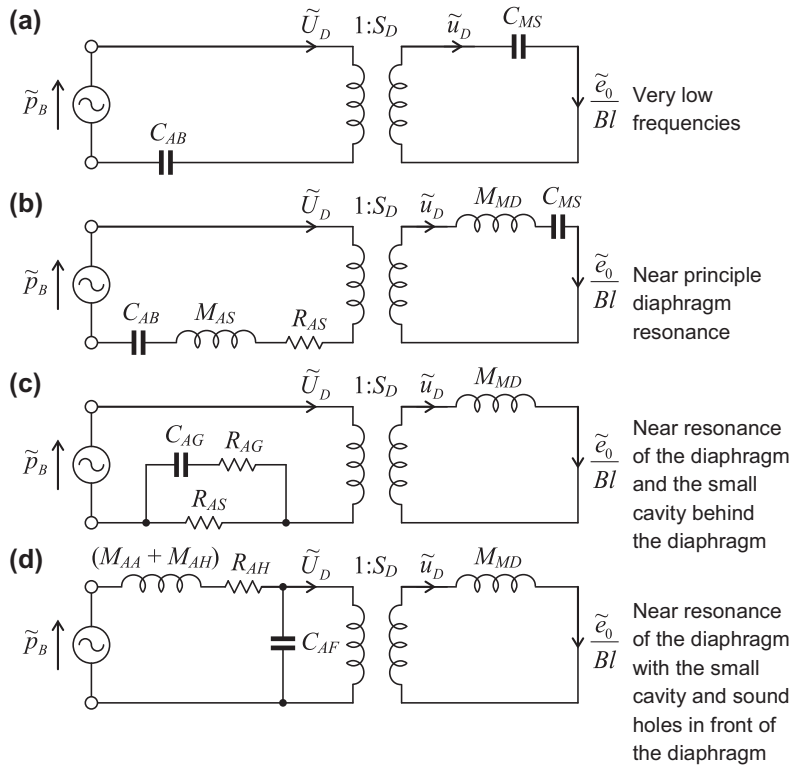


Figure 5.16 Moving-coil microphones. Simplified circuits for four frequency regions (impedance analogy). The excess pressure produced by the sound wave at the front of the microphone with the sound holes blocked off is \tilde{p}_B and the open-circuit voltage is \tilde{e}_0 .

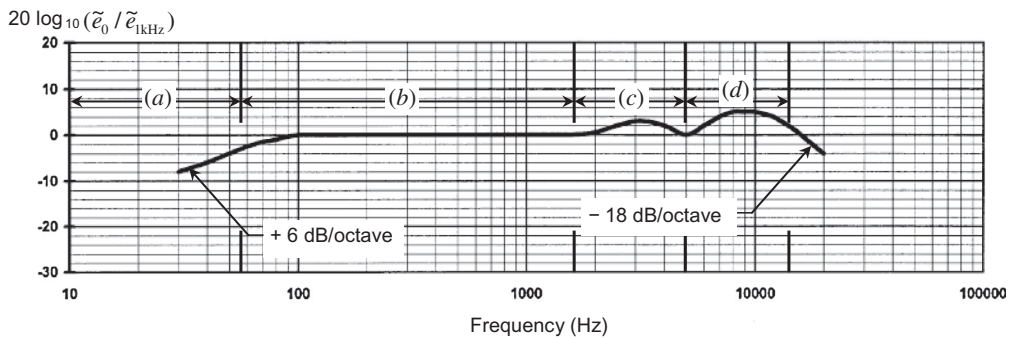


Figure 5.17 Open-circuit voltage response characteristic of a moving-coil microphone of the type shown in Fig. 5.9. The vertical scale is in dB and the reference voltage $\tilde{e}_{1\text{kHz}}$ is the value of \tilde{e}_0 at 1 kHz. Courtesy of AKG.

As the frequency increases (see Fig. 5.16b), a highly damped resonance condition occurs involving the resistance and mass of the screens behind the diaphragm, R_{AS} and M_{AS} , and the diaphragm constants themselves, M_{MD} and C_{MS} , together with the compliance C_{AB} back of the back cavity. This is region (b) of Fig. 5.17. A highly important design feature, therefore, is a resistance of the screens R_{AS} large enough so that the response curve in region (b) is as flat as possible. The damping is so great that it makes more sense to define this region by two break frequencies ω_L and ω_U , which define the upper and lower limits of this region rather than a single resonance frequency ω_0 . These are defined by

$$\omega_L = \frac{C_{AB} + S_D^2 C_{MS}}{R_{AS} C_{AB} S_D^2 C_{MS}} \quad (5.24)$$

$$\omega_U = \frac{R_{AS}}{M_{AS} + M_{MD}/S_D^2} \quad (5.25)$$

and

$$\omega_0 = \sqrt{\omega_L \omega_U} \quad (5.26)$$

The lower frequency ω_L marks the beginning of the 6 dB/octave low-frequency roll-off, which occurs at 55 Hz in Fig. 5.17, where the response is 3 dB less than that in the flat region. The upper frequency ω_U occurs somewhere near the upper limit of region (b). At the resonance frequency ω_0 , the mass and compliance elements cancel each other's reactances leaving just resistive element R_{AS} . At this frequency, the midband sensitivity is given by

$$\tilde{e}_0 = \frac{Bl \tilde{p}_B}{S_D R_{AS}} \quad (5.27)$$

In the case of the microphone shown in Fig. 5.9, the sensitivity is 2.4 mV/Pa or -52 dBV/Pa.

Above region (b) (see Fig. 5.16c), a resonance condition results that involves primarily the mass of the diaphragm M_{MD} and the stiffness of the air immediately behind it, C_{AG} . This yields the response shown in region (c) of Fig. 5.17. The resonance frequency ω_C at the center of region (c) is given by

$$\omega_C = \frac{S_D}{\sqrt{M_{MD} C_{AG}}} \quad (5.28)$$

Because the air gap is so small, the viscous air flow therein has a damping effect on this resonance, as represented by R_{AG} , which is important for keeping the frequency response reasonably flat. The large value of R_{AS} damps the antiresonance of C_{AG} with M_{AS} , which would otherwise produce a suck-out in the frequency response.

Finally, a third resonance occurs involving primarily the acoustical elements in front of the diaphragm (see Fig. 5.16d and region (d) of Fig. 5.17). The resonance frequency ω_D at the center of region (d) is given by

$$\omega_D = \frac{1}{\sqrt{(M_{AA} + M_{AH})C_{AF}}} \quad (5.29)$$

Because there are three reactive elements in the circuit ($M_{AA} + M_{AH}$, C_{AF} , and M_{MD}), the response then drops off at the rate of -18 dB per doubling of frequency. Of course, this is the open-circuit roll-off and a steeper rate is likely to occur if the microphone is loaded with a capacitive cable that will resonate with the coil inductance at some frequency. A step-up transformer also has a limited bandwidth, although through careful design this need not compromise the performance of the microphone. The low-frequency response depends on the inductance, which is maximized through the use of a generous core size and an ample number of turns. The high-frequency response is extended through the use of a split bobbin to reduce the interwinding capacitance and several interleaving primary and secondary sections, which reduces the leakage inductance.

These various resonance conditions result in a microphone whose response is substantially flat from 50 to 20,000 Hz except for diffraction effects around the microphone. These diffraction effects will influence the response in different ways, depending on the direction of travel of the sound wave relative to the position of the microphone. The usual effect is that the response is enhanced in regions (c) and (d) if the sound wave impinges on the front of the microphone at normal (perpendicular) incidence compared with grazing incidence. One purpose of the outer protective screen is to minimize this enhancement.



5.5 ELECTROSTATIC MICROPHONE (CAPACITOR MICROPHONE)

General features

The electrostatic type of microphone is used extensively as a standard microphone for the measurement of sound pressure and as a studio microphone for the high-fidelity pickup of music. It can be made small in size so it does not disturb the sound field appreciably in the frequency region below 1000 Hz.

Sound-pressure levels as low as 10 dB and as high as 185 dB re 0.0002 μ bar can be measured with standard instruments. The mechanical impedance of the diaphragm is that of a stiffness and is high enough so that measurement of sound pressures in cavities is possible. The electrical impedance is that of a pure capacitance.

The temperature coefficient for a well-designed capacitor microphone is less than 0.025 dB for each degree Celsius rise in temperature.

Continued operation at high relative humidities may give rise to noisy operation because of leakage across the insulators inside. Quiet operation can be restored by desiccation.

Construction

In principle, the electrostatic microphone consists of a thin diaphragm, a very small distance behind which there is a back plate (see Fig. 5.18). The diaphragm and back plate are electrically insulated from each other and form an electric capacitor. In precision measuring-microphones, commonly used diaphragm materials are nickel, stainless alloy, and titanium. Sometimes there can be problems with pin holes in nickel and wrinkles in stainless alloy. Titanium suffers from neither of these problems. The thickness of the diaphragm is typically a few micrometers, and the tension is usually greater than 2000 N/m.

A commercial form of this type of microphone is shown in Fig. 5.19. The holes in the back plate form an acoustic resistance that serves to damp the diaphragm at resonance. One manner in which the microphones are operated is shown in Fig. 5.18b. The resistances R_1 and R_2 are made very large to keep the membrane charge constant at low frequencies and thus preserve the bass response. The direct voltage E is several hundred volts and acts to polarize the microphone. A JFET buffer amplifier is usually located close to the microphone capsule; otherwise the capacitance of the microphone leads would exceed that of the microphone itself and therefore attenuate its output.

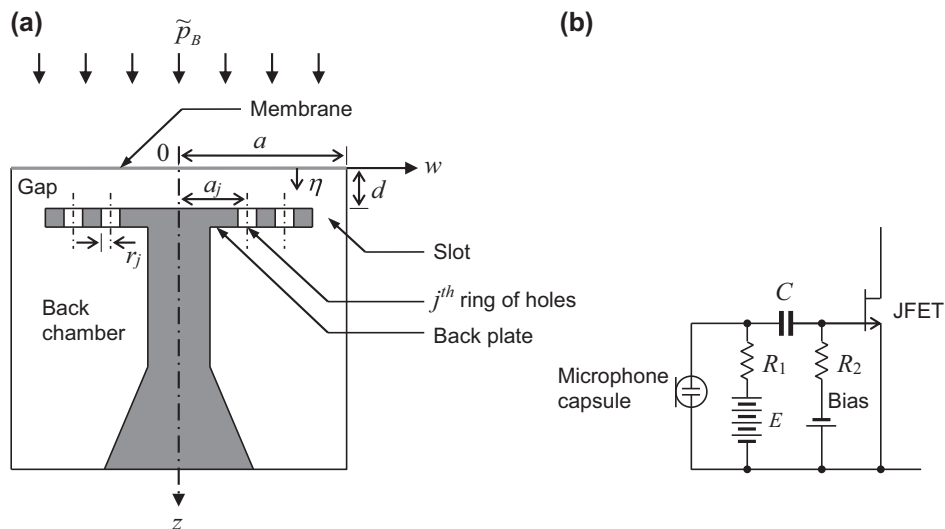


Figure 5.18 (a) Cross-sectional sketch of an electrostatic microphone. (b) Simple FET circuit for use with capacitor microphone.

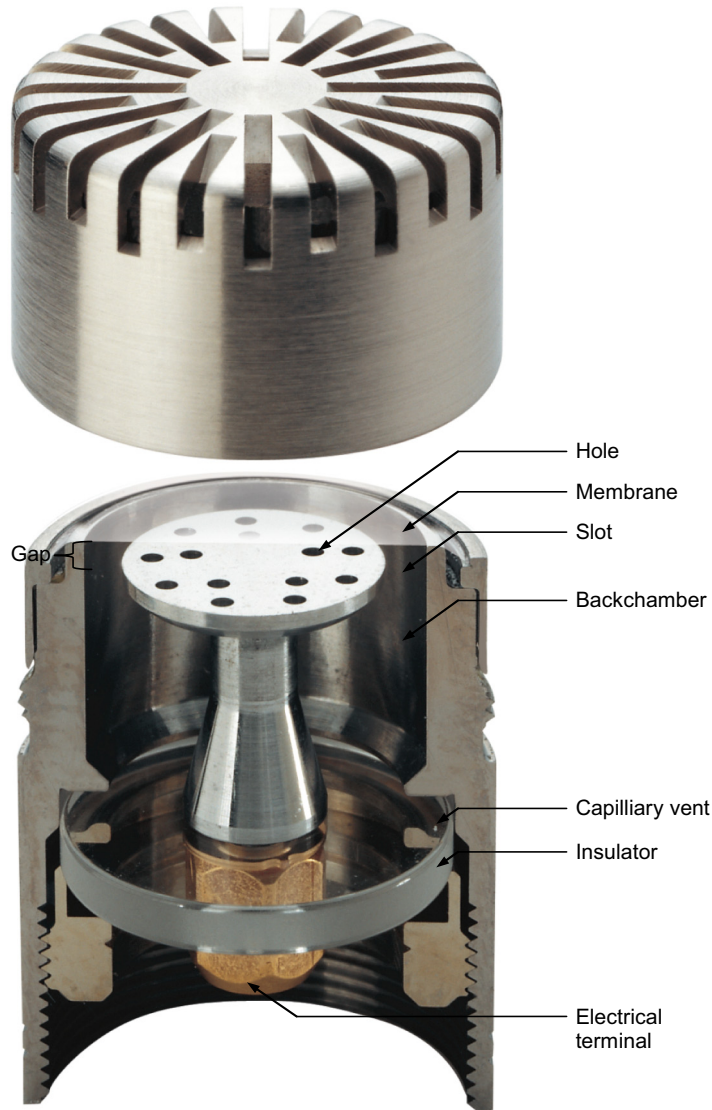


Figure 5.19 Cutaway view of the B&K type 4190 capacitor microphone. The perforated back plate serves both as the second terminal of the condenser and as a means for damping the principal resonant mode of the diaphragm. The cap with holes in it serves both for protection and as an acoustic network at high frequencies. This microphone has a polarizing voltage of $E = 200$ V. *Courtesy of Brüel & Kjær Sound & Vibration Measurement A/S.*

Electromechanical relations

Electrically, the electrostatic microphone is a capacitor with a capacitance that varies with time so that the total charge $Q(t)$ is

$$Q(t) = q_0 + q(t) = C_E(t)(E + e(t)), \quad (5.30)$$

where q_0 is the quiescent charge in coulombs, $q(t)$ is the incremental charge in coulombs, $C_E(t)$ is the capacitance in farads, E is the quiescent polarizing voltage in volts, and $e(t)$ is the incremental voltage in volts.

The capacitance $C_E(t)$ in farads is equal to (see Fig. 5.18a)

$$\begin{aligned} C_E(t) &= C_{E0} + C_{E1}(t) = \frac{\epsilon_0 S}{d - \eta(t)} \approx \frac{\epsilon_0 S}{d} \left(1 + \frac{\eta(t)}{d}\right), \\ &\approx C_{E0} \left(1 + \frac{\eta(t)}{d}\right) \end{aligned} \quad (5.31)$$

where C_{E0} is the capacitance in farads for $\eta(t) = 0$ and $C_{E1}(t)$ is the incremental capacitance in farads, ϵ_0 is a factor of proportionality that for air equals 8.85×10^{-12} , S is the effective area of one of the plates in square meters, d is the quiescent separation in meters, and $\eta(t)$ is the average incremental separation in meters. It is assumed in writing the right-hand term of Eq. (5.31) that the square of the maximum value of $\eta(t)$ is small compared with d^2 .

If we similarly assume that $[e(t)]_{\max}^2 \ll E^2$, then Eqs. (5.30) and (5.31) yield

$$q_0 + q(t) = C_{E0}E + C_{E0}E \left(\frac{e(t)}{E} + \frac{\eta(t)}{d} \right) \quad (5.32)$$

so that

$$q(t) = C_{E0} \left(e(t) + \frac{E}{d} \eta(t) \right). \quad (5.33)$$

The total stored potential energy $W(t)$ at any instant is equal to the sum of the stored electrical and mechanical energies,

$$\frac{1}{2} Q(t)^2 / C_E(t) \text{ plus } \frac{1}{2} \eta(t)^2 / C_{MS},$$

where C_{MS} is the mechanical compliance of the moving plate in m/N. That is,

$$\begin{aligned} W(t) &= \frac{1}{2} \frac{(q_0 + q(t))^2}{C_{E0} + C_{E1}(t)} + \frac{1}{2} \frac{\eta(t)^2}{C_{MS}} \approx \frac{1}{2} \frac{q_0^2 + 2q_0q(t)}{C_{E0} \left(1 + \frac{\eta(t)}{d}\right)} + \frac{1}{2} \frac{\eta(t)^2}{C_{MS}} \\ &= \frac{1}{2} \frac{q_0}{C_{E0}} (q_0 + 2q(t)) \left(1 - \frac{\eta(t)}{d}\right) + \frac{1}{2} \frac{\eta(t)^2}{C_{MS}}. \end{aligned} \quad (5.34)$$

The force in N at any instant acting to move the plate is, from the equation for work, $dW = f d\eta$,

$$f_0 + f(t) = \frac{dW(t)}{d\eta} \quad (5.35)$$

so that, by differentiation of Eq. (5.34),

$$\begin{aligned} f_0 + f(t) &\approx -\frac{q_0}{2dC_{E0}}(q_0 + 2q(t)) + \frac{\eta(t)}{C_{MS}} \\ &= -\frac{q_0^2}{2dC_{E0}} + \left(\frac{\eta(t)}{C_{MS}} - \frac{q(t)q_0}{dC_{E0}} \right). \end{aligned} \quad (5.36)$$

Hence, because $E = q_0/C_{E0}$,

$$f(t) = \frac{\eta(t)}{C_{MS}} - \frac{Eq(t)}{d}. \quad (5.37)$$

Rearranging Eq. (5.33) gives

$$e(t) \approx -\frac{E\eta(t)}{d} + \frac{q(t)}{C_{E0}}. \quad (5.38)$$

In the steady state,

$$\begin{aligned} j\omega \tilde{q} &= \tilde{i} \\ j\omega \tilde{n} &= \tilde{u} \end{aligned} \quad (5.39)$$

where \tilde{q} , \tilde{i} , \tilde{n} , and \tilde{u} are now taken to be complex harmonically varying quantities; so Eqs. (5.37) and (5.38) become, in z -parameter matrix form,

$$\begin{bmatrix} \tilde{f} \\ -\tilde{e} \end{bmatrix} = \begin{bmatrix} \frac{1}{j\omega C_{MS}} & \frac{E}{j\omega d} \\ \frac{E}{j\omega d} & \frac{1}{j\omega C_{E0}} \end{bmatrix} \cdot \begin{bmatrix} \tilde{u} \\ -\tilde{i} \end{bmatrix} \quad (5.40)$$

with \tilde{e} and \tilde{f} also being complex harmonically varying quantities.

Analogous circuits

Eq. (5.40) may be represented by either of the networks shown in Fig. 5.20, or the simplified versions shown in Fig. 5.21 where

$$C'_{E0} = \frac{-C_{E0}C_{MS}(d^2/E^2C_{MS}^2)}{C_{E0} - C_{MS}(d^2/E^2C_{MS}^2)} = \frac{C_{E0}d^2}{-E^2C_{MS}C_{E0} + d^2}, \quad (5.41)$$

$$= \frac{C_{E0}}{1 - (E^2/d^2)C_{MS}C_{E0}}$$

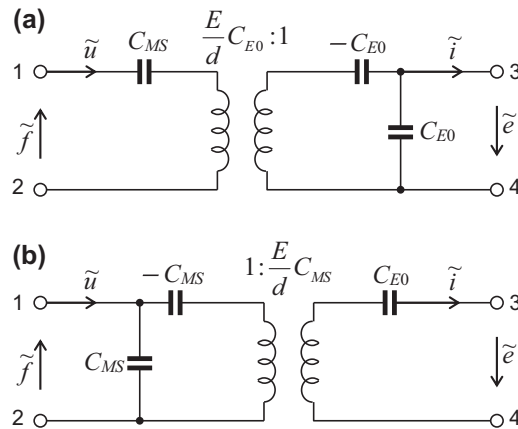


Figure 5.20 Alternate electromechanical analogous circuits for electrostatic microphones (impedance analogy).

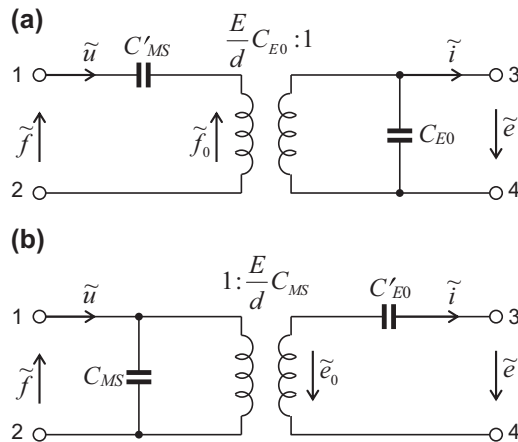


Figure 5.21 Simplified alternate electromechanical analogous circuits for electrostatic microphones (impedance analogy).

$$C'_{MS} = \frac{C_{MS}}{1 - (E^2/d^2)C_{MS}C_{E0}}. \quad (5.42)$$

The negative polarity of \tilde{e} makes sense when we consider that in Fig. 5.18a: a positive incident pressure causes a reduction in separation d , which in turn increases the capacitance $C_E(t)$ in Eq. (5.30). If the total charge remains constant, then the incremental voltage $e(t)$ must be negative. If we were to reverse the polarity of the bias voltage E , however, \tilde{e} would become positive.

Note in particular that:

C_{E0} is electrical capacitance measured with the mechanical “terminals” blocked so that no motion occurs ($\tilde{u} = 0$).

C'_{E0} is electrical capacitance measured with the mechanical “terminals” operating into zero mechanical impedance so that no force is built up ($\tilde{f} = 0$).

C_{MS} is mechanical compliance measured with the electrical terminals open circuited ($\tilde{i} = 0$).

C'_{MS} is mechanical compliance measured with the electrical terminals short circuited ($\tilde{e} = 0$).

The negative elements $-C_{E0}$ and $-C_{MS}$ in Fig. 5.20a,b respectively are due to the force of electrostatic attraction toward the back plate. These circuits were first shown as Fig. 3.37 and Fig. 3.38, and the element sizes were given in Eqs. (3.36) and (3.37). In practice, the circuit of Fig. 5.21b is ordinarily used for electrostatic microphones.

When the microphone shown in Fig. 5.19 is radiating sound into air, the force built up at the face of the microphone when a voltage is applied to electrical terminals (3–4 of Fig. 5.21b) is very small. Hence, when an electric-impedance bridge is used to measure the capacitance of the microphone, the capacitance obtained is approximately equal to C'_{E0} .

By Thévenin's theorem, the capacitor microphone in a free field can be represented by Fig. 5.22. The quantity \tilde{e}_0 is the open-circuit voltage produced at the terminals of the microphone by the sound wave and equals (from Eq. (5.40) and Fig. 5.21)

$$\tilde{e}_0 = -\frac{\tilde{u}E}{j\omega d} = -\frac{C_{MS}S\tilde{p}_B E}{d}, \quad (5.43)$$

where the force \tilde{f}_B , acting on the microphone with the diaphragm blocked so that $\tilde{u} = 0$, is equal to the blocked pressure \tilde{p}_B times the area of the diaphragm S .

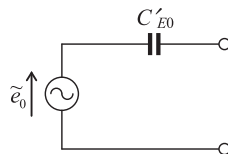


Figure 5.22 Thévenin's circuit of a capacitor microphone of the type shown in Fig. 5.18 situated in free space.

Acoustical relations

The microphone of Fig. 5.19 has a diaphragm with the property of mass M_{MD} in addition to the mechanical compliance C_{MS} assumed so far. However, unlike with the dynamic microphone, the two parameters are not separable and it is difficult to evaluate them with any accuracy over the whole frequency range because of the localized nature of the loading on the membrane, which is strongly coupled to the motion of the air in the gap and back-plate openings. However, we will use lumped-parameter elements with approximations to gain insight. For the 4190 microphone, the complete acoustical and mechanical circuit in the impedance-type analogy is seen in Fig. 5.23. The internal acoustical circuit consists of an air gap directly behind the diaphragm with an acoustic compliance C_{AG} , a back plate, including holes and a slot, with acoustic resistance and mass R_{AS} and M_{AS} , and a back cavity behind the plate with an acoustic stiffness C_{AB} . The radiation impedance looking outward from the front side of the diaphragm is $R_{AA} + j\omega M_{AA}$, where R_{AA} and M_{AA} are found from Table 4.6. In this circuit \tilde{p}_B is the incident pressure at the diaphragm when it is restrained from moving, $M_{AD} = M_{MD}/S^2$ is the acoustic mass of the diaphragm, S is the effective area of the diaphragm, and $\tilde{U}_D = S\tilde{u}_D$ is the volume velocity of the diaphragm.

When Fig. 5.21b is combined with Fig. 5.23, the complete circuit for the electrostatic microphone shown in Fig. 5.24 is obtained.

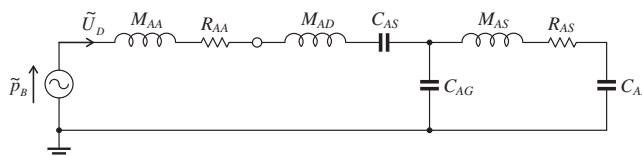


Figure 5.23 Acoustical circuit of a capacitor microphone including the radiation mass and the acoustical elements behind the diaphragm (impedance analogy).

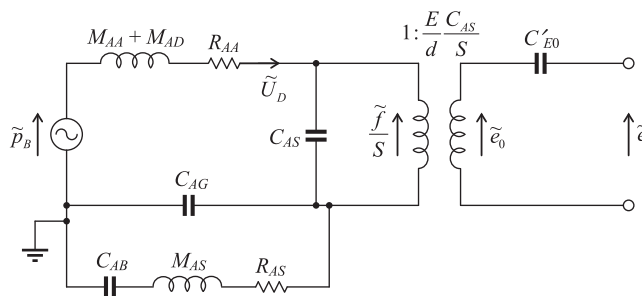


Figure 5.24 Complete electroacoustical circuit of a capacitor microphone (impedance analogy).

Performance

The performance of the capacitor microphone shown in Fig. 5.19, viz., the B&K type 4190, can best be understood by reference to Figs. 5.25 and 5.26, which are derived from Fig. 5.24. At low frequencies the circuit is essentially that of Fig. 5.25a. From this circuit, the open-circuit voltage \tilde{e}_0 is equal to

$$\tilde{e}_0 = \frac{E}{d} \frac{C_{AB} C_{AS}}{C_{AB} + C_{AS}} \frac{\tilde{p}_B}{S}. \quad (5.44)$$

At low frequencies, therefore, \tilde{e}_0 is independent of frequency. This is the frequency region shown as (a) in Fig. 5.26. Note that C_{AS} is inversely proportional to the diaphragm tension T , and C_{AB} is proportional to the back cavity volume V but inversely proportional to the atmospheric pressure P_0 (see Eq. (4.13)). In a measuring microphone the tension is set high enough so that $C_{AB} \gg C_{AS}$, which makes the microphone relatively insensitive to changes in atmospheric pressure.

In the vicinity of the first major resonance, the circuit becomes that of Fig. 5.25b. At resonance, the volume velocity through the compliance C_{AB} is limited only by the magnitude of the acoustic resistance R_{AS} . In general, this resistance is chosen to be large enough so that the resonance peak is less than 2 db (26%) higher than the response at lower frequencies. The response near resonance is shown at (b) in Fig. 5.26.

Above the resonance frequency, the circuit becomes that of Fig. 5.25c. The volume velocity is controlled entirely by the mass reactance. Hence,

$$\tilde{e}_0 = \frac{E}{\omega^2 (M_{AA} + M_{AD} + M_{AS}) d} \frac{\tilde{p}_B}{S}. \quad (5.45)$$

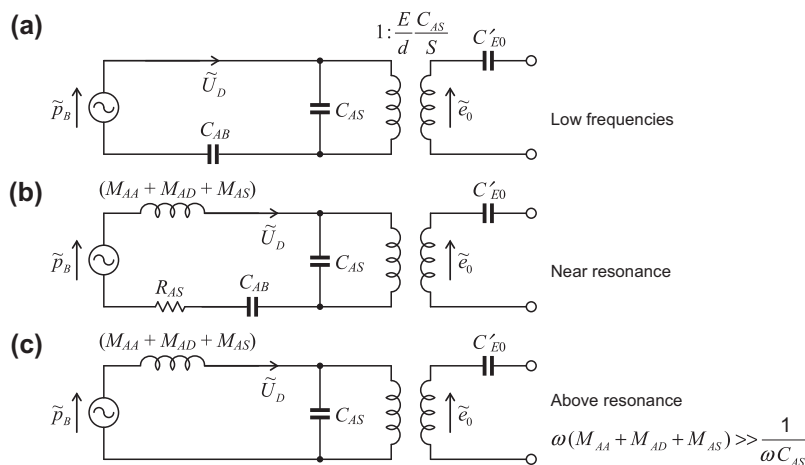


Figure 5.25 Capacitor microphone—simplified circuits (impedance analogy) for low frequencies (a), near resonance (b), and above resonance (c). The excess pressure produced by the sound wave at the diaphragm of the microphone with the microphone held motionless is \tilde{p}_B , and the open-circuit voltage is \tilde{e}_0 .

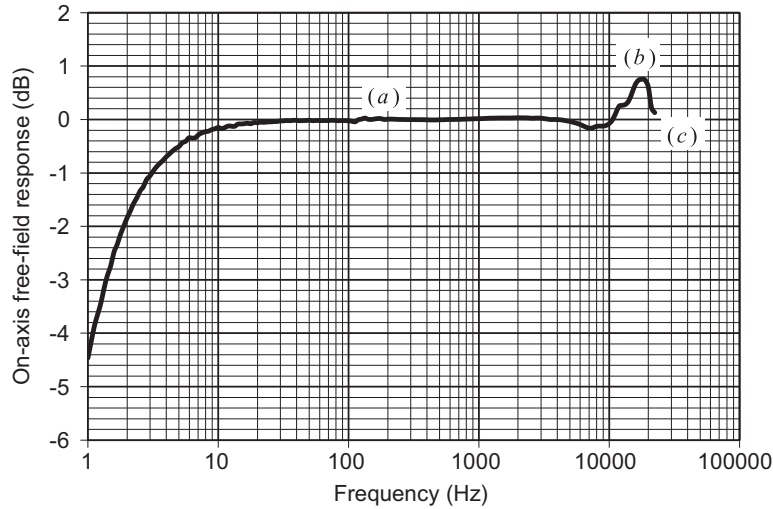


Figure 5.26 Free-field response of the B&K type 4190 capacitor microphone shown in Fig. 5.19. Courtesy of Brüel & Kjær Sound & Vibration Measurement A/S.

In this frequency region the response decreases at the rate of 12 dB per octave (see region (c) of Fig. 5.26).

At higher frequencies, further resonances could occur, but if they are not completely damped by the radiation resistance R_{AA} (which is no longer negligible compared with $j\omega M_{AA}$), the resonance peaks are likely to be limited by the viscous air flow resistance R_{AS} in the holes or gap.

In a detailed analysis, which we shall not reproduce here, Zuckerwar [1] finds that the membrane mass and compliance elements can be approximated by Ref. [1].

$$C_{AS} = \frac{S^2}{8\pi T}, \quad (5.46)$$

$$M_{AS} = \frac{4\rho_M h}{3S}, \quad (5.47)$$

which gives a resonant frequency of

$$\omega_0 = \frac{\sqrt{6}}{a} \sqrt{\frac{T}{\rho_M h}}. \quad (5.48)$$

The fundamental resonant frequency of a membrane is

$$\omega_1 = \frac{\alpha_1}{a} \sqrt{\frac{T}{\rho_M h}}, \quad (5.49)$$

where $\alpha_1 = 2.4048$ is the first zero of the Bessel function $J_0(x)$. The two frequencies ω_0 and ω_1 differ by only 2%, which implies that the lumped-element model is an accurate representation of the membrane up to ω_0 . If we assume the back plate is virtually as large as the membrane, the membrane deflection $\tilde{\eta}(w)$ at low frequencies is given by

$$\tilde{\eta}(w) = \left(1 - \frac{w^2}{a^2}\right)\tilde{\eta}_0, \quad (5.50)$$

where $\tilde{\eta}_0$ is the maximum deflection at the center. Hence the average deflection is given by

$$\langle \tilde{\eta} \rangle = \frac{2\pi}{S} \int_0^a \tilde{\eta}(w) w dw = \frac{\tilde{\eta}_0}{2}. \quad (5.51)$$

Thus the average deflection is half of that at the center, which means that the effective membrane area is half of the total area S . The optimum back-plate radius b is given by Ref. [1].

$$b = \sqrt{\frac{2}{3}}a. \quad (5.52)$$

When designing a capacitor microphone, it is desirable to minimize the air gap width d to maximize the sensitivity and hence also the signal to noise ratio. Obviously this limits the diaphragm excursion and thus also the maximum sound pressure that can be detected, but this is not generally a problem unless the microphone is designed to record very high sound pressure levels such as those produced by jet engines. Using a small gap, Paschen's law [2] works in our favor because larger electric field strengths (E/d) can be obtained before break down than in larger gaps. Once the gap width and maximum electric field strength have been established, we have to apply enough tension to the membrane for it to resist the electrostatic force of attraction toward the back plate. In other words, the positive mechanical compliance C_{MS} in Fig. 5.20a must be less than the negative electrical compliance $-C_{E0}$ when referred to the mechanical side

$$C_{MS} < \frac{d^2}{E^2 C_{E0}}. \quad (5.53)$$

However, because $C_{MS} = 1/(8\pi T)$ and $C_{E0} = \epsilon_0 S/d$ from Eqs. (5.46) and (5.31) respectively, we can write

$$T > \frac{\epsilon_0 a^2 E^2}{8d^3}, \quad (5.54)$$

which is similar to a more rigorous solution [3] based on the static membrane wave equation

$$T > \frac{\epsilon_0 a^2 E^2}{\alpha_1^2 d^3}. \quad (5.55)$$

PART XVII: PRESSURE-GRADIENT MICROPHONES

5.6 ELECTROMAGNETIC RIBBON MICROPHONES

General features

The ribbon microphone has approximately the same sensitivity and impedance as a moving-coil microphone when used with a suitable impedance-matching transformer. Because of its figure 8 directivity pattern, it used to be extensively used in broadcast and public-address applications to eliminate unwanted sounds that are situated in space, relative to the microphone, about 90 degrees from those sounds that are wanted but fell from favor because the delicate ribbon material was too prone to damage. However, because newer more rugged materials have emerged, the ribbon microphone has seen a significant revival of interest in recent years. This has also been helped by the reduction in size and weight made possible by the introduction of neodymium magnets. The ribbon microphone is often preferred by singers to introduce a “throaty” or “bassy” quality into their voices. Similarly, it produces a rich, full sound when placed close to amplified instruments. A disadvantage of the ribbon microphone is that, unless elaborate wind screening is resorted to, it is often very noisy when used outdoors.

Construction

A typical form of a pressure-gradient microphone is that represented by Fig. 5.27. It consists of a ribbon with a very low resonant frequency hung in a slot in a baffle. A magnetic field transverses the slot so that a movement of the ribbon causes a potential difference to appear across its ends. In this way, the moving conductor also serves as the diaphragm. In modern design, the ribbon element might be 38-mm long, 3.5-mm wide, and 4- μm thick with a clearance of 0.25 mm at each side.

From Eq. (5.11) we see that the pressure difference acting to move the diaphragm is

$$\tilde{p}_R = \tilde{f}_R / S = \tilde{u} \omega \rho_0 \Delta l \cos \theta, \quad (5.56)$$

where

\tilde{f}_R is the net force acting to move the ribbon.

\tilde{u} is the particle velocity in the wave in the direction of propagation of the wave.

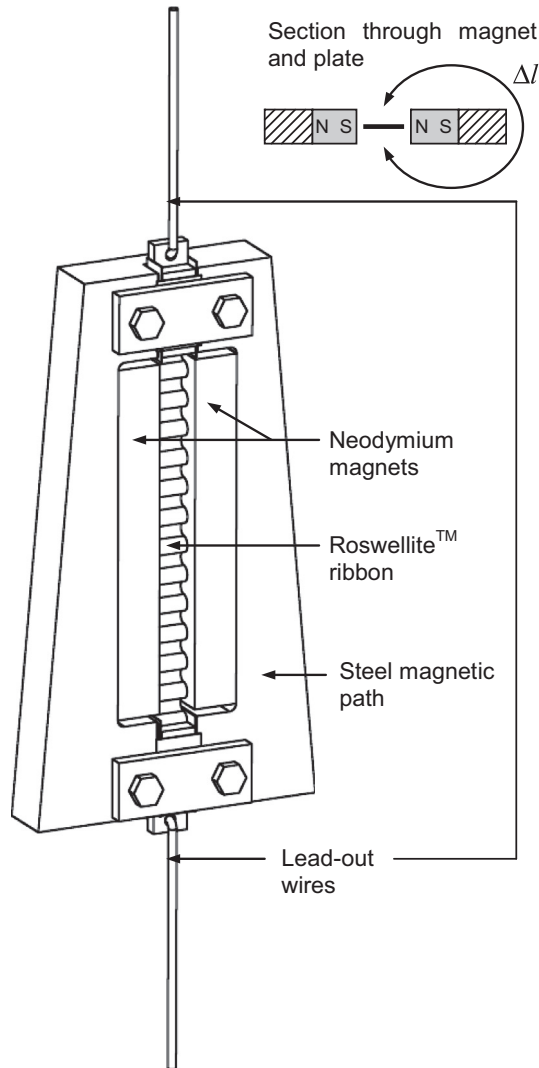


Figure 5.27 Sketch of the ribbon and magnetic structure for a velocity microphone type KSM313 ©2012, Shure Incorporated. The lead-out wires are soldered to metal blocks, and these blocks are clamped against the ribbon by the rectangular plates and the hex-shaped screws that thread into the steel frame. *Courtesy of Shure Incorporated.*

S is the effective area of ribbon.

Δl is the effective distance between the two sides.

θ is the angle the normal to the ribbon makes with the direction of travel of the wave.

This equation is valid as long as the height of the baffle is less than approximately one-half of the wavelength.

Analogous circuit

The equivalent circuit (impedance analogy) for this type of microphone is shown in Fig. 5.28. There \tilde{p}_R is the pressure difference that would exist between the two sides of the ribbon if it were held rigid and no air could leak around it; Z_{AA} is the acoustic impedance of the medium viewed from one side of the ribbon; $\tilde{U}_R = S\tilde{u}_R$ is the volume velocity of the ribbon; \tilde{u}_R is the linear velocity of the ribbon; M_{AR} , C_{AR} , and R_{AR} are the acoustic constants of the ribbon itself (for example, $M_{AR} = M_{MR}/S^2$, where M_{MR} is the mass of the ribbon); M_{AS} and R_{AS} are the acoustic mass and resistance, respectively, of the slots at either edge of the ribbon; and \tilde{U}_S is the volume velocity of movement of the air through the slot on the two sides of the ribbon.

Over nearly all the frequency range, the radiation impedance Z_{AA} is a pure mass reactance corresponding to an acoustic mass M_{AA} (see Eq. (4.172)). In a properly designed microphone, $\tilde{U}_S \ll \tilde{U}_R$. Also, the microphone is operated above the resonance frequency so that $\omega M_{AR} \gg 1/(\omega C_{AR})$. Usually, also, $\omega M_{AR} \gg R_{AR}$. Hence, the circuit of Fig. 5.28 simplifies into a single acoustic mass of magnitude $2M_{AA} + M_{AR}$.

When the admittance analogy is used and the electrical circuit is considered, we get the complete circuit of Fig. 5.29. Here, $M_{MA} = M_{AA}S^2$, $M_{MR} = M_{AR}S^2$, B is flux density, l is length of the ribbon, and $\tilde{f}_R = \tilde{p}_R/S$.

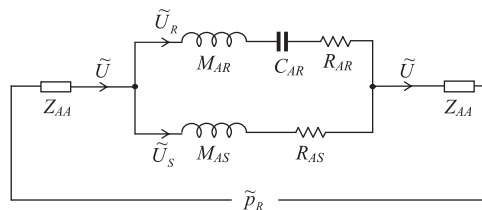


Figure 5.28 Analogous acoustical circuit for a ribbon microphone (impedance analogy).

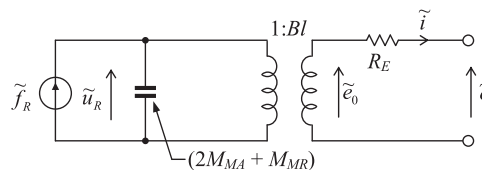


Figure 5.29 Simplified electromechanical analogous circuit for a ribbon microphone (admittance analogy).

Performance

The open-circuit voltage \tilde{e}_0 of the microphone is found from solution of Fig. 5.29 to be

$$\tilde{e}_0 = \frac{Bl\tilde{f}_R}{j\omega(2M_{MA} + M_{MR})}. \quad (5.57)$$

Substitution of Eq. (5.56) in Eq. (5.57) yields

$$|\tilde{e}_0| = |\tilde{u}| \frac{(Bl)\rho_0\Delta l}{2M_{MA} + M_{MR}} S \cos \theta. \quad (5.58)$$

The open-circuit voltage is directly proportional to the component of the particle velocity perpendicular to the plane of the ribbon. In a well-designed ribbon microphone, this relation holds true over the frequency range from 50 to 10,000 Hz. The lower resonance frequency is usually about 15–25 Hz. The effects of diffraction begin at frequencies of about 2000 Hz but are counterbalanced by appropriate shaping of the magnetic pole pieces.

PART XVIII: COMBINATION MICROPHONES

5.7 ELECTRICAL COMBINATION OF PRESSURE AND PRESSURE-GRADIENT TRANSDUCERS

One possible way of producing a directivity pattern that has a single maximum (so-called unidirectional characteristic) is to combine electrically the outputs of a pressure and a pressure-gradient microphone. The two units must be located as near to each other in space as possible so that the resulting directional characteristic will be substantially independent of frequency.

Microphones with unidirectional, or cardioid, characteristics are used primarily in broadcast or public-address applications where it is desired to suppress unwanted sounds that are situated, with respect to the microphone, about 180 degrees from wanted sounds. With respect to impedance and sensitivity, this type of cardioid microphone is similar to a ribbon or to a moving-coil microphone when suitable impedance-matching transformers are used.

The equation for the magnitude of the open-circuit output voltage of a pressure microphone in the frequency range where its response is “flat” is

$$\tilde{e}_0 = A\tilde{p}. \quad (5.59)$$

The equation for the open-circuit output voltage of a magnetic or ribbon type of pressure-gradient microphone in the same frequency range is

$$\tilde{e}'_0 = C\tilde{p} \cos \theta. \quad (5.60)$$

Adding Eqs. (5.59) and (5.60) and letting $C/A = B$ gives

$$\tilde{e}_0 = A\tilde{p}(1 + B \cos \theta). \quad (5.61)$$

B will be a real positive number only if \tilde{e}_0 and \tilde{e}'_0 have the same phase.

The directional characteristic for a microphone obeying Eq. (5.61) will depend on the value of B . For $B = 0$, the microphone is a nondirectional type; for $B = 1$, the microphone is a cardioid type; for $B = \infty$, the microphone is a figure 8 type. The value of B can also take on other values that are optimized for particular characteristics. For example, we may wish to maximize the rejection of ambient or nondirect sound. The directivity factor Q as defined in Eq. (3.142) is given by

$$Q(B) = \frac{2D^2(0)}{\int_0^\pi D^2(\theta) \sin \theta d\theta} = \frac{3(1+B)^2}{3+B^2}, \quad (5.62)$$

where the directivity function is given by

$$D(\theta) = \frac{1 + B \cos \theta}{1 + B} \quad (5.63)$$

and on-axis $D(0) = 1$. The condition for maximum off-axis rejection is

$$\frac{\partial}{\partial B} Q(B) = \frac{6(1+B)(3-B)}{(3+B^2)^2} = 0, \quad (5.64)$$

which is met when $B = 3$ and $Q(3) = 4$. This gives what is known as the *hypercardioid* pattern. Alternatively, we may wish to maximize the ratio of the sound captured from the front to that received from the rear, where the rear is defined as anything at an angle of greater than 90 degrees. Let us define the function P such that

$$P(B) = \frac{\int_0^{\pi/2} D^2(\theta) \sin \theta d\theta}{\int_{\pi/2}^\pi D^2(\theta) \sin \theta d\theta} = \frac{3 + 3B + B^2}{3 - 3B + B^2}. \quad (5.65)$$

The condition for maximum front-to-rear ratio is

$$\frac{\partial}{\partial B} P(B) = \frac{6(3-B^2)}{(3-3B+B^2)^2} = 0, \quad (5.66)$$

which is met when $B = \sqrt{3}$ and $P(\sqrt{3}) = (2 + \sqrt{3})/(2 - \sqrt{3}) = 13.9$. This gives what is known as the *supercardioid* pattern. In Fig. 5.30 directional characteristics for six values of B are shown.

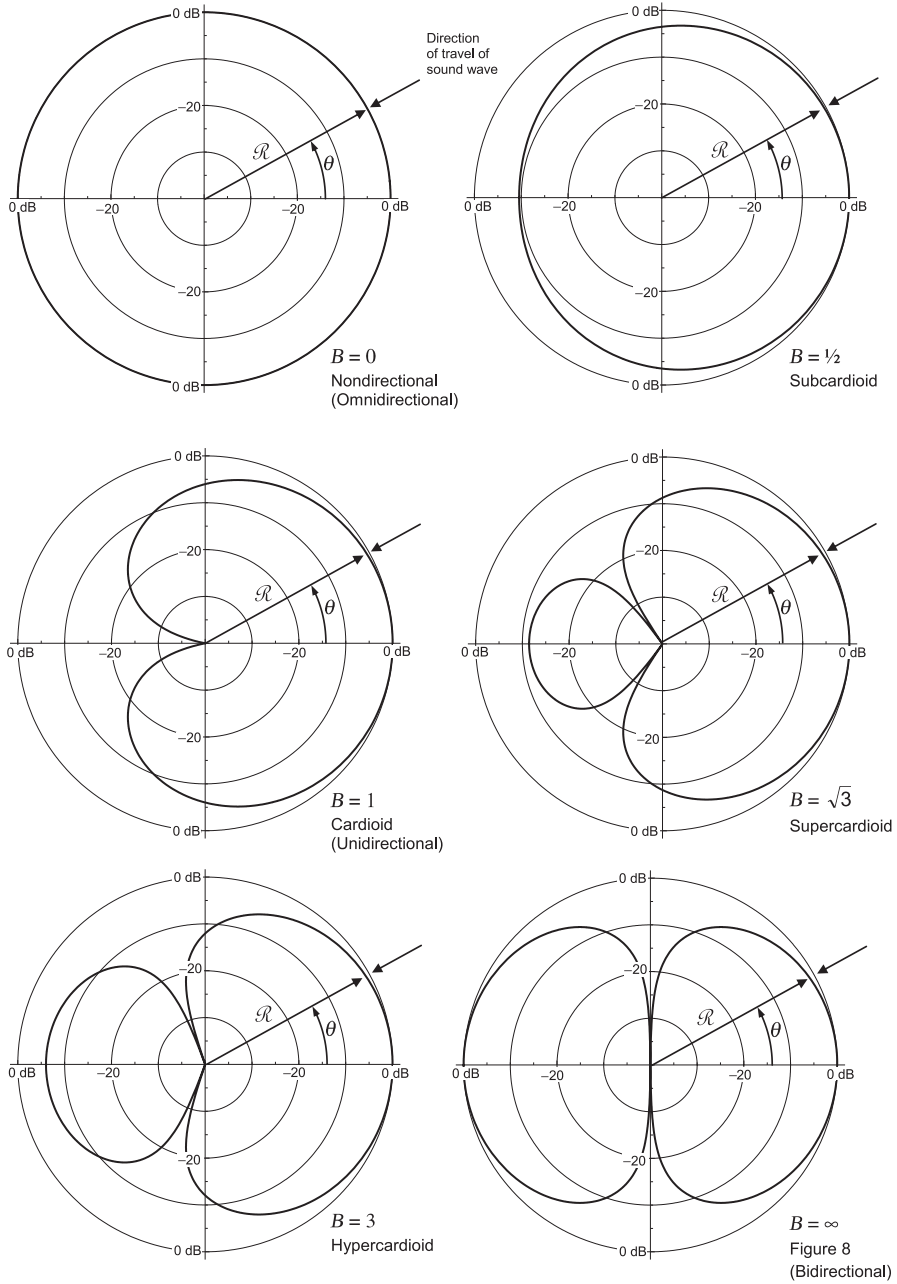


Figure 5.30 Graphs of the expression $R = 20 \log_{10}((1 + B \cos \theta)/(1 + B))$ as a function of θ for $B = 0, \frac{1}{2}, 1, \sqrt{3}, 3,$ and ∞ .

The voltage \tilde{e}'_0 is a function of kr , as discussed in Section 5.3, so that the voltage \tilde{e}_0 as given by Eq. (5.61) will vary as a function of frequency for small values of $\omega r/c$, where r is the distance between the microphone and a small source of sound. Here, as is the case for a pressure-gradient microphone, a “bassy” quality is imparted to a person’s voice if he stands very close to the microphone.



5.8 ACOUSTICAL COMBINATION OF PRESSURE AND PRESSURE-GRADIENT MICROPHONES

One example of an acoustical design responding to both pressure and pressure gradient in a sound wave was described earlier in Section 5.3 (p. 206). The directional patterns for this type of design are the same as those shown for Fig. 5.30.

Because this type of microphone has a flat response as a function of frequency for \tilde{p} constant (i.e., constant sound pressure at all frequencies in the sound wave), a transducer must be chosen whose output voltage for a constant differential force acting on the diaphragm is inversely proportional to the quantity A defined in Eq. (5.23), i.e.,

$$\tilde{e}_0 \propto 1/|A| = \left| \frac{Z_{AD} - j[(R_A + Z_{AD})/\omega C_A R_A]}{Z_{AD}} \right| \quad (5.67)$$

As an example, let us take the case of a microphone for which $Z_{AD} \gg R_A$ and $1/\omega C_A R_A \gg 1$. In this case the response of the transducer must be proportional to

$$1/|A| = \frac{1}{\omega C_A R_A} = \frac{cB}{\Delta l \omega}, \quad (5.68)$$

where B is given by Eq. (5.21).

Restated, the transducer must have an output voltage for a constant net force acting on the diaphragm that is inversely proportional to frequency, if a flat frequency response is desired. This is the case for a moving-coil or ribbon transducer above the natural resonance frequency of the diaphragm.



5.9 DUAL-DIAPHRAGM COMBINATION OF PRESSURE AND PRESSURE-GRADIENT MICROPHONES

A versatile microphone that is popular in recording studios and for recording ensembles on location is the dual-diaphragm variable-pattern capacitor microphone, the schematic of which is shown in Fig. 5.31. It has two diaphragms: one mounted in front (F) of and the other mounted at the back (B) of a common central plate (P). An array of holes in the central plate provides a mixture of resistance and reactance. When the slider of the potentiometer is at position “k,” the polarizing voltages on both diaphragms are equal so that they behave like a pair of back-to-back pressure microphones. Hence the

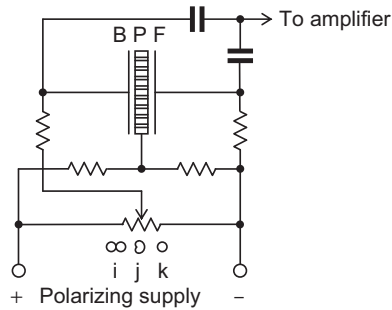


Figure 5.31 Schematic of a dual-diaphragm capacitor microphone with a variable directivity pattern. In switch positions “i,” “j,” and “k,” bi-, uni-, and omnidirectional directivity patterns are obtained respectively.

resulting directivity pattern is omnidirectional. The low compliance of the air in the holes of the plate ensures that the resonance frequencies of the diaphragms are high to provide a suitably wide working bandwidth. As with all pressure microphones, it is stiffness-controlled and displacement-sensitive in this mode.

When the slider is at the other end of its range in position “i,” the polarizing voltages on the two diaphragms are of equal magnitude but opposite polarity. Therefore, the microphone is only sensitive to the difference in pressures at the two diaphragms so that they behave more or less as a single diaphragm. Hence the resulting directivity pattern is figure 8. The resonance frequency is now determined by the diaphragm tension instead of the stiffness of the trapped air, which now travels back and forth through the holes providing a high viscous damping resistance. It is this damping resistance that determines the bandwidth of the microphone, which is resistance-controlled and velocity-sensitive in this mode. Without this resistance, the frequency response would be just one sharp resonant peak.

When the slider is at position “j,” no polarizing voltage is supplied to the diaphragm at the back (B), which in turn no longer contributes to the output voltage. Because it has low mass and high compliance, the back diaphragm is also acoustically transparent so that we have essentially the same configuration as an acoustic combination of pressure and pressure-gradient microphones shown in Fig. 5.7.

The analogous circuit for this kind of microphone is shown in Fig. 5.32, where \tilde{p}_1 and \tilde{p}_2 are the pressures on the outer surfaces of the front and back diaphragms, \tilde{U}_1 and \tilde{U}_2 are their respective volume velocities, E_1 and E_2 are the front and back polarizing voltages, and \tilde{e} is the microphone output voltage. Also, C_{E0} is the static capacitance of each diaphragm when blocked, $S = \pi a^2$ is the surface area of each diaphragm, d is distance between each diaphragm and the central plate, C_{AP} is the compliance of the air in the holes of the plate, C_{AG} is the compliance of the air in the gap between each diaphragm and the plate, and Z_{AD} is the impedance of each diaphragm that includes the

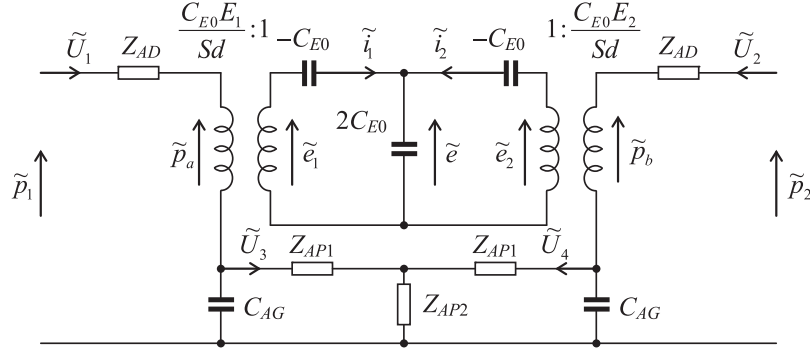


Figure 5.32 Analogous circuit for a dual-diaphragm capacitor microphone with a variable directivity pattern.

mass, compliance, radiation mass, and resistance. The holes in the plate are represented by the T-circuit impedances Z_{AP1} and Z_{AP2} using the tube model shown in Fig. 4.45 except that the holes are assumed to be so narrow that the pressure variations are effectively isothermal and hence R_T can be ignored. The elements C_{E0} and C_{AG} are defined by

$$C_{E0} = \frac{\epsilon_0 S}{d}, \quad (5.69)$$

$$C_{AG} = \frac{Sd}{\rho_0 c^2}, \quad (5.70)$$

where $\epsilon_0 = 8.85 \times 10^{-12}$ is the permittivity of free space, $\rho_0 = 1.18 \text{ kg/m}^3$ is the static density of air, and $c = 345 \text{ m/s}$ is the speed of sound in free space. From Fig. 5.32 we can write the following equations:

$$\tilde{p}_1 = \tilde{p}_a + \left(Z_{AD} + \frac{1}{j\omega C_{AG}} \right) \tilde{U}_1 - \frac{1}{j\omega C_{AG}} \tilde{U}_3, \quad (5.71)$$

$$\tilde{p}_2 = \tilde{p}_b - \frac{1}{j\omega C_{AG}} \tilde{U}_4 + \left(Z_{AD} + \frac{1}{j\omega C_{AG}} \right) \tilde{U}_2, \quad (5.72)$$

$$0 = -\frac{1}{j\omega C_{AG}} \tilde{U}_1 \left(Z_{AP1} + Z_{AP2} + \frac{1}{j\omega C_{AG}} \right) \tilde{U}_3 + Z_{AP2} \tilde{U}_4, \quad (5.73)$$

$$0 = -\frac{1}{j\omega C_{AG}} \tilde{U}_2 + Z_{AP2} \tilde{U}_3 + \left(Z_{AP1} + Z_{AP2} + \frac{1}{j\omega C_{AG}} \right) \tilde{U}_4, \quad (5.74)$$

$$\tilde{e}_1 = \frac{Sd}{E_1 C_{E0}} \tilde{p}_a = \left(\frac{1}{-j\omega C_{E0}} + \frac{1}{2j\omega C_{E0}} \right) \tilde{i}_1 + \frac{1}{2j\omega C_{E0}} \tilde{i}_2, \quad (5.75)$$

$$\tilde{e}_2 = \frac{Sd}{E_2 C_{E0}} \tilde{p}_b = \frac{1}{2j\omega C_{E0}} \tilde{i}_1 + \left(\frac{1}{-j\omega C_{E0}} + \frac{1}{2j\omega C_{E0}} \right) \tilde{i}_2, \quad (5.76)$$

$$\tilde{U}_1 = \frac{Sd}{E_1 C_{E0}} \tilde{i}_1, \quad (5.77)$$

$$\tilde{U}_2 = \frac{Sd}{E_2 C_{E0}} \tilde{i}_2, \quad (5.78)$$

$$\tilde{e} = \frac{\tilde{i}_1 + \tilde{i}_2}{2j\omega C_{E0}}. \quad (5.79)$$

Firstly we solve Eqs. (5.73) and (5.74) for \tilde{U}_3 and \tilde{U}_4 and insert these into Eqs. (5.71) and (5.72). If we then insert $\tilde{p}_a, \tilde{p}_b, \tilde{U}_1,$ and \tilde{U}_2 from Eqs. (5.75–5.78) respectively into Eqs. (5.71) and (5.72), and solve for \tilde{i}_1 and \tilde{i}_2 before inserting the latter in Eq. (5.79), we obtain an expression for the output voltage \tilde{e} . Furthermore, we use the expression for \tilde{p}_2 given by Eq. (5.17).

Omnidirectional performance

If $E_2 = E_1$, which corresponds to the slider being at position “k” in Fig. 5.31, we have a pressure microphone and the sensitivity is given by

$$\tilde{e}_k = \frac{E_1 \left(2 - j \frac{\omega}{c} \Delta l \cos \theta \right)}{2j\omega Sd \left(Z_{AD} + \frac{(Z_{AP1} + 2Z_{AP2}) \frac{1}{j\omega C_{AG}}}{Z_{AP1} + 2Z_{AP2} + \frac{1}{j\omega C_{AG}}} \right)} \tilde{p}_1, \quad (5.80)$$

where we let

$$\Delta l = (l + \pi a/4) \quad (5.81)$$

in accordance with Eq. (5.15) for a resilient disk. Using this formula, the exact on-axis response with the switch in position “i” for an omnidirectional pattern is plotted in Fig. 5.33. We see from this formula that the directivity pattern is essentially omnidirectional provided that

$$f \ll \frac{c}{3a + \pi l} \quad (5.82)$$

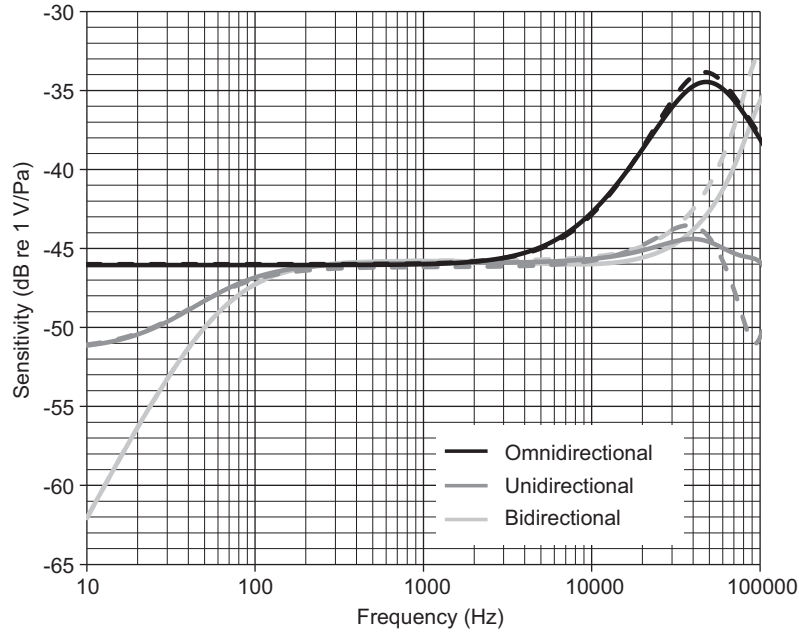


Figure 5.33 Exact (solid) and approximate (dashed) curves of the on-axis responses of a dual-diaphragm condenser microphone in three different modes: omni-, uni-, and bidirectional. Exact results from Eqs. (5.80, 5.98, 5.103) are shown by black, dark gray, and light gray solid curves respectively. Approximate results from Eqs. (5.95, 5.99, 5.104) are shown by black, dark gray, and light gray dashed curves respectively. The parameters are given in Table 5.2.

so that the $\cos \theta$ term becomes insignificant. The impedances can be expanded as follows:

$$Z_{AD} = j\omega M_{AD} + \frac{1}{j\omega C_{AD}} + \frac{1}{\frac{1}{j\omega M_{AR}} + \frac{1}{R_{AR}}}, \quad (5.83)$$

$$Z_{AP1} = \frac{R_{AP}}{2} + j\omega \frac{M_{AP}}{2}, \quad (5.84)$$

$$Z_{AP2} = \frac{1}{j\omega C_{AP}} - \frac{R_{AP}}{6} - j\omega \frac{M_{AP}}{6}, \quad (5.85)$$

where dynamic mass M_{AD} and compliance C_{AD} of the membrane are given by Ref. [1].

$$M_{AD} = \frac{4\rho_D h}{3S}, \quad (5.86)$$

Table 5.2 Dual-diaphragm condenser microphone parameters

Membrane		
Radius	a	12.6 mm
Thickness	h	2.5 μm
Density	ρ_D	1400 kg/m ³
Tension	T	50 N/m
Air		
Density	ρ_0	1.18 kg/m ³
Absolute viscosity	μ	17.9 $\mu\text{N s/m}^2$
Mean free path	λ	60 nm
Accommodation coefficient	α	0.9
Adiabatic sound speed	c	345 m/s
Specific heat ratio	γ	1.403
Gap	d	50 μm
Permittivity	ϵ_0	8.85 pF/m
Polarizing voltage	E_1	100 V
Plate		
Hole radius	a_p	6 μm
Hole pitch (center to center)	p	18 μm
Depth	l	1.15 mm

$$C_{AD} = \frac{S^2}{8\pi T}, \quad (5.87)$$

where ρ_D is the density of the membrane material, h is its thickness, $S = \pi a^2$ is its surface area, a is its radius, and T is its tension. The acoustic radiation mass and resistance are given by

$$R_{AR} = \frac{\rho_0 c}{S}, \quad (5.88)$$

$$M_{Ar} = \frac{\rho_0}{4a}. \quad (5.89)$$

From Chapter 4 the plate mass, compliance, and resistance are given by

$$R_{AP} = \frac{8\mu l}{(1 + 4B_u) a_p^2 S f_f}, \quad (5.90)$$

$$M_{AP} = \frac{1 + 3B_u}{1 + 4B_u} \frac{4\rho_0 l}{3S f_f}, \quad (5.91)$$

$$C_{AP} = \frac{lSf_f}{\rho_0 c^2}, \quad (5.92)$$

where l is the thickness of the plate, a_p is the hole diameter, $\mu = 18.6 \times 10^{-6} \text{ N} \cdot \text{s/m}^2$ is the viscosity of air, and f_f is the fill factor, which for a rectangular hole grid is given by

$$f_f = \frac{\pi a_p^2}{p^2}, \quad (5.93)$$

where p is the hole pitch. Also B_u is the boundary slip factor that is given by

$$B_u = \left(\frac{2}{\alpha_u} - 1 \right) \frac{\lambda_m}{a_p}, \quad (5.94)$$

where $\alpha_u = 0.9$ is the accommodation coefficient and $\lambda_m = 60 \text{ nm}$ is the mean free path length of an air molecule between collisions. It is assumed that the holes are so narrow that the pressure variations within them are isothermal because of heat conduction through the walls. Hence the specific heat ratio γ is absent from the expression for C_{AP} . Because the membrane is flexible as opposed to rigid, the radiation mass M_{AR} is that of a resilient disk in free space as derived in Chapter 13. If we ignore M_{AB} , M_{AR} , R_{AR} , C_{AD} , and ω^3 in Eq. (5.80), we obtain the following approximate formula for the sensitivity

$$\tilde{e}_k \approx \frac{E_1 \left(1 - j \frac{\omega}{2c} \Delta l \cos \theta \right) \left(\left(C_{AG} + \frac{C_{AP}}{2} \right) + j \omega \frac{R_{AP} C_{AG} C_{AP}}{12} \right)}{Sd \left(1 - \omega^2 M_{AD} \left(C_{AG} + \frac{C_{AP}}{2} \right) + j \omega \frac{R_{AP} C_{AP}}{12} \right)} \tilde{p}_1. \quad (5.95)$$

Using this formula, the approximate on-axis response with the switch in position “k” for an omnidirectional pattern is plotted in Fig. 5.33 and also in Fig. 5.34 along with the 180 degrees off-axis response. We see that at low to mid frequencies, where $\omega \rightarrow 0$, the reference sensitivity is given by

$$\tilde{e}_{k(\text{ref})} = \frac{E_1 \left(C_{AG} + \frac{C_{AP}}{2} \right)}{Sd} \tilde{p}_1. \quad (5.96)$$

The upper limit of the working range is roughly determined by the resonance frequency

$$f_U = \frac{1}{2\pi \sqrt{M_{AD} \left(C_{AG} + \frac{C_{AP}}{2} \right)}}. \quad (5.97)$$

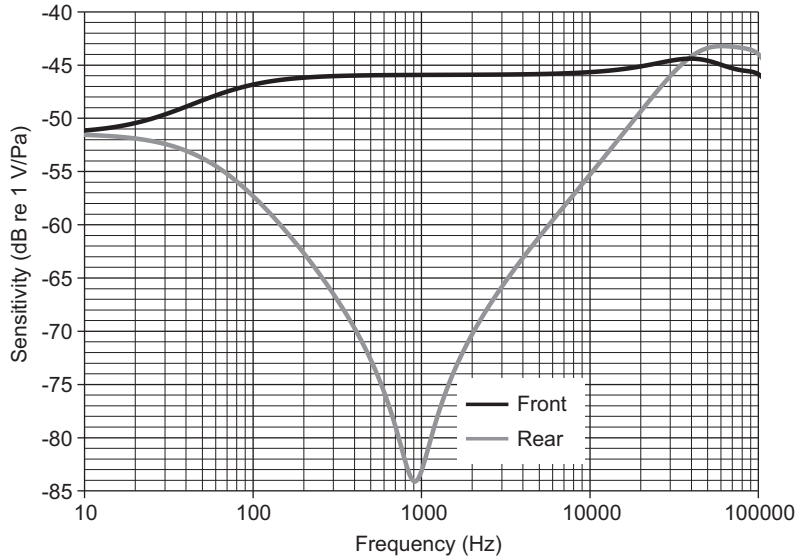


Figure 5.34 Plots of the on-axis responses at the front (*black*) and rear (*gray*) of a dual-diaphragm condenser microphone in unidirectional mode. The parameters are given in [Table 5.2](#).

Bidirectional performance

If $E_2 = -E_1$, which corresponds to the slider being at position “i” in [Fig. 5.31](#), we have a pressure-gradient microphone and the exact sensitivity is given by

$$\tilde{e}_i = \frac{E_1 \Delta l \cos \theta}{2cSd \left(Z_{AD} + \frac{Z_{AP1} \frac{1}{j\omega C_{AG}}}{Z_{AP1} + \frac{1}{j\omega C_{AG}}} \right)} \tilde{p}_1, \quad (5.98)$$

which gives a bidirectional directivity pattern at all frequencies. Using this formula, the on-axis response is plotted in [Fig. 5.33](#) and also in [Fig. 5.34](#) along with the 180 degrees off-axis response. If we ignore M_{AP} , M_{AR} , and R_{AR} , we obtain the following approximate formula for the sensitivity

$$\tilde{e}_i \approx \frac{E_1 \Delta l \cos \theta}{2cSd \left(\frac{R_{AP}}{2 + j\omega R_{AP} C_{AG}} + j\omega M_{AD} + \frac{1}{j\omega C_{AD}} \right)} \tilde{p}_1, \quad (5.99)$$

which is also plotted in [Fig. 5.33](#). We also see that at mid frequencies, where $j\omega C_{AD} > 2/R_{AP}$ but $j\omega M_{AD} < R_{AP}/2$ and $j\omega R_{AP} C_{AG} < 2$, the reference sensitivity is given by

$$\tilde{e}_{i(\text{ref})} = \frac{E_1 \Delta l}{cSd R_{AP}} \tilde{p}_1. \quad (5.100)$$

The lower cut-off frequency is

$$f_L = \frac{1}{\pi R_{AP} C_{AD}} \quad (5.101)$$

and the upper limit of the working range is roughly determined by the resonance frequency:

$$f_U = \frac{1}{2\pi\sqrt{M_{AD}C_{AG}}}. \quad (5.102)$$

Unidirectional performance

If $E_2 = 0$, which corresponds to the slider being at position “j” in Fig. 5.31, we have a combination of pressure and pressure-gradient microphones and the exact sensitivity is given by

$$\tilde{e}_j = \frac{\frac{1}{2}(\tilde{e}_i + \tilde{e}_k)}{1 - \frac{C_{E0}E_1^2}{4j\omega S^2 d^2} \left\{ \left(Z_{AD} + \frac{(Z_{AP1} + 2Z_{AP2})\frac{1}{j\omega C_{AG}}}{Z_{AP1} + 2Z_{AP2} + \frac{1}{j\omega C_{AG}}} \right)^{-1} + \left(Z_{AD} + \frac{Z_{AP1}\frac{1}{j\omega C_{AG}}}{Z_{AP1} + \frac{1}{j\omega C_{AG}}} \right)^{-1} \right\}}, \quad (5.103)$$

which is plotted in Fig. 5.33. The expression in the numerator is a pure summation of the pressure and pressure-gradient responses obtained with the switch in positions “k” and “i” respectively. In those positions, all terms containing C_{E0} are balanced out, but in position “j” there is no such balance, which explains the presence of the complicated denominator term in Eq. (5.103). However, the denominator only contributes at low frequencies so that after removing all the high-frequency terms we can make the following approximation:

$$\tilde{e}_j = \frac{\frac{2}{R_{AP}C_{AD}} + j\omega}{\frac{2}{R_{AP}} \left(\frac{1}{C_{AD}} - \frac{C_{E0}E_1^2}{4S^2 d^2} \right) + j\omega} \cdot \frac{\tilde{e}_i + \tilde{e}_k}{2}, \quad (5.104)$$

which produces a shelf at low frequencies that is determined by the amount of negative stiffness produced by the force of electrostatic attraction. This in fact helps to equalize the amount of low-frequency attenuation, which would otherwise be 6 dB because of taking the half sum of the pressure and pressure-gradient responses, where the former is flat at

low frequencies and the latter rolls-off at a rate of 6 dB per octave. The low-frequency shelf starts to rise at the upper frequency of

$$f_{SU} = \frac{1}{\pi R_{AP} C_{AD}} \quad (5.105)$$

and levels off at the lower frequency of

$$f_{SL} = \frac{1}{\pi R_{AP}} \left(\frac{1}{C_{AD}} - \frac{C_{E0} E_1^2}{4 S^2 d^3} \right). \quad (5.106)$$

The approximate on-axis response with the switch in position “j” for a unidirectional pattern is plotted in Fig. 5.33 where the approximate expressions for \tilde{e}_i and \tilde{e}_k obtained from Eqs. (5.95) and (5.99) respectively are inserted into Eq. (5.104).

Condition for equal sensitivity in all three switch positions

Ideally we would like the sensitivity of the microphone to be the same at all three switch positions “i”, “j”, and “k”. It turns out that this is also the condition for obtaining the optimum cardioid directivity pattern in position “j”, which is met by setting $\tilde{e}_i = \tilde{e}_k$ in Eqs. (5.95) and (5.99) to yield

$$R_{AP} = \frac{\Delta l}{\left(C_{AG} + \frac{C_{AP}}{2} \right) c}, \quad (5.107)$$

which after inserting the path length difference from Eq. (5.15) gives

$$R_{AP} = \frac{l + \frac{\pi a}{4}}{\left(C_{AG} + \frac{C_{AP}}{2} \right) c}. \quad (5.108)$$

Quite a large resistance is needed to meet this condition so that the holes through the plate have to be very narrow.

Condition for stability

Another condition that must be met is for the restoring force of the membrane tension to be greater than the force of electrostatic attraction towards the plate. We see from the schematic that this is met if

$$C_{A0} = \left(\frac{Sd}{C_{E0} E_1} \right)^2 C_{E0} > C_{AD} \quad (5.109)$$

or using the expressions from Eqs. (5.69) and (5.87), we obtain the minimum tension value:

$$T > \frac{\epsilon_0 a^2 E_1^2}{8d^3}. \quad (5.110)$$

Typically the tension should be about three times the minimum value to allow for slackening through age and environmental conditions.

NOTES

- [1] Zuckerwar AJ. In: Wong GSK, Embleton TFW, editors. AIP handbook of condenser microphones. New York: AIP Press; 1995. p. 47–58. Chap. 3.
- [2] Paschen F. Über die zum Funkenübergang in Luft, Wasserstoff und Kohlensäure bei verschiedenen Drucken erforderliche Potentialdifferenz (On the Potential Difference Required to Cause Spark-over in Air, Hydrogen and Carbon Dioxide Under Different Pressures). Ann Phys 1889;273(5):69–75.
- [3] Streng JH. Sound radiation from a circular stretched membrane in free space. J Audio Eng Soc 1989;37(3):107–18.

Electrodynamic loudspeakers

PART XIX: BASIC THEORY OF ELECTRODYNAMIC LOUDSPEAKERS

6.1 INTRODUCTION

An electrodynamic or moving-coil loudspeaker is an electromagnetic transducer for converting electrical signals into sounds. When the original version of this book was published in 1954 under the title *Acoustics*, the only practical amplifying device available was the vacuum tube, so output power was expensive. Hence, the efficiency of the electrodynamic loudspeaker was one of the most important factors. As the cost of amplifier watts has decreased, there has been a steady trend toward smaller loudspeakers coupled with ever more powerful amplifiers, which are needed to compensate for the reduced radiating efficiency of the smaller diaphragms. Two developments have spurred this trend: the replacement of the vacuum tube with silicon transistor and the introduction of the so-called digital amplifiers using various coding schemes, the most popular being pulse-width modulation or Class D. In mobile devices, which rely on battery power, the efficiency issue has not gone away. The most important development for mobile devices has been the introduction of rare-earth neodymium magnets, which have enabled significant miniaturization. One trend which has enabled loudspeakers of all sizes to be used with smaller enclosures has been the development of high-compliance suspensions which are stable enough not to cause rocking modes. The term “acoustic suspension” has been dubbed [1] to describe a loudspeaker which has an enclosure so small that the air inside the enclosure is stiffer than the suspension.

There are two principal types of loudspeakers: those in which the vibrating surface (called the diaphragm) radiates sound directly into the air, and those in which a horn is interposed between the diaphragm and the air. The direct-radiator type is used in most home and car entertainment, mobile devices, and in small public-address systems. The horn type is used in more exotic hi-fi systems (especially those using tubes), in large sound systems in theaters and auditoriums, and in music and outdoor-announcing systems.

The principal advantages of the direct-radiator type are (1) small size, (2) low cost, and (3) a satisfactory response over a comparatively wide frequency range. The principal disadvantages are (1) low efficiency and (2) narrow directivity pattern at high frequencies. For use in home, car, and mobile audio, where little acoustic power is necessary, the

advantages far outweigh the disadvantages. In theater and outdoor sound systems, where large amounts of acoustic power are necessary and where space is not important, the more efficient horn-type loudspeaker is generally used.

All the types of transduction discussed in the previous chapter on Microphones might be used for loudspeakers. In this text, however, we shall limit ourselves to electrodynamic loudspeakers, the type most commonly used in home, car, mobile, and professional audio.

6.2 CONSTRUCTION [2]

A cross-sectional sketch of a typical loudspeaker drive unit is shown in Fig. 6.1. The diaphragm (1) is a cone made from a suitably light and stiff material, although most of the stiffness comes from the fact that it is curved. In the center is a dust cap (2), which guards against metallic dust fouling the magnetic gap and prevents sound from the back of the diaphragm leaking through to the outside world. If the loudspeaker were mounted in a bass-reflex enclosure, such leakage could seriously reduce the Q of the port resonance. Attached to the top of the cone is a coil former on which the coil (3) is wound. This coil is located in the gap of a magnetic path, comprising a pole piece (4) and pole plate (5), where the magnetic flux is produced by a permanent magnet (6), which is

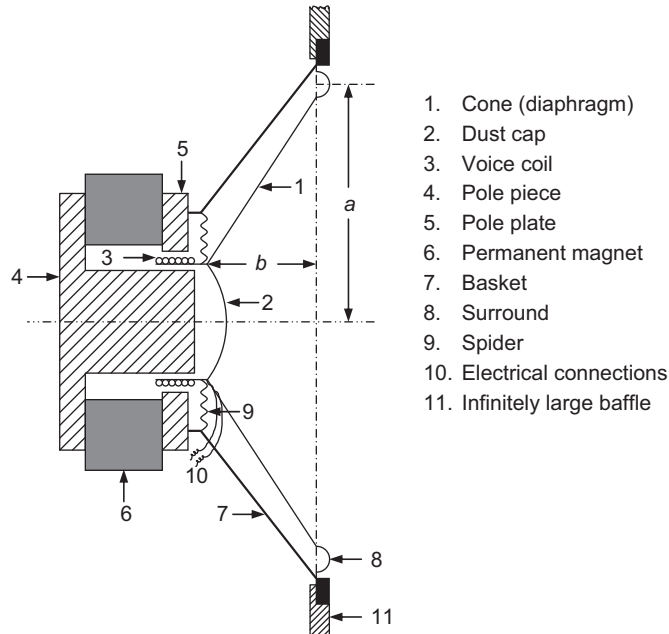


Figure 6.1 Cross-sectional sketch of a direct-radiator loudspeaker assumed to be mounted in an infinite baffle.

held in place by a basket structure (7). The diaphragm is supported at the perimeter and near the voice coil by a surround (8) and spider (9), respectively, so that it is free to move only in an axial direction. The name “spider” originates from the early electrodynamic loudspeakers in which the cone was supported by a spider-like slotted disk that was anchored to the pole piece in place of the dust cap. Apart from this modification and the switch from electromagnets to alnico (aluminum–nickel–cobalt) permanent magnets in the 1930s and then to ferrite magnets in the 1970s (for economic reasons, not performance related), there has been very little change in the construction of electrodynamic loudspeakers since the Rice–Kellogg [3] patent of 1924. We will refer to the spider and surround as the suspension. In general, sound from the back of the cone exits through holes in the basket (7), whereas sound from the back of the dome (2) leaks through the magnetic gap and spider (9), which is often made from a phenolic resin-impregnated textile, before exiting through the basket.

When an audio signal is applied to the electrical connections (10), the resulting current through the voice coil creates a magnetomotive force which interacts with the air-gap flux of the permanent magnet and causes a translatory movement of the voice coil and, hence, of the cone to which it is attached. The movement of the cone in turn displaces the air molecules at its surface thus producing sound waves. Usually, the cone is sufficiently stiff at low frequencies to move as a whole. At high frequencies, however, vibrations from the center travel outward toward the edge in the form of waves. The results of these traveling waves and of resonances in the cone itself are to produce irregularities in the frequency–response curve at the higher frequencies and to influence the relative amounts of sound radiated in different directions. Unless treated, metal cones have relatively low internal damping and tend to produce high Q resonances, but at frequencies higher than paper or polymer cones due to their high ratio of flexural rigidity to density. Care needs to be taken in the choice of surround material and means of attachment to the coil former to minimize such resonances. Paper and polymer cones have greater damping so that the compression waves propagating through the cone from the coil are mainly absorbed at higher frequencies. This leads to an interesting phenomenon whereby the effective radiating area of the cone decreases with frequency, which is beneficial for maintaining a widely dispersed sound field. Eventually, only the dust cap radiates and the stationary cone acts as a horn. We will discuss the vibration modes of the cone later in this chapter.

In Fig. 6.1, the drive unit is shown mounted in a flat baffle (11) assumed to be of infinite extent. Obviously, this is not possible in practice, but it is an ideal configuration which simplifies our analysis of the drive unit. By definition, a baffle is any means for acoustically isolating the front side of the diaphragm from the rear side. For purposes of analysis, the diaphragm may be considered at low frequencies to be a planar piston of radius a moving with uniform velocity over its entire surface. This is a fair approximation at frequencies for which the distance b on Fig. 6.1 is less than about one-tenth

wavelength. The piston in an infinite baffle is the only sound source which gives a uniformly flat far-field on-axis response under constant acceleration, and this phenomenon is explained in [Section 6.6](#).



6.3 ELECTRO-MECHANO-ACOUSTICAL CIRCUIT

Before drawing a circuit diagram for a loudspeaker, we must identify the various elements involved. The voice coil has inductance and resistance, which we shall call L_E and R_E , respectively. The diaphragm and the wire on the voice coil have a total mass M_{MD} . The diaphragm is mounted on flexible suspensions at the center and at the edge. The total effect of these suspensions may be represented by a mechanical compliance C_{MS} and a mechanical resistance $R_{MS} = 1/G_{MS}$, where G_{MS} is the mechanical conductance. The air cavity and the holes at the rear of the center portion of the diaphragm form an acoustic network which, in most loudspeakers, can be neglected in analysis because they have no appreciable influence on the performance of the loudspeaker. However, both the rear and the front side of the main part of the diaphragm radiate sound into the open air.

An acoustic radiation impedance is assigned to each side and is designated as $Z_{AR} = 1/Y_{AR}$, where Y_{AR} is the acoustic radiation admittance. Thus, the mechanical radiation admittance seen by each side of the diaphragm is $Y_{MR} = S_D^2 Y_{AR}$, where S_D is the effective diaphragm area. Approximate equivalent circuits for Y_{MR} and Y_{AR} are given in Fig. 4.37c and d, respectively.

We observe that one side of each flexible suspension is at zero velocity. For the mechanical resistance, this also must be true because it is contained in the suspensions. We already know from earlier chapters that one side of the mass and one side of the radiation admittance must be considered as having zero velocity. Similarly, we note that the other sides of the masses, the compliance, the conductance, and the radiation admittances all have the same velocity, viz., that of the voice coil.

From inspection, we are able to draw a mechanical circuit and the electromechanical analogous circuit using the admittance analogy. These are shown in [Fig. 6.2a and b](#), respectively. The symbols have the following meanings:

\tilde{e}_g is open-circuit voltage of the generator (audio amplifier) in volts (V).

R_g is generator resistance in electrical ohms (Ω).

L_E is inductance of voice coil in henrys (H), measured with the voice-coil movement blocked, i.e., for $\tilde{u}_c = 0$.

R_E is resistance of voice coil in electrical ohms (Ω), measured in the same manner as L_E .

B is steady air-gap magnetic field or flux density in Tesla (T).

l is length of wire in m on the voice-coil winding.

\tilde{i} is electric current in amperes (A) through the voice-coil winding.

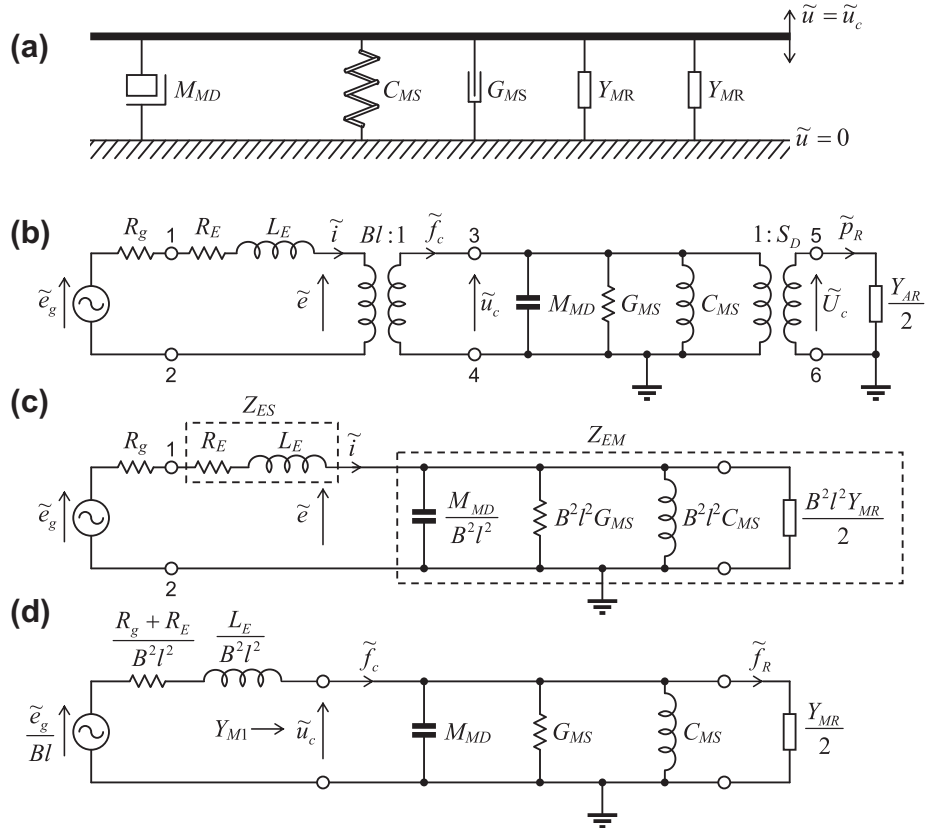


Figure 6.2 (a) Mechanical circuit of direct-radiator loudspeaker; (b) electro-mechano-acoustical analogous circuit of the admittance type; (c) electrical circuit showing static electrical impedance Z_{ES} and motional electrical impedance Z_{EM} ; and (d) analogous circuit of the admittance type with electrical quantities referred to the mechanical side.

\tilde{f}_c is force in N generated by interaction between the alternating and steady mmfs, that is, $\tilde{f}_c = Bl\tilde{i}$.

\tilde{u}_c is voice-coil velocity in m/s, that is, $\tilde{u}_c = \tilde{e}/Bl$, where \tilde{e} is the so-called counter emf.

a is radius of diaphragm in m.

M_{MD} is mass of the diaphragm and the voice coil in kg.

C_{MS} is total mechanical compliance of the suspensions in m/N.

$G_{MS} = 1/R_{MS}$ is mechanical conductance of the suspension in $\text{m} \cdot \text{N}^{-1} \cdot \text{s}^{-1}$.

R_{MS} is mechanical resistance of the suspensions in $\text{N} \cdot \text{s}/\text{m}$.

$Y_{MR} = 1/Z_{MR} = \mathbf{G}_{MR} + jB_{MR}$ is mechanical radiation admittance in $\text{m} \cdot \text{N}^{-1} \cdot \text{s}^{-1}$ from one side of the diaphragm (see Fig. 4.36). The bold \mathbf{G} indicates that \mathbf{G}_{MR} varies with frequency.

$Z_{MR} = \mathbf{R}_{MR} + jX_{MR}$ is mechanical radiation impedance in $\text{N}\cdot\text{s}/\text{m}$ from one side of a piston of radius a mounted in an infinite baffle (see Fig. 4.35). The bold \mathbf{R} indicates that \mathbf{R}_{MS} varies with frequency.

$S_D = \pi a^2$ is effective area of diaphragm in m^2 .

\tilde{p}_R is pressure on the diaphragm due to the radiation load, that is, $\tilde{p}_R = 2\tilde{U}_c/Y_{MR}$.

\tilde{U}_c is volume velocity produced by the diaphragm, that is, $\tilde{U}_c = S_D\tilde{u}_c$.

It should be noted that the coil inductance L_E is highly nonlinear. In practice, the reactive coil impedance does not rise linearly with frequency but is roughly proportional to the square root of frequency. A more accurate model [4] can be made by adding a second inductor with a resistor in parallel with it, but in this text we shall use the simple model with a single inductor.

The circuit of Fig. 6.2b with the mechanical side brought through the transformer to the electrical side is shown in Fig. 6.2c. Hence, this represents the circuit as seen from the input terminals. It is important for several reasons. Firstly, we have to take the electrical impedance into account when considering the load presented by the loudspeaker to the amplifier driving it. The loading effect will also modify the frequency response of any passive crossover network that may be used. In addition, we can calculate the parameters of a drive unit by measuring the input impedance, as will be explained in Section 6.10, without the need for an anechoic chamber. The mechanical admittance $Y_{M1} = \tilde{u}_c/\tilde{f}_c$ is zero if the diaphragm is blocked so that there is no motion ($\tilde{u}_c = 0$) but has a value different from zero whenever there is motion. For this reason, the quantity $Z_{EM} = B^2l^2Y_{M1}$ is usually called the motional electrical impedance. A quantity often found on data sheets is the electrical suspension resistance $R_{ES} = B^2l^2G_{MS} = B^2l^2/R_{MS}$. This resistance is in series with the coil resistance R_E at resonance. When the electrical side is brought over to the mechanical side, we have the circuit of Fig. 6.2d.

The circuit of Fig. 6.2d will be easier to solve if its form is modified. First, we recognize the equivalence of the two circuits shown in Fig. 6.3a and b according to

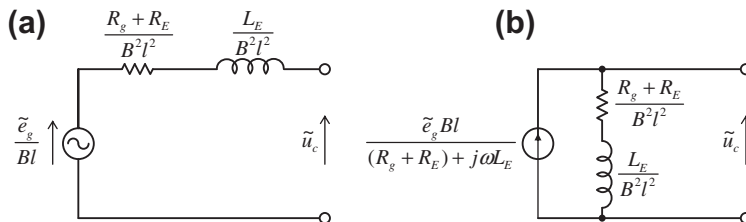


Figure 6.3 The electrical circuit (referred to the mechanical side) is shown here in two equivalent forms (a and b) according to Norton's theorem. The circuits are of the admittance type. (Note: The generator in (b) is of constant flow type.).

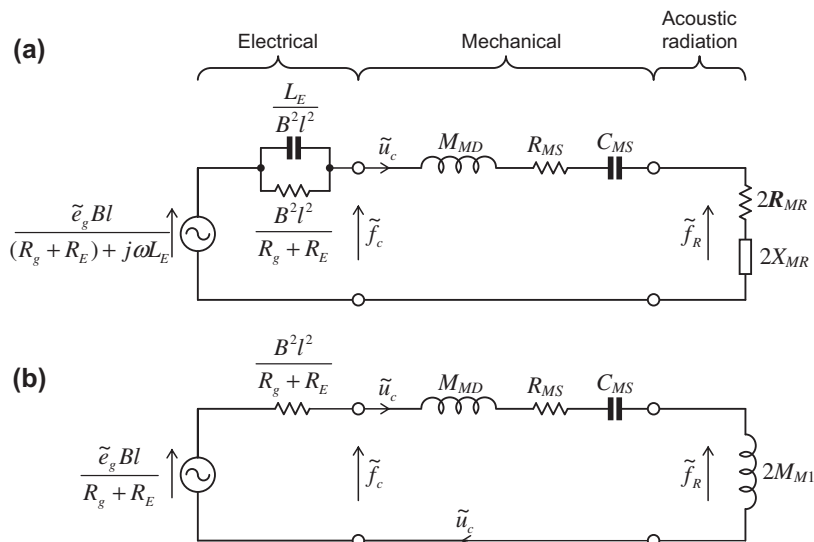


Figure 6.4 (a) Low-frequency analogous circuit of the impedance type with electrical quantities referred to mechanical side. Z_{MR} is given by Fig. 4.35. The quantity \tilde{f}_c represents the total force acting in the equivalent circuit to produce the voice-coil velocity \tilde{u}_c . (b) Single-loop approximation to Fig. 6.4a valid for $X_{MR}^2 \gg R_{MR}^2$.

Norton's theorem (see Fig. 14.4). Next, we substitute Fig. 6.3b for its equivalent in Fig. 6.2d. Then, we take the dual of Fig. 6.2d to obtain Fig. 6.4a. (See Figs. 3.41 and 3.42).

The performance of a direct-radiator loudspeaker is directly related to the diaphragm velocity. Having solved for it, we may compute the acoustic power radiated and the sound pressure produced at any given distance from the loudspeaker in the far field.

Voice-coil velocity at medium and low frequencies

The voice-coil velocity \tilde{u}_c , neglecting $\omega^2 L^2$ compared with $(R_g + R_E)^2$, is found from Fig. 6.4a,

$$\tilde{u}_c \approx \frac{\tilde{e}_g Bl}{(R_g + R_E)(R_M + jX_M)} \quad (6.1)$$

where

$$R_M = \frac{B^2 l^2}{R_g + R_E} + R_{MS} + 2R_{MR} \quad (6.2)$$

$$X_M = \omega M_M = \omega M_{MD} + 2X_{MR} - \frac{1}{\omega C_{MS}} \quad (6.3)$$

Voice-coil velocity at low frequencies

At low frequencies, assuming in addition that $X_{MR}^2 \gg R_{MR}^2$, we have from Fig. 6.4b that

$$(X_M)_{\text{low } f} = \omega(M_{MD} + 2M_{M1}) - \frac{1}{\omega C_{MS}} \quad (6.4)$$

where

$$M_{M1} = 2.67a^3\rho_0 \quad (6.5)$$

is the mass in kg contributed by the air load on one side of the piston for the frequency range in which $ka < 0.5$. (See Table 4.4). The quantity ka equals the ratio of the circumference of the diaphragm to the wavelength.

The voice-coil velocity is found from Eq. (6.1), using Eqs. (6.2) and (6.4) for R_M and X_M , respectively, so that

$$\tilde{u}_c = \frac{\tilde{e}_g}{BlQ_{ES}}\beta_c(f) \quad (6.6)$$

where $\beta_c(f)$ is a dimensionless frequency response function given by

$$\beta_c(f) = \frac{j\frac{f}{f_S}}{1 - \frac{f^2}{f_S^2} + j\frac{1}{Q_{TS}}\frac{f}{f_S}} \quad (6.7)$$

The suspension resonance frequency f_S is given by

$$f_S = \frac{1}{2\pi\sqrt{M_{MS}C_{MS}}}, \quad (6.8)$$

where $M_{MS} = M_{MD} + 2M_{M1}$ is the combined diaphragm and air-load mass, and

$$Q_{TS} = \left(\frac{B^2 l^2}{R_g + R_E} + R_{MS} \right)^{-1} \sqrt{\frac{M_{MS}}{C_{MS}}}. \quad (6.9)$$

When $f = f_S$, the real terms in the denominator of Eq. (6.7) vanish, and we see from Eq. (6.9) that the total Q value of the suspension resonance equals Q_{TS} where Q_{TS} is the reciprocal of the effective resistance in the mechanical circuit multiplied by the square root of the ratio of the mass to the compliance of the diaphragm. If we define f_1 and f_2 as the frequencies at which the velocity is 3 dB below its peak value, then $Q_{TS} = f_S/(f_2 - f_1)$. Therefore, increasing the Q value increases the height of the

resonance peak while decreasing its width. At f_S , the inertial and static reactances in Fig. 6.4b cancel each other so that the velocity \tilde{u}_c is simply the driving force (first term in Eq. 6.6) divided by the total resistance in the loop, as shown in Fig. 6.6b. The total Q can be separated into two parts

$$Q_{TS} = \frac{1}{\frac{1}{Q_{ES}} + \frac{1}{Q_{MS}}} = \frac{Q_{ES}Q_{MS}}{Q_{ES} + Q_{MS}} \quad (6.10)$$

namely the electrical Q

$$Q_{ES} = \frac{R_g + R_E}{B^2 l^2} \sqrt{\frac{M_{MS}}{C_{MS}}} \quad (6.11)$$

and the mechanical Q

$$Q_{MS} = \frac{1}{R_{MS}} \sqrt{\frac{M_{MS}}{C_{MS}}} \quad (6.12)$$

The normalized velocity is plotted in Fig. 6.5 using $20 \log_{10} |\beta_c|$. It is a universal resonance curve. Below the resonance frequency, it has a slope of +6 dB per octave of frequency. Above the resonance frequency, it has a slope of -6 dB per octave. The acceleration is given by the first time derivative of the velocity

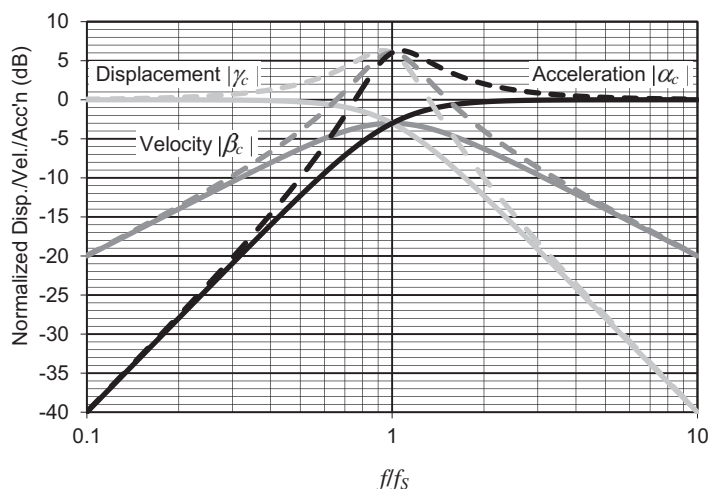


Figure 6.5 Normalized voice-coil displacement, velocity, and acceleration. The solid line is for $Q_{TS} = 1/\sqrt{2}$. The dashed line is for $Q_{TS} = 2$.

$$\tilde{a}_c = j\omega\tilde{u}_c = \frac{2\pi f_S \tilde{e}_g}{BlQ_{ES}} \alpha_c(f) \quad (6.13)$$

where $\alpha_c(f)$ is a dimensionless frequency response function given by

$$\alpha_c(f) = \frac{\frac{f^2}{f_S^2}}{1 - \frac{f^2}{f_S^2} + j \frac{1}{Q_{TS}} \cdot \frac{f}{f_S}} \quad (6.14)$$

The displacement is given by the first time integral of the velocity

$$\tilde{\eta}_c = \frac{\tilde{u}_c}{j\omega} = \frac{\tilde{e}_g}{2\pi f_S BlQ_{ES}} \gamma_c(f) \quad (6.15)$$

where $\gamma_c(f)$ is a dimensionless frequency response function given by

$$\gamma_c(f) = \frac{1}{1 - \frac{f^2}{f_S^2} + j \frac{1}{Q_{TS}} \cdot \frac{f}{f_S}} \quad (6.16)$$

The normalized displacement and acceleration are also plotted in Fig. 6.5 along with the velocity. We see that when $f/f_S \leq 1/3$, the displacement is virtually constant. This is the *stiffness-controlled* range in which the displacement is simply the static deflection as determined by Hooke's law, that is, the product of the driving force and the compliance:

$$\tilde{\eta}_c|_{f \leq 1/3f_S} \approx \frac{\tilde{e}_g Bl}{R_g + R_E} C_{MS} \quad (6.17)$$

The displacement curve is that of a second-order low-pass filter with a 12 dB/octave slope when $f/f_S \geq 3$. As is seen from Eq. (6.16), the displacement in this range is proportional to $1/f^2$, and the equivalent circuit is that shown in Fig. 6.6a. When $f/f_S \geq 3$, the acceleration is virtually constant. This is the *mass-controlled* range in which the acceleration is simply the driving force divided by the mass in accordance with Newton's second law of motion

$$\tilde{a}_c|_{f \leq 3f_S} \approx \frac{\tilde{e}_g Bl}{(R_g + R_E) M_{MS}} \quad (6.18)$$

The acceleration curve is that of a second-order high-pass filter with a 12 dB/octave slope when $f/f_S \leq 1/3$. As can be seen from Eq. (6.16), the acceleration in this range is proportional to f^2 , and the equivalent circuit is that shown in Fig. 6.6c.

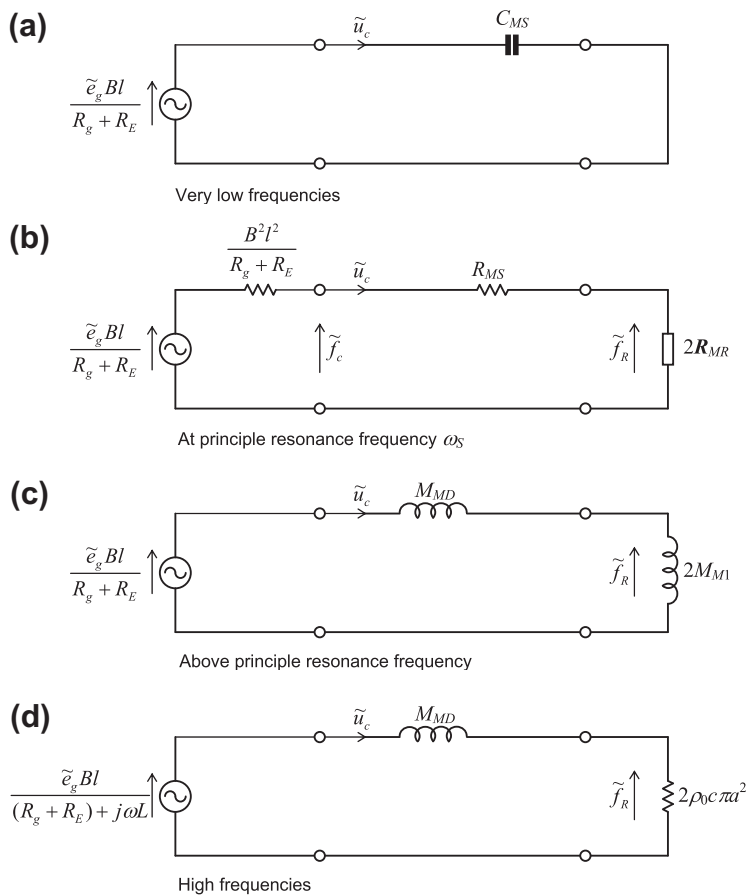


Figure 6.6 Simplified forms of the circuit of Fig. 6.4a valid for very low frequencies (a), at principle resonance frequency (b), above principle resonance frequency (c), and at high frequencies (d).



6.4 POWER OUTPUT

The acoustic power radiated in watts from both the rear and the front sides of the loudspeaker is

$$W = \left| \frac{\tilde{u}_c}{\sqrt{2}} \right|^2 (2\mathbf{R}_{MR}) \quad (6.19)$$

Hence, assuming $\omega^2 L^2 \ll (R_g + R_E)^2$, and using Eq. (6.1) for \tilde{u}_c , we obtain

$$W = \left| \frac{\tilde{e}_g}{\sqrt{2}} \right|^2 \frac{2B^2 l^2 \mathbf{R}_{MR}}{(R_g + R_E)^2 (R_M^2 + X_M^2)} \quad (6.20)$$

Above the suspension resonance frequency, the diaphragm mass dominates so that $X_M \gg R_M$ where $X_M \approx j\omega M_{MS}$. In addition, when the wavelength is small compared with the diameter of the diaphragm, we see from Table 4.4 that

$$\mathbf{R}_{MR} = \frac{\omega^2 S_D^2 \rho_0}{2\pi c} \quad (6.21)$$

where

$$S_D = \pi a^2 \quad (6.22)$$

is the *effective* area of the diaphragm of Fig. 6.1. Inserting these into Eq. (6.20) yields

$$W = \frac{e_{g(\text{rms})}^2 B^2 l^2 S_D^2 \rho_0}{\pi (R_g + R_E)^2 M_{MS}^2 c}, \quad 2f_0 < f < \frac{c}{4\pi a} \quad (6.23)$$

where

$$e_{g(\text{rms})} = \left| \frac{\tilde{e}_g}{\sqrt{2}} \right| \quad (6.24)$$

In this frequency range, the radiated power is fairly constant because, as the frequency increases, the falling velocity is compensated for by the rising radiation resistance. At higher frequencies where $\mathbf{R}_{MR} = S_D \rho_0 c$, we have

$$W = \frac{2e_{g(\text{rms})}^2 B^2 l^2 S_D \rho_0 c}{(R_g + R_E)^2 \omega^2 M_{MS}^2}, \quad f > \frac{5c}{2\pi a} \quad (6.25)$$

Hence, the radiated power is proportional to the inverse square of the frequency when the radiation impedance is mainly resistive and the equivalent circuit is that shown in Fig. 6.6d.



6.5 THIELE—SMALL PARAMETERS [5]

A complete low-frequency model of a loudspeaker drive unit can be defined by just six parameters known as the Thiele—Small parameters, which are

$$R_E, Q_{ES}, Q_{MS}, f_s, S_D, \text{ and } V_{AS}.$$

So far, we have introduced all of these except for V_{AS} . The parameters Q_{ES} , Q_{MS} , f_s , and S_D are defined by Eqs. (6.11), (6.12), (6.8), and (6.22), respectively. The parameter V_{AS} is the *equivalent suspension volume*. In other words, it is the volume of air having the same acoustic compliance as the suspension and is defined as

$$V_{AS} = C_{AS} \rho_0 c^2 = C_{MS} S_D^2 \rho_0 c^2 \quad (6.26)$$

The use of this parameter will make more sense when we consider the performance of the loudspeaker with an enclosure of volume V_B , which in its simplest approximation is an extra compliance in the loop of Fig. 6.4b. Straight away, we can say that mounting the drive unit in a box of volume $V_B = V_{AS}$ will result in a total compliance that is half that of the drive unit in free space or an infinite baffle. Hence, the suspension resonance frequency will be raised by a factor of $\sqrt{2}$. From these six parameters, we can furnish our equivalent circuit of Fig. 6.4b with all the required element values:

$$C_{MS} = \frac{V_{AS}}{S_D^2 \rho_0 c^2} \quad (6.27)$$

Then from Eq. (6.8)

$$M_{MS} = \frac{1}{(2\pi f_S)^2 C_{MS}} \quad (6.28)$$

and from Eq. (6.12)

$$R_{MS} = \frac{1}{Q_{MS}} \sqrt{\frac{M_{MS}}{C_{MS}}} \quad (6.29)$$

Inserting Eq. (6.28) into Eq. (6.11) yields

$$Bl = \sqrt{\frac{R_E}{2\pi f_S Q_{ES} C_{MS}}} \quad (6.30)$$

where we have ignored R_g because this is not a drive unit parameter. Finally, $M_{MD} = M_{MS} - 2M_{M1}$, where M_{M1} is given by Eq. (6.5). Another parameter that is commonly found in loudspeaker data sheets, although it is not a Thiele–Small parameter, is the maximum (linear) displacement or x_{\max} . It is a difficult parameter to specify in any meaningful way because it depends on how much distortion can be tolerated and varies with frequency [6].



6.6 SOUND PRESSURE PRODUCED AT DISTANCE R

We show in Eq. (13.104) that the far-field on-axis pressure produced by a plane circular piston in an infinite baffle is given by

$$\begin{aligned} \tilde{p}(r) &= jf \rho_0 \tilde{U}_c \frac{e^{-jkr}}{r} \\ &= \rho_0 S_D \tilde{a}_c \frac{e^{-jkr}}{2\pi r} \end{aligned} \quad (6.31)$$

where \tilde{a}_c is given by Eqs. (6.8), (6.9), and (6.13) so that

$$\tilde{p}(r) = \frac{\tilde{e}_g B l S_D \rho_0}{(R_g + R_E) M_{MS}} \cdot \frac{e^{-jkr}}{2\pi r} \alpha_c \quad (6.32)$$

The frequency response is then given by α_c in Eq. (6.14). In other words, the frequency response is proportional to the cone acceleration and remains flat above the suspension resonance.

The fact that the on-axis frequency response remains flat, even though the radiated power decreases when the wavelength is small in comparison with the circumference of the piston, may seem slightly surprising. However, what we have not taken into account here is the spatial distribution of the radiated sound pressure which becomes increasingly narrow at high frequencies. Although we are not dealing with an ideal flat piston and have not included the effect of the coil inductance, Eq. (6.32) is useful for defining the voltage sensitivity of a loudspeaker within its working frequency range between the suspension resonance and cone break-up (which we will discuss later in this chapter). It shows that for a given coil resistance R_E , the sensitivity is increased by maximizing the $B l$ factor and diaphragm area S_D while minimizing the total moving mass M_{MS} , which includes the radiation mass M_{MR} , although it is usually very small in comparison with M_{MD} . These requirements are usually in conflict with each other, so it is not possible to optimize all of them in a practical design. Because the most common nominal impedance of a loudspeaker is 8Ω , the rms generator voltage $e_{g(\text{rms})}$ is usually taken as $\sqrt{8}$ or $2.83 \text{ V}_{\text{rms}}$ to deliver 1 W of power into an 8Ω load. Hence, Eq. (6.32) can then be used to give the power sensitivity which is usually expressed in dB SPL (sound pressure level) (relative to $20 \mu\text{Pa}$, see Eq. 1.18) for $W_E = 1 \text{ W}$ at $r = 1 \text{ m}$, so that

$$\text{Sensitivity} = 20 \log_{10} \left(\frac{\sqrt{Z_{\text{nom}} W_E} B l S_D \rho_0}{2\pi r (R_g + R_E) M_{MS} \times 20 \times 10^{-6}} \right) \text{dB SPL/W/m} \quad (6.33)$$

where Z_{nom} is the *nominal* electrical impedance of the drive unit. Theoretically, it is the average value over the loudspeaker's working frequency range, but in practice it is about 10%–30% greater than R_E so that at some frequencies, especially those below resonance, more than 1 W will be supplied at the nominal voltage. Alternatively, by combining Eqs. (6.8), (6.11), (6.26), and (6.33), we may conveniently express the sensitivity in terms of the Thiele–Small parameters V_{AS} and Q_{ES} :

$$\text{Sensitivity} = 20 \log_{10} \left(\frac{1}{rc \times 20 \times 10^{-6}} \sqrt{\frac{Z_{\text{nom}} W_E 2\pi f_S^3 V_{AS} \rho_0}{(R_g + R_E) Q_{ES}}} \right) \text{dB SPL/W/m} \quad (6.34)$$

Sometimes, we wish to determine how far a diaphragm must travel to produce a target SPL. From Eqs. (1.18) and (6.31), we obtain

$$\eta_{\text{peak}} = \frac{\sqrt{2}r \times 10^{\left(\frac{\text{SPL}}{20} - 5\right)}}{\pi f^2 \rho_0 S_D} \quad (6.35)$$

Low frequencies

From Eq. (13.101), we see that the magnitude of the pressure at a point in free space a distance r from *either* side of the loudspeaker in an infinite baffle is that of a point source multiplied by a directivity function:

$$\tilde{p}(r, \theta) = jka^2 \rho_0 \tilde{u}_c \frac{e^{-jkr}}{2r} D(\theta), \quad (6.36)$$

where the directivity function $D(\theta)$ is given by

$$D(\theta) = \frac{2J_1(ka \sin \theta)}{ka \sin \theta}. \quad (6.37)$$

A piston whose diameter is less than one-third wavelength ($ka < 1.0$) is essentially nondirectional at low frequencies, that is $D(\theta) \approx 1$ for any value of θ . Hence, we can approximate it by a hemisphere whose volume velocity is $\tilde{U}_c = S_D \tilde{u}_c$. It is assumed in writing this equation that the distance r is great enough so that it is situated in the “far field.” Assuming a loss-free medium, the total radiated power distributed over a spherical surface in the far field is

$$W = 4\pi r^2 I = \frac{4\pi r^2}{\rho_0 c} \left| \frac{\tilde{p}(r)}{\sqrt{2}} \right|^2 \quad (6.38)$$

where I is the intensity at distance r in W/m^2 . From this, we see for a point source radiating to *both sides* of an infinite baffle (or free space) that

$$p_{\text{rms}}(r) = \sqrt{\frac{W \rho_0 c}{4\pi r^2}} \quad (6.39)$$

It is worth noting that it only takes 1 W of acoustic power to produce 6.7 Pa or 109 dB SPL at 1 m, which is as loud as a pneumatic drill! The fact that it takes much more than 1 W of input power to achieve this with a loudspeaker is due to the low efficiency of most loudspeakers.

Medium frequencies

At medium frequencies, where the radiation from the diaphragm becomes directional but yet where the diaphragm vibrates as one unit, i.e., as a rigid piston, the pressure produced at a distance r depends on the power radiated and the directivity factor Q .

The directivity factor Q was defined in Chapter 4 as the ratio of the intensity on a designated axis of a sound radiator to the intensity that would be produced at the same position by a point source radiating the same acoustic power.

For a directional source in an infinite baffle such as we are considering here,

$$p_{\text{rms}}(r) = \sqrt{\frac{W_1 Q \rho_0 c}{4\pi r^2}} \quad (6.40)$$

where, W_1 is acoustic power in W radiated from one side of the loudspeaker. Q is directivity factor for *one* side of a piston in an infinite plane baffle. Values of Q are found from Fig. 4.30. Note that W_1 equals $W/2$ and, at low frequencies where there is no directionality, $Q = 2$, so that Eq. (6.40) reduces to Eq. (6.39) at low frequencies.

We see from Eq. (6.40) that, as frequency increases, Q increases while W_1 decreases. In other words, the reduction in radiated power is compensated for by the concentration of the radiated sound pressure over a decreasing beamwidth. The transition is so smooth that the frequency response remains flat. This can also be explained by the fact that the on-axis sound pressure is due to an infinite number of point sources over the surface of the piston, the radiation from which arrives in phase, where the frequency response of each point source is flat.



6.7 FREQUENCY—RESPONSE CURVES

A frequency—response curve of a loudspeaker is defined as the variation in sound pressure or acoustic power as a function of frequency, with some quantity such as voltage or electrical power held constant. To calculate the full frequency response, we refer to Fig. 6.4 but using Eqs. (13.116)–(13.118) for the exact acoustic radiation impedance instead of lumped elements. The total impedance in the loop with all quantities referred to the mechanical side is

$$Z_{MT} = \frac{B^2 l^2}{R_g + R_E + j\omega L_E} + j\omega M_{MD} + R_{MS} + \frac{1}{j\omega C_{MS}} + 2S_D \rho_0 c \left(1 - \frac{J_1(2ka)}{ka} + j \frac{\mathbf{H}_1(2ka)}{ka} \right) \quad (6.41)$$

where $k = \omega/c$. The diaphragm velocity is then given by the driving force divided by the total impedance

$$u_{c(\text{rms})} = \left| \frac{e_{g(\text{rms})} Bl}{(R_g + R_E + j\omega L_E) Z_{MT}} \right| \quad (6.42)$$

We then calculate the on-axis pressure using

$$p_{\text{rms}}(r) = \frac{\rho_0 f_S D u_{c(\text{rms})}}{r} \quad (6.43)$$

and

$$\text{SPL} = 20 \log_{10} \left(\frac{p_{\text{rms}}(r)}{p_{\text{ref}}} \right) \quad (6.44)$$

where $p_{\text{ref}} = 20 \mu\text{Pa}$ rms. The on-axis pressure of a typical 100 mm loudspeaker in an infinite baffle is plotted in Fig. 6.7. For this application, the mass of the cone is made as light as possible and the compliance of the suspension as high as possible consistent with mechanical stability. The high frequency response is aided by means of a concentric secondary or “whizzer” cone.

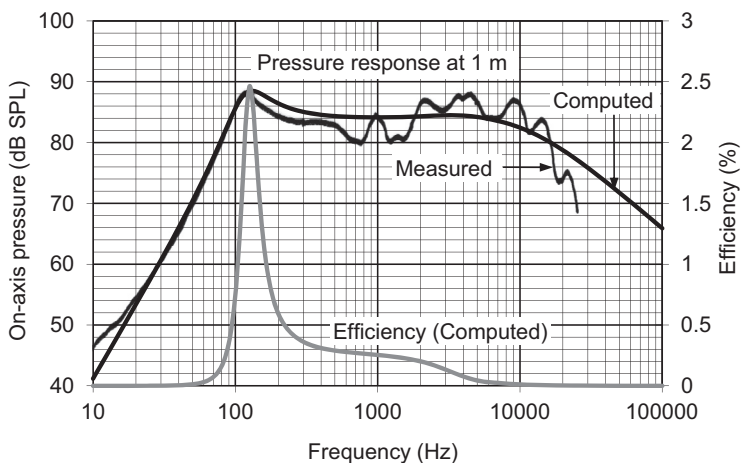


Figure 6.7 On-axis pressure response and efficiency of an electrodynamic loudspeaker in an infinite baffle for which $e_{g(\text{rms})} = 2.83 \text{ Vrms}$, $R_E = 7 \Omega$, $L_E = 100 \mu\text{H}$, $Q_{ES} = 2.2$, $Q_{MS} = 5$, $f_s = 125 \text{ Hz}$, $S_D = 56 \text{ cm}^2$, and $V_{AS} = 2 \text{ L}$.



6.8 ELECTRICAL INPUT IMPEDANCE

If we ignore the radiation resistance, which is a negligibly small part of the input impedance, and add the radiation mass to the mechanical mass so that $M_{MS} = M_{MD} + 2M_{M1}$, we can write the electrical input impedance Z_E from inspection of Fig. 6.2:

$$\begin{aligned}
 Z_E &= Z_{ES} + Z_{EM} = R_E + j\omega L_E + \left(j\omega \frac{M_{MS}}{B^2 l^2} + \frac{1}{B^2 l^2 G_{MS}} + \frac{1}{j\omega B^2 l^2 C_{MS}} \right)^{-1} \\
 &= R_E + j\omega L_E + \frac{B^2 l^2}{R_{MS}} \left(\frac{\frac{j}{Q_{MS}} \cdot \frac{f}{f_S}}{1 - \frac{f^2}{f_S^2} + \frac{j}{Q_{MS}} \cdot \frac{f}{f_S}} \right)
 \end{aligned} \tag{6.45}$$

The electrical impedance curve of a typical 100 mm loudspeaker in an infinite baffle is plotted in Fig. 6.8. The peak at 125 Hz coincides with the suspension resonance frequency f_S . If we ignore the effect of the coil inductance L_E , the input impedance at f_S is approximately $Z_E = R_E + R_{ES}$, where $R_{ES} = B^2 l^2 / R_{MS}$ ($= R_E Q_{MS} / Q_{ES}$). Therefore, a high peak indicates a large Bl factor or small mechanical damping resistance or both. At high frequencies, the impedance rises due to the increasing contribution of the coil inductance L_E . At very low frequencies, the impedance approaches the DC resistance R_E asymptotically, which in this case is 7Ω .

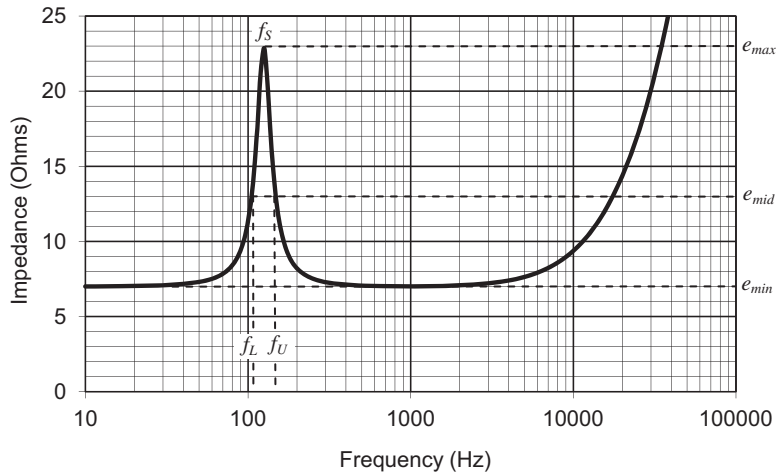


Figure 6.8 Electrical impedance Z_E of an electrodynamic loudspeaker in an infinite baffle with the same parameters as those in Fig. 6.7.



6.9 EFFICIENCY

Medium frequencies

The efficiency of a loudspeaker is defined as 100 times the ratio of the acoustic power radiated to the power supplied by the electrical generator. In the medium frequency range between the suspension resonance and the point where the coil inductance starts to contribute to the electrical impedance, the power supplied by the generator is approximately

$$W_E \approx \frac{e_g^2}{R_E} \quad (6.46)$$

where we are assuming that $R_g \ll R_E$. Using W from Eq. (6.23), the reference efficiency E_{ff} is then given by

$$E_{ff} = 100 \frac{W}{W_E} \approx 100 \frac{B^2 l^2 S_D^2 \rho_0}{\pi R_E M_{MS}^2 c}, \quad 2f_0 < f < \frac{c}{4\pi a} \quad (6.47)$$

Not surprisingly, if we compare this with Eq. (6.32), we find that the same parameters which contribute to a high SPL also make for an efficient loudspeaker, namely high field strength, low mass, and a large radiating area. By combining Eqs. (6.8), (6.11), (6.26), and (6.47), we obtain a convenient expression for the reference efficiency in terms of Thiele–Small parameters:

$$E_{ff} = 100 \frac{W}{W_E} \approx 100 \frac{8\pi^2 V_{AS} f_S^3}{Q_{ES} c^3}, \quad 2f_0 < f < \frac{c}{4\pi a} \quad (6.48)$$

At resonance

When $f = f_S$, the cone velocity is at a maximum value which is found by letting $X_M = 0$ in Eq. (6.1) so that

$$\tilde{u}_c = \frac{\tilde{e}_g B l}{(R_g + R_E) R_M} \quad (6.49)$$

From Eqs. (6.19) and (6.21),

$$W = \frac{e_g^2 (\text{rms}) B^2 l^2 \omega_S^2 S_D^2 \rho_0}{\pi c (R_g + R_E)^2 R_M^2} \quad (6.50)$$

The input power at resonance, assuming $R_{MS} \gg 2\mathbf{R}_{MR}$, is given by

$$W_E = \frac{e_g^2(\text{rms})}{R_g + R_E + (B^2 l^2)/R_{MS}} \quad (6.51)$$

Then the efficiency at resonance, assuming $R_E \gg R_g$, is given by

$$E_{ffS} = 100 \frac{W}{W_E} = 100 \frac{B^2 l^2 \omega_S^2 S_D^2 \rho_0}{\pi c (B^2 l^2 + R_E R_{MS}) R_{MS}} \quad (6.52)$$

Noting that $Q_{MS} = \omega_S M_{MS}/R_{MS}$ and $Q_{ES} = \omega_S M_{MS} R_E / (Bl)^2$, we obtain

$$E_{ffS} = 100 \frac{W}{W_E} = 100 \frac{Q_{ES} Q_{MS}^2 B^2 l^2 S_D^2 \rho_0}{(Q_{ES} + Q_{MS}) \pi R_E M_{MS}^2 c} \quad (6.53)$$

Comparing this with Eq. (6.47) and using the relationship of Eq. (6.10) yields the following relationship between the efficiency at resonance E_{ffS} and the midband reference efficiency E_{ff} :

$$\frac{E_{ffS}}{E_{ff}} = Q_{TS} Q_{MS} \quad (6.54)$$

All frequencies

The power supplied by the generator at all frequencies is

$$W_E = e_g^2(\text{rms}) \Re\left(\frac{1}{Z_E}\right) \quad (6.55)$$

where the electrical impedance Z_E is given by Eq. (6.45). The radiated power is given by Eq. (6.19) where the cone velocity is given by Eq. (6.42) and \mathbf{R}_{MR} by

$$\mathbf{R}_{MR} = S_D \rho_0 c \left(1 - \frac{J_1(2ka)}{ka}\right) \quad (6.56)$$

from Eq. (13.117). Hence,

$$E_{ff} = 100 \frac{W}{W_E} = 100 \left| \frac{Bl}{(R_E + j\omega L_E) Z_{MT}} \right|^2 \frac{2S_D \rho_0 c}{\Re(1/Z_E)} \left(1 - \frac{J_1(2ka)}{ka}\right) \quad (6.57)$$

where Z_{MT} is given by Eq. (6.41). The efficiency of a typical 100 mm loudspeaker in an infinite baffle is plotted in Fig. 6.7. Not surprisingly, the loudspeaker is most efficient at the suspension resonance f_S where the input impedance is also at a maximum so that relatively little current is drawn. The efficiency falls off at high frequencies due to diaphragm and coil inertia, where most of the input power is dissipated in heating the voice coil.



6.10 MEASUREMENT OF THIELE—SMALL PARAMETERS

Before embarking on a loudspeaker enclosure design, we need to know the six Thiele—Small parameters that will be used to calculate the low-frequency response of our chosen drive unit in the enclosure. Most drive unit manufacturers now provide these on their data sheets, but if they are not available, we have to measure them. Even if they are available, production tolerances are such that we cannot always expect our computed frequency response to match the measured one unless the model used for computation is based on parameters obtained from the measured sample. In this section, it is shown how to obtain the Thiele—Small parameters purely by measuring the electrical input voltage at different frequencies using a multimeter and a calibrated variable-frequency oscillator.

During the tests, the electrodynamic loudspeaker is preferably mounted in a baffle such as the IEC 268-5 baffle [7], which is the standard baffle used by manufacturers. We see from Fig. 12.28 that if the outer diameter of the baffle is at least four times that of the loudspeaker, the radiation mass or reactive load is that of a piston in an infinite baffle. It should be borne in mind that if the loudspeaker is measured without any baffle, the radiation mass is halved which will result in a small error that can be corrected. It is not essential to perform the tests in an anechoic chamber: A large room that is not too noisy or reverberant will suffice. A variable-frequency source of sound with an output impedance R_g greater than 20 times the nominal impedance of the loudspeaker is connected to the loudspeaker terminals. An AC voltmeter is then connected across the terminals. The value of R_g should include both the inherent output impedance of the generator and any external resistor connected to in order to make up the desired impedance. The value of $e_{g(\text{rms})}$ is that measured by the meter before the loudspeaker is connected. Some AC meters are only designed to work at around 50–60 Hz, so it is worth checking to see if the reading varies with frequency with the loudspeaker disconnected. If it does, the open-circuit readings should be used to calibrate the measurements to the loudspeaker. The parameters are then determined as follows.

Measurement of suspension resonance frequency f_s

To measure f_s , the frequency is varied until a maximum meter reading is obtained (see Fig. 6.9). From Fig. 6.2 and Fig. 6.8, we see that maximum electrical loudspeaker

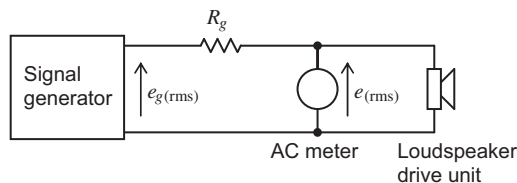


Figure 6.9 Circuit for determining the Thiele—Small parameters of a loudspeaker.

impedance corresponds to maximum mechanical admittance, which in turn occurs at the resonance frequency f_S or ω_S . The reading obtained at this frequency is e_{\max} .

Measurement of Q_{MS} and Q_{ES}

The minimum reading e_{\min} in Fig. 6.8 is found by reducing the frequency until the voltage reading no longer changes. Increase the frequency again until the voltage reading gives a value of $e_{\text{mid}} = \sqrt{e_{\max}e_{\min}}$. The frequency at this point is f_L . Then, increase the frequency beyond f_S (maximum voltage reading) until the voltage reading gives a value of $\sqrt{e_{\max}e_{\min}}$ for a second time. The frequency at this point is f_U . Note that $f_S = \sqrt{f_L f_U}$. The mechanical Q is then given by

$$Q_{MS} = \frac{f_S}{f_U - f_L} \left(\frac{e_g - e_{\min}}{e_g - e_{\max}} \right) \sqrt{\frac{e_{\max}}{e_{\min}}} \quad (6.58)$$

and the electrical Q by

$$Q_{ES} = \left(1 - \frac{e_{\max}}{e_g} \right) \frac{e_{\min} Q_{MS}}{e_{\max} - e_{\min}} \quad (6.59)$$

If the signal generator is a current source, then $e_g \rightarrow \infty$ and the bracketed terms become unity. These equations assume that the effect of the coil inductance L_E at around f_S is negligible.

Measurement of R_E

The electrical resistance of the voice coil is measured with a milliohm meter.

Measurement of S_D

The effective area of the diaphragm can be determined by coupling its front side to a closed box. The volume of air V_0 enclosed in the space bounded by the diaphragm and the sides of the box must be determined accurately. Then a slant manometer for measuring air pressure is connected to the airspace. The cone is then displaced a known distance ξ meters, the manometer is read, and the incremental pressure p is determined. Then,

$$p = \frac{P_0}{V_0} \xi S_D \quad (6.60)$$

or

$$S_D = \frac{P_0}{V_0} \frac{p}{\xi} \quad (6.61)$$

where P_0 is the ambient pressure. The pressures P_0 and p both must be measured in the same units, and V_0/ξ should be determined in m^2 .

Usually, S_D can be determined accurately enough for most calculations from Fig. 6.1, that is, $S_D = \pi a^2$. To determine the effective radius a more accurately, we assume that the displacement of the surround (8) decreases linearly between its inner and outer edges which have radii a_1 and a_2 , respectively. Then, the effective radius is given by

$$a = \sqrt{\frac{a_1^2 + a_1 a_2 + a_2^2}{3}} \quad (6.62)$$

and, hence, the effective area by

$$S_D = \frac{\pi}{3} (a_1^2 + a_1 a_2 + a_2^2) \quad (6.63)$$

Measurement of V_{AS}

The equivalent suspension volume V_{AS} (see Eq. 6.26) can be obtained in two ways. Either we add mass to the diaphragm and observe the change in resonance frequency or we add stiffness in the form of a sealed enclosure. The first method is simplest and is suitable for most loudspeakers. However, in the case of microspeakers used in mobile devices, it is impractical to attach masses as the risk of destabilizing the diaphragm is too great.

The added mass is usually a rod of nonferrous metal (e.g., enameled copper wire or solder) bent into a circle or spiral and attached to the diaphragm using tape or blu tack so that it does not bounce.

If the original resonance frequency was f_S and the resonance frequency after addition of a mass M_x kg is f'_S , then

$$f_S = \frac{1}{2\pi\sqrt{M_{MS}C_{MS}}} \quad (6.64)$$

and

$$f'_S = \frac{1}{2\pi\sqrt{(M_{MS} + M_x)C_{MS}}} \quad (6.65)$$

where C_{MS} is mechanical compliance of the suspension in m/N . Simultaneous solution of Eqs. (6.64) and (6.65) yields

$$M_{MS} = \frac{M_x}{(f_S/f'_S)^2 - 1} \quad (6.66)$$

Combining this with Eqs. (6.27) and (6.28) yields

$$V_{AS} = \left(1 - \frac{f'^2}{f_S^2}\right) \frac{S_D^2 \rho_0 c^2}{(2\pi f'_S)^2 M_x} \quad (6.67)$$

Alternatively, if the drive unit is mounted in a sealed enclosure of known volume V_B , then the new resonance frequency is given by

$$f_C = \frac{1}{2\pi} \sqrt{\frac{C_{MS} + C_{MB}}{M_{MC} C_{MS} C_{MB}}} \quad (6.68)$$

where C_{MB} is the mechanical stiffness due to the air in the enclosure given by

$$C_{MB} = \frac{V_B}{S_D^2 \rho_0 c^2} \quad (6.69)$$

Because of the air mass loading within the box, the total moving mass may be modified slightly, in which case we denote a new value M_{MC} and a new electrical Q_{EC} :

$$Q_{EC} = \frac{R_E}{B^2 l^2} \sqrt{\frac{M_{MC}(C_{MS} + C_{MB})}{C_{MS} C_{MB}}} \quad (6.70)$$

Simultaneous solution of Eqs. (6.11), (6.64), (6.68), and (6.70) yields

$$C_{MS} = \left(\frac{f_C Q_{EC}}{f_S Q_{ES}} - 1\right) C_{MB} \quad (6.71)$$

Hence, from Eq. (6.27)

$$V_{AS} = \left(\frac{f_C Q_{EC}}{f_S Q_{ES}} - 1\right) V_B \quad (6.72)$$

In Chapter 7 of this book, on Loudspeaker Enclosures, design charts are presented from which it is possible to determine, without laborious computation, the sound pressure from a direct-radiator loudspeaker as a function of frequency including the directivity characteristics. Methods for determining the constants of box and bass-reflex enclosures are also presented. If the reader is interested only in learning how to choose a baffle for a loudspeaker, he or she may proceed directly to Chapter 7. The next part deals with the factors in design that determine the overall response and efficiency of the loudspeaker.



6.11 EXAMPLES OF LOUDSPEAKER CALCULATIONS

Example 6.1. Given the efficiency of Eq. (6.47) for a loudspeaker in an infinite baffle, determine the reference sound pressure equivalent to the efficiency assuming that the directivity factor Q (for radiation to one side) equals 2.

Solution. The sound pressure at distance r , assuming no directivity, is related to the acoustic power radiated to one side as follows (see Eqs. 6.40 and 6.46):

$$p_{\text{rms}}(r) = \sqrt{\rho_0 c I} = \sqrt{\frac{\rho_0 c W_1}{2\pi r^2}}$$

where I is intensity at distance r . $W_1 = W/2$ is total acoustic power radiated from one side of the diaphragm.

The reference sound pressure is

$$\begin{aligned} p_{\text{rms}}(r) &= \sqrt{\frac{\rho_0 c}{2\pi r^2}} \sqrt{\frac{E_{\text{ff}}}{200} W_E} \\ &= \frac{e_{g(\text{rms})} \rho_0 B I S_D}{2\pi r R_E (M_{MD} + 2M_{M1})} \end{aligned}$$

which is that given by Eq. (6.32) in the passband where $\alpha_c \approx 1$ and it is assumed that $R_g \ll R_E$.

Example 6.2. As an example of the efficiency to be expected from an electrodynamic loudspeaker of conventional design mounted in an infinite baffle and radiating directly from both sides of the baffle, let us calculate the reference efficiency E_{ff} from Eq. (6.48) for the case of a commercial loudspeaker with an advertised diameter of 10 cm. In addition, let us calculate the ratio of the efficiency at the suspension resonance frequency to the reference efficiency. The values of the six Thiele–Small parameters are as follows:

$$R_E = 7 \Omega$$

$$Q_{ES} = 2.2$$

$$Q_{MS} = 5$$

$$f_S = 125 \text{ Hz}$$

$$S_D = 56 \text{ cm}^2$$

$$V_{AS} = 0.002 \text{ m}^3 \text{ (2 L)}$$

Also

$$a = \sqrt{S_D/\pi} = 42.22 \text{ mm}$$

$$Q_{TS} = \frac{Q_{ES} Q_{MS}}{Q_{ES} + Q_{MS}} = 1.528$$

ρ_0 , density of air = 1.18 kg/m³

c , speed of sound = 344.8 m/s.

Solution. From Eq. (6.48), we obtain

$$E_{ff} = 100 \frac{8 \times (3.14)^2 \times 0.002 \times (125)^3}{2 \times (344.8)^3} = 0.342\%$$

For radiation from one side of the loudspeaker only, divide this figure by 2. Hence, only 0.171% of the available electrical power is radiated to one side of the diaphragm at mid to low frequencies. This illustrates the statement made at the beginning of this chapter that the efficiency of this type of loudspeaker is usually low.

For our example, the transition frequency at which the loudspeaker starts to become more directional and the efficiency decreases rapidly occurs when ka lies approximately between 1 and 2. For our example, $ka = 1$ corresponds to a frequency of

$$f = \frac{c}{2\pi a} = \frac{344.8}{2\pi \times 0.04222} = 1.3 \text{ kHz}$$

Obviously, a smaller diaphragm of lighter weight would result in this transition extending to a higher frequency. However, a reduction in the mass M_{MD} occasioned by a smaller diaphragm will cause an increase in the first resonance frequency with a resulting loss in bass response. A further disadvantage of a smaller diaphragm is that, for a given sound pressure, a greater voice-coil velocity \tilde{u}_c is needed. A longer air gap and a larger magnet structure must therefore be provided.

From Eq. (6.54), we obtain the efficiency at the suspension resonance:

$$E_{ffS} = 1.528 \times 5 \times 0.342 = 2.61\%$$

Hence, the ratio E_{ffS}/E_{ff} equals 7.64, and efficiency at f_S equals 1.3% for radiation from one side only.



PART XX: DESIGN FACTORS AFFECTING DIRECT-RADIATOR LOUSPEAKER PERFORMANCE

A loudspeaker generally is designed to provide an efficient transfer of electric power into acoustic power and to effect this transfer uniformly over as wide a frequency range as possible. To accomplish this, the voice coil, diaphragm, and amplifier must be properly chosen. The choice of the elements and their effect on efficiency, directivity, and transient response are discussed here.

6.12 MAGNET SIZE

A cross-sectional sketch of a typical microspeaker is shown in Fig. 6.10. In this discussion, it is assumed that the coil fills the gap in the magnetic path without any air spaces and that it has the same permeability as free space. For the sake of argument, the wire cross section might be rectangular so that any gap width or length could accommodate an integer number of turns or layers, respectively. It is also assumed that the reluctances of the pole pieces are negligible in comparison with that of the gap, so these are ignored. The radii of the diaphragm, magnet, and coil are a , a_m , and a_c , respectively.

Suppose the solid curve in Fig. 6.11 to represent the demagnetizing portion of the hysteresis loop for a magnetizing force H_{sat} obtained with the coil gaps in Fig. 6.10 closed, where B_R is the remanent flux density. To neutralize the residual magnetism, it is necessary to apply, by means of a suitable field winding, a demagnetizing magnetomotive force \mathfrak{F} in ampere-turns. If H_C is the coercive force and l_m the length of the magnet, then $\mathfrak{F} = H_C l_m$. Therefore, \mathfrak{F} may be termed *the inherent magnetomotive force* for maintaining the remanent flux density B_R .

With the coil gaps in Fig. 6.10 closed, let us reduce the magnetic field strength from H_{sat} to zero and then increase it to H_1 in the reverse direction, so that the flux density is reduced to B_1 . The net magnetomotive force available to produce this flux density in the magnet is $H_C l_m - H_1 l_m$ or in other words, the difference between the inherent MMF and applied MME.

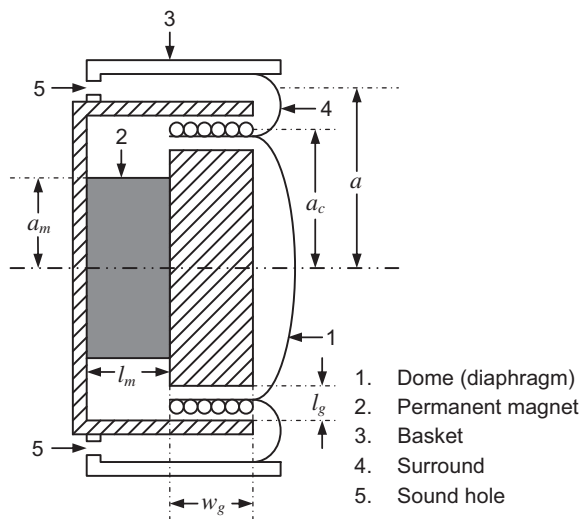


Figure 6.10 Cross-sectional sketch of a microspeaker.

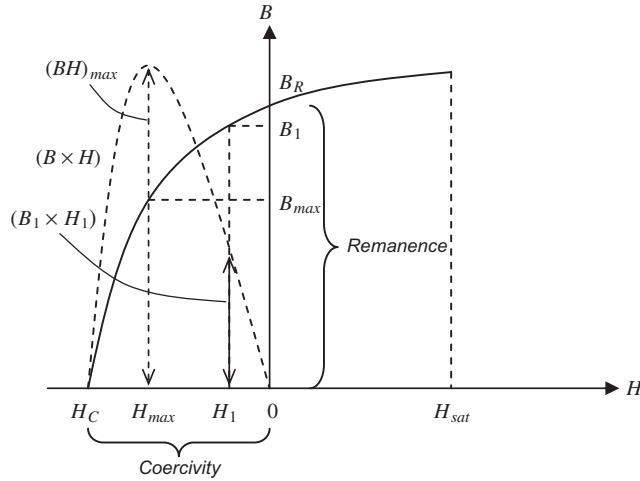


Figure 6.11 A typical demagnetization curve.

Next, let us gradually pull the pole pieces apart and at the same time reduce the demagnetizing current in the field coil so as to keep the flux density constant at B_1 . Suppose the procedure to be continued until the current has been reduced to zero and suppose l_g in Fig. 6.10 to be the corresponding gap length. Because this gap has been introduced without any change of flux density in the magnet, it follows that the magnetomotive force now available to send the flux ϕ across the gap is therefore $H_1 l_m$, namely that neutralized by the negative magnetomotive force of the field coil before the gap was introduced. The flux ϕ across the gap is given by

$$\phi = B_1 \pi a_m^2 = B_g \times 2\pi a_c w_g \quad (6.73)$$

where B_1 is the flux density in the magnet and B_g is the flux density in the gap. In addition, the magnetomotive force required to send flux across the gap is given by

$$\mathfrak{F}_g = \frac{B_g l_g}{\mu_o}, \quad (6.74)$$

where $\mu_o = 4\pi \times 10^{-7}$ H/m is the permeability of free space, but it was shown that the magnetomotive force required to send flux across the gap is given by $H_1 l_m$. Therefore,

$$H_1 l_m = \frac{B_g l_g}{\mu_o}. \quad (6.75)$$

From Eqs. (6.73) and (6.75), it follows that the volume V_m of the magnet is given by

$$\begin{aligned} V_m &= \pi a_m^2 l_m \\ &= \frac{B_g \times 2\pi a_c w_g}{B_1} \cdot \frac{B_g l_g}{H_1 \mu_o} \\ &= \frac{2\pi a_c w_g l_g B_g^2}{\mu_o B_1 H_1} \end{aligned} \quad (6.76)$$

From Eq. (6.76), it is evident that for a given flux density in the given dimensions of the gap, the volume of the magnet is a minimum when the product $B_1 H_1$ is a maximum. The variation of this product with H in the *magnet core* is shown in Fig. 6.11 as a dashed curve from which it follows that the volume of the magnet is a minimum when it is operated at magnetomotive force H_{\max} . The value of the product $(BH)_{\max}$, also known as the *maximum energy product*, for a magnetic material is the best criterion of its suitability for use as a permanent magnet and the volume is then given by

$$V_m = \frac{2\pi a_c w_g l_g B_g^2}{\mu_o (BH)_{\max}} \quad (6.77)$$

Notice that

$$V_g = 2\pi a_c w_g l_g \quad (6.78)$$

is the volume occupied by the gap. In addition, let us assume that the field in the pole pieces is in saturation so that $B_g = B_{\text{sat}}$. This prevents the field from varying significantly with the driving current in the coil and thus improves linearity. Hence, the magnet volume can be written as

$$V_m = \frac{B_{\text{sat}}^2}{\mu_o (BH)_{\max}} V_g \quad (6.79)$$

If the demagnetization curve were perfectly linear, the values of H_{\max} and B_{\max} would be exactly half of the values of the coercivity and remanence, respectively, which are more commonly found in manufacturer's data than H_{\max} and B_{\max} . However, because of nonlinearity, a factor of 2/3 should give a reasonably good estimate for many materials, although neodymium iron boron (NdFeB) magnets [8] are remarkably close to ideal, as can be seen in Fig. 6.12. The upper curves are the *intrinsic B* versus H values which show the flux density excluding the flux due to the external applied field, and the

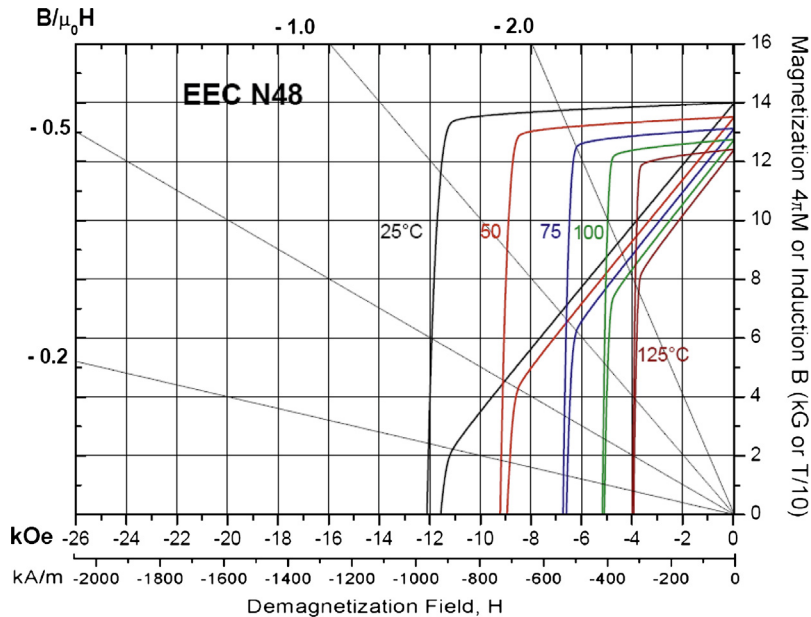


Figure 6.12 Demagnetization curves for a commercial neodymium iron boron magnet at five different temperatures ranging from 25 to 125°C. Upper curves are intrinsic values and lower curves are actual values including applied field.

lower curves are the *actual* “normal” B versus H values including the total net flux. It should be noted that the intrinsic coercivity is slightly greater than the actual coercivity. Commercial NdFeB magnets are denoted by a grade which specifies the maximum energy product in mega-gauss-oersteds and the minimum intrinsic coercivity in kilo-oersteds. For example, a Grade N4811 NdFeB magnet has a maximum energy product BH_{\max} of 48 MGOe and a minimum intrinsic coercivity H_{ci} of 11 kOe. For our calculations, it is more convenient to use MKS units, in which case the conversions can be made using

$$1 \text{ G} = 10^{-4} \text{ T} \quad (6.80)$$

$$1 \text{ Oe} = \frac{10^3}{4\pi} \text{ A/m} \quad (6.81)$$

Hence, a Grade N4811 NdFeB magnet has a maximum energy product BH_{\max} of 382 kTA/m and a minimum intrinsic coercivity H_{ci} of 875 kA/m.



6.13 VOICE-COIL DESIGN

Effect of coil size on efficiency

Let us now reconsider Eq. (6.47) to see how to maximize the efficiency in terms of the actual coil dimensions. The resistance R_E can be expressed in terms of the mass of the voice-coil winding M_{MC} by writing

$$R_E = \frac{k l}{\pi a_w^2} \quad (6.82)$$

where κ is resistivity of voice-coil conductor in units of $\Omega \cdot \text{m}$. The value of κ for different materials is given in Table 6.1. a_w is radius of wire in m. l is length of voice-coil winding in m.

We also note that the volume occupied by the coil wire is

$$V_w = \pi a_w^2 l \quad (6.83)$$

where for simplicity we are assuming that the space occupied by the coil former and insulation is negligible compared with the conductor. Inserting Eqs. (6.82) and (6.83) into Eq. (6.47) yields

$$E_{ff} \approx 100 \frac{V_w B^2 S_D^2 \rho_0}{\pi k M_{MS}^2 c}, \quad 2f_0 < f < \frac{c}{4\pi a} \quad (6.84)$$

We now define the total moving mass by

$$M_{MS} = M'_{MS} + M_{MC} \quad (6.85)$$

where M'_{MS} is the combined mass of the diaphragm and radiation load excluding the coil, and M_{MC} is the mass of the coil given by

$$M_{MC} \approx V_w \rho_w = \frac{\pi}{4} V_g \rho_w \quad (6.86)$$

where ρ_w is the density of the voice-coil wire in kg/m^3 (see Table 6.1). Inserting Eqs. (6.85) and (6.86) into Eq. (6.84) yields

$$E_{ff} \approx 100 \frac{V_w B^2 S_D^2 \rho_0}{\pi k (V_w \rho_w + M'_{MS})^2 c}, \quad 2f_0 < f < \frac{c}{4\pi a} \quad (6.87)$$

Table 6.1 Resistivity and density of various metals

Metal element	Resistivity k , $10^{-6} \Omega \cdot \text{m}$	Density ρ_w , 10^3 kg/m^3	$k\rho^2w$, $\Omega \cdot \text{kg}^2/\text{m}^5$	Ranking
Aluminum	0.0283	2.70	0.206	6
Antimony	0.417	6.6	18.2	21
Bismuth	1.190	9.8	114.2876	27
Cadmium	0.075	8.7	5.68	14
Calcium	0.046	1.54	0.109	4
Carbon	8.0	2.25	40.5	25
Cesium	0.22	1.9	0.794	8
Chromium	0.026	6.92	1.25	9
Cobalt	0.097	8.71	7.36	19
Copper	0.0172	8.7	1.30	10
Gold	0.0244	19.3	9.09	20
Iridium	0.061	22.4	30.6	24
Iron	0.1	7.9	6.24	18
Lead	0.220	11.0	26.6	23
Lithium	0.094	0.534	0.0268	1
Magnesium	0.046	1.74	0.139	5
Manganese	0.050	7.42	2.75	12
Mercury	0.958	13.5	174	28
Molybdenum	0.057	10.2	5.93	15
Nickel	0.078	8.8	6.04	16
Platinum	0.10	21.4	45.8	26
Potassium	0.071	0.87	0.0537	3
Silver	0.0163	10.5	1.80	11
Sodium	0.046	0.97	0.0433	2
Tin	0.115	7.3	6.13	17
Titanium	0.032	4.5	0.648	7
Tungsten	0.055	19.0	19.9	22
Zinc	0.059	7.1	2.97	13

To find the optimum coil volume, we differentiate with respect to V_w and set the result to zero:

$$\frac{\partial}{\partial V_w} E_{ff} = 100 \frac{(M'_{MS} - V_w \rho_w) B^2 S_D^2 \rho_0}{\pi k (V_w \rho_w + M'_{MS})^2 c} = 0 \quad (6.88)$$

so that the optimum coil volume is given by

$$V_w = M'_{MS} / \rho_w \quad (6.89)$$

Hence, the optimum mass for the coil is that of the diaphragm (less the coil) combined with the radiation mass. However, this optimum is quite broad and in practice one

can err on the side of greater coil mass. If the coil wire has a circular cross section, then the gap volume is $V_g = 4V_w/\pi$, otherwise for a square cross section $V_g = V_w$. Let us suppose for the sake of argument that we can make the diaphragm as light as we wish and that it remains perfectly rigid. Then, setting $M'_{MS} = M_{MC}$ gives

$$E_{ff} \approx 100 \frac{2B^2 S_D^2 \rho_0}{\pi^2 k \rho_w^2 V_g c}, \quad 2f_0 < f < \frac{c}{4\pi a}, \quad M'_{MS} \approx M_{MC} \quad (6.90)$$

From this equation, we see that the efficiency is independent of the coil resistance, number of turns, or wire diameter. It is only dependent on the volume of the gap and the properties of the conductor, namely the resistivity κ and the density ρ_w . The product $\kappa\rho_w^2$ which appears in the denominator of Eq. (6.90) is given in Table 6.1 for various materials and ranked in ascending order. Unfortunately, the top-ranked four materials—lithium, sodium, potassium, and calcium—are not practicable for loudspeakers because they are highly reactive metals. Although copper is the material most commonly used in voice coils, there are many instances where aluminum has been successfully deployed to give increased efficiency and sensitivity. The problem in microspeakers is that aluminum lead out wires are somewhat brittle and liable to break after repeated flexing, although an alloy could be used. We have already deduced in Eq. (6.79) that the size of the magnet V_M is directly related to that of the magnetic gap V_G . Hence, reducing the gap volume not only makes the loudspeaker more efficient but also reduces the required magnet size and therefore saves cost and weight.

Number of turns and wire diameter

The length l of the coil wire is

$$l = 2\pi a_c N \quad (6.91)$$

where N is the number of turns and the cross-sectional area S_w of the wire is

$$S_w = \pi a_w^2 = \frac{\pi w_g l_g}{4N} \quad (6.92)$$

Inserting Eqs. (6.91) and (6.92) into Eq. (6.82) for the coil resistance and solving for N yields

$$N = \sqrt{\frac{w_g l_g R_E}{8a_c k}} \quad (6.93)$$

Then the wire radius is given by

$$a_w = \sqrt{\frac{w_g l_g}{4N}} = \left(\frac{V_g k}{4\pi R_E} \right)^{1/4} \quad (6.94)$$

from Eqs. (6.78), (6.82) and (6.91). Therefore, we conclude that while reducing the coil volume is beneficial for efficiency and reducing the magnet size, there is a limit to how much the volume can be reduced because eventually the wire becomes so thin that it is difficult to manufacture with any reasonable tolerance. In addition, smaller coils are more difficult to cool, although with the increased efficiency they should not run so hot. Interestingly, the efficiency and wire radius are both independent of the coil geometry, and only dependent on its volume. This means there is a certain amount of flexibility regarding the diameter d or length l_g of the coil. Ideally, we would like to maximize l_g as this would also maximize the linear displacement x_{\max} . In microspeakers, however, the gap length cannot be increased too much as the thickness of the component is an important factor in the design of the host product, especially if it is a mobile device. It is obvious from Eq. (6.94) that thinner wire is needed for high impedance loudspeakers in which R_E is large. However, reducing R_E usually results in greater losses in the amplifier and associated power source, so it is rarely less than about 3Ω .



6.14 DIAPHRAGM BEHAVIOR

The simple theory using the method of equivalent circuits, which we have just derived, is not valid above some frequency between 300 and 1000 Hz. In the higher frequency range, the cone, diaphragm mass M_{MD} , and also the radiation impedance change no longer move as a single unit. These changes may occur with great rapidity as a function of frequency. As a result, no exact mathematical treatment is available by which the performance of a loudspeaker can be predicted in the higher frequency range, unless the geometry is very simple, as in the case of a shallow spherical shell [9]. Cones are often approximated by concentric rings [10] or finite element models. Modern finite element models include the magnetic path and nonlinear behavior [11].

A detailed study of one particular loudspeaker is reported here as an example of the behavior of the diaphragm [12]. The diaphragm is a felted-paper cone, about 170 mm in effective diameter (see Fig. 6.13), having an included angle of 118 degrees. The sound—pressure—level response curve for this loudspeaker measured on the principal axis is shown in Fig. 6.14.

This particular loudspeaker has, in addition to its fundamental resonance, other peaks and dips in the response at points 1–8 as indicated on the curve. The major resonance at 90 Hz is the principal suspension resonance f_S and has the relative amplitude given by $20 \log Q_{TS}$ from Eq. (6.14). Immediately above that is a fairly flat region. At point 1, which is located at 420 Hz, the cone breaks up into a resonance of the form shown by the first sketch in Fig. 6.15. Here, there are four nodal lines on the cone extending radially, and four regions of maximum movement. As indicated by the plus and minus signs, two regions move outward while two regions move inward. The net effect is a pumping of air

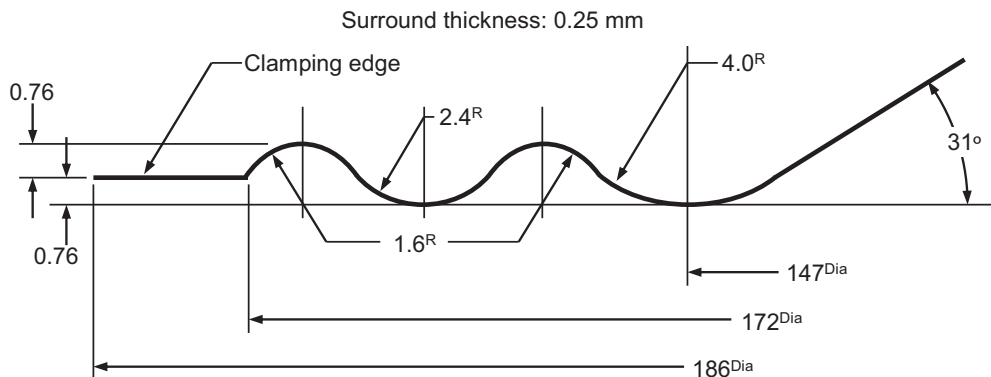


Figure 6.13 Detail of the edge of a felted-paper loudspeaker cone from a 200 mm loudspeaker. After Corrington. Amplitude and phase measurements on loudspeaker cones. Proc IRE 1951;39:1021–26.

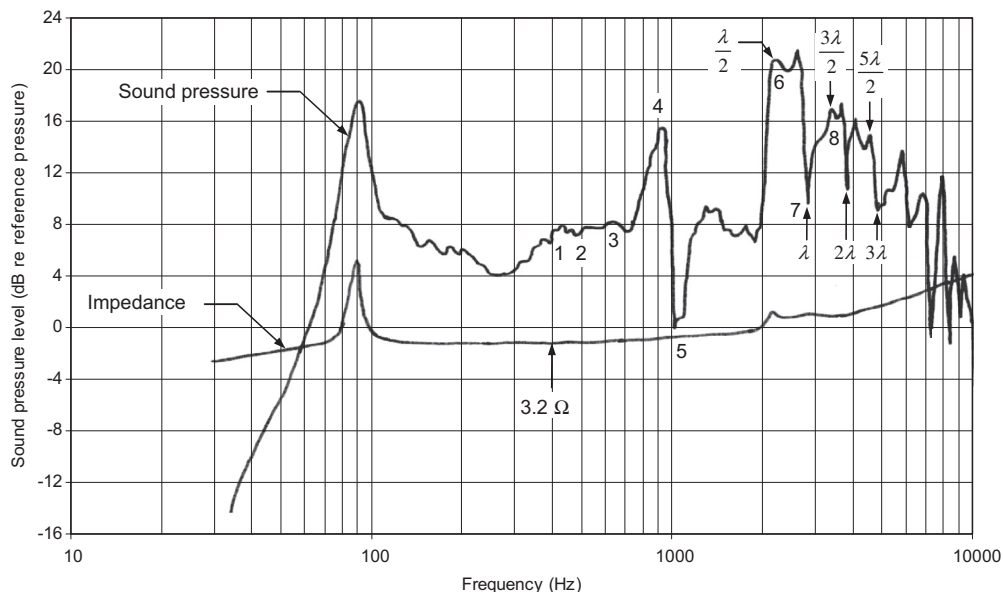


Figure 6.14 On-axis response of a 200 mm diameter loudspeaker mounted in an infinite baffle. After Corrington [12].

back and forth across the nodal lines. The cone is also vibrating as a whole in and out of the page. The net change in the output is an increase of about 5 dB relative to that which it would be if the cone were perfectly rigid. A similar situation exists at point 2 at 500 Hz, except that the number of nodal lines is increased from 4 to 6. At point 3, 650 Hz, the vibration becomes more complex. Nodal lines are no longer well defined, and the speaker vibrates in such a way that the increase in pressure level is again about 5 dB.

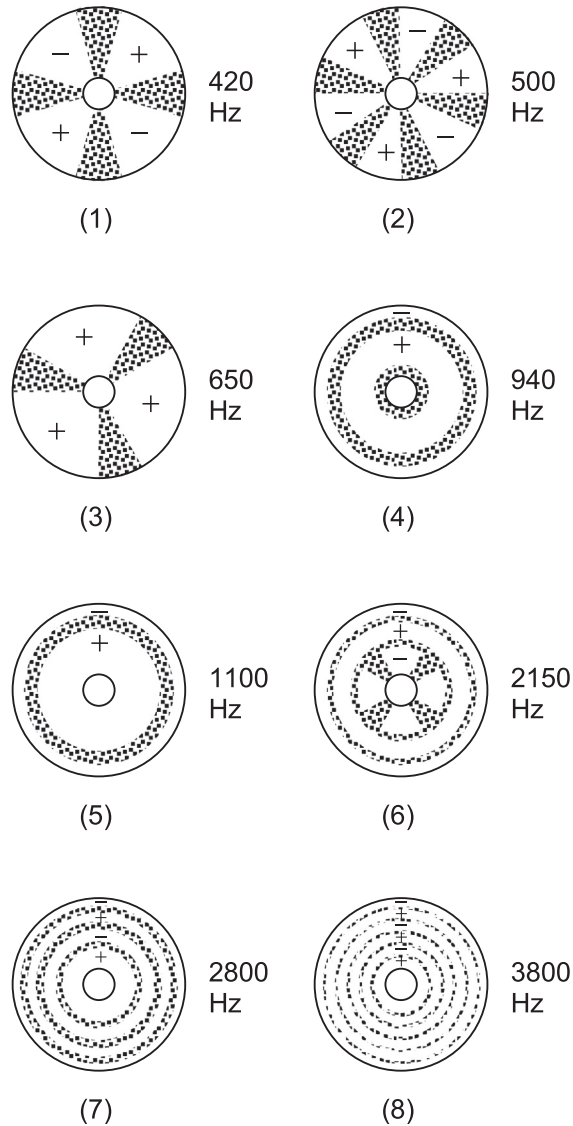


Figure 6.15 Nodal pattern of the cone of the loudspeaker whose response curve is given in Fig. 6.14 at 420 Hz (1), 500 Hz (2), 650 Hz (3), 940 Hz (4), 1100 Hz (5), 2150 Hz (6), 2800 Hz (7), and 3800 Hz (8). The shaded and dashed lines indicate lines of small amplitude of vibration. The (+) and (−) signs indicate regions moving in opposite directions, i.e., opposite phases. After Corrington [12] with changes.

For point 4 at 940 Hz, a new type of vibration has become quite apparent. The diaphragm moves in phase everywhere except at the surround. Looking at the surround construction shown in Fig. 6.13 and at the vibration pattern of Fig. 6.15(4), we can deduce what happens. The center part of the cone vibrates at a fairly small amplitude,

whereas the main part of the cone has a larger amplitude. At the 147 mm diameter, the amplitude of vibration is very small. At this point the corrugation has a large radius (4 mm). As the cone moves to and fro, the paper tends to roll around this curve, and this excites the 2.4 mm corrugation that follows into violent oscillation at its resonance frequency. The surround resonance is 180 degrees out of phase with respect to the main part of the cone. However, the main part of the cone has a high amplitude produced by the rocking motion around the 147 mm diameter, and because of its greater area, only part of its effect in producing a high sound level is canceled out by the surround motion. The net result is a peak in output (see point 4 of Fig. 6.14).

At point 5, 1100 Hz, a sharp decrease in response is observed. The decrease seems to be the result of a movement of the nodal line toward the apex of the cone, and a reduction of the amplitude of the (+) portion. Here, the effect is a pumping of air back and forth across the nodal line, with a cancellation in output. This vibration is very characteristic, and at the time such motion occurs, the response drops vigorously.

As frequency is increased, the loudspeaker breaks up into still different characteristic modes of vibration. As shown in Fig. 6.15, case 6, several nodal lines appear concentric to the surround of the loudspeaker. When these occur, a large increase in output is obtained, as shown at point 6 of Fig. 6.14. As frequency is increased, other such resonances occur, with more nodal lines becoming apparent. These nodal lines are the result of waves traveling from the voice coil out to the edge of the cone and being reflected back again. These outwardly and inwardly traveling waves combine to produce a standing-wave pattern that will radiate a maximum of power at some particular angle with the principal axis of the loudspeaker.

To reduce standing-wave patterns of the type shown in cases 6, 7, and 8 of Fig. 6.15, it is necessary that a termination of proper mechanical impedance be placed at the outer edge of the diaphragm. This termination must be one that absorbs waves traveling outward from the center of the cone so that no wave is reflected back. In practical design, a synthetic foam or rubber supporting edge is frequently employed. A rubber supporting edge is also effective in reducing the surround resonance. The resulting effect is to produce a more uniform response in the frequency region between 700 and 1500 Hz of Fig. 6.14.

The finite delay time it takes for higher frequency waves, which may be transverse or longitudinal, to travel through the cone from the edge of the voice coil to an absorbent surround has the effect of widening the directivity pattern, although the nonplanar geometry of the cone also has this effect (see Section 12.10), but due to a phase advance toward the surround as opposed to a phase delay. In theory, the two effects could be arranged to cancel each other so that the cone would act largely as a planar source, which would produce a maximally flat axial response, albeit with cup resonances and an increasingly narrow beamwidth at high frequencies.

Often a highly damped cone material is chosen, such as paper, so that the waves propagating within it are absorbed at high frequencies. Consequently, an ever decreasing portion of the cone radiates at high frequencies until the sound is coming mainly from the edge of the coil. If the mass of the coil were negligible compared with that of the cone, the moving mass would also progressively decrease with frequency and the radiated power would remain constant. Furthermore, the shrinking radiating area would maintain a wide directivity pattern as well as a flat on-axis response. Although this sounds like an ideal solution, greatest efficiency is actually obtained by making the coil and diaphragm masses equal (see Eq. 6.89), so there is a limit to how much the total mass can decrease with frequency.



6.15 DIRECTIVITY CHARACTERISTICS

The response curve of Fig. 6.7 and the information of the previous three paragraphs reveal that above the frequency where $ka = 2$ (usually between 800 and 2000 Hz), a direct-radiator loudspeaker can be expected to radiate less and less power. The rate at which the radiated power would decrease, if the cone were a rigid piston, is between 6 and 12 dB for each doubling of frequency. This decrease in power output is not as apparent directly in front of the loudspeaker as at the sides because of directivity. That is to say, at high frequencies, the cone directs a larger proportion of the power along the axis than in other directions. In addition, the decrease in power is overcome in part by the resonances that occur in the diaphragm, as we have seen from Fig. 6.14.

Directivity patterns for typical loudspeakers

Typical directivity patterns for a 5-inch-diameter direct-radiator loudspeaker, mounted in one of the two largest sides of a closed box having the dimensions 285 by 189 by 178 mm, were shown in Fig. 4.31. These data are approximately correct for loudspeakers of other diameters if the frequencies beneath the graphs are multiplied by the ratio of 5 inch to the diameter of the loudspeaker in inches.

Comparison with the directivity patterns for a flat rigid piston in a sphere, as shown in Fig. 12.23, reveals that the directivity patterns for a flat piston are different from those for an actual loudspeaker. This difference results from the cone angle, the speed of propagation of sound in the cone relative to that in the air, and the resonances in the cone. In this connection, it is interesting to see how the speed varies with frequency in an actual cone.

Speed of propagation of sound in cone

Let us define the average speed of propagation of sound in the cone as the distance between the apex and the surround, divided by the number of wavelengths in that distance, multiplied by the frequency in cycles per second. For the particular 200 mm loudspeaker of Figs. 6.13–6.15, the phase shift and the average speed of propagation of the sound wave from the apex to the surround of the cone are given in Fig. 6.16. At low frequencies, the

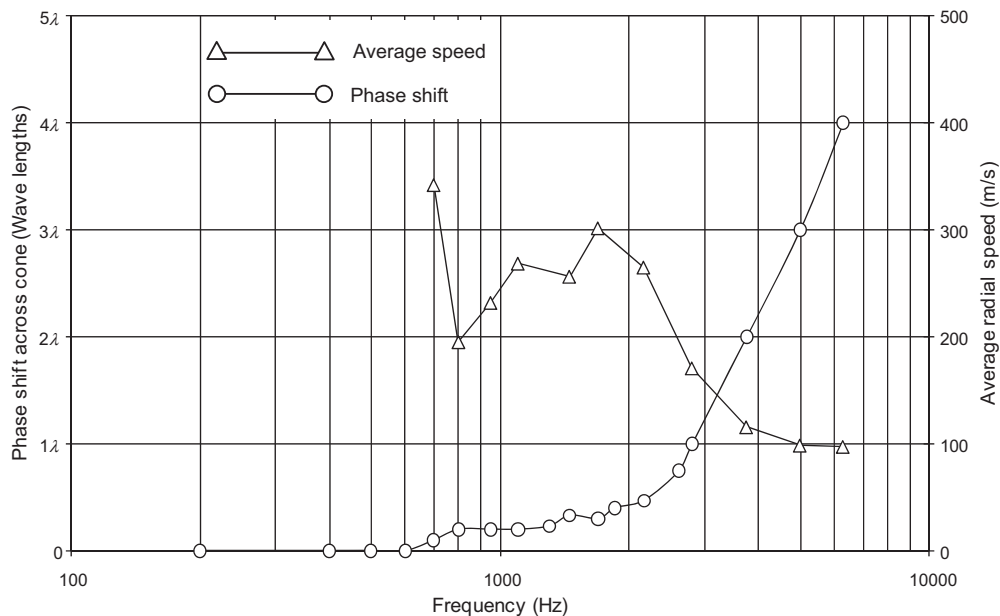


Figure 6.16 Phase shift and average wave speed in the cone of a 200 mm loudspeaker. After Corington. Amplitude and phase measurements on loudspeaker cones. Proc IRE 1951;39:1021–20.

cone moves in phase so that the speed can be considered infinite. At high frequencies, the speed asymptotically approaches that in a flat sheet of the same material, infinite in size.

Intensity level on designated axis

We have stated already that at high frequencies a loudspeaker diaphragm becomes directional. To calculate the enhancement of the sound pressure on the axis of the loudspeaker as compared with that indicated by Eqs. (4.65) and (4.66) for an omnidirectional source, it is convenient to use the concepts of directivity factor and of directivity index as defined in Part XII (pages 163 to 168). For example, we might wish to know the intensity (or the SPL) on the axis of the loudspeaker, given the efficiency response and the directivity factor. This is done as follows.

The intensity as a function of frequency on the axis of symmetry of the loudspeaker divided by the electrical power available is equal to the product of (1) the efficiency response characteristic, (2) the directivity factor, and (3) $1/4\pi r^2$, where r is the distance at which the intensity is being measured. In decibels, we have

$$10 \log_{10} \frac{I_{ax}}{W_E} = 10 \log_{10} E_{ff} - 20 + DI - 10 \log_{10} 4\pi r^2 \quad (6.95)$$

where $I_E = |p_{ax}|^2 / \rho_0 c$ is intensity in watts per square meter on the designated axis at a particular frequency. p_{ax} is SPL in Pa measured on the designated axis at a particular

frequency. $E_{ff} = 100W/W_E$ is ratio of total acoustic power radiated by the front side of the loudspeaker to the power supplied by the electrical generator. DI is given by Eq. (4.138) and Fig. 4.30. Note that, for the piston in an infinite baffle, the DI at low frequencies is 3 dB because the power is radiated into a hemisphere, and that the last term of Eq. (6.95) is the area of a sphere, in decibels.

Expressed in terms of the SPL on the designated axis re 20 μPa , Eq. (6.95) becomes (see Eq. 6.40)

$$\begin{aligned} \text{SPL re 20 } \mu\text{Pa} &= 20 \log_{10} \frac{p_{ax}}{0.00002} = 10 \log_{10} W_E \\ &+ 10 \log_{10} E_{ff} + \text{DI} - \log_{10} 4\pi r^2 \\ &+ 10 \log_{10} \rho_0 c + 74 \text{ dB} \end{aligned} \quad (6.96)$$



6.16 TRANSFER FUNCTIONS AND THE LAPLACE TRANSFORM

If we substitute $s = j\omega$ in Eq. (6.14), we obtain

$$\alpha_c(s) = \frac{s^2}{s^2 + \frac{\omega_S}{Q_{TS}}s + \omega_S^2} \quad (6.97)$$

where s is the imaginary frequency variable. The roots of the denominator polynomial are known as *poles*. If $Q_{TS} \leq 0.5$, the roots of the denominator polynomial are real and given by

$$s = -\omega_S \left(\frac{1}{2Q_{TS}} \pm \sqrt{\frac{1}{4Q_{TS}^2} - 1} \right) \quad (6.98)$$

If $Q_{TS} > 0.5$, the roots of are complex and given by

$$s = -\omega_S \left(\frac{1}{2Q_{TS}} \pm j \sqrt{1 - \frac{1}{4Q_{TS}^2}} \right) \quad (6.99)$$

or expressed as magnitude and phase as

$$s = -\omega_S \angle \pm \arccos(1/(2Q_{TS})).$$

The dotted curves in Fig. 6.17 are plotted from Eq. (6.97), but solid lines are linear approximations plotted from the poles or roots of the denominator polynomial. The locus of these poles is shown in Fig. 6.18. The arrows on the negative real axis show the direction in which the poles move as Q_{TS} is increased. When $Q_{TS} = 0.5$, the poles are

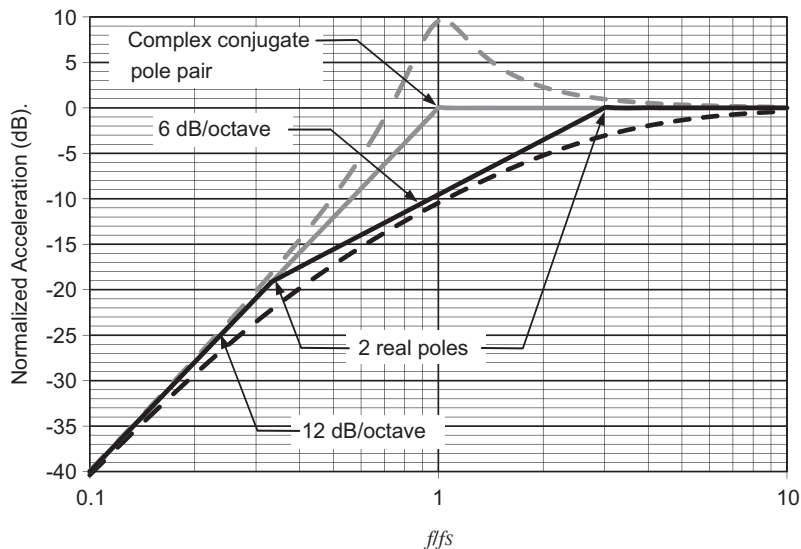


Figure 6.17 Linear approximations of the acceleration frequency response function. The *black curves* are for $Q_{TS} = 0.3$ and the *gray* for $Q_{TS} = 3$. The *solid lines* are linear approximations and the *dotted curves* are calculated from the exact expressions.

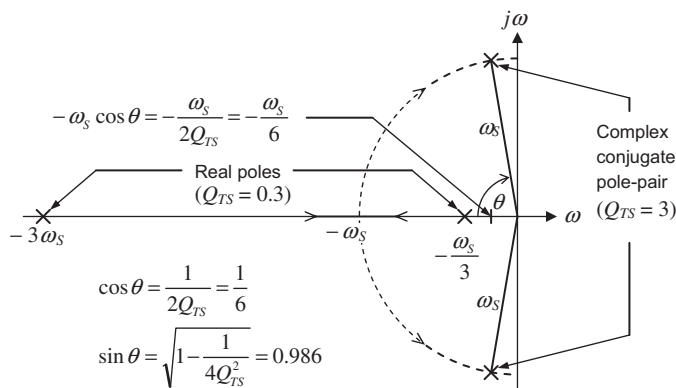


Figure 6.18 Root loci of the poles in Fig. 6.17.

real and coincident at $-\omega_s$. When $Q_{TS} > 0.5$, they become a complex conjugate pair and follow the arrows on the semicircular path. If there were no damping such that $Q_{TS} = \infty$, the poles would lie on the imaginary axis.

A more general transfer function is represented by

$$F(s) = \frac{Q_N s^N + Q_{N-1} s^{N-1} + \cdots + Q_2 s^2 + Q_1 s + Q_0}{P_M s^M + P_{M-1} s^{M-1} + \cdots + P_2 s^2 + P_1 s + P_0} = \frac{\sum_{n=0}^N Q_n s^n}{\sum_{m=0}^M P_m s^m} \quad (6.100)$$

which includes N zeros in the numerator as well as M poles in the denominator. Although we are unlikely to encounter zeros when dealing with larger loudspeakers, they do occur in cell phone designs which are generally more complicated, having small sound holes with viscous losses. Certainly, when we consider loudspeakers in bass-reflex enclosures or with auxiliary filters we will encounter higher order denominator polynomials. After solving the denominator and numerator polynomials for the poles p_m and zeros q_n respectively, we can rewrite the transfer function as

$$F(s) = \frac{(s + q_1)(s + q_2) \cdots (s + q_{N-1})(s + q_N)}{(s + p_1)(s + p_2) \cdots (s + p_{M-1})(s + p_M)} = \frac{\prod_{n=1}^N (s + q_n)}{\prod_{m=1}^M (s + p_m)} \quad (6.101)$$

This is a convenient form which enables us to tailor the frequency response by manipulating the roots of the denominator polynomial and to calculate the transient response by means of the inverse Laplace transform.



6.17 TRANSIENT RESPONSE

The design of a loudspeaker enclosure and the choice of amplifier impedance eventually must be based on subjective judgments as to what constitutes “quality” or perhaps simply on listening “satisfaction.” It is believed by many observers that a flat sound—pressure—level response over at least the frequency range between 70 and 7000 Hz is found desirable by most listeners. Some observers believe that the response should be flat below 1000 Hz but that between 1000 and 4000 Hz it should be about 5 dB higher than its below-1000-Hz value. Above 4000 Hz, the response should return to its low-frequency value. It is also believed by some observers that those loudspeakers which sound best generally reproduce tone bursts [13] well, although this requirement is better substantiated in the literature for the high frequencies than for the low.

An important factor determining the transient response of the circuits of Fig. 6.4 is the amount of damping of the motion of the loudspeaker diaphragm that is present. For a given loudspeaker, the damping may be changed (1) by choice of the amplifier impedance R_g , or (2) by adjustment of the resistive component of the impedance of the enclosure for the loudspeaker, or (3) by choosing a drive unit with a smaller Q_{TS} value, or (4) by any combination of (1) to (3). The amplifier impedance may be adjusted using negative current feedback to increase Q_{TS} or positive current feedback to reduce it. The latter provides a negative output impedance which is subtracted from R_E .

Before we can apply the transform to Eq. (6.101), we must split the expression into a sum of partial fractions, each containing a single factor in its denominator:

$$F(s) = \frac{A_1}{s + p_1} + \frac{A_2}{s + p_2} + \cdots + \frac{A_{M-1}}{s + p_{M-1}} + \frac{A_M}{s + p_M} = \sum_{m=1}^M \frac{A_m}{s + p_m} \quad (6.102)$$

This is achieved using a technique known as the residues theorem. The residues A_m are found from the formula

$$A_m = (s + p_m)F(s)|_{s \rightarrow -p_m} \quad (6.103)$$

For the expression of Eq. (6.97) this gives

$$\begin{aligned} \alpha_c(s) &= \frac{s^2}{(s + p_1)(s + p_2)} \\ &= (1) + \frac{p_1^2}{(p_2 - p_1)(s + p_1)} + \frac{p_2^2}{(p_1 - p_2)(s + p_2)} \end{aligned} \quad (6.104)$$

The extra unity term in parentheses comes from the fact that the numerator polynomial is of the same order as the denominator. However, we shall drop it from subsequent handling. If $M < N$, then this term vanishes anyway. The poles p_1 and p_2 are given by

$$p_1 = \omega_S \left(\frac{1}{2Q_{TS}} - j \sqrt{1 - \frac{1}{4Q_{TS}^2}} \right) \quad (6.105)$$

$$p_2 = \omega_S \left(\frac{1}{2Q_{TS}} + j \sqrt{1 - \frac{1}{4Q_{TS}^2}} \right) \quad (6.106)$$

To obtain the response in the time domain, we apply the inverse Laplace transform:

$$f(t) = L^{-1}(F(s)) = \frac{1}{2\pi j} \int_{\gamma - j\infty}^{\gamma + j\infty} F(s) e^{st} ds \quad (6.107)$$

where γ is an arbitrary positive constant chosen so that the contour of integration lies to the right of all singularities in $F(s)$. The Laplace transform is a variant of the Fourier transform that converts a function of time to one of imaginary frequency as opposed to real frequency.

$$F(s) = L(f(t)) = \frac{1}{2\pi j} \int_0^{\infty} f(t) e^{-st} ds \quad (6.108)$$

Table 6.2 Laplace transforms of various functions of time

$\mathbf{f(t)}$	$\delta(t)$	$H(t)$	$\sin \omega t$	$\cos \omega t$	$e^{-\omega t}$	$1 - e^{-\omega t}$	$\frac{\alpha e^{-\alpha t} - \beta e^{-\beta t}}{\alpha - \beta}$	$1 - \frac{\alpha e^{-\beta t} - \beta e^{-\alpha t}}{\alpha - \beta}$
$\mathbf{F(s)}$	1	$\frac{1}{s}$	$\frac{\omega}{s^2 + \omega^2}$	$\frac{s}{s^2 + \omega^2}$	$\frac{1}{s + \omega}$	$\frac{\omega}{s(s + \omega)}$	$\frac{s}{(s + \alpha)(s + \beta)}$	$\frac{\alpha\beta}{S(S + \alpha)(S + \beta)}$

Table 6.2 shows the Laplace transforms of some input waveforms that we may wish to use to investigate the time response of a loudspeaker system with its associated enclosure and electrical filters.

We see that the Laplace transform of an infinite impulse at $t = 0$, which is represented by the Dirac delta function $\delta(t)$, is simply unity. Therefore, applying the inverse Laplace transform directly to the frequency response function in s will give us the infinite impulse response of the system. Applying the inverse Laplace transform to Eq. (6.104) is fairly straightforward because according to Table 6.2 the $1/(s + p_m)$ terms become exponents:

$$\alpha_c = \frac{p_1^2}{(p_2 - p_1)} e^{-p_1 t} + \frac{p_2^2}{(p_1 - p_2)} e^{-p_2 t} \quad (6.109)$$

If we wish to evaluate the time response to an input waveform other than an infinite impulse, we may multiply Eq. (6.104) by the Laplace transform of the waveform before applying the inverse Laplace transform. For example, if we wished to evaluate the response to a Heaviside step function $H(t)$, which represents a step from 0 to 1 at $t = 0$, we could multiply Eq. (6.104) by $1/s$ before applying the inverse Laplace transform. Alternatively, we could convolve the impulse response of Eq. (6.109) with the Heaviside step function in the time domain using the convolution integral:

$$\begin{aligned} \alpha_c(t) * H(t) &= \int_{-\infty}^{\infty} \alpha_c(x) H(t - x) dx \\ &= \frac{p_1 e^{-p_1 t} - p_2 e^{-p_2 t}}{p_1 - p_2} \\ &= \begin{cases} \frac{\sin(\theta - \omega_S t \sin \theta)}{\sin \theta} e^{-\omega_S t \cos \theta}, & Q_{TS} > 0.5 \\ \frac{\sinh(\theta - \omega_S t \sinh \theta)}{\sinh \theta} e^{-\omega_S t \cosh \theta}, & Q_{TS} \leq 0.5 \end{cases} \end{aligned} \quad (6.110)$$

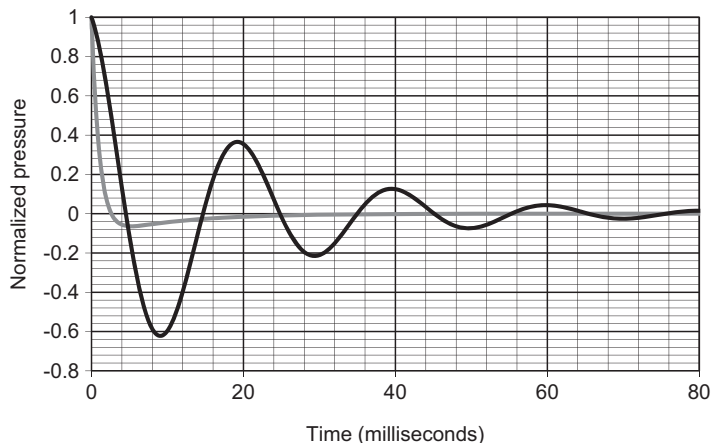


Figure 6.19 Time response to a unity step function where $f_S = 50$ Hz. The *black curve* is for $Q_{TS} = 3$ and the *gray* for $Q_{TS} = 0.3$.

where

$$\cos \theta = \frac{1}{2Q_{TS}}, \quad \sin \theta = \sqrt{1 - \frac{1}{4Q_{TS}^2}}, \quad Q_{TS} > 0.5 \quad (6.111)$$

$$\cosh \theta = \frac{1}{2Q_{TS}}, \quad \sinh \theta = \sqrt{\frac{1}{4Q_{TS}^2} - 1}, \quad Q_{TS} \leq 0.5 \quad (6.112)$$

which gives the same result as multiplying Eq. (6.104) by $1/s$ before applying the inverse Laplace transform. Hence, the impulse response is a powerful expression which can be used to predict the response to any input waveform.

We see from Eq. (6.110) that when $Q_{TS} > 0.5$, the time response to a step function has an oscillatory component represented by the sine and cosine functions of $\omega_S t$ and a decaying component represented by the exponent term which contains the *decay constant* $\omega_S/(2Q_{TS})$. The response to a step function is plotted in Fig. 6.19 with $f_S = 50$ Hz. The black curve for $Q_{TS} = 3$ gives an undershoot value of 62% and ringing for several cycles, each about 20 ms in duration. The gray curve for $Q_{TS} = 0.3$ shows just 6.4% undershoot and no ringing.

An input waveform of particular interest is that of a finite tone burst¹ of frequency ω_0 and duration t_0 involves a somewhat more complicated expression:

$$F(t) = (1 - H(t - t_0)) \sin \omega_0 t \quad (6.113)$$

¹ A tone burst is a wave-train pulse that contains a number of waves of a frequency.

which yields the pressure waveform

$$\begin{aligned}
 a_c(t) * F(t) = & (\omega^4 + \omega_S^4 + 2\omega^2\omega_S^2 \cos 2\theta)^{-1} \\
 & \times \left\{ \csc \theta (\omega\omega_S^3 \sin(\omega_S t \sin \theta) + \omega^3\omega_S \sin(\omega_S t \sin \theta - 2\theta)) e^{-\omega_S t \cos \theta} + H(t - t_0) \right. \\
 & \times \left\{ \csc \theta \sin \omega t_0 (\omega_S^4 \sin(\omega_S(t - t_0) \sin \theta - \theta) + \omega^2\omega_S^2 \sin(\omega_S(t - t_0) \sin \theta - 3\theta)) \right. \\
 & \left. \left. - \csc \theta \cos \omega t_0 (\omega\omega_S^3 \sin(\omega_S(t - t_0) \sin \theta) + \omega^3\omega_S \sin(\omega_S(t - t_0) \sin \theta - 2\theta)) \right\} \right. \\
 & \left. \times e^{-\omega_S(t-t_0)\cos(\theta)} + (1 - H(t - t_0))(2\omega^3\omega_S \cos \theta \cos \omega t + \omega^2(\omega^2 - \omega_S^2)\sin \omega t) \right\}
 \end{aligned} \tag{6.114}$$

We see from Fig. 6.20 that the beginning of the tone burst excites the suspension resonance frequency which is superimposed on the tone burst even though the tone-burst frequency is three times higher than that of the suspension resonance. As a result, the tone takes a while to settle before it is switched off, at which point the suspension resonance is triggered again before finally decaying. Hence, loudspeakers with a high Q_{TS} tend to produce bass with a “one-note” quality. Not only is the suspension resonance frequency boosted in the frequency response, but it also adds overhang to transients at other frequencies.

It is known that the reverberation time in the average living room is about 0.5 s, which corresponds to a decay constant of 13.8 s^{-1} . Psychological studies also indicate that if a transient sound in a room has decreased to less than 0.1 of its initial value within 0.1 s, most listeners are not disturbed by the “overhang” of the sound. This corresponds to a decay constant of 23 s^{-1} , which is a more rapid decay that occurs in the average

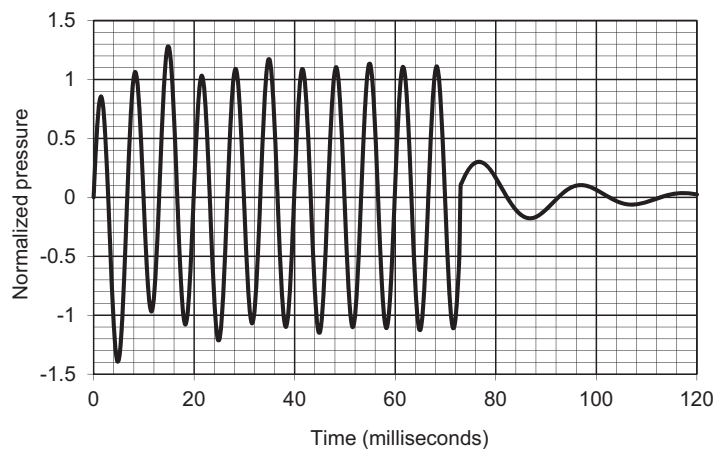


Figure 6.20 Transient response to a tone burst of frequency $f_0 = 150 \text{ Hz}$ and duration $t_0 = 73 \text{ ms}$, where the suspension resonance frequency $f_S = 50 \text{ Hz}$ and $Q_{TS} = 3$.

living room. Although criteria for acceptable transient distortion have not been established for loudspeakers, it seems reasonable to assume that if the decay constant for a loudspeaker is greater than four times this quantity, i.e., greater than 92 s^{-1} , no serious objection will be met from most listeners to the transient occurring with a tone burst. Accordingly, the criterion that is suggested here as representing satisfactory transient performance is

$$\frac{\omega_S}{2Q_{TS}} > 92 \text{ s}^{-1} \quad (6.115)$$

Eq. (6.110) reveals that the greater $\omega_S/(2Q_{TS})$, the shorter the transient. Eq. (6.115) should be construed as setting a lower limit on the amount of damping that must be introduced into the system. It is not known how much damping ought to be introduced beyond this minimum amount.

In the next chapter, we shall discuss the relation between the criterion of Eq. (6.115) and the response curve with baffle.

Each of the diaphragm resonances (e.g., points 1–8 in Fig. 6.14) has associated with it a transient decay time determined from an equation like Eq. (6.110). To fulfill the criterion of Eq. (6.115), it is usually necessary to damp the loudspeaker cone and to terminate the edges so that a response curve smoother than that shown in Fig. 6.14 is obtained. With the very best direct-radiator loudspeakers, much smoother response curves are obtained. The engineering steps and the production control necessary to achieve low transient distortion and a smooth response curve may result in a high cost for the completed loudspeaker.



6.18 NONLINEARITY [14]

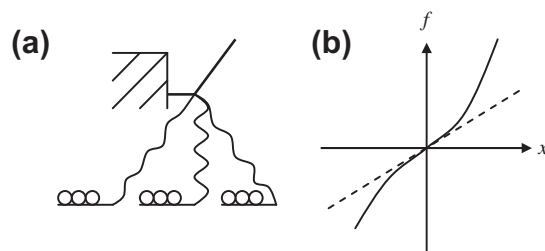
There are a number of nonlinear mechanisms in electrodynamic loudspeakers which give rise to harmonic distortion. They tend to be dominant at different frequencies. In some cases, the nonlinearity is a function of input current and in others of displacement, or even both. An overview is given in Table 6.3.

Suspension compliance

The purpose of the suspension (see (9) in Fig. 6.1) is to provide a linear restoring force that moves the coil back to its rest position and to ensure that it is correctly centered. However, from Fig. 6.21a, we see that for large excursions, the suspension becomes stiffer as it stretches and so the compliance becomes nonlinear, typically in an asymmetrical manner, as shown in Fig. 6.21b. It is also common for hysteresis losses to prevent the coil from returning to the same position as before. To combat this, a “regressive” spider design [15] has been proposed in which the corrugations diminish in height with increasing radius.

Table 6.3 Overview of nonlinearities in electrodynamic loudspeakers

Nonlinearity	As a function of	Frequency range	Mechanism
Compliance C_{MS}	Displacement x	Below f_S	Nonlinear restoring force
Force factor Bl	Displacement x , current i	Low frequencies (where x is greatest)	Nonlinear force, $f = Bli$
Coil inductance L_E	Displacement x , velocity u		Nonlinear damping, $e = Blu$
	Displacement x	High frequency modulated by low frequency	Inductance varies with position of coil relative to pole piece
	Displacement x , current i	Ditto	Extra reluctance force, $f \propto i^2$
	Current i	High frequencies	Nonlinear permeability of steel
Coil resistance R_E	Current i	All frequencies	Resistance increases with temperature
Young's modulus E of cone material	Strain ϵ	At normal vibration mode frequencies of cone	Stress σ is nonlinear function of strain, $\sigma = E\epsilon$. For large amplitude vibrations, further nonlinearity caused by change in geometry
Doppler effect	Displacement x	High frequency modulated by low frequency	Variable time shift $t = x/c$ in propagated sound causes frequency modulation distortion

**Figure 6.21** (a) Sketch of suspension at center and extreme end positions and (b) nonlinear force versus displacement curve (*solid curve*) with ideal linear curve (*dashed line*).

Force factor

If the coil length h_c is equal to the gap length h_g (see Fig. 6.22a), the force factor decreases as soon as the coil starts to move in the x direction because the part of the coil which is then outside the gap experiences a much smaller force. This typically produces the

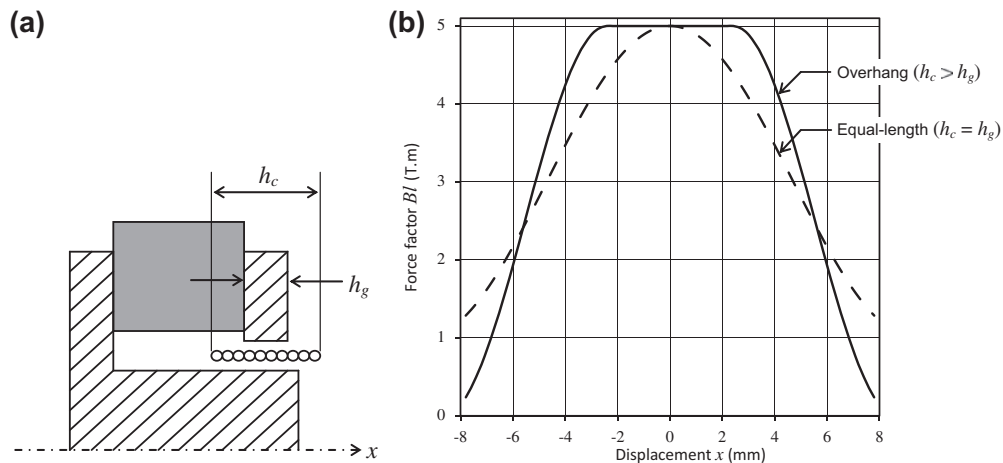


Figure 6.22 (a) Sketch of a coil of length h_c in a magnetic gap of length h_g and (b) force factor versus displacement curves with $h_c = h_g$ (dashed line) and $h_c > h_g$ (solid line).

dashed curve shown in Fig. 6.22b. To improve linearity and to extend the maximum excursion, the length of the coil is often extended beyond the length of the gap and this is known as *overhang*. This typically produces the solid curve shown in Fig. 6.22b. Alternatively, it can be shorter, which is known as *underhang*. One disadvantage of overhang is that the ratio of force factor Bl to moving mass M_{MS} is decreased, which tends to reduce efficiency somewhat (see Eq. 6.47). Although force-factor nonlinearity is most noticeable at low frequencies, where the coil excursion is greatest, if the Q_{TS} value of the drive unit is fairly high, then the distortion has a minimum at the suspension resonance frequency. In other words, the peak at the resonance frequency has a filtering effect on the distortion harmonics. By the same token, distortion harmonics of frequencies in the roll-off region (below resonance) are augmented.

Coil inductance

Like the force factor Bl , the coil inductance L_E also varies according to the position of the coil in the gap, albeit in a somewhat less symmetrical manner. In fact, the inductance is greatest when the coil is in its innermost position and completely surrounded by iron, as we see from Fig. 6.23. Conversely, it is smallest when the coil is in its outermost position and partly surrounded by air, which has a much smaller relative permeability than iron. Although the inductance alone would only affect the high frequencies, the fact that the excursion is greatest at low frequencies means that the effect of the nonlinearity is for the low frequencies to modulate the high frequencies.

Not only does the inductance vary with coil position x , but it also varies with current i . The flux density B varies in a nonlinear fashion with the magnetizing force H (see Fig. 6.11) and hence in turn with the current i . To minimize this effect, the pole piece

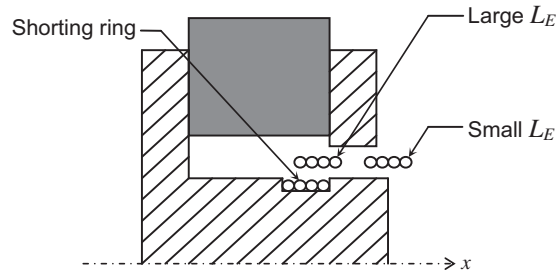


Figure 6.23 Sketch of a coil in two extreme positions along its journey back and forth in the x direction. In the innermost position, the inductance L_E is greatest and in the outermost position it is smallest. The inclusion of the shorting ring minimizes the amount of variation of L_E .

and pole plate are normally saturated as much as possible so that there is relatively little variation of B with H . In addition, the inclusion of a shorting ring around the pole piece, as shown in Fig. 6.23, reduces the variation of L_E with both x and i . It is usually made of aluminum and behaves like a short-circuited secondary winding of a transformer in which the voice coil forms the primary.

A third nonlinear mechanism due to the coil inductance is the reluctance force. This was actually the driving force used in the receivers of early telephone handsets. In the receiver, an electromagnet would actuate a steel plate in close proximity to it. Then the first loudspeakers were simply receivers with horns attached. Although the transduction was inherently nonlinear, the vibrations of the plate were small enough for the distortion not to be too serious. However, in a modern dynamic speaker, such a driving force is an undesirable by-product of the principal transduction mechanism.

Coil resistance

As the power dissipated by the coil is increased, its temperature also increases, which leads to an increase in resistance. At very low frequencies, the temperature increases during every half cycle of the input signal, thus leading to odd harmonic distortion. At higher frequencies, the thermal inertia of the coil smoothes out the temperature variations so that instead we have a phenomenon known as *power compression* whereby the rise in coil resistance temporarily reduces the sensitivity of the loudspeaker. The use of a current-source amplifier [16] with motional feedback to provide damping has been proposed to minimize this effect. Alternatively, a ferrofluid [17] may be suspended within the magnetic gap. This will effectively conduct heat away from the coil to the pole plate, which acts as a heat sink. Another advantage is that the magnetic fluid reduces the width of the gap to the diameter of the coil wire plus the thickness of the former. A slight disadvantage is that viscosity of the fluid increases mechanical damping and hence reduces Q_{MS} . Ideally, to maintain maximum efficiency at resonance, we would prefer all of the damping to be provided electrically so that $Q_{TS} \approx Q_{ES}$ and $Q_{MS} \gg Q_{ES}$.

Young's modulus of cone material

At low to mid frequencies, the cone should move as a perfectly rigid piston in which case there is no flexing and the nonlinear stress versus strain relationship should have no effect whatsoever. However, at higher frequencies, vibration modes within the cone will occur and the motion is likely to be nonlinear depending on the amplitude. This can be mitigated by ensuring that either the cone material has sufficient internal damping or that the radial waves are absorbed by a lossy surround. One should also use a crossover which diverts the higher frequencies to another drive unit.

Doppler effect

Suppose that a loudspeaker reproduces two tones simultaneously, one at a sufficiently low frequency to produce significant excursion and the other at a much higher frequency. As the cone moves toward the listener during a positive half cycle of the low note, the pitch of the high note will be raised by a small amount. In addition, as the cone moves away from the listener during a negative half cycle, the pitch will be lowered. This is the same phenomenon that causes the apparent frequency of a siren to change when an ambulance drives past. Hence, the low note frequency modulates the high note. In practice, the effect is usually minimized through careful choice of crossover frequency [18].

Example 6.3. If the circular gap in the permanent magnet has a radial length of 0.2 cm, a circumference of 8 cm, and an axial length of 1.0 cm, determine the energy stored in the air gap if the flux density is 10,000 G.

Solution

$$\text{Volume of air gap} = (0.002)(0.08)(0.01) = 1.6 \times 10^{-6} \text{ m}^3$$

$$\text{Flux density} = 1 \text{ T.}$$

From books on magnetic devices, we find that the energy stored is

$$W = \frac{B^2 V}{2\mu}$$

where the permeability μ for air is $\mu_0 = 4\pi \times 10^{-7}$ H/m. Hence, the air-gap energy is

$$W = \frac{(1)(1.6 \times 10^{-6})}{(2)(4\pi \times 10^{-7})} = \frac{2}{\pi} = 0.636 \text{ J}$$

Example 6.4. A 5-inch loudspeaker is mounted in one of the two largest sides of a closed box having the dimensions 285 by 189 by 178 mm. Determine and plot the relative power available efficiency and the relative SPL on the principal axis.

Solution. Typical directivity patterns for this loudspeaker are shown in Fig. 4.31. The directivity index on the principal axis as a function of frequency is shown in Fig. 4.32. It is interesting to note that the transition frequency from low directivity to high directivity is about 1 kHz. Because the effective radius of the radiating cone for this loudspeaker is about 0.055 m, ka at this transition frequency is

$$ka = \frac{2\pi fa}{c} = \frac{1000\pi \times 0.13}{344.8} = 1.18$$

or unity, as would be expected from our previous studies. The transition from the circuit of Fig. 6.6c (where we assumed that $\omega^2 M_{M1}^2 \gg \Re_{MR}^2$ and $\omega^2 L^2 \ll (R_g + R_E)^2$) to Fig. 6.6d also occurs at about $ka = 1$. Now, let us model the loudspeaker as a spherical cap in a sphere. From the box dimensions, the equivalent radius R of the equivalent sphere is

$$R = \sqrt[3]{\frac{3(285 \times 189 \times 178)}{4\pi}} = 132 \text{ mm}$$

Because the effective radius a of the cap is 55 mm, the half-angle of the cap is given by $\alpha = \arcsin(55/132) = 25$ degrees. The directivity patterns of a cap of half-angle 30 degrees are shown in Fig. 6.24. Considering the approximate nature of the model, these directivity patterns are remarkably consistent with those shown in Fig. 4.31 for the

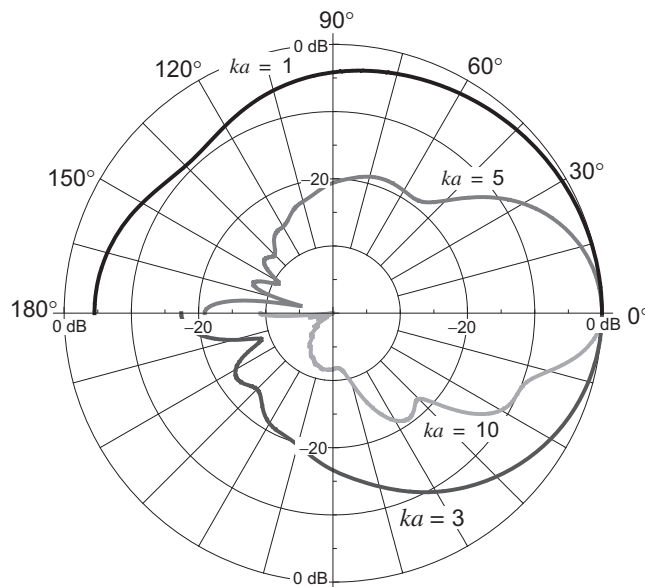


Figure 6.24 Plots of the directivity patterns of a typical 5-inch-diameter loudspeaker in a closed box baffle using an oscillating spherical cap in a sphere as a model.

actual loudspeaker. One advantage of this model is its simplicity because Eq. (12.59) for the directivity pattern is in the form of a fast-converging expansion.

Now, let us determine the SPL on the principal axis of the loudspeaker, using Eqs. (12.58) and (12.61) together with

$$\tilde{u}_c = \frac{Bl}{(R_E + j\omega L_E)j\omega M_{MS}} \tilde{e}_g$$

which is derived from Fig. 6.4a, assuming that above resonance M_{MS} dominates the loop impedance. In addition, let us assume that the amplifier impedance is very low. The results are given by the dashed curve in Fig. 6.25. Above 200 Hz, the pressure level starts to rise due to the baffle effect of the enclosure, although the amount of lift is limited by the coil inductance which starts to have effect at around the same point. The cupped shape of the diaphragm helps to maintain a wide directivity pattern at higher frequencies, but the radiated power is falling off, so the sound pressure must also start to fall (unlike with a flat piston where the concentration of sound on its axis maintains a level output). The fact that the model uses a convex dome as opposed to a concave cone will introduce errors but a quick comparison of Fig. 12.28 with Fig. 12.32 for a convex and a concave dome, respectively, shows that the trends are broadly similar. Hence, we see a second-order or 12 dB/octave high frequency roll-off due to the compounded effect of the diaphragm inertia and coil inductance. In addition, at higher frequencies, cone resonances occur, as we said before, and the typical response curve of Fig. 6.14 is obtained.

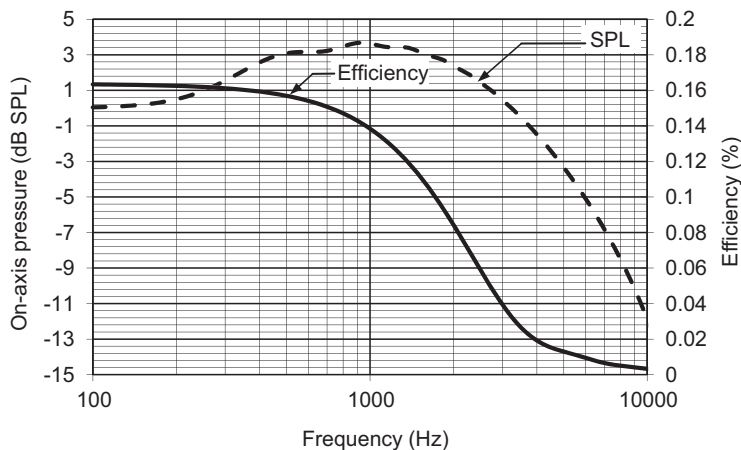


Figure 6.25 Graphs of the computed efficiency and sound pressure level measured on the principal axis of a typical 5-inch-diameter loudspeaker in a closed box baffle. $R_E = 6.6 \Omega$, $L_E = 0.5 \text{ mH}$, $Bl = 4.5 \text{ Tm}$, and $M_{MS} = 9.6 \text{ g}$. The reference level is chosen arbitrarily. SPL, sound pressure level.

To calculate the efficiency, let us assume that it is mounted in an infinite baffle and that one-half the power is radiated to each side.

The efficiency, *from one side of the loudspeaker*, is given by Eq. (6.57) divided by 2, where for the frequency range well above resonance, we have used the approximations

$$Z_{MT} \approx j\omega M_{MS} \text{ and } Z_E \approx R_E + j\omega L_E.$$

From this we obtain the solid curve of Fig. 6.25a. It is seen that, above $f = 1000$ Hz, the efficiency drops off.

REFERENCES

- [1] Villchur EM. Problems of bass reproduction in loudspeakers. *J Audio Eng Soc* 1957;5(3):122–6.
- [2] For supplemental reading, the student will find the following publication valuable. In: Borwick J, editor. *Loudspeaker and headphone handbook*. 3rd ed. Oxford: Focal Press; 2001.
- [3] Rice CW, Kellogg EW. Notes on the development of a new type of hornless loudspeaker. *J Audio Eng Soc* 1982;30(7/8):512–21. Abridgment of paper presented at the Spring convention of the A.I.E.E., St. Louis, April 13–17, 1925. U.S. Patent No. 1,795,214. Previous patents for moving-coil transducers were granted to Ernest Siemens in 1874 (US patent no. 149797) and Sir Oliver Lodge in 1898 (British patent no. 9712).
- [4] Klippel W. Prediction of speaker performance at high amplitudes, in the 111th AES convention. 2001. Paper no. 5418.
- [5] Small RH. Direct radiator loudspeaker system Analysis. *J Audio Eng Soc* 1972;20(5):383–95.
- [6] Klippel W. Assessment of voice-coil peak displacement X_{\max} . *J Audio Eng Soc* 2003;51(5):307–23.
- [7] See IEC 60268–5, ed. 3.1, Sound system equipment – part 5: loudspeakers. Available from: <http://webstore.iec.ch/>. For example, for a nominal 8-in (200 mm) diameter loadspeaker, the baffle size would be 1.65 m long by 1.35 m wide, with the loadspeaker offset from the center by 22.5 cm lengthways and 15 cm widthways.
- [8] <http://www.electronenergy.com/>.
- [9] Mellow TJ, Kärkkäinen LM. On the sound field of a shallow spherical shell in an infinite baffle. *J Acoust Soc Am* 2007;121(6):3527–41.
- [10] Frankort FJM. Vibration patterns and radiation behavior of loudspeaker cones. *J Audio Eng Soc* 1978;26(9):609–22.
- [11] Lerch R, Kaltenbacher M, Meiler M. Virtual prototyping of electrodynamic loudspeakers by utilizing a finite element model. *J Acoust Soc Am* 2008;123:3643.
- [12] Corrington MS. Amplitude and phase measurements on loudspeaker cones. *Proc IRE* 1951;39:1021–6.
- [13] A tone burst is a wave-train pulse that contains a number of waves of a certain frequency.
- [14] Klippel W. Tutorial: loudspeaker nonlinearities – causes, parameters, symptoms. *J Audio Eng Soc* 2006;54(10):907–39.
- [15] Hutt S. Loudspeaker spider linearity, in the 108th AES convention. 2000. Paper no. 5159.
- [16] Mills PG, Hawksford MJ. Distortion reduction in moving-coil loudspeaker systems using current-drive technology. *J Audio Eng Soc* 1989;37(3):129–48.
- [17] Bottenberg W, Melillo L, Raj K. The dependence of loudspeaker design parameters on the properties of magnetic fluids. *J Audio Eng Soc* 1980;28(1/2):17–24.
- [18] Allison R, Villchur E. The audibility of Doppler distortion in loudspeakers, in the 70th AES convention. 1981. Paper no. 1844.

Loudspeaker systems

PART XXI: SIMPLE ENCLOSURES

Loudspeaker enclosures are the subject of more controversy than any other item connected with modern high-fidelity music reproduction. Even though the behavior of enclosures is well understood, opinions and pseudo theories as to the effects of enclosures on loudspeaker response still persist. For instance, the very mention of directivity is guaranteed to spark a lively debate among audio engineers, with some favoring a wide pattern, whereas others prefer a narrow pattern, although virtually all agree that a constant pattern is desirable to ensure that the room reflections produced by the off-axis sound have the correct frequency balance. Personal preferences aside, it could be that the choice depends on the program material. A narrow pattern with fewer room reflections allows the listener to hear the acoustics of the recording location more clearly, as well as the positions of the individual performers on the stage. Hence, we might expect a narrow pattern to favor recordings made in a natural acoustic space such as a concert hall, church, or theater. On the other hand, for close-miked studio recordings, a greater sense of presence and listener envelopment may be created by employing a wide pattern that produces many reflections around the room to produce some sense of a live performance, albeit in a flawed domestic listening space. After all, unlike the majority of loudspeakers, musical instruments do not generally fire in one direction only at higher frequencies. One thing that we cannot control is the fact that at low frequencies, where the wavelength is much larger than the diaphragm, loudspeakers are invariably omnidirectional, except for a few dipole/cardioid designs. More directive patterns at low frequencies come at the cost of reduced efficiency.

The design of an enclosure should be undertaken only with full knowledge of the characteristics of the loudspeaker and of the amplifier available, but fortunately most reputable manufacturers now provide the Thiele—Small parameters in their data sheets along with other useful figures such as sensitivity, α_{\max} , and power rating.

A large part of the difficulty of selecting a loudspeaker and its enclosure arises from the fact that the psychoacoustic factors involved in the reproduction of speech and music are not understood. Listeners will rank order differently four apparently identical loudspeakers placed in four identical enclosures. It has been remarked that if one selects his own components, builds his own enclosure, and is convinced he has made a wise choice of design, then his own loudspeaker sounds better to him than does anyone else's

loudspeaker. In this case, the frequency response of the loudspeaker seems to play only a minor part in forming a person's opinion.

Many working in the field of loudspeaker design believe that it is as much an art as a science because it involves many choices which reflect personal preferences such as maximum loudness versus bass extension, physical size, directivity characteristics, and so forth. In this chapter, we shall discuss only the physics of the problem. Designers should be able to achieve, from this information, any reasonable frequency-response curve that they may desire. Furthermore, they will have to seek information elsewhere or to decide for themselves which shape of frequency-response curve will give greatest pleasure to themselves and to other listeners.

With the information of this chapter, the high-fidelity enthusiast should be able to calculate, if he or she understands AC circuit theory, the frequency-response curve for his or her amplifier-loudspeaker-baffle combination. Design graphs are presented to simplify the calculations, and three complete examples are worked out in detail. Unfortunately, the calculations are sometimes tedious, but there is no short cut to the answer.



7.1 BRIEF SUMMARY OF COMMON LOUSPEAKER SYSTEMS

In the sections that follow, information is given on the detail design of loudspeaker systems. A brief summary of the four most common systems is given here as an aid to understanding the relative advantages of each of those that are discussed.

Loudspeaker in closed box

It is not practical to mount a loudspeaker in the wall of a residence. Alternatively, an unbaffled speaker would behave like a dipole radiator and at low frequencies would radiate little power. To eliminate radiation from the rear side, all loudspeakers before 1950 were mounted in a simple box. In the equivalent circuit, see Fig. 7.1a, the presence of the box appears as a series compliance C_{MB} which equals $S_D^2 V_B / 1.4P_0$, where V_B is the volume of the box. Its presence raises the speaker's resonance frequency above that if it were in an infinite baffle. Obviously, to minimize this increase, the volume of the box must be made very large. Historically, increasing the compliance C_{MS} to compensate would result in too large an excursion of the voice coil at low frequencies.

Air-suspension loudspeaker system

A unique solution to box size came with the perception that if the suspension compliance C_{MS} were made very large, the compliance of the box C_{MB} (i.e., its volume) could be made much smaller, actually equaling the magnitude of the C_{MS} of the usual loudspeaker. A different method of suspending the cone was used and, after about 1950, box volumes were often as small as 20 L.

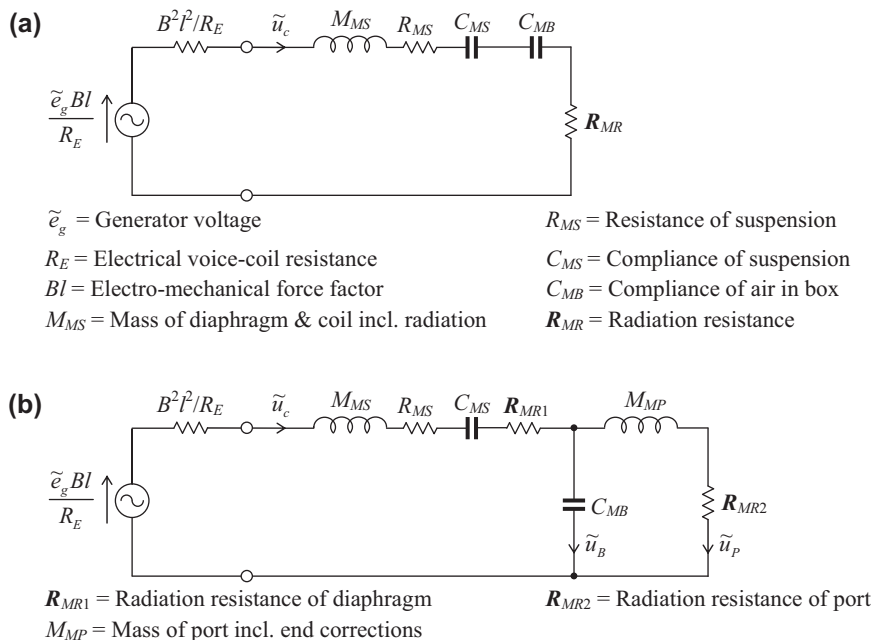


Figure 7.1 Low-frequency analogous circuits for (a) a closed-box loudspeaker and (b) a bass-reflex loudspeaker with electrical quantities referred to mechanical side. For simplicity, generator, box, leakage, and port resistances are omitted.

Bass-reflex loudspeaker system

The bass-reflex system is a means for obtaining a greater response at low frequencies than that from the same loudspeaker in a closed box. Actually, it is often used to boost the output at low frequencies from a system using a relatively small box. Its special feature is a port in the box from which sound emerges that adds to that directly radiated by the loudspeaker. The port is a tube with a cross-sectional area about equal to the area of the loudspeaker cone and a length that is chosen to give the desired resonance frequency.

The simplified equivalent circuit is shown in Fig. 7.1b. Two resonant frequencies occur: that of the loudspeaker (ω_0) and that of the box/port. Usually, $M_{MS}C_{MS} = M_{MP}C_{MB} = 1/\omega_0$. At ω_0 , \tilde{u}_c approaches zero and \tilde{u}_p becomes very large. Below ω_0 , \tilde{u}_c and \tilde{u}_p are out of phase, and the response is not enhanced by the addition of the port. However, for one to two octaves above ω_0 the response is usually enhanced by about 5 dB.

Transmission-line enclosures

A transmission-line enclosure is the result of research leading to a small box containing a small loudspeaker and yet producing a strong bass sound. The box may have a volume as little as 2 L. The loudspeaker drive unit usually has a stiff cone with a diameter between

5 and 12 cm, and its voice coil is capable of large excursions without generating appreciable distortion. The front side of the cone radiates directly into the listening space. Connected to the rear side is a tube whose length is one-fourth that of the lowest desired bass frequency, and the open end of which also radiates into the listening space. A small displacement of the cone will result in a large displacement of the air particles at the end of the tube. For strong bass at 100 Hz, this means a length of 86 cm. The difficulty in the overall design of the system is that the tube also resonates at frequencies higher than the 100 Hz. Their strength at the opening end of the tube is diminished by tapering the tube and filling it with a porous acoustical material of low flow resistance.



7.2 UNBAFFLED DIRECT-RADIATOR LOUDSPEAKER

A baffle is a structure for shielding the front-side radiation of a loudspeaker diaphragm from the rear-side radiation which can potentially cancel it at low frequencies. The necessity for shielding the front side from the rear side can be understood if we consider that an un baffled loudspeaker at low frequencies is the equivalent of a pair of simple spherical sources of equal strength located near each other and pulsing out of phase (see Fig. 7.2). The rear side of the diaphragm of the loudspeaker is equivalent to one of these sources, and the front side is equivalent to the other.

If we measure, as a function of frequency f , the magnitude of the rms sound pressure p at a point A , fairly well removed from these two sources, and if we hold the volume velocity of each constant, we find from Eq. (4.117) that

$$|\tilde{p}| = \frac{\rho_0 f^2 |\tilde{U}_0| b \pi}{rc} \cos \theta \quad (7.1)$$

where

\tilde{U}_0 is strength of each simple source in m^3/s .

b is separation between the simple sources in m.

ρ_0 is density of air in kg/m^3 ($1.18 \text{ kg}/\text{m}^3$ for ordinary temperature and pressure).

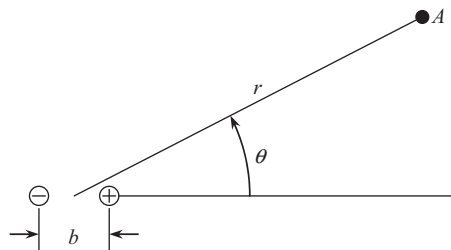


Figure 7.2 Doublet sound source equivalent at low frequencies to an un baffled vibrating diaphragm. The point A is located at a distance r and at an angle θ with respect to the axis of the loudspeaker.

r is distance in m from the sources to the point A . It is assumed that $r \gg b$.

θ is angle shown in Fig. 7.2.

c is speed of sound in m/s (344.8 m/s, normally).

In other words, for a constant-volume velocity of the loudspeaker diaphragm, the pressure \tilde{p} measured at a distance r is proportional to the square of the frequency f and to the cosine of the angle θ and is inversely proportional to r . In terms of decibels, the sound pressure \tilde{p} increases at the rate of 12 dB for each octave (doubling) in frequency.

In the case of an actual un baffled loudspeaker, below the first resonance frequency where the system is stiffness-controlled, the velocity of the diaphragm is not constant but doubles with each doubling of frequency. This is an increase in velocity of 6 dB per octave. Hence, the pressure \tilde{p} from a loudspeaker *without* a baffle increases $12 + 6 = 18$ dB for each octave increase in frequency. Above the first resonance frequency, where the system is mass-controlled, the velocity of the diaphragm decreases 6 dB for each octave in frequency. Hence, in that region, the pressure \tilde{p} increases $12 - 6 = 6$ dB for each octave increase in frequency and we can use the curve shown in Fig. 13.22 for an un baffled circular piston ($b = a$).

The un baffled loudspeaker has the same analogous circuit as that shown in Fig. 6.4, but there are two important differences. Instead of the radiation impedance being approximated by that of a *piston in an infinite baffle* as plotted in Fig. 4.35 from Eqs. (13.117) and (13.118), with approximations given in Table 4.4, we use the radiation impedance of a *free disk* as plotted in Fig. 4.38 from Eqs. (13.249) and (13.250) (with $b = a$), with approximations given in Table 4.5. The other difference is that the on-axis sound pressure is proportional to the total radiation force \tilde{F}_0 rather than the *volume velocity* \tilde{U}_0 . From Eqs. (13.237), (13.249), and (13.250), we obtain

$$\begin{aligned} \tilde{p}(r) &= jf \rho_0 \tilde{U}_0 \frac{Z_S}{\rho_0 c} \frac{e^{-jkr}}{r} = jf \tilde{u}_0 Z_M \frac{e^{-jkr}}{rc} \\ &= jf \tilde{F}_0 \frac{e^{-jkr}}{2rc}, \end{aligned} \tag{7.1a}$$

where we have substituted $kb \sum_{n=0}^N A_n = Z_S/(\rho_0 c)$, $\tilde{U}_0 = \pi a^2 \tilde{u}_0$, $Z_S = Z_M/(\pi a^2)$, and $\tilde{F}_0 = 2Z_M \tilde{u}_0$, taking into account the mechanical radiation impedance Z_M on *both* sides. Hence, if the diaphragm acceleration is constant, the on-axis response is simply the magnitude of the radiation impedance and is shown in Fig. 13.22 ($b = a$). However, in practice, the acceleration varies with frequency, which is what determines the baffled response. Because the radiation impedance is small compared with the mechanical impedance of the driver in most cases and therefore has little influence on the velocity, we see that the un baffled response is the product of the baffled response and the radiation

impedance. Eq. (7.1a) happens to be the same as Eq. (13.128) for the on-axis pressure of a resilient disk in free space.

The absence of a baffle makes the loudspeaker more directional because, in the plane of the baffle, the sound pressure tends to reduce to zero. Hence, there are fewer reflections from side walls. This figure 8 directivity pattern may be used to extend the width of the stereo “sweet spot” in a room. If the listener moves toward one side of the listening area, he or she will move further off the main axis of the nearest loudspeaker than that of the furthest one. Hence, the sound pressure of the nearest loudspeaker will be reduced automatically relative to that of the furthest one, which will compensate for its proximity.

Certain kinds of loudspeaker that have very low moving mass, such as electrostatic or planar magnetic types, are used almost exclusively without a baffle because the extra stiffness provided by a closed box would push the fundamental resonance frequency up too high. The problem of low-frequency cancellation is compensated for by using a very large radiating area. Full-range electrostatic or planar magnetic loudspeakers have radiating areas of at least 0.5 m^2 .



7.3 INFINITE BAFFLE

In the previous chapter, we talked about direct-radiator loudspeakers in infinite baffles. Reference to Fig. 6.7 reveals that with an infinite baffle, the response of a direct-radiator loudspeaker is enhanced over that just indicated for no baffle. It was shown that if one is above the suspension resonance frequency, but below the first diaphragm break-up mode, usually the response is flat with frequency (unless the Bl product is very large), and that if one is below the first resonance frequency, the response decreases at the rate of 12 dB per octave instead of 18 dB per octave. Hence, the isolation of the front side from the back side by an infinite baffle is definitely advantageous.

In practice, the equivalent of an infinite baffle is a very large enclosure, well damped by absorbing material. One practical example is to mount the loudspeaker in one side of a closet filled with clothing, allowing the front side of the loudspeaker to radiate into the adjoining listening room.

Design charts covering the performance of a direct-radiator loudspeaker in an infinite baffle are identical to those for a closed box. We shall present these charts in [Section 7.6](#).



7.4 FINITE-SIZED FLAT BAFFLE

The discussion above indicated that it is advisable to shield completely one side of the loudspeaker from the other, as by mounting the loudspeaker in a closet. Another possible alternative is to mount the loudspeaker in a flat baffle of finite size, free to stand at one end of the listening room. The worst shape for such a baffle is circular because

sound from the rear arrives at the front at the same time whichever radial path is taken. Hence, at some frequencies, where the radial path length is a multiple of the wavelength λ , the front radiation is partially canceled, and we have a comb filter effect, as shown in Fig. 13.22. The effect is considerably smeared if we use a rectangular baffle with the drive unit offset from the center as is the case with the IEC 268-5 baffle [1].

The performance of a loudspeaker in a free-standing flat baffle leaves much to be desired, however. If the wavelength of a tone being radiated is greater than twice the smallest lateral dimension of the baffle, the loudspeaker will act according to Eq. (7.1). This means that for a finite flat baffle to act approximately like an infinite baffle at 50 Hz, its smallest lateral dimension must be about 3.5 m (11.5 ft), which limits its use to midrange units or above. However, even above this frequency, sound waves traveling from behind the loudspeaker reflect off walls and meet with those from the front and cause alternate cancellations and reinforcements of the sound as the two waves come into phase or out of phase at particular frequencies in particular parts of the room. Hence, the loudspeaker must be located away from walls or reflecting objects to minimize this effect.

7.5 OPEN-BACK CABINETS

An open-back cabinet is simply a box with one side missing and with the loudspeaker mounted in the side opposite the open back. Many portable stereos are of this type. Such a cabinet performs nearly the same as a flat baffle that provides the same path length between the front and back of the loudspeaker. One additional effect, usually undesirable, occurs at the frequency where the depth of the box approaches a quarter wavelength. At this frequency, the box acts as a resonant tube, and more power is radiated from the rear side of the loudspeaker than at other frequencies. Furthermore, the sound from the rear may combine in phase with that from the front at about this same frequency, and an abnormally large peak in the response may be obtained.

7.6 CLOSED-BOX BAFFLE [2,3]

The most commonly used type of loudspeaker baffle is a closed box in one side of which the loudspeaker is mounted. In this type, discussed here in considerable detail, the back side of the loudspeaker is completely isolated from the front. A customary type of closed-box baffle is shown in Fig. 7.3. The sides are made as rigid as possible using some material like 5-ply plywood or MDF, 0.75–1.0 in. thick, and braced to prevent resonance. A slow air leak must be provided in the box so that changes in atmospheric pressure do not displace the neutral position of the diaphragm.

When selecting a loudspeaker, the first two questions that arise are how loud must it go and what bass cutoff frequency can be tolerated? This of course will depend on the application, and the radiated sound pressure will need to be greater for an auditorium

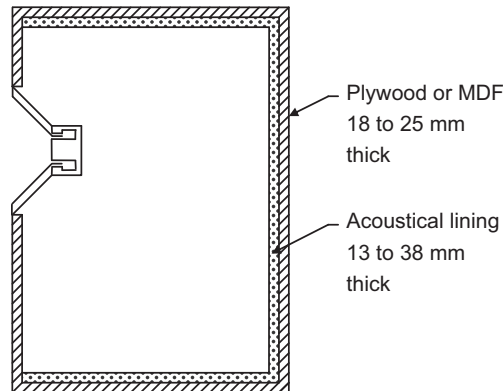


Figure 7.3 Typical plywood box with loudspeaker mounted off center in one side and lined with a layer of soft absorbent acoustical material.

than for a domestic living room. For a cellphone ringtone, it must be possible to hear it in a noisy street environment. In general, the low-frequency sound pressure is limited by the displacement limit x_{\max} , and the high-frequency sound pressure is limited by the power rating. In fact, at higher frequencies, the situation is worse because at least the larger low-frequency displacement pumps air through the magnetic gap, which helps to cool the voice coil. If the suspension alone is not stiff enough to limit the full-power displacement at low frequencies, then part of the function of the box is to provide the extra stiffness needed to keep the displacement in check. Otherwise, an auxiliary high-pass filter must be employed. As more stable suspension materials have been developed, the trend has been toward more compliant suspensions so that an ever greater proportion of the stiffness can be provided by air in the box which in turn makes the volume of the box correspondingly smaller. This principle is known as *air suspension* [4].

Summary of closed-box baffle design

To determine the volume of the closed box and the -3 dB cutoff frequency:

If the Thiele–Small parameters (R_E , Q_{ES} , Q_{MS} , f_s , S_D and V_{AS}) of the chosen drive unit are not supplied by the manufacturer, they may be measured according to Section 6.10. Then $Q_{TS} = Q_{ES}Q_{MS}/(Q_{ES} + Q_{MS})$.

From Table 7.2, select the frequency-response shape, taking into account that the closed-box Q_{TC} value must be higher than the infinite baffle Q_{TS} of the drive unit. The effect of various Q_{TC} values on the frequency-response shape can be seen from Fig. 7.16. Further advice regarding Q_{TC} is given in the paragraph following Eq. (7.56).

Estimate the volume of air in the box V_A using Eq. (7.61). However, if the box is filled or has a thick lining, then the Q_{TC} value will be modified. Using the manufacturer's or measured value of flow resistance R_f for the lining material, compute R_{AB} from

Eq. (7.7) and Q_{MB} from Eq. (7.58). Determine the volume V_A from Eq. (7.60). The total internal volume is then $V_B = V_A + V_M$, where V_M is the volume of the lining material.

Determine the closed-box resonance frequency f_C from Eq. (7.28). From the value of f_{3dB}/f_C given in Table 7.2, compute the cutoff frequency f_{3dB} .

To determine the maximum sound pressure level (SPL):

If the loudspeaker is to be used near a wall or a rigid planar surface, which is large compared with the longest wavelength to be reproduced, then the maximum sound pressure SPL_{max} is obtained from Eq. (6.34) to give

$$SPL_{max} = 20 \log_{10} \left(\frac{1}{rc \times 20 \times 10^{-6}} \frac{\sqrt{Z_{nom} W_{max} 2\pi f_S^3 V_{AS} \rho_0}}{R_E Q_{ES}} \right) \text{ dB SPL @ 1m}$$

where W_{max} is the maximum rated input power. Otherwise, if it is to be used in the free field, subtract 6 dB from SPL_{max} .

To determine the excursion limit:

The maximum peak diaphragm displacement at frequencies well below the closed-box resonance is obtained from Eq. (7.64) to give

$$\eta_{max} = \frac{1}{S_{DC}(1 + V_{AS}/V_{AB})} \frac{\sqrt{Z_{nom} W_{max} V_{AS}}}{R_E Q_{ES} \pi f_S \rho_0}$$

However, we see from Fig. 7.17 that at frequencies below the closed-box resonance, the displacement peaks at a higher value in the case of Chebyshev alignments. For example, the displacement peaks at $1.4\eta_{max}$ in the case of the 3-dB Chebyshev alignment or $2\eta_{max}$ in the case of the 6-dB Chebyshev alignment. If this peak value is greater than the rated x_{max} limit of the drive unit, then it should be arranged for the box resonance frequency f_C to be placed below the lower limit of the frequency range of the program material to be reproduced. If this is not possible, a high-pass filter should be employed to remove all content below the box resonance frequency. If this is not possible either, then an alternate drive unit with a greater x_{max} limit should be considered.

Fig. 7.4 shows the effective diameter of a drive unit required to achieve a given SPL, with a peak displacement of 1 mm, when radiating omnidirectionally into free space from a closed-box enclosure. This is obtained from Eq. (6.35), but adjusted by a factor of $\sqrt{2}$ for free-space omnidirectional radiation. Hence, for loudspeakers that are to be placed near a wall, the required diameter should be divided by $\sqrt{2}$. Because the diameter has an inverse square-root relationship with the displacement, quadrupling the peak displacement halves the required diameter. Hence, there has been a trend toward smaller drive units with greater x_{max} values, usually achieved by extending the coil beyond the

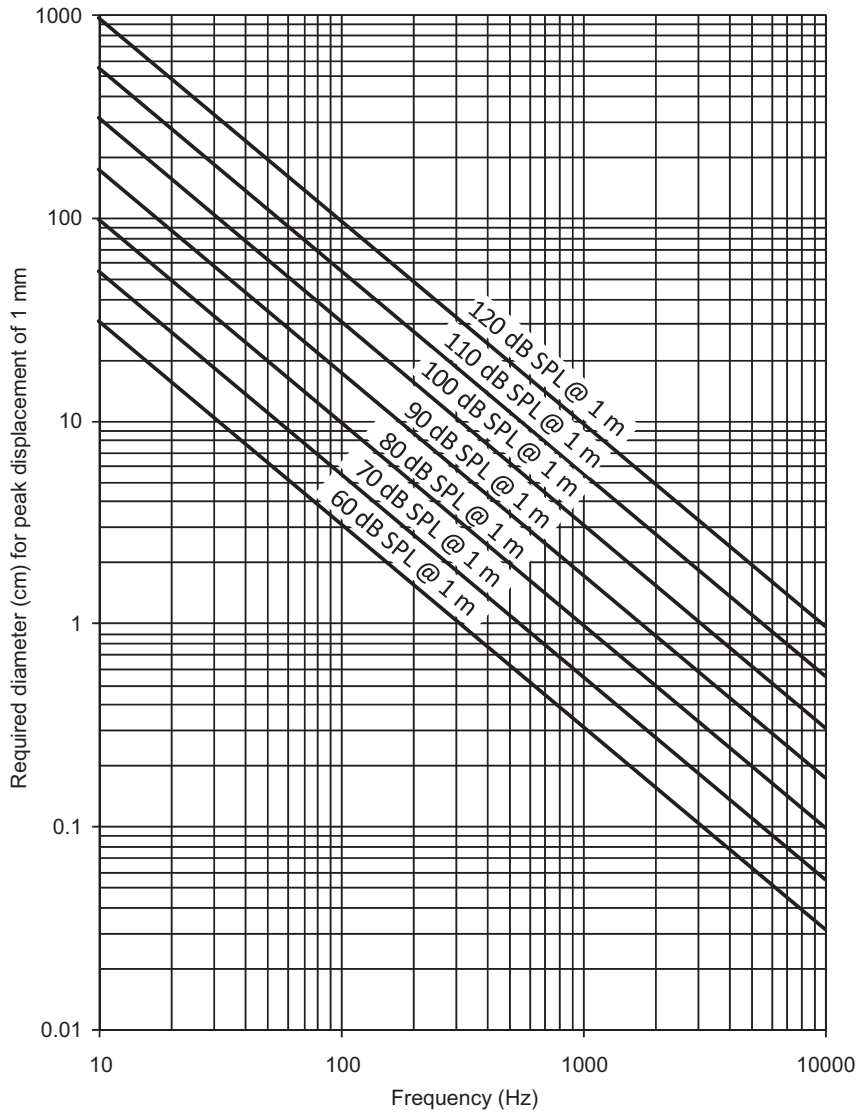


Figure 7.4 Drive unit effective diameter required to produce a given sound pressure level, with a peak displacement of 1 mm, when radiating omnidirectionally into free space from a closed-box enclosure. If the peak displacement is quadrupled (say a peak displacement of 4 mm is allowed), then the required diameter is halved.

magnetic gap, although this reduces sensitivity and efficiency. Considering that the maximum effective diameter of an individual drive unit is around 40 cm, the difficulty of producing very low frequencies at high sound pressures is evident. For large auditoriums, the very large diameters are made up by stacking multiple loudspeakers.

Analogous circuit

A closed box reacts on the back side of the loudspeaker diaphragm. This reaction may be represented by an acoustic impedance which at low frequencies is a compliance operating to stiffen the motion of the diaphragm and to raise the resonance frequency. At high frequencies, the reaction of the box, if unlined, is that of a multiresonant circuit. This is equivalent to an impedance that varies cyclically with frequency from zero to infinity to zero to infinity, and so on. This varying impedance causes the frequency-response curve to have corresponding peaks and dips.

If the box is lined with a sound-absorbing material, these resonances are damped, and at high frequencies the rear side of the diaphragm is loaded with an impedance equal to that for the diaphragm in an infinite baffle radiating into free space. The acoustical circuit for the box and radiation load on the diaphragm is given in Fig. 7.5. The reactance and resistance of the box are X_{AB} and R_{AB} . The radiation mass and resistance on the front of the diaphragm are M_{AR} and R_{AR} , respectively.

At low frequencies, where the diaphragm vibrates as one unit so that it can be treated as a rigid piston, a complete electromechanoacoustical circuit can be drawn that describes the behavior of the box-enclosed loudspeaker. This circuit is obtained by combining Fig. 6.4(b) and Fig. 7.5. To do this, the acoustical radiation element of the circuit labeled “ $2M_{M1}$ ” in Fig. 6.4(b) is removed, and the circuit of Fig. 7.5 is substituted in its place. The resulting circuit with the transformer removed and everything referred to the acoustical side is shown in Fig. 7.6.

Some interesting facts about loudspeakers are apparent from this circuit. First, the electrical generator (power amplifier) resistance R_g and the voice-coil resistance R_E appear in the denominator of one of the resistances shown. This means that if one desires a highly damped or an overdamped system, it is possible to achieve this by using a power

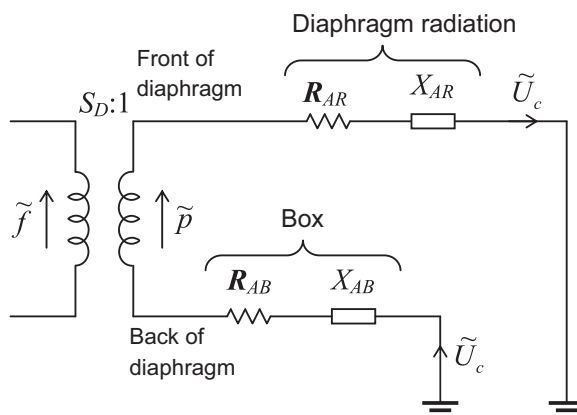


Figure 7.5 Analogous acoustical circuit for a loudspeaker box. The volume velocity of the diaphragm is U_c .

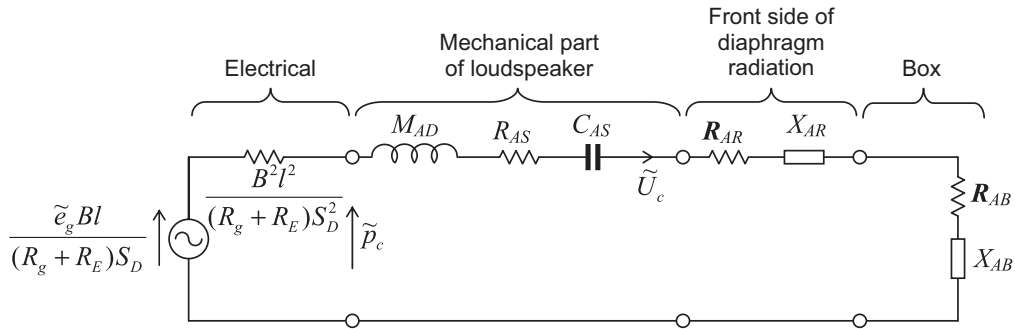


Figure 7.6 Circuit diagram for a direct-radiator loudspeaker mounted in a closed-box baffle. This circuit is valid for frequencies below about 400 Hz.

amplifier with very low output impedance. Second, the circuit is of the simple resonant type so that we can solve for the voice-coil volume velocity (equal to the linear velocity times the effective area of the diaphragm) by the use of universal resonance curves. Our problem becomes, therefore, one of evaluating the circuit elements and then determining the performance by using standard theory for electrical series *LRC* circuits.

Values of electrical-circuit elements

All the elements shown in Fig. 7.6 are in units that yield acoustic impedances in $\text{N}\cdot\text{s}/\text{m}^5$, which means that all elements are transformed to the acoustical side of the circuit. This accounts for the effective area of the diaphragm S_D appearing in the electrical part of the circuit. The quantities shown are

- \tilde{e}_g is open-circuit voltage in V of the audio amplifier driving the loudspeaker.
- B is flux density in the air gap in T ($1 \text{ T} = 10^4 \text{ G}$).
- l is length of the wire wound on the voice coil in m.
- R_g is output electrical impedance (assumed resistive) in Ω of the audio amplifier.
- R_E is electrical resistance of the wire on the voice coil in Ω .
- a is effective radius in m of the diaphragm.
- $S_D = \pi a^2$ is effective area in m^2 of the diaphragm.

Values of the mechanical-circuit elements

The elements for the mechanical part of the circuit differ here from those of Part XIX in that they are transformed over to the acoustical part of the circuit so that they yield acoustic impedances in $\text{N}\cdot\text{s}/\text{m}^5$.

- $M_{AD} = M_{MD}/S_D^2$ is acoustic mass of the diaphragm and voice coil in kg/m^4 .
- M_{MD} is mass of the diaphragm and voice coil in kg.
- $C_{AS} = C_{MS}S_D^2$ is acoustic compliance of the diaphragm suspensions in m^5/N .
- C_{MS} is mechanical compliance in m/N .

$R_{AS} = R_{MS}/S_D^2$ is acoustic resistance of the suspensions in $\text{N}\cdot\text{s}/\text{m}^5$.

R_{MS} is mechanical resistance of the suspensions in $\text{N}\cdot\text{s}/\text{m}$.

These quantities may readily be measured with a simple setup in the laboratory, as described in Section 6.10. It is helpful, however, to have typical values of loudspeaker constants available for rough computations, and these are shown in Figs. 7.7 and 7.8. The average value of R_E for a drive unit with an advertised impedance of $8\ \Omega$ is around $6.3\ \Omega$. The magnitude of the air-gap flux density B varies from 0.6 to 1.4 T depending on the cost and size of the loudspeaker.

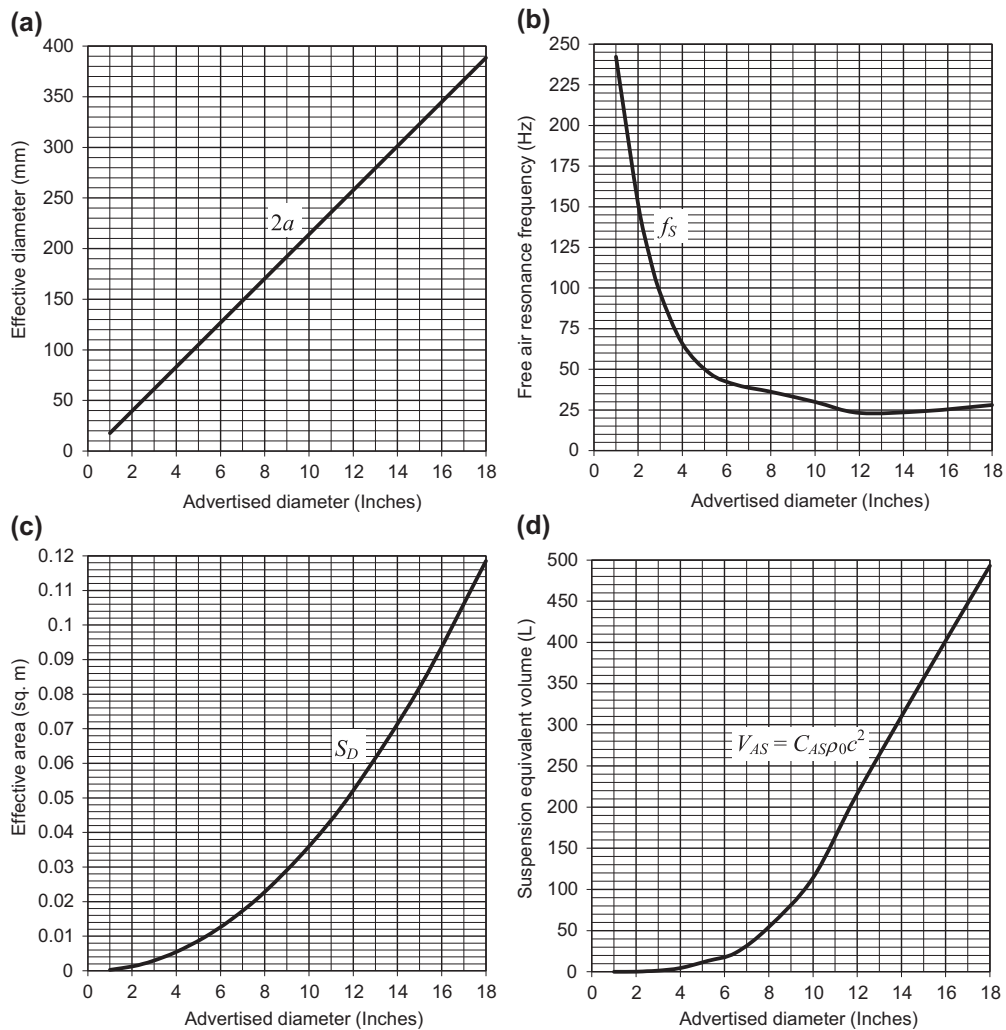


Figure 7.7 (a) Relation between effective diameter of a loudspeaker and its advertised diameter. (b) Average resonance frequencies of direct-radiator loudspeakers when mounted in IEC 268-5 baffles [1] versus the advertised diameters. (c) Average effective radiating areas of loudspeakers versus the advertised diameters. (d) Average compliances of suspensions of loudspeakers versus the advertised diameters, where the compliance is expressed as an equivalent volume in liters.

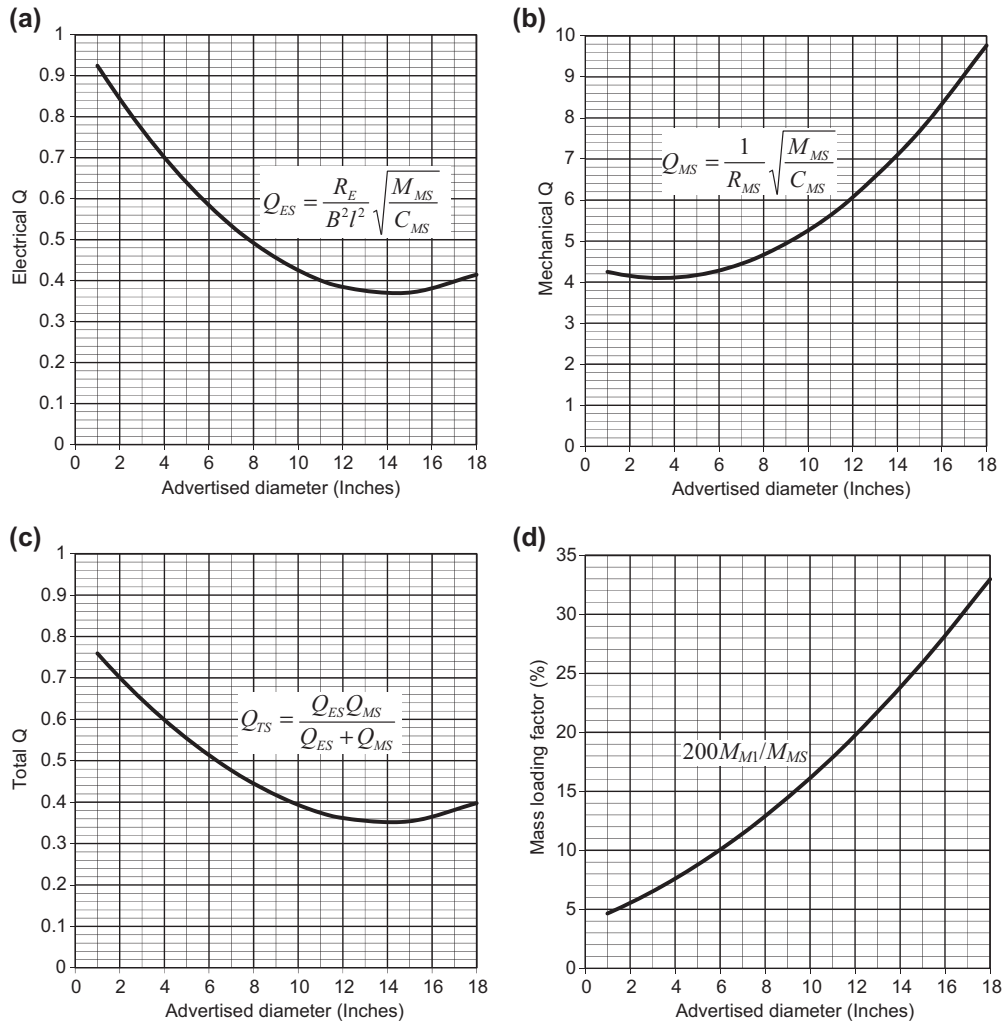


Figure 7.8 (a) Average electrical Q_{ES} values of loudspeaker drive units versus the advertised diameters. (b) Average mechanical Q_{MS} values of loudspeaker drive units versus the advertised diameters. (c) Average total Q_{TS} values of loudspeaker drive units versus the advertised diameters. (d) Average mass loading factors of loudspeaker drive units versus the advertised diameters, where the mass loading factor is the ratio of the radiation mass on *both sides* in an infinite baffle ($2M_{M1}$) to the total moving mass of the drive unit (M_{MS}), where $M_{MS} = M_{MD} + 2M_{M1}$.

Impedance of closed box with absorbent lining

The type of reactance function shown in Fig. 7.12 without absorbent lining is not particularly desirable because of the very high value that X_{AB} reaches at the first normal mode of vibration (resonance) for the box, which occurs when the depth of the box equals one-half wavelength. A high reactance reduces the power radiated to a very

small value. To reduce the magnitude of X_{AB} at the first normal mode of vibration, an acoustical lining is placed in the box. This lining should be highly absorbent at the frequency of this mode of vibration and at all higher frequencies. For normal-sized boxes, a satisfactory lining is a 25 mm-thick layer of bonded mineral wool, bonded Fiberglass, bonded hair felt, Cellufoam (bonded wood fibers), etc. For small cabinets, where the largest dimension is less than 0.5 m, a 12.5 mm-thick layer of absorbing material may be satisfactory.

At low frequencies, where the thickness of the lining is less than 0.05 wavelength, the impedance of the box presented to the rear side of the diaphragm is represented by the analogous circuit of Fig. 7.9 and equals

$$Z_{AB} = R_{AB} + jX_{AB} \quad (7.2)$$

where

$$X_{AB} \approx \omega M_{AB} - \frac{1}{\omega(C_{AA} + C_{AM})} \quad (7.3)$$

and C_{AA} and M_{AB} are the acoustic compliance and mass, respectively, of the air inside the box given by

$$C_{AA} = \frac{V_A}{\gamma P_0} \quad (7.4)$$

$$M_{AB} = \frac{B\rho_0}{\pi a} \quad (7.5)$$

where

V_A is volume of air in the box in m^3 excluding that contained within the pores of the lining material. The volume of the loudspeaker should also be subtracted from the

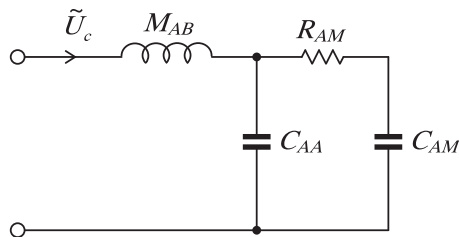


Figure 7.9 Analogous circuit for the acoustic impedance Z_{AB} presented to the rear side of the diaphragm at low frequencies where the smallest dimension of the box is less than one-sixteenth wavelength. The volume velocity of the diaphragm = \tilde{U}_c ; M_{AB} = acoustic mass of the air load on the rear side of diaphragm; C_{AA} = acoustic compliance of the air in the box excluding the lining; C_{AM} = acoustic compliance of the air in the pores of the lining; and R_{AM} = acoustic resistance of the lining.

actual volume of the box to obtain this number. To a first approximation, the volume of the speaker in m^3 equals $0.4 \times$ the fourth power of the advertised diameter in m. $\gamma = 1.4$ for air for adiabatic compressions.

P_0 is atmospheric pressure in Pa (about 10^5 on normal days).

$\pi a = \sqrt{S_D \pi}$ if the loudspeaker is not circular.

B is a constant, given in Fig. 7.10 for a box of the type shown in Fig. 7.11, which is dependent on the ratio of the effective area of the loudspeaker diaphragm S_D to the area L^2 of the side of the box in which it is mounted.

We see from Fig. 7.10 that when the diaphragm has the same area as the cross-sectional area of the box, that is $S_D/L^2 = 1$, the box becomes a closed tube of length $L/2$ and the mass load on the rear of the diaphragm is one-third of the total mass in the box, so that $B = \sqrt{\pi}/6$. On the other hand, when the area of the diaphragm is very small compared with the cross-sectional area of the box, that is $S_D/L^2 \rightarrow 0$, the mass on the rear of the diaphragm is that of a piston in an infinite baffle so that $B \rightarrow 8/(3\pi)$.

It is assumed that the pressure variations in the pores of the lining material are isothermal so that the compliance of the lining material is given by

$$C_{AM} = \frac{V_M}{P_0} \quad (7.6)$$

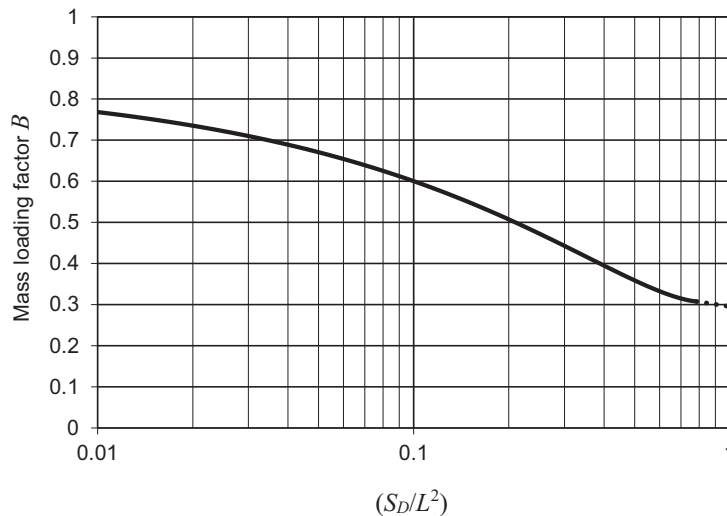


Figure 7.10 End-correction factor B for the reactance term of the impedance at the rear side of the loudspeaker diaphragm mounted in a box of the type shown in Fig. 7.11. Because the diaphragm is circular, it cannot have the same area as the wall in which it is mounted ($S_D/L^2 = 1$). Hence, the last part of the curve beyond $S_D/L^2 = \pi/4$ is only applicable to square diaphragms and is thus dotted. The acoustic reactance of the box on the diaphragm is given by $X_{AB} = -\gamma P_0/\omega V_A + \omega B \rho_0/\pi a$. For a noncircular diaphragm of area S_D , $\pi a = \sqrt{S_D \pi}$.

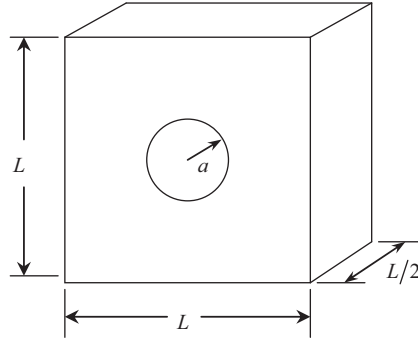


Figure 7.11 Loudspeaker mounted in a closed box with internal dimensions $L \times L \times L/2$ when unlined and a diaphragm of area $S_D = \pi a^2$ at the center of the $L \times L$ face where $L^2/S_D = 16$. When lining of thickness $d = L/10$ is added to the rear surface, the internal depth is increased to $0.6L$. While this type of box is convenient for analysis, the construction shown in [Fig. 7.3](#) is more commonly used.

where V_M is the total volume of the pores. Then, from [Fig. 7.9](#), the resistance is defined by

$$\begin{aligned}
 R_{AB} &= \Re \left(\left(j\omega C_{AA} + \frac{1}{R_{AM} + (j\omega C_{AM})^{-1}} \right)^{-1} \right) \\
 &= \frac{R_{AM}}{\left(1 + \frac{V_A}{\gamma V_M} \right)^2 + \omega^2 R_{AM}^2 C_{AA}^2}
 \end{aligned} \tag{7.7}$$

where

$R_{AM} = dR_f/(3S_M)$ is one-third of the total flow resistance of a layer of thickness d of the acoustical material that lines the box divided by the area of the acoustical material S_M . The units are $\text{N}\cdot\text{s}/\text{m}^5$. The flow resistance equals the ratio of the pressure drop across the sample of the material to the linear air velocity through it. For lightweight materials the flow resistance R_f is about 100 rayls for each 25 mm of thickness. For dense materials like PF Fiberglass board or rockwool duct liner, the flow resistance may be as high as 2000 rayls for each 25 mm of thickness of the material. For example, if the flow resistance per 25 mm of material is 500 rayls, the thickness is 75 mm, and the area is 0.2 m^2 , then $R_{AM} = 1500/(3 \times 0.2) = 2500 \text{ N}\cdot\text{s}/\text{m}^5$.

It is assumed in writing this equation that the material does not occupy more than 20% of the volume of the box.

Sound propagation in homogeneous absorbent materials [\[5\]](#)

The sound propagation in fibrous or porous acoustical materials can be described with a relatively simple analytical model if the constituent (the solid part of the material) is assumed to be rigid [\[6\]](#). A model taking into account the flexibility of the constituent [\[7\]](#)

would better describe behavior of the relatively low-density absorbents used in loudspeakers, but such a model requires parameters that are quite difficult to obtain. A good empirical description of sound propagation in absorbents has been presented by Delany and Bazley [8], with extensions by Miki [9]. Flow resistance is needed to compute the acoustical properties of a porous material. It can be determined when the porosity and the average (rms) fiber diameter are known, by using an equation derived by Sides et al. [10]:

$$R_f = \frac{\Delta p}{ud} = \frac{4\mu(1-\varphi)}{\varphi r^2} \left(\frac{1 - \frac{4}{\pi}(1-\varphi)}{2 + \ln \frac{\mu\varphi}{2r\rho_0 u}} + \frac{6}{\pi}(1-\varphi) \right) \quad (7.8)$$

where

R_f is flow resistance of material in rayls/m.

Δp is pressure difference across material in Pa.

u is flow velocity in the material in m/s.

d is thickness of the material in m.

μ is viscosity coefficient. For air, $\mu = 1.86 \times 10^{-5} \text{ N}\cdot\text{s}/\text{m}^2$ at 20°C and 0.76 m Hg.

φ is porosity of the material.

r is fiber diameter (rms average).

ρ_0 is density of air in kg/m^3 .

As Eq. (7.8) shows, the flow resistance is a function of flow velocity. Eq. (7.8) is actually the equation of the static flow resistance, and so with sound the rms value of flow velocity should be used. With flow velocities associated with sound pressures of interest, the variation of the flow resistance is rather small, and so this nonlinear effect can be ignored and a typical value of flow velocity can be used; Sides et al. recommend a value of $u = 0.03 \text{ m/s}$. If the flexibility of the constituent were taken into account, the resistance values would be somewhat lower. The porosity φ is defined as the proportion of the constituent material to the total volume of the absorbent and is defined by

$$\varphi = 1 - \frac{\rho_M}{\rho_C} \quad (7.9)$$

where

ρ_M is density of absorbent material in kg/m^3 .

ρ_C is density of the constituent material (e.g., glass 2200–2900 kg/m^3).

Typical values of porosity in acoustical absorbents range from 0.95 to 0.99. When the flow resistance is determined, then the characteristic impedance Z_s can be determined by

$$Z_s = \rho_0 c \left\{ \left(1 + a_1 \left(\frac{R_f}{f} \right)^{b_1} \right) - ja_2 \left(\frac{R_f}{f} \right)^{b_2} \right\} \quad (7.10)$$

Table 7.1 Values of coefficients used in Eqs. (7.10) and (7.11) for characteristic impedance and wave number, respectively, of a homogenous absorbent material.

Coefficient	Delany and Bazley	Miki
a_1	0.0511	0.070
a_2	0.0768	0.107
a_3	0.0858	0.109
a_4	0.175	0.160
b_1	0.75	0.632
b_2	0.73	0.632
b_3	0.70	0.618
b_4	0.59	0.618

and the wave number \mathbf{k} by

$$\mathbf{k} = \frac{\omega}{c} \left\{ \left(1 + a_3 \left(\frac{R_f}{f} \right)^{b_3} \right) - ja_4 \left(\frac{R_f}{f} \right)^{b_4} \right\} \quad (7.11)$$

where

ρ_0 is density of air in kg/m^3 .

c is speed of sound in air in m/s.

f is frequency in Hz.

ω is angular frequency ($2\pi f$).

The coefficients a_1 to b_4 are given in Table 7.1.

The original coefficients given by Delany and Bazley give an excellent match to experimental results when $0.01 < f/R_f < 1$, but the coefficients should not be used for extrapolation outside this range; using these coefficients with low values of flow resistance and frequency (such as those usually applied in loudspeakers) can yield negative values of attenuation. In such cases, the coefficients given by Miki should be used instead. The lower limit of validity for Miki's equations is $f/R_f > 0.0005$. Other conditions for validity of these equations are that the porosity is close to unity and that the flow resistance R_f is between 20 and 800 rayls/cm. In practice, the soft bulk fibrous absorbents, such as natural and synthetic organic fibers and soft glass wool, used in loudspeakers meet these additional conditions. The more rigid absorbent sheets commonly used for room acoustics treatment have anisotropic acoustical characteristics, and these models cannot be applied as such.

Impedance of closed box with or without absorbent lining at all frequencies

Until now, we have only dealt with low frequencies using the circuit shown in Fig. 7.9, which is valid when the wavelength is greater than 8 times the smallest dimension of the box. To see the effect of the internal standing wave modes on the impedance or to

investigate the effect of placing lining material on the rear surface, we need a full model of the enclosed space. Such a model will be developed in Section 7.18 resulting in Eq. (7.131) for the self- and mutual impedances of a closed box with two pistons in one wall and an impedance boundary condition on the opposite wall as shown in Fig. 7.34. The second piston is intended to represent the coupling to a bass-reflex port. The width, length, and depth of the box are l_x , l_y , and l_z , respectively. The dimensions of the pistons are $a_1 \times b_1$ and $a_2 \times b_2$. However, for a closed box with no bass-reflex port, we just use Z_{11} from Eq. (7.128a) and divide through by a_1^2 to obtain the acoustic impedance, which is in the form of an eigenfunction expansion. In the case of a box with the dimensions shown in Fig. 7.11, where $l_x = l_y = L$, $l_z = x_1 = y_1 = L/2$, and $a_1 = a$, this reduces to:

$$Z_{AB} = \frac{z_{11}}{(\pi a^2)^2} = -j\rho_0 c \left\{ \frac{1}{L^2} \cot \frac{kL}{2} + \frac{k}{\pi^2 a^2} \sum_{m=0}^{\infty} \sum_{n=0}^{\infty} \frac{(2 - \delta_{m0})(2 - \delta_{n0})}{k_{mn}(n^2 + m^2) + \delta_{m0}\delta_{n0}} \right. \\ \left. \times J_1^2 \left(\frac{2\pi a \sqrt{m^2 + n^2}}{L} \right) \cot \frac{k_{mn}L}{2} \right\}, \quad (7.12)$$

where k_{mn} is given by

$$k_{mn} = \sqrt{k^2 - \left(\frac{2m\pi}{l_x} \right)^2 - \left(\frac{2n\pi}{l_y} \right)^2}. \quad (7.13)$$

Although this expansion looks complicated, it is highly amenable to numerical computation, and the impedance can be used as part of a matrix expression for the equivalent circuit, as will be demonstrated in Examples 7.2 and 7.3. The first term is simply that of a tube with the same depth l_z as that of the box and a termination impedance Z_s . The impedance of a tube was given by Eq. (2.60). For the impedance of the lining we set

$$Z_s = \frac{R_f d}{3} + \frac{P_0}{j\omega d} \quad (7.14)$$

where d is the thickness of the lining, and we are assuming that the material is so porous that it is mainly air. For simplicity, we will let $l_z = L/2$, $l_x = l_y = L$, $a_1 = b_1 = \sqrt{S_D}$, and $y_1 = L/2$. In Fig. 7.12, the specific impedance is plotted for the box of Fig. 7.11 with acoustic lining on the rear surface only to a depth of $d = L/10$ in addition to the box

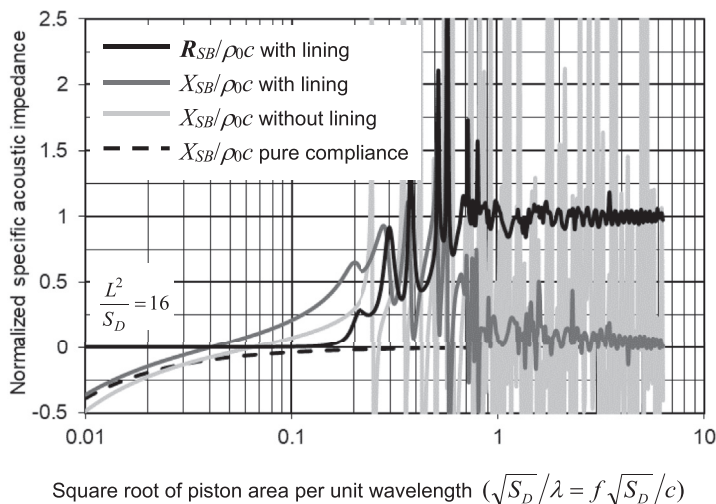


Figure 7.12 Normalized specific acoustic impedance ($Z_{SB}/\rho_0c = Z_{MB}/(S_D\rho_0c) = Z_{AB}S_D/\rho_0c$) of the closed box shown in Fig. 7.11. The lining has a specific flow resistance of $R_f d = 3\rho_0c$, which provides optimum sound absorption at higher frequencies. The position of the first normal mode of vibration occurs when $L/2 = \lambda/2$, that is, it occurs at $\sqrt{S_D}/\lambda = 0.25$ for $L^2/S_D = 16$. Without the lining, $R_{SB} = 0$.

depth of $L/2$. Hence, the air volume is $V_A = L^3/2$, and the material volume is $V_M = L^3/10$. The flow resistance of the lining is $R_f d = 3\rho_0c$ to maximize absorption at high frequencies.

We see from Fig. 7.12 that at high frequencies the unlined box impedance varies dramatically with frequency between zero reactance and very high reactance. With lining, the box resonances (normal modes of vibration) are damped out so that R_{SB} has a constant value of around ρ_0c and X_{SB} approaches zero. If this behaved simply like an acoustic transformer (see Eq. (4.38)), we might expect the high-frequency value of R_{SB} to be $\rho_0c/16$, that is, the impedance of the lining divided by the ratio of the area of the lining to that of the diaphragm. However, the transformer model is only valid when the wavelength is large compared with the depth $L/2$. Instead, we see a much higher value of R_{SB} because, as the size of the box is increased, the impedance seen by the diaphragm approaches that of a piston in an infinite baffle, which is ρ_0c .

Acoustical material may also be used to enlarge effectively the volume of enclosed air. Gaseous compressions in a sound wave are normally adiabatic. If the air space is completely filled with a soft, lightweight material such as kapok or Cellufoam (foamed wood fibers), the compressions become isothermal. This means that the speed of sound decreases from $c = 344.8$ m/s to $c = 292$ m/s. Reference to Fig. 7.12 shows that this lowers the reactance at low frequencies just as does an increase in box dimension L . This also means that in Eq. (7.4) the value of γ is 1.0 instead of 1.4. In some designs, activated

carbon is used to increase the apparent volume of the box even further. The pores within the material have a vast internal surface area on which air molecules are adsorbed when the pressure increases. When the pressure decreases, they are released again, the effect of which is to reduce the stiffness of the air in the box. However, the flow resistance of the material will have the effect of reducing the Q of the closed-box resonance, which may or may not be a good thing depending on what the value was to begin with [11,12].

Unlined closed box at low frequencies

In an unlined box, X_{AB} is not well behaved for wavelengths shorter than eight times the smallest dimension of the box [13], as is seen from Fig. 7.12. If the dimension behind the loudspeaker is less than about $\lambda/4$, the reactance is negative (compliance dominated). If that dimension is greater than $\lambda/4$, the reactance is usually positive (mass dominated). When that dimension is equal to $\lambda/2$, the reactance becomes very large and the sound pressure radiated from the loudspeaker is attenuated. However, in many applications, such as tweeters, cellphones, and MP3-player docking stations, the box is small compared with the wavelength over most of the working frequency range and so these typically have unlined enclosures. For those frequencies where the wavelength of sound is greater than eight times the smallest dimension of the box, the acoustic reactance presented to the rear side of the loudspeaker is a series mass and compliance as given by Eq. (7.3), but with $C_{AM} = 0$. For example, if the depth of the box is 2 cm, then the maximum frequency for Eq. (7.3) is 2.18 kHz, and the reactance will become very large at 8.72 kHz. The impedance at all frequencies is given by Eq. (7.12), but with $Z_s \rightarrow \infty$, so that

$$\frac{\frac{k_{mn}Z_s}{k\rho_0c} + j \tan k_{mn}l_z}{1 + j \frac{k_{mn}Z_s}{k\rho_0c} \tan k_{mn}l_z} = -j \cot k_{mn}l_z \quad (7.15)$$

To determine the end-correction factor B used in Eq. (7.5) and for the plot of Fig. 7.10 (where for simplicity we let $l_z = L/2$, $l_x = l_y = L$, $a_1 = b_1 = \sqrt{S_D}$, and $\gamma_1 = L/2$), we make the following low-frequency ($k \rightarrow 0$) approximations:

$$\cot \frac{kL}{2} \approx \frac{2}{kL} - \frac{kL}{6} \quad (7.16)$$

$$k_{mn} \approx j \frac{2\pi}{L} \sqrt{m^2 + n^2} \quad (7.17)$$

and

$$\frac{k}{k_{mn}} \cot \frac{k_{mn}L}{2} \approx - \frac{kL}{2\pi\sqrt{m^2 + n^2}} \quad (7.18)$$

Noting that $Z_{AB} = jX_{AB}$, where X_{AB} is given by Eq. (7.3), we obtain the following expression for the end-correction factor B :

$$B = \frac{\sqrt{\pi S_D}}{\rho_0} M_{AB} = \frac{\pi^{1/2} \sqrt{S_D}}{6L} + \frac{L}{2\sqrt{S_D}} \sum_{m=0}^{\infty} \sum_{n=0}^{\infty} \frac{(2 - \delta_{m0})(2 - \delta_{n0})}{(\pi(m^2 + n^2))^{3/2} + \delta_{m0}\delta_{n0}} J_1^2 \left(2\sqrt{\pi(m^2 + n^2)} \frac{\sqrt{S_D}}{L} \right), \quad (7.19)$$

which is valid for lined or unlined boxes.

Location of loudspeaker drive unit in box

The results shown in Fig. 7.12 for the reactance of the closed box apply to a loudspeaker mounted in the center of one of the L by L sides. This location of the loudspeaker leaves something to be desired, because waves traveling outward from the diaphragm reach the outside edges of the box simultaneously and in combination set up a strong diffracted wave in the listening space. To reduce the magnitude of the diffracted wave, the loudspeaker should be moved off center by several inches—preferably in the direction of one corner. The use of rounded corners also helps to mitigate diffraction effects.

Note that if an ideal flat drive unit occupies the whole of one wall, no modes will occur between the adjacent walls, only between the drive unit and opposite (rear) wall. This is because the drive unit itself and the opposite wall are both reflected in the adjacent walls, which act like mirrors. Hence, the drive unit behaves like an infinite piston facing an infinite reflective surface.

The front face of the box of Fig. 7.11 need not be square. It is possible to make the ratio of the two front edges vary between one and three without destroying the validity of the charts, for the same total volume. In hi-fi loudspeaker enclosures, it is not unusual for all the sides to be of different lengths with a “golden ratio” of $2^{1/3}$ (≈ 1.26) between the two smallest sides and the two largest ones so that the largest side is $2^{2/3}$ (≈ 1.6) times longer than the shortest one. The purpose of this is to interleave the internal vibration modes so that they do not reinforce each other. It is also common to make the width of the front panel as narrow as possible (hence, there will be little in the way of modes between the side walls) and also to extend the height of the box so that the loudspeaker is floor standing. It is advisable to locate the drive unit at about one-third of the internal height from either the top or bottom so as not to coincide with the antinodes of the first or second vertical modes.

Effect of box compliance on resonance frequency and Q

Let us analyze the effect of the closed-box baffle on the lowest resonance frequency of a direct-radiator loudspeaker. For convenience, let us define a net compliance C_{AB} for a lined box:

$$C_{AB} = C_{AA} + C_{AM} \quad (7.20)$$

where C_{AM} is the compliance of the air in the lining material (we assume that it is highly porous so that it is mainly air) given by Eq. (7.6) and C_{AA} is the compliance of the remaining free space given by Eq. (7.4). Let us define an apparent box volume V_{AB} for a lined box in terms of the volume of the lining material V_M and the remaining internal free space V_A so that

$$V_{AB} = V_A + \gamma V_M \quad (7.21)$$

However, the total physical internal volume of the box V_B is

$$V_B = V_A + V_M \quad (7.22)$$

which is smaller than the apparent volume V_{AB} due to the isothermal pressure fluctuations within the lining material. For a loudspeaker mounted in an infinite baffle, the frequency for zero reactance is

$$f_{SB} = \frac{1}{2\pi\sqrt{C_{AS}(M_{AD} + 2M'_{A1})}} \quad (7.23)$$

where we have assumed that the radiation reactance X_{AR} from each side of the diaphragm equals $\omega M'_{A1}$ and that $M'_{A1} = 0.27\rho_0/a$.

From Fig. 7.6, we see that the resonance frequency f_C for the loudspeaker in a closed-box baffle with a volume less than about 200 L is

$$f_C = \frac{1}{2\pi}\sqrt{\frac{C_{AS} + C_{AB}}{C_{AS}C_{AB}(M_{AD} + M_{A1} + M_{AB})}} \quad (7.24)$$

where C_{AB} and M_{AB} are given by Eqs. (7.20) and (7.5) and M_{A1} is the radiation mass of a closed-back piston given by $M_{A1} = {}^{3/4}M'_{A1} \approx 0.2\rho_0/a$.

The ratio of (7.24) to (7.23) is equal to the ratio of the resonance frequency with the box to the resonance frequency with an infinite baffle. This ratio is

$$\frac{f_C}{f_{SB}} = \sqrt{\left(1 + \frac{C_{AS}}{C_{AB}}\right)\left(1 + \frac{2M'_{A1} - M_{A1} - M_{AB}}{M_{AD} + M_{A1} + M_{AB}}\right)}. \quad (7.25)$$

Let us assume that M_{AB} is approximately the radiation mass of a piston in an infinite baffle and that $M'_{A1} \approx 0.043M_{AD}$ so that Eq. (7.25) is approximately:

$$\frac{f_C}{f_{SB}} = \sqrt{1.01 \left(1 + \frac{C_{AS}}{C_{AB}} \right)} \quad (7.26)$$

Hence, the 1% difference in mass loading alone between the loudspeaker in a closed box and in an infinite baffle will produce a 0.5% increase in resonance frequency.

Often, it is difficult to find an “infinite” baffle in which to determine the resonance frequency. If the loudspeaker is held in free space without a baffle, the mass loading M''_{A1} on the diaphragm will be exactly one-half its value in an infinite baffle, that is, $M''_{A1} = 0.135\rho_0/a$. Hence, the ratio of the resonance frequency in the closed box f_C to the resonance frequency without baffle f_{SA} is approximately

$$\frac{f_C}{f_{SA}} = \sqrt{0.97 \left(1 + \frac{C_{AS}}{C_{AB}} \right)} \quad (7.27)$$

Ignoring the mass loading effect, the above equations for the frequency shift due to a lined box can be conveniently expressed in terms of the Thiele–Small parameters f_S and V_{AS} (IEC-baffle [1] resonance frequency and equivalent suspension volume, respectively), and the apparent box volume V_{AB} :

$$\frac{f_C}{f_S} = \sqrt{1 + \frac{V_{AS}}{V_{AB}}} \quad (7.28)$$

This equation is plotted in Fig. 7.13.

Values of radiation (front-side) impedance

Acoustical elements always give the newcomer to the field of acoustics some difficulty because they are not well behaved. That is to say, the resistances vary with frequency, and, when the wavelengths are short, so do the masses.

The radiation impedance for the radiation from the front side of the diaphragm is simply a way of indicating schematically that the air has mass, that its inertia must be overcome by the movement of the diaphragm, and that it is able to accept power from the loudspeaker. The magnitude of the front-side radiation impedance depends on whether the box is very large so that it approaches being an infinite baffle or whether the box has dimensions of less than about 0.6 by 0.6 by 0.6 m (7.6 ft³), in which case the behavior is quite different.

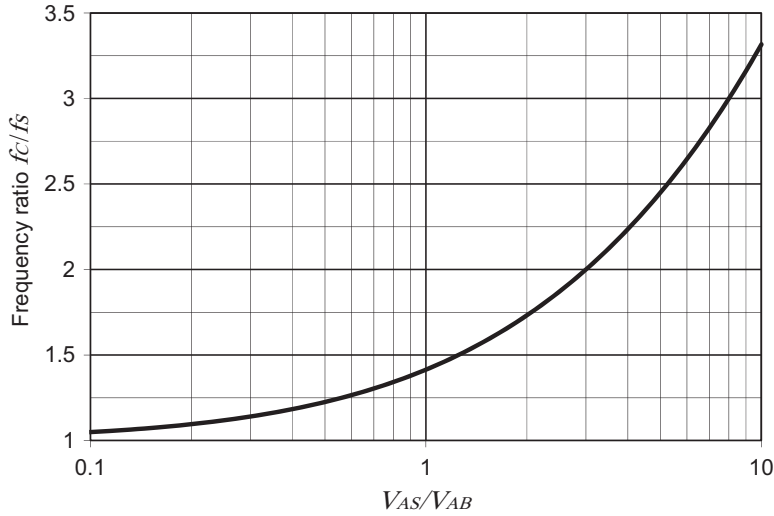


Figure 7.13 Frequency ratio f_c/f_s = ratio of the resonance frequency for a loudspeaker in a closed-box baffle to the resonance frequency for the same loudspeaker in an IEC 268-5 baffle [1].

Very large box (approximating infinite baffle)

R_{AR} is radiation resistance for a piston in an infinite baffle in $\text{N}\cdot\text{s}/\text{m}^5$. This resistance is determined from the ordinate of Fig. 4.35 multiplied by $407/S_D$. If the frequency is low, so that the effective circumference of the diaphragm ($2\pi a$) is less than λ , that is, $ka < 1$ (where $k = 2\pi/\lambda$), R_{AR} may be computed from

$$R_{AR} \approx \frac{0.159\omega^2\rho_0}{c} \approx 0.0215f^2 \quad (7.29)$$

X_{AR} is radiation reactance for a piston in an infinite baffle. This reactance is determined from the ordinate of Fig. 4.35, multiplied by $407/S_D$. For $ka < 1$, X_{AR} is given by

$$X_{AR} = \omega M_{A1} \approx \frac{0.270\omega\rho_0}{a} \approx \frac{2.0f}{a} \quad (7.30a)$$

and

$$M_{A1} = \frac{0.270\rho_0}{a} \approx \frac{0.318}{a} \quad (7.30b)$$

Small- to medium-sized box (less than 200 L)

R_{AR} is approximately the radiation impedance for a one-sided piston in free space. This resistance is determined from the ordinate of Fig. 4.39 multiplied by $407/S_D$. If the

frequency is low so that the effective circumference of the diaphragm ($2\pi a$) is less than λ , R_{AR} may be computed from

$$R_{AR} = \frac{\pi f^2 \rho_0}{c} \approx 0.01076 f^2 \quad (7.31)$$

X_{AR} is approximately the radiation reactance for a one-sided piston in free space. This reactance is determined from the ordinate of Fig. 4.39 multiplied by $407/S_D$. For $ka < 1$, X_{AR} is given by

$$X_{AR} = \omega M_{A1} \approx \frac{\omega(0.2026)\rho_0}{a} \approx \frac{1.5f}{a} \quad (7.32a)$$

and

$$M_{A1} = \frac{0.2026\rho_0}{a} \approx \frac{0.239}{a} \quad (7.32b)$$

Radiation equation

At very low frequencies where the diaphragm has not yet become a directional radiator (i.e., its circumference is less than about a wavelength), the loudspeaker in a closed-box baffle may be treated as though it were a simple spherical source of sound. We find from Eq. (4.71) that the sound pressure a distance r away from such a source in a free field is given by

$$\tilde{p}(r) = -jf\rho_0\tilde{U}_c\frac{e^{-jkr}}{2r}, \quad kR \ll 1 \quad (7.33)$$

where

\tilde{p} is sound pressure in Pa at a distance r from the loudspeaker.

$\tilde{U}_c = \tilde{u}_c S_D$ is volume velocity of the diaphragm in m^3/s .

ρ_0 is density of air in kg/m^3 (about $1.18 \text{ kg}/\text{m}^3$ for normal room conditions).

r is distance from the loudspeaker in m.

f is frequency in Hz.

$R = (3V_B/4\pi)^{1/3}$ is average dimension of the enclosure.

At higher frequencies, where the diaphragm is becoming more directional but yet is still vibrating substantially as a rigid piston, we use Eq. (13.104) for a piston in an infinite baffle. When the wavelength is small compared with the dimensions of the box, it acts as a large baffle so that the pressure at a distance r in a free field is

$$\tilde{p}(r) = -jf\rho_0\tilde{U}_c\frac{e^{-jkr}}{r}, \quad kR \gg 1 \quad (7.34)$$

Hence, there is a 6 dB lift at higher frequencies due to the baffle effect. Examples of this can be seen in Figs. 12.24 and 13.30, which show the on-axis pressure responses of a piston in a sphere and a closed-back circular baffle, respectively. If the corners of the box are square, the rise will be accompanied by some ripples in the on-axis response due to reflections from the corners. No exact solution exists for this kind of problem, although some useful approximations can be made [14–16]. Otherwise, if the corners are rounded, the transition will be smoother like that of a point source in a sphere shown in Fig. 12.15. Let us now modify Eq. (7.33) by adding an on-axis directivity function $D(0)$ so that it covers the transition region:

$$\tilde{p}(r) = -jf\rho_0\tilde{U}_c\frac{e^{-jkr}}{2r}D(0) \quad (7.35)$$

The type of approximation we use for $D(0)$ will depend on the form of the enclosure. If it is very rounded, the following expression provides a reasonably good approximation to a point source on a sphere:

$$D(0) \approx \frac{1 + jkR}{1 + jkR/2} \quad (7.36)$$

where R is the radius of the sphere and $k = 2\pi f/c$, so that the pressure magnitude is

$$|p(r)| \approx \frac{f\rho_0|U_c|}{2r} \sqrt{\frac{1 + k^2R^2}{1 + k^2R^2/4}} \quad (7.37)$$

The approximation of Eq. (7.36) is plotted in Fig. 7.14 along with the exact expression for a point source on a sphere from Eq. (12.47). For an enclosure in which the loudspeaker occupies the full width, a closed-back piston model is more appropriate, in which case

$$D(0) \approx \frac{1 - 2(ka/\sqrt{5})^2 + j2(ka/\sqrt{5})}{1 - (ka/\sqrt{5})^2 + j(ka/\sqrt{5})} \quad (7.38)$$

where a is the radius of the piston so that the pressure magnitude is

$$|p(r)| \approx \frac{f\rho_0|U_c|}{2r} \sqrt{\frac{(5 - 2k^2a^2)^2 + 20k^2a^2}{(5 - k^2a^2)^2 + 5k^2a^2}}. \quad (7.39)$$

The approximation of Eq. (7.38) is plotted in Fig. 7.15 along with the exact expression for a closed-back piston in free space from Eq. (13.253). This gives a more rapid 6 dB transition than the point source on a sphere. Because most drive units are designed to have as flat a response as possible in a flat baffle, the only way to correct for

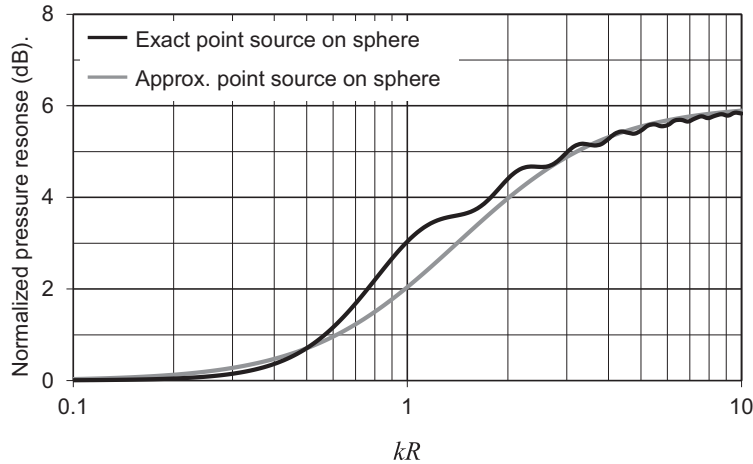


Figure 7.14 Plot of $20 \log_{10} D(0)$ for a point source in a sphere of radius R , which is used to model the baffle effect of a loudspeaker in a rounded closed-box baffle with constant diaphragm acceleration. The *black curve* shows the exact result from Eq. (12.47) and the *gray curve* shows the approximation from Eq. (7.36).

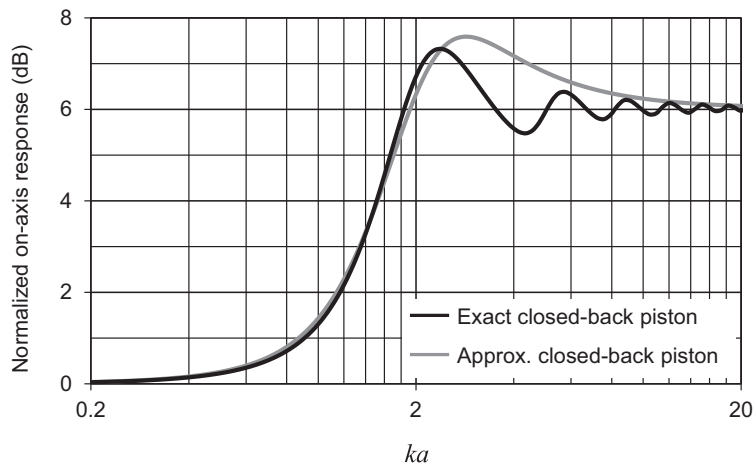


Figure 7.15 Plot of $20 \log_{10} D(0)$ for a closed-back piston of radius a in free space, which is used to model the baffle effect of a loudspeaker in a narrow closed-box baffle with constant diaphragm acceleration. The *black curve* shows the exact result from Eq. (13.253) and the *gray curve* shows the approximation from Eq. (7.38). It is interesting to note that the exact on-axis response of the closed-back piston is obtained from the sum of the on-axis responses of a free piston and a piston in an infinite baffle, where the latter is just unity under constant acceleration. The on-axis response of a free piston is simply the magnitude of its radiation impedance shown in Fig. 4.38.

this 6 dB lift is to include the inverse of the function $D(0)$ in the crossover network as will be discussed in Section 7.20. At even higher frequencies, the on-axis response starts to roll off, even if the diaphragm is rigid and perfectly well behaved, because of the cone shape, which can be thought of as an approximate concave dome. See Fig. 12.32. The roll-off is somewhat irregular due to “cup” resonances. The directivity pattern then becomes constant with an angle of dispersion that corresponds to the arc angle of the concave dome, as shown in Fig. 12.31.

Diaphragm volume velocity \tilde{U}_c

We determine the volume velocity \tilde{U}_c from Fig. 7.6:

$$\tilde{U}_c = \frac{\tilde{e}_g B l}{S_D (R_g + R_E) \left(\frac{B^2 l^2}{(R_g + R_E) S_D^2} + R_A + j X_A \right)} \quad (7.40)$$

where, from Fig. 7.6,

$$R_A = R_{AS} + \mathbf{R}_{AB} + \mathbf{R}_{AR} \quad (7.41)$$

$$X_A = \omega M_A - 1/(\omega C_A) \quad (7.42)$$

$$M_A = M_{AD} + M_{A1} + M_{AB} \quad (7.43)$$

$$C_A = \frac{C_{AS} C_{AB}}{(C_{AS} + C_{AB})} \quad (7.44)$$

The radiation mass and resistance \mathbf{R}_{AR} and M_{A1} are generally given by Eqs. (7.31) and (7.32) but for very large boxes or for infinite baffles are given by Eqs. (7.29) and (7.30).

In an effort to simplify Eq. (7.40), let us define a Q_{TC} in the same manner as we do for electrical circuits. First, let us set

$$\omega_C = 2\pi f_C = \frac{1}{\sqrt{M_A C_A}} \quad (7.45)$$

where ω_C = angular resonance frequency for zero reactance. Then,

$$Q_{EC} = \frac{(R_g + R_E) S_D^2}{B^2 l^2} \sqrt{\frac{M_A}{C_A}} \quad (7.46)$$

$$Q_{MC} = \frac{1}{R_A} \sqrt{\frac{M_A}{C_A}} \quad (7.47)$$

$$Q_{TC} = \frac{Q_{EC}Q_{MC}}{Q_{EC} + Q_{MC}} \quad (7.48)$$

so that we can write

$$\tilde{U}_c = \frac{S_D \tilde{e}_g}{BlQ_{EC}} B_C(f) \quad (7.49)$$

where the frequency-response function $B_C(f)$ is given by

$$B_C(f) = \frac{j \frac{f}{f_C}}{1 - \frac{f^2}{f_C^2} + j \frac{1}{Q_{TC}} \cdot \frac{f}{f_C}} \quad (7.50)$$

This has the same form as $\beta_c(f)$ in Eq. (6.7) for a loudspeaker in an infinite baffle, which is plotted in Fig. 6.5, except that the parameters have been modified by the enclosure.

Reference volume velocity and sound pressure

A reference diaphragm volume velocity is arbitrarily defined here by the equation

$$U_{c(\text{rms})} = \frac{e_{g(\text{rms})} Bl S_D}{(R_g + R_E) \omega M_M} \quad (7.51)$$

where we have set the total mass to $M_A = M_M / S_D^2$. This reference volume velocity is equal to the actual volume velocity above the resonance frequency under the special condition that R_A^2 of Eq. (7.41) is small compared with $\omega^2 M_A^2$. This reference volume velocity is consistent with the efficiency defined in Section 6.9.

The reference sound pressure at low frequencies, where it can be assumed that there is unity directivity factor, is found from Eqs. (7.33) and (7.51):

$$p_{\text{rms}} = \frac{e_{g(\text{rms})} Bl S_D \rho_0}{(R_g + R_E) M_M 4\pi r} \quad (7.52)$$

It is emphasized that the reference sound pressure will not be the actual sound pressure in the region above the resonance frequency unless the motion of the diaphragm is mass-controlled and unless the directivity factor is nearly unity. The reference pressure is, however, a convenient way of locating “zero” decibels on a relative SPL response curve, and this is the reason for defining it here.

Radiated sound pressure for $ka < 1$

The radiated sound pressure in the frequency region where the circumference of the diaphragm ($2\pi a$) is less than a wavelength (i.e., where there is negligible directivity) is found by inserting the volume velocity from Eqs. (7.49) and (7.50) into Eq. (7.33) so that

$$\tilde{p}(r) = -\frac{\tilde{e}_g B l S_D \rho_0}{(R_g + R_E) M_M} \cdot \frac{e^{-jkr}}{4\pi r} \alpha_C(f), \quad kR \ll 1 \quad (7.53)$$

where $\alpha_C(f)$ is a frequency-response function in the form of a second-order high-pass filter which is proportional to the acceleration of the cone. It is defined by

$$\alpha_C(f) = \frac{\frac{-f^2}{f_C^2}}{1 - \frac{f^2}{f_C^2} + j \frac{1}{Q_{TC}} \cdot \frac{f}{f_C}} \quad (7.54)$$

Notice that Eq. (7.53) is very similar to Eq. (6.32) for the sound pressure radiated from a loudspeaker in an infinite baffle, the only difference being the factor of 4 in the denominator instead of 2. The reason for this is that the sound pressure is doubled when radiating into half space instead of whole space. Otherwise, there are very little differences in the reference sensitivity apart from that due to the change in mass loading when the loudspeaker is mounted in the enclosure. However, this will be negligible in most cases. Similarly, the sensitivity is the same as that given in Eq. (6.33) but with a factor of 4 in the denominator:

$$\text{Sensitivity} = 20 \log_{10} \left(\frac{\sqrt{Z_{\text{nom}}} W_E B l S_D \rho_0}{4\pi r (R_g + R_E) M_M \times 20 \times 10^{-6}} \right) \text{dB SPL/W/m} \quad (7.55)$$

Alignments for predetermined frequency-response shapes

The normalized SPL is plotted in Fig. 7.16 using $20 \log_{10} |\alpha_C|$ from Eq. (7.54). Note that at the resonance frequency f_C , the SPL is simply $20 \log_{10} Q_{TC}$ so that it is 6 dB for $Q_{TC} = 2$, 3 dB for $Q_{TC} = \sqrt{2}$, 0 dB for $Q_{TC} = 1$, and so forth.

We should observe that, even in the frequency range where the diaphragm diameter is less than one-third wavelength, the value of Q_{TC} is not strictly constant because R_{AR} increases with the square of the frequency. In using Eq. (7.54) and Fig. 7.16, therefore, R_A in Q_{TC} probably ought to be calculated as a function of ω/ω_C . Usually, however, the value of R_A at ω_C is the only case for which calculation is necessary.

The curve for $Q_{TC} = 1/\sqrt{2}$, also known as critical damping, has a Butterworth high-pass frequency-response shape. It gives the flattest possible response down to f_C where it is 3 dB below the passband level. Hence, we see that we can choose a

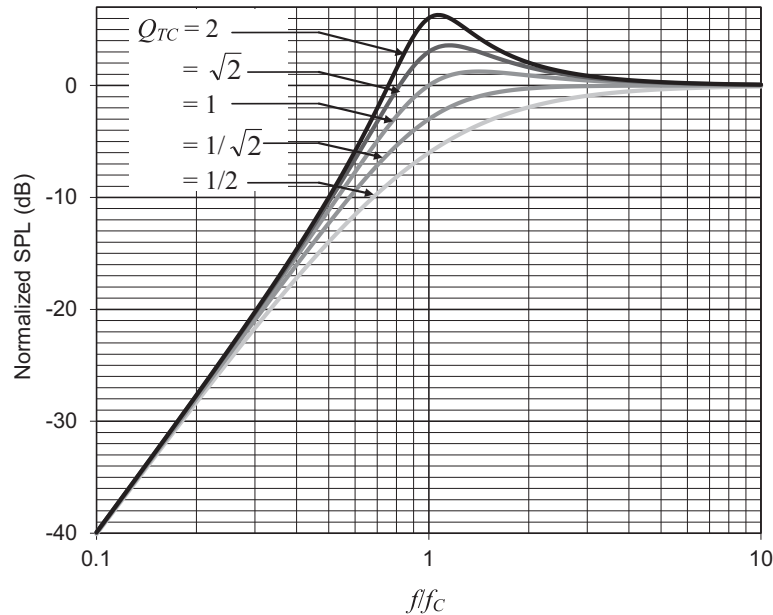


Figure 7.16 Normalized sound pressure level (SPL) response of a loudspeaker in a closed box at low frequencies using $20 \log_{10} |\alpha_C|$ from Eq. (7.54). An infinite baffle or a closed-box enclosure is assumed. Q_{TC} is the same as Q_{TC} of Eq. (7.48), and ω_C is found from Eq. (7.45). The graph applies only to the frequency range where the wavelengths are greater than about three times the advertised diameter of the diaphragm.

frequency-response shape and engineer the loudspeaker accordingly. Instead of defining the shape by the Q_{TC} factor, which only tells us the magnitude at the resonance frequency f_C , it is more convenient to define the largest amount of deviation from the flat level that we wish to allow, or ripple factor, in dB. Chebyshev alignments are defined in this way, and the Q_{TC} values needed for various ripple factors are given in Table 7.2. These are calculated from the formulae given in Appendix I. Small loudspeakers are often deliberately designed with a peak in the bass response to make them sound more impressive on first hearing and thus compensate for the lack of deep bass. On the other hand, if this is overdone, the effect of the poor transient response (see Section 6.17), with the resulting “one note” bass, can be fatiguing. For larger loudspeakers with more extended bass, the Bessel frequency-response shape, which has a maximally linear phase response, offers a useful compromise between bass extension and good transient response. If the loudspeaker is to be situated in a relatively small listening room where the low frequencies are likely to be augmented by room modes, then a gentle roll-off is desirable, as provided by the synchronous shape, which has two real coincident poles. In this case, a relatively small room is one in which the largest dimension is less than 6 m.

Table 7.2 Resonance frequencies and Q values for various second-order frequency-response shapes.

Frequency-response shape	f_{3dB}/f_C	Q_{TC}
Synchronous	1.5538	0.5000
Bessel	1.2720	0.5774
Butterworth	1.0000	0.7071
Chebyshev with 0.1 dB ripple	0.93682	0.76736
Chebyshev with 0.5 dB ripple	0.88602	0.86372
Chebyshev with 1.0 dB ripple	0.86234	0.9565
Chebyshev with 2.0 dB ripple	0.84461	1.1287
Chebyshev with 3.0 dB ripple	0.84090	1.3047
Chebyshev with 4.0 dB ripple	0.84312	1.4934
Chebyshev with 5.0 dB ripple	0.84842	1.6996
Chebyshev with 6.0 dB ripple	0.85544	1.9269

Referring back to Eq. (6.115), we find that we suggested for satisfactory transient response that $\omega_S/(2Q_{TS}) > 92 \text{ s}^{-1}$. Let us see what this means in terms of Q_{TC} .

In terms of Q_{TC} , the suggested criterion for satisfactory transient response is

$$Q_{TC} < \frac{\omega_C}{184} \quad (7.56)$$

As an example, if $\omega_C = 2\pi f_C = 2\pi 40 = 251 \text{ rad/s}$, then Q_{TC} should be less than 1.37. This would mean that the peak in the response curve must be less than 2.7 dB. Methods for achieving desired Q_{TC} values will be discussed as part of the example below.

Setting the value of Q_{TC} and determination of the total box volume V_T

The Q_{TC} of a loudspeaker in a closed box is never the same as its free-space Q_{TS} unless the box is extremely large and empty. However, it is the closed-box Q_{TC} which determines the final frequency-response shape. Its value obviously depends on the inherent mechanical resistance [see Q_{MC} from Eq. (7.47)] and electrical damping [see Q_{EC} from Eq. (7.46)] of the drive unit, which we cannot change very easily in the case of a passive loudspeaker design except through the choice of drive unit. However, we can control the box volume and filling material. If we ignore the acoustic mass loading effect so that $M_A = S_D^2 M_{MS}$, the ratio of Q_{TC} to Q_{TS} is found from Eqs. (7.48) and (6.9):

$$\frac{Q_{TC}}{Q_{TS}} = \frac{\frac{B^2 l^2}{R_g + R_E} + R_{MS}}{\frac{B^2 l^2}{R_g + R_E} + R_{MS} + R_{MB}} \sqrt{1 + \frac{C_{AS}}{C_{AB}}} \quad (7.57)$$

Let us define Q_{MB} for the box:

$$Q_{MB} = \frac{1}{R_{MB}} \sqrt{\frac{M_{MS}}{C_{MS}}} = \frac{\rho_0 c^2}{R_{AB} \omega_S V_{AS}} \quad (7.58)$$

where R_{AB} is calculated from Eq. (7.7). Hence,

$$\frac{Q_{TC}}{Q_{TS}} = \frac{\frac{1}{Q_{ES}} + \frac{1}{Q_{MS}}}{\frac{1}{Q_{ES}} + \frac{1}{Q_{MS}} + \frac{1}{Q_{MB}}} \sqrt{1 + \frac{V_{AS}}{V_{AB}}} \quad (7.59)$$

where $V_{AB} = V_A + \gamma V_M$, which is solved for V_A to yield

$$V_A = V_{AB} - \gamma V_M = \frac{V_{AS}}{Q_{TC}^2 \left(\frac{1}{Q_{TS}} + \frac{1}{Q_{MB}} \right)^2 - 1} - \gamma V_M \quad (7.60)$$

where V_M is the volume of the lining material and V_A the remaining free space. Although a value of V_A is required to calculate R_{AB} from Eq. (7.7), a first approximation is given by letting $Q_{MB} = \infty$ so that

$$V_A \approx \frac{V_{AS}}{(Q_{TC}/Q_{TS})^2 - 1} - \gamma V_M \quad (7.61)$$

The total internal volume of the box is then $V_B = V_A + V_M$.

Cone displacement

The first time integral of the velocity from Eqs. (7.49) and (7.50) gives the displacement:

$$\tilde{\eta}_C = \frac{\tilde{u}_C}{j\omega} = \frac{\tilde{U}_C}{j\omega S_D} = \frac{\tilde{e}_g}{\omega_C B l Q_{EC}} \gamma_C(f) \quad (7.62)$$

where $\gamma_C(f)$ is a dimensionless frequency-response function given by

$$\gamma_C(f) = \frac{1}{1 - \frac{f^2}{f_C^2} + j \frac{1}{Q_{TC}} \cdot \frac{f}{f_C}} \quad (7.63)$$

This is plotted in Fig. 7.17. At very low frequencies, we have

$$\tilde{\eta}_0 = \frac{\tilde{e}_g}{\omega_C B l Q_{EC}} = \frac{\tilde{e}_g}{\omega_S B l Q_{ES} (1 + V_{AS}/V_{AB})} \quad (7.64)$$

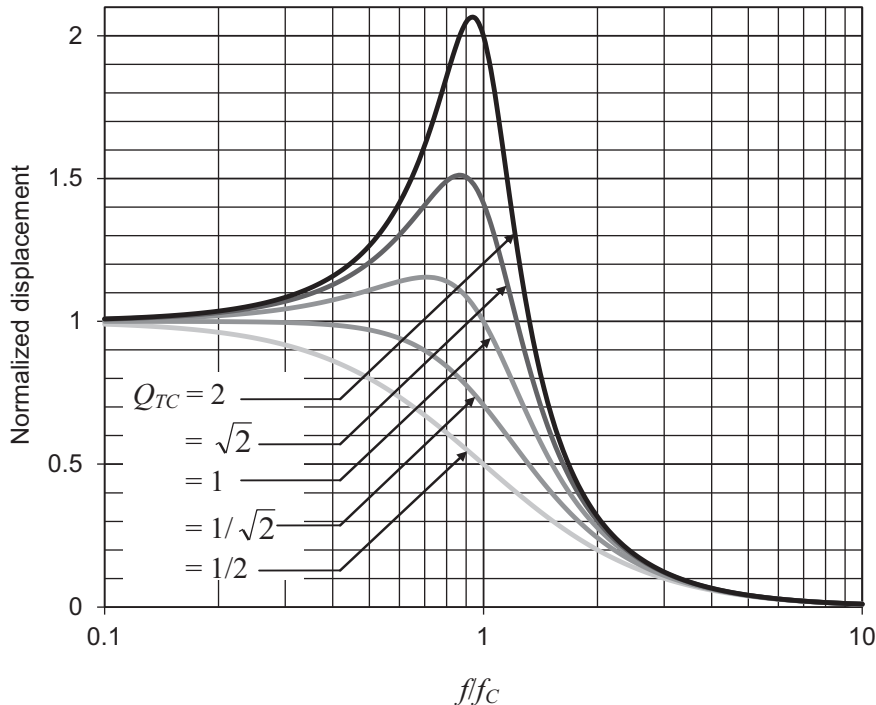


Figure 7.17 Normalized cone displacement of a loudspeaker in a closed box at low frequencies using $|\gamma_C(f)|$ from Eq. (7.63). Q_{TC} is the same as Q_{TC} of Eq. (7.48), and ω_C is found from Eq. (7.45).

Hence, reducing the size of the box reduces the amount of displacement at low frequencies below ω_C and thus enables greater sound pressure to be obtained at higher frequencies above ω_C with less risk of displacement limiting due to the low frequencies present. On the other hand, reducing the box volume raises ω_C and therefore reduces the sound pressure at low frequencies, so a compromise has to be reached somewhere.



7.7 MEASUREMENT OF BAFFLE CONSTANTS

The constants of the baffle may be measured after the loudspeaker constants are known. Refer to Fig. 7.6. The quantities R_{AR} and X_{AR} are determined from Eqs. (7.31) and (7.32). The electrical and mechanical quantities are measured directly.

Measurement of C_{AB}

Using the same procedure as for measuring f_S and Q_{EC} in Section 6.10, determine a new f_C and Q_{EC} and solve for C_{AB} from Eq. (6.71) so that

$$C_{AB} = \frac{V_{AS}}{\rho_0 c^2 \left(\frac{f_C Q_{EC}}{f_S Q_{ES}} - 1 \right)} \quad (7.65)$$

Measurement of R_{AB}

Using the same procedure as for measuring Q_{ES} and Q_{MS} in Section 6.10, determine a new Q_{EC} and Q_{MC} and solve for R_{AB} from

$$R_{AB} = \frac{\omega_C(M_{AD} + M_{A1} + M_{AB})}{Q_{MC}} - (R_{AS} + R_{AR})$$

where $M_{AD} = M_{MD}/S_D^2$; M_{A1} is given by Eq. (7.32b), and

$$R_{AS} + R_{AR} = \frac{R_{MS} + R_{MR}}{S_D^2}$$

Example 7.1. Miniature loudspeaker. A miniature loudspeaker intended for use in mobile products has the Thiele–Small parameters given below:

$$R_E = 7.2 \Omega$$

$$Q_{ES} = 2.05$$

$$Q_{MS} = 3.48$$

$$f_S = 476 \text{ Hz}$$

$$S_D = 1.40 \text{ cm}^2$$

$$V_{AS} = 4.81 \text{ cm}^3$$

It is assumed that the loudspeaker will be used mainly near a large flat surface such as a table.

Determine the reference sound pressure at a distance of 0.1 m for 0.5 W input.

Determine the percentage shift in the first resonance frequency of the loudspeaker from the value for an infinite baffle if an unlined box having a volume of 1 cm^3 is used.

Determine the sound pressure at the closed-box resonance frequency, assuming $R_{AB} = 0$.

Determine the volume of a box that will cause a shift in infinite baffle resonance frequency of only 25%.

Determine the sound pressure at the closed-box resonance frequency for the box of (c).

Solution 1. To calculate the maximum SPL, we first obtain C_{MS} , M_{MS} , and Bl from Eqs. (6.27), (6.28), and (6.30), respectively:

$$C_{MS} = \frac{4.81 \times 10^{-6}}{(1.40 \times 10^{-4})^2 \times 1.18 \times 345^2} = 1.75 \text{ mm/N}$$

$$M_{MS} = \frac{1}{(2 \times 3.14 \times 476)^2 \times 0.00175} = 64 \text{ mg}$$

$$Bl = \sqrt{\frac{7.2}{2 \times 3.14 \times 476 \times 2.05 \times 0.00175}} = 0.82 \text{ T} \cdot \text{m}$$

From Eq. (6.33), we obtain the reference sound pressure:

$$20 \log_{10} \left(\frac{\sqrt{8} \times 0.5 \times 0.82 \times 1.401 \times 10^{-4} \times 1.18}{2 \times 3.14 \times 0.1 \times 7.2 \times 64 \times 10^{-6} \times 20 \times 10^{-6}} \right) = 93.4 \text{ dB SPL}$$

Solution 2. From Eq. (7.28), we obtain the closed-box resonance frequency:

$$f_C = f_S \sqrt{1 + \frac{V_{AS}}{V_B}} = 476 \times \sqrt{1 + \frac{4.81}{1}} = 1147 \text{ Hz}$$

Solution 3. The sound pressure at resonance is simply increased by a factor of Q_{TC} compared with the reference level. From Eq. (6.10), $Q_{TS} = 2.05 \times 3.48 / (2.05 + 3.48) = 1.29$. At resonance,

$$Q_{TC} = \frac{f_C}{f_S} Q_{TS} = \frac{1147}{476} \times 1.29 = 3.11$$

Then the sound pressure is simply $93.4 + 20 \log_{10} 3.11 = 103.3$ dB SPL.

Solution 4. We rearrange the equation of part 2 of the solution to obtain

$$V_B = \frac{V_{AS}}{(f_C/f_S)^2 - 1}$$

so that for a 25% shift in resonance frequency, where $f_C/f_S = 1.25$ or $f_C = 595$ Hz, we have

$$V_B = \frac{4.81}{1.25^2 - 1} = 8.55 \text{ cm}^2$$

which is too large a volume for most mobile products and, in any case, the diaphragm displacement becomes unacceptably large because of the greater compliance of air in the larger box.

Solution 5. Using the same procedure as in part 3 of the solution, we obtain the sound pressure at the new resonance frequency of 595 Hz:

$$93.4 + 20 \log_{10} \left(\frac{595}{476} \times 1.29 \right) = 97.6 \text{ dB SPL}$$

Example 7.2. Low-frequency loudspeaker (woofer). Design a loudspeaker to be used with a 600-Hz crossover network and which is intended for use in a small- to medium-sized room where the bass response will be augmented by room modes. A maximum sound pressure of 99 dB SPL will be sufficient. Let us choose the Bandor type 100DW/8A drive unit which has a 6-in. diameter aluminum cone that is free from

resonances until well above the crossover frequency. The Thiele–Small parameters are as follows:

$$R_E = 6.27 \, \Omega$$

$$Q_{ES} = 0.55$$

$$Q_{MS} = 2.2$$

$$f_S = 39 \, \text{Hz}$$

$$S_D = 120 \, \text{cm}^2$$

$$V_{AS} = 21.6 \, \text{L}$$

which gives a Q_{TS} value of

$$Q_{TS} = \frac{Q_{ES}Q_{MS}}{Q_{ES} + Q_{MS}} = 0.44$$

For a small listening room, we desire a smooth low-frequency roll-off, so we choose the Butterworth alignment from Table 7.2, which returns a Q_{TC} value of $1/\sqrt{2}$ and gives a good transient response without ringing. The frequency-response shape for this value is shown in Fig. 7.16. However, to reuse this design with a bass-reflex port in a future example, we set $Q_{TC} = 0.7$, which is close enough. In addition, we will not fill the box completely with lining material because this would kill the bass-reflex resonance when the port is added. Therefore, we set the volume of the lining material to be one-third of that of the remaining free space or one-quarter of the total volume. That is, $V_M = V_A/3 = V_B/4$ because $V_B = V_A + V_M$. We estimate V_A from Eq. (7.61):

$$V_A \approx \frac{V_{AS}}{(1 + \gamma/3)(Q_{TC}^2/Q_{TS}^2 - 1)} = \frac{21.6}{(1 + 1.4/3)(0.7^2/0.44^2 - 1)} = 9.6 \, \text{L}$$

and $V_M = 9.6/3 = 3.2 \, \text{L}$, which we use to compute R_{AB} from Eq. (7.7), where $C_{AA} = V_A/(\gamma P_0)$. First though, we have to calculate $R_{AM} = R_f d/(3S_M)$, where R_f is the flow resistance of the lining material chosen such that $R_f d/3 = \rho_0 c = 412 \, \text{rayl}$, which is the impedance of free space and thus provides optimum sound absorption at higher frequencies. In addition, S_M is the area of the lining material, which in this case is the area of the back panel given by $S_M = lxy = 0.15 \times 0.3175 = 0.04763 \, \text{m}^2$, so that $R_{AM} = 412/0.047625 = 8651 \, \text{N} \cdot \text{s}/\text{m}^5$. We just need to find the internal depth lz from the volume after computing the following from Eq. (7.7)

$$\begin{aligned} R_{AB} &\approx \frac{8651}{\left(1 + \frac{3}{1.4}\right)^2 + \left(2 \times 3.14 \times \frac{0.7}{0.44} \times 39\right)^2 \times 8651^2 \times \left(\frac{0.0096}{1.4 \times 10^5}\right)^2} \\ &= 871 \, \text{N} \cdot \text{s}/\text{m}^5 \end{aligned}$$

Then, from Eq. (7.58), the box Q is determined:

$$Q_{MB} = \frac{1.18 \times 345^2}{871 \times 2 \times 3.14 \times 39 \times 0.0216} = 30.5$$

so that after inserting this into Eq. (7.60) we obtain the air volume:

$$\begin{aligned} V_A &= \frac{V_{AS}}{\left(1 + \frac{\gamma}{3}\right) \left\{ Q_{TC}^2 \left(\frac{1}{Q_{TS}} + \frac{1}{Q_{MB}} \right)^2 - 1 \right\}} \\ &= \frac{21.6}{\left(1 + \frac{1.4}{3}\right) \left\{ 0.7^2 \left(\frac{1}{0.44} + \frac{1}{30.5} \right)^2 - 1 \right\}} = 9.15 \text{ L} \end{aligned}$$

from which $V_M = 9.15/3 = 3.05$ L, $V_B = 9.15 + 3.05 = 12.2$ L, and $V_{AB} = 9.15 + (1.4 \times 3.05) = 13.42$ L. The internal depth is then $l_z = V_A/S_M = 0.00915/0.04763 = 0.192$ m. The box is shown in Fig. 7.18. The internal width l_x is 15 cm, which is the smallest width that will accommodate the drive unit. The acoustic center of the drive unit is about one-third of the internal height from the bottom so as not to coincide with the antinodes of the first or second vertical modes. The box contains one 31.8 by 15 by 6.4 cm piece of lining material. From Eq. (7.28), we obtain the closed-box resonance frequency:

$$f_C = \sqrt{1 + \frac{21.6}{13.42}} \times 39 = 63 \text{ Hz}$$

From Table 7.2, we see that the cutoff frequency is $f_{3dB} = 1 \times 63 = 63$ Hz. From Eq. (6.48), we can calculate the reference efficiency, noting that a loudspeaker in a box is half as efficient as one radiating from both sides in an infinite baffle:

$$E_{ff} = 100 \frac{8 \times 3.14^2 \times 0.0216 \times 39^3}{2 \times 0.55 \times 345^3} = 0.224\%$$

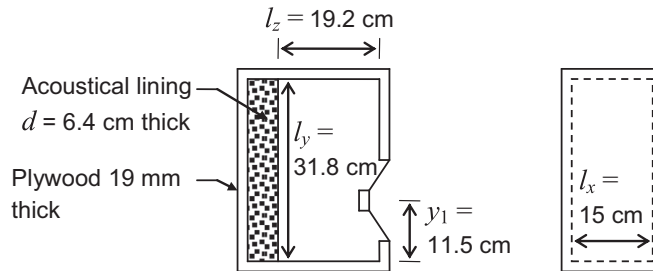


Figure 7.18 Example of closed-box enclosure design.

To calculate the maximum SPL, we first obtain C_{MS} , M_{MS} , and Bl from Eqs. (6.27), (6.28), and (6.30), respectively:

$$C_{MS} = \frac{0.0216}{0.012^2 \times 1.18 \times 345^2} = 1.07 \text{ mm/N}$$

$$M_{MS} = \frac{1}{(2 \times 3.14 \times 39)^2 \times 0.00107} = 0.0156 \text{ kg}$$

$$Bl = \sqrt{\frac{6.27}{2 \times 3.14 \times 39 \times 0.55 \times 0.00107}} = 6.59 \text{ T}\cdot\text{m}$$

Knowing that the power rating W_{\max} is 100 W, we obtain from Eq. (6.33)

$$\text{SPL}_{\max} = 20 \log_{10} \left(\frac{\sqrt{6.27 \times 100} \times 6.59 \times 0.012 \times 1.18}{4 \times 3.14 \times 6.27 \times 0.0156 \times 20 \times 10^{-6}} \right) = 99.6 \text{ dB SPL @ 1 m}$$

where a drive unit in a box produces the half the pressure of one in an infinite baffle. Next, use Eq. (7.64) to check the peak displacement at low frequencies at full power:

$$\eta_{\max} = \frac{\sqrt{2 \times 6.27 \times 100}}{2 \times 3.14 \times 39 \times 6.59 \times 0.55 \times (1 + 21.6/13.42)} = 15.3 \text{ mm}$$

but at the resonance frequency $f_C = 63 \text{ Hz}$, the maximum displacement is $Q_{TC}\eta_{\max} = 0.7 \times 15.3 = 10.7 \text{ mm}$. It turns out that the x_{\max} value of the drive unit is 14 mm, so there should be no problems with this design as most program material is above this frequency.

Let us now create a semianalytical simulation model of the design of Fig. 7.18 using two-port networks and transmission matrices, as introduced in Section 3.10 and Fig. 4.43. The schematic is shown in Fig. 7.19. Although it is based on the circuit of Fig. 7.6, a gyrator has been inserted between the electrical elements and the mechanical ones, which enables us to calculate more easily the generator current \tilde{i}_g from which we obtain the electrical impedance. We are ignoring the generator impedance R_g because in the experimental setup this is negligible compared with R_E . The dashed boxes are lumped-element two-port networks and the solid boxes are analytical ones. From the schematic, we create the transmission matrices required to represent each two-port network as follows:

1. *Coil.*

$$\begin{bmatrix} \tilde{e}_g \\ \tilde{i}_g \end{bmatrix} = \begin{bmatrix} 1 & Z_E \\ 0 & 1 \end{bmatrix} \cdot \begin{bmatrix} \tilde{e}_1 \\ \tilde{i}_1 \end{bmatrix} = \mathbf{C} \cdot \begin{bmatrix} \tilde{e}_1 \\ \tilde{i}_1 \end{bmatrix}$$

where $Z_E = R_E + j\omega L_E$

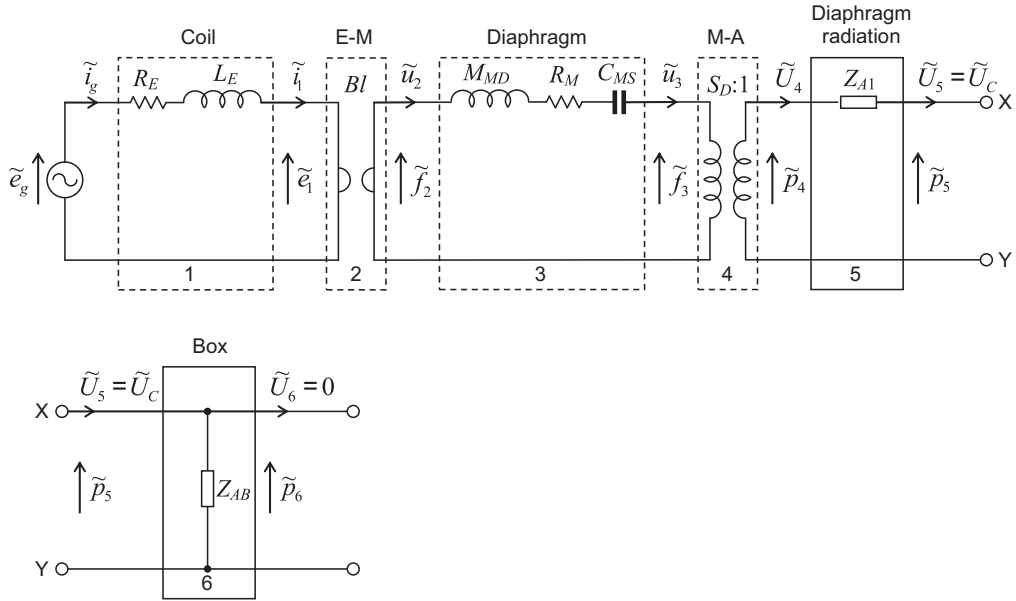


Figure 7.19 Semianalytical model of example closed-box enclosure design shown in Fig. 7.18, using transmission matrices. The dashed boxes are lumped-element two-port networks, and the solid boxes are analytical ones.

2. Electromechanical transduction.

$$\begin{bmatrix} \tilde{e}_1 \\ \tilde{i}_1 \end{bmatrix} = \begin{bmatrix} 0 & Bl \\ (Bl)^{-1} & 0 \end{bmatrix} \cdot \begin{bmatrix} \tilde{f}_2 \\ \tilde{u}_2 \end{bmatrix} = \mathbf{E} \cdot \begin{bmatrix} \tilde{f}_2 \\ \tilde{u}_2 \end{bmatrix}$$

3. Diaphragm.

$$\begin{bmatrix} \tilde{f}_2 \\ \tilde{u}_2 \end{bmatrix} = \begin{bmatrix} 1 & Z_{MD} \\ 0 & 1 \end{bmatrix} \cdot \begin{bmatrix} \tilde{f}_3 \\ \tilde{u}_3 \end{bmatrix} = \mathbf{D} \cdot \begin{bmatrix} \tilde{f}_3 \\ \tilde{u}_3 \end{bmatrix}$$

where $Z_{MD} = j\omega M_{MD} + R_{MS} + 1/(j\omega C_{MS})$. We must exclude the radiation mass from the diaphragm so that $M_{MD} = M_{MS} - 16\rho_0 a^3/3$, where $a = \sqrt{S_D/\pi}$.

4. Mechanoacoustical transduction.

$$\begin{bmatrix} \tilde{f}_3 \\ \tilde{u}_3 \end{bmatrix} = \begin{bmatrix} S_D & 0 \\ 0 & S_D^{-1} \end{bmatrix} \cdot \begin{bmatrix} \tilde{p}_4 \\ \tilde{U}_4 \end{bmatrix} = \mathbf{M} \cdot \begin{bmatrix} \tilde{p}_4 \\ \tilde{U}_4 \end{bmatrix}$$

5. Diaphragm radiation.

$$\begin{bmatrix} \tilde{p}_4 \\ \tilde{U}_4 \end{bmatrix} = \begin{bmatrix} 1 & Z_{A1} \\ 0 & 1 \end{bmatrix} \cdot \begin{bmatrix} \tilde{p}_5 \\ \tilde{U}_5 \end{bmatrix} = \mathbf{F} \cdot \begin{bmatrix} \tilde{p}_5 \\ \tilde{U}_5 \end{bmatrix}$$

where Z_{A1} is the acoustic-radiation impedance of the diaphragm given by Eqs. (13.116)–(13.118) with $a = \sqrt{S_D/\pi}$.

6. Box.

$$\begin{bmatrix} \tilde{p}_5 \\ \tilde{U}_5 \end{bmatrix} = \begin{bmatrix} 1 & 0 \\ Z_{AB}^{-1} & 1 \end{bmatrix} \cdot \begin{bmatrix} \tilde{p}_6 \\ \tilde{U}_6 \end{bmatrix} = \mathbf{B} \cdot \begin{bmatrix} \tilde{p}_6 \\ \tilde{U}_6 \end{bmatrix}$$

where Z_{AB} is given by Eq. (7.12) and

$$Z_s = \frac{R_f d}{3} + \frac{P_0}{j\omega d},$$

where the value of the lining flow resistance R_f is chosen such that $R_f d/3 = \rho_0 c = 412$ rayl, which is the impedance of free space and thus provides optimum sound absorption at higher frequencies. The dimensions are given in Fig. 7.18 except for $a_1 = b_1 \sqrt{S_D}$. First, we evaluate \tilde{p}_6 at the end of the chain:

$$\begin{bmatrix} \tilde{e}_g \\ \tilde{i}_g \end{bmatrix} = \mathbf{A} \cdot \begin{bmatrix} \tilde{p}_6 \\ 0 \end{bmatrix}$$

where

$$\mathbf{A} = \mathbf{C} \cdot \mathbf{E} \cdot \mathbf{D} \cdot \mathbf{M} \cdot \mathbf{F} \cdot \mathbf{B} = \begin{bmatrix} a_{11} & a_{12} \\ a_{21} & a_{22} \end{bmatrix}$$

Hence, $\tilde{p}_6 = \tilde{e}_g/a_{11}$. Then, we work backward to obtain the volume velocities we wish to evaluate. In particular, we are interested in the far-field pressure which, according to Eq. (7.33), is a function of $\tilde{U}_c = \tilde{U}_5$. This procedure is fairly straightforward and does not involve any matrix inversion. From the box matrix (6), we obtain the diaphragm volume velocity:

$$\tilde{U}_c = \tilde{U}_5 = p_6/Z_{AB}$$

To plot the normalized far-field on-axis pressure, we simply divide \tilde{U}_c by a reference volume velocity

$$\tilde{U}_{ref} = \frac{\tilde{e}_g B l S_D}{\omega M_{MS} R_E}$$

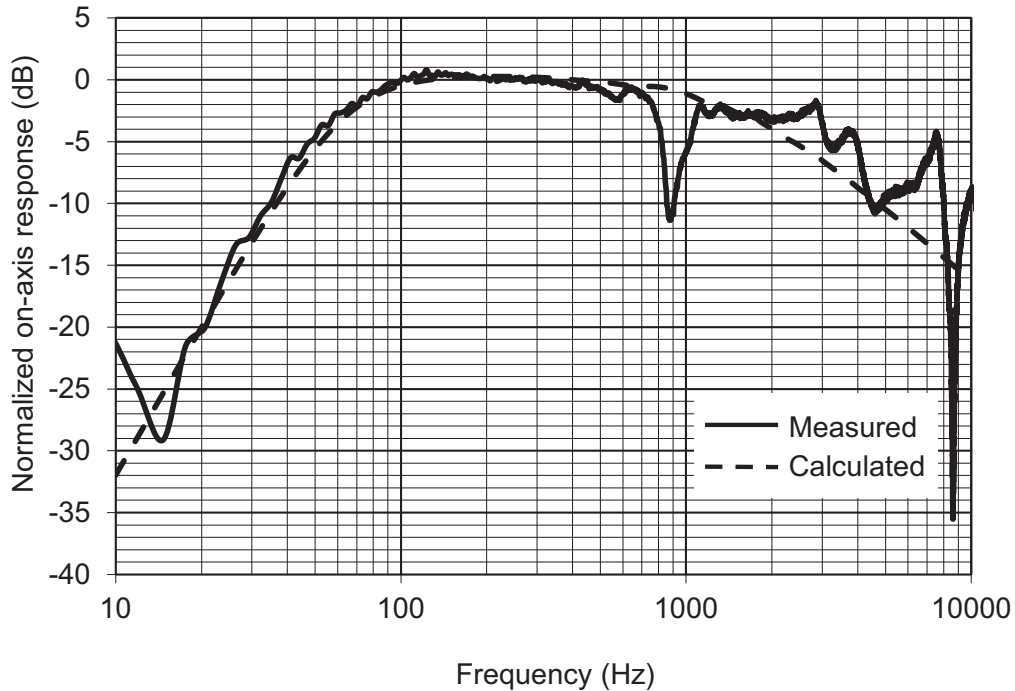


Figure 7.20 Graphs of the on-axis sound pressure level produced by the closed-box enclosure design shown in Fig. 7.18. The *dashed* curves are calculated from $20 \log_{10} |\tilde{U}_c / \tilde{U}_{ref}|$. *Solid* curves are measured.

and plot $20 \log_{10} |\tilde{U}_c / \tilde{U}_{ref}|$ as shown in Fig. 7.20. The output from the diaphragm is fairly smooth apart from one small feature at 430 Hz, which is due to the fundamental vertical mode of the box. Finally, we can obtain the input impedance from $\tilde{e}_g / \tilde{i}_g$ where $\tilde{i}_g = a_{21} \tilde{p}_6$ and from above $\tilde{p}_6 = \tilde{e}_g / a_{11}$. Therefore, the input impedance is simply $Z_E = a_{11} / a_{21}$, as plotted in Fig. 7.21.

PART XXII: BASS-REFLEX ENCLOSURES

7.8 GENERAL DESCRIPTION

The bass-reflex enclosure is a closed box in which an opening, usually called the *port*, has been made [17–26]. The area of the port is commonly made equal to or smaller than the effective area of the diaphragm of the drive unit. A common construction of this type of loudspeaker is shown in Fig. 7.22. When the diaphragm vibrates, part of its displacement compresses the air inside the box and the remainder of its displacement moves air outward through the port. Thus, the port is a second “diaphragm,” driven by

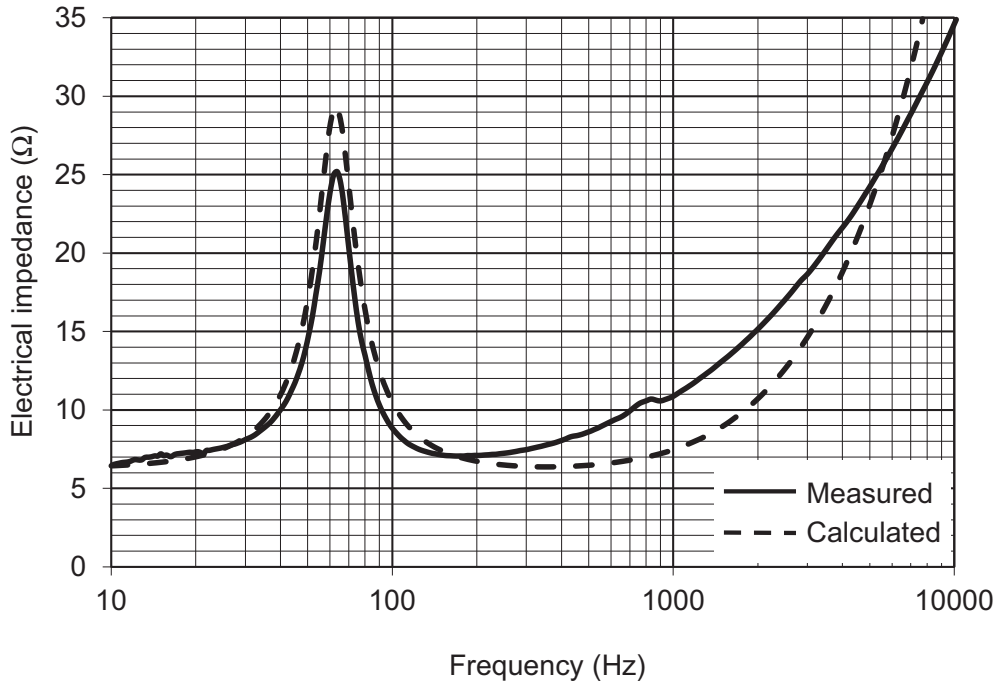


Figure 7.21 Graphs of the electrical input impedance of the closed-box enclosure design shown in Fig. 7.18. The dashed curves are calculated from $Z_E = |\tilde{e}_g/\tilde{i}_g| = a_{11}/a_{21}$. Solid curves are measured.

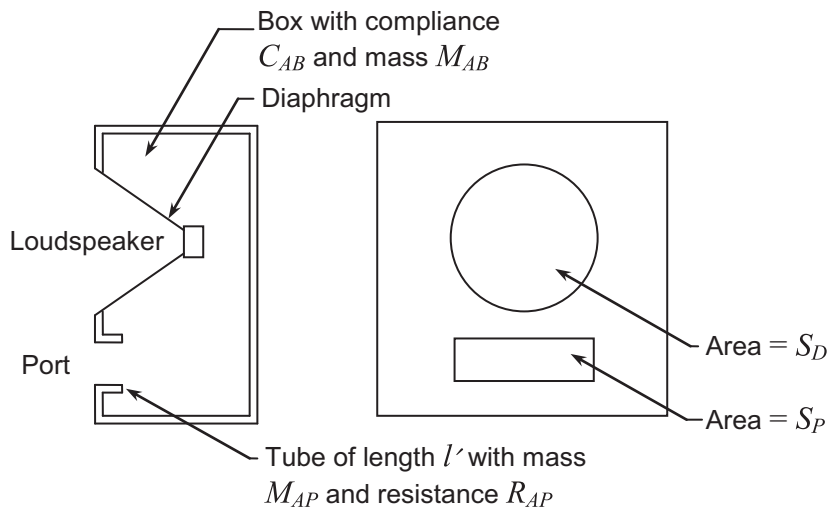


Figure 7.22 Bass-reflex baffle. The port has an area S_p , and the diaphragm has an area S_D . The inner end correction for the tube is included in the magnitude of M_{AP} .

the back side of the loudspeaker diaphragm. The port is, at low frequencies, equivalent to a short length of tube with an acoustic mass reactance and a series acoustic resistance. This tube has an end correction on the inner end and a radiation impedance on the outer, or radiating, end.

We shall assume for the remainder of this analysis that $ka < 0.5$. In other words, we are restricting ourselves to the very low-frequency region where the radiation from both the port and the loudspeaker is nondirectional.

7.9 ACOUSTICAL CIRCUIT

The acoustical circuit for the box and the port is given in Fig. 7.23. The series radiation mass and resistance on the front side of the diaphragm are, respectively, M_{A1} and R_{AR1} . The mass loading on the back side of the diaphragm is M_{AB} . The resistance due to leakage through the walls of the box, or even through a woven dust cap or gasket, is R_{AL} . The compliance and resistance of the lined box are C_{AB} and R_{AB} . The mass and resistance of the air in the port that penetrates the side of the box, including the inner end correction, are M_{AP} and R_{AP} respectively. Finally, the series radiation mass and resistance from the front side of the port are, respectively, M_{A2} and R_{AR2} . The values of these quantities are M_{AB} as in Eq. (7.5); R_{AB} as in Eq. (7.7); C_{AB} as in Eq. (7.20); M_{A2} as in Eq. (7.32), but with a_2 instead of a , that is, $M_{A2} = 0.64a_2\rho_0/(\pi a_2^2)$; R_{AR2} as in Eq. (7.31); and

M_{A1} is acoustic-radiation mass for the front side of the loudspeaker diaphragm $= 0.2026\rho_0/a \text{ kg/m}^4$. Note that we assume the loudspeaker unit is equivalent to a piston radiating from one side only in free space.

$R_{AR1} = 0.01075f^2$ is acoustic-radiation resistance for the front side of the loudspeaker diaphragm in $\text{N}\cdot\text{s/m}^5$ (see Fig. 4.39 for $ka > 1.0$).

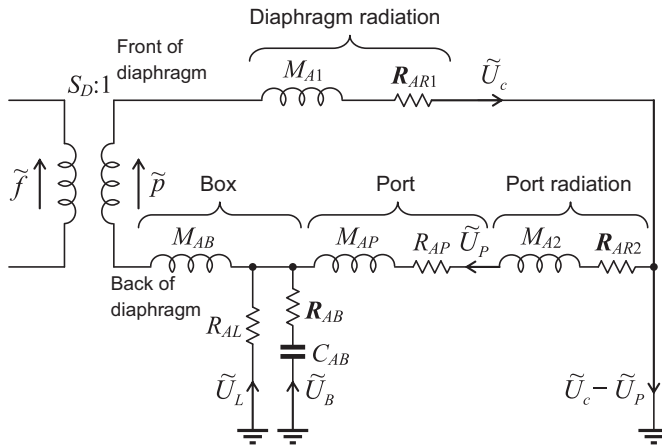


Figure 7.23 Analogous acoustical circuit for a loudspeaker box with a port. The volume velocity of the diaphragm is \tilde{U}_c , that of the port is \tilde{U}_p , that of the box is \tilde{U}_B , and that due to leakage is \tilde{U}_L .

$M_{AP} = (t + 0.64a_2)\rho_0/(\pi a_2^2)$ is acoustic mass of the air in the port in kg/m^4 . This quantity includes the inner end correction.

R_{AP} is acoustic resistance of the air in the port in $\text{N}\cdot\text{s}/\text{m}^5$. [See Eq. (4.23). Use the number (1) in the parentheses.]

ρ_0 is density of air in kg/m^3 (normally about $1.18 \text{ kg}/\text{m}^3$).

a_2 is effective radius in m of the port in the vented enclosure. If the port is not circular, then let $a_2 = \sqrt{S_p/\pi}$, where S_p is the effective area of the opening in m^2 .

$S_p = \pi a_2^2$ is effective area of the port in m^2 .

t is length of the tube or the thickness of the wall of the enclosure in which the port is cut in m.

In case, the port is composed of a number of identical small openings or tubes, the following procedure is followed.

Let N equal the number of such openings in the enclosure. For each opening, the acoustic mass and resistance including M_{A2} and R_{AR2} are as follows:

$M_A = (t + 1.7a_3)\rho_0/(\pi a_3^2) \text{ kg}/\text{m}^4$ [see Eq. (4.26)]

R_A is acoustic resistance of each opening in $\text{N}\cdot\text{s}/\text{m}^5$ [see Eq. (4.25)]

a_3 is effective radius of each opening in m.

The total acoustic mass and resistance for the N identical openings are as follows:

$M_{A2} + M_{AP} = M_A/N \text{ kg}/\text{m}^4$

$R_{AR2} + R_{AP} = R_A/N \text{ N}\cdot\text{s}/\text{m}^5$.

The directivity factor for a group of holes is about equal to that for a piston with an area equal to the area within a line circumscribing the entire group of holes.

7.10 ELECTROMECHANOACOUSTICAL CIRCUIT

The complete circuit for a loudspeaker in a bass-reflex enclosure is obtained by combining Figs. 6.4(b) and 7.23. To do this, the acoustical radiation element of the circuit labeled “ $2M_{M1}$ ” in Fig. 6.4(b) is removed, and the circuit of Fig. 7.23 is substituted in its place. The resulting circuit with the transformer removed and everything referred to the acoustical side is shown in Fig. 7.24.

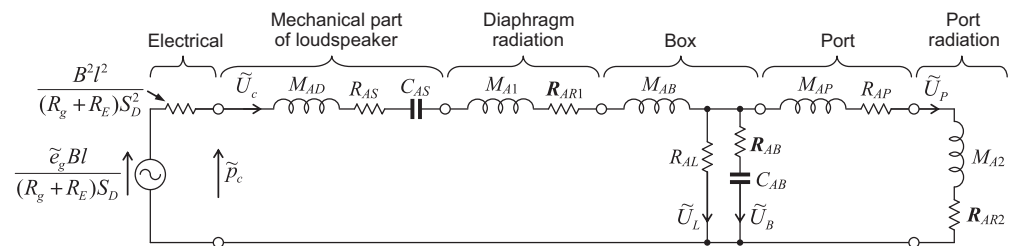


Figure 7.24 Complete electromechanoacoustical circuit for a bass-reflex loudspeaker. The total force produced at the voice coil by the electric current is $\tilde{p}_c S_D$, where S_D is the area of the diaphragm. The volume velocity of the diaphragm is \tilde{U}_c , that of the port is \tilde{U}_p , that of the box is \tilde{U}_B , and that due to leakage is \tilde{U}_L . Note that M_{AP} includes the inner mass loading for the port.

If the port is closed off so that \tilde{U}_P , the volume velocity of the air in the port, equals zero, then Fig. 7.24 essentially reduces to Fig. 7.6. At very low frequencies, the mass of air moving *out* of the lower opening is nearly equal to that moving into the upper opening at all instants. In other words, at very low frequencies, the volume velocities at the two openings are nearly equal in magnitude and opposite in phase.

Summary of bass-reflex design

To determine the cutoff frequency, frequency response, and the volume of the box:

If the Thiele–Small parameters (R_E , Q_{ES} , Q_{MS} , f_S , S_D and V_{AS}) of the chosen drive unit are not supplied by the manufacturer, they may be measured according to Section 6.10. Then $Q_{TS} = Q_{ES}Q_{MS}/(Q_{ES} + Q_{MS})$.

From Table 7.4, select the frequency-response shape for which the Q_{TS} value is closest to that of the chosen drive unit (or choose a drive unit whose Q_{TS} value is closest to that of the desired frequency-response shape).

From the values of f_{3dB}/f_S , f_B/f_S , and V_{AB}/V_{AS} given in the table, compute the cutoff frequency f_{3dB} , box resonance frequency f_B , and apparent box volume V_{AB} , respectively, from the Thiele–Small parameters f_S and V_{AS} .

The frequency-response shape below the first diaphragm break-up mode is shown in Fig. 7.26.

To determine the maximum SPL:

If the loudspeaker is to be used near a wall or a rigid planar surface, which is large compared with the longest wavelength to be reproduced, then the maximum sound pressure SPL_{max} at a distance r is obtained from Eq. (6.34) to give

$$SPL_{max} = 20 \log_{10} \left(\frac{1}{rc \times 20 \times 10^{-6}} \sqrt{\frac{Z_{nom} W_{max} 2\pi f_S^3 V_{AS} \rho_0}{R_E Q_{ES}}} \right) \text{ dB SPL @ 1 m}$$

where W_{max} is the maximum rated input power. Otherwise, if it is to be used in the free field, subtract 6 dB from SPL_{max} .

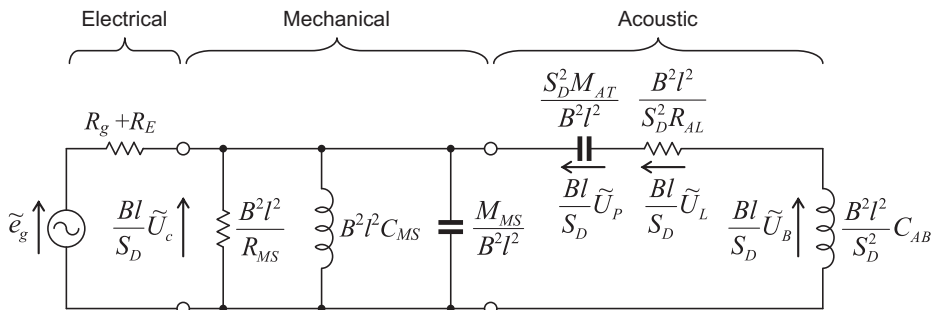


Figure 7.25 Simplification of the circuit of Fig. 7.24, where the mechanical and acoustical quantities are referred to the electrical side using the admittance type analogy.

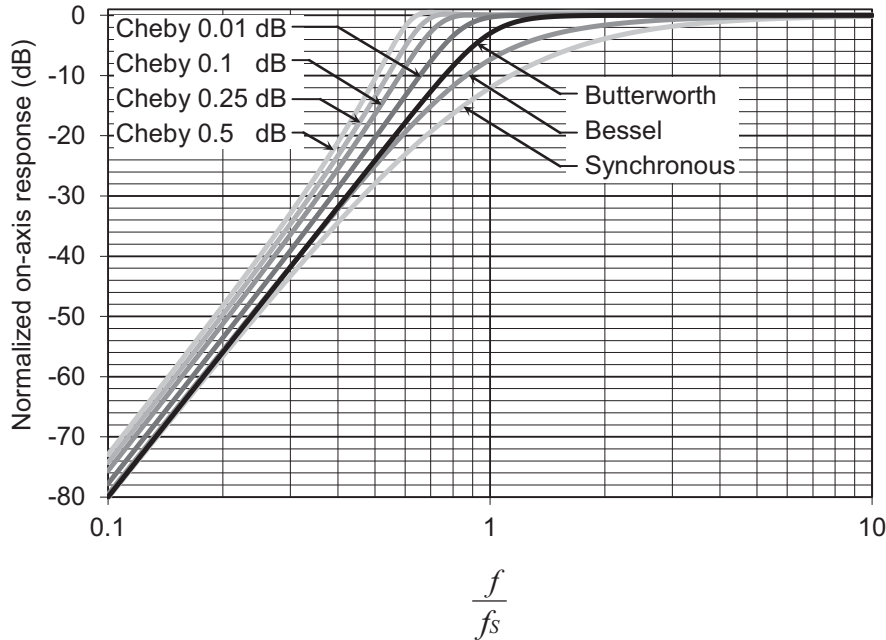


Figure 7.26 On-axis frequency responses of fourth-order bass-reflex alignments generated from Table 7.4 by taking 20 times the logarithm of Eq. (7.73).

To determine the excursion limit:

The maximum peak diaphragm displacement at frequencies well below the box resonance is obtained from Eq. (7.101) to give

$$\eta_{\max} = \frac{1}{S_{Dc}} \sqrt{\frac{Z_{\text{nom}} W_{\max} V_{AS}}{R_E Q_{ES} \pi f_s \rho_0}}$$

However, we see from Fig. 7.27 that at frequencies above the box resonance, the displacement peaks at a smaller value. For example, the displacement peaks at $0.5\eta_{\max}$ in the case of the 0.25 dB Chebyshev alignment or $0.25\eta_{\max}$ in the case of the Butterworth alignment. If this peak value is greater than the rated x_{\max} limit of the drive unit, then an alternate drive unit with a greater x_{\max} limit should be considered. If, however, the subresonance η_{\max} value is greater than the rated x_{\max} limit of the drive unit, it should be arranged for the box resonance frequency to be placed at the lower limit of the frequency range of the program material to be reproduced. If this is not possible, a high-pass filter should be employed to remove all content below the box resonance frequency. Best results are obtained when the filter is designed as part of the overall system [20,25,26]. If this is not possible either, then an alternate drive unit with a greater x_{\max} limit should be considered.

To determine the port dimensions:

The maximum peak pressure p_{\max} in Pa is obtained from SPL_{\max} using

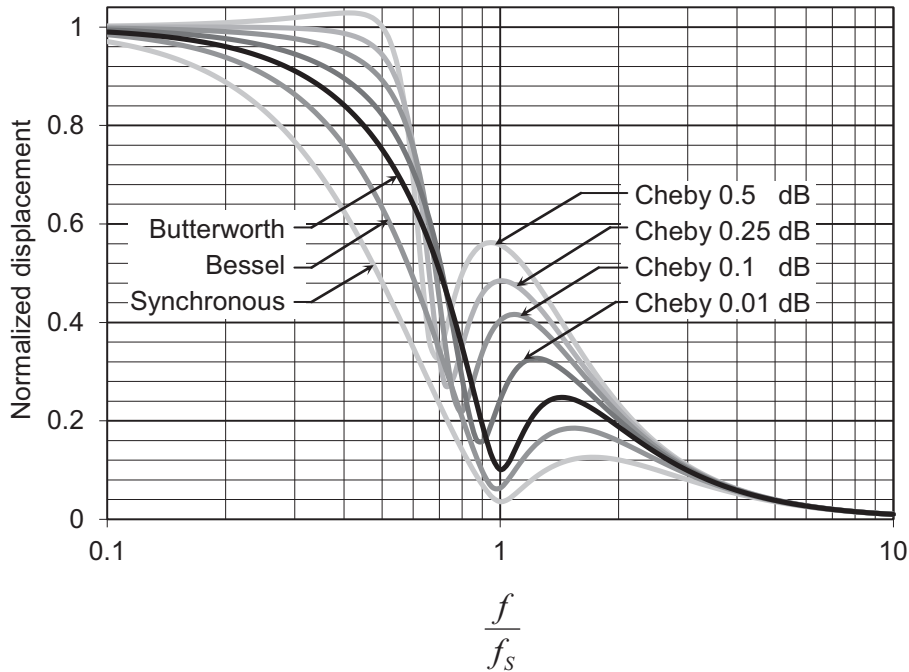


Figure 7.27 Plots of normalized displacement $\tilde{\eta}/\tilde{\eta}_0$ for the fourth-order bass-reflex alignments of Table 7.4. For simplicity, we assume that $Q_{MS} \gg Q_{ES}$ so that $Q_{ES} \approx Q_{TS}$.

$$p_{\max} = 2\sqrt{2} \times 10^{\left(\frac{\text{SPL}_{\max} - 5}{20}\right)} \text{ Pa}$$

Determine the peak volume displacement V_{\max} required to produce p_{\max} at the box resonance frequency f_B , which is obtained from Eq. (13.104) to yield

$$V_{\max} = \frac{r p_{\max}}{2\pi f_B^2 \rho_0} \text{ m}^3$$

Choose the volume of the port V_P to be several times larger than V_{\max} but within a reasonable limit. Then calculate the approximate length t of the port using Eq. (7.97) and the approximate cross-sectional area $S_P = V_P/t$. Either choose a convenient area S_P and calculate the exact length t using Eq. (7.98) or choose a convenient length t and calculate the exact area S_P using Eq. (7.99).

Study Sections 7.16 and 7.17 (pages 342–343) for construction, adjustment, and performance.

The quantities not listed in the previous paragraph are

\tilde{e}_g is open-circuit voltage in V of the audio amplifier.

B is flux density in the air gap in T (1 T = 10^4 G).

l is length in m of voice-coil wire.

R_g is output electrical resistance in Ω of the audio amplifier.

R_E is electrical resistance in Ω of the voice coil.

a is effective radius of the diaphragm in m.

$M_{AD} = M_{MD}/S_D^2$ is acoustic mass of the diaphragm and the voice coil in kg/m^4 .

$C_{AS} = C_{MS}S_D^2$ is acoustic compliance of the diaphragm suspension in m^5/N .

$R_{AS} = R_{MS}/S_D^2$ is acoustic resistance of the diaphragm suspension in $\text{N}\cdot\text{s}/\text{m}^5$.

7.11 RADIATED SOUND

The port in the box of a bass-reflex baffle is generally effective only at fairly low frequencies. At those frequencies, its dimensions are generally so small that it can be treated as though it were a simple source. The loudspeaker diaphragm can also be treated as a simple source because its area is often nearly the same as that of the opening.

Referring to Eq. (4.71), we find that the sound pressure a distance r away from the bass-reflex loudspeaker is

$$\tilde{p} = \tilde{p}_1 + \tilde{p}_2 + \tilde{p}_3 \approx \frac{j\omega\rho_0}{4\pi r} \left(\tilde{U}_c e^{-jkr_1} - \tilde{U}_p e^{-jkr_2} - \tilde{U}_L e^{-jkr_3} \right) \quad (7.66)$$

where

\tilde{p}_1 , \tilde{p}_2 , and \tilde{p}_3 are complex sound pressures, respectively, from the diaphragm, port, and leakage outlet at distance r .

r is average distance of the point of observation from the diaphragm and the port. Note that r is large compared with the diaphragm and port radii.

r_1 , r_2 , and r_3 are actual distances, respectively, of the point of observation from the diaphragm, port, and leakage outlet.

\tilde{U}_c is complex volume velocity of the diaphragm.

\tilde{U}_p is complex volume velocity of the port. Note that the negative sign is used for \tilde{U}_p because, except for phase shift introduced by C_{AB} and M_{AB} the air from the port moves outward when the air from the diaphragm moves inward.

\tilde{U}_L is complex volume velocity of the leakage path.

In addition, the complex volume velocity necessary to compress and expand the air in the box is

$$\tilde{U}_B = \tilde{U}_c - \tilde{U}_p - \tilde{U}_L \quad (7.67)$$

If we now let $r_1 = r_2 = r_3 = r$ by confining our attention to a particular point in space in front of the loudspeaker where this is true, we get

$$\tilde{p} \approx \frac{j\omega\rho_0}{4\pi r} (\tilde{U}_c - \tilde{U}_p - \tilde{U}_L) e^{-jkr} \quad (7.68)$$

Because $\tilde{U}_c - \tilde{U}_p - \tilde{U}_L = \tilde{U}_B$, we have simply that

$$|\tilde{p}| \approx \frac{f\rho_0|\tilde{U}_B|}{2r} \quad (7.69)$$

Amazing as it seems, the sound pressure produced at faraway points equidistant from cone and port of a bass-reflex loudspeaker is directly proportional to the volume velocity necessary to compress and expand the air inside the box!

At very low frequencies, where the reactance of C_{AB} is very high, \tilde{U}_c becomes nearly equal to \tilde{U}_p , and \tilde{U}_L becomes insignificant so that the pressure, measured at points $r = r_1 = r_2 = r_3$, approaches zero. In fact, the two sources \tilde{U}_c and \tilde{U}_p behave like a dipole so that the radiated sound pressure decreases by a factor of 4 for each halving of frequency. In addition, if we are below the lowest resonance frequency of the circuit of Fig. 7.24, the diaphragm velocity \tilde{U}_c halves for each halving of frequency. Hence, in this very low-frequency region, the sound pressure decreases by a factor of 16, which is 24 dB, for each halving of frequency. In other words, the slope is fourth order. Note that this decrease is greater than that for a loudspeaker in a closed box or in an infinite baffle.



7.12 ALIGNMENTS FOR PREDETERMINED FREQUENCY-RESPONSE SHAPES

As with the loudspeaker in a closed-box enclosure, we can choose a predetermined frequency-response shape and engineer the loudspeaker accordingly using an alignment table, which we shall generate in this section. In the interest of simplifying our analysis, let us redraw Fig. 7.24 to be as shown in Fig. 7.25, referring the mechanical and acoustical quantities to the electrical side. Furthermore, we have assumed that at low frequencies we can ignore \mathbf{R}_{AR1} and \mathbf{R}_{AR2} , and that the effects of the box and port resistances, \mathbf{R}_{AB} and \mathbf{R}_{AP} , respectively, can be accounted for by adjusting the value of \mathbf{R}_{AL} . It has been found in practice that \mathbf{R}_{AL} is the dominant source of damping of the box resonance [21]. The new quantities shown on that circuit are defined as follows:

$$M_{MS} = M_{MD} + S_D^2(M_{A1} + M_{AB}) \quad (7.70)$$

$$M_{AT} = M_{A2} + M_{AP} \quad (7.71)$$

This circuit is exactly that which appears across the generator, which makes it easier to evaluate the electrical input impedance. In addition, it looks more like an electrical filter network. The electrical and mechanical sections form a first-order band-pass filter, which in conjunction with the first-order time derivative in Eq. (7.69) given by the

frequency term f , produces a net second-order high-pass filter. The acoustical section forms a second second-order high-pass filter so that the overall response is fourth order. However, these two second-order filters do not operate in isolation but are coupled to a degree which depends on their relative resonance frequencies and the size of the box. Hence, we shall introduce a coupling factor V_{AS}/V_{AB} during the following analysis, commonly known as the *compliance ratio*. As the volume of the box V_{AB} is increased relative to the suspension equivalent volume V_{AS} , the amount of coupling is weakened. From the circuit of Fig. 7.25 we obtain

$$\tilde{p}(r) = \frac{\tilde{c}_g B I S_D \rho_0}{(R_g + R_E) M_{MS}} \cdot \frac{e^{-jkr}}{4\pi r} G(s) \quad (7.72)$$

where the frequency-response function $G(s)$ is given by

$$G(s) = \frac{s^4}{s^4 + P_3 s^3 + P_2 s^2 + P_1 s + P_0} \quad (7.73)$$

and the coefficients of the denominator polynomial in $s = j\omega$ are given by

$$P_3 = \frac{\omega_S}{Q_{TS}} + \frac{\omega_B}{Q_L} \quad (7.74)$$

$$P_2 = \left(1 + \frac{V_{AS}}{V_{AB}}\right) \omega_S^2 + \omega_B^2 + \frac{\omega_S \omega_B}{Q_{TS} Q_L} \quad (7.75)$$

$$P_1 = \frac{\omega_S \omega_B^2}{Q_{TS}} + \frac{\omega_S^2 \omega_B}{Q_L} \quad (7.76)$$

$$P_0 = \omega_S^2 \omega_B^2 \quad (7.77)$$

where ω_S is the angular suspension resonant frequency in an infinite baffle given by

$$\omega_S = \frac{1}{\sqrt{M_{MS} C_{MS}}} \quad (7.78)$$

Q_{ES} is the electrical Q factor

$$Q_{ES} = \omega_S \frac{R_g + R_E}{(B I)^2} M_{MS} \quad (7.79)$$

Q_{MS} is the mechanical Q factor

$$Q_{MS} = \omega_S \frac{1}{R_{MS}} M_{MS} \quad (7.80)$$

Q_{TS} is the total Q factor

$$Q_{TS} = \frac{Q_{ES}Q_{MS}}{Q_{ES} + Q_{MS}} \quad (7.81)$$

ω_B is the angular resonant frequency of the box and port (including end corrections) given by

$$\omega_B = \frac{1}{\sqrt{M_{AT}C_{AB}}} \quad (7.82)$$

Q_L is the acoustical Q factor due to box and port losses

$$Q_L = \omega_B R_{AL} C_{AB} \quad (7.83)$$

V_{AB} is the apparent box volume, including the lining, which is related to the acoustic compliance by

$$V_{AB} = \rho_0 c^2 C_{AB} \quad (7.84)$$

and V_{AS} is the suspension equivalent volume

$$V_{AS} = S_D^2 \rho_0 c^2 C_{MS} \quad (7.85)$$

To solve Eqs. (7.74)–(7.77) for ω_S , ω_B , Q_{TS} , and V_{AS}/V_{AB} , we first eliminate Q_{TS} from Eqs. (7.74) and (7.76) and insert $\omega_S^2 = P_0/\omega_B^2$ from Eq. (7.77), which gives

$$\frac{\omega_B^4}{Q_L} - P_3 \omega_B^3 + P_1 \omega_B - \frac{P_0}{Q_L} = 0 \quad (7.86)$$

which is a quartic equation that has to be solved for ω_B so that

$$\omega_B = \frac{1}{4} \left(S + Q_L P_3 - \sqrt{3Q_L^2 P_3^2 - S^2 - \frac{2Q_L(8P_1 - Q_L^2 P_3^2)}{S}} \right),$$

where

$$S = \sqrt{Q_L^2 P_3^2 + 8 \sqrt{\frac{Q_L^2 P_1 P_3 - 4P_0}{3}} \cos\left(\frac{\phi}{3}\right)}$$

and

$$\phi = \arccos\left(\frac{\sqrt{27} Q_L^2 (P_1^2 - P_0 P_3^2)}{2(Q_L^2 P_1 P_3 - 4P_0)^{3/2}}\right).$$

Then, from Eq. (7.77), (7.74), and (7.75), respectively, we obtain the other three quantities:

$$\omega_S = \frac{\sqrt{P_0}}{\omega_B} \quad (7.87)$$

$$Q_{TS} = \frac{Q_L \omega_S}{P_3 Q_L - \omega_B} \quad (7.88)$$

$$\frac{V_{AS}}{V_{AB}} = \frac{P_2 - \omega_B^2}{\omega_S^2} - \frac{\omega_B}{Q_{TS} Q_L \omega_S} - 1 \quad (7.89)$$

Let a predefined fourth-order frequency-response function be given by

$$G(s) = \frac{s^4}{\left(s^2 + \frac{\omega_1}{Q_1} s + \omega_1^2\right) \left(s^2 + \frac{\omega_2}{Q_2} s + \omega_2^2\right)} \quad (7.90)$$

which has a value of $1/\sqrt{2}$ or -3 dB when $\omega = 1$. The values of ω_1 , ω_2 , Q_1 , and Q_2 for a number of frequency-response shapes are given in Table 7.3, which are calculated from the formulas given in Appendix I. Because the suspension and box resonance frequencies are the same in the Butterworth alignment, the two complex-conjugate pole pairs lie on a semicircle in the complex plane with angles of $\pi/4$ between them. We shall see in Section 7.15 that these coincident resonance frequencies are useful when it comes to evaluating Q_L . We may create a range of sub-Butterworth alignments with such coincident resonance frequencies by multiplying the angles between the poles and the negative real axis by a scaling factor B , which has values between 0 and 1. When $B = 0$, we have the synchronous alignment in which all four poles are coincident and real. These sub-Butterworth alignments are generated by solving the quartic equation

Table 7.3 Resonance frequencies and Q values for various fourth-order frequency-response shapes.

Frequency-response shape	ω_1	Q_1	ω_2	Q_2
Synchronous ($B = 0$)	0.4350	0.5000	0.4350	0.5000
Sub-Butterworth ($B = 0.6$)	0.5634	0.5142	0.5634	0.6575
Bessel (close to $B = 0.77$)	0.6992	0.5219	0.6237	0.8055
Sub-Butterworth ($B = 0.9$)	0.8482	0.5329	0.8482	1.0233
Butterworth ($B = 1$)	1.0000	0.5412	1.0000	1.3066
Chebyshev with 0.01 dB ripple	1.2870	0.5746	1.0356	1.7237
Chebyshev with 0.1 dB ripple	1.5370	0.6188	1.0519	2.1829
Chebyshev with 0.25 dB ripple	1.6900	0.6573	1.0574	2.5361
Chebyshev with 0.5 dB ripple	1.8310	0.7051	1.0600	2.9406

Table 7.4 Fourth-order alignments for bass-reflex enclosures for $Q_L = 7$.

Frequency-response shape	f_{3dB}/f_S	V_{AB}/V_{AS}	Q_{TS}	f_B/f_S
Synchronous ($B = 0$)	2.2990	0.2899	0.2593	1.0000
Sub-Butterworth ($B = 0.6$)	1.7748	0.4028	0.3010	1.0000
Bessel (close to $B = 0.77$)	1.4941	0.5242	0.3312	0.9735
Sub-Butterworth ($B = 0.9$)	1.1790	0.6914	0.3689	1.0000
Butterworth ($B = 1$)	1.0000	0.9422	0.4048	1.0000
Chebyshev with 0.01 dB ripple	0.8143	1.5511	0.4572	0.8838
Chebyshev with 0.1 dB ripple	0.6963	2.3308	0.5120	0.7839
Chebyshev with 0.25 dB ripple	0.6374	2.9747	0.5553	0.7259
Chebyshev with 0.5 dB ripple	0.5894	3.7464	0.6073	0.6742

$\Omega^4 + 2(a + b)\Omega^3 + 2(1 + 2ab)\Omega^2 + 2(a + b)\Omega - 1 = 0$ for Ω , where $a = \cos(B\pi/4)$ and $b = \cos(3B\pi/4)$. Although there are four solutions for Ω , only one is real and positive. Then $\omega_1 = \omega_2 = \sqrt{\Omega}$, $Q_1 = 0.5 \sec(B\pi/8)$, and $Q_2 = 0.5 \sec(3B\pi/8)$.

Equating the denominator of Eq. (7.90) with that of Eq. (7.73) gives

$$P_3 = \frac{\omega_1}{Q_1} + \frac{\omega_2}{Q_2} \quad (7.91)$$

$$P_2 = \omega_1^2 + \omega_2^2 + \frac{\omega_1\omega_2}{Q_1Q_2} \quad (7.92)$$

$$P_1 = \frac{\omega_1\omega_2^2}{Q_1} + \frac{\omega_1^2\omega_2}{Q_2} \quad (7.93)$$

$$P_0 = \omega_1^2\omega_2^2 \quad (7.94)$$

Then after inserting these values for P_0 to P_3 into Eqs. (7.86)–(7.89), we can generate the alignments given in Table 7.4.

Shown in Fig. 7.26 are frequency responses generated from Table 7.4 using Eq. (7.73). The frequency scale is normalized using f_S as the reference point because this is a fixed parameter of the loudspeaker drive unit. We see that the Chebyshev alignments give greater low-frequency extension at the cost of increased box size.



7.13 PORT DIMENSIONS

Knowing the Thiele–Small parameters of the drive unit (R_E , Q_{ES} , Q_{MS} , f_S , S_D , and V_{AS}), we choose a suitable alignment from Table 7.4, which gives us the required box volume V_{AB} and resonance frequency f_B . The total acoustic mass of the port

including end corrections and assuming that it behaves as a flanged tube at one end only is given by

$$M_{AT} = \frac{\rho_0}{S_P} (t + 0.84\sqrt{S_P}) \quad (7.95)$$

Otherwise, if it is flanged at both ends, the correction factor is changed from 0.84 to 0.96, or to 0.72 if unflanged at both ends. The volume of air in the port V_P , which is simply the product of its cross-sectional area S_P and its length t , should be chosen to be several times greater than the amount of air it has to displace to produce the maximum sound pressure at full power. Hence,

$$S_P = V_P/t \quad (7.96)$$

Inserting Eqs. (7.84), (7.95), and (7.96) into Eq. (7.82) but ignoring the end-correction factor yields the following approximate equation for the port length t :

$$t \approx \frac{c}{\omega_B} \sqrt{\frac{V_P}{V_{AB}}} \quad (7.97)$$

in which case the approximate cross-sectional area S_P is given by Eq. (7.96). However, we may wish to choose a more convenient area S_P and readjust the length t accordingly using the following exact formula:

$$t = \frac{S_P c^2}{V_{AB} \omega_B^2} - 0.84\sqrt{S_P} \quad (7.98)$$

or we may wish to choose a length t and calculate the exact area S_P using

$$S_P = \frac{0.84^2 V_{AB}^2 \omega_B^4}{4c^4} \left(1 + \sqrt{1 + \frac{4c^2 t}{0.84^2 V_{AB} \omega_B^2}} \right)^2 \quad (7.99)$$



7.14 DIAPHRAGM DISPLACEMENT

From the circuit of Fig. 7.25, we can derive the diaphragm volume velocity \tilde{U}_c from which we obtain the diaphragm displacement:

$$\begin{aligned} \tilde{\eta} &= \tilde{U}_c / (j\omega S_D) \\ &= \frac{\omega_S \tilde{e}_g}{Bl Q_{ES}} \left(\frac{s^2 + (\omega_B/Q_L)s + \omega_B^2}{s^4 + P_3 s^3 + P_2 s^2 + P_1 s + P_0} \right) \end{aligned} \quad (7.100)$$

At very low frequencies, the loudspeaker is virtually open at the back because the acoustic impedances of the box and port present very little opposition. Hence, the low-frequency displacement $\tilde{\eta}_0$ is determined purely by the mechanical compliance C_{MS} of the suspension:

$$\tilde{\eta}|_{\omega \rightarrow 0} = \tilde{\eta}_0 = \frac{\tilde{e}_g}{BlQ_{ES}\omega_S} = C_{MS}Bl\frac{\tilde{e}_g}{R_E} \left(\text{i.e. Hooke's law where } Bl\frac{\tilde{e}_g}{R_E} = \tilde{f} \right) \quad (7.101)$$

This makes a useful reference point with which to normalize the displacement curves which are shown in Fig. 7.27 for the alignments of Table 7.4. We see that the Chebyshev alignments, which give greater low-frequency extension, not only require a larger box size but also require a loudspeaker drive unit with a greater excursion limit x_{\max} .



7.15 ELECTRICAL INPUT IMPEDANCE AND EVALUATION OF Q_L

Also from the circuit of Fig. 7.25, we can derive the electrical input impedance Z_E as seen across the loudspeaker terminals:

$$\begin{aligned} Z_E &= \frac{\tilde{e}_g R_E}{\tilde{e}_g - Bl\tilde{U}_c/S_D} \\ &= R_E \left\{ 1 + \frac{\omega_S s}{Q_{ES}} \left(\frac{s^2 + (\omega_B/Q_L)s + \omega_B^2}{s^4 + E_3 s^3 + E_2 s^2 + E_1 s + E_0} \right) \right\} \end{aligned} \quad (7.102)$$

where the denominator polynomial coefficients are given by

$$E_3 = \frac{\omega_S}{Q_{MS}} + \frac{\omega_B}{Q_L} \quad (7.103)$$

$$E_2 = \left(1 + \frac{V_{AS}}{V_{AB}} \right) \omega_S^2 + \omega_B^2 + \frac{\omega_S \omega_B}{Q_{MS} Q_L} \quad (7.104)$$

$$E_1 = \frac{\omega_S \omega_B^2}{Q_{MS}} + \frac{\omega_S^2 \omega_B}{Q_L} \quad (7.105)$$

$$E_0 = \omega_S^2 \omega_B^2 \quad (7.106)$$

The coefficients E_0 to E_3 differ from the coefficients P_0 to P_3 of Eqs. (7.74)–(7.77), respectively, in that Q_{TS} is replaced by Q_{MS} . Normalized impedance curves are plotted in Fig. 7.28 for the alignments of Table 7.4. When comparing these curves with the impedance of a loudspeaker in an infinite baffle, as shown in Fig. 6.8, we see that the peak at f_S due to the parallel resonance of M_{MS} with C_{MS} has been split into two peaks with a minima in between at f_B due to the series resonance of M_{AT} with C_{AB} . For the

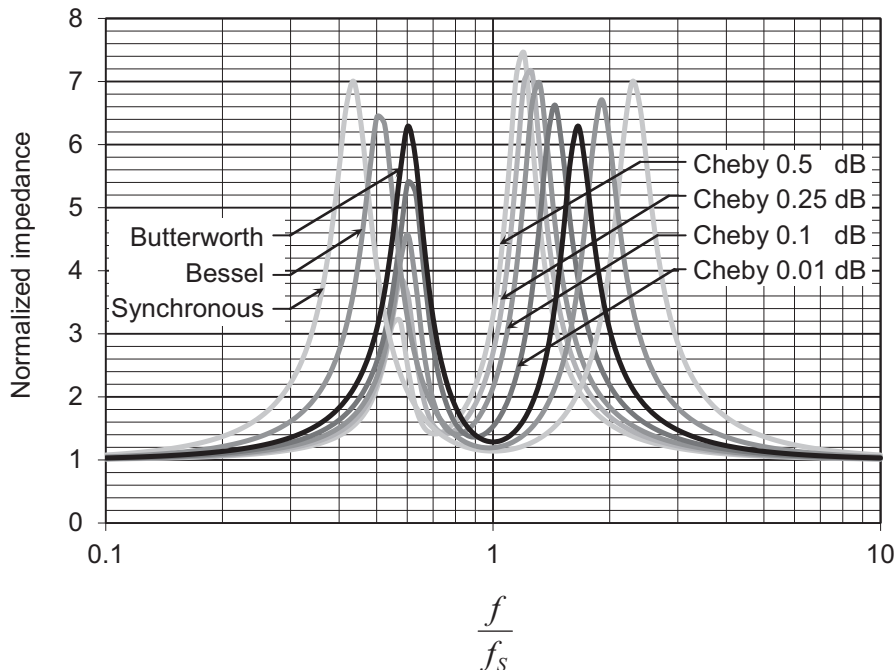


Figure 7.28 Plots of normalized electrical impedance $|Z_E/R_E|$ for the fourth-order bass-reflex alignments of [Table 7.4](#). We let $Q_{MS} = 9Q_{TS}$ so that $Q_{ES} = 1.125Q_{TS}$.

Synchronous, Bessel, and Butterworth alignments, where $f_B = f_S$, the two peaks are symmetrical either side of f_B . However, in the case of the Chebyshev alignments, the peaks are asymmetrical with the smaller peak occurring below f_B which indicates that the low-frequency response is extended at the cost of extra power.

The minima at f_B is particularly useful for checking the tuning of the port. Furthermore, in the case of alignments where $f_B = f_S$ (e.g., Synchronous, Bessel, and Butterworth), we can simplify [Eq. \(7.102\)](#) at $f = f_B$ to give the impedance at the box resonance dip:

$$Z_E|_{\omega=\omega_s=\omega_B} = Z_{EB} = R_E \left(1 + \frac{\frac{1}{Q_{ES}Q_L}}{\frac{V_{AS}}{V_{AB}} + \frac{1}{Q_{MS}Q_L}} \right) \quad (7.107)$$

from which we obtain

$$Q_L = \frac{V_{AB}}{V_{AS}} \left(\frac{1}{Q_{ES}((Z_{EB}/R_E) - 1)} - \frac{1}{Q_{MS}} \right) \quad (7.108)$$

which enables us to measure the Q_L value for the box and port resonance. See [Section 7.17](#).



7.16 PERFORMANCE

With the formulas and charts just given, it is possible to calculate the response of the loudspeaker in a bass-reflex enclosure. A complete example is given after [Section 7.17](#).

From [Fig. 7.25](#), we see that for frequencies below ω_B , radiation from the port (proportional to $-\tilde{U}_p$) is out of phase with the radiation from the diaphragm (proportional to \tilde{U}_d). As a result, the response at very low frequencies is usually not enhanced by the addition of the port. Above the resonance frequency ω_B , radiation from the port is in phase with that from the diaphragm, with a resulting enhancement over the closed-baffle response. The amount of the increase in response generally averages about 3 dB over a frequency range of one to two octaves.

An important reason for using a bass-reflex enclosure is that the loudspeaker produces less distortion at frequencies of around ω_B for a given acoustic power radiated than would be the case if the box were closed. The assumption on which this statement is made is that the motion of the air in the port is distortionless even though the amplitude of vibration is large. This is true generally because there is no suspension or magnetic circuit in the port in which nonlinear effects can occur. However, to avoid turbulence, the port should be as smooth as possible with filleted edges at each end. A large loudspeaker diaphragm usually is superior to a small one because the amplitude of its motion is less, thereby reducing nonlinear distortion.

One disadvantage of a bass-reflex enclosure is that the port can produce pipe modes at higher frequencies, and these cannot be damped using absorbent material without negating the benefit of the port. However, their effect can be mitigated by locating the mouth of the port on the rear of the box so that they are less audible at the front. At the box resonance, the wavelength is usually very large compared with the box dimensions, so the small resulting phase difference between the outputs of the port and diaphragm will have little effect on the performance [27].

An advantage of a bass-reflex enclosed loudspeaker is that, where room space is a factor, a properly tuned bass-reflex system helps to offset the effect of the small box volume.



7.17 CONSTRUCTION AND ADJUSTMENT NOTES

Bear in mind that many drive units nowadays are designed for use in “air-suspension” closed-box enclosures and can be identified by their very low resonance frequencies. In a bass-reflex design, the high compliance of their suspensions could lead to excessive diaphragm excursion below the box resonance frequency.

The box should be very rigid to resist vibration. The joints should be tight-glued, and the larger panels should be braced by gluing reinforcing strips to them. The access side should be screwed on securely with strips of sealing material such as neoprene. Most drive units are now supplied with sealing gaskets.

When the cabinet has been completed and the loudspeaker has been installed, the correctness of the tuning may be determined by connecting an audio oscillator with an output impedance about 100 times that of the loudspeaker to the electrical terminals. Next, connect a voltmeter across the loudspeaker terminals. Then, vary the frequency of the oscillator to find the minimum reading between the two peaks (see Fig. 7.28). This should occur at the calculated frequency ω_B if the design is correct. The ratio of the voltage reading at this frequency to that at some very low frequency, where it reaches an absolute minimum, gives the ratio Z_{EB}/R_E from which we can calculate Q_L using Eq. (7.108).

The resonance frequency ω_B of the enclosure can be adjusted by varying the length of the port. A typical value of Q_L is around 7. If it is much lower than this, there is probably a problem with leakage caused by a poor seal. To find the source of leakage, block the port and drive the loudspeaker (with minimum source impedance) at a very low frequency and listen around the box for any turbulent “hissing” sounds.

Example 7.3. Bass-reflex enclosure design. In the previous part, we discussed in detail the design of a closed-box baffle for a low-frequency (woofer) loudspeaker. We presented methods for the determination of its physical constants, and we showed a comparison between measurements and calculations.

In this part, we shall use the same loudspeaker drive unit as part of a pair with double the box volume, so that each unit “sees” the same volume as before. If a pair of $8\ \Omega$ drive units is used, this provides a choice of $4\ \Omega$ or $16\ \Omega$ loads for parallel or series combinations, respectively. A port will be introduced into the box that resonates with the box compliance to the same frequency as the mechanical or driver part of the circuit of Fig. 7.25, that is,

$$\omega_S = 1/\sqrt{M_{MS}C_{MS}}.$$

Your brief is to design a compact floor-standing loudspeaker that can produce 105 dB SPL at 1 m so that it will be suitable for a medium to large listening area. In other words, the low frequencies will not be augmented by room modes. Therefore, the frequency response should be as flat as possible down to 41 Hz, the lowest note on a bass guitar. To give the widest possible dispersion and for cosmetic reasons, the drive unit should not be too large. A suitable drive unit is the Bandor type 100DW/8A used in the previous closed-box example. To reach the required SPL, we will need to use two of these, one above the other, which doubles the radiating area without increasing the width and therefore maintains the horizontal directivity pattern. From actual measurements (see Section 6.10), the Thiele—Small parameters are as follows:

$$R_E = 6.27\ \Omega$$

$$Q_{ES} = 0.522$$

$$Q_{MS} = 1.9$$

$$f_S = 37\ \text{Hz}$$

$$S_D = 120 \text{ cm}^2$$

$$V_{AS} = 24 \text{ L}$$

If we reuse the same volume per drive unit as the closed-box design, then $V_{AB} = 13.42 \text{ L}$. Hence, $V_{AB}/V_{AS} = 13.42/24 = 0.56$, which from Table 7.4 would suggest the use of a Bessel alignment where $V_{AB}/V_{AS} = 0.52$, and the frequency response is plotted in Fig. 7.26. At $f_S = 37 \text{ Hz}$, the response is -7.4 dB with the -3 dB point at $1.49f_S = 55 \text{ Hz}$. However, the Q_{TS} value of

$$Q_{TS} = \frac{Q_{ES}Q_{MS}}{Q_{ES} + Q_{MS}} = 0.41$$

is somewhat higher than the optimum value of 0.33 given by Table 7.4 for a Bessel alignment. This may be corrected by using an amplifier with a negative output impedance of $R_g = -1.45 \Omega$ (due to positive current feedback [28]). However, for the purpose of this analysis, we shall proceed with an “underdamped” Bessel alignment by setting $R_g = 0$.

$$V_{AB} = 2 \times 0.5242 \times 24 = 25.2 \text{ L}$$

From Eq. (6.48), we can calculate the reference efficiency, noting that on one hand a loudspeaker in a box is half as efficient as one radiating from both sides in an infinite baffle, but on the other, this is compensated for by having two of them:

$$E_{ff} = 100 \frac{8 \times 3.14^2 \times 0.024 \times 37^3}{0.522 \times 345^3} = 0.448\%$$

To calculate the maximum SPL, we first obtain C_{MS} , M_{MS} , and Bl from Eqs. (6.27), (6.28), and (6.30), respectively

$$C_{MS} = \frac{0.024}{0.012^2 \times 1.18 \times 345^2} = 1.19 \text{ mm/N}$$

$$M_{MS} = \frac{1}{(2 \times 3.14 \times 37)^2 \times 0.00119} = 0.0156 \text{ kg}$$

$$Bl = \sqrt{\frac{6.27}{2 \times 3.14 \times 37 \times 0.522 \times 0.00119}} = 6.59 \text{ T}\cdot\text{m}$$

Knowing that the power rating W_{\max} is 100 W , we obtain from Eq. (6.33)

$$\begin{aligned} \text{SPL}_{\max} &= 20 \log_{10} \left(\frac{\sqrt{6.27 \times 100 \times 6.59 \times 0.012 \times 1.18}}{2 \times 3.14 \times 6.27 \times 0.0156 \times 20 \times 10^{-6}} \right) \\ &= 105.6 \text{ dB SPL @ } 1 \text{ m} \end{aligned}$$

where two drive units in a box produce the same pressure as a single one in an infinite baffle. Next, use Eq. (7.101) to check the peak displacement at low frequencies at full power:

$$\eta_{\max} = \frac{\sqrt{2 \times 6.27 \times 100}}{6.59 \times 0.522 \times 2 \times 3.14 \times 37} = 44.3 \text{ mm}$$

but from Fig. 7.27 we see that for the Bessel alignment the maximum above f_S frequency is 0.126 times this value, or 5.6 mm. It turns out that the x_{\max} value of the drive unit is 14 mm, with a linear limit of 4.5 mm, so there should be no problems with this design. Now, we turn to the port dimensions, but first we must calculate the volume displacement V_{\max} required from the maximum pressure p_{\max} (see Summary of bass-reflex design section, p. 334).

$$p_{\max} = 2 \times 1.414 \times 10^{\frac{105.6-7.4}{20}-5} = 2.3 \text{ Pa}$$

so that from Eq. (6.35)

$$V_{\max} = \frac{1 \times 2.3}{2 \times 3.14 \times 37^2 \times 1.18} = 0.23 \text{ L}$$

Let the volume of the port be 10 times the maximum volume displacement, or $V_P = 10V_{\max} = 2.3 \text{ L}$. From Table 7.4, the box resonance frequency is $f_B = 0.9735f_S = 36 \text{ Hz}$. The approximate length of the port excluding end effects is obtained from Eq. (7.97):

$$t \approx \frac{345}{2 \times 3.14 \times 36} \sqrt{\frac{2.3}{25.2}} = 46.1 \text{ cm}$$

so that the approximate cross-sectional area is

$$S_P = V_P/t = 0.0023/0.461 = 50 \text{ cm}^2, \text{ say } 15 \text{ cm} \times 3.4 \text{ cm} = 51 \text{ cm}^2$$

Then, the actual length is calculated from Eq. (7.98):

$$t = \frac{0.0051 \times 345^2}{0.0252 \times (2 \times 3.14 \times 36)^2} - 0.84 \times \sqrt{0.0051} = 41.1 \text{ cm}$$

We let the lining material occupy one-quarter of the total box volume so that $V_M = V_B/4 = V_A/3$ because $V_B = V_A + V_M$. We already know that $V_{AB} = V_A + \gamma V_M = 25.2 \text{ L}$ where $\gamma = 1.4$. Hence,

$$V_A = \frac{25.2}{1 + 1.4/3} = 17.2 \text{ L}$$

and $V_M = 17.2/3 = 5.7 \text{ L}$ so that $V_B = 17.2 + 5.7 = 22.9 \text{ L}$. Hence, the compliance of the air in the box is $C_{AA} = V_A/(\gamma P_0) = 0.0172/(1.4 \times 10^5) = 1.23 \times 10^{-7}$ and the

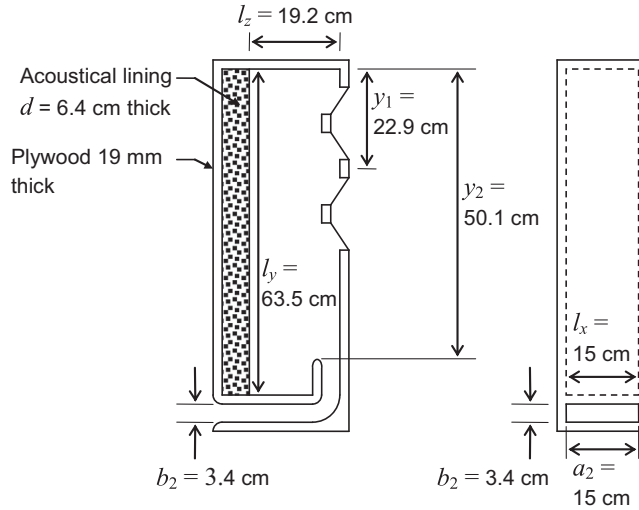


Figure 7.29 Example of bass-reflex enclosure design.

lining material $C_{AM} = V_M/P_0 = 0.0061/10^5 = 6.1 \times 10^{-8}$ so that the apparent compliance is $C_{AB} = C_{AA} + \gamma C_{AM} = 1.23 \times 10^{-7} + 6.1 \times 10^{-8} = 1.84 \times 10^{-7}$. The box and port dimensions are shown in Fig. 7.29. The internal width W is 15 cm, which is the smallest width that will accommodate the drive units. The acoustic center of the two drive units is about one-third of the internal height from the top so as not to coincide with the antinodes of the first or second vertical modes. The box contains one 63.5 by 15 by 6.4 cm piece of lining material. Let us now calculate the box and port losses. If the flow resistance is $R_f = 200$ rayl/cm, then acoustic resistance of the lining material with a depth of 6.4 cm becomes

$$R_{AM} = \frac{6.4 \times 200}{3 \times 0.635 \times 0.15} = 4480 \text{ N}\cdot\text{s}/\text{m}^5$$

so that the box resistance from Eq. (7.7) is

$$\begin{aligned} R_{AB} &= \frac{4480}{\left(1 + \frac{17.2}{1.4 \times 6.1}\right)^2 + (2 \times 3.14 \times 36 \times 4480 \times 1.23 \times 10^{-7})^2} \\ &= 492 \text{ N}\cdot\text{s}/\text{m}^5 \end{aligned}$$

from which we obtain Q_A due to absorption within the box:

$$Q_A = \frac{1}{\omega_B R_{AB} C_{AB}} = \frac{1}{2 \times 3.14 \times 36 \times 492 \times 1.84 \times 10^{-7}} = 49$$

The resistance of the port is given by Eq. (4.23):

$$R_{AP} = \frac{\sqrt{4 \times 3.14 \times 36 \times 1.18 \times 1.86 \times 10^{-5}}}{0.15 \times 0.034} \left(\frac{0.411}{\sqrt{0.15 \times 0.034/3.14}} + 2 \right)$$

$$= 238 \text{ N}\cdot\text{s}/\text{m}^5$$

from which we obtain Q_p of the port:

$$Q_p = \frac{1}{\omega_B R_{AP} C_{AB}} = \frac{1}{2 \times 3.14 \times 36 \times 238 \times 1.84 \times 10^{-7}} = 101$$

These Q values are very high, which supports the commonly held view that leakage losses dominate. Unfortunately, the effect of leakage cannot be determined until the loudspeaker and its enclosure are assembled and measured. A common value of Q_L due to all losses is around 7.

Let us now create a semianalytical simulation model of the design of Fig. 7.29 using two-port networks and transmission matrices, as introduced in Section 3.10 and Fig. 4.43. The schematic is shown in Fig. 7.30. Although it is based on the circuit of Fig. 7.24, a gyrator has been inserted between the electrical elements and the mechanical ones, which enables us to calculate more easily the generator current \tilde{i}_g from which we

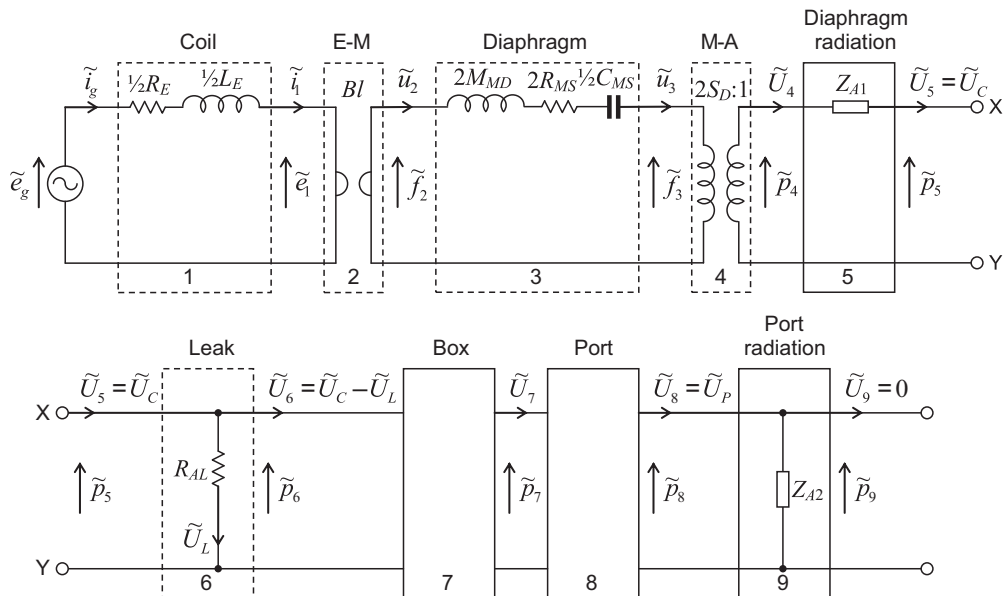


Figure 7.30 Semianalytical model of example bass-reflex enclosure design shown in Fig. 7.29 using transmission matrices. The dashed boxes are lumped-element two-port networks, and the solid boxes are analytical ones. Here, the two drive units are connected in parallel so that the net coil resistance R_E is halved. If the drive units are connected in series, replace $\frac{1}{2}R_E$, $\frac{1}{2}L_E$, and Bl with $2R_E$, $2L_E$, and $2Bl$.

obtain the electrical impedance. We are ignoring the generator impedance R_g because in the experimental setup this is negligible compared with R_E . The dashed boxes are lumped-element two-port networks, and the solid boxes are analytical ones. Here, the two drive units are connected in parallel so that the net coil resistance R_E is halved. If the drive units are connected in series, replace $\frac{1}{2}R_E$, $\frac{1}{2}L_E$, and Bl with $2R_E$, $2L_E$, and $2Bl$. From the schematic, we create the transmission matrices required to represent each two-port network as follows:

1. *Coil.*

$$\begin{bmatrix} \tilde{e}_g \\ \tilde{i}_g \end{bmatrix} = \begin{bmatrix} 1 & \frac{1}{2}Z_E \\ 0 & 1 \end{bmatrix} \cdot \begin{bmatrix} \tilde{e}_1 \\ \tilde{i}_1 \end{bmatrix} = \mathbf{C} \cdot \begin{bmatrix} \tilde{e}_1 \\ \tilde{i}_1 \end{bmatrix}$$

where $Z_E = R_E + j\omega L_E$.

2. *Electromechanical transduction.*

$$\begin{bmatrix} \tilde{e}_1 \\ \tilde{i}_1 \end{bmatrix} = \begin{bmatrix} 0 & Bl \\ (Bl)^{-1} & 0 \end{bmatrix} \cdot \begin{bmatrix} \tilde{f}_2 \\ \tilde{u}_2 \end{bmatrix} = \mathbf{E} \cdot \begin{bmatrix} \tilde{f}_2 \\ \tilde{u}_2 \end{bmatrix}$$

3. *Diaphragm.*

$$\begin{bmatrix} \tilde{f}_2 \\ \tilde{u}_2 \end{bmatrix} = \begin{bmatrix} 1 & 2Z_{MD} \\ 0 & 1 \end{bmatrix} \cdot \begin{bmatrix} \tilde{f}_3 \\ \tilde{u}_3 \end{bmatrix} = \mathbf{D} \cdot \begin{bmatrix} \tilde{f}_3 \\ \tilde{u}_3 \end{bmatrix}$$

where $Z_{MD} = j\omega M_{MD} + R_{MS} + 1/(j\omega C_{MS})$. We must exclude the radiation mass from the diaphragm so that $M_{MD} = M_{MS} - 16\rho_0 a^3/3$, where $a = \sqrt{S_D/\pi}$.

4. *Mechanoacoustical transduction.*

$$\begin{bmatrix} \tilde{f}_3 \\ \tilde{u}_3 \end{bmatrix} = \begin{bmatrix} 2S_D & 0 \\ 0 & 2S_D^{-1} \end{bmatrix} \cdot \begin{bmatrix} \tilde{p}_4 \\ \tilde{U}_4 \end{bmatrix} = \mathbf{M} \cdot \begin{bmatrix} \tilde{p}_4 \\ \tilde{U}_4 \end{bmatrix}$$

5. *Diaphragm radiation.*

$$\begin{bmatrix} \tilde{p}_4 \\ \tilde{U}_4 \end{bmatrix} = \begin{bmatrix} 1 & Z_{A1} \\ 0 & 1 \end{bmatrix} \cdot \begin{bmatrix} \tilde{p}_5 \\ \tilde{U}_5 \end{bmatrix} = \mathbf{F} \cdot \begin{bmatrix} \tilde{p}_5 \\ \tilde{U}_5 \end{bmatrix}$$

where Z_{A1} is the acoustic-radiation impedance of the diaphragm, taking into account the mutual radiation impedance, given by Eqs. (13.339) and (13.345) where $Z_{A1} = (Z_{11} + Z_{12})/S_D$ and $a = \sqrt{S_D/\pi}$.

6. Leak.

$$\begin{bmatrix} \tilde{p}_5 \\ \tilde{U}_5 \end{bmatrix} = \begin{bmatrix} 1 & 0 \\ R_{AL}^{-1} & 1 \end{bmatrix} \cdot \begin{bmatrix} \tilde{p}_6 \\ \tilde{U}_6 \end{bmatrix} = \mathbf{L} \cdot \begin{bmatrix} \tilde{p}_6 \\ \tilde{U}_6 \end{bmatrix}$$

where the leakage resistance is given by

$$R_{AL} = Q_L / (2\pi f_B C_{AB}) = 7 / (2 \times 3.14 \times 36 \times 1.84 \times 10^{-7}) = 168,200 \text{ N}\cdot\text{s}/\text{m}^5.$$

7. Box.

$$\begin{bmatrix} \tilde{p}_6 \\ \tilde{U}_6 \end{bmatrix} = \begin{bmatrix} b_{11} & b_{12} \\ b_{21} & b_{22} \end{bmatrix} \cdot \begin{bmatrix} \tilde{p}_7 \\ \tilde{U}_7 \end{bmatrix} = \mathbf{B} \cdot \begin{bmatrix} \tilde{p}_7 \\ \tilde{U}_7 \end{bmatrix}$$

The mechanical z -parameters of the two-port network for the bass-reflex enclosure are given by the following equation, which is derived in a similar manner to Eq. (7.131) in Section 7.18, except that the circular pistons are replaced by rectangular pistons of width a_p in the x direction and b_p in the y direction. In addition, the drivers and port are mounted half way between the side walls so that $x_1 = x_2 = l_x/2$. We obtain the acoustical z -parameters by dividing through by $a_p b_p a_q b_q$ to yield

$$\begin{aligned} Z_{pq} = \rho_0 c & \left\{ \frac{1}{l_x l_y} \frac{Z_s}{\rho_0 c} + j \tan kl_z + \frac{8l_y}{\pi^2 b_p b_q l_x} \right. \\ & \times \sum_{n=1}^{\infty} \frac{k}{n^2 k_{0n}} \cos\left(\frac{n\pi\gamma_p}{l_y}\right) \cos\left(\frac{n\pi\gamma_q}{l_y}\right) \sin\left(\frac{n\pi b_p}{2l_y}\right) \sin\left(\frac{n\pi b_q}{2l_y}\right) \frac{\frac{k_{0n} Z_s}{\rho_0 c} + j \tan k_{0n} l_s}{1 + j \frac{k_{0n} Z_s}{\rho_0 c} \tan k_{0n} l_s} \\ & + \frac{2l_x}{\pi^2 a_p a_q l_y} \sum_{m=1}^{\infty} \frac{k}{m^2 k_{m0}} \sin\left(\frac{m\pi a_p}{l_x}\right) \sin\left(\frac{m\pi a_q}{l_x}\right) \frac{\frac{k_{m0} Z_s}{\rho_0 c} + j \tan k_{m0} l_z}{1 + j \frac{k_{m0} Z_s}{\rho_0 c} \tan k_{m0} l_z} \\ & + \frac{16l_x l_y}{\pi^4 a_p a_q b_p b_q} \sum_{m=1}^{\infty} \sum_{n=1}^{\infty} \frac{k}{m^2 n^2 k_{mn}} \sin\left(\frac{m\pi a_p}{l_x}\right) \sin\left(\frac{m\pi a_q}{l_x}\right) \cos\left(\frac{m\pi\gamma_p}{l_y}\right) \\ & \left. \times \cos\left(\frac{n\pi\gamma_q}{l_y}\right) \sin\left(\frac{n\pi b_p}{2l_y}\right) \sin\left(\frac{n\pi b_q}{2l_y}\right) \frac{\frac{k_{mn} Z_s}{\rho_0 c} + j \tan k_{mn} l_z}{1 + j \frac{k_{mn} Z_s}{\rho_0 c} \tan k_{mn} l_z} \right\} \end{aligned}$$

where

$$k_{mn} = \sqrt{k^2 - \left(\frac{2m\pi}{l_x}\right)^2 - \left(\frac{n\pi}{l_y}\right)^2}$$

and

$$Z_s = \frac{R_f d}{3} + \frac{P_0}{j\omega d}$$

where the value of the lining flow resistance R_f is chosen such that $R_f d/3 = \rho_0 c = 412$ rayl, which is the impedance of free space and thus provides optimum sound absorption at higher frequencies. Then, the transmission-matrix parameters for the box are given by $b_{11} = Z_{11}/Z_{21}$, $b_{12} = (Z_{11}Z_{22} - Z_{12}Z_{21})/Z_{21}$, $b_{21} = 1/Z_{21}$, and $b_{22} = Z_{22}/Z_{21}$. The dimensions are given in Fig. 7.29 except for $a_1 = b_1 = \sqrt{S_D}$.

8. Port.

$$\begin{bmatrix} \tilde{p}_7 \\ \tilde{U}_7 \end{bmatrix} = \begin{bmatrix} \cos k_p t & jZ_p \sin k_p t \\ jZ_p^{-1} \sin k_p t & \cos k_p t \end{bmatrix} \cdot \begin{bmatrix} \tilde{p}_9 \\ \tilde{U}_9 \end{bmatrix} = \mathbf{P} \cdot \begin{bmatrix} \tilde{p}_8 \\ \tilde{U}_8 \end{bmatrix}$$

where the port wave number k_p and characteristic impedance Z_p are obtained from Eqs. (4.215) and (4.217), respectively. The port is assumed to be large enough to ignore boundary slip and thermal conduction so that we only consider the viscous flow losses to obtain $k_p = \omega\xi/c = 2\pi f\xi/c$, $Z_p = \rho_0 c\xi/S_p$, and $S_p = a_2 b_2$ where

$$\xi = \sqrt{1 - \frac{2J_1(k_V a_p)}{k_V a_p J_0(k_V a_p)}}, \quad a_p = \sqrt{a_2 b_2 / \pi}, \quad \text{and } k_V = \sqrt{-j\pi 2f \rho_0 / \mu}$$

where $\mu = 1.86 \times 10^{-5} \text{ m}^2/\text{s}$ is the viscosity coefficient for air at 20°C.

9. Port radiation.

$$\begin{bmatrix} \tilde{p}_8 \\ \tilde{U}_8 \end{bmatrix} = \begin{bmatrix} 1 & 0 \\ Z_{A2}^{-1} & 1 \end{bmatrix} \cdot \begin{bmatrix} \tilde{p}_9 \\ \tilde{U}_9 \end{bmatrix} = \mathbf{R} \cdot \begin{bmatrix} \tilde{p}_9 \\ \tilde{U}_9 \end{bmatrix}$$

In this case, the port outlet is rectangular and close to the floor so that Z_{A2} may be given by the impedance of a rectangular piston in an infinite baffle using Eqs. (13.326) and (13.327), where $Z_{A2} = (\mathbf{R}_s + jX_s)/(a_2 b_2)$.

First, we evaluate \tilde{p}_9 at the end of the chain:

$$\begin{bmatrix} \tilde{e}_g \\ \tilde{i}_g \end{bmatrix} = \mathbf{A} \cdot \begin{bmatrix} \tilde{p}_9 \\ 0 \end{bmatrix}$$

where

$$\mathbf{A} = \mathbf{C} \cdot \mathbf{E} \cdot \mathbf{D} \cdot \mathbf{M} \cdot \mathbf{F} \cdot \mathbf{L} \cdot \mathbf{B} \cdot \mathbf{P} \cdot \mathbf{R} = \begin{bmatrix} a_{11} & a_{12} \\ a_{21} & a_{22} \end{bmatrix}$$

Hence, $\tilde{p}_9 = \tilde{e}_g/a_{11}$. Then, we work backward to obtain the volume velocities we wish to evaluate. In particular, we are interested in the far-field pressure, which according to Eq. (7.69) is a function of

$$\tilde{U}_B = \tilde{U}_c - \tilde{U}_L - \tilde{U}_p = \tilde{U}_6 - \tilde{U}_8.$$

This procedure is fairly straightforward and does not involve any matrix inversion. From the port radiation matrix (9), we obtain

$$\tilde{U}_p = \tilde{U}_8 = \tilde{p}_9/Z_{A2}$$

and working back further to the box matrix (7) we obtain

$$\begin{bmatrix} \tilde{p}_6 \\ \tilde{U}_6 \end{bmatrix} = \mathbf{N} \cdot \begin{bmatrix} \tilde{p}_9 \\ 0 \end{bmatrix}$$

where

$$\mathbf{N} = \mathbf{B} \cdot \mathbf{P} \cdot \mathbf{R} = \begin{bmatrix} n_{11} & n_{12} \\ n_{21} & n_{22} \end{bmatrix}$$

so that

$$\tilde{U}_c - \tilde{U}_L = \tilde{U}_6 = n_{21}\tilde{p}_9$$

and therefore

$$\tilde{U}_B = \tilde{U}_c - \tilde{U}_L - \tilde{U}_p = \tilde{U}_6 - \tilde{U}_8 = (n_{21} - 1/Z_{A2})e_g/a_{11}$$

The port volume velocity is given by

$$\tilde{U}_p = \tilde{U}_8 = e_g/(a_{11}Z_{A2})$$

and the diaphragm volume velocity by

$$\tilde{U}_c - \tilde{U}_L = \tilde{U}_6 = n_{21}\tilde{e}_g/a_{11}$$

To plot the normalized far-field on-axis pressure, we simply divide \tilde{U}_B by a reference volume velocity

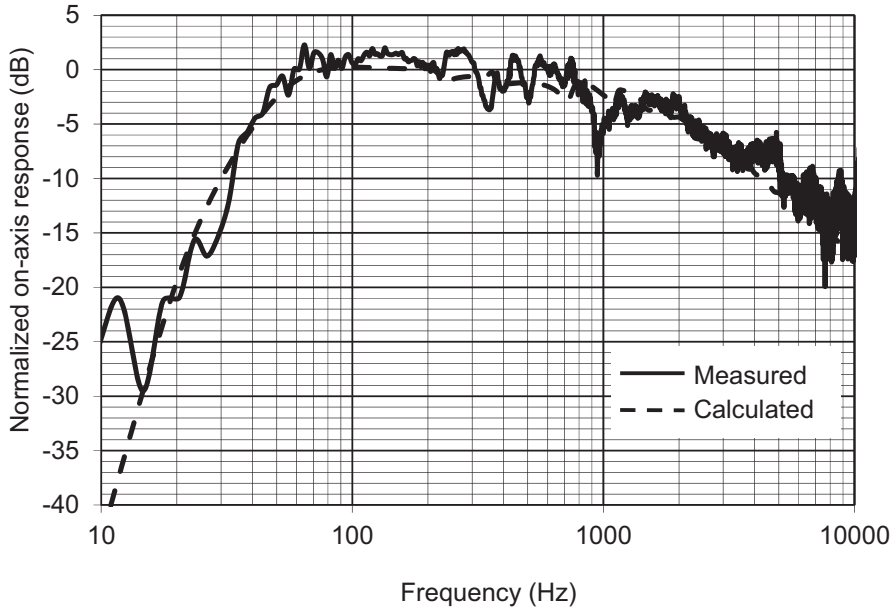


Figure 7.31 Graphs of the on-axis sound pressure level produced by the bass-reflex enclosure design shown in Fig. 7.29. The *dashed curves* are calculated from $20 \log_{10} |\tilde{U}_B / \tilde{U}_{ref}|$. *Solid curves* are measured.

$$\tilde{U}_{ref} = \frac{2\tilde{e}_g B I S_D}{\omega M_{MSR_E}}$$

and plot $20 \log_{10} |\tilde{U}_B / \tilde{U}_{ref}|$ as shown in Fig. 7.31. The port and diaphragm volume velocities,

$$20 \log_{10} |\tilde{U}_P / \tilde{U}_{ref}| \text{ and } 20 \log_{10} |(\tilde{U}_c - \tilde{U}_L) / \tilde{U}_{ref}|,$$

respectively, are plotted separately in Fig. 7.32. Although the effects of box and port modes are clearly seen in the calculated response of Fig. 7.31, most of the irregularities are emanating from the mouth of the port as is seen from Fig. 7.32. By contrast, the output from the diaphragm is fairly smooth apart from one small feature at 220 Hz, which is due to the fundamental vertical mode of the box. At 375, 750, and 1125 Hz, we see the first, second, and third port modes, respectively. The effect of these will be mitigated somewhat by mounting the port on the rear of the enclosure as is seen from the measured response of Fig. 7.31. Finally, we can obtain the input impedance from $\tilde{e}_g / \tilde{i}_g$ where $\tilde{i}_g = a_{21} \tilde{p}_9$ and from above $\tilde{p}_9 = \tilde{e}_g / a_{11}$. Therefore, the input impedance is simply $Z_E = a_{11} / a_{21}$, as plotted in Fig. 7.33.

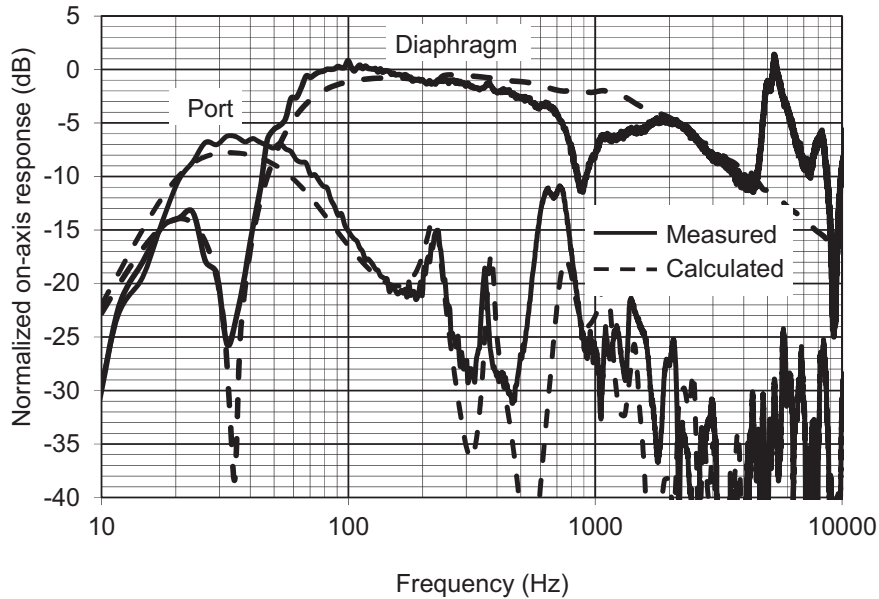


Figure 7.32 Graphs of the on-axis sound pressure level produced by port and diaphragm of the bass-reflex enclosure design shown in Fig. 7.29. The dashed curves are calculated from $20 \log_{10} |\tilde{U}_p / \tilde{U}_{ref}|$ and $20 \log_{10} |(\tilde{U}_c - \tilde{U}_l) / \tilde{U}_{ref}|$ for the port and diaphragm, respectively. Solid curves are measured.

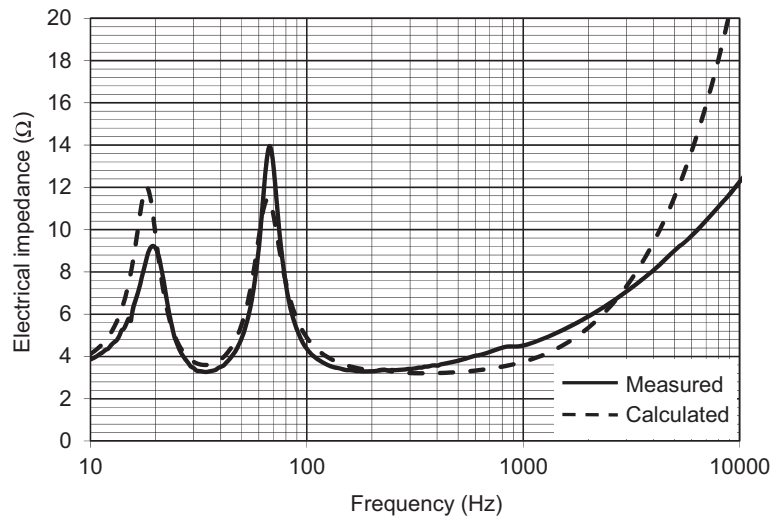


Figure 7.33 Graphs of the electrical input impedance of the bass-reflex enclosure design shown in Fig. 7.29, where the two drive units are connected in parallel. The dashed curves are calculated from $Z_E = |\tilde{e}_g / \tilde{i}_g| = a_{11} / a_{21}$. Solid curves are measured.

PART XXIII: TWO-PORT NETWORK FOR SMALL ENCLOSURES

In this part, we shall use the two-port network theory, introduced in Section 3.10 and Fig. 4.43, to create a z -parameter matrix that describes a bass-reflex enclosure in which the rear of the loudspeaker diaphragm connects to one port and the bass-reflex port connects to the other. Absorbent lining material is located on the internal wall opposite to the diaphragm and bass-reflex port. This matrix is valid for all wavelengths because it is based on eigenfunction expansions of the internal modes.

For a closed-box enclosure, we simply set the velocity at the bass-reflex port to zero so that we are left with one-port network or impedance at the rear of the diaphragm, which is given by the first element of the matrix z_{11} .

7.18 TWO-PORT NETWORK FOR A BASS-REFLEX ENCLOSURE

A sketch of the two-port enclosure is shown in Fig. 7.34. It is a generic enclosure, which we shall use for purposes other than the bass-reflex enclosure in Example 7.3, such as the simple enclosure in Section 7.6, normal modes of a rectangular enclosure in Section 10.3, and horn bends in Section 9.14.

The two ports, represented by piston 1 and piston 2, are circular and planar. To simplify the problem, there is only acoustic lining on the surface opposite to the two ports, represented by a termination impedance at $z = 0$. For a bass-reflex enclosure, this avoids having too much absorption which would negate the advantage of the port, the resonance of which is best damped by the acousto-mechano-electrical coupling to the voice-coil resistance. If the force and velocity at piston 1 are given by \tilde{F}_1 and \tilde{u}_1 , respectively, and the force and velocity at piston 2 by \tilde{F}_2 and \tilde{u}_2 , then

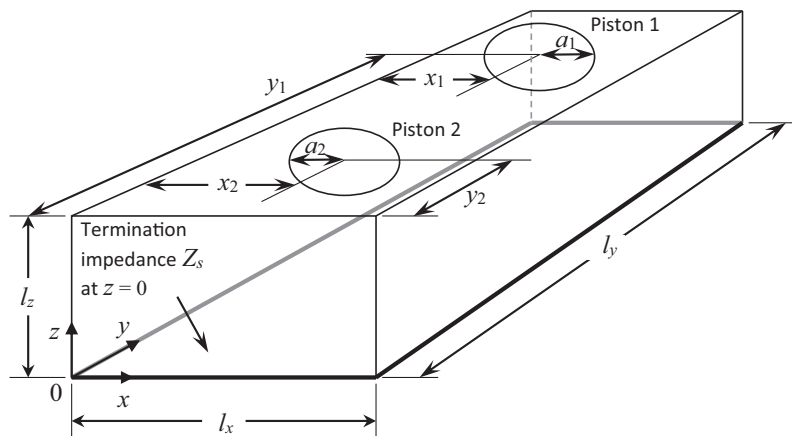


Figure 7.34 Sketch of the bass-reflex enclosure as a two-port network.

$$\begin{bmatrix} \tilde{F}_1 \\ \tilde{F}_2 \end{bmatrix} = \begin{bmatrix} z_{11} & z_{12} \\ z_{21} & z_{22} \end{bmatrix} \begin{bmatrix} \tilde{u}_1 \\ -\tilde{u}_2 \end{bmatrix}, \quad (7.109)$$

where the mechanical self-impedance z_{11} of piston 1 is the ratio of the force to velocity at piston 1 with piston 2 blocked

$$z_{11} = \left. \frac{\tilde{F}_1}{\tilde{u}_1} \right|_{\tilde{u}_2=0}. \quad (7.110)$$

Similarly, the mechanical self-impedance z_2 of piston 2 is the ratio of the force to velocity at piston 2 with piston 1 blocked

$$z_{22} = \left. \frac{\tilde{F}_2}{-\tilde{u}_2} \right|_{\tilde{u}_1=0}, \quad (7.111)$$

which is obtained by interchanging “1” and “2” in the expression for z_{11} . In a passive network such as this, the mutual impedances z_{12} and z_{21} are equal and given by

$$z_{12} = \left. \frac{\tilde{F}_1}{-\tilde{u}_2} \right|_{\tilde{u}_1=0} = z_{21} = \left. \frac{\tilde{F}_2}{\tilde{u}_1} \right|_{\tilde{u}_2=0}. \quad (7.112)$$

For simplicity, we let either $\tilde{u}_1 = \tilde{u}_0$ when $\tilde{u}_2 = 0$ or $\tilde{u}_2 = \tilde{u}_0$ when $\tilde{u}_1 = 0$, although in practice they will be different and, according to the superposition of fields, the pressure field will be the sum of those produced by the velocity at each inlet, which in turn depends on the inlet pressure and impedance. However, this simplification enables us to write a single expression for the internal pressure due to the velocity \tilde{u}_0 at any inlet

$$\tilde{p}(x, y, z) = \rho_0 c \tilde{u}_0 \sum_{m=0}^{\infty} \sum_{n=0}^{\infty} (A_{mn} e^{-jk_{mn}z} + B_{mn} e^{jk_{mn}z}) \cos(m\pi x/l_x) \cos(n\pi y/l_y), \quad (7.113)$$

where

$$k_{mn} = \sqrt{k^2 - \left(\frac{m\pi}{l_x}\right)^2 - \left(\frac{n\pi}{l_y}\right)^2}. \quad (7.114)$$

The boundary condition of zero pressure gradient at the perfectly rigid side walls ($x = 0$, $x = l_x$, $y = 0$, $y = l_y$) is accounted for by the cosine expansions in m and n . In other words, only standing waves whose wavelengths are integer or half-integer divisions of l_x and l_y can exist in the x and y directions, respectively. The term with the coefficient

B_{mn} represents plane waves traveling from the pistons in the negative z direction and the term with the coefficient A_{mn} represents reflected plane waves traveling in the positive z direction. The strengths of the reflections depend on the value of the impedance specific Z_s in the plane $z = 0$. The unknown expansion coefficients A_m and B_n are found by applying the boundary conditions at the pistons in the front baffle ($z = l_z$) and at the rear wall ($z = 0$), which is terminated in a specific impedance Z_s . The velocity in the z direction is given by

$$\begin{aligned}\tilde{u}_z(x, y, z) &= \frac{1}{-jk\rho_0c} \frac{\partial}{\partial z} \tilde{p}(x, y, z) \\ &= \frac{1}{k} \tilde{u}_0 \sum_{m=0}^{\infty} \sum_{n=0}^{\infty} k_{mn} (A_{mn} e^{-jk_{mn}z} - B_{mn} e^{jk_{mn}z}) \cos(m\pi x/l_x) \cos(n\pi y/l_y).\end{aligned}\quad (7.115)$$

At $z = 0$,

$$\tilde{p}(x, y, 0) = -Z_s \tilde{u}_z(x, y, 0), \quad (7.116)$$

so that

$$B_{mn} = \frac{k_{mn}Z_s + k\rho_0c}{k_{mn}Z_s - k\rho_0c} A_{mn}. \quad (7.117)$$

To evaluate the pressure field due to a velocity \tilde{u}_0 at piston 1, we set the following boundary conditions at $z = l_z$,

$$\tilde{u}_z(x, y, l_z) = \begin{cases} \tilde{u}_0, & x_1 - \sqrt{a_1^2 - (y - y_1)^2} \leq x \leq x_1 + \sqrt{a_1^2 - (y - y_1)^2}, \quad y_1 - a \leq y \leq y_1 + a. \\ 0, & \text{everywhere else} \end{cases} \quad (7.118)$$

After inserting Eq. (7.117) into Eq. (7.115), we then multiply through by $\cos(p\pi x/l_x)$ and $\cos(q\pi y/l_y)$ and integrate over x and y as follows:

$$\begin{aligned}\tilde{u}_z(x, y, z) &= \frac{2}{k} \tilde{u}_0 \sum_{m=0}^{\infty} \sum_{n=0}^{\infty} k_{mn} A_{mn} \frac{k\rho_0c \cos k_{mn}l_z + jk_{mn}Z_s \sin k_{mn}l_z}{k\rho_0c - k_{mn}Z_s} \\ &\quad \times \int_0^{l_x} \cos(m\pi x/l_x) \cos(p\pi x/l_x) dx \int_0^{l_y} \cos(n\pi y/l_y) \cos(q\pi y/l_y) dy \\ &= \tilde{u}_0 \int_{y_1-a_1}^{y_1+a_1} \cos(q\pi y/l_y) \int_{x_1-\sqrt{a_1^2-(y-y_1)^2}}^{x_1+\sqrt{a_1^2-(y-y_1)^2}} \cos(p\pi x/l_x) dx dy.\end{aligned}\quad (7.119)$$

Using the property of orthogonality such that $p = m$ and $q = n$ together with the integral identities

$$\int_0^{l_x} \cos(m\pi x/l_x) \cos(p\pi x/l_x) dx = \begin{cases} (1 + \delta_{m0})l_x/2, & p = m \\ 0, & p \neq m \end{cases} \quad (7.120)$$

$$\int_0^{l_y} \cos(n\pi y/l_y) \cos(q\pi y/l_y) dy = \begin{cases} (1 + \delta_{n0})l_y/2, & q = n \\ 0, & q \neq n \end{cases} \quad (7.121)$$

$$\int_{x_1 - \sqrt{a_1^2 - (y - \gamma_1)^2}}^{x_1 + \sqrt{a_1^2 - (y - \gamma_1)^2}} \cos(p\pi x/l_x) dx = \begin{cases} 2\sqrt{a_1^2 - (y - \gamma_1)^2}, & p = 0 \\ \frac{2l_x}{p\pi} \cos\left(\frac{p\pi x_1}{l_x}\right) \sin\left(\frac{p\pi}{l_x} \sqrt{a_1^2 - (y - \gamma_1)^2}\right), & p \neq 0 \end{cases} \quad (7.122)$$

$$\begin{aligned} \int_{\gamma_1 - a_1}^{\gamma_1 + a_1} \cos\left(\frac{n\pi y}{l_y}\right) \sin\left(\frac{m\pi}{l_x} \sqrt{a_1^2 - (y - \gamma_1)^2}\right) dy \\ = \frac{\pi a_1 m l_y}{\sqrt{n^2 l_x^2 + m^2 l_y^2}} \cos\left(\frac{n\pi \gamma_1}{l_y}\right) J_1\left(\frac{\pi a_1 \sqrt{n^2 l_x^2 + m^2 l_y^2}}{l_x l_y}\right), \end{aligned} \quad (7.123)$$

we obtain

$$A_{00} = \frac{\pi a_1^2}{2l_x l_y} \frac{\rho_0 c - Z_s}{\rho_0 c \cos kl_z + jZ_s \sin kl_z}, \quad (7.124)$$

$$\begin{aligned} A_{0n} = \frac{2k}{l_x l_y k_{0n}} \int_{\gamma_1 - a_1}^{\gamma_1 + a_1} \cos\left(\frac{n\pi y}{l_y}\right) \sqrt{a_1^2 - (y - \gamma_1)^2} dy \\ \times \frac{k\rho_0 c - k_{0n} Z_s}{k\rho_0 c \cos k_{0n} l_z + jk_{0n} Z_s \sin k_{0n} l_z}, \end{aligned} \quad (7.125)$$

$$\begin{aligned} A_{m0} = \frac{2k}{m\pi k_{m0} l_y} \cos\left(\frac{m\pi x_1}{l_x}\right) \int_{\gamma_1 - a_1}^{\gamma_1 + a_1} \sin\left(\frac{m\pi \sqrt{a_1^2 - (y - \gamma_1)^2}}{l_x}\right) dy \\ \times \frac{k\rho_0 c - k_{m0} Z_s}{k\rho_0 c \cos k_{m0} l_z + jk_{m0} Z_s \sin k_{m0} l_z}, \end{aligned} \quad (7.126)$$

$$A_{mn} = \frac{(2 - \delta_{m0})(2 - \delta_{n0})ka_1}{k_{mn}\sqrt{n^2l_x^2 + m^2l_y^2}} \cos\left(\frac{m\pi x_1}{l_x}\right) \cos\left(\frac{n\pi y_1}{l_y}\right) J_1\left(\frac{\pi a_1 \sqrt{n^2l_x^2 + m^2l_y^2}}{l_x l_y}\right) \\ \times \frac{k\rho_0 c - k_{mn}Z_s}{k\rho_0 c \cos k_{mn}l_z + jk_{mn}Z_s \sin k_{mn}l_z}, \quad (7.127)$$

where δ_{m0} is the Kronecker delta function. Inserting Eqs. (7.117) and (7.127) into Eq. (7.113) gives

$$\tilde{p}(x, y, z) = -\rho_0 c \tilde{u}_0 \left\{ \frac{\pi a_1^2}{l_x l_y} \cdot \frac{Z_s \cos kz + j\rho_0 c \sin kz}{\rho_0 c \cos kl_z + jZ_s \sin kl_z} + 2ka_1 \sum_{m=0}^{\infty} \sum_{n=0}^{\infty} \cos\left(\frac{m\pi x_1}{l_x}\right) \right. \\ \times \cos\left(\frac{n\pi y_1}{l_y}\right) \frac{(2 - \delta_{m0})(2 - \delta_{n0})}{k_{mn}\sqrt{n^2l_x^2 + m^2l_y^2} + \delta_{m0}\delta_{n0}} J_1\left(\frac{\pi a_1 \sqrt{n^2l_x^2 + m^2l_y^2}}{l_x l_y}\right) \\ \left. \times \cos\left(\frac{m\pi x}{l_x}\right) \cos\left(\frac{n\pi y}{l_y}\right) \frac{k_{mn}Z_s \cos k_{mn}z + jk\rho_0 c \sin k_{mn}z}{k\rho_0 c \cos k_{mn}l_z + jk_{mn}Z_s \sin k_{mn}l_z} \right\} \quad (7.127a)$$

where we have inserted the term $\delta_{m0}\delta_{n0}$ to avoid a singularity in the denominator when $m = n = 0$ and to ensure a zero result. Otherwise, we see that as $m = n \rightarrow 0$, $J_1(x)/x \rightarrow x/2$ for small x , so that the first term of the expansion is nonzero and equal to the first term in the braces. This is the “tube” term as it describes the pressure field that would result if the piston were as large as the wall in which it is mounted, in which case all the other terms would vanish. In the opposite extreme, to derive the expression for the pressure field when the piston is so small that it can be considered as a point source, let us replace \tilde{u}_0 with a volume velocity \tilde{U}_0 divided by the area of the piston πa_1^2 and again use the relationship $J_1(x)/x \rightarrow x/2$ for small x to yield

$$\tilde{p}(x, y, z)|_{a_1 \rightarrow 0} = -\rho_0 c \tilde{U}_0 \frac{k}{l_x l_y} \sum_{m=0}^{\infty} \sum_{n=0}^{\infty} \frac{(2 - \delta_{m0})(2 - \delta_{n0})}{k_{mn}} \cos\left(\frac{m\pi x_1}{l_x}\right) \cos\left(\frac{n\pi y_1}{l_y}\right) \\ \times \cos\left(\frac{m\pi x}{l_x}\right) \cos\left(\frac{n\pi y}{l_y}\right) \frac{k_{mn}Z_s \cos k_{mn}z + jk\rho_0 c \sin k_{mn}z}{k\rho_0 c \cos k_{mn}l_z + jk_{mn}Z_s \sin k_{mn}l_z}. \quad (7.127b)$$

The mechanical self-impedance is given by

$$z_{11} = \frac{1}{-\tilde{u}_0} \int_{y_1-a_1}^{y_1+a_1} \int_{x_1-\sqrt{a_1^2-(y-y_1)^2}}^{x_1+\sqrt{a_1^2-(y-y_1)^2}} \tilde{p}(x, y, l_z) dx dy \quad (7.128)$$

Using the integral of Eq. (7.123) gives

$$\begin{aligned} z_{11} = \rho_0 c \left\{ \frac{\pi^2 a_1^4}{l_x l_y} \cdot \frac{\frac{Z_s}{\rho_0 c} + j \tan kl_z}{1 + j \frac{Z_s}{\rho_0 c} \tan kl_z} + 4ka_1^2 l_x l_y \sum_{m=0}^{\infty} \sum_{n=0}^{\infty} \frac{\frac{k_{mn} Z_s}{k\rho_0 c} + j \tan k_{mn} l_z}{1 + j \frac{k_{mn} Z_s}{k\rho_0 c} \tan k_{mn} l_z} \right. \\ \left. \times \frac{(2 - \delta_{m0})(2 - \delta_{n0})}{k_{mn} (n^2 l_x^2 + m^2 l_y^2) + \delta_{m0} \delta_{n0}} \cos^2 \left(\frac{m\pi x_1}{l_x} \right) \cos^2 \left(\frac{n\pi y_1}{l_y} \right) J_1^2 \left(\frac{\pi a_1 \sqrt{n^2 l_x^2 + m^2 l_y^2}}{l_x l_y} \right) \right\}. \end{aligned} \quad (7.128a)$$

The mutual mechanical impedance z_{12} is given by

$$z_{12} = \frac{1}{-\tilde{u}_0} \int_{y_2-a_2}^{y_2+a_2} \int_{x_2-\sqrt{a_2^2-(y-y_2)^2}}^{x_2+\sqrt{a_2^2-(y-y_2)^2}} \tilde{p}(x, y, l_z) dx dy \quad (7.129)$$

Using the integral of Eq. (7.123) gives

$$\begin{aligned} z_{12} = \rho_0 c \left\{ \frac{\pi^2 a_1^2 a_2^2}{l_x l_y} \cdot \frac{\frac{Z_s}{\rho_0 c} + j \tan kl_z}{1 + j \frac{Z_s}{\rho_0 c} \tan kl_z} \right. \\ \left. + 4ka_1 a_2 l_x l_y \sum_{m=0}^{\infty} \sum_{n=0}^{\infty} \frac{\frac{k_{mn} Z_s}{k\rho_0 c} + j \tan k_{mn} l_z}{1 + j \frac{k_{mn} Z_s}{k\rho_0 c} \tan k_{mn} l_z} \cdot \frac{(2 - \delta_{m0})(2 - \delta_{n0})}{k_{mn} (n^2 l_x^2 + m^2 l_y^2) + \delta_{m0} \delta_{n0}} \right. \\ \left. \times \cos \left(\frac{m\pi x_1}{l_x} \right) \cos \left(\frac{n\pi y_1}{l_y} \right) J_1 \left(\frac{\pi a_1 \sqrt{n^2 l_x^2 + m^2 l_y^2}}{l_x l_y} \right) \right. \\ \left. \times \cos \left(\frac{m\pi x_2}{l_x} \right) \cos \left(\frac{n\pi y_2}{l_y} \right) J_1 \left(\frac{\pi a_2 \sqrt{n^2 l_x^2 + m^2 l_y^2}}{l_x l_y} \right) \right\}. \end{aligned} \quad (7.130)$$

All the self- and mutual mechanical impedances are given by the single expression

$$\begin{aligned}
 \tilde{z}_{pq} = \rho_0 c \left\{ \frac{S_p S_q}{l_x l_y} \cdot \frac{\frac{Z_s}{\rho_0 c} + j \tan kl_z}{1 + j \frac{Z_s}{\rho_0 c} \tan kl_z} \right. \\
 + 4ka_p a_q l_x l_y \sum_{m=0}^{\infty} \sum_{n=0}^{\infty} \frac{\frac{k_{mn} Z_s}{k\rho_0 c} + j \tan k_{mn} l_z}{1 + j \frac{k_{mn} Z_s}{k\rho_0 c} \tan k_{mn} l_z} \cdot \frac{(2 - \delta_{m0})(2 - \delta_{n0})}{k_{mn} (n^2 l_x^2 + m^2 l_y^2) + \delta_{m0} \delta_{n0}} \\
 \times \cos\left(\frac{m\pi x_p}{l_x}\right) \cos\left(\frac{n\pi y_p}{l_y}\right) J_1\left(\frac{\pi a_p \sqrt{n^2 l_x^2 + m^2 l_y^2}}{l_x l_y}\right) \\
 \left. \times \cos\left(\frac{m\pi x_q}{l_x}\right) \cos\left(\frac{n\pi y_q}{l_y}\right) J_1\left(\frac{\pi a_q \sqrt{n^2 l_x^2 + m^2 l_y^2}}{l_x l_y}\right) \right\}
 \end{aligned} \tag{7.131}$$

where

$$k_{mn} = \sqrt{k^2 - \left(\frac{m\pi}{l_x}\right)^2 - \left(\frac{n\pi}{l_y}\right)^2}. \tag{7.132}$$

and $S_p = \pi a_p^2$, $S_q = \pi a_q^2$. The self- and mutual mechanical Z -parameters of Eq. (7.131) may be converted into specific or acoustic ones, but we have to be careful when converting into mutual-specific Z -parameters. Let us denote the mechanical Z -parameters by

$$Z_{Mpq} = \left. \frac{\tilde{f}_p}{\tilde{u}_q} \right|_{\tilde{u}_p=0} = \tilde{z}_{pq}.$$

Although the conversion to self-specific Z -parameters is straightforward, the mutual ones depend on whether we define the specific impedance as the ratio of pressure to velocity or the ratio of force to volume velocity

$$Z_{Spq} = \left. \frac{\tilde{p}_p}{\tilde{u}_q} \right|_{\tilde{u}_p=0} = \frac{Z_{Mpq}}{S_p} \quad \text{or} \quad Z'_{Spq} = \left. \frac{\tilde{f}_p}{\tilde{U}_q} \right|_{\tilde{U}_p=0} = \frac{Z_{Mpq}}{S_q}$$

The same care has to be taken in converting mutual-specific Z -parameters into acoustic ones, although the conversion from mechanical into acoustic is straightforward

$$Z_{Apq} = \left. \frac{\tilde{p}_p}{\tilde{U}_q} \right|_{\tilde{U}_p=0} = \frac{Z_{Spq}}{S_q} = \frac{Z'_{Spq}}{S_p} = \frac{Z_{Mpq}}{S_p S_q}$$

PART XXIV: TRANSMISSION-LINE ENCLOSURES

7.19 TRANSMISSION-LINE ENCLOSURES

General description

A transmission-line enclosure has a duct or tube between the rear side of the loudspeaker and an opening to the outside world, which is usually folded to save space. Sound is radiated both from the front of the loudspeaker and from the opening. Unlike a bass-reflex enclosure where the dimensions of the enclosure and port are usually small compared with the wavelength, the duct is long enough for it to introduce significant phase shifts at low frequencies. If the length of the duct is one-quarter of a wavelength, a small movement of the loudspeaker diaphragm creates a large movement of air at the duct opening. Thus, the enclosure causes a large response at the quarter-wavelength frequency, and this permits a small loudspeaker (2–4 in. diameter) to radiate appreciable sound at frequencies down to 100 Hz. But there is a problem. When the frequency is increased, the sound radiated from the tube opening becomes opposite in phase from that radiated from the front of the loudspeaker. Thus, a sizable dip in the total radiated sound will occur. This dip in response will happen at half-wavelength multiples. In practice, two solutions to this problem have been employed. One is to use a digital signal processor (DSP) to change the phases and the other is to fill the tube with a lightweight sound-absorbing material. Both solutions remove or greatly modify the “bumpiness” in the response curve. When the latter solution is selected, the tube is usually tapered in length so that it acts like in inverse horn loudspeaker. Although the extent is not known to which DSP is used in practice and/or adding sound-absorbing material in the duct, two transmission-line loudspeakers are shown in [Fig. 7.35](#).

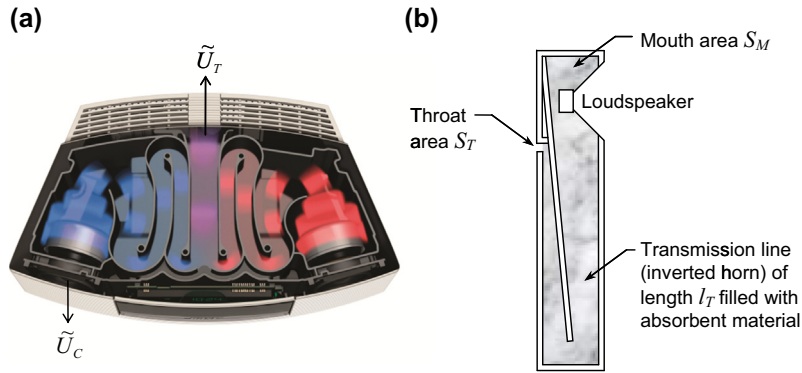


Figure 7.35 Transmission-line enclosures: (a) Substantially “straight” transmission line, except for some flaring near the drive unit, as used in the Bose Wave[®] music system. *Courtesy of Bose Corporation.* (b) “Tapered” transmission line. The diaphragm has an area S_D .

Fig. 7.35a shows a substantially straight transmission line as used in the Bose Wave[®] music system. Fig. 7.35b shows a tapered transmission line. A commercial example is the Bowers and Wilkins Nautilus[™], which as the name suggests, uses a tapered transmission line rolled into a spiral.

Summary of transmission-line design

To determine the cutoff frequency, frequency response, and the volume of the box:

If the Thiele—Small parameters (R_E , Q_{ES} , Q_{MS} , f_s , S_D , and V_{AS}) of the chosen drive unit are not supplied by the manufacturer, they may be measured according to Section 6.10. Then $Q_{TS} = Q_{ES}Q_{MS}/(Q_{ES} + Q_{MS})$.

If we assume that the drive unit will behave more or less as if it were mounted in an infinite baffle, we can select the frequency-response shape from Table 7.2 for which the Q_{TC} value is closest to the Q_{TS} value of the chosen drive unit (or choose a drive unit whose Q_{TS} value is closest to that of the desired frequency-response shape).

From the value of f_{3dB}/f_C in the table, compute the cutoff frequency f_{3dB} assuming that $f_C \approx f_s$.

The frequency-response shape below the first diaphragm break-up mode but above the transmission-line cutoff frequency f_T is shown in Fig. 7.16. Below f_T , the roll-off increases from second-order (12 dB/octave) to third-order (18 dB/octave).

To determine the maximum SPL:

If the loudspeaker is to be used near a wall or a rigid planar surface, which is large compared with the longest wavelength to be reproduced, then the maximum sound pressure SPL_{max} at a distance r is obtained from Eq. (6.34) to give

$$\text{SPL}_{\max} = 20 \log_{10} \frac{1}{rc \times 20 \times 10^{-6}} \sqrt{\frac{Z_{\text{nom}} W_{\max} 2\pi f_s^3 V_{AS} \rho_0}{R_E Q_{ES}}} \text{ dB SPL @ 1 m}$$

where W_{\max} is the maximum rated input power. Otherwise, if it is to be used in the free field, subtract 6 dB from SPL_{\max} .

To determine the excursion limit:

The maximum peak diaphragm displacement at frequencies well below the suspension resonance is obtained from Eq. (6.15) to give

$$\eta_{\max} = \frac{1}{S_{DC}} \sqrt{\frac{Z_{\text{nom}} W_{\max} V_{AS}}{R_E Q_{ES} \pi f_s \rho_0}}$$

If this value is greater than the rated x_{\max} limit of the drive unit, then a high-pass filter should be employed to remove all content below the suspension resonance frequency. If this is not possible, then an alternate drive unit with a greater x_{\max} limit should be considered.

To determine the transmission-line dimensions and filling material:

Determine the flow velocity u from Eq. (7.137) and the flow resistance of the filling material from Eq. (7.8).

Calculate the length l_T of the transmission-line using Eq. (7.138). Choose a convenient mouth area S_M to fit around the back of the drive unit and choose a throat area S_T which is about 4–8 times smaller. The volume of the transmission line V_T is then given by Eq. (7.139).

Calculate the specific acoustic resistance R_{ST} of the filling material from Eq. (7.140) and the transmission-line cutoff frequency from Eq. (7.141).

The cutoff frequency should be less than one-half of the suspension resonance frequency f_s . If it is not, then consider a different filling material with a higher flow resistance R_f . Alternatively, increase the length l_T of the transmission line or reduce the throat area S_T or both.

To obtain a smooth frequency response from passive loudspeaker, without equalization, the tapered transmission line shown in Fig. 7.35b is preferable. Although a horn is commonly used as a high-pass filter because it increases the radiated volume velocity above its cutoff frequency, here we have an inverted parabolic horn which, as we shall see, acts as a low-pass filter because it attenuates the volume velocity radiated from its outlet or throat. To obtain the smoothest possible response, it is tuned to roll-off well below the fundamental resonance frequency of the drive unit, which in turn behaves as though it is mounted in large sealed enclosure except that the filling material may damp the fundamental resonance slightly. The low-frequency roll-off of a loudspeaker with a

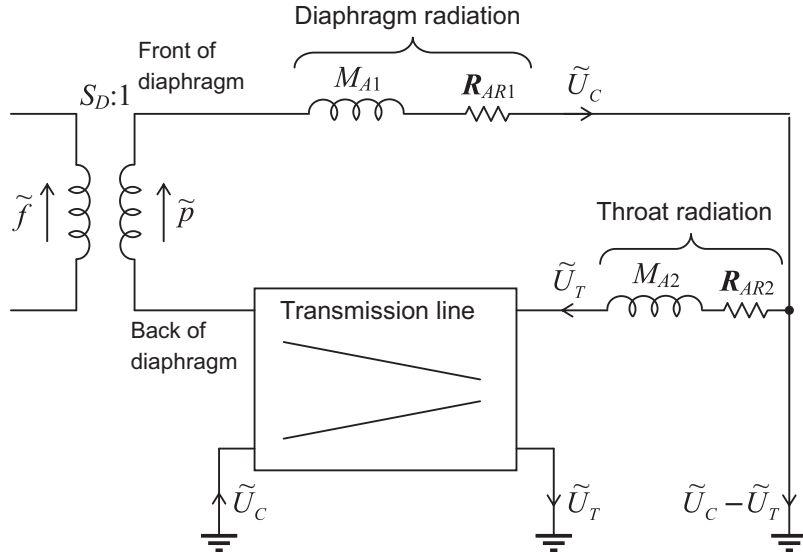


Figure 7.36 Analogous acoustical circuit for a loudspeaker box with a transmission line, which is a reverse finite horn and may be modeled using the transmission-parameter matrices given in Section 9.13. In the case of Fig. 7.35(b), it is parabolic. The volume velocity of the diaphragm is \tilde{U}_C and that of the transmission-line throat outlet is \tilde{U}_T .

transmission-line enclosure has a second-order slope initially, increasing to third-order below the transmission-line cutoff frequency.

We shall assume for the remainder of this analysis that $ka < 0.5$. In other words, we are restricting ourselves to the very low-frequency region where the radiation from both the port and the loudspeaker is nondirectional. Hence, we can draw the simplified model of Fig. 7.36.

Acoustical circuit

The acoustical circuit for the transmission line and radiation is given in Fig. 7.36 using lumped elements, except for the transmission line, which is treated as a two-port network. The series radiation mass and resistance on the front side of the diaphragm are, respectively, M_{A1} and R_{AR1} . Unlike with the bass-reflex enclosure, we omit leakage losses as we shall assume that the losses within the lining material will dominate over all others. Finally, the series radiation mass and resistance from the throat of the transmission line are, respectively, M_{A2} and R_{AR2} . The values of these quantities are M_{A2} as in Eq. (7.32), but with a_T instead of a , that is,

$$M_{A2} = 0.2026\rho_0/a_T$$

R_{AR2} as in Eq. (7.31), and

M_{A1} is acoustic-radiation mass for the front side of the loudspeaker diaphragm = $0.2026\rho_0/a$ kg/m⁴. Note that we assume the loudspeaker unit is equivalent to a piston radiating from one side only in free space.

$R_{AR1} = 0.01075f^2$ is acoustic-radiation resistance for the front side of the loudspeaker diaphragm in N·s/m⁵ (see Fig. 4.39 for $ka > 1.0$).

ρ_0 is density of air in kg/m³ (normally about 1.18 kg/m³).

a_T is effective radius in m of the transmission-line throat. If it is not circular, then let $a_T = \sqrt{S_T/\pi}$, where S_T is the effective area of the throat opening in m².

$S_M = \pi a_M^2$ is effective cross-sectional area of the transmission-line mouth in m².

$S_T = \pi a_T^2$ is effective cross-sectional area of transmission-line throat outlet in m².

l_T is length of the transmission line in m.

Electromechanoacoustical circuit

The complete circuit for a loudspeaker with a transmission-line enclosure is obtained by combining Figs. 6.4(b) and 7.36. To do this, the acoustical radiation element of the circuit labeled “ $2M_{M1}$ ” in Fig. 6.4(b) is removed, and the circuit of Fig. 7.36 is substituted in its place. The resulting circuit with the transformer removed and everything referred to the acoustical side is shown in Fig. 7.37.

The quantities not listed in the previous paragraph are

\tilde{e}_g is open-circuit voltage in V of the audio amplifier.

B is flux density in the air gap in T (1 T = 10⁴ G).

l is length in m of voice-coil wire.

R_g is output electrical resistance in Ω of the audio amplifier.

R_E is electrical resistance in Ω of the voice coil.

a is effective radius of the diaphragm in m.

$M_{AD} = M_{MD}/S_D^2$ is acoustic mass of the diaphragm and the voice coil in kg/m⁴.

$C_{AS} = C_{MS}S_D^2$ is acoustic compliance of the diaphragm suspension in m⁵/N.

$R_{AS} = R_{MS}/S_D^2$ is acoustic resistance of the diaphragm suspension in N·s/m⁵.

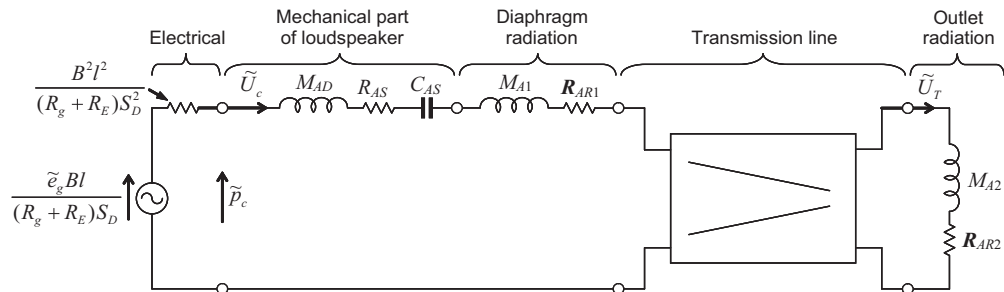


Figure 7.37 Complete electromechanoacoustical circuit for a transmission-line loudspeaker. The total force produced at the voice coil by the electric current is $\tilde{p}_c S_D$, where S_D is the area of the diaphragm. The volume velocity of the diaphragm is \tilde{U}_c and that of the transmission-line throat outlet is \tilde{U}_T .

If the outlet of the transmission line is closed off so that \tilde{U}_T equals zero, then Fig. 7.37 essentially reduces to Fig. 7.6. At very low frequencies, the mass of air moving *out* of the lower opening is nearly equal to that moving into the upper opening at all instants. In other words, at very low frequencies, the volume velocities at the two openings are nearly equal in magnitude and opposite in phase.

Radiated sound

The outlet in the box of a transmission-line baffle is generally effective only at fairly low frequencies. At those frequencies, its dimensions are generally so small that it can be treated as though it were a simple source. The loudspeaker diaphragm can also be treated as a simple source because its area is often nearly the same as that of the opening.

Referring to Eq. (4.71), we find that the sound pressure at a distance r away from the transmission-line loudspeaker is

$$\tilde{p} = \tilde{p}_1 + \tilde{p}_2 \approx \frac{j\omega\rho_0}{4\pi r} \left(\tilde{U}_c e^{-jkr_1} - \tilde{U}_T e^{-jkr_2} \right), \quad (7.133)$$

where

\tilde{p}_1 and \tilde{p}_2 are complex sound pressures, respectively, from the diaphragm and transmission-line outlet at distance r .

r is average distance of the point of observation from the diaphragm and the transmission-line outlet. Note that r is large compared with the diaphragm and port radii.

r_1 and r_2 are actual distances, respectively, of the point of observation from the diaphragm and transmission-line outlet.

\tilde{U}_c is complex volume velocity of the diaphragm.

\tilde{U}_T is complex volume velocity of the transmission-line outlet. Note that the negative sign is used for \tilde{U}_T because, except for phase shift introduced by the transmission line, the air from its throat outlet moves outward when the air from the diaphragm moves inward.

In addition, the complex volume velocity necessary to compress and expand the air inside the transmission line is

$$\tilde{U}_B = \tilde{U}_c - \tilde{U}_T. \quad (7.134)$$

If we now let $r_1 = r_2 = r$ by confining our attention to a particular point in space in front of the loudspeaker where this is true, we get

$$\tilde{p} \approx \frac{j\omega\rho_0}{4\pi r} (\tilde{U}_c - \tilde{U}_T) e^{-jkr}. \quad (7.135)$$

Because $\tilde{U}_c - \tilde{U}_T = \tilde{U}_B$, we have simply that

$$|\tilde{p}| \approx \frac{f\rho_0|\tilde{U}_B|}{2r}. \quad (7.136)$$

As with the bass-reflex enclosure, the sound pressure produced at faraway points equidistant from cone and outlet of a transmission-line loudspeaker is directly proportional to the volume velocity necessary to compress and expand the air inside the transmission line.

At very low frequencies, where the wavelength is much greater than the length l_T of the transmission line, \tilde{U}_c becomes nearly equal to \tilde{U}_T , and the pressure, measured at points $r = r_1 = r_2$, approaches zero. In fact, the two sources behave like a dipole so that the radiated sound pressure decreases by a factor of 2 for each halving of frequency. In addition, if we are below the lowest resonance frequency of the circuit of Fig. 7.37, the diaphragm velocity \tilde{U}_c halves for each halving of frequency. Hence, in this very low-frequency region, the sound pressure decreases by a factor of 8, which is 18 dB, for each halving of frequency. In other words, the slope is third order. Note that this decrease is greater than that for a loudspeaker in a closed box or in an infinite baffle (which is second order) but less than that for a loudspeaker in a vented box (which is fourth order). The effect is somewhat similar to mounting the loudspeaker in a very large flat open baffle (which is also third order).

The flow resistance R_f of the filling material, given by Eq. (7.8) is dependent on the flow velocity u and is therefore nonlinear. The problem is that the flow velocity varies with frequency and with position along the tapered transmission line. This could lead to a very complicated analysis, but if we make sure that there is enough attenuation within the transmission line for the radiation from the throat outlet not to interfere too much with the direct radiation from the diaphragm, we need not worry too much about the accuracy of the model. The flow resistance will mainly affect the damping of the fundamental resonance of the drive unit over a relatively small range of frequencies. Therefore, we set the rms velocity value to that of the diaphragm at resonance at its maximum displacement:

$$u \approx \frac{\omega_s x_{\max}}{\sqrt{2}}. \quad (7.137)$$

We then obtain the flow resistance R_f from Eq. (7.8). Usually, we set the length l_T to be one-quarter of the wavelength at the suspension resonance frequency f_s so that

$$l_T = \frac{c}{4f_s}. \quad (7.138)$$

This rather naïve formula assumes the free-space speed of sound c , whereas in the lossy filling material it is somewhat slower [see Eqs. (2.115) and (2.117) for the speed of sound in a material with flow resistance R_f]. However, this is largely compensated for by

the fact that the resonance in a tapered duct is not a true quarter-wavelength one, but rather occurs when $l_T = \alpha\lambda/(2\pi)$, where $J_0(\alpha) = 0$, or $l_T = \lambda/2.61274$ (assuming $S_T \ll S_M$). The volume occupied by the transmission line is

$$V_T = \frac{S_T + S_M}{2} l_T. \quad (7.139)$$

By examining the asymptotic low-frequency behavior of the tapered transmission line, we find that its specific resistance R_{ST} as seen from the mouth, is

$$R_{ST} = \frac{S_M}{S_M - S_T} l_T R_f \ln \frac{S_M}{S_T}. \quad (7.140)$$

If the filling material has ample overall specific resistance (>400 rayls), we can use the following empirical formula for the transmission-line cutoff frequency

$$f_T \approx \frac{2P_0}{3R_{ST}l_T}. \quad (7.141)$$

Performance

With the information just given, it is possible to calculate the response of the loudspeaker in a transmission-line enclosure. A complete example is given in the next section.

From Fig. 7.37, we see that, for frequencies below ω_T radiation from the transmission-line outlet (proportional to $-\tilde{U}_0$) is out of phase with the radiation from the diaphragm (proportional to \tilde{U}_c). As a result, the response at very low frequencies is usually not enhanced by the transmission line. Above the cutoff frequency ω_T radiation from the throat is in phase with that from the diaphragm at some frequencies but out of phase at others. However, because the radiation from the throat is attenuated, it has relatively little influence on the overall response. Consequently, a transmission-line enclosure behaves somewhat like a large open baffle, and the need for a reasonably stiff suspension is even greater than in the case of a bass-reflex enclosure. A large loudspeaker diaphragm usually is superior to a small one because the amplitude of its motion is less, thereby reducing nonlinear distortion.

At low frequencies, the wavelength is usually very large compared with the box dimensions if the transmission line is folded, so the small resulting phase difference between the outputs of the transmission line and diaphragm will have little effect on the performance.

An advantage of a transmission-line loaded loudspeaker is that the buildup of pressure inside the enclosure is much less than inside a closed-box or even a bass-reflex enclosure above the box resonance. Therefore, pressure waves from the rear of the diaphragm are less likely to couple to the walls of the enclosure and cause unwanted vibrations.

Example 7.4. Transmission-line enclosure design. In the previous part, we discussed in detail the design of a bass-reflex baffle for a low-frequency (woofer) loudspeaker. We presented methods for the determination of its physical constants, and we showed a comparison between measurements and calculations.

In this part, we shall use a single full-range unit loaded at the rear with a transmission line. The brief here is to design a compact loudspeaker for domestic use with extended bass response at moderate listening levels in an enclosure no larger than 2½ liters. We aim to produce 86 dB SPL at 1 m using just 2 W of input power, or 92 dB SPL from a stereo pair. We wish to extend the frequency response down to 140 Hz. We assume that the loudspeaker will be placed near a wall to support the low frequencies.

A suitable drive unit is the Peerless 2½-inch “Tympany” type 830,985. The Thiele–Small parameters are as follows:

$$R_E = 3.7 \Omega$$

$$Q_{ES} = 0.83$$

$$Q_{MS} = 3.46$$

$$f_S = 140 \text{ Hz}$$

$$S_D = 22 \text{ cm}^2$$

$$V_{AS} = 0.472 \text{ L}$$

Then

$$Q_{TS} = \frac{Q_{ES} Q_{MS}}{Q_{ES} + Q_{MS}} = 0.67.$$

From Eq. (6.48), we can calculate the reference efficiency

$$E_{ff} = 100 \frac{8 \times 3.14^2 \times 472 \times 10^{-6} \times 140^3}{0.83 \times 344.8^3} = 0.3\%.$$

To calculate the maximum SPL, we first obtain C_{MS} , M_{MS} , and Bl from Eqs. (6.27), (6.28), and (6.30), respectively:

$$C_{MS} = \frac{472 \times 10^{-6}}{0.0022^2 \times 1.18 \times 344.8^2} = 0.695 \text{ mm/N},$$

$$M_{MS} = \frac{1}{(2 \times 3.14 \times 140)^2 \times 695 \times 10^{-6}} = 0.0019 \text{ kg},$$

$$Bl = \sqrt{\frac{3.7}{2 \times 3.14 \times 140 \times 0.83 \times 695 \times 10^{-6}}} = 2.7 \text{ T}\cdot\text{m}.$$

We obtain from Eq. (6.33)

$$\text{SPL}_{2W} = 20 \log_{10} \left(\frac{\sqrt{3.7 \times 2} \times 2.7 \times 0.0022 \times 1.18}{2 \times 3.14 \times 3.7 \times 0.0019 \times 20 \times 10^{-6}} \right) = 86.7 \text{ dB SPL @ 1 m.}$$

Next we use Eq. (6.35) to check the peak displacement at f_S for 86 dB SPL:

$$\eta_{\text{peak}} = \frac{\sqrt{2} \times 1 \times 10^{\left(\frac{86}{20} - 5\right)}}{\pi \times 140^2 \times 1.18 \times 0.0022} = 1.8 \text{ mm.}$$

However, $Q_{TS} = 0.66$ so that at resonance the actual displacement is $0.66 \times 1.8 = 1.2 \text{ mm}$ and the sound pressure is $86 + 20 \log_{10} 0.66 = 82.4 \text{ dB SPL}$. It turns out that the x_{max} value of the drive unit is 2 mm, so there should be no problems with this design provided that the input power is limited to just 2 W at low frequencies. For the purpose of evaluating the flow resistance of the filling material, we take the flow velocity u from Eq. (7.137) as follows:

$$u \approx \frac{2\pi 140 \times 0.0012}{\sqrt{2}} = 0.75 \text{ m/s.}$$

Suppose that our filling material, which in this case is lamb's wool, has a porosity $\varphi = 0.98$ and an average fiber diameter of 50 μm . From Eq. (7.8), we obtain the flow resistance:

$$\begin{aligned} R_f &= \frac{4 \times 1.86 \times 10^{-5} \times 0.02}{0.98 \times 50^2 \times 10^{-12}} \left(\frac{1 - \frac{4}{\pi} \times 0.02}{2 + \ln \frac{1.86 \times 10^{-5} \times 0.98}{2 \times 50 \times 10^{-6} \times 1.18 \times 0.75}} + \frac{6}{\pi} \times 0.02 \right) \\ &= 1433 \text{ rayls/m.} \end{aligned}$$

Now, we turn to the transmission-line dimensions. Let us make the length l_T equal to one-quarter wavelength at f_S from Eq. (7.138), so that

$$l_T = \frac{344.8}{4 \times 140} = 0.62 \text{ m.}$$

For convenience, we make the mouth area a square large enough to fit the diameter of the drive unit:

$$S_M = 7 \text{ cm} \times 7 \text{ cm} = 49 \text{ cm}^2$$

and

$$S_T = S_M/4 = 12.25 \text{ cm}^2,$$

which from Eq. (7.139) makes the total volume

$$V_T = \frac{(12.25 + 49) \times 10^{-4}}{2} \times 0.62 = 1.9 \times 10^{-3} \text{ m}^3 \text{ or } 1.9 \text{ L.}$$

From Eq. (7.140), this gives a specific resistance value of

$$R_{ST} = \frac{49}{49 - 12.25} \times 0.62 \times 1433 \times \ln \frac{49}{12.25} = 1642 \text{ rayls.}$$

Now from Eq. (7.141), we can calculate the cutoff frequency

$$f_T \approx \frac{2 \times 10^5}{3 \times 1642 \times 0.62} = 65.5 \text{ Hz,}$$

which is well below the suspension resonance frequency f_S of the drive unit.

Let us now create a semianalytical simulation model of the design of Fig. 7.38 using two-port networks and transmission matrices, as introduced in Section 3.10 and Fig. 4.43. The schematic is shown in Fig. 7.39. Although it is based on the circuit of Fig. 7.37, a gyrator has been inserted between the electrical elements and the mechanical ones, which enables us to calculate more easily the generator current \tilde{i}_g from which we obtain the electrical impedance. We are ignoring the generator impedance R_g because in the experimental setup this is negligible compared with R_E . The dashed boxes are lumped-element two-port networks and the solid boxes are analytical ones. From the schematic, we create the transmission matrices required to represent each two-port network as follows:

1. *Coil.*

$$\begin{bmatrix} \tilde{e}_g \\ \tilde{i}_g \end{bmatrix} = \begin{bmatrix} 1 & Z_E \\ 0 & 1 \end{bmatrix} \cdot \begin{bmatrix} \tilde{e}_1 \\ \tilde{i}_1 \end{bmatrix} = \mathbf{C} \cdot \begin{bmatrix} \tilde{e}_1 \\ \tilde{i}_1 \end{bmatrix}$$

where $Z_E = R_E + j\omega L_E$.

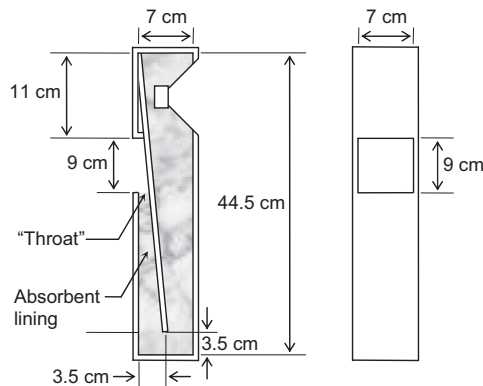


Figure 7.38 Example of transmission-line enclosure design.

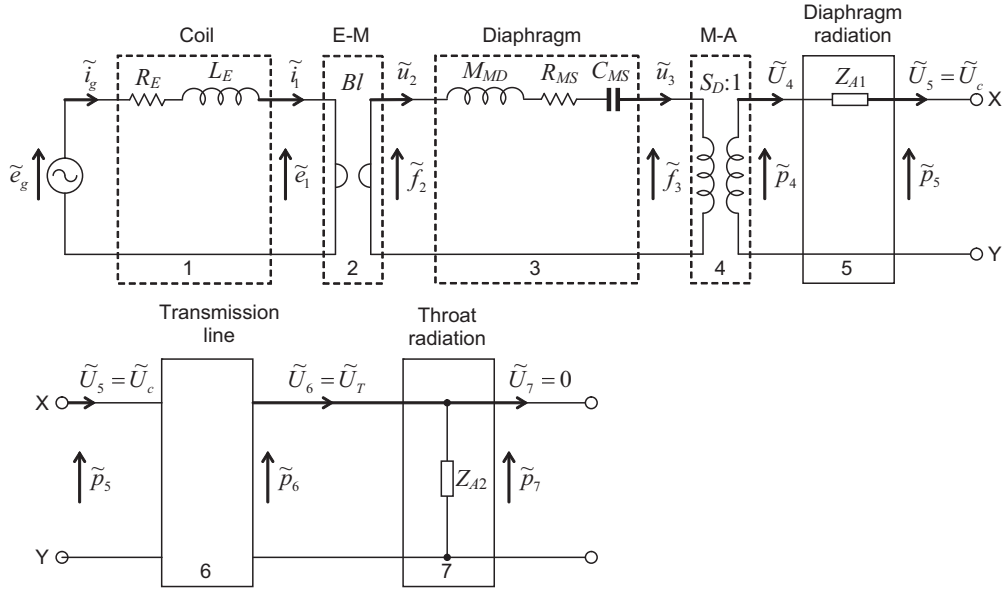


Figure 7.39 Semianalytical model of example transmission-line enclosure design shown in Fig. 7.38 using transmission matrices. The matrix for the transmission line is given in Eq. (9.65) for a reverse parabolic horn.

2. Electromechanical transduction.

$$\begin{bmatrix} \tilde{e}_1 \\ \tilde{i}_1 \end{bmatrix} = \begin{bmatrix} 0 & Bl \\ (Bl)^{-1} & 0 \end{bmatrix} \cdot \begin{bmatrix} \tilde{f}_2 \\ \tilde{u}_2 \end{bmatrix} = \mathbf{E} \cdot \begin{bmatrix} \tilde{f}_2 \\ \tilde{u}_2 \end{bmatrix}$$

3. Diaphragm.

$$\begin{bmatrix} \tilde{f}_2 \\ \tilde{u}_2 \end{bmatrix} = \begin{bmatrix} 1 & Z_{MD} \\ 0 & 1 \end{bmatrix} \cdot \begin{bmatrix} \tilde{f}_3 \\ \tilde{u}_3 \end{bmatrix} = \mathbf{D} \cdot \begin{bmatrix} \tilde{f}_3 \\ \tilde{u}_3 \end{bmatrix}$$

where $Z_{MD} = j\omega M_{MD} + R_{MS} + 1/(j\omega C_{MS})$. We must exclude the radiation mass from the diaphragm so that $M_{MD} = M_{MS} - 16\rho_0 a^3/3$, where $a = \sqrt{S_D/\pi}$.

4. Mechanoacoustical transduction.

$$\begin{bmatrix} \tilde{f}_3 \\ \tilde{u}_3 \end{bmatrix} = \begin{bmatrix} S_D & 0 \\ 0 & S_D^{-1} \end{bmatrix} \cdot \begin{bmatrix} \tilde{p}_4 \\ \tilde{U}_4 \end{bmatrix} = \mathbf{M} \cdot \begin{bmatrix} \tilde{p}_4 \\ \tilde{U}_4 \end{bmatrix}$$

5. Diaphragm radiation.

$$\begin{bmatrix} \tilde{p}_4 \\ \tilde{U}_4 \end{bmatrix} = \begin{bmatrix} 1 & Z_{A1} \\ 0 & 1 \end{bmatrix} \cdot \begin{bmatrix} \tilde{p}_5 \\ \tilde{U}_5 \end{bmatrix} = \mathbf{D} \cdot \begin{bmatrix} \tilde{p}_5 \\ \tilde{U}_5 \end{bmatrix}$$

where Z_{A1} is the acoustic-radiation impedance of the diaphragm given by Eqs. (13.116)–(13.118) with $a = \sqrt{S_D/\pi}$.

6. Transmission line. Distributed parameter model:

$$\begin{bmatrix} \tilde{p}_5 \\ \tilde{U}_5 \end{bmatrix} = \frac{1}{a_{11}a_{22} - a_{12}a_{21}} \begin{bmatrix} a_{22} & a_{12} \\ a_{21} & a_{11} \end{bmatrix} \cdot \begin{bmatrix} \tilde{p}_6 \\ \tilde{U}_6 \end{bmatrix} = \mathbf{T} \cdot \begin{bmatrix} \tilde{p}_6 \\ \tilde{U}_6 \end{bmatrix}$$

where

$$a_{11} = -\frac{\pi}{2} \mathbf{k}x_M (J_0(\mathbf{k}x_T)Y_1(\mathbf{k}x_M) - J_1(\mathbf{k}x_M)Y_0(\mathbf{k}x_T))$$

$$a_{12} = j \frac{Z_{ST}}{S_M} \frac{\pi}{2} \mathbf{k}x_M (J_0(\mathbf{k}x_T)Y_0(\mathbf{k}x_M) - J_0(\mathbf{k}x_M)Y_0(\mathbf{k}x_T))$$

$$a_{21} = j \frac{S_T}{Z_{ST}} \frac{\pi}{2} \mathbf{k}x_M (J_1(\mathbf{k}x_T)Y_1(\mathbf{k}x_M) - J_1(\mathbf{k}x_M)Y_1(\mathbf{k}x_T))$$

$$a_{22} = \frac{S_T}{S_M} \frac{\pi}{2} \mathbf{k}x_M (J_1(\mathbf{k}x_T)Y_0(\mathbf{k}x_M) - J_0(\mathbf{k}x_M)Y_1(\mathbf{k}x_T))$$

where

$$x_T = S_T l_T / (S_M - S_T) \quad \text{and} \quad x_M = S_M l_T / (S_M - S_T).$$

For Z_{ST} and \mathbf{k} , we use Eqs. (7.10) and (7.11), respectively. The ratio of the throat volume velocity to the mouth volume velocity

$$\tilde{U}_T / \tilde{U}_c = \tilde{U}_6 / \tilde{U}_5 = 1/a_{11}$$

is plotted in Fig. 7.40, assuming that the pressure at the throat is virtually zero. We see that the volume velocity rolls off smoothly above $f_T = 65.5$ Hz.

7. Throat radiation.

$$\begin{bmatrix} \tilde{p}_6 \\ \tilde{U}_6 \end{bmatrix} = \begin{bmatrix} 1 & 0 \\ Z_{A2}^{-1} & 1 \end{bmatrix} \cdot \begin{bmatrix} \tilde{p}_7 \\ \tilde{U}_7 \end{bmatrix} = \mathbf{R} \cdot \begin{bmatrix} \tilde{p}_7 \\ \tilde{U}_7 \end{bmatrix}$$

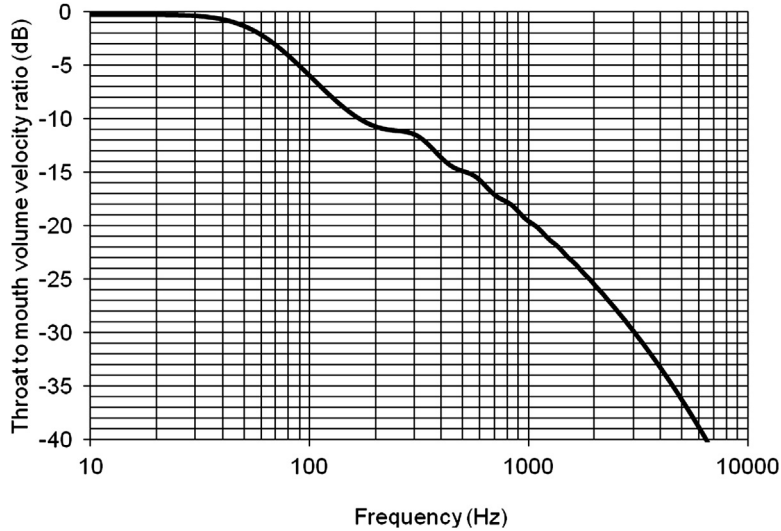


Figure 7.40 Graph of the volume velocity attenuation produced by the transmission-line enclosure design shown in Fig. 7.38. Curve is calculated from $20 \log_{10} |\tilde{U}_T / \tilde{U}_c|$.

In this case, the throat outlet is rectangular and close to a large planar surface so that Z_{A2} may be given by the impedance of a rectangular piston in an infinite baffle using Eqs. (13.326) and (13.327), where

$$Z_{A2} = (\mathbf{R}_s + jX_s) / S_T.$$

First, we evaluate \tilde{p}_7 at the end of the chain:

$$\begin{bmatrix} \tilde{e}_g \\ \tilde{i}_g \end{bmatrix} = \mathbf{A} \cdot \begin{bmatrix} \tilde{p}_7 \\ 0 \end{bmatrix}$$

where

$$\mathbf{A} = \mathbf{C} \cdot \mathbf{E} \cdot \mathbf{D} \cdot \mathbf{M} \cdot \mathbf{F} \cdot \mathbf{T} \cdot \mathbf{R} = \begin{bmatrix} a_{11} & a_{12} \\ a_{21} & a_{22} \end{bmatrix}$$

Hence, $\tilde{p}_7 = \tilde{e}_g / a_{11}$. Then, we work backward to obtain the volume velocities we wish to evaluate. In particular, we are interested in the far-field pressure, which according to Eq. (7.136) is a function of

$$\tilde{U}_B = \tilde{U}_c - \tilde{U}_T = \tilde{U}_5 - \tilde{U}_6.$$

This procedure is fairly straightforward and does not involve any matrix inversion. From the outlet radiation matrix (7), we obtain

$$\tilde{U}_T = \tilde{U}_6 = \tilde{p}_7 / Z_{A2}$$

and working back further to the transmission-line matrix (6) we obtain

$$\begin{bmatrix} \tilde{p}_5 \\ \tilde{U}_5 \end{bmatrix} = \mathbf{N} \cdot \begin{bmatrix} \tilde{p}_7 \\ 0 \end{bmatrix}$$

where

$$\mathbf{N} = \mathbf{T} \cdot \mathbf{R} = \begin{bmatrix} n_{11} & n_{12} \\ n_{21} & n_{22} \end{bmatrix}$$

so that

$$\tilde{U}_c = \tilde{U}_5 = n_{21} \tilde{p}_7$$

and therefore

$$\tilde{U}_B = \tilde{U}_c - \tilde{U}_T = \tilde{U}_5 - \tilde{U}_6 = (n_{21} - 1/Z_{A2}) \tilde{e}_g / a_{11}$$

The throat volume velocity is given by

$$\tilde{U}_T = \tilde{U}_6 = \tilde{e}_g / (a_{11} Z_{A2})$$

and the diaphragm volume velocity by

$$\tilde{U}_c = \tilde{U}_5 = n_{21} \tilde{e}_g / a_{11}$$

To plot the normalized far-field on-axis pressure, we simply divide \tilde{U}_B by a reference volume velocity

$$\tilde{U}_{ref} = \frac{\tilde{e}_g B I S_D}{\omega M_{MS} R_E}$$

and plot $20 \log_{10} |\tilde{U}_B / \tilde{U}_{ref}|$ as shown in Fig. 7.41. The throat and diaphragm volume velocities,

$$20 \log_{10} |\tilde{U}_T / \tilde{U}_{ref}| \text{ and } 20 \log_{10} |\tilde{U}_c / \tilde{U}_{ref}|$$

respectively, are plotted separately in Fig. 7.42. Individually, the outputs from the diaphragm and throat are very smooth, but their combined output shown in Fig. 7.41 does exhibit some very small 1 dB ripples which will be hardly audible. Obviously, the response at 90 Hz is not increased much by the tube, only about 2.6 dB. If the added sound-absorbing material is a lot less attenuating, the bass response will be greater, but the radiation from the port will become very “peaky” and the combined response will be

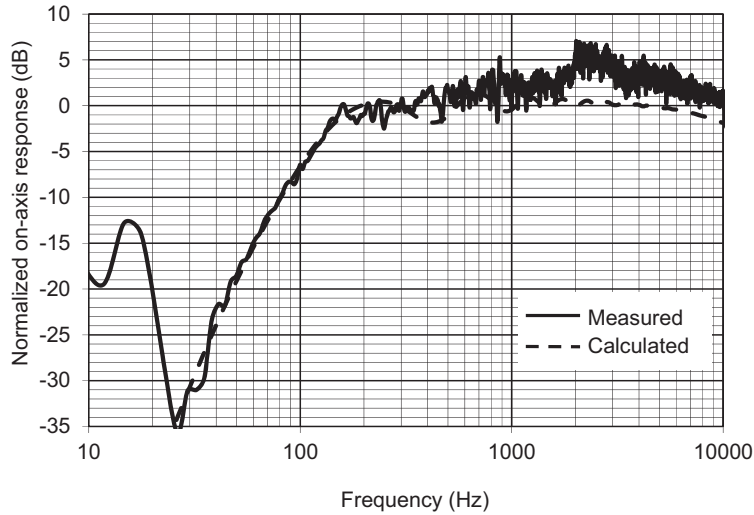


Figure 7.41 Graphs of the on-axis sound pressure level produced by the transmission-line enclosure design shown in Fig. 7.38. The *dashed curves* are calculated from $20 \log_{10} |\tilde{U}_B / \tilde{U}_{ref}|$. *Solid curves* are measured.

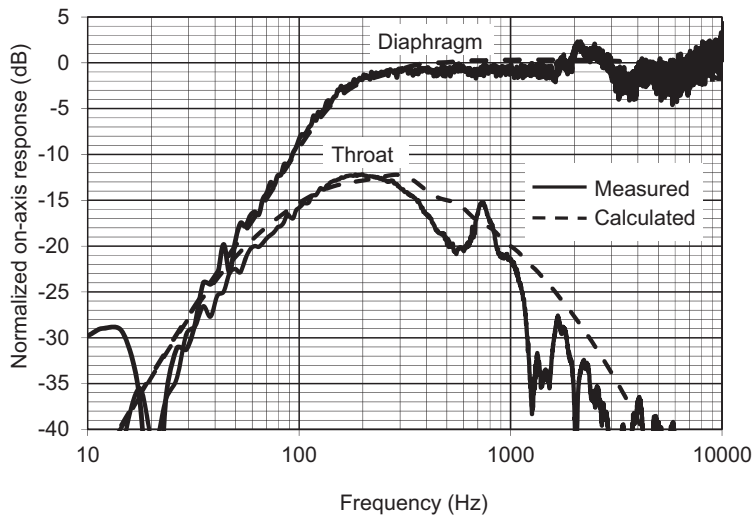


Figure 7.42 Graphs of the on-axis sound pressure level produced by throat and diaphragm of the transmission-line enclosure design shown in Fig. 7.38. The *dashed curves* are calculated from $20 \log_{10} |\tilde{U}_T / \tilde{U}_{ref}|$ and $20 \log_{10} |\tilde{U}_c / \tilde{U}_{ref}|$ for the transmission-line outlet and diaphragm, respectively. *Solid curves* are measured.

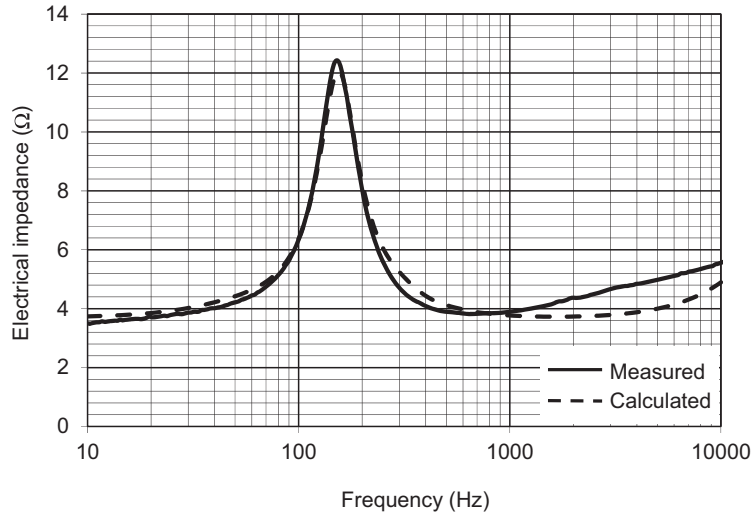


Figure 7.43 Graphs of the electrical input impedance of the transmission-line enclosure design shown in Fig. 7.38. The *dashed curves* are calculated from $Z_E = |\tilde{e}_g/\tilde{i}_g| = a_{11}/a_{21}$. *Solid curves* are measured.

irregular. The design goal is to allow only enough “peakiness” that the irregularities will not be perceived by the listener. If the “peakiness” is great enough to give a substantial boost to the lowest frequencies, digital signal processing will have to be employed to make the total radiation adequately smooth with frequency. Finally, we can obtain the input impedance from \tilde{e}_g/\tilde{i}_g where $\tilde{i}_g = a_{21}\tilde{p}_7$ and from above $\tilde{p}_7 = \tilde{e}_g/a_{11}$. Therefore, the input impedance is simply $Z_E = a_{11}/a_{21}$, as plotted in Fig. 7.43.

PART XXV: MULTIPLE DRIVE UNITS

7.20 CROSSOVER FILTERS

Many high-fidelity sound systems employ two or more loudspeaker drive units. One, called a *woofer*, covers the low-frequency range, whereas the other, called a *tweeter*, covers the high-frequency range. Sometimes, a third unit or *squawker* is included to cover the midrange. An electrical network, called a *crossover* network, is used to divide the output energy from the amplifier into the different frequency regions covered by the multiple drive units. Here, we shall concentrate on two-way crossovers as the same rules can be applied when designing loudspeakers with three or more drive units.

Classical crossover filters

Fig. 7.44 shows an outline schematic of a two-way loudspeaker with a classical crossover network. The woofer is fed via an n th-order low-pass filter and the tweeter via an n th-order high-pass filter. The transfer functions of the low-pass and high-pass filters are $L_n(s)$ and $H_n(s)$, respectively, where $s = j\omega$ is the complex frequency. These filters are designed such that when their outputs are summed, they form all-pass filters $F_n(s) = L_n(s) + H_n(s)$, that is, $|F_n(s)| = 1$ at all frequencies, although the phase varies except in the case of $n = 1$. Furthermore, the input impedance is R at all frequencies, so that the power dissipation is uniform. Low-pass filter circuits of orders $n = 1$ to 6 are shown in Fig. 7.45 along with their transfer functions. The complementary high-pass filter circuits and transfer functions are shown in Fig. 7.46. The filters in these figures are labeled B1, B1², and so forth, where the B stands for Butterworth and the superscript denotes the number of cascaded sections. The even-order filters are commonly referred to as Linkwitz–Riley [29,30] and are often favored because the woofer and tweeter are in phase at the crossover frequency, whereas in the case of odd-order filters, they are 90 degrees out of phase, as is seen from the Nyquist plots of Fig. 7.47. This is cited as reducing the chances of off-axis nulls occurring in the directivity pattern around the crossover frequency [31], although this also largely depends on the ratio of the wavelength to drive unit spacing. Obviously, the drive unit spacing should be as small as possible.

On the other hand, odd-order filters have a constant power response [32], regardless of drive unit spacing, and the coil inductance of the woofer can be included as part of the last inductor in the filter, thus eliminating the need for a Zobel network for correcting the load impedance as well as giving greater accuracy. Another feature of odd-order filters is that they form all-pass filters regardless of the polarity of the drives. This is a useful feature when combining a dipole open-baffle driver with a monopole woofer because the response will be flat both on-axis and 180 degrees off-axis, even though the polarity of the dipole is reversed at the rear. However, the time-domain response is affected by the polarity as we will discuss. All-pass filters need not be symmetrical [33–35]. If we include the low-frequency roll-off of the tweeter in its high-pass filter transfer function, the overall order of the filter is increased by 2. It would be making

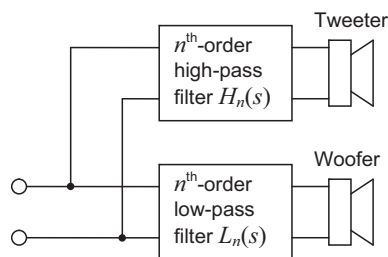


Figure 7.44 Outline schematic of a two-way loudspeaker with a classical crossover network.

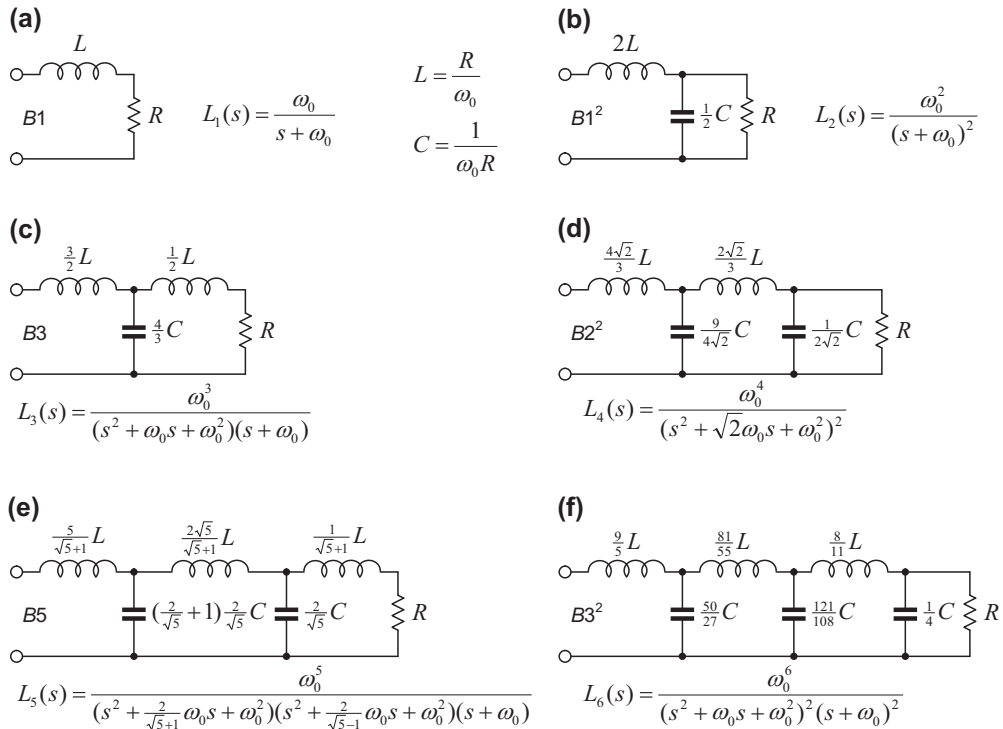


Figure 7.45 Classical low-pass crossover filters: (a) first-order; (b) second-order; (c) third-order; (d) fourth-order; (e) fifth-order; and (f) sixth-order. In each case, the inductor and capacitor values are given by $L = R/\omega_0$ and $C = 1/(\omega_0 R)$, respectively, where $\omega_0 = 2\pi f_0$ is the crossover frequency and R is the coil resistance of the woofer. The labels $B1$, $B3^2$, and so forth are the names of the transfer functions where B stands for Butterworth and the number is the order of the function. Note that the square in $B3^2$ means that it is equivalent to two cascaded third-order Butterworth filters, making a net sixth-order filter.

the low-pass filter to the woofer unnecessarily complicated to increase its order by the same amount.

High-pass crossover filters which take into account the native response of the tweeter

Classical crossover filters make two assumptions about the loudspeaker drive units. First, they assume that the load impedance is a constant resistance at all frequencies. Second, they assume that the frequency responses of the drive units are flat with zero phase shift in the crossover frequency range. If we were to select drive units and crossover frequencies such that these assumptions were approximately true, we would end up with more drive units than necessary in a complicated and expensive design, because each unit would be working over only part of its usable frequency range.

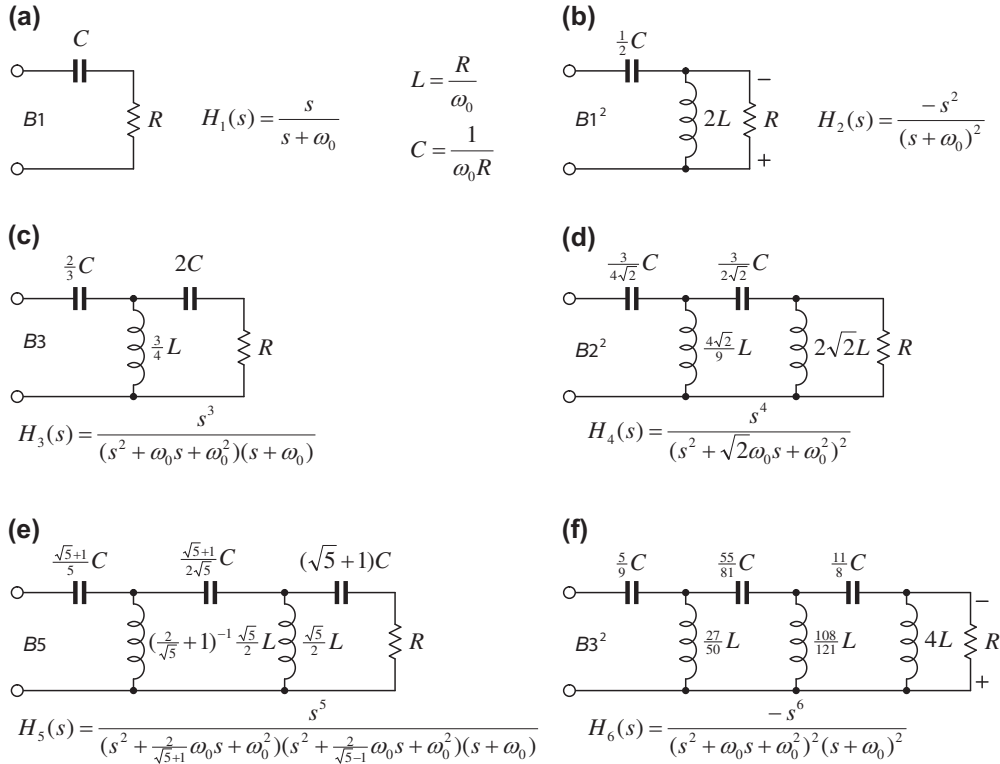


Figure 7.46 Classical high-pass crossover filters: (a) first-order; (b) second-order; (c) third-order; (d) fourth-order; (e) fifth-order; and (f) sixth-order. In each case, the inductor and capacitor values are given by $L = R/\omega_0$ and $C = 1/(\omega_0 R)$, respectively, where $\omega_0 = 2\pi f_0$ is the crossover frequency and R is the coil resistance of the tweeter. Note that in the case of the second- and sixth-order functions, the tweeter terminals must be reversed. The labels $B1$, $B3^2$, and so forth are the names of the transfer functions where B stands for Butterworth and the number is the order of the function. Note that the square in $B3^2$ means that it is equivalent to two cascaded third-order Butterworth filters, making a net sixth-order filter.

Third-order high-pass filter with a series capacitor

The simplest high-pass filter is just a series capacitor, as shown in Fig. 7.48. Using the same methodology as in Sections 7.6 and 7.12, we can write the following expression for the radiated sound:

$$\tilde{p}(r) = \frac{\tilde{e}_g B I S_D \rho_0}{(R_g + R_E) M_{MS}} \cdot \frac{e^{-jkr}}{4\pi r} G(s) \tag{7.142}$$

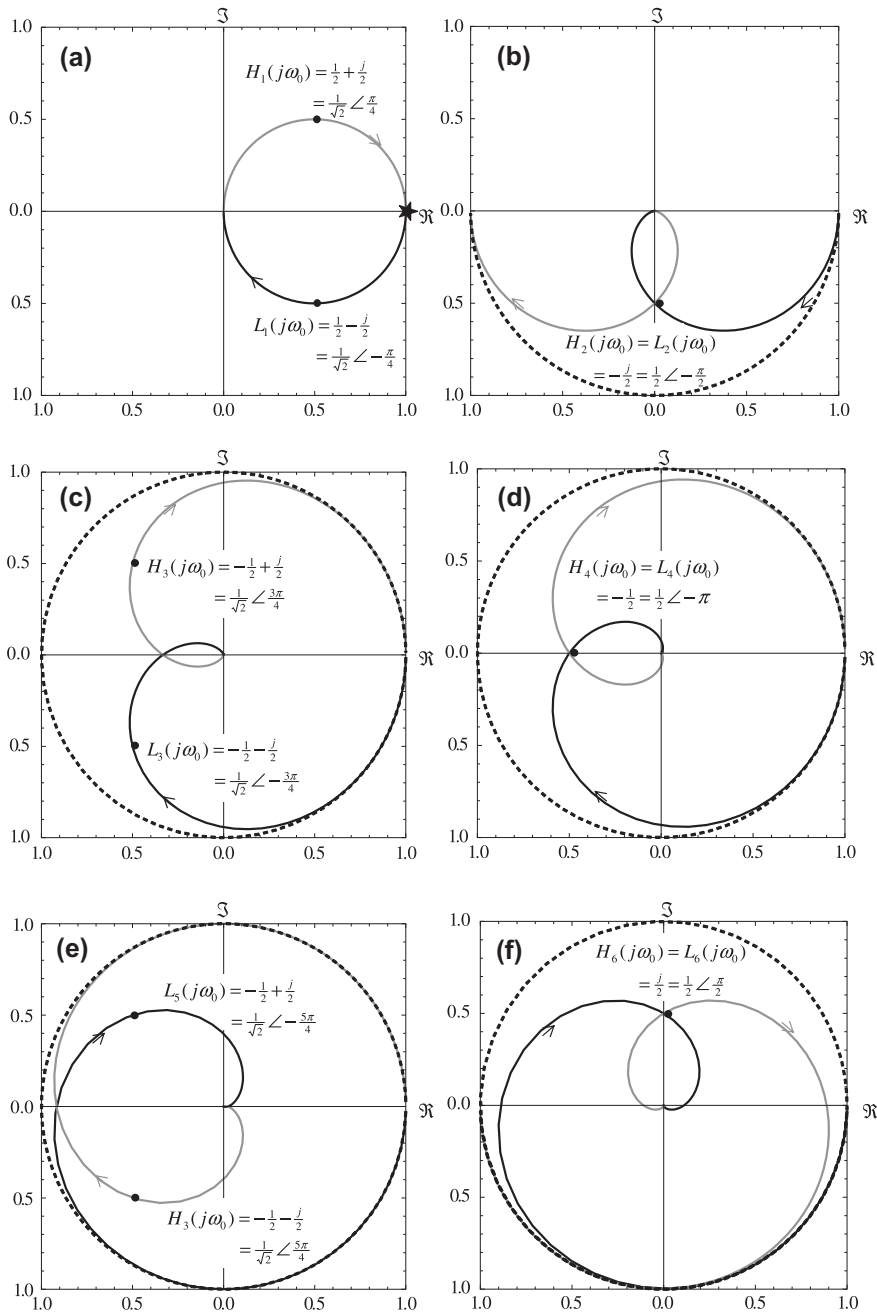


Figure 7.47 Nyquist plots for classical crossover filters in the complex plane: (a) first-order; (b) second-order; (c) third-order; (d) fourth-order; (e) fifth-order; and (f) sixth-order. *Black solid curves* show the low-pass transfer functions $L_n(s)$, *gray solid curves* show the high-pass transfer functions $H_n(s)$, and *black dotted curves* show the resultant all-pass transfer functions $F_n(s) = L_n(s) + H_n(s)$, where $s = j\omega$ is the complex frequency and n is the order of the crossover. Note that for the first-order crossover, there is *no dotted curve* because the resultant is always $+1$, marked by a pentagram. *Black dots* indicate the crossover frequencies at which $\omega = \omega_0$, and *arrows* show the direction of increasing frequency. The maximum phase shift of $F_n(s)$ is 0 for $n = 1$, π for $n = 2$, 2π for $n = 3, 4, 5$, and 3π for $n = 6$.

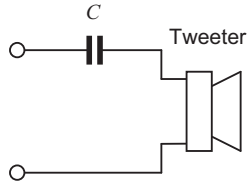


Figure 7.48 Third-order high-pass filter in which the native response of tweeter provides the second-order part of the transfer function and the series capacitor provides the first-order part.

where the third-order frequency-response function $G(s)$ is given by

$$G(s) = \frac{s^3}{s^3 + P_2s^2 + P_1s + P_0} \quad (7.143)$$

and the coefficients of the denominator polynomial in $s = j\omega$ are given by

$$P_2 = \frac{\omega_C}{Q_{TC}} + \omega_E \quad (7.144)$$

$$P_1 = \left(\omega_C + \frac{\omega_E}{Q_{MC}} \right) \omega_C \quad (7.145)$$

$$P_0 = \omega_C^2 \omega_E \quad (7.146)$$

where ω_C is the angular resonant frequency of the tweeter in its closed-box enclosure, Q_{MC} is its mechanical Q factor, Q_{TC} is its total Q factor, and ω_E is the cutoff frequency of the electrical filter comprising the external capacitor C and inductor R_E :

$$\omega_E = \frac{1}{R_EC} \quad (7.147)$$

The electrical Q factor is given by

$$Q_{EC} = \frac{Q_{MC}Q_{TC}}{Q_{MC} - Q_{TC}} \quad (7.148)$$

The transfer function of a third-order Butterworth high-pass filter is shown in Fig. 7.46(c) so that

$$P_2 = 2\omega_0 \quad (7.149)$$

$$P_1 = 2\omega_0^2 \quad (7.150)$$

$$P_0 = \omega_0^3 \quad (7.151)$$

where ω_0 is the angular crossover frequency. Equating Eqs. (7.144)–(7.146) with Eqs. (7.149)–(7.151) and solving for ω_0 , ω_E , and Q_{TC} gives

$$\omega_0^3 - 2Q_{MC}\omega_C\omega_0^2 + Q_{MC}\omega_C^2 = 0 \quad (7.152)$$

which has to be solved for ω_0 . Then,

$$\omega_E = \frac{\omega_0^3}{\omega_C^2} \quad (7.153)$$

and

$$Q_{TC} = \frac{\omega_C}{2\omega_0 - \omega_E} \quad (7.154)$$

Numerical values for these solutions are given in Table 7.5. A tweeter unit should be chosen which has Q_{MC} and Q_{EC} values that match, as closely as possible, those in one of the rows of the table, remembering that the Q_{EC} value will be modified by any series resistance added to match the sensitivity of the tweeter to that of the woofer. Then, the crossover frequency f_0 is given as a multiple of f_C . For example, if the Q_{MC} and Q_{EC} values are 2 and 1.7, respectively, and the resonance frequency is $f_C = 2$ kHz, we use the fourth row of Table 7.5 to arrive at a crossover frequency of

$$f_0 = 0.7892 \times 2 = 1.56 \text{ kHz}$$

and an electrical cutoff frequency of

$$f_E = 0.4916 \times 2 = 0.98 \text{ kHz}$$

If the coil resistance is 6Ω , the value of the capacitor is then given by

$$C = \frac{1}{2\pi f_E R_E} = \frac{1}{2 \times 3.14 \times 980 \times 6} = 27 \mu\text{F}$$

Table 7.5 Parameters for third-order Butterworth high-pass crossover filter using a series capacitor.

Q_{MC}	Q_{EC}	Q_{TC}	f_0/f_C	f_E/f_C
1.0	∞	1.0000	1.0000	1.0000
1.2	4.1510	0.9309	0.8921	0.7099
1.5	2.3729	0.9191	0.8318	0.5754
2.0	1.7039	0.9201	0.7892	0.4916
3.0	1.3392	0.9259	0.7564	0.4327
4.0	1.2112	0.9297	0.7424	0.4091
5.0	1.1457	0.9322	0.7346	0.3964
10	1.0343	0.9374	0.7202	0.3735
∞	0.9428	0.9428	0.7071	0.3535

Unfortunately, choosing a tweeter to use with this type of filter is not so easy, as few manufacturers provide much information about their tweeters, which is strange considering that woofers now come with a full set of Thiele—Small parameters practically as standard (Thiele—Small parameters are discussed in Section 6.5). Let this be considered as a plea to manufacturers to rectify the situation and provide all the data necessary to design the crossover filter.

Note that for higher values of Q_{MC} , the crossover frequency f_0 is about half an octave below the resonance frequency f_C . Hence, the working range of the tweeter is extended. In fact many commercial closed-box loudspeakers have a capacitor in series with the woofer to augment the bass response [36]. However, this advantage is reduced as Q_{MC} approaches unity.

Fourth-order high-pass filter with a series capacitor and shunt inductor

The fourth-order high-pass filter is shown in Fig. 7.49. Using the same methodology as in Sections 7.6 and 7.12, we can write the following expression for the radiated sound:

$$\tilde{p}(r) = \frac{\tilde{c}_g B I S_D \rho_0}{(R_g + R_E) M_{MS}} \cdot \frac{e^{-jkr}}{4\pi r} G(s) \quad (7.155)$$

where the fourth-order frequency-response function $G(s)$ is given by

$$G(s) = \frac{s^4}{s^4 + P_3 s^3 + P_2 s^2 + P_1 s + P_0} \quad (7.156)$$

and the coefficients of the denominator polynomial in $s = j\omega$ are given by

$$P_3 = \frac{\omega_C}{Q_{TC}} + \frac{\omega_E}{Q_E} \quad (7.157)$$

$$P_2 = \omega_C^2 + \omega_E^2 + \frac{\omega_C \omega_E}{Q_{MC} Q_E} \quad (7.158)$$

$$P_1 = \left(\frac{\omega_E}{Q_{TC}} + \frac{\omega_C}{Q_E} \right) \omega_C \omega_E \quad (7.159)$$

$$P_0 = \omega_C^2 \omega_E^2 \quad (7.160)$$

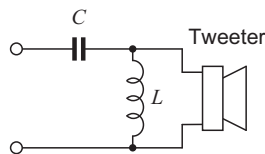


Figure 7.49 Fourth-order high-pass filter in which the native response of tweeter provides one second-order part of the transfer function and the series capacitor and shunt inductor provide the other.

where ω_C is the angular resonant frequency of the tweeter in its closed-box enclosure, Q_{MC} is its mechanical Q factor, Q_{TC} is its total Q factor, and ω_E is the cutoff frequency of the electrical filter comprising the external capacitor C and coil resistance L :

$$\omega_E = \frac{1}{LC} \quad (7.161)$$

The electrical Q factor of the filter is given by

$$Q_E = \omega_E R_E C \quad (7.162)$$

The electrical Q factor of the tweeter is given by

$$Q_{EC} = \frac{Q_{MC} Q_{TC}}{Q_{MC} - Q_{TC}} \quad (7.163)$$

The transfer function of a fourth-order Linkwitz–Riley or B2² high-pass filter is shown in Fig. 7.46(d), so that

$$P_3 = 2\sqrt{2}\omega_0 \quad (7.164)$$

$$P_2 = 4\omega_0^2 \quad (7.165)$$

$$P_1 = 2\sqrt{2}\omega_0^3 \quad (7.166)$$

$$P_0 = \omega_0^4 \quad (7.167)$$

where ω_0 is the angular crossover frequency. Equating Eqs. (7.157)–(7.160) with Eqs. (7.164)–(7.167) and solving for ω_0 , ω_E , and Q_{TC} gives

$$\omega_0^6 - 3\omega_C^2\omega_0^2 + \frac{2\sqrt{2}\omega_C^3\omega_0^3}{Q_{MC}} - 3\omega_C^4\omega_0^2 + \omega_C^6 = 0 \quad (7.168)$$

which has to be solved for ω_0 . Then,

$$\omega_E = \frac{\omega_0^2}{\omega_C} \quad (7.169)$$

$$Q_E = \frac{\omega_0^2\omega_C^2}{Q_{MC}(4\omega_0^2\omega_C^2 - \omega_0^2 - \omega_C^2)} \quad (7.170)$$

and

$$Q_{TC} = \frac{Q_E\omega_C^2}{\omega_0(2\sqrt{2}Q_E\omega_C - \omega_0)} \quad (7.171)$$

Table 7.6 Solution 1 parameters for fourth-order Linkwitz–Riley ($B2^2$) high-pass crossover filter using a series capacitor and shunt inductor.

Q_{MC}	Q_{EC}	Q_{TC}	f_0/f_C	f_E/f_C	Q_E
$1/\sqrt{2}$	∞	0.7071	1.0000	1.0000	0.7071
1.0	3.2743	0.7660	0.6666	0.4444	0.7660
2.0	1.3924	0.8209	0.5712	0.3263	0.8209
3.0	1.1604	0.8368	0.5506	0.3031	0.8368
4.0	1.0703	0.8444	0.5415	0.2932	0.8444
5.0	1.0224	0.8489	0.5363	0.2876	0.8489
10	0.9380	0.8576	0.5266	0.2773	0.8576
∞	0.8660	0.8660	0.5176	0.2679	0.8660

In this solution, the crossover frequency f_0 is below the tweeter resonance frequency f_C .

Numerical values for these solutions are given in [Tables 7.6 and 7.7](#). In [Table 7.6](#), the crossover frequency f_0 is *below* the tweeter's resonance frequency f_C and in [Table 7.7](#) f_0 is *above* f_C . The latter is a safer solution as it is less likely to lead to excessive diaphragm excursion or a dip in the input impedance. A tweeter unit should be chosen which has Q_{MC} and Q_{EC} values that match, as closely as possible, those in one of the rows of the table, remembering that the Q_{EC} value will be modified by any series resistance added to match the sensitivity of the tweeter to that of the woofer. Then, the crossover frequency f_0 is given as a multiple of f_C . For example, if the Q_{MC} and Q_{EC} values are 3 and 1.2, respectively, and the resonance frequency is $f_C = 2$ kHz, we use the fourth row of [Table 7.7](#) to arrive at a crossover frequency of

$$f_0 = 1.8161 \times 2 = 3.63 \text{ kHz}$$

and an electrical cutoff frequency of

$$f_E = 3.2985 \times 2 = 6.60 \text{ kHz}$$

Table 7.7 Solution 2 parameters for fourth-order Linkwitz–Riley ($B2^2$) high-pass crossover filter using a series capacitor and shunt inductor.

Q_{MC}	Q_{EC}	Q_{TC}	f_0/f_C	f_E/f_C	Q_E
$1/\sqrt{2}$	∞	0.7071	1.0000	1.0000	0.7071
1.0	3.2743	0.7660	1.5001	2.2502	0.7660
2.0	1.3924	0.8209	1.7506	3.0646	0.8209
3.0	1.1604	0.8368	1.8161	3.2985	0.8368
4.0	1.0703	0.8444	1.8468	3.4107	0.8444
5.0	1.0224	0.8489	1.8646	3.4767	0.8489
10	0.9380	0.8576	1.8989	3.6061	0.8576
∞	0.8660	0.8660	1.9318	3.7321	0.8660

In this solution, the crossover frequency f_0 is above the tweeter resonance frequency f_C .

If the coil resistance is $6\ \Omega$, the value of the capacitor is then given by

$$C = \frac{Q_E}{2\pi f_E R_E} = \frac{1}{2 \times 3.14 \times 6600 \times 6} = 3.9\ \mu\text{F}$$

and the value of the inductor is given by

$$L = \frac{1}{(2\pi f_E)^2 C} = \frac{1}{(2 \times 3.14 \times 6600)^2 \times 3.9 \times 10^{-6}} = 150\ \mu\text{H}$$

Effect of phase delay of second-order crossover on time-domain response to square waves

Although we have already discounted the use of a second-order crossover when taking into account the frequency response of the tweeter, this serves as a relatively simple example of what the phase delay of a crossover does to the shape of a square wave. Obviously, the effects will only be more pronounced in higher-order crossover filters. A square wave $W(t)$ can be described by an infinite series of sinusoidal waves:

$$W(t) = \frac{4}{\pi} \sum_{n=0}^{\infty} \frac{\sin \omega_n t}{2n+1} \quad (7.172)$$

where $\omega_n = (2n+1)\omega$ are *odd* harmonics. According to Table 6.2, the Laplace transform of the square wave is

$$W(s) = \frac{4}{\pi} \sum_{n=0}^{\infty} \frac{\omega_n}{(2n+1)(s^2 + \omega_n^2)} \quad (7.173)$$

Thus, the frequency-domain response of the second-order filter to a square wave is

$$\begin{aligned} G(s) &= (L_2(s) + H_2(s)) \cdot W(s) \\ &= F_2(s) \cdot W(s) = \frac{\omega_0^2 - s^2}{(\omega_0 + s)^2} \cdot \frac{4}{\pi} \sum_{n=0}^{\infty} \frac{\omega_n}{(2n+1)(s^2 + \omega_n^2)} \end{aligned} \quad (7.174)$$

In other words, $G(s)$ is the sum of the outputs of the low-pass and high-pass filters and thus constitutes an all-pass filter. Taking the inverse Laplace transform then gives us the time-domain response to a square wave:

$$g(t) = \frac{1}{2\pi j} \int_{\gamma-j\infty}^{\gamma+j\infty} G(s) e^{st} ds = \frac{4}{\pi} \sum_{n=0}^{\infty} \frac{2\omega_0 \omega_n (e^{-\omega_0 t} - \cos \omega_n t) + (\omega_0^2 - \omega_n^2) \sin \omega_n t}{(2n+1)(\omega_0^2 + \omega_n^2)} \quad (7.175)$$

The distortion of a square wave produced by the phase delay of a second-order all-pass crossover filter is shown in Fig. 7.50, where the square wave frequency is $f = 1$ kHz and the crossover frequency is $f_0 = 4$ kHz. Clearly, the output waveform is radically different from the input one. The spikes are a result of the tweeter being out of phase with the woofer. Also shown is the effect on a square wave of a third-order all-pass filter in which the tweeter is *in phase* with the woofer and here the spikes are inverted. We mentioned previously that the phase of the tweeter may be reversed in the case of odd-order all-pass filters without affecting the all-pass magnitude. However, we see in Fig. 7.50 that when the tweeter of a first- or third-order all-pass filter is connected in *antiphase*, the square wave becomes the same as that for a second-order all-pass filter.

Note that the first-order all-pass filter with the tweeter connected *in phase* with the woofer is the only one which faithfully preserves the shape of the square wave but unfortunately, like the second-order filter, is impractical for real nonideal tweeters.

What we have is an imperfect time delay filter. If it were ideal, the phase would increase linearly with frequency in Fig. 7.47 so that it would keep wrapping round indefinitely, whereas in reality it stops at π for $n = 2$, 2π for $n = 3, 4, 5$, and 3π for $n = 6$. Hence, the time delay τ decreases above the crossover frequency according to

$$\tau = \frac{\angle F_2(s)}{\omega} = -\frac{2}{\omega} \arctan \frac{\omega}{\omega_0}$$

The effect of this is to delay the low frequencies relative to the high ones so that the sound from the tweeter arrives at the listener before that from the woofer.

The audibility of phase distortion has provoked a lively debate over the years [37–41], but why not design the loudspeaker correctly in the first place so that there need not be any doubt about its accuracy? As we shall see in the next section, the solution to this problem need not be complicated if we approach it holistically and take into account all the factors that affect the response of the loudspeaker, including the baffle effect.

Crossover filters with zero phase shift

In the previous section, we studied the waveform distortion produced by classical crossover networks. We also saw that the simplest high-pass filter $H(s)$ is a series capacitor (see Fig. 7.48). Let us now take its transfer function and deduce what low-pass filter $L(s)$ when summed with it will produce an output which is real and constant at all frequencies, that is, simply unity:

$$L(s) + H(s) = 1 \quad (7.176)$$

where

$$H(s) = \frac{s^3}{(s + \omega_0)(s^2 + \omega_0 s + \omega_0^2)} \quad (7.177)$$

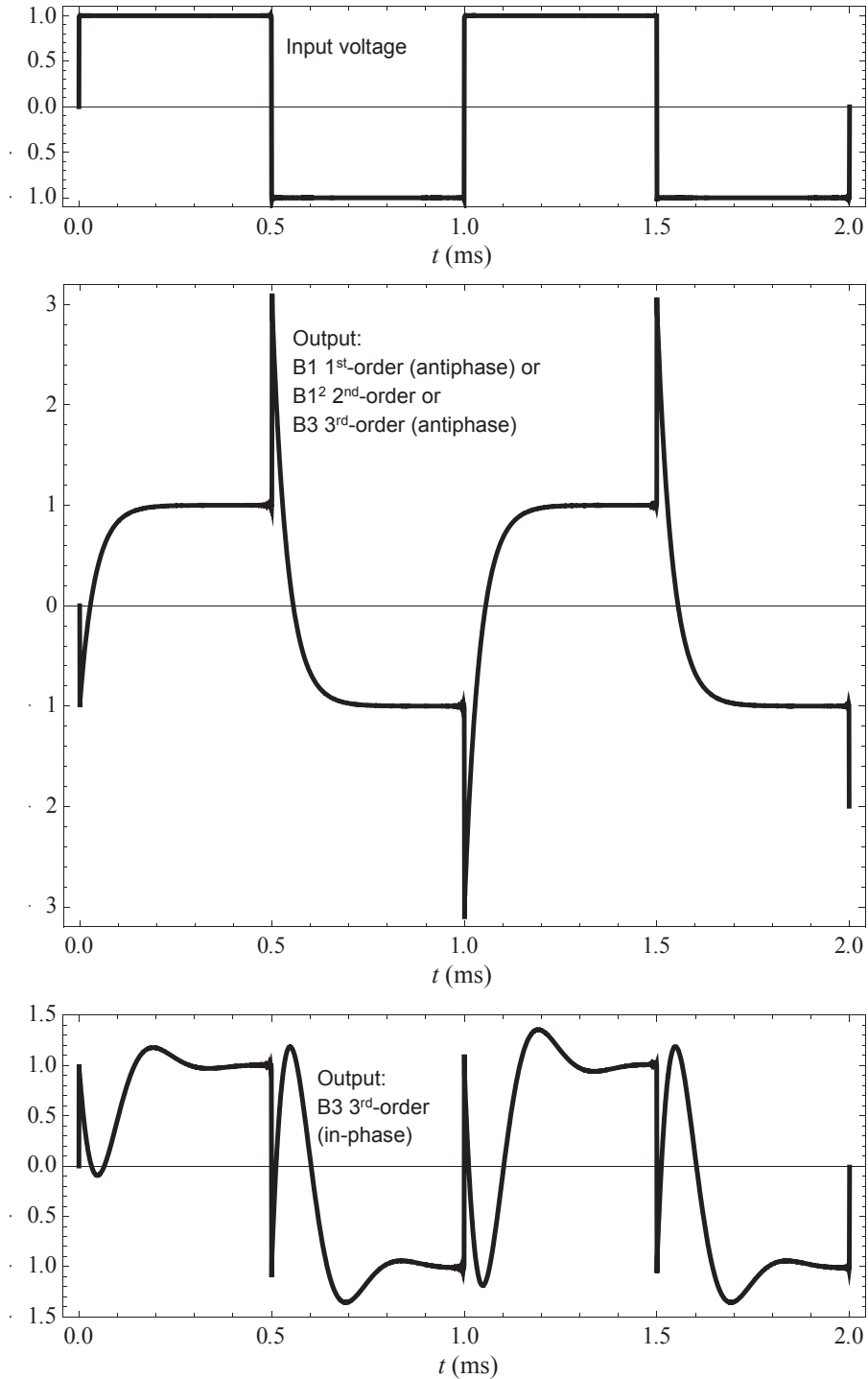


Figure 7.50 Distortion of a square wave produced by the phase delay of a second-order all-pass crossover filter, where the output voltage is the sum of the output voltages of the low-pass and high-pass filters. The square wave frequency is 1 kHz, and the crossover frequency is 4 kHz.

Hence,

$$L(s) = 1 - H(s) = \frac{\omega_0}{s + \omega_0} \cdot \frac{2s^2 + 2\omega_0s + \omega_0^2}{s^2 + \omega_0s + \omega_0^2} \quad (7.178)$$

The first part of this transfer function is just simple first-order low-pass filter. The second part is a shelf with a 6 dB boost at frequencies above the crossover frequency ω_0 . As it happens, such a boost is provided by the baffle effect whereby the woofer acts as a point source when the wavelength is large compared with the dimensions of the box but behaves like a piston in an infinite baffle when the wavelength is small. Comparing Eq. (7.178) with Eq. (7.38) for the on-axis response of a closed-back piston in free space, we deduce that the ideal crossover frequency is

$$f_0 = \sqrt{5}c/(2\pi a) \quad (7.179)$$

It should be noted that the methods developed in this chapter are by no means perfect, because of the assumptions we have made about the baffle effect and the drive units behaving as perfectly rigid flat pistons. However, computer algorithms have been developed [42] which can optimize the crossover component values taking into account the measured responses of the drivers.

Example 7.4. Crossover for woofer of Example 7.2. In this example, we shall implement a third-order Butterworth high-pass filter using a series capacitor for the first-order section and the native response of the tweeter for the second-order section. Because the tweeter will be mounted in a sphere, we shall design a crossover to compensate for the 6 dB lift associated with a point source in a sphere (see Fig. 7.14) so that it provides part of the first-order section. The low-pass section will be designed to give an all-pass overall response with zero phase shift, as discussed in the previous section. Hence, the low-pass section will use just a series inductor together with the 6 dB lift due to the baffle effect, using a closed-back piston as a model (see Fig. 7.15). Because the woofer occupies almost the full width of the box, we will take a as 9.4 cm which, using Eq. (7.179), gives us a crossover frequency of

$$f_0 = 2.24 \times 344.8 / (2 \times 3.14 \times 0.094) = 1305 \text{ Hz}$$

Hence, the value of the series inductance needed is

$$L_1 = \frac{R_E}{2\pi f_0} = \frac{6.27}{2 \times 3.14 \times 1305} = 0.766 \text{ mH}$$

However, the coil inductance is 0.71 mH, so to make up the difference we will use an inductor with a value of $0.766 - 0.71 = 56 \mu\text{H}$. Next, we need to choose a tweeter suitable for a crossover frequency of 1305 Hz. The SEAS model 27TFF (H0831) has a resonance frequency of $f_C = 1200 \text{ Hz}$, which is close enough. The effective area of the dome is

$S_D = 7.5 \text{ cm}^2$. The maximum sound pressure of the woofer has already been specified as 99.6 dB SPL at a distance of $r = 1 \text{ m}$. At the crossover frequency f_0 , the sound pressure produced by the tweeter is 3 dB less than this, that is 96.6 dB SPL, and decreases at a rate of 18 dB/octave below f_0 . The peak displacement at f_0 is obtained from Eq. (6.35) to give

$$\eta_{\text{peak}} = \frac{\sqrt{2}r \times 10^{\frac{\text{SPL}}{20}-5}}{\pi f^2 \rho_0 S_D} = \frac{1.414 \times 1 \times 10^{\frac{96.6}{20}-5}}{3.14 \times 1305^2 \times 1.18 \times 7.5 \times 10^{-4}} = 0.2 \text{ mm}$$

which is within the linear excursion limit of 0.5 mm and at frequencies above and below f_0 the displacement is reduced. Using the method described in Section 6.10 for measuring the Thiele–Small parameters, we estimate the Q factors from the impedance curve to be

$$Q_{EC} = \omega_S M_{MD} R_{ES} / (Bl)^2 = 2\pi \times 1200 \times 0.0003 \times 4.8 / 3.5^2 = 0.89$$

$$Q_{MC} = \omega_S M_{MD} R_E / (Bl)^2 = 2\pi \times 1200 \times 0.0003 \times 10.2 / 3.5^2 = 1.88$$

In addition, the quoted sensitivity is 92 dB SPL in a baffle at 1 m with an input voltage of 2.83 Vrms (or 86 dB SPL in free space). However, the woofer has a sensitivity of 79.6 dB SPL in free space, so the tweeter needs a series resistor to match its sensitivity to that of the woofer. If $R_E = 4.8 \Omega$, then the series resistor value is

$$\begin{aligned} R_1 &= R_E \left(10^{(\text{TweeterSensitivity} - \text{WooferSensitivity})/20} - 1 \right) \\ &= 4.8 \times \left(10^{(92-79.6)/20} - 1 \right) = 15.2 \Omega \approx 15\Omega \end{aligned}$$

This will modify the values of Q_{EC} and Q_{TC} as follows:

$$Q'_{EC} = \left(1 + \frac{R_1}{R_E} \right) Q_{EC} = \left(1 + \frac{15}{4.8} \right) \times 0.89 = 3.67$$

$$Q'_{TC} = Q'_{EC} Q_{MC} / (Q'_{EC} + Q_{MC}) = 1.24$$

which is close enough to unity for a third-order Butterworth response. We need to correct for the 6 dB lift in the response of the tweeter due to the baffle effect. We will simplify this by mounting the tweeter on a wooden sphere so that we can model it as a point source on a sphere of radius R . Then, the transfer function of the point source on a sphere from Eq. (7.36) (producing a 6 dB lift) provides the shelf filter response

$$\frac{s + c/R}{s + 2c/R} = \frac{s + \omega_E}{s + \omega_0}$$

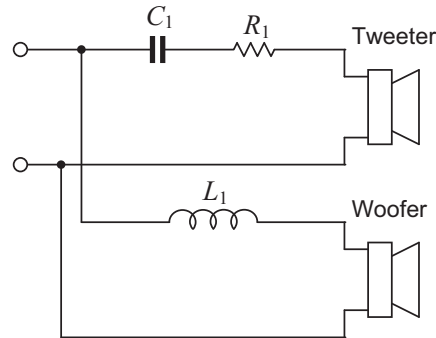


Figure 7.51 Crossover network of Example 7.4 with a crossover frequency of $f_0 = 1305$ Hz. The values of the crossover circuit elements are $R_1 = 15 \text{ W}$ (25 W), $L_1 = 56 \text{ mH}$, and $C_1 = 12 \text{ }\mu\text{F}$. The woofer is a Bandor type 100DW/8A mounted in a closed-box baffle as described in Example 7.2 and shown Fig. 7.18. The tweeter is a SEAS type 27TFF (H0831) mounted in a 16 cm diameter sphere.

where the radius of the sphere is given by

$$R = 2c/\omega_0 = 344.8/(3.14 \times 1305) = 84.1 \text{ mm}$$

Thus, the 6 dB transition takes place between $f_E = f_0/2 = 1305/2 = 653$ Hz and $f_0 = 1305$ Hz with a first-order slope. Hence, we need the series capacitor to continue the first-order slope from f_E downward and its value is determined by

$$C_1 = \frac{1}{2\pi f_E(R_E + R_1)} = \frac{1}{2 \times 3.14 \times 653 \times (4.8 + 15)} = 12.3 \text{ }\mu\text{F} \approx 12 \text{ }\mu\text{F}$$

The network is shown in Fig. 7.51.

7.21 DUAL-CONCENTRIC DRIVE UNITS

A difficulty with mounting a woofer and tweeter side by side or one above the other is that the path that the sound has to travel from each of the loudspeakers to a listener will be different in different parts of the listening room. Hence, in the vicinity of the crossover frequencies, cancellation of the sound will result at some parts of the room, and addition will occur at others.

To avoid this effect, the loudspeakers are sometimes mounted *concentrically*, i.e., the tweeter is placed behind and on the axis of the woofer (see Fig. 7.52). In this arrangement, the diaphragm of the woofer acts as a horn and the tweeter usually has a phase plug in front of it. Horn loudspeakers will be discussed in greater detail in Chapter 9.

Problem 7.1. A loudspeaker drive unit with a fiberglass cone has the Thiele-Small parameters: $R_E = 5.6 \text{ }\Omega$, $Q_{ES} = 0.46$, $Q_{MS} = 7.58$, $f_S = 50$ Hz, $S_D = 137 \text{ cm}^3$, and $V_{AS} = 19.5$ L.

Calculate the box volume and port dimensions needed to give a Chebyshev frequency response with 0.01 dB ripple and a maximum sound pressure of $SPL_{\text{max}} = 100$

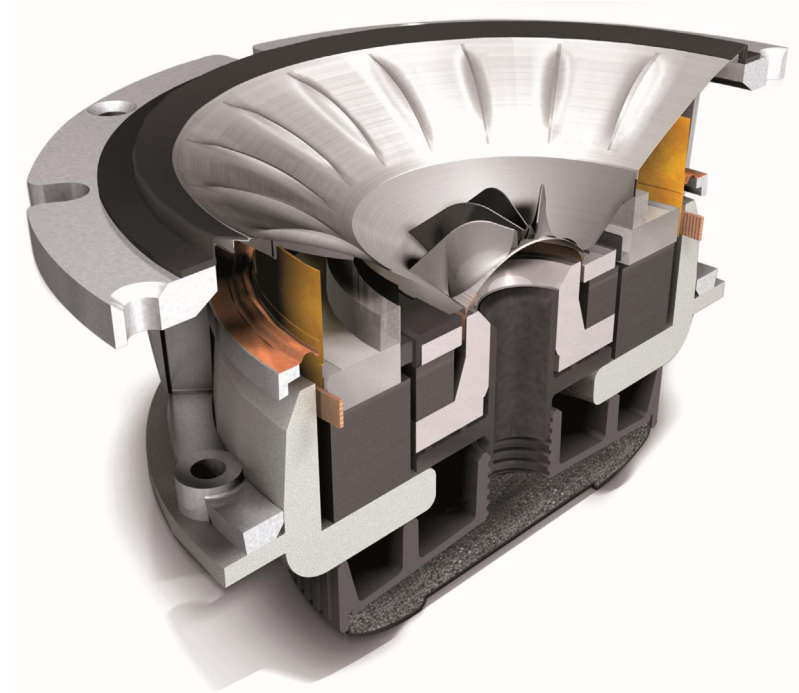


Figure 7.52 Section view of a Blade UniQ two-way drive unit. The tweeter is located at the center of the woofer behind a “tangerine” phase plug and has its own independent voice coil. Note that the woofer diaphragm is driven half way along its radius to eliminate the first radial mode together with its odd-order harmonics. Courtesy of KEF.

dB SPL at 1 m. Show that to make the port volume ten times the volume displacement needed to produce 100 dB SPL, the optimum bore diameter is around 9 cm. Also, calculate the cut-off frequency.

Hint: Obtain Q_{TS} from Eq. (6.10). Obtain V_{AB} and f_B from Table 7.4. Calculate the maximum peak pressure and volume displacement required to produce that pressure using formulas from “Summary of bass-reflex design” on p. 334. Let the port volume be $V_P = 10V_{\max}$ and use Eqs. (7.97) and (7.96) to calculate the approximate length t and cross-sectional area S_P respectively so that the diameter is $d_P = 2\sqrt{S_P/\pi}$. Using a diameter of 9 cm, then calculate the exact length t from Eq. (7.98). Obtain the cut-off frequency f_{3dB} from Table 7.4.

REFERENCES

- [1] See IEC 60268–5, ed. 3.1. Sound system equipment - part 5: loudspeakers. Available from: <http://webstore.iec.ch/>. For example, for a nominal 8-in (200 mm) diameter loudspeaker, the baffle size would be 1.65 m long by 1.35 m wide, with the loudspeaker offset from the center by 22.5 cm lengthways and 15 cm widthways.

- [2] Small RH. Closed-box loudspeaker systems Part I: analysis. *J Audio Eng Soc* 1972;20(10):798–808.
- [3] Small RH. Closed-box loudspeaker systems Part II: synthesis. *J Audio Eng Soc* 1973;21(1):11–8.
- [4] Villchur EM. Problems of bass reproduction in loudspeakers. *J Audio Eng Soc* 1957;5(3):122–6.
- [5] Backman J. Improvement of one-dimensional loudspeaker models, in the 123rd AES convention. Paper No. 7253. 2007.
- [6] Attenborough K. Acoustical characteristics of porous materials. *Phys Rep* 1982;82(2):179–227.
- [7] Zarek JHB. Sound absorption in flexible porous materials. *J Sound Vib* 1978;61(2):205–34.
- [8] Delany ME, Bazley EN. Acoustical properties of fibrous absorbent materials. *Appl Acoust* 1970;3:105–16.
- [9] Miki Y. Acoustical properties of porous materials, modification of Delany-Bazley models. *J Acoust Soc Jpn* 1990;11:19–24.
- [10] Sides DJ, Attenborough K, Mulholland KA. Application of a generalized acoustic propagation theory of fibrous absorbents. *J Sound Vib* 1971;19:49–64.
- [11] Wright JR. The virtual loudspeaker cabinet. *J Audio Eng Soc* 2003;51(4):244–7.
- [12] Venegas R, Umnova O. Acoustical properties of double porosity granular materials. *J Acoust Soc Am* 2011;130(5):2765–76.
- [13] At 1000 Hz, a wavelength at 22°C is about 35 cm; at 500 Hz, 70 cm; at 2000 Hz, 17.5 cm; and so on.
- [14] Backman J. Computation of diffraction for loudspeaker enclosures. *J Audio Eng Soc* 1989;37(5):353–62.
- [15] Vanderkooy J. A simple theory of cabinet edge diffraction. *J Audio Eng Soc* 1991;39(12):923–33.
- [16] Svensson UP. Line integral model of transient radiation from planar pistons in baffles. *Acta Acust* 2001;87:307–15.
- [17] Thuras AL. U.S. Patent No. 1,869,178 sound translating device. July 1932 (filed 1930).
- [18] Locanthi BN. Applications of electric circuit analogies to loudspeaker design problems, *IRE trans. Audio, PGA-6*: 15 (1952); republished in. *J Audio Eng Soc* 1971;19(9):778–85.
- [19] Novak JF. Performance of enclosures for high-compliance loudspeakers. *J Audio Eng Soc* 1959;7(1):29–37.
- [20] Thiele AN. Loudspeakers in vented boxes. *Proc IREE* 1961;22:487 [republished in *J Audio Eng Soc* 1971;19(5):382–392 and 1971;19(6):471–83].
- [21] Small RH. Vented-box loudspeaker systems Part I: small-signal analysis. *J Audio Eng Soc* 1973;21(5):363–72.
- [22] Small RH. Vented-box loudspeaker systems Part II: large-signal analysis. *J Audio Eng Soc* 1973;21(6):438–44.
- [23] Small RH. Vented-box loudspeaker systems Part III: synthesis. *J Audio Eng Soc* 1973;21(7):549–54.
- [24] Small RH. Vented-box loudspeaker systems Part IV: appendices. *J Audio Eng Soc* 1973;21(8):635–9.
- [25] Mellow TJ. A new set of fifth and sixth-order vented-box loudspeaker system alignments using a loudspeaker-enclosure matching filter: Part I, in the 112th AES convention. Paper No. 5505. 2002.
- [26] Mellow TJ. A new set of fifth and sixth-order vented-box loudspeaker system alignments using a loudspeaker-enclosure matching filter: Part II, in the 112th AES convention. Paper No. 5506. 2002.
- [27] Thiele AN. Estimating the loudspeaker response when the vent output is delayed. *J Audio Eng Soc* 2002;50(3):173–5.
- [28] Werner RE. Effect of negative impedance source on loudspeaker performance. *J Audio Eng Soc* 1957;29(3):335–40.
- [29] Linkwitz SH. Active crossover networks for noncoincident drivers. *J Audio Eng Soc* 1976;24(1):2–8.
- [30] Linkwitz SH. Passive crossover networks for noncoincident drivers. *J Audio Eng Soc* 1978;28(3):149–50.
- [31] Bullock III RM. Loudspeaker-crossover systems: an optimal crossover choice. *J Audio Eng Soc* 1982;30(7/8):486–95.
- [32] Vanderkooy J, Lipshitz SP. Power response of loudspeakers with noncoincident drivers – the influence of crossover design. *J Audio Eng Soc* 1986;34(4):236–44.
- [33] Hawksford MOJ. Asymmetric all-pass crossover alignments. *J Audio Eng Soc* 1993;41(2):123–34.
- [34] Thiele AN. Passive all-pass crossover system of order 3 (low pass) + 5 (high pass), incorporating driver parameters. *J Audio Eng Soc* 2002;50(12):1030–8.

- [35] Thiele AN. Implementing asymmetrical crossovers. *J Audio Eng Soc* 2007;55(10):819–32.
- [36] Recklinghausen DR. Low-frequency range extension of loudspeakers. *J Audio Eng Soc* 1985;33(6):440–6.
- [37] Mathes RC, Miller RL. Phase effects in monaural perception. *J Acoust Soc Am* 1947;19(5):780–97.
- [38] Craig JH, Jeffress LA. Effect of phase on the quality of a two-component tone. *J Acoust Soc Am* 1962;34(11):1752–60.
- [39] Cabot RC, Mino MG, Dorans DA, Tackel IS, Breed HE. Detection. Of phase shifts in harmonically related tones. *J Audio Eng Soc* 1976;24(7):568–71.
- [40] Ashley JR. Group and phase delay requirements for loudspeaker systems. In: *Proc. IEEE int. conf. on acoustics, speech, and signal processing* (Denver, CO, 1980 Apr. 9–11), vol. 3; 1980. p. 1030–3.
- [41] Lipshitz SP, Pockock M, Vanderkooy J. On the audibility of midrange phase distortion in audio systems. *J Audio Eng Soc* 1982;30(9):580–95.
- [42] Schuck PL. Design of optimized loudspeaker crossover networks using a personal computer. *J Audio Eng Soc* 1986;34(3):124–42.

Cell phone acoustics

PART XXVI: ACOUSTICAL TRANSDUCERS FOR CELL PHONES

The number of cell phones in the world is approaching 6 billion. These range from those that provide simple telephone services to those that serve as full business and entertainment centers. For all these, acoustical design is very important, but such design is involved because of limitations of space, ergonomics, and frequently the requirement of producing good-sounding music.

Shown in Fig. 8.1 is a cell phone with the characteristics of an entertainment center. The three main electroacoustic elements are the handsfree loudspeaker, the receiver, and the microphone. The basic principles for the loudspeakers are the same as that for a loudspeaker in a closed baffle as presented in Chapter 7.

8.1 LOUSPEAKER AND MICROPHONE

Basic considerations

The sound-producing part in all cell phones is a flat radiating surface, i.e., the diaphragm, which is analogous to the cone in a hi-fi loudspeaker. The diaphragm is set in motion by an attached moving coil located in a magnetic field. The diaphragm and the coil may be circular or square. In the cell phone of Fig. 8.1, there are two flat diaphragms and driving coils, one of which feeds into the handsfree loudspeaker opening and the other into the call receiver opening. The small fully enclosed space behind either diaphragm is analogous to an acoustic compliance. The combined mass of the diaphragm and coil is analogous to an acoustic mass. These elements at resonance determine the low-frequency cutoff of the radiated sound.

Handsfree loudspeaker

In the simplest cell phones, the ringtone is a buzz or a repeated ring resembling that of an old landline phone. In an entertainment center type, the ringtone is often an excerpt from a musical composition. Also, continuous music may be played through it. As shown, the handsfree loudspeaker opening is on the side of the cell phone so that the phone can be laid on a flat surface and thus is “handsfree.” If the surface is large enough, the energy output of the loudspeaker will be double that compared with the handheld



Figure 8.1 Cell phone Nokia model 7.1 showing the positions of the receiver, handsfree loudspeaker, and microphone openings. Courtesy of HMD Global OY.

position because the opening is radiating into half space. Like any small closed-box loudspeaker the trend in cell phones is toward the “acoustic suspension” concept, i.e., the stiffness of the suspension for the diaphragm is a small fraction of that of the airspace behind. The volume of the backspace is about 1 cm^3 . This design is only practical if the diaphragm is fairly stable and the resonant frequencies are constant. Surprisingly, in the cell phone of Fig. 8.1, the user can carry on a telephone conversation with it on a surface, despite the proximity of the microphone to the handsfree opening. This is possible because the output of the microphone has an “echo canceling” feature in the digital circuitry and its output is also attenuated while the loudspeaker is operating. Nowadays handsfree loudspeakers are very loud, often producing as much as 105 phons at a distance of 10 cm.

Receiver

The receiver is similar to the handsfree loudspeaker. In Fig. 8.1, the volume of the space behind its diaphragm is larger and it contains the electronics and the keyboard. There is greater chance of leakage from this space and, if it should occur, the low-frequency output will be diminished. The opening is always held close to the ear, which mitigates the effect of leakage from the rear space.

Microphone

The microphone is an electret or microelectromechanical system (MEMS) type, more of which will be discussed later. It is only actuated when voice transmission is required.



8.2 CIRCUIT DIAGRAM FOR A CELL PHONE LOUDSPEAKER/RECEIVER

The circuit diagram for a cell phone loudspeaker system is given in Fig. 8.2. The elements are derived from the circuit of a loudspeaker in a closed box baffle as given in Fig. 7.6. The symbols are as follows:

\tilde{e}_g is open-circuit voltage of the generator (audio amplifier) in volts (V).

R_g is generator resistance in electrical ohms (Ω).

R_E is resistance of voice coil in electrical ohms (Ω).

B is steady air-gap magnetic field or flux density in Tesla (T).

l is length of wire on the voice coil winding in m.

\tilde{i} is electric current through the voice coil winding in amperes (A).

a is radius of diaphragm in m.

$S_D = \pi a^2$ is area of diaphragm in m^2 .

$\tilde{P}_c \cdot S_D$ is force produced by the current in the coil in $\text{Pa} \cdot \text{m}^2$.

\tilde{U}_c is volume velocity produced by the diaphragm in m^3/s .

M_{AD} is acoustic mass of the diaphragm and the voice coil in kg/m^4 .

C_{AS} is total acoustic compliance of the suspensions in m^5/N .

R_{AS} is acoustic resistance of the suspensions in $\text{N} \cdot \text{s}/\text{m}^5$.

C_{AB} is total acoustic compliance of the back enclosure in m^5/N .

C_{AF} is acoustic compliance of the front cavity in m^5/N .

R_{AB} is acoustic resistance of the leak path through the enclosure (needed to relieve changes in atmospheric pressure) in $\text{N} \cdot \text{s}/\text{m}^5$.

M_{AH} is acoustic mass of the sound hole(s) in kg/m^4 .

R_{AH} is acoustic resistance of the dust screen in $\text{N} \cdot \text{s}/\text{m}^5$.

Z_{AE} is radiation impedance (including the effect of proximity to the ear).

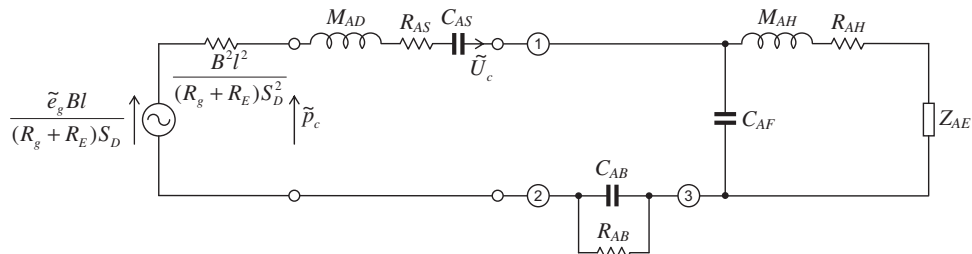


Figure 8.2 Analogous circuit of a handsfree loudspeaker or receiver in a cell phone. All circuit elements are referred to the acoustical side. In the case of a receiver, Z_{AE} is the impedance of the ear including any leakage because it is unlikely to be sealed. In the case of a handsfree loudspeaker near a flat surface, Z_{AE} can be considered to be the radiation impedance of a piston in an infinite baffle.

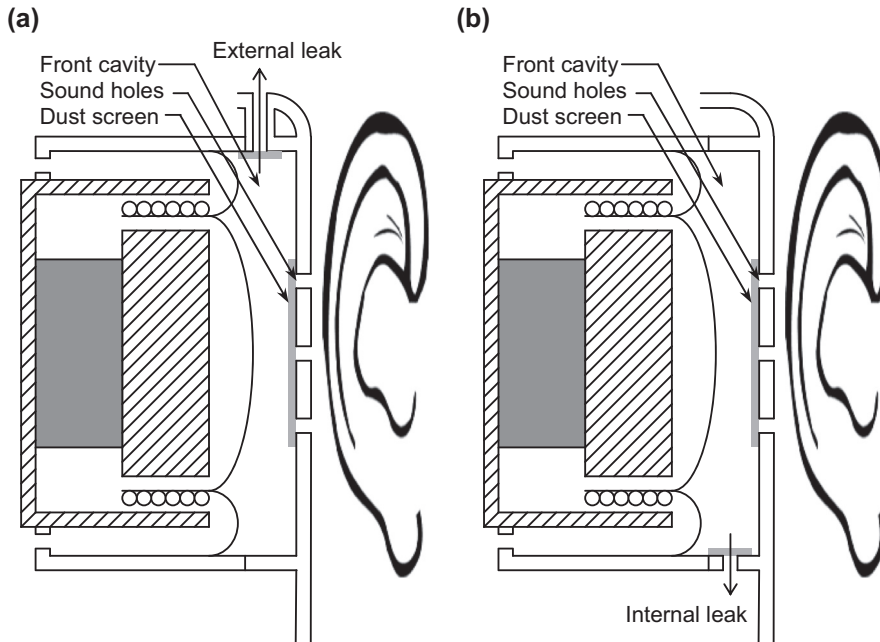


Figure 8.3 Cross section of leak-tolerant receiver in cell phone with (a) external leak and (b) internal leak [1].

The radiation impedance, Z_{AE} , is difficult to specify because the impedance for the receiver opening is highly dependent on how the user uses the handset. Because both of the openings are small, the radiation impedance when not too near the ear will approximate that for a small diaphragm in the end of a tube. Possible means for assuring a known radiation impedance in the receiver opening are to deliberately build a degree of controlled leakage that is at least as great as the uncontrolled leakage that would occur in normal usage. The controlled leakage path may lead to the outside space as shown in Fig. 8.3(a) or to the internal space as shown in Fig. 8.3(b). The more probable solution is that shown in Fig. 8.3(a), and for it a series acoustic resistance and acoustic mass must be connected between the circles “1” and “3” in Fig. 8.2. For the solution of Fig. 8.3(b), the mass and resistance should be connected between the circles “1” and “2.” Obviously the controlled leakage addition will reduce the output strength. The solution of Fig. 8.3(b) in particular will cause loss of low frequencies because of the acoustic short circuit between the front and back of the diaphragm, unless the space inside the handset is very large ($>60 \text{ cm}^3$).

Acoustic low-pass filter (helmholtz resonator)

In cell phones, for both the handsfree loudspeaker and the receiver, the compliance of the front cavity C_{AF} and the mass of the sound opening M_{AH} form a

Helmholtz resonator. This is a second-order low-pass filter. The angular resonance frequency is

$$\omega_0^2 = 1/(M_{AH}C_{AF}). \quad (8.1)$$

When listening to music, the resonance frequency is normally set at the upper limit of the required frequency range, and the Q of the resonance is controlled by the resistance R_{AH} of the dust screen. To calculate the dimensions of the resonator, we can either choose the radius a of the opening and calculate the length l according to $l = nc^2a^2/(4\pi f_0^2V) - \zeta a$ or choose the length and calculate the radius according to

$$a = \frac{2\pi\zeta f_0^2 V}{nc^2} \left(1 + \sqrt{1 + \frac{nc^2 l}{\pi\zeta^2 f_0^2 V}} \right). \quad (8.2)$$

These are general formulas for a Helmholtz resonator, such as a bottle, which are derived from those given in Sections 4.2 and 4.3 for an acoustic mass M_{AH} and acoustic compliance C_{AF} respectively.

The quantities are defined as follows:

l is length of opening in m.

a is radius of opening in m.

ζ is end correction factor.

f_0 is resonance frequency in Hz.

V is volume of cavity in m^3 .

c is speed of sound = 348.8 m/s at $P_0 = 10^5$ Pa and $T = 22^\circ\text{C}$.

The end correction factor for the opening is given by

$$\zeta = \begin{cases} 1.28, & \text{unflanged at both ends} \\ 1.49, & \text{flanged at one end, unflanged at the other} \\ 1, 7, & \text{flanged at both ends} \end{cases} \quad (8.3)$$



8.3 DESIGN CONSIDERATIONS

Dust screens

All of the openings, for the loudspeakers and microphone, must be covered by a dust screen, which not only protects against the ingress of magnetic dust but also helps damp out the various Helmholtz resonances. Data on dust screens are given in Section 4.4.

Magnetic fields

High strength neodymium magnets have generally improved the performance of miniature loudspeakers; however, their proximity to sound holes means that magnetic dust can be sucked in and clog the coil gap. Magnetic fields can also affect magnetic strips on credit cards.

Acoustic shock

The location of a loudspeaker opening is very important because, if it is tightly held against the ear, damage to hearing may result. Loudspeaker openings are often located on the sides of a phone so that they cannot be sealed against the ear. Another frequent location is on a rear surface that is curved, which also prevents closure of the opening when laid on a table.

Protection against damage to the loudspeaker

It is vital that all seals be secure. If the back enclosure leaks, the stiff cushion of the air that limits the excursion of the diaphragm no longer exists and physical damage may result. At low frequencies, the generated sound pressure is limited by diaphragm excursion and at high frequencies by power dissipation. The input voltage to a voice coil is often limited according to a digital signal processor model [2] of the loudspeaker parameters and how they change according to conditions such as temperature. In addition, audio peak clipping, called dynamic range compression, is used extensively to make the sound louder.

Turbulence

At low particle velocities, the flow of air in a tube is linear. In other words, the velocity increases with radial distance from the wall as discussed in Chapter 4. As the velocity is increased beyond a certain point, the flow becomes turbulent with the formation of chaotic eddies and vortices. The Reynolds number is given by

$$\text{Re} = \frac{\rho_0 u d}{\mu} \quad (8.4)$$

where

ρ_0 is density of air in kg/m^3 .

u is particle velocity in m/s .

d is diameter of tube in m .

μ is viscosity coefficient in $\text{N}\cdot\text{s}/\text{m}^2$ (see Eq. (4.23)).

The point at which the flow becomes turbulent varies considerably with both geometry and surface finishes. As a rule of thumb, the Reynolds number should be kept below

1000 and the particle velocity below 10 m/s. All surfaces should be smooth with no sharp edges.

Wind noise [3]

The location of the microphone on the handset is critical with respect to wind noise. The worst location is on a large flat area such as a front cover because there is greater boundary layer turbulence than on a small area. The bottom edge is better and the best position is away from the center of the bottom edge. The direction of the wind also makes a significant difference. When the microphone is on the surface facing the wind, there is generally less noise than when it is facing away because turbulence builds up as air flows past an obstacle. Trailing edge vortex shedding also contributes to wind noise, but to a lesser degree than boundary layer turbulence. In general, all surfaces should be as smooth as possible with no sharp edges.

Handling noise

Handling noise is generated by friction when a handset is held. Smooth surfaces produce less noise than rough ones. The noise is amplified by structural vibrations within housing as well as normal modes within the internal space, although the latter will be reduced by the presence of electronic components. Therefore, the housing should be either rigid or well damped, or both. Adding ribs to the inner surfaces of the housing increases its rigidity. These precautions will also help to reduce unwanted resonance peaks and dips in the handsfree loudspeaker and receiver frequency responses.



8.4 HEAD AND TORSO SIMULATOR

The most commonly used device for testing the receiver of a cell phone is a head and torso simulator or HATS, which has a pair of “soft” ears (pinna) on a head with shoulders, as shown in Fig. 8.4. The HATS microphone is located at the eardrum position. Unfortunately, acoustical simulation of the head and torso simulator is not so simple because to date there is no reliable equivalent circuit available using lumped elements. Not only is the model complicated by leakage into open air, but the loading varies with force and handset position. Therefore, finite element modeling would have to be used. However, once a finite element model has been made for the acoustic path between the receiver and microphone, which is mainly the ear plus the space surrounding it and the phone, the results can be converted into a two-port model. The two-port model is then imported into an equivalent circuit for the receiver and microphone.

It should be noted that the head and torso simulator is a multipurpose device. Although the head beyond the immediate vicinity of the ear has little influence on the

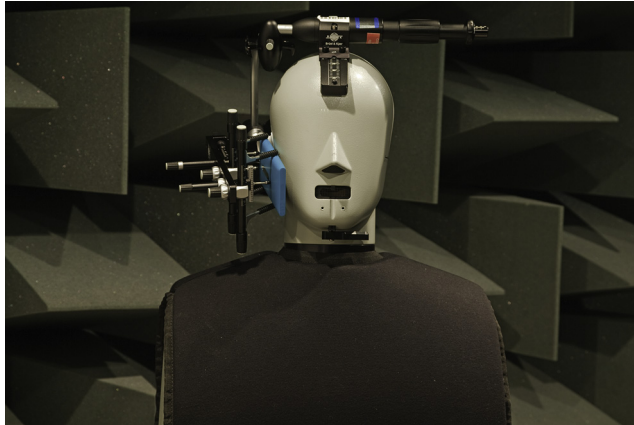


Figure 8.4 B&K type 4128D head and torso simulator with cell phone Nokia model Lumia 800. The simulator has a sound source inside the mouth and a microphone inside the ear. Courtesy of Brüel and Kjær Sound and Vibration Measurement A/S and Nokia OY. Photograph by Enrico Pascucci.

testing of a receiver, it is important for testing the microphone in a cell phone, in which case the sound source is in the mouth. Because the receiver opening is not in tight contact with the ear opening, it is probably sufficient to assume that the radiation impedance for it is similar to that for a diaphragm in the end of a tube. In testing, the head and torso simulator has largely replaced the older ear simulators, which looked nothing like real human ears. They were originally used for testing of the receivers in a conventional phone handset. For readers who are interested to find out what the impedance of an ear or that of an older simulator looks like, the data sheets [4] for the B&K 4185 sealed ear simulator or B&K 4195 nonsealed ear simulator with IEC low-leak and high-leak couplers are informative.



8.5 MICROPHONES

Electret microphones

Until the electret condenser microphone (ECM) was invented by Sessler and West [5–8], all condenser microphones required a polarizing voltage supply. Such condenser microphones are treated in Section 5.5. The name electret literally means “electrostatic magnet.” It is a dielectric in which a permanent charge is embedded. In Sessler and West’s invention, as shown in Fig. 8.5(a), the dielectric was a metalized Teflon foil which formed the diaphragm and the electrode was a stationary plate located behind it. In recent years, the charge storage capacity has been increased by using porous membranes [9]. Metalized electrets have a dipole charge because a charge of opposite polarity to that contained by the membrane is induced in the metallic coating. Although this gives a more stable charge, it means that, for a given membrane charge, the resulting field decays

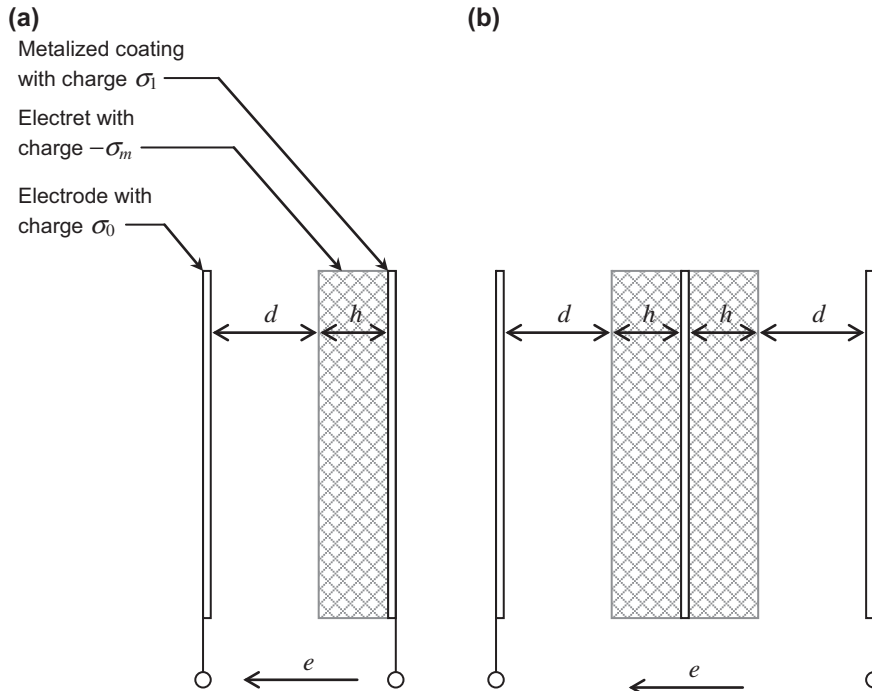


Figure 8.5 Simplified cross section of an electret transducer: (a) Single-ended and (b) Push-pull.

with increasing electrode separation, whereas in an externally polarized condenser microphone, the field remains constant. However, this is not a major issue in a microphone where the electrode spacing is usually very small. The capacitance of the electret membrane is given by

$$C_M = \frac{\epsilon_0 \epsilon_r S}{h} \quad (8.5)$$

where ϵ_0 is the permittivity of air, ϵ_r is the relative permittivity of the dielectric, S is the area of the membrane, and h is the thickness of the electret membrane. This voltage then also appears across the air gap when the microphone terminals are at the same potential. The capacitance of the air gap is given by

$$C_G = \frac{\epsilon_0 S}{d} \quad (8.6)$$

where d is the width of the gap. Then the total capacitance across the input terminals is

$$C_{E0} = \frac{C_M C_G}{C_M + C_G} \quad (8.7)$$

The negative membrane charge is usually expressed as a charge per unit area $-\sigma_m$ or charge density so that the total charge is $-\sigma_m S$. The charge induced in the electrode is given by

$$\sigma_0 = \frac{C_G \sigma_m}{2(C_M + C_G)}. \quad (8.8)$$

The charge induced in the membrane coating is given by

$$\sigma_1 = \frac{(2C_M + C_G) \sigma_m}{2(C_M + C_G)}. \quad (8.9)$$

so that when $d = \infty$, there is zero charge on the electrode ($\sigma_0 = 0$) and the charge on the coating is equal and opposite to the electret charge so that $\sigma_1 = \sigma_m$. In general, the total induced charge on the electrode and coating is equal and opposite to the electret charge. When $d = 0$, the induced charge is shared equally so that $\sigma_0 = \sigma_1 = \sigma_m/2$. Although the charge may be distributed throughout the electret, we may model it as a concentrated layer somewhere near the middle, depending on how symmetrical the charge distribution is. Inevitably some charge is lost both near the outer surface and near the coating, where there will be some recombination of positive and negative charge. Hence we may treat the concentrated charge layer and coating as electrodes of a capacitor across which there is a polarizing voltage E , where the dielectric thickness is $h/2$, so that

$$E = \frac{S \sigma_m}{2(C_M + C_G)}. \quad (8.10)$$

Hence we can use the same equivalent circuits as those for an externally polarized electrostatic microphone shown in Fig. 5.20.

The voltage sensitivity versus average diaphragm displacement $\Delta\delta$ is given by Ref. [10].

$$\Delta e_{\text{in}} = -\frac{E}{d} \Delta\delta = -\frac{h \sigma_m}{2 \epsilon_0 (\epsilon_r d + h)} \Delta\delta \quad (8.11)$$

It is well known that single-ended electrostatic transducers are nonlinear because the charge varies with displacement. This is not such a problem with microphones at moderate sound pressures because the displacement is very small and hence almost linear. However, for microphones at high sound pressures or loudspeakers, which have to displace a significant volume of air, a linear transducer may be created using the constant-charge push-pull principle. All conventional electrostatic loudspeakers with external polarizing supplies use this principle, which was first proposed by Frederick Hunt and then commercialized by Peter Walker [11–13]. An electret equivalent of this is shown in

Fig. 8.5(b), which has been proven to be linear both theoretically [10] and experimentally [14]. Fig. 8.6 shows a cutaway view of an electret microphone.

So far we have only considered the foil electret microphone. In fact there are three types:

Foil-type or diaphragm-type. The diaphragm itself is made of an electret dielectric. However, the electret may not be strong enough to maintain tension over a long period, especially if it is porous, and may therefore require support from an additional membrane.

Back electret. The electret film is adhered to the back plate of the microphone capsule, which forms an electrode, and the diaphragm is made of a metalized but uncharged material.

Front electret. This is a newer design, which is essentially the reverse of the back electret. The back plate is eliminated from the design, and the condenser is formed by the metalized diaphragm and the inside surface of the capsule. The electret film is adhered to the inside front cover, which is perforated to let sound through.

The circuit for an electret microphone as shown in Fig. 8.7 is simpler than that for an externally polarized microphone, shown in Fig. 5.18, because the electret provides the polarization for the capsule, although the bias for the FET usually settles to zero due to leakage.

When ECMs were first introduced, they were only expected to last for the lifetimes of the products in which they were used. However, with improved materials and processes, the ability to store charge over long periods has steadily increased. The loss of charge is compensated for by slackening of the diaphragm. Hence the sensitivity change over 28 years [15] has been found to be less than 1 dB.

Microelectromechanical system microphones

At the time of writing, most low-cost cell phones use analogue electret microphones, whereas midmarket models use both analogue microelectromechanical system

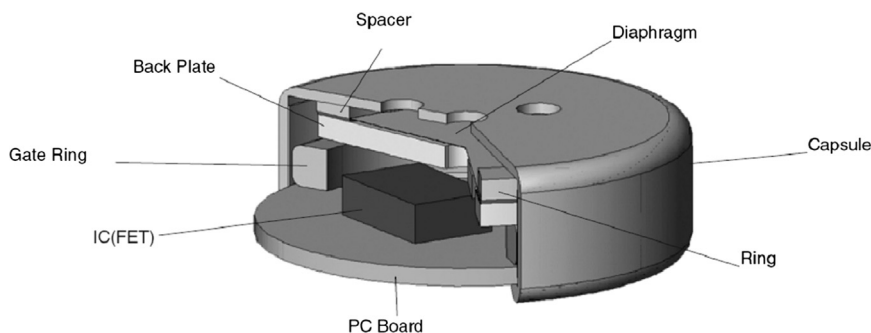


Figure 8.6 Cutaway view of an electret microphone. Courtesy of Hosiden.

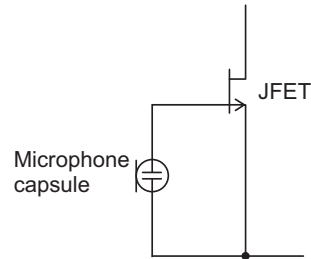


Figure 8.7 FET circuit for an electret microphone.

microphones and digital electret microphones, where the latter are analogue electret microphones with onboard analogue-to-digital converters. This has the advantage of immunity to electrical noise pickup by the connections between the microphone and baseband chip. Many top-end models now use digital MEMS microphones because these have better signal-to-noise ratios (typically 69 dB). Also, MEMS microphones are smaller and can be surface mounted, which is an advantage in products that may have stereo microphones for recording as well as multiple microphones for noise cancellation. The sensitivity of a MEMS microphone is typically -38 to -42 dBV/Pa, and the acoustic performance is very stable.

A cross section of a MEMS microphone [16,17] is shown in Fig. 8.8. Although its operation is the same as that of a conventional capacitor microphone, as described in Section 5.5, the fabrication is somewhat different and is more akin to that of an integrated circuit. The substrate is made of silicon. On this rests a “free” diaphragm of polysilicon which is $1\ \mu\text{m}$ thick. The patented free diaphragm design avoids film stress which would otherwise stiffen it. The backplate has a $0.5\ \mu\text{m}$ layer of polysilicon coated with a $1.5\ \mu\text{m}$ layer of low-stress silicon nitride. The various layers are deposited and etched to form the entire structure. The gap between the diaphragm and substrate is

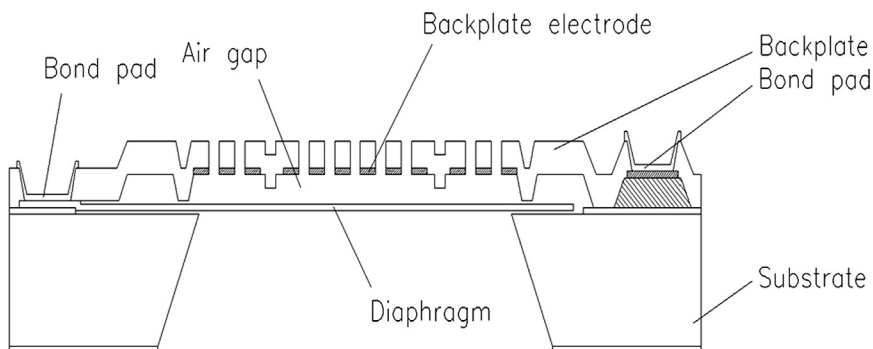


Figure 8.8 Cross section of a SiSonic microelectromechanical system microphone. Courtesy of Knowles Electronics, LLC.

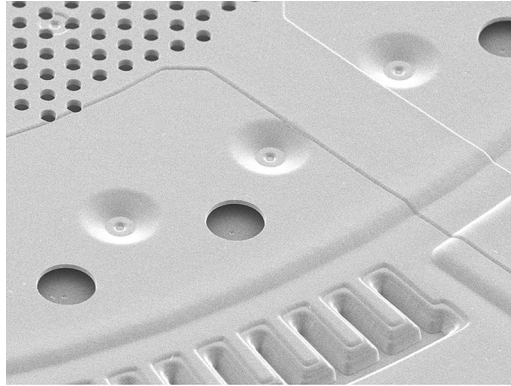


Figure 8.9 Detailed SEM photograph of a SiSonic microelectromechanical system microphone. The diaphragm is visible through the holes in the backplate. The small holes provide acoustic damping because of viscous flow losses. Courtesy of Knowles Electronics, LLC.

created by means of a sacrificial layer of phosphorus-doped glass, which is removed using an HF acid release process. The same method is also used to create the gap between the diaphragm and backplate. A detailed view of the backplate and diaphragm is shown in Fig. 8.9.

Because the cost of silicon wafer is fixed, the price of each MEMS microphone depends on how many can be made from a single wafer. Hence it is necessary for the diaphragm to be small for economic reasons as well as for miniaturization. The diaphragm is typically 0.6 mm in diameter with a gap of about 4 μm . The polarizing voltage of 11 V is developed by a charge pump within a separate integrated circuit (see Fig. 8.10), which also contains the amplifier and analogue-to-digital converter, if there is one.

PART XXVII: TYPE APPROVAL TESTING OF CELL PHONES

The most commonly used standard for the acoustical testing of cell phones today is the 3GPP Technical Specification [18,19], which is part of the overall set of specifications for the third generation network, although many network operators have their own type approval requirements which are usually variations of or additions to 3GPP. However, this only provides the acceptable limits for the test results. The test setups and methods for calculating the results are specified in other documents [20,21].

8.6 MEASUREMENTS FOR TYPE APPROVAL

Because there are many measurements in type approval testing, we shall only discuss the basic acoustic ones.

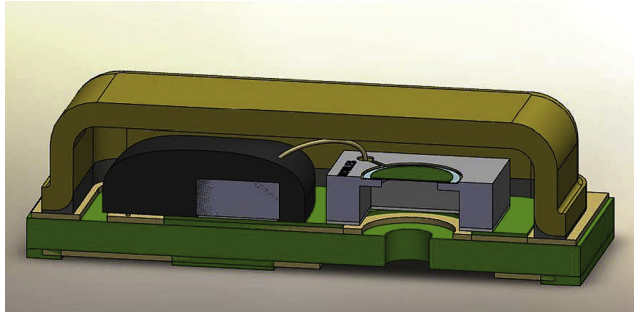


Figure 8.10 Cross section of a SiSonic microelectromechanical system microphone inside its package which provides an environmental and interference shield. The integrated circuit, which provides the polarizing voltage and amplification, is on the left. Courtesy of Knowles Electronics, LLC.

Frequency response

Here we shall confine ourselves to broadband telephony (100 Hz–8 kHz) as opposed to narrowband (100 Hz–4 kHz). To measure the send frequency response, the sound source is calibrated by means of a microphone holder attached to the head and torso simulator (see Fig. 8.4). Then the calibration microphone is attached to the microphone holder with the diaphragm at the mouth reference point (MRP), which is 25 mm in front of the lip plane. The sound source is equalized to give a constant sound pressure of typically -4.7 dB Pa at all test frequencies. The frequency response is measured by connecting an analyzer to the point of interconnection (POI). In a landline phone, this is an analogue connection to the public switched telephone network, but in a cell phone it is usually the digital interface point (formerly digital air interface). The measured frequency response is plotted between upper and lower limits known as a mask. Thus, to meet the requirements of type approval, the plot must fall within this mask. A typical frequency response is shown in Fig. 8.11.

To measure the receive frequency response, a signal is applied to the POI, and the microphone at the drum reference point (DRP) within the HATS is connected to an analyzer. A typical frequency response is shown in Fig. 8.12.

Loudness rating

The loudness rating LR is calculated from the measured response over a set of frequencies which are spaced 1/3 octave apart according to the following formula:

$$\text{LR} = -\frac{10}{m} \log_{10} \sum_{i=N_1}^{N_2} 10^{0.1m(S_i - W_i)} \quad (8.12)$$

where

$m = 0.175$ is a constant.

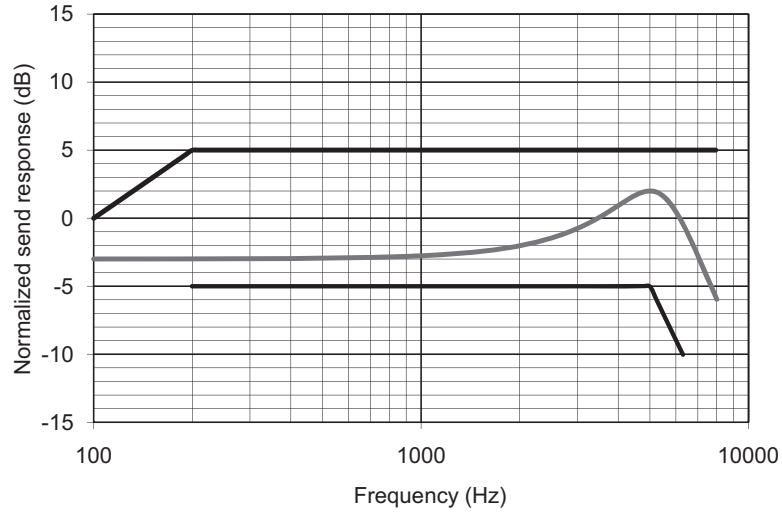


Figure 8.11 Typical send frequency response (*gray*) with mask (*black*).

S_i refers to the sensitivities at frequency f_i of the send or receive electroacoustic path. W_i refers to the weighting factors given in [Table 8.1](#), where SLR refers to the send loudness rating and RLR to the receive loudness rating.

Notice the minus sign in [Eq. \(8.12\)](#), which means that the larger the loudness rating, the quieter the phone.

However, care has to be taken in evaluating the sensitivities from the digital POI of a cell phone. They are expressed in dB re V/Pa in the send direction and dB re Pa/V in the receive direction.

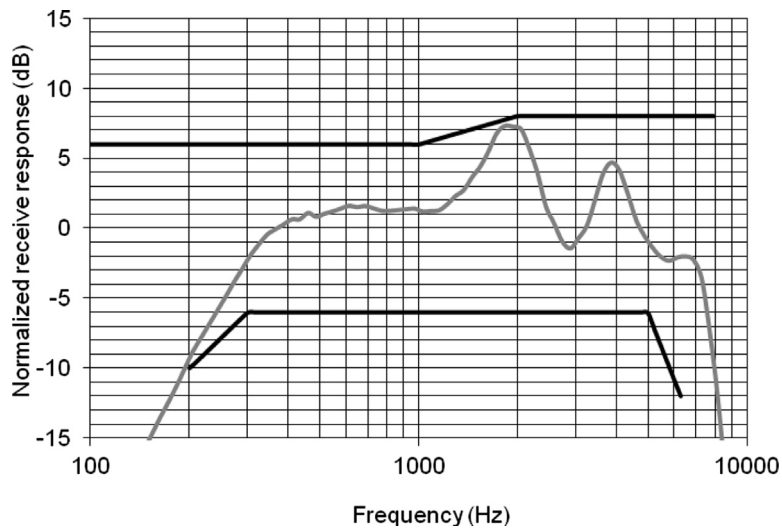


Figure 8.12 Typical receive frequency response (*gray*) with mask (*black*).

Table 8.1 Weights for wideband SLR and RLR calculations.

Frequency (Hz)	W_{Si} (SLR)	W_{Ri} (RLR)
100	103.0	115.4
125	75.3	87.5
160	60.2	72.3
200	59.5	72.1
250	52.9	67.2
315	59.4	75.8
400	45.4	63.6
500	56.6	74.6
630	53.5	70.4
800	53.8	69.9
1000	55.9	70.9
1250	64.2	78.4
1600	60.6	74.9
2000	73.7	85.2
2500	70.4	81.6
3150	87.1	95.4
4000	68.2	77.0
5000	84.5	91.7
6300	86.5	92.4
8000	71.0	89.0

receive direction, which are analogue quantities. This is fairly straightforward in a landline phone where we are simply concerned with the analogue voltage across a 600Ω termination. In a digital system, it is convenient to use the maximum “full-scale” level before clipping as the reference point or 0 dBFS. This has been defined as equivalent to the voltage which is required to deliver 2.06 mW of power into a 600Ω load. Hence

$$0 \text{ dBFS} = 3.14 \text{ dBm}_0 = 0.922 \text{ dBV (or } 1.112 \text{ V}_{\text{rms}}) \text{ for send and receive} \quad (8.13)$$

For type approval, the send and receive loudness ratings must be

$$\text{SLR} = 8 \pm 3 \text{ dB}$$

$$\text{RLR} = 2 \pm 3 \text{ dB}$$

Sidetone

When we talk, we normally hear our own voices via the external acoustic path between our mouths and ears. It is unnatural to have one ear obscured by a cell phone, so the acoustic path is replaced by an electrical one between the microphone and receiver. This is known as sidetone. There are two kinds, one being a deliberate path within the handset

and the other the result of echo from an imperfect analogue interface, or hybrid, to a two-wire line within the network. The latter is minimized through use of a digital echo canceler because delayed sidetone is extremely irritating to the caller. Other sidetone paths may be carried by the mechanical structure of the phone or the space within it.

The sidetone rating is calculated using Eq. (8.12) as before except that the sensitivities S_i are for the path between the MRP and DRP and are thus dimensionless because pressure is measured (in Pa) at both points. In addition, $m = 0.225$ and the weights are given in Table 8.2.

There are two sidetone ratings. One is the sidetone masking rating (STMR) and the other is the listener sidetone rating (LSTR). In the case of the STMR, the test signal comes from the mouth simulator, whereas in the case of the LSTR, it is an external diffuse field. Hence the latter is a characterization of the room noise picked up via the electrical sidetone path. However, it is often more useful to evaluate the listener's sidetone performance of a handset indirectly by the difference

$$D = \text{LSTR} - \text{STMR} \quad (8.14)$$

where D is a parameter of the phone which is *independent* of the network.

Table 8.2 Weights for wideband sidetone masking rating and listener sidetone rating calculations.

Band No.	Midfrequency (Hz)	W_i
1	100	115.4
2	125	87.5
3	160	72.3
4	200	72.1
5	250	67.2
6	315	75.8
7	400	63.6
8	500	74.6
9	630	70.4
10	800	69.9
11	1000	70.9
12	1250	78.4
13	1600	74.9
14	2000	85.2
15	2500	81.6
16	3150	95.4
17	4000	77.0
18	5000	91.7
19	6300	92.4
20	8000	89.0

REFERENCES

- [1] Andersen MK. Telephone handset, a cordless telephone or a mobile telephone, Kirk acoustics. Patent no. WO 9824214. 1998.
- [2] Bright AP. Paper No. 22. In: Adaptive HR filters for loudspeaker parameter tracking, in the second AES conference; 2007.
- [3] Bradley S, Wu T, von Hünenbein S, Backman J. The mechanisms creating wind noise in microphones, in the 114th AES convention. paper no. 5718. 2003.
- [4] <http://www.bksv.com/>.
- [5] Sessler GM, Hill M, West JE. Electroacoustic transducer. U.S. Patent No. 3,118,022. 1962.
- [6] Sessler GM, West JE. Self-biased condenser microphone with high capacitance. *J Acoust Soc Am* 1962;34(11):1787–8.
- [7] Sessler GM. Electrostatic microphones with electret foils. *J Acoust Soc Am* 1963;35(9):1357–534.
- [8] Sessler GM. Electric fields and forces due to charged dielectrics. *J Appl Phys* 1972;43(2):405–8.
- [9] Chiang D-M, Liu W-L, Chen J-L, Susuki R. PALS and SPM/EFM investigation of charged nanoporous electret films. *Chem Phys Lett* 2005;412:50–4.
- [10] Mellow TJ, Kärkkäinen LM. On the forces in single-ended and push-pull electret transducers. *J Acoust Soc Am* 2008;124(3):1497–504.
- [11] Walker PJ. Wide range electrostatic loudspeakers, Part 1. *Wireless World* 1955;61:208–11.
- [12] Walker PJ. Wide range electrostatic loudspeakers, Part 2. *Wireless World* 1955;61:265–9.
- [13] Walker PJ. Wide range electrostatic loudspeakers, Part 3. *Wireless World* 1955;61:381–4.
- [14] Bai MR, Wang CJ, Chiang DM, Lin SR. Experimental modeling and design optimization of push-pull electret loudspeakers. *J Acoust Soc Am* 2010;127(4):2274–81.
- [15] Yasuno Y, Miura K. Sensitivity change with practical use of electret condenser microphone. *J Acoust Soc Am* 2006;120(5):3233.
- [16] Loeppert PV, Graber WS. Silicon-on-Silicon differential input sensors. U.S. Patent No. 5,178,015. 1993.
- [17] Loeppert PV. Solid state sensor and microphone devices. U.S. Patent No. 5,490,220. 1994.
- [18] 3rd Generation partnership project; technical specification group services and system aspects; terminal acoustic characteristics for telephony; requirements (release 10), 3GPP TS 26.131, V10.3.0 (2011-09). <http://www.3gpp.org>.
- [19] 3rd Generation partnership project; technical specification group services and system aspects; Terminal acoustic characteristics for telephony; test (release 10), 3GPP TS 26.132 V10.2.0 (2011-09). <http://www.3gpp.org>.
- [20] Series P: Telephone transmission quality, telephone installations, local line networks; measurements related to speech; calculation of loudness ratings for telephone sets, ITU-T P.79 (11/2007). <http://www.itu.int>.
- [21] Series P: Telephone transmission quality, telephone installations, local line networks; measurements related to speech; calculation of loudness ratings for telephone sets; annex G: wideband loudness rating algorithm, ITU-T P.79, annex G (11/2001). <http://www.itu.int>.

Horn loudspeakers

PART XXVIII: HORN DRIVE UNITS

9.1 INTRODUCTION

Horn loudspeakers usually consist of an electrodynamic drive unit coupled to a horn. When well designed, the large end of the horn, called the “mouth,” has an area sufficiently large to radiate sound efficiently at the lowest frequency desired. The small end of the horn, called the “throat,” has an area selected to match the acoustic impedance of the drive unit and to produce as little nonlinear distortion of the acoustic signal as possible.

Horn loudspeakers are in widespread use in cinemas, theaters, concert halls, stadiums, and arenas where large acoustic powers must be radiated and where control of the direction of sound radiation is desired. The efficiency of radiation of sound from one side of a well-designed direct-radiator loudspeaker was shown in Chapters 6 and 7 to be typically less than 1%. By comparison, the efficiency of radiation from a horn loudspeaker usually lies between 10% and 50%.

The principal disadvantages of horn loudspeakers compared with the direct-radiator loudspeakers are higher cost and larger size.

Before proceeding with an analysis of the horn loudspeaker, it should be mentioned again that the radiating efficiency of a direct-radiator loudspeaker can be increased at low frequencies by mounting several units side by side in a single baffle. The mutual interaction among the radiating units serves to increase the radiation resistance of each unit substantially. For example, two identical direct-radiator loudspeakers very close to each other in an infinitely large plane baffle, and vibrating in phase, will produce four times the intensity on the principal axis as will one of them alone.

Direct-radiator loudspeakers used in an array often are not as satisfactory at high frequencies as one horn loudspeaker because of the difficulty of obtaining uniform phase conditions from different direct-radiator diaphragms. That is to say, the conditions of vibration of a loudspeaker cone are complex, so that normal variations in the uniformity of cones result in substantial differences in the phases of the radiated signals of different cones at high frequencies. A very irregular and unpredictable response curve and directivity pattern result.

This problem does not arise with a horn where only a single drive unit is employed. When two or more drive units are used to drive a single horn, the frequency range in which the response curve is not adversely affected by the multiplicity of drive units is that where the diaphragms vibrate in one phase.



9.2 ELECTRO-MECHANO-ACOUSTICAL CIRCUIT [1]

The drive unit for a horn loudspeaker is essentially a small direct-radiator loudspeaker that couples to the throat of a flaring horn as shown in Fig. 9.1. In the next part we shall discuss the characteristics of the horn itself. In this section we restrict ourselves to that part of the frequency range where the complex mechanical impedance Z_{MT} looking into the throat of a horn is a pure resistance:

$$Z_{MT} = \frac{1}{Y_{MT}} = \rho_0 c S_T N \cdot s/m \quad (9.1)$$

where

ρ_0 is density of air in kg/m^3

c is velocity of sound in m/s

$\rho_0 c = 406$ rayls at 22°C and 10^5 Pa ambient pressure

S_T is area of the throat in m^2

Y_{MT} is mechanical admittance at the throat of the horn in $\text{m}/\text{N s}$

A cross-sectional drawing of a compression drive unit for a horn loudspeaker is shown in Fig. 9.2. It has a diaphragm and voice coil with a total mass M_{MD} , a mechanical compliance C_{MS} , and a mechanical resistance $R_{MS} = 1/G_{MS}$. The quantity G_{MS} is the mechanical conductance of the diaphragm in $\text{m}/\text{N s}$.

Behind the diaphragm is a back cavity that is usually filled with a soft acoustical material. At low frequencies this space acts as a compliance C_{MB} , which can be lumped in with the compliance of the diaphragm. At high frequencies the reactance of this space

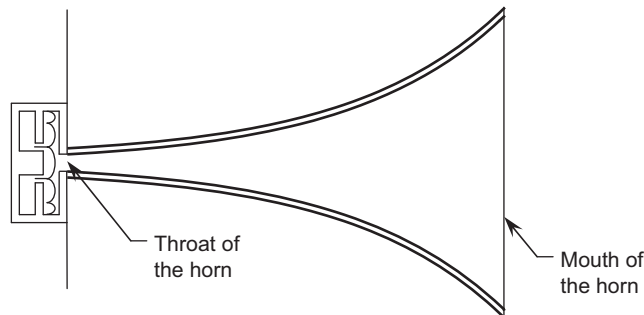


Figure 9.1 Cross section of a simple horn loudspeaker with an exponential cross section. For this design, the radius of the throat is 0.1, the radius of the mouth 1.7, and the length is 5.0 (arbitrary units).

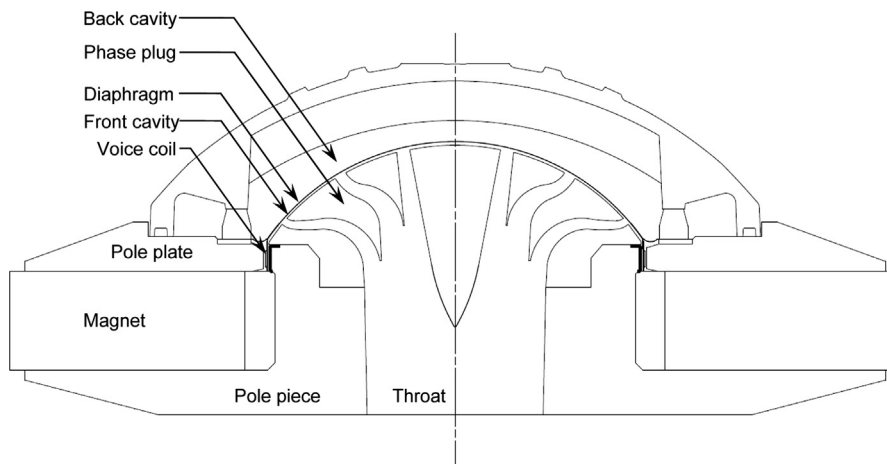


Figure 9.2 Cross section of a horn compression drive unit. The diaphragm couples to the throat of the horn through a small cavity with a mechanical compliance C_{M1} . Note that in this design, the annular channels within the phase plug meet the front cavity at nodal points so as to suppress the normal modes, which would otherwise occur [19]. Such modes would produce a somewhat uneven frequency response. Courtesy of Celestion.

becomes small so that the space behind the diaphragm becomes a mechanical radiation resistance $R_{MB} = 1/G_{MB}$ with a magnitude equal to that given in Eq. (9.1). This resistance combines with the mechanical radiation resistance of the throat, and the diaphragm must develop power both to its front and its back. Obviously, any power developed behind the diaphragm is wasted, and at high frequencies this sometimes becomes as much as one-half of the total generated acoustic power.

In front of the diaphragm there is an air space or front cavity with compliance C_{M1} . At low frequencies the air in this space behaves like an incompressible fluid, that is, ωC_{M1} is small, and all the air displaced by the diaphragm passes into the throat of the horn. At high frequencies, the mechanical reactance of this air space becomes sufficiently low (i.e., the air becomes compressible), so that all the air displaced by the diaphragm does not pass into the throat of the horn.

The voice coil has an electrical resistance R_E and inductance L_E . As stated above, Y_{MT} is the mechanical admittance at the throat of the horn.

By inspection, we draw the admittance-type analogous circuit shown in Fig. 9.3. In this circuit, forces “flow” through the elements, and the velocity “drops” across them. The generator open-circuit voltage and resistance are \tilde{e}_g and R_g . The electric current is \tilde{i} ; the linear velocity of the voice coil and diaphragm is \tilde{u}_c ; the linear velocity of the air at the throat of the horn is \tilde{u}_T ; and the force at the throat of the horn is \tilde{f}_T . As before, the area of the diaphragm is S_D and that of the throat is S_T .

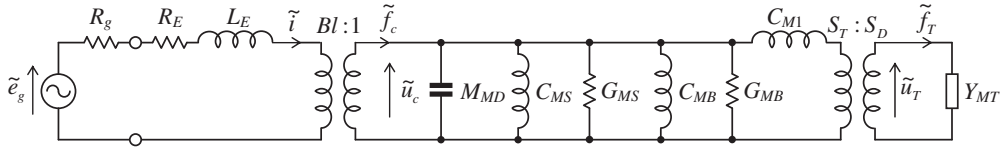


Figure 9.3 Electro-mechano-acoustical analogous circuit of the admittance type for the drive unit. To derive this, we assume that the mechanical impedance at the horn throat is $\rho_0 c S_T$, that is, the mechanical admittance is $Y_{MT} = 1/(\rho_0 c S_T)$.

9.3 REFERENCE EFFICIENCY

In the middle-frequency range many approximations usually can be made to simplify the analogous circuit of Fig. 9.3. Because the drive unit is very small, the mass of the diaphragm and the voice coil M_{MD} is very small. This in turn usually means that the compliance of the suspension C_{MS} is large to keep the resonance frequency low. Also, the conductance of the suspension G_{MS} usually is large, and the reactance ωC_{M1} is small. Hence, in this frequency range, the circuit reduces essentially to that of Fig. 9.4a, where the conductance behind the diaphragm is

$$G_{MB} \equiv \frac{1}{\rho_0 c S_D} \text{ m} \cdot \text{N/s}. \tag{9.2}$$

With the area-changing and electromechanical transformers removed, we get Fig. 9.4b, where the radiation conductance at the throat is

$$G_{MT} \equiv \frac{S_T}{\rho_0 c S_D^2} \text{ m} \cdot \text{N/s}. \tag{9.3}$$

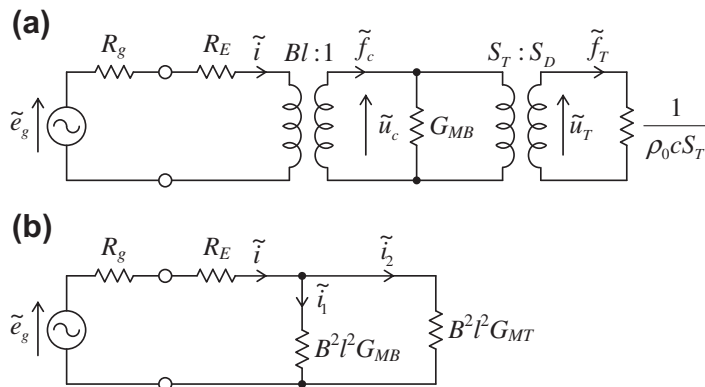


Figure 9.4 Simplified analogous circuits of the admittance type for the drive unit in the region where the motion of the diaphragm is resistance-controlled by the horn (a) and with the transformers removed (b).

As before, S_T is the area of the throat and S_D is the area of the diaphragm in m^2 . We have assumed here that the cavity behind the diaphragm in this frequency range is nearly perfectly absorbing, which may not always be true. Usually, however, this circuit is valid over a considerable frequency range because of the heavy damping provided by the conductance of the horn G_{MT} . Also, G_{MT} usually is smaller than G_{MB} so that most of the power supplied by the diaphragm goes into the horn.

Solution of Fig. 9.4b gives us

$$\tilde{i}_2 = \frac{G_{MB}}{G_{MB} + G_{MT}} \tilde{i}. \quad (9.4)$$

Assuming that the output resistance R_g of the generator is small compared with the coil resistance R_E of the drive unit, the total electrical power supplied from the generator is

$$\text{Total power supplied} = \left| \frac{\tilde{i}}{\sqrt{2}} \right|^2 \left(R_E + B^2 l^2 \frac{G_{MB} G_{MT}}{G_{MB} + G_{MT}} \right). \quad (9.5)$$

Using the solution of Eq. (9.4), the reference efficiency E_{ff} is equal to the power delivered to the horn,

$$\left| \tilde{i}_2 / \sqrt{2} \right|^2 B^2 l^2 G_{MT},$$

times 100 divided by the total power supplied:

$$E_{ff} = \frac{(G_{MB}/(G_{MB} + G_{MT}))^2 B^2 l^2 G_{MT}}{R_E + B^2 l^2 G_{MB} G_{MT}/(G_{MB} + G_{MT})} \times 100. \quad (9.6)$$

From Eqs. (9.2, 9.3 and 9.6) we get

$$E_{ff} = \frac{100 B^2 l^2 (S_T/S_D)}{(1 + S_T/S_D)((B^2 l^2 + S_D \rho_0 c R_E)(S_T/S_D) + S_D \rho_0 c R_E)} \quad (9.7)$$

or, in terms of Thiele–Small parameters,

$$E_{ff} = \frac{100 (S_T/S_D) S_D c}{(1 + S_T/S_D)((S_D c + \omega_S Q_{ES} V_{AS})(S_T/S_D) + \omega_S Q_{ES} V_{AS})}, \quad (9.8)$$

where we have used Eqs. (6.27) and (6.30) for the Bl factor. We note that the value of G_{MT} and hence the ratio S_T/S_D would seem to need to be large for high efficiency. However, if S_T/S_D becomes too large, reference to Fig. 9.4b shows that too much power will be dissipated in G_{MB} and the efficiency will be low. To optimize the efficiency, let us

now differentiate the above with respect to (S_T/S_D) and equate the result to zero. Hence maximum efficiency occurs when

$$\frac{S_T}{S_D} = \sqrt{\frac{S_D \rho_0 c R_E}{B^2 l^2 + S_D \rho_0 c R_E}} = \sqrt{\frac{\omega_S Q_{ES} V_{AS}}{S_{Dc} + \omega_S Q_{ES} V_{AS}}}, \quad (9.9)$$

so that the maximum efficiency is

$$E_{ff}(\max) = \frac{100 B^2 l^2}{\left(\sqrt{B^2 l^2 + S_D \rho_0 c R_E} + \sqrt{S_D \rho_0 c R_E}\right)^2}, \quad (9.10)$$

which can also be given in terms of Thiele–Small parameters:

$$E_{ff}(\max) = \frac{100 S_{Dc}}{\left(\sqrt{S_{Dc} + \omega_S Q_{ES} V_{AS}} + \sqrt{\omega_S Q_{ES} V_{AS}}\right)^2}. \quad (9.11)$$

To increase the efficiency further, it is seen from Eq. (9.10) that the length l of the wire on the voice coil should be increased as much as possible without altering electrical resistance R_E . Within given space limitations, this can be done by winding the voice coil from wire with a rectangular cross section rather than with a circular cross section. This means that the voice-coil mass will be increased. Increasing l further will demand a wire of larger cross section, which will require a larger air gap, with a corresponding reduction in B or increase in magnet size. Also, the voice coil must not become too large as its mass will limit the high-frequency response.



9.4 FREQUENCY RESPONSE

The frequency response of a complete horn loudspeaker, in the range where the throat impedance of the horn is a resistance as given by Eq. (9.1), is determined by solution of the circuit of Fig. 9.3. A horn-loaded drive unit behaves very differently from a direct radiator. The diaphragm of a direct-radiator loudspeaker is *mass controlled* because a flat on-axis response is given at frequencies where the acceleration of the diaphragm is constant. Because the velocity decreases with frequency, so does the radiated power for $\omega > c/a$, but this is compensated for by an increasingly narrow directivity pattern, which is how the flat on-axis response is maintained. By contrast, a horn has a fairly constant directivity pattern over its operating frequency range. Hence, for a flat frequency response, the radiated power must also be constant, which can only be achieved if the velocity is constant. Hence the diaphragm of horn-loaded drive unit is *resistance controlled*. For purposes of analysis, we shall divide the frequency range into three parts, *A*, *B*, and *C*, as shown in Fig. 9.5.

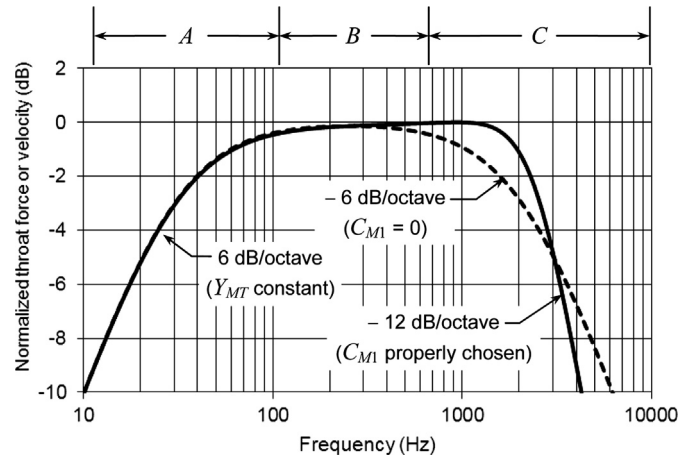


Figure 9.5 Normalized frequency response of the mechanical force \tilde{f}_T or velocity \tilde{u}_T at the throat of a horn drive unit, in the frequency region where the mechanical impedance at the throat is a pure resistance $\rho_0 c S_T$. The ordinate is a logarithmic scale, proportional to decibels.

Midfrequency range

In the midfrequency range, designated as B in Fig. 9.5, the response is equal to the reference efficiency given by Eq. (9.8). Here, the response is “flat” with frequency, and, for the usual high-frequency units used in auditoriums with 300-Hz cutoff frequencies, the flat region extends from a little above 500 to a little below 3000 Hz. In this region the velocity of the diaphragm is constant with frequency, rather than decreasing in inverse proportion to frequency as was the case for a direct-radiator loudspeaker.

Resonance frequency

It is apparent from Fig. 9.3 that because ωC_{M1} is small, zero reactance will occur at the frequency where

$$f_0 = \frac{1}{2\pi\sqrt{M_{MD}(C_{MS}C_{MB}/(C_{MS} + C_{MB}))}} \quad (9.12)$$

In practice, this resonance usually is located in the middle of region B of Fig. 9.5 and is heavily damped by the conductance G_{MT} , so that the velocity of the diaphragm is resistance controlled.

Low frequencies

At frequencies well below the resonance frequency, the response will drop off 6 dB for each octave decrease in frequency if the throat impedance is a resistance as given by Eq. (9.1). This case is shown as region A in Fig. 9.5.

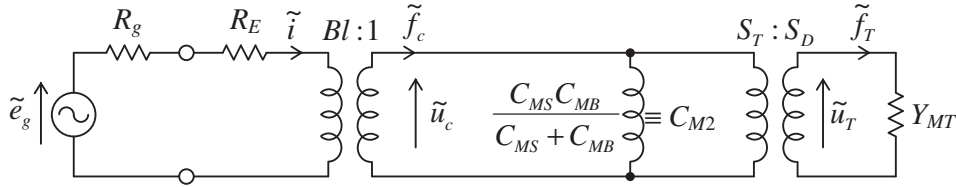


Figure 9.6 Analogous circuit for a horn drive unit in the region where the diaphragm would be stiffness controlled if the horn admittance were infinite. The actual value of the mechanical admittance of the horn at the throat is Z_{MT} .

Let us simplify Fig. 9.3 so that it is valid only for the low-frequency region, well below the resonance of the diaphragm. Then the inductance L_E , the mass M_{MD} , the compliance C_{M1} , and the conductances G_{MS} and G_{MB} may all be dropped from the circuit, giving us Fig. 9.6.

Assuming the throat admittance of the horn is a pure conductance as given by Eq. (9.3), the frequency at which the frequency response is 3 dB down is given in terms of the Thiele–Small parameters by

$$\omega_L = \left(1 + \frac{V_{AS}}{V_B}\right) \frac{\omega_S Q_{ES} S_{Dc}}{S_{Dc} + (1 + S_D/S_T)\omega_S Q_{ES} V_{AS}}. \quad (9.13)$$

where V_B is the volume of the back cavity. In practice, however, the throat impedance Z_{MT} of the horn near the lowest frequency at which one wishes to radiate sound is *not* a pure resistance. Hence, region *A* needs more careful study. Solving for the mechanical admittance at the diaphragm of the drive unit yields

$$Y_{Mc} = \frac{\tilde{u}_c}{\tilde{f}_c} = \frac{j\omega C_{M2} (S_T/S_D)^2 Y_{MT}}{j\omega C_{M2} + (S_T/S_D)^2 Y_{MT}} \quad (9.14)$$

where

$$C_{M2} = \frac{C_{MS} C_{MB}}{C_{MS} + C_{MB}} \quad (9.15)$$

and Y_{MT} is the mechanical admittance at the throat of the horn with area S_T . The mechanical impedance at the diaphragm of the drive unit is the reciprocal of Y_{Mc} ,

$$Z_{Mc} = \frac{\tilde{f}_c}{\tilde{u}_c} = \left(\frac{S_D}{S_T}\right)^2 Z_{MT} - j \frac{1}{\omega C_{M2}} \quad (9.16)$$

where $Z_{MT} = 1/Y_{MT}$ is the mechanical impedance at the throat of the horn with area S_T .

As we shall show in the next part, the mechanical impedance at the throat of ordinary types of horn at the lower end of the useful frequency range is equal to a mechanical resistance in series with a negative compliance. That is to say,

$$Z_{MT} \equiv \mathbf{R}_{MT} + j \frac{1}{\omega C_{MT}}. \quad (9.17)$$

The bold \mathbf{R}_{MT} indicates that this resistance varies with frequency. Usually, its variation is between zero at very low frequencies and $\rho_0 c S_T$ (as given by Eq. 9.1) at some frequency in region *A* of Fig. 9.5. Hence, the admittance $Y_{MT} = 1/Z_{MT}$ is a resistance in series with a negative mass reactance. In the frequency range where this is true, therefore, the reactive part of the impedance Z_{Mc} can be canceled out by letting (see Eqs. 9.16 and 9.17)

$$\frac{S_D^2}{S_T^2} \frac{1}{C_{MT}} = \frac{1}{C_{M2}} = \left(\frac{1}{C_{MB}} + \frac{1}{C_{MS}} \right). \quad (9.18)$$

Then,

$$Z_{Mc} = \mathbf{R}_{MT} \left(\frac{S_D}{S_T} \right)^2 \equiv \frac{1}{\mathbf{G}_{Mc}} \quad (9.19)$$

where \mathbf{G}_{Mc} is the acoustic conductance of the throat of the horn at low frequencies transformed to the diaphragm.

The efficiency for frequencies where the approximate circuit of Fig. 9.6 holds, and where the conditions of Eq. (9.18) are met, is

$$E_{ff} = \frac{100 B^2 l^2 \mathbf{G}_{Mc}}{R_E + B^2 l^2 \mathbf{G}_{Mc}} \quad (9.20)$$

assuming $R_g \gg R_E$. The conductance \mathbf{G}_{Mc} usually varies from “infinity” at very low frequencies down to $S_T / (S_D^2 \rho_0 c)$ at some frequency in region *A* of Fig. 9.5.

High frequencies

At very high frequencies, the response is limited principally by the combined mass of the diaphragm and the voice coil M_{MD} . If the compliance C_{M1} of the front cavity were zero, the response would drop off at the rate of 6 dB per octave (see region *C* of Fig. 9.5). It is possible to choose C_{M1} to resonate with M_{MD} at a frequency that extends the response upward beyond where it would extend if it were limited by M_{MD} alone. We can understand this situation by deriving a circuit valid for the higher frequencies as shown in

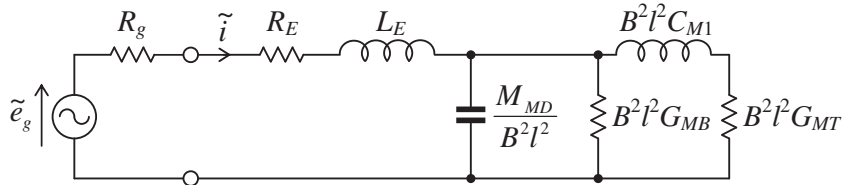


Figure 9.7 Analogous circuit for a horn drive unit at high frequencies where the diaphragm mass reactance is much larger than its compliance reactance.

Fig. 9.7. It is seen that a damped antiresonance occurs at a selected high frequency ω_U , which is given in terms of the Thiele–Small parameters of the drive unit by

$$\omega_U = \omega_S \sqrt{\frac{V_{AS}}{V_F} \left\{ 1 + \frac{S_T}{S_D} \left(1 + \frac{S_{Dc}}{\omega_S Q_{ES} V_{AS}} \right) \right\}} \quad (9.21)$$

with a Q_U value of

$$Q_U = \omega_U \left\{ \frac{S_{Tc}}{V_F} + \omega_S \left(\frac{1}{Q_{ES}} + \frac{\omega_S V_{AS}}{S_{Dc}} \right) \right\}^{-1} \quad (9.22)$$

where V_F is the volume of the front cavity. Above this resonance frequency, the response drops off 12 dB for each octave increase in frequency (see region *C* of Fig. 9.5).

Because the principal diaphragm resonance (Eq. 9.12) is highly damped by the throat resistance of the horn, it is possible to extend the region of flat response of a drive unit over a range of four octaves by proper choice of C_{M1} at higher frequencies and by meeting the conditions of Eq. (9.18) at lower frequencies.



9.5 EXAMPLES OF HORN CALCULATIONS

Example 9.1. Find the maximum efficiency of a 2-inch theater horn drive unit designed to operate in the frequency range above 500 Hz with the following Thiele–Small parameters:

$$\begin{aligned} R_E &= 6.4 \, \Omega \\ Q_{ES} &= 0.8 \\ f_S &= 250 \, \text{Hz} \\ S_D &= 13.2 \, \text{cm}^2 \\ V_{AS} &= 0.1 \, \text{L.} \end{aligned}$$

Solution. From Eq. (9.9) the optimum throat area is

$$\begin{aligned} S_T &= 13.2 \times 10^{-4} \times \sqrt{\frac{2 \times 3.14 \times 250 \times 0.8 \times 0.1 \times 10^{-3}}{13.2 \times 10^{-4} \times 348.8 + 2 \times 3.14 \times 250 \times 0.8 \times 0.1 \times 10^{-3}}} \\ &= 6.11 \text{ cm}^2, \end{aligned}$$

which from Eq. (9.11) gives a maximum efficiency of

$$\begin{aligned} E_{ff}(\text{max}) &= \frac{100S_{Dc}}{\left(\sqrt{13.2 \times 10^{-4} \times 348.8 + 2 \times 3.14 \times 250 \times 0.8 \times 0.1 \times 10^{-3}} + \sqrt{2 \times 3.14 \times 250 \times 0.8 \times 0.1 \times 10^{-3}}\right)^2} \\ &= 36.7\%. \end{aligned}$$

Example 9.2. To extend the high-frequency response of the previous example, reduce the throat area to $S_T = 0.66 \text{ cm}^2$ ($S_T/S_D = 0.05$) and recalculate the efficiency. Also determine the upper resonance frequency and the Q of the resonance, as well as the theoretical lower cutoff frequency that would be obtained with an infinite horn of low cutoff frequency and a 0.1 L back cavity (i.e., $V_B = V_{AS}$).

Solution. Then we obtain the efficiency from Eq. (9.8), which gives

$$\begin{aligned} E_{ff} &= \frac{100 \times 0.05 \times 13.2 \times 10^{-1} \times 348.8}{(1 + 0.05)((13.2 \times 10^{-1} \times 348.8 + 2 \times 3.14 \times 250 \times 0.8 \times 0.1) \times 0.05 + 2 \times 3.14 \times 250 \times 0.8 \times 0.1)} \\ &= 14.2\%, \end{aligned}$$

which is still quite good. If we set the depth d of the front cavity to $d = 1 \text{ mm}$ so that $V_F \approx dS_D = 1.32 \text{ cm}^3$, we obtain the high-frequency resonance from Eq. (9.21), which gives

$$\begin{aligned} f_U &= 250 \sqrt{\frac{0.1 \times 10^{-3}}{1 \times 10^{-3} \times 13.2 \times 10^{-4}} \left\{ 1 + 0.05 \times \left(1 + \frac{13.2 \times 10^{-4} \times 348.8}{2 \times 3.14 \times 250 \times 0.8 \times 0.1 \times 10^{-3}} \right) \right\}} \\ &= 2.42 \text{ kHz}. \end{aligned}$$

Using Eq. (9.22) we obtain a Q value of

$$\begin{aligned} Q_U &= 2 \times 3.14 \times 2420 \times \left\{ \frac{0.66 \times 10^{-4} \times 348.8}{10^{-3} \times 13.2 \times 10^{-4}} + 2 \times 3.14 \times 250 \left(\frac{1}{0.8} + \frac{2 \times 3.14 \times 250 \times 0.1 \times 10^{-3}}{13.2 \times 10^{-4} \times 348.8} \right) \right\}^{-1} \\ &= 0.762, \end{aligned}$$

which is fairly optimal for a flat frequency-response with a smooth roll-off. Finally, from Eq. (9.13) we obtain the following lower cutoff frequency with an ideal infinite horn:

$$f_L = \frac{1}{2 \times 3.14} (1 + 1) \frac{2 \times 3.14 \times 250 \times 0.8 \times 13.2 \times 10^{-4} \times 348.8}{13.2 \times 10^{-4} \times 348.8 + (1 + 20) \times 2 \times 3.14 \times 250 \times 0.8 \times 0.1 \times 10^{-3}}$$

$$= 59.4 \text{ Hz.}$$

Of course this is unrealistic in practice as the lower cutoff frequency is more likely to be determined by the characteristics of the horn, which we shall examine in the next section. The full frequency response is plotted in Fig. 9.5.

PART XXIX: HORNS

9.6 GENERAL DESCRIPTION

A horn is in effect an acoustic transformer. It transforms a small-area diaphragm into a large-area diaphragm without the difficulties of cone resonances discussed in Section 6.14. A large-area diaphragm has a radiation impedance that is more nearly resistive over the desired frequency range than is the radiation impedance for a small-area diaphragm (see Fig. 4.35). As a result, more power is radiated at low frequencies for a given volume velocity of air. A horn is also a directivity controlling device, which radiates over an angle defined by the flare angle of the mouth.

In designing a horn for a particular application, we usually wish to select the parameters so as to radiate the maximum amount of acoustic power over the desired frequency range with suitably low nonlinear distortion. Once we have stated the frequency range, tolerable distortion, and desired radiated power, we can choose the drive unit and then proceed to calculate the throat and the mouth diameters and the length and shape of the horn.

9.7 POSSIBLE PROFILES [2]

When it comes to considering various horn profiles, there are only a limited number with exact analytical solutions to the wave equation. For a start, an exact solution relies upon a profile that fits a coordinate system which leads to a separable wave equation. In other words, the coordinate system must be orthogonal, having coordinate surfaces that all meet at right angles. In Part V we presented solutions to the three-dimensional Helmholtz wave equation in three such coordinate systems, namely, rectangular, cylindrical, and spherical. Generally, cylindrical coordinates lead to parabolic

horns (with two parallel and two nonparallel side walls), while spherical coordinates lead to conical horns.

There are only a few other three-dimensional orthogonal coordinate systems that lead to practical horn profiles. Of these are spheroidal coordinates, which come in two flavors: prolate and oblate. Although they are too complicated to deal with in this text, they are worth mentioning. Spheroidal coordinates are constructed from overlapping families of ellipses and hyperbolas, which share two focal points. If the ellipses are rotated about an axis passing through the focal points, they become prolate spheroids (cigar shaped) and we have a prolate—spheroidal coordinate system. Then any one of the rotated hyperbolas can be chosen as a horn profile. Such a profile looks parabolic near the throat but becomes more conical as the distance from the throat increases. Similarly, if the ellipses are rotated about an axis passing between the two focal points, they become oblate spheroids (flying saucer shaped) and we have an oblate—spheroidal coordinate system. Again, any one of the rotated hyperbolas can be chosen as a horn profile [3]. In this case, however, the profile looks hyperbolic near the throat but becomes more conical as the distance from the throat increases. However, spheroidal wave functions [4,20], unlike Bessel and Legendre functions, are not frequency independent. The fact that a whole series of harmonics must be calculated at each frequency step somewhat complicates the analysis. Ellipsoidal coordinates lead to similar horn profiles but with cross sections that are not circular.

Some other three-dimensional coordinate systems are simply two-dimensional systems translated through parallel planes. For example, elliptical—cylindrical coordinates are formed by translating the ellipses and hyperbolas of the spheroidal system. From this we can form horn profiles having two straight parallel walls and two curved walls that are hyperbolas. Again, we have the problem that the resulting Mathieu functions [4] are not frequency independent.

A rigorous treatment of a horn profile would involve solving the wave equation in three dimensions with the correct boundary conditions at the throat, walls, and mouth, but the analysis would be somewhat complicated. It is much simpler if we can reduce the wave equation down to one dimension by assuming that pressure variations over the cross section of the horn are minimal. In practice, the errors produced by such an assumption are fairly small. We have already introduced Webster's equation [21], Eq. (2.27), which is one-dimensional, but allows for a number of different functions $S(x)$ to describe the variation of cross-sectional area S with distance x along its length. However, this equation assumes that the wave front does not change shape as it progresses along the length of the horn; otherwise it is not truly one-dimensional. In the case of a parabolic horn (with two parallel walls and two nonparallel) or conical horn, this assumption is generally true. However, we shall also consider exponential and hyperbolic horns in which case the wave front starts off substantially planar near the throat and becomes more curved as it progresses along the length of the horn. As a result, the infinite horn exhibits

an abrupt cutoff frequency below which no power is transmitted. However, for a finite horn, the errors produced by this one-dimensional assumption are not too bad. It should be noted that there is no orthogonal coordinate system for an exponential or hyperbolic horn that leads to a separable wave equation with an exact solution, but proposals have been made to improve Webster's one-dimensional theory that include recasting it [5], applying expansions [6] or correction factors [7,8], and smoothing the cutoff discontinuity with a complex wave number [9].

First we shall consider infinite horns, as these provide the simplest solutions for the throat impedance and hence radiated power under idealized conditions. If the horn is a number of wavelengths long and if the mouth circumference is larger than the wavelength, we may call it "infinite" in length. This simplification leads to equations that are easy to understand and are generally useful in design. Then we shall develop 2-port transmission matrices for finite horns, which can be used as part of an overall loudspeaker system design. Our analysis will be limited to parabolic, conical, exponential, and hyperbolic horns.

For a horn to be a satisfactory transformer, its cross-sectional area near the throat end should increase gradually with axial distance x . If it does, the transformation ratio remains reasonably constant with frequency over a wide range. Exponential and hyperbolic horns are closer to this ideal, but the more gradual cutoff of a conical horn makes it easier to integrate into a loudspeaker system when used as a high-frequency unit or tweeter. The parabolic horn is often used in reverse as a transmission line because it is the easiest to construct.

We already mentioned that the directivity is largely defined by the flare angle at the mouth. This is certainly the case for parabolic and conical horns when the wavelength is smaller than the diameter of the mouth. The mouth of a conical horn behaves somewhat like a spherical cap in a sphere because it produces spherical waves that are largely confined within the angle of the apex of the cone at high frequencies. A conical horn may not necessarily have a circular cross-section though. A rectangular cross-section enables different angles of dispersion in the horizontal and vertical planes. It also produces a smoother on-axis response. Pulsating spherical and rectangular caps in spheres are discussed in Example 9.4 and covered in detail in Section 12.7. The high-frequency directivity factor is

$$Q(f) = \frac{4\pi R^2}{S_M} \quad (9.23)$$

where R is the radius of the mouth and S_M is the area of the mouth. In the case of a rectangular cone, the area is given by Eq. (12.69). Unfortunately, exponential and hyperbolic horns produce a more planar wave in the middle of the flare at high frequencies, resulting in a somewhat narrower directivity pattern. Multiple horns or "multicell"

horns are often used to mitigate this effect. They may either comprise multiple horns with each having its own drive unit or horns with a common drive unit. Another option is to use a hybrid exponential/conical horn [10].



9.8 MOUTH SIZE

The large end (mouth) of the horn should have a circumference large enough so that the radiation impedance is nearly resistive over the desired frequency range. Reference to Fig. 4.35 shows that this will be true for $ka > 1$: that is, $C/\lambda > 1$, where C is the circumference of the mouth of the horn and λ is the wavelength of the lowest tone that it is desired to radiate. If the mouth of the horn is not circular but square, it will behave in nearly the same way, as far as radiated power is concerned, for equal mouth areas. Hence, for good design, the mouth circumference C or mouth area S_M ,

$$C = 2\sqrt{\pi S_M} > \lambda \quad (9.24)$$

where λ is the longest wavelength of sound that is to be radiated efficiently.



9.9 INFINITE PARABOLIC HORN [11]

Theoretical considerations

A parabolic horn can either have a rectangular cross section with two parallel straight walls and two nonparallel straight walls, or a circular cross section with a curved wall following a parabola. The former gives more accurate results using the one-dimensional wave equation and is easier to construct, but in the figures we shall use the latter for convenience. The equation describing the cross-sectional area $S(x)$ as a function of the distance x along the axis is

$$S(x) = S_T x/x_T \quad (9.25)$$

where S_T is the area of the throat, which is located at a distance $x = x_T$ ahead of the apex at $x = 0$. In the steady state, the Helmholtz equation for the parabolic horn is obtained by inserting $S(x)$ from Eq. (9.25) into Eq. (2.27) to yield

$$\left(\frac{\partial^2}{\partial x^2} + \frac{1}{x} \frac{\partial}{\partial x} + k^2 \right) \tilde{p}(x) = 0 \quad (9.26)$$

where

$$k = \frac{2\pi}{\lambda} = \frac{\omega}{c} \quad (9.27)$$

and

\tilde{p} is harmonically varying sound pressure at a point along the length of the horn in Pa.
(It is assumed that the pressure is uniform across the cross section of the horn.)

c is speed of sound in m/s.

x is distance along the length of the horn from the apex in m.

x_T is distance from the apex to the throat in m.

S_T is cross-sectional area of the throat in m^2 .

S is cross-sectional area at x in m^2 .

The general solution for the pressure in a parabolic horn of any length is

$$\tilde{p}(x) = \tilde{p}_+ H_0^{(2)}(kx) + \tilde{p}_- H_0^{(1)}(kx) \quad (9.28)$$

where \tilde{p}_+ denotes the pressure amplitude of the forward traveling wave and \tilde{p}_- that of the backwards traveling wave. The tilde replaces the factor $e^{j\omega t}$. Using Eq. (2.122), the velocity is given by

$$\begin{aligned} \tilde{u}(x) &= -\frac{1}{jk\rho_0 c} \frac{\partial}{\partial x} \tilde{p}(x) \\ &= \frac{1}{j\rho_0 c} \left(\tilde{p}_+ H_1^{(2)}(kx) + \tilde{p}_- H_1^{(1)}(kx) \right). \end{aligned} \quad (9.29)$$

Throat impedance

Noting that in an infinite horn there are no reflections from the mouth, we set $\tilde{p}_- = 0$ to obtain the acoustic throat impedance, which is the ratio of the pressure \tilde{p} to the volume velocity \tilde{U} at $x = x_T$ so that

$$\begin{aligned} Z_{AT} &= \frac{\tilde{p}(x_T)}{\tilde{U}(x_T)} = \frac{\tilde{p}(x_T)}{S_T \tilde{u}(x_T)} = j \frac{\rho_0 c}{S_T} \frac{H_0^{(2)}(kx_T)}{H_1^{(2)}(kx_T)} \\ &= \frac{\rho_0 c}{S_T} \left(\frac{2}{\pi k x_T (J_1^2(kx_T) + Y_1^2(kx_T))} + j \frac{J_0(kx_T) J_1(kx_T) + Y_0(kx_T) Y_1(kx_T)}{J_1^2(kx_T) + Y_1^2(kx_T)} \right) \text{N} \cdot \text{s} / \text{m}^5 \end{aligned} \quad (9.30)$$

where we have used the relationships of Eqs. (A2.75) and (A2.111) from Appendix II. This is the same as the radiation impedance of an infinitely long pulsating cylinder of radius x_T . If we equate the real and imaginary parts of the impedance, we find that the *cutoff frequency* occurs at $kx_T = 0.268$, which we shall designate as f_c , where

$$f_c = \frac{0.268c}{2\pi x_T}. \quad (9.31)$$

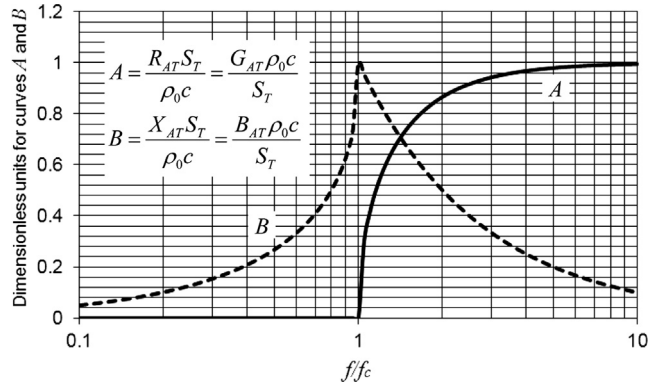


Figure 9.8 Plot of the quantities A and B , which are defined by the relations given on the graph.

The throat impedance of an infinite parabolic horn is plotted in [Fig. 9.9](#).

9.10 INFINITE CONICAL HORN

Theoretical considerations

The equation describing the cross-sectional area $S(x)$ as a function of the distance x along the axis is

$$S(x) = S_T (x/x_T)^2 \quad (9.32)$$

where S_T is the area of the throat, which is located at a distance $x = x_T$ ahead of the apex at $x = 0$. In the steady state, the Helmholtz equation for the conical horn is obtained by inserting $S(x)$ from [Eq. \(9.32\)](#) into [Eq. \(2.27\)](#) to yield

$$\left(\frac{\partial^2}{\partial x^2} + \frac{2}{x} \frac{\partial}{\partial x} + k^2 \right) \tilde{p}(x) = 0 \quad (9.33)$$

where

$$k = \frac{2\pi}{\lambda} = \frac{\omega}{c} \quad (9.34)$$

and

\tilde{p} is harmonically varying sound pressure at a point along the length of the horn in Pa. (It is assumed that the pressure is uniform across the cross section of the horn.)

c is speed of sound in m/s.

x is distance along the length of the horn from the apex in m.

x_T is distance from the apex to the throat in m.

S_T is cross-sectional area of the throat in m^2 .

S is cross-sectional area at x in m^2 .

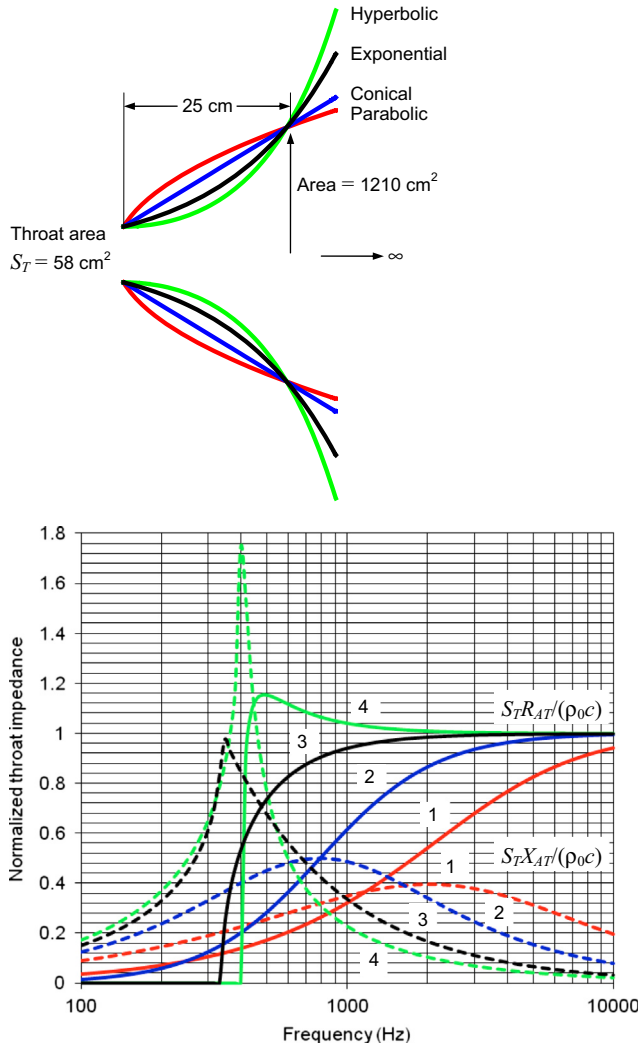


Figure 9.9 Plot of normalized throat impedances for infinite parabolic (1), conical (2), exponential (3), and hyperbolic (4) horns using Eqs. (9.30, 9.37, 9.45, and 9.57) respectively. Real impedances $S_T R_{AT}/(\rho_0 c)$ are represented by solid curves and the imaginary impedances $S_T X_{AT}/(\rho_0 c)$ are represented by dashed curves. The value of α for the hyperbolic horn is $1/2$. The cutoff frequencies of the parabolic, conical, exponential, and hyperbolic horns are 1182 Hz, 792 Hz, 337 Hz, and 399 Hz respectively.

The general solution for the pressure in a conical horn of any length is

$$\tilde{p}(x) = \tilde{p}_+ \frac{e^{-jkx}}{x} + \tilde{p}_- \frac{e^{jkx}}{x} \tag{9.35}$$

where \tilde{p}_+ denotes the pressure amplitude of the forward traveling wave and \tilde{p}_- that of the backwards traveling wave. The tilde replaces the factor $e^{j\omega t}$. Using Eq. (2.122), the velocity is given by

$$\begin{aligned}\tilde{u}(x) &= -\frac{1}{jk\rho_0c} \frac{\partial}{\partial x} \tilde{p}(x) \\ &= \frac{1}{\rho_0c} \left\{ \tilde{p}_+ \left(1 - \frac{j}{kx}\right) \frac{e^{-jkx}}{x} - \tilde{p}_- \left(1 + \frac{j}{kx}\right) \frac{e^{jkx}}{x} \right\}.\end{aligned}\quad (9.36)$$

Throat impedance

Noting that in an infinite horn there are no reflections from the mouth, we set $\tilde{p}_- = 0$ to obtain the acoustic throat impedance, which is the ratio of the pressure \tilde{p} to the volume velocity \tilde{U} at $x = x_T$, so that

$$\begin{aligned}Z_{AT} &= \frac{\tilde{p}(x_T)}{\tilde{U}(x_T)} = \frac{\tilde{p}(x_T)}{S_T \tilde{u}(x_T)} = \frac{\rho_0c}{S_T} \frac{jkx_T}{1 + jkx_T} \\ &= \frac{\rho_0c}{S_T} \left(\frac{k^2 x_T^2}{1 + k^2 x_T^2} + j \frac{kx_T}{1 + k^2 x_T^2} \right) \text{N}\cdot\text{s}/\text{m}^5.\end{aligned}\quad (9.37)$$

This is the same as the radiation impedance of a pulsating sphere of radius x_T . The special case of $kx_T = 1$ occurs at the *cutoff frequency*, which we shall designate as f_c , where

$$f_c = \frac{c}{2\pi x_1}.\quad (9.38)$$

The throat impedance of an infinite conical horn is plotted in Fig. 9.9.



9.11 INFINITE EXPONENTIAL HORN

Theoretical considerations

The equation describing the cross-sectional area $S(x)$ as a function of the distance x along the axis is

$$S(x) = S_T e^{mx}\quad (9.39)$$

where S_T is the area of the throat, which is located at $x = 0$. In the steady state, the Helmholtz equation for the exponential horn is obtained by inserting $S(x)$ from Eq. (9.39) into Eq. (2.27) to yield

$$\left(\frac{\partial^2}{\partial x^2} + m \frac{\partial}{\partial x} + k^2\right)\tilde{p}(x) = 0 \quad (9.40)$$

where

$$k = \frac{2\pi}{\lambda} = \frac{\omega}{c} \quad (9.41)$$

and

\tilde{p} is harmonically varying sound pressure at a point along the length of the horn in Pa. (It is assumed that the pressure is uniform across the cross section of the horn.)

c is speed of sound in m/s.

x is distance along the length of the horn from the throat in m.

m is flare constant in m^{-1} . Obviously, m determines the magnitude of the second term of the equation above, which expresses the rate at which the sound pressure changes with distance down the horn. If $m = 0$, Eq. (9.40) becomes the equation for propagation in a cylindrical tube, i.e., a horn with zero flare.

S_T is cross-sectional area of the throat in m^2 .

S is cross-sectional area at x in m^2 .

The general solution for the pressure in an exponential horn of any length is

$$\tilde{p}(x) = e^{-mx/2} \left(\tilde{p}_+ e^{-jkx\sqrt{1-\frac{m^2}{4k^2}}} + \tilde{p}_- e^{jkx\sqrt{1-\frac{m^2}{4k^2}}} \right) \quad (9.42)$$

where \tilde{p}_+ denotes the pressure amplitude of the forward traveling wave and \tilde{p}_- that of the backwards traveling wave. The tilde replaces the factor $e^{j\omega t}$. Using Eq. (2.122), the velocity is given by

$$\begin{aligned} \tilde{u}(x) &= -\frac{1}{jk\rho_0 c} \frac{\partial}{\partial x} \tilde{p}(x) \\ &= \frac{e^{-mx/2}}{\rho_0 c} \left\{ \tilde{p}_+ \left(\sqrt{1-\frac{m^2}{4k^2}} - j\frac{m}{2k} \right) e^{-jkx\sqrt{1-\frac{m^2}{4k^2}}} - \tilde{p}_- \left(\sqrt{1-\frac{m^2}{4k^2}} + j\frac{m}{2k} \right) e^{jkx\sqrt{1-\frac{m^2}{4k^2}}} \right\}. \end{aligned} \quad (9.43)$$

Throat impedance

Noting that in an infinite horn there are no reflections from the mouth, we set $\tilde{p}_- = 0$ to obtain the acoustic throat admittance, which is the ratio of the volume velocity \tilde{U} to the pressure \tilde{p} at $x = x_T$, so that

$$Y_{AT} = \frac{\tilde{U}(x_T)}{\tilde{p}(x_T)} = \frac{S_T \tilde{u}(x_T)}{\tilde{p}(x_T)} = \frac{S_T}{\rho_0 c} \left(\sqrt{1 - \frac{m^2}{4k^2}} - j \frac{m}{2k} \right) m^5 \cdot N^{-1} \cdot S^{-1} \quad (9.44)$$

$$= G_{AT} + jB_{AT}.$$

The acoustic impedance $Z = 1/Y_{AT}$ at the throat is

$$Z_{AT} = \frac{\rho_0 c}{S_T} \left(\sqrt{1 - \frac{m^2}{4k^2}} + j \frac{m}{2k} \right) \quad (9.45)$$

$$= R_{AT} + jX_{AT} \text{ N} \cdot \text{s} / \text{m}^5.$$

The real and imaginary parts of Z and Y_{AT} behave alike with frequency and differ only by the magnitude $(S/\rho_0 c)^2$ and the sign of the imaginary part. Note also that, unlike with the parabolic or conical horns, this impedance is independent of the distance x along the axis of the horn. Next, we shall examine how varying the flare constant m affects the acoustic impedance Z_{AT} .

Flare constant and throat impedance

When the flare constant m is *greater* than 4π divided by the wavelength ($m > 2k$, low frequencies), the acoustic resistance R_{AT} and the acoustic reactance X_{AT} at the throat of the horn where the area is S_T are

$$R_{AT} = 0$$

$$X_{AT} = \frac{\rho_0 c}{S_T} \left(\frac{m}{2k} - \sqrt{\frac{m^2}{4k^2} - 1} \right). \quad (9.46)$$

When the flare constant m *equals* 4π divided by the wavelength, the acoustic resistance, and reactance are

$$R_{AT} = 0$$

$$X_{AT} = \frac{\rho_0 c m}{2k S_T} = \frac{\rho_0 c}{S_T}. \quad (9.47)$$

For all cases where m is *less* than 4π divided by the wavelength ($m < 2k$, high frequencies), the acoustic resistance and reactance at any point x along the horn where the cross-sectional area is S are

$$R_{AT} = \frac{\rho_0 c}{S_T} \sqrt{1 - \frac{m^2}{4k^2}} \quad (9.48)$$

$$X_{AT} = \frac{\rho_0 c m}{2k S_T} = \frac{\rho_0 c^2 m}{2\omega S_T} \equiv \frac{1}{\omega C_{AT}}$$

where $C_{AT} = 2S_T/\rho_0 c^2 m$.

For very high frequencies, the reactance approaches zero and the resistance approaches $\rho_0 c/S_T$ or $\rho_0 c/S$ in general. This is also the impedance for a plane progressive sound wave in a tube of uniform cross section S .

Cutoff frequency

The special case of $m = 4\pi/\lambda$ occurs at a frequency that we shall designate as f_c , where

$$f_c = \frac{mc}{4\pi}. \quad (9.49)$$

This frequency f_c is called the cutoff frequency because, for frequencies lower than this, no power will be transmitted down the horn, i.e., the impedance at all positions along the horn is purely reactive (see Eq. 9.46). The throat impedance of an infinite exponential horn is plotted in Fig. 9.9.

To obtain the acoustic impedance at the throat of the horn in terms of the cutoff frequency, we observe that $f_c/f = m/2k$. Substituting in Eq. (9.45) yields

$$Z_{AT} = \frac{\rho_0 c}{S_T} \left(\sqrt{1 - \left(\frac{f_c}{f}\right)^2} + j\frac{f_c}{f} \right) = R_{AT} + jX_{AT} \quad (9.50)$$

where

S_T is throat area in m^2 .

$\rho_0 c$ is characteristic impedance of air in rayls.

f_c is cutoff frequency.

f is driving frequency.

Graphs of two quantities A and B that are directly proportional to the resistive and reactive parts of the acoustic impedance at the throat of an infinitely long exponential horn are shown in Fig. 9.8. The quantities A and B also are directly proportional to the real and imaginary parts of the acoustic admittance at the throat. The relations among A , B , R_{AT} , X_{AT} , G_{AT} and B_{AT} are given on the graph. When the frequency is greater than approximately double the cutoff frequency f_c , the throat impedance is substantially resistive and very near its maximum value in magnitude.



9.12 INFINITE HYPERBOLIC HORN (HYPEX) [12]

Theoretical considerations

The equation describing the cross-sectional area $S(x)$ as a function of the distance x along the axis is

$$S(x) = S_T \left(\cosh \frac{x}{x_T} + \alpha \sinh \frac{x}{x_T} \right)^2 \quad (9.51)$$

where S_T is the area of the throat, which is located at $x = 0$ and $0 \leq \alpha \leq 1$. We can vary the parameter α to create any profile between hyperbolic ($\alpha = 0$) and exponential ($\alpha = 1$). In the steady state, the Helmholtz equation for the hyperbolic horn is obtained by inserting $S(x)$ from Eq. (9.51) into Eq. (2.27) to yield

$$\left(\frac{\partial^2}{\partial x^2} + \frac{2}{x_T} \cdot \frac{\sinh(x/x_T) + \alpha \cosh(x/x_T)}{\cosh(x/x_T) + \alpha \sinh(x/x_T)} \cdot \frac{\partial}{\partial x} + k^2 \right) \tilde{p}(x) = 0 \quad (9.52)$$

where

$$k = \frac{2\pi}{\lambda} = \frac{\omega}{c} \quad (9.53)$$

and

\tilde{p} is harmonically varying sound pressure at a point along the length of the horn in Pa. (It is assumed that the pressure is uniform across the cross section of the horn.)

c is speed of sound in m/s.

x_T is reference axial distance from the throat in m.

x is distance along the length of the horn from the throat in m.

α is parameter that never exceeds unity.

S_T is cross-sectional area of the throat in m^2 .

S is cross-sectional area at x in m^2 .

The general solution for the pressure in an hyperbolic horn of any length is

$$\tilde{p}(x) = \frac{1}{\cosh(x/x_T) + \alpha \sinh(x/x_T)} \left(\tilde{p}_+ e^{-jkx \sqrt{1 - \frac{1}{k^2 x_T^2}}} + \tilde{p}_- e^{jkx \sqrt{1 - \frac{1}{k^2 x_T^2}}} \right) \quad (9.54)$$

where \tilde{p}_+ denotes the pressure amplitude of the forward traveling wave and \tilde{p}_- that of the backwards traveling wave. The tilde replaces the factor $e^{j\omega t}$. Using Eq. (2.122), the velocity is given by

$$\tilde{u}(x) = -\frac{1}{jk\rho_0 c} \frac{\partial}{\partial x} \tilde{p}(x). \quad (9.55)$$

Throat impedance

Noting that in an infinite horn there are no reflections from the mouth, we set $\tilde{p}_- = 0$ to obtain the acoustic throat admittance, which is the ratio of the volume velocity \tilde{U} to the pressure \tilde{p} at $x = x_T$, so that

$$Y_{AT} = \frac{\tilde{U}(x_T)}{\tilde{p}(x_T)} = \frac{S_T \tilde{u}(x_T)}{\tilde{p}(x_T)} = \frac{S_T}{\rho_0 c} \left(\sqrt{1 - \frac{1}{k^2 x_T^2}} - j \frac{\alpha}{k x_T} \right) \text{m}^5/\text{N}\cdot\text{s} \quad (9.56)$$

$$= G_{AT} + jB_{AT}.$$

The acoustic impedance $Z_{AT} = 1/Y_{AT}$ at the throat is

$$Z_{AT} = \frac{\rho_0 c}{S_T} \left(\sqrt{1 - \frac{1}{k^2 x_T^2}} - j \frac{\alpha}{k x_T} \right)^{-1} \text{N}\cdot\text{s}/\text{m}^5 \quad (9.57)$$

$$= R_{AT} + jX_{AT}.$$

The real and imaginary parts of Z_{AT} and Y_{AT} behave alike with frequency and differ only by the magnitude $(S/\rho_0 c)^2$ and the sign of the imaginary part. Note also that like with an exponential horn, but unlike the parabolic or conical horns, this impedance is independent of the distance x along the axis of the horn.

Cutoff frequency

The special case of $x_T = \lambda/2\pi$ occurs at a frequency that we shall designate f_c , where

$$f_c = \frac{c}{2\pi x_T}. \quad (9.58)$$

This frequency f_c is called the cutoff frequency because, for frequencies lower than this, no power will be transmitted down the horn, i.e., the impedance at all positions along the horn is purely reactive. The throat impedance of an infinite hyperbolic horn is plotted in Fig. 9.9.

In Fig. 9.9, the throat impedances for the parabolic, conical, exponential, and hyperbolic horn types are shown. At very high frequencies, all these types behave about alike. At low frequencies, however, there are considerable differences. These differences can be shown by comparison of the throat impedances for the conical and hyperbolic horns with that for the exponential horn.

For all horns, the throat resistance is very low, or zero, below the cutoff frequency. Above the cutoff frequency, the specific throat resistance rises rapidly to its ultimate value of $\rho_0 c$ for those cases where the rate of taper is *small* near the throat of the horn. For

example, the specific throat resistance for the hyperbolic horn reaches $\rho_0 c$ at about one-twentieth the frequency at which the specific throat resistance for the conical horn reaches this value. Similarly for the hyperbolic horn, the specific throat resistance approaches unity at about one-third the frequency for the exponential horn.

It would seem that for best loading conditions on the horn drive unit over the frequency range above the cutoff frequency, one should use the hyperbolic horn. However, it should also be remembered that the nonlinear distortion will be higher for the hyperbolic horn because the wave travels further in the horn before the pressure drops off owing to area increase than is the case for the other horns. For minimum distortion at given power per unit area, the conical horn is obviously the best of the three. The exponential horn is usually a satisfactory compromise in design because it falls between these two extremes.



9.13 FINITE HORNS

Transmission parameters

A horn can be represented as a 2-port network, which is described by the following transmission-parameter matrix:

$$\begin{bmatrix} \tilde{p}_T \\ \tilde{U}_T \end{bmatrix} = \begin{bmatrix} a_{11} & a_{12} \\ a_{21} & a_{22} \end{bmatrix} \cdot \begin{bmatrix} \tilde{p}_M \\ \tilde{U}_M \end{bmatrix} = A \cdot \begin{bmatrix} \tilde{p}_M \\ \tilde{U}_M \end{bmatrix} \quad (9.59)$$

where \tilde{p}_T and \tilde{U}_T are the pressure and volume velocity respectively at the throat and \tilde{p}_M and \tilde{U}_M are the pressure and volume velocity respectively at the mouth. The matrix elements are given by

$$a_{11} = \left. \frac{\tilde{p}_T}{\tilde{p}_M} \right|_{\tilde{U}_M=0} \quad (9.60)$$

$$a_{12} = \left. \frac{\tilde{p}_T}{\tilde{U}_M} \right|_{\tilde{p}_M=0} \quad (9.61)$$

$$a_{21} = \left. \frac{\tilde{U}_T}{\tilde{p}_M} \right|_{\tilde{U}_M=0} \quad (9.62)$$

$$a_{22} = \left. \frac{\tilde{U}_T}{\tilde{U}_M} \right|_{\tilde{p}_M=0} \quad (9.63)$$

Throat impedance

The acoustic impedance at the throat of the horn is given by

$$Z_{AT} = \frac{a_{11}Z_{AM} + a_{12}}{a_{21}Z_{AM} + a_{22}} \quad (9.64)$$

where Z_{AM} is the acoustic radiation impedance at the mouth.

Reverse horn

If the horn is used in reverse, as a tapered transmission line for example, we write

$$\begin{bmatrix} \tilde{p}_M \\ \tilde{U}_M \end{bmatrix} = \frac{1}{\text{Det}(A)} \cdot \begin{bmatrix} a_{22} & a_{12} \\ a_{21} & a_{11} \end{bmatrix} \cdot \begin{bmatrix} \tilde{p}_T \\ \tilde{U}_T \end{bmatrix}. \quad (9.65)$$

If no energy is added or dissipated within the horn

$$\text{Det}(A) = a_{11}a_{22} - a_{12}a_{21} = 1. \quad (9.66)$$

However, this does not apply in the case of a transmission line filled with absorbent material.

Finite parabolic horn

The matrix elements are given by

$$a_{11} = -\frac{\pi}{2} kx_M (J_0(kx_T)Y_1(kx_M) - J_1(kx_M)Y_0(kx_T)) \quad (9.67)$$

$$a_{12} = j \frac{\rho_0 c}{S_M} \cdot \frac{\pi}{2} kx_M (J_0(kx_T)Y_0(kx_M) - J_0(kx_M)Y_0(kx_T)) \quad (9.68)$$

$$a_{21} = j \frac{S_T}{\rho_0 c} \cdot \frac{\pi}{2} kx_M (J_1(kx_T)Y_1(kx_M) - J_1(kx_M)Y_1(kx_T)) \quad (9.69)$$

$$a_{22} = \frac{S_T}{S_M} \cdot \frac{\pi}{2} kx_M (J_1(kx_T)Y_0(kx_M) - J_0(kx_M)Y_1(kx_T)) \quad (9.70)$$

where S_T is the area of the throat, S_M is the area of the mouth, and the length l of the horn from the throat to the mouth is given by $l = x_M - x_T$ so that $x_T = l / ((S_M/S_T) - 1)$. The throat impedance of a finite parabolic horn is plotted in [Fig. 9.10](#).

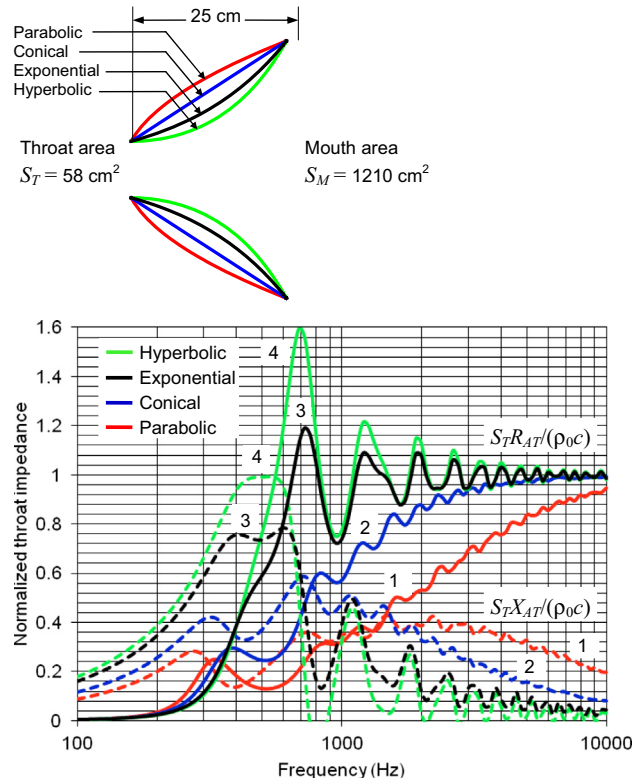


Figure 9.10 Plot of normalized throat impedances for finite parabolic (1), conical (2), exponential (3), and hyperbolic (4) horns using Eq. (9.64) and Eq. (13.116) for $Z_{AM} = Z_s/S_M$, assuming termination in an infinite baffle. Real impedances $S_T R_{AT}/(\rho_0 c)$ are represented by solid curves and the imaginary impedances $S_T X_{AT}/(\rho_0 c)$ are represented by dashed curves. The value of α for the hyperbolic horn is $1/2$. The cutoff frequencies of the parabolic, conical, exponential, and hyperbolic horns are 1182 Hz, 792 Hz, 337 Hz, and 399 Hz respectively.

Finite conical horn

The matrix elements are given by

$$a_{11} = \sqrt{\frac{S_M}{S_T}} \left(\cos kl - \frac{1}{kx_M} \sin kl \right) \quad (9.71)$$

$$a_{12} = j \frac{\rho_0 c}{\sqrt{S_T S_M}} \sin kl \quad (9.72)$$

$$a_{21} = j \frac{\sqrt{S_T S_M}}{\rho_0 c} \left\{ \left(\frac{1}{k x_M} - \frac{1}{k x_T} \right) \cos kl + \left(1 + \frac{1}{k^2 x_M x_T} \right) \sin kl \right\} \quad (9.73)$$

$$a_{22} = \sqrt{\frac{S_T}{S_M}} \left(\cos kl + \frac{1}{k x_T} \sin kl \right) \quad (9.74)$$

where S_T is the area of the throat, S_M is the area of the mouth, and the length l of the horn from the throat to the mouth is given by $l = x_M - x_T$ so that $x_T = l / (\sqrt{S_M S_T} - 1)$. The throat impedance of a finite conical horn is plotted in Fig. 9.10.

Finite exponential horn [13]

The matrix elements are given by

$$a_{11} = \sqrt{\frac{S_M}{S_T}} (\cos(kl \cos \theta) - \tan \theta \sin(kl \cos \theta)) \quad (9.75)$$

$$a_{12} = j \frac{\rho_0 c}{\sqrt{S_T S_M}} \sec \theta \sin(kl \cos \theta) \quad (9.76)$$

$$a_{21} = j \frac{\sqrt{S_T S_M}}{\rho_0 c} \sec \theta \sin(kl \cos \theta) \quad (9.77)$$

$$a_{22} = \sqrt{\frac{S_T}{S_M}} (\cos(kl \cos \theta) + \tan \theta \sin(kl \cos \theta)) \quad (9.78)$$

where S_T is the area of the throat, $S_M = S_T e^{ml}$ is the area of the mouth, l is the length of the horn from the throat to the mouth, and $\theta = \arcsin(m/2k)$. The throat impedance of a finite exponential horn is plotted in Fig. 9.10.

Finite hyperbolic horn

The matrix elements are given by

$$a_{11} = \sqrt{\frac{S_M}{S_T}} (\cos(kl \cos \theta) - \beta \tan \theta \sin(kl \cos \theta)) \quad (9.79)$$

$$a_{12} = j \frac{\rho_0 c}{\sqrt{S_T S_M}} \sec \theta \sin(kl \cos \theta) \quad (9.80)$$

$$a_{21} = j \frac{\sqrt{S_T S_M}}{\rho_0 c} ((\beta - \alpha) \sin \theta \cos(kl \cos \theta) + (1 + (\alpha\beta - 1) \sin^2 \theta) \sec \theta \sin(kl \cos \theta)) \quad (9.81)$$

$$a_{22} = \sqrt{\frac{S_T}{S_M}} (\cos(kl \cos \theta) + \alpha \tan \theta \sin(kl \cos \theta)) \quad (9.82)$$

where S_T is the area of the throat,

$$S_M = S_T (\cosh(l/x_T) + \alpha \sinh(l/x_T))^2$$

is the area of the mouth, l is the length of the horn from the throat to the mouth, and $\theta = \arcsin(1/kx_T)$. The quantity β is given by

$$\beta = \sqrt{\frac{S_T}{S_M}} (\sinh(l/x_T) + \alpha \cosh(l/x_T)). \quad (9.83)$$

The throat impedance of a finite hyperbolic horn is plotted in [Fig. 9.10](#).

Truncation effects

Whenever the bell diameter is not large or when the horn length is short, it is not possible to use the infinite approximation for the throat impedance. Instead we must use the exact equation of [Eq. \(9.64\)](#). However, we see from [Fig. 9.10](#) that, for a given size horn, the parabolic and conical horns are closer to the infinite ideal of [Fig. 9.9](#) than are the exponential and hyperbolic types. To illustrate what the words “large bell diameter” and “long length” mean, let us refer to [Fig. 9.11](#) for a finite exponential horn of various sizes.

If the circumference of the mouth of the horn divided by the wavelength is less than about 0.5 (i.e., the diameter of the mouth divided by the wavelength is less than about 0.16), the horn will resonate like a cylindrical tube, i.e., at multiples of that frequency where the length is equal to a half wavelength. This condition is shown clearly by the two lower-frequency resonances in [Fig. 9.11a](#).

When the circumference of the mouth of the horn divided by the wavelength is greater than about 3 (i.e., diameter divided by wavelength greater than about 1.0), the horn acts nearly like an infinite horn. This is shown clearly by comparison of c and d of [Fig. 9.11](#), for the region where f/f_c is greater than about 2, which is the case where the ratio of mouth diameter to wavelength exceeds 0.5.

In the frequency region where the circumference of the mouth to wavelength ratio lies between about 1 and 3, the exact equation for a finite exponential horn ([Eq. \(3.49\)](#)) must be used, or the results may be estimated from a and b of [Fig. 9.11](#).

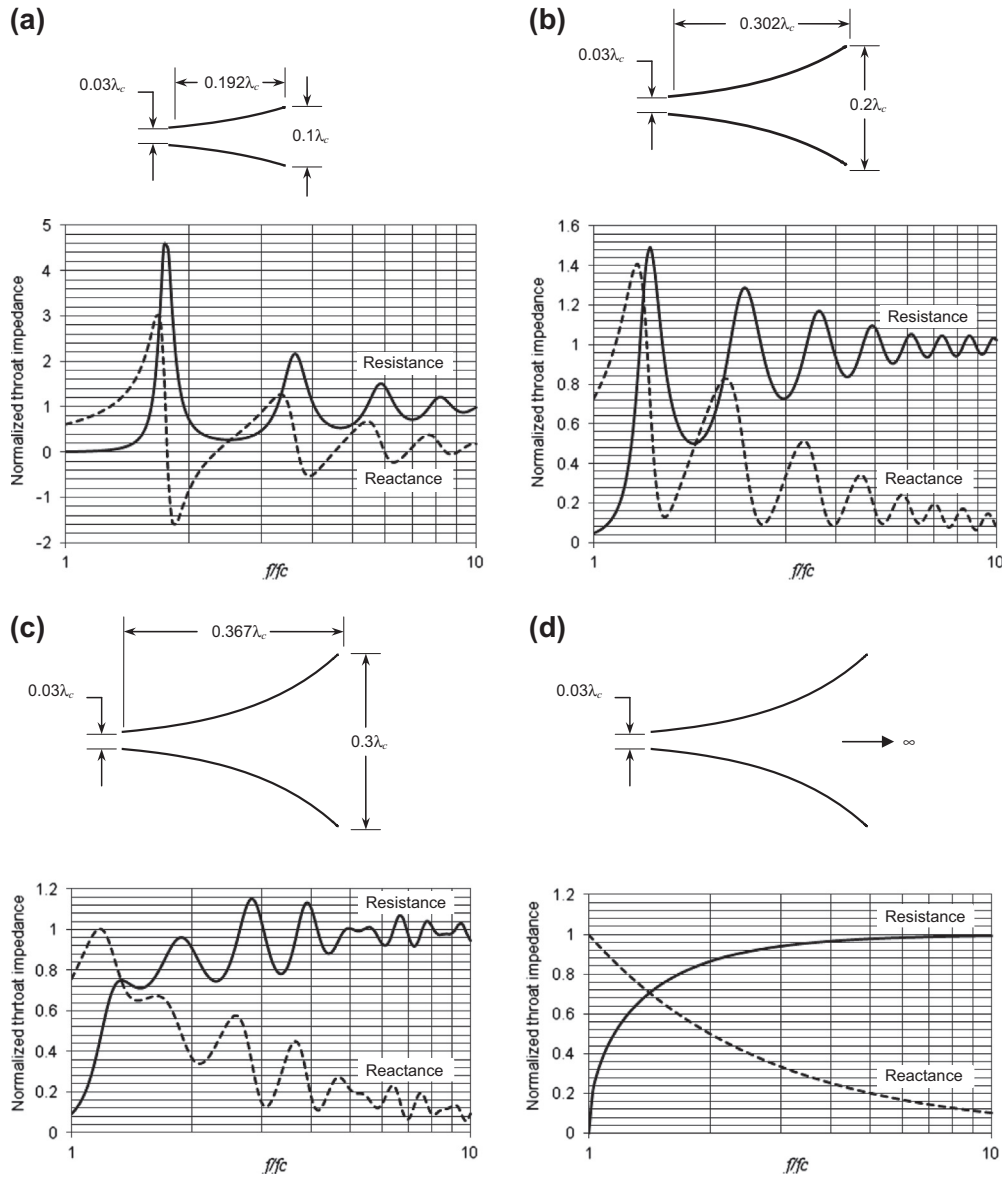


Figure 9.11 Graphs showing the variation in specific acoustic impedance at the throat of four exponential horns as a function of frequency with bell diameter as the parameter. The cutoff frequency $f_c = mc/4\pi$ and the throat diameter $= 0.03 c/f_c$; both are held constant. Bell circumferences are (a) $C = 0.314\lambda_c$, (b) $C = 0.628\lambda_c$, (c) $C = 0.942\lambda_c$ and (d) $C = \infty$. The mouth of the horn is assumed to be terminated in an infinite baffle.

When the length of the horn becomes less than one-quarter wavelength, it may be treated as a simple discontinuity of area such as was discussed in Section 4.8 (pp. 131 to 133).

Obviously, if one chooses a certain mouth area and a throat area to obtain maximum efficiency, the length of the horn is automatically set by the flare constant m , which is in turn directly dependent on the desired cutoff frequency.

Nonlinear distortion

A sound wave produces an expansion and a compression of the air in which it is traveling. We find from Eq. (2.6) that the relation between the pressure and the volume of a small “box” of the air at 20°C through which a sound wave is passing is

$$P = \frac{0.726}{V^{1.4}} \quad (9.84)$$

where

V is specific volume of air in $\text{m}^3/\text{kg} = 1/\rho_0$

P is absolute pressure in bars, where 1 bar = 10^5 Pa

This equation is plotted as curve AB in Fig. 9.12.

Assuming that the displacement of the diaphragm of the drive unit is sinusoidal, it acts to change the volume of air near it sinusoidally. For large changes in volume, the pressure built up in the throat of the horn is no longer sinusoidal, as can be seen from Fig. 9.12. The pressure wave so generated travels away from the throat toward the mouth.

If the horn were simply a long cylindrical pipe, the distortion would increase the distance the wave progressed according to the formula (air assumed) [14,15]

$$\frac{p_2}{p_1} = \frac{\gamma + 1}{2\sqrt{2\gamma}} k \frac{p_1}{P_0} x = 1.21k \frac{p_1}{P_0} x \quad (9.85)$$

where

p_1 is rms sound pressure of the fundamental frequency in Pa.

p_2 is rms sound pressure of the second harmonic in Pa.

P_0 is atmospheric pressure in Pa.

$k = \omega/c = 2\pi/\lambda$ is wave number in m^{-1} .

$\gamma = 1.4$ for air.

x is distance the wave has traveled along the cylindrical tube in m.

Eq. (9.85) breaks down when the second-harmonic distortion becomes large, and a more complicated expression, not given here, must be used.

In the case of an exponential horn, the amplitude of the fundamental decreases as the wave travels away from the throat, so that the second-harmonic distortion does not increase linearly with distance. Near the throat it increases about that given by Eq. (9.85),

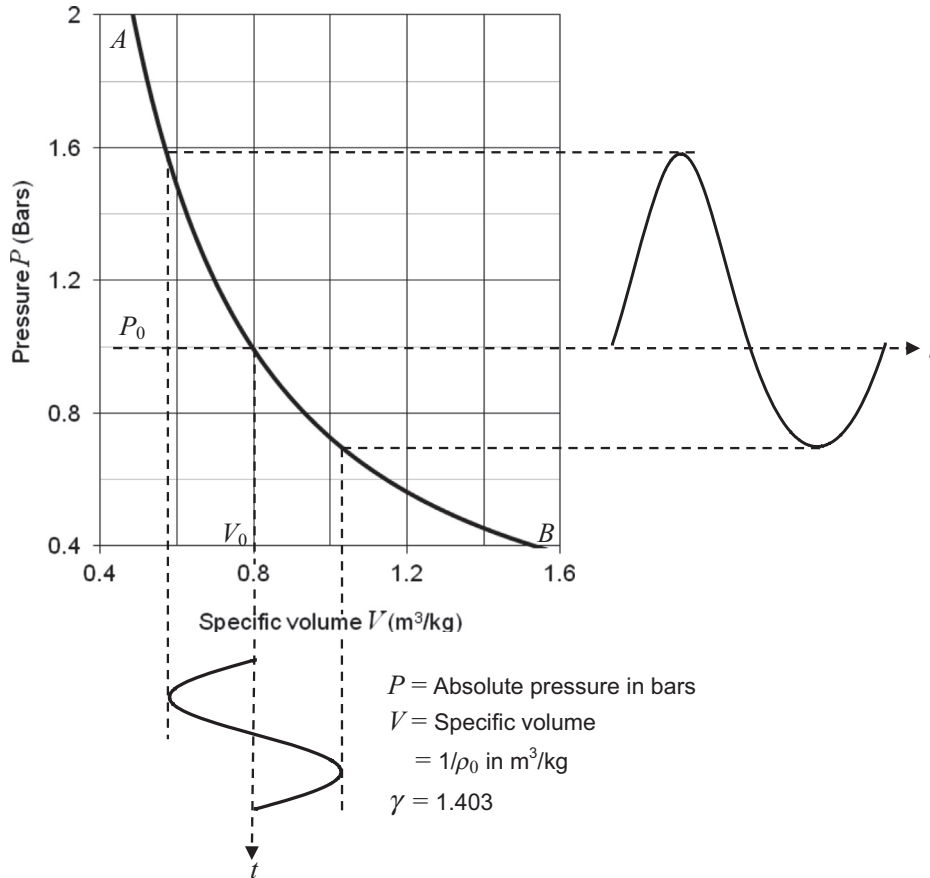


Figure 9.12 Plot of the gas equation $PV^\gamma = 1.26 \times 10^4$, valid at 20°C . Normal atmospheric pressure (0.76 m Hg) is shown as $P_0 = 1$ bar.

but near the mouth the pressure amplitude of the fundamental is usually so low that very little additional distortion occurs.

The distortion introduced into a sound wave after it has traveled a distance x down an exponential horn for the case of a constant power supplied to unit area of the throat is found as follows:

1. Differentiate both sides of Eq. (9.85) with respect to x , so as to obtain the rate of change in p_2 with x for a constant p_1 . Call this Eq. (9.85a).
2. In Eq. (9.85a), substitute for p_1 the pressure $p_T e^{-mx/2}$, where p_T is the rms pressure of the fundamental at the throat of the horn in Pa and m is the flare constant.
3. Then let $p_T = \sqrt{I_T \rho_0 c}$, where I_T is the intensity of the sound at the throat in W/m^2 and $\rho_0 c$ is the characteristic acoustic impedance of air in rayls.
4. Integrate both sides of the resulting equation with respect to x .

This yields:

$$\text{percent second - harmonic distortion} = \frac{50(\gamma + 1)}{\gamma P_0} \sqrt{\frac{I_T \rho_0 c}{2}} \frac{f}{f_c} \left(1 - e^{-mx/2}\right). \quad (9.86)$$

For an infinitely long exponential horn, at normal atmospheric pressure and temperature, the equation for the total distortion introduced into a wave that starts off sinusoidally at the throat is

$$\text{Percent second - harmonic distortion} = 1.22 \frac{f}{f_c} \sqrt{I_T} \times 10^{-2} \quad (9.87)$$

where

f is driving frequency in Hz.

f_c is cutoff frequency in Hz.

I_T is intensity in W/m^2 at the throat of the horn.

Eq. (9.87) is shown plotted in Fig. 9.13. Actually, this equation is nearly correct for finite horns because most of the distortion occurs near the throat.

Eq. (9.87) reveals that, for minimum distortion, the cutoff frequency f_c should be as large as possible, which in turn means as large a flare constant as possible. In other words, the horn should flare out rapidly to reduce the intensity rapidly as one travels along the horn toward the mouth.

Unfortunately, a high cutoff frequency is not a feasible solution for horns that are designed to operate over a wide frequency range. In this case, it is necessary to operate the horn at low power at the higher frequencies if the distortion is to be low at these

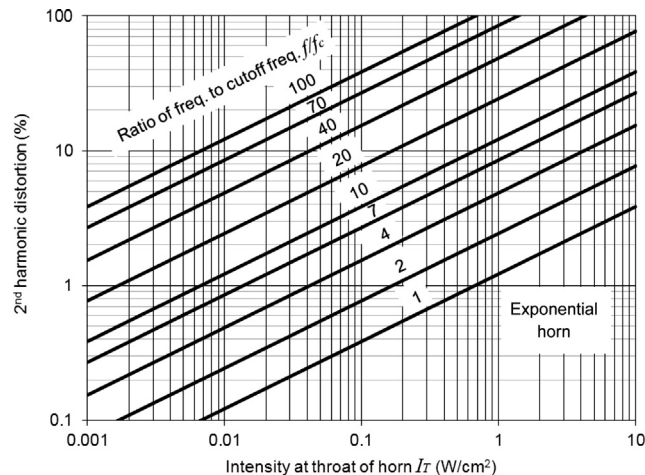


Figure 9.13 Percentage second-harmonic distortion in an exponential horn as a function of the intensity at the horn throat with the ratio of the frequency to the cutoff frequency as parameter.

frequencies. This goal is achieved automatically to some extent in reproducing speech and music because above 1000 Hz the intensity for these sounds decreases by about a factor of 10 for each doubling of frequency.

9.14 BENDS IN HORNS

A horn loudspeaker for use at low frequencies is very large and long, because the flare rate m must be small for a low cutoff frequency and the area of the mouth must be large to radiate sound properly. As a consequence, it has become popular to “fold” the horn so that it will fit conveniently into a cabinet of reasonable size.

Many types of folded horns have been devised that are more or less successful in reproducing music and speech with satisfactory frequency response. To be successful, the bends in folded horns must not be sharp when their lateral dimensions approach a half wavelength, or they will change the spectrum of the radiated sound.

Useful data on the comparative performance of folded horns are not available. This is partly because it is difficult to measure the response of large folded horns in an anechoic chamber and partly because commercial companies guard their data. To get some idea of the effect of an abrupt 180 degrees bend as shown in Fig. 9.14, we can use the 2-port model for a cavity developed in Section 7.18, except that the circular pistons are replaced by rectangular pistons of width l_x in the x direction and $l = l_y/2$ in the y direction. Also, $x_1 = x_2 = l_x/2$, $y_1 = 3l/2$, and $y_2 = l/2$. The 2-port model is shown in Fig. 9.15. The volume velocity entering the bend is \tilde{U}_{in} and the volume velocity leaving the bend is \tilde{U}_{out} . We assume that the two ducts that are joined at the bend are both infinitely long so that the acoustic source and termination impedances, z_S and z_T respectively, of the network are given by

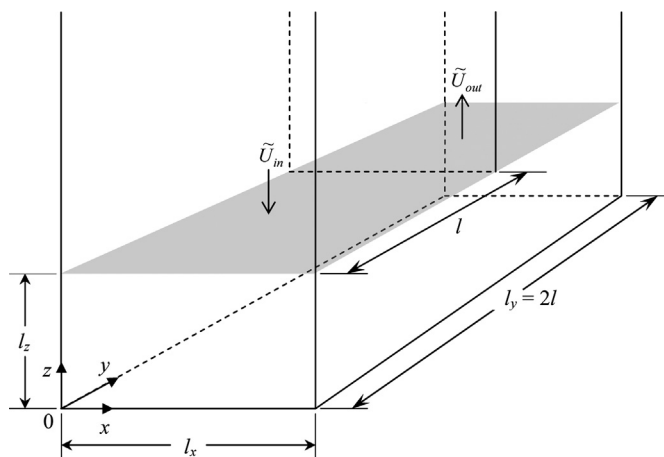


Figure 9.14 Geometry of 180 degrees bend.

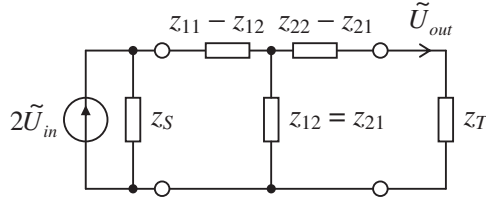


Figure 9.15 Equivalent electrical circuit for a 180 degrees bend.

$$z_S = z_T = \frac{\rho_0 c}{l_x l}. \quad (9.88)$$

The self-impedances of the network are

$$z_{11} = z_{22} = -j \frac{\rho_0 c}{l_x l} \left(\frac{\cot kl_z}{2} + kl \sum_{n=0}^{\infty} \frac{\cot \left(\sqrt{k^2 l^2 - \left(n + \frac{1}{2}\right)^2 \pi^2 l_z / l} \right)}{\left(n + \frac{1}{2}\right)^2 \pi^2 \sqrt{k^2 l^2 - \left(n + \frac{1}{2}\right)^2 \pi^2}} \right) \quad (9.89)$$

and the mutual impedances are

$$z_{12} = z_{21} = -j \frac{\rho_0 c}{l_x l} \left(\frac{\cot kl_z}{2} - kl \sum_{n=0}^{\infty} \frac{\cot \left(\sqrt{k^2 l^2 - \left(n + \frac{1}{2}\right)^2 \pi^2 l_z / l} \right)}{\left(n + \frac{1}{2}\right)^2 \pi^2 \sqrt{k^2 l^2 - \left(n + \frac{1}{2}\right)^2 \pi^2}} \right). \quad (9.90)$$

We define the transmission coefficient α by

$$\begin{aligned} \alpha &= 20 \log_{10} \frac{\tilde{U}_{out}}{2\tilde{U}_{in}} \\ &= 20 \log_{10} \frac{z_{12} z_S}{z_{11}^2 - z_{12}^2 + z_{11}(z_S + z_T) + z_S z_T}. \end{aligned} \quad (9.91)$$

This is plotted in Fig. 9.16 as a function of kl .

We see that there are strong transverse modes when

$$kl = (n + 1/2)\pi, \quad n = 0, 1, 2, \dots \quad (9.92)$$

or $2l = (n + 1/2)\lambda$. Such modes of vibration may be reduced by curving the bend or simply by chamfering the corners. If possible, the wavelength should be long compared with the width of the duct at the bend. Then the attenuation will be very small.

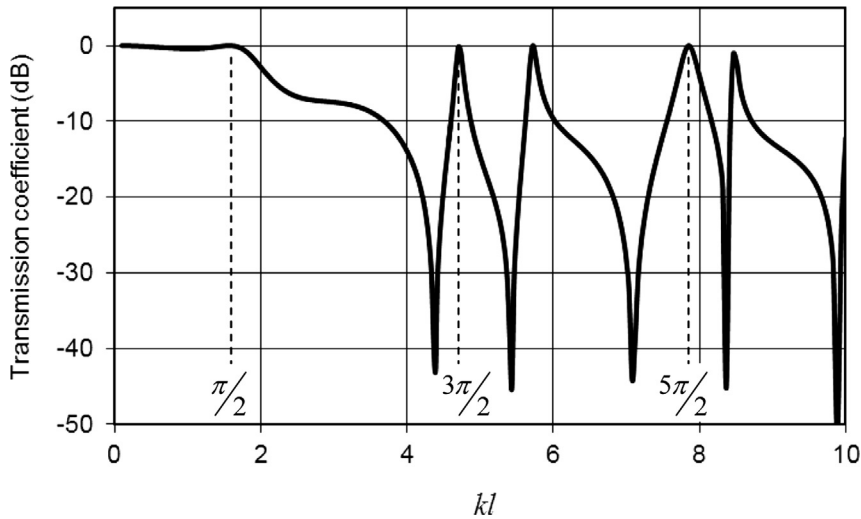


Figure 9.16 Transmission of sound through a 180 degrees bend as a function of kl .

We note that this model of the bend does not take into account normal modes resulting from sound reflected back from the bend into the preceding duct because we do not know its length, so we just assume it to be infinite. Supposing we let $z_S = \infty$, we then have a rigid piston with a volume velocity \tilde{U}_{in} where the sound enters the bend at $z = l_z$. This would produce strong normal modes at

$$kl_z = n\pi, \quad n = 1, 2, \dots \quad (9.93)$$

However, such reflections are also reduced by curving the bend or chamfering the corners.



9.15 CROSS-SECTIONAL SHAPES

Earlier it was stated that the cross-sectional shape of a horn is not too important. This is true provided the lateral dimensions of the horn are not comparable with a wavelength. When the lateral dimensions are large enough, standing waves exist across the duct, similar to the standing waves in a closed end tube. These waves are usually not important in an exponential horn that is circular or square in cross section because, generally, only that section of the horn near the mouth is greater than a half wavelength.

In a rectangular horn that is constructed with two sides parallel and the other two sides varying according to the exponential or hyperbolic law, standing waves may exist between the two parallel walls. These resonances occur at wavelengths that are sub-multiples of the width of the duct, i.e., at frequencies equal to

$$f = \frac{nc}{2l_x} \quad (9.94)$$

or wavelengths equal to

$$\lambda = \frac{2l_x}{n} \quad (9.95)$$

where n is an integer, that is, 1, 2, 3, 4,...

For example, suppose that the width of the horn were 0.5 m. Then resonances (standing waves) would occur at 345, 690, 1034, etc., Hz. At these frequencies, reduced power output generally occurs. In general, the upper frequency limit for operation of a horn should be chosen sufficiently low so that troubles from transverse standing waves are avoided.



9.16 MATERIALS

The material from which a horn is constructed is very important. If the side walls of the horn resonate mechanically at one or more frequencies in the range of operation, “dips” in the power output curve will occur. Undamped thin metal is the least desirable material because the horn from which it is made will resonate violently at fairly low frequencies. Heavy metals, covered on the outside with thick mastic material so that mechanical resonances are damped, are much better. A concrete or plaster horn 1 or 2 inch in thickness is best because of its weight and internal damping.

Plywood is commonly used in the construction of large horns. Although it is not as satisfactory as concrete, it gives satisfactory results if its thickness exceeds $\frac{3}{4}$ inch and if it is braced with wooden pieces glued on at frequent, irregular intervals.

Example 9.3. Low-frequency horn design. A horn for radiating low frequencies is required. It is desired that the frequency response be flat between 40 and 600 Hz and that the horn be designed to be heard throughout a 500-seat auditorium with a volume of 5000 m^3 . Therefore, from Fig. 10.17, we see that we need to radiate an acoustic power of 3.6 W if we wish to reproduce the sound of a large orchestra. We shall select the exponential horn as the best compromise shape of horn for our use. Because the lowest frequency at which good radiation is desired is 40 Hz, we choose the mouth area from Eq. (9.24).

$$\text{Mouth area } S_M = \frac{\lambda^2}{4\pi} = \frac{c^2}{4\pi f^2} = 6.05 \text{ m}^2.$$

This is probably too large for a mouth area in most applications, so that a compromise in design is necessary.

Let us choose arbitrarily a mouth area of 2.4 m^2 . This corresponds to the bell opening shown in Fig. 9.11b. We see from this chart that below $f = 3f_c$, there will be two resonances that are not desirable, but they are fairly well damped.

Let us design for a cutoff frequency of

$$f_c = 40 \text{ Hz.}$$

The flare constant m equals (see Eq. 9.49)

$$m = \frac{4\pi f_c}{c} = \frac{4\pi \times 40}{344.8} = 1.44 \text{ m}^{-1}.$$

Let us choose a 12-inch direct-radiator unit with the following Thiele—Small parameters:

$$R_E = 6 \Omega$$

$$Q_{ES} = 0.2$$

$$Q_{MS} = 4.4$$

$$f_S = 20 \text{ Hz}$$

$$S_D = 0.0486 \text{ m}^2$$

$$V_{AS} = 0.368 \text{ m}^3.$$

From Eq. (9.9), it appears that for maximum efficiency S_D/S_T should equal $1^2/3$. However, to keep the length down, let us make

$$\frac{S_D}{S_T} = 1.$$

Then,

$$G_{MT} = \frac{S_T}{\rho_0 c S_D^2} = \frac{1}{1.18 \times 348.8 \times 0.0486} = 0.05 \text{ m} \cdot \text{N/s}.$$

Let us calculate the reference efficiency. From Eq. (9.8),

$$E_{ff} = \frac{100 \times 0.05 \times 348.8}{2 \times (0.05 \times 348.8 + 2 \times 2\pi \times 20 \times 0.2 \times 0.368)} = 23.9\%.$$

As a trial, let us make $S_D/S_T = 2.0$. Then $G_{MT} = 0.025$, and $E_{ff} = 25.3\%$. Finally, let $S_T/S_D = 2$. Then, $G_{MT} = 0.1$, and $E_{ff} = 18.3\%$.

It is seen that the ratio of the throat and diaphragm areas may be made equal with little loss of efficiency, thereby making our horn of reasonably short length. However, for good high frequency response, it is desirable to have as small a throat area as possible. To reconcile this, we shall employ a “rubber neck” [16], which is a short section of horn with a higher flare rate than the rest of the horn (see Fig. 4.10). At low frequencies it behaves as a simple discontinuity so that the throat area is that of the mouth of the neck, but at high frequencies it is that of the throat of the neck. Hence we shall make the area of

the mouth of the neck equal to S_D , but the throat area of the neck will be equal to $S_D/2$. Let the neck have a cutoff frequency of 100 Hz. Then its flare constant is

$$m_n = \frac{4\pi f_n}{c} = \frac{4\pi \times 100}{344.8} = 3.65 \text{ m}^{-1}.$$

The length of the neck x_n is found from Eq. (9.39):

$$e^{m_n x_n} = 2$$

or

$$m_n x_n = \ln(2) = 0.693$$

$$x_n = \frac{0.693}{3.65} = 0.19 \text{ m}$$

The length of the rest of our horn is found from Eq. (9.39):

$$e^{mx} = \frac{2.4}{0.0486} = 49.4$$

or

$$mx = \ln(49.4) = 3.90$$

$$x = \frac{3.90}{1.44} = 2.71 \text{ m}.$$

The intensity for a horn with a throat area of $0.5 \times 0.0486 \text{ m}^2$ radiating 3.6 W of acoustic power is 0.015 W/cm^2 , assuming uniform pressure distribution. Let us set the upper limit of operation at 600 Hz. Then $f/f_c = 10$. The line for 10 in Fig. 9.13 at 0.015 W/cm^2 shows that the percent second-harmonic distortion in the horn will be about 1.5%, which, bearing in mind that this is for peaks of short duration, will hardly be audible.

This calculation would seem to indicate that the low-frequency unit could be operated successfully above 600 Hz. However, it seems from experience that for psychological reasons the crossover from the low-frequency to the high-frequency horn should occur at a frequency below 600 Hz for best auditory results.

Let us see what back enclosure volume V_B the drive-unit circuit ought to have if the total compliance C_{M2} is to balance out the mass reactance of the horn at frequencies below the diaphragm resonance frequency. The quantity C_{M2} includes the combined compliance of the loudspeaker C_{MS} and that of the enclosure behind it C_{MB} . From Eqs. (9.17, 9.18) and (9.45), we have the condition

$$\frac{1}{C_{M2}} = \frac{S_D^2}{S_T^2 C_{MT}} = \frac{S_D^2 \rho_0 c^2 m}{2S_T}$$

where

$$\frac{1}{C_{M2}} = \frac{1}{C_{MB}} + \frac{1}{C_{MS}} = \frac{S_D^2 \rho_0 c^2}{V_B} + \frac{S_D^2 \rho_0 c^2}{V_{AS}}$$

so that after canceling all the $S_D^2 \rho_0 c^2$ terms, we have

$$V_B = \left(\frac{m}{2S_T} - \frac{1}{V_{AS}} \right)^{-1} = \left(\frac{1.44}{2 \times 0.0486} - \frac{1}{0.368} \right)^{-1} = 0.0826 \text{ m}^3 \quad \text{or} \quad 82.6 \text{ L.}$$

Two possible horns for our design are the straight square horn shown in Fig. 9.17 or the folded horn of the Klipsch type [17] shown in Fig. 9.18, which has the dimensions given in Table 9.1.

By placing the Klipsch horn in the corner of the room, the three adjoining walls form the final part of the horn flare. Of course, this is not the only way to fold a horn [18]. If the straight horn is used, it will probably be necessary to put it partially above the ceiling or below the floor to make its presence nonobjectionable in the room.

Example 9.4. High-frequency horn design. In this example we shall design a horn-loaded tweeter for use with the bass-reflex loudspeaker design of Example 7.3. The tweeter will be the same type as that used for the closed-box design of Example 7.2 and for which a crossover is designed in Example 7.4. However, because the bass-reflex design uses two bass drive units, we shall design a horn for the tweeter to increase its sensitivity. The horn, which is shown in Fig. 9.19, is mounted in a sphere so that we can model the radiation from the mouth as a rectangular cap in a sphere, which will be described in detail in Chapter 12. The horn has conical profile to give a smooth response

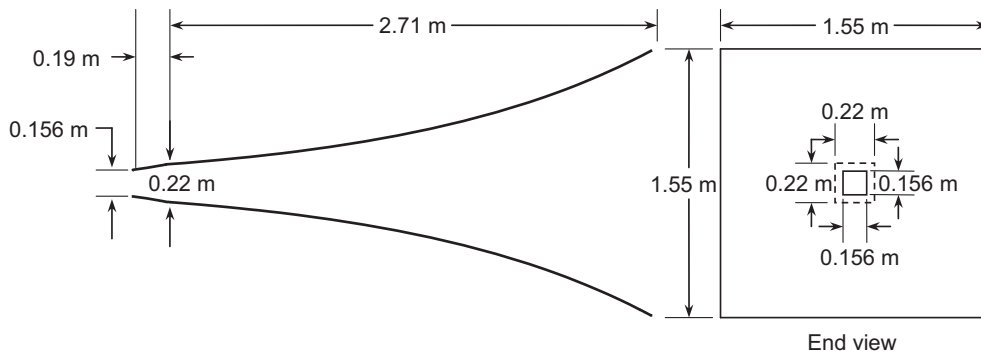


Figure 9.17 Plans for a simple straight exponential horn with a cutoff frequency of 40 Hz, a throat area of 0.0243 m^2 , and a mouth area of 2.4 m^2 .

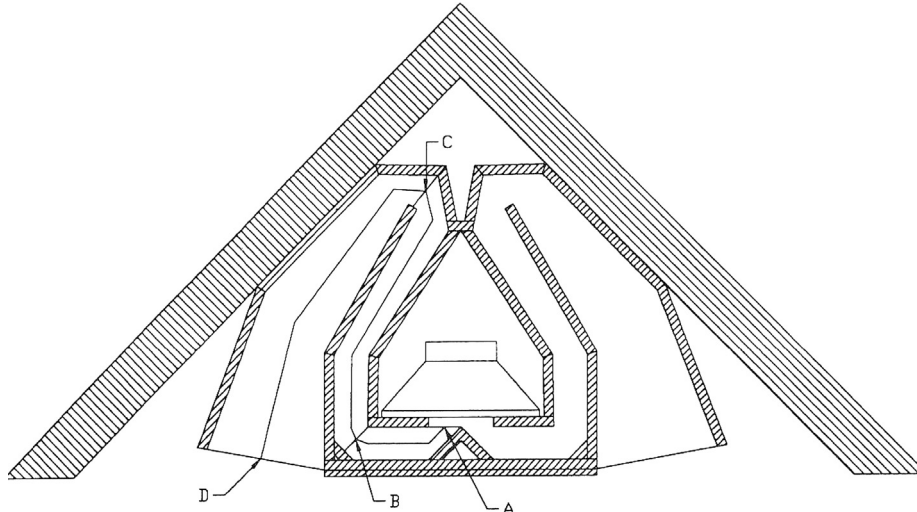


Figure 9.18 Horizontal section for a Klipsch type of folded exponential horn. This particular horn is about 1 m high and has smooth response below 600 Hz. There are two 12-inch drive units, one above the other.

Table 9.1 Dimensions of horn in Example 9.3

Location	Length (m)	Area of horn (m ²)	Flare rate (Hz)
Point A	0	0.029	0
Point B	0.209	0.061	97
Point C	0.741	0.075	35
Point C	1.402	0.232	40

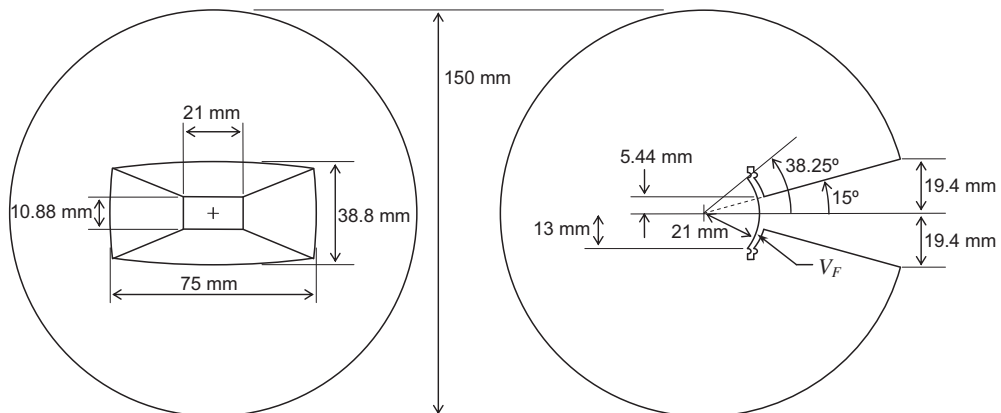


Figure 9.19 Example of high-frequency horn design. For clarity, only the diaphragm of the drive unit is shown. The front plate, coil, and magnet, etc. are omitted.

with a gentle roll-off (see Fig. 9.10). This makes it easier to design a simple crossover than in the case of exponential or hyperbolic types, which have more abrupt transitions. Also, its cross section is rectangular to smooth out any deep nulls, which would otherwise appear in its on-axis response if it were circular (see Fig. 12.21).

From the manufacturer's data we have

$$R_E = 4.9 \Omega$$

$$L_E = 50 \mu\text{H}$$

$$f_C = 750 \text{ Hz}$$

$$M_{MS} = 0.32 \text{ g}$$

$$S_D = 7 \text{ cm}^2$$

Because the tweeter is supplied with its own integral closed-box enclosure, the resonance frequency f_C is the closed-box resonance frequency. From this we shall deduce the total mechanical compliance C_{MC} , which combines the compliance of the suspension with that of the air in the enclosure. Similarly, the total resistance R_{MC} combines the resistance of the suspension with that of the enclosure. From actual measurements we deduce that

$$Q_{EC} = 0.75,$$

$$Q_{MC} = 1.64.$$

Also

$$C_{MC} = \frac{1}{(2\pi f_C)^2 M_{MS}} = \frac{10^3}{(2\pi \times 750)^2 \times 0.32} = 0.141 \text{ mm/N}.$$

Hence from Eqs. (6.10–6.12) we obtain

$$Q_{TC} = \frac{Q_{EC} Q_{MC}}{Q_{EC} + Q_{MC}} = 0.515,$$

$$R_{MC} = \frac{1}{Q_{MC}} \sqrt{\frac{M_{MS}}{C_{MC}}} = \frac{1}{1.64} \sqrt{\frac{0.32}{0.141}} = 0.92 \text{ N}\cdot\text{s/m},$$

$$Bl = \sqrt{\frac{R_E}{Q_{EC}}} \sqrt{\frac{M_{MS}}{C_{MC}}} = \sqrt{\frac{4.9}{0.75}} \sqrt{\frac{0.32}{0.141}} = 3.14 \text{ T}\cdot\text{m}.$$

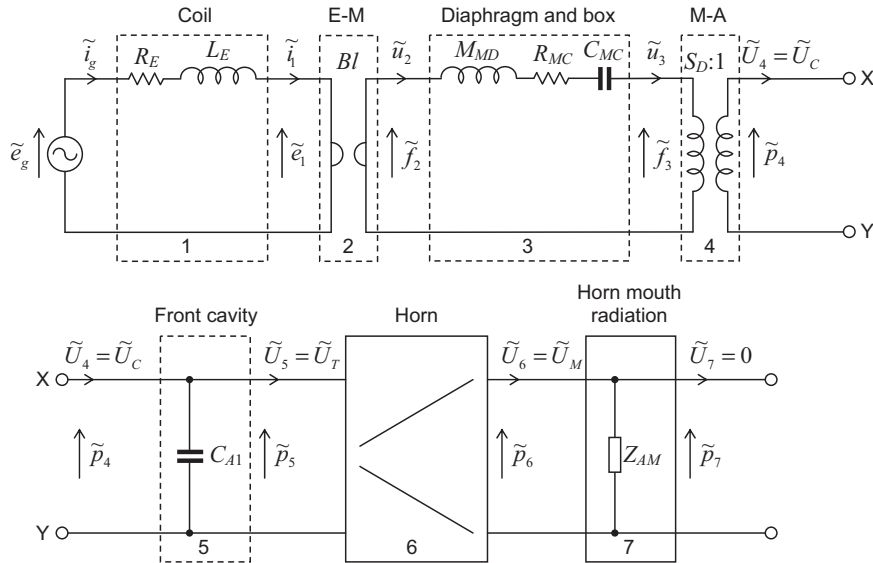


Figure 9.20 Semianalytical model of example high-frequency horn design shown in Fig. 9.19 using transmission matrices. The dashed boxes are lumped-element 2-port networks and the solid boxes are analytical ones.

Let us now create a semianalytical simulation model of the design of Fig. 9.19 using 2-port networks and transmission matrices, as introduced in Section 3.10 and Fig. 4.43. The schematic is shown in Fig. 9.20. Although the drive unit part is based on the circuit of Fig. 9.3, a gyrator has been inserted between the electrical elements and the mechanical ones so that the whole circuit is written using the impedance analogy. Also, we have added the horn and horn mouth impedance to the circuit. We are ignoring the generator impedance R_g because in the experimental setup this is negligible compared with R_E . The dashed boxes are lumped-element 2-port networks and the solid boxes are analytical ones. From the schematic we create the transmission matrices required to represent each 2-port network as follows:

1. *Coil.*

$$\begin{bmatrix} \tilde{e}_g \\ \tilde{i}_g \end{bmatrix} = \begin{bmatrix} 1 & Z_E \\ 0 & 1 \end{bmatrix} \cdot \begin{bmatrix} \tilde{e}_1 \\ \tilde{i}_1 \end{bmatrix} = \mathbf{C} \cdot \begin{bmatrix} \tilde{e}_1 \\ \tilde{i}_1 \end{bmatrix}$$

where $Z_E = R_E + j\omega L_E$.

2. *Electro-Mechanical Transduction.*

$$\begin{bmatrix} \tilde{e}_1 \\ \tilde{i}_1 \end{bmatrix} = \begin{bmatrix} 0 & Bl \\ (Bl)^{-1} & 0 \end{bmatrix} \cdot \begin{bmatrix} \tilde{f}_2 \\ \tilde{u}_2 \end{bmatrix} = \mathbf{E} \cdot \begin{bmatrix} \tilde{f}_2 \\ \tilde{u}_2 \end{bmatrix}.$$

3. *Diaphragm.*

$$\begin{bmatrix} \tilde{f}_2 \\ \tilde{u}_2 \end{bmatrix} = \begin{bmatrix} 1 & Z_M \\ 0 & 1 \end{bmatrix} \cdot \begin{bmatrix} \tilde{f}_3 \\ \tilde{u}_3 \end{bmatrix} = \mathbf{D} \cdot \begin{bmatrix} \tilde{f}_3 \\ \tilde{u}_3 \end{bmatrix}$$

where $Z_M = j\omega M_{MD} + R_{MC} + 1/(j\omega C_{MC})$. We must exclude the radiation mass from the diaphragm so that

$$M_{MD} = M_{MS} - 16\rho_0 a^3/3, \quad \text{where } a = \sqrt{S_D/\pi}.$$

4. *Mechano-acoustical transduction.*

$$\begin{bmatrix} \tilde{f}_3 \\ \tilde{u}_3 \end{bmatrix} = \begin{bmatrix} S_D & 0 \\ 0 & S_D^{-1} \end{bmatrix} \cdot \begin{bmatrix} \tilde{p}_4 \\ \tilde{U}_4 \end{bmatrix} = \mathbf{M} \cdot \begin{bmatrix} \tilde{p}_4 \\ \tilde{U}_4 \end{bmatrix}.$$

5. *Front cavity.*

$$\begin{bmatrix} \tilde{p}_4 \\ \tilde{U}_4 \end{bmatrix} = \begin{bmatrix} 1 & 0 \\ j\omega C_{A1} & 1 \end{bmatrix} \cdot \begin{bmatrix} \tilde{p}_5 \\ \tilde{U}_5 \end{bmatrix} = \mathbf{F} \cdot \begin{bmatrix} \tilde{p}_5 \\ \tilde{U}_5 \end{bmatrix}$$

where the acoustic compliance of the front cavity, which has a total volume of 1.4 cm^3 , is given by

$$C_{A1} = \frac{V_F}{\rho_0 c^2} = \frac{1.4 \times 10^{-6}}{1.18 \times 344.8^2} = 4.99 \times 10^{-12} \text{ m}^5/\text{N}.$$

6. *Horn.*

$$\begin{bmatrix} \tilde{p}_5 \\ \tilde{U}_5 \end{bmatrix} = \begin{bmatrix} b_{11} & b_{12} \\ b_{21} & b_{22} \end{bmatrix} \cdot \begin{bmatrix} \tilde{p}_6 \\ \tilde{U}_6 \end{bmatrix} = \mathbf{H} \cdot \begin{bmatrix} \tilde{p}_6 \\ \tilde{U}_6 \end{bmatrix}$$

where

$$b_{11} = \sqrt{\frac{S_M}{S_T}} \left(\cos kl - \frac{1}{kr_M} \sin kl \right),$$

$$b_{12} = j \frac{\rho_0 c}{\sqrt{S_T S_M}} \sin kl,$$

$$b_{21} = j \frac{\sqrt{S_T S_M}}{\rho_0 c} \left\{ \left(\frac{1}{kr_M} - \frac{1}{kr_T} \right) \cos kl + \left(1 + \frac{1}{k^2 r_M r_T} \right) \sin kl \right\},$$

$$b_{22} = \sqrt{\frac{S_T}{S_M}} \left(\cos kl + \frac{1}{kr_T} \sin kl \right),$$

and $l = r_M - r_T$. We see from Fig. 9.19 that $r_T = 22$ mm and $r_M = 75$ mm. The horn is defined by the angles $\alpha = 15$ degrees in the vertical direction and $\beta = 30$ degrees in the horizontal direction. Hence from Eq. (12.69) we can calculate the throat area S_T and mouth area S_M as follows:

$$S_T = 4R_T^2 \left\{ \arctan \left(\frac{\tan \frac{\pi}{12} \tan \frac{\pi}{6}}{\sec^2 \frac{\pi}{12} + \sqrt{\sec^2 \frac{\pi}{12} + \tan^2 \frac{\pi}{6}}} \right) + \arctan \left(\frac{\tan \frac{\pi}{12} \tan \frac{\pi}{6}}{\sec^2 \frac{\pi}{6} + \sqrt{\sec^2 \frac{\pi}{6} + \tan^2 \frac{\pi}{12}}} \right) \right\}$$

$$= 4 \times 0.022^2 \times 0.13 = 2.52 \text{ cm}^2$$

$$S_M = 4 \times 0.075^2 \times 0.13 = 29.3 \text{ cm}^2.$$

7. Horn Mouth Radiation.

$$\begin{bmatrix} \tilde{p}_6 \\ \tilde{U}_6 \end{bmatrix} = \begin{bmatrix} 1 & 0 \\ Z_{AM}^{-1} & 1 \end{bmatrix} \cdot \begin{bmatrix} \tilde{p}_7 \\ \tilde{U}_7 \end{bmatrix} = \mathbf{R} \cdot \begin{bmatrix} \tilde{p}_7 \\ \tilde{U}_7 \end{bmatrix}.$$

The horn mouth radiation impedance Z_{AM} is reasonably well approximated by that of a rectangular cap in a sphere using Eqs. (12.122) and (12.123), where

$$Z_{AM} = (\mathbf{R}_s + jX_s)/S.$$

First we evaluate \tilde{p}_7 at the end of the chain

$$\begin{bmatrix} \tilde{e}_g \\ \tilde{i}_g \end{bmatrix} = \mathbf{A} \cdot \begin{bmatrix} \tilde{p}_7 \\ 0 \end{bmatrix}$$

where

$$\mathbf{A} = \mathbf{C} \cdot \mathbf{E} \cdot \mathbf{D} \cdot \mathbf{M} \cdot \mathbf{F} \cdot \mathbf{H} \cdot \mathbf{R} = \begin{bmatrix} a_{11} & a_{12} \\ a_{21} & a_{22} \end{bmatrix}.$$

Hence $\tilde{p}_7 = \tilde{e}_g/a_{11}$. Then we work backwards to obtain the volume velocities we wish to evaluate. In particular, we are interested in the far-field pressure, which according to Eq. (12.117) is a function of $\tilde{U}_M = \tilde{U}_6$. This procedure is fairly straightforward and does not involve any matrix inversion. From the mouth radiation matrix (7), we obtain

$$\tilde{U}_M = \tilde{U}_6 = \tilde{p}_7/Z_{AM}.$$

To plot the normalized far-field on-axis pressure, we simply divide \tilde{U}_M by a reference volume velocity

$$\tilde{U}_{ref} = \frac{\tilde{e}_g B I S_D}{\omega M_{MD} R_E}$$

and multiply it by the on-axis response $D(0, \phi)$ of the spherical cap from Eq. (12.120). A plot of

$$20 \log_{10} |D(0, \phi) \tilde{U}_M / \tilde{U}_{ref}|$$

is shown in Fig. 9.21. The maximum gain we may expect to see from the horn is $20 \log_{10}(S_M/S_T) = 21.3$ dB. However, the actual gain is usually less than this and we see

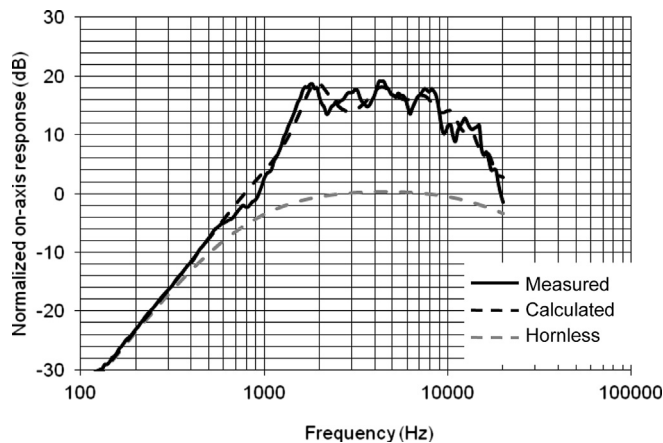


Figure 9.21 Graphs of the on-axis sound pressure level produced by the high-frequency horn design shown in Fig. 9.19. The dashed curves are calculated from $20 \log_{10} |D(0, \phi) \tilde{U}_M / \tilde{U}_{ref}|$. Solid curves are measured. During testing it was found that placing a small sphere of about 1 cm in diameter in front of the diaphragm improved the correlation between the measured and calculated responses at high frequencies.

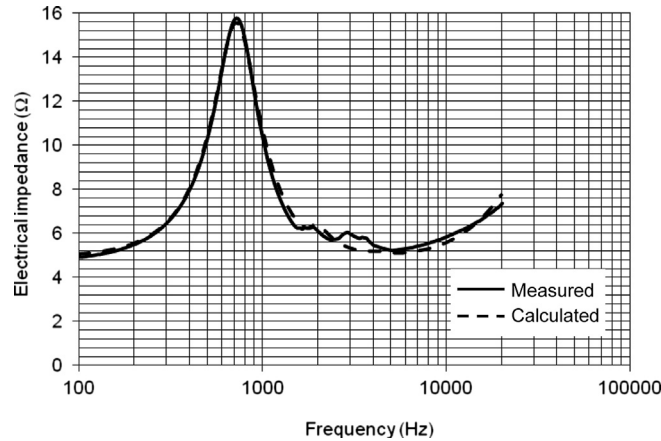


Figure 9.22 Graphs of the electrical input impedance of the high-frequency horn design shown in Fig. 9.19. The dashed curves are calculated from $Z_E = |\tilde{e}_g/\tilde{i}_g| = a_{11}/a_{21}$. Solid curves are measured.

that in this example the combined gain of the horn and baffle effect of the sphere is 14–20 dB between 1.5 and 11 kHz. Finally, we can obtain the input impedance from \tilde{e}_g/\tilde{i}_g where $\tilde{i}_g = a_{21}\tilde{p}_7$ and from above $\tilde{p}_7 = \tilde{e}_g/a_{11}$. Therefore the input impedance is simply $Z_E = a_{11}/a_{21}$, as plotted in Fig. 9.22.

REFERENCES

- [1] An authoritative discussion of horn loudspeakers is found in H, F Olson. Elements of acoustical engineering. 2nd ed. New York: D. Van Nostrand Company, Inc.; 1947 [Chap. VII].
- [2] Geddes ER, Lee LW. Audio transducers. Michigan: GedLee; 2002. p. 126–63.
- [3] Freehafer JE. The acoustical impedance of an infinite hyperbolic horn. J Acoust Soc Am 1940;11:467–76.
- [4] Abramowitz M, Stegun IA. Handbook of mathematical functions. New York: Dover; 1964. p. 721–69.
- [5] Salmon V. Generalized plane wave horn theory. J Acoust Soc Am 1946;17(3):199–211.
- [6] Martin PA. On Webster's horn equation and some generalizations. J Acoust Soc Am 2004;116(3):1381–8.
- [7] Hélie T. Unidimensional models of acoustic propagation in axisymmetric waveguides. J Acoust Soc Am 2003;114(5):2633–47.
- [8] Nederveen CJ, Dalmont J-P. Corrections to the plane-wave approximation in rapidly flaring horns. Acta Acoust Acust 2008;94:461–73.
- [9] Fryer PA. Horn acoustics: calculation through the horn cutoff frequency. J Audio Eng Soc 2003;51(1/2):45–51.
- [10] Keele DB. What's so sacred about exponential horns? In: The 51st AES convention; 1975. p. 1038.
- [11] Olson HF, Wolff I. Sound concentrator for microphones. J Acoust Soc Am 1930;1(3):410–7.
- [12] Salmon V. A new family of horns. J Acoust Soc Am 1946;17(3):212–8.
- [13] Olson HF. RCA Rev 1937;1(4):68.
- [14] Thuras AL, Jenkins RT, O'Neil HT. Extraneous frequencies generated in air carrying intense sound waves. J Acoust Soc Am 1935;6:173–80.

- [15] Black LH. A physical analysis of the distortion produced by the non-linearity of the medium. *J Acoust Soc Am* 1940;12:266–7.
- [16] Olson HF. A horn consisting of manifold exponential sections. *J Soc Motion Pict Eng* 1938;30(5):511.
- [17] Delgado Jr R, Klipsch PW. A revised low-frequency horn of small dimensions. *J Audio Eng Soc* 2000;48(10):922–9.
- [18] Bright A, Holland K, Fahy FJ. Analysis of a folded acoustic horn. *J Audio Eng Soc* 2004;52(10):1029–42.
- [19] Dodd M, Oclec-Brown J. New methodology for the acoustic design of compression driver phase plugs with concentric annular channels. *J Audio Eng Soc* 2009;57(10):771–87.
- [20] Bouwkamp CJ. Theoretical and numerical treatment of diffraction through a circular aperture. *IEEE Trans Antenn Propag* 1970;AP18-2:152–76. This is a translation of his PhD dissertation originally published in Dutch in 1941.
- [21] Webster AG. Acoustical impedance, and the theory of horns and of the phonograph. *Proc Natl Acad Sci USA* 1919;5:275–82.

Sound in enclosures



PART XXX: SOUND FIELDS IN SMALL REGULARLY SHAPED ENCLOSURES

10.1 INTRODUCTION

The study of sound in enclosures involves not only a search into how sounds are reflected backward and forward in an enclosure but also investigations into how to measure sound under such conditions and the effect various materials have in absorbing and controlling this sound. Also of great importance in applying one's engineering knowledge of the behavior of sound in such enclosed spaces is an understanding of the personal preferences of listeners, whether listening in the room where the music is produced or listening at a remote point to a microphone pickup. Psychological criteria for acoustic design have occupied the attention of many investigators and should always be borne in mind. This chapter is confined to physical acoustics.

Two extremes to the study of sound in enclosures can be analyzed and understood easily. At one extreme, we have small enclosures of simple shape, such as rectangular boxes, cylindrical tubes, or spherical shells. In these cases, the interior sound field is describable in precise mathematical terms, although the analysis becomes complicated if the walls of the enclosures are covered in whole or in part with acoustical absorbing materials.

At the other extreme, we have very large irregularly shaped enclosures where no precise description can be made of the sound field but where a statistically reliable statement can be made of the average conditions in the room. This is analogous to a study that a physician might make of a particular man to determine the number of years he will live, as opposed to a study of the entire population on a statistical basis to determine how long a man, on the average, will live. As might be expected, the statistical study leads to simpler formulas than the detailed study of a particular case.



10.2 STATIONARY AND STANDING WAVES

One type of small regularly shaped enclosure, the rigidly closed tube, has been discussed already in Part IV. This case provides an excellent example of the acoustical situation that exists in large enclosures.

First, we noted that along the x axis of the tube, the sound field could be described as the combination of an outward-traveling wave and a backward-traveling wave. Actually, the outward-traveling wave is the sum of the original free-field wave that started out from the source plus the outward-going waves that are making their second, third, fourth, and so on round trips. Similarly, the backward-traveling wave is a combination of the first reflected wave and of waves that are making the return leg of their second, third, fourth, and so on round trips. These outward- and backward-traveling waves add in magnitude to produce what is called a *stationary wave* if the intensity along the tube is zero. If there is some, but not complete, absorption at the terminating end of the tube so that power flows along the tube away from the source (intensity not equal to zero), it is called a *standing wave*. In the case of complete absorption, we have a *traveling* or *progressive wave*.



10.3 NORMAL MODES AND NORMAL FREQUENCIES

We saw from Eq. (2.70) that whenever the driving frequency is such that $\sin kl \rightarrow 0$, the pressure in the tube reaches a very large value. That is to say, the pressure is very large whenever

$$kl = n\pi \quad (10.1)$$

Then, because

$$k = \frac{2\pi f}{c} = \frac{2\pi}{\lambda}, \quad (10.2)$$

we have

$$f_n = \frac{nc}{2l} \quad (10.3)$$

or

$$\frac{l}{\lambda_n} = \frac{n}{2} \quad (10.4)$$

where

$$n = 1, 2, 3, 4, \dots \infty$$

f_n is n th resonance (normal) frequency of the tube.

$\lambda_n c/f_n$ is n th resonance (normal) wavelength of the tube.

Eq. (10.3) tells us that the pressure is very large whenever the length of the tube equals some integral multiple of a half wavelength ($\lambda/2$).

The condition where the frequency equals $nc/2l$ so that a very large sound pressure builds up in the tube is called a *resonance condition* or a *normal mode of vibration* of the air space in the tube. The frequency f_n of a normal mode of vibration is called a *normal frequency*. There are an infinite number of normal modes of vibration for a tube because n can take on all integral values between 0 and ∞ . We may look on the tube, or in fact on any enclosure, as a large number of acoustic resonators, each with its own normal frequency.

In the closed-tube discussion of Part IV, we made no mention of the effect on the results of the cross-sectional shape or size of the tube. It was assumed that the transverse dimensions were less than about 0.1 wavelength so that no transverse resonances would occur in the frequency region of interest.

If the transverse dimensions are greater than one-half wavelength, we have a small room which, if rectangular, can be described by the dimensions shown in Fig. 10.1. Waves can travel in the room backward and forward between any two opposing walls. They can travel also around the room involving the walls at various angles of incidence. If these angles are chosen properly, the waves will return on themselves and set up stationary or standing waves. Each standing wave is a normal mode of vibration for the enclosure.

In Sec. 7.18, we solve such a rectangular enclosure mathematically and describe exactly the distribution of sound as determined by the strength of a piston source in one of the walls. In this section, however, we shall describe the simplest cases to gain insight into the problem.

The number of modes of vibration in a rectangular enclosure is much greater than that for the rigidly closed tube whose diameter is small compared with a wavelength. In fact, the normal frequencies of such an enclosure are given by the equation

$$f_n = \frac{\omega_n}{2\pi} = \frac{c}{2} \sqrt{\left(\frac{n_x}{l_x}\right)^2 + \left(\frac{n_y}{l_y}\right)^2 + \left(\frac{n_z}{l_z}\right)^2} \quad (10.5)$$

where

f_n is the n th normal frequency in Hz.

n_x , n_y , and n_z are integers that can be chosen separately. They may take on all integral values between 0 and ∞ .

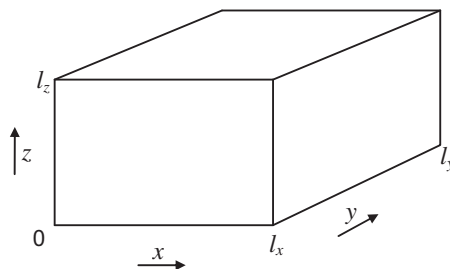


Figure 10.1 Dimensions and coordinate system for a rectangular enclosure.

l_x , l_y , and l_z are dimensions of the room in m.
 c is speed of sound in m/s.

As an example, let us assume that the z dimension, l_z , is less than 0.1 of all wavelengths being considered. This corresponds to n_z being zero at all times. Hence,

$$f_{n_x, n_y, 0} = \frac{c}{2} \sqrt{\left(\frac{n_x}{l_x}\right)^2 + \left(\frac{n_y}{l_y}\right)^2} \quad (10.6)$$

Let $l_x = 4$ m and $l_y = 3$ m. Find the normal frequencies of the $n_x = 1$, $n_y = 1$, and the $n_x = 3$, $n_y = 2$ normal modes of vibration. We have

$$f_{1,1,0} = \frac{344.8}{2} \sqrt{\frac{1}{16} + \frac{1}{9}} = 71.8\text{Hz}$$

and

$$f_{3,2,0} = \frac{344.8}{2} \sqrt{\frac{9}{16} + \frac{4}{9}} = 237\text{Hz}$$

The sound-pressure distribution in a rectangular box for each normal mode of vibration with a normal frequency ω_n is proportional to the product of three cosines:

$$p_{n_x, n_y, n_z} \propto \cos \frac{\pi n_x x}{l_x} \cos \frac{\pi n_y y}{l_y} \cos \frac{\pi n_z z}{l_z} e^{j\omega_n t} \quad (10.7)$$

where the origin of coordinates is at the corner of the box. It is assumed in writing Eq. (10.7) that the walls have very low absorption. If the absorption is high, the sound pressure cannot be represented by a simple product of cosines.

If we inspect Eq. (10.7) in detail, we see that n_x , n_y , and n_z indicate the number of planes of zero pressure occurring along the x , y , and z coordinates, respectively. Such a distribution of sound pressure levels (SPLs) can be represented by forward- and backward-traveling waves in the room. This situation is analogous to that for the closed tube (one-dimensional case). Examples of pressure distributions for three modes of vibration in a rectangular room are shown in Fig. 10.2. The lines indicate planes of constant pressure extending from floor to ceiling along the z dimension. Note that n_x and n_y indicate the number of planes of zero pressure occurring along the x and y coordinates, respectively.

The angles θ_x , θ_y , and θ_z at which the forward- and backward-traveling waves are incident on and reflect from the walls are given by the relations

$$\theta_x = \arctan \frac{\sqrt{(n_y/l_y)^2 + (n_z/l_z)^2}}{n_x/l_x} = \arccos \frac{n_x c}{2l_x f_n} \quad (10.8)$$

$$\theta_y = \arctan \frac{\sqrt{(n_x/l_x)^2 + (n_z/l_z)^2}}{n_y/l_y} = \arccos \frac{n_y c}{2l_y f_n} \quad (10.9)$$

$$\theta_z = \text{similarly} \quad (10.10)$$

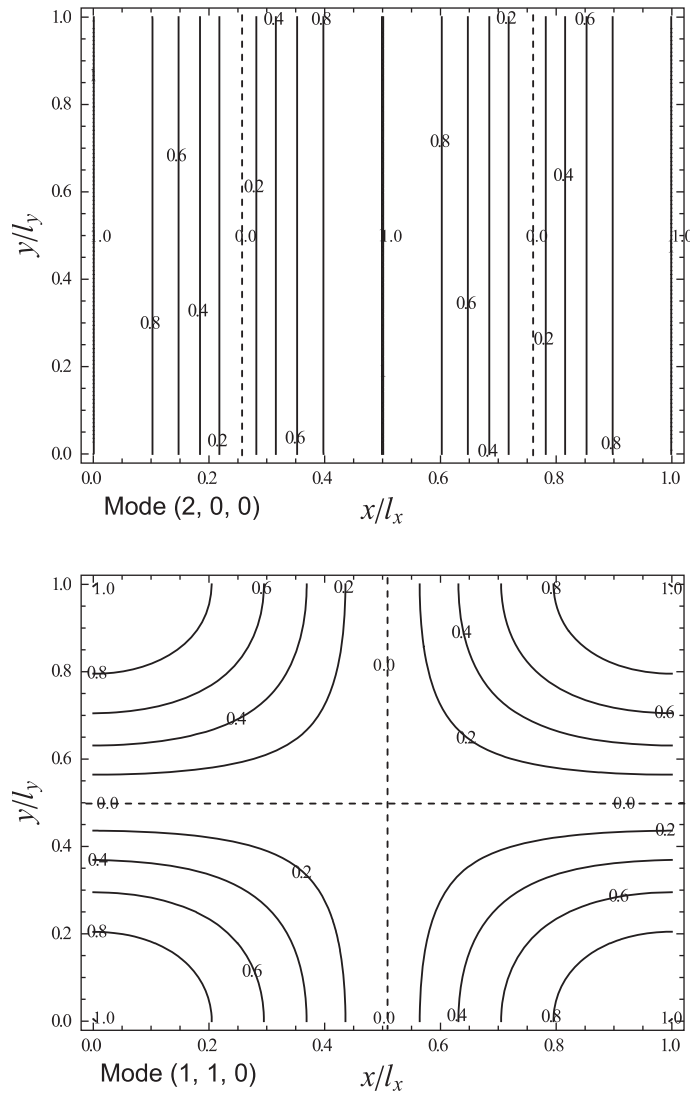


Figure 10.2 Sound-pressure contour plots on a section through a rectangular room. The numbers on the plots indicate the relative sound pressure.

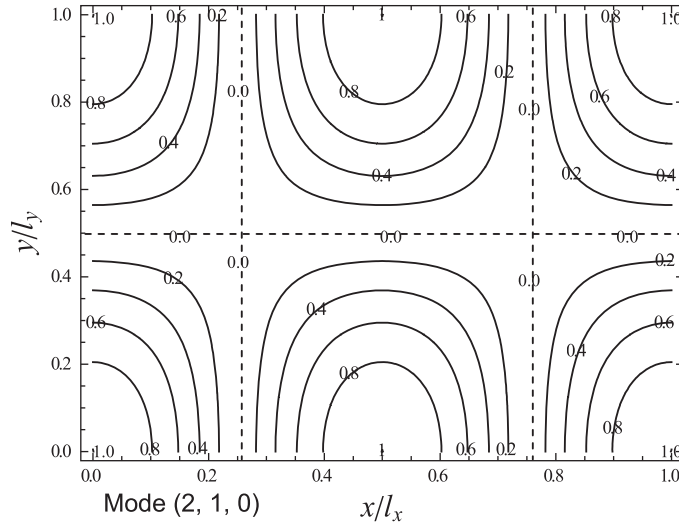


Figure 10.2 (continued).

For the examples where $n_x = 1$, $n_y = 1$ and $n_x = 3$, $n_y = 2$, the traveling waves reflect from the $x = 0$ and $x = l_x$ walls at

$$(\theta_x)_{1,1,0} = \arctan \frac{l_x}{l_y} = \arctan \frac{4}{3} = 53.1^\circ$$

$$(\theta_x)_{3,2,0} = \arctan \frac{2l_x}{3l_y} = \arctan \frac{8}{9} = 41.6^\circ$$

The angles of reflection at the $y = 0$ and $y = l_y$ walls are

$$(\theta_y)_{1,1,0} = \arctan \frac{l_y}{l_x} = \arctan \frac{3}{4} = 36.9^\circ$$

$$(\theta_y)_{3,2,0} = \arctan \frac{3l_y}{2l_x} = \arctan \frac{9}{8} = 48.4^\circ$$

The wave fronts travel as shown in (a) and (b) of Fig. 10.3. It is seen that there are two forward-traveling waves (1 and 3) and two backward-traveling waves (2 and 4). In the three-dimensional case, there will be four forward- and four backward-traveling waves.

When the acoustical absorbing materials are placed on some or all surfaces in an enclosure, energy will be absorbed from the sound field at these surfaces and the

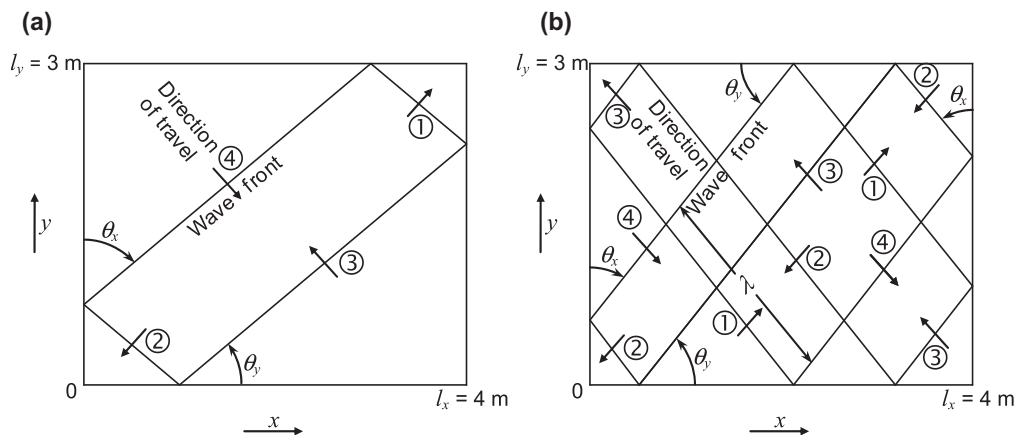


Figure 10.3 Wave fronts and direction of travel for (a) $n_x = 1, n_y = 1$ normal mode of vibration; and (b) $n_x = 3$ and $n_y = 2$ normal mode of vibration. These represent two-dimensional cases where $n_z = 0$. The numbers 1 and 3 indicate forward-traveling waves, and the numbers 2 and 4 indicate backward-traveling waves.

sound-pressure distribution will be changed from that for the hard wall case. For example, if an absorbing material were put on one of the $l_x l_z$ walls, the sound pressure at that wall would be lower than at the other $l_x l_z$ wall and the traveling wave would undergo a phase shift as it is reflected from the absorbing surface.

All normal modes of vibration cannot be excited to their fullest extent by a sound source placed at other than a maximum pressure point in the room. In Fig. 10.2, for example, the source of sound can excite only a normal mode to its fullest extent if it is at a 1.0 contour. Obviously, because the peak value of sound pressure occurs on a 1.0 contour, the microphone also must be located on a 1.0 contour to measure the maximum pressure.

If the source is at a corner of a rectangular room, it will be possible for it to excite every mode of vibration to its fullest extent, provided it radiates sound energy at every normal frequency. Similarly, if a microphone is at the corner of the room, it will measure the peak sound pressure for every normal mode of vibration, provided the mode is excited.

If either the source or the microphone is at the center of a rectangular room, only one-eighth of the normal modes of vibration will be excited or detected because at the center of the room, seven-eighths of the modes have contours of zero pressure. In Fig. 10.2, as an illustration, two out of the three normal modes portrayed have contours of zero pressure at the center of the room. In fact, only those modes of vibration having even numbers simultaneously for $n_x, n_y,$ and n_z will not have zero sound pressure at the center.

Examples of the transmission of sound from a point source to an observation point in a model sound chamber are shown in Figs. 10.4 and 10.5. The curves were obtained using the following equation for the pressure at the observation point (x, y, z) :

$$\begin{aligned} \tilde{p}(x, y, z) = & -\frac{4\rho_0 c \tilde{U}_0}{l_x l_y} \sum_{m=0}^{\infty} \sum_{n=0}^{\infty} \frac{k \cos(m\pi x_0/l_x) \cos(n\pi y_0/l_y) \cos(m\pi x/l_x) \cos(n\pi y/l_y)}{k_{mn}(1+\delta_{m0})(1+\delta_{0n})} \\ & \times \frac{\frac{k_{mn} Z_s}{k\rho_0 c} \cos k_{mn} z + j \sin k_{mn} z}{\cos k_{mn} l_z + j \frac{k_{mn} Z_s}{k\rho_0 c} \sin k_{mn} l_z} \end{aligned} \quad (10.11)$$

where

$$k_{mn} = \sqrt{k^2 - \left(\frac{m\pi}{l_x}\right)^2 - \left(\frac{n\pi}{l_y}\right)^2} \quad (10.12)$$

and $k = \omega/c = 2\pi/\lambda$, which is derived in the same way as we derive the 2-port network for a bass reflex enclosure in Part XXIV, except that the rectangular pistons are replaced by a point source of volume velocity \tilde{U}_0 at a point (x_0, y_0, l_z) described by the Dirac delta function

$$\delta(x - x_0)\delta(y - y_0).$$

The absorbing material at $z = 0$ has a specific impedance Z_s , which is related to the flow resistance R_f of the material by

$$Z_s = \frac{R_f d}{3} + \frac{P_0}{j\omega d} \quad (10.13)$$

where d is the thickness for the material, which is subtracted from l_z . The eightfold increase in the number of modes of vibration that were excited with the source at the corner over that with the source at the center is apparent. It is apparent also that the addition of sound-absorbing material decreases the height of resonance peaks and smoothes the transmission curve, particularly at the higher frequencies, where the sound-absorbing material is most effective.

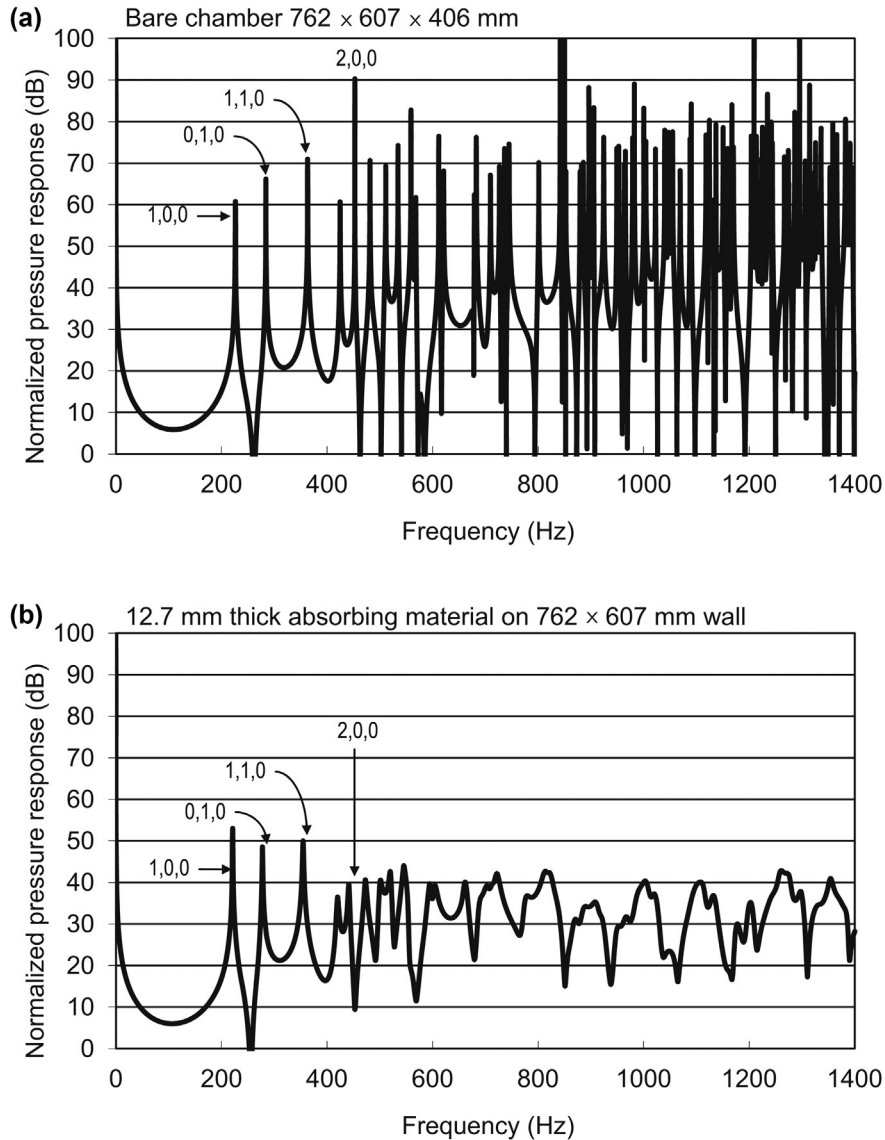


Figure 10.4 Comparison of two transmission curves calculated with and without an absorbing sample on a 762 by 607 mm wall of a model chamber with dimensions 762 by 607 by 406 mm. (a) Bare chamber, (b) one wall absorbent, where $R_f d/3 \approx \rho_0 c$. The source was in one corner (l_x, l_y, l_z) , and the observation point was diagonally opposite $(0, 0, 0)$. The plots are of $20 \log_{10}(l_x l_y \tilde{p}(x, y, z) / (\rho_0 c \tilde{U}_0))$, where $\tilde{p}(x, y, z)$ is calculated from Eq. (10.11). This result has also been verified experimentally [1].

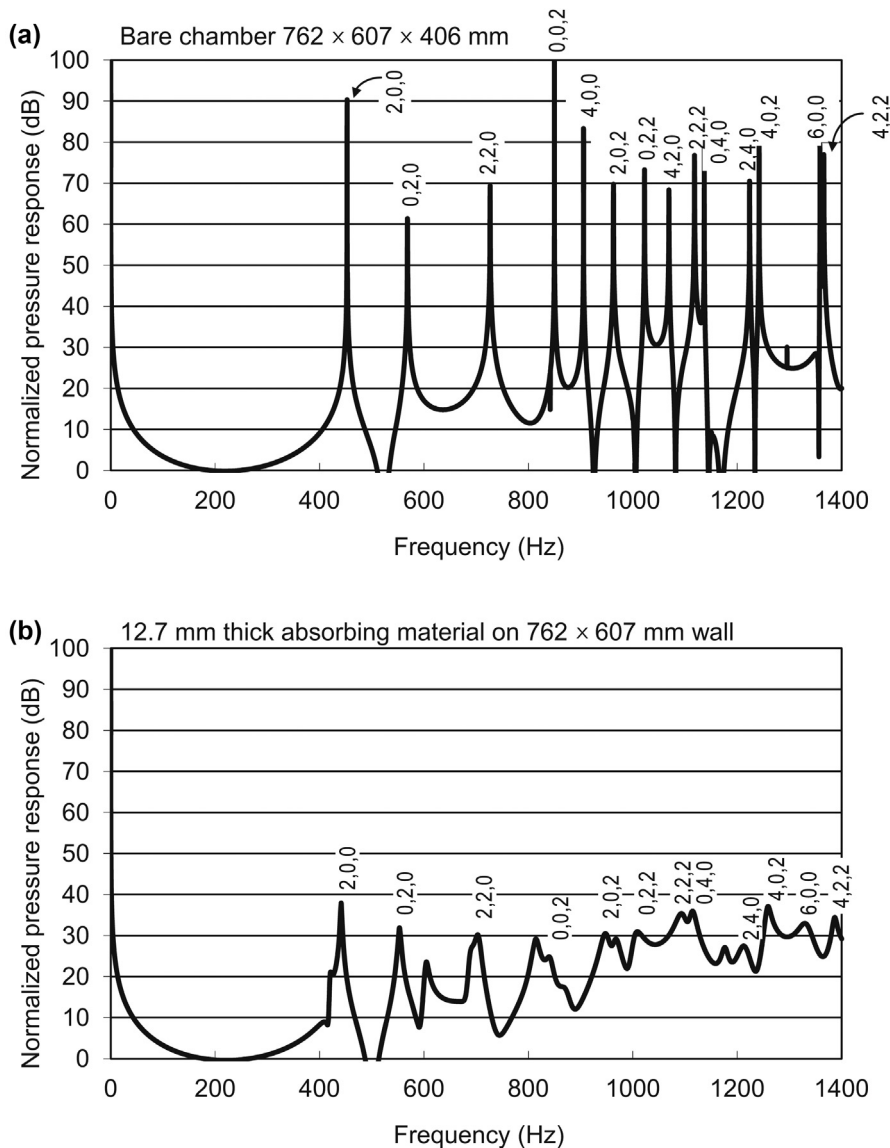


Figure 10.5 Same as Fig. 10.4, except that the point of observation is in the center of the room ($l_x/2, l_y/2, l_z/2$). (a) Bare chamber, (b) one wall absorbent.



10.4 STEADY-STATE AND TRANSIENT SOUND PRESSURES

Sound pressure at normal modes

When a source of sound is turned on in a small enclosure, such as that of Fig. 10.1, it will excite one or more of the stationary-wave possibilities, i.e., normal modes of vibration in

the room. Let us assume that the source is constant in strength and is of a single frequency and that its frequency coincides with one of the normal frequencies of the enclosure. The sound pressure for that normal mode of vibration will build up until the magnitude of its rms value (averaged in time and also in space by moving the microphone backward and forward over a wavelength) equals [1]

$$|p_n| = \frac{K}{k_n} \quad (10.14)$$

where

K is a source constant determined principally by the strength and location of the source and by the volume of the room.

k_n is damping constant determined principally by the amount of absorption in the room and by the volume of the room. The more absorbing material that is introduced into the room, the greater k_n becomes, and the smaller the value of the average pressure. The value of k_n is inversely proportional to the value of Q_n .

Blocked-tube impedance and equivalent circuit

To illustrate what happens when the driving frequency does not necessarily coincide with the normal frequency, we shall simplify the problem by considering only those modes of vibration which occur in one direction only. Hence, we may model the room as a one-dimensional tube. Furthermore, although absorption mainly occurs at boundary surfaces, we may simplify the problem even further by assuming that it occurs everywhere. Also, we assume the acoustic resistance to have the same value at all frequencies, although this is unlikely in practice. However, if the variation of resistance with frequency is known, the resistance value at each normal frequency may be used to improve accuracy.

According to Eq. (2.72), the specific impedance Z_T of a blocked tube is given by

$$Z_T = -jZ_s \cot \mathbf{k}l \quad (10.15)$$

which is expanded using Eq. (A2.43) from Appendix II:

$$Z_T = -jZ_s \sum_{n=0}^{\infty} \frac{(2 - \delta_{0n})\mathbf{k}l}{(\mathbf{k}l)^2 - n^2\pi^2} \quad (10.16)$$

where from Eqs. (2.115), (2.119), and (2.120), the complex wave number \mathbf{k} and characteristic impedance Z_s are given by

$$\mathbf{k} = \omega \sqrt{\frac{1}{P_0} \left(\rho_0 + \frac{R_f}{j\omega} \right)} \quad (10.17)$$

$$Z_s = \sqrt{P_0 \left(\rho_0 + \frac{R_f}{j\omega} \right)} \quad (10.18)$$

where P_0 is the static pressure, ρ_0 is the density of air, and R_f is the flow resistance per unit length of the filling material. Hence, the impedance of the tube may be written as

$$Z_T = \frac{1}{C_0 s} + \sum_{n=1}^{\infty} Z_n \quad (10.19)$$

where each impedance term is represented by a parallel resonance circuit in which

$$Z_n = \frac{1}{C_n} \cdot \frac{s + \frac{R_n}{L_n}}{s^2 + \frac{R_n}{L_n} s + \frac{1}{L_n C_n}} \quad (10.20)$$

where $s = \omega$, and the specific compliance C_n , mass L_n , and resistance R_n element values are given by

$$C_0 = \frac{l}{P_0}, \quad C_n = \frac{l}{2P_0}, \quad L_n = \frac{2\rho_0 l}{n^2 \pi^2}, \quad R_n = \frac{2R_f l}{n^2 \pi^2} \quad (10.21)$$

or

$$Z_n = \frac{1}{C_n} \cdot \frac{s + \frac{\omega_n}{Q_n}}{s^2 + \frac{\omega_n}{Q_n} s + \omega_n^2} \quad (10.22)$$

where the angular normal frequency ω_n and Q_n values are given by

$$\omega_n = \frac{1}{\sqrt{L_n C_n}} = \frac{n\pi c}{1/\sqrt{\gamma}}, \quad Q_n = \omega_n \frac{\rho_0}{R_f} = \frac{n\pi \rho_0 c}{\sqrt{\gamma} R_f l} \quad (10.23)$$

The equivalent circuit for a blocked tube using this impedance expansion is shown in Fig. 10.6a.

Alternatively, we may use the expansion of Eq. (A2.42) from Appendix II for the admittance:

$$Z_T = -j \frac{Z_s}{\tan \mathbf{k}l} = \left(\sum_{n=0}^{\infty} Y_n \right)^{-1} \quad (10.24)$$

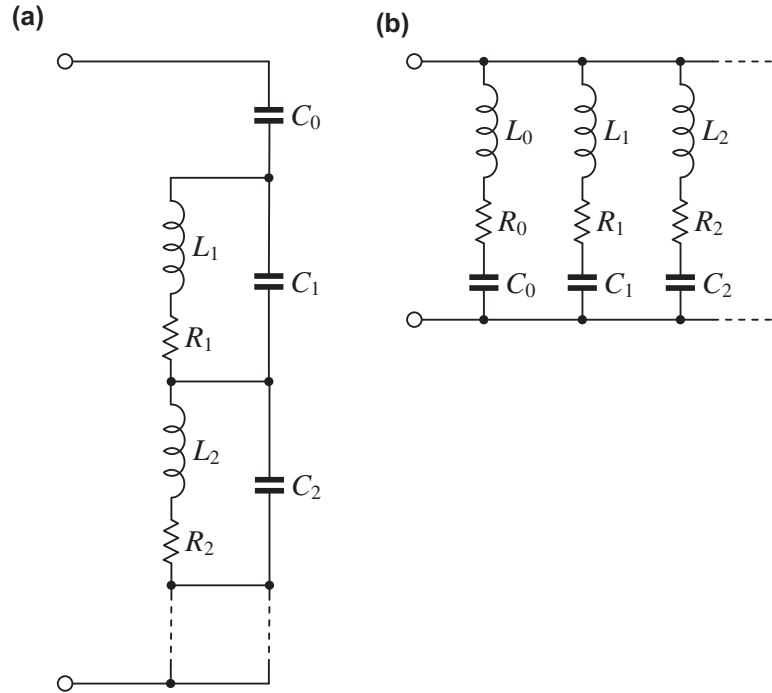


Figure 10.6 Equivalent circuits for the impedance Z_T of a blocked tube using an impedance expansion (a) and an admittance expansion (b).

where

$$Y_n = \frac{\frac{1}{L_n} s}{s^2 + \frac{R_n}{L_n} s + \frac{1}{L_n C_n}} \quad (10.25)$$

and

$$C_n = \frac{2l}{\left(n + \frac{1}{2}\right)^2 \pi^2 P_0}, \quad L_n = \frac{\rho_0 l}{2}, \quad R_n = \frac{R_f l}{2} \quad (10.26)$$

so that

$$\omega_n = \frac{1}{\sqrt{L_n C_n}} = \frac{\left(n + \frac{1}{2}\right) \pi c}{l \sqrt{\gamma}}, \quad Q_n = \omega_n \frac{\rho_0}{R_f} = \frac{\left(n + \frac{1}{2}\right) \pi \rho_0 c}{\sqrt{\gamma} R_f l} \quad (10.27)$$

The equivalent circuit for a blocked tube using this admittance expansion is shown in Fig. 10.6b. In general, we use the impedance expansion to calculate the time response of the pressure as a function of an input velocity and the admittance expansion to calculate the time response of the velocity as a function of an input pressure.

Open-tube impedance and equivalent circuit

Although we shall only consider the decay of sound in a blocked tube, the equivalent circuit of an open tube is derived here just for completeness as it is frequently encountered in the field of acoustics.

According to Eq. (2.60) with $Z_T = 0$, the specific impedance Z_T of an open tube is given by

$$Z_T = jZ_s \tan kl \quad (10.28)$$

which is expanded using Eq. (A2.42) from Appendix II:

$$Z_T = \sum_{n=0}^{\infty} Z_n \quad (10.29)$$

where

$$Z_n = \frac{1}{C_n} \cdot \frac{s + \frac{R_n}{L_n}}{s^2 + \frac{R_n}{L_n}s + \frac{1}{L_n C_n}} \quad (10.30)$$

and

$$C_n = \frac{l}{2P_0}, \quad L_n = \frac{2\rho_0 l}{\left(n + \frac{1}{2}\right)^2 \pi^2}, \quad R_n = \frac{2R_f l}{\left(n + \frac{1}{2}\right)^2 \pi^2} \quad (10.31)$$

or

$$Z_n = \frac{1}{C_n} \cdot \frac{s + \frac{\omega_n}{Q_n}}{s^2 + \frac{\omega_n}{Q_n}s + \omega_n^2} \quad (10.32)$$

where

$$\omega_n = \frac{1}{\sqrt{L_n C_n}} = \frac{\left(n + \frac{1}{2}\right) \pi c}{1/\sqrt{\gamma}}, \quad Q_n = \omega_n \frac{\rho_0}{R_f} = \frac{\left(n + \frac{1}{2}\right) \pi \rho_0 c}{\sqrt{\gamma} R_f l} \quad (10.33)$$

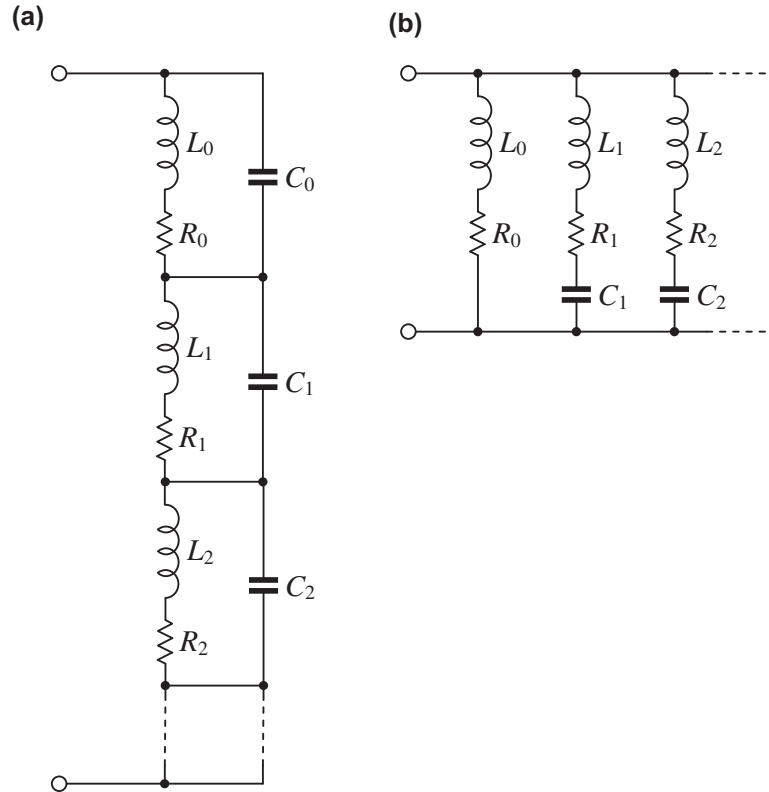


Figure 10.7 Equivalent circuits for the impedance Z_T of an open tube using an impedance expansion (a) and an admittance expansion (b).

The equivalent circuit for an open tube using this impedance expansion is shown in Fig. 10.7a.

Alternatively, we may use the expansion of Eq. (A2.43) from Appendix II for the admittance:

$$Z_T = j \frac{Z_s}{\cot kl} = \left(\frac{1}{\frac{L_0}{s} + \frac{R_0}{s} + \sum_{n=1}^{\infty} Y_n} \right)^{-1} \quad (10.34)$$

where

$$Y_n = \frac{\frac{1}{L_n} s}{s^2 + \frac{R_n}{L_n} s + \frac{1}{L_n C_n}} \quad (10.35)$$

and

$$C_n = \frac{2l}{n^2\pi^2 P_0}, \quad L_0 = \rho_0 l, \quad L_n = \frac{\rho_0 l}{2}, \quad R_0 = R_f l, \quad R_n = \frac{R_f l}{2} \quad (10.36)$$

so that

$$\omega_n = \frac{1}{\sqrt{L_n C_n}} = \frac{n\pi c}{l\sqrt{\gamma}}, \quad Q_n = \omega_n \frac{\rho_0}{R_f} = \frac{n\pi\rho_0 c}{\sqrt{\gamma}R_f l} \quad (10.37)$$

The equivalent circuit for an open tube using this admittance expansion is shown in Fig. 10.7b.

Resonance curve

When the driving frequency does not coincide with the normal frequency, the pressure for that particular mode of vibration builds up according to a standard resonance curve as shown in Fig. 10.8. The maximum value of the resonance curve is given by

$$\begin{aligned} Z_n|_{\omega=\omega_n} &= (Q_n + j)Q_n R_n \\ &\approx Q_n^2 R_n, \quad Q_n \geq 3 \end{aligned} \quad (10.38)$$

The width of the resonance curve at the half-power (3 dB down) points is equal to Ref. [2].

$$f'' - f \approx \frac{f_n}{Q_n} \quad (10.39)$$

When driven by an excitation velocity u_0 , the magnitude of the sound pressure p_n for a single mode as a function of frequency is given by

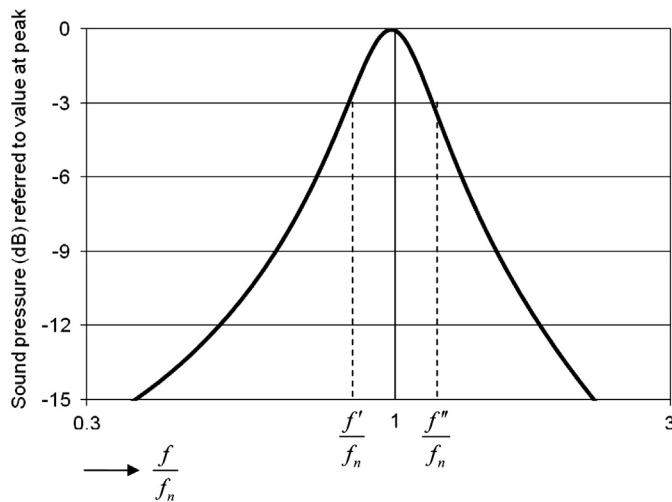


Figure 10.8 Resonance curve for a normal mode of vibration with $Q_n = 3$. Sound pressure level versus the ratio of frequency to f_n .

$$|p_n| = u_0 |Z_n| = \frac{u_0}{C_n} \sqrt{\frac{Q_n^2 \omega^2 + \omega_n^2}{Q_n^2 (\omega_n^2 - \omega^2)^2 + \omega_n^2 \omega^2}} \quad (10.40)$$

where ω is the angular driving frequency and ω_n is the angular normal frequency given approximately by Eq. (10.5).

Obviously, if the driving frequency lies between two normal frequencies or if k_n is large so that the resonance curve is broad, more than one normal mode of vibration will be excited significantly, each to the extent shown by Eq. (10.40). Because the phase above a normal frequency is opposite to that below it, there will be a cancellation at some frequency between a pair of adjacent normal frequencies, leading to a minimum impedance value. These minimum impedance frequencies correspond to the resonance frequencies ω_n in the admittance expansion.

Transient response

When the source of sound is turned off, each normal mode of vibration behaves like an electrical parallel resonance circuit in which energy has been stored initially. The pressure for each normal mode of vibration will decay exponentially at its own normal frequency as shown in Fig. 10.9. To simulate the decay of sound, let us apply an impulse to our tube model, rather like a hand clap in a room. We simply take the expression for the impedance of each mode given by Eq. (10.22) and apply the inverse Laplace transform given by Table 6.2 in Sec. 6.17 to obtain

$$p_n(t) = u_0 Z_n(t) = \frac{u_0}{C_n} e^{-\omega_n t \cos \theta_n} \frac{\sin(\theta_n + \omega_n t \sin \theta_n)}{\sin \theta_n} \quad (10.41)$$

where $\cos \theta_n = 1/(2Q_n)$. If only one mode of vibration is excited, the decay is as shown in Fig. 10.9a. Stated differently, on a log p_n scale versus time, the magnitude of the rms SPL decays linearly with time.

If two or more modes of vibration are decaying simultaneously, beats will occur because each has its own normal frequency (Fig. 10.9b). However, as we superimpose an ever greater number of modes, the waveform becomes a series of impulses (Fig. 10.9c), as we would expect, due to the original impulse being reflected at each end of the tube and thus making multiple round journeys along it. In a real room, as opposed to a simple one-dimensional tube, early reflections would behave in a similar manner, being distinct and thus *specular* in nature. However, later reflections resulting from random reflections of multiple surfaces tend to cluster together and are termed *diffuse*.

In this illustration, each mode has the same decay constant ($\omega_n/2Q_n = R_f/2\rho_0$) because the specific flow resistance per unit length R_f has been assumed to be independent of frequency. However, it is very possible that each will have its own decay constant, dependent on the position of the absorbing materials in the room.

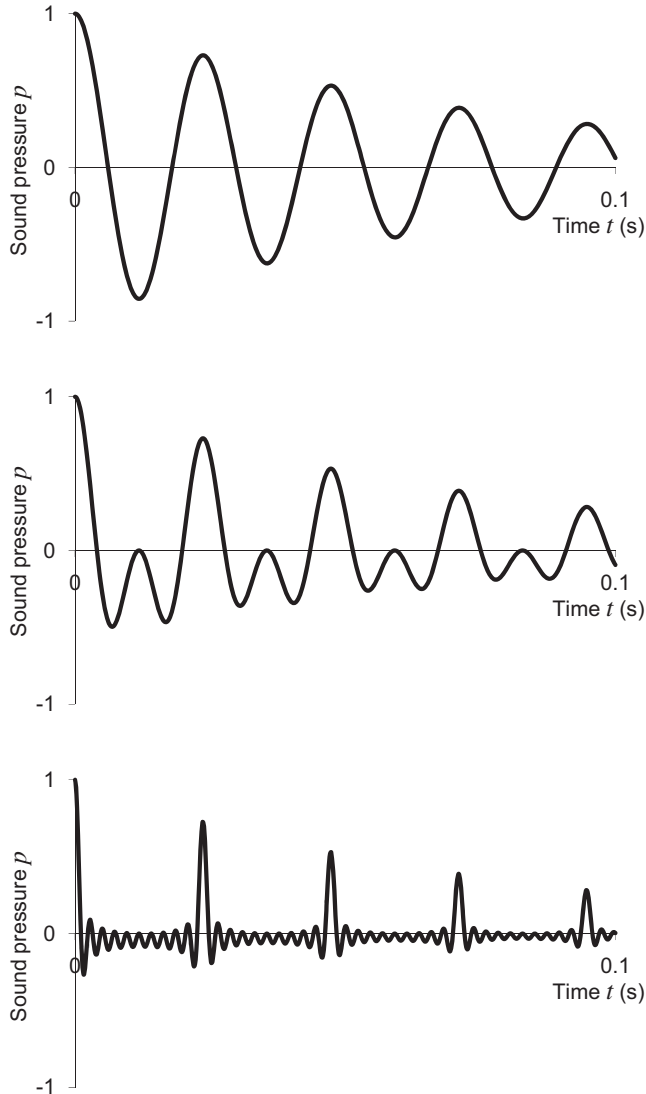


Figure 10.9 (a) Sound-pressure decay curve for the first mode of vibration. (b) Sound-pressure decay curve for the first two modes of vibration. (c) Sound-pressure decay curve for the first 10 modes of vibration in a blocked tube, where $l = 3.5$ m and $R_f = 10$ rays/m.

In actual measurements of sound in rooms, it is quite common to use fast Fourier transforms (FFTs) to create waterfall plots of the sound pressure decay against both time T and frequency f , which in this case is obtained as follows:

$$p_n(f, T) = \int_{T-\delta t}^{T+\delta t} \left(0.54 - 0.46 \cos\left(\frac{t-T+\delta t}{\delta t} \pi\right) \right) p_n(t) e^{j2\pi ft} dt \quad (10.42)$$

where the integration is performed over a sliding interval or “window” of width $2\delta t$ centered on the time of interest T . The term in parenthesis is the Hamming window function, which minimizes any unwanted frequency components that may otherwise appear in the spectrum because of the finite integral limits. In this way, we can plot the variation of the frequency spectrum with time and thus see how the individual normal modes of vibration decay relative to each other, as shown in Fig. 10.10.

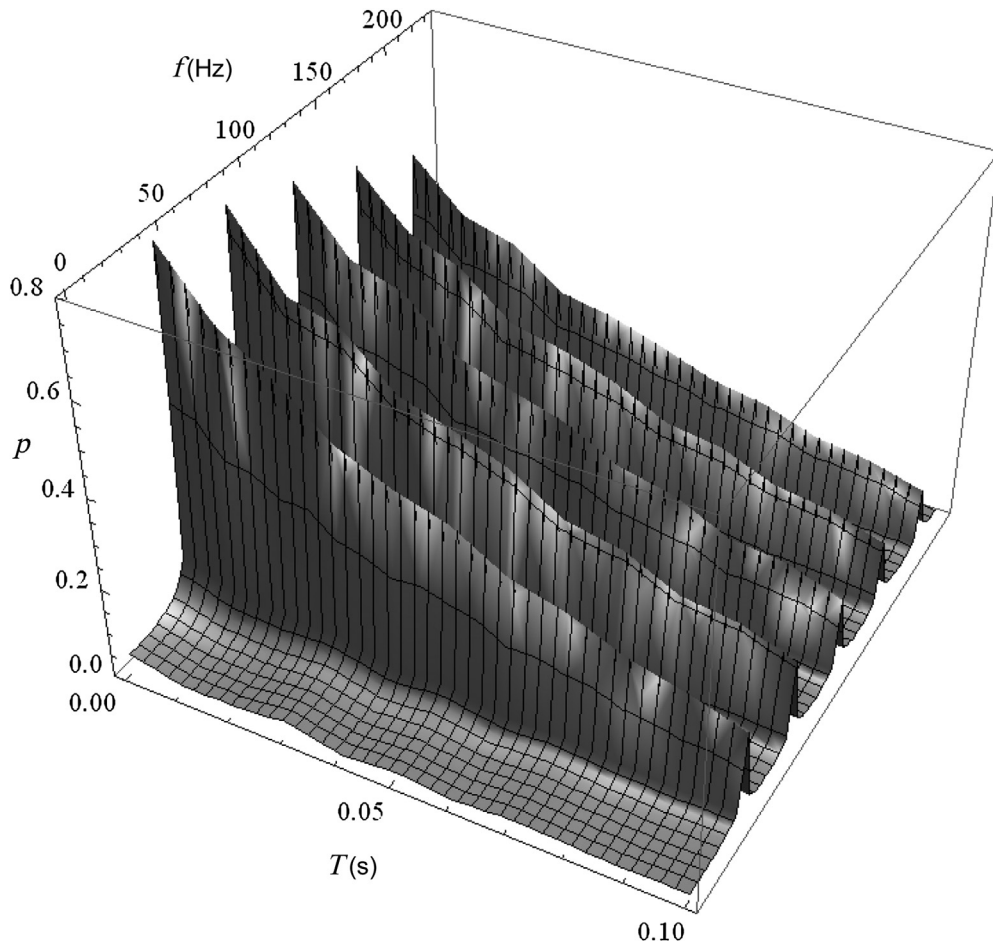


Figure 10.10 Waterfall plot of sound-pressure decay in a tube in which $l = 3.5$ m, $R_f = 10$ rays/m, $\delta t = 0.5$ s, and the first five modes are summed in the calculation. The 0th mode is ignored because it simply gives a constant change in pressure.

In summary, we see that when a sound source of a given frequency is placed in an enclosure, it will excite one or more of the infinity of resonance conditions called normal modes of vibration. Each of those normal modes of vibration has a different distribution of sound pressures in the enclosure, its own normal frequency, and its own damping constant. The damping constant determines the maximum height and the width of the steady-state sound-pressure resonance curve.

In addition, when the source of sound is turned off, the sound pressure associated with each mode of vibration decays exponentially with its own normal frequency and at a rate determined by its damping constant. The room is thus an assemblage of resonators that act independently of each other when the sound source is turned off. The larger the room and the higher the frequency, the nearer together will be the normal frequencies and the larger will be the number of modes of vibration excited by a single-frequency source or by a source with a narrow band of frequencies.



10.5 EXAMPLES OF RECTANGULAR ENCLOSURES

Example 10.1. Determine the normal frequencies and directional cosines for the lowest six normal modes of vibration in a room with dimensions $5 \times 4 \times 3$ m.

Solution. From Eq. (10.5), we see that

$$f_{1,0,0} = \frac{348.8}{2} \times \frac{1}{5} = 34.9 \text{ Hz}$$

$$f_{0,1,0} = \frac{348.8}{2} \times \frac{1}{4} = 40.4 \text{ Hz}$$

$$f_{1,1,0} = \frac{348.8}{2} \sqrt{\frac{1}{25} + \frac{1}{16}} = 55.8 \text{ Hz}$$

$$f_{2,0,0} = \frac{348.8}{2} \times \frac{2}{5} = 69.8 \text{ Hz}$$

$$f_{2,1,0} = \frac{348.8}{2} \sqrt{\frac{4}{25} + \frac{1}{16}} = 82.3 \text{ Hz}$$

$$f_{0,0,1} = \frac{348.8}{2} \times \frac{1}{3} = 58.1 \text{ Hz}$$

From Eqs. (10.8–10.10) we find the direction cosines for the various modes as follows:

$$(1, 0, 0) \text{ mode: } \theta_x = 0; \theta_y = 90^\circ; \theta_z = 90^\circ$$

$$(0, 1, 0) \text{ mode: } \theta_x = 90^\circ; \theta_y = 0^\circ; \theta_z = 90^\circ$$

$$(1, 1, 0) \text{ mode: } \theta_x = \arccos \frac{348.8}{2 \times 5 \times 55.8} = 51.3^\circ$$

$$\theta_y = \arccos \frac{348.8}{2 \times 4 \times 55.8} = 38.6^\circ$$

$$\theta_z = 90^\circ$$

$$(2, 0, 0) \text{ mode: } \theta_x = 0; \theta_y = 90^\circ; \theta_z = 90^\circ$$

$$(2, 1, 0) \text{ mode: } \theta_x = \arccos \frac{2 \times 348.8}{2 \times 5 \times 82.3} = 32.1^\circ$$

$$\theta_y = \arccos \frac{348.8}{2 \times 4 \times 82.3} = 58.0^\circ$$

$$\theta_z = 90^\circ$$

$$(0, 0, 1) \text{ mode: } \theta_x = 90^\circ; \theta_y = 90^\circ; \theta_z = 0^\circ$$

Example 10.2. A rectangular room with dimensions $l_x = 3$ m, $l_y = 4$ m, and $l_z = 5$ m is excited by a sound source located in one corner of the room. The SPL developed is measured at another corner of the room. The sound source produces a continuous band of frequencies between 450 and 550 Hz, with a uniform spectrum level, and a total acoustic power output of 1 W. When the sound source is turned off, a linear decay curve ($\log p$ vs. t) is obtained, which has a slope of 30 dB/s. (a) Determine graphically the number of normal modes of vibration excited by the source; (b) determine the approximate angle of incidence of the traveling-wave field involving the walls at $x = 0$ and $x = l_x$ in each of the principal groupings of normal frequencies shown in the graphical construction.

Solution. (a) A graphical solution to Eq. (10.5) is given in Fig. 10.11. The frequency of any given normal mode of vibration is the distance from the origin of coordinates to one of the black spheres shown. That frequency will be made up of three components given

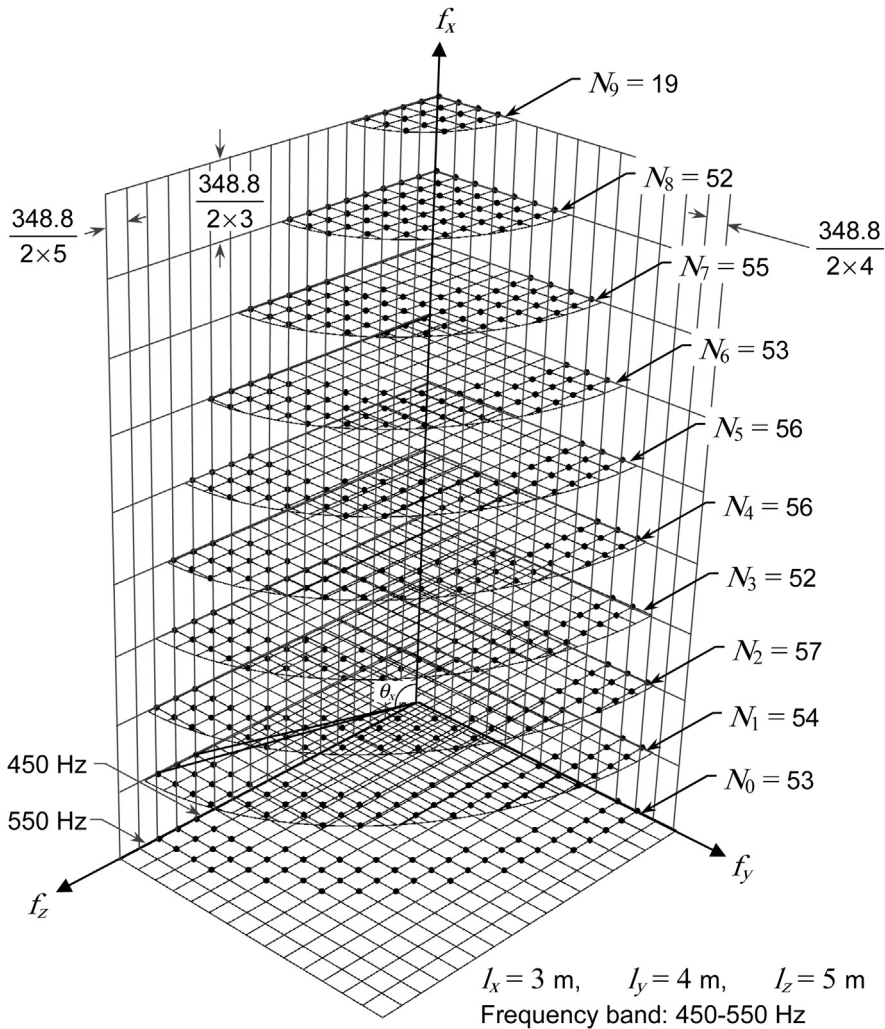


Figure 10.11 Normal frequency diagram, drawn to scale for a 3 by 4 by 5 m rectangular room with hard walls. Most of the vertical lines are omitted to avoid confusion. After Hunt, Beranek, and Maa, [1] *Analysis of Sound Decay in Rectangular Rooms, J. Acoust. Soc. Am.*, **11**: 80–94 (1939).

by $cn_x/2l_x$, $cn_y/2l_y$, and $cn_z/2l_z$. Notice that along the vertical coordinate, the normal frequencies occur in increments of $348.8/6$ along the right-hand axis in increments of $348.8/8$ and along the remaining axis in increments of $348.8/10$. On the layer labeled N_0 , there are 53 normal frequencies. The total number of normal frequencies between 450 and 550 Hz for this room is 507. The average frequency is 500 Hz.

Solution. (b) The θ_x angles of incidence can be divided into 10 principal groups as shown in Fig. 10.11. The angles are as follows:

$$\theta_x(0, n_y, n_z) \approx 90^\circ$$

$$\theta_x(1, n_y, n_z) \approx \cos^{-1}\left(\frac{345}{6} \cdot \frac{1}{500}\right) \approx 83^\circ$$

$$\theta_x(2, n_y, n_z) \approx \cos^{-1}\left(\frac{2.345}{6.500}\right) \approx 77^\circ$$

$$\theta_x(3, n_y, n_z) \approx \cos^{-1}(0.345) \approx 70^\circ$$

$$\theta_x(4, n_y, n_z) \approx \cos^{-1}(0.46) \approx 63^\circ$$

$$\theta_x(5, n_y, n_z) \approx \cos^{-1}(0.575) \approx 55^\circ$$

$$\theta_x(6, n_y, n_z) \approx \cos^{-1}(0.69) \approx 46^\circ$$

$$\theta_x(7, n_y, n_z) \approx \cos^{-1}(0.805) \approx 36^\circ$$

$$\theta_x(8, n_y, n_z) \approx \cos^{-1}(0.92) \approx 23^\circ$$

$$\theta_x(9, n_y, n_z) \approx \cos^{-1}(0.995) \approx 6^\circ$$

PART XXXI: SOUND IN LARGE ENCLOSURES

10.6 BASIC MATTERS

When a sound source, having components that extend over a band of frequencies, radiates sound into a large irregular enclosure, a microphone that is moved about will experience fluctuations in sound pressure. The maxima and minima of these fluctuations will lie much closer together in such an enclosure than in a small or regular enclosure because there are a large number of room resonances in all bands except for the very lowest frequency bands. Thus, in these enclosures, the mean square sound pressure can be determined by moving the microphone back and forth over a short distance. The sound field is largely a superposition of plane waves traveling in all directions with equal probability. This condition is called a *diffuse sound field*. To avoid the influence of the direct sound, this condition is experienced at a reasonable distance from the source.

The number of reflections from surfaces in such a room per second is equal to c/d , where d is the *mean free path of the wave* and c is the *speed of sound*. By actual measurements in rooms of varying shapes and sizes, it has been found that mean free path is equal to

$$d = \frac{4V}{S} \text{ m} \quad (10.43)$$

where V is the volume of the room in m^3 and S is the total area of the surfaces of the room in m^2 . If, after establishing a steady-state sound field, the source of sound is turned off, the sound energy stored in the enclosure will decrease with each reflection (See Fig. 10.12) according to

$$D(n) = D'(1 - \alpha)^n \quad (10.44)$$

where D' is the steady-state energy density before the source was turned off, n is the number of reflections that have occurred, and α is the sound absorption coefficient, which is taken to be averaged for all angles of incidence. By replacing n with $ct/d = (cS/4V)t$, the decay formula is

$$D(t) = D'(1 - \alpha)^{(cS/4V)t} = D'e^{-(cS/4V)(-\ln(1-\alpha))t} \quad (10.45)$$

where \ln is the logarithm to the base e . In a reverberant sound field, the energy density is proportional to the mean square sound pressure. Hence,

$$p_{av}^2(t) = p_{av}^2(0)e^{-(cS/4V)(-\ln(1-\alpha))t} \quad (10.46)$$

Because $10 \log_{10}$ of the exponential function equals

$$10(cS/4V)(\log_{10}(1 - \alpha))t,$$

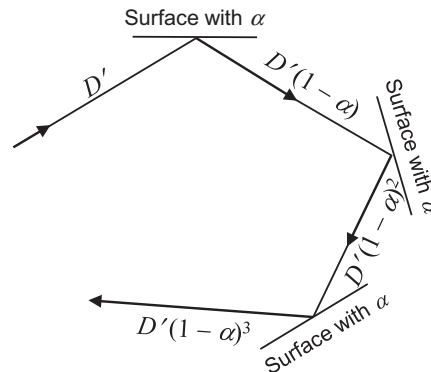


Figure 10.12 Path of a sound wave with energy density D' as it travels distances of $4V/S$ and reflects off surfaces with average absorption coefficient α .

where we have used the relationship $\log_{10} x = \log_{10} e \cdot \ln x$, the SPL decays at the rate of

$$-\frac{10cS}{4V} \log_{10}(1 - \alpha) \text{ dB/s} \quad (10.47)$$



10.7 THE REVERBERATION EQUATIONS

The reverberation time of the enclosure is defined as the time required for the SPL to fall 60 dB. Thus, the well-known **Eyring equation** [3], which gives the reverberation time T for an energy drop of 60 dB (often denoted by T_{60}), is obtained from Eq. (10.47), with $S = S_{tot} = \sum S_i$, where S_i 's are areas of particular surfaces in the room, such as audience area and ceiling area:

$$T = \frac{24V}{-cS_{tot} \log_{10}(1 - \alpha_{ey})} \text{ s} \quad (10.48)$$

where V is the volume of room in m^3 , S_{tot} is the area of all surfaces in the room, and α_{ey} is the average sound absorption coefficient for the surface S_i as shown in Fig. 10.12. The Eyring equation is usually presented with either the natural logarithm or \log_{10} in the denominator and with c taken as 343.5 m/s at 20°C so that

$$T = \frac{0.161V}{S_{tot}(-\ln(1 - \alpha_{ey}))} = \frac{0.161V}{S_{tot}(-2.30 \log_{10}(1 - \alpha_{ey}))} \text{ s} \quad (10.49)$$

Note that if the surfaces are perfectly absorbing, i.e., $\alpha_{ey} = 1.0$, the reverberation time T goes to zero.

The **Sabine equation** [4] was derived by Wallace Sabine from measurements he made in a number of rooms at Harvard University:

$$T = \frac{0.161V}{S_{tot}\alpha_{tot}} \text{ s (metric units)} \quad (10.50)$$

$$T = \frac{0.049V}{S_{tot}\alpha_{tot}} \text{ s (English units)} \quad (10.51)$$

Note that, in the Sabine equation, T only goes to zero if α_{tot} approaches infinity. Even today, most published data on acoustical materials and the absorption of audiences and the like have been obtained using the Sabine equation, partly because the formula is simpler to use and partly because for α_{ey} less than 0.26, α_{tot} is decreasingly less than 0.3.

It is possible to derive the absorption coefficients in one equation from the absorption coefficients in the other equation [5]. In the Sabine equation, let

$$\alpha_{tot} = \frac{\sum \alpha_{s,i} S_i}{S_{tot}} \quad (10.52)$$

where $\alpha_{s,i}$ is the Sabine absorption coefficient for a particular area S_i and $S_{tot} = \sum S_i$.

In the Eyring equation, let

$$\alpha_{ey} = \frac{\sum \alpha_{e,i} S_i}{S_{tot}} \quad (10.53)$$

where $\alpha_{e,i}$ is the Eyring absorption coefficient for a particular area S_i .

Then, we find

$$\frac{\alpha_{ey}}{\alpha_{tot}} = \frac{\sum \alpha_{e,i} S_i}{\sum \alpha_{s,i} S_i} \quad (10.54)$$

Hence,

$$\alpha_{e,i} = (\alpha_{ey}/\alpha_{tot})\alpha_{s,i}. \quad (10.55)$$

10.8 AIR ABSORPTION

As a sound wave travels from one reflection to another in a room, some energy is lost in the air itself. Such absorption in all but very large rooms is appreciable only at frequencies above 1000 Hz. When the reverberation equations are corrected to account for air absorption, they read as follows.

Eyring equation, metric units:

$$T = \frac{0.161V}{S_{tot}(-\ln(1 - \alpha_{ey})) + 4mV} = \frac{0.161V}{S_{tot}(-2.30 \log_{10}(1 - \alpha_{ey})) + 4mV}. \quad (10.56)$$

Sabine equation, metric units:

$$T = \frac{0.161V}{S_{tot}\alpha_{tot} + 4mV}, \quad (10.57)$$

where m is the energy attenuation constant in units of reciprocal length. Measured values of $4m$ under some typical atmosphere conditions are shown in [Table 10.1](#).

10.9 TOTAL STEADY SOUND PRESSURE LEVEL

We are now in a position to incorporate the direct sound field from a source into the energy equations and calculate the total steady-state SPL.

Table 10.1 Measured values of air attenuation constant m (multiplied by 4) in m^{-1} as a function of frequency, temperature, and relative humidity

Relative humidity	Temperature °C (°F)	2000 Hz	4000 Hz	6300 Hz	8000 Hz
30%	15° (59°)	0.0147	0.0519	0.1144	0.1671
	20° (68°)	0.0122	0.0411	0.0937	0.1431
	25° (77°)	0.0111	0.0335	0.0759	0.1178
	30° (86°)	0.0114	0.0292	0.0633	0.0975
50%	15° (59°)	0.0096	0.0309	0.0712	0.1102
	20° (68°)	0.0092	0.0258	0.0577	0.0896
	25° (77°)	0.0101	0.0234	0.0489	0.0748
	30° (86°)	0.0119	0.0234	0.0443	0.0655
70%	15° (59°)	0.0081	0.0231	0.0519	0.0808
	20° (68°)	0.0088	0.0208	0.0437	0.0671
	25° (77°)	0.0105	0.0208	0.0396	0.0586
	30° (86°)	0.0131	0.0231	0.0391	0.0548

Direct steady-state sound pressure

The space average sound pressure in a room (determined by moving a microphone back and forth over at least one wavelength) at a distance r from a small directional source radiating W watts is

$$p^2(r) = \frac{\rho_0 c W}{4\pi r^2} Q \text{ N}^2/\text{m}^4, \quad (10.58)$$

where Q is the directivity index (not in decibels) (see Sec. 4.16).

Reverberant steady-state sound pressure

The sound power absorbed by the first reflection is $W\alpha$; hence, the power remaining for the reverberant field is $W_r = W(1 - \alpha)$. Let t' be the length of time it takes for the sound to travel one mean free path length:

$$t' = \frac{4V}{cS} \text{ s}. \quad (10.59)$$

Let the steady-state value of the reverberant energy density be D'_r . Then, the total energy per second removed from the room is

$$\frac{D'_r V \alpha}{t'} = W_r, \quad (10.60)$$

which yields, where $p_r^2 = D_r' \rho_0 c^2$,

$$p_r^2 = \frac{4\rho_0 c W}{S\alpha} (1 - \alpha) N^2 / \text{m}^4. \quad (10.61)$$

Total steady-state sound pressure

Combining Eqs. (10.58) and (10.61) yields

$$p^2(r) = W\rho_0 c \left[\frac{Q}{4\pi r^2} + \frac{4(1 - \alpha)}{S\alpha} \right] N^2 / \text{m}^4. \quad (10.62)$$

The restrictions on this equation are that α not be too large and the mean free path is about $4V/S$. The absorption coefficient α is the Eyring coefficient.



10.10 OPTIMUM REVERBERATION TIME

The following formula [6–11] gives the average optimum reverberation time T for a given auditorium volume V based on subjective results:

$$\log_{10} V = 5.72 + \log_{10} T - \frac{2.43}{\sqrt{T}}, \quad (10.63)$$

which is solved numerically for T and plotted in Fig. 10.13.

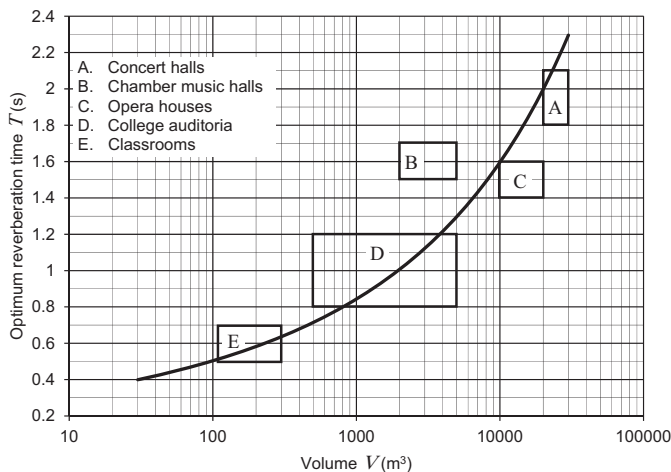


Figure 10.13 Optimum reverberation T versus auditorium volume V .

10.11 SOUND STRENGTH G

It is now customary in auditorium acoustics to express Eq. (10.61) in terms of sound strength G [12]. Sound strength G , in decibels, is the ratio of the sound energy that comes from a nondirectional source ($Q = 1$) measured at a distance r in the auditorium to the same sound energy from the same source but measured in an anechoic chamber at $r = 10$ m. Thus, the reference sound pressure is

$$p_{ref}^2 = \frac{W\rho_0c}{4\pi \cdot 100} \quad (10.64)$$

Division of Eq. (10.62) by (10.64) and taking 10 log to get decibels yields the sound strength G :

$$G = 10 \log_{10} \left(\frac{100}{r^2} + \frac{1600\pi(1 - \alpha_{tot})}{S_{tot}\alpha_{tot}} \right) \text{dB}. \quad (10.65)$$

The reason α_{tot} is used here instead of α_{ey} because it has been found that if T is measured in an actual hall and if $S\alpha$ is determined from the Sabine formula ($T = 0.161V/S_{tot}\alpha_{tot}$) and if this value for $S\alpha$ is used in the G equation to calculate G , the calculated G equals the actual measured values of G in the hall very closely (when using the reverberation method of calibrating the standard dodecahedral source) (see Fig. 10.14). If the Eyring equation is used, this means that the $[-2.30 \log(1 - \alpha_{ey})]$ must be used and not just α_{ey} to calculate G . If α_{ey} is used, the calculated G will be about 2.5 dB higher than the measured G .

The second term in Eq. (10.65) would seem to indicate that the reverberant sound field is uniform in an auditorium, but SPLs measure larger in the front part of an auditorium than toward the rear (see Section 10.12). This term actually indicates the average of the SPLs determined from measurements at a large number of positions in the auditorium (with r large enough that the first term does not appreciably influence the second).

10.12 EARLY AND REVERBERANT SOUND IN CONCERT HALLS

It can be shown that the second term of Eq. (10.65) may be divided into two parts, one for early sound (that arriving within 80 ms of the direct sound) and the other for late (reverberant) sound (after 80 ms), both varying with distance r [13]. These equations are

$$E_{early} = \frac{31200T}{V} e^{-0.04r/T} \left(1 - e^{-1.11/T} \right), \quad (10.66)$$

$$E_{reverberant} = \frac{31200T}{V} e^{-0.04r/T} \left(e^{-1.11/T} \right). \quad (10.67)$$

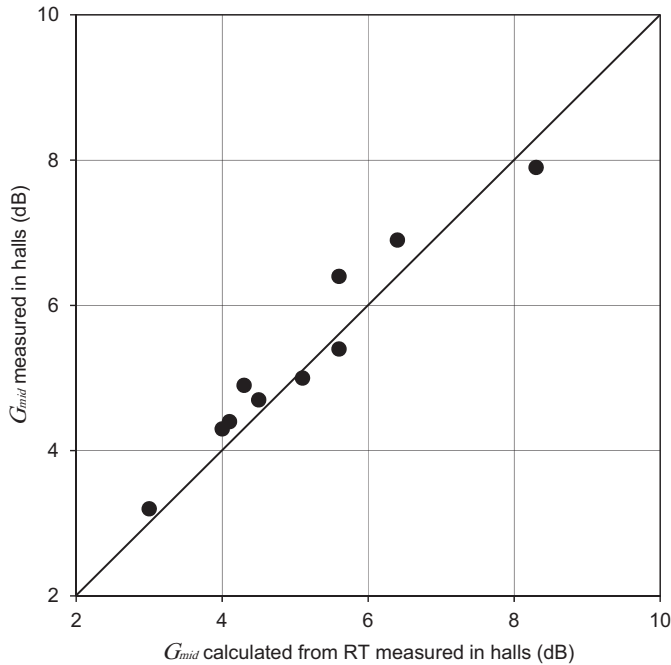


Figure 10.14 Values of G at middle frequencies measured in 10 concert halls (4 shoebox shaped, 4 surround, and 2 fan shaped) versus G_{mid} calculated from measurements of RT in these halls.

As an example, these equations, with $V = 20,000 \text{ m}^3$ and $T = 2 \text{ s}$, are plotted in Fig. 10.15. Zero on the ordinate is set for the direct sound with $r = 10 \text{ m}$. For r between 10 and 40 m, the top curve predicts the difference in $G(\text{total})$ to be 3.8 dB. Measurements made in nine shoebox-shaped halls, with average $V = 16,500 \text{ m}^3$ and $T = 2.5 \text{ s}$, found that for r between 10 and 40 m, $G(\text{total})$ drops about 2 dB, while in 11 surround halls, with average $V = 23,000 \text{ m}^3$ and $T = 2.2 \text{ s}$, it drops by about 5 dB. The quantity of 3.8 dB above for $V = 20,000 \text{ m}^3$ and $T = 2 \text{ s}$ is correctly between these two numbers. In addition, measurements show that the levels drop off faster if the reverberation times are less than about 1.5 s—the drop-off rate significantly increasing (nearer the drop in direct sound level) as RT's become less than 0.7 s.



10.13 DISTANCE FOR EQUALITY OF DIRECT AND REVERBERANT SOUND FIELDS

We will define the distance r_{rev} at which the reverberant field takes over as the distance at which the direct and reverberant fields are equal. Hence,

$$r_{rev} = \frac{1}{4} \sqrt{\frac{QS_{tot}\alpha_{tot}}{\pi(1 - \alpha_{tot})}}. \quad (10.68)$$

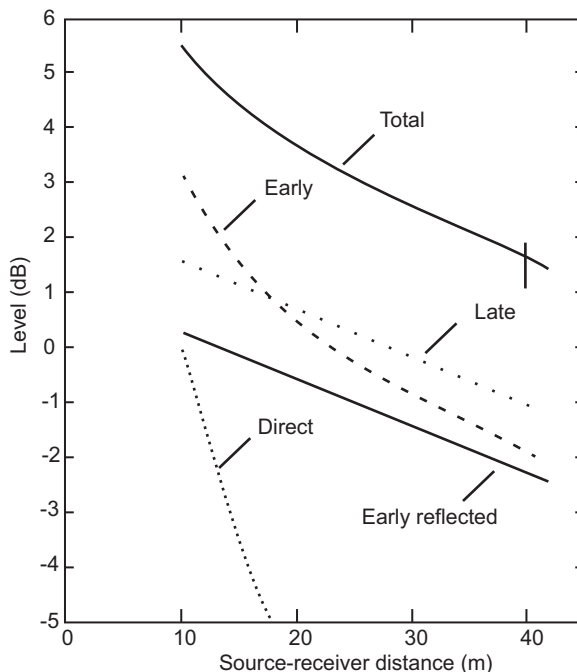


Figure 10.15 Calculation of the component values of G with $V = 20,000 \text{ m}^3$ and $T = 2 \text{ s}$. The reference sound pressure level at 10 m distance is 0 dB. “Total” at top is the sum of “Direct,” “Early Reflected,” and “Late.” “Early” is the sum of “Direct” and “Early Reflected.” “Early reflected” is from Eq. (10.66) and “Late” is from Eq. (10.67). From Barron M, Lee LJ. Energy relations in concert auditoriums. *J Acoust Soc Am* 1988;84(2):618–628.

The total absorbent area S_{tot} and absorption coefficient α_{tot} are both related to the volume of the auditorium. On average [8]

$$S_{tot} = 2.2V^{2/3}. \quad (10.69)$$

Let us also assume the reverberation time is the optimum value given by Eq. (10.63) and plotted in Fig. 10.13, and that we have a point source with $Q = 1$. From Eqs. (10.48) and (10.50),

$$\alpha_{tot} = \frac{0.161V}{S_{tot}T}, \quad \alpha_{ey} = 1 - e^{-0.161V/(S_{tot}T)} \quad (10.70)$$

We can now deduce the distance r_{rev} , which is shown in Fig. 10.16.

We note that r_{rev} will be greater for sources which are more directional than a point source ($Q > 1$). It is common to use directional loudspeakers such as horns or column arrays in more reverberant spaces where satisfactory speech intelligibility is needed. The reference distance is generally taken as 10 m, which is valid for even the larger concert halls.

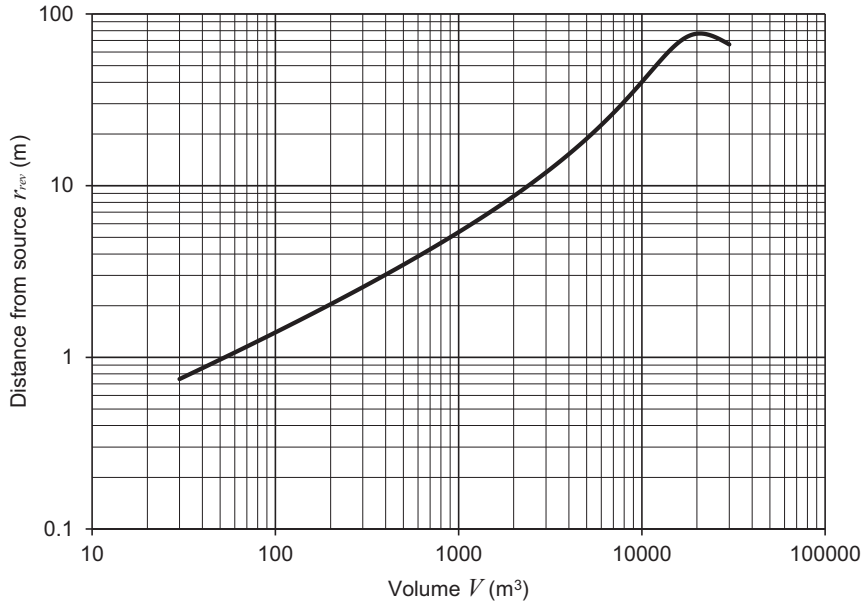


Figure 10.16 Distance r_{rev} from an omnidirectional source, at which the reverberant sound is equal to the direct sound, versus auditorium volume V . Optimum reverberation time T is assumed (see Fig. 10.13).

10.14 SOUND LEVELS FOR SPEECH AND MUSIC

When designing a sound system for a specific auditorium, we need to know how much sound pressure is required to produce realistic volumes for music or speech or both. The second column of Table 10.2 shows the maximum peak SPL at 10 m from various sources. However, conversational speech at such a distance is too quiet so the third column gives an SPL value adjusted for a distance of 1 m, which is more natural. The orchestra is adjusted for a distance of 3 m, which represents a good seat a few rows back from the stage. For speech, the crest factor (the difference between the maximum peak SPL and average rms SPL) is about 13 dB. For music, it is about 20 dB.

Knowing the required pressure from the third column of Table 10.2, S_{tot} from Eq. (10.69), and α_{ey} from Eq. (10.70), we can evaluate the acoustic power required [17] from Eq. (10.62) as follows:

$$W = \frac{4 \times 10^{(SPL/10)-10}}{\rho_0 c} \left(\frac{Q}{4\pi r_{ref}^2} + \frac{4(1 - \alpha_{ey})}{S_{tot} \alpha_{ey}} \right)^{-1}, \quad (10.71)$$

where $r_{ref} = 10$ m and the SPL value is taken from the third column of Table 10.2. The maximum peak acoustic power is plotted against auditorium volumes in Fig. 10.17. Of

Table 10.2 Maximum peak sound pressure levels (SPLs) due to various sound sources [14]

Sound source	Maximum peak SPL (dB) at 10 m from source	Maximum peak SPL (dB) adjusted for 1 m (conversational speech) and 3 m (others)
Conversational speech [15]	56	76
Declamatory speech [15]	67.5	78
Large orchestra [16]	92	102.5

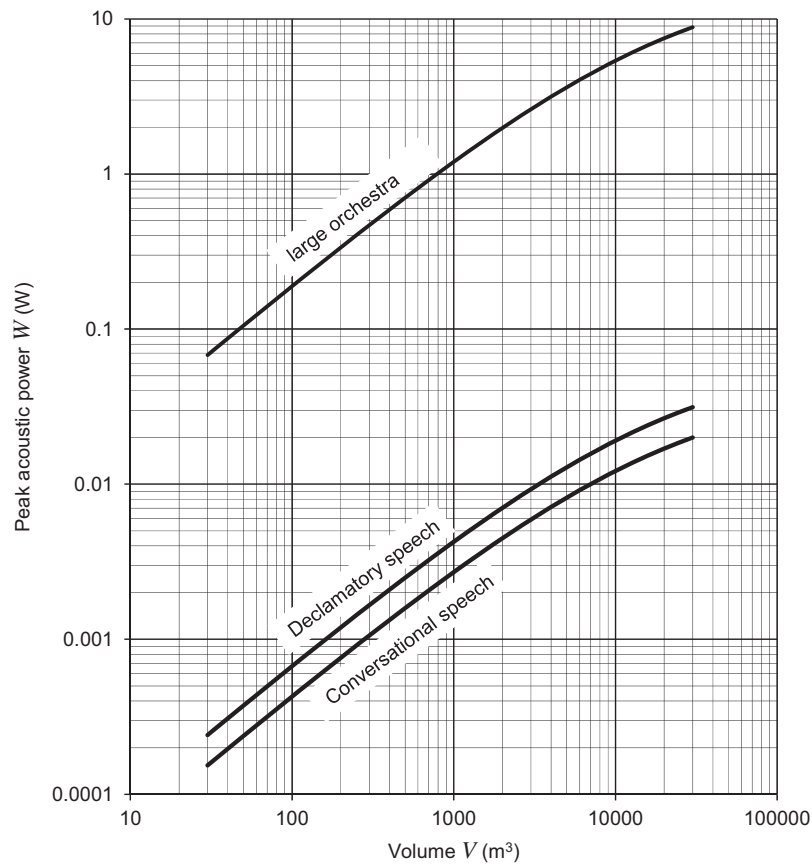


Figure 10.17 Peak acoustic power W versus auditorium volume V for various sound sources. Optimum reverberation time T is assumed (see Fig. 10.13). The maximum peak sound pressure levels are given in Table 10.2.

course, the required amplifier output power will depend on the choice of loudspeaker. For example, a living room with a volume of 60 m^3 will require a stereo amplifier with a power rating of 6 W per channel to reproduce a large orchestra if the loudspeakers have an efficiency of 1%. If loudspeakers with an efficiency of 10% can be employed, the power rating of the amplifier can be reduced to 0.6 W per channel.

Problem 10.1. An auditorium is 12.5 m long by 10 m wide by 8 m high. We assume all surfaces to be perfectly reflective except for those in the table below for which the Sabine absorption coefficients α_s are given.

Surface	Area (m^2)	α_s @ 500 Hz
Seating (half occupied)	100	0.7
Acoustic ceiling tiles	125	0.6
Drapes	32	0.5

Calculate the total volume V of the auditorium, the total absorptive area S_{tot} , the average Sabine absorption coefficient α_{tot} , the reverberation time T , sound strength G , the distance r_{rev} from a source to equal direct and reverberant fields, and the average Eyring absorption coefficient α_{ey} . Is the reverberation time optimum for the size of auditorium? Also, calculate the amplifier power needed in a sound system to reproduce the sound of a large orchestra assuming the loudspeakers have an efficiency of 0.5%.

REFERENCES

- [1] Hunt FV, Beranek LL, Maa DY. Analysis of sound decay in rectangular rooms. *J Acoust Soc Am* 1939;11:80–94.
- [2] Beranek LL. *Acoustic measurements*. New York: John Wiley & Sons, Inc; 1949. p. 329–36.
- [3] Eyring CF. Reverberation time in dead rooms. *J Acoust Soc Am* 1929;1:217–41.
- [4] Sabine WC. *Collected papers on acoustics*. Cambridge, MA: Harvard University Press; 1922.
- [5] Beranek LL. Analysis of sabine and eyring equations and their application to concert hall audience and chair absorption. *J Acoust Soc Am* 2006;120:1399–410.
- [6] MacNair WA. Optimum reverberation time for auditoriums. *J Acoust Soc Am* 1930;1(1):242–8.
- [7] Lifshitz S. Acoustics of large auditoriums. *J Acoust Soc Am* 1932;4:112–21.
- [8] Beranek L. *Concert halls and opera houses*. Springer; 2004.
- [9] Hidaka T, Nishihara N. Chamber music halls in Europe and Japan. *J Acoust Soc Am* 2004;116(1):357–72.
- [10] Amer. Nat'l. Standard (ANSI-S12.60). *Design requirements and guidelines for schools*. 2010.
- [11] Beranek LL. *Acoustics*. McGraw-Hill; 1954. p. 425. Fig. 13.25. The material here is from the literature and from the experience of Bolt, Beranek and Newman, consultants in acoustics.
- [12] Beranek LL. The sound strength parameter G and its importance in evaluating and planning the acoustics of halls for music. *J Acoust Soc Am* 2011;129(5):3020–6.
- [13] Barron M, Lee LJ. Energy relations in concert auditoriums. *J Acoust Soc Am* 1988;84(2):618–28.

- [14] Fletcher H. Hearing, the determining factor for high-fidelity transmission. Proc IRE 1942;20:266–77.
- [15] Beranek LL. The design of speech communication systems. Proc IRE 1947;35:880–90.
- [16] Hidaka T Nishihara N, From unpublished data relating to Suntory Hall, Tokyo, which has $V = 21000 \text{ m}^3$, $S_{tot} = 6674 \text{ m}^2$, and $T = 2 \text{ s}$. Hence $a_{ey} = 0.221$. Although readings were taken at 34 m, similar levels can be expected at 10 m because it is still beyond the r_{eq} distance of 7.5 m.
- [17] Hopkins HF, Stryker NR. A proposed loudness–efficiency rating for loudspeakers and the determination of system power requirements for enclosures. Proc IRE 1948;36:315–35 [Modified with more recent data].

FURTHER READING

- [1] Barron M. Auditorium acoustics and architectural design. Spon Press; 2010.



Room design for loudspeaker listening

In the light of various caveats about room and loudspeaker design, there are no precise answers to the questions: “What precautions should be taken in typical living rooms toward making listening to recorded music over loudspeakers as pleasant as possible?” and “How should loudspeaker outputs be adjusted to go with different room characteristics?” Sean Olive et al. [1] boldly state “Given that today the sound quality of commercial phonograph recordings remains highly variable, there are always opportunities for good room corrections to sound bad and for bad room corrections to sound good.” Added to this is what some call “Beranek’s Law” [2]: “If one selects his own components, builds his own loudspeaker enclosure, and is convinced he made a wise choice of design, then his own loudspeaker sounds better to him than does anyone else’s loudspeaker.”

The following discussion is offered as a general guide to listening to recorded music with loudspeakers located in a living room.



PART XXXII: HOME ROOM DESIGN



11.1 CONCERT HALL ACOUSTICS

Because listening to music in your home is an alternative to listening to music in a concert hall, the acoustical factors that make a concert hall satisfactory must be considered when planning room and loudspeaker configurations. These concert hall factors include direct sound, loudness, adequacy of bass, degree of source spreading, reverberation time, strength and quality of the reverberant field, envelopment, freedom from distortion, freedom from echoes, and quietness.

Direct sound

Wherever one sits in a concert hall, the direct sound should be clearly heard before the energy in early reflections and reverberation have risen to the level that starts masking that sound. Freedom from masking of the direct sound is particularly important in the frequency region above 700 Hz. If the direct sound is not clearly heard, the music lacks impact and the listener may tend to go to sleep. This problem is particularly important in shoebox-shaped halls with small seating capacities because the sidewalls that reflect early sound are nearer to the listener, which means that the reflections start masking the direct

sound sooner. One possible design for a hall with limited seating is to make it fan shaped. This way, all listeners are nearer the stage, and the sidewalls do not reflect early sound toward the audience areas. In Boston Symphony Hall, which is shoebox-shaped, the statues and niches and edges of high-up windows reflect sound above 700 Hz back toward the stage, which decreases the energy that would otherwise reflect from the sidewalls and thus preserves audibility of the direct sound.

Loudness

In a concert hall, the music must be loud enough as measured by the quantity Sound Strength G in dB. The magnitude of G is determined by the total overall sound-absorbing quantities of the audience, sidewalls, ceiling, and performers on stage. The greater their absorption, the lesser is G .

Loudness of the bass sounds

A common complaint in concert halls is inadequate loudness of the bass sounds. A measure of bass loudness is a quantity called Bass Index, which is the strength of the sound G in the 125 Hz octave frequency band *minus* the strength of the sound at midfrequencies (average of the strength G in the 500 and 1000 Hz bands). Generally, if the walls are adequately heavy and the absorption of the audience seats at low frequencies is not too high, the bass loudness will be satisfactory.

Degree of source spreading

The sound in a concert hall is more pleasant if there are early reflections that come from lateral directions—the sidewalls in a shoebox-shaped hall. Early lateral reflections spread the source, which results in a fuller tone. Of course, these reflections must not come so soon as to mask the direct sound, but they must occur in the interval between 30 and 80 ms after arrival of the direct sound. The optimum shoebox-hall width for meeting this requirement is about 24 m. It is difficult to achieve sufficient early lateral reflections in halls where the audience surrounds the orchestra. In fan-shaped halls, early lateral reflections are nonexistent.

Reverberation time

Reverberation is part of the music that one hears in a concert hall. No symphonic piece sounds good outdoors where there is no reverberation. Optimum reverberation time for the current symphonic repertoire is 1.8–2.1 s. For chamber music, the optimum time is 1.5–1.7 s. Reverberation does not contribute to loudness.

Strength and quality of the reverberant sound field

The quality of the reverberant field is enhanced if there are substantial irregularities on the sidewalls and ceiling. In some halls, this is accomplished by niches on the sidewalls

above the top balcony and by coffered in the ceiling. These irregularities must be of depths of up to 0.5 m. Such great depths are not desirable below the upper balcony because lateral sound reflections of high quality are needed from there.

Envelopment

In the best halls, the audience feels enveloped by the reverberant sound. This is a matter of the strength G of the reverberant sound measured 80 ms after arrival of the direct sound—the higher the strength, the greater the envelopment. However, the design of concert halls of the future may be influenced by a trend in modern phonograph recordings. In these, some of the recording microphones are placed near the performers. The others record the reverberant sound. The relative strength of the two is then adjusted by the tonmeister and the tendency is to make the strength of the reverberant field relative to the direct sound lower than is experienced in the actual concert hall. The strength of the reverberant sound field may be reduced in a hall by adding appropriate sound absorption materials in the sidewalls and ceiling.

Freedom from distortion, noise, and echoes

It almost goes without saying that these must be avoided in a concert hall. Distortion can come from repetitive small-scale irregularities on the sidewalls below the top balcony. This is sometimes called the “picket fence” effect. Noise generally comes from the ventilating system. Echoes are easy to identify in computer simulation of a hall during the planning stage.



11.2 LISTENING ROOM ACOUSTICS

Typical space

The typical American living room has dimensions of, say, 7×9 m with a ceiling height of 2.7 m. Window frames, draperies, and pictures on the walls provide diffusion of the sound field at high frequencies, but at frequencies below 1000 Hz, the sound field is generally not diffused. The reverberation times are often greatly different at different frequencies depending on the sound absorption qualities of furniture, wall hangings, and carpets.

Reverberation times

There is general agreement that reverberation times at midfrequencies (500 and 1000 Hz octave frequency bands) should not exceed 0.5 s, and at low frequencies (62 and 125 Hz bands), it may rise somewhat, say, to 1.25 times that at midfrequencies. Control of the low-frequency sound is possible by selecting heavily upholstered furniture. In other words, the room should neither sound “dead” nor very reverberant, partly because the reverberation time of the recorded sound should come through in its pristine form.

Loudness

Loudness is generally not a problem because the amplification of the playback system is easily adjustable.

Placement of loudspeakers

Of course, the answer to this question depends on the system purchased. A five-loudspeaker system will be handled differently from a two- or three-speaker system. Let us first talk about the interaction of room resonances with loudspeaker location.

The four lowest modes of vibration in the above-mentioned typical living room will have frequencies of 19.2, 24.5, 31.2, and 38.4 Hz. These will only be excited if the loudspeaker is put in the corner of the room. Even if the loudspeaker is in the corner, the listener would also have to be in another corner to hear those resonances. If either the loudspeaker or the listener is located in the center of the room, the four lowest modes that the listener would hear would be double in frequency, 38.2, 49, 62.4, and 76.4 Hz. Because neither the listener nor the loudspeaker will likely be in either place, the frequencies of the first four modes that are heard will probably lie between about 30 and 60 Hz.

From Fig. 11.1, we see that the lowest note of the double bass is 41 Hz and that of the cello is 65 Hz, so these notes may be better served by their harmonics. It is well known that if the harmonics of a musical note are heard, the hearing mechanism will supply the missing fundamentals.

If the typical five- or six-loudspeaker system is employed, the woofer will be at the front of the room and the others will circle the listener. In this case, the question arises as to the directivity characteristics of the side and rear loudspeakers.

Directivity of loudspeakers above the cutoff frequency

This category includes all loudspeakers surrounding the listener. Some listeners prefer the sound to come from loudspeakers that have relatively narrow directivity patterns at all of these frequencies. The reason is that they wish to hear only the sound that is recorded. If the patterns are broad, they will overlap in the room, and the recorded sounds from the different loudspeakers will arrive at different times, and a “smearing” effect results. Others feel that the smear is equivalent to increased “envelopment,” which they feel is a good thing.

Some subjective tests

There are electrical systems that are sold to “correct” the reproduced sound in the room. Olive et al. [1] made subjective tests of several such electrical systems. For the tests, they used a high-quality loudspeaker operating above a crossover frequency at 80 Hz and a high-quality subwoofer. The woofer was located in a left-front corner, and the other

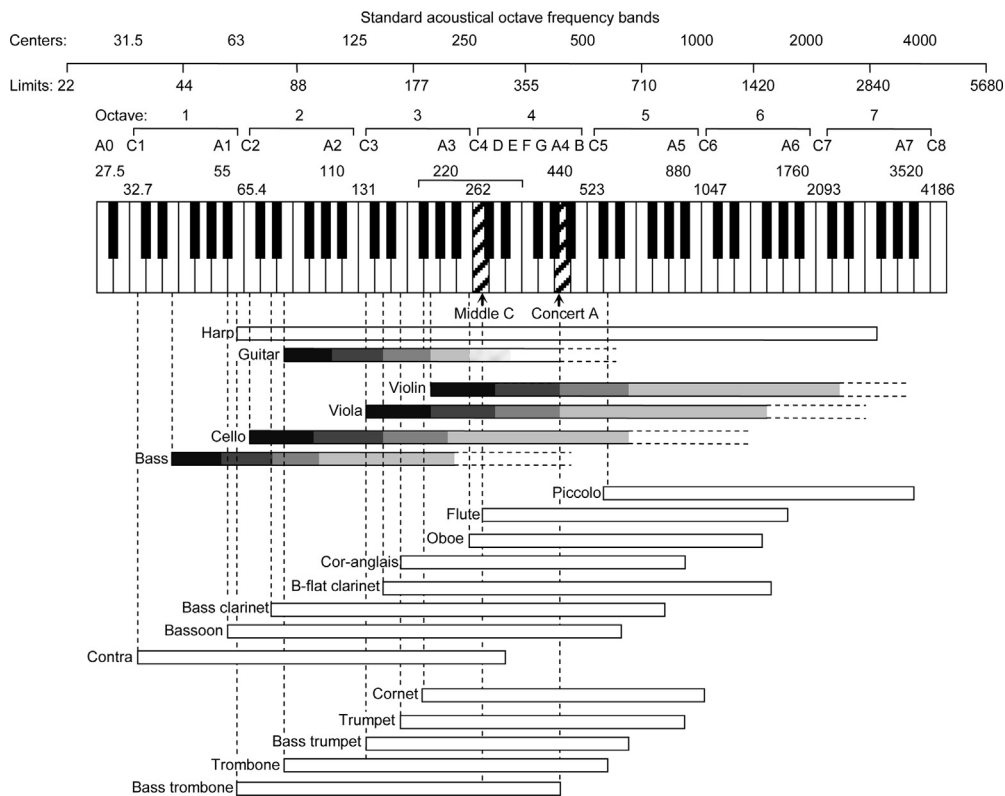


Figure 11.1 Musical scale.

loudspeaker was located in a direction about halfway between the center of the room and the location of the woofer. Eight subjects were seated on chairs in the center. The reverberation time for the room was 0.4 s, and the levels for all of the correcting systems being compared were adjusted to be the same as determined by dBA measurements at the listening positions.

According to the test subjects, the most preferred systems had the flattest spectral balances and they were rated as “full and neutral.” This could be accomplished by rolling off the response below the cutoff frequency by, say, 6 dB per octave, to compensate for the rise in reverberation time and loudness owing to uneven sound absorption in the listening room. The lowest preferred systems were rated as “colored, harsh, and thin.” Surprisingly, the best-rated systems had a downward-sloping frequency response toward the high end of the frequency spectrum.

A more elaborate system was described in some detail in the *Science Times* section of the *New York Times* (9/6/2011) as providing sound of the quality heard in the best shoebox-shaped halls. To quote with some editing, the company Audyssey in Los Angeles said “That listening tests showed that speakers directly ahead and to either side of

the listener provided the most attractive sound stage. The ‘wide speakers’ mimicked the reflections from the side walls of a concert hall. For ‘depth of stage’, listeners preferred speakers in front and high above. This sound—also slightly delayed—gave a sense of where the different instruments were. For full concert-hall-effect three speakers were in front; two were elevated; two were wide; two were slightly behind, and two were directly behind.’ Of course a subwoofer in the corner of the room was used. It was emphasized that the levels had to be adjusted so that a flat frequency response was achieved at the listeners’ positions. No mention was made of how the loudspeakers were driven by present-day symphonic recordings.

Concluding remarks

There is not much more to be said. When setting up a listening system, it is recommended that a suitable room-correction system be used to obtain the best response of the combined room/loudspeaker system.

REFERENCES

- [1] Olive SE, Jackson J, Devantier A, Hunt D, Hess SM. The subjective and objective evaluation of room correction products, in the 127th AES convention. 2009. Paper No. 7960.
- [2] Beranek LL. Acoustics. McGraw-Hill; 1954. p. 208.



Radiation and scattering of sound by the boundary value method

In this chapter and the next, we will derive results that were used in previous chapters to study transducers and their radiation characteristics. The aim is to provide insight into how the shape of a transducer determines its behavior as well as an understanding of how to solve acoustical problems analytically. In each problem, a new concept or method is introduced so that each problem is slightly more complicated than the previous one. Formulas are given which the interested reader may use as part of his or her own simulations. In this chapter, we will take the wave equation solutions of Chapter 2 and apply the appropriate boundary conditions to them to determine the unknown coefficients. This is known as the boundary value method. In fact, we have already used this method to solve for the reflection of a plane wave from a plane in Section 4.9, radiation from a pulsating sphere in Section 4.10, and an oscillating sphere Section 4.15. In Chapter 13, we will treat sound sources as arrays of point sources, which are integrated using the boundary integral method.



PART XXXIII: RADIATION IN CYLINDRICAL COORDINATES



12.1 RADIATION FROM A PULSATING INFINITE CYLINDER

The infinitely long pulsating cylinder is a useful model for vertical loudspeaker arrays. If the height of the array is much greater than the wavelength of the sound being radiated, then we can use a two-dimensional model of infinite extent. Because of axial symmetry, it can be treated as a one-dimensional problem with just a single radial ordinate w .

Pressure field

Because the cylinder is radiating into free space, where there are no reflections, we take the outward-going part of the solution to the cylindrical wave Eq. (2.125) given by Eq. (2.129), where \tilde{p}_+ is an unknown coefficient to be determined from the

boundary conditions. Let us now impose a boundary condition at the surface of the cylinder whereby the particle velocity normal to the surface, given by Eq. (2.130), is equal to the uniform surface velocity \tilde{u}_0 so that $\tilde{u}(a) = \tilde{u}_0$, where a is the radius, which gives

$$\tilde{p}_+ = \frac{j\rho_0 c \tilde{u}_0}{H_1^{(2)}(ka)}. \quad (12.1)$$

Inserting this into Eq. (2.129) and substituting $\tilde{U}_0/l = 2\pi a \tilde{u}_0$, where \tilde{U}_0/l is the total volume velocity per unit length, yields

$$\tilde{p}(w) = \frac{j\rho_0 c (\tilde{U}_0/l)}{2\pi a H_1^{(2)}(ka)} H_0^{(2)}(kw). \quad (12.2)$$



12.2 RADIATION FROM AN INFINITE LINE SOURCE

In the limit as the radius of the cylinder shrinks to zero, we have an infinite line source. In Section 13.14, we will use this as a building block for an infinite ribbon, which can be treated as an array of line sources using the Huygens–Fresnel principle. When the radius is very small, we find that

$$H_1^{(2)}(ka)|_{a \rightarrow 0} = \frac{2j}{\pi ka}, \quad (12.3)$$

which, after inserting into Eq. (12.2), gives the pressure field of an infinite line source:

$$\tilde{p}(w) = \frac{k\rho_0 c (\tilde{U}_0/l)}{4} H_1^{(2)}(kw). \quad (12.4)$$

In the far field, we find that

$$H_1^{(2)}(kw)|_{w \rightarrow \infty} = \sqrt{\frac{2}{\pi kw}} e^{-j(kw - \frac{\pi}{4})}, \quad (12.5)$$

so that the far-field pressure for a line source is given by

$$\tilde{p}(w) = \frac{\rho_0 c (\tilde{U}_0/l)}{2} \sqrt{\frac{k}{2\pi w}} e^{-j(kw - \frac{\pi}{4})}. \quad (12.6)$$

Interestingly, the far-field pressure given by Eq. (12.6) varies with the inverse square root of the radial distance w from the source so that the sound pressure falls by 3 dB for

every doubling of distance, which is a characteristic of cylindrically diverging waves. This is in contrast to a spherically diverging wave, where the pressure given by Eq. (2.142) varies with the inverse square of the radial distance r from the source so that the SPL falls by 6 dB for every doubling of distance. Hence, line sources, in the form of vertical stacks of loudspeakers, are popular in auditoriums because they give a more uniform sound pressure distribution.

PART XXXIV: RADIATION AND SCATTERING IN SPHERICAL COORDINATES

12.3 SCATTERING OF A PLANE WAVE FROM A RIGID SPHERE

In this example, the expression *scattering* has been applied rather than *reflection* because not only does a sphere reflect sound but sound waves can bend around it, a phenomenon known as *diffraction*. Generally, scattering refers to a mixture of reflection and diffraction. In the case of reflection from a plane (see Section 4.9), we used rectangular coordinates in x and y . Here, we are considering a sphere [1], so it is convenient to use axially symmetrical spherical coordinates in r and θ as shown in Fig. 12.1. In general, the solution for the *resultant field* is the sum of the *incident field* in the absence of any obstacle and the *scattered field* which is that which would be produced if the obstacle itself were radiating with a notional surface velocity which is normal to its surface. If the object is rigid, this notional velocity must be equal and opposite to the component of velocity of the incident wave that is normal to the surface of the obstacle in its absence. The result of this is to produce zero net velocity normal to the surface of the obstacle when it is present in the resultant field. Because the incident wave front arrives at different parts of the surface at different times, the normal surface velocity varies in magnitude and phase over θ , except when the wavelength is very large compared with the diameter of the sphere, in which case it behaves as a simple omnidirectional source or pulsating sphere as discussed in Section 4.10.

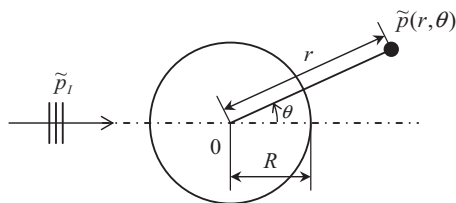


Figure 12.1 Geometry of plane wave and sphere.

Incident field

In spherical coordinates, the incident plane wave pressure is

$$\tilde{p}_I(r, \theta) = \tilde{p}_0 e^{-jkr \cos \theta}. \quad (12.7)$$

Fortunately, this expression can be expanded in terms of spherical Bessel functions j_n and Legendre functions P_n as follows:

$$\tilde{p}_I(r, \theta) = \tilde{p}_0 \sum_{n=0}^{\infty} (-j)^n (2n+1) j_n(kr) P_n(\cos \theta). \quad (12.8)$$

This expression, which is similar in form to Eq. (2.199) for the solution to the wave equation in spherical coordinates, is treated more rigorously later in the derivation of Eq. (13.63).

Scattered field

We assume that the pressure field scattered from the sphere is a solution to Eq. (2.180), the Helmholtz wave equation in spherical coordinates. However, due to axial symmetry, we can ignore Eq. (2.197) for the azimuthal part of the solution. Furthermore, because the sphere is in free space, there are no waves reflected back toward the sphere (Sommerfeld condition). Hence, we can take just the outward-traveling part of Eq. (2.186) for the radial part of the solution. Combining this with Eq. (2.195) for the inclinational part of the solution gives

$$\tilde{p}_s(r, \theta) = \tilde{p}_0 \sum_{n=0}^{\infty} A_n h_n^{(2)}(kr) P_n(\cos \theta), \quad (12.9)$$

where A_n are unknown series coefficients that are determined by applying appropriate boundary conditions.

Resultant field

Using the principle of *superposition of fields*, we now express the resultant field $\tilde{p}(r, \theta)$ as the sum of the incident and scattered fields:

$$\tilde{p}(r, \theta) = \tilde{p}_I(r, \theta) + \tilde{p}_s(r, \theta). \quad (12.10)$$

At the rigid surface of the sphere, where $r = R$, we have the boundary condition of zero normal velocity. Hence, from Eq. (2.4a), the pressure gradient must also be zero:

$$\frac{\partial}{\partial r} \tilde{p}(r, \theta)|_{r=R} = 0, \quad (12.11)$$

so that

$$\frac{\partial}{\partial r} \tilde{p}_s(r, \theta)|_{r=R} = -\frac{\partial}{\partial r} \tilde{p}_I(r, \theta)|_{r=R}. \quad (12.12)$$

What this equation tells us is that the scattered field is that which would be produced if the surface of the sphere itself were oscillating with a velocity equal and opposite to the normal velocity of the incident wave at the surface in the absence of the sphere. Inserting the expressions for \tilde{p}_s and \tilde{p}_I from Eqs. (12.9) and (12.8), respectively, into Eq. (12.12) gives

$$\sum_{n=0}^{\infty} A_n h_n^{(2)}(kR) P_n(\cos \theta) = -\sum_{n=0}^{\infty} (-j)^n (2n+1) j_n'(kR) P_n(\cos \theta), \quad 0 \leq \theta \leq \pi, \quad (12.13)$$

where

$$j_n'(kR) = \frac{\partial}{\partial r} j_n(kr)|_{r=R} = \frac{k}{2n+1} (nj_{n-1}(kR) - (n+1)j_{n+1}(kR)), \quad (12.14)$$

$$h_n^{(2)}(kR) = \frac{\partial}{\partial r} h_n^{(2)}(kr)|_{r=R} = \frac{k}{2n+1} (nh_{n-1}^{(2)}(kR) - (n+1)h_{n+1}^{(2)}(kR)). \quad (12.15)$$

Straight away, by matching the coefficients of $P_n(\cos \theta)$ on both sides of Eq. (12.13), we can see that the unknown coefficients A_n are given by

$$A_n = -(-j)^n (2n+1) \frac{j_n'(kR)}{h_n^{(2)}(kR)}. \quad (12.16)$$

Inserting Eq. (12.16) into Eq. (12.9) gives the scattered field as

$$\tilde{p}_s(r, \theta) = -\tilde{p}_0 \sum_{n=0}^{\infty} (-j)^n (2n+1) \frac{j_n'(kR)}{h_n^{(2)}(kR)} h_n^{(2)}(kr) P_n(\cos \theta). \quad (12.17)$$

The resultant field $\tilde{p}(r, \theta)$ is then given by Eq. (12.10) using Eq. (12.7) for $\tilde{p}_I(r, \theta)$ and Eq. (12.17) for $\tilde{p}_s(r, \theta)$. The magnitude of the normalized pressure $|\tilde{p}(w, z)/\tilde{p}_0|$ is plotted in Figs. 12.2 and 12.3 in cylindrical coordinates w and z where $r = \sqrt{w^2 + z^2}$ and $\cos \theta = z/\sqrt{w^2 + z^2}$. It can be seen from Fig. 12.2 that the incident field is hardly disturbed at all when $kR = 0.1$, i.e., when the wavelength is much greater than its circumference. On the other hand, at the other end of the spectrum, the plot for $kR = 10$ in Fig. 12.3 tells us that there are significant interference patterns in the vicinity of the sphere when the wavelength is considerably shorter than the circumference of the sphere.

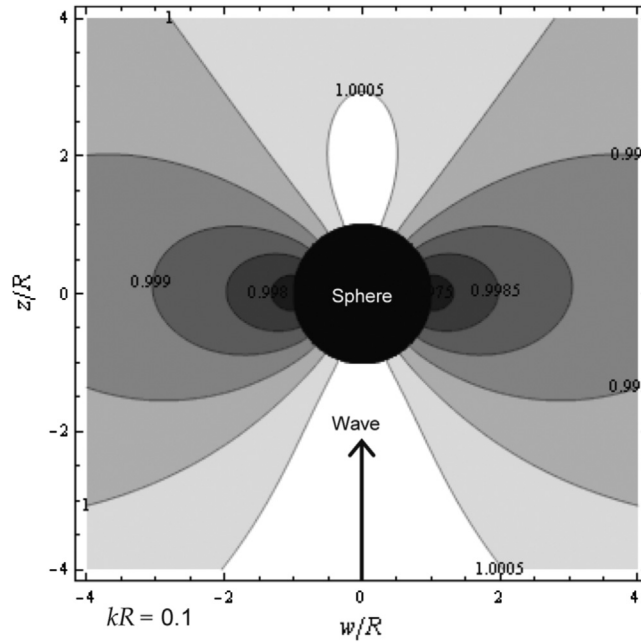


Figure 12.2 Resultant pressure field $|\tilde{p}(w, z)|/\tilde{p}_0$ due to the scattering of a plane wave from a sphere for $kR = 0.1$. The arrow shows the direction of the incident wave.

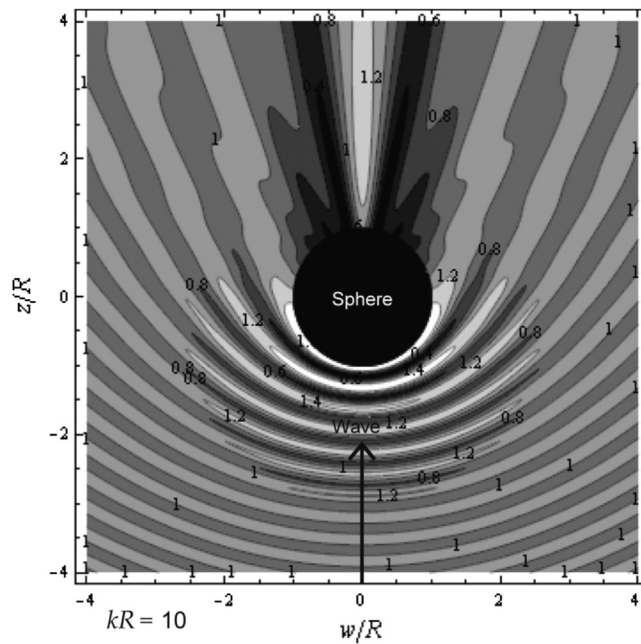


Figure 12.3 Resultant pressure field $|\tilde{p}(w, z)|/\tilde{p}_0$ due to the scattering of a plane wave from a sphere for $kR = 10$. The arrow shows the direction of the incident wave.

Far-field pressure

As the distance r from the center of the sphere is increased to many wavelengths, the asymptotic expression for the spherical Hankel function becomes

$$h_n^{(2)}(kr)|_{r \rightarrow \infty} = \frac{j^{n+1}}{kr} e^{-jkr}. \quad (12.18)$$

Inserting this into Eq. (12.17) yields

$$\tilde{p}_s(r, \theta)|_{r \rightarrow \infty} = \frac{-jR \tilde{p}_0}{2r} e^{-jkr} D(\theta), \quad (12.19)$$

where $D(\theta)$ is a directivity function given by

$$D(\theta) = \frac{2}{kR} \sum_{n=0}^{\infty} (2n+1) \frac{j_n'(kR)}{h_n^{(2)'}(kR)} P_n(\cos \theta). \quad (12.20)$$

The directivity pattern $20 \log_{10}(D(\theta)/D(0))$ is plotted in Fig. 12.4 for various values of kR .

Let a reflection coefficient be defined by

$$D(\pi) = \frac{2}{kR} \sum_{n=0}^{\infty} (-1)^n (2n+1) \frac{j_n'(kR)}{h_n^{(2)'}(kR)} \approx \begin{cases} -5jk^2R^2/3, & kR < 0.5 \\ -1, & kR > 2, \end{cases} \quad (12.21)$$

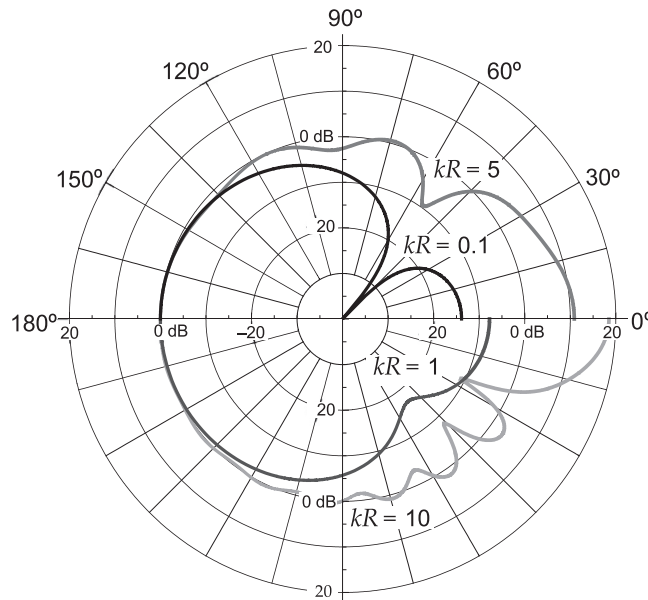


Figure 12.4 Directivity pattern $20 \log_{10}(|D(\theta)|/|D(\pi)|)$ of the far-field pressure due to the scattering of a plane wave from a rigid sphere (excluding the incident field).

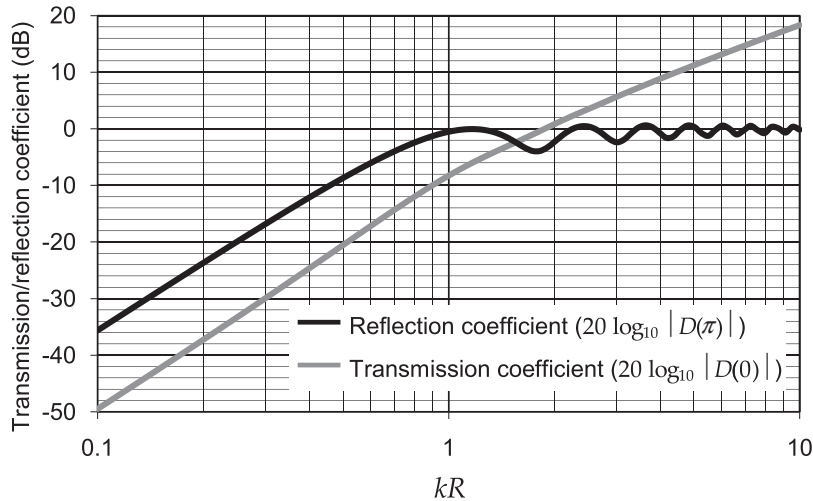


Figure 12.5 Transmission and reflection coefficients for the scattering of a plane wave by a rigid sphere.

where we have used the identity $P_n(-1) = (-1)^n$. Similarly, let a transmission coefficient be defined by

$$D(0) = \frac{2}{kR} \sum_{n=0}^{\infty} (2n+1) \frac{j'_n(kR)}{h_n^{(2)}(kR)} \approx \begin{cases} jk^2 R^2 / 3, & kR < 0.5 \\ kR, & kR > 10, \end{cases} \quad (12.22)$$

where we have used the identity $P_n(1) = 1$. These reflection and transmission coefficients are plotted against kR in Fig. 12.5.

For small values of kR , the transmission and reflection coefficients are both fairly weak. We see that, above $kR = 2$, the reflection coefficient remains virtually constant, whereas the transmission coefficient shows that energy is concentrated in the direction of the incident wave. This can also be seen from Fig. 12.3. This may seem somewhat counterintuitive because one might expect an obstacle to cast a shadow at high frequencies, and we will see later that this is indeed the case when the obstacle is planar. However, in this case, the smooth continuous contours of the sphere enable sound waves to be diffracted around it at high frequencies. The fact that higher frequency waves are scattered more than lower frequency ones is also true for light, which explains why the sky is blue.



12.4 SCATTERING FROM A RIGID SPHERE BY A POINT SOURCE

Refer to Fig. 12.6. Let a point source of volume velocity \tilde{U}_0 be located at a distance d from a sphere of radius R . We wish to calculate the resultant pressure field

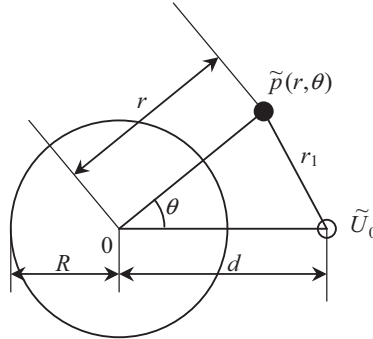


Figure 12.6 Geometry of point source and sphere.

$\tilde{p}(r, \theta)$ at a distance r from the center of the sphere and at an angle θ with the axis passing through the point source and center of the sphere. The distance r_1 between the observation point and the point source is given by

$$r_1 = \sqrt{r^2 + d^2 - 2rd \cos \theta}. \quad (12.23)$$

Incident field

In spherical coordinates, the incident pressure field due to the point source is obtained by substituting $r = r_1$ in Eq. (4.71) to give

$$\tilde{p}_I(r, \theta) = jk\rho_0c\tilde{U}_0 \frac{e^{-jkr_1}}{4\pi r_1}. \quad (12.24)$$

This expression can be expanded in terms of spherical Bessel functions j_n and Legendre functions P_n from Eq. (13.68) as follows:

$$\tilde{p}_I(r, \theta) = \frac{k^2\rho_0c\tilde{U}_0}{4\pi} \sum_{n=0}^{\infty} (2n+1)h_n^{(2)}(kd)j_n(kr)P_n(\cos \theta), \quad r \leq d. \quad (12.25)$$

Scattered field

As in the case of the previous problem of the plane wave and a sphere, we assume that the pressure field scattered from the sphere is a general axisymmetric solution to Eq. (2.180), the Helmholtz wave equation in spherical coordinates:

$$\tilde{p}_s(r, \theta) = \frac{\rho_0c\tilde{U}_0}{4\pi R^2} \sum_{n=0}^{\infty} A_n h_n^{(2)}(kr)P_n(\cos \theta), \quad (12.26)$$

where A_n are unknown series coefficients that are determined by applying appropriate boundary conditions. However, this time the solution is in terms of the source volume

velocity instead of pressure. To keep the coefficients A_n dimensionless, the volume velocity has been converted into a particle velocity by dividing it by the surface area of the sphere $S = 4\pi R^2$ and then converted into a pressure term by multiplying it by the specific acoustic impedance of free space $\rho_0 c$.

Resultant field

Using the principle of superposition of fields, we now express the resultant field $\tilde{p}(r, \theta)$ as the sum of the incident and scattered fields:

$$\tilde{p}(r, \theta) = \tilde{p}_1(r, \theta) + \tilde{p}_s(r, \theta). \quad (12.27)$$

At the rigid surface of the sphere, where $r = R$, we have the boundary condition of zero normal velocity. Hence, from Eq. (2.4a), the pressure gradient must also be zero:

$$\frac{\partial}{\partial r} \tilde{p}(r, \theta)|_{r=R} = 0, \quad (12.28)$$

so that

$$\frac{\partial}{\partial r} \tilde{p}_s(r, \theta)|_{r=R} = -\frac{\partial}{\partial r} \tilde{p}_I(r, \theta)|_{r=R}, \quad (12.29)$$

which, after inserting the expressions for \tilde{p}_s and \tilde{p}_I from Eqs. (12.26) and (12.25), respectively, gives

$$\sum_{n=0}^{\infty} A_n h_n^{(2)}(kR) P_n(\cos \theta) = -k^2 R^2 \sum_{n=0}^{\infty} (2n+1) h_n^{(2)}(kd) j_n'(kR) P_n(\cos \theta),$$

$$0 \leq \theta \leq \pi, \quad (12.30)$$

where

$$j_n'(kR) = \frac{\partial}{\partial r} j_n(kr)|_{r=R} = \frac{k}{2n+1} (n j_{n-1}(kR) - (n+1) j_{n+1}(kR)), \quad (12.31)$$

$$h_n^{(2)}(kR) = \frac{\partial}{\partial r} h_n^{(2)}(kr)|_{r=R} = \frac{k}{2n+1} (n h_{n-1}^{(2)}(kR) - (n+1) h_{n+1}^{(2)}(kR)). \quad (12.32)$$

Straight away, by matching the coefficients of $P_n(\cos \theta)$ on both sides of Eq. (12.30), we can see that the unknown coefficients A_n are given by

$$A_n = -k^2 R^2 (2n+1) h_n^{(2)}(kd) \frac{j_n'(kR)}{h_n^{(2)}(kR)}. \quad (12.33)$$

Inserting Eq. (12.33) into Eq. (12.26) gives the scattered field as

$$\tilde{p}_s(r, \theta) = -k^2 R^2 \rho_0 c \tilde{U}_0 \sum_{n=0}^{\infty} (2n+1) h_n^{(2)}(kd) \frac{j_n'(kR)}{h_n^{(2)'(kR)} h_n^{(2)}(kr)} P_n(\cos \theta), \quad (12.34)$$

where $S = 4\pi R^2$ is the total surface area of the sphere. The resultant field $\tilde{p}(r, \theta)$ is then given by Eq. (12.27) using Eq. (12.24) for $\tilde{p}_I(r, \theta)$ and Eq. (12.34) for $\tilde{p}_s(r, \theta)$. We see that the resultant field obeys the principle of *reciprocity* in that it is not affected by exchanging the source and observation point, which can be verified by exchanging d and r in Eqs. (12.24) and (12.34). We will apply this principle in Section 13.3. The magnitude of the normalized pressure,

$$|S\tilde{p}(w, z)/(\rho c \tilde{U}_0)|,$$

is plotted in Figs. 12.7 and 12.8 in cylindrical coordinates w and z where

$$r = \sqrt{w^2 + z^2} \quad \text{and} \quad \cos \theta = z / \sqrt{w^2 + z^2}.$$

It can be seen from Fig. 12.7 that the incident field is hardly disturbed at all when $kR = 0.1$, i.e., when the wavelength is much greater than the circumference of the sphere, except that the constant pressure contours are distorted slightly so that they

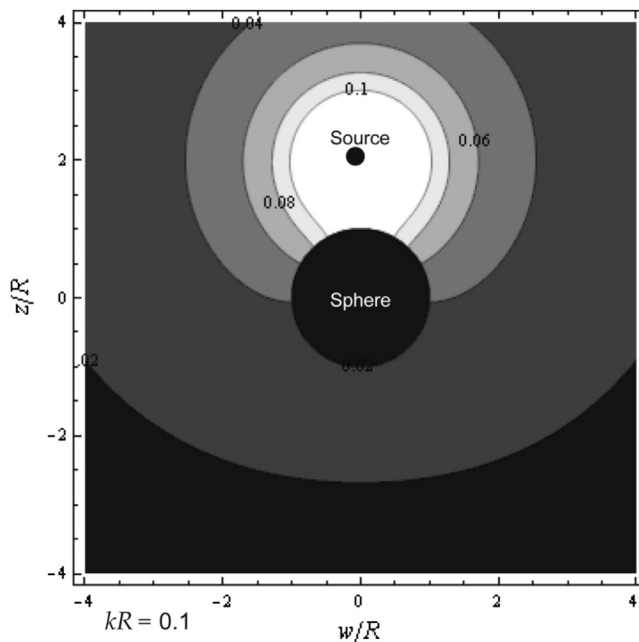


Figure 12.7 Resultant pressure $|S\tilde{p}(w, z)/\rho c \tilde{U}_0|$ field due to the scattering of a point source from a rigid sphere for $kR = 0.1$.

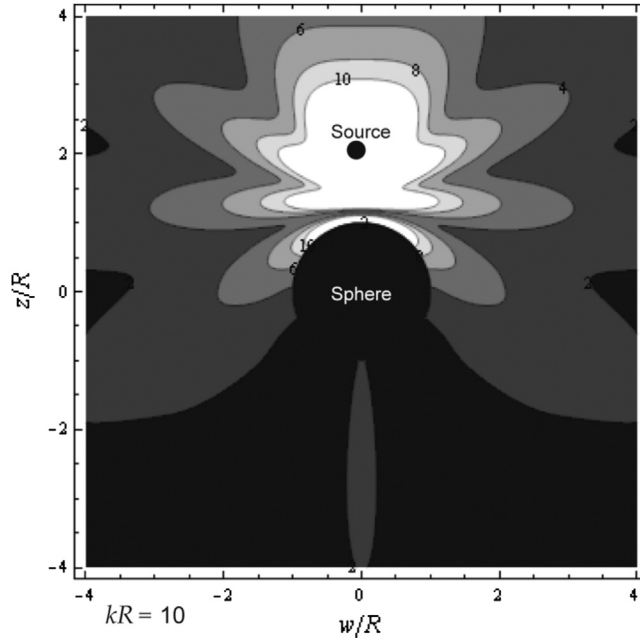


Figure 12.8 Resultant pressure field $|\tilde{S}\tilde{p}(w, z)|/\rho c\tilde{U}_0$ due to the scattering of a field from a point source by a rigid sphere where $kR = 10$.

become normal to the surface of the sphere. On the other hand, at the other end of the spectrum, the plot for $kR = 10$ in Fig. 12.3 tells us that there are significant interference patterns in the vicinity of the sphere when the wavelength is considerably shorter than the circumference of the sphere. In addition, the shadow regions are more distinct than those that are produced by an incident plane wave in Fig. 12.3.

Far-field pressure

As the distance r from the center of the sphere is increased to many wavelengths, the asymptotic expression for the spherical Hankel function becomes that of Eq. (12.18). Inserting Eq. (12.18) into Eq. (12.34) yields

$$\tilde{p}_s(r, \theta)|_{r \rightarrow \infty} = \frac{jk\rho_0 c \tilde{U}_0}{4\pi r} e^{-jkr} D(\theta), \quad (12.35)$$

where $D(\theta)$ is a directivity function given by

$$D(\theta) = - \sum_{n=0}^{\infty} j^n (2n+1) h_n^{(2)}(kd) \frac{j'_n(kR)}{h_n^{(2)}(kR)} P_n(\cos \theta). \quad (12.36)$$

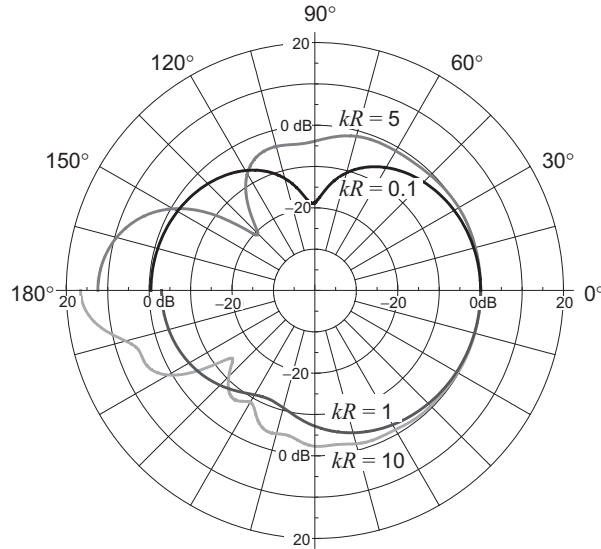


Figure 12.9 Directivity pattern $20 \log_{10}(|D(\theta)|/|D(0)|)$ of the far-field pressure for $d = 2R$ due to the scattering of a point source from a rigid sphere (excluding the incident field).

The directivity pattern $20 \log_{10}(D(\theta)/D(0))$ is plotted in Fig. 12.9 for various values of kR . Let a reflection coefficient be defined by

$$D(0) = - \sum_{n=0}^{\infty} j^n (2n+1) h_n^{(2)}(kd) \frac{j'_n(kR)}{h_n^{(2)}(kR)}, \quad (12.37)$$

where we have used the identity $P_n(1) = 1$. Similarly, let a transmission coefficient be defined by

$$D(\pi) = - \sum_{n=0}^{\infty} (-j^n) (2n+1) h_n^{(2)}(kd) \frac{j'_n(kR)}{h_n^{(2)}(kR)}, \quad (12.38)$$

where we have used the identity $P_n(-1) = (-1)^n$. These reflection and transmission coefficients are plotted against kR in Figs. 12.10 and 12.11. For small values of kR , the transmission and reflection coefficients are both fairly weak, but more or less equal because the sound is scattered in all directions. It can be seen that above $kR = 2$, the reflection coefficient remains virtually constant. In the plot for $d = R$, the point source is on the surface of the sphere and the reflection coefficient above $kR = 2$ is 100% because the point source is behaving as though it is on an infinite plane. In the plot for $d = 2R$, the reflected wave has decayed over twice the distance between the point source and the sphere. We will study the behavior of a point source on a sphere in greater detail when

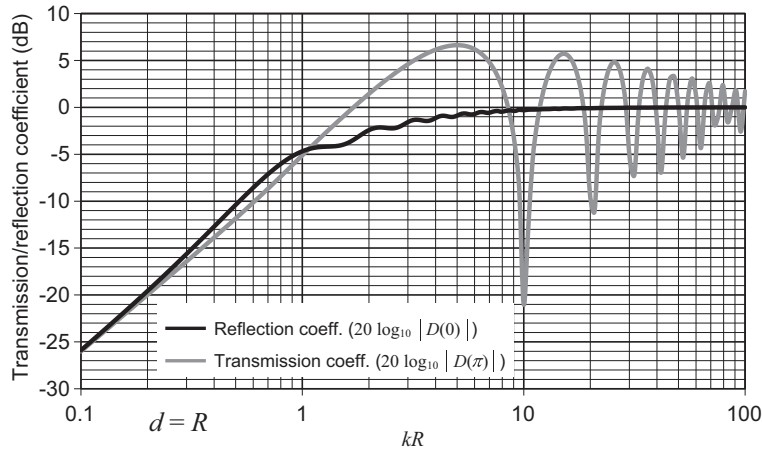


Figure 12.10 Transmission and reflection coefficients for the scattering of a point source by a rigid sphere for $d = R$. Frequency is plotted on a normalized scale, where $kR = 2\pi R/\lambda = 2\pi fR/c$.

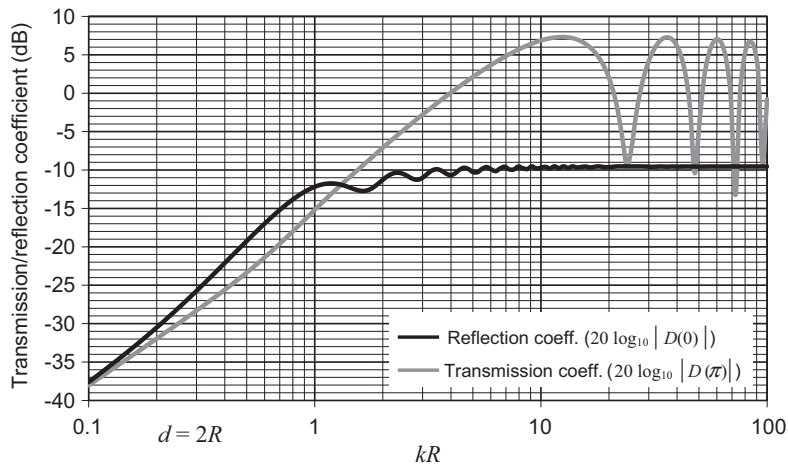


Figure 12.11 Transmission and reflection coefficients for the scattering of a point source by a rigid sphere for $d = 2R$. Frequency is plotted on a normalized scale, where $kR = 2\pi R/\lambda = 2\pi fR/c$.

dealing with sound sources. Above $kR = 10$, we do not see the rising transmission coefficient that we saw with the plane wave. Instead, it oscillates around unity (0 dB) due to constructive and destructive interference. Hence, the sound from a point source is not concentrated by the sphere like that from a plane wave. The reason for this is that components of the plane wave strike the sphere from many different directions, including the sides, and these components can be diffracted around it.



12.5 RADIATION FROM A POINT SOURCE ON A SPHERE

This problem is essentially the same as the last one when $d = R$. However, this time we shall introduce the property of orthogonality to obtain a simple solution. By *reciprocity*, the resulting expression can be used to obtain the pressure at a point on the sphere due to a source at some point in space. This is a useful model for the diffraction effects of the human head on sound arriving at one ear, assuming a hard sphere model of the head. Unlike the pulsating sphere, only an infinitesimally small part of the surface is oscillating, so that the velocity distribution is described by

$$\tilde{u}(R, \theta) = \begin{cases} \tilde{u}_0, & 0 \leq \theta \leq \delta \\ 0, & \delta \leq \theta \leq \pi \end{cases}, \quad (12.39)$$

where δ is a vanishingly small angle.

Near-field pressure

We assume that the pressure field generated is a general axisymmetric solution to Eq. (2.180), the Helmholtz wave equation in spherical coordinates:

$$\tilde{p}(r, \theta) = \rho_0 c \tilde{u}_0 \sum_{n=0}^{\infty} A_n h_n^{(2)}(kr) P_n(\cos \theta). \quad (12.40)$$

Applying the velocity boundary condition gives

$$\begin{aligned} \tilde{u}(R, \theta) &= \frac{1}{-jk\rho_0 c} \frac{\partial}{\partial r} p(r, \theta)|_{r=R} \\ &= \frac{\tilde{u}_0}{-jk} \sum_{n=0}^{\infty} A_n h_n^{\prime(2)}(kR) P_n(\cos \theta) = \begin{cases} \tilde{u}_0, & 0 \leq \theta \leq \delta \\ 0, & \delta \leq \theta \leq \pi, \end{cases} \end{aligned} \quad (12.41)$$

where the derivative of the spherical Hankel function $h_n^{\prime(2)}(kR)$ is given by Eq. (12.32). We now multiply both sides of Eq. (12.41) with the orthogonal function $P_m(\cos \theta)$ and integrate over the surface of the sphere, where the area of each surface element is given by

$$\delta S = 2\pi R^2 \sin \theta \delta \theta,$$

so that

$$\frac{1}{-jk} \sum_{n=0}^{\infty} A_n h_n^{\prime(2)}(kR) \int_0^{\pi} P_n(\cos \theta) P_m(\cos \theta) R \sin \theta d\theta = \int_0^{\delta} P_m(\cos \theta) R \sin \theta d\theta \quad (12.42)$$

It can be seen from Eq. (12.42) that we have effectively exchanged θ dependency for m dependency. Hence, Eq. (12.42) represents an infinite set of simultaneous equations where $m = 0, 1, 2, \dots$. The integral identities are given by Eqs. (A2.66) and (A2.67) in Appendix II. However, δ_{mn} is the Kronecker delta function which is zero unless $m = n$ in which case its value is 1. In other words, we have a matrix in which only the diagonal terms are nonzero, so that the coefficients are given directly by

$$A_n = -jk \frac{(2n+1)\delta^2}{4h_n^{(2)}(kR)} \quad (12.43)$$

without having to solve a system of equations. Finally, by inserting (12.43) in (12.40) and letting $\tilde{U}_0 = \pi(\delta R)^2 \tilde{u}_0$, we can write the near-field pressure as

$$\tilde{p}(r, \theta) = -j\rho_0 c \frac{\tilde{U}_0}{S} \sum_{n=0}^{\infty} \frac{(2n+1)^2 h_n^{(2)}(kr) P_n(\cos \theta)}{nh_{n-1}^{(2)}(kR) - (n+1)h_{n+1}^{(2)}(kR)}, \quad (12.44)$$

where $S = 4\pi R^2$ is the total surface area of the sphere. The magnitude of the normalized pressure,

$$|S\tilde{p}(w, z)/(\rho_0 c \tilde{U}_0)|,$$

is plotted in Figs. 12.12 and 12.13 in cylindrical coordinates w and z where

$$r = \sqrt{w^2 + z^2} \quad \text{and} \quad \cos \theta = z / \sqrt{w^2 + z^2}.$$

We can see from Fig. 12.12 that at low frequencies the pressure contours are more or less concentric with the acoustic center at a distance of around $\frac{1}{2}R$ in front of the point source. By contrast, the contours in Fig. 12.13 are eccentric so that at high frequencies, the further you are from the source, the further the source appears to be from its actual position.

Far-field pressure

In the far field, we can use the asymptotic expression for the spherical Hankel function from Eq. (12.18), which when inserted into Eq. (12.44) gives

$$\tilde{p}(r, \theta)|_{r \rightarrow \infty} = jk\rho_0 c \frac{\tilde{U}_0}{4\pi r} e^{-jkr} D(\theta), \quad (12.45)$$

where

$$D(\theta) = -\frac{1}{k^2 R^2} \sum_{n=0}^{\infty} \frac{j^{n+1} (2n+1)^2 P_n(\cos \theta)}{nh_{n-1}^{(2)}(kR) - (n+1)h_{n+1}^{(2)}(kR)}. \quad (12.46)$$

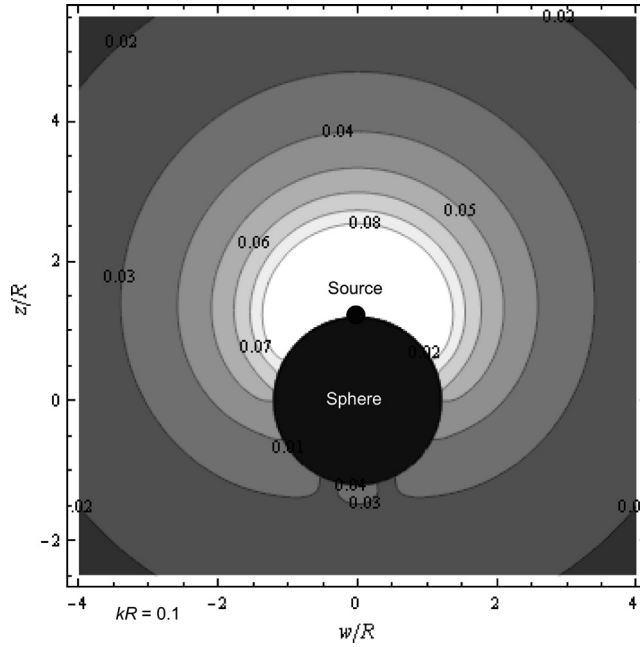


Figure 12.12 Pressure field $|\tilde{S}\tilde{p}(w,z)|/\rho_0 c \tilde{U}_0$ due to a point source on a rigid sphere for $kR = 0.1$.

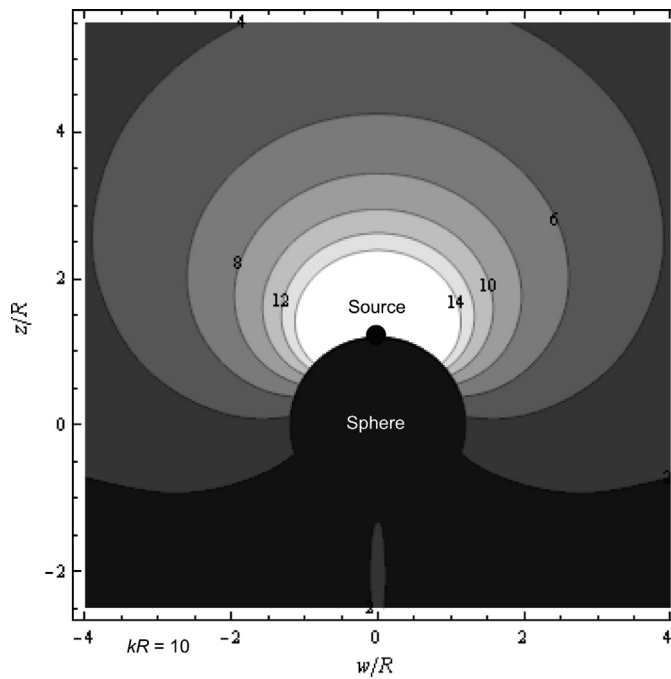


Figure 12.13 Pressure field $|\tilde{S}\tilde{p}(w,z)|/\rho_0 c \tilde{U}_0$ due to a point source on a rigid sphere for $kR = 10$.

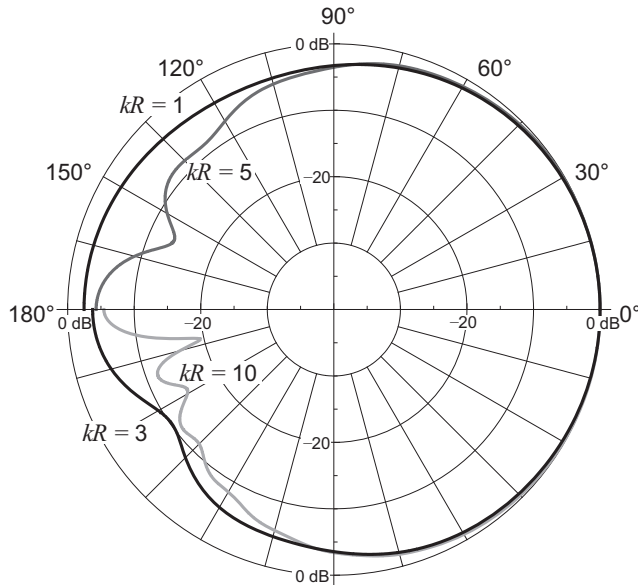


Figure 12.14 Far-field directivity pattern $20 \log_{10}(|D(\theta)|/|D(0)|)$ of the far-field pressure due to a point source on a rigid sphere of radius R .

The directivity pattern $20 \log_{10}(|D(\theta)|/|D(0)|)$ is plotted in Fig. 12.14 for various values of kR . The far-field on-axis response is given by

$$D(0) = \frac{1}{k^2 R^2} \sum_{n=0}^{\infty} \frac{j^n (2n+1)^2}{n h_{n-1}^{(2)}(kR) - (n+1) h_{n+1}^{(2)}(kR)}. \quad (12.47)$$

The on-axis response $20 \log_{10}|D(0)|$ and 180 degrees off-axis response $20 \log_{10}|D(\pi)|$ are plotted against kR in Fig. 12.15. It can be seen that there is a 6 dB lift in the on-axis response when the wavelength is approximately equal to the circumference of the sphere. This is due to the fact that the point source acts as a pure monopole radiator at low frequencies as though the sphere were not present. However, at high frequencies, the sphere acts as a large baffle and the radiated sound is concentrated in half space thus doubling the pressure value. Because the sphere is smooth and continuous with no reflecting edges, the transition from whole-space to half-space radiation is also smooth, producing just some very small ripples in the on-axis response. We shall see that this is not so in the case of radiators with edges. Hence, the sphere represents an idealized loudspeaker enclosure.



12.6 RADIATION FROM A SPHERICAL CAP IN A SPHERE

In reality, loudspeakers do not have vanishingly small diaphragms, and at high frequencies the size and shape of the radiator strongly influences the resulting sound field.

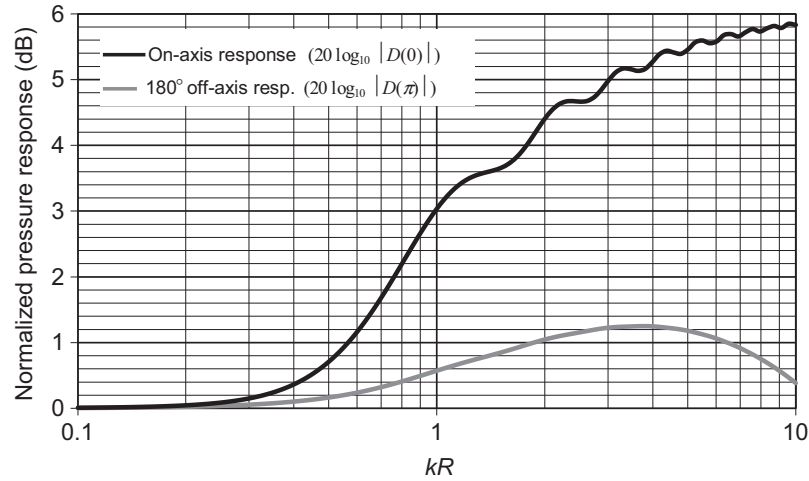


Figure 12.15 Plots of $20 \log_{10}|D(0)|$ and $20 \log_{10}|D(\pi)|$ where $D(\theta)$ is the directivity function of a point source on a rigid sphere of radius R . Frequency is plotted on a normalized scale, where $kR = 2\pi R/\lambda = 2\pi fR/c$.

The spherical cap [2] represents a curved finite diaphragm which follows the contour of the sphere. This makes it easier to analyze than a flat piston, which we shall consider in Section 12.8. The spherical cap shown in Fig. 12.16 is set in a rigid sphere of radius R and moves with an axial velocity \tilde{u}_0 such that the velocity distribution is described by

$$\tilde{u}(R, \theta) = \begin{cases} \tilde{u}_0 \cos \theta & 0 \leq \theta \leq \alpha \\ 0, & \alpha \leq \theta \leq \pi \end{cases}, \quad (12.48)$$

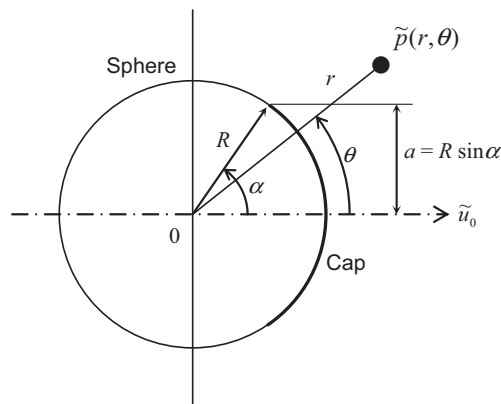


Figure 12.16 Geometry of oscillating cap in a rigid sphere.

where α is the half angle of the arc formed by the cap. Although the cap is rigid in this case, other velocity distributions are possible [6]. The total volume velocity is given by

$$\tilde{U}_0 = \tilde{u}_0 R^2 \int_0^{2\pi} \int_0^\alpha \cos \theta \sin \theta \, d\phi = S \tilde{u}_0, \quad (12.49)$$

where S is the *effective* surface area of the cap given by

$$S = \pi R^2 \sin^2 \alpha. \quad (12.50)$$

If the cap were radially pulsating, we would drop the $\cos \theta$ term from Eqs. (12.48) and (12.49) and the effective surface area would be

$$S = 2\pi R^2(1 - \cos \alpha) = 4\pi R^2 \sin^2(\alpha/2).$$

Near-field pressure

Again we assume that the pressure field generated is a general axisymmetric solution to Eq. (2.180), the Helmholtz wave equation in spherical coordinates:

$$\tilde{p}(r, \theta) = \rho_0 c \tilde{u}_0 \sum_{n=0}^{\infty} A_n h_n^{(2)}(kr) P_n(\cos \theta). \quad (12.51)$$

Applying the velocity boundary condition of Eq. (2.4a) gives

$$\begin{aligned} \tilde{u}(R, \theta) &= \frac{1}{-jk\rho_0 c} \frac{\partial}{\partial r} p(r, \theta) \Big|_{r=R} \\ &= \frac{\tilde{u}_0}{-jk} \sum_{n=0}^{\infty} A_n h_n^{(2)'}(kR) P_n(\cos \theta) = \begin{cases} \tilde{u}_0 \cos \theta, & 0 \leq \theta \leq \alpha \\ 0 & \alpha \leq \theta \leq \pi, \end{cases} \end{aligned} \quad (12.52)$$

where the derivative of the spherical Hankel function $h_n^{(2)'}(kR)$ is given by Eq. (12.32). We now multiply both sides of (12.41) with the orthogonal function $P_m(\cos \theta)$ and integrate over the surface of the sphere, where the area of each surface element is given by

$$\delta S = 2\pi R^2 \sin \theta \, \delta\theta,$$

so that

$$\frac{1}{-jk} \sum_{n=0}^{\infty} A_n h_n^{(2)'}(kR) \int_0^\pi P_n(\cos \theta) P_m(\cos \theta) \sin \theta \, d\theta = \int_0^\alpha P_m(\cos \theta) \cos \theta \sin \theta \, d\theta \quad (12.53)$$

from which we obtain the coefficients as follows:

$$A_0 = jk \frac{-\sin^2 \alpha}{4h_0^{(2)}(kR)}, \quad (12.54)$$

$$A_1 = jk \frac{\cos^3 \alpha - 1}{2h_1^{(2)}(kR)}, \quad (12.55)$$

$$A_n = jk(2n+1)\sin \alpha \frac{\sin \alpha P_n(\cos \alpha) + \cos \alpha P_n^1(\cos \alpha)}{2(n-1)(n+2)h_n^{(2)}(kR)}, \quad n \geq 2, \quad (12.56)$$

where we have used the integral identities from Eqs. (A2.66) and (A2.68) in Appendix II. Separate terms have been derived for $n = 0$ and 1 in Eq. (A2.68) because the expression for $n \geq 2$ is singular at $n = 1$. Alternatively, if the cap were radially pulsating, we would drop the $\cos \theta$ term from the right-hand side of Eqs. (12.48) and (12.52) and use Eq. (A2.69) from Appendix II. Finally, by inserting Eqs. (12.54), (12.55) and (12.56) in Eq. (12.51), we can write the near-field pressure as

$$\begin{aligned} \tilde{p}(r, \theta) = & -jk\rho_0 c \tilde{u}_0 \left(\frac{\sin^2 \alpha}{4h_0^{(2)}(kR)} h_0^{(2)}(kr) + \frac{1 - \cos^3 \alpha}{2h_1^{(2)}(kR)} h_1^{(2)}(kr) \cos \theta \right. \\ & \left. - \sin \alpha \sum_{n=2}^{\infty} (2n+1) \frac{\sin \alpha P_n(\cos \alpha) + \cos \alpha P_n^1(\cos \alpha)}{2(n-1)(n+2)h_n^{(2)}(kR)} h_n^{(2)}(kr) P_n(\cos \theta) \right) \end{aligned} \quad (12.57)$$

Far-field pressure

In the far field, we can use the asymptotic expression for the spherical Hankel function from Eq. (12.18), which when inserted into Eq. (12.57) gives

$$\tilde{p}(r, \theta)|_{r \rightarrow \infty} = -jk\rho_0 c S \frac{\tilde{u}_0}{4\pi r} e^{-jkr} D(\theta), \quad (12.58)$$

where S is the dome effective area given by $S = \pi a^2$ and

$$\begin{aligned} D(0) = & -\frac{2}{k^2 R^2} \left(\frac{j}{2h_1^{(2)}(kR)} + \frac{3(1 - \cos^3 \alpha)}{\sin^2 \alpha (h_0^{(2)}(kR) - 2h_2^{(2)}(kR))} \cos \theta \right. \\ & \left. + \sum_{n=2}^{\infty} \frac{j^{n+1} (2n+1)^2 (\sin \alpha P_n(\cos \alpha) + \cos \alpha P_n^1(\cos \alpha))}{(n-1)(n+2) \sin \alpha (nh_{n-1}^{(2)}(kR) - (n+1)h_{n+1}^{(2)}(kR))} P_n(\cos \theta) \right). \end{aligned} \quad (12.59)$$

When $\alpha = 1/2 \pi$, the second term simplifies to that for an oscillating sphere, as described in Section 4.15, and odd terms in the expansion vanish so that Eq. (12.59) simplifies to

$$D(\theta)|_{\alpha=\frac{\pi}{2}} = -j \frac{2k R e^{jkR}}{2 - k^2 R^2 + j2kR} \cos \theta$$

$$-j \frac{2}{k^2 R^2} \sum_{n=0}^{\infty} \frac{(-1)^n (4n+1)^2 P_{2n}(0)}{(2n-1)(2n+2) \left(2n h_{2n-1}^{(2)}(kR) - (2n+1) h_{2n+1}^{(2)}(kR) \right)} P_{2n}(\cos \theta),$$
(12.60)

which represents the superposition of two fields. The first term represents an oscillating sphere and the second two diametrically opposed hemispherical caps or a hemispherical dome in an infinite baffle, which will be discussed in greater detail in Sec. 12.9. The same kind of superposition of fields, or “Gutin concept,” will be used in Section 13.11 to describe a single-sided piston. The directivity pattern $20 \log_{10}(|D(\theta)|/|D(0)|)$ for $\alpha = 60$ degrees is plotted in Fig. 12.17 for various values of ka . As expected, we see that at low frequencies the pattern is almost omnidirectional. However, at high frequencies, the spherical cap shows a fairly constant angle of dispersion, which is approximately

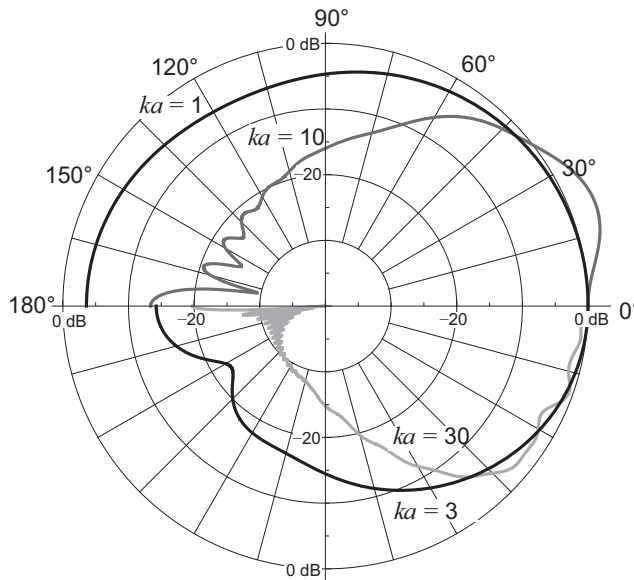


Figure 12.17 Far-field directivity pattern $20 \log_{10}(|D(\theta)|/|D(0)|)$ of the far-field pressure due to a spherical cap of radius a in a rigid sphere for $\alpha = 60$ degrees, where α is the half angle of the arc formed by the cap.

equal to the angle of arc formed by the cap itself. The far-field on-axis response is given by

$$D(0) = -\frac{2}{k^2 R^2} \left(\frac{j}{2h_1^{(2)}(kR)} + \frac{3(1 - \cos^3 \alpha)}{\sin^2 \alpha (h_0^{(2)}(kR) - 2h_2^{(2)}(kR))} \right. \\ \left. + \sum_{n=2}^{\infty} \frac{j^{n+1} (2n+1)^2 (\sin \alpha P_n(\cos \alpha) + \cos \alpha P_n^1(\cos \alpha))}{(n-1)(n+2) \sin \alpha (nh_{n-1}^{(2)}(kR) - (n+1)h_{n+1}^{(2)}(kR))} \right). \quad (12.61)$$

The on-axis response $20 \log_{10}|D(0)|$ is plotted against ka in Fig. 12.18. Like the point source on a sphere, we see a rise in the response around $kR = 1$ (i.e., the wavelength is roughly equal to the circumference of the sphere), due to the transition from whole-space to half-space radiation. However, like the oscillating sphere, the response starts to fall above $ka = 5$ because the response is proportional to the cap velocity when the radiation resistance is mainly resistive, as indicated in Fig. 12.19. Unlike the oscillating sphere, the falling response is accompanied by ripples due to the discontinuity at the edge of the cap. This produces cancellation effects due to path length differences from different parts of the cap.

Radiation impedance

The total radiation force \tilde{F} is given by

$$\tilde{F} = R^2 \int_0^{2\pi} \int_0^\alpha \tilde{p}(R, \theta) \cos \theta \sin \theta \, d\theta \, d\phi \quad (12.62)$$

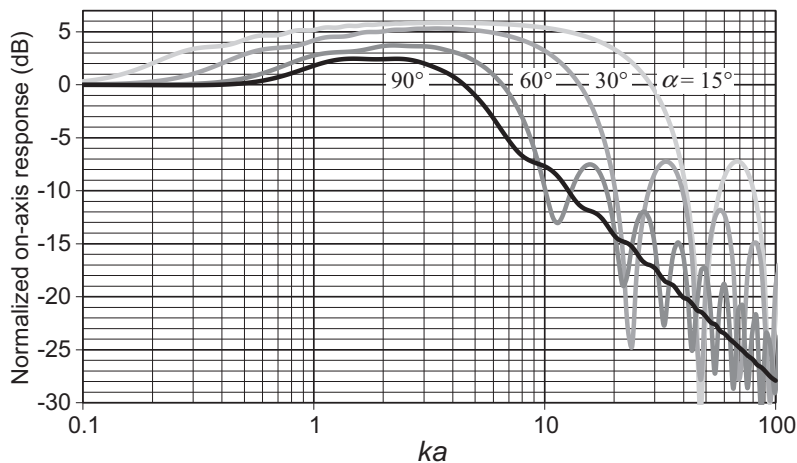


Figure 12.18 Plot of $20 \log_{10}|D(0)|$ where $D(\theta)$ is the directivity function of a spherical cap of radius a in a rigid sphere, where α is the half angle of the arc formed by the cap. The axial acceleration of the cap is constant. Frequency is plotted on a normalized scale, where $ka = 2\pi a/\lambda = 2\pi fa/c$.

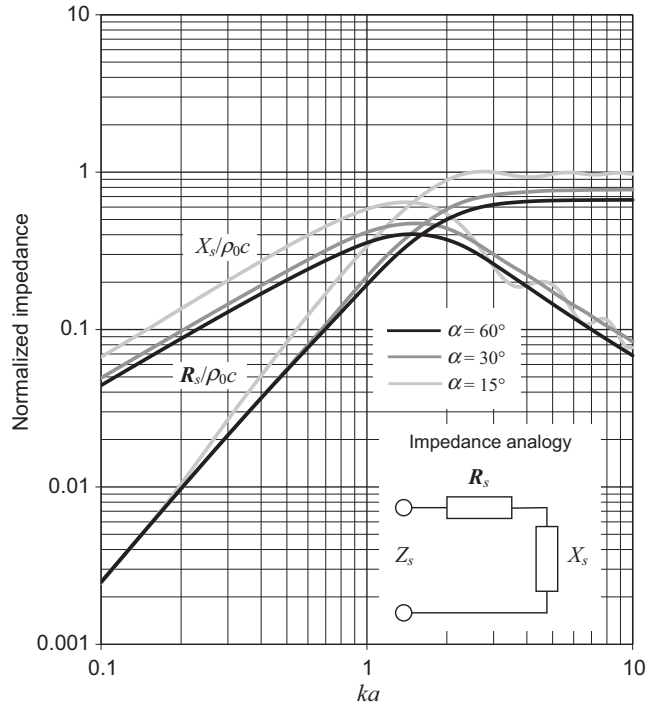


Figure 12.19 Real and imaginary parts of the normalized specific radiation impedance Z_s/ρ_0c of the air load on an oscillating spherical cap of radius a in a rigid sphere, where α is the half angle of the arc formed by the cap. Frequency is plotted on a normalized scale, where $ka = 2\pi a/\lambda = 2\pi fa/c$.

using the identity of Eq. (A2.68) from Appendix II. The specific impedance Z_s is then given by

$$Z_S = \frac{\tilde{F}}{\tilde{U}_0} = j\rho_0c \left(\frac{\sin^2 \alpha h_0^{(2)}(kR)}{4h_1^{(2)}(kR)} - \frac{(1 - \cos^3 \alpha)^2 h_1^{(2)}(kR)}{\sin^2 \alpha (h_0^{(2)}(kR) - 2h_2^{(2)}(kR))} \right) \quad (12.63)$$

$$- \sum_{n=2}^{\infty} \frac{(2n+1)^2 (\sin \alpha P_n(\cos \alpha) + \cos \alpha P_n^1(\cos \alpha))^2 h_n^{(2)}(kR)}{(n-1)^2 (n+2)^2 (nh_{n-1}^{(2)}(kR) - (n+1)h_{n+1}^{(2)}(kR))},$$

where we have used the expression for \tilde{U}_0 from Eq. (12.49). When $\alpha = 1/2\pi$, the odd terms of the expansion vanish, except for the second term, which simplifies to

that for an oscillating sphere, as described in Section 4.15. Hence, Eq. (12.63) simplifies to

$$Z_s|_{\alpha=\frac{\pi}{2}} = \rho_0 c \left(\frac{k^4 a^4 + j(k^3 a^3 + 2ka)}{3(k^4 a^4 + 4)} - j \sum_{n=0}^{\infty} \frac{(4n+1)^2 (P_{2n}(0))^2 h_{2n}^{(2)}(kR)}{(2n-1)^2 (2n+2)^2 (2nh_{2n-1}^{(2)}(kR) - (2n+1)h_{2n+1}^{(2)}(kR))} \right), \quad (12.64)$$

which represents the superposition of two fields. The first term represents an oscillating sphere and the second two diametrically opposed hemispherical caps or a hemispherical dome in an infinite baffle, which will be discussed in greater detail in Section 12.9. The same kind of superposition of fields, or “Gutin concept,” will be used in Section 13.11 to describe a single-sided piston. The real and imaginary parts, \mathbf{R}_s and X_s , are plotted in Fig. 12.19 where

$$Z_s = \mathbf{R}_s + jX_s = \Re(Z_s) + j\Im(z_s). \quad (12.65)$$

We can see that the impedance of the 90 degrees cap is roughly the average of the pulsating and oscillating spheres. At 15 degrees, the cap approaches a piston in an infinite baffle, which we will study later. There are ripples in the impedance curves above $ka = 2$ due to interference patterns in the immediate vicinity of the radiator.



12.7 RADIATION FROM A RECTANGULAR CAP IN A SPHERE

A useful model for the mouth of a circular horn is the spherical cap in a sphere [3]. However, this can be shown to have a somewhat irregular on-axis response with peaks and dips due to interference between sound radiated from the center of the cap and its perimeter. In addition, circular horns are rarely used these days, and it is more common to find a rectangular horn with an aspect ratio chosen so that its horizontal radiation is concentrated over an angle which covers the auditorium area. However, one additional advantage of this arrangement is that on-axis irregularities are less likely. The question we wish to answer is what is the optimum aspect ratio for a smooth on-axis response? Until now we have only dealt with problems with axial symmetry, which are independent of the azimuthal angle ϕ . In other words, they are really two dimensional in r and θ . The rectangular cap in a sphere is our first genuinely three-dimensional problem in spherical coordinates (r, θ, ϕ) , and its geometry is shown in Fig. 12.20. The rectangular cap, which is defined by the half angles α and β , is set in a rigid sphere of radius R and pulsates with a velocity \tilde{u}_0 such that the velocity distribution is described by

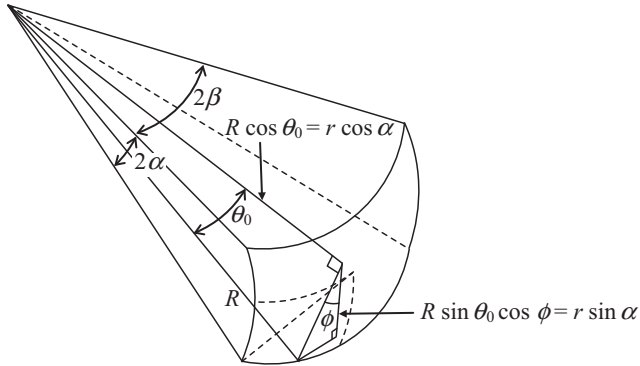


Figure 12.20 Geometry of rectangular cap in sphere. For clarity the sphere is not shown.

$$\tilde{u}(R, \theta, \phi) = \begin{cases} \tilde{u}_0, & \begin{cases} 0 \leq \theta \leq \theta_0, & 0 \leq \phi \leq \arctan(\tan \beta / \tan \alpha) \\ 0 \leq \theta \leq \theta_1, & 0 \leq \phi \leq \arctan(\tan \alpha / \tan \beta) \end{cases} \\ 0, & \begin{cases} \theta_0 \leq \theta \leq \pi, & 0 \leq \phi \leq \arctan(\tan \beta / \tan \alpha) \\ \theta_1 \leq \theta \leq \pi, & 0 \leq \phi \leq \arctan(\tan \alpha / \tan \beta) \end{cases} \end{cases}, \quad (12.66)$$

where

$$\theta_0 = \arctan(\tan \alpha / \cos \phi), \quad (12.67)$$

$$\theta_1 = \arctan(\tan \beta / \cos \phi). \quad (12.68)$$

To calculate the *effective* surface area S of the cap, where the area of each surface element is given by

$$\delta S = R^2 \sin \theta \delta \theta \delta \phi,$$

we need only integrate over one quarter of the cap and multiply the result by four:

$$\begin{aligned} S &= 4R^2 \left(\int_0^{\arctan \frac{\tan \beta}{\tan \alpha}} \int_0^{\arctan \frac{\tan \alpha}{\cos \phi}} \sin \theta \, d\theta \, d\phi + \int_0^{\arctan \frac{\tan \alpha}{\tan \beta}} \int_0^{\arctan \frac{\tan \beta}{\cos \phi}} \sin \theta \, d\theta \, d\phi \right) \\ &= 4R^2 \left\{ \arctan \left(\frac{\tan \alpha \tan \beta}{\sec^2 \alpha + \sqrt{\sec^2 \alpha + \tan^2 \beta}} \right) + \arctan \left(\frac{\tan \alpha \tan \beta}{\sec^2 \beta + \sqrt{\sec^2 \beta + \tan^2 \alpha}} \right) \right\} \\ &\approx 4R^2 \sin \alpha \sin \beta, \quad \alpha < \frac{\pi}{4}, \quad \beta < \frac{\pi}{4} \end{aligned}$$

(12.69)

Near-field pressure

The Helmholtz wave equation in spherical coordinates is given by

$$\nabla^2 = \frac{\partial^2}{\partial r^2} + \frac{2}{r} \frac{\partial}{\partial r} + \frac{1}{r^2} \frac{\partial^2}{\partial \theta^2} + \frac{1}{r^2 \tan \theta} \frac{\partial}{\partial \theta} + \frac{1}{r^2 \sin^2 \theta} \frac{\partial^2}{\partial \phi^2}, \quad (12.70)$$

The resulting pressure field is given by the following solution:

$$\tilde{p}(r, \theta, \phi) = \rho_0 \tilde{c} u_0 \sum_{n=0}^{\infty} \sum_{m=0}^{n/2} A_{mn} h_n^{(2)}(kr) P_n^{2m}(\cos \theta) \cos 2m\phi, \quad (12.71)$$

where A_{mn} are the as-yet unknown power series coefficients, which are evaluated by applying appropriate boundary conditions. To meet the boundary condition of symmetry at $\phi = 0$, we use only cosine terms in the solution. Applying the velocity boundary condition gives

$$\begin{aligned} \tilde{u}(R, \theta, \phi) &= \frac{1}{-jk\rho_0 c} \frac{\partial}{\partial r} p(r, \theta, \phi) \Big|_{r=R} \\ &= \frac{\tilde{u}_0}{-jk} \sum_{n=0}^{\infty} \sum_{m=0}^{n/2} A_{mn} h_n^{\prime(2)}(kR) P_n^{2m}(\cos \theta) \cos 2m\phi \end{aligned} \quad (12.72)$$

where the derivative of the spherical Hankel function $h_n^{\prime(2)}(kR)$ is given by

$$h_n^{\prime(2)}(k, R) = \frac{\partial}{\partial r} h_n^{(2)}(kr) \Big|_{r=R} = \frac{k}{2n+1} \left(n h_{n-1}^{(2)}(kR) - (n+1) h_{n+1}^{(2)}(kR) \right). \quad (12.73)$$

We now equate Eq. (12.66) with Eq. (12.72) while truncating the infinite series limit to N . Then multiplying both sides with the orthogonal function

$$P_q^{2p}(\cos \theta) \cos 2p\phi$$

and integrating over the surface of the sphere gives

$$\begin{aligned} \frac{1}{-jk} \sum_{n=0}^N \sum_{m=0}^{n/2} A_{mn} h_n^{\prime(2)}(kR) \int_0^{\pi} P_n^{2m}(\cos \theta) P_q^{2p}(\cos \theta) \sin \theta \, d\theta \int_0^{2\pi} \cos 2m\phi \cos 2p\phi \, d\phi \\ = \int_0^{\arctan \frac{\tan \beta}{\tan \alpha}} \cos 2p\phi \int_0^{\arctan \frac{\tan \alpha}{\tan \phi}} P_q^{2p}(\cos \theta) \sin \theta \, d\theta \, d\phi \\ + \int_{\frac{\pi}{2} - \arctan \frac{\tan \alpha}{\tan \beta}}^{\frac{\pi}{2} + \arctan \frac{\tan \alpha}{\tan \beta}} \cos 2p\phi \int_0^{\arctan \frac{\tan \beta}{(\cos \phi - \pi/2)}} P_q^{2p}(\cos \theta) \sin \theta \, d\theta \, d\phi \\ + \int_{\pi - \arctan \frac{\tan \beta}{\tan \alpha}}^{\pi} \cos 2p\phi \int_0^{\arctan \frac{\tan \alpha}{\cos(\phi - \pi)}} P_q^{2p}(\cos \theta) \sin \theta \, d\theta \, d\phi \end{aligned} \quad (12.74)$$

from which we obtain the coefficients:

$$A_{mn} = \frac{(2n+1)^2(n-2m)! I_{mn}}{j2\pi(n+2m)! \left(nh_{n-1}^{(2)}(kR) - (n+1)_{n+1}^{(2)}(kR) \right)}, \quad (12.75)$$

where

$$\begin{aligned} I_{mn} = & \int_0^{\arctan \frac{\tan \beta}{\tan \alpha}} \cos 2m\phi \int_0^{\arctan \frac{\tan \alpha}{\cos \phi}} P_n^{2m}(\cos \theta) \sin \theta \, d\theta \, d\phi \\ & + \int_{\frac{\pi}{2} - \arctan \frac{\tan \alpha}{\tan \beta}}^{\frac{\pi}{2} + \arctan \frac{\tan \alpha}{\tan \beta}} \cos 2m\phi \int_0^{\arctan \frac{\tan \beta}{\sin \phi}} P_n^{2m}(\cos \theta) \sin \theta \, d\theta \, d\phi \\ & + \int_{\pi - \arctan \frac{\tan \beta}{\tan \alpha}}^{\pi} \cos 2m\phi \int_0^{\arctan \frac{\tan \alpha}{-\cos \phi}} P_n^{2m}(\cos \theta) \sin \theta \, d\theta \, d\phi, \end{aligned} \quad (12.76)$$

$$\begin{aligned} I_{0n} = & \int_0^{\arctan \frac{\tan \beta}{\tan \alpha}} \frac{\tan \alpha}{\sqrt{\cos^2 \phi + \tan^2 \alpha}} P_n^{-1} \left(\frac{\cos \phi}{\sqrt{\cos^2 \phi + \tan^2 \alpha}} \right) d\phi \\ & + \int_{\frac{\pi}{2} - \arctan \frac{\tan \alpha}{\tan \beta}}^{\frac{\pi}{2} + \arctan \frac{\tan \alpha}{\tan \beta}} \frac{\tan \alpha}{\sqrt{\sin^2 \phi + \tan^2 \beta}} P_n^{-1} \left(\frac{\sin \phi}{\sqrt{\sin^2 \phi + \tan^2 \beta}} \right) d\phi \\ & + \int_{\pi - \arctan \frac{\tan \beta}{\tan \alpha}}^{\pi} \frac{\tan \alpha}{\sqrt{\cos^2 \phi + \tan^2 \alpha}} P_n^{-1} \left(\frac{-\cos \phi}{\sqrt{\cos^2 \phi + \tan^2 \alpha}} \right) d\phi, \end{aligned} \quad (12.77)$$

and we have used the integral identities (12.78)

$$\int_0^{2\pi} \cos 2m\phi \cos 2p\phi \, d\phi = \begin{cases} \pi, & m = p \\ 0, & m \neq p \end{cases} \quad (12.78)$$

$$\int_0^{\pi} P_n^{2m}(\cos \theta) P_q^{2q}(\cos \theta) \sin \theta \, d\theta = \begin{cases} \frac{2(n+2m)!}{(2n+1)(n-2m)!}, & m = p \text{ and } n = q \\ 0, & m \neq p \text{ or } n \neq q \end{cases} \quad (12.79)$$

$$\int_0^{\psi} P_n(\cos \theta) \sin \theta \, d\theta = P_n^{-1}(\cos \psi) \sin \psi \quad (12.80)$$

Far-field pressure

In the far field, we can use the asymptotic expression for the spherical Hankel function:

$$h_n^{(2)}(kr) \Big|_{r \rightarrow \infty} = \frac{j^{n+1}}{kr} e^{-jkr}, \quad (12.81)$$

which when inserted into Eq. (12.71) gives

$$\tilde{p}(r, \theta, \phi) \Big|_{r \rightarrow \infty} = -jk\rho_0 c S \frac{\tilde{u}_0}{4\pi r} e^{-jkr} D(\theta, \phi), \quad (12.82)$$

where S is the cap effective area given by Eq. (12.49) and

$$D(\theta, \phi) = -\frac{4\pi}{k^2 S} \sum_{n=0}^N \sum_{m=0}^{n/2} A_{mn} j^n P_n^{2m}(\cos \theta) \cos 2m\phi. \quad (12.83)$$

The far-field on-axis response is obtained using the relationship

$$P_n^{2m}(1) = \delta_{m0} \quad (12.84)$$

so that

$$D(0, 0) = -\frac{4\pi}{k^2 S} \sum_{n=0}^N A_{0n} j^n. \quad (12.85)$$

The on-axis response $20 \log_{10}|D(0,0)|$ is plotted against kR in Fig. 12.21. The black curve shows the response of a pulsating circular cap in a sphere [from Eq. (13.83)], which

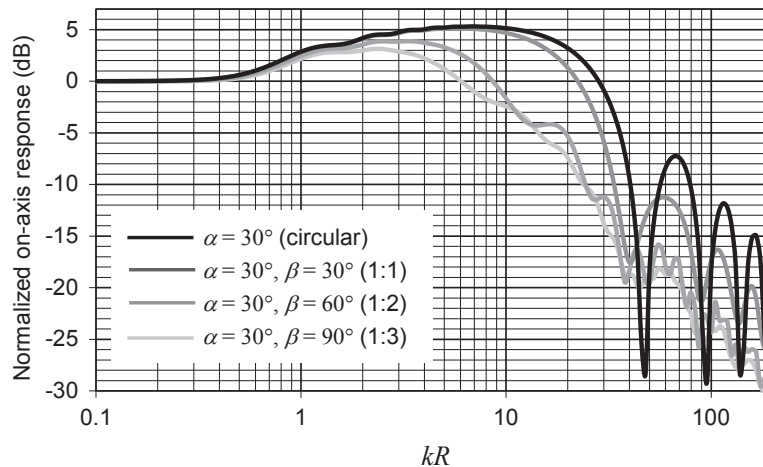


Figure 12.21 Plot of $20 \log_{10}|D(0,0)|$ where $D(\theta, \phi)$ is the directivity function of a rectangular cap in a rigid sphere of radius R , where α and β are the two half angles of the arc formed by the cap. The axial acceleration of the cap is constant. Frequency is plotted on a normalized scale, where $kR = 2\pi R/\lambda = 2\pi fR/c$.

has even deeper nulls than those of the oscillating cap shown in Fig. 12.18. Replacing it with a square cap, shown by the dark gray trace, immediately reduces the heights of the peaks and depths of the nulls. The smoothest response is that of the rectangular cap with an aspect ratio of 1:3 shown by the light gray trace. The worst shape is circular because at certain frequencies, the sound from near the perimeter arrives out of phase with that from the center and cancels it. At other frequencies, it is in phase and reinforces it. By making the cap rectangular, the cancellations are never complete because the amount of sound radiated from near the corners is reduced compared with what it would be if the cap were circular.

Radiation impedance

The total radiation force \tilde{F} is given by

$$\begin{aligned} \tilde{F} = 2R^2 & \left(\int_0^{\arctan \frac{\tan \beta}{\tan \alpha}} \int_0^{\arctan \frac{\tan \alpha}{\cos \phi}} \tilde{p}(R, \theta, \phi) \sin \theta \, d\theta \, d\phi \right. \\ & + \int_{\frac{\pi}{2} - \arctan \frac{\tan \alpha}{\tan \beta}}^{\frac{\pi}{2} + \arctan \frac{\tan \alpha}{\tan \beta}} \int_0^{\arctan \frac{\tan \beta}{\sin \phi}} \tilde{p}(R, \theta, \phi) \sin \theta \, d\theta \, d\phi \\ & \left. + \int_{\pi - \arctan \frac{\tan \beta}{\tan \alpha}}^{\pi} \int_0^{\arctan \frac{\tan \beta}{-\cos \phi}} \tilde{p}(R, \theta, \phi) \sin \theta \, d\theta \, d\phi \right) \end{aligned} \quad (12.86)$$

The specific impedance Z_s is then given by

$$Z_s = \frac{\tilde{F}}{\tilde{U}_0} = \frac{\tilde{F}}{S \tilde{u}_0} = \frac{2R^2 \rho_0 c}{S} \sum_{n=0}^{\infty} \sum_{m=0}^{n/2} A_{mn} h_n^{(2)}(kR) I_{mn}, \quad (12.87)$$

where we use the expression for S from Eq. (12.69). The real and imaginary parts, \mathbf{R}_s and X_s , are given by

$$Z_s = \mathbf{R}_s + jX_s = \Re(Z_s) + j\Im(Z_s). \quad (12.88)$$



12.8 RADIATION FROM A PISTON IN A SPHERE

The geometry of the piston of radius a in a sphere of radius R is shown in Fig. 12.22. In this example, we shall see the effect of having a planar radiator as opposed to the curved ones in all the previous examples. In the previous problem, the spherical

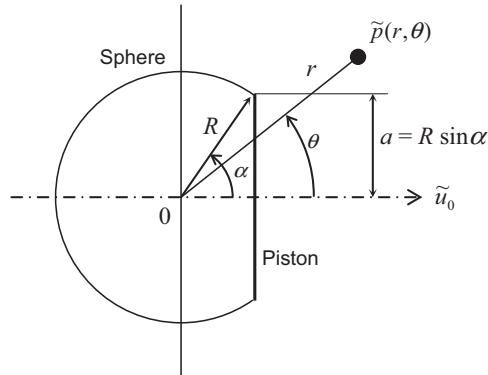


Figure 12.22 Geometry of piston in a rigid sphere.

cap followed the contour of the sphere so that there was only angular dependency in the velocity boundary condition with no radial dependency. This led to a direct solution for the expansion coefficients. Here, a flat circular piston [4] oscillates with a uniform axial velocity of \tilde{u}_0 . Hence, the velocity boundary condition is more complicated so that the expansion coefficients can only be obtained by solving a set of simultaneous equations.

Near-field pressure

Again we assume that the pressure field generated is a general axisymmetric solution to Eq. (2.180), the Helmholtz wave equation in spherical coordinates:

$$\tilde{p}(r, \theta) = \rho_0 \tilde{c} \tilde{u}_0 \sum_{n=0}^{\infty} A_n h_n^{(2)}(kr) P_n(\cos \theta), \quad (12.89)$$

where A_n are the as-yet unknown expansion coefficients, which will be calculated by means of a set of simultaneous equations in matrix form. Now, we define the velocity boundary condition on the piston as

$$\tilde{u}_z(r_1, \theta) = \tilde{u}_0, \quad 0 \leq \theta \leq \alpha, \quad r = r_1, \quad (12.90)$$

where

$$r_1 = \frac{R \cos \alpha}{\cos \theta}, \quad (12.91)$$

and the velocity boundary condition on the sphere as

$$\tilde{u}_r(R, \theta) = \frac{1}{-jk\rho_0 c} \cdot \frac{\partial}{\partial r} \tilde{p}(r, \theta) \Big|_{r=R} = 0, \quad \alpha < \theta < \pi, \quad r = R, \quad (12.92)$$

where the subscript z denotes the axial direction, or normal to the piston, and the subscript r denotes the radial direction, or normal to the sphere. The piston velocity boundary condition can be obtained using

$$\tilde{u}_z(r_1, \theta) = \frac{1}{-jk\rho_0 c} \frac{\partial}{\partial z} p(r, \theta)|_{r=r_1}, \quad (12.93)$$

where

$$\frac{\partial}{\partial z} = \frac{\partial r}{\partial z} \frac{\partial}{\partial r} + \frac{\partial \theta}{\partial z} \frac{\partial}{\partial \theta}, \quad (12.94)$$

$$\frac{\partial r}{\partial z} = \cos \theta, \quad (12.95)$$

$$\frac{\partial \theta}{\partial z} = -\frac{\sin \theta}{r}, \quad (12.96)$$

so that

$$\tilde{u}_z(r_1, \theta) = \frac{\tilde{u}_0}{-jk} \sum_{n=0}^{\infty} A_n \left(h_n^{(2)}(kr_1) P_n(\cos \theta) \cos \theta - \frac{1}{r_1} h_n^{(2)}(kr_1) P_n'(\cos \theta) \sin \theta \right), \quad (12.97)$$

where the derivative of the spherical Hankel function $h_n^{(2)}(kr_1)$ is given by Eq. (12.32) and the derivative of the Legendre function $P_n'(\cos \theta)$ is given from Eq. (A2.65) in Appendix II by

$$P_n'(\cos \theta) = \frac{\partial}{\partial \theta} P_n(\cos \theta) = \frac{n(n+1)}{(2n+1) \sin \theta} (P_{n-1}(\cos \theta) - P_{n+1}(\cos \theta)). \quad (12.98)$$

The sphere boundary condition is the same as that for the spherical cap in a sphere given by Eq. (12.52). We also note that the area of each surface element on the piston and the sphere are given, respectively, by

$$\delta S_p = 2\pi \frac{r_1^2}{\cos \theta} \sin \theta \delta \theta, \quad (12.99)$$

$$\delta S_s = 2\pi R^2 \sin \theta \delta \theta. \quad (12.100)$$

Hence, we can create an infinite set of simultaneous equations by multiplying Eqs. (12.90) and (12.92) through by $P_m(\cos \theta)$ and integrating over the surfaces of the piston and sphere:

$$\begin{aligned} & \int_0^\alpha \tilde{u}_z(r_1, \theta) P_m(\cos \theta) r_1^2 \tan \theta d\theta + R^2 \int_\alpha^\pi \tilde{u}_r(R, \theta) P_m(\cos \theta) \sin \theta d\theta \\ & = \tilde{u}_0 \int_0^\alpha P_m(\cos \theta) r_1^2 \tan \theta d\theta, \quad m = 0, 1, 2, \dots \end{aligned} \quad (12.101)$$

In matrix form, this becomes

$$\mathbf{M} \cdot \mathbf{a} = \mathbf{b} \Rightarrow \mathbf{a} = \mathbf{M}^{-1} \cdot \mathbf{b}, \quad (12.102)$$

where the matrix \mathbf{M} and vectors \mathbf{a} and \mathbf{b} are given by

$$\mathbf{M}(m+1, n+1) = \frac{I_{mn} + \left(nh_{n-1}^{(2)}(kR) - (n+1)h_{n+1}^{(2)}(kR) \right) K_{mn}}{2n+1}, \quad \begin{cases} m = 0, 1, \dots, N \\ n = 0, 1, \dots, N \end{cases}, \quad (12.103)$$

$$\mathbf{b}(m+1) = -jL_m, \quad m = 0, 1, \dots, N, \quad (12.104)$$

$$\mathbf{a}(n+1) = A_n, \quad n = 0, 1, \dots, N, \quad (12.105)$$

where

$$I_{mn} = \int_0^\alpha \left\{ \left(nh_{n-1}^{(2)}(kr_1) - (n+1)h_{n+1}^{(2)}(kr_1) \right) P_n(\cos \theta) \cos \theta \right. \\ \left. + n(n+1)h_n^{(2)}(kr_1)(P_{n-1}(\cos \theta) - P_{n+1}(\cos \theta)) / kr_1 \right\} P_m(\cos \theta) \frac{r_1^2}{R^2} \tan \theta d\theta, \quad (12.106)$$

$$K_{mn} = \int_\alpha^\pi P_n(\cos \theta) P_m(\cos \theta) \sin \theta d\theta, \quad (12.107)$$

$$L_m = \int_0^\alpha P_m(\cos \theta) \frac{r_1^2}{R^2} \tan \theta d\theta. \quad (12.108)$$

A solution to the integral K_{mn} is given by Eq. (A2.70) in Appendix II. Unfortunately, integrals I_{mn} and L_m have no analytical solutions and, therefore, have to be evaluated numerically using, for example,

$$\int_0^\alpha f(\theta) d\theta = \frac{\alpha}{P} \sum_{p=1}^P f(\theta_p), \quad \text{where } \theta_p = \frac{p-1/2}{P} \alpha. \quad (12.109)$$

Far-field pressure

In the far field, we can use the asymptotic expression for the spherical Hankel function from Eq. (12.18), which when inserted into Eq. (12.89) gives

$$\tilde{p}(r, \theta)|_{r \rightarrow \infty} = -jk\rho_0 c S \frac{\tilde{u}_0}{4\pi r} e^{-jkr} D(\theta). \quad (12.110)$$

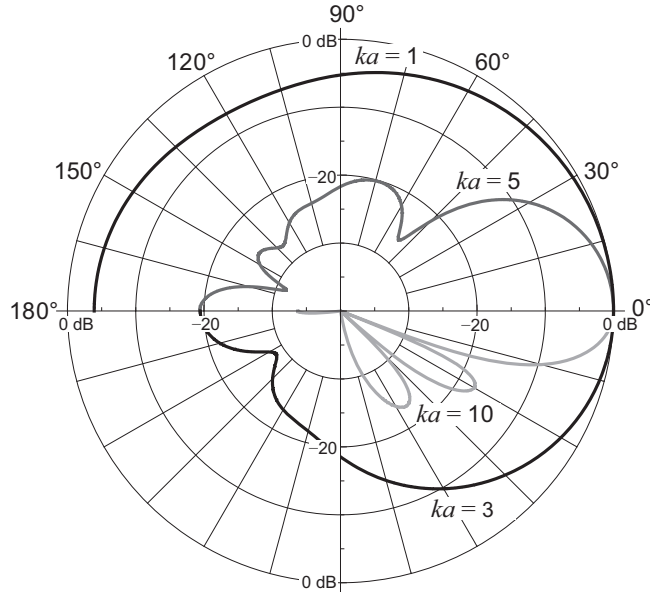


Figure 12.23 Far-field directivity pattern $20 \log_{10}(|D(\theta)|/|D(0)|)$ of the far-field pressure due to a piston of radius a in a rigid sphere for $\alpha = 60$ degrees, where $R = a/\sin \alpha$ is the radius of the sphere.

where S is the piston area given by $S = \pi a^2$ and

$$D(\theta) = -\frac{4}{k^2 R^2 \sin^2 \alpha} \sum_{n=0}^N A_n j^n P_n(\cos \theta). \quad (12.111)$$

The directivity pattern $20 \log_{10}(|D(\theta)|/|D(0)|)$ for $\alpha = 60$ degrees is plotted in Fig. 12.23 for various values of ka . The far-field on-axis response is given by

$$D(0) = -\frac{4}{k^2 R^2 \sin^2 \alpha} \sum_{n=0}^N A_n j^n. \quad (12.112)$$

The on-axis response $20 \log_{10}|D(0)|$ is plotted against ka in Fig. 12.24. Comparing the directivity pattern of Fig. 12.23 with that of a spherical cap shown in Fig. 12.17 we see that the piston is more directional at high frequencies, concentrating its output over a decreasing angle. By contrast, the spherical cap shows a fairly constant angle of dispersion at high frequencies, which is approximately equal to the angle of arc formed by the cap itself. The on-axis responses of Fig. 12.24 are quite interesting. They all show an overall 6 dB rise due to the transition from whole-space radiation at low frequencies to half-space radiation at high frequencies. In addition, there are ripples in the response above $ka = 1.5$ due to reflections from the edge of the piston, which acts as a secondary radiator interfering with the direct radiation. Furthermore, the 15 degrees

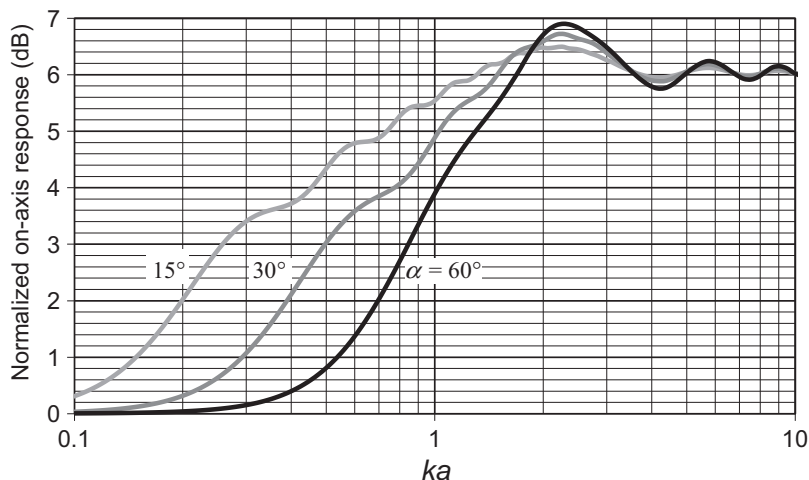


Figure 12.24 Plot of $20 \log_{10}|D(0)|$ where $D(\theta)$ is the directivity function of a piston of radius a in a rigid sphere, where $R = a/\sin \alpha$ is the radius of the sphere. The axial acceleration of the piston is constant. Frequency is plotted on a normalized scale, where $ka = 2\pi a/\lambda = 2\pi fa/c$.

cap behaves rather like the point source on a sphere and produces ripples below $ka = 1.5$ due to diffraction around the sphere. An important difference between planar sources and curved “constant directivity” sources such as the spherical cap (see Fig. 12.18), driven with constant acceleration, is that the on-axis response of the latter rolls off in the region where the radiation impedance is resistive and the radiated pressure is thus proportional to the velocity of the radiating surface. With a planar source, the narrowing of the directivity pattern and subsequent concentration of the radiated pressure on axis tends to compensate for this and maintain a level response. At lower frequencies, where the radiation load is mainly mass, both have a level pressure response with constant acceleration due to Newton’s second law: force = mass \times acceleration.

Radiation impedance

The total radiation force \tilde{F} is given by

$$\tilde{F} = \int_0^{2\pi} \int_0^\alpha \tilde{p}(r_1, \theta) r_1^2 \tan \theta \, d\theta \, d\phi. \quad (12.113)$$

The specific impedance Z_s is then given by

$$Z_s = \frac{\tilde{F}}{\tilde{U}_0} = \frac{2\rho_0 c}{R^2 \sin^2 \alpha} \sum_{n=0}^{\infty} A_n \int_0^\alpha h_n^{(2)}(kr_1) P_n(\cos \theta) r_1^2 \tan \theta \, d\theta, \quad (12.114)$$

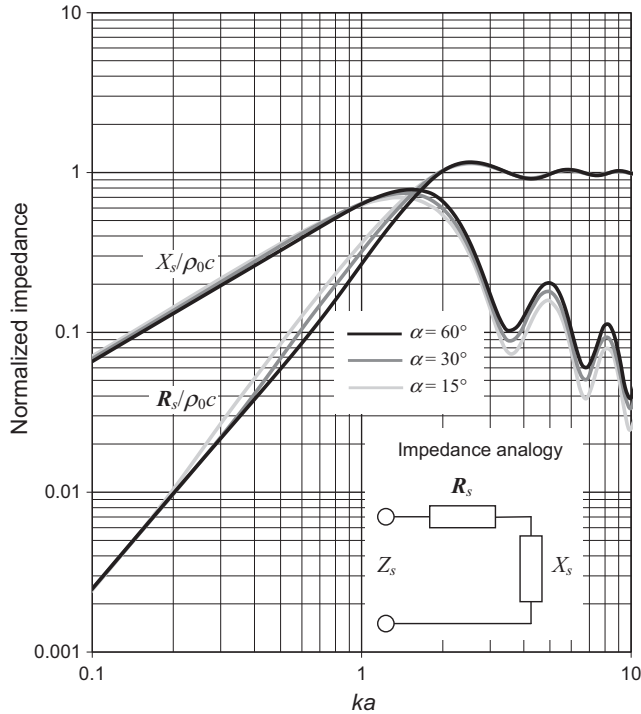


Figure 12.25 Real and imaginary parts of the normalized specific radiation impedance Z_s/ρ_0c of the air load on an oscillating piston of radius a in a rigid sphere, where $R = a/\sin \alpha$ is the radius of the sphere. Frequency is plotted on a normalized scale, where $ka = 2\pi a/\lambda = 2\pi fa/c$.

where $\tilde{U}_0 = \pi R^2 \sin^2 \alpha \tilde{u}_0$. The real and imaginary parts, \mathbf{R}_s and X_s , are plotted in Fig. 12.25 where

$$Z_s = \mathbf{R}_s + jX_s = \Re(Z_s) + j\Im(Z_s). \tag{12.115}$$

The main difference between these curves and those of Fig. 12.19 for the spherical cap is that they all show ripples due to interference patterns in the immediate vicinity of the piston.

➤ 12.9 RADIATION FROM AN OSCILLATING CONVEX DOME IN AN INFINITE BAFFLE

A convex dome [5] of radius a and radius of curvature R in an infinite baffle is shown in Fig. 12.26. We shall solve this problem using field matching, whereby we make use of the fact that the dome in an infinite baffle produces the same field as that of two back-to-back domes in free space that oscillate in opposite directions. The latter produces a symmetrical field which is identical to that of the single dome together with its image field due to reflection from the baffle. In this way,

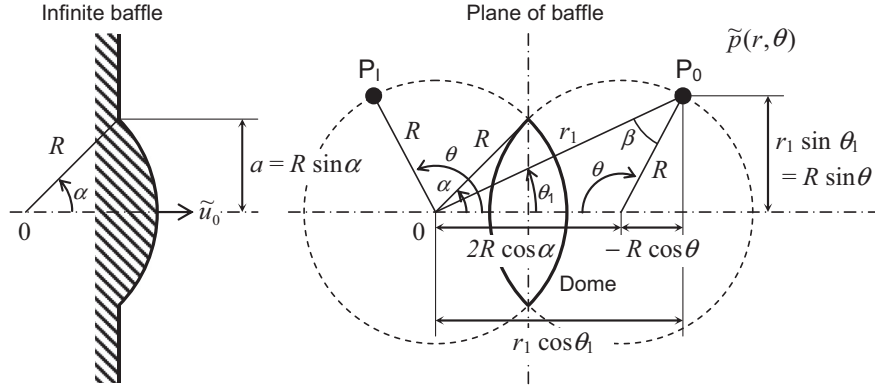


Figure 12.26 Geometry of convex dome in infinite baffle.

the boundary condition of zero velocity or pressure gradient at the baffle is satisfied automatically.

Near-field pressure

Again we assume that the pressure field generated is a general axisymmetric solution to Eq. (2.180), the Helmholtz wave equation in spherical coordinates:

$$\tilde{p}(r, \theta) = \rho_0 c \tilde{u}_0 \sum_{n=0}^{\infty} A_n h_n^{(2)}(kr) P_n(\cos \theta), \quad (12.116)$$

where A_n are the as-yet unknown expansion coefficients, which will be calculated by means of a set of simultaneous equations in matrix form. The normal particle velocity $\tilde{u}_s(R, \theta)$ at the surface of the dome is given by

$$\begin{aligned} \tilde{u}_s(R, \theta) &= \frac{1}{-jk\rho_0 c} \frac{\partial}{\partial r} p(r, \theta) \Big|_{r=R} \\ &= \frac{\tilde{u}_0}{-jk} \sum_{n=0}^{\infty} A_n h_n^{\prime(2)}(kR) P_n(\cos \theta). \end{aligned} \quad (12.117)$$

where the derivative of the spherical Hankel function $h_n^{\prime(2)}(kR)$ is given by Eq. (12.32). For $\theta \leq \alpha$, this is simply equal to the normal velocity of the dome. However, for $\theta > \alpha$, we are in the image field to the left of the baffle plane, as indicated by P_1 in Fig. 12.26, and we need to match this velocity with that of the particle velocity $\tilde{u}_1(\theta)$ at the corresponding point P_0 to the right of the plane. The latter is defined by

$$\tilde{u}_1(r_1, \theta_1) = \frac{1}{-jk\rho_0 c} \frac{\partial}{\partial r} \tilde{p}(r, \theta) \Big|_{r=r_1, \theta=\theta_1}, \quad (12.118)$$

where the derivative is taken with respect to the normal n of the surface such that

$$\frac{\partial}{\partial n} = \frac{\partial r}{\partial n} \cdot \frac{\partial}{\partial r} + \frac{\partial \theta}{\partial n} \cdot \frac{\partial}{\partial \theta}, \quad (12.119)$$

$$\frac{\partial r}{\partial n} = \cos \beta, \quad (12.120)$$

$$\frac{\partial \theta}{\partial n} = \frac{\sin \beta}{r}. \quad (12.121)$$

The following useful relationships can be derived from the geometry of the problem:

$$\cos \beta = \frac{R}{r_1} (1 - 2 \cos \alpha \cos \theta), \quad (12.122)$$

$$r_1 = R \sqrt{1 + 4 \cos \alpha (\cos \alpha - \cos \theta)}, \quad (12.123)$$

$$\cos \theta_1 = \frac{R}{r_1} (2 \cos \alpha - \cos \theta). \quad (12.124)$$

Inserting all of the above into Eq. (12.118) leads to

$$\tilde{u}_1(r_1, \theta_1) = \frac{\tilde{u}_0}{-jk} \sum_{n=0}^{\infty} A_n \left(h_n^{(2)}(kr_1) \cos \beta P_n(\cos \theta_1) + h_n^{(2)}(kr_1) \frac{\sin \beta}{r_1} P_n'(\cos \theta_1) \right), \quad (12.125)$$

where the derivative of the spherical Hankel function $h_n^{(2)}(kR)$ is given by Eq. (12.32) and the derivative of the Legendre function $P_n'(\cos \theta_1)$ is given by Eq. (A2.65) from Appendix II. By matching the fields, the velocity boundary condition can be expressed by

$$\tilde{u}_s(R, \theta) = \begin{cases} \tilde{u}_0 \cos \theta, & 0 \leq \theta \leq \alpha \\ \tilde{u}_1(r_1, \theta_1) & \alpha < \theta \leq \pi \end{cases}. \quad (12.126)$$

As before, we multiply through with the orthogonal function $P_m(\cos \theta)$ and integrate over the surface of the sphere, where the area of each surface element is given by

$$\delta S = 2\pi R^2 \sin \theta \delta \theta,$$

to yield the following infinite set of simultaneous equations:

$$\int_0^\pi \tilde{u}_s(R, \theta) P_m(\cos \theta) \sin \theta d\theta = \tilde{u}_0 \int_0^\alpha P_m(\cos \theta) \cos \theta \sin \theta d\theta \\ + \int_\alpha^\pi \tilde{u}_1(r_1, \theta_1) P_m(\cos \theta) \sin \theta d\theta, \quad m = 0, 1, 2, \dots \quad (12.127)$$

Inserting Eqs. (12.117) and (12.125) for $\tilde{u}_s(R, \theta)$ and $\tilde{u}_1(r_1, \theta_1)$, respectively, into Eq. (12.127), while truncating the infinite summation limits to order N , gives

$$\sum_{n=0}^N A_n \left(\frac{2\delta_{mn} \left(nh_{n-1}^{(2)}(kR) - (n+1)h_{n+1}^{(2)}(kR) \right)}{(2n+1)^2} - I_{mn} \right) = -jK_m, \quad m = 0, 1, 2, \dots, N \quad (12.128)$$

where

$$I_{mn} = \int_\alpha^\pi \left(\frac{nh_{n-1}^{(2)}(kr_1) - (n+1)h_{n+1}^{(2)}(kr_1)}{2n+1} P_n(\cos \theta_1) \cos \beta \right. \\ \left. - \frac{n(n+1)h_n^{(2)}(kr_1)}{(2n+1)kr_1} (P_{n-1}(\cos \theta_1) - P_{n+1}(\cos \theta_1)) \frac{\sin \beta}{\sin \theta_1} \right) P_m(\cos \theta) \sin \theta d\theta, \quad (12.129)$$

$$K_m = \int_0^\alpha P_m(\cos \theta) \cos \theta \sin \theta d\theta \\ = \begin{cases} (1 - \cos^3 \alpha)/3, & m = 1 \\ -\sin \alpha \frac{\sin \alpha P_m(\cos \alpha) + \cos \alpha P_m^1(\cos \alpha)}{(m-1)(m+2)}, & m \neq 1 \end{cases} \quad (12.130)$$

where the identities of Eqs. (A2.66) and (A2.68) from Appendix II have been applied. Unfortunately, the integral I_{mn} has no analytical solution and has to be evaluated numerically using, for example,

$$\int_\alpha^\pi f(\theta) d\theta = \frac{\pi - \alpha}{P} \sum_{p=1}^P f(\theta_p), \quad \text{where } \theta_p = \alpha + \frac{p-1/2}{P}(\pi - \alpha). \quad (12.131)$$

In matrix form, Eq. (12.128) becomes

$$\mathbf{M} \cdot \mathbf{a} = \mathbf{b} \Rightarrow \mathbf{a} = \mathbf{M}^{-1} \cdot \mathbf{b}, \quad (12.132)$$

where the $N \times N$ matrix elements are given by

$$\mathbf{M}(m+1, n+1) = \frac{2\delta_{mn} \left(nh_{n-1}^{(2)}(kR) - (n+1)h_{n+1}^{(2)}(kR) \right)}{(2n+1)^2} - I_{mn}, \quad \begin{cases} m = 0, 1, \dots, N \\ n = 0, 1, \dots, N \end{cases}, \quad (12.133)$$

$$\mathbf{b}(m+1) = -jK_m, \quad m = 0, 1, \dots, N, \quad (12.134)$$

$$\mathbf{a}(n+1) = A_n, \quad n = 0, 1, \dots, N, \quad (12.135)$$

Far-field pressure

In the far field, we can use the asymptotic expression for the spherical Hankel function from Eq. (12.18), which when inserted into Eq. (12.116) gives

$$\tilde{p}(r, \theta)|_{r \rightarrow \infty} = -jk\rho_0 c S \frac{\tilde{u}_0}{2\pi r} e^{-jkr} D(\theta), \quad (12.136)$$

where S is the dome effective area given by $S = \pi a^2$ and

$$D(\theta) = -\frac{2}{k^2 R^2 \sin^2 \alpha} \sum_{n=0}^N A_n j^n P_n(\cos \theta). \quad (12.137)$$

In the case where $\alpha = \frac{1}{2}\pi$, we obtain the following simple expansion solution from Eq. (12.60):

$$D(\theta)_{\alpha=\frac{\pi}{2}} \Big| = -j \frac{2}{k^2 R^2} \sum_{n=0}^N \frac{(-1)^n (4n+1)^2 P_{2n}(0) P_{2n}(\cos \theta)}{(2n-1)(2n+1) \left(2nh_{2n-1}^{(2)}(kR) - (2n+1)h_{2n+1}^{(2)}(kR) \right)}. \quad (12.138)$$

The directivity pattern $20 \log_{10}(|D(\theta)|/|D(0)|)$ for $\alpha = 60$ degrees is plotted in Fig. 12.27 for various values of ka . The results are fairly similar to those of the spherical cap in a sphere in that at low frequencies the pattern is almost omnidirectional and at high frequencies the dome cap shows a fairly constant angle of dispersion which is

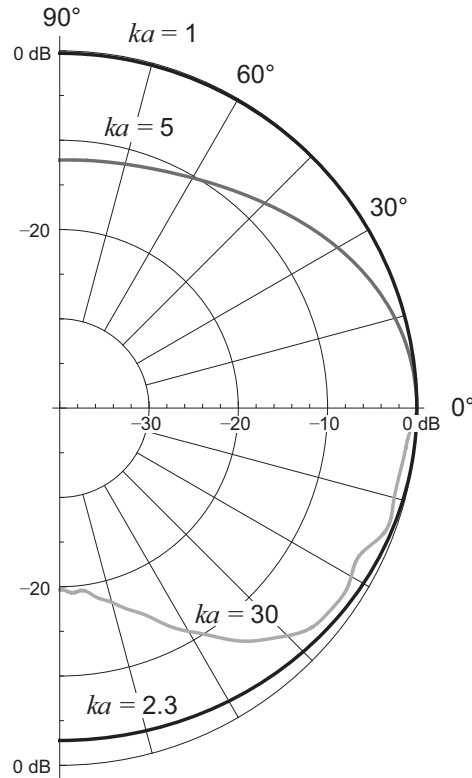


Figure 12.27 Far-field directivity pattern $20 \log_{10}(|D(\theta)|/|D(0)|)$ of the far-field pressure due to a convex dome of radius a in an infinite baffle for $\alpha = 60$ degrees, where α is the half angle of the arc formed by the dome.

approximately equal to the angle of arc formed by the dome itself. The far-field on-axis response is given by

$$D(0) = -\frac{2}{k^2 R^2 \sin^2 \alpha} \sum_{n=0}^N A_n j^n. \quad (12.139)$$

The on-axis response $20 \log_{10}|D(0)|$ is plotted against ka in Fig. 12.28. Again, the response is fairly similar to that of the spherical cap in a sphere except that there is no 6 dB level shift between low and high frequencies due to that fact that the sound is radiated into half space at all frequencies.

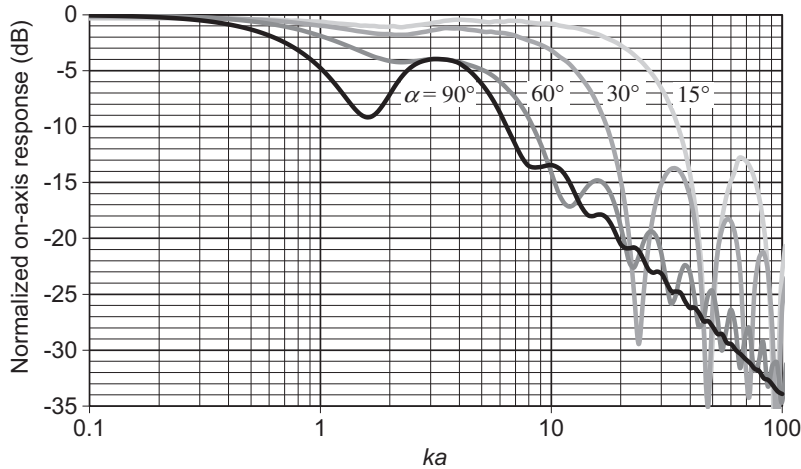


Figure 12.28 Plot of $20 \log_{10}|D(0)|$ where $D(\theta)$ is the directivity function of a convex dome of radius a in an infinite baffle, where α is the half angle of the arc formed by the dome. The axial acceleration of the dome is constant. Frequency is plotted on a normalized scale, where $ka = 2\pi a/\lambda = 2\pi fa/c$.

Radiation impedance

The total radiation force \tilde{F} is given by

$$\tilde{F} = R^2 \int_0^{2\pi} \int_0^\alpha \tilde{p}(R, \theta) \cos \theta \sin \theta \, d\theta \, d\phi, \quad (12.140)$$

using the identity of Eq. (A2.68) from Appendix II. The specific impedance Z_s is then given by

$$Z_s = \frac{\tilde{F}}{\tilde{U}_0} = \frac{2\rho_0 c}{\sin^2 \alpha} \sum_{n=0}^N A_n h_n^{(2)}(kR) K_n, \quad (12.141)$$

where we have used the expression for \tilde{U}_0 from Eq. (12.49). The real and imaginary parts, \mathbf{R}_s and X_s , are plotted in Fig. 12.29 where

$$Z_s = \mathbf{R}_s + jX_s = \Re(Z_s) + j\Im(Z_s). \quad (12.142)$$

Again the results are fairly similar to those for a spherical cap in a sphere except at low frequencies where the radiation impedance is greater due to the half-space radiation load.



12.10 RADIATION FROM AN OSCILLATING CONCAVE DOME IN AN INFINITE BAFFLE

A concave dome [5] of radius a and radius of curvature R in an infinite baffle is shown in Fig. 12.30. In this problem, we shall introduce the concept of coupling whereby

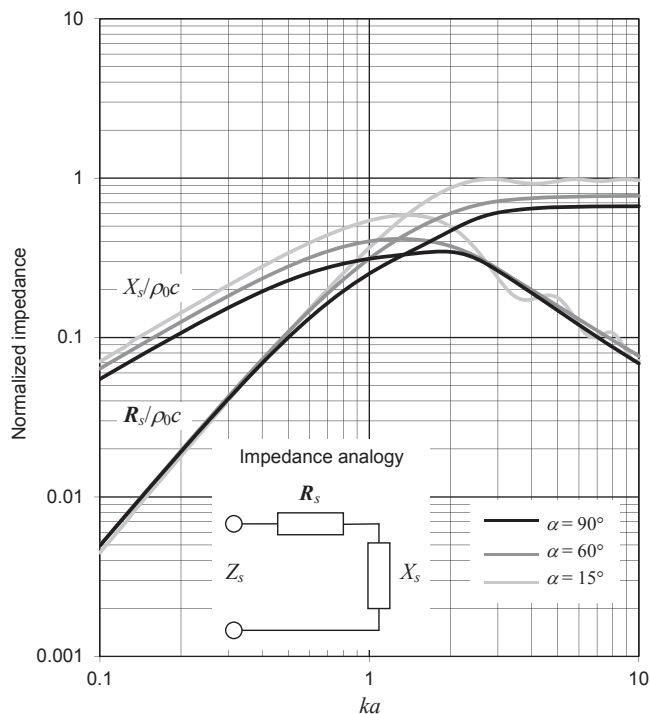


Figure 12.29 Real and imaginary parts of the normalized specific radiation impedance Z_s/ρ_0c of the air load on a convex dome of radius a in an infinite baffle, where α is the half angle of the arc formed by the dome. Frequency is plotted on a normalized scale, where $ka = 2\pi a/\lambda = 2\pi fa/c$.

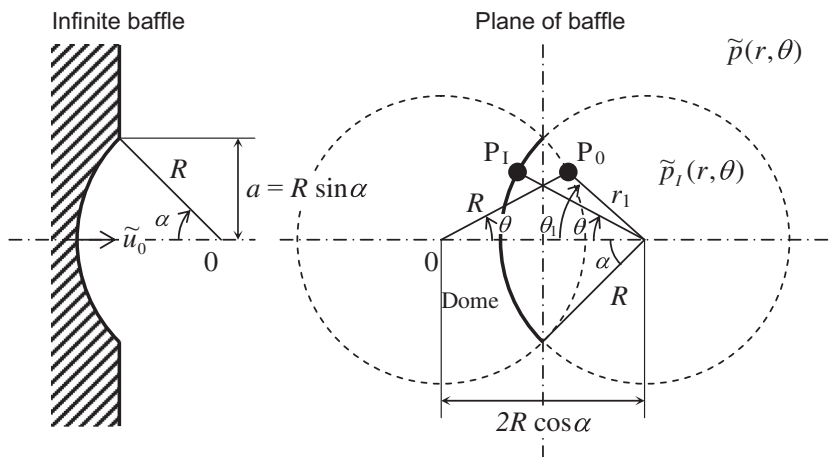


Figure 12.30 Geometry of concave dome in infinite baffle.

the field $\tilde{p}_I(r, \theta)$ inside the imaginary sphere, which includes the space inside the dome, is coupled to an external field $\tilde{p}(r, \theta)$. Again, the baffle can be removed so that we have an equivalent field which is symmetrical either side of the plane of the baffle. However, in the external field, we completely ignore the dome as if it inhabited some other universe. What we have in effect is a breathing disk in free space with identical pressure distributions on both faces, which are also the same as that of the mouth of the dome. The velocity distributions are also equal in magnitude to that of the mouth, but have opposite directions. This enables us to apply the same field-matching condition as in the convex dome.

Near-field pressure

We assume that the external pressure field $\tilde{p}(r, \theta)$ in the region $r \geq R$ is a general axisymmetric solution to Eq. (2.180), the Helmholtz wave equation in spherical coordinates:

$$\tilde{p}(r, \theta) = \rho_0 c \tilde{u}_0 \sum_{n=0}^{\infty} x_n h_n^{(2)}(kr) P_n(\cos \theta), \quad (12.143)$$

where x_n are the as-yet unknown expansion coefficients, which will be calculated by means of a set of simultaneous equations in matrix form. The normal particle velocity $\tilde{u}_S(R, \theta)$ at the surface of the sphere is given by

$$\begin{aligned} \tilde{u}(R, \theta) &= \frac{1}{-jk\rho_0 c} \frac{\partial}{\partial r} \tilde{p}(r, \theta)|_{r=R} \\ &= \frac{\tilde{u}_0}{-jk} \sum_{n=0}^{\infty} x_n h_n^{\prime(2)}(kR) P_n(\cos \theta), \end{aligned} \quad (12.144)$$

where the derivative of the spherical Hankel function $h_n^{\prime(2)}(kR)$ is given by Eq. (12.32). The internal field $\tilde{p}_I(r, \theta)$ must be continuous everywhere in the region $r \leq R$. Hence, we omit the spherical Bessel function of the second kind, which has a singularity at $r = 0$, from the spherical Hankel function so that

$$\tilde{p}_I(r, \theta) = \rho_0 c \tilde{u}_0 \sum_{n=0}^{\infty} \gamma_n j_n(kr) P_n(\cos \theta), \quad (12.145)$$

where γ_n are the unknown expansion coefficients. The normal particle velocity $\tilde{u}_I(R, \theta)$ at the surface of the sphere is given by

$$\begin{aligned} \tilde{u}_I(R, \theta) &= \frac{1}{-jk\rho_0 c} \frac{\partial}{\partial r} p_I(r, \theta)|_{r=R} \\ &= \frac{\tilde{u}_0}{-jk} \sum_{n=0}^{\infty} \gamma_n j_n^{\prime}(kR) P_n(\cos \theta). \end{aligned} \quad (12.146)$$

At the surface of the dome, the normal particle velocity has to match the axial velocity \tilde{u}_0 of the dome. Hence,

$$\tilde{u}_I(R, \theta) = -\tilde{u}_0 \cos \theta, \quad 0 \leq \theta \leq \alpha. \quad (12.147)$$

In addition, we have the coupling condition whereby the normal particle velocity on the inner surface of the imaginary sphere has to match that on its outer surface

$$\tilde{u}_I(R, \theta) = \tilde{u}(R, \theta), \quad \alpha \leq \theta \leq \pi. \quad (12.148)$$

Likewise, the pressure on the inner surface of the sphere has to match that on its outer surface:

$$\tilde{p}(R, \theta) = \tilde{p}_I(R, \theta), \quad \alpha < \theta \leq \pi. \quad (12.149)$$

Finally, we apply the field matching whereby the pressure on the outer surface of the imaginary sphere is equal to that of its mirror image, which lies inside the image sphere:

$$\tilde{p}(R, \theta) = \tilde{p}_I(r_1, \theta_1), \quad 0 < \theta \leq \alpha. \quad (12.150)$$

From the geometry of the problem, we can write

$$r_1 = R\sqrt{1 + 4 \cos \alpha (\cos \alpha - \cos \theta)}, \quad (12.151)$$

$$\cos \theta_1 = \frac{R}{r_1} (2 \cos \alpha - \cos \theta). \quad (12.152)$$

Now, we have all of the boundary conditions in place, we can create the following pair of infinite simultaneous equations in the unknown coefficients x_n and y_n in the usual manner by multiplying through $P_m(\cos \theta)$ and integrating over the surface of the imaginary sphere together with its image and the surface of the dome:

$$\begin{aligned} \int_0^\pi \tilde{p}(R, \theta) P_m(\cos \theta) \sin \theta \, d\theta &= \int_0^\alpha \tilde{p}_I(r_1, \theta_1) P_m(\cos \theta) \sin \theta \, d\theta \\ &+ \int_\alpha^\pi \tilde{p}_I(R, \theta) P_m(\cos \theta) \sin \theta \, d\theta, \quad m = 0, 1, 2, \dots, \end{aligned} \quad (12.153)$$

$$\begin{aligned} \int_0^\pi \tilde{u}_I(R, \theta) P_m(\cos \theta) \sin \theta \, d\theta &= -\tilde{u}_0 \int_0^\alpha P_m(\cos \theta) \cos \theta \sin \theta \, d\theta \\ &+ \int_\alpha^\pi \tilde{u}(R, \theta) P_m(\cos \theta) \sin \theta \, d\theta, \quad m = 0, 1, 2, \dots. \end{aligned} \quad (12.154)$$

In matrix form, this becomes

$$\mathbf{x} = \mathbf{A} \cdot \mathbf{y}, \quad (12.155)$$

$$\mathbf{y} = \mathbf{B} \cdot \mathbf{x} + \mathbf{c}, \quad (12.156)$$

where

$$\mathbf{x} = [x_0, x_1, \dots, x_m], \mathbf{y} = [y_0, y_1, \dots, y_m],$$

where the matrices \mathbf{A} and \mathbf{B} and vector \mathbf{c} are given by

$$\mathbf{A}(m+1, n+1) = \frac{m+1/2}{h_m^{(2)}(kR)} (I_{mn} + j_n(kR)K_{mn}), \quad \begin{cases} m = 0, 1, \dots, N \\ n = 0, 1, \dots, N \end{cases}, \quad (12.157)$$

$$\mathbf{B}(m+1, n+1) = \frac{m+1/2}{j'_m(kR)} h_n^{(2)}(kR)K_{mn}, \quad \begin{cases} m = 0, 1, \dots, N \\ n = 0, 1, \dots, N \end{cases}, \quad (12.158)$$

$$\mathbf{c}(m+1) = jk \frac{m+1/2}{j'_m(kR)} L_m, \quad m = 0, 1, \dots, N, \quad (12.159)$$

where

$$I_{mn} = \int_0^a j_n(kr_1) P_n(\cos \theta_1) P_m(\cos \theta) \sin \theta \, d\theta, \quad (12.160)$$

$$K_{mn} = \int_\alpha^\pi P_n(\cos \theta) P_m(\cos \theta) \sin \theta \, d\theta$$

$$= \begin{cases} \frac{\sin \alpha (P_m(\cos \alpha) P'_n(\cos \alpha) - P_n(\cos \alpha) P'_m(\cos \alpha))}{m(m+1) - n(n+1)}, & m \neq n \\ \frac{1 + (P_m(\cos \alpha))^2 \cos \alpha + 2 \sum_{j=1}^{m-1} P_j(\cos \alpha) (P_j(\cos \alpha) \cos \alpha - P_{j+1}(\cos \alpha))}{2m+1}, & m = n \end{cases}, \quad (12.161)$$

$$L_m = \int_0^\alpha P_m(\cos \theta) \cos \theta \sin \theta \, d\theta$$

$$= \begin{cases} (1 - \cos^3 \alpha)/3, & m = 1 \\ -\sin \alpha \frac{\sin \alpha P_m(\cos \alpha) + \cos \alpha P_m^1(\cos \alpha)}{(m-1)(m+2)}, & m \neq 1, \end{cases} \quad (12.162)$$

where the identities of Eqs. (A2.66), (A2.68), and (A2.70) from Appendix II have been applied. Unfortunately, the integral I_{mm} has no analytical solution and has to be evaluated numerically using, for example,

$$\int_0^{\alpha} f(\theta) d\theta = \frac{\alpha}{P} \sum_{p=1}^P f(\theta_p), \quad \text{where } \theta_p = \frac{p-1/2}{P} \alpha. \quad (12.163)$$

Solving Eqs. (12.155) and (12.156) for \mathbf{x} and \mathbf{y} gives

$$\mathbf{y} = [\mathbf{I} - \mathbf{B} \cdot \mathbf{A}]^{-1} \cdot \mathbf{c}, \quad (12.164)$$

$$\mathbf{x} = \mathbf{A} \cdot \mathbf{y}. \quad (12.165)$$

Far-field pressure

In the far field, we can use the asymptotic expression for the spherical Hankel function from Eq. (12.18), which when inserted into Eq. (12.143) gives

$$\tilde{p}(r, \theta)|_{r \rightarrow \infty} = -jk\rho_0 c S \frac{\tilde{u}_0}{2\pi r} e^{-jkr} D(\theta), \quad (12.166)$$

where S is the dome effective area given by $S = \pi a^2$ and

$$D(\theta) = -\frac{2}{k^2 R^2 \sin^2 \alpha} \sum_{n=0}^N x_n j^n P_n(\cos \theta). \quad (12.167)$$

The directivity pattern $20 \log_{10}(|D(\theta)|/|D(0)|)$ for $\alpha = 60$ degrees is plotted in Fig. 12.31 for various values of ka . Not surprisingly, the directivity is similar to that of the convex dome. The far-field on-axis response is given by

$$D(0) = -\frac{2}{k^2 R^2 \sin^2 \alpha} \sum_{n=0}^N x_n j^n. \quad (12.168)$$

The on-axis response $20 \log_{10}|D(0)|$ is plotted against ka in Fig. 12.32. This shows some interesting features. The dips in the responses of the convex dome shown in Fig. 12.28 for various values α are now replaced with resonant peaks. In each case, the resonant frequency is determined by the compliance of the dome cavity and the radiation mass. The peak is fairly broad due to the damping effect of the radiation resistance. At $ka = 4.1$, we see a sharp dip due to a radial standing wave across the mouth of the dome, where the air just circulates back and forth between points of maximum and minimum pressure. Above this frequency, the response is fairly uneven due to standing wave harmonics.

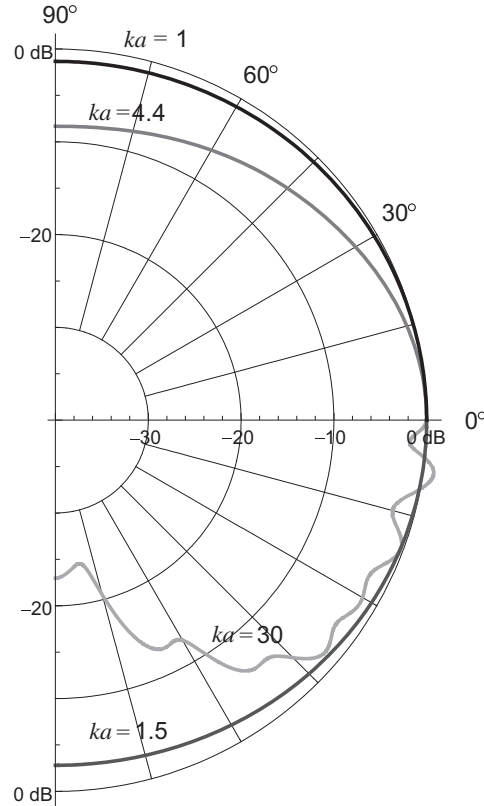


Figure 12.31 Far-field directivity pattern $20 \log_{10}(|D(\theta)|/|D(0)|)$ of the far-field pressure due to a concave dome of radius a in an infinite baffle for $\alpha = 60$ degrees, where α is the half angle of the arc formed by the dome.

Radiation impedance

The total radiation force \tilde{F} is given by

$$\tilde{F} = R^2 \int_0^{2\pi} \int_0^a \tilde{p}(R, \theta) \cos \theta \sin \theta \, d\theta \, d\phi \quad (12.169)$$

using the identity of equation (A2.68) from Appendix II. The specific impedance Z_s is then given by

$$Z_s = \frac{\tilde{F}}{\tilde{U}_0} = \frac{2\rho_0 c}{\sin^2 \alpha} \sum_{n=0}^N \gamma_n j_n(kR) L_n, \quad (12.170)$$

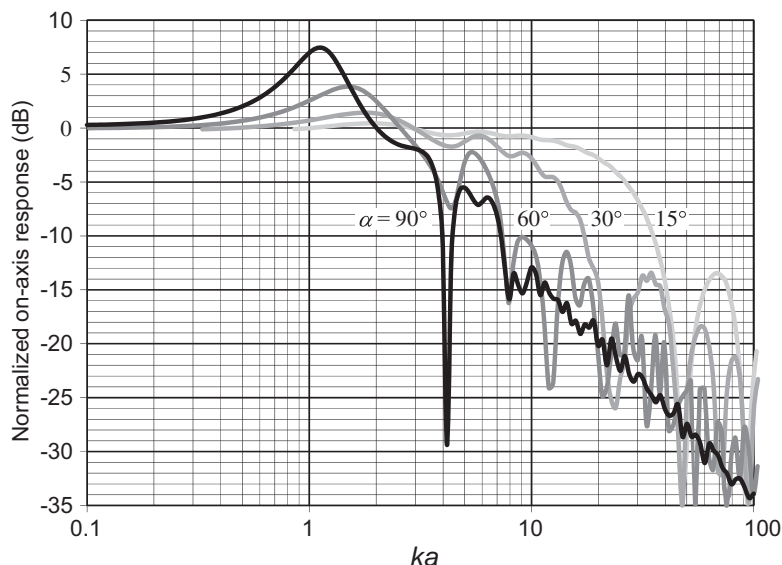


Figure 12.32 Plot of $20 \log_{10}|D(0)|$ where $D(\theta)$ is the directivity function of a concave dome of radius a in an infinite baffle, where α is the half angle of the arc formed by the dome. The axial acceleration of the dome is constant. Frequency is plotted on a normalized scale, where $ka = 2\pi a/\lambda = 2\pi fa/c$.

where we have used the expression for \tilde{U}_0 from Eq. (12.49). The real and imaginary parts, \mathbf{R}_s and X_s , are plotted in Fig. 12.33, where

$$Z_s = \mathbf{R}_s + jX_s = \Re(Z_s) + j\Im(Z_s). \quad (12.171)$$

We can see from these curves that at the first peak in the radiation resistance, which more or less corresponds with the first peak in the on-axis response, the radiation reactance is at a minimum, so that the radiation efficiency is enhanced. Below this resonance, the reactance is positive due to the radiation mass. Immediately above it, the reactance is negative due to the compliance of the dome cavity. However, due to standing wave modes, the reactance is alternately positive and negative as the frequency increases above $ka = 4$.

Problem 12.1. In Section 12.1, we derived the sound pressure at a radial distance w from the axis of an infinitely long pulsating cylinder of radius a . Divide the pressure at the surface (where $w = a$) by the surface velocity \tilde{u}_0 to obtain the specific radiation impedance, after substituting $\tilde{U}_0 = 2\pi a\tilde{u}_0$. Separate the impedance into real and imaginary parts by multiplying the numerator and denominator by the complex conjugate of the denominator $H_1^{(1)}(ka)$ and applying the Hankel function identities of

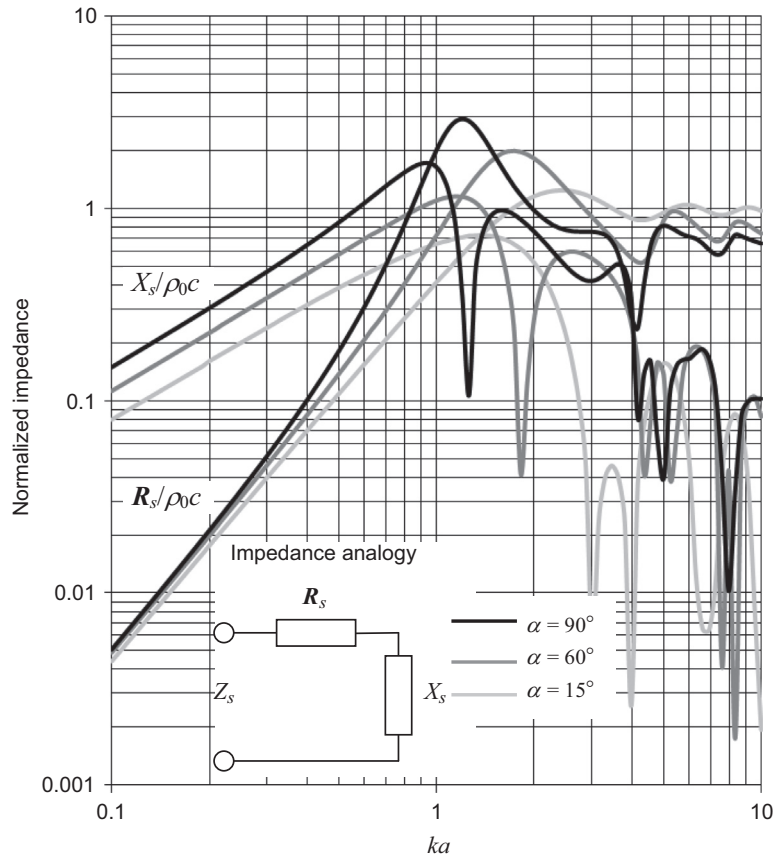


Figure 12.33 Real and imaginary parts of the normalized specific radiation impedance Z_s/ρ_0c of the air load on a concave dome of radius a in an infinite baffle, where α is the half angle of the arc formed by the dome. Frequency is plotted on a normalized scale, where $ka = 2\pi a/\lambda = 2\pi fa/c$.

Eqs. (A2.74) and (A2.75) of Appendix II. Use the Wronskian of Eq. (A2.111) to simplify the real part and thus show that it is the throat impedance of an infinite hyperbolic horn given by Eq. (9.30) if we set $a = x_T$.

Problem 12.2. In Section 12.6, we derived the nearfield pressure, far-field pressure and radiation impedance of an *oscillating* spherical cap in a sphere. Derive the same for a *pulsating* spherical cap in a sphere using the same methods. In other words, instead of the cap oscillating axially, it moves radially with a velocity $u_0%$, which removes the $\cos\theta$ terms from Eqs. (12.48), (12.49), (12.52), (12.53), and (12.62). Instead of Eq. (A2.68), use Eq. (A2.69) from Appendix II to evaluate the integral on the right-hand-side of Eq. (12.53) and the integral of Eq. (12.62). Show that the results are the same as those obtained in Section 13.5 using the boundary integral method.

REFERENCES

- [1] Stenzel H. Über die von einer starren Kugel hervorgerufene Störung des schallfeldes (On the Interference of a Sound Field Produced by a Rigid Ball). *ENT* 1938;15:71–8.
- [2] Skudrzyk E. *The foundations of acoustics: basic mathematics and basic acoustics*. Wien: Springer-Verlag; 1971. p. 396–400 [Although Skudrzyk's equations are in a different form, the results agree well with those presented here].
- [3] Morse PM, Ingard KU. *Theoretical acoustics*. New York: McGraw-Hill; 1968. p. 343–6.
- [4] Skudrzyk E. *The foundations of acoustics: basic mathematics and basic acoustics*. Wien: Springer-Verlag; 1971. p. 400–7 [Skudrzyk's solution was obtained by a slightly different method from the one presented here and used least squares minimization whereas here it is obtained directly using the property of orthogonality. However, the two solutions show good agreement].
- [5] Suzuki H, Tichy J. Sound radiation from convex and concave domes in an infinite baffle. *J Acoust Soc Am* 1981;69(1):41–9 [Their solution was obtained by a slightly different method from the one presented here and used least squares minimization. However, the two solutions show good agreement].
- [6] Aarts RM, Janssen AJEM. Sound radiation from a resilient spherical cap on a rigid sphere. *J Acoust Soc Am* 2010;127(4):2262–73.

Radiation and scattering of sound by the boundary integral method

PART XXXV: BOUNDARY INTEGRALS AND THE GREEN'S FUNCTION

13.1 THE HUYGENS—FRESNEL PRINCIPLES

The Huygens—Fresnel principle states that each point on the wave front of a propagating wave can be replaced with a point source as illustrated in Fig. 13.1, thus creating an array of wavelets whereby each wavelet is unaffected by the presence of all the other wavelets. Some time later, the wave front is equivalent to the envelope of these wavelets. In other words, the resultant field is due to the sum of the point sources, using the principle of superposition. The point sources can be monopoles or dipoles. Although the forward propagating wave remains unaltered, the principle does not explain the creation of a backward propagating wave that was not present in the original. However, if the surface over which the point sources are distributed encloses the original source(s) fully, we can use the principle to analyze the internal or external fields separately. It can also be used to

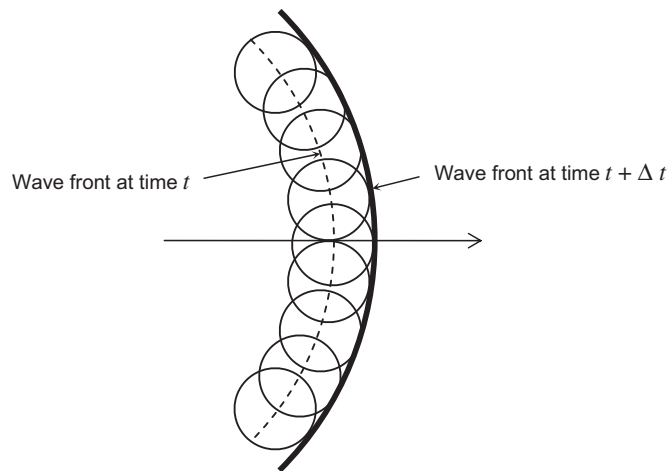


Figure 13.1 Huygens—Fresnel principle.

analyze sound radiation from vibrating surfaces, which may or may not be closed, provided that the boundary conditions are correct.



13.2 THE RAYLEIGH INTEGRALS AND GREEN'S FUNCTION

In this section, monopole and dipole boundary integrals are derived in an intuitive way based on the Huygens–Fresnel principle whereby monopole and dipole point sources are summed over surfaces. A more mathematically rigorous treatment follows in [Section 13.3](#). We have treated all problems so far in this text as *boundary value problems* based on solutions to the following *homogeneous* Helmholtz wave equation in an arbitrary coordinate system:

$$(\nabla^2 + k^2)\tilde{p}(\mathbf{r}) = 0, \quad (13.1)$$

where, for example, in rectangular coordinates $(\mathbf{r}) = (x, y, z)$ and the Laplace operator ∇^2 is given in rectangular, cylindrical, and spherical coordinates by Eqs. (2.147), (2.160), and (2.181), respectively. By *homogeneous*, we mean that the equation describes waves that could exist, but there are no driving forces or velocities present in the equation to create them. These come later from the boundary conditions. In general, the boundary value method involves solving the homogeneous Helmholtz wave equation in a suitable orthogonal coordinate system such that it becomes a separable equation. That is, the equation is split into a set of differential equations, each with respect to one ordinate only, as described in Sections 2.9–2.11. The solutions to those equations then contain constants, which can be determined by applying boundary conditions. By a suitable coordinate system, we mean one that first must lead to a separable wave equation (if there is more than one ordinate involved) and second fits the geometry of the problem, by which we mean that boundary conditions can be applied by setting pressure or velocity to specific values at constant ordinate values. The simplest example is the pulsating sphere that is solved by setting the particle velocity at the surface of the sphere, where the radial ordinate is equal to the sphere's radius. In the limit, when the radius approaches zero, this leads to the pressure field due to a point source as defined in Eq. (4.71). Let us now recast this equation in the following form:

$$\tilde{p}(\mathbf{r}|\mathbf{r}_0) = jk\rho_0c\tilde{U}_0g(\mathbf{r}|\mathbf{r}_0), \quad (13.2)$$

where \mathbf{r} and \mathbf{r}_0 are the positions of the observation point and source respectively in an arbitrary coordinate system. The function $g(\mathbf{r}|\mathbf{r}_0)$ is known as the *Green's function* and is defined by

$$g(\mathbf{r}|\mathbf{r}_0) = \frac{e^{-jk(\mathbf{r}-\mathbf{r}_0)}}{4\pi(\mathbf{r}-\mathbf{r}_0)}. \quad (13.3)$$

For example, in rectangular coordinates, we would write

$$g(x, y, z|x_0, y_0, z_0) = \frac{e^{-jk\sqrt{(x-x_0)^2+(y-y_0)^2+(z-z_0)^2}}}{4\pi\sqrt{(x-x_0)^2+(y-y_0)^2+(z-z_0)^2}}. \quad (13.4)$$

The Green's function is a useful short hand for the spatial distribution due to a point source, but it does not indicate its absolute strength. In this instance, it tells us that the sound pressure varies sinusoidally as it spreads outwards from the source, and its amplitude is inversely proportional to the distance from the source. It should be noted that there is a singularity at $\mathbf{r} = \mathbf{r}_0$. Using the Huygens–Fresnel principle we can treat a vibrating surface as an array of point sources, or rather surface elements that in the limit shrink to points. In the case of a closed surface (i.e., that which fully encloses a volume), we need not worry about the back wave when considering the external field. The volume velocity of each surface element is given by

$$\tilde{U}_0(\mathbf{r}_0) = \tilde{u}_0(\mathbf{r}_0)\delta S_0, \quad (13.5)$$

where δS_0 is the area of the surface element and $\tilde{u}_0(\mathbf{r}_0)$ is the velocity *normal to the surface* at point \mathbf{r}_0 . The radiated field is the sum of the fields due to all the point sources so that

$$\tilde{p}_M(\mathbf{r}) = jk\rho_0c \iint \tilde{u}_0(\mathbf{r}_0)g(\mathbf{r}|\mathbf{r}_0)dS_0, \quad (13.6)$$

which is known as the *monopole Rayleigh integral*. Furthermore, using the relationship

$$\tilde{u}_0(\mathbf{r}_0) = \frac{1}{-jk\rho_0c} \frac{\partial}{\partial n_0} \tilde{p}(\mathbf{r}_0) \quad (13.7)$$

leads to

$$\tilde{p}_M(\mathbf{r}) = - \iint \frac{\partial}{\partial n_0} \tilde{p}(\mathbf{r}_0)g(\mathbf{r}|\mathbf{r}_0)dS_0. \quad (13.8)$$

Similarly, the surface can be made up of dipole point sources, each comprising two monopole point sources of opposite polarity, separated by a distance Δz_0 that tends to zero. Let the Green's function be defined in axisymmetric spherical–cylindrical coordinates by

$$g(r, \theta|z_0) = \frac{e^{-jkr_1}}{4\pi r_1}, \quad (13.9)$$

where

$$r_1^2 = r^2 + z_0^2 - 2rz_0 \cos \theta$$

and θ is the inclination angle of the observation point relative to the z -axis, which passes through the two monopole point sources. The dipole point source is located at a distance z_0 from the origin and r is the distance from the observation point to the origin. The gradient of the Green's function in the z direction is then given by

$$\frac{\partial}{\partial z_0} g(r, \theta | z_0) \Big|_{z_0=0} = \left(\frac{1}{r} + jk \right) \cos \theta \frac{e^{-jkr}}{4\pi r}. \quad (13.10)$$

From Eq. (4.114), the field due to a single dipole point source has previously been shown to be

$$\tilde{p}(r, \theta) = jk\rho_0 c \tilde{U}_0 b \left(\frac{1}{r} + jk \right) \cos \theta \frac{e^{-jkr}}{4\pi r}, \quad (13.11)$$

which after substituting Eq. (13.10) and letting $b = \Delta z_0$ becomes

$$\tilde{p}(r, \theta) = jk\rho_0 c \tilde{U}_0 \Delta z_0 \frac{\partial}{\partial z_0} g(r, \theta | z_0) \Big|_{z_0=0}. \quad (13.12)$$

Again, using the relationships of Eqs. (13.5) and (13.7), together with

$$\Delta_{z_0} \frac{\partial \tilde{p}_0}{\partial z_0} \Big|_{\Delta z_0 \rightarrow 0} = -\tilde{p}_0, \quad (13.13)$$

leads to

$$\tilde{p}(r, \theta) = \tilde{p}_0 \frac{\partial}{\partial z_0} g(r, \theta | z_0) \Big|_{z_0=0} \delta S_0, \quad (13.14)$$

which is then integrated over the surface to give

$$\tilde{p}_D(\mathbf{r}) = \iint \tilde{p}(\mathbf{r}_0) \frac{\partial}{\partial n_0} g(\mathbf{r} | \mathbf{r}_0) dS_0 \quad (13.15)$$

in any coordinate system. This is known as the *dipole Rayleigh integral*. We note that the derivative of the Green's function is taken with respect to the normal n_0 to the surface because the axis of each dipole element must be normal to the surface.



13.3 THE KIRCHHOFF–HELMHOLTZ BOUNDARY INTEGRAL

In the previous section we introduced the Green's function

$$g(\mathbf{r}|\mathbf{r}_0) = \frac{e^{-jk(\mathbf{r}-\mathbf{r}_0)}}{4\pi(\mathbf{r}-\mathbf{r}_0)}, \quad (13.16)$$

which turns out to be a solution of the following *inhomogeneous* wave equation:

$$(\nabla^2 + k^2)g(\mathbf{r}|\mathbf{r}_0) = -\delta(\mathbf{r}-\mathbf{r}_0). \quad (13.17)$$

An important principle in acoustics is that of *reciprocity* whereby the locations of the sound source \mathbf{r}_0 and its observation point \mathbf{r} are interchangeable. It can be seen that Eqs. (13.16) and (13.17) are unaffected by interchanging \mathbf{r} and \mathbf{r}_0 . Hence

$$g(\mathbf{r}|\mathbf{r}_0) = g(\mathbf{r}_0|\mathbf{r}) \quad (13.18)$$

and

$$\delta(\mathbf{r}-\mathbf{r}_0) = \delta(\mathbf{r}_0-\mathbf{r}). \quad (13.19)$$

Eq. (13.17) differs from the *homogeneous* wave Eq. (13.1) in that the Dirac delta function δ on the right hand side represents the excitation at the point \mathbf{r}_0 . Eq. (13.17) describes the normalized pressure field (that is, divided by $ik\rho c\tilde{U}_0$) of a point source. However, it is desirable to solve the following inhomogeneous wave equation for *any* source distribution:

$$(\nabla^2 + k^2)\tilde{p}(\mathbf{r}) = -\tilde{f}(\mathbf{r}), \quad (13.20)$$

where $\tilde{f}(\mathbf{r})$ is a source pressure distribution in Pa/m². This can be achieved [1,2] by multiplying Eq. (13.17) by $\tilde{p}(\mathbf{r})$ and then subtracting it from Eq. (13.20) multiplied by $g(\mathbf{r}|\mathbf{r}_0)$, which leads to

$$g(\mathbf{r}|\mathbf{r}_0)\nabla^2\tilde{p}(\mathbf{r}) - \tilde{p}(\mathbf{r})\nabla^2g(\mathbf{r}|\mathbf{r}_0) = \tilde{p}(\mathbf{r})\delta(\mathbf{r}-\mathbf{r}_0) - g(\mathbf{r}|\mathbf{r}_0)\tilde{f}(\mathbf{r}). \quad (13.21)$$

Using the reciprocity relationships of Eqs. (13.18) and (13.19), we can exchange \mathbf{r} and \mathbf{r}_0 in Eq. (13.21) and integrate over an arbitrary volume containing all the sources to obtain

$$\begin{aligned} & \iiint (g(\mathbf{r}|\mathbf{r}_0)\nabla_0^2\tilde{p}(\mathbf{r}_0) - \tilde{p}(\mathbf{r}_0)\nabla_0^2g(\mathbf{r}|\mathbf{r}_0))dV_0 \\ &= \iiint\int\tilde{p}(\mathbf{r}_0)\delta(\mathbf{r}-\mathbf{r}_0)dV_0 - \iiint\int g(\mathbf{r}|\mathbf{r}_0)\tilde{f}(\mathbf{r}_0)dV_0, \end{aligned} \quad (13.22)$$

where the zero subscripts indicate differentiation with respect to the \mathbf{r}_0 coordinates. Using Green's theorem [3], which essentially states that anything created within a diverging volume passes through its outer surface, the volume integral of the term in parentheses can be replaced with a surface integral:

$$\begin{aligned}
 & \iiint \left(g(\mathbf{r}|\mathbf{r}_0) \nabla_0^2 \tilde{p}(\mathbf{r}_0) - \tilde{p}(\mathbf{r}_0) \nabla_0^2 g(\mathbf{r}|\mathbf{r}_0) \right) dV_0 \\
 &= \iiint \nabla_0 \left(g(\mathbf{r}|\mathbf{r}_0) \nabla_0 \tilde{p}(\mathbf{r}_0) - \tilde{p}(\mathbf{r}_0) \nabla_0 g(\mathbf{r}|\mathbf{r}_0) \right) dV_0 \quad (13.23) \\
 &= \iint \left(g(\mathbf{r}|\mathbf{r}_0) \frac{\partial}{\partial n_0} \tilde{p}(\mathbf{r}_0) - \tilde{p}(\mathbf{r}_0) \frac{\partial}{\partial n_0} g(\mathbf{r}|\mathbf{r}_0) \right) dS_0,
 \end{aligned}$$

where the surface of integration bounds the volume of the original volume integral, and the Laplace operator is replaced with a first-order derivative normal to the surface, pointing away from the space enclosed by the surface integral. We can verify the first step of Eq. (13.23) by working backwards. Although taking the derivative of the two products in the second line leads to four terms, two of them cancel to leave the remaining two terms in the first line. The third line is obtained from the second by the divergence theorem of Gauss. Inserting Eq. (13.23) into Eq. (13.22) and using the property of the Dirac delta function to solve the volume integral $\tilde{p}(\mathbf{r}_0) \delta(\mathbf{r} - \mathbf{r}_0)$ yields

$$\tilde{p}(\mathbf{r}) = \tilde{p}_V(\mathbf{r}) + \tilde{p}_S(\mathbf{r}), \quad (13.24)$$

where $\tilde{p}_V(\mathbf{r})$ is a volume integral given by

$$\tilde{p}_V(\mathbf{r}) = \iiint g(\mathbf{r}|\mathbf{r}_0) \tilde{f}(\mathbf{r}_0) dV_0 \quad (13.25)$$

and $\tilde{p}_S(\mathbf{r})$ is the Kirchhoff–Helmholtz surface integral given by

$$\tilde{p}_S(\mathbf{r}) = \tilde{p}_M(\mathbf{r}) + \tilde{p}_D(\mathbf{r}) \quad (13.26)$$

where $\tilde{p}_M(\mathbf{r})$ is the monopole integral given by

$$\tilde{p}_M(\mathbf{r}) = \iint g(\mathbf{r}|\mathbf{r}_0) \frac{\partial}{\partial n_0} \tilde{p}(\mathbf{r}_0) dS_0 \quad (13.27)$$

and $\tilde{p}_D(\mathbf{r})$ is the dipole integral given by

$$\tilde{p}_D(\mathbf{r}) = - \iint \tilde{p}(\mathbf{r}_0) \frac{\partial}{\partial n_0} g(\mathbf{r}|\mathbf{r}_0) dS_0. \quad (13.28)$$

What is remarkable about Eq. (13.24) is that, merely given a solution $g(\mathbf{r}|\mathbf{r}_0)$ to the wave equation for a point source, it provides a solution for the pressure field $\tilde{p}(\mathbf{r})$ everywhere in the presence of an arbitrary source distribution $\tilde{f}(\mathbf{r}_0)$ within the volume of integration.

It should be noted that in this instance, the integrals $\tilde{p}_M(\mathbf{r})$ and $\tilde{p}_D(\mathbf{r})$ have nothing to do with reflections, although they can be applied to problems of scattering surfaces when appropriate boundary conditions are applied. The volume of integration does not have a physical reflecting boundary surface but a transparent notional one. Inside the volume, $\tilde{p}_M(\mathbf{r})$ and $\tilde{p}_D(\mathbf{r})$ cancel each other so that there is no net contribution from $\tilde{p}_S(\mathbf{r})$, and the field is entirely given by the volume integral, or

$$\tilde{p}(\mathbf{r})|_{\mathbf{r} \in V_0} = \tilde{p}_V(\mathbf{r}), \quad \tilde{p}_S(\mathbf{r}) = 0, \quad \tilde{p}_M(\mathbf{r}) = -\tilde{p}_D(\mathbf{r}). \quad (13.29)$$

However, outside the boundary, the field due to the surface integral cancels the field due to the volume integral:

$$\tilde{p}(\mathbf{r})|_{\mathbf{r} \notin V_0} = 0, \quad \tilde{p}_S(\mathbf{r}) = -\tilde{p}_V(\mathbf{r}), \quad \left(\begin{array}{l} \tilde{p}_M(\mathbf{r}) = \tilde{p}_D(\mathbf{r}) = -\tilde{p}_V(\mathbf{r})/2 \\ \text{if planar infinite surface} \end{array} \right). \quad (13.30)$$

Hence, $\tilde{p}_S(\mathbf{r})$ is a discontinuous solution to Eq. (13.20), which is only valid outside the volume containing the sources (provided that the sign is reversed). If the volume is infinitely large, the Sommerfeld condition applies and the boundary integrals vanish so that $\tilde{p}(\mathbf{r}) = \tilde{p}_V(\mathbf{r})$ is a solution to Eq. (13.20) everywhere. In practice, however, the volume of integration only has to include all the sources under consideration, but not necessarily all the observation points. The usefulness of the boundary surface integral of Eq. (13.26) for solving acoustical problems cannot be overstated; it forms the basis for many numerical methods such as Boundary Element Modeling (or BEM). It is an embodiment of the Huygens–Fresnel principle discussed in Section 13.1. The surface of integration must be a closed one, which fully encloses all the sources, although they may form part or all of the surface. By a closed surface, we could also mean an infinite plane that isolates the sources on one side of the plane (or within the plane itself) from the observation field on the other. Although $\tilde{p}_M(\mathbf{r})$ and $\tilde{p}_D(\mathbf{r})$ are both needed in the case of general surfaces, such as the spherical cap in a sphere in Section 13.5, we shall see that in the case of planar sources, one of the integrals can often be eliminated because of the symmetry of the problem. Before we apply the boundary integral to some problems of practical importance, we shall take a further look at the Green's function.



13.4 THE GREEN'S FUNCTION IN DIFFERENT COORDINATE SYSTEMS

Rectangular coordinates

Rectangular coordinates—near-field

The Green's function in rectangular coordinates was given by Eq. (13.4) as

$$g(x, y, z|x_0, y_0, z_0) = e^{-jkR}/(4\pi R), \quad (13.31)$$

where R is the Euclidean distance, which is given by

$$R = \sqrt{(x - x_0)^2 + (y - y_0)^2 + (z - z_0)^2}. \quad (13.32)$$

However, problems are often encountered when using this expression because the space variables are all enclosed in a square-root sign and therefore cannot be separated. This makes finding analytical solutions very difficult, and one often has to resort to using moveable-origin coordinate systems. This limits its use to numerical integration in the Kirchhoff–Helmholtz surface integral. Unfortunately, the Green's function of Eq. (13.31) is not particularly amenable to numerical integration because it is singular at the origin and leads to oscillatory integrands at high frequencies. The dipole integral is even more problematic because the Green's function normal gradient has a $1/R^2$ term, which leads to diverging numerical and analytical integrals. Furthermore, where the surface of integration encloses one or more sources, we can only calculate the field on the side of the surface where there are no sources and the waves are diverging. In other words we cannot solve the *reverse* problem and calculate the field in which there are sources and the waves converge toward them. A more powerful formula is given by

$$g(x, y, z|x_0, y_0, z_0) = \frac{-j}{8\pi^2} \int_{-\infty}^{\infty} \int_{-\infty}^{\infty} \frac{e^{-j(k_x(x-x_0)+k_y(y-y_0)+k_z|z-z_0|)}}{k_z} dk_x dk_y \quad (13.33)$$

where

$$k_z = \begin{cases} \sqrt{k^2 - k_x^2 - k_y^2}, & k_x^2 + k_y^2 \leq k^2 \\ -j\sqrt{k_x^2 + k_y^2 - k^2}, & k_x^2 + k_y^2 > k^2 \end{cases} \quad (13.34)$$

where k_x , k_y , and k_z represent the spatial frequency components in the x , y , and z directions respectively of a plane wave of spatial frequency k traveling in an arbitrary direction. For example, if the direction of travel subtends an angle θ with the z -axis, then the trace velocity seen along the z -axis is $c/\cos \theta$ and the wave number is $k_z = k \cos \theta$.

Hence the wavelength will appear to be longer along the z -axis. To gain a better understanding of Eq. (13.33) we may compare it with Eq. (7.113) for the pressure field inside an enclosure by letting $k_x = m\pi/l_x$, $k_y = n\pi/l_y$, and $k_z = k_{mn}$. We also replace the infinite integrals with summations. In other words, Eq. (13.33) may be thought of as the spatial distribution of an infinite enclosure in which traveling plane waves of any wavelength may exist as opposed to standing ones of particular wavelengths that correspond to the dimensions of the finite enclosure. The fact that a point source can be represented as integral over all spatial frequencies is not so surprising when we consider that an infinite impulse contains all frequencies.

It may seem counterintuitive to introduce two extra integrals, but the troublesome $1/R$ term has vanished along with the square-root sign in the exponent. When used in the Kirchhoff–Helmholtz integrals, we will show in Section 13.19 that this integral form of the Green's function is an inverse Fourier transform. This leads to an important theorem that forms the basis of near-field acoustical holography in which the dipole Kirchhoff–Helmholtz integral evaluated over one plane is the Fourier transform of the pressure distribution in that plane. The sound field spectra is then propagated in k -space to another parallel plane in which the Green's function is the inverse Fourier transform that gives the pressure in that plane. Furthermore, we can solve the so-called reverse problem where there are one or more sources in the field of interest. This method of calculation is particularly amenable to the digital processing of sound fields captured by planar microphone arrays to calculate the entire sound field of interest. In other words, if there are sources on one side of the array, we can plot the pressure field on *both* sides of the array. This is not possible using the Euclidean form of the Green's function of Eq. (13.31).

Proof of the Fourier Green's function in rectangular coordinates

To derive the Fourier Green's function, we shall apply a triple Fourier transform, one for each Cartesian ordinate, to the Green's function in the spatial domain to convert it to the spatial frequency domain or k -space.

$$G(k_x, k_y, k_z) = \int_{-\infty}^{\infty} \int_{-\infty}^{\infty} \int_{-\infty}^{\infty} g(x, y, z|x_0, y_0, z_0) e^{j(k_x x + k_y y + k_z z)} dx dy dz, \quad (13.35)$$

where $G(k_x, k_y, k_z)$ is the Fourier transform of $g(x, y, z|x_0, y_0, z_0)$. The inverse transform is

$$g(x, y, z|x_0, y_0, z_0) = \frac{1}{8\pi^3} \int_{-\infty}^{\infty} \int_{-\infty}^{\infty} \int_{-\infty}^{\infty} G(k_x, k_y, k_z) e^{-j(k_x x + k_y y + k_z z)} dk_x dk_y dk_z. \quad (13.36)$$

To solve for $G(k_x, k_y, k_z)$, we take the Fourier transform of Eq. (13.17)

$$\begin{aligned} & \int_{-\infty}^{\infty} \int_{-\infty}^{\infty} \int_{-\infty}^{\infty} (\nabla^2 + k^2) g(x, y, z | x_0, y_0, z_0) e^{j(k_x x + k_y y + k_z z)} dx dy dz \\ &= - \int_{-\infty}^{\infty} \int_{-\infty}^{\infty} \int_{-\infty}^{\infty} \delta(x - x_0) \delta(y - y_0) \delta(z - z_0) e^{j(k_x x + k_y y + k_z z)} dx dy dz, \end{aligned} \quad (13.37)$$

where

$$\nabla^2 = \frac{\partial^2}{\partial x^2} + \frac{\partial^2}{\partial y^2} + \frac{\partial^2}{\partial z^2}. \quad (13.38)$$

Using the general property of the Dirac delta function from Eq. (154) of Appendix II and noting that

$$\nabla^2 e^{-j(k_x x + k_y y + k_z z)} = \left(-k_x^2 - k_y^2 - k_z^2 \right) e^{-j(k_x x + k_y y + k_z z)}$$

yields

$$\begin{aligned} & \left(k^2 - k_x^2 - k_y^2 - k_z^2 \right) \int_{-\infty}^{\infty} \int_{-\infty}^{\infty} \int_{-\infty}^{\infty} g(x, y, z | x_0, y_0, z_0) e^{j(k_x x + k_y y + k_z z)} dx dy dz \\ &= -e^{jk(k_x x_0 + k_y y_0 + k_z z_0)}, \end{aligned} \quad (13.39)$$

which after substituting in Eq. (13.35) gives us the Green's function in k -space:

$$G(k_x, k_y, k_z) = \frac{e^{j(k_x x_0 + k_y y_0 + k_z z_0)}}{k_x^2 + k_y^2 + k_z^2 - k^2}. \quad (13.40)$$

Applying the inverse Fourier transform of Eq. (13.36) then gives us a Fourier Green's function in terms of k -parameters:

$$\begin{aligned} g(x, y, z | x_0, y_0, z_0) &= \frac{1}{8\pi^3} \int_{-\infty}^{\infty} \int_{-\infty}^{\infty} \int_{-\infty}^{\infty} \frac{e^{-j(k_x(x-x_0) + k_y(y-y_0) + k_z(z-z_0))}}{k_x^2 + k_y^2 + k_z^2 - k^2} dk_x dk_y dk_z \\ &= \frac{1}{8\pi^3} \int_{-\infty}^{\infty} \int_{-\infty}^{\infty} \int_{-\infty}^{\infty} \frac{e^{-j(k_x(x-x_0) + k_y(y-y_0) + k_z(z-z_0))}}{\left(k_z + \sqrt{k^2 - k_x^2 - k_y^2} \right) \left(k_z - \sqrt{k^2 - k_x^2 - k_y^2} \right)} dk_x dk_y dk_z, \end{aligned} \quad (13.41)$$

which has two poles: one at $k_z = +\sigma$ and the other at $k_z = -\sigma$, where

$$\sigma = \sqrt{k^2 - k_x^2 - k_y^2}.$$

We now convert Eq. (13.41) from a volume integral to a surface one by integrating over k_z using the *residue theorem*, which states that

$$\int_{-\infty}^{\infty} f(x)e^{-jxt} dx = \begin{cases} -2\pi j \text{ (sum of residues of } f(x)e^{jxt} \text{ at all its poles } \alpha_i \\ \text{above the real axis), } & t \geq 0 \\ 2\pi j \text{ (sum of residues of } f(x)e^{jxt} \text{ at all its poles } \alpha_i \\ \text{on or below the real axis), } & t < 0 \end{cases}, \quad (13.42)$$

where each residue is defined by

$$(x - \alpha_i)f(x)e^{-jxt} \Big|_{x \rightarrow \alpha_i}. \quad (13.43)$$

Applying this to Eq. (13.41) to solve the integral over k_z gives

$$g(x, y, z | x_0, y_0, z_0) = \frac{-j}{8\pi^2} \int_{-\infty}^{\infty} \int_{-\infty}^{\infty} \frac{e^{-j(k_x(x-x_0)+k_y(y-y_0)+\sigma|z-z_0|)}}{\sigma} dk_x dk_y. \quad (13.44)$$

If we let $k_z = \sigma$, this then gives us Eq. (13.33).

Rectangular coordinates—far-field

At a large distance R , Eq. (13.31) simplifies to

$$\begin{aligned} g(x, y, z | x_0, y_0, z_0) \Big|_{R \rightarrow \infty} &= \frac{e^{-jk(x(x-x_0)+y(y-y_0)+z(z-z_0))/r}}{4\pi r} \\ &= \frac{e^{-jkr}}{4\pi r} e^{jk(x x_0 + y y_0 + z z_0)/r}, \end{aligned} \quad (13.45)$$

where

$$r = \sqrt{x^2 + y^2 + z^2}. \quad (13.46)$$

Cylindrical coordinates

If we substitute

$$x = w \cos \phi, \quad y = w \sin \phi, \quad x_0 = w_0 \cos \phi_0, \quad y_0 = w_0 \sin \phi_0 \quad (13.47)$$

in Eq. (13.31) and use

$$\sin \phi \sin \phi_0 + \cos \phi \cos \phi_0 = \cos(\phi - \phi_0),$$

we obtain

$$g(w, \phi, z|w_0, \phi_0, z_0) = e^{-jkR}/(4\pi R), \quad (13.48)$$

where

$$R = \sqrt{w^2 + w_0^2 - 2ww_0 \cos(\phi - \phi_0) + (z - z_0)^2}. \quad (13.49)$$

However, this expression is of limited use and suffers from all the same drawbacks as were described in reference to the Euclidean Green's function in rectangular coordinates given by Eq. (13.31). A more powerful formula [4] is given by

$$\begin{aligned} g(w, \phi, z|w_0, \phi_0, z_0) &= \frac{-j}{4\pi} \sum_{n=0}^{\infty} (2 - \delta_{n0}) \cos n(\phi - \phi_0) \\ &\times \int_0^{\infty} J_n(k_w w) J_n(k_w w_0) \frac{e^{-jk_z |z - z_0|}}{k_z} k_w dk_w, \end{aligned} \quad (13.50)$$

where

$$k_z = \begin{cases} \sqrt{k^2 - k_w^2}, & 0 \leq k_w \leq k \\ -j\sqrt{k_w^2 - k^2}, & k_w > k, \end{cases} \quad (13.51)$$

which is known as the Lamb–Sommerfeld integral [5,6]. This equation can be considered as the integral over all spatial frequencies of radial standing waves in an infinite cylinder, which are also summed over all azimuthal harmonics of order n . The component in the z direction is planar as represented by the exponent term. The reason why we have radial standing waves is that incoming waves pass through the z axis (or $w = 0$) before traveling back out again. In doing so, the imaginary part of the Hankel function, or Y_n function, changes sign. Thus the Y_n function is canceled leaving just the J_n function. This can be considered as the same phenomena as the incoming waves being reflected back from a rigid termination at $w = 0$. Hence the standing waves. In the case of axial symmetry, we exclude all azimuthal harmonics but the $n = 0$ term:

$$g(w, z|w_0, z_0) = \frac{-j}{4\pi} \int_0^{\infty} J_0(k_w w) J_0(k_w w_0) \frac{e^{-jk_z |z - z_0|}}{k_z} k_w dk_w. \quad (13.52)$$

We will apply this formula to problems with cylindrical symmetry such as circular sources.

Proof of the Fourier Green's function in cylindrical coordinates

If we substitute $x_0 = w_0 \cos \phi_0$, $y_0 = w_0 \sin \phi_0$, $x = w \cos \phi$, $y = w \sin \phi$, $k_x = k_w \cos \phi$, and $k_y = k_w \sin \phi$ in Eq. (13.33) and use the identity of Eq. (46) in Appendix II, we obtain

$$g(w, \phi, z | w_0, \phi_0, z_0) = \frac{-j}{8\pi^2} \int_0^{2\pi} \int_0^\infty e^{-jk_w(w \cos(\phi-\phi) - w_0 \cos(\phi-\phi_0))} \\ \times \frac{e^{-j\sqrt{k^2 - k_w^2}|z-z_0|}}{\sqrt{k^2 - k_w^2}} k_w dk_w d\phi. \quad (13.53)$$

We then expand the first exponent term using Eq. (110) of Appendix II to give

$$g(w, \phi, z | w_0, \phi_0, z_0) = \frac{-j}{8\pi^2} \sum_{m=0}^{\infty} \sum_{n=0}^{\infty} (2 - \delta_{m0})(2 - \delta_{n0}) j^{m-n} \\ \times \int_0^{2\pi} \int_0^\infty \cos m(\phi - \phi_0) \cos n(\phi - \phi) J_m(k_w w_0) J_n(k_w w) \frac{e^{-j\sqrt{k^2 - k_w^2}|z-z_0|}}{\sqrt{k^2 - k_w^2}} k_w dk_w d\phi, \quad (13.54)$$

where the angular integral over ϕ is solved using

$$\int_0^{2\pi} \cos m(\phi - \phi_0) \cos n(\phi - \phi) d\phi = \begin{cases} \frac{2\pi \cos n(\phi - \phi_0)}{2 - \delta_{n0}} & m = n \\ 0, & m \neq n \end{cases}, \quad (13.55)$$

so that the double expansion of Eq. (13.54) reduces to the single one of Eq. (13.50).

Spherical coordinates

The Green's function in rectangular coordinates was given by Eq. (13.4):

$$g(x, y, z | x_0, y_0, z_0) = e^{-jkR} / (4\pi R), \quad (13.56)$$

where

$$R = \sqrt{(x - x_0)^2 + (y - y_0)^2 + (z - z_0)^2}. \quad (13.57)$$

If we substitute

$$\begin{aligned} x &= r \sin \theta \cos \phi, & y &= r \sin \theta \sin \phi, & z &= r \cos \theta \\ x_0 &= r_0 \sin \theta_0 \cos \phi_0, & y_0 &= r_0 \sin \theta_0 \sin \phi_0, & z_0 &= r_0 \cos \theta_0 \end{aligned} \quad (13.58)$$

and use

$$\sin \phi \sin \phi_0 + \cos \phi \cos \phi_0 = \cos(\phi - \phi_0),$$

we obtain

$$g(r, \theta, \phi | r_0, \theta_0, \phi_0) = e^{-jkR} / (4\pi R), \quad (13.59)$$

where

$$R = \sqrt{r^2 + r_0^2 - 2rr_0(\sin \theta \sin \theta_0 \cos(\phi - \phi_0) + \cos \theta \cos \theta_0)}. \quad (13.60)$$

However, as in the cylindrical and rectangular cases, this expression is of limited use and suffers from all the same drawbacks as were described in reference to the Euclidean Green's function in rectangular coordinates given by Eq. (13.31). A more powerful formula [7] is given by

$$\begin{aligned} g(r, \theta, \phi | r_0, \theta_0, \phi_0) &= \frac{-jk}{4\pi} \sum_{n=0}^{\infty} (2n+1) \sum_{m=0}^n (2 - \delta_{m0}) \frac{(n-m)!}{(n+m)!} \cos m(\phi - \phi_0) \\ &\quad \times P_n^m(\cos \theta_0) P_n^m(\cos \theta) \begin{cases} j_n(kr_0) h_n^{(2)}(kr), & r > r_0 \\ j_n(kr) h_n^{(2)}(kr_0), & r < r_0. \end{cases} \end{aligned} \quad (13.61)$$

In the case of axial symmetry, we exclude all terms from the summation in m except for the $m = 0$ term:

$$g(r, \theta | r_0, \theta_0) = \frac{-jk}{4\pi} \sum_{n=0}^{\infty} (2n+1) P_n(\cos \theta_0) P_n(\cos \theta) \begin{cases} j_n(kr_0) h_n^{(2)}(kr), & r > r_0 \\ j_n(kr) h_n^{(2)}(kr_0), & r < r_0. \end{cases} \quad (13.62)$$

By relocating the source to $\theta_0 = \pi$, $r_0 \rightarrow \infty$, we obtain the expansion for a plane wave:

$$e^{-jkr \cos \theta} = \sum_{n=0}^{\infty} (-j)^n (2n+1) j_n(kr) P_n(\cos \theta). \quad (13.63)$$

Like the Fourier Green's functions in rectangular and cylindrical coordinates, this expansion form in spherical coordinates can be applied to reverse problems (see Ref. [8], pp. 210–211, Eqs. (6.107)–(6.110) for compact Kirchhoff–Helmholtz integrals. Note that G_N and G_D are not equivalent to the Green's function given by Eq. (13.61) above or its normal derivative but can be derived from it using the method we shall apply in Section 13.5).

Spherical–cylindrical coordinates

Spherical–cylindrical coordinates—near-field

If we substitute

$$x = r \sin \theta \cos \phi, \quad y = r \sin \theta \sin \phi, \quad z = r \cos \theta, \quad x_0 = w_0 \cos \phi_0, \quad y_0 = w_0 \sin \phi_0 \quad (13.64)$$

in Eq. (13.31) and use

$$\sin \phi \sin \phi_0 + \cos \phi \cos \phi_0 = \cos(\phi - \phi_0),$$

we obtain

$$g(r, \theta | w_0, \phi_0) = e^{-jkR} / (4\pi R), \quad (13.65)$$

where

$$R^2 = r^2 + w_0^2 + z_0^2 - 2r(w_0 \sin \theta \cos(\phi - \phi_0) + z_0 \cos \theta). \quad (13.66)$$

If we set $z_0 = 0$ and $\phi = 0$, this simplifies to

$$R^2 + r^2 + w_0^2 - 2rw_0 \sin \theta \cos \phi_0. \quad (13.67)$$

Again, this expression is of limited use, and a more powerful formula [9] is given by

$$g(r, \theta, \phi | w_0, \phi_0) = \begin{cases} \frac{-jk}{4\pi} \sum_{n=0}^{\infty} (2n+1) h_n^{(2)}(kr) j_n(kw_0) P_n(\sin \theta \cos(\phi - \phi_0)), & w_0 \leq r \\ \frac{-jk}{4\pi} \sum_{n=0}^{\infty} (2n+1) j_n(kr) h_n^{(2)}(kw_0) P_n(\sin \theta \cos(\phi - \phi_0)), & w_0 \geq r \end{cases}, \quad (13.68)$$

where

$$P_n(\sin \theta \cos(\phi - \phi_0)) = \sum_{m=0}^{\infty} (2 - \delta_{m0}) (-1)^m P_n^{-m}(0) P_n^m(\cos \theta) \cos(m(\phi - \phi_0)),$$

which is a modified form of the Gegenbauer addition theorem or multipole expansion. We shall use it to derive near-field expressions for axisymmetric planar sources.

Spherical–cylindrical coordinates—far-field

At a large distance r , the terms containing r in Eq. (13.66) dominate. Hence the remaining terms can be replaced with ones that enable R to be factorized as follows:

$$\begin{aligned} R^2 &= r^2 - 2r(w_0 \sin \theta \cos(\phi - \phi_0) + z_0 \cos \theta) + w_0^2 + z_0^2 \\ &\approx r^2 - 2r(w_0 \sin \theta \cos(\phi - \phi_0) + z_0 \cos \theta) \\ &\quad + (w_0 \sin \theta \cos(\phi - \phi_0) + z_0 \cos \theta)^2 \\ &= (r - w_0 \sin \theta \cos(\phi - \phi_0) - z_0 \cos \theta)^2. \end{aligned} \quad (13.69)$$

Thus we can write the far-field Green's function as

$$g(r, \theta, \phi | w_0, \phi_0, z_0) \Big|_{r \rightarrow \infty} = \frac{e^{-jk(r - w_0 \sin \theta \cos(\phi - \phi_0) - z_0 \cos \theta)}}{4\pi r}. \quad (13.70)$$

We will use this formula to derive far-field expressions for axisymmetric planar sources.



13.5 BOUNDARY INTEGRAL METHOD CASE STUDY: RADIALY PULSATING CAP IN A RIGID SPHERE

In this section, we shall apply the boundary integral method to a pulsating cap in a sphere to illustrate its application to an elementary acoustical problem that has already been treated in Section 12.6 using the boundary value method. The geometry of the problem is shown in Fig. 12.16. From Eq. (13.26), we can write the pressure field as a surface integral:

$$\begin{aligned} \tilde{p}(r, \theta) &= \int_0^{2\pi} \int_0^\pi g(r, \theta | r_0, \theta_0) \Big|_{r_0=R} \frac{\partial}{\partial r_0} \tilde{p}(r_0, \theta_0) \Big|_{r_0=R} R^2 \sin \theta_0 d\theta_0 d\phi_0 \\ &\quad - \int_0^{2\pi} \int_0^\pi \tilde{p}(r_0, \theta_0) \Big|_{r_0=R} \frac{\partial}{\partial r_0} g(r, \theta | r_0, \theta_0) \Big|_{r_0=R} R^2 \sin \theta_0 d\theta_0 d\phi_0, \end{aligned} \quad (13.71)$$

where the Green's function in axisymmetric spherical coordinates is given from Eq. (13.62) by

$$g(r, \theta | r_0, \theta_0) \Big|_{r_0=R} = \frac{-jk}{4\pi} \sum_{n=0}^{\infty} (2n+1) P_n(\cos \theta_0) P_n(\cos \theta) j_n(kR) h_n^{(2)}(kr), \quad (13.72)$$

and its normal gradient is given by

$$\frac{\partial}{\partial r_0} g(r, \theta | r_0, \theta_0) \Big|_{r_0=R} = \frac{-jk}{4\pi} \sum_{n=0}^{\infty} (2n+1) P_n(\cos \theta_0) P_n(\cos \theta) j'_n(kR) h_n^{(2)}(kr), \quad (13.73)$$

where the derivative of the spherical Bessel function is given by Eq. (12.31). We see from Eq. (13.71) that we have a superposition of two fields. The first integral (monopole) represents the incident sound field due to the velocity source, formed by the cap. The normal pressure gradient, or velocity distribution, is obtained from the boundary conditions at the surface of the sphere:

$$\frac{\partial}{\partial r_0} \tilde{p}(r_0, \theta_0) \Big|_{r_0=R} = \begin{cases} -jk\rho_0\tilde{c}\tilde{u}_0, & 0 \leq \theta \leq \alpha \\ 0, & \alpha < \theta \leq \pi. \end{cases} \quad (13.74)$$

The second integral (dipole) represents the sound field reflected by the sphere. The surface pressure distribution, which is a function of θ_0 , is not yet known and is thus represented as a Legendre series:

$$\tilde{p}(r_0, \theta_0) \Big|_{r_0=R} = \rho_0\tilde{c}\tilde{u}_0 \sum_{m=0}^{\infty} A_m P_m(\cos \theta_0), \quad (13.75)$$

where the unknown coefficients A_m have to be determined. Inserting Eqs. (13.72)–(13.75) into Eq. (13.71) yields

$$\begin{aligned} \tilde{p}(r, \theta) = & -k^2 R^2 \rho_0 \tilde{c} \tilde{u}_0 \sum_{n=0}^{\infty} \left(n + \frac{1}{2} \right) P_n(\cos \theta) j_n(kR) h_n^{(2)}(kr) \int_0^{\alpha} P_n(\cos \theta_0) \sin \theta_0 d\theta_0 \\ & + jkR^2 \rho_0 \tilde{c} \tilde{u}_0 \sum_{n=0}^{\infty} \left(n + \frac{1}{2} \right) P_n(\cos \theta) j'_n(kR) h_n^{(2)}(kr) \sum_{m=0}^{\infty} A_m \int_0^{\pi} P_m(\cos \theta_0) P_n(\cos \theta_0) \sin \theta_0 d\theta_0, \end{aligned} \quad (13.76)$$

where the integrals can be solved using the identities of Eqs. (66) and (69) from Appendix II to give

$$\tilde{p}(r, \theta) = kR^2 \rho_0 \tilde{c} \tilde{u}_0 \sum_{n=0}^{\infty} P_n(\cos \theta) h_n^{(2)}(kr) \left(j_n A_n j'_n(kR) - k \left(n + \frac{1}{2} \right) j_n(kR) \sin \alpha P_n^{-1}(\cos \alpha) \right). \quad (13.77)$$

To solve for the unknown coefficients A_n , we apply the following boundary condition to the above pressure field:

$$\frac{\partial}{\partial r} \tilde{p}(r, \theta)|_{r=R} = -jk\rho_0 c \tilde{u}(R, \theta) = \begin{cases} -jk\rho_0 c \tilde{u}_0, & 0 \leq \theta \leq \alpha \\ 0, & \alpha < \theta \leq \pi. \end{cases} \quad (13.78)$$

The surface velocity can be represented by the following Legendre series:

$$\tilde{u}(R, \theta) = \tilde{u}_0 \sum_{n=0}^{\infty} B_n P_n(\cos \theta), \quad (13.79)$$

where the coefficients B_n are found by multiplying through by the orthogonal function $P_m(\cos \theta)$ and integrating over the surface as follows:

$$\int_0^{\alpha} P_m(\cos \theta) \sin \theta d\theta = \sum_{n=0}^{\infty} B_n \int_0^{\pi} P_m(\cos \theta) P_n(\cos \theta) \sin \theta d\theta \quad (13.80)$$

and applying the identities of Eqs. (66) and (69) from Appendix II to yield

$$B_n = \left(n + \frac{1}{2}\right) \sin \alpha P_n^{-1}(\cos \alpha). \quad (13.81)$$

The coefficients are finally solved by applying Eq. (13.78) to Eq. (13.77) and equating the coefficients of $P_n(\cos \theta)$ to give

$$A_n = -\left(n + \frac{1}{2}\right) \sin \alpha P_n^{-1}(\cos \alpha) \frac{1 + jkR^2 j_n(kR) h_n'^{(2)}(kR)}{R^2 j_n'(kR) h_n'^{(2)}(kR)}, \quad (13.82)$$

which, after inserting into Eq. (13.77), gives

$$\tilde{p}(r, \theta) = -jk\rho_0 c \tilde{u}_0 \sum_{n=0}^{\infty} \left(n + \frac{1}{2}\right) \sin \alpha P_n^{-1}(\cos \alpha) P_n(\cos \theta) \frac{h_n^{(2)}(kr)}{h_n'^{(2)}(kR)}. \quad (13.83)$$

This is exactly the same equation as would be obtained using the boundary value method described in Section 12.6. In the far field, applying the asymptotic expression for the spherical Hankel function from Eq. (12.18) gives

$$\tilde{p}(r, \theta) = -jk\rho_0 c S \frac{\tilde{u}_0}{4\pi r} e^{-jkr} D(\theta), \quad (13.84)$$

where the directivity function is given by

$$D(\theta) = \frac{\sin \alpha}{2k^2 R^2 \sin^2(\alpha/2)} \sum_{n=0}^{\infty} \frac{j^{n+1} (2n+1)^2 P_n^{-1}(\cos \alpha) P_n(\cos \theta)}{n h_{n-1}^{(2)}(kR) - (n+1) h_{n+1}^{(2)}(kR)}, \quad (13.85)$$

and $S = 4\pi R^2 \sin^2 \alpha/2$. The radiation impedance is given by

$$\begin{aligned} Z_s &= \frac{\tilde{F}}{\tilde{U}_0} = \frac{2\pi R^2}{S \tilde{u}_0} \int_0^\alpha \tilde{p}(r, \theta) \sin \theta \, d\theta \\ &= -j\rho_0 c \frac{\sin^2 \alpha}{\sin^2(\alpha/2)} \sum_{n=0}^{\infty} \frac{\left(n + \frac{1}{2}\right)^2 (P_n^{-1}(\cos \alpha))^2 h_n^{(2)}(kR)}{n h_{n-1}^{(2)}(kR) - (n+1) h_{n+1}^{(2)}(kR)}. \end{aligned} \quad (13.86)$$



13.6 REFLECTION OF A POINT SOURCE FROM A PLANE

Here we consider what happens when a point source is placed near an infinite reflective planar boundary. Essentially, a hard reflecting surface is the acoustic equivalent to a mirror in optics whereby each reflecting element on its surface acts as a light source. A mirror can be regarded as a perfect hologram because it produces an intensity that varies with direction in accordance with the law of reflection. That is, the angle of reflection is equal to the angle of incidence. Hence, when you walk past a mirror, the view changes, whereas when you walk past a picture or video screen, it does not. This is because the latter provides only intensity information and no directional information. The directional information comes from the *phase* of each point source on the surface. For analytical purposes, it is often convenient to replace the reflecting plane with a transparent plane of symmetry, which has a symmetrically identical source behind it as shown in Fig. 13.2.

This property of symmetry has already been applied in previous examples such as the domes in Sections 12.9 and 12.10. The source and its image both have the same perpendicular distance d from the plane. With the image source present, the pressure fields with and without the reflecting plane can be shown to be identical if we consider that in both cases the field is symmetrical to either side of the plane. Therefore, the pressures must be equal on opposite faces of the plane, in which case the pressure gradient in the plane must be zero. Because it takes a pressure gradient to generate a particle velocity, this also satisfies the boundary condition of zero particle velocity normal to the plane. Of course, there is no physical image source, so this model is only valid on the source side of the surface.

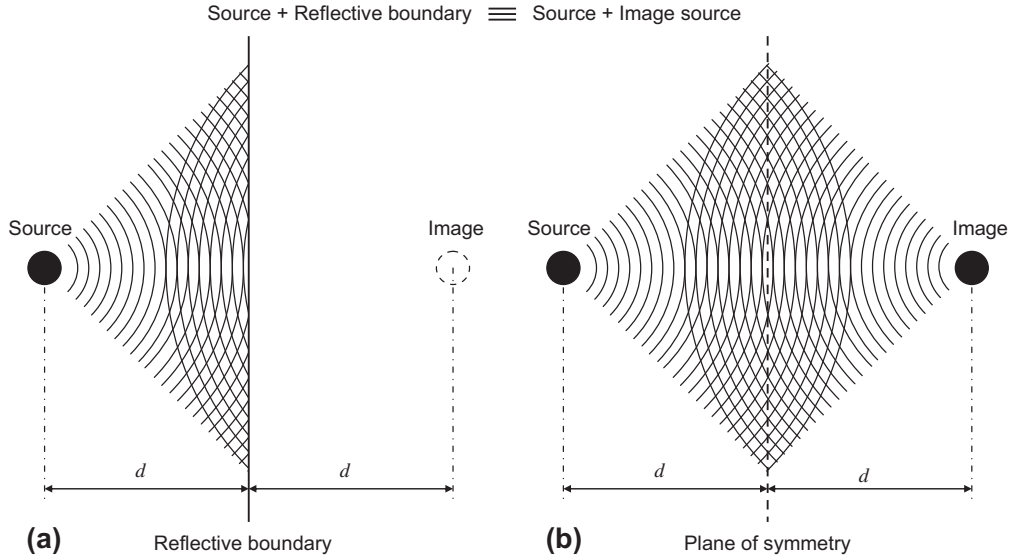


Figure 13.2 Reflection of a point source from (a) a plane and (b) equivalent source and image.

The principle can be expressed by the superposition of fields as follows. If the point source is located at a distance z_0 from an infinite screen at $z = 0$, there will be an extra field superimposed on the original because of a virtual source behind the screen. Using Eqs. (13.2), (13.31), (13.48), and (13.49) for a point source, the field $\tilde{p}_S(w, \phi, z)$ produced by the source in cylindrical coordinates is given by

$$\tilde{p}_S(w, \phi, z) = jk\rho_0c\tilde{U}_S \frac{e^{-jkR_S}}{4\pi R_S}, \quad (13.87)$$

where

$$R_S = \sqrt{w^2 + w_0^2 - 2ww_0 \cos(\phi - \phi_0) + (z + z_0)^2}. \quad (13.88)$$

The field $\tilde{p}_I(w, \phi, z)$ produced by the image is then

$$\tilde{p}_I(w, \phi, z) = jk\rho_0c\tilde{U}_S \frac{e^{-jkR_I}}{4\pi R_I}, \quad (13.89)$$

where

$$R_I = \sqrt{w^2 + w_0^2 - 2ww_0 \cos(\phi - \phi_0) + (z - z_0)^2}, \quad (13.90)$$

which produces a resultant field

$$\begin{aligned}\tilde{p}(w, \phi, z) &= \tilde{p}_S(w, \phi, z) + \tilde{p}_I(w, \phi, z) \\ &= jk\rho_0 c \tilde{U}_S \left(\frac{e^{-jkR_S}}{4\pi R_S} + \frac{e^{-ikR_I}}{4\pi R_I} \right).\end{aligned}\quad (13.91)$$

Let us now recast this equation in the form

$$\tilde{p}(w, \phi, z) = jk\rho_0 c \tilde{U}_S G(w, \phi, z|w_0, \phi_0, z_0), \quad (13.92)$$

where

$$G(w, \phi, z|w_0, \phi_0, z_0) = \frac{e^{-jkR_S}}{4\pi R_S} + \frac{e^{-ikR_I}}{4\pi R_I} \quad (13.93)$$

is a *bounded* Green's function. Notice that we use the upper case G . An interesting feature of this bounded Green's function is that its normal derivative with respect to the plane (i.e., with respect to z) is zero. Now suppose that part of the plane is in motion and radiating sound. Points on the plane can be represented by G if we let $z_0 \rightarrow 0$ so that the source and its image coalesce. Hence

$$G(w, \phi, z|w_0, \phi_0, 0) = \frac{e^{-jkR}}{2\pi R} = 2g(w, \phi, z|w_0, \phi_0, 0), \quad (13.94)$$

where

$$R = \sqrt{w^2 + w_0^2 - 2ww_0 \cos(\phi - \phi_0) + z^2}. \quad (13.95)$$

We can use this Green's function in the monopole Rayleigh integral to represent a planar source in an infinite baffle. Because the normal derivative of G is zero, the dipole Rayleigh integral vanishes, and the point sources on the surface become monopole point sources of double strength.



PART XXXVI: RADIATION AND SCATTERING IN CYLINDRICAL-SPHERICAL COORDINATES



13.7 RADIATION FROM A RIGID CIRCULAR PISTON IN AN INFINITE BAFFLE

The simplest monopole planar source is the oscillating circular piston (or rigid disk) in an infinite baffle. The piston is assumed to be rigid so that all parts of its surface vibrate in

phase, and its velocity amplitude is independent of the mechanical or acoustic loading on its radiating surface. Remarkably, its radiation impedance was first derived by Rayleigh [10] before the direct radiator loudspeaker had even been invented [11], yet it has been widely accepted as an idealized model for such when mounted in an enclosure situated near a wall or, even better, mounted directly in a wall as commonly found in recording studios. The model is useful in the frequency range up to the first diaphragm break-up mode. It should be noted that here the term “infinite baffle” refers to an infinitely large plane rigid wall that surrounds the piston and not a finite sealed enclosure, which is often referred to as an infinite baffle enclosure. The only thing they have in common is that they both block the transmission path between the back and the front of the radiating surface. However, the infinitely large wall model does not take into account reflections from the edges of a real finite enclosure. Also both sides of the radiating surface are open to half space so that the loading effects of a real finite enclosure such as compliance, standing waves, absorption, and wall vibration, etc. are ignored. The original derivation of the radiation impedance by Rayleigh over 100 years ago used the nonintegral Green’s function of Eq. (13.16) with an ingenious coordinate system. Here we shall follow the approach of King [12] using the integral Green’s function in cylindrical coordinates given by Eq. (13.52).

Boundary conditions

The circular piston of radius a shown in Fig. 13.3 is mounted in an infinite baffle in the xy plane with its center at the origin and oscillates in the z direction with a harmonically time-dependent velocity \tilde{u}_0 , thus radiating sound into a homogeneous loss-free medium. The area of each surface element is given by

$$\delta S_0 = w_0 \delta w_0 \delta \phi_0. \quad (13.96)$$

The monopole source elements shown in Fig. 13.4, together with their images, form the piston source. As they are coincident in the plane of the baffle, they coalesce to form elements of double strength. Hence the piston in an infinite baffle can be modeled as a “breathing” disk in free space. It may also be considered as a pulsating sphere of the same radius compressed into the plane of the disk. Because of the symmetry of the pressure fields on either side of the baffle,

$$\tilde{p}(w, z) = \tilde{p}(w, -z). \quad (13.97)$$

Consequently, there is the following Neumann boundary condition on its surface:

$$\frac{\partial}{\partial z} \tilde{p}(w, z) \Big|_{z=0+} = 0, \quad a < w \leq \infty, \quad (13.98)$$

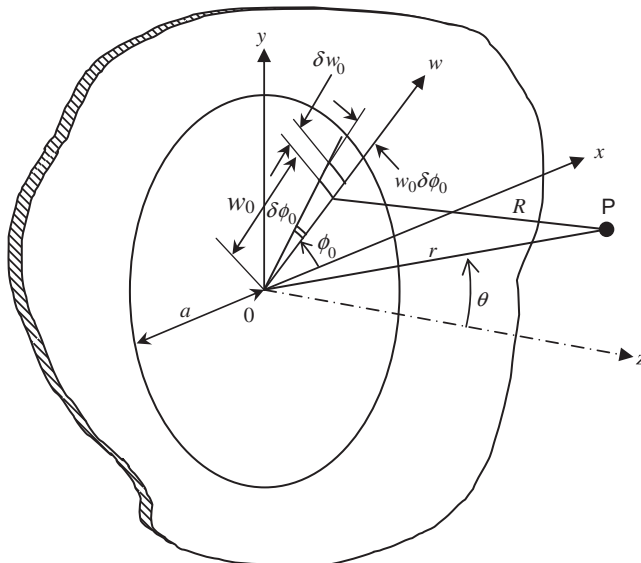


Figure 13.3 Geometry of rigid circular piston in infinite baffle. The point of observation P is located at a distance r and angle θ with respect to the origin at the center of the piston.

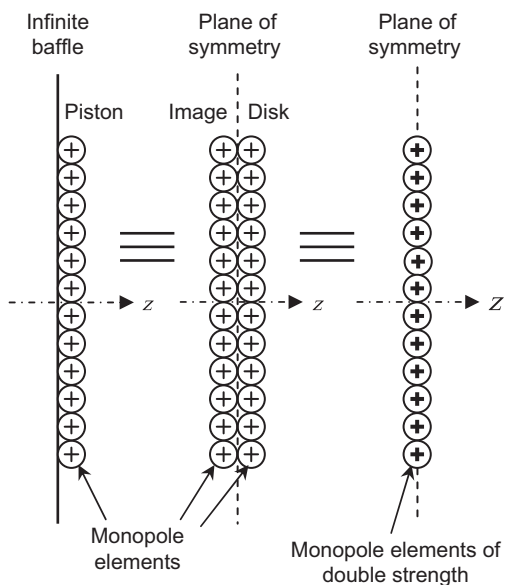


Figure 13.4 Equivalence between circular piston in infinite baffle and double-sided monopole piston in free space or “breathing” disk in free space.

which is satisfied automatically. On the surface of the disk there is the coupling condition

$$\frac{\partial}{\partial z} \tilde{p}(w, z)|_{z=0+} = -jk\rho_0 c \tilde{u}_0, \quad 0 \leq w \leq a \quad (13.99)$$

and k is the wave number given by $k = \omega/c = 2\pi/\lambda$, ω is the angular frequency of excitation, ρ_0 is the density of the surrounding medium, c is the speed of sound in that medium, and λ is the wavelength.

Far-field pressure

The far-field pressure distribution is given by Eq. (13.27) taking into account the double strength source:

$$\tilde{p}(r, \theta) = -2 \int_0^{2\pi} \int_0^a g(r, \theta|w_0, \phi_0) \frac{\partial}{\partial z_0} \tilde{p}(w_0, z_0)|_{z_0=0+} w_0 dw_0 d\phi_0, \quad (13.100)$$

where the far-field Green's function in spherical-cylindrical coordinates given by Eq. (13.70) is used. Inserting Eqs. (13.70) and (13.99) into Eq. (13.100) and integrating over the surface, using Eqs. (76) and (95) from Appendix II (with $z = kw_0 \sin \theta$, $b = k \sin \theta$, and letting $\phi = \pi/2$ so that $\cos(\phi - \phi_0) = \sin \phi_0$), gives

$$\tilde{p}(r, \theta) = jka^2 \rho_0 c \tilde{u}_0 \frac{e^{-jkr}}{2r} D(\theta), \quad (13.101)$$

where the directivity function $D(\theta)$ is given by

$$D(\theta) = \frac{2J_1(ka \sin \theta)}{ka \sin \theta}, \quad (13.102)$$

which is often referred to as the Fraunhofer or Airy diffraction pattern. The normalized directivity function $20 \log_{10}|D(\theta)|$ is plotted in Fig. 13.5 for four values of $ka = 2\pi a/\lambda$, that is, for four values of the ratio of the circumference of the piston to the wavelength. When the circumference of the piston ($2\pi a$) is less than one-half wavelength, that is, $ka < 0.5$, the piston behaves essentially like a point source. When ka becomes greater than 3, the piston is highly directional.

The on-axis pressure is evaluated by setting $\theta = 0$ in Eq. (13.70) before inserting it in Eq. (13.100) and integrating over the surface to give

$$D(0) = 1, \quad (13.103)$$

which means that the on-axis far-field pressure is proportional to the piston *acceleration* at all frequencies and is often written as

$$\tilde{p}(r, 0) = j\rho_0 f \tilde{U}_0 \frac{e^{-jkr}}{r}, \quad (13.104)$$

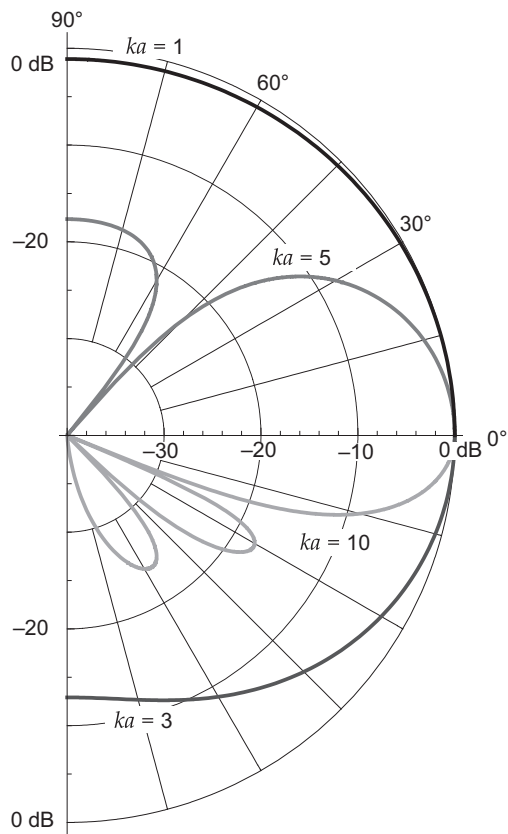


Figure 13.5 Far-field directivity patterns for a rigid circular piston in an infinite baffle as a function of $ka = 2\pi a/\lambda = 2\pi fa/c$, where a is the radius of the piston. The directivity index never becomes less than 3 dB because the piston radiates only into half space.

where $\tilde{U}_0 = \pi a^2 \tilde{u}_0$ is the total volume velocity. This is a general expression for a planar source in an infinite baffle and also applies to nonuniform velocity distributions where the volume velocity is the product of the average velocity and the radiating area, which can be of arbitrary shape.

Although the piston behaves as a more or less omnidirectional source for $ka \leq 1$, similar to a pulsating sphere, the output of the piston is 6 dB less than that of the pulsating sphere at very low frequencies. Because the piston is radiating into half space, its output per unit surface area is double that of the pulsating sphere, which is radiating into whole space. However, the sphere has four times the surface area of a piston of the same radius. Therefore it produces twice the output. Unlike the pulsating sphere, the on-axis response of the piston does not roll-off at high frequencies, which is a property of planar sources in general, as already discussed in Section 12.8 regarding a piston in a

sphere. Unlike the piston in a sphere, there is no 6 dB level shift between low and high frequencies because the baffled piston effectively radiates into half space at all frequencies. As we shall see, its radiation impedance, like that of a pulsating sphere, is dominated by mass reactance at low frequencies and resistance at high frequencies.

In the low-frequency region, the radiated sound pressure and hence also intensity are held constant under constant piston acceleration. This is because the decreasing velocity is compensated for by the rising radiation resistance, as discussed in greater detail in Section 4.10.

At higher frequencies, where the impedance starts to become more resistive, the beam pattern, coincidentally, becomes increasingly narrow. This phenomenon compensates for the fall in on-axis output that would otherwise occur. Indeed, in the case of the pulsating sphere, the radiated sound pressure is proportional to the surface velocity in the region where the load is resistive and therefore falls under constant acceleration and falling velocity. It seems a remarkable coincidence of nature that this transition occurs so smoothly as to produce a completely flat on-axis response, although it does not seem so surprising when we consider that the on-axis response results from the sum of an array of point sources that are all in phase, where the field of each point source is frequency invariant under constant volume acceleration.

Near-field pressure

The near-field pressure distribution is given by the boundary integral of Eq. (13.27) taking into account the double-strength source:

$$\tilde{p}(r, \theta) = -2 \int_0^{2\pi} \int_0^a g(r, \theta | w_0, \phi_0) \frac{\partial}{\partial z_0} \tilde{p}(w_0, z_0) \Big|_{z_0=0^+} w_0 dw_0 d\phi_0, \quad (13.105)$$

where the Green's function in spherical-cylindrical coordinates given by Eq. (13.68) is used. Mast and Yu [13] show that inserting Eqs. (13.68) and (13.99) into Eq. (13.105) and integrating over the surface gives [46]

$$\begin{aligned} \tilde{p}(r, \theta) = & 2\rho_0 \tilde{c} \tilde{u}_0 \sum_{n=0}^{\infty} \frac{(-1)^n \Gamma(n + 1/2)}{\Gamma(n + 2) \Gamma(2n + 1/2)} \left(\frac{ka}{2}\right)^{2n+2} \\ & \times {}_1F_2\left(n + 1; n + 2, 2n + \frac{3}{2}; -\frac{k^2 a^2}{4}\right) h_{2n}^{(2)}(kr) P_{2n}(\cos \theta), \end{aligned} \quad (13.106)$$

which converges for $r > a$ but is generally used for $w \geq a$. The other part of the Green's function of Eq. (13.68) could be used to derive an expression for $r < a$ as was done previously by Stenzel [14]. However, a better expression is provided by Mast and Yu [13],

which is derived by moving the origin of the coordinate system to a point on the z axis that lies in the same plane as the observation point to give

$$\tilde{p}(w, z) = \frac{\rho_0 c \tilde{u}_0}{\sqrt{\pi}} \sum_{n=0}^{\infty} (-1)^n (4n+1) \frac{\Gamma\left(n + \frac{1}{2}\right)}{\Gamma(n+1)} j_{2n}(kw) f_{2n}, \quad (13.107)$$

where f_{2n} is given by the following recursion formulas:

$$f_0 = e^{-jkz} - e^{-jkr_a}, \quad (13.108)$$

$$f_{2n} = -f_{2n-2} - kr_a h_{2n-1}^{(2)}(kr_a) (P_{2n}(z/r_a) - P_{2n-2}(z/r_a)), \quad (13.109)$$

and

$$r_a = \sqrt{z^2 + a^2}, \quad (13.110)$$

which converges for $w^2 < a^2 + z^2$ but is generally used for $w < a$ and is thus termed the *paraxial* solution. These equations are an elegant and important result for ultrasound because they eliminate the need for inefficient numerical integration at high frequencies. In particular, the number of terms needed for convergence in the paraxial expansion decreases linearly toward the z -axis until just a single term remains. This is the closed-form Backhaus axial solution [47]:

$$\tilde{p}(0, z) = \rho_0 c \tilde{u}_0 (e^{-jkz} - e^{-jkr_a}). \quad (13.111)$$

The first term represents a point source at the center of the piston and the second term radiation from the perimeter. The magnitude of the axial pressure is $|\tilde{p}(0, z)| = 2\rho_0 c |\tilde{u}_0 \sin k(r_a - z)/2|$. Near the surface of the piston, it is approximately $|\tilde{p}(0, z)| \approx \rho_0 c k a |\tilde{u}_0| / (1 + z/a)$ for $ka < 0.5$ and $z < 0.5a$. Hence, at low frequencies, the radiated sound pressure of a loudspeaker may be calculated from the diaphragm velocity [see Eq. 13.101], which in turn may be measured using a probe microphone close to the center. The pressure field for three values of ka is plotted in Fig. 13.6 and for $ka = 12\pi$ in Fig. 13.7. From these figures, we can see the formation of the central and side lobes of the directivity patterns at the start of the far-field or Fraunhofer diffraction zone, where the waves are spherically diverging. The near-field or Fresnel region is dominated by nonpropagating interference patterns due to the differences in path lengths from different parts of the radiating surface. However, in the immediate near field of Fig. 13.7, the pressure fluctuations are relatively small and we see here the formation of a plane wave, which extends outwards with increasing frequency. The furthest axial peak is a

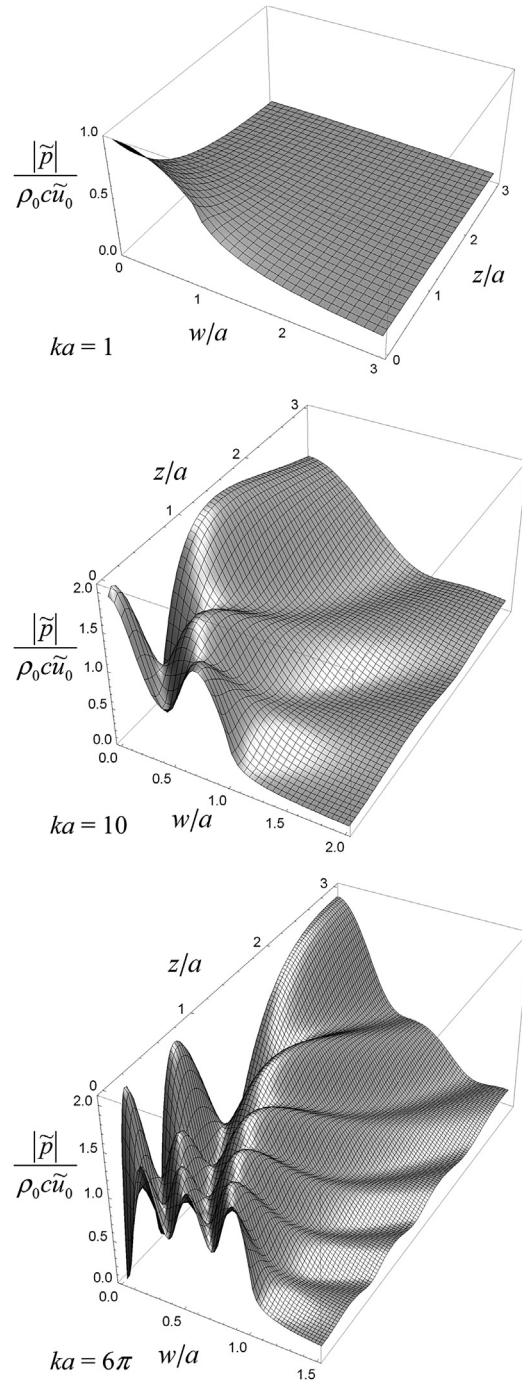


Figure 13.6 Normalized near-field pressure plots for a rigid circular piston in an infinite baffle as a function of $ka = 2\pi a/\lambda = 2\pi fa/c$. Where a is the radius of the piston, $|\tilde{p}|$ is the pressure magnitude, \tilde{u}_0 is the piston velocity, ρ_0 is the density of the acoustic medium, and c is the speed of sound in that medium.

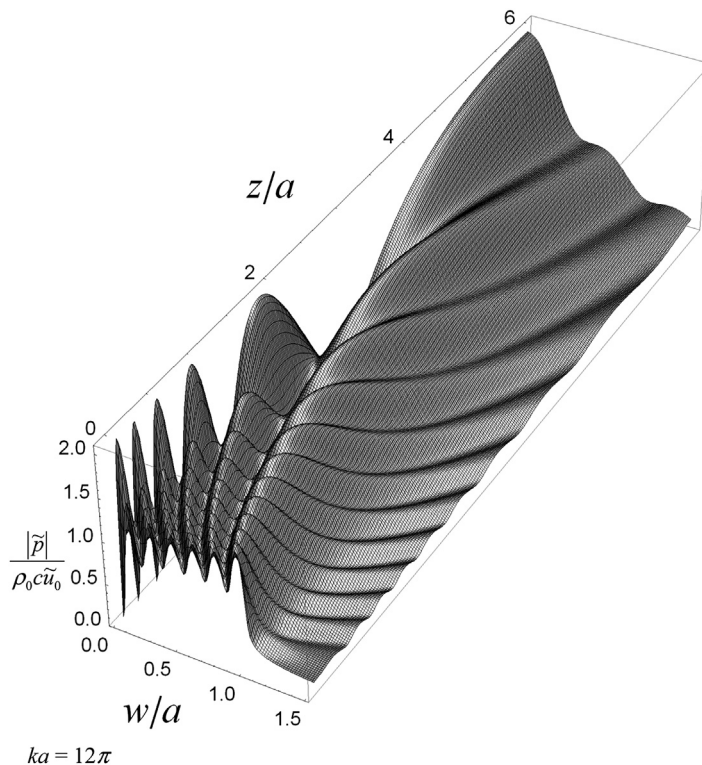


Figure 13.7 Normalized near-field pressure plots for a rigid circular piston in an infinite baffle as a function of $ka = 2\pi a/\lambda = 2\pi fa/c$. Where a is the radius of the piston, $|\tilde{p}|$ is the pressure magnitude, \tilde{u}_0 is the piston velocity, ρ_0 is the density of the acoustic medium, and c is the speed of sound in that medium.

focal point, which is useful for ultrasound applications. Also, we can make the following observations:

1. At low frequencies, where $ka < 3$, the on-axis pressure of Eq. (13.111) converges to the far-field approximation of Eq. (13.104) at around $z = \pi a/2$.
2. At high frequencies, where $ka > 3$, the on-axis pressure converges to the far-field approximation at around $z = ka^2/2$, which is known as the Rayleigh distance [15,16]. The on-axis near-field pressure is oscillatory and there are $ka/(2\pi)$ or a/λ cycles before it converges to the far-field response, where one cycle spans two magnitude peaks or two nulls. The pressure on the face of the piston also oscillates radially with a total of $ka/2\pi$ or a/λ cycles between the center and perimeter. Furthermore, if $ka = n\pi$ or $n\lambda = 2a$, where n is an integer, the pressure at the center of the piston is at a null for even n and at a peak for odd n .
3. The number of lobes in the directivity pattern corresponds to the number of axial peaks plus the number of peaks along the radius of the piston.

An alternative expression to Eq. (13.107) is given in Reference [48].

Radiation impedance and high-frequency asymptotic expression

The near-field pressure distribution is given by Eq. (13.27) taking into account the double-strength source:

$$\tilde{p}(w, z) = 2 \int_0^{2\pi} \int_0^a g(r, \theta | w_0, z_0) \frac{\partial}{\partial z_0} \tilde{p}(w_0, z_0) \Big|_{z_0=0^+} w_0 dw_0 d\phi_0, \quad (13.112)$$

where the Green's function in cylindrical coordinates given by Eq. (13.52) is used. In this form Eq. (13.112) is known as the monopole King integral [12]. Inserting Eqs. (13.52) and (13.99) into Eq. (13.112) and integrating over the surface gives

$$\tilde{p}(w, z) = -ka\rho_0 c\tilde{u}_0 \int_0^\infty J_0(k_w w) J_1(k_w a) \frac{1}{k_z} e^{-jk_z z} dk_w, \quad (13.113)$$

where we have used the integral solution of Eq. (95) from Appendix II and k_z is given by Eq. (13.51). To investigate the asymptotic high-frequency behavior, we let $k \rightarrow \infty$ in Eq. (13.113) to give

$$\begin{aligned} \tilde{p}(w, z) \Big|_{k \rightarrow \infty} &= -\rho_0 c\tilde{u}_0 e^{-jkz} a \int_0^\infty J_1(k_w a) J_0(k_w w) dk_w \\ &= \begin{cases} -\rho_0 c\tilde{u}_0 e^{-jkz}, & 0 \leq w \leq a \\ 0, & w > a. \end{cases} \end{aligned} \quad (13.114)$$

This slightly trivial solution describes the sound being radiated as a laser beam confined within the diameter of the piston. It can also be regarded as a virtual infinite tube or transmission line in space starting from the perimeter of the piston. At first sight, this may appear to contradict Eq. (13.111), because the axial nulls and peaks never actually disappear. On the contrary, they become more numerous and travel out further with increasing frequency. However, in the high frequency limit, the radial width of this range of hills and dales shrinks so much that they become insignificant.

The total radiation force is found by integrating the pressure from Eq. (13.113) over the surface of the piston and again using the integral of Eq. (95) from Appendix II to give

$$\begin{aligned} \tilde{F} &= - \int_0^{2\pi} \int_0^a \tilde{p}(w, z) \Big|_{z=0^+} w dw d\phi \\ &= 2\pi ka^2 \rho_0 c\tilde{u}_0 \left(\int_0^k \frac{J_1^2(k_w a)}{k_w \sqrt{k^2 - k_w^2}} dk_w + j \int_k^\infty \frac{J_1^2(k_w a)}{k_w \sqrt{k_w^2 - k^2}} dk_w \right). \end{aligned} \quad (13.115)$$

King [12] shows the solution to be

$$Z_s = \frac{\tilde{F}}{\tilde{U}_0} = \mathbf{R}_s + j X_s, \quad (13.116)$$

where $\tilde{U}_0 = \pi a^2 \tilde{u}_0$ is the total volume velocity and \mathbf{R}_s is the specific radiation resistance in $\text{N}\cdot\text{s}/\text{m}^3$ (rayl) given by

$$\mathbf{R}_s = \rho_0 c \left(1 - \frac{J_1(2ka)}{ka} \right) \approx \rho_0 c \frac{k^2 a^2}{2}, \quad ka < 0.5, \quad (13.117)$$

where the bold \mathbf{R} indicates that the quantity varies with frequency. X_s is the specific radiation reactance in $\text{N}\cdot\text{s}/\text{m}^3$ (rayl) given by

$$X_s = \rho_0 c \frac{\mathbf{H}_1(2ka)}{ka} \approx \rho_0 c \frac{8ka}{3\pi}, \quad ka < 0.5, \quad (13.118)$$

where J_1 and \mathbf{H}_1 are Bessel and Struve functions respectively as defined by Eqs. (71) and (125) in Appendix II. Plots of the real and imaginary parts of

$$\frac{Z_s}{\rho_0 c} = \frac{\mathbf{R}_s + jX_s}{\rho_0 c} \quad (13.119)$$

are shown in Fig. 4.35 as a function of ka . Similar graphs of the real and imaginary parts of the specific admittance

$$\begin{aligned} Y_s \rho_0 c &= \rho_0 c (\mathbf{G}_s + jB_s) = \rho_0 c \left(\frac{\mathbf{R}_s}{\mathbf{R}_s^2 + X_s^2} - j \frac{X_s}{\mathbf{R}_s^2 + X_s^2} \right) \\ &\approx \frac{9\pi^2}{128} - j \frac{3\pi}{8ka}, \quad ka < 0.5 \end{aligned} \quad (13.120)$$

are shown in Fig 4.36. The specific admittance is in $\text{m}^3 \cdot \text{N}^{-1} \text{s}^{-1}$ (rayl⁻¹).

We see from Fig. 4.35 that, for $ka < 0.5$, the reactance varies as the first power of frequency while the resistance varies as the second power of frequency. At high frequencies, for $ka > 5$, the reactance becomes small compared with the resistance, and the resistance approaches a constant value.

The admittance, on the other hand, is better behaved. The conductance is constant for $ka < 0.5$, and it is also constant for $ka > 5$ although its value is larger.

13.8 RADIATION FROM A RESILIENT CIRCULAR DISK WITHOUT A BAFFLE [17]

The resilient circular disk in free space is the simplest dipole planar source and the dipole complement of the rigid circular piston in an infinite baffle. It can be used as an approximate model for unbaffled loudspeakers of the electrostatic or planar magnetic type, in which it is assumed that a perfectly uniform driving pressure is applied to a very light flexible membrane diaphragm in free space. Because of the dipole nature of the source, there is zero pressure in the plane of the disk extending beyond its perimeter. Walker [18] pointed out that such a source is acoustically transparent, in that it does not disturb the field around it, and used this idealized model to derive the far-field on-axis pressure response of an electrostatic loudspeaker, which provides a useful approximation over the loudspeaker's working range. However, it should be noted that the model assumes a freely suspended membrane, whereas in reality it is usually clamped at the perimeter, which effectively removes the singularity from the perimeter of the idealized model [19].

Boundary conditions

The basic configuration is shown in Fig. 13.8. The infinitesimally thin membrane-like resilient disk is assumed to be perfectly flexible, has zero mass, and is free at its perimeter. It is driven by a uniformly distributed harmonically varying pressure \tilde{p}_0 and thus radiates sound from both sides into a homogeneous loss-free acoustic medium. In fact,

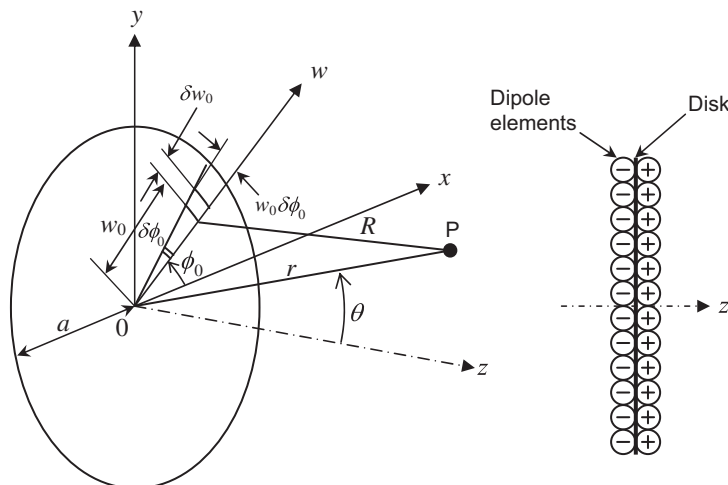


Figure 13.8 Geometry of resilient circular disk in free space. The point of observation P is located at a distance r and angle θ with respect to the origin at the center of the disk.

there need not be a disk present at all and instead the driving pressure could be acting on the air particles directly. However, for expedience, the area over which this driving pressure is applied shall be referred to as a disk from here onwards. The pressure field on one side of the xy plane is the symmetrical “negative” of that on the other, so that

$$\tilde{p}(w, z) = -\tilde{p}(w, -z). \quad (13.121)$$

Consequently, there is a Dirichlet boundary condition in the plane of the disk where these equal and opposite fields meet.

$$\tilde{p}(w, 0) = 0, \quad a < w \leq \infty. \quad (13.122)$$

On the front and rear surfaces of the disk, the pressures are \tilde{p}_+ and \tilde{p}_- respectively, which are given by

$$\tilde{p}_+(w_0) = -\tilde{p}_-(w_0) = \tilde{p}_0/2, \quad 0 \leq w_0 \leq a \quad (13.123)$$

and k is the wave number given by $k = \omega/c = 2\pi/\lambda$, where ω is the angular frequency of excitation, ρ_0 is the density of the surrounding medium, c is the speed of sound in that medium, and λ is the wavelength.

Far-field pressure

The far-field pressure distribution is given by the dipole boundary integral of Eq. (13.28), taking into account the surface pressure on both sides:

$$\tilde{p}(r, \theta) = \int_0^{2\pi} \int_0^a (\tilde{p}_+(w_0) - \tilde{p}_-(w_0)) \frac{\partial}{\partial z_0} g(r, \theta | w_0, \phi_0) \Big|_{z_0=0^+} dw_0 d\phi_0, \quad (13.124)$$

where the far-field Green's function in spherical-cylindrical coordinates given by Eq. (13.70) is used. Inserting Eqs. (13.70), (13.121) and (13.123) into Eq. (13.124) and integrating over the surface, using Eqs. (76) and (95) from Appendix II [with $z = kw_0 \sin \theta$, $b = k \sin \theta$, and letting $\phi = \pi/2$ so that $\cos(\phi - \phi_0) = \sin \phi_0$], gives

$$\tilde{p}(r, \theta) = jka^2 \tilde{p}_0 \frac{e^{-jkr}}{4r} D(\theta), \quad (13.125)$$

where the directivity function $D(\theta)$ is given by

$$D(\theta) = \frac{2J_1(ka \sin \theta)}{ka \sin \theta} \cos \theta. \quad (13.126)$$

The on-axis pressure is evaluated by setting $\theta = 0$ in Eq. (13.70) before inserting it in Eq. (13.124) and integrating over the surface to give

$$D(0) = 1 \quad (13.127)$$

so that the on-axis response can be written as

$$\tilde{p}(r, 0) = jf\tilde{F}_0 \frac{e^{-jkr}}{2rc}, \quad (13.128)$$

which just gives a constant 6 dB/octave rising response at all frequencies for a given driving force $\tilde{F}_0 = S\tilde{p}_0$, where $S = \pi a^2$ is the area. Eq. (13.128) is true for a planar resilient radiator of *any* shape. The normalized directivity function $20 \log_{10}|D(\theta)/D(0)|$ is plotted in Fig. 13.9 for four values of $ka = 2\pi a/\lambda$, that is, for four values of the ratio of the circumference of the disk to the wavelength. *The directivity pattern is that of a rigid piston in an infinite baffle multiplied by $\cos \theta$.* When the circumference of the disk ($2\pi a$) is less than one-half wavelength, that is, $ka < 0.5$, the resilient disk behaves essentially like a dipole point source. When ka becomes greater than 3, the resilient disk is highly directional, like the piston in an infinite baffle. In fact, at very high frequencies, they both radiate sound as a narrow central lobe (Airy disk) accompanied by a number of very small side lobes, in which case the factor of $\cos \theta$ makes relatively little difference. In the case of a push-pull electrostatic loudspeaker,

$$\tilde{p}_0 = \frac{E_p}{d} \cdot \frac{2\tilde{I}_{in}}{j\omega\pi a^2}, \quad (13.129)$$

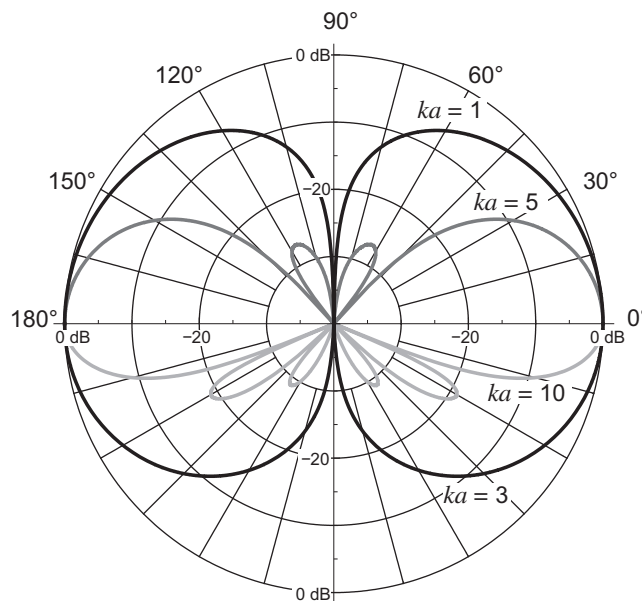


Figure 13.9 Far-field directivity patterns for a resilient circular disk in free space as a function of $ka = 2\pi a/\lambda = 2\pi fa/c$, where a is the radius of the disk.

where E_p is the polarizing voltage, d is the membrane–electrode separation, and \tilde{I}_{in} is the static input current to each electrode, assuming that the motional current is negligible in comparison. Substituting this in Eq. (13.128) yields

$$\tilde{p}(r, 0) = \frac{E_p}{d} \cdot \frac{\tilde{I}_{in} e^{-jkr}}{2\pi r c}, \quad (13.130)$$

which is Walker's equation [18], albeit obtained by a slightly different method.

Near-field pressure

The near-field pressure distribution is given by Eq. (13.28) taking into account the surface pressure on both sides:

$$\tilde{p}(r, \theta) = \int_0^{2\pi} \int_0^a (\tilde{p}_+(w_0) - \tilde{p}_-(w_0)) \frac{\partial}{\partial z_0} g(r, \theta | w_0, \phi_0) \Big|_{z_0=0^+} w_0 dw_0 d\phi_0, \quad (13.131)$$

where the Green's function in spherical–cylindrical coordinates given by Eq. (13.68) is used. It has been shown [17] that inserting Eqs. (13.68) and (13.123) into Eq. (13.131) and integrating over the surface gives

$$\begin{aligned} \tilde{p}(r, \theta) = & -j\tilde{p}_0 \sum_{n=0}^{\infty} \frac{(-1)^n \Gamma(n + 3/2)}{\Gamma(n + 2) \Gamma(2n + 3/2)} \left(\frac{ka}{2}\right)^{2n+2} \\ & \times {}_1F_2\left(n + 1; n + 2, 2n + \frac{5}{2}; -\frac{k^2 a^2}{4}\right) h_{2n+1}^{(2)}(kr) P_{2n+1}(\cos \theta), \end{aligned} \quad (13.132)$$

which converges for $r > a$ but is generally used for $w \geq a$. The other part of the Green's function of Eq. (13.68) could be used to derive an expression for $r < a$. However, a better expression is provided by moving the origin of the coordinate system to a point on the z axis that lies on the same plane as the observation point to give

$$\tilde{p}(w, z) = \frac{j\tilde{p}_0}{\sqrt{\pi k w}} \sum_{n=0}^{\infty} (-1)^n (4n + 3) \frac{\Gamma(n + 3/2)}{\Gamma(n + 1)} j_{2n+1}(kw) f_{2n+1}, \quad (13.133)$$

where f_{2n+1} is given by the following recursion formulas:

$$f_1 = j \left(\frac{z}{r_a} e^{-jkr_a} - e^{-jkz} \right), \quad (13.134)$$

$$f_{2n+1} = -f_{2n-1} + kr_a h_{2n}^{(2)}(kr_a)(P_{2n+1}(z/r_a) - P_{2n-1}(z/r_a)), \quad (13.135)$$

and

$$r_a = \sqrt{z^2 + a^2}, \quad (13.136)$$

which converges for $w^2 < a^2 + z^2$ but is generally used for $w < a$ and is thus termed the *paraxial* solution. The number of terms in the expansion needed for convergence decreases linearly toward the z -axis until just a single term is needed. This is the closed-form axial solution:

$$\tilde{p}(0, z) = \frac{\tilde{p}_0}{2} \left(e^{-jkz} - \frac{z}{\sqrt{z^2 + a^2}} e^{-jk\sqrt{z^2 + a^2}} \right). \quad (13.137)$$

The pressure field for three values of ka is plotted in Fig. 13.10. We can see that the plane wave region near the surface forms more readily than in the case of the rigid piston (see Fig. 13.6), no doubt aided by the uniform pressure distribution at the surface of the resilient disk. At $ka = 6\pi$, the pressure field fluctuations in the vicinity of the resilient disk are smaller than for the rigid piston. Furthermore, the axial pressure response of a rigid disk given by Eq. (13.111) has nulls, whereas the resilient disk axial response given by Eq. (13.137) is oscillatory but with decreasing magnitude toward the face of the disk. An alternative expression to Eq. (13.133) is given in Reference [48].

Surface velocity

Using the solutions for the near-field pressure from Eqs. (13.133)–(13.135), and taking the normal pressure gradient at the surface of the disk, the surface velocity is given by

$$\begin{aligned} \tilde{u}_0(w) &= \frac{j}{\rho c} \frac{d}{dz} \tilde{p}(w, z)|_{z=0+} \\ &= -\frac{\tilde{p}_0}{\rho c \sqrt{\pi}} \sum_{n=0}^{\infty} (-1)^n (4n+3) \frac{\Gamma\left(n + \frac{3}{2}\right)}{\Gamma(n+1)} f_{2n}' \frac{j_{2n+1}(kw)}{kw}, \end{aligned} \quad (13.138)$$

where

$$f_0' = 1 - j \frac{e^{-jka}}{ka}, \quad (13.139)$$

$$f_{2n}' = -f_{2n-2}' - h_{2n}^{(2)}(ka)((2n+1)P_{2n}(0) - (2n-1)P_{2n-2}(0)). \quad (13.140)$$

The magnitude and phase of the normalized velocity are shown in Figs. 13.11 and 13.12, respectively, for four values of ka . For small k , it can be shown to agree well with

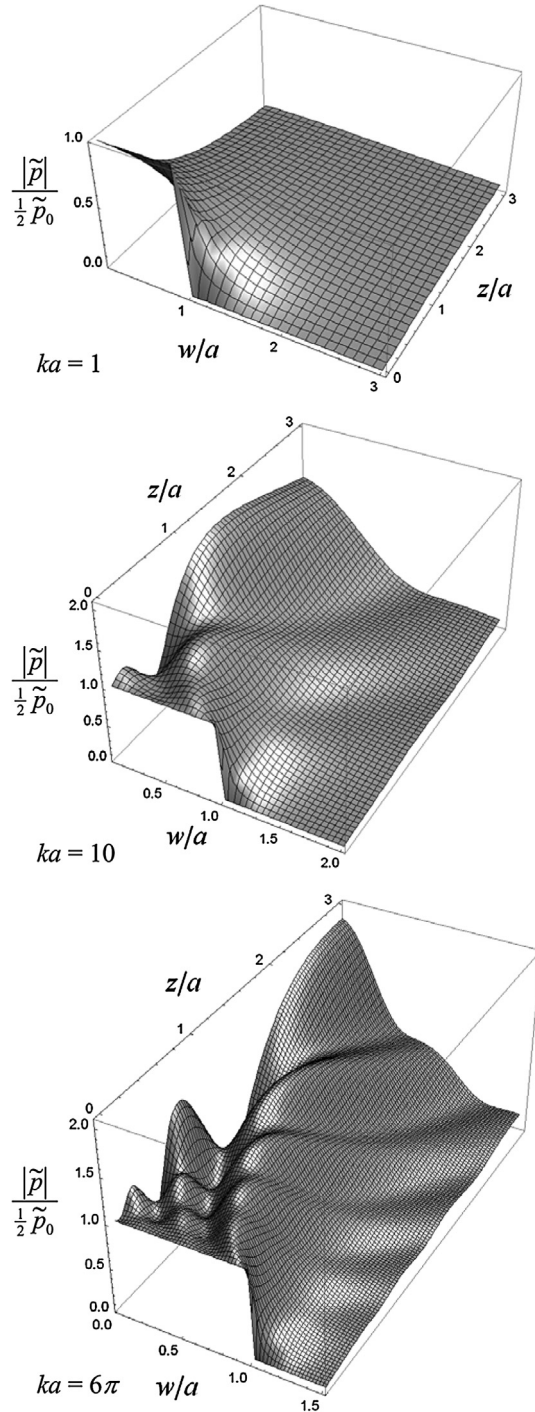


Figure 13.10 Normalized near-field pressure plots for a resilient circular disk in free space as a function of $ka = 2\pi a/\lambda = 2\pi fa/c$, where a is the radius of the disk. $|\tilde{p}|$ is the pressure magnitude, \tilde{p}_0 is the driving pressure.

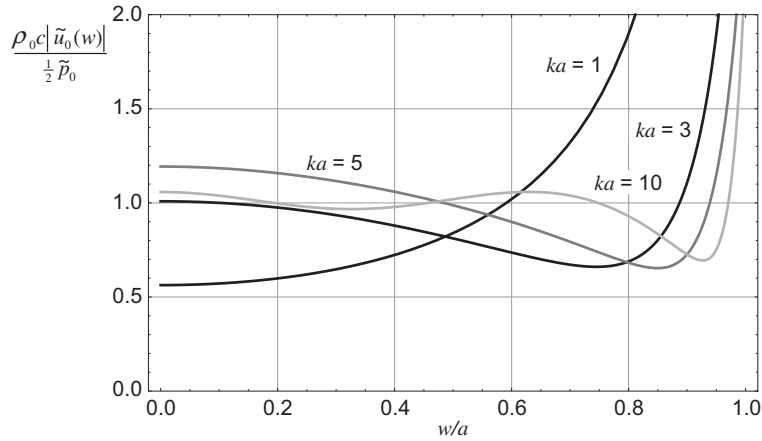


Figure 13.11 Normalized surface velocity magnitude for a resilient circular disk in free space as a function of w/a , where w is the radial ordinate and $ka = 2\pi a/\lambda = \omega/c$, where a is the radius of the disk.

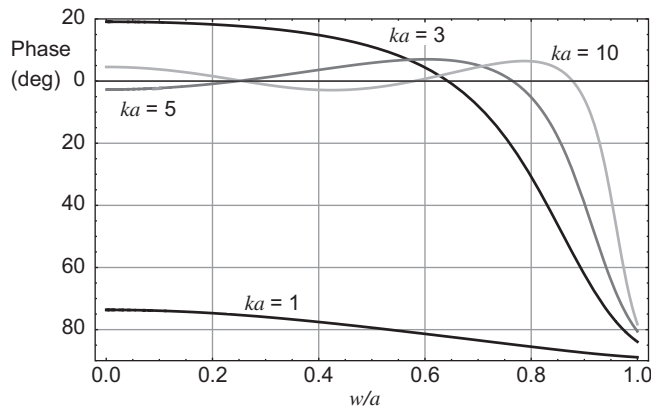


Figure 13.12 Surface velocity phase for a resilient circular disk in free space as a function of w/a , where w is the radial ordinate and $ka = 2\pi a/\lambda = \omega/c$, where a is the radius of the disk.

the asymptotic expression given by Eq. (13.144). We see that the velocity increases rapidly toward the perimeter, where it is singular. This is a feature of uniform pressure sources in general due to the discontinuity at the perimeter. However, it is exacerbated in this case by the acoustic short circuit between the front and rear surfaces of the dipole source.

Radiation admittance and low-frequency asymptotic surface velocity

The near-field pressure distribution is given by Eq. (13.28) taking into account the surface pressure on both sides:

$$\tilde{p}(w, z) = \int_0^{2\pi} \int_0^a (\tilde{p}_+(w_0) - \tilde{p}_-(w_0)) \frac{\partial}{\partial z_0} g(w, z | w_0, z_0) \Big|_{z_0=0+} w_0 dw_0 d\phi_0, \quad (13.141)$$

where the integral Green's function in cylindrical coordinates given by Eq. (13.52) is used. In this form Eq. (13.141) is known as the dipole King integral. Inserting Eqs. (13.52) and (13.123) into Eq. (13.141) and integrating over the surface gives

$$\tilde{p}(w, z) = -ka \rho_0 c \tilde{u}_0 \int_0^\infty J_0(k_w w) J_1(k_w a) \frac{1}{k_z} e^{-jk_z z} dk_w, \quad (13.142)$$

where we have again used the integral of Eq. (95) from Appendix II and k_z is given by Eq. (13.51). The disk velocity $\tilde{u}_0(w)$ can be derived using the following relationship for the normal pressure gradient:

$$\begin{aligned} \tilde{u}_0(w) &= \frac{1}{-jk\rho_0 c} \frac{\partial}{\partial z} \tilde{p}(w, z) \Big|_{z=0+} \\ &= \frac{\tilde{a}\tilde{p}_0}{2k\rho_0 c} \int_0^\infty J_1(k_w a) J_0(k_w w) k_z dk_w. \end{aligned} \quad (13.143)$$

For small k , we obtain

$$\begin{aligned} \tilde{u}_0(w) \Big|_{k \rightarrow 0} &= \frac{j\tilde{a}\tilde{p}_0}{2k\rho_0 c} \int_0^\infty J_1(k_w a) J_0(k_w w) k_w dk_w \\ &= \frac{j\tilde{p}_0 \mathbf{E}(w^2/a^2)}{\pi k a \rho_0 c} \left(1 - \frac{w^2}{a^2}\right)^{-1}, \end{aligned} \quad (13.144)$$

where \mathbf{E} is the complete elliptic integral of the second kind. Hence there is a singularity at the perimeter. The total volume velocity \tilde{U}_0 is found by integrating the velocity from Eq. (13.143) over the surface of the disk and again using the integral of Eq. (95) from Appendix II to give

$$\begin{aligned} \tilde{U}_0 &= \int_0^{2\pi} \int_0^a \tilde{u}_0(w) w dw d\phi \\ &= \frac{\pi a^2 \tilde{p}_0}{k\rho_0 c} \left(\int_0^k J_1^2(k_w a) \frac{\sqrt{k^2 - k_w^2}}{k_w} dk_w - j \int_k^\infty J_1^2(k_w a) \frac{\sqrt{k_w^2 - k^2}}{k_w} dk_w \right), \end{aligned} \quad (13.145)$$

The solution [17,20] has been shown to be

$$Y_s = \frac{\tilde{U}_0}{S\tilde{p}_0} = \mathbf{G}_s + jB_s, \quad (13.146)$$

where $\tilde{U}_0 = \pi a^2 \tilde{u}_0$ is the total volume velocity and \mathbf{G}_s is the specific radiation conductance in $\text{m}^3 \cdot \text{N}^{-1} \text{s}^{-1}$ (rayl^{-1}) given by

$$\begin{aligned} \mathbf{G}_s &= \frac{1}{\rho_0 c} \left(1 + \frac{J_1(2ka)}{ka} - 2J_0(2ka) - \pi(J_1(2ka)\mathbf{H}_0(2ka) - J_0(2ka)\mathbf{H}_1(2ka)) \right) \\ &\approx \frac{1}{\rho_0 c} \cdot \frac{k^2 a^2}{6}, \quad ka < 0.5, \end{aligned} \quad (13.147)$$

where the bold \mathbf{G} indicates that the quantity varies with frequency and B_s is the specific radiation susceptance in $\text{m}^3 \cdot \text{N}^{-1} \text{s}^{-1}$ (rayl^{-1}) given by

$$\begin{aligned} B_s &= -\frac{1}{\rho_0 c} \left(\frac{4}{\pi ka} - \frac{\mathbf{H}_1(2ka)}{ka} + \frac{4ka}{\pi} {}_2F_3 \left(1, 1; \frac{3}{2}, \frac{3}{2}, 2; -k^2 a^2 \right) \right) \\ &\approx \frac{1}{\rho_0 c} \cdot \frac{4}{\pi ka}, \quad ka < 0.5, \end{aligned} \quad (13.148)$$

where J_n and \mathbf{H}_n are Bessel and Struve functions respectively and ${}_2F_3$ is a hypergeometric function. Plots of the real and imaginary parts of

$$\rho_0 c Y_s = \rho_0 c (\mathbf{G}_s + jB_s) \quad (13.149)$$

are shown in Fig. 13.13 as a function of ka . Similar graphs of the real and imaginary parts of the specific impedance

$$\begin{aligned} \frac{Z_s}{\rho_0 c} &= \frac{\mathbf{R}_s + jX_s}{\rho_0 c} = \frac{1}{\rho_0 c} \left(\frac{\mathbf{G}_s}{\mathbf{G}_s^2 + B_s^2} - j \frac{B_s}{\mathbf{G}_s^2 + B_s^2} \right) \\ &\approx \frac{\pi k^4 a^4}{96} - j \frac{\pi ka}{4}, \quad ka < 0.5 \end{aligned} \quad (13.150)$$

are shown in Fig. 13.14. The specific admittance is in $\text{m}^3 \cdot \text{N}^{-1} \text{s}^{-1}$ (rayl^{-1}). Although the impedance and admittance functions of the rigid disk in an infinite baffle show ripples (see Figs. 13.35 and 13.36, respectively), those of the resilient disk are

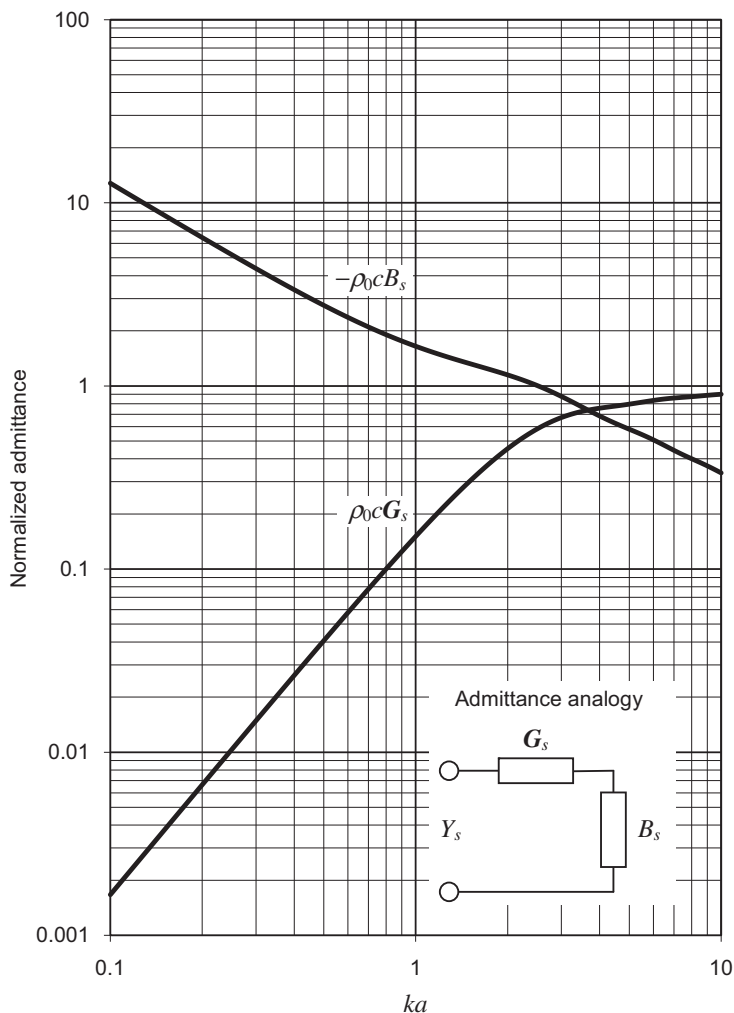


Figure 13.13 Real and imaginary parts of the normalized specific radiation admittance $\rho_0 c Y_s$ of the air load on one side of a plane circular resilient disk of radius a in free space. Frequency is plotted on a normalized scale, where $ka = 2\pi a/\lambda = 2\pi f a/c$.

smooth almost monotonic functions. We can see that at low frequencies the impedance and admittance curves are more reactive than those of a piston in an infinite baffle, so that less power is radiated. This is due to the cancellation of the acoustic output by the rear wave or acoustic “short circuit,” which is generally the case with all dipole sources.

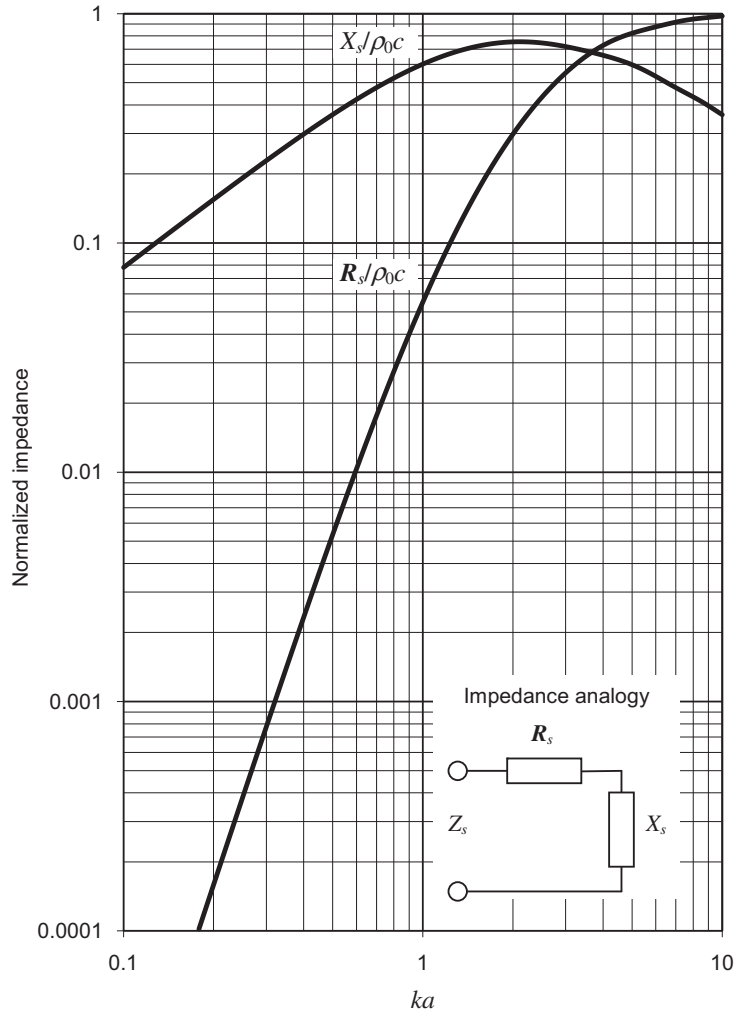


Figure 13.14 Real and imaginary parts of the normalized specific radiation impedance Z_s/ρ_0c of the air load on one side of a plane circular resilient disk of radius a in free space. Frequency is plotted on a normalized scale, where $ka = 2\pi a/\lambda = 2\pi fa/c$.

Relationship between a resilient disk in free space and a rigid piston in an infinite baffle

Suppose that the radiation resistance and reactance of a rigid disk in an infinite baffle are denoted by R_s and X_s respectively and G_s and B_s are the radiation conductance and susceptance respectively of a resilient disk in free space as defined in Eqs. (13.147) and (13.148), then

$$(\rho_0c)^2 \frac{d}{d(ka)} ka G_s(ka) = R_s(ka) = \rho_0c \left(1 - \frac{J_1(2ka)}{ka} \right), \quad (13.151)$$

or

$$\mathbf{G}_s(ka) = \frac{1}{ka(\rho_0 c)^2} \int \mathbf{R}_s(ka) d(ka), \quad (13.152)$$

and

$$(\rho_0 c)^2 \frac{d}{d(ka)} ka B_s(ka) = X_s(ka) = \rho_0 c \left(\frac{\mathbf{H}_1(2ka)}{ka} \right), \quad (13.153)$$

or

$$B_s(ka) = \frac{1}{ka(\rho_0 c)^2} \left(\int X_s(ka) d(ka) + \frac{4}{\pi} \right). \quad (13.154)$$



13.9 RADIATION FROM A RESILIENT DISK IN AN INFINITE BAFFLE [21]

A resilient disk in an infinite baffle, like the previous example, represents a source with a uniform pressure distribution over its radiating surface, unlike the rigid piston where the velocity is uniform. This makes the problem slightly harder to solve because we have to include a trial function for the disk velocity distribution in the surface integral. The trial function is in the form of a series expansion, the unknown coefficients of which have to be calculated via a set of simultaneous equations. However, it is worth the effort because, as we shall see, this particular source represents the diffraction pattern due to a plane wave passing through a circular aperture in an infinite screen, which is an important result in optics too. The transmission coefficient, or radiation conductance, was first calculated by Bouwkamp [20] in his PhD dissertation using the boundary value method in the oblate-spheroidal coordinate system. Less than a decade later, Spence [22] calculated the surface velocity distribution and directivity pattern. However, oblate-spheroidal functions are rather complicated, so instead we shall use the boundary integral method with the Green's function in cylindrical coordinates and a trial function first used by Streng [23] for a membrane.

Boundary conditions

The configuration is the same as that shown in Fig. 13.3. The infinitesimally thin membrane-like resilient disk is mounted in an infinite baffle in the xy plane with its center at the origin. It is assumed to be perfectly flexible, has zero mass, and is free at its perimeter. It is driven by a uniformly distributed harmonically varying pressure \tilde{p}_0 and

thus radiates sound from both sides into a homogeneous loss-free acoustic medium. In fact, there need not be a disk present at all and instead the driving pressure could be acting on the air particles directly. However, for expedience, the area over which this driving pressure is applied shall be referred to as a disk from here onwards. As with the rigid piston in an infinite baffle, we will model this as a “breathing” disk in free space. Because of the symmetry of the pressure fields on either side of the baffle

$$\tilde{p}(w, z) = \tilde{p}(w, -z). \quad (13.155)$$

Consequently, there is a Neumann boundary condition in the plane of the disk where these fields meet:

$$\frac{\partial}{\partial z} \tilde{p}(w, z)|_{z=0} = 0, \quad a < w \leq \infty, \quad (13.156)$$

which is satisfied automatically. On the front and rear surfaces of the disk, the pressures are \tilde{p}_+ and \tilde{p}_- respectively, which are given by

$$\tilde{p}_+(w_0) = \tilde{p}_-(w_0) = \tilde{p}_0/2, \quad 0 \leq w_0 \leq a. \quad (13.157)$$

The pressure gradient is given by

$$\frac{\partial}{\partial z_0} \tilde{p}(w_0, z_0)|_{z_0=0+} = \begin{cases} -jk\rho_0 c \tilde{u}(w_0), & 0 \leq w_0 \leq a, \\ 0, & w_0 > a, \end{cases} \quad (13.158)$$

where $\tilde{u}(w_0)$ is the unknown surface velocity distribution and k is the wave number given by $k = \omega/c = 2\pi/\lambda$, where ω is the angular frequency of excitation, ρ_0 is the density of the surrounding medium, c is the speed of sound in that medium, and λ is the wavelength. We will use the following trial function, which is itself a solution to the free-space Helmholtz wave equation in oblate-spheroidal coordinates [20],

$$\tilde{u}_0(w_0) = \frac{\tilde{p}_0}{2\rho_0 c} \sum_{n=0}^{\infty} A_n \left(n + \frac{1}{2} \right) \left(1 - \frac{w_0^2}{a^2} \right)^{n-\frac{1}{2}}, \quad (13.159)$$

where A_n are the as-yet unknown power series coefficients that will be evaluated by means of a set of simultaneous equations in matrix form. Note that the $n = 0$ term is singular when $w_0 = a$. This is due to the discontinuity at the perimeter, which is inherent in the problem [2]. Otherwise, if we were modeling a problem with zero velocity at the perimeter, such as a membrane with a clamped perimeter [19], we would replace $(n + 1/2)$ in the index with $(n - 1/2)$. Using a trial function, any velocity distribution is possible, and this is not the only trial function that may be used [24,25].

Calculation of the velocity series coefficients

The near-field pressure distribution is given by Eq. (13.27) taking into account the double strength source

$$\tilde{p}(w, z) = -2 \int_0^{2\pi} \int_0^a g(w, z|w_0, z_0) \frac{\partial}{\partial z_0} \tilde{p}(w_0, z_0)|_{z_0=0} w_0 dw_0 d\phi_0, \quad (13.160)$$

where the Green's function in cylindrical coordinates given by Eq. (13.52) is used. In this form Eq. (13.160) is known as the monopole King integral. Inserting Eqs. (13.52), (13.158), (13.159), and (13.99) into Eq. (13.160) and integrating over ϕ_0 gives

$$\tilde{p}(w, z) = k \frac{\tilde{p}_0}{2} \sum_{n=0}^{\infty} A_n \left(n + \frac{1}{2} \right) \int_0^a \left(1 - \frac{w_0^2}{a^2} \right)^{n-\frac{1}{2}} \int_0^{\infty} J_0(k_w w) J_0(k_w w_0) \frac{e^{-jk_z z}}{k_z} k_w dk_w w_0 dw_0, \quad (13.161)$$

where k_z is given by Eq. (13.51). At the surface of the disk, we have the coupling condition

$$\tilde{p}(w, z)|_{z=0+} = \frac{\tilde{p}_0}{2}, \quad 0 \leq w \leq a \quad (13.162)$$

which leads to the following coupled equation

$$\sum_{n=0}^{\infty} A_n I_n(w) = \Phi(w) \quad (13.163)$$

which is to be solved for the power series coefficients A_n , where

$$\Phi(w) = 1, \quad 0 \leq w \leq a \quad (13.164)$$

and

$$I_n(w) = k \left(n + \frac{1}{2} \right) \int_0^a \left(1 - \frac{w_0^2}{a^2} \right)^{n-\frac{1}{2}} \int_0^{\infty} J_0(k_w w) J_0(k_w w_0) \frac{k_w}{k_z} dk_w w_0 dw_0. \quad (13.165)$$

The infinite integral [49-51] is given by Eq. (A2.106a), together with Eqs. (A2.11a) and (A2.150), from Appendix II with $m = n = 0$ and $\gamma = 1$

$$\int_0^\infty J_0(k_w w) J_0(k_w w_0) \frac{k_w}{\sqrt{k^2 - k_w^2}} dk_w = \frac{\sqrt{\pi} k}{2} \sum_{m=0}^\infty \frac{1}{(m!)^2} \left(\frac{w}{w_0}\right)^{2m} \\ \times \sum_{r=0}^\infty \frac{\Gamma\left(\frac{r}{2} + \frac{1}{2}\right)}{\Gamma\left(\frac{r}{2} + 1\right) \Gamma^2\left(\frac{r}{2} - m + \frac{1}{2}\right)} \left(\frac{-jk w_0}{2}\right)^{r-1}, \quad (13.166)$$

so that

$$I_n(w) = k \left(n + \frac{1}{2}\right) \frac{\sqrt{\pi} k}{2} \sum_{m=0}^\infty \frac{w^{2m}}{(m!)^2} \\ \times \sum_{r=0}^\infty \frac{\Gamma\left(\frac{r}{2} + \frac{1}{2}\right)}{\Gamma\left(\frac{r}{2} + 1\right) \Gamma^2\left(\frac{r}{2} - m + \frac{1}{2}\right)} \left(\frac{-jk}{2}\right)^{r-1} \int_0^a \left(1 - \frac{w_0^2}{a^2}\right)^{n-\frac{1}{2}} w_0^{r-2m} dw_0, \quad (13.167)$$

which is simplified with help of the integral

$$\int_0^a \left(1 - \frac{w_0^2}{a^2}\right)^{n-\frac{1}{2}} w_0^\mu dw_0 = \frac{a^{\mu+1} \Gamma\left(n + \frac{1}{2}\right) \Gamma\left(\frac{\mu+1}{2}\right)}{2\Gamma\left(n + \frac{\mu}{2} + 1\right)} \quad (13.168)$$

to give

$$I_n(w) = -\sqrt{\pi} \Gamma\left(n + \frac{3}{2}\right) \sum_{m=0}^\infty \frac{1}{(m!)^2} \\ \times \sum_{r=0}^\infty \frac{\Gamma\left(\frac{r}{2} + \frac{1}{2}\right)}{\Gamma\left(\frac{r}{2} + 1\right) \Gamma\left(\frac{r}{2} - m + \frac{1}{2}\right) \Gamma\left(n - m + \frac{r}{2} + 1\right)} \left(\frac{-jka}{2}\right)^{r+1} \left(\frac{w}{a}\right)^{2m}, \quad (13.169)$$

which is an expansion in $(w/a)^{2m}$. We also note that

$$\Phi(w) = \sum_{m=0}^{\infty} \delta_{m0} \left(\frac{w}{a}\right)^{2m}, \quad 0 \leq w \leq a \quad (13.170)$$

where δ_{m0} is the Kronecker delta function. Inserting Eqs. (13.169) and (13.170) into Eq. (13.163) and equating the coefficients of $(w/a)^{2m}$ yields the following $(N+1) \times (N+1)$ matrix equation

$$\mathbf{M} \cdot \mathbf{a} = \mathbf{b} \Rightarrow \mathbf{a} = \mathbf{M}^{-1} \cdot \mathbf{b}, \quad (13.171)$$

where the matrix \mathbf{M} and vectors \mathbf{a} and \mathbf{b} are given by

$$\mathbf{M}(m+1, n+1) = {}_n\mathbf{T}_m(ka), \quad \begin{cases} m = 0, 1, \dots, N \\ n = 0, 1, \dots, N \end{cases} \quad (13.172)$$

$$\mathbf{b}(m+1) = \delta_{m0}, \quad m = 0, 1, \dots, N \quad (13.173)$$

$$\mathbf{a}(n+1) = A_n, \quad n = 0, 1, \dots, N \quad (13.174)$$

and the infinite power series limits have been truncated to order N . The monopole cylindrical wave function ${}_n\mathbf{T}_m$ is named the Stenzel–Spence function in tribute to their pioneering work and is defined by

$${}_n\mathbf{T}_m(ka) = -\sqrt{\pi} \frac{\Gamma\left(n + \frac{3}{2}\right)}{(m!)^2} \sum_{r=0}^N {}_n\mathbf{P}_m(r) \left(\frac{-jka}{2}\right)^{r+1} \quad (13.175)$$

$${}_n\mathbf{P}_m(r) = \frac{\Gamma\left(\frac{r}{2} + \frac{1}{2}\right)}{\Gamma\left(\frac{r}{2} + 1\right)\Gamma\left(\frac{r}{2} - m + \frac{1}{2}\right)\Gamma\left(\frac{r}{2} - m + n + 1\right)} \quad (13.176)$$

Now that we have the surface velocity series coefficients A_n , we can derive some radiation characteristics for the resilient disk.

Far-field pressure

The far-field pressure distribution is given by Eq. (13.27) taking into account the double-strength source:

$$\tilde{p}(r, \theta) = -2 \int_0^{2\pi} \int_0^a g(r, \theta|w_0, \phi_0) \frac{\partial}{\partial z_0} \tilde{p}(w_0, z_0)|_{z_0=0^+} w_0 dw_0 d\phi_0, \quad (13.177)$$

where the far-field Green's function in spherical-cylindrical coordinates given by Eq. (13.70) is used. Inserting Eqs. (13.70), (13.158) and (13.159) into Eq. (13.177) and integrating over the surface, using Eqs. (76) and (96) from Appendix II [with $z = kv_0 \sin \theta$, $b = k \sin \theta$, and letting $\phi = \pi/2$ so that $\cos(\phi - \phi_0) = \sin \phi_0$], gives

$$\tilde{p}(r, \theta) = jka^2 \tilde{p}_0 \frac{e^{-jkr}}{4r} D(\theta), \quad (13.178)$$

where the directivity function $D(\theta)$ is given by

$$D(\theta) = \sum_{n=0}^N A_n \Gamma \left(n + \frac{3}{2} \right) \left(\frac{2}{ka \sin \theta} \right)^{n+\frac{1}{2}} J_{n+\frac{1}{2}}(ka \sin \theta). \quad (13.179)$$

The on-axis pressure is evaluated by setting $\theta = 0$ in Eq. (13.70) before inserting it in Eq. (13.177) and integrating over the surface to give

$$D(0) = \sum_{n=0}^N A_n \approx \begin{cases} 4j/(\pi ka), & ka < 0.5 \\ 1, & ka > 2. \end{cases} \quad (13.180)$$

It is worth noting that $D(0)$ is simply the normalized radiation admittance, that is

$$D(0) = \rho_0 c (\mathbf{G}_S + jB_S),$$

where \mathbf{G}_S and B_S are given by Eqs. (13.193) and (13.194) respectively. The asymptotic expression for low-frequency on-axis pressure is then simply

$$\tilde{p}(r, 0) \approx -\frac{a}{\pi r} \tilde{p}_0 e^{-jkr}, \quad ka < 0.5 \quad (13.181)$$

and at high frequencies

$$\tilde{p}(r, 0) \approx j \frac{ka^2}{4r} \tilde{p}_0 e^{-jkr}, \quad ka > 2, \quad (13.182)$$

which is the same as for a resilient disk in free space at all frequencies. The on-axis response is shown in Fig. 13.15, calculated from the magnitude of $D(0)$. The normalized directivity function $20 \log_{10} |D(\theta)/D(0)|$ is plotted in Fig. 13.16 for four values of $ka = 2\pi a/\lambda$, that is, for four values of the ratio of the circumference of the piston to the wavelength. When the circumference of the piston ($2\pi a$) is less than one-half wavelength, that is, $ka < 0.5$, the disk behaves essentially like a point source. When ka becomes greater than 3, the resilient disk is highly directional, rather like the rigid piston in an infinite baffle except without the nulls.

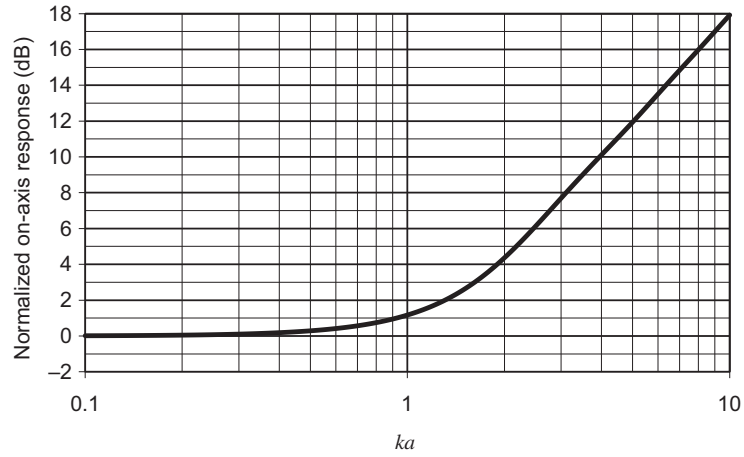


Figure 13.15 Plot of $20 \log_{10} (\pi ka |D(0)/4|)$ where $D(\theta)$ is the directivity function of a resilient disk of radius a in an infinite baffle. The uniform driving pressure is constant. Frequency is plotted on a normalized scale, where $ka = 2\pi a/\lambda = 2\pi fa/c$.

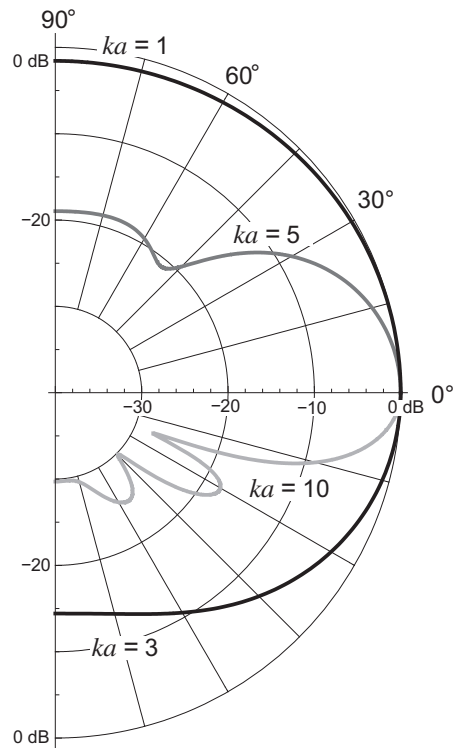


Figure 13.16 Far-field directivity patterns for a resilient disk in an infinite baffle as a function of $ka = 2\pi a/\lambda = 2\pi fa/c$, where a is the radius of the disk.

Near-field pressure

The near-field pressure distribution is given by Eq. (13.27) taking into account the surface pressure on both sides:

$$\tilde{p}(r, \theta) = 2 \int_0^{2\pi} \int_0^a g(r, \theta | w_0, \phi_0) \frac{\partial}{\partial z_0} \tilde{p}(w_0, z_0)_{z_0=0+} w_0 dw_0 d\phi_0, \quad (13.183)$$

where the Green's function in spherical-cylindrical coordinates given by Eq. (13.68) is used. It has been shown [21] that inserting Eqs. (13.68), (13.158) and (13.159) into Eq. (13.183) and integrating over the surface gives

$$\begin{aligned} p(r, \theta) = \tilde{p}_0 \sum_{n=0}^N A_n \sum_{p=0}^P \frac{(-1)^p \Gamma(p + 1/2) \Gamma(n + 3/2) h_{2p}^{(2)}(kr) P_{2p}(\cos \theta)}{\Gamma(2p + 1/2) \Gamma(p + n + 3/2)} \\ \times \left(\frac{ka}{2}\right)^{2p+2} {}_1F_2\left(p + 1; p + n + \frac{3}{2}, 2p + \frac{3}{2}; -\frac{k^2 a^2}{4}\right), \end{aligned} \quad (13.184)$$

which converges for $r > a$. For $r \leq a$, we derive a suitable expression from Eq. (13.161), which is weakly singular at $k_w = k$. However, we can remove this singularity as follows: First, we substitute

$$k_w = k\sqrt{1 - t^2} \text{ for } k_w \leq k$$

and

$$k_w = k\sqrt{1 + t^2} \text{ for } k_w > k$$

in Eq. (13.161) to obtain

$$\tilde{p}(w, z) = \tilde{p}_0 \sum_{n=0}^{\infty} A_n \Gamma\left(n + \frac{3}{2}\right) (I_{Fin} + jI_{Inf}), \quad (13.185)$$

where

$$I_{Fin} = \left(\frac{2}{ka}\right)^{n-\frac{3}{2}} \int_0^1 \left(\frac{1}{1-t^2}\right)^{\frac{n+1}{2}} J_{n+\frac{1}{2}}(ka\sqrt{1-t^2}) J_0(kw\sqrt{1-t^2}) e^{-jkzt} dt, \quad (13.186)$$

$$I_{Inf} = \left(\frac{2}{ka}\right)^{n-\frac{3}{2}} \int_0^{\infty} \left(\frac{1}{1+t^2}\right)^{\frac{n+1}{2}} J_{n+\frac{1}{2}}(ka\sqrt{1+t^2}) J_0(kw\sqrt{1+t^2}) e^{-kzt} dt. \quad (13.187)$$

We then apply the expansion of Eq. (109) from Appendix II to give

$$I_{Fin} + jI_{Inf} = \sum_{p=0}^{\infty} \frac{(-1)^p}{p! \Gamma(n+p+3/2)} \left(\frac{ka}{2}\right)^{2p+2} {}_2F_1\left(-p, -n-p-\frac{1}{2}; 1; \frac{w^2}{a^2}\right) \\ \times \left(\int_0^1 (1-t^2)^p e^{-jkzt} dt + j \int_0^{\infty} (1+t^2)^p e^{-kzt} dt \right), \quad (13.188)$$

which, after integrating, yields

$$I_{Fin} = \frac{\sqrt{\pi}}{2} \sum_{p=0}^{\infty} \frac{(-1)^p}{\Gamma(n+p+3/2)} \left(\frac{ka}{2}\right)^{2p+2} {}_2F_1\left(-p, -n-p-\frac{1}{2}; 1; \frac{w^2}{a^2}\right) \\ \times \left(\frac{2}{kz}\right)^{p+\frac{1}{2}} \left(J_{p+\frac{1}{2}}(kz) - j\mathbf{H}_{p+\frac{1}{2}}(kz)\right), \\ I_{Inf} = \frac{\sqrt{\pi}}{2} \sum_{p=0}^{\infty} \frac{(-1)^p}{\Gamma(n+p+3/2)} \left(\frac{ka}{2}\right)^{2p+2} {}_2F_1\left(-p, -n-p-\frac{1}{2}; 1; \frac{w^2}{a^2}\right) \\ \times \left(\frac{2}{kz}\right)^{p+\frac{1}{2}} \left(\mathbf{H}_{p+\frac{1}{2}}(kz) - Y_{p+\frac{1}{2}}(kz)\right). \quad (13.190)$$

Eq. (13.189) converges everywhere and is therefore suitable for $r < a$. Unfortunately, Eq. (13.190) only converges for $z^2 > w^2 + a^2$ and is therefore not suitable. However, Eq. (13.187) converges everywhere and can be calculated numerically without problem and is therefore suitable for $r < a$. Using the Babinet–Bouwkamp principle, this represents the field scattered by a hole in an infinite screen in the presence of an incident plane wave, as plotted in Fig. 13.39 for three values of ka .

Surface velocity

The magnitude and phase of the normalized velocity from Eq. (13.159) are shown in Figs. 13.17 and 13.18, respectively, for four values of ka . We see that the velocity increases rapidly toward the perimeter where it is singular. This is a feature of uniform pressure sources in general because of the discontinuity at the perimeter.

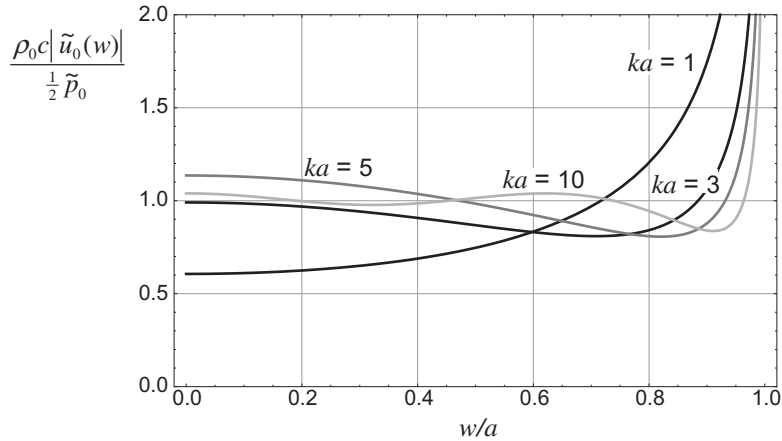


Figure 13.17 Normalized surface velocity magnitude for a resilient circular disk in an infinite baffle as a function of w/a where w is the radial ordinate and $ka = 2\pi a/\lambda = \omega/c$, where a is the radius of the disk.

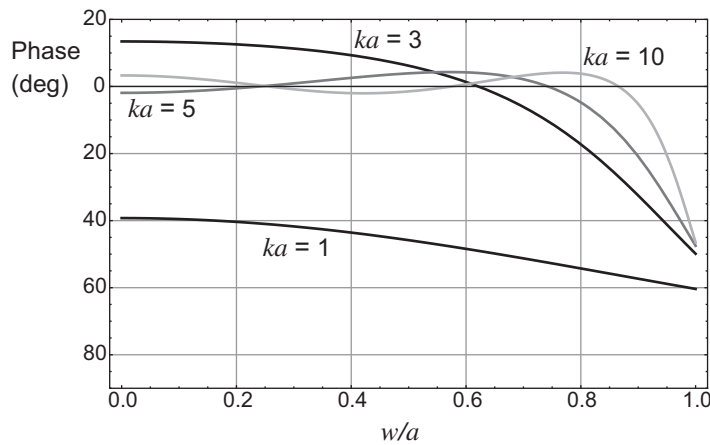


Figure 13.18 Surface velocity phase for a resilient circular disk in an infinite baffle as a function of w/a where w is the radial ordinate and $ka = 2\pi a/\lambda = \omega/c$, where a is the radius of the disk.

Radiation admittance

The total volume velocity \tilde{U}_0 is found by integrating the velocity from Eq. (13.159) over the surface of the disk to give

$$\tilde{U}_0 = \int_0^{2\pi} \int_0^a \tilde{u}_0(w_0) w_0 dw_0 d\phi_0 = \frac{\pi a^2 \tilde{p}_0}{2\rho_0 c} \sum_{n=0}^N A_n. \quad (13.191)$$

The specific radiation admittance is then given by

$$Y_s = \frac{\tilde{U}_0}{\tilde{S}p_0} = \mathbf{G}_s + jB_s, \quad (13.192)$$

where \tilde{U}_0 is the total volume velocity and \mathbf{G}_s is the specific radiation conductance in $\text{m}^3 \cdot \text{N}^{-1} \text{s}^{-1}$ (rayl⁻¹) given by

$$\begin{aligned} \mathbf{G}_s &= \frac{1}{\rho_0 c} \Re \left(\sum_{n=0}^N A_n \right) \\ &\approx \frac{1}{\rho_0 c} \cdot \frac{8}{\pi^2}, \quad ka < 0.5, \end{aligned} \quad (13.193)$$

where the bold \mathbf{G} indicates that the quantity varies with frequency. B_s is the specific radiation susceptance in $\text{m}^3 \cdot \text{N}^{-1} \text{s}^{-1}$ (rayl⁻¹) given by

$$\begin{aligned} B_s &= \frac{1}{\rho_0 c} \Im \left(\sum_{n=0}^N A_n \right) \\ &\approx \frac{1}{\rho_0 c} \cdot \frac{4}{\pi ka}, \quad ka < 0.5. \end{aligned} \quad (13.194)$$

Plots of the real and imaginary parts of

$$\rho_0 c Y_s = \rho_0 c (\mathbf{G}_s + jB_s) \quad (13.195)$$

are shown in Fig. 13.19 as a function of ka . Similar graphs of the real and imaginary parts of the specific impedance

$$\begin{aligned} \frac{Z_s}{\rho_0 c} = \frac{\mathbf{R}_s + jX_s}{\rho_0 c} &= \frac{1}{\rho_0 c} \left(\frac{\mathbf{G}_s}{\mathbf{G}_s^2 + B_s^2} - j \frac{B_s}{\mathbf{G}_s^2 + B_s^2} \right) \\ &\approx \frac{k^2 a^2}{2} - j \frac{\pi ka}{4}, \quad ka < 0.5 \end{aligned} \quad (13.196)$$

are shown in Fig. 13.20. The specific admittance is in $\text{m}^3 \cdot \text{N}^{-1} \text{s}^{-1}$ (rayl⁻¹). Although the impedance and admittance functions of the rigid disk in an infinite baffle show ripples (see Figs. 13.35 and 13.36 respectively), those of the resilient disk are smooth, almost monotonic functions.

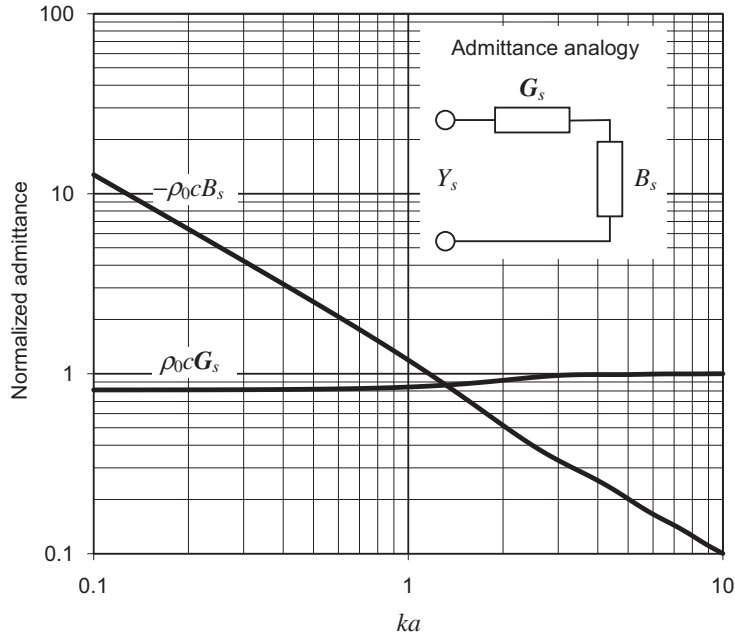


Figure 13.19 Real and imaginary parts of the normalized specific radiation admittance $Y_s/\rho_0 c$ of the air load on one side of a plane circular resilient disk of radius a in an infinite baffle. Frequency is plotted on a normalized scale, where $ka = 2\pi a/\lambda = 2\pi f a/c$.

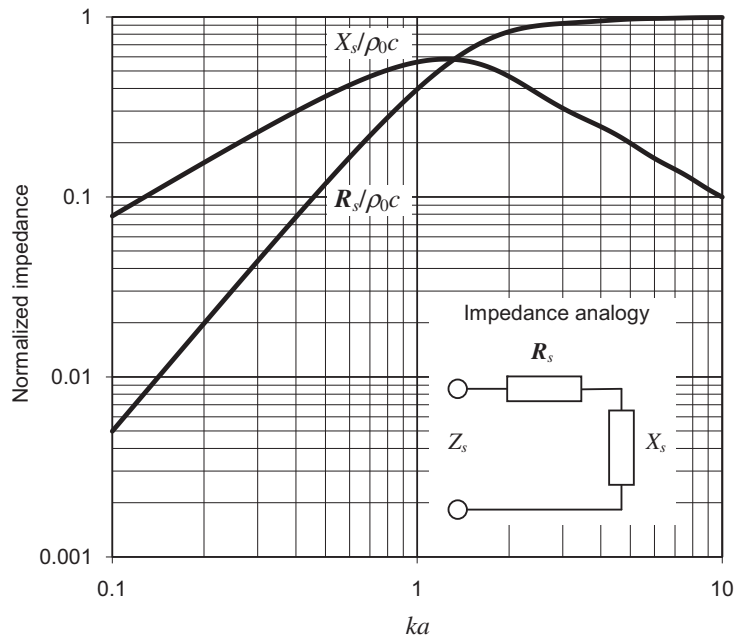


Figure 13.20 Real and imaginary parts of the normalized specific radiation impedance $Z_s/\rho_0 c$ of the air load on one side of a plane circular resilient disk of radius a in an infinite baffle. Frequency is plotted on a normalized scale, where $ka = 2\pi a/\lambda = 2\pi f a/c$.



13.10 RADIATION FROM A RIGID CIRCULAR PISTON IN A FINITE CIRCULAR OPEN BAFFLE [26,27]

A disk in a circular baffle is a useful model for an open-baffle type loudspeaker and in the limiting case a loudspeaker without a baffle of any sort. Loudspeaker drive units are often measured in a finite baffle such as the rectangular IEC 268-5 baffle. See IEC 60268-5, ed. 3.1, “Sound system equipment – Part 5: Loudspeakers,” available from <http://webstore.iec.ch/>. For example, for a nominal 8-in (200 mm) diameter loudspeaker, the baffle size would be 1.65 m long by 1.35 m wide, with the loudspeaker offset from the center by 22.5 cm lengthways and 15 cm widthways. If we have a rigorous model of the baffle, we can subtract its diffraction effects from the measurement to reveal the true response of the drive unit. The problem was first solved by Nimura and Watanabe [28] using the boundary value method in the oblate-spheroidal coordinate system. However, oblate-spheroidal functions are rather complicated, so instead we shall use the boundary integral method with the Green’s function in cylindrical coordinates and a trial function first used by Streng [23] for a membrane. Previous solutions for the limiting case of a disk in free space have been obtained by Bouwkamp [20] using the boundary value method and Sommerfeld [29] using the boundary integral method in cylindrical coordinates. Meixner and Fritze [30] plotted the near-field pressure, a formidable task without the benefit of modern computing power, and Wiener [31] plotted the far-field directivity pattern.

Boundary conditions

The circular piston of radius a shown in Fig. 13.21 is mounted in a finite circular baffle of radius b in the xy plane with its center at the origin and oscillates in the z direction with a harmonically time-dependent velocity \tilde{u}_0 , thus radiating sound from both sides into a homogeneous loss-free medium. The dipole source elements shown in Fig. 13.21 form the piston source. The area of each surface element is given by

$$\delta S_0 = w_0 \delta w_0 \delta \phi_0. \quad (13.197)$$

The pressure field on one side of the xy plane is the symmetrical “negative” of that on the other, so that

$$\tilde{p}(w, z) = -\tilde{p}(w, -z). \quad (13.198)$$

Consequently, there is a Dirichlet boundary condition in the plane of the disk where these equal and opposite fields meet:

$$\tilde{p}(w, 0) = 0, \quad b < w \leq \infty, \quad (13.199)$$

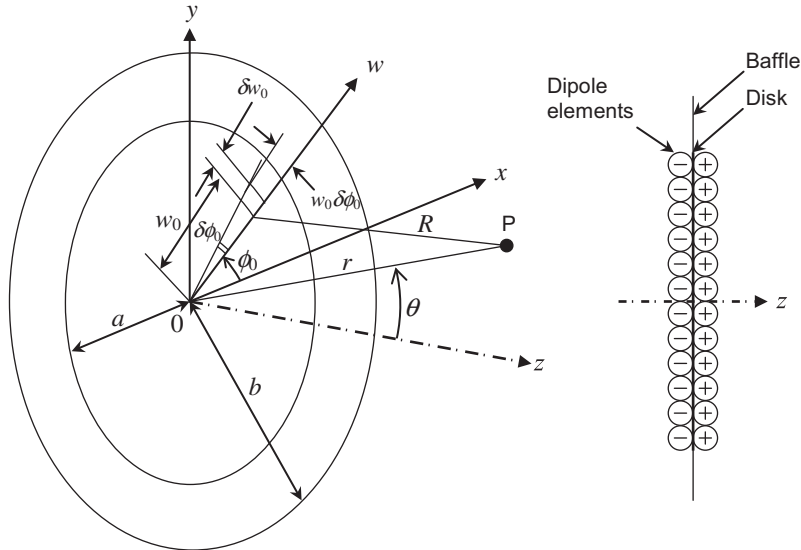


Figure 13.21 Geometry of rigid circular piston in finite baffle. The point of observation P is located at a distance r and angle θ with respect to the origin at the center of the piston.

which is satisfied automatically. On the front and rear surfaces of the baffle, there is a Neumann boundary condition

$$\frac{\partial}{\partial z} \tilde{p}(w, z)|_{z=0\pm} = 0, \quad a < w \leq b. \quad (13.200)$$

Also, on the front and rear surfaces of the disk, there is the coupling condition

$$\frac{\partial}{\partial z} \tilde{p}(w, z)|_{z=0\pm} = -jk\rho_0 c \tilde{u}_0, \quad 0 \leq w \leq a, \quad (13.201)$$

where k is the wave number given by $k = \omega/c = 2\pi/\lambda$, ω is the angular frequency of excitation, ρ_0 is the density of the surrounding medium, c is the speed of sound in that medium, and λ is the wavelength. To tackle this problem, we shall use the *dipole* surface integral of Eq. (13.28). However, some prior expression for the frontal surface pressure distribution $\tilde{p}_+(w_0)$ is needed. In addition, because the disk can radiate from both sides, the rear surface pressure distribution $\tilde{p}_-(w_0)$ must be included too, where $\tilde{p}_+(w_0) = -\tilde{p}_-(w_0)$. Streng [23] showed that the surface pressure distribution for any flat axially symmetric un baffled source (or sink), based on Bouwkamp's solution [20] to the free-space wave equation in oblate-spheroidal coordinates, could be written as

$$\tilde{p}_+(w_0) = -\tilde{p}_-(w_0) = kb\rho_0 c \tilde{u}_0 \frac{a^2}{b^2} \sum_{n=0}^{\infty} A_n \left(n + \frac{3}{2}\right) \left(1 - \frac{w_0^2}{b^2}\right)^{n+\frac{1}{2}}, \quad 0 \leq w_0 \leq b. \quad (13.202)$$

where A_n are the as-yet unknown power series coefficients, which will be evaluated by means of a set of simultaneous equations in matrix form.

Formulation of the coupled equation

The near-field pressure distribution is given by the boundary integral of Eq. (13.28) taking into account the surface pressure on both sides

$$\tilde{p}(w, z) = \int_0^{2\pi} \int_0^b (\tilde{p}_+(w_0) - \tilde{p}_-(w_0)) \frac{\partial}{\partial z_0} g(w, z | w_0, z_0) \Big|_{z_0=0^+} w_0 dw_0 d\phi_0, \quad (13.203)$$

where the Green's function in cylindrical coordinates given by Eq. (13.52) is used. In this form Eq. (13.203) is known as the dipole King integral. Inserting Eqs. (13.52), (13.198) and (13.202) into Eq. (13.203) and integrating over ϕ_0 gives

$$\begin{aligned} \tilde{p}(w, z) &= kb\rho_0\tilde{c}u_0\frac{a^2}{b^2} \sum_{n=0}^{\infty} A_n \left(n + \frac{3}{2}\right) \int_0^b \left(1 - \frac{w_0^2}{b^2}\right)^{n+\frac{1}{2}} \\ &\quad \times \int_0^{\infty} J_0(k_w w) J_0(k_w w_0) e^{-jk_z|z|} k_w dk_w w_0 dw_0, \end{aligned} \quad (13.204)$$

where k_z is given by Eq. (13.51). At the surface of the disk, we have the coupling condition

$$\frac{\partial}{\partial z} \tilde{p}(w, z) \Big|_{z=0} = -jk\rho_0\tilde{c}u_0\Phi(w), \quad (13.205)$$

where $\Phi(w)$ is a dimensionless function of the surface velocity distribution. We will use different expressions for $\Phi(w)$ when considering a piston in free space and a piston or point source in a circular baffle. This leads to the following coupled equation

$$\sum_{n=0}^{\infty} A_n I_n(w) = \Phi(w), \quad (13.206)$$

where

$$I_n(w) = \frac{a^2}{b} \left(n + \frac{3}{2}\right) \int_0^b \left(1 - \frac{w_0^2}{b^2}\right)^{n+\frac{1}{2}} \int_0^{\infty} J_0(k_w w) J_0(k_w w_0) \sqrt{k^2 - k_w^2} k_w dk_w w_0 dw_0. \quad (13.207)$$

The infinite integral [46–48] is given by Eq. (A2.106b), together with Eqs. (A2.11a) and (A2.150), from Appendix II with $m = n = 0$ and $\gamma = 1$

$$\begin{aligned}
& \int_0^\infty J_0(k_w w) J_0(k_w w_0) \sqrt{k^2 - k_w^2} k_w dk_w \\
&= -\frac{2j\sqrt{\pi}}{w_0^3} \sum_{m=0}^\infty \frac{1}{(m!)^2} \left(\frac{w}{w_0}\right)^{2m} \sum_{r=0}^\infty \frac{\Gamma\left(\frac{r}{2} - \frac{1}{2} + \delta_{r,1}\right)}{\Gamma\left(\frac{r}{2} + 1\right) \Gamma^2\left(\frac{r}{2} - m - \frac{1}{2}\right)} \left(\frac{-jk_w w_0}{2}\right)^r,
\end{aligned} \tag{13.208}$$

where $\delta_{r,1}$ is the Kronecker delta function that is included to ensure that the $r = 1$ term goes to zero in an orderly way without having a singularity due to $\Gamma(0)$ in the numerator. Hence

$$\begin{aligned}
I_n(w) &= -2j\sqrt{\pi} \frac{a^2}{b} \left(n + \frac{3}{2}\right) \sum_{m=0}^\infty \frac{w^{2m}}{(m!)^2} \\
&\times \sum_{r=0}^\infty \frac{\Gamma\left(\frac{r}{2} - \frac{1}{2} + \delta_{r,1}\right)}{\Gamma\left(\frac{r}{2} + 1\right) \Gamma^2\left(\frac{r}{2} - m - \frac{1}{2}\right)} \left(\frac{-jk}{2}\right)^r \int_0^b \left(1 - \frac{w_0^2}{b^2}\right)^{n+\frac{1}{2}} w_0^{r-2m-2} dw_0,
\end{aligned} \tag{13.209}$$

which is simplified with help of the integral

$$\int_0^b \left(1 - \frac{w_0^2}{b^2}\right)^{n+\frac{1}{2}} w_0^\mu dw_0 = \frac{b^{\mu+1} \Gamma\left(n + \frac{3}{2}\right) \Gamma\left(\frac{\mu+1}{2}\right)}{2\Gamma\left(n + \frac{\mu}{2} + 2\right)} \tag{13.210}$$

to give

$$\begin{aligned}
I_n(w) &= -j\sqrt{\pi} \frac{a^2}{b^2} \Gamma\left(n + \frac{5}{2}\right) \sum_{m=0}^\infty \frac{1}{(m!)^2} \left(\frac{w}{b}\right)^{2m} \\
&\times \sum_{r=0}^\infty \frac{\Gamma\left(\frac{r}{2} - \frac{1}{2} + \delta_{r,1}\right)}{\Gamma\left(\frac{r}{2} + 1\right) \Gamma\left(\frac{r}{2} - m - \frac{1}{2}\right) \Gamma\left(\frac{r}{2} + n - m + 1\right)} \left(\frac{-jkb}{2}\right)^r.
\end{aligned} \tag{13.211}$$

Solution of the power series coefficients for a piston in free space

Eq. (13.211) is an expansion in $(w/b)^{2m}$. Hence, to solve for the expansion coefficients, it is useful to also express the disk and baffle velocity distribution $\Phi(w)$ as a function of $(w/b)^{2m}$. In the case of a disk in free space where $b = a$, we have

$$\Phi(w)|_{b=a} = 1 = \sum_{m=0}^{\infty} \delta_{m,0} \left(\frac{w}{a}\right)^{2m}, \quad 0 \leq w \leq a \quad (13.212)$$

where δ_{m0} is the Kronecker delta function. Inserting Eqs. (13.211) and (13.212) in Eq. (13.206) and equating the coefficients of $(w/a)^{2m}$ yields the $(N+1) \times (N+1)$ matrix equation

$$\mathbf{M} \cdot \mathbf{a} = \mathbf{b}, \quad (13.213)$$

where the matrix \mathbf{M} and vectors \mathbf{a} and \mathbf{b} are given by

$$\mathbf{M}(m+1, n+1) = {}_n\mathbf{B}_m(ka), \quad \begin{cases} m = 0, 1, \dots, N \\ n = 0, 1, \dots, N \end{cases}, \quad (13.214)$$

$$\mathbf{b}(m+1) = \delta_{m,0}, \quad m = 0, 1, \dots, N, \quad (13.215)$$

$$\mathbf{a}(n+1) = A_n, \quad n = 0, 1, \dots, N, \quad (13.216)$$

and the infinite power series limits have been truncated to order N . The dipole cylindrical wave function ${}_n\mathbf{B}_m$ is named the Bouwkamp–Streng function in tribute to their pioneering work and is defined by

$${}_n\mathbf{B}_m(ka) = -j\sqrt{\pi}\Gamma\left(n + \frac{5}{2}\right) \frac{1}{(m!)^2} \sum_{r=0}^{\infty} {}_n\mathbf{S}_m(r) \left(\frac{-jka}{2}\right)^r, \quad (13.217)$$

where

$${}_n\mathbf{S}_m(r) = \frac{\Gamma\left(\frac{r}{2} - \frac{1}{2} + \delta_{r,1}\right)}{\Gamma\left(\frac{r}{2} + 1\right)\Gamma\left(\frac{r}{2} - m - \frac{1}{2}\right)\Gamma\left(\frac{r}{2} + n - m + 1\right)}. \quad (13.218)$$

Solution of the power series coefficients for a piston in a circular baffle

For a finite baffle, where $b \neq a$, we can employ the following *least-mean-squares* (LMS) algorithm. From Eq. (13.206), let an error function be defined by

$$E(A_n) = \int_0^b \left| \sum_{n=0}^N A_n I_n(w) - \Phi(w) \right|^2 w dw. \quad (13.219)$$

where

$$\Phi(w) = \begin{cases} 1, & 0 \leq w \leq a \\ 0, & a < w \leq b, \end{cases} \quad (13.220)$$

To find the values of A_n that minimize the error, we take the derivative of E with respect to A_n and equate the result to zero

$$\frac{\partial}{\partial A_n} E(A_n) = 2 \int_0^b I_m^*(w) \left(\sum_{n=0}^N A_n I_n(w) - \Phi(w) \right) w dw = 0, \quad (13.221)$$

which, after truncating the infinite series limit to order N , yields the following set of $N + 1$ simultaneous equations

$$\sum_{n=0}^{\infty} A_n \int_0^b I_m^*(w) I_n(w) w dw = \int_0^a I_m^*(w) w dw, \quad m = 0, 1, \dots, N, \quad (13.222)$$

where

$$I_m^*(w) = \frac{a^2}{b^2} \sum_{p=0}^P m \mathbf{B}_p^*(kb) \left(\frac{w}{b} \right)^{2p}, \quad (13.223)$$

$$I_n(w) = \frac{a^2}{b^2} \sum_{q=0}^Q n \mathbf{B}_q(kb) \left(\frac{w}{b} \right)^{2q}. \quad (13.224)$$

Integrating over w yields the following $(N + 1) \times (N + 1)$ matrix equation

$$\mathbf{M} \cdot \mathbf{a} = \mathbf{b}, \quad (13.225)$$

where the matrix \mathbf{M} and vectors \mathbf{a} and \mathbf{b} are given by

$$\mathbf{M}(m + 1, n + 1) = \sum_{p=0}^P \sum_{q=0}^Q \frac{m \mathbf{B}_q^*(kb)_n \mathbf{B}_q(kb)}{p + q + 1}, \quad \begin{cases} m = 0, 1, \dots, N \\ n = 0, 1, \dots, N \end{cases}, \quad (13.226)$$

$$\mathbf{b}(m + 1) = - \sum_{p=0}^P \frac{m \mathbf{B}_p^*(kb)}{p + 1} \left(\frac{a}{b} \right)^{2p}, \quad m = 0, 1, \dots, N, \quad (13.227)$$

$$\mathbf{a}(n + 1) = A_n, \quad n = 0, 1, \dots, N \quad (13.228)$$

Solution of the power series coefficients for a point or ring source in a circular baffle

In the case of a ring source of radius a in a circular baffle, we have

$$\Phi(w) = \frac{a}{2} \delta(w - a), \quad (13.229)$$

where δ is the Dirac delta function. Inserting this into Eq. (13.221) and truncating the infinite series limit to order N , yields the following set of $N + 1$ simultaneous equations

$$\sum_{n=0}^N A_n \int_0^b I_m^*(w) I_n(w) w dw = \frac{a}{2} \int_0^b \delta(w - a) I_m^*(w) w dw, \quad m = 0, 1, \dots, N, \quad (13.230)$$

where $I_m^*(w)$ and $I_n(w)$ are given by Eqs. (13.223) and (13.224), respectively. Integrating over w and using the property of the Dirac delta function yields the same matrix equations as Eqs. (13.225)–(13.228) except that

$$\mathbf{b}(m+1) = \sum_{p=0}^P {}_m \mathbf{B}_p^*(kb) \left(\frac{a}{b}\right)^{2p}. \quad (13.231)$$

In the limiting case of a point source at the center of a circular baffle, we let $a \rightarrow 0$ so that

$$\mathbf{b}(m+1) = {}_m \mathbf{B}_0^*(kb). \quad (13.232)$$

Now that we have the surface pressure series coefficients A_n , we can derive some radiation characteristics for the disk in free space or open circular baffle or a point source in a circular baffle.

Far-field pressure

The far-field pressure distribution is given by the dipole boundary integral of Eq. (13.28), taking into account the surface pressure on both sides:

$$\tilde{p}(r, \theta) = \int_0^{2\pi} \int_0^b (\tilde{p}_+(w_0) - \tilde{p}_-(w_0)) \frac{\partial}{\partial z_0} g(r, \theta | w_0, \phi_0) \Big|_{z_0=0^+} w_0 dw_0 d\phi_0, \quad (13.233)$$

where the far-field Green's function in spherical-cylindrical coordinates given by Eq. (13.70) is used. Inserting Eqs. (13.70), (13.198), and (13.202) into Eq. (13.233) and

integrating over the surface, using Eqs. (76) and (96) from Appendix II [with $z = k\omega_0 \sin \theta$, $b = k \sin \theta$, and letting $\phi = \pi/2$ so that $\cos(\phi - \phi_0) = \sin \phi_0$], gives

$$\tilde{p}(r, \theta) = jka^2 \rho_0 \tilde{u}_0 \frac{e^{-jkr}}{2r} D(\theta), \quad (13.234)$$

where the directivity function $D(\theta)$ is given by

$$D(\theta) = kb \cos \theta \sum_{n=0}^N A_n \Gamma \left(n + \frac{5}{2} \right) \left(\frac{2}{kb \sin \theta} \right)^{n+\frac{3}{2}} J_{n+\frac{3}{2}}(kb \sin \theta). \quad (13.235)$$

The on-axis pressure is evaluated by setting $\theta = 0$ in Eq. (13.70) before inserting it into Eq. (13.233) and integrating over the surface to give

$$D(0) = kb \sum_{n=0}^N A_n, \quad (13.236)$$

so that the on-axis response can be written as

$$\tilde{p}(r, 0) = j\rho_0 f \tilde{U}_0 \frac{e^{-jkr}}{r} kb \sum_{n=0}^N A_n. \quad (13.237)$$

where $\tilde{U}_0 = \pi a^2 \tilde{u}_0$ is the total volume velocity. It is worth noting that in the un baffled case, where $b = a$, $D(0)$ is simply the normalized radiation impedance, that is $D(0) = (\mathbf{R}_s + jX_s)/(\rho_0 c)$ where \mathbf{R}_s and X_s are given by Eqs. (13.249) and (13.250), respectively. Using standard curve-fitting methods, the following asymptotic expression can be written as

$$D(0) \approx j0.66 \left(\frac{b}{a} - 0.3 \right) ka, \quad kb < 0.5. \quad (13.238)$$

The on-axis response for five values of b is shown in Fig. 13.22, calculated from the magnitude of $D(0)$.

We can see from Fig. 13.22 that, in the case of an un baffled piston ($b = a$) radiating from both sides, the on-axis sound pressure falls at 6 dB/octave for small values of ka owing to the decreasing path difference (as a proportion of wavelength λ) between the antiphase rear radiation and the front radiation, which it partially cancels. This is also true of the oscillating sphere (see Fig. 4.26), but the attenuation is not as great because of the longer path difference around the sphere.

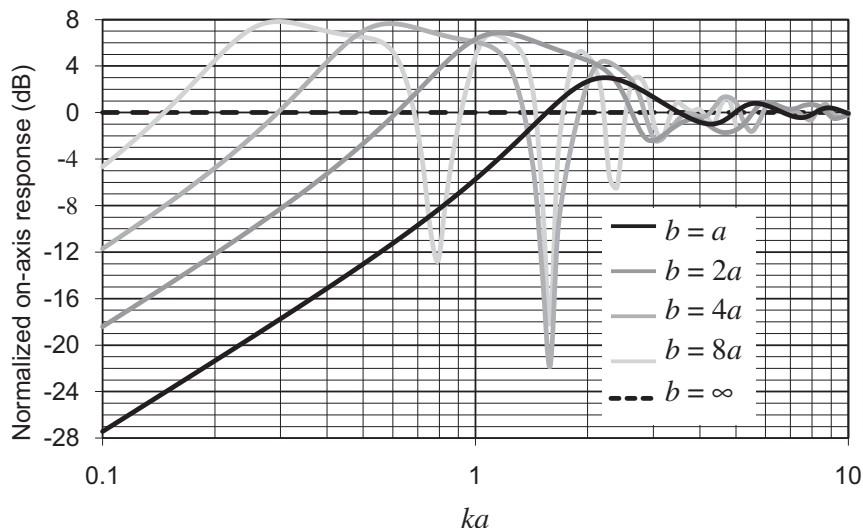


Figure 13.22 Plot of $20 \log_{10}(D(0))$ where $D(\theta)$ is the directivity function of a plane circular piston of radius a in a flat open circular baffle of radius b . When $b = a$ (solid black curve), there is no baffle and the piston is radiating from both sides in free space. When $b = \infty$ (dotted black curve), the piston is in an infinite baffle. The axial acceleration of the piston is constant. Frequency is plotted on a normalized scale, where $ka = 2\pi a/\lambda = 2\pi fa/c$.

At larger values of ka , the rear radiation moves in and out of phase with that from the front. However, the comb-filter effect is fairly “smeared,” the largest peak being 3 dB at $ka = \pi/\sqrt{2}$ (or $\lambda = 2\sqrt{2} a$), the reason being that rear radiation is due to the sum of many ring sources spread over the radius of the piston, each with a different path length to the front, so that at no particular frequency do they combine to produce a source that is either directly in phase or out of phase with that from the front. Unlike the oscillating sphere, the on-axis response does not roll-off at high frequencies, which is a property of planar sources, as already discussed in Section 12.8.

By contrast, when we include a circular baffle and increase its size, the actual radiating area decreases in proportion to the total so that it behaves more like a coherent point source at the center. Hence, when $b = 4a$, a deep null can be seen at $ka = \pi/2$ or $\lambda = 4a$, which is the distance from the center to the edge. Of course, a piston at the center of a circular baffle is the “worst case,” and it would be interesting to compare these results with those of an offset piston in a circular, rectangular, or elliptical baffle, for example, to “smear” the path difference effect.

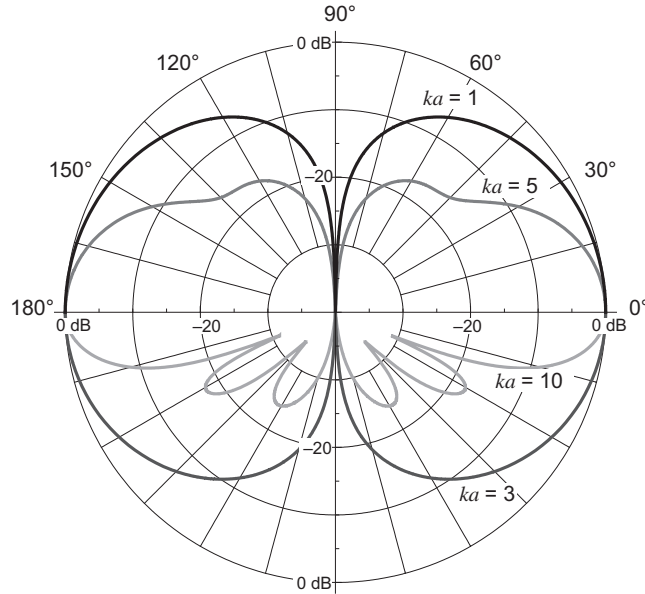


Figure 13.23 Far-field directivity patterns for a plane circular piston radiating from both sides into free space as a function of $ka = 2\pi a/\lambda = 2\pi fa/c$, where a is the radius of the piston.

The normalized directivity function $20 \log_{10}|D(\theta)/D(0)|$ for a piston in free space is plotted in Fig. 13.23 for four values of $ka = 2\pi a/\lambda$, that is, for four values of the ratio of the circumference of the disk to the wavelength. When the circumference of the piston ($2\pi a$) is less than one-half wavelength, that is, $ka < 0.5$, it behaves essentially like a dipole point source. In fact, to a first approximation, an unbaffled thin piston is simply a doublet because an axial movement in one direction compresses the air on one side of it and causes a rarefaction of the air on the other side. When ka becomes greater than 3, the piston is highly directional, like the piston in an infinite baffle. Also, the directivity function for a piston in a finite open baffle is plotted in Fig. 13.24 for four values of ka with $b = 2a$ and in Fig. 13.25 for four values of b .

Near-field pressure

The near-field pressure distribution is given by Eq. (13.28) taking into account the surface pressure on both sides:

$$\tilde{p}(r, \theta) = \int_0^{2\pi} \int_0^b \left(\tilde{p}_+(w_0) - \tilde{p}_-(w_0) \right) \frac{\partial}{\partial z_0} g(r, \theta | w_0, \phi_0) \Big|_{z_0=0^+} w_0 dw_0 d\phi_0, \quad (13.239)$$

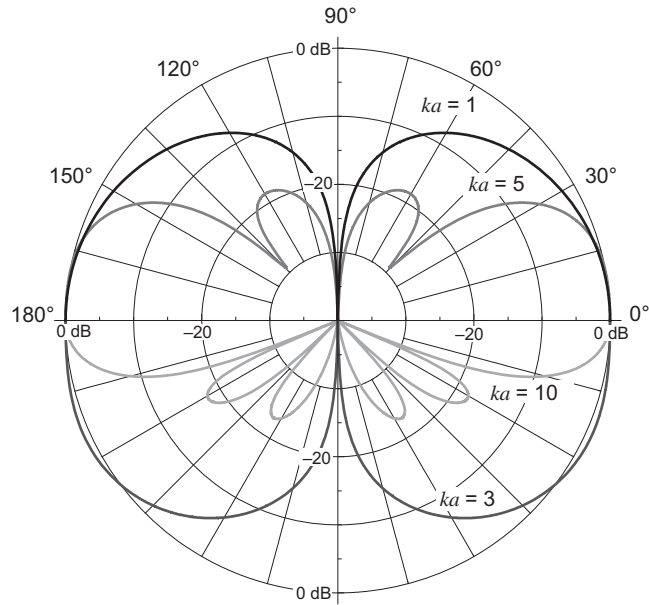


Figure 13.24 Far-field directivity patterns for a circular piston in a plane open circular baffle as a function of $ka = 2\pi a/\lambda = 2\pi fa/c$, where a is the radius of the piston and $b = 2a$ is the radius of the baffle.

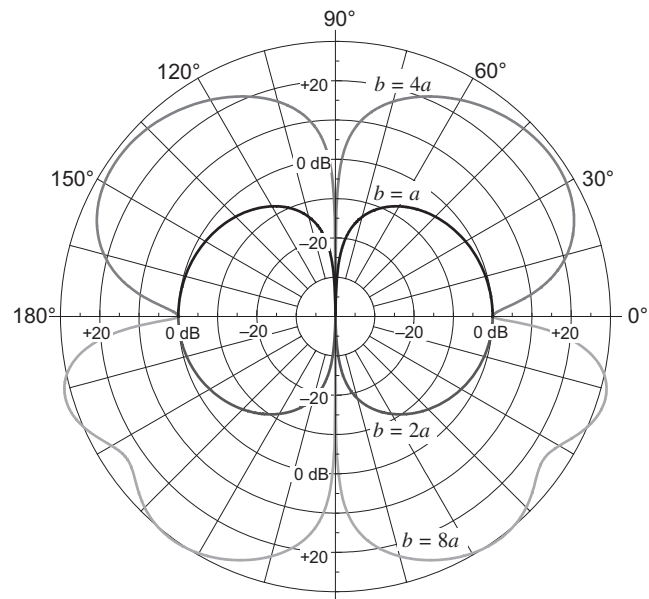


Figure 13.25 Far-field directivity patterns for a circular piston in a plane open circular baffle as a function of b at $ka = \pi/2$ or $\lambda = 4a$, where a is the radius of the piston and b is the radius of the baffle.

where the Green's function in spherical-cylindrical coordinates given by Eq. (13.68) is used. It has been shown [17] that inserting Eqs. (13.68), (13.198) and (13.202) into Eq. (13.239) and integrating over the surface gives

$$\begin{aligned} \tilde{p}(r, \theta) = & 2jkb\rho_0\tilde{c}u_0\frac{a^2}{b^2} \sum_{n=0}^N A_n \sum_{p=0}^P \frac{(-1)^p \Gamma\left(p + \frac{3}{2}\right) \Gamma\left(n + \frac{5}{2}\right) h_{2p+1}^{(2)}(kr) P_{2p+1}(\cos \theta)}{\Gamma\left(2p + \frac{3}{2}\right) \Gamma\left(p + n + \frac{5}{2}\right)} \\ & \times \left(\frac{kb}{2}\right)^{2p+2} {}_1F_2\left(p + 1; p + n + \frac{5}{2}, 2p + \frac{5}{2}; -\frac{k^2 b^2}{4}\right), \end{aligned} \quad (13.240)$$

which converges for $r > b$. For $r \leq b$, we derive a suitable expression from Eq. (13.204), which is weakly singular at $k_w = k$. However, we can remove this singularity as follows: Firstly, we substitute

$$k_w = k\sqrt{1 - t^2} \text{ for } k_w \leq k$$

and

$$k_w = k\sqrt{1 + t^2} \text{ for } k_w > k$$

in Eq. (13.204) to obtain

$$\tilde{p}(w, z) = k^2 a^2 \rho_0 \tilde{c} u_0 \sum_{n=0}^{\infty} A_n \Gamma\left(n + \frac{5}{2}\right) (I_{Fin} + I_{Inf}), \quad (13.241)$$

where

$$I_{Fin} = -\left(\frac{2}{kb}\right)^{n+\frac{1}{2}} \int_0^1 \left(\frac{1}{1-t^2}\right)^{\frac{n+\frac{3}{2}}{2}} J_{n+\frac{3}{2}}(kb\sqrt{1-t^2}) J_0(kw\sqrt{1-t^2}) e^{-jkzt} t dt, \quad (13.242)$$

$$I_{Inf} = -\left(\frac{2}{kb}\right)^{n+\frac{1}{2}} \int_0^{\infty} \left(\frac{1}{1+t^2}\right)^{\frac{n+\frac{3}{2}}{2}} J_{n+\frac{3}{2}}(kb\sqrt{1+t^2}) J_0(kw\sqrt{1+t^2}) e^{-kzt} t dt. \quad (13.243)$$

We then apply the expansion of Eq. (109) from Appendix II to give

$$I_{Fin} + I_{Inf} = - \sum_{p=0}^{\infty} \frac{(-1)^p}{p! \Gamma\left(n + p + \frac{5}{2}\right)} \left(\frac{kb}{2}\right)^{2p+1} {}_2F_1\left(-p, -n - p - \frac{3}{2}; 1; \frac{w^2}{b^2}\right) \\ \times \left(\int_0^1 (1-t^2)^p e^{-jkzt} dt + \int_0^{\infty} (1+t^2)^p e^{-kzt} dt \right), \quad (13.244)$$

which after integrating yields

$$I_{Fin} = \frac{\sqrt{\pi}}{2} \sum_{p=0}^{\infty} \frac{(-1)^p}{\Gamma\left(n + p + \frac{5}{2}\right)} \left(\frac{kb}{2}\right)^{2p+1} {}_2F_1\left(-p, -n - p - \frac{3}{2}; 1; \frac{w^2}{b^2}\right) \quad (13.245)$$

$$\times \left\{ \left(\frac{2}{kz}\right)^{p+\frac{1}{2}} \left(j^J_{p+\frac{3}{2}}(kz) + \mathbf{H}_{p+\frac{3}{2}}(kz) \right) - \frac{1}{\sqrt{\pi}(p+1)!} \right\},$$

$$I_{Inf} = \frac{\sqrt{\pi}}{2} \sum_{p=0}^{\infty} \frac{(-1)^p}{p! \Gamma\left(n + p + \frac{5}{2}\right)} \left(\frac{kb}{2}\right)^{2p+1} {}_2F_1\left(-p, -n - p - \frac{3}{2}; 1; \frac{w^2}{b^2}\right) \quad (13.246)$$

$$\times \left\{ \left(\frac{2}{kz}\right)^{p+\frac{1}{2}} \left(Y_{p+\frac{3}{2}}(kz) - \mathbf{H}_{p+\frac{3}{2}}(kz) \right) + \frac{1}{\sqrt{\pi}(p+1)!} \right\}.$$

Eq. (13.245) converges everywhere and is therefore suitable for $r < b$. Unfortunately, Eq. (13.246) only converges for $z^2 > w^2 + b^2$ and is therefore not suitable. However, Eq. (13.243) converges everywhere and can be calculated numerically without problem and is therefore suitable for $r < b$. The pressure field of a rigid piston in free space is plotted in Fig. 13.26 for three values of ka . At $ka = 6\pi$, the sound field of the un baffled piston shows similar characteristics to the baffled one, except that the radial pressure beyond its perimeter is zero, as with any planar dipole source. This suggests that, at high frequencies, objects on either side of the source have less effect on the sound field, except that the axial nulls are not as deep and the peaks are slightly higher. It can be shown that at low frequencies, where $ka < 1$, the on-axis pressure converges to the far-field approximation at increasingly greater distances due to the proximity effect (bass tip-up). The pressure field of a rigid piston in a circular baffle of radius $b = 2a$ is plotted in Fig. 13.27 for two values of ka .

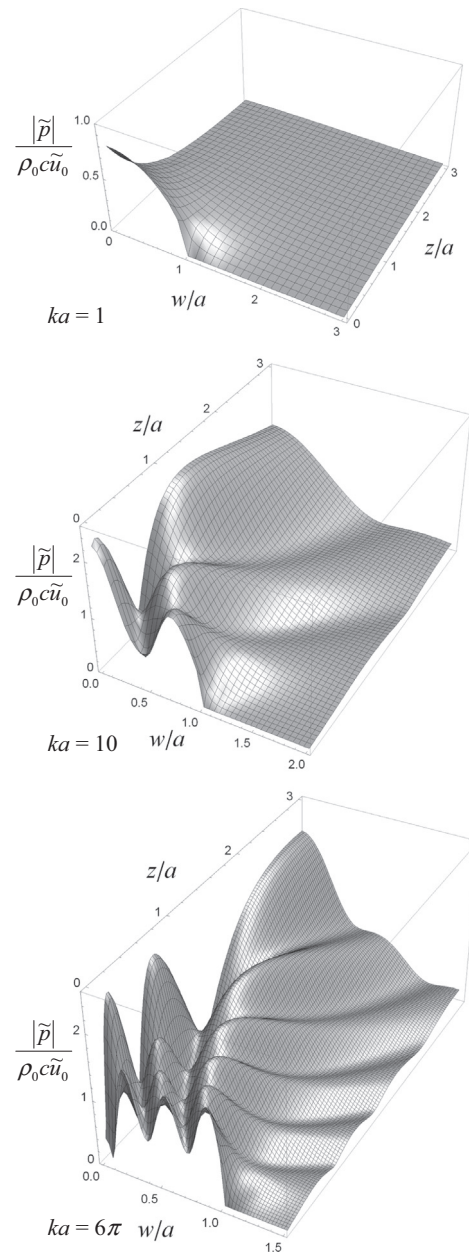


Figure 13.26 Normalized near-field pressure plots for a rigid circular piston in free space as a function of $ka = 2\pi a/\lambda = 2\pi fa/c$, where a is the radius of the piston. $|\tilde{p}|$ is the pressure magnitude, \tilde{u}_0 is the piston velocity, ρ_0 is the density of the acoustic medium, and c is the speed of sound in that medium.

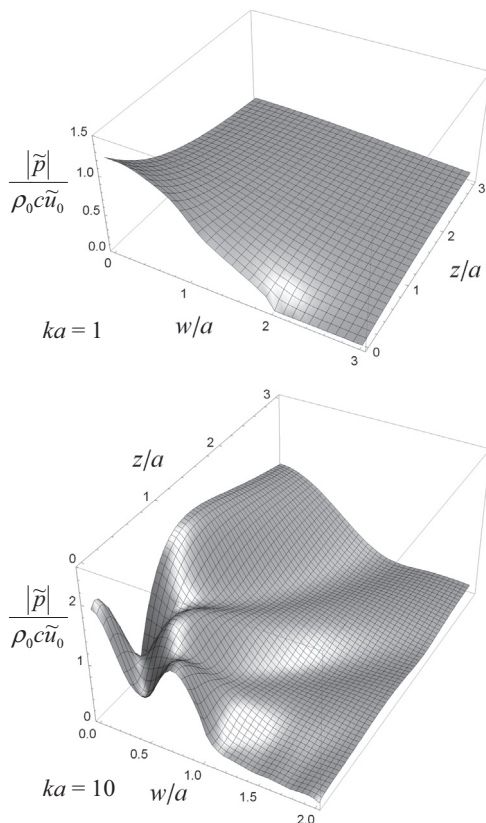


Figure 13.27 Normalized near-field pressure plots for a rigid circular piston in a finite open circular baffle of radius $b = 2a$ as a function $ka = 2\pi a/\lambda = 2\pi fa/c$, where a is the radius of the piston. $|\tilde{p}|$ is the pressure magnitude, \tilde{u}_0 is the piston velocity, ρ_0 is the density of the acoustic medium, and c is the speed of sound in that medium.

Radiation impedance of a piston in a circular baffle

The total radiation force is found by integrating the pressure from Eq. (13.202) over the surface of the disk on both sides to give

$$\begin{aligned}
 \tilde{F} &= \int_0^{2\pi} \int_0^a \left(\tilde{p}_+(w_0) - \tilde{p}_-(w_0) \right) w dw d\phi \\
 &= 2\pi a^2 \rho_0 \tilde{c} \tilde{u}_0 \sum_{n=0}^N A_n \left\{ 1 - \left(1 - \frac{a^2}{b^2} \right)^{n+\frac{3}{2}} \right\}.
 \end{aligned} \tag{13.247}$$

The specific radiation impedance Z_s is then given by

$$Z_s = \frac{\tilde{F}}{\tilde{U}_0} = \mathbf{R}_s + jX_s, \quad (13.248)$$

where $\tilde{U}_0 = \pi a^2 \tilde{u}_0$ is the total volume velocity and \mathbf{R}_s is the specific radiation resistance in $\text{N}\cdot\text{s}/\text{m}^3$ (rayl) given by

$$\mathbf{R}_s|_{b \neq a} = kb\rho_0c\Re\left(\sum_{n=0}^N A_n \left\{1 - \left(1 - \frac{a^2}{b^2}\right)^{n+\frac{3}{2}}\right\}\right) \quad (13.249)$$

$$\mathbf{R}_s|_{b=a} = ka\rho_0c\Re\left(\sum_{n=0}^N A_n\right) \approx \rho_0c \frac{8k^4 a^4}{27\pi^2}, \quad ka < 0.5,$$

where the bold \mathbf{R} indicates that the quantity varies with frequency and X_s is the specific radiation reactance in $\text{N}\cdot\text{s}/\text{m}^3$ (rayl) given by

$$X_s|_{b \neq a} = kb\rho_0c\Im\left(\sum_{n=0}^N A_n \left\{1 - \left(1 - \frac{a^2}{b^2}\right)^{n+\frac{3}{2}}\right\}\right) \quad (13.250)$$

$$X_s|_{b=a} = ka\rho_0c\Im\left(\sum_{n=0}^N A_n\right) \approx \rho_0c \frac{4ka}{3\pi}, \quad ka < 0.5.$$

Plots of the real and imaginary parts of

$$\frac{Z_s}{\rho_0c} = \frac{\mathbf{R}_s + jX_s}{\rho_0c} \quad (13.251)$$

are shown in Fig. 13.28 as a function of ka .

The data of Fig. 13.28 are used in dealing with impedance analogies. The complex admittance can be obtained by taking the reciprocal of the complex impedance.

The specific admittance is given by

$$Y_s = \mathbf{G}_s + jB_s = \frac{\mathbf{R}_s}{\mathbf{R}_s^2 + X_s^2} - j \frac{X_s}{\mathbf{R}_s^2 + X_s^2}$$

$$Y_s|_{b=a} = (\mathbf{G}_s + jB_s)|_{b=a} \approx \frac{1}{\rho_0c} \left(\frac{k^2 a^2}{6} - j \frac{3\pi}{4ka} \right), \quad ka < 0.5.$$

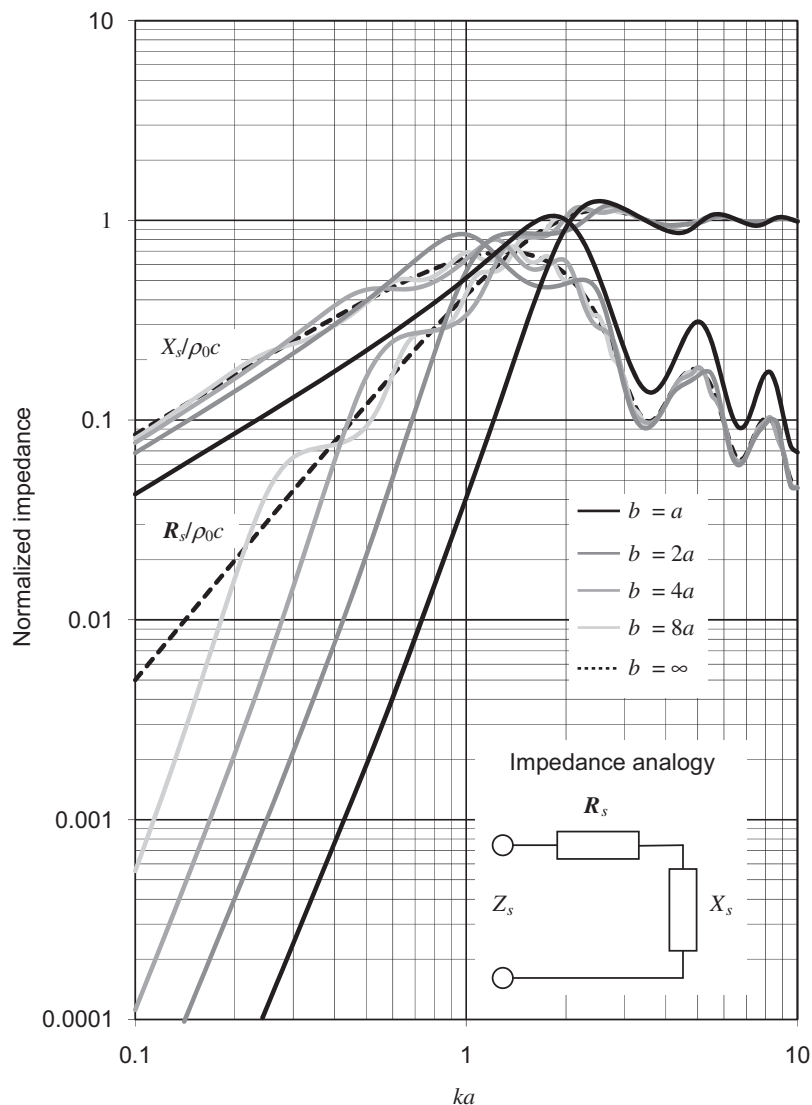


Figure 13.28 Real and imaginary parts of the normalized specific radiation impedance Z_s/ρ_0c of the air load on one side of a plane circular piston of radius a in a flat circular open baffle of radius b . When $b = a$ (solid black curve), there is no baffle and the piston is radiating from both sides into free space. When $b = \infty$ (dotted black curve), the piston is in an infinite baffle. Frequency is plotted on a normalized scale, where $ka = 2\pi a/\lambda = 2\pi fa/c$.



13.11 RADIATION FROM A RIGID CIRCULAR PISTON IN A FINITE CIRCULAR CLOSED BAFFLE [32] (ONE-SIDED RADIATOR)

The configuration is the same as that shown in Fig. 13.21 for a piston in an open baffle except that the velocity on the rear of the piston is zero. We can achieve this boundary condition by superposition of fields (or Gutin concept) whereby we combine the field of a piston in an open finite baffle with that of a piston in an infinite baffle. The former has negative velocity $-\tilde{u}_0$ on its rear surface, whereas the latter, if treated as a “breathing” disk in free space, has positive velocity \tilde{u}_0 on its rear surface. Hence, when the two fields are combined, their rear surface velocities cancel to produce a zero velocity boundary condition as illustrated in Fig. 13.29. However, if we wish the front velocity to be \tilde{u}_0 and not $2\tilde{u}_0$, we must halve the result.

Although the piston and baffle are both infinitesimally thin in this model, it can be used to model a finite cylindrical enclosure with reasonable accuracy. In fact, the radiation characteristics of the single-sided piston without a baffle ($b = a$) are remarkably similar to those of a piston at the end of an infinite tube [33]. In the case of a finite cylinder, there will be secondary reflections from the far end, but they will be considerably weaker than the primary ones from the perimeter of the baffle.

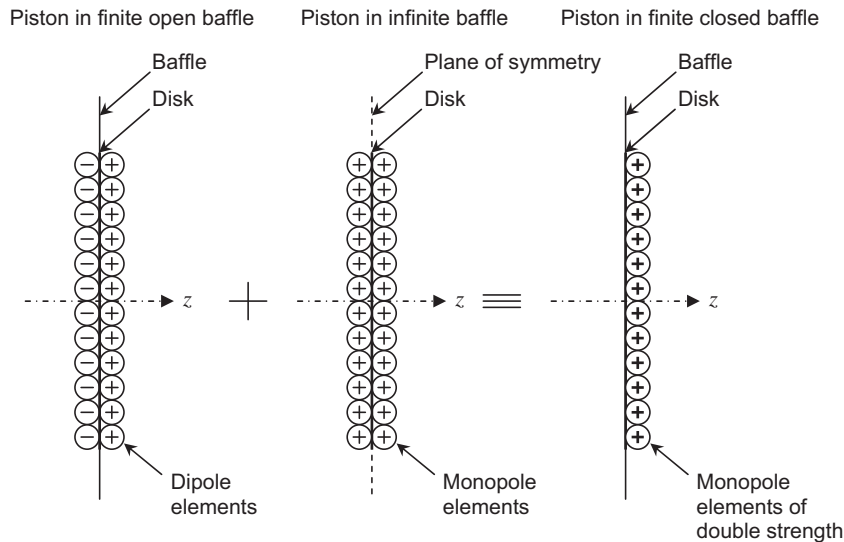


Figure 13.29 Gutin concept: By superposition of fields, a one-sided piston in a finite closed baffle is equivalent to the sum of a double-sided dipole piston in a finite open baffle and a monopole piston in an infinite baffle. Also see Fig.13.4 for the monopole piston model.

Far-field pressure

The directivity function $D(\theta)$ is half the sum of that from Eq. (13.102) for a piston in an infinite baffle and that from Eq. (13.235) for a piston in a finite open baffle:

$$D(\theta) = \frac{J_1(ka \sin \theta)}{ka \sin \theta} + \frac{kb}{2} \cos \theta \sum_{n=0}^N A_n \Gamma\left(n + \frac{5}{2}\right) \left(\frac{2}{kb \sin \theta}\right)^{n+\frac{3}{2}} J_{n+\frac{3}{2}}(kb \sin \theta). \quad (13.252)$$

Similarly, the on-axis pressure is obtained from Eqs. (13.103) and (13.236) to give

$$D(0) = \frac{1}{2} \left(1 + kb \sum_{n=0}^N A_n \right). \quad (13.253)$$

The on-axis response for five values of b is shown in Fig. 13.30, calculated from the magnitude of $D(0)$. The normalized directivity function $20 \log_{10}|D(\theta)/D(0)|$ for a one-sided piston in free space is plotted in Fig. 13.31 for four values of $ka = 2\pi a/\lambda$, that is, for four values of the ratio of the circumference of the disk to the wavelength. Also, the directivity function for a piston in a finite closed baffle is plotted in Fig. 13.32 for four values of ka with $b = 2a$ and in Fig. 13.33 for four values of b .

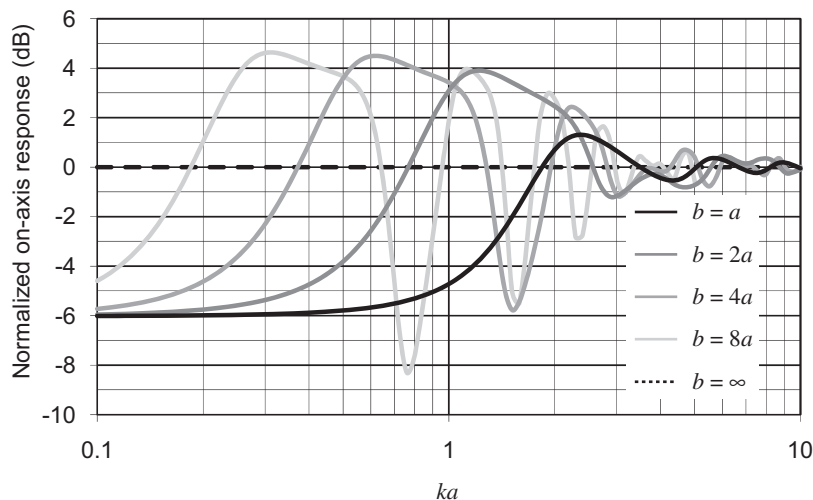


Figure 13.30 Plot of $20 \log_{10}(D(0))$ where $D(\theta)$ is the directivity function of a plane circular piston of radius a in a plane closed circular baffle of radius b . When $b = a$ (solid black curve), there is no baffle and the piston is radiating from one side only in free space. When $b = \infty$ (dotted black curve), the piston is in an infinite baffle. The axial acceleration of the piston is constant. Frequency is plotted on a normalized scale, where $ka = 2\pi a/\lambda = 2\pi fa/c$.

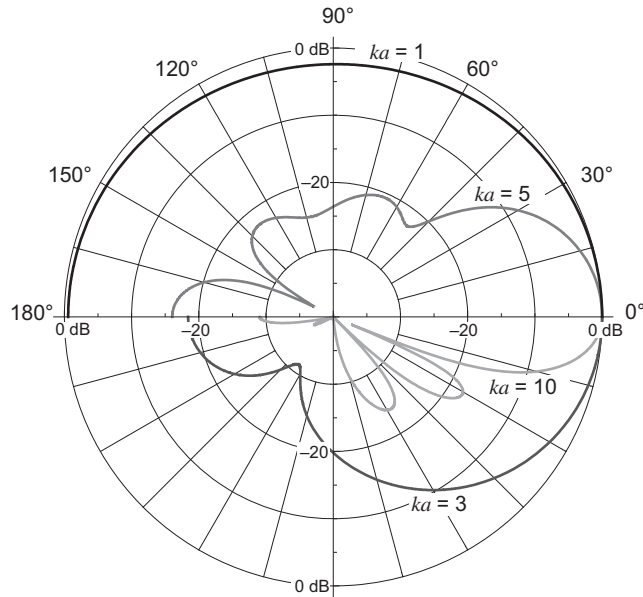


Figure 13.31 Far-field directivity patterns for a plane circular piston radiating from one side only into free space as a function of $ka = 2\pi a/\lambda = 2\pi fa/c$, where a is the radius of the piston.

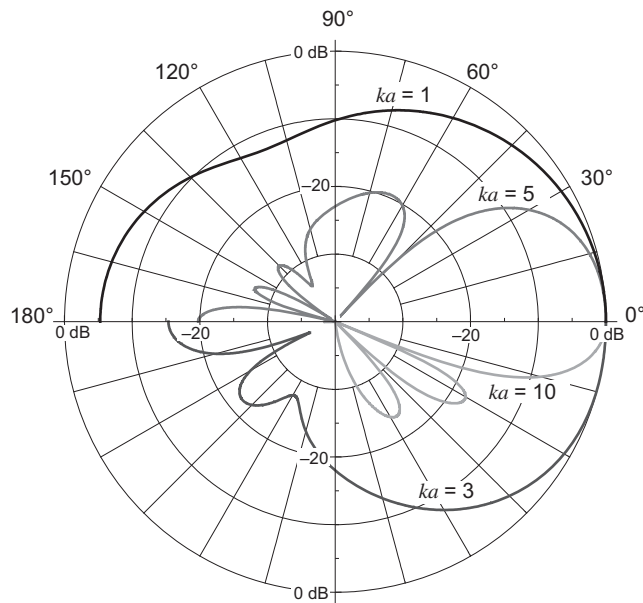


Fig. 13.32 Far-field directivity patterns for a circular piston in a plane closed circular baffle as a function of $ka = 2\pi a/\lambda = 2\pi fa/c$, where a is the radius of the piston and $b = 2a$ is the radius of the baffle.

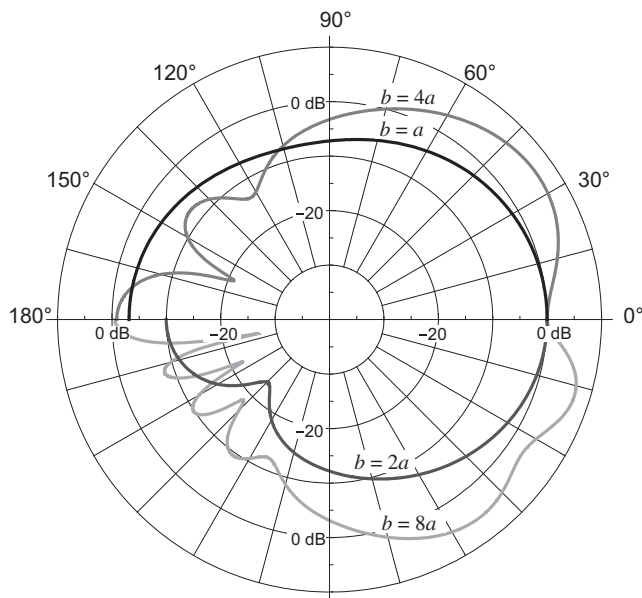


Fig. 13.33 Far-field directivity patterns for a circular piston in a plane closed circular baffle as a function of b at $ka = \pi/2$ or $\lambda = 4a$, where a is the radius of the piston and b is the radius of the baffle.

Near-field pressure

The near-field pressure is simply the average of the pressures from Eqs. (13.106) and (13.240) for $r > a$ or Eqs. (13.107) and (13.241) for $r \leq a$. The pressure field for a one-sided piston in free space is plotted in Fig. 13.34 for three values of ka . The pressure response on the shadow side of the one-sided radiator is interesting not only for what it reveals about the diffraction effects around an infinitesimally thin edge but also for the fact that this pressure field is actually the difference between the baffled (monopole) and unbaffled (dipole) responses of the rigid piston. In particular, the differences persist into the high-frequency range. The pressure field for a rigid circular piston in a closed circular baffle of radius $b = 2a$ is plotted in Fig. 13.35 for two values of ka .

Radiation impedance

The same principle can also be applied to the radiation impedance, which is proportional to the sum of the surface pressures of a piston in a finite baffle and an infinite baffle. Hence the real part can be obtained from Eqs. (13.117) and (13.249) as follows:

$$\mathbf{R}_s|_{b \neq a} = \frac{\rho_0 c}{2} \left\{ 1 - \frac{J_1(2ka)}{ka} + kb \Re \left(\sum_{n=0}^N A_n \left\{ 1 - \left(1 - \frac{a^2}{b^2} \right)^{n+\frac{3}{2}} \right\} \right) \right\} \quad (13.254)$$

$$\mathbf{R}_s|_{b=a} = \frac{\rho_0 c}{2} \left\{ 1 - \frac{J_1(2ka)}{ka} + ka \Re \left(\sum_{n=0}^N A_n \right) \right\} \approx \rho_0 c \frac{k^2 a^2}{4}, \quad ka < 0.5,$$

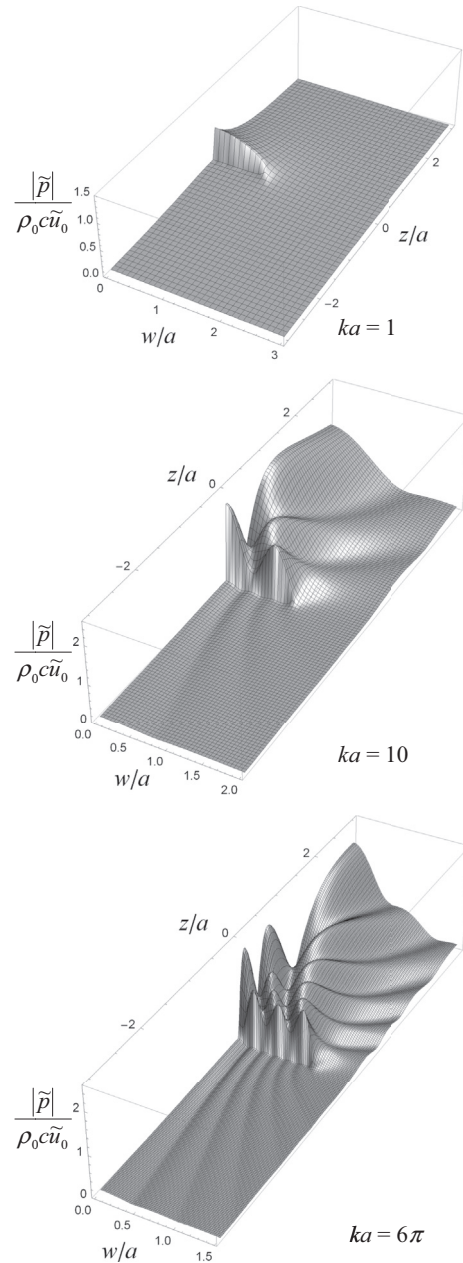


Figure 13.34 Normalized near-field pressure plots for a rigid circular piston radiating from one side only into free space as a function of $ka = 2\pi a/\lambda = 2\pi fa/c$, where a is the radius of the piston. $|\tilde{p}|$ is the pressure magnitude, \tilde{u}_0 is the piston velocity, ρ_0 is the density of the acoustic medium, and c is the speed of sound in that medium.

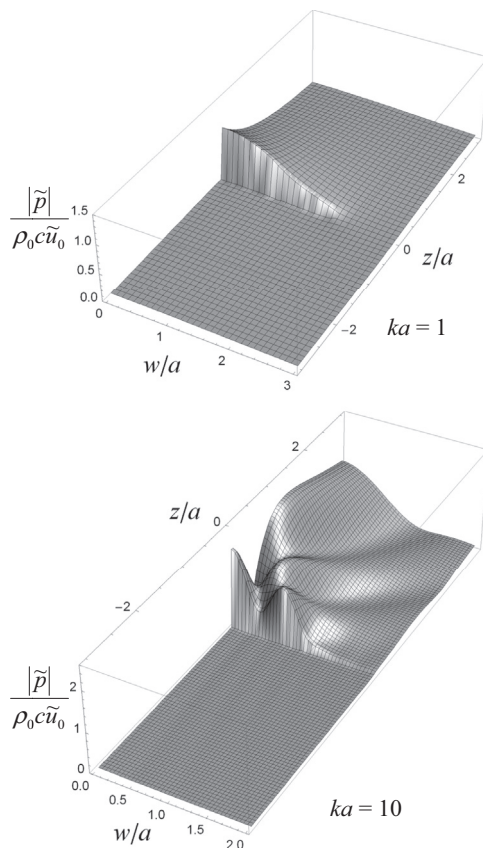


Figure 13.35 Normalized near-field pressure plots for a rigid circular piston in a closed circular baffle of radius $b = 2a$ as a function of $ka = 2\pi a/\lambda = 2\pi fa/c$, where a is the radius of the piston. $|\tilde{p}|$ is the pressure magnitude, \tilde{u}_0 is the piston velocity, ρ_0 is the density of the acoustic medium, and c is the speed of sound in that medium.

Likewise, the imaginary part can be obtained from Eqs. (13.118) and (13.250) as follows:

$$X_s|_{b \neq a} = \frac{\rho_0 c}{2} \left\{ \frac{\mathbf{H}_1(2ka)}{ka} + kb \Im \left(\sum_{n=0}^N A_n \left\{ 1 - \left(1 - \frac{a^2}{b^2} \right)^{n+\frac{3}{2}} \right\} \right) \right\} \quad (13.255)$$

$$X_s|_{b=a} = \frac{\rho_0 c}{2} \left\{ \frac{\mathbf{H}_1(2ka)}{ka} + ka \Im \left(\sum_{n=0}^N A_n \right) \right\} \approx \rho_0 c \frac{2ka}{\pi}, \quad ka < 0.5.$$

Plots of the real and imaginary parts of

$$\frac{Z_s}{\rho_0 c} = \frac{R_s + jX_s}{\rho_0 c} \quad (13.256)$$

are shown in Fig. 13.36 as a function of ka .

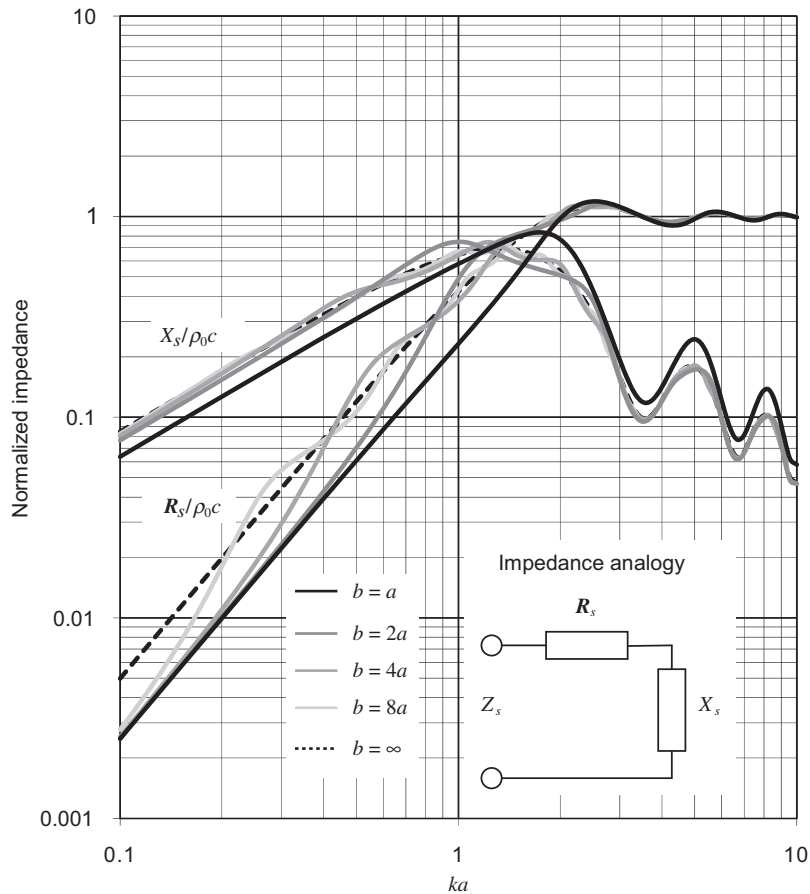


Figure 13.36 Real and imaginary parts of the normalized specific radiation impedance $Z_s/\rho_0 c$ of the air load on one side of a plane circular piston of radius a in a flat circular closed baffle of radius b . When $b = a$ (solid black curve), there is no baffle and the piston is radiating from one side only into free space. When $b = \infty$ (dotted black curve), the piston is in an infinite baffle. Frequency is plotted on a normalized scale, where $ka = 2\pi a/\lambda = 2\pi fa/c$.

The specific admittance is given by

$$Y_s = \mathbf{G}_s + jB_s = \frac{\mathbf{R}_s}{\mathbf{R}_s^2 + X_s^2} - j \frac{X_s}{\mathbf{R}_s^2 + X_s^2}$$

$$Y_s|_{b=a} = (\mathbf{G}_s + jB_s)|_{b=a} \approx \frac{1}{\rho_0 c} \left(\frac{\pi^2}{16} - j \frac{\pi}{2ka} \right), \quad ka < 0.5.$$



13.12 THE BABINET–BOUWKAMP PRINCIPLE

Kirchhoff theory

In its original form, Babinet's principle [34] simply states that the diffraction pattern resulting from the transmission of a plane wave through an aperture in an infinite screen is equivalent to that produced by the scattering of the same incident wave by the complementary disk. In the Kirchhoff theory of diffraction [35], it is assumed that the screen and complementary disk are either both rigid or both resilient, in which case the field scattered by an aperture in a rigid screen or complementary rigid disk can be represented by radiation from a rigid piston in an infinite baffle. Similarly, the field scattered by an aperture in a resilient screen or complementary resilient disk can be represented by radiation from a resilient disk in free space. If this were true, it would make life much simpler as everything could be calculated from closed-form solutions. The problem is that the former assumes that the velocity of the scattered wave at the aperture or complementary rigid disk is the same as that of the incident wave, as if it were unaffected by the presence of the scattering object. Similarly, the latter assumes that the pressure of the scattered wave at the aperture or complementary resilient disk is the same as that of the incident wave. At best, this is an approximation [22] that can only be used when the wavelength is much smaller than the aperture or disk.

Bouwkamp theory

Bouwkamp's modified version [20] of Babinet's principle states that the diffraction pattern resulting from the transmission of a plane wave through an aperture in an infinite *rigid* screen (see Fig. 13.37c) is equivalent to that produced by the scattering of the same incident wave by the complementary *resilient* disk (see Fig. 13.37f). Also, the flip side of this is that the diffraction pattern resulting from the transmission of a plane wave through an aperture in an infinite *resilient* screen (see Fig. 13.38c) is equivalent to that produced by the scattering of the same incident wave by the complementary *rigid* disk (see Fig. 13.38f). Furthermore, Bouwkamp states that:

- The sound field scattered by a *rigid* disk is equivalent to that produced if the disk itself were radiating in *free space*, provided that the *velocity* at the surface of the disk is equal to that of the incident plane wave in the absence of any scattering obstacle.

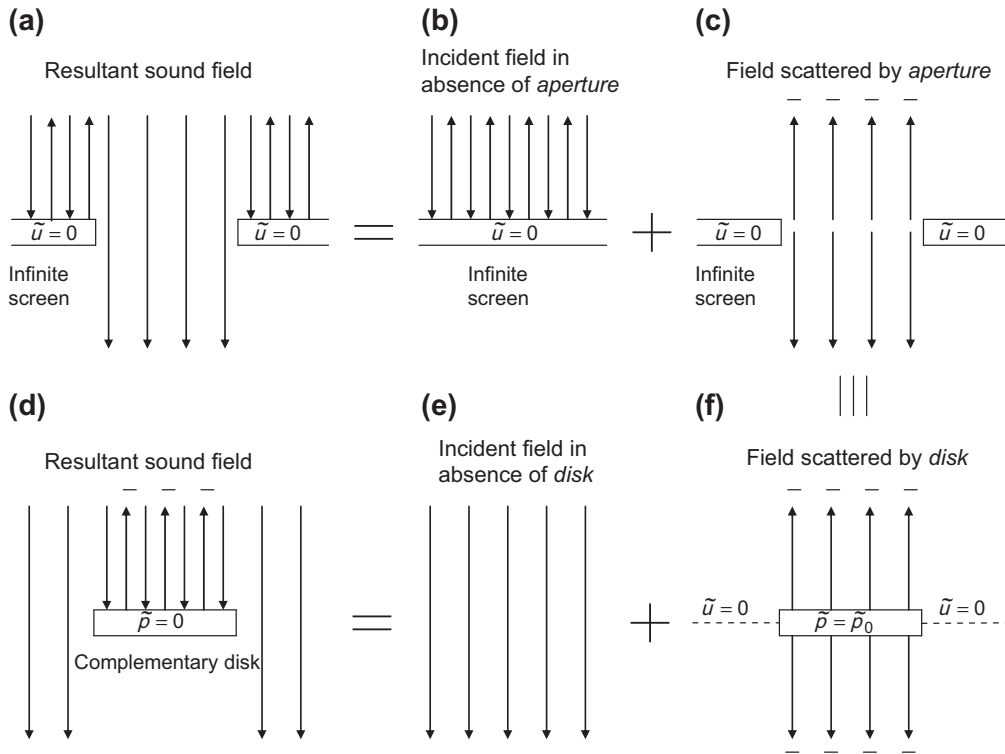


Figure 13.37 The Babinet–Bouwkamp principle for a circular aperture in an infinite *rigid* screen.

- The sound field scattered by a *resilient* disk is equivalent to that produced if the disk itself were radiating in an *infinite rigid baffle*, provided that the *pressure* at the surface of the disk is equal to that of the incident plane wave in the absence of any scattering obstacle.

The general principle is illustrated in [Figs. 13.37 and 13.38](#), but before we discuss apertures, we will consider the scattering from plane objects.

Reflection from plane rigid objects [31]

We have already discussed the radiation of sound from moving surfaces using the boundary integral method. It often happens in acoustics that once you have found a solution for one problem, you get another for free. This is certainly the case with reflection from plane objects, and here it will be shown how. Imagine a plane wave being

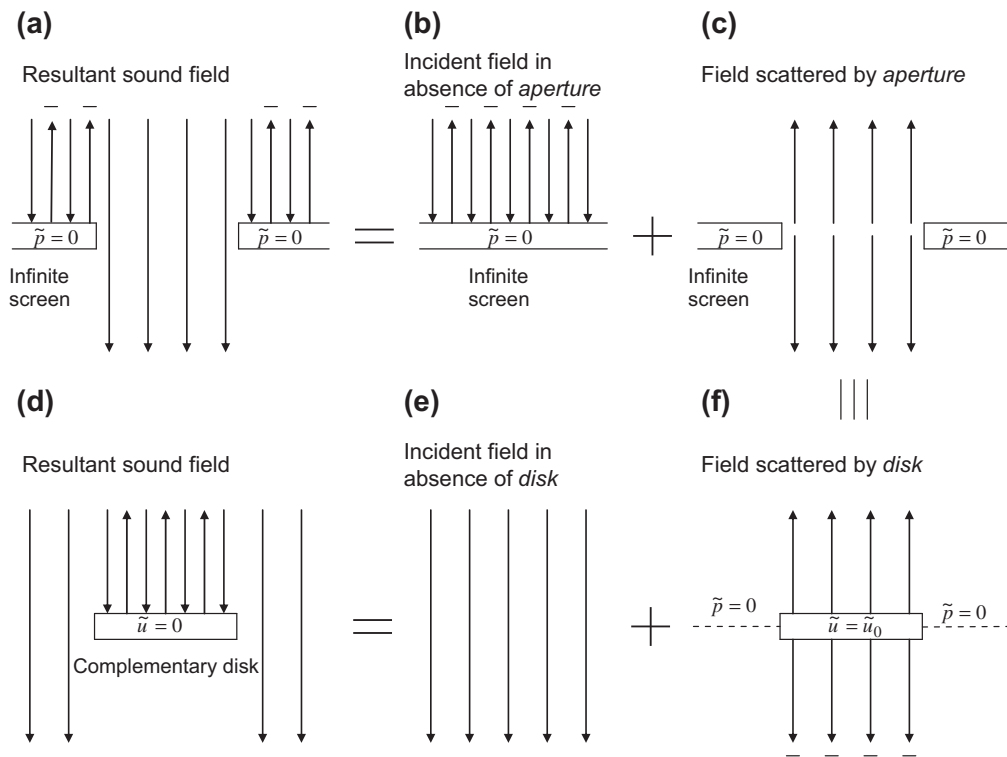


Figure 13.38 The Babinet–Bouwkamp principle for a circular aperture in an infinite *resilient* screen.

reflected from an arbitrary rigid surface. At the surface, the normal velocity is zero. Now we let the resulting pressure field $\tilde{p}(\mathbf{r})$ comprise two components as follows:

$$\tilde{p}(\mathbf{r}) = \tilde{p}_I(\mathbf{r}) + \tilde{p}_S(\mathbf{r}) \quad (13.257)$$

where $\tilde{p}_I(\mathbf{r})$ is the incident wave in the absence of any obstacles and $\tilde{p}_S(\mathbf{r})$ is the scattered wave. To satisfy the boundary condition of zero normal velocity at the surface, the normal velocity of the surface producing the scattered wave must be equal and opposite to the component of the velocity of the incident wave that is normal to the surface. This is easiest to illustrate with a planar obstacle such as a circular disk in free space, as shown in Fig. 13.8 except that in this case it is perfectly rigid. Let $\tilde{p}_{ID}(z)$ be a simple plane incident wave traveling along the disk's axis of symmetry, which in this case is defined as the z -axis, and let the disk be located at $z = 0$. At the disk, the velocity and hence also the gradient of the resultant field $\tilde{p}_D(z)$ are both zero:

$$\tilde{u}_0 = -jk\rho_0c \frac{\partial \tilde{p}_D(w, z)}{\partial z} \Big|_{z=0} = 0, \quad 0 \leq w \leq a, \quad (13.258)$$

where w is the radial ordinate and a is the radius of the disk. Also, from Eq. (13.257) and to preserve continuity, the resultant pressure gradient is the sum of the incident and scattered pressure gradients:

$$\frac{\partial \tilde{p}_D(w, z)|_{z=0}}{\partial z} = \frac{\partial \tilde{p}_{ID}(w, z)|_{z=0}}{\partial z} + \frac{\partial \tilde{p}_{SD}(w, z)|_{z=0}}{\partial z} = 0, \quad 0 \leq w \leq a. \quad (13.259)$$

Hence, the velocity \tilde{u}_0 of the disk is equal and opposite to the velocity \tilde{u}_{ID} of the incident wave in the absence of any scattering obstacles:

$$\tilde{u}_0 = -jk\rho_0 c \frac{\partial \tilde{p}_{SD}(w, z)|_{z=0}}{\partial z} = jk\rho_0 c \frac{\partial \tilde{p}_{ID}(w, z)|_{z=0}}{\partial z} = -\tilde{u}_{ID}, \quad 0 \leq w \leq a. \quad (13.260)$$

Therefore, the scattered field $\tilde{p}_{SD}(w, z)$ is that which would be produced if the disk were oscillating back and forth with the same velocity as the incident wave, but with opposite phase, and the resultant field $\tilde{p}_D(w, z)$ is the sum of the incident and scattered fields:

$$\tilde{p}_D(w, z) = \tilde{p}_{ID}(w, z) + \tilde{p}_{SD}(w, z), \quad (13.261)$$

as expressed in Fig. 13.38d–f. However, we have to ask whether scattered field $\tilde{p}_{SD}(w, z)$ is the same as that of a disk in free space or one in an infinite baffle. To answer that, we have to consider another boundary condition, which lies in the plane of the disk beyond its perimeter. We can already assume that the field on one side of this plane will be the symmetrical negative of that on the other. This can be explained by the fact that on the “bright” side (facing the incident wave), the radiated sound represents the reflected sound, whereas on the “dark” side, it is of opposite phase and therefore cancels the incident wave that would otherwise be present in the absence of the disk. However, in a baffle, these equal and opposite pressure values on either side of the baffle would produce a discontinuous field when added to the original incident wave. Therefore, the disk must behave as though it is oscillating in free space, thus producing a continuous field with zero pressure in the plane beyond its perimeter as shown in Fig. 13.38f. Hence, the resultant pressure in that region is simply that of the incident wave in the absence of any obstacles. The scattered field $\tilde{p}_{SD}(w, z)$ is that of a rigid disk oscillating in free space, which has already been evaluated in Section 13.10, using the dipole part of the Kirchhoff–Helmholtz boundary integral.

Reflection from plane resilient objects

In the case of a resilient disk in the presence of an incident plane wave traveling toward it along its axis of symmetry, the boundary condition at its surface is that of zero pressure:

$$\tilde{p}_D(w, z)|_{z=0} = \tilde{p}_{ID}(w, z)|_{z=0} + \tilde{p}_{SD}(w, z)|_{z=0} = 0, \quad 0 \leq w \leq a. \quad (13.262)$$

Hence, the pressure of the scattered field at the surface must be equal and opposite to the pressure of the incident wave in the absence of any scattering obstacles:

$$\tilde{p}_0 = \tilde{p}_{SD}(w, z)|_{z=0} = -\tilde{p}_{ID}(w, z)|_{z=0}, \quad 0 \leq w \leq a. \quad (13.263)$$

Therefore, the scattered field $\tilde{p}_{SD}(w, z)$ is that which would be produced if the disk were in motion with the same pressure as the incident wave, but opposite phase, and the resultant field $\tilde{p}_D(w, z)$ is the sum of the incident and scattered fields:

$$\tilde{p}_D(w, z) = \tilde{p}_{ID}(w, z) + \tilde{p}_{SD}(w, z), \quad (13.264)$$

as expressed in Fig. 13.37d–f. Furthermore, the scattered fields on each side of the disk are symmetrical and both of opposite polarity to the incident wave. This has the effect of creating a shadow on the “dark” side and reversing the phase of the reflected wave on the “bright” side because of the boundary condition of zero pressure, as opposed to zero velocity. If the boundary condition in the plane beyond the perimeter of the disk were one of zero pressure, the velocities on each side would be equal and opposite thus adding to and subtracting from the velocity of the incident wave on consecutive sides. This would in turn lead to a discontinuity in the velocity distribution of the resultant field at the plane. Hence, the scattered field is that of a resilient disk in an infinite baffle with symmetrical fields on each side, or a “breathing” resilient disk, which we have already evaluated in Section 13.9, using the monopole part of the Kirchhoff–Helmholtz boundary integral.

The Babinet–Bouwkamp principle for diffraction through a circular aperture in a rigid screen

Essentially, the boundary conditions for a circular aperture in an infinite rigid screen are the same as those for the complementary rigid disk in free space above and Fig. 13.38d, except that they are interchanged as shown in Fig. 13.37a. Hence, the resultant velocity is zero at the screen, which is the scattering obstacle, and the pressure in the aperture is the same as that of the incident wave in the absence of any scattering obstacles. However, although the rigid disk itself was treated as the source of the scattered wave, it is not so convenient to treat the infinite rigid screen as such. Instead, the aperture is treated as the source whereby the pressure is uniform everywhere within it and the aperture acts as a pressure source, namely a resilient disk in an infinite baffle, which we have already evaluated in Section 13.9, using the monopole part of the Kirchhoff–Helmholtz boundary integral, and satisfies the boundary condition of zero velocity on the screen. To calculate the resultant field on *both* sides of the screen, we simply add the scattered field to the incident field in the absence of an aperture, i.e., the incident plane wave plus its reflection from a continuous infinite rigid screen plus the radiation from the resilient disk. This is illustrated in Fig. 13.37a–c. For clarity, the diagram portrays the scattering

of a sound wave at some very high frequency where there is minimal diffraction. However, the principle applies at all frequencies. In general, for diffraction through a circular aperture in a rigid screen,

$$\tilde{p}_{IH}(z) = \begin{cases} \tilde{p}_0(e^{jkz} + e^{-jkz}), & \text{bright side of rigid screen} \\ 0, & \text{dark side of rigid screen} \\ \tilde{p}_0 e^{jkz}, & \text{without disk(or screen)} \end{cases} \quad (13.265)$$

and

$$\tilde{p}_{SH}(z) = \begin{cases} \tilde{p}_0, & z = 0+ \\ -\tilde{p}_0, & z = 0- . \end{cases} \quad (13.266)$$

These expressions are plotted in Fig. 13.39 for $ka = 1, 5,$ and 10 .

The Babinet–Bouwkamp principle for diffraction through a circular aperture in a resilient screen

Here we interchange the boundary conditions for a resilient disk in free space, described above. Hence, the resultant pressure is zero at the screen, which is the scattering obstacle, and the velocity in the aperture is the same as that of the incident wave in the absence of any scattering obstacles. The aperture is treated as the source, namely a rigid disk in free space, which we have already evaluated in Section 13.10, using the dipole part of the Kirchhoff–Helmholtz boundary integral, and satisfies the boundary condition of zero pressure on the screen. To calculate the resultant field on *both* sides of the screen, we simply add the scattered field to the incident field in the absence of an aperture, i.e., the incident plane wave plus its reflection from a continuous infinite resilient screen plus the radiation from the rigid disk. This is illustrated in Fig. 13.38a–c. For clarity, the diagram portrays the scattering of a sound wave at some very high frequency where there is minimal diffraction. However, the principle applies at all frequencies. In general, for diffraction through a circular aperture in a resilient screen,

$$\tilde{p}_{IH}(z) = \begin{cases} \tilde{p}_0(e^{jkz} - e^{-jkz}), & \text{bright side of resilient screen} \\ 0, & \text{dark side of resilient screen} \\ \tilde{p}_0 e^{jkz}, & \text{without disk(or screen)} \end{cases} \quad (13.267)$$

and

$$-jk\rho_0c \frac{\partial \tilde{p}_{SH}(z)}{\partial z} \Big|_{z=0} = \tilde{u}_0. \quad (13.268)$$

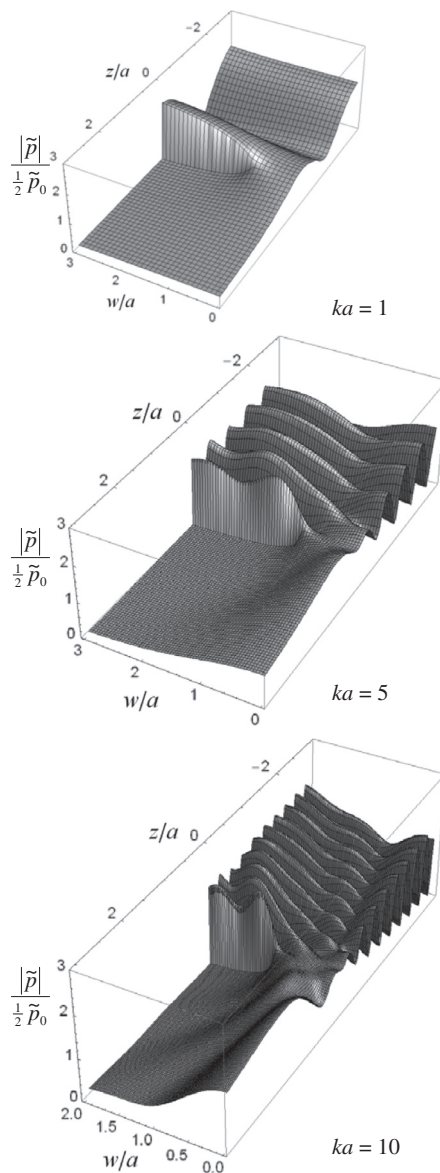


Figure 13.39 Normalized plots of pressure field due to a plane wave diffracted through a circular hole in an infinite rigid screen as a function of $ka = 2\pi a/\lambda = 2\pi fa/c$, where a is the radius of the hole. $|\tilde{p}|$ is the pressure magnitude, \tilde{p}_0 is the incident pressure at the hole in the absence of a screen, ρ is the density of the acoustic medium, and c is the speed of sound in that medium.

PART XXXVII: RADIATION THEOREMS, RADIATION IN RECTANGULAR-SPHERICAL COORDINATES, MUTUAL IMPEDANCE

13.13 THE BOUWKAMP IMPEDANCE THEOREM [36]

To find the radiation impedance of a piston in an infinite baffle, we used an expression for the near-field pressure and integrated the pressure over the surface of the piston to find the total force. However, the far-field pressure is generally given by a much simpler expression. According to Bouwkamp's impedance theorem, if the acoustic medium is loss free, we can obtain the radiation resistance of a piston, or combination of pistons, of any shape, vibrating in an infinite baffle or free space (assuming antisymmetry) as follows: We integrate the square of the far-field pressure over a hemispherical surface, while letting the radius tend to infinity, and then divide the result by the specific impedance of free space to obtain the total radiated power. We then obtain the acoustic radiation resistance by dividing the power by the square of the volume velocity of the piston(s). Furthermore, we can obtain the radiation reactance by integrating the square of the far-field pressure over certain complex values of the spherical inclination angle θ . In general, the far-field pressure is given in spherical coordinates (r, θ, ϕ) by

$$\tilde{p}(r, \theta, \phi) = \frac{jk\rho_0c\tilde{U}_0}{2\pi r}D(\theta, \phi), \quad (13.269)$$

although, in the case of an axisymmetric source such as the circular piston, there is no ϕ dependency. The total radiated power W is given by

$$W = \left| \frac{\tilde{U}_0}{\sqrt{2}} \right|^2 \mathbf{R}_{AR} = \frac{1}{\rho_0c} \int_0^{2\pi} \int_0^{\frac{\pi}{2}} \left| \frac{\tilde{p}(r, \theta, \phi)}{\sqrt{2}} \right|^2 r^2 \sin \theta \, d\theta \, d\phi \Big|_{r \rightarrow \infty}, \quad (13.270)$$

where \mathbf{R}_{AR} is the acoustic radiation resistance of the source and \tilde{U}_0 is its total volume velocity. Hence the specific radiation resistance is given by

$$\mathbf{R}_s = S\mathbf{R}_{AR} = \frac{k^2\rho_0cS}{4\pi^2} \int_0^{2\pi} \int_0^{\frac{\pi}{2}} |D(\theta, \phi)|^2 \sin \theta \, d\theta \, d\phi. \quad (13.271)$$

Also, the specific radiation reactance is given by

$$X_s = S X_{AR} = -j \frac{k^2\rho_0cS}{4\pi^2} \int_0^{2\pi} \int_{\frac{\pi}{2}+j0}^{\frac{\pi}{2}+j\infty} |D(\theta, \phi)|^2 \sin \theta \, d\theta \, d\phi. \quad (13.272)$$

It is fairly straightforward to verify this result by inserting the directivity function of Eq. (13.102) together with $k_w = k \sin \theta$ into Eqs. (13.271) and (13.272). In this way, the

expressions for the radiation impedance given by Eqs. (13.118) and (13.117) can be duplicated, bearing in mind that $\sin(\pi/2 + j\infty) = \cos j\infty = \cosh \infty = \infty$. Of course, this theorem is not limited to radiators with uniform surface velocity. Bouwkamp's expression [36] includes the square of average surface velocity divided by the square of the velocity at some reference point, although we have omitted this here. We will use this theorem to derive an expression for the radiation impedance of a rectangular piston in an infinite baffle.

We can extend Bouwkamp's impedance theorem to a pressure (resilient) source, where the far-field pressure is given by

$$\tilde{p}(r, \theta, \phi) = \frac{jkS\tilde{p}_0}{4\pi r} D(\theta, \phi)$$

so that the total radiated power is given by

$$W = \left| \frac{\tilde{p}_0}{2\sqrt{2}} \right|^2 \mathbf{G}_{AR} = \frac{1}{\rho_0 c} \int_0^{2\pi} \int_0^{\pi/2} \left| \frac{\tilde{p}(r, \theta, \phi)}{\sqrt{2}} \right|^2 r^2 \sin \theta \, d\theta \, d\phi \Big|_{r \rightarrow \infty},$$

where \mathbf{G}_{AR} is the acoustic radiation conductance of the source and $\tilde{p}_0/2$ is the driving pressure on one side only of the baffle or plane. Hence the specific radiation conductance is given by

$$\mathbf{G}_S = \frac{\mathbf{G}_{AR}}{S} = \frac{k^2 S}{4\pi^2 \rho_0 c} \int_0^{2\pi} \int_0^{\pi/2} |D(\theta, \phi)|^2 \sin \theta \, d\theta \, d\phi$$

and the specific radiation susceptance is given by

$$B_S = \frac{B_{AR}}{S} = j \frac{k^2 S}{4\pi^2 \rho_0 c} \int_0^{2\pi} \int_{\frac{\pi}{2}+j0}^{\frac{\pi}{2}+j\infty} |D(\theta, \phi)|^2 \sin \theta \, d\theta \, d\phi.$$



13.14 RADIATION FROM AN INFINITELY LONG OSCILLATING STRIP IN AN INFINITE BAFFLE [37,38]

Boundary conditions

Essentially this is the limiting case of a rectangular piston as one of its dimensions tends to infinity. The infinitely long strip of width d shown in Fig. 13.40 is mounted in an infinite baffle in the xy plane and oscillates in the z direction with a harmonically time-dependent velocity \tilde{u}_0 . As with the circular piston in an infinite baffle, the monopole source elements, together with their images, coalesce to form elements of double

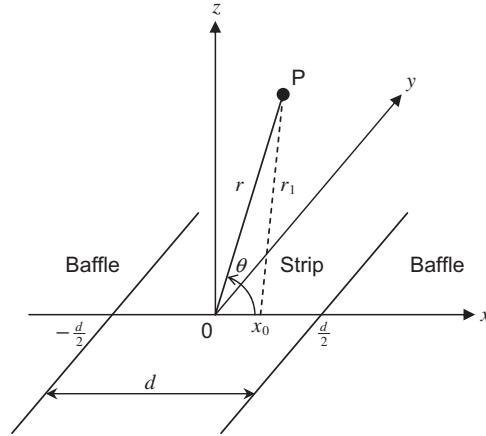


Figure 13.40 Geometry of infinitely long rigid strip in infinite baffle. The point of observation P is located at position (x,y,z) in rectangular coordinates.

strength. Because of the symmetry of the pressure fields on either side of the baffle, there is the following Neumann boundary condition on its surface:

$$\frac{\partial}{\partial z} \tilde{p}(x, z) \Big|_{z=0+} = 0, \quad \begin{cases} -\infty \leq x < -\frac{d}{2}, \\ -\frac{d}{2} < x \leq \infty \end{cases} \quad (13.273)$$

which is satisfied automatically. On the surface of the strip there is the coupling condition

$$\frac{\partial}{\partial z} \tilde{p}(x, y) \Big|_{z=0+} = -jk\rho_0 c \tilde{u}_0, \quad -\frac{d}{2} \leq x \leq \frac{d}{2}, \quad (13.274)$$

where ρ_0 is the density of air or any other surrounding medium, c is the speed of sound in that medium, and $k = 2\pi/\lambda = \omega/c$ is the wave number.

Far-field pressure

The pressure at point P due to a single line source at x_0 is obtained from Eq. (12.6) to give

$$\tilde{p}(r, \theta) = \frac{\rho_0 c (\tilde{U}_0/l)}{2} \sqrt{\frac{k}{2\pi r_1}} e^{-j\left(kr_1 - \frac{\pi}{4}\right)}, \quad (13.275)$$

where (\tilde{U}_0/l) is the volume velocity per unit length, $k = \omega/c = 2\pi/\lambda$ is the wave number, and

$$r_1^2 = r^2 \cos^2 \theta + (r \sin \theta - x_0)^2. \quad (13.276)$$

Hence, the pressure due to the strip is the integral across its width of Eq. (13.275) for a single line source taking into account the double strength sources and letting $\tilde{U}_0 = l\tilde{u}_0$ as follows:

$$\tilde{p}(r, \theta) = \rho_0 c \tilde{u}_0 \int_{-\frac{d}{2}}^{\frac{d}{2}} \sqrt{\frac{k}{2\pi r_1}} e^{-j\left(kr_1 - \frac{\pi}{4}\right)} dx_0. \quad (13.277)$$

At a large distance r , the terms containing r in Eq. (13.276) dominate. Hence the remaining terms can be replaced with ones that enable r_1 to be factorized as follows

$$\begin{aligned} r_1^2 &= r^2 + x_0^2 - 2rx_0 \sin \theta \\ &\approx r^2 + x_0^2 \sin^2 \theta - 2rx_0 \sin \theta \\ &= (r - x_0 \sin \theta)^2, \end{aligned} \quad (13.278)$$

which after inserting into Eq. (13.277) gives

$$\begin{aligned} \tilde{p}(r, \theta) &= \rho_0 c \tilde{u}_0 \sqrt{\frac{k}{2\pi r}} e^{-j\left(kr - \frac{\pi}{4}\right)} \int_{-\frac{d}{2}}^{\frac{d}{2}} e^{jkx_0 \sin \theta} dx_0 \\ &= \frac{kd\rho_0 c \tilde{u}_0}{2} \sqrt{\frac{d}{\pi r}} e^{-j\left(kr - \frac{\pi}{4}\right)} D(\theta), \end{aligned} \quad (13.279)$$

where the directivity function $D(\theta)$ is given by

$$D(\theta) = \frac{\sin\left(\frac{1}{2}kd \sin \theta\right)}{\left(\frac{1}{2}kd\right)^{3/2} \sin \theta}, \quad (13.280)$$

which is the same as that of a finite line source of length d in its plane, as given by Eq. (4.89). The directivity pattern is shown in Fig. 4.18. The on-axis pressure is given by

$$D(0) = 1 \left/ \sqrt{\frac{1}{2}kd} \right.$$

In Section 2.1, we saw that in the case of a piston radiating into an infinitely long tube, the pressure \tilde{p} along the tube is directly proportional to the piston velocity \tilde{u}_0 .

Assuming the tube is much narrower than the wavelength, this represents a one-dimensional system. In three-dimensional space, such as that of a piston in an infinite baffle radiating into free space, the radiated pressure is proportional to the acceleration of the piston $j\omega\tilde{u}_0$. Not surprisingly, in the two-dimensional space of an infinite strip we find that the pressure is proportional to $\sqrt{j\omega\tilde{u}_0}$.

Radiation impedance

Using the Bouwkamp impedance theorem (see [Section 13.13](#)), the radiated power per unit length l is given by

$$W = \left| \frac{\tilde{U}_0}{\sqrt{2}} \right|^2 \mathbf{R}_{AR} = \frac{l}{\rho_0 c} \int_{-\pi/2}^{\pi/2} \left| \frac{\tilde{p}(r, \theta)}{\sqrt{2}} \right|^2 r d\theta \Big|_{r \rightarrow \infty}, \quad (13.281)$$

where the integration is taken over a half-cylindrical surface in the extreme far field. Using the pressure from [Eq. \(13.279\)](#), we obtain the real and imaginary parts of the impedance as follows:

$$\mathbf{R}_s = l d \mathbf{R}_{AR} = \rho_0 c \frac{kd}{\pi} \int_0^{\pi/2} D^2(\theta) d\theta, \quad (13.282)$$

$$X_s = l d X_{AR} = \rho_0 c \frac{kd}{\pi} \int_{\pi/2 + j0}^{\pi/2 + j\infty} D^2(\theta) d\theta, \quad (13.283)$$

where \mathbf{R}_s is the specific radiation resistance in $\text{N} \cdot \text{s} / \text{m}^3$ (rayl), where the bold \mathbf{R} indicates that the quantity varies with frequency, and X_s is the specific radiation reactance in $\text{N} \cdot \text{s} / \text{m}^3$ (rayl). Substituting $t = \sin \theta$ yields

$$\begin{aligned} \mathbf{R}_s = l d \mathbf{R}_{AR} &= \rho_0 c \frac{kd}{\pi} \int_0^1 \left(\frac{\sin\left(\frac{kd}{2}t\right)}{\frac{kd}{2}t} \right)^2 \frac{dt}{\sqrt{1-t^2}} \\ &= \rho_0 c \frac{kd}{2} {}_1F_2\left(\frac{1}{2}; \frac{3}{2}, 2; -\frac{k^2 d^2}{4}\right) \\ &\approx \rho_0 c \frac{kd}{2}, \quad kd < 0.5, \end{aligned} \quad (13.284)$$

$$\begin{aligned}
X_s = ldX_{AR} &= \rho_0 c \frac{kd}{\pi} \int_0^\infty \left(\frac{\sin\left(\frac{kd}{2}t\right)}{\frac{kd}{2}t} \right)^2 \frac{dt}{\sqrt{t^2-1}} \\
&= \rho_0 c \frac{1}{kd} G_{2,4}^{2,1} \left(\frac{k^2 d^2}{4} \middle|_{1,1,0,\frac{1}{2}}^{1,\frac{3}{2}} \right) \\
&\approx \rho_0 c \frac{kd}{\pi} \left(\frac{3}{2} - \gamma - \ln\left(\frac{kd}{2}\right) \right), \quad kd < 0.5,
\end{aligned} \tag{13.285}$$

where F is the hypergeometric function, G is the Meijer G function, and $\gamma = 0.5772$ is Euler's constant. Separate plots of $\mathbf{R}_s/\rho_0 c$ and $X_s/\rho_0 c$ are shown in Figs. 13.43 and 13.44, respectively, as a function of kd .



13.15 THE FAR-FIELD PRESSURE DISTRIBUTION AS A SPATIAL FREQUENCY SPECTRUM OF THE SOURCE VELOCITY DISTRIBUTION

Two-dimensional system

In a two-dimensional system with a planar source, the far-field pressure distribution is given by a generalized version of Eq. (13.279), where $\tilde{u}_0(x_0)$ is the source velocity distribution:

$$\begin{aligned}
\tilde{p}(r, \theta) &= \rho_0 c \sqrt{\frac{k}{2\pi r}} e^{-j\left(kr - \frac{\pi}{4}\right)} \int_{-\infty}^{\infty} \tilde{u}_0(x) e^{jkx_0 \sin \theta} dx_0 \\
&= -j \frac{e^{-j\left(kr + \frac{\pi}{4}\right)}}{\sqrt{2\pi kr}} \tilde{F}(k_x),
\end{aligned} \tag{13.286}$$

where

$$\tilde{F}(k_x) = \int_{-\infty}^{\infty} \tilde{f}(x_0) e^{jk_x x_0} dx_0, \tag{13.287}$$

which is simply the Fourier transform or spatial frequency spectrum of the normal pressure gradient distribution $\tilde{f}(x_0)$ in the xy plane:

$$\tilde{f}(x_0) = -\frac{\partial}{\partial z_0} \tilde{p}(x_0, z_0) \Big|_{z_0=0} = jk \rho_0 c \tilde{u}(x_0), \tag{13.288}$$

where k_x is the spatial frequency of the component of a wave in the x direction given by

$$k_x = k \sin \theta. \quad (13.289)$$

In the case of a strip of infinite extent in the y direction, the velocity distribution is just a step function in the x direction:

$$f(x_0) = \begin{cases} 0, & x < -\frac{d}{2} \\ 1, & -\frac{d}{2} \leq x \leq \frac{d}{2} \\ 0, & x > \frac{d}{2}. \end{cases} \quad (13.290)$$

By inspection of Eq. (13.279) we see that

$$D(k_x) = \frac{2\pi}{jkd\rho_0\tilde{c}u_0} F(k_x) = \frac{\sin\left(\frac{1}{2}k_x d\right)}{\frac{1}{2}k_x d}. \quad (13.291)$$

Now let us convert from polar coordinates in r and θ to rectangular coordinates in x and z , using

$$r = \sqrt{z^2 + x^2}, \quad (13.292)$$

$$\sin \theta = \frac{x}{\sqrt{z^2 + x^2}} \quad (13.293)$$

and project the polar directivity pattern onto a distant parallel screen. Hence, the spatial frequency k_x at a point on the screen a horizontal distance x from the z axis is scaled by

$$k_x = k \sin \theta = \frac{kx}{\sqrt{z^2 + x^2}}. \quad (13.294)$$

At a given frequency $\omega = kc$, only the spectrum up to spatial frequency $k_x = k$ is displayed on the screen as θ varies from 0 to $\pi/2$. As the frequency is increased, more of the spectrum is shown but never the whole spectrum. We also note that the amplitude of the spectrum is scaled by $(z^2 + x^2)^{-1/4}$ because of the $1/\sqrt{r}$ term in Eq. (13.279).

Three-dimensional system

Here we consider a three-dimensional system in rectangular coordinates (x, y, z) with an arbitrary source velocity distribution in an infinite baffle in the xy plane, which radiates into half space. The pressure field is given by the Rayleigh integral of Eq. (13.6) using the Green's function given by Eq. (13.4), which for $z_0 = 0$ can be written as

$$g(x, y, z|x_0, y_0, 0) = \frac{e^{-jkr_1}}{4\pi r_1}, \quad (13.295)$$

where

$$r_1^2 = (x - x_0)^2 + (y - y_0)^2 + z^2. \quad (13.296)$$

If we let $x = r \sin \theta_x$, $y = r \sin \theta_y$, and $z^2 = r^2 - x^2 - y^2$, then

$$\begin{aligned} r_1^2 &= r^2 - 2rx_0 \sin \theta_x - 2ry_0 \sin \theta_y + x_0^2 + y_0^2 \\ &\approx (r - x_0 \sin \theta_x - y_0 \sin \theta_y)^2, \quad r^2 \gg x_0^2 + y_0^2, \end{aligned} \quad (13.297)$$

where θ_x is the angle of elevation subtended with the z axis in the x direction, and θ_y is that subtended with the z axis in the y direction as follows:

$$\sin \theta_x = \frac{x}{\sqrt{x^2 + y^2 + z^2}} = \frac{x}{r}, \quad (13.298)$$

$$\sin \theta_y = \frac{y}{\sqrt{x^2 + y^2 + z^2}} = \frac{y}{r}. \quad (13.299)$$

Alternatively, in cylindrical coordinates we have $\sin \theta_x = \sin \theta \cos \phi$ and $\sin \theta_y = \sin \theta \sin \phi$. Inserting the Green's function of Eq. (13.295) into the Rayleigh integral of Eq. (13.6), while doubling the source strength due to half-space radiation, yields

$$\begin{aligned} \tilde{p}(x, y, z) &= jk\rho_0 c \frac{e^{-jkr}}{2\pi r} \int_{-\infty}^{\infty} \int_{-\infty}^{\infty} \tilde{u}(x_0, y_0) e^{jk(x_0 \sin \theta_x + y_0 \sin \theta_y)} dx_0 dy_0 \\ &= \frac{e^{-jkr}}{2\pi r} \tilde{F}(k_x, k_y), \end{aligned} \quad (13.300)$$

where

$$\tilde{F}(k_x, k_y) = \int_{-\infty}^{\infty} \int_{-\infty}^{\infty} \tilde{f}(x_0, y_0) e^{j(k_x x_0 + k_y y_0)} dx_0 dy_0, \quad (13.301)$$

which is simply the Fourier transform or spatial frequency spectrum of the normal pressure gradient distribution $\tilde{f}(x_0, y_0)$ in the xy plane:

$$\tilde{f}(x_0, y_0) = -\frac{\partial}{\partial z_0} \tilde{p}(x_0, y_0, z_0) \Big|_{z_0=0} = jk\rho_0 c \tilde{u}(x_0, y_0), \quad (13.302)$$

where k_x and k_y are the spatial frequencies given by

$$k_x = k \sin \theta_x, \quad (13.303)$$

$$k_y = k \sin \theta_y, \quad (13.304)$$

and the amplitude in the distant plane is scaled by $(x^2 + y^2 + z^2)^{-1/2}$.

Axisymmetric three-dimensional system

In an axisymmetric system with a planar source, such as a piston in an infinite baffle, the pressure distribution is given by the Rayleigh integral of Eq. (13.6) using the Green's function given by Eq. (13.70), which for $z_0 = 0$ and $\phi = \pi/2$ can be written as

$$\begin{aligned} p(r, \theta) &= jk\rho_0 c \frac{e^{jkr}}{2\pi r} \int_0^{2\pi} \int_0^\infty \tilde{u}(w_0) e^{jk w_0 \sin \theta \sin \phi_0} w_0 dw_0 d\phi_0 \\ &= \frac{e^{jkr}}{r} \int_0^\infty \tilde{f}(w_0) J_0(k w_0 \sin \theta) w_0 dw_0 \\ &= \frac{e^{jkr}}{r} \tilde{F}(k_w), \end{aligned} \quad (13.305)$$

where we have used Eq. (76) from Appendix II to solve the integral and

$$\tilde{F}(k_w) = \int_0^\infty \tilde{f}(w_0) J_0(k_w w_0) w_0 dw_0, \quad (13.306)$$

which is simply the Hankel transform or spatial frequency spectrum of the normal pressure gradient distribution $\tilde{f}(w_0)$ in the w plane:

$$\tilde{f}(w_0) = -\frac{\partial}{\partial z_0} \tilde{p}(w_0, z_0) \Big|_{z_0=0} = jk\rho_0 c \tilde{u}(w_0), \quad (13.307)$$

where k_w is the spatial frequency given by

$$k_w = k \sin \theta. \quad (13.308)$$

In the case of a piston in an infinite baffle, the velocity distribution is just a step function in the w direction:

$$\tilde{f}(w_0) = \begin{cases} jk\rho_0\tilde{c}u_0, & 0 \leq w_0 \leq a \\ 0, & w_0 > a \end{cases}, \quad (13.309)$$

so that applying the integral solution of Eq. (95) from Appendix II yields

$$\begin{aligned} \tilde{F}(k_w) &= jk\rho_0\tilde{c}u_0 \int_0^a J_0(kw_0 \sin \theta) w_0 dw_0 \\ &= jka^2\rho_0\tilde{c}u_0 \frac{J_1(ka \sin \theta)}{ka \sin \theta}. \end{aligned} \quad (13.310)$$

By inspection of Eq. (13.102), we see that

$$D(k_w) = \frac{2}{jka^2\rho_0\tilde{c}u_0} \tilde{F}(k_w). \quad (13.311)$$

Now let us convert from polar coordinates in r and θ to cylindrical coordinates in w and z , using

$$r = \sqrt{z^2 + w^2}, \quad (13.312)$$

$$\sin \theta = \frac{w}{\sqrt{z^2 + w^2}}, \quad (13.313)$$

and project the polar directivity pattern onto a distant parallel screen. Hence, the spatial frequency k_w at a point on the screen a horizontal distance w from the z axis is scaled by

$$k_w = k \sin \theta = \frac{k w}{\sqrt{z^2 + w^2}}. \quad (13.314)$$

At a given frequency $\omega = kc$, only the spectrum up to spatial frequency $k_w = k$ is displayed on the screen as θ varies from 0 to $\pi/2$. As the frequency is increased, more of the spectrum is shown but never the whole spectrum. We also note that the amplitude of the spectrum is scaled by $(z^2 + w^2)^{-1/2}$ because of the $1/r$ term in Eq. (13.101).



13.16 THE BRIDGE PRODUCT THEOREM

This important theorem in acoustics is a corollary of the fact that the pressure distribution in one plane is a Fourier transform of the velocity distribution in another one that is far away and parallel to it, as discussed in the previous section. For simplicity, let us consider a two-dimensional system in the xz plane of infinite extent in the y

direction. We then multiply the Fourier transform of an arbitrary velocity distribution $f(x)$ by that of a line source at x_0 as follows:

$$\begin{aligned} F(K) &= \int_{-\infty}^{\infty} f(x)e^{jKx} dx \times \int_{-\infty}^{\infty} \delta(x - x_0)e^{jKx} dx \\ &= \int_{-\infty}^{\infty} f(x)e^{jK(x+x_0)} dx, \end{aligned} \quad (13.315)$$

where $\delta(x - x_0)$ is the Dirac delta function and we have used the property that

$$\int_{-\infty}^{\infty} \delta(x - x_0)e^{jKx} dx = e^{jKx_0}. \quad (13.316)$$

If we now substitute $x' = x + x_0$, we obtain

$$F(K) = \int_{-\infty}^{\infty} f(x' - x_0)e^{jKx'} dx', \quad (13.317)$$

which is simply the Fourier transform of the original distribution $f(x)$ shifted to a new origin at x_0 as illustrated in Fig. 13.41. This is somewhat analogous to the principle of amplitude modulation whereby multiplying a baseband signal by a single tone in the time domain produces a modulated tone with “sideband” spectrums on either side of the tone in the frequency domain. Here the space domain is analogous to the frequency domain and the spatial frequency domain is analogous to the time domain, as the product is taken

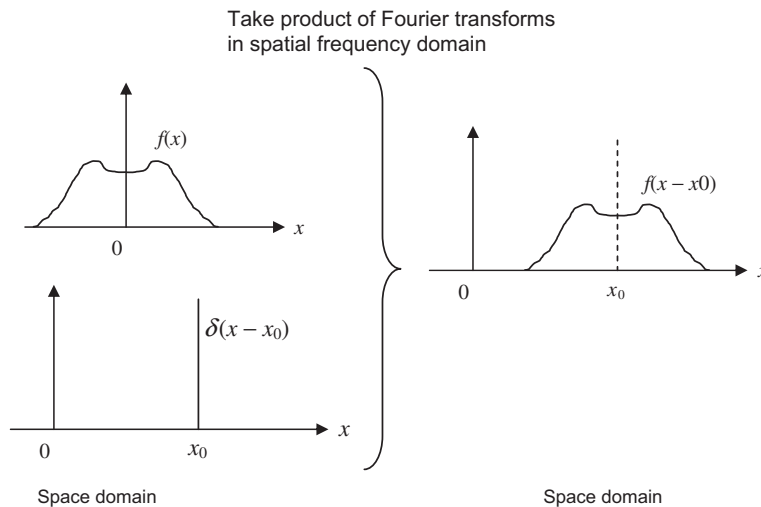


Figure 13.41 Product theorem: origin shifting.

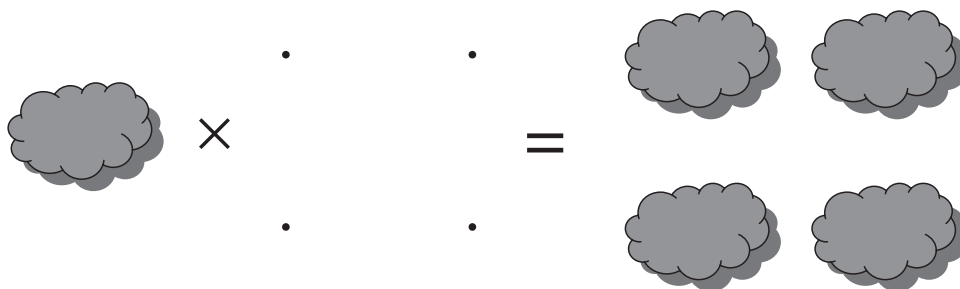


Figure 13.42 Product theorem: array creation.

in the latter. Seeing that the far-field pressure of a planar source is the Fourier transform of the source velocity distribution, we can use the product theorem to derive the far-field pressure for a transducer array by simply taking the product of the directivity function for a single transducer and that of any number of point sources located in the array positions, as illustrated in Fig. 13.42.

13.17 RADIATION FROM A RIGID RECTANGULAR PISTON IN AN INFINITE BAFFLE [39,40]

Far-field pressure

Using the product theorem given in Section 13.16, the directivity pattern is equal to the product of the directivity patterns for two line arrays at right angles to each other [see Eq. (4.89)]. The directivity pattern for this type of radiating source with dimensions l_x and l_y is given by the formula

$$D(\theta_x, \theta_y) = \frac{\sin\left(\frac{1}{2}kl_x \sin \theta_x\right)}{\frac{1}{2}kl_x \sin \theta_x} \cdot \frac{\sin\left(\frac{1}{2}kl_y \sin \theta_y\right)}{\frac{1}{2}kl_y \sin \theta_y}, \quad (13.318)$$

where θ_x is the angle between the normal to the surface of the piston and the projection of the line joining the middle of the surface and the observation point on the plane normal to the surface and parallel to l_x ; θ_y is the same as θ_x , with l_y substituted for l_x .

It is often more convenient to express Eq. (13.318) using spherical coordinates using

$$\sin \theta_x = \sin \theta \cos \phi, \quad \sin \theta_y = \sin \theta \sin \phi. \quad (13.319)$$

Also, we shall substitute $\text{sinc } x = (\sin x)/x$ to obtain

$$D(\theta, \phi) = \text{sinc}\left(\frac{1}{2}kl_x \sin \theta \cos \phi\right) \cdot \text{sinc}\left(\frac{1}{2}kl_y \sin \theta \sin \phi\right). \quad (13.320)$$

Radiation impedance

Using the Bouwkamp impedance theorem, the radiation resistance and reactance can be found by inserting Eq. (13.320) into Eqs. (13.271) and (13.272) respectively to give

$$\mathbf{R}_s = kl_x kl_y \frac{\rho_0 c}{\pi^2} \int_0^{\pi/2} \int_0^{\pi/2} \text{sinc}^2\left(\frac{1}{2} kl_x \sin \theta \cos \phi\right) \cdot \text{sinc}^2\left(\frac{1}{2} kl_y \sin \theta \sin \phi\right) \sin \theta \, d\theta \, d\phi, \quad (13.321)$$

$$X_s = -jkl_x kl_y \frac{\rho_0 c}{\pi^2} \int_0^{\pi/2} \int_{\pi/2+j0}^{\pi/2+j\infty} \text{sinc}^2\left(\frac{1}{2} kl_x \sin \theta \cos \phi\right) \cdot \text{sinc}^2\left(\frac{1}{2} kl_y \sin \theta \sin \phi\right) \sin \theta \, d\theta \, d\phi, \quad (13.322)$$

where \mathbf{R}_s is the specific radiation resistance in $\text{N}\cdot\text{s}/\text{m}^3$ (rayl). The bold \mathbf{R} indicates that the quantity varies with frequency, and X_s is the specific radiation reactance in $\text{N}\cdot\text{s}/\text{m}^3$ (rayl). Substituting $t = \sin \theta$ in Eqs. (13.321) and (13.322) yields

$$\mathbf{R}_s = \frac{kl_x l_y \rho_0 c}{4\pi^2} \int_0^{\pi/2} \int_0^1 \text{sinc}^2\left(\frac{kl_x}{2} t \cos \phi\right) \text{sinc}^2\left(\frac{kl_y}{2} t \sin \phi\right) \frac{t \, dt \, d\phi}{\sqrt{1-t^2}}, \quad (13.323)$$

$$X_s = \frac{kl_x l_y \rho_0 c}{4\pi^2} \int_0^{\pi/2} \int_1^{\infty} \text{sinc}^2\left(\frac{kl_x}{2} t \cos \phi\right) \text{sinc}^2\left(\frac{kl_y}{2} t \sin \phi\right) \frac{t \, dt \, d\phi}{\sqrt{t^2-1}}, \quad (13.324)$$

where we note that $\sin(\pi/2 + j\infty) = \cos j\infty = \cosh \infty = \infty$. An analytical solution to Eq. (13.323) can be found by substituting $s = \sin \phi$ and expanding the sinc functions using

$$\text{sinc}^2 x = (\sin x)^2 / x^2 = \sum_{n=1}^{\infty} \frac{(-1)^{n+1} 2^{2n-1}}{(2n)!} x^{2n-2}, \quad (13.325)$$

which gives

$$\mathbf{R}_s = \frac{\rho_0 c}{\sqrt{\pi}} \sum_{m=0}^{\infty} \sum_{n=0}^{\infty} \frac{(-1)^{m+n}}{(2m+1)(2n+1)(m+1)!(n+1)! \Gamma\left(m+n+\frac{3}{2}\right)} \left(\frac{kl_x}{2}\right)^{2m+1} \left(\frac{kl_y}{2}\right)^{2n+1}. \quad (13.326)$$

A somewhat more complicated evaluation of the integrals in Eq. (13.324) is given in Ref. [40]. Firstly, the sine squared terms have to be expanded into cosine terms using Eqs. (A2.46) and (A2.50) from Appendix II. Then the infinite integral is evaluated before

expanding the resulting Bessel and Struve functions. The range of the remaining finite integral has to be split into two at $l_x / \sqrt{l_x^2 + l_y^2}$ yielding

$$X_s = \frac{2\rho c}{\pi} \left(\frac{1 - \text{sinc}(kl_x)}{qkl_x} + \frac{1 - \text{sinc}(qkl_x)}{kl_x} + \sum_{m=0}^M \frac{(-1)^m f_m(q)}{(2m+1)m!(m+1)!} \left(\frac{kl_x}{2}\right)^{2m+1} \right), \quad (13.327)$$

where $q = l_y/l_x$,

$$f_m(q) = \frac{{}_2F_1\left(1, m + \frac{1}{2}; m + \frac{3}{2}, \frac{1}{1+q^2}\right) + {}_2F_1\left(1, m + \frac{1}{2}; m + \frac{3}{2}, \frac{1}{1+q^{-2}}\right)}{(2m+1)(1+q^{-2})^{m+1/2}} + \frac{1}{2m+3} \sum_{n=0}^m g_{mn}(q), \quad (13.328)$$

and

$$g_{mn}(q) = \binom{2m+3}{2n} \sum_{p=n}^m \frac{(-1)^{p-n} q^{2n-1}}{(2p-1)(1+q^2)^{p-1/2}} \binom{m-n}{p-n} + \binom{2m+3}{2n+3} \sum_{p=m-n}^m \frac{(-1)^{p-m+n} q^{2n+2}}{(2p-1)(1+q^{-2})^{p-1/2}} \binom{n}{p-m+n}. \quad (13.329)$$

Separate plots of $\mathbf{R}_s/\rho_0 c$ and $X_s/\rho_0 c$ are shown in Figs. 13.43 and 13.44 respectively as a function of kl , where $l = l_x$ is the smallest dimension. Separate plots of $\mathbf{R}_s/\rho_0 c$ and $X_s/\rho_0 c$ are also shown in Figs. 13.45 and 13.46 respectively as a function of ka , where a is a notional radius that gives the same circular area S as the actual area of the rectangular piston, which is given by $S = \pi a^2 = l_x l_y$.

13.18 MUTUAL RADIATION IMPEDANCE BETWEEN RIGID CIRCULAR PISTONS IN AN INFINITE BAFFLE [41–43]

Boundary conditions

When sound sources are radiating in close proximity to each other, their radiation characteristics may be affected by their acoustic interaction, depending on their spacing and the frequency. Here we consider two circular pistons of radii a_1 and a_2 , as shown in Fig. 13.47, which are mounted in an infinite rigid baffle in the xy plane with a separation

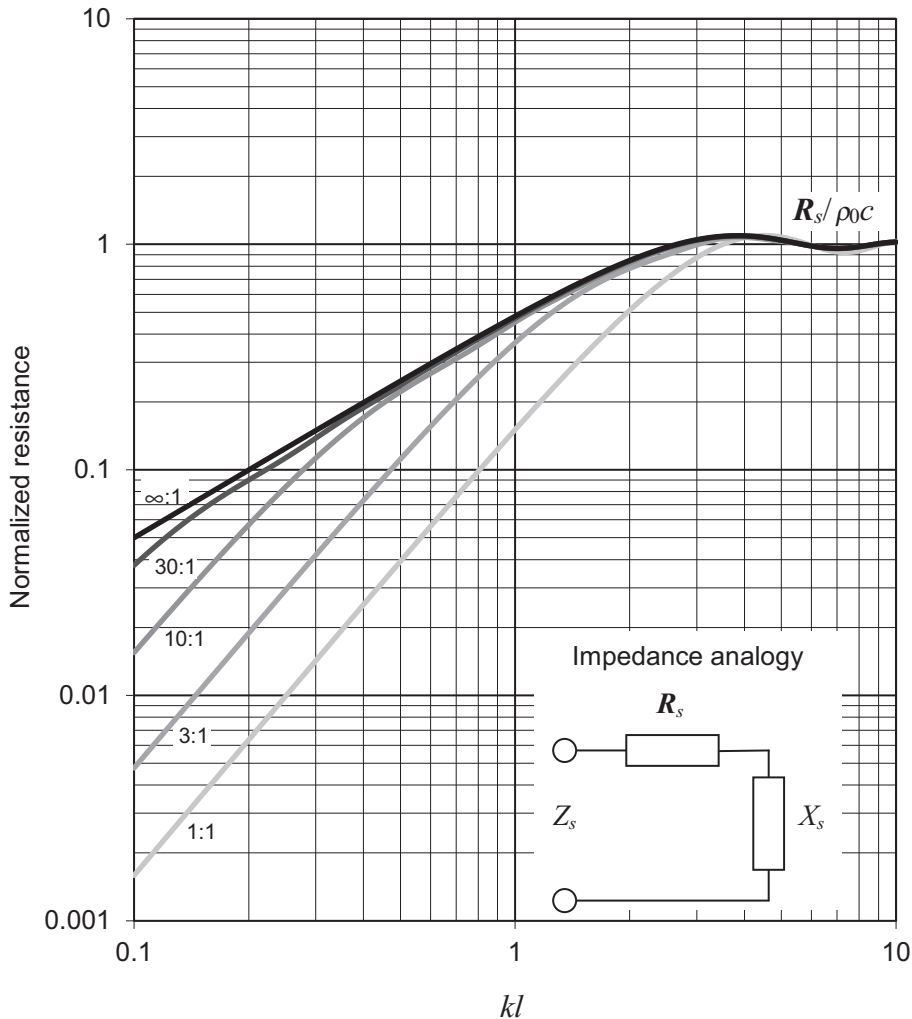


Figure 13.43 Normalized specific radiation resistance $R_s/\rho_0 c$ of the air load on one side of a plane rectangular piston in an infinite flat baffle for five different aspect ratios $q = l_y/l_x$, where l_x and l_y are the dimensions of the piston. Frequency is plotted on a normalized scale, where $kl = 2\pi l/\lambda = 2\pi l/c$ and $l = l_x$ is the smallest dimension. In the case of $q = \infty$, the impedance is that of an infinitely long strip.

distance d between their centers and oscillate in phase in the z direction with a harmonically time-dependent velocity \tilde{u}_0 .

According to the principle of superposition of fields, we obtain the directivity pattern from the combinations shown in Fig. 13.48.

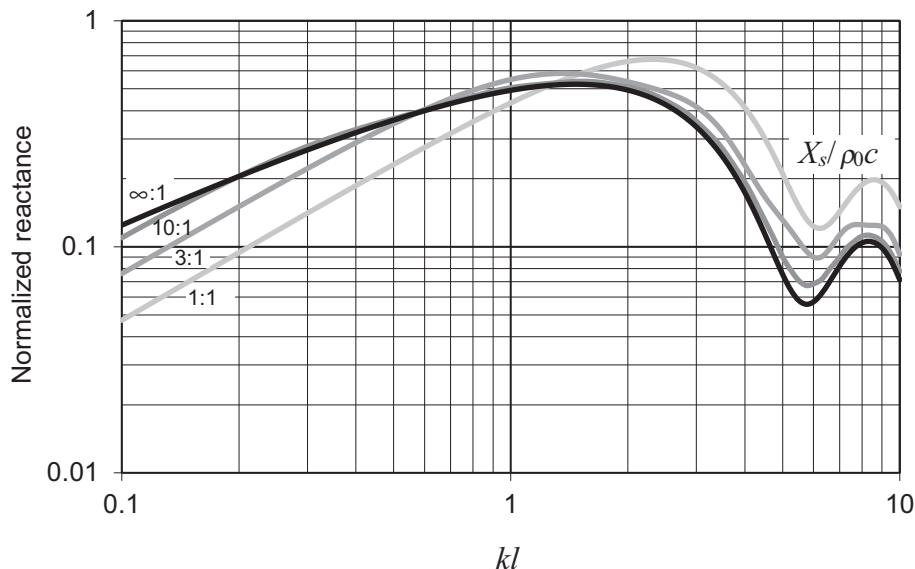


Figure 13.44 Normalized specific radiation reactance $X_s/\rho_0 c$ of the air load on one side of a plane rectangular piston in an infinite flat baffle for four different aspect ratios $q = l_y/l_x$, where l_x and l_y are the dimensions of the piston. Frequency is plotted on a normalized scale, where $kl = 2\pi l/\lambda = 2\pi l/c$ and $l = l_x$ is the smallest dimension. In the case of $q = \infty$, the impedance is that of an infinitely long strip.

Directivity

According to the product theorem of Section 13.16, we multiply the directivity pattern of a single piston from Eq. (13.102) by that of two point sources *in phase* from Eq. (4.79) to produce the directivity patterns of Fig. 13.48(b) and (d). Similarly, we multiply the directivity pattern of a single piston by that of two point sources *in antiphase* from Eq. (4.80) to produce the directivity patterns of Fig. 13.48(c) and (e). Hence, the directivity pattern of Fig. 13.48(a) is given by

$$D(\theta, \phi) = \frac{a_1^2 D_1(\theta)}{a_1^2 + a_2^2} e^{j \frac{kd}{2} \sin \theta \sin \phi} + \frac{a_2^2 D_2(\theta)}{a_1^2 + a_2^2} e^{-j \frac{kd}{2} \sin \theta \sin \phi}, \quad (13.330)$$

where

$$e^{\pm j \frac{kd}{2} \sin \theta \sin \phi} = \cos\left(\frac{kd}{2} \sin \theta \sin \phi\right) \pm j \sin\left(\frac{kd}{2} \sin \theta \sin \phi\right) \quad (13.331)$$

and $D_1(\theta)$ is the directivity pattern of the piston of radius a_1 as given by

$$D_1(\theta) = \frac{2J_1(ka_1 \sin \theta)}{ka_1 \sin \theta} \quad (13.332)$$

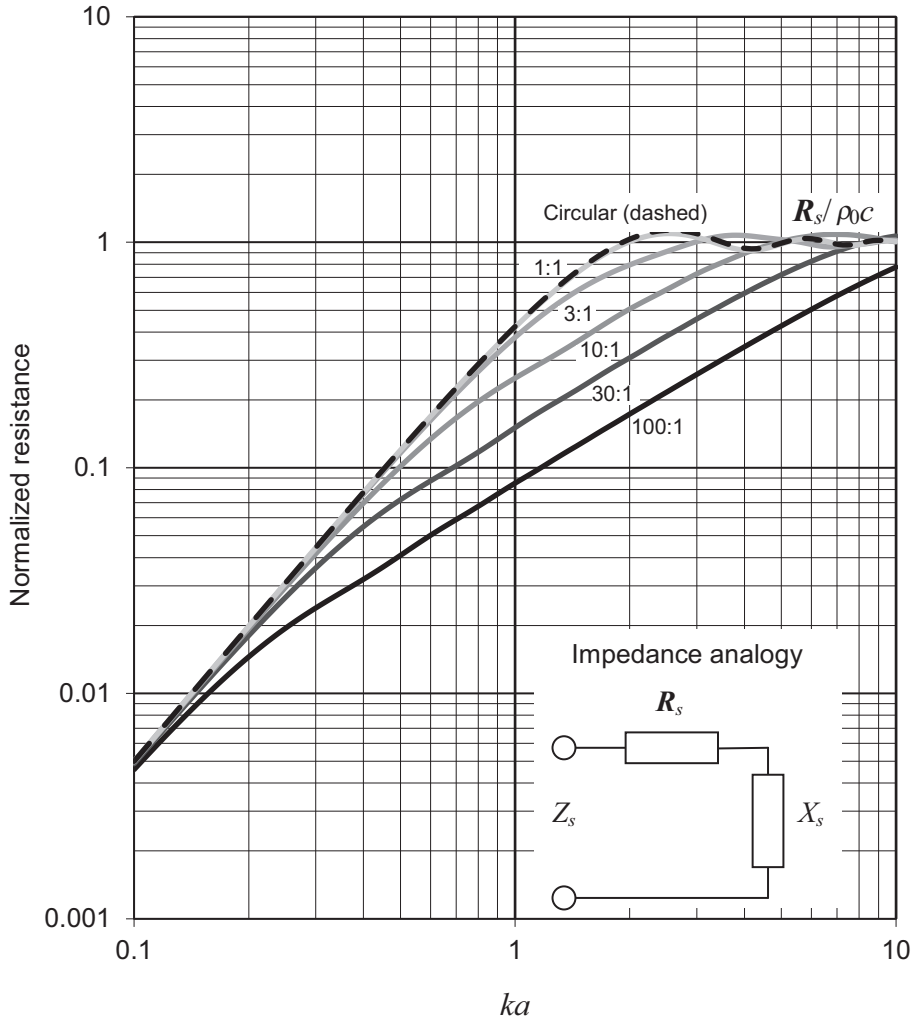


Figure 13.45 Normalized specific radiation resistance $R_s/\rho_0 c$ of the air load on one side of a plane rectangular piston in an infinite flat baffle for five different aspect ratios $q = l_y/l_x$, where l_x and l_y are the dimensions of the piston. Frequency is plotted on a normalized scale, where $ka = 2\pi a/\lambda = 2\pi a/c$ and a is a notional radius that gives the same circular area S as the actual area of the rectangular piston, which is given by $S = \pi a^2 = l_y l_x$.

and $D_2(\theta)$ is the directivity pattern of the piston of radius a_2 as given by

$$D_2(\theta) = \frac{2J_1(ka_2 \sin \theta)}{ka_2 \sin \theta}. \quad (13.333)$$

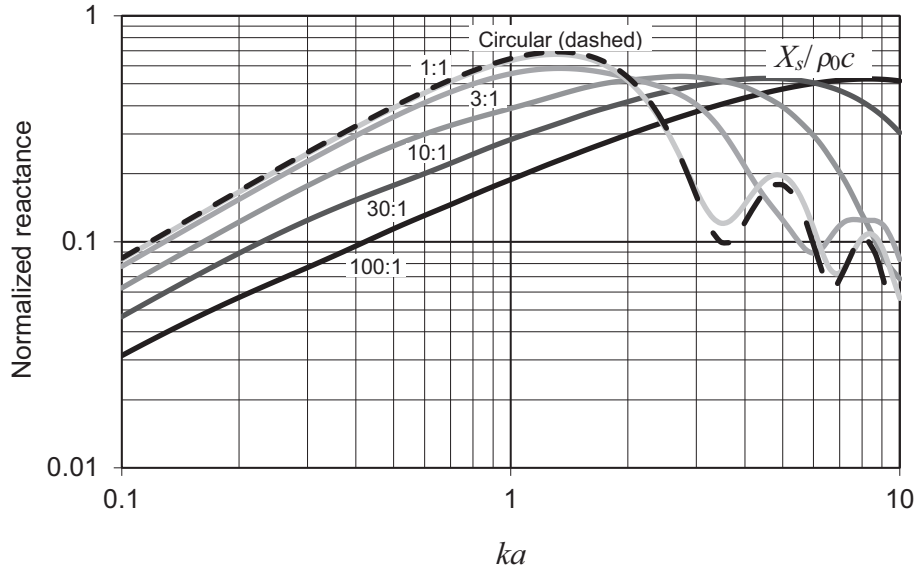


Figure 13.46 Normalized specific radiation reactance $X_s/\rho_0 c$ of the air load on one side of a plane rectangular piston in an infinite flat baffle for five different aspect ratios $q = l_y/l_x$, where l_x and l_y are the dimensions of the piston. Frequency is plotted on a normalized scale, where $ka = 2\pi a/\lambda = 2\pi f a/c$ and a is a notional radius that gives the same circular area S as the actual area of the rectangular piston, which is given by $S = \pi a^2 = l_x l_y$.

Note that Eqs. (4.79) and (4.80) have been modified to include the ϕ dependency. Then

$$|D(\theta, \phi)|^2 = \frac{a_1^4 D_1^2(\theta) + a_2^4 D_2^2(\theta) + 2a_1^2 a_2^2 D_1(\theta) D_2(\theta) \cos(kd \sin \theta \sin \phi)}{(a_1^2 + a_2^2)^2}, \quad (13.334)$$

where we have noted that $\sin^2(kd \sin \theta \sin \phi) = 1 - \cos^2(kd \sin \theta \sin \phi)$.

Impedance

We now obtain the total radiation impedance of the two pistons using Bouwkamp's impedance theorem of Eqs. (13.271) and (13.272)

$$Z_S = \mathbf{R}_S + jX_S = \frac{k^2 \rho_0 c S}{4\pi^2} \int_0^{2\pi} \left(\int_0^{\frac{\pi}{2}} |D(\theta, \phi)|^2 + \int_{\frac{\pi}{2}+j0}^{\frac{\pi}{2}+j\infty} |D(\theta, \phi)|^2 \right) \sin \theta \, d\theta \, d\phi, \quad (13.335)$$

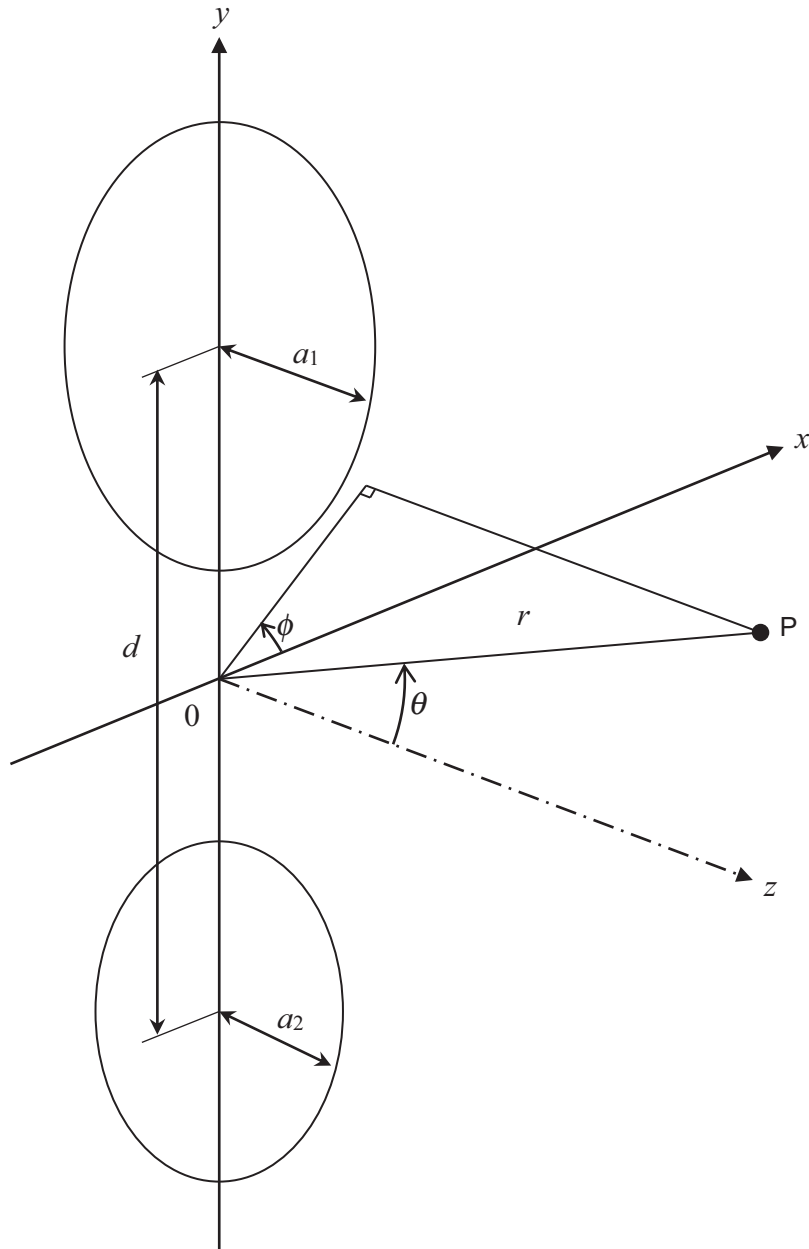


Figure 13.47 Geometry of two circular pistons in an infinite baffle. The point of observation P is located at a distance r from the origin at an inclination angle θ with respect to the z axis.

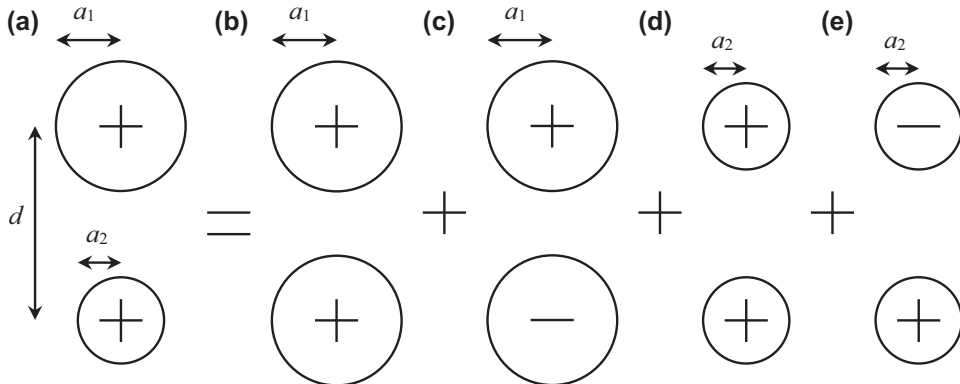


Figure 13.48 Combination of pistons of radii a_1 and a_2 .

where $S = \pi(a_1^2 + a_2^2)$ is the total radiating area. The total specific radiation resistance is given by

$$\begin{aligned} \mathbf{R}_S &= \frac{a_1^2}{a_1^2 + a_2^2} \mathbf{R}_{11} + \frac{a_2^2}{a_1^2 + a_2^2} \mathbf{R}_{22} + \frac{2a_1 a_2}{a_1^2 + a_2^2} \mathbf{R}_{12} \\ &= \frac{4k^2 \rho_0 c}{\pi(a_1^2 + a_2^2)} \int_0^{2\pi} \int_0^{\frac{\pi}{2}} (a_1^4 D_1^2(\theta) + a_2^4 D_2^2(\theta) \\ &\quad + a_1^2 a_2^2 D_1(\theta) D_2(\theta) \cos(kd \sin \theta \sin \phi)) \sin \theta \, d\theta \, d\phi, \end{aligned} \quad (13.336)$$

where \mathbf{R}_{11} and \mathbf{R}_{22} are the *self-resistances* of each piston and \mathbf{R}_{12} is the *mutual resistance* between the two pistons. The specific radiation reactance is given by

$$\begin{aligned} X_S &= \frac{a_1^2}{a_1^2 + a_2^2} X_{11} + \frac{a_2^2}{a_1^2 + a_2^2} X_{22} + \frac{2a_1 a_2}{a_1^2 + a_2^2} X_{12} \\ &= -j \frac{4k^2 \rho_0 c}{\pi(a_1^2 + a_2^2)} \int_0^{2\pi} \int_{\frac{\pi}{2}+j0}^{\frac{\pi}{2}+j\infty} (a_1^4 D_1^2(\theta) + a_2^4 D_2^2(\theta) \\ &\quad + a_1^2 a_2^2 D_1(\theta) D_2(\theta) \cos(kd \sin \theta \sin \phi)) \sin \theta \, d\theta \, d\phi, \end{aligned} \quad (13.337)$$

where X_{11} and X_{22} are the *self-reactances* of each piston and X_{12} is the *mutual reactance* between the two pistons. The first term in each integral, which is independent of the spacing d , may be identified as the self-impedance Z_{11} of the first piston

$$Z_{11} = 2\rho_0 c \left(\int_0^{\frac{\pi}{2}} \frac{J_1^2(ka_1 \sin \theta)}{\sin \theta} d\theta + \int_{\frac{\pi}{2}+j0}^{\frac{\pi}{2}+j\infty} \frac{J_1^2(ka_1 \sin \theta)}{\sin \theta} d\theta \right), \quad (13.338)$$

which after substituting $\mu = k \sin \theta$, as discussed in [Section 13.13](#), gives

$$Z_{11} = \mathbf{R}_{11} + jX_{11} = \rho_0 c \left\{ \left(1 - \frac{J_1^2(ka_1)}{ka_1} \right) + j \frac{\mathbf{H}_1(ka_1)}{ka_1} \right\}. \quad (13.339)$$

Similarly, the second term in each integral may be identified as the self-impedance Z_{22} of the second piston

$$Z_{22} = \mathbf{R}_{22} + jX_{22} = \rho_0 c \left\{ \left(1 - \frac{J_1^2(ka_2)}{ka_2} \right) + j \frac{\mathbf{H}_1(ka_2)}{ka_2} \right\}. \quad (13.340)$$

The third term in each integral then gives the mutual impedance Z_{12} so that, after integrating over ϕ using the integral solution of Eq. (A2.77) from Appendix II (with $z = kd \sin \theta$), we have

$$Z_{12} = 2\rho_0 c \left(\int_0^{\frac{\pi}{2}} \frac{J_1(ka_1 \sin \theta) J_1(ka_2 \sin \theta)}{\sin \theta} J_0(kd \sin \theta) d\theta \right. \\ \left. + \int_{\frac{\pi}{2}+j0}^{\frac{\pi}{2}+j\infty} \frac{J_1(ka_1 \sin \theta) J_1(ka_2 \sin \theta)}{\sin \theta} J_0(kd \sin \theta) d\theta \right), \quad (13.341)$$

which after substituting $s = \sin \theta$ becomes

$$Z_{12} = 2\rho_0 c \left(\int_0^1 \frac{J_1(ka_1 s) J_1(ka_2 s)}{s\sqrt{1-s^2}} J_0(kds) ds + \int_1^\infty \frac{J_1(ka_1 s) J_1(ka_2 s)}{s\sqrt{1-s^2}} J_0(kds) ds \right). \quad (13.342)$$

We then expand the J_1 functions using the following Lommel expansion

$$J_\nu(kas) = s^\nu \sum_{m=0}^{\infty} \left(\frac{ka}{2} \right)^m \frac{(1-s^2)^m}{m!} J_{\nu+m}(ka) \quad (13.343)$$

to give

$$Z_{12} = 2\rho_0 c \sum_{m=0}^{\infty} \sum_{n=0}^{\infty} \left(\frac{ka_1}{2}\right)^m \left(\frac{ka_2}{2}\right)^n \frac{J_{m+1}(ka_1)J_{n+1}(ka_2)}{m!n!} \\ \times \left(\int_0^1 J_0(kds)(1-s^2)^{m+n-1/2} s ds + j(-1)^{m+n} \int_1^{\infty} J_0(kds)(s^2-1)^{m+n-1/2} s ds \right), \quad (13.344)$$

which can be solved with help from Eqs. (A2.96), (A2.97), and (A2.98) of Appendix II to yield

$$Z_{12} = \frac{2\rho_0 c}{\sqrt{\pi}} \sum_{m=0}^{\infty} \sum_{n=0}^{\infty} \left(\frac{ka_1}{kd}\right)^m \left(\frac{ka_2}{kd}\right)^n \frac{\Gamma(m+n+1/2)J_{m+1}(ka_1)J_{n+1}(ka_2)}{m!n!} h_{m+n}^{(2)}(kd), \quad (13.345)$$

where the total specific radiation impedance is given by

$$Z_S = \frac{a_1^2}{a_1^2 + a_2^2} Z_{11} + \frac{a_2^2}{a_1^2 + a_2^2} Z_{22} + \frac{2a_1 a_2}{a_1^2 + a_2^2} Z_{12} \quad (13.346)$$

and $h_{m+n}^{(2)}$ is the spherical Hankel function defined in Eq. (A2.133) of Appendix II. For very large wavelengths and separations, where $ka \ll 1$ and $d \gg a$, we have

$$Z_{12} \approx \rho_0 c \frac{(ka_1)(ka_2)}{2} \left(\frac{\sin(kd)}{kd} + j \frac{\cos(kd)}{kd} \right), \quad (ka_1)(ka_2) \ll 1, \quad \frac{\sqrt{a_1 a_2}}{d} \ll 1, \quad (13.347)$$

where $\mathbf{R}_{11} = (ka)^2/2$. Plots of the real normalized mutual radiation resistance ($\mathbf{R}_{12}/\mathbf{R}_{11}$) and reactance (X_{12}/\mathbf{R}_{11}) for $ka = 1$ are shown in Fig. 13.49 as a function of kd .

Array of pistons

We now extend the model to an array of N pistons, each of radius a_p , where the p th and q th pistons are separated by a distance d_{pq} . Multiplying Eq. (13.346) through by the total area $\pi(a_1^2 + a_2^2)$ yields the total mechanical impedance

$$Z_M = \pi(a_1^2 + a_2^2) Z_S = \pi a_1^2 Z_{11} + \pi a_2^2 Z_{22} + 2\pi a_1 a_2 Z_{12}. \quad (13.348)$$

We may represent this with an N -port model in the following matrix form

$$\mathbf{F} = \mathbf{Z} \cdot \mathbf{u}, \quad (13.349)$$

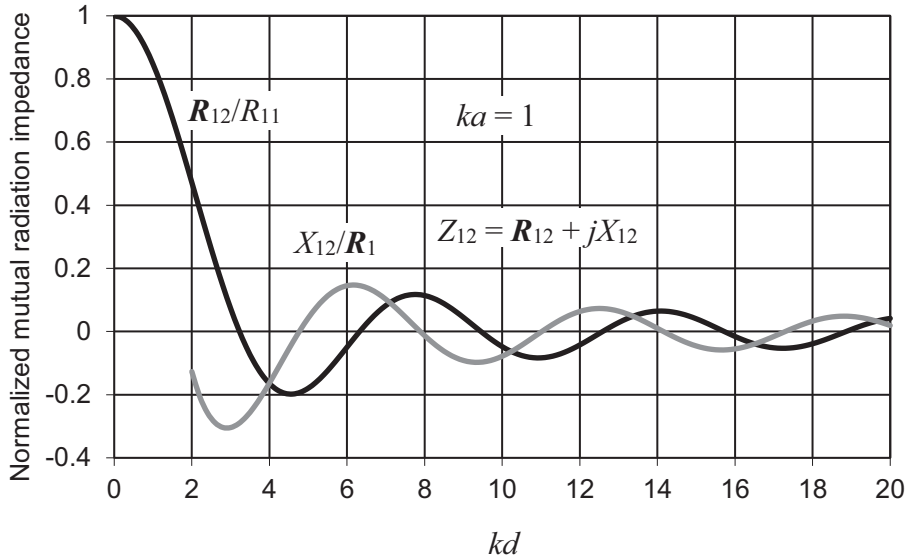


Figure 13.49 Real and imaginary parts of the normalized mutual radiation impedance Z_{12} of the air load on one side of two plane circular pistons of radius a and separation d in an infinite baffle.

where \mathbf{u} is the velocity vector

$$\mathbf{u} = [\tilde{u}_1 \quad \tilde{u}_2 \quad \cdots \quad \tilde{u}_p \quad \cdots \quad \tilde{u}_N]^T. \quad (13.350)$$

Because we are extending this model to an unlimited number of ports, we define all the velocities as positive flowing *into* the ports. Then \mathbf{Z} is the mechanical impedance matrix

$$\mathbf{Z} = \begin{bmatrix} z_{11} & z_{12} & \cdots & z_{1q} & \cdots & z_{1N} \\ z_{21} & z_{22} & \cdots & z_{2q} & \cdots & z_{2N} \\ \vdots & \vdots & & \vdots & & \vdots \\ z_{p1} & z_{p2} & \cdots & z_{pq} & \cdots & z_{pN} \\ \vdots & \vdots & & \vdots & & \vdots \\ z_{N1} & z_{N2} & \cdots & z_{Nq} & \cdots & z_{NN} \end{bmatrix}, \quad (13.351)$$

and \mathbf{F} is the force vector

$$\mathbf{F} = [\tilde{F}_1 \quad \tilde{F}_2 \quad \cdots \quad \tilde{F}_q \quad \cdots \quad \tilde{F}_N]^T. \quad (13.352)$$

The mechanical self-impedance elements on the diagonal are given by

$$z_{pp} = \pi a_p^2 (\mathbf{R}_{pp} + jX_{pp}) = \pi a_p^2 \rho_0 c \left\{ \left(1 - \frac{J_1^2(ka_p)}{ka_p} \right) + j \frac{\mathbf{H}_1(ka_p)}{ka_p} \right\} \quad (13.353)$$

and the symmetrical mutual-impedance elements are given by

$$\begin{aligned} z_{pq} &= z_{qp} = \pi a_p a_q (\mathbf{R}_{pq} + jX_{pq}) \\ &= 2\sqrt{\pi} a_p a_q \rho_0 c \sum_{m=0}^{\infty} \sum_{n=0}^{\infty} \left(\frac{ka_p}{kd_{pq}} \right)^m \left(\frac{ka_q}{kd_{pq}} \right)^n \\ &\quad \times \frac{\Gamma(m+n+1/2) J_{m+1}(ka_p) J_{n+1}(ka_q)}{m!n!} h_{m+n}^{(2)}(kd_{pq}). \end{aligned} \quad (13.354)$$

The self- and mutual acoustic impedances are given by

$$Z_{pq} = \frac{z_{pq}}{\pi^2 a_p^2 a_q^2}. \quad (13.355)$$



13.19 NEAR-FIELD ACOUSTICAL HOLOGRAPHY [8]

The forward problem

In [Section 13.3](#) we stated that an infinite plane counts as a closed surface over which a boundary surface integral may be evaluated because it isolates the sources on one side of the plane from the observation field on the other. You will also recall from [Section 13.15](#) that the far-field pressure distribution is the Fourier transform of the velocity distribution over an infinite plane. To calculate the near-field pressure we also have to take the inverse Fourier transform, and this technique is known as near-field acoustical holography. If we take the Fourier Green's function of [Eq. \(13.33\)](#) and insert it into the dipole part of the Kirchhoff–Helmholtz boundary integral of [Eq. \(13.28\)](#) or dipole Rayleigh integral, we obtain

$$\begin{aligned} \tilde{p}(x, y, z) &= \frac{1}{8\pi^2} \int_{-\infty}^{\infty} \int_{-\infty}^{\infty} 2\tilde{p}_0(x_0, y_0, z_0) \\ &\quad \times \int_{-\infty}^{\infty} \int_{-\infty}^{\infty} e^{-j(k_x(x-x_0)+k_y(y-y_0)+k_z(z-z_0))} dk_x dk_y dx_0 dy_0, \end{aligned} \quad (13.356)$$

which gives the pressure $\tilde{p}(x, y, z)$ in the z -plane in terms of the pressure $\tilde{p}_0(x_0, y_0, z_0)$ on *both* faces of the z_0 -plane. The *forward* problem is defined as the one where the field is calculated for $z \geq z_0$, and all sources are located in the region $z \leq z_0$. Rearranging the integrals gives

$$\begin{aligned} \tilde{p}(x, y, z) &= \frac{1}{4\pi^2} \int_{-\infty}^{\infty} \int_{-\infty}^{\infty} e^{-jk_z(z-z_0)} \\ &\times \int_{-\infty}^{\infty} \int_{-\infty}^{\infty} \tilde{p}_0(x_0, y_0, z_0) e^{j(k_x x_0 + k_y y_0)} dx_0 dy_0 e^{-j(k_x x + k_y y)} dk_x dk_y, \end{aligned} \quad (13.357)$$

where

$$k_z = \begin{cases} \sqrt{k^2 - k_x^2 - k_y^2}, & k_x^2 + k_y^2 \leq k^2 \\ -j\sqrt{k_x^2 + k_y^2 - k^2}, & k_x^2 + k_y^2 > k^2 \end{cases}. \quad (13.358)$$

We shall now reconstruct this equation by a different method in three simple steps. First, we take the spatial Fourier transform of the pressure in the z_0 -plane:

$$\tilde{P}(k_x, k_y, z_0) = \int_{-\infty}^{\infty} \int_{-\infty}^{\infty} \tilde{p}_0(x_0, y_0, z_0) e^{j(k_x x_0 + k_y y_0)} dx_0 dy_0. \quad (13.359)$$

The transformed pressure $\tilde{P}(k_x, k_y, z_0)$ contains no references to the spatial ordinates x and y . It is simply the wave-number spectra, each component of which represents a plane harmonic traveling wave, provided that the associated wave number is real. However, nonpropagating evanescent fields can exist, in which case the transform component represents a field of uniform phase that oscillates in time, but not in space, and decays exponentially with distance. Next, the wave-number spectra is propagated in k -space to the parallel z -plane by multiplying it with an exponent propagator term as follows

$$\tilde{P}(k_x, k_y, z_0, z) = e^{-jk_z(z-z_0)} \tilde{P}(k_x, k_y, z_0). \quad (13.360)$$

Over values of k_x and k_y for which k_z is real, the propagator is simply a phase term that does not affect the amplitude of the spectra. However, when k_z is imaginary, the propagator becomes a decaying exponent that when multiplied with the spectra represents nonpropagating evanescent waves. Finally, we take the inverse Fourier transform to construct the pressure field in the z -plane, which is essentially the sum of all the fields produced by each component of the wave-number spectra:

$$\tilde{p}(x, y, z) = \frac{1}{4\pi^2} \int_{-\infty}^{\infty} \int_{-\infty}^{\infty} \tilde{P}(k_x, k_y, z_0, z) e^{-j(k_x x + k_y y)} dk_x dk_y. \quad (13.361)$$

Combining Eq. (13.361) with Eqs. (13.358) and (13.360) gives Eq. (13.357). However, Eq. (13.361) has computational and interpretational advantages over the Rayleigh integral and is particularly amenable to the digital processing of sound fields captured by planar microphone arrays to calculate the entire sound field of interest.

The reverse problem

It turns out that we can apply exactly the same equations that were used for the forward problem, above, to the inverse problem, where the field is calculated for $z \leq z_0$ and all sources are also located in the region $z \leq z_0$. The only difference now is that over values of k_x and k_y for which k_z is imaginary, the propagator becomes a growing exponent because the nonpropagating evanescent waves increase in strength when approaching the sources.



13.20 TIME REVERSAL

Imagine that we place a planar array of microphones between a stage and an audience and then make a recording of a performance by musicians on the stage. We assume that the extent of the array is large enough to be considered infinite and that the microphones are small enough and far enough apart not to disturb the sound field produced. We also assume that the ratio of the smallest wavelength to the microphone pitch is large enough not to introduce spatial aliasing. If we play back the recording through an infinite array of either omnidirectional (monopole) or bidirectional (dipole) loudspeakers in place of the microphones (making the same assumptions as with the microphones), we will faithfully reproduce the concert when listening from the audience side of the array. However, if we listen from the stage side, we will not hear what was heard by the musicians, but that which was heard by the audience. Reproducing a sound field with sources in it is not so easy. Near-field acoustical holography, as described in the previous section, only provides a way to *calculate* the sound field on the stage side. In other words, we only have a virtual field, not a real one.

In time reversal, we play the recording backwards. Although this obviously makes no sense for music, it does have an interesting effect in the case of signals such as a continuous tone or an impulse. During the recording, an impulse arrives at the middle microphone first and then the ones on either side of that and works its way progressively toward the outermost microphones. During normal playback, the impulse leaves the loudspeakers in the same order as it arrived at the corresponding microphones, but if the recording is played backwards the sound emanates in reverse order starting from the outermost loudspeakers and finishing from the middle one. The effect of this is to focus the sound toward the source from which it was originally produced during the recording. If the sound was produced by a point source [see Eq. (4.71)], will the original source be faithfully reproduced?

To answer that question, let us now consider a simpler example. Suppose now that we have a spherical wave converging toward a point. If there is no source or sink at the focal point, the spherical wave will pass through the focal point and reemerge as a diverging wave. From Eq. (2.134) we have

$$\tilde{p}(r) = \tilde{A}_+ \frac{e^{-jkr}}{r} + \tilde{A}_- \frac{e^{jkr}}{r}, \quad (13.362)$$

where \tilde{A}_- is the amplitude of the sound pressure in the incoming wave at unit distance from the center of the sphere and \tilde{A}_+ is the same for the outgoing wave. To meet the boundary condition of pressure continuity, or zero pressure gradient, at the center, we set $\tilde{A}_+ = -\tilde{A}_-$ so that

$$\tilde{p}(r) = 2j\tilde{A}_- \frac{\sin kr}{r}. \quad (13.362)$$

The incoming wave is reflected back out again as if there were a rigid termination point at the center. To absorb it we have to place a point sink $-\tilde{A}_+e^{-jkr}/r$ at the center. It has been pointed out that, when time reversing the waves produced by dropping a pebble into a pond, a pebble must rise out of the water at the end of the sequence [44]. In the case of a plane wave, it is relatively straight forward to absorb it using a ρ_0c termination as was shown in Section 2.4. In the case of a converging spherical wave, the characteristic impedance is only approximately ρ_0c at a distance of several wavelengths from the center, as demonstrated by Eq. (2.144). At closer distances, the impedance is mainly massive. Therefore, a sphere whose surface impedance is ρ_0c can only be used as an acoustic sink to absorb an incoming spherical wave if it has a diameter of several wavelengths.

If we now return to the problem of the planar loudspeaker array, the same principle applies. In the absence of any acoustic sink, the waves converge on the point from which the sound originally emanated and reemerge on the opposite side. As they pass through the focal point, there is a transition from the positive phase angle of the converging wave to the negative phase angle of the diverging one [45]. Hence the imaginary part of the pressure field is zero in the plane of the focal point where the converging and diverging waves meet. In this way, the singularity of the original point source is removed and we are left with an approximation of it.

Problem 13.1. In Section 13.17, we derived the far-field directivity of a rectangular piston in an infinite baffle using the Bridge product theorem. Show that Eq. (13.318) may also be derived using the far-field Green's function of Eqs. (13.45) and (13.46) in the Rayleigh integral of Eq. (13.6), taking into account the double-strength source as illustrated in Fig. 13.4 for a circular piston. The rectangular piston lies in the xy plane with its center located at the origin of the rectangular coordinate system and oscillates with a velocity \tilde{u}_0 in the z -direction.

Hint: Use the integral $\int_{-l_x/2}^{l_x/2} e^{jkxx_0/R} dx_0 = \left[\frac{e^{jkxx_0/R}}{jkx/R} \right]_{-l_x/2}^{l_x/2} = \frac{\sin(kl_x x/2R)}{kx/2R}$ together with

$\sin \theta_1 = x/R$ and $\sin \theta_2 = y/R$. Show that the far-field pressure is of the form $\tilde{p}(x, y, z) = jkl_x l_y \rho_0 c \tilde{u}_0 \frac{e^{-jkR}}{2\pi R} D(\theta_x, \theta_y)$

Problem 13.2. In Section 13.17, we derived the radiation impedance of a rectangular piston in an infinite baffle from the far-field directivity using Bouwkamp's impedance theorem. Show that Eqs. (13.323) and (13.324) may also be derived using the

Fourier Green's function of Eqs. (13.33) and (13.34) in the Rayleigh integral of Eq. (13.6), taking into account the double-strength source as illustrated in Fig. 13.4 for a circular piston. The rectangular piston lies in the xy plane with its center located at the origin of the rectangular coordinate system and oscillates with a velocity \tilde{u}_0 in the z -direction.

Hint: Because the sinusoidal function is odd, the imaginary parts of the complex exponents cancel out over the positive and negative values of k_x and k_y in the infinite integrals. After evaluating the surface integrals to derive the expression for the specific impedance Z_s , use polar coordinates, where $k_x = kt \cos \phi$, $k_y = kt \sin \phi$, and $dk_x dk_y = k^2 t dt d\phi$, to reduce the double infinite integral to a single infinite one over t and a single finite one over ϕ . Then separate the infinite integral into real and imaginary parts to produce the resistance R_s and reactance X_s , respectively.

Problem 13.3. Use the Bridge product theorem to derive the far-field directivity pattern of four pistons of radius a in an infinite baffle regularly spaced in a straight line at intervals of d , where the directivity of an array of N point sources is given by Eq. (4.85) and that of a circular piston in an infinite baffle is given by Eq. (13.102). Use the identity $(\sin 4x)/(\sin x) = 4 \cos x \cos 2x$ and do not forget to include the ϕ dependency in Eq. (4.85) as was done in Section 13.8.

REFERENCES

- [1] Morse PM, Ingard KU. Theoretical acoustics. New York: McGraw-Hill; 1968. p. 319–21. It should be noted that their derivation uses a bounded Green's function which accounts for the reflections from the boundary which have nothing to do with the boundary integral.
- [2] Rayleigh JWS. The theory of sound, vol. II. New York: Dover; 1945. p. 107–9. Interestingly, Rayleigh derives Eqs. (13.27) and (13.28) by shrinking the volume integral of Eq. (13.25) down to a plane and then applying the appropriate boundary conditions in the plane.
- [3] Arfken GB, Weber HJ. Mathematical methods for physicists. 6th ed. Florida: Academic Press; 2005. p. 60. Eq. (1.101a), p. 61, Eq. (1.104).
- [4] Morse PM, Ingard KU. Theoretical acoustics. New York: McGraw-Hill; 1968. p. 364–5.
- [5] Lamb H. On the propagation of tremors over the surface of an elastic solid. Philos Trans R Soc London, Ser A 1904;203:1–42.
- [6] Sommerfeld A. Über die Ausbreitung der Wellen in der drahtlosen Telegraphie [On the propagation of waves in wireless telegraphy]. Ann Phys 1909;4(28):665–736.
- [7] Skudrzyk E. The foundations of acoustics: basic mathematics and basic acoustics. Wien: Springer-Verlag; 1971. p. 658.
- [8] Williams EG. Fourier acoustics: sound radiation and nearfield acoustical holography. San Diego: Academic Press; 1999.
- [9] Watson GN. A treatise on the theory of Bessel functions. 2nd ed. London: Cambridge University Press; 1944 [chapter XI].
- [10] Rayleigh JWS. The theory of sound, vol. II. New York: Dover; 1945. p. 107–62.
- [11] Chester Rice W, Kellogg Edward W. Notes on the development of a new type of hornless loudspeaker. Trans Am Inst Elec Eng 1925;44:461–75. Reprinted J Audio Eng Soc (1982);30(7/8):512–521. U.S. Patent No. 1,795,214.
- [12] King LV. On the acoustic radiation field of the piezoelectric oscillator and the effect of viscosity on the transmission. Can J Res 1934;11:135–46.

- [13] Mast TD, Yu F. Simplified expansions for radiation from a baffled circular piston. *J Acoust Soc Am* 2005;118(6):3457–64.
- [14] Stenzel H. Über die Berechnung des Schallfeldes einer kreisförmigen Kolbenmembran [On the calculation of the sound field of a circular piston diaphragm]. *Electr Nacr Tech* 1935;12:16–30.
- [15] Rayleigh JWS. *The theory of sound*, vol. II. New York: Dover; 1945. p. 138–46.
- [16] Kuntz HL. Radiated sound and the geometric nearfield. *Noise Control Eng J* 2008;56(4):269–81.
- [17] Mellow TJ. On the sound field of a resilient disk in free space. *J Acoust Soc Am* 2008;123(4):90–101.
- [18] Walker PJ. New developments in electrostatic loudspeakers. *J Audio Eng Soc* 1980;28(11):795–9.
- [19] Mellow TJ, Kärkkäinen LM. On the sound field of a circular membrane in free space and an infinite baffle. *J Acoust Soc Am* 2006;120(5):2460–77.
- [20] Bouwkamp CJ. Theoretical and numerical treatment of diffraction through a circular aperture. *IEEE Trans Antennas Propag* 1970;18(2):152–76. This is a translation of his PhD dissertation originally published in Dutch in 1941.
- [21] Mellow TJ. On the sound field of a resilient disk in an infinite baffle. *J Acoust Soc Am* 2006;120(1):90–101.
- [22] Spence RD. A note on the Kirchhoff approximation in diffraction theory. *J Acoust Soc Am* 1949;21(2):98–100.
- [23] Streng JH. Calculation of the surface pressure on a vibrating circular stretched membrane in free space. *J Acoust Soc Am* 1987;82(2):679–86.
- [24] Aarts RM, Janssen AJEM. On-axis and far-field sound radiation from resilient flat and dome-shaped radiators. *J Acoust Soc Am* 2009;125(3):1444–55.
- [25] Mellow TJ, Kärkkäinen LM. Comparison of spheroidal and eigenfunction-expansion trial functions for a membrane in an infinite baffle. *J Acoust Soc Am* 2008;123(5):2598–602.
- [26] Mellow TJ, Kärkkäinen LM. On the sound field of an oscillating disk in an open and closed circular baffle. *J Acoust Soc Am* 2005;118(3):1311–25.
- [27] Mellow TJ, Kärkkäinen LM. A dipole loudspeaker with a balanced directivity pattern. *J Acoust Soc Am* 2010;128(5):2749–57.
- [28] Nimura T, Watanabe Y. Effect of a finite circular baffle board on acoustic radiation. *J Acoust Soc Am* 1952;25(1):76–80.
- [29] Sommerfeld A. Die frei schwingende Kolbenmembran [The freely oscillating piston membrane]. *Ann Phys* 1942/3;5(42):389–420.
- [30] Meixner J, Fritze U. Das Schallfeld in der Nähe einer frei schwingenden Kolbenmembran [The sound field in the vicinity of a freely oscillating piston diaphragm]. *Z Angew Physik* 1949;1:535–42.
- [31] Wiener FM. On the relation between the sound fields radiated and diffracted by plane obstacles. *J Acoust Soc Am* 1951;23(6):697–700.
- [32] Mellow TJ, Kärkkäinen LM. On the sound field of an oscillating disk in an open and closed circular baffle. *J Acoust Soc Am* 2005;118(3):1–15.
- [33] Levine H, Schwinger J. On the radiation of sound from an unflanged circular pipe. *Phys Rev* February 15, 1948;73:383–406.
- [34] Babinet J. Mémoires d'optique météorologique [Memoirs on meteorological optics]. *C R Acad Sci Paris* 1837;4:638.
- [35] Kirchhoff G. Zur Theorie der Lichtstrahlen [On the theory of light radiation]. *Sitz-Ber kgl preuß Akad Wiss June 22, 1882:641–69.*
- [36] Bouwkamp CJ. A contribution to the theory of acoustic radiation. *Philips Res Rep* 1945;1:251–77.
- [37] Lipshitz SP, Scott TC, Salvy B. On the acoustic impedance of baffled strip radiators. *J Audio Eng Soc* 1995;43(7/8):573–80.
- [38] Mellow TJ, Kärkkäinen LM. On the sound fields of infinitely long strips. *J Acoust Soc Am* 2011;130(1):153–67.
- [39] Stenzel H. Die akustische Strahlung der rechteckigen Kolbenmembran [The acoustic radiation of the rectangular piston diaphragm]. *Acustica* 1952;2:263–81.
- [40] Mellow TJ, Kärkkäinen LM. Expansions for the radiation impedance of a rectangular piston in an infinite baffle. *J Acoust Soc Am* 2016;140(4):2867–75.

- [41] Pritchard RL. Mutual acoustic impedance between radiators in an infinite baffle. *J Acoust Soc Am* 1960;32(6):730–7. The paper also includes an illustrative example of how the mutual radiation impedance can be calculated for a seven-piston hexagonal array.
- [42] Porter DT. Two FORTRAN programs for computing electroacoustical behavior of transmitting sonar arrays. U.S. Navy Underwater Sound Lab; 1967. Rep No. 791.
- [43] Thompson Jr W. The computation of self- and mutual-radiation impedances for annular and elliptical pistons using Bouwkamp's integral. *J Sound Vib* 1971;17(2):221–33.
- [44] Anderson BE, Griffa M, Larmar C, Ulrich AJ, Johnson PA. Timing reversal. *Acoust Today* 2008;4(1):5–15.
- [45] Mellow TJ, Kärkkäinen LM. Expansions for infinite or finite plane circular time-reversal mirrors and acoustic curtains for wave-field-synthesis. *J Acoust Soc Am* 2014;135(3):1256–77.
- [46] Zeitler B, Zeitler E. The field of sound of a circular membrane. *J Acoust Soc Am* 2004;116(2):916–7.
- [47] Backhaus H, Trendelenburg F. Ueber die richtwirkung von kolbenmembranen (On the directivity of piston membranes). *Z Tech Phys (Leipzig)* 1927;7:630.
- [48] Poletti MA. Spherical expansions of sound radiation from resilient and rigid disks with reduced error. *J Acoust Soc Am* 2018;144(3):1180–9.
- [49] Bouwkamp CJ. On integrals occurring in the theory of diffraction of electromagnetic waves by a circular disk. *Proc Koninklijke Nederl Akademie Wetenschappen Ser A Math Sci* 1950;53(5):654–61. <http://www.dwc.knaw.nl/DL/publications/PU00018814.pdf>.
- [50] Aarts RM, Janssen AJEM. Sound radiation quantities arising from a resilient circular radiator. *J Acoust Soc Am* 2009;126(4):1776–87.
- [51] Rdzanek WP. Sound scattering and transmission through a circular cylindrical aperture revisited using the radial polynomials. *J Acoust Soc Am* 2018;143(3):1259–82. See Appendix E.

Vibroacoustics (membranes, plates, and shells)

PART XXXVIII: MEMBRANES

14.1 INTRODUCTION TO VIBROACOUSTICS

Apart from a brief overview of loudspeaker diaphragm behavior in Section 6.14, until now we have treated all sound sources as if they were either perfectly rigid or perfectly flexible (resilient). Real diaphragms, of course, fall somewhere between these two extremes in their behavior. Until now, we have concentrated on airborne waves (or sound fields) radiating from sound sources into free space or confined within cavities or ducts. Vibroacoustics is the subject that deals with waves within structures such as membranes, plates, and shells. We shall begin with membranes, which are plates so thin that they can be treated as if they have zero-bending stiffness. Membranes are used as diaphragms in high-end electrostatic or planar-magnetic loudspeakers. However, unlike a resilient disk, which we treated in Section 13.8 and 13.9, a membrane is clamped at its perimeter and can therefore support standing waves. Plates are slightly more complicated because they have finite bending stiffness. We will examine how these can be used as loudspeaker diaphragms in Section 14.19, but for now we will simply calculate their modes with various boundary conditions.

The third kind of structure we shall consider is the spherical shell which is the most common kind of diaphragm and is found in devices ranging from microspeakers to hi-fi dome tweeters. These are more rigid than plates for the same thickness and therefore resonate at higher frequencies. We will examine the behavior of membranes, plates, and shells as loudspeaker diaphragms fully coupled into their surrounding air loads. Hence, we will introduce the concept of *fluid–structure interaction*.

14.2 MEMBRANE WAVE EQUATION IN RECTANGULAR COORDINATES

A membrane is normally pretensioned, so we will define a force per unit length T that we can assume to be uniformly distributed throughout the membrane. As we shall see, the membrane tension is analogous to static pressure in the case of pressure waves in

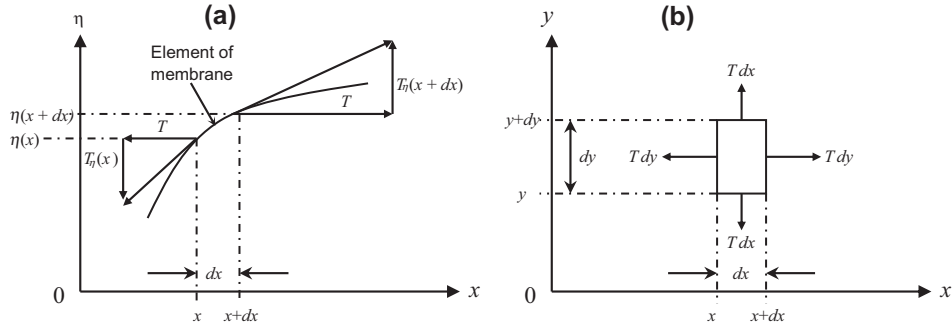


Figure 14.1 Membrane element in rectangular coordinates shown as (a) cross section and (b) from above.

air as it determines the restoring force. Although pressure waves in air are *longitudinal*, in a membrane we have *transverse* waves. In other words, the displacement η at each point is normal to the direction of travel rather than back and forth in the direction of travel. Let the density of the membrane be ρ_D and its thickness be h . Referring to Fig. 14.1, we wish to find the restoring force F_x acting on the element of the membrane when it is displaced from the position of equilibrium (at $\eta = 0$). The net restoring force is proportional to the difference between the normal components $T_\eta(x + dx)$ and $T_\eta(x)$ of the tension T at the points $x + dx$ and x , respectively.

We can write

$$\begin{aligned}
 F_\eta(x) &= (T_\eta(x + dx) - T_\eta(x)) dy \\
 &= T \left(\frac{\partial}{\partial x} \eta(x + dx) - \frac{\partial}{\partial x} \eta(x) \right) dy \\
 &= T \frac{\partial^2 \eta}{\partial x^2} dx dy.
 \end{aligned} \tag{14.1}$$

The second-order differential in (Eq. 14.1) is termed the *curvature* of the membrane and is equal to the inverse of the radius of curvature. Similarly, the restoring force in the y direction is given by

$$\begin{aligned}
 F_\eta(y) &= (T_\eta(y + dy) - T_\eta(y)) dx \\
 &= T \left(\frac{\partial}{\partial y} \eta(y + dy) - \frac{\partial}{\partial y} \eta(y) \right) dx \\
 &= T \frac{\partial^2 \eta}{\partial y^2} dx dy.
 \end{aligned} \tag{14.2}$$

In accordance with Newton's second law, the sum of the restoring forces must equal the element's mass $\rho_D h dx dy$ times its normal acceleration. Hence

$$F_\eta(x) + F_\eta(y) = T \left(\frac{\partial^2 \eta}{\partial x^2} + \frac{\partial^2 \eta}{\partial y^2} \right) dx dy = \rho_D h \frac{\partial^2 \eta}{\partial t^2} dx dy. \quad (14.3)$$

The wave equation for the membrane in rectangular coordinates is therefore

$$\nabla^2 \eta = \frac{1}{c_D^2} \frac{\partial^2 \eta}{\partial t^2}, \quad (14.4)$$

where the Laplace operator ∇^2 is given by

$$\nabla^2 = \frac{\partial^2}{\partial x^2} + \frac{\partial^2}{\partial y^2} \quad (14.5)$$

and the speed of sound in the membrane c_D is given by

$$c_D = \sqrt{\frac{T}{\rho_D h}} \quad (14.6)$$

In the steady state, we replace the first time derivative in (Eq. 14.4) with $j\omega$ to obtain

$$(\nabla^2 + k_D^2) \tilde{\eta} = 0, \quad (14.7)$$

where the wavenumber k_D of the membrane is given by

$$k_D = \frac{\omega}{c_D} = \sqrt{k_x^2 + k_y^2}. \quad (14.8)$$

The general form of this wave equation is the same as the Helmholtz wave equation for sound pressure waves given by Eq. (2.146) except that the speed of sound is different, and the z -term is missing from the Laplace operator because here we have a 2-dimensional wave instead of a 3-dimensional one. Hence, the general unbounded solution is

$$\tilde{\eta}(x, y) = \tilde{\eta}_+ e^{-j(k_x x + k_y y)} + \tilde{\eta}_- e^{j(k_x x + k_y y)}. \quad (14.9)$$



14.3 SOLUTION OF THE MEMBRANE WAVE EQUATION FOR A RECTANGULAR MEMBRANE

Consider a finite rectangular membrane of dimensions l_x and l_y , which is clamped at its perimeter, where $x = 0$ or l_x and $y = 0$ or l_y , so that we have the boundary conditions

$$\tilde{\eta}(x, 0) = \tilde{\eta}(x, l_y) = \tilde{\eta}(0, y) = \tilde{\eta}(l_x, y) = 0. \quad (14.10)$$

Only modes that satisfy these boundary conditions can exist so that

$$k_x = m\pi/l_x \quad (14.11)$$

$$k_y = n\pi/l_y. \quad (14.12)$$

Hence, the solution of Eq. (14.7) for a finite rectangular membrane is the form of an *eigenfunction* expansion

$$\tilde{\eta}(x, y) = \sum_{m=1}^{\infty} \sum_{n=1}^{\infty} \tilde{A}_{mn} \sin\left(\frac{m\pi x}{l_x}\right) \sin\left(\frac{n\pi y}{l_y}\right) \quad (14.13)$$

where the products of the two cosine terms for each value of m and n are the *eigenfunctions* and the expansion coefficients \tilde{A}_{mn} depend on the excitation conditions. Although an infinite membrane can support any frequency, just like open space, a finite membrane that is clamped at its perimeter can only support specific frequencies, known as *eigenfrequencies*. In the case of a rectangular membrane, these are given by

$$f_{mn} = \frac{\omega_{mn}}{2\pi} = \frac{c_D}{2} \sqrt{\left(\frac{m}{l_x}\right)^2 + \left(\frac{n}{l_y}\right)^2}, \quad (14.14)$$

which has a similar form to Eq. (10.5) for the eigenfrequencies of pressure waves within a rectangular enclosure.

14.4 MODES OF A RECTANGULAR MEMBRANE

The eigenfunctions $\sin(m\pi x/l_x) \sin(n\pi y/l_y)$ are plotted in Fig. 14.2.

14.5 GREEN'S FUNCTION FOR A RECTANGULAR MEMBRANE

So far, we have only solved the *homogeneous* membrane wave equation (see Eq. 14.7) to find out what vibration modes may be possible, but which ones will actually be excited depends on the specific driving conditions. Different modes will occur depending on whether the membrane is driven with a uniform pressure distribution, for example, or a driving velocity is applied at a point off-center. Let us now write an *inhomogeneous* membrane equation by adding an arbitrary driving pressure distribution $\tilde{p}_0(x, y)$ to the *homogeneous* one of Eq. (14.7)

$$(\nabla^2 + k_D^2)\tilde{\eta}(x, y) = -\frac{\tilde{p}_0(x, y)}{T}, \quad (14.15)$$

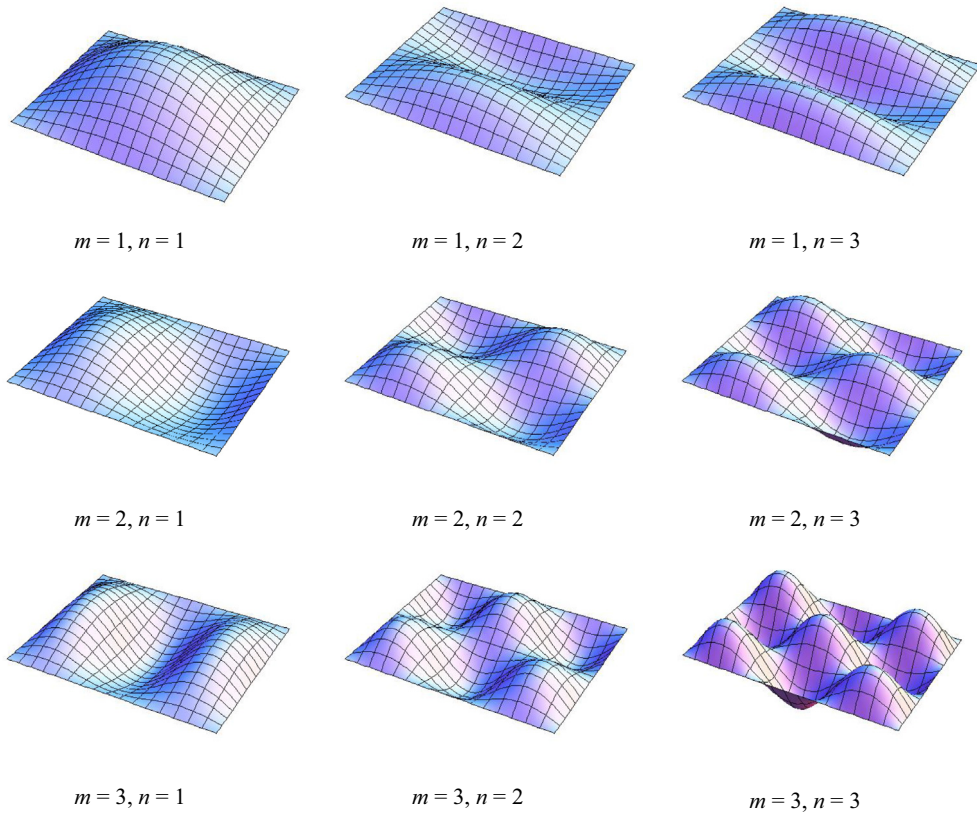


Figure 14.2 Eigenfunctions of a rectangular membrane.

where

$$\nabla^2 \tilde{\eta}(x, y) = -\pi^2 \left(\frac{m^2}{l_x^2} + \frac{n^2}{l_y^2} \right) \tilde{\eta}(x, y) \quad (14.16)$$

We then multiply both sides by a normalizing function, which in this case is $\sin(p\pi x/l_x) \sin(q\pi y/l_y)$, and integrate over the surface of the membrane

$$\begin{aligned} & \left(k_D^2 - \pi^2 \left(\frac{m^2}{l_x^2} + \frac{n^2}{l_y^2} \right) \right) \sum_{m=1}^{\infty} \sum_{n=1}^{\infty} \tilde{A}_{mn} \int_0^{l_x} \sin\left(\frac{m\pi x}{l_x}\right) \sin\left(\frac{p\pi x}{l_x}\right) dx \int_0^{l_y} \sin\left(\frac{n\pi y}{l_y}\right) \sin\left(\frac{q\pi y}{l_y}\right) dy \\ &= -\frac{1}{T} \int_0^{l_y} \int_0^{l_x} \tilde{p}_0(x, y) \sin\left(\frac{p\pi x}{l_x}\right) \sin\left(\frac{q\pi y}{l_y}\right) dx dy. \end{aligned} \quad (14.17)$$

Using the orthogonal integral from Eq. (A2.57) of Appendix II

$$\int_0^{l_x} \sin\left(\frac{m\pi x}{l_x}\right) \sin\left(\frac{p\pi x}{l_x}\right) dx = \begin{cases} 0, & m \neq p \\ (1 - \delta_{m0})l_x/2, & m = p, \end{cases} \quad (14.18)$$

together with the same integral with m, p, x , and l_x exchanged for n, q, γ , and l_y , yields

$$\tilde{A}_{mn} = \frac{4}{T(k_{mn}^2 - k_D^2)l_x l_y} \int_0^{l_y} \int_0^{l_x} \tilde{P}_0(x, \gamma) \sin\left(\frac{m\pi x}{l_x}\right) \sin\left(\frac{n\pi \gamma}{l_y}\right) dx d\gamma, \quad (14.19)$$

where

$$k_{mn} = \pi \sqrt{\frac{m^2}{l_x^2} + \frac{n^2}{l_y^2}}. \quad (14.20)$$

Hence, the displacement $\tilde{\eta}(w, \phi)$ for a given pressure distribution $\tilde{p}_0(w_0, \phi_0)$ is

$$\begin{aligned} \tilde{\eta}(x, \gamma) &= \frac{4}{T} \sum_{m=1}^{\infty} \sum_{n=1}^{\infty} \frac{\sin(m\pi x/l_x) \sin(n\pi \gamma/l_y)}{(k_{mn}^2 - k_D^2)l_x l_y} \\ &\quad \times \int_0^{l_y} \int_0^{l_x} \tilde{p}_0(x_0, \gamma_0) \sin(m\pi x_0/l_x) \sin(n\pi \gamma_0/l_y) dx_0 d\gamma_0 \end{aligned} \quad (14.21)$$

This can also be written as

$$\tilde{\eta}(x, \gamma) = \frac{1}{T} \int_0^{l_y} \int_0^{l_x} \tilde{p}_0(x_0, \gamma_0) G(x, \gamma|x_0, \gamma_0) dx_0 d\gamma_0, \quad (14.22)$$

where $G(x, \gamma|x_0, \gamma_0)$ is the Green's function for the membrane given by

$$G(x, \gamma|x_0, \gamma_0) = 4 \sum_{m=1}^{\infty} \sum_{n=1}^{\infty} \frac{\sin(m\pi x/l_x) \sin(n\pi \gamma/l_y) \sin(m\pi x_0/l_x) \sin(n\pi \gamma_0/l_y)}{(k_{mn}^2 - k_D^2)l_x l_y}, \quad (14.23)$$

which can be shown to satisfy the inhomogeneous wave equation for excitation by a point source at (x_0, γ_0)

$$(\nabla^2 + k_D^2) G(x, \gamma|x_0, \gamma_0) = -\delta(x - x_0)\delta(\gamma - \gamma_0). \quad (14.24)$$

Notice that the Dirac delta functions on the right-hand side denotes a concentrated point excitation at (x_0, γ_0) in a similar manner to the point source in space described by the Green's function of Eqs. (13.16) and (13.17). However, in this case we have a *bounded* Green's function denoted by the upper case G.

14.6 MEMBRANE WAVE EQUATION IN POLAR COORDINATES

As the Laplace operator of Eq. (14.5) is the same as that of the wave equation in three dimensions given by Eq. (2.147) but without the z -term, it follows that the Laplace operator for the membrane in polar coordinates, which is given by

$$\nabla^2 = \frac{\partial^2}{\partial w^2} + \frac{1}{w} \frac{\partial}{\partial w} + \frac{1}{w^2} \frac{\partial^2}{\partial \phi^2}. \quad (14.25)$$

A rigorous derivation of this is given in Ref. [1]. Following the same procedure as in Section 2.10, where we separate the wave equation into its radial and angular (azimuthal) parts, we arrive at the solution to the homogeneous membrane wave equation

$$(\nabla^2 + k_D^2)\tilde{\eta}(w, \phi) = 0. \quad (14.26)$$

The general unbounded solution is

$$\tilde{\eta}_m(w, \phi) = (\tilde{A}_m \cos(m\phi) + \tilde{B}_m \sin(m\phi)) \left(\tilde{\eta}_+ H_m^{(2)}(k_D w) + \tilde{\eta}_- H_m^{(1)}(k_D w) \right). \quad (14.27)$$

14.7 SOLUTION OF THE MEMBRANE WAVE EQUATION FOR A CIRCULAR MEMBRANE

Consider a finite circular membrane of radius a with its center at the origin, which is clamped at its perimeter, where $w = a$, so that we have the boundary condition

$$\tilde{\eta}(a, \phi) = 0. \quad (14.28)$$

We assume that the membrane is continuous at the center so that we can disregard the Neumann functions in Eq. (14.27). These would only be needed in special cases such as an annular membrane. Hence, the Hankel functions reduce to a Bessel function. Only modes that satisfy these boundary conditions can exist so that

$$k_D = \alpha_{mn}/a, \quad (14.29)$$

where α_{mn} are zeros of the Bessel function such that $J_m(\alpha_{mn}) = 0$. Hence, the solution to Eq. (14.26) for a finite circular membrane is in the form of an eigenfunction expansion

$$\tilde{\eta}(w, \phi) = \sum_{m=0}^{\infty} \sum_{n=1}^{\infty} (\tilde{A}_{mn} \cos(m\phi) + \tilde{B}_{mn} \sin(m\phi)) J_m(\alpha_{mn} w/a), \quad (14.30)$$

where the expansion coefficients \tilde{A}_{mn} and \tilde{B}_{mn} depend on the excitation conditions. Here we shall assume $\tilde{B}_{mn} = 0$. Some eigenvalues are given in Table 14.1.

Table 14.1 Zeros α_{mn} of the Bessel function $J_m(\alpha_{mn})$

α_{01}	2.4048	α_{02}	5.5201	α_{03}	8.6537	α_{04}	11.792
α_{11}	3.8317	α_{12}	7.0156	α_{13}	10.173	α_{14}	13.324
α_{21}	5.1356	α_{22}	8.4172	α_{23}	11.620	α_{24}	14.796
α_{31}	6.3802	α_{32}	9.7610	α_{33}	13.015	α_{34}	16.223

For large values

$$\alpha_{mn}|_{n \rightarrow \infty} = \left(\frac{m}{2} + n - \frac{1}{4} \right) \pi. \quad (14.31)$$

The eigenfrequencies are given by

$$f_n = \frac{\omega_n}{2\pi} = \frac{c_D \alpha_{mn}}{2\pi a}. \quad (14.32)$$

where the speed of sound in the membrane c_D is given by Eq. (14.6).



14.8 MODES OF A CIRCULAR MEMBRANE [2]

The eigenfunctions $\cos(m\phi)J_m(\alpha_{mn}w/a)$ are plotted in Fig. 14.3. The modes for $m = 0$ are known as *axisymmetric* modes and the values of α_{0n} for these are given in the first row of Table 14.1.



14.9 GREEN'S FUNCTION FOR A CIRCULAR MEMBRANE

Let us now write an *inhomogeneous* membrane equation by adding a driving pressure distribution $\tilde{p}_0(w, \phi)$ to the *homogeneous* one of Eq. (14.26)

$$(\nabla^2 + k_D^2)\tilde{\eta}(w, \phi) = -\frac{\tilde{p}_0(w, \phi)}{T}, \quad (14.33)$$

where

$$\tilde{\eta}(w, \phi) = \sum_{m=0}^{\infty} \sum_{n=1}^{\infty} \tilde{A}_{mn} \cos(m\phi) J_m(\alpha_{mn}w/a). \quad (14.34)$$

Using the recursion formulas of Eqs. (A2.83) and (A2.84) from Appendix II it can be shown that

$$\nabla^2 \tilde{\eta}(w, \phi) = -\frac{\alpha_{mn}^2}{a^2} \tilde{\eta}(w, \phi). \quad (14.35)$$

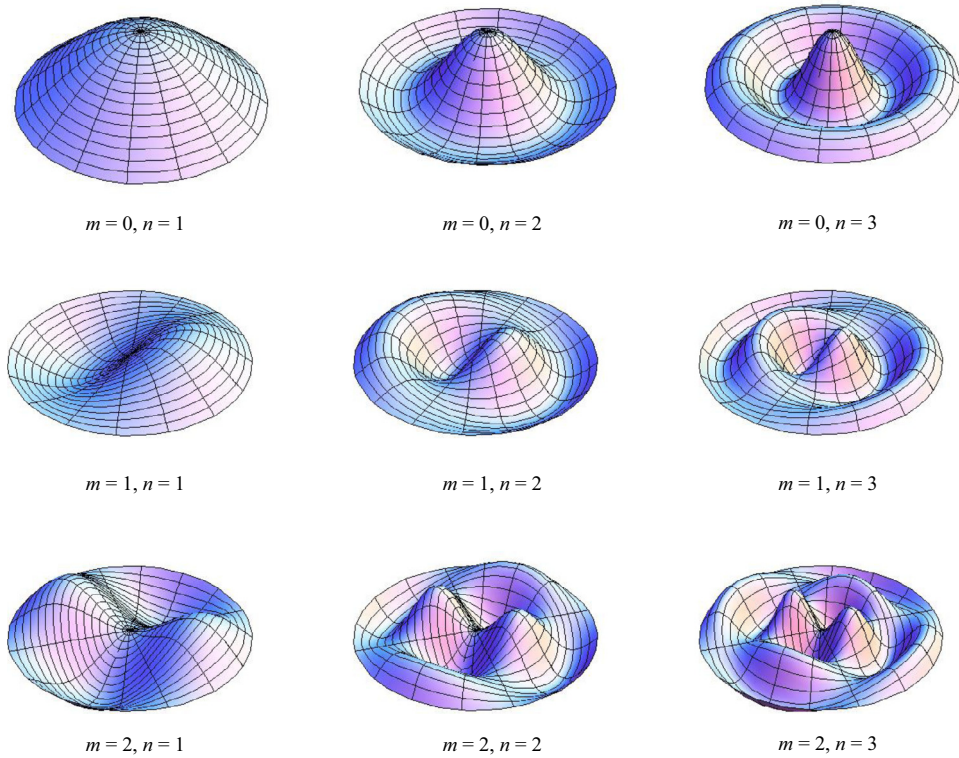


Figure 14.3 Eigenfunctions of a circular membrane.

From Eqs. (14.6) and (14.8), the wave number for the membrane is

$$k_D = \frac{\omega}{c_D} = \omega \sqrt{\frac{\rho_D h}{T}}. \quad (14.36)$$

The tension T is included in the denominator on the right-hand side of Eq. (14.33) to ensure consistency of units on both sides of the equation. As usual, we multiply both sides by a normalizing function, which in this case is $\cos(p\phi)J_p(\alpha_{pq}w/a)$, and integrate over the surface of the membrane

$$\begin{aligned} & \sum_{m=0}^{\infty} \sum_{n=1}^{\infty} \tilde{A}_{mn} \left(k_D^2 - \frac{\alpha_{mn}^2}{a^2} \right) \int_0^{2\pi} \cos(m\phi) \cos(p\phi) d\phi \int_0^a J_m(\alpha_{mn}w/a) J_p(\alpha_{pq}w/a) w dw \\ &= -\frac{1}{T} \int_0^{2\pi} \int_0^a \tilde{p}_0(w, \phi) \cos(p\phi) J_p(\alpha_{pq}w/a) w dw d\phi. \end{aligned} \quad (14.37)$$

Using the orthogonal integrals from Eqs. (A2.56) and (A2.101) of Appendix II

$$\int_0^{2\pi} \cos(m\phi)\cos(p\phi)d\phi = \begin{cases} 0, & m \neq p \\ (1 + \delta_{m0})\pi, & m = p \end{cases} \quad (14.38)$$

$$\int_0^a J_m(\alpha_{mn}w/a)J_m(\alpha_{mq}w/a)wdw = \begin{cases} 0, & n \neq q \\ a^2 J_{m+1}^2(\alpha_{mn})/2, & n = q \end{cases} \quad (14.39)$$

yields

$$\tilde{A}_{mn} = \frac{2 \int_0^{2\pi} \int_0^a \tilde{p}_0(w, \phi)\cos(m\phi)J_m(\alpha_{mn}w/a)wdwd\phi}{\pi T(1 + \delta_{m0})(\alpha_{mn}^2 - k_D^2 a^2)J_{m+1}^2(\alpha_{mn})}. \quad (14.40)$$

Hence, the displacement $\tilde{\eta}(w, \phi)$ for a given pressure distribution $\tilde{p}_0(w_0, \phi_0)$ is

$$\begin{aligned} \tilde{\eta}(w, \phi) &= \frac{2}{\pi T} \sum_{m=0}^{\infty} \sum_{n=1}^{\infty} \frac{\cos(m\phi)J_m(\alpha_{mn}w/a)}{(1 + \delta_{m0})(\alpha_{mn}^2 - k_D^2 a^2)J_{m+1}^2(\alpha_{mn})} \\ &\quad \times \int_0^{2\pi} \int_0^a \tilde{p}_0(w_0, \phi_0)\cos(m\phi_0)J_m(\alpha_{mn}w_0/a)w_0dw_0d\phi_0. \end{aligned} \quad (14.41)$$

This can also be written as

$$\tilde{\eta}(w, \phi) = \frac{1}{T} \int_0^{2\pi} \int_0^a \tilde{p}_0(w_0, \phi_0)G(w, \phi|w_0, \phi_0)w_0dw_0d\phi_0, \quad (14.42)$$

where $G(w, \phi|w_0, \phi_0)$ is the Green's function for the membrane given by

$$G(w, \phi|w_0, \phi_0) = \frac{2}{\pi} \sum_{m=0}^{\infty} \sum_{n=1}^{\infty} \frac{\cos(m\phi)J_m(\alpha_{mn}w/a)\cos(m\phi_0)J_m(\alpha_{mn}w_0/a)}{(1 + \delta_{m0})(\alpha_{mn}^2 - k_D^2 a^2)J_{m+1}^2(\alpha_{mn})}, \quad (14.43)$$

which can be shown to satisfy the inhomogeneous wave equation [1] for excitation by a point source at (w_0, ϕ_0)

$$(\nabla^2 + k_D^2)G(w, \phi|w_0, \phi_0) = -\frac{1}{w}\delta(w - w_0)\delta(\phi - \phi_0). \quad (14.44)$$



14.10 RADIATION FROM A CIRCULAR MEMBRANE WITHOUT A BAFFLE—ANALYTICAL MODEL OF AN ELECTROSTATIC LOUDSPEAKER COUPLED TO ITS SURROUNDING AIR [3]

In this section, we will introduce the concept of fluid—structure coupling. So far, we have only considered sound radiation from a pure pressure source in free space as if the uniform electrostatic force were driving the air particles directly without any structure, as described in Section 13.8 under the heading “Radiation from a resilient circular disk without a baffle”. However, a real membrane has mass and stiffness, because of its tension, as well as the boundary condition of zero velocity at its perimeter where it is clamped. Without this boundary condition, the velocity of the resilient disk was infinite at the perimeter.

Also, in the previous section, we only considered the behavior of the membrane in vacuum. When surrounded by a fluid medium such as air, there is a strong and highly localized interaction between the membrane and the surrounding air. The radiation mass, which is usually considerably greater than the mass of the membrane, lowers the lowest resonance frequencies while the radiation resistance damps the higher ones. Hence the membrane and free space wave equations must be solved simultaneously. Using the Fourier free-space Green’s function enables all the integrals to be evaluated analytically and thus avoids numerical integration.

Boundary conditions

The membrane of radius a lies in the xy plane, as shown in Fig. 13.8, with its center at the origin and the uniform driving pressure \tilde{p}_1 is applied to its surface in the z direction. The pressure field on one side of the xy plane is the symmetrical “negative” of that on the other, so that

$$\tilde{p}(w, z) = -\tilde{p}(w, -z). \quad (14.45)$$

Consequently, there is a *Dirichlet* boundary condition in the plane of the membrane where these equal and opposite fields meet, so that

$$\tilde{p}(w, 0) = 0, \quad w \geq a. \quad (14.46)$$

On the front and rear outer surfaces of the membrane, there is the coupling condition

$$\begin{aligned} \left. \frac{\partial}{\partial z} \tilde{p}(w, z) \right|_{z=0\pm} &= -jk\rho c \tilde{u}_0(w), \\ &= k^2 \rho_0 c^2 \tilde{\eta}(w), \quad 0 \leq w \leq a, \end{aligned} \quad (14.47)$$

where $\tilde{u}_0(w)$ is the normal particle velocity in the z direction at the surfaces, $\tilde{\eta}(w)$ is the membrane displacement, and k is the wave number given by

$$k = \frac{\omega}{c} = \frac{2\pi}{\lambda}, \quad (14.48)$$

ω is the angular frequency of excitation, ρ_0 is the density of air or any other surrounding medium, c is the speed of sound in that medium, and λ is the wavelength. We will represent the unknown surface pressure distribution $\tilde{p}_+(w_0)$ by a power-series trial or basis function [4,5], which is itself based on a solution to the free-space wave equation in oblate spheroidal coordinates [6].

$$\tilde{p}_+(w_0) = -\tilde{p}_-(w_0) = \frac{\tilde{p}_I}{2} \sum_{n=0}^{\infty} A_n \left(n + \frac{3}{2} \right) \left(1 - \frac{w_0^2}{a^2} \right)^{n+1/2}, \quad (14.49)$$

where \tilde{A}_n are the power-series coefficients, which have to be solved for. Notice that the surface pressure is zero at $w_0 = a$, which satisfies the boundary condition of Eq. (14.46).

Wave equation for the membrane in free space

The construction of the electrostatic loudspeaker is shown in Fig. 14.4, with stationary electrodes on either side of the membrane, each at a distance d from it. The membrane is assumed to be circular with a radius a , and its conductive coating is charged by the polarizing voltage E_P via the high-value resistor R_B which keeps the membrane charge reasonably constant at all but the very lowest frequencies. The inhomogeneous steady-state wave equation for the displacement $\tilde{\eta}(w)$ of the circular membrane, which is clamped at its perimeter, can be written with the inherent membrane forces on the left and the external forces on the right

$$(T\nabla^2 - j\omega z_s - \omega^2 \rho_D h) \tilde{\eta}(w) = \tilde{p}_+(w) - \tilde{p}_-(w) - \tilde{p}_I, \quad \tilde{\eta}(a) = 0, \quad (14.50)$$

where the Laplace operator is given by

$$\nabla^2 = \frac{\partial^2}{\partial w^2} + \frac{1}{w} \frac{\partial}{\partial w}, \quad (14.51)$$

and $\tilde{p}_+(w)$ and $\tilde{p}_-(w)$ are the front and rear pressure distributions, respectively, due to the surrounding acoustic medium, T is the tension (which is evenly distributed throughout the membrane), ρ_D is the density of the membrane material, and h is its thickness. The driving pressure \tilde{p}_I is related to the input voltage \tilde{e}_{in} by

$$\tilde{p}_I = \frac{\beta}{S_D} \tilde{e}_{in}, \quad (14.52)$$

where β is the electromechanical conversion factor, which is given by

$$\beta = 2C_{ED} \frac{E_P}{d}, \quad (14.53)$$

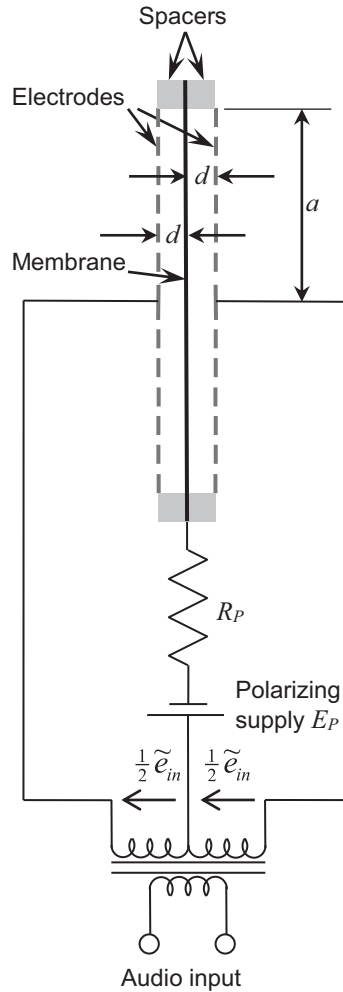


Figure 14.4 Construction of electrostatic loudspeaker.

and the interelectrode capacitance of the loudspeaker is given by

$$C_{ED} = \frac{\epsilon_0 S_D}{2d}, \quad (14.54)$$

where S_D is the membrane surface area, given by $S_D = \pi a^2$, and ϵ_0 is the permittivity of free space. The arbitrary specific acoustic impedance z_s is defined by

$$z_s = R_S + j\omega M_S - \frac{\beta^2}{i\omega C_{ED} S_D}, \quad (14.55)$$

where R_S and M_S are the distributed resistance and mass respectively of the dust screen (not shown) and perforations in the electrodes either side of the membrane, which are usually designed to damp its vibration modes. For this analysis, it is assumed that the mass is negligible and that the resistance is linear and will not vary with frequency. The remaining term is the “negative impedance” that results from the increase in electrostatic attraction toward each electrode as the membrane approaches it. We rewrite Eq. (14.50) in the “Helmholtz” form using the modified diaphragm wavenumber k'_D as follows

$$(\nabla^2 + k_D'^2)\tilde{\eta} = \frac{1}{T}(\tilde{p}_+(w) - \tilde{p}_-(w) - \tilde{p}_I), \quad \tilde{\eta}(a) = 0, \quad (14.56)$$

where

$$k_D' = k_D \sqrt{1 - j \frac{z_S}{k_D(k) \sqrt{\rho_D h T}}}, \quad (14.57)$$

$$k_D = \omega/c_D = kc/c_D, \quad (14.58)$$

and

$$c_D = \sqrt{\frac{T}{\rho_D h}}, \quad (14.59)$$

where c_D is the speed of sound in the membrane.

Solution of the membrane wave equation

The solution to membrane wave equation, Eq. (14.56), subject to the edge constraint $\tilde{\eta}(a) = 0$, is given by Eq. (14.30), but with the azimuthal ordinate ϕ suppressed because of axial symmetry.

$$\tilde{\eta}(w) = \frac{1}{T} \int_0^{2\pi} \int_0^a (\tilde{p}_+(w_0) - \tilde{p}_-(w_0) - \tilde{p}_I) G(w|w_0) w_0 dw_0 d\phi_0. \quad (14.60)$$

We rewrite the Green's function of Eq. (14.43) for the membrane using the modified wavenumber k'_D as follows

$$G(w|w_0) = \frac{1}{\pi} \sum_{m=1}^{\infty} \frac{J_0(\alpha_m w/a) J_0(\alpha_m w_0/a)}{J_1^2(\alpha_m) (\alpha_m^2 - k_D'^2 a^2)}, \quad 0 \leq w \leq a, \quad (14.61)$$

where α_m is the m th zero of $J_0(k'_D a)$ such that $J_0(k'_D a) = 0$ when $k'_D a = \alpha_m$. Inserting Eqs. (14.45), (14.49) and (14.61) in Eq. (14.60), while integrating over the surface of the membrane and baffle, yields

$$\begin{aligned} \tilde{\eta}(w) = & -\frac{a^2}{T} \tilde{p}_I \sum_{m=1}^{\infty} \frac{J_0(\alpha_m w/a)}{J_1(\alpha_m)(\alpha_m^2 - k_D^2 a^2)} \\ & \times \left(\frac{2}{\alpha_m} - \sum_{n=0}^{\infty} A_n \Gamma\left(n + \frac{5}{2}\right) \left(\frac{2}{\alpha_m}\right)^{n+3/2} \frac{J_{n+3/2}(\alpha_m)}{J_1(\alpha_m)} \right). \end{aligned} \quad (14.62)$$

where we have used the integrals of Eqs. (A2.95) and (A2.96) from Appendix II.

Solution of the free-space wave equation

We write the free-space wave equation in axisymmetric cylindrical coordinates as

$$\left(\frac{\partial^2}{\partial w^2} + \frac{1}{w} \frac{\partial}{\partial w} + \frac{\partial^2}{\partial z^2} + k^2 \right) \tilde{p}(w, z) = 0. \quad (14.63)$$

The solution is that same as that for a rigid circular piston in a finite open circular baffle given by Eq. (13.203) but with $b = a$. Hence, after inserting Eqs. (13.52), (14.45) and (14.49) into Eq. (13.203) and integrating over the surface of the membrane, we obtain

$$\tilde{p}(w, z) = \frac{\tilde{p}_I}{2} \sum_{n=0}^{\infty} A_n \left(n + \frac{3}{2} \right) \int_0^a \left(1 - \frac{w_0^2}{a^2} \right)^{n+1/2} \int_0^{\infty} J_0(k_w w) J_0(k_w w_0) e^{-jk_z |z|} k_w dk_w w_0 dw_0, \quad (14.64)$$

which is the same as Eq. (13.204) if we substitute $b = a$ and

$$kb\rho_0 \tilde{c} u_0 \frac{a^2}{b^2} = \frac{\tilde{p}_I}{2}. \quad (14.65)$$

Applying the boundary condition of Eq. (14.47) to Eq. (14.64) leads to an expression for the surface particle displacement $\tilde{\eta}(w)$ as follows

$$\begin{aligned} \tilde{\eta}(w) &= \frac{1}{k^2 \rho_0 c^2} \frac{\partial}{\partial z} \tilde{p}(w, z) \Big|_{z=0\pm} \\ &= \frac{-j\tilde{p}_I}{2k^2 a \rho_0 c^2} \sum_{n=0}^{\infty} A_n I_n(w) \end{aligned} \quad (14.66)$$

where $I_n(w)$ is given by Eq. (13.211) with the substitutions $b = a$ and $m = q$ to give

$$I_n(w) = \sum_{q=0}^{\infty} {}_n\mathbf{B}_q \left(\frac{w}{a} \right)^{2q}, \quad (14.67)$$

where ${}_n\mathbf{B}_q(ka)$ is given by Eqs. (13.217) and (13.218). To solve the membrane and free-space wave equations simultaneously, we wish to equate the two displacements given in

Eqs. (14.62) and (14.66). However, Eq. (14.62) is in the form of a Bessel series, with the radial ordinate w in the argument of the Bessel function, whereas Eq. (14.66) is in the form of a power series in w . Therefore, we let

$$\left(\frac{w}{a}\right)^{2q} = \sum_{m=1}^{\infty} a_m J_0(\alpha_m w/a), \quad (14.68)$$

where α_m is the m th zero of $J_0(\alpha_m)$ (i.e., m th solution of $J_0(\alpha_m) = 0$). Multiplying through by the normalizing function $J_0(\alpha_k w/a)$ and integrating over w while applying the property of orthogonality leads to

$$\begin{aligned} a_m &= \frac{\int_0^a (w/a)^{2q} J_0(\alpha_k w/a) w dw}{\int_0^a J_0(\alpha_m w/a) J_0(\alpha_k w/a) w dw} \\ &= \frac{{}_1F_2(q+1; 1, q+2; -\alpha_m^2/4)}{(q+1)J_1^2(\alpha_m)}, \end{aligned} \quad (14.69)$$

where we have used the integrals of Eqs. (A2.95) and (A2.100) from Appendix II. Hence, after substituting Eqs. (14.67) to (14.69) into Eq. (14.66), we obtain

$$\tilde{\eta}(w) = \frac{-\tilde{f}p_I}{2k^2 a \rho_0 c^2} \sum_{n=0}^{\infty} A_n \sum_{q=0}^{\infty} {}_n\mathbf{B}_q(ka) \sum_{m=1}^{\infty} \frac{{}_1F_2(q+1; 1, q+2; -\alpha_m^2/4)}{(q+1)J_1^2(\alpha_m)} J_0(\alpha_m w/a). \quad (14.70)$$

Final set of simultaneous equations for the power-series coefficients

Equating the right-hand sides of Eqs. (14.62) and (14.70) and then equating the coefficients of $J_0(\alpha_n w/a)$, yields the following set of $N+1$ simultaneous equations in A_n

$$\sum_{n=0}^N {}_n\Psi_m(k'_D a, ka) A_n = 1, \quad m = 1, 2, \dots, N+1, \quad (14.71)$$

where

$$\begin{aligned} {}_m\Psi_n(k'_D a, ka) &= \frac{\alpha_m}{2J_1(\alpha_m)} \left\{ \Gamma\left(n + \frac{5}{2}\right) \left(\frac{2}{\alpha_m}\right)^{n+3/2} J_{n+3/2}(\alpha_m) \right. \\ &\quad \left. - j \frac{\alpha_m^2 - k'_D{}^2 a^2}{\alpha^2 (ka)} \sum_{q=0}^Q {}_n\mathbf{B}_q(ka) \frac{{}_1F_2(q+1; 1, q+2; -\alpha_m^2/4)}{q+1} \right\} \end{aligned} \quad (14.72)$$

and α is the fluid-loading factor defined by

$$\alpha(ka) = a\omega\sqrt{\frac{2a\rho_0}{T}} = ka\sqrt{\frac{2a\gamma P_0}{T}}, \quad (14.73)$$

where the infinite series have been truncated to orders N , Q , and R , ${}_n\mathbf{B}_q(ka)$ is the dipole cylindrical wave function defined in Eqs. (13.217) and (13.218), and ${}_1F_2$ is the hypergeometric function.

Radiation impedance

The total volume velocity \tilde{U}_0 produced by the membrane is equal to the integral of its velocity $\tilde{u}_0(w)$ ($= j\omega\tilde{\eta}(w)$) from Eqs. (14.66) and (14.67) over its surface, without making the substitution of Eqs. (14.68) and (14.69), as follows

$$\begin{aligned} \tilde{U}_0 &= jkc \int_0^{2\pi} \int_0^a \tilde{\eta}(w) w dw d\varphi \\ &= \frac{S_D \tilde{p}_I}{2ka\rho c} \sum_{n=0}^N A_n \sum_{q=0}^Q \frac{{}_n\mathbf{B}_q(ka)}{q+1} \end{aligned} \quad (14.74)$$

The total radiation force \tilde{F}_R acting on both sides of the membrane can be found by integrating the surface pressure from Eq. (14.49) over its surface as follows

$$\tilde{F}_R = 2 \int_0^{2\pi} \int_0^a \tilde{p}_+(w_0) w_0 dw_0 d\varphi_0 = \varsigma S_D \tilde{p}_I. \quad (14.75)$$

where ς is the *force transmission coefficient* defined by

$$\varsigma = \frac{\tilde{F}_R}{S_D \tilde{p}_I} = \frac{\tilde{F}_R}{\tilde{F}_I} = \sum_{n=0}^N A_n \quad (14.76)$$

In other words, it is the proportion of the electrostatic driving force that acts on the radiation load on *both* sides of the membrane. The rest just acts on the membrane itself. The specific radiation impedance Z_{SR} for just one side of the membrane is then given by

$$Z_{SR} = \frac{\tilde{F}_R}{2\tilde{U}_0} = ka\rho c \varsigma \left(\sum_{n=0}^N A_n \sum_{q=0}^Q \frac{{}_n\mathbf{B}_q(ka)}{q+1} \right)^{-1}. \quad (14.77)$$

The specific diaphragm impedance Z_{SD} is given by

$$Z_{SD} = \frac{\tilde{F}_I - \tilde{F}_R}{\tilde{U}_0} = 2ka\rho c(1 - \varsigma) \left(\sum_{n=0}^N A_n \sum_{q=0}^Q \frac{{}_n\mathbf{B}_q(ka)}{q+1} \right)^{-1}, \quad (14.78)$$

where $\tilde{F}_I = S_D \tilde{p}_I$ and the total specific motional (input) impedance Z_{SI} is given by

$$Z_{SI} = \frac{\tilde{F}_I}{\tilde{U}_0} = 2k\alpha\rho c \left(\sum_{n=0}^N A_n \sum_{q=0}^Q \frac{n \mathbf{B}_q(ka)}{q+1} \right)^{-1}. \quad (14.79)$$

Far-field pressure

The far-field pressure is the same as that given by Eq. (13.234) for a rigid circular piston in a finite open circular baffle after making the substitution of Eq. (14.65)

$$\begin{aligned} \tilde{p}(r, \theta) &= jka^2 \tilde{p}_I \frac{e^{-jkr}}{4r} D(\theta) \\ &= j\epsilon_0 ka^2 \frac{E_P}{d} \cdot \frac{\tilde{e}_{in}}{2d} \cdot \frac{e^{-jkr}}{2r} D(\theta), \end{aligned} \quad (14.80)$$

where \tilde{p}_I is given by Eqs. (14.52) and (14.53) and the directivity function $D(\theta)$ by

$$D(\theta) = \cos \theta \sum_{n=0}^{\infty} A_n \Gamma \left(n + \frac{5}{2} \right) \left(\frac{2}{ka \sin \theta} \right)^{n+\frac{3}{2}} J_{n+3/2}(ka \sin \theta), \quad (14.81)$$

which, for $\theta = 0$ (i.e., on-axis), simplifies to

$$D(0) = \sum_{n=0}^N A_n = \zeta, \quad (14.82)$$

using ζ from Eq. (14.76). (The on-axis response of a resilient disk in free space is given by setting $\zeta = 1$). The on-axis pressure then simplifies to

$$\begin{aligned} \tilde{p}(r, 0) &= jka^2 \zeta \tilde{p}_I \frac{e^{-jkr}}{4r} \\ &= j\epsilon_0 ka^2 \zeta \frac{E_P}{d} \cdot \frac{\tilde{e}_{in}}{2d} \cdot \frac{e^{-jkr}}{2r}, \end{aligned} \quad (14.83)$$

which is plotted in Fig. 14.5 for $z_S = 0$ so that there is no viscous damping or electrostatic force of attraction. We see that the response is highly modal at the lower frequencies but becomes increasingly smoother at the higher frequencies, where the radiation impedance becomes more resistive. Although the finite element modal (FEM) agrees well with the rigorous calculation from Eq. (14.83) at lower frequencies, it becomes increasingly irregular above 1 kHz because of insufficient resolution of the

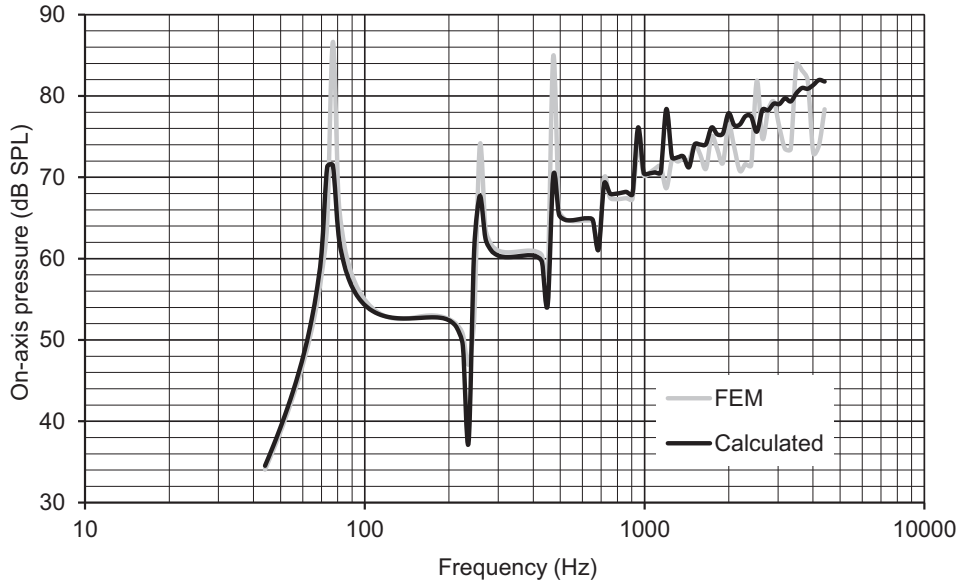


Figure 14.5 Comparison of on-axis response of a 250 mm diameter membrane in free space calculated from Eq. (14.83) (black curve) with a FEM simulation (gray curve), where $p_i = 1 \text{ N/m}^2$, $a = 0.125 \text{ m}$, $h = 12 \text{ }\mu\text{m}$, $\rho_D = 1667 \text{ kg/m}^3$, $T = 100 \text{ N/m}$, $r = 1 \text{ m}$, and $z_S = 0$.

elements. From Eqs. (14.6) and (14.32), we obtain the fundamental in vacuo resonance frequency

$$f_0 = \frac{\alpha_0}{2\pi a} \sqrt{\frac{T}{\rho_D h}} = 217 \text{ Hz}, \quad (14.84)$$

where $\alpha_0 = 2.4048$. However, the radiation mass brings this down to 75 Hz in Fig. 14.5. Substituting $\tilde{I}_{\text{in}} \approx j\omega C_{ED} \tilde{e}_{\text{in}}$ in Eq. (14.83) leads to

$$\tilde{p}(r, 0) \approx \zeta \frac{E_P}{d} \cdot \frac{\tilde{I}_{\text{in}}}{c} \cdot \frac{e^{-jkr}}{2\pi r}, \quad (14.85)$$

which, in the case of $\zeta = 1$, is Walker's equation [7] A better approximation is given by

$$\zeta \approx 2\rho_0 c / (R_S + 2\rho_0 c). \quad (14.86)$$

In this “modified Walker's equation” a dust screen of specific acoustic resistance R_S is used to damp the modes. A total resistance of around 100 rayls (including both front and back covers) is usually sufficient.

PART XXXIX: PLATES

14.11 PLATE WAVE EQUATION IN POLAR COORDINATES

Essentially, a plate is a membrane that is thick enough to have a bending stiffness that significantly modifies its vibrational behavior. When a plate bends, its outer surface is under tension while its inner one is under compression. Between the two surfaces is a middle layer, known as the neutral layer, which is neither under tension nor compression. The surface under tension shrinks and thus pulls the material from either side toward it while the surface under compression tends to spread out. As a result, if a plate is bent downwards, the edges on either side will tend to curl upwards. The degree to which this happens is a property of the material known as the Poisson's ratio ν . Here we shall assume a value of $\nu = 0.3$.

The homogeneous wave equation in any coordinate system for the displacement η is obtained by adding the inertia term to Eq. (105) of Ref. [8].

$$D\nabla^4\eta + \rho_D h \frac{d^2\eta}{dt^2} = 0, \quad (14.87)$$

where h is the thickness of the plate and ρ_D is the density of the plate material. The flexural rigidity D is given by

$$D = \frac{Yh^3}{12(1-\nu^2)}, \quad (14.88)$$

where Y is the Young's modulus of the plate material and ν is the Poisson's ratio. We can rewrite the above wave equation in the following steady-state Helmholtz form as

$$(\nabla^4 - k_D^4)\tilde{\eta} = 0, \quad (14.89)$$

where the wavenumber is given by

$$k_D = \left(\omega^2 \frac{\rho_D h}{D} \right)^{1/4} = \frac{\omega}{c_D} = \frac{2\pi}{\lambda_D}. \quad (14.90)$$

Hence the bending-wave velocity in the plate c_D is given by

$$c_D = \sqrt{\omega \sqrt{\frac{D}{\rho_D h}}}. \quad (14.91)$$

Therefore, high frequencies travel faster in a plate than low ones, which makes it a *dispersive* medium. This contrasts with the membrane in which the speed of sound is constant. The wave Eq. (14.89) gets factorized as follows

$$(\nabla^2 + k_D^2)(\nabla^2 - k_D^2)\tilde{\eta} = 0. \quad (14.92)$$

Hence, η can either be a solution of

$$\nabla^2\tilde{\eta} + k_D^2\tilde{\eta} = 0 \quad (14.93)$$

or

$$\nabla^2\tilde{\eta} - k_D^2\tilde{\eta} = 0, \quad (14.94)$$

where, in the case of polar coordinates, the Laplace operator is given by

$$\nabla^2 = \frac{\partial^2}{\partial w^2} + \frac{1}{w} \cdot \frac{\partial}{\partial w} + \frac{1}{w^2} \cdot \frac{\partial^2}{\partial \phi^2}. \quad (14.95)$$



14.12 SOLUTION OF THE PLATE WAVE EQUATION FOR A CIRCULAR PLATE

In the case of the first solution, we see that Eq. (14.93) is identical to Eq. (14.26) for a circular membrane, for which the solution was found to be

$$\tilde{\eta}(w, \phi) = \sum_{m=0}^{\infty} \sum_{n=1}^{\infty} (\tilde{A}_{mn} \cos(m\phi) + \tilde{B}_{mn} \sin(m\phi)) J_m(\alpha_{mn}w/a), \quad (14.96)$$

where

$$\alpha_{mn} = k_D a. \quad (14.97)$$

These eigenvalues depend on the boundary conditions while the expansion coefficients \tilde{A}_{mn} and \tilde{B}_{mn} depend on the excitation as well as the boundary conditions. However, in the case of the second solution, we rewrite Eq. (14.94) as

$$\nabla^2\tilde{\eta} + (jk_D)^2\tilde{\eta} = 0, \quad (14.98)$$

which is like having an imaginary wavenumber. Hence the solution is

$$\tilde{\eta}(w, \phi) = \sum_{m=0}^{\infty} \sum_{n=1}^{\infty} (\tilde{A}_{mn} \cos(m\phi) + \tilde{B}_{mn} \sin(m\phi)) I_m(\alpha_{mn}w/a), \quad (14.99)$$

where I_m is the hyperbolic Bessel function defined by

$$I_m(x) = j^{-m} J_m(jx). \quad (14.100)$$

Hence, the full solution can be written as

$$\begin{aligned} \tilde{\eta}(w, \phi) = & \sum_{m=0}^{\infty} \sum_{n=1}^{\infty} (\tilde{A}_{mn} \cos(m\phi) + \tilde{B}_{mn} \sin(m\phi)) \\ & \times (C_{mn} J_m(\alpha_{mn} w/a) + D_{mn} I_m(\alpha_{mn} w/a)). \end{aligned} \quad (14.101)$$

For simplicity, let us suppress the sinusoidal part of the angular modes such that $\tilde{B}_{mn} = 0$. Hence, Eq. (14.101) becomes

$$\tilde{\eta}(w, \phi) = \sum_{m=0}^{\infty} \sum_{n=1}^{\infty} \tilde{A}_{mn} \eta_{mn}, \quad (14.102)$$

where the eigenfunctions are given by

$$\eta_{mn} = \cos(m\phi) (C_{mn} J_m(\alpha_{mn} w/a) + D_{mn} I_m(\alpha_{mn} w/a)). \quad (14.103)$$



14.13 MODES OF A CLAMPED CIRCULAR PLATE

In the case of a clamped plate, we have two boundary conditions at the perimeter. Firstly, there is zero displacement

$$\eta_{mn}|_{w=a} = \cos(m\phi) (C_{mn} J_m(\alpha_{mn}) + D_{mn} I_m(\alpha_{mn})) = 0. \quad (14.104)$$

Secondly, there is no bending so that the gradient of the displacement is zero

$$\begin{aligned} \frac{\partial}{\partial w} \eta_{mn}|_{w=a} = & \frac{\alpha_{mn}}{2a} \cos(m\phi) \times \{C_{mn} (J_{m-1}(\alpha_{mn}) - J_{m+1}(\alpha_{mn})) \\ & + D_{mn} (I_{m-1}(\alpha_{mn}) + I_{m+1}(\alpha_{mn}))\} = 0. \end{aligned} \quad (14.105)$$

We obtain the eigenvalues α_{mn} by solving Eqs. (14.104) and (14.105) as a set of simultaneous equations

$$\begin{vmatrix} J_m(\alpha_{mn}) & J_{m-1}(\alpha_{mn}) - J_{m+1}(\alpha_{mn}) \\ I_m(\alpha_{mn}) & I_{m-1}(\alpha_{mn}) + I_{m+1}(\alpha_{mn}) \end{vmatrix} = 0. \quad (14.106)$$

Some eigenvalues are given in Table 14.2. Unlike a simply supported or free plate, which we will consider next, the clamped plate has eigenvalues that are independent of ν .

For large values

$$\alpha_{mn}|_{n \rightarrow \infty} = \left(\frac{m}{2} + n - \frac{1}{2} \right) \pi. \quad (14.107)$$

Table 14.2 Eigenvalues for a clamped circular plate

α_{01}	3.1962	α_{02}	6.3064	α_{03}	9.4395	α_{04}	12.577
α_{11}	4.1609	α_{12}	7.7993	α_{13}	10.958	α_{14}	14.109
α_{21}	5.9057	α_{22}	9.1969	α_{23}	12.402	α_{24}	15.580
α_{31}	7.1435	α_{32}	10.537	α_{33}	13.795	α_{34}	17.005

From Eqs. (14.88), (14.90) and (14.97), the eigenfrequencies are given by

$$f_{mn} = \frac{\alpha_{mn}^2 h}{4\pi a^2} \sqrt{\frac{Y}{3(1-\nu^2)\rho_D}}. \quad (14.108)$$

In other words, to keep the eigenfrequencies as high as possible, it is necessary to use a material with a high ratio of Young's modulus to density. Increasing the thickness also raises the eigenfrequencies but increases the mass which leads to reduced sensitivity when used as a transducer diaphragm. From Eq. (14.104),

$$D_{mn} = -C_{mn} \frac{J_m(\alpha_{mn})}{I_m(\alpha_{mn})}, \quad (14.109)$$

so that the eigenfunctions become

$$\eta_{mn} = C_{mn} \cos(m\phi) \left(J_m(\alpha_{mn}w/a) - \frac{J_m(\alpha_{mn})}{I_m(\alpha_{mn})} I_m(\alpha_{mn}w/a) \right), \quad (14.110)$$

which are plotted in Fig. 14.6.



14.14 MODES OF A SIMPLY SUPPORTED CIRCULAR PLATE

In the case of a simply supported plate, the first boundary condition of zero displacement at the perimeter is identical to that for a clamped plate, as given by Eq. (14.104). However, instead of zero *bending* for the second boundary condition, we have zero *bending moment* because the edge is free to rotate

$$\begin{aligned} M_w|_{w=a} &= -D \left(\frac{\partial^2}{\partial w^2} + \frac{\nu}{w} \frac{\partial}{\partial w} \right) \eta_{mn}|_{w=a} \\ &= -\frac{D}{a^2} \cos(m\phi) (C_{mn} W_{mn} + D_{mn} X_{mn}) = 0, \end{aligned} \quad (14.111)$$

where

$$W_{mn} = (m(m+\nu-1) - \alpha_{mn}^2) J_m(\alpha_{mn}) + (1-\nu) \alpha_{mn} J_{m+1}(\alpha_{mn}), \quad (14.112)$$

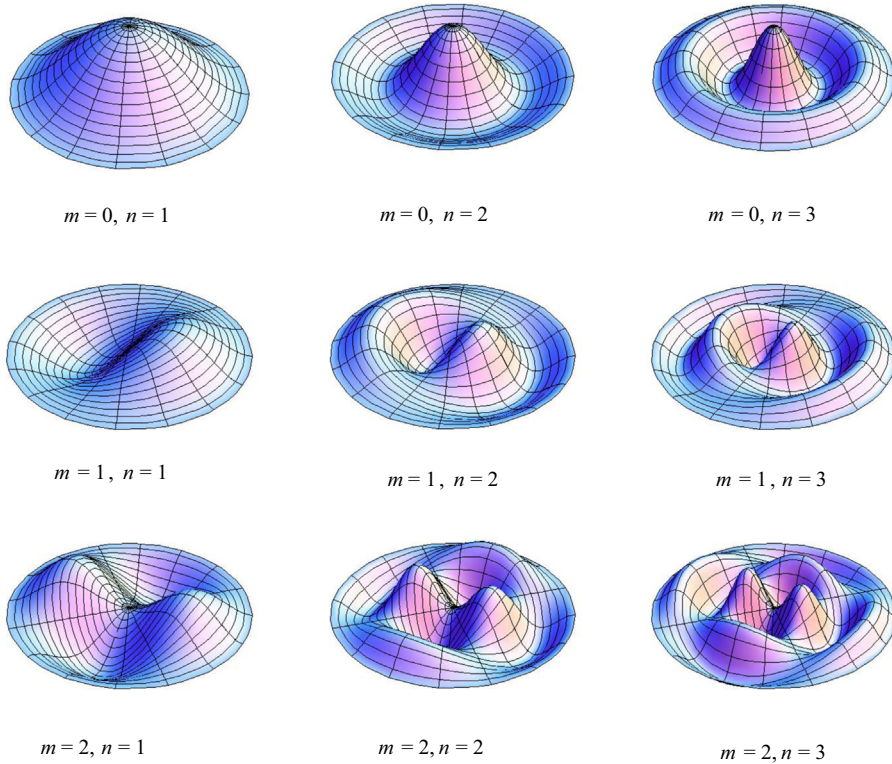


Figure 14.6 Eigenfunctions of a clamped circular plate.

$$X_{mn} = (m(m + \nu - 1) + \alpha_{mn}^2)I_m(\alpha_{mn}) - (1 - \nu)\alpha_{mn}I_{m+1}(\alpha_{mn}). \quad (14.113)$$

We obtain the eigenvalues α_{mn} by solving Eqs. (14.104) and (14.113) as a set of simultaneous equations

$$\begin{vmatrix} J_m(\alpha_{mn}) & W_{mn} \\ I_m(\alpha_{mn}) & X_{mn} \end{vmatrix} = 0. \quad (14.114)$$

Some eigenvalues are given in Table 14.3, which are fairly close to those shown in Table 14.1 for a circular membrane, especially the larger values.

For large values

$$\alpha_{mn}|_{n \rightarrow \infty} = \left(\frac{m}{2} + n - \frac{3}{4} \right) \pi. \quad (14.115)$$

Table 14.3 Eigenvalues for a simply supported circular plate ($\nu = 0.3$)

α_{01}	2.2215	α_{02}	5.4516	α_{03}	8.6114	α_{04}	11.761
α_{11}	3.7280	α_{12}	6.9627	α_{13}	10.138	α_{14}	13.297
α_{21}	5.0610	α_{22}	8.3736	α_{23}	11.589	α_{24}	14.772
α_{31}	6.3212	α_{32}	9.7236	α_{33}	12.988	α_{34}	16.201

From Eq. (14.104),

$$D_{mn} = -C_{mn} \frac{J_m(\alpha_{mn})}{I_m(\alpha_{mn})}, \quad (14.116)$$

so that the eigenfunctions become

$$\eta_{mn} = C_{mn} \cos(m\varphi) \left(J_m(\alpha_{mn}w/a) - \frac{J_m(\alpha_{mn})}{I_m(\alpha_{mn})} I_m(\alpha_{mn}w/a) \right), \quad (14.117)$$

which are plotted in Fig. 14.7. These shapes are similar to those shown in Fig. 14.3 for a circular membrane.

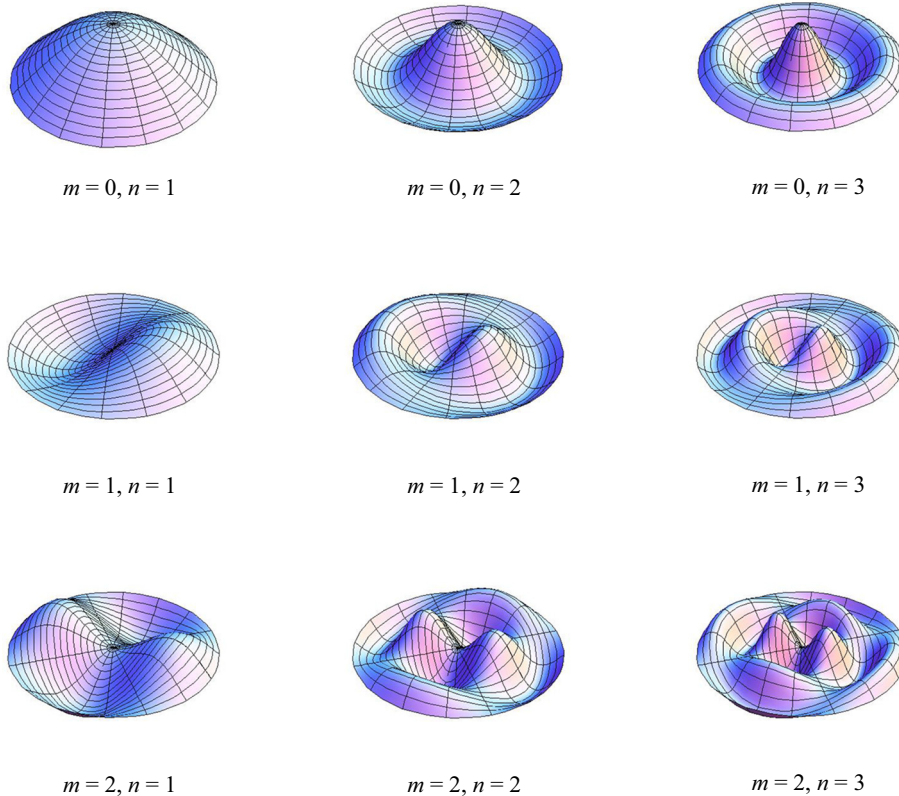


Figure 14.7 Eigenfunctions of a simply supported circular plate.



14.15 MODES OF A FREE CIRCULAR PLATE

In the case of a plate with a free edge, the second boundary condition of zero *bending moment* at the perimeter is identical to that for a simply supported plate, as given by Eq. (14.253). However, instead of zero *displacement* for the first boundary condition, we have zero *shear force* because the edge can move freely

$$\begin{aligned} Q_w|_{w=a} &= -D \frac{\partial}{\partial w} \left(\frac{\partial^2}{\partial w^2} + \frac{1}{w} \cdot \frac{\partial}{\partial w} \right) \eta_{mn}|_{w=a} \\ &= -\frac{D}{a^3} \cos(m\phi) (C_{mn} Y_{mn} + D_{mn} Z_{mn}) = 0, \end{aligned} \quad (14.118)$$

where

$$Y_{mn} = m(m(m-2) - \alpha_{mn}^2) J_m(\alpha_{mn}) - (m^2 - \alpha_{mn}^2) \alpha_{mn} J_{m+1}(\alpha_{mn}), \quad (14.119)$$

$$Z_{mn} = m(m(m-2) + \alpha_{mn}^2) I_m(\alpha_{mn}) + (m^2 + \alpha_{mn}^2) \alpha_{mn} I_{m+1}(\alpha_{mn}). \quad (14.120)$$

We obtain the eigenvalues α_{mn} by solving Eqs. (14.111) and (14.118) as a set of simultaneous equations

$$\begin{vmatrix} W_{mn} & Y_{mn} \\ X_{mn} & Z_{mn} \end{vmatrix} = 0. \quad (14.121)$$

Some eigenvalues are given in Table 14.4.

For large values

$$\alpha_{mn}|_{n \rightarrow \infty} = \left(\frac{m}{2} + n - \frac{3}{4} \right) \pi. \quad (14.122)$$

From Eq. (14.104),

$$D_{mn} = -C_{mn} \frac{J_m(\alpha_{mn})}{I_m(\alpha_{mn})}, \quad (14.123)$$

Table 14.4 Eigenvalues for a free circular plate ($\nu = 0.3$)

α_{01}	0.0000	α_{02}	3.0005	α_{03}	6.2003	α_{04}	9.3675
α_{11}	1.5756	α_{12}	4.4808	α_{13}	7.7153	α_{14}	10.897
α_{21}	2.6494	α_{22}	5.8163	α_{23}	9.1294	α_{24}	12.350
α_{31}	3.6817	α_{32}	7.0792	α_{33}	10.481	α_{34}	13.750

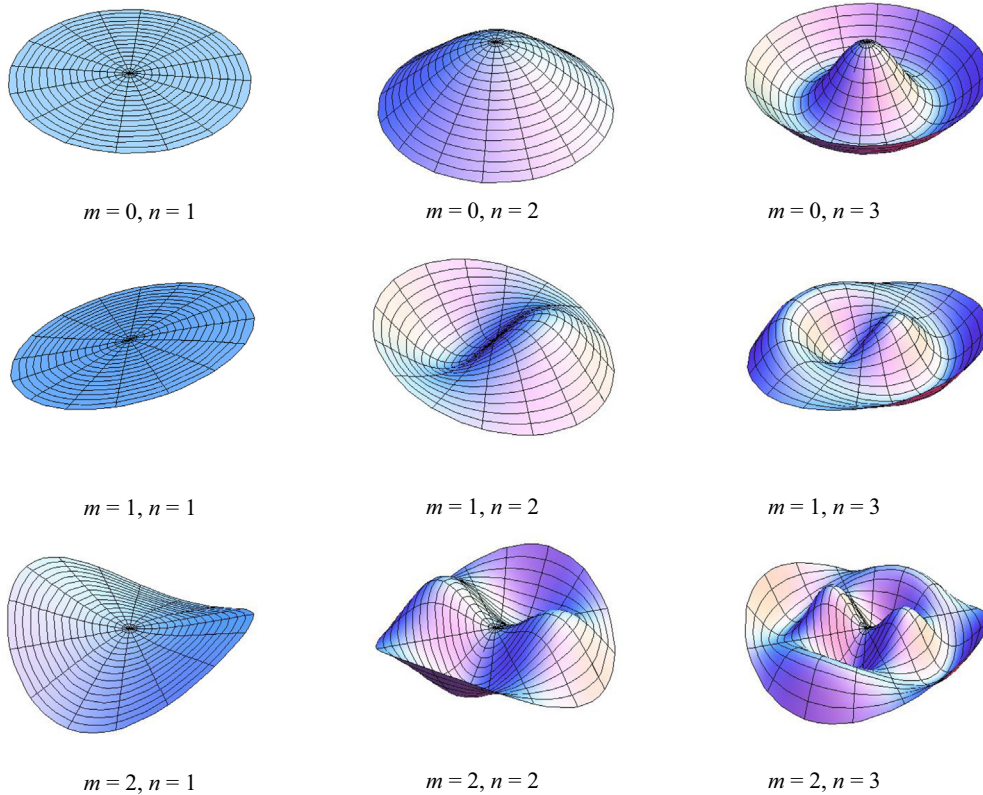


Figure 14.8 Eigenfunctions of a free circular plate.

so that the eigenfunctions become

$$\eta_{mn} = C_{mn} \cos(m\phi) \left(J_m(\alpha_{mn}w/a) - \frac{Y_{mn}}{Z_{mn}} I_m(\alpha_{mn}w/a) \right), \quad (14.124)$$

which are plotted in Fig. 14.8. For the $m = 0, n = 0$ mode, the whole plate just moves continuously through space in the axial direction.

PART XXXX: SHELLS

14.16 SHELL WAVE EQUATION IN POLAR COORDINATES

Like a plate, a shell has bending stiffness, but it has additional stiffness because of its curvature. If you hold a sheet of paper by the edge, it will hang down because it has no stiffness. However, if you curve it even slightly, it will support small objects such as a

pencil. The dynamic shell wave equations [9] are obtained by adding an axial inertia term to the static shell equations [8]. We shall simplify our analysis by assuming that the shell is *shallow*, or the radius of curvature R is large, so that we can ignore radial and tangential components of the displacement $\tilde{\eta}$. This is a reasonable assumption for height/radius ratios up to around 0.25. The following simultaneous steady-state equations for a spherical shell with an applied external harmonic load distribution $\tilde{p}_0(w, \phi)$ need to be solved for the displacement $\tilde{\eta}$ and an Airy stress function \tilde{F}

$$D\nabla^4\tilde{\eta}(w, \phi) - \frac{1}{R}\nabla^2\tilde{F}(w, \phi) - \omega^2\rho_D h\tilde{\eta}(w, \phi) = -\tilde{p}_0(w, \phi), \quad (14.125)$$

$$\nabla^4\tilde{F}(w, \phi) + \frac{hY}{R}\nabla^2\tilde{\eta}(w, \phi) = 0, \quad (14.126)$$

where, in the case of polar coordinates, the Laplace operator is defined by

$$\nabla^2 = \frac{\partial^2}{\partial w^2} + \frac{1}{w}\frac{\partial}{\partial w} + \frac{1}{w^2}\frac{\partial^2}{\partial \phi^2}. \quad (14.127)$$

The flexural rigidity D is defined by

$$D = \frac{Yh^3}{12(1-\nu^2)}, \quad (14.128)$$

where h is the thickness of the shell, Y is the Young's modulus of elasticity of the shell material, ν is its Poisson's ratio, and ρ_D is its density. Let a harmonic function $\tilde{\psi}$ be defined, which satisfies

$$\nabla^2\tilde{\psi} = 0 \quad (14.129)$$

so that

$$\nabla^2\tilde{F}(w, \phi) = -\frac{hY}{R}(\tilde{\eta}(w, \phi) - \tilde{\psi}), \quad (14.130)$$

which, in turn, satisfies Eq. (14.126). Substituting Eq. (14.130) in Eq. (14.125) gives the following single steady-state homogeneous wave equation for the displacement

$$\left(D\nabla^4 + \frac{hY}{R^2} - \omega^2\rho_D h\right)\tilde{\eta}(w, \phi) = \frac{hY}{R}\tilde{\psi} - \tilde{p}_0(w, \phi), \quad (14.131)$$

which can be written in the Helmholtz form as follows

$$(\nabla^4 - k_D^4)\tilde{\eta}(w, \phi) = \frac{hY}{DR}\tilde{\psi} - \frac{\tilde{p}_0(w, \phi)}{D}, \quad (14.132)$$

where k_D is the wavenumber of the shell, which is given by

$$k_D = \frac{2\pi}{\lambda_D} = \frac{\omega}{c_D} = \left(\frac{\rho_D h}{D} \omega^2 - \frac{hY}{R^2 D} \right)^{\frac{1}{4}}. \quad (14.133)$$

The bending-wave velocity c_D in the shell is given by

$$c_D = \omega/k_D. \quad (14.134)$$

As with a plate, high frequencies travel faster in the shell than low frequencies, which makes the shell a dispersive medium. We see that at some transition frequency f_{INF} the speed of sound becomes infinite, as does also the wavelength. Below f_{INF} the wavelength is complex with a phase angle of $\pi/4$. Hence static solutions [8,10] are usually written in terms of Thomson (a.k.a. Kelvin) functions, which can be defined as Bessel functions with $e^{i\pi/4}$ in their arguments [11]. This transition frequency is given by

$$f_{\text{INF}} = \frac{1}{2\pi R} \sqrt{\frac{Y}{\rho_D}}. \quad (14.135)$$



14.17 GREEN'S FUNCTION FOR A SHALLOW SPHERICAL SHELL

Let the solution to Eq. (14.132) for a shallow spherical shell of radius a be in the form of the eigenfunction expansion

$$\tilde{\eta}(w, \phi) = \sum_{m=0}^{\infty} \sum_{n=1}^{\infty} \tilde{A}_{mn} \eta_{mn}(w, \phi), \quad (14.136)$$

where the eigenfunctions are given by

$$\eta_{mn}(w, \phi) = \cos(m\phi) (J_m(\alpha_{mn}w/a) - B_{mn}I_m(\alpha_{mn}w/a) + C_{mn}). \quad (14.137)$$

We use the following identity for the Laplace operator in Eq. (14.132)

$$\nabla^4 \eta_{mn}(w, \phi) = \frac{\alpha_{mn}^4}{a^4} \eta_{mn}(w, \phi) + C_{mn} \left(\frac{m^2(m^2-3)}{w^4} - \frac{\alpha_{mn}^4}{a^4} \right) \cos m\phi \quad (14.138)$$

so that Eq. (14.132) is satisfied if $k_D a = \alpha_{mn}$ and

$$\tilde{\psi} = \frac{RD}{hY} \sum_{m=0}^{\infty} \sum_{n=1}^{\infty} \tilde{A}_{mn} C_{mn} \left(\frac{m^2(m^2-3)}{w^4} - \frac{\alpha_{mn}^4}{a^4} \right) \cos m\phi. \quad (14.139)$$

After inserting Eq. (14.136) into Eq. (14.132), while using the identities of Eqs. (14.138) and (14.139), we multiply both sides by the normalizing function

$$\eta_{pq}^*(w, \phi) = \cos(p\phi) \left(J_p(\alpha_{pq}^* w/a) - B_{pq}^* I_p(\alpha_{pq}^* w/a) + C_{pq}^* \right) \quad (14.140)$$

and integrate over the surface of the shell to yield

$$\pi a^2 \sum_{m=0}^{\infty} \sum_{n=1}^{\infty} \tilde{A}_{mn} \left(\frac{\alpha_{mn}^4}{a^4} - k_D^4 \right) \Delta_{mn} = -\frac{1}{D} \int_0^{2\pi} \int_0^a \tilde{p}_0(w, \phi) \eta_{pq}^*(w, \phi) w dw d\phi, \quad (14.141)$$

where

$$\Delta_{mn} = \frac{1}{\pi a^2} \int_0^{2\pi} \int_0^a \eta_{pq}^*(w, \phi) \eta_{mn}(w, \phi) w dw d\phi. \quad (14.142)$$

Because of the property of orthogonality, only terms where $m = p$ and $n = q$ are nonzero so that

$$\tilde{A}_{mn} = \frac{a^2 \int_0^{2\pi} \int_0^a \tilde{p}_0(w, \phi) \eta_{mn}^*(w, \phi) w dw d\phi}{\pi D \Delta_{mn} (k_D^4 a^4 - \alpha_{mn}^4)}. \quad (14.143)$$

If there is resistance in the system, so that $\alpha_{mn}^* \neq \alpha_{mn}$, the integrals in Eq. (14.142) are evaluated using Eqs. (56), (95) and (102) of Appendix II to give

$$\begin{aligned} \Delta_{mn} = & \frac{1 + \delta_{m0}}{2} \left(C_{mn} C_{mn}^* + 2 \frac{\alpha_{mn} J_m(\alpha_{mn}^*) J_{m+1}(\alpha_{mn}) - \alpha_{mn}^* J_m(\alpha_{mn}) J_{m+1}(\alpha_{mn}^*)}{\alpha_{mn}^2 - \alpha_{mn}^{*2}} \right. \\ & - 2B_{mn} \frac{\alpha_{mn} J_m(\alpha_{mn}^*) I_{m+1}(\alpha_{mn}) + \alpha_{mn}^* I_m(\alpha_{mn}) J_{m+1}(\alpha_{mn}^*)}{\alpha_{mn}^2 + \alpha_{mn}^{*2}} \\ & - 2B_{mn}^* \frac{\alpha_{mn}^* J_m(\alpha_{mn}) I_{m+1}(\alpha_{mn}^*) + \alpha_{mn} I_m(\alpha_{mn}^*) J_{m+1}(\alpha_{mn})}{\alpha_{mn}^{*2} + \alpha_{mn}^2} \\ & + 2B_{mn} B_{mn}^* \frac{\alpha_{mn} I_m(\alpha_{mn}^*) I_{m+1}(\alpha_{mn}) - \alpha_{mn}^* I_m(\alpha_{mn}) I_{m+1}(\alpha_{mn}^*)}{\alpha_{mn}^2 - \alpha_{mn}^{*2}} \\ & \left. + 2C_{mn} \frac{J_m(\alpha_{mn}^*) - B_{mn}^* I_{m+1}(\alpha_{mn}^*)}{\alpha_{mn}^*} + 2C_{mn}^* \frac{J_{m+1}(\alpha_{mn}) - B_{mn} I_{m+1}(\alpha_{mn})}{\alpha_{mn}} \right). \end{aligned} \quad (14.144)$$

Otherwise, if there are no losses, so that $\alpha_{mn}^* = \alpha_{mn}$, then

$$\begin{aligned} \Delta_{mn} = & \frac{1 + \delta_{m0}}{2} \{ J_m^2(\alpha_{mn}) - J_{m-1}(\alpha_{mn})J_{m+1}(\alpha_{mn}) \\ & + B_{mn}^2 (I_m^2(\alpha_{mn}) - I_{m-1}(\alpha_{mn})I_{m+1}(\alpha_{mn})) + C_{mn}^2 \\ & + 4C_{mn} \left(\frac{\alpha_{mn}}{2} \right)^{m_1} \frac{{}_1F_2 \left(\frac{m}{2} + 1; \frac{m}{2} + 2, m + 1; -\frac{\alpha_{mn}^2}{4} \right)}{(m+1)m!} \\ & - 4B_{mn}C_{mn} \left(\frac{\alpha_{mn}}{2} \right)^{m_1} \frac{{}_1F_2 \left(\frac{m}{2} + 1; \frac{m}{2} + 2, m + 1; \frac{\alpha_{mn}^2}{4} \right)}{(m+1)m!} \\ & - \frac{2}{\alpha_{mn}} B_{mn} (J_m(\alpha_{mn})I_{m+1}(\alpha_{mn}) + J_{m+1}(\alpha_{mn})I_m(\alpha_{mn})) \}, \end{aligned} \quad (14.145)$$

where ${}_1F_2$ is the hypergeometric function.

Hence, after inserting A_{mn} from Eq. (14.143) into Eq. (14.136), the displacement $\tilde{\eta}(w, \phi)$ for a given pressure distribution $\tilde{p}_0(w_0, \phi_0)$ is

$$\tilde{\eta}(w, \phi) = \frac{a^2}{\pi D} \sum_{m=0}^{\infty} \sum_{n=1}^{\infty} \frac{\eta_{mn}(w, \phi)}{\Delta_{mn}(k_D^4 a^4 - \alpha_{mn}^4)} \int_0^{2\pi} \int_0^a \tilde{p}_0(w_0, \phi_0) \eta_{mn}^*(w_0, \phi_0) w_0 dw_0 d\phi_0. \quad (14.146)$$

This can also be written as

$$\tilde{\eta}(w, \phi) = \frac{1}{D} \int_0^{2\pi} \int_0^a \tilde{p}_0(w_0, \phi_0) G(w, \phi | w_0, \phi_0) w_0 dw_0 d\phi_0, \quad (14.147)$$

where $G(w, \phi | w_0, \phi_0)$ is the Green's function for the shell given by

$$G(w, \phi | w_0, \phi_0) = \frac{a^2}{\pi} \sum_{m=0}^{\infty} \sum_{n=1}^{\infty} \frac{\eta_{mn}(w, \phi) \eta_{mn}^*(w_0, \phi_0)}{\Delta_{mn}(k_D^4 a^4 - \alpha_{mn}^4)}, \quad (14.148)$$

which can be shown to satisfy the inhomogeneous wave equation for excitation by a point source at (w_0, ϕ_0)

$$\begin{aligned} (\nabla^4 - k_D^4) G(w, \phi | w_0, \phi_0) - \sum_{m=0}^{\infty} \sum_{n=1}^{\infty} A_{mn} C_{mn} \left(\frac{m^2(m^2 - 3)}{w^4} - \frac{\alpha_{mn}^4}{a^4} \right) \cos m\phi \\ = -\frac{1}{w} \delta(w - w_0) \delta(\phi - \phi_0). \end{aligned} \quad (14.149)$$

where

$$A_{mn} = \frac{a^2 \eta_{mn}^*(w_0, \phi_0)}{\pi \Delta_{mn} (k_D^4 a^4 - \alpha_{mn}^4)}. \quad (14.150)$$



14.18 RADIATION FROM A CIRCULAR SHALLOW SPHERICAL SHELL IN AN INFINITE BAFFLE—MODEL OF A DOME-SHAPED DYNAMIC LOUDSPEAKER COUPLED TO ITS SURROUNDING AIR [12]

The spherical shell is a somewhat commonly used structure for dynamic loudspeaker diaphragms ranging from small Bluetooth devices to hi-fi midrange units and tweeters. To simplify our analysis, we shall exclude the ring surround, basket, magnet, and rear cavity from the model and instead assume that the dome is open to free space on both sides and mounted in a planar baffle, which extends to infinity from its perimeter. However, a specific acoustic impedance z_S is included in the complex wavenumber, which may be used to model distributed impedances such as external resistance (e.g., a screen) or mixed mass and resistance in the form of an array of sound outlet holes. Internal damping can also be modeled using complex flexural rigidity. The specific impedance may even be used to approximate lumped elements such as the compliance of a rear cavity. In addition to making the shallow shell assumption by ignoring the radial and tangential components of the displacement, we will assume the radiation load to be that of a planar circular source.

Boundary conditions

An elastic spherical shell with radius a and thickness h , as shown in Fig. 14.9, is set in an infinite baffle of the same thickness with its center located on the z axis, which forms the axis of symmetry. Hence, there is no ϕ dependency and we set $m = 0$ in the equations from here onwards. The spherical shell surface is defined by

$$z = R \left(\sqrt{1 - w^2/R^2} - \sqrt{1 - a^2/R^2} \right) \quad (14.151)$$

$$\approx \frac{a^2 - w^2}{2R}, \quad R > 2a \text{ (for surface average error } < 10\%).$$

The radius of curvature R is related to the dome height H by

$$R = \frac{a^2}{2H} \quad (14.152)$$

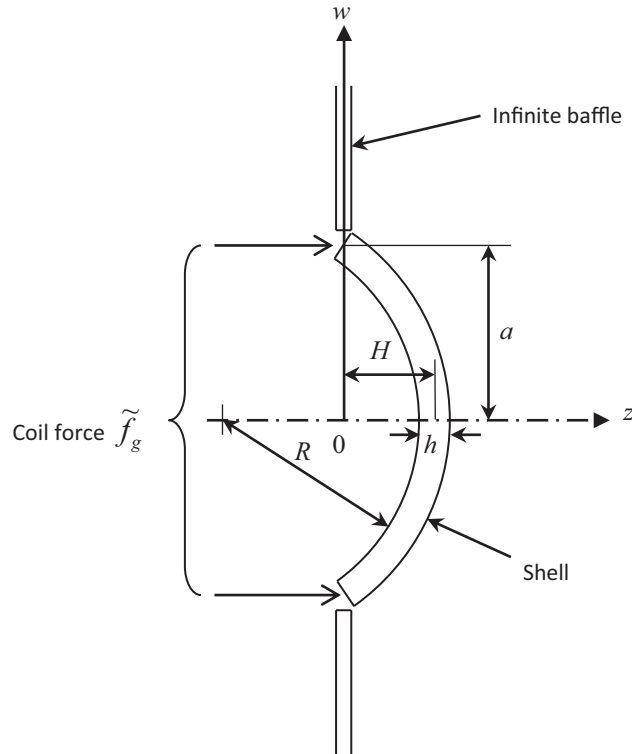


Figure 14.9 Geometry of the shell in an infinite baffle.

and the surface area S_D of a shallow shell is

$$S_D = 2\pi R \left(R - \sqrt{R^2 - a^2} \right) \quad (14.153)$$

$$\approx \pi a^2, \quad R > 2a.$$

Within its perimeter, the shell is homogenous and continuous and is fabricated from an isotropic material with a Poisson's ratio of $\nu = 0.3$. In this model, the shell and coil former are formed from the same piece of material and have the same thickness. Hence, at the perimeter, there is assumed to be neither bending nor radial strain. Also, the coil force \tilde{f}_g is applied to the perimeter in the z direction. A separate suspension is assumed to be attached either to the coil or directly to the shell perimeter. It is assumed to provide pure linear compliance C_{MS} in the z direction with mechanical damping R_{MS} , and its mass is included with that of the voice coil, which is denoted by M_{MC} . The coil driving force \tilde{f}_g is used as the input in a wave equation for the shell, which is defined in terms of the input voltage \tilde{e}_g by

$$\tilde{f}_g = Bl\tilde{e}_g/R_E, \quad (14.154)$$

where R_E is the electrical resistance of the coil and Bl is the product of magnetic flux and coil length. The total mechanical damping resistance R_{MT} is then given by

$$R_{MT} = R_{MS} + (Bl)^2/R_E. \quad (14.155)$$

The displacement $\tilde{\eta}(w)$ of the shell is then be used as a parameter to couple it to the surrounding loss-free acoustic medium. Hence the shell and free space wave equations must be solved simultaneously.

Axisymmetric solutions to the shell wave equations

The axisymmetric solutions to Eqs. (14.125) and (14.126), where we have suppressed any ϕ dependency, are eigenfunctions of the form

$$\tilde{\eta}_n(w) = \tilde{C}_{1n}J_0(k_D w) + \tilde{C}_{2n}Y_0(k_D w) + \tilde{C}_{3n}I_0(k_D w) + \tilde{C}_{4n}K_0(k_D w) + \tilde{C}_{5n} \quad (14.156)$$

$$\begin{aligned} \tilde{F}_n(w) = & -\frac{2HhY}{k_D^2 a^2} (\tilde{C}_{1n}J_0(k_D w) + \tilde{C}_{2n}Y_0(k_D w) - \tilde{C}_{3n}I_0(k_D w) - \tilde{C}_{4n}K_0(k_D w)) \\ & + \frac{\rho_D h a^2 \omega^2}{8H} \tilde{C}_{5n} w^2 + \tilde{C}_{6n} \log w + \tilde{C}_{7n} \end{aligned} \quad (14.157)$$

where $\tilde{C}_{5n} = \tilde{\psi}_n$ and n is the eigen index. Using Eqs. (14.128) and (14.152), let us rewrite the wavenumber from Eq. (14.133) as

$$k_D^4 = \frac{\rho_D h}{D} \omega^2 - \frac{\xi^4}{a^4}, \quad (14.158)$$

where

$$\xi^4 = 48(1 - \nu^2)H^2/h^2 \quad (14.159)$$

In Eqs. (14.156) and (14.157), the arguments of the Bessel functions J , Y , I , and K can only have specific values, or eigenvalues, which satisfy the boundary conditions. The eigenvalues of the system are represented by setting $k_D a = \beta_n$. The eigenvalues and constants are then determined by applying boundary conditions, which are evaluated with help from the following identities:

$$\frac{d}{dw} Z_0(k_D w) = \mp k_D Z_1(k_D w), \quad (14.160)$$

$$\frac{d^2}{dw^2} Z_0(k_D w) = k_D^2 \left(\pm \frac{Z_1(k_D w)}{k_D w} \mp Z_0(k_D w) \right), \quad (14.161)$$

$$\frac{d^3}{dw^3}Z_0(k_D w) = k_D^3 \left\{ \left(1 \mp \frac{2}{k_D^2 w^2} \right) Z_1(k_D w) \pm \frac{Z_0(k_D w)}{k_D w} \right\}, \quad (14.162)$$

where Z can represent either J (upper sign) or I (lower sign).

Boundary condition of continuity at the center

In this configuration, $\tilde{\eta}_n$ and \tilde{F}_n must be continuous at the apex ($w = 0$). Therefore, we have

$$\tilde{C}_{2n} = \tilde{C}_{4n} = \tilde{C}_{6n} = 0 \quad (14.163)$$

Boundary condition of zero bending at the perimeter

We assume zero bending at the perimeter. Therefore

$$\frac{\partial}{\partial w} \tilde{\eta}_n(w)|_{w=a} = -\frac{\beta_n}{a} \tilde{C}_{1n} J_1(\beta_n) + \frac{\beta_n}{a} \tilde{C}_{3n} I_1(\beta_n) = 0 \quad (14.164)$$

so that

$$\tilde{C}_{3n} = \frac{J_1(\beta_n)}{I_1(\beta_n)} \tilde{C}_{1n} \quad (14.165)$$

Boundary condition of zero radial strain at the perimeter

We assume zero radial strain at the perimeter. Hence

$$\begin{aligned} \left(\frac{\partial^2}{\partial w^2} - \frac{\nu}{w} \frac{\partial}{\partial w} \right) \tilde{F}_n(w)|_{w=a} &= \frac{2hHY}{a^2} \left\{ \tilde{C}_{1n} \left(J_0(\beta_n) - \frac{1+\nu}{\beta_n} J_1(\beta_n) \right) \right. \\ &\quad \left. + \tilde{C}_{3n} \left(I_0(\beta_n) - \frac{1+\nu}{\beta_n} I_1(\beta_n) \right) \right\} + (1-\nu) \omega_n^2 \frac{a^2 \rho_D h}{4H} \tilde{C}_{5n} = 0, \end{aligned} \quad (14.166)$$

where from Eq. (14.158)

$$\omega_n^2 = \frac{D(\beta_n^4 + \xi^4)}{a^4 \rho_D h} \quad (14.167)$$

so that

$$\begin{aligned} \tilde{C}_{5n} &= -\frac{2\xi^4}{(1-\nu)(\beta_n^4 + \xi^4)} \left\{ \tilde{C}_{1n} \left(J_0(\beta_n) - \frac{1+\nu}{\beta_n} J_1(\beta_n) \right) \right. \\ &\quad \left. + \tilde{C}_{3n} \left(I_0(\beta_n) - \frac{1+\nu}{\beta_n} I_1(\beta_n) \right) \right\}. \end{aligned} \quad (14.168)$$

Coil impedance at the perimeter

The coil mass and suspension produce an axially symmetric (vertical) shear force resultant Q_v at the perimeter. Hence, assuming that $a \ll R$,

$$\begin{aligned}\tilde{Q}_{vn}(w)|_{w=a} &= \left(\tilde{Q}_n(w) + \tilde{N}_n(w) \frac{w}{R} \right)_{w=a} \\ &= - \left(\frac{1}{C_{MS}} + j\omega_n R_{MT} - \omega_n^2 M_{MC} \right) \frac{\tilde{\eta}_n(a)}{2\pi a},\end{aligned}\quad (14.169)$$

where M_{MC} is the mass of the coil and its former, C_{MS} is the compliance of the suspension, and R_{MT} is the total damping resistance. Also, the shear force is defined by

$$\begin{aligned}\tilde{Q}_n(w) &= -D \frac{\partial}{\partial w} \nabla^2 \tilde{\eta}_n(w) \Big|_{w=a} \\ &= -\frac{\beta_n^3}{a^3} D (\tilde{C}_{1n} J_1(\beta_n) + \tilde{C}_{3n} I_1(\beta_n))\end{aligned}\quad (14.170)$$

and the radial membrane force is defined by

$$\begin{aligned}\tilde{N}_n(w) &= -\frac{1}{w} \frac{\partial}{\partial w} \tilde{F}(w) \\ &= -\frac{2HhY}{a^2 \beta_n} (\tilde{C}_{1n} J_1(\beta_n) + \tilde{C}_{3n} I_1(\beta_n)) - \tilde{C}_{5n} \frac{\omega_n^2 a^2 \rho_D h}{4H},\end{aligned}\quad (14.171)$$

so that inserting Eqs. (14.167), (14.170) and (14.171) into Eq. (14.169) yields

$$\begin{aligned}\tilde{C}_{5n} &= -\tilde{C}_{1n} J_0(\beta_n) - \tilde{C}_{3n} I_0(\beta_n) - (\beta_n^4 + \xi^4) \\ &\quad \times \frac{4\tilde{C}_{1n} J_1(\beta_n) - \beta_n (\tilde{C}_{1n} J_0(\beta_n) + \tilde{C}_{3n} I_0(\beta_n))}{\beta_n \left(\frac{M_{MD}}{M_{MS}} (\beta_n^4 + \xi^4) - \frac{a^2 K_S}{\pi D} - j \frac{R_S}{\pi} \sqrt{\frac{\beta_n^4 + \xi^4}{\rho_S h D}} \right)},\end{aligned}\quad (14.172)$$

where the mass M_{MS} of the shell is

$$M_{MS} = \pi a^2 \rho_D h \quad (14.173)$$

and the total mass of the shell and coil is

$$M_{MD} = M_{MS} + M_{MC}. \quad (14.174)$$

Let ω_0 be a notional angular frequency, representing the suspension resonance of a perfectly rigid shell (including its coil mass). Hence, the compliance may be defined by

$$C_{MS} = \frac{1}{\omega_0^2 M_{MD}}. \quad (14.175)$$

From Eqs. (14.167), (14.173) and (14.175), the compliance may be expressed as follows

$$C_{MS} = \frac{\zeta a^2}{\pi D (\beta_0^4 + \xi^4)}, \quad (14.176)$$

where β_0 is a notional zeroth eigenvalue and ζ is the mass loading factor defined by

$$\zeta = \frac{M_{MS}}{M_{MD}}. \quad (14.177)$$

Also, let the total Q of the fundamental resonance ω_0 be defined by

$$Q_{TS} = \frac{1}{R_{MT}} \sqrt{\frac{M_{MD}}{C_{MS}}}. \quad (14.178)$$

Calculation of the eigenvalues

Equating Eq. (14.168) with Eq. (14.172) and inserting the expressions for C_{MS} and R_{MT} from Eqs. (14.176) and (14.178) respectively, together with the identity for \tilde{C}_{3n} from Eq. (14.165), produces a characteristic equation that can be solved for the eigenvalues

$$\begin{aligned} & \frac{1}{\zeta} \left(\beta_n^4 - \beta_0^4 - j \frac{\sqrt{(\beta_0^4 + \xi^4)(\beta_n^4 + \xi^4)}}{Q_{TS}} \right) \\ & \times \left\{ ((1 - \nu)\beta_n^4 - (1 + \nu)\xi^4) W(\beta_n) + 4\xi^4 \frac{1 + \nu}{\beta_n} J_1(\beta_n) I_1(\beta_n) \right\} \\ & - (1 - \nu)(\beta_n^4 + \xi^4)^2 \left(W(\beta_n) - \frac{4}{\beta_n} J_1(\beta_n) I_1(\beta_n) \right) = 0, \end{aligned} \quad (14.179)$$

where

$$W(\beta_n) = J_0(\beta_n) I_1(\beta_n) + J_1(\beta_n) I_0(\beta_n) \quad (14.180)$$

and the notional zeroth eigenvalue β_0 is defined by

$$\beta_0^4 = \frac{a^2 M_{MS}}{\pi D} \omega_0^2 - \xi^4, \quad (14.181)$$

which is then used as a parameter in the characteristic equation (not a solution) to define the suspension stiffness.

Eigenvalues with zero load at the perimeter

If there is no loading at the perimeter, then $M_{MC} = 0$ and $\omega_0 = 0$. Hence, Eq. (14.179) reduces to

$$(\beta_n^4 + \xi^4) \left\{ W(\beta_n) - 2 \frac{(1-\nu)\beta_n^4 + 2\xi^4}{\beta_n \xi^4} J_1(\beta_n) I_1(\beta_n) \right\} = 0. \quad (14.182)$$

For zero height, setting $\xi^4 = 0$, yields the following eigenvalues:

$$\beta_1 = 0 \quad \beta_2 = 3.8317 \quad \beta_3 = 7.0156 \quad \beta_4 = 10.174 \quad \beta_5 = 13.324,$$

whereas setting $\xi^4 = \infty$ gives

$$\beta_1 = e^{j\pi/4} \infty \quad \beta_2 = 5.9057 \quad \beta_3 = 9.1969 \quad \beta_4 = 12.402 \quad \beta_5 = 15.580.$$

Using the asymptotic expression for the Bessel function from Eq. (90) of Appendix II, it can be shown that

$$\beta_n|_{n \rightarrow \infty} \approx (n - 3/4)\pi, \quad H/h = 0. \quad (14.183)$$

From Eq. (14.158), the eigenfrequencies are obtained using

$$f_n = \frac{h}{4\pi a^2} \sqrt{\frac{Y}{3\rho_D} \left(\frac{\beta_n^4}{1-\nu^2} + 48 \frac{H^2}{h^2} \right)}. \quad (14.184)$$

Note that for any height H , the factor $(\beta_n^4 + \xi^4)$ in Eq. (14.182) determines the first eigenvalue, which is given by $\beta_1 = e^{j\pi/4} \xi$ and returns a zero value for the first eigenfrequency f_1 when entered into Eq. (14.184). Not surprisingly, when $H = 0$, Eq. (14.184) reduces to the eigenfrequency equation for a plate. However, when $H > 10h$, say, the equation for the fundamental shell eigenfrequency in asymptotic form becomes

$$\begin{aligned} f_2 &\approx \frac{H}{\pi a^2} \sqrt{\frac{Y}{\rho_D}}, \quad H > 10h \\ &= \frac{1}{2\pi R} \sqrt{\frac{Y}{\rho_D}} = f_{\text{INF}}. \end{aligned} \quad (14.185)$$

This slightly surprising result [9] indicates that when the height of the apex is much greater than the wall thickness, the fundamental resonant frequency (second eigenfrequency f_2) of the shell is dependent only on its radius of curvature and material properties regardless of the wall thickness. (This does not apply to the first eigenfrequency, or piston eigenfrequency, which remains zero.) This effect is demonstrated in Fig. 14.10 where the eigenfrequencies are plotted against the height to thickness ratio.

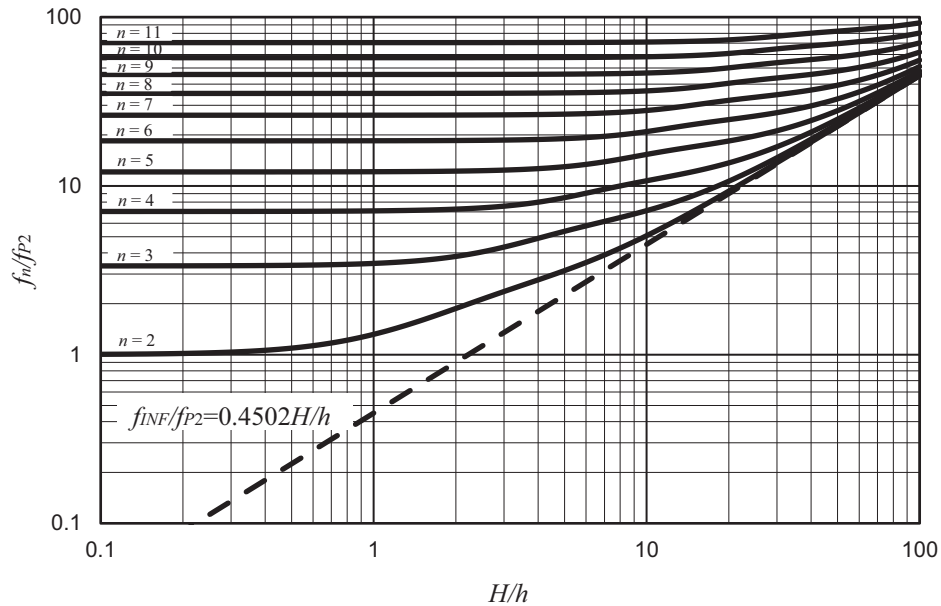


Figure 14.10 Eigenfrequencies of a shallow spherical shell with zero load at the perimeter.

The eigenfrequencies f_n are normalized to the fundamental eigenfrequency f_{p2} of the corresponding flat circular plate, where

$$f_{p2} = \frac{\beta_2^2 h}{4\pi a^2} \sqrt{\frac{Y}{3(1-\nu^2)\rho_D}} \quad \text{and} \quad \beta_2 = 3.8317. \quad (14.186)$$

On the left-hand side of the plot, the eigenfrequencies converge to those of the flat circular plate with the same boundary conditions. On the right-hand side, the asymptotic value is $f_{\text{INF}}/f_{p2} = 0.4502 H/h$. However, $f_1 = 0$ for any height because the shell is free to float through space, and so this is the “piston” eigenfrequency. Notice how as we increase the curvature by increasing the height/thickness ratio (H/h), the lower-order eigenfrequencies increase more than the higher-order ones. This is because the curvature appears to be greater for larger wavelengths than it does for smaller ones. As an analogy, the earth appears to be flat to us because we are small, whereas if we were giants, we would see that it is spherical.

Eigenvalues with infinite load at the perimeter

If $M_{MC} = \infty$ and $\omega_0 = 0$, then the shell’s dynamic axial movement is blocked, although it can still move through space at constant velocity and hence returns a zero value for the first eigenfrequency. Eq. (14.179) reduces to

$$(\beta_n^4 + \xi^4) \left\{ W(\beta_n) + \frac{4(1 + \nu)\xi^4 J_1(\beta_n) I_1(\beta_n)}{\beta_n((1 - \nu)\beta_n^4 - (1 + \nu)\xi^4)} \right\} = 0, \quad (14.187)$$

which is identical to that for a clamped shell, [9] except for the factor $(\beta_n^4 + \xi^4)$, which gives the piston mode. For zero height, setting $\xi^4 = 0$ yields the following eigenvalues:

$$\beta_1 = 0 \quad \beta_2 = 3.1962 \quad \beta_3 = 6.3064 \quad \beta_4 = 9.4395 \quad \beta_5 = 12.577,$$

whereas setting $\xi^4 = \infty$ gives

$$\beta_1 = e^{j\pi/4} \infty \quad \beta_2 = 5.9057 \quad \beta_3 = 9.1969 \quad \beta_4 = 12.402 \quad \beta_5 = 15.580.$$

Again, using the asymptotic expression from Eq. (90) of Appendix II, expressions for the large eigenvalues can be obtained:

$$\beta_n|_{n \rightarrow \infty} \approx (n - 1)\pi, \quad H/h = 0, \quad (14.188)$$

$$\beta_n|_{n \rightarrow \infty} \approx n\pi, \quad H/h = \infty. \quad (14.189)$$

In Fig. 14.11, the eigenfrequencies f_n of a simply supported shell are normalized to the fundamental eigenfrequency f_{P2} of the corresponding flat circular plate where

$$f_{P2} = \frac{\beta_2^2 h}{4\pi a^2} \sqrt{\frac{Y}{3(1 - \nu^2)\rho_D}}. \quad (14.190)$$

On the left-hand side of the plot, the eigenfrequencies converge to those of a clamped flat circular plate. On the right-hand side, the asymptotic value is $f_{INF}/f_{P1} = 0.6470H/h$.

Eigenvalues with finite load at the perimeter

With a low stiffness boundary condition, β_1 and f_1 have values fairly close to β_0 and f_0 respectively but are not coincident because of the interaction between the modes. As the stiffness is increased, β_1 and f_1 approach asymptotic values representing blocked axial movement no matter how large β_0 and f_0 are. The perimeter damping changes the angle of all the eigenvalues such that the angle of the complex eigenvalues is no longer 45 degrees and the imaginary parts of the remainder are no longer zero.

Eigenfunctions

Substituting Eqs. (14.163), (14.165) and (14.168) in Eq. (14.156) yields the following eigenfunctions

$$\eta_n(w) = J_0(\beta_n w/a) - B_n I_0(\beta_n w/a) + C_n, \quad (14.191)$$

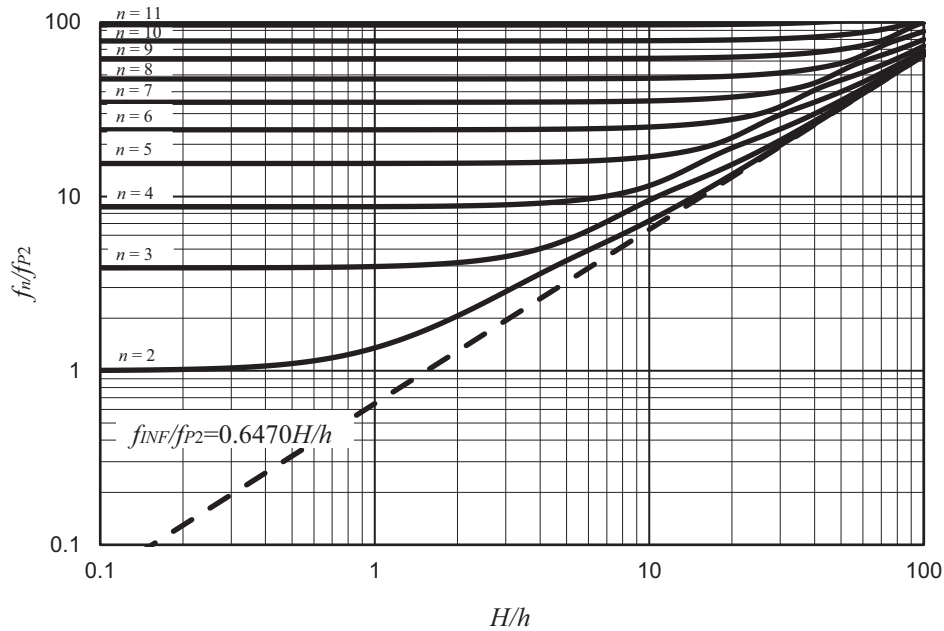


Figure 14.11 Eigenfrequencies of a shallow spherical shell with infinite load at the perimeter.

which are the solutions to the following homogeneous wave equation

$$(\nabla^4 - k_D^4)\eta_n(w) + \frac{\alpha_n^4}{a^4}C_n = 0, \quad (14.192)$$

where the Laplace operator is given by

$$\nabla^2 = \frac{\partial^2}{\partial w^2} + \frac{1}{w} \frac{\partial}{\partial w} \quad (14.193)$$

and the coefficients B_n and C_n by

$$B_n = -\frac{\tilde{C}_{3n}}{\tilde{C}_{1n}} = \frac{J_1(\beta_n)}{I_1(\beta_n)}, \quad (14.194)$$

$$C_n = \frac{\tilde{C}_{5n}}{\tilde{C}_{1n}} = -\frac{2\xi^4(W(\beta_n) - 2(1+\nu)J_1(\beta_n)I_1(\beta_n)/\beta_n)}{(1-\nu)I_1(\beta_n)(\beta_n^4 + \xi^4)}. \quad (14.195)$$

Solution of the wave equation for the shell in an infinite baffle

The inhomogeneous steady-state wave equation for the displacement $\tilde{\eta}(w)$ of the circular shallow spherical shell, with the above boundary conditions at its perimeter, can be written with the inherent shell forces on the left and the external forces on the right as

$$D(\nabla^4 - k_D'^4)\tilde{\eta}(w) + D \sum_{n=1}^{\infty} \tilde{A}_n \frac{\alpha_n^4}{a^4} C_n = \zeta \left(\tilde{p}_+(w) - \tilde{p}_-(w) - \frac{\delta(w-b)\tilde{f}_g}{2\pi b} \right) \quad (14.196)$$

where the Laplace operator is given by Eq. (14.193) and $\tilde{p}_+(w)$ and $\tilde{p}_-(w)$ are the front and rear pressure distributions, respectively, due to the surrounding acoustic medium, D is the flexural rigidity of the shell material, and a is its radius. The concentrated ring force due to the coil of radius b is represented by Dirac delta function. Although we will set $b = a$ to model the shell shown in Fig. 14.9, we will also use this equation in Section 14.19 to investigate a free plate with a coil of zero mass where $b \neq a$. The solution is given by

$$\tilde{\eta}(w) = \frac{\zeta}{D} \int_0^{2\pi} \int_0^a \left(2\tilde{p}_+(w_0) - \frac{\delta(w_0-b)\tilde{f}_g}{2\pi b} \right) G(w|w_0) w_0 dw_0 d\varphi_0, \quad (14.197)$$

where k_D' is the complex wavenumber of the shell defined by

$$k_D'^4 = k_D^4 - j\omega \frac{\zeta}{D} z_S, \quad (14.198)$$

$$k_D^4 = \frac{\rho_D h}{D} \omega^2 - \frac{\zeta^4}{a^4}, \quad (14.199)$$

$$\zeta^4 = 48(1 - \nu^2) H^2 / h^2, \quad (14.200)$$

ρ_D is the density of the shell material, h is its thickness, and H is the dome height. A specific acoustic impedance such as that due to a mesh with flow resistance is define by z_S . The Green's function for the shell from Eq. (14.148) can be rewritten suppressing the axial term in ϕ and ϕ_0 as follows

$$G(w|w_0) = \frac{a^2}{\pi} \sum_{n=1}^{\infty} \frac{\eta_n(w)\eta_n^*(w_0)}{\Delta_n(\beta_n^4 - k_D'^4 a^4)}, \quad 0 \leq w \leq a. \quad (14.201)$$

where

$$\eta_n^*(w_0) = J_0(\beta_n^* w_0/a) - B_n^* I_0(\beta_n^* w_0/a) + C_n^*. \quad (14.202)$$

Velocity distribution

On the surface of the shell, let the velocity distribution $\tilde{u}_0(w)$ be defined as

$$\tilde{u}_0(w) = \frac{\tilde{f}_g}{2\rho_0 c S_D} \sum_{m=1}^{\infty} A_m \eta_m(w), \quad (14.203)$$

where $\eta_m(w)$ is given by Eq. (14.191) above.

Solution of the free-space wave equation

The free-space wave equation is the same as that given by Eq. (14.63) for a membrane in free space, but because of the presence of an infinite baffle, we use the monopole solution which is the same as that for a resilient disk in an infinite baffle given by Eq. (13.160). Hence, after inserting Eqs. (13.52), (13.158), and (14.203) into Eq. (13.160) and integrating over ϕ_0 , we obtain

$$\tilde{p}(w, z) = \frac{k\tilde{f}_g}{2S_D} \sum_{m=1}^{\infty} A_m \int_0^a \eta_m(w_0) \int_0^{\infty} J_0(k_w w) J_0(k_w w_0) \frac{e^{-jk_z z}}{k_z} k_w dk_w w_0 dw_0. \quad (14.204)$$

Then setting $z = 0$ yields the surface pressure

$$\tilde{p}_+(w) = \frac{\tilde{f}_g}{S_D} \sum_{m=1}^{\infty} A_m I_m(k, w), \quad (14.205)$$

where

$$I_m(k, w) = \frac{k}{2} \int_0^a \eta_m(w_0) \int_0^{\infty} J_0(k_w w) J_0(k_w w_0) \frac{k_w}{\sqrt{k^2 - k_w^2}} dk_w w_0 dw_0 \quad (14.206)$$

and the infinite integral is given by Eq. (13.166). Hence,

$$I_m(k, w) = \frac{k}{2} \frac{\sqrt{\pi} k}{2} \sum_{q=0}^{\infty} \frac{w^{2q}}{(q!)^2} \times \sum_{r=0}^{\infty} \frac{\Gamma\left(\frac{r}{2} + \frac{r}{2}\right)}{\Gamma\left(\frac{r}{2} + 1\right) \Gamma^2\left(\frac{r}{2} - q + \frac{r}{2}\right)} \left(\frac{-jk}{2}\right)^{r-1} \int_0^a \eta_m(w_0) w_0^{r-2q} dw_0 \quad (14.207)$$

which is simplified with help of the integrals

$$\int_0^a J_0(\beta_m w_0/a) w_0^{r-2q} dw_0 = \frac{a^{r-2q+1}}{r-2q+1} {}_1F_2\left(\frac{r}{2} - q + \frac{1}{2}; \frac{r}{2} - q + \frac{3}{2}, 1; -\frac{\beta_m^2}{4}\right) \quad (14.208)$$

$$\int_0^a I_0(\beta_m w_0/a) w_0^{r-2q} dw_0 = \frac{a^{r-2q+1}}{r-2q+1} {}_1F_2\left(\frac{r}{2} - q + \frac{r}{2}; \frac{r}{2} - q + \frac{3}{2}, 1; \frac{\beta_m^2}{4}\right) \quad (14.209)$$

$$\int_0^a w_0^{r-2q} dw_0 = \frac{a^{r-2q+1}}{r-2q+1} \quad (14.210)$$

so that

$$\begin{aligned}
 I_m(k, w) = & -\frac{\sqrt{\pi}}{2} \sum_{r=0}^{\infty} \frac{\Gamma\left(\frac{r}{2} + \frac{1}{2}\right)}{\Gamma\left(\frac{r}{2} + 1\right)} \left(\frac{-jka}{2}\right)^{r+1} \sum_{q=0}^{\infty} \frac{1}{(q!)^2 \Gamma\left(\frac{r}{2} - q + \frac{1}{2}\right)} \left(\frac{w}{a}\right)^{2q} \\
 & \times \left({}_1\tilde{F}_2\left(\frac{r}{2} - q + \frac{1}{2}; \frac{r}{2} - q + \frac{3}{2}, 1; \frac{-\alpha_m^2}{4}\right) \right. \\
 & \left. - B_{m1} \tilde{F}_2\left(\frac{r}{2} - q + \frac{1}{2}; \frac{r}{2} - q + \frac{3}{2}, 1; \frac{\alpha_m^2}{4}\right) + \frac{C_m}{\Gamma\left(\frac{r}{2} - q + \frac{3}{2}\right)} \right), \tag{14.211}
 \end{aligned}$$

where ${}_1\tilde{F}_2$ is the regularized hypergeometric function.

Formulation of the coupled shell

Substituting Eqs. (14.205) and (14.201) in Eq. (14.197), integrating over the surface of the shell, and then equating the displacement with that given in Eq. (14.203) (where $\tilde{\eta}(w) = -j\tilde{u}_0(w)/kc$), while replacing w with w_0 in Eq. (14.205) and equating the coefficients of $\eta_n(w)$, leads to the following coupled equation

$$A_n \frac{jD(\beta_n^4 - k_D^4 a^4)}{4\zeta ka^4 \rho_0 c^2} + \sum_{m=1}^{\infty} A_m \frac{2}{a^2 \Delta_n} \int_0^a I_m(k, w_0) \eta_n^*(w_0) w_0 dw_0 = \frac{\eta_n^*(b)}{2\Delta_n}, \tag{14.212}$$

where we have used the property of the Dirac delta function.

Final set of simultaneous equations for the power-series coefficients

From Eq. (14.212), together with the identity of Eq. (14.208), the following set of M simultaneous equations in A_m can be written as

$$\sum_{m=1}^M {}_m\Psi_n(k_D' a, ka) A_m = 1, \quad n = 1, 2, \dots, M, \tag{14.213}$$

where ${}_m\Psi_n$ is an element of the m th column and n th row of the $M \times M$ matrix given by

$${}_m\Psi_n(k_D' a, ka) = \frac{jka \delta_{mn} \Delta_n (\beta_n^4 - k_D^4 a^4)}{\zeta \alpha^2 (ka) \eta_n^*(b)} + \frac{\sqrt{\pi}}{\eta_n^*(b)} \sum_{r=1}^{\infty} \left(\frac{-jka}{2}\right)^r H_{nmr}, \tag{14.214}$$

where Δ_n is given by Eq. (14.144) with $m = 0$, δ_{mn} is the Kronecker delta function, and the infinite series limit has been truncated to order M . The dimensionless quantity α is the fluid-loading factor given by

$$\alpha(ka) = a^2\omega\sqrt{2a\rho_0/D} = ka^2\sqrt{2a\gamma P_0/D}, \quad (14.215)$$

where P_0 is the static pressure defined by $P_0 = \rho_0 c^2/\gamma$. The function H_{mmr} is defined by

$$\begin{aligned} H_{mmr} &= \frac{\Gamma\left(\frac{r}{2}\right)}{\Gamma\left(\frac{r}{2} + \frac{1}{2}\right)} \sum_{q=0}^{\infty} \frac{1}{q! \Gamma\left(\frac{r}{2} - q\right)} \\ &\times \left({}_1\tilde{F}_2\left(\frac{r}{2} - q; \frac{r}{2} - q + 1, 1; -\frac{\beta_m^2}{4}\right) - B_{m1}\tilde{F}_2\left(\frac{r}{2} - q; \frac{r}{2} - q + 1, 1; \frac{\beta_m^2}{4}\right) + \frac{C_m}{\Gamma\left(\frac{r}{2} - q + 1\right)} \right) \\ &\times \left({}_1\tilde{F}_2\left(q + 1; q + 2, 1; -\frac{\beta_n^{*2}}{4}\right) - B_{n1}^*\tilde{F}_2\left(q + 1; q + 2, 1; \frac{\beta_n^{*2}}{4}\right) + \frac{C_n^*}{\Gamma(q + 2)} \right), \end{aligned} \quad (14.216)$$

Far-field pressure

The far-field pressure is derived by inserting the far-field Green's function in spherical–cylindrical coordinates from Eq. (13.70), together with Eq. (14.203) and (13.158), into Eq. (13.177) and integrating over the surface of the shell using Eqs. (76) and (95) from Appendix II (with $z = kw_0 \sin \theta$, $b = k \sin \theta$, and letting $\phi = \pi/2$ so that $\cos(\phi - \phi_0) = \sin \phi_0$) together with the following integrals:

$$\int_0^a J_0(kw_0 \sin \theta) J_0(\beta_m w_0/a) w_0 dw_0 = a^2 \frac{\beta_m J_1(\beta_m) J_0(ka \sin \theta) - (ka \sin \theta) J_1(ka \sin \theta) J_0(\beta_m)}{\beta_m^2 - (ka \sin \theta)^2} \quad (14.217)$$

$$\int_0^a J_0(kw_0 \sin \theta) I_0(\beta_m w_0/a) w_0 dw_0 = a^2 \frac{\beta_m I_1(\beta_m) J_0(ka \sin \theta) + (ka \sin \theta) J_1(ka \sin \theta) I_0(\beta_m)}{\beta_m^2 + (ka \sin \theta)^2} \quad (14.218)$$

to give

$$\tilde{p}(r, \theta) = \frac{jaf_g}{4rS_D} e^{-ikr} D(\theta), \quad (14.219)$$

where r is the distance from the origin to the observation point and θ is the angle subtended to the axis of symmetry. The directivity function $D(\theta)$ is given by

$$D(\theta) = 2ka \sum_{m=1}^{\infty} A_m \left(\frac{\beta_m J_1(\beta_m) J_0(ka \sin \theta) - (ka \sin \theta) J_1(ka \sin \theta) J_0(\beta_m)}{\beta_m^2 - (ka \sin \theta)^2} - B_m \frac{\beta_m I_1(\beta_m) J_0(ka \sin \theta) + (ka \sin \theta) J_1(ka \sin \theta) I_0(\beta_m)}{\beta_m^2 + (ka \sin \theta)^2} + C_m \frac{J_1(ka \sin \theta)}{ka \sin \theta} \right). \quad (14.220)$$

For $\theta = 0$ (i.e., on-axis), this simplifies to

$$D(0) = ka \sum_{m=1}^M A_m \left(2 \frac{J_1(\beta_m)}{\beta_m} - 2B_m \frac{I_1(\beta_m)}{\beta_m} + C_m \right). \quad (14.221)$$

The far-field on-axis responses of a 25 mm dia. aluminum dome loudspeaker are plotted in Figs. 14.12 and 14.13 with $h = 10$ and $20 \mu\text{m}$, respectively. The remaining quantities are given in Tables 14.5 and 14.6 with the in vacuo eigenfrequencies given in Table 14.7.

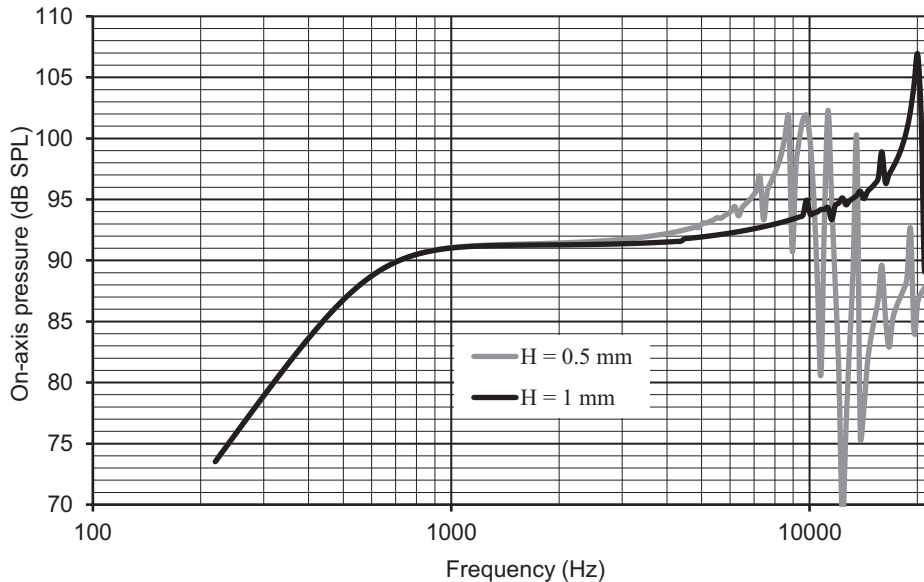


Figure 14.12 Far-field on-axis pressure response of the fully coupled 25 mm dia. aluminum dome loudspeaker in an infinite baffle with $h = 10 \mu\text{m}$ and 1 W input. The remaining quantities are given in Tables 14.5 and 14.6, with the in vacuo eigenfrequencies given in Table 14.7.

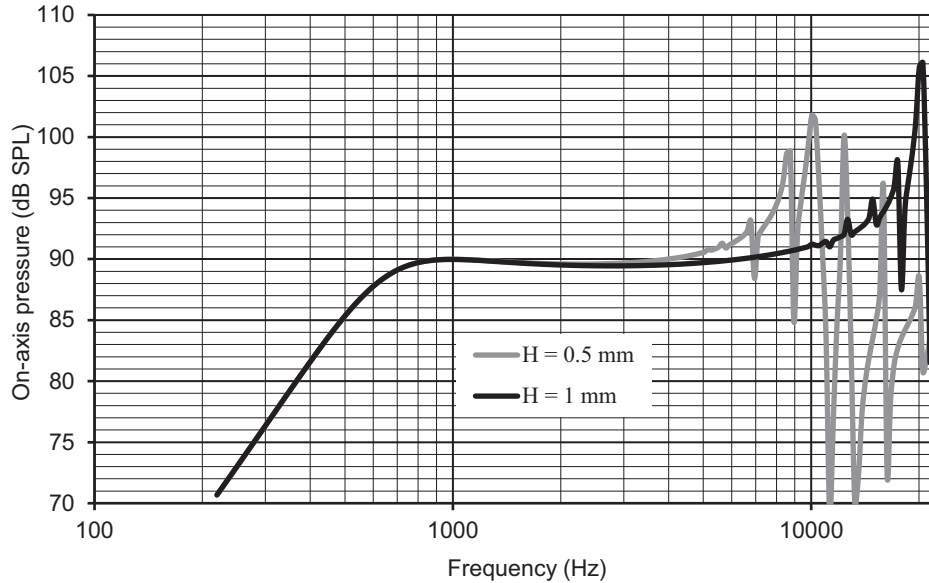


Figure 14.13 Far-field on-axis pressure response of the fully coupled 25 mm dia. aluminum dome loudspeaker in an infinite baffle with $h = 20 \mu\text{m}$ and 1 W input. The remaining quantities are given in Tables 14.5 and 14.6, with the in vacuo eigenfrequencies given in Table 14.7.

To provide maximum efficiency according to the criteria of Section 6.13, the coil wire diameter t is calculated to make the mass M_{MW} of the coil wire equal to the remaining moving mass. This is achieved by solving

$$M_{MW} = M_{MS} + M_{AR} + M_{MF} \quad (14.222)$$

Table 14.5 Aluminum shell quantities for the 25 mm dia. dynamic loudspeaker

Radius	$a = 12.5 \text{ mm}$
Thickness	$h = 10/20 \mu\text{m}$
Apex height	$H = 0.5/1.0 \text{ mm}$
Young's modulus	$Y = 69 \text{ GN/m}^2$
Poisson's ratio	$\nu = 0.3$
Density of shell	$\rho_D = 2700 \text{ kg/m}^3$
Shell mass	$M_{MS} = 13.3/26.6 \text{ mg}$
Density of air	$\rho_0 = 1.18 \text{ kg/m}^3$
Speed of sound in air	$c = 345 \text{ m/s}$
Damping/loading	$z_S = 0 \text{ kg/s}$
Observation distance	$r = 1 \text{ m}$

Table 14.6 Coil and suspension quantities for the 25 mm dia. dynamic loudspeaker

Suspension frequency	$f_0 = 700$ Hz
Suspension resistance	$R_{MS} = 0.06$ N s m
Coil electrical resistance	$R_E = 8$ Ω
Coil wire diameter	$t = 56/65$ μ m
Coil wire density	$\rho_C = 8700$ kg/m ³
Coil wire resistivity	$\sigma_C = 17.2$ n Ω m
Coil wire total length	$l = 1.09/1.47$ m
Coil wire length per turn	$l_T = 78.5$ mm
Coil number of turns	$n = 14/18$
Coil mass	$M_{MC} = 25.0/47.3$ mg
Magnetic flux density	$B = 1$ T
Flux coil-length product	$Bl = B \times l = 0.87/1.47$ T m
Input voltage for 1 W	$e_{g(\text{rms})} = \sqrt{R_E W} _{W=1 \text{ W}_{\text{rms}}} = 2.83$ V

Table 14.7 Eigenfrequencies for the 25 mm aluminum shell

Frequency no.	$h = 10$ μ m		$h = 20$ μ m	
	$H = 0.5$ mm	$H = 1.0$ mm	$H = 0.5$ mm	$H = 1.0$ mm
$n = 1$	699.98	699.99	699.69	699.92
$n = 2$	5177.8	10,313	5261.8	10,356
$n = 3$	5314.6	10,382	5774.5	10,629
$n = 4$	5676.1	10,573	6976.8	11,352
$n = 5$	6375.3	10,969	8834.5	12,751
$n = 6$	7471.1	11,658	10,367	14,947
$n = 7$	8903.7	12,713	12,531	17,849
$n = 8$	11,358	14,175	16,092	20,464
$n = 9$	13,589	16,048	20,468	22,859
$n = 10$	16,291	18,258	25,542	27,221

for t . The wire mass M_{MW} is given by

$$M_{MW} = \pi t^2 l \rho_C / 4, \quad (14.223)$$

where ρ_C is the density of the coil wire. The total length l of the coil wire is related to the coil resistance R_E by

$$l = \pi t^2 R_E / (4 \sigma_C), \quad (14.224)$$

where σ_C is the resistivity of the coil wire. The shell mass M_{MS} is given by Eq. (14.173), M_{MR} is the radiation mass on *both* sides of a piston in an infinite baffle given by

$$M_{MR} = 16a^3\rho_0/3, \quad (14.225)$$

and M_{MF} is the mass of the coil former given by

$$M_{MF} = 2\pi ant\rho_D h, \quad (14.226)$$

where n is the number of turns given by

$$n = l/l_T, \quad (14.227)$$

and

$$l_T = 2\pi a \quad (14.228)$$

is the length per turn. Then the total coil mass M_{MC} is given by

$$M_{MC} = M_{MW} + M_{MF}. \quad (14.229)$$

Comparing Figs. 14.12 and 14.13, we see that the main effect of increasing the thickness h of the shell from 10 to 20 μm is to produce a dip in the midband sensitivity due to the increased inertia. Otherwise, the two figures are remarkably similar. Changing the dome height H has a much more significant effect. In each case, the diaphragm break-up starts just above 5 kHz (gray curve) when the dome height is 0.5 mm, but this rises to above 10 kHz (black curve) when it is 1 mm. We see from Table 14.7 that the lower eigenfrequencies are largely determined by the dome height, whereas the higher ones are determined more by the dome thickness. Because of the high overall mechanical impedance, the radiation resistance acting on the coupled shell does not appear to have the damping effect on the higher-order modes that it does in the case of the membrane response shown in Fig. 14.5.

PART XXXXI: INDUCTION LOUDSPEAKERS

14.19 RADIATION FROM A CIRCULAR PLATE IN AN INFINITE Baffle—MODEL OF AN INDUCTION LOUDSPEAKER COUPLED TO ITS SURROUNDING AIR [13,14]

So far, we have analyzed membrane and shell type loudspeaker diaphragms but only looked briefly at plates to calculate their mode frequencies with various boundary conditions. With the shell, we followed the traditional approach of using curvature, together with the material properties, to maximize the stiffness and thus raise the eigenfrequencies

as high as possible. This in turn made the pressure response relatively flat until the first break-up frequencies occurred, above which it became highly irregular. The ideal material has a high ratio of Young's modulus to density. With an ultra-light membrane, there is no bending stiffness and instead we can use the combination of a dust-screen and radiation resistance to damp the modes, as will be demonstrated in Chapter 15.

Here we explore a third way, which is to use the phenomenon whereby the modes of a free circular plate are not propagated on-axis when driven by a concentrated ring force, such as that produced by a voice coil. Hence, the on-axis response looks as flat as that of a rigid piston, provided that the acoustic load is very light. However, the free plate differs from a piston in that if the radius of the ring force is reduced until it effectively becomes a point force at the center, the radiated power becomes constant! Hence, the directivity pattern of the free plate does not shrink with increasing frequency as does that of a rigid piston.

Unfortunately, if the circular plate is used as the diaphragm of a dynamic, or moving-coil, loudspeaker, the coil mass introduces irregularities into the on-axis response. The edge suspension, or surround, also detracts slightly from the ideal free plate, so it is important to set the suspension resonance frequency well before the first plate mode. One way to compensate for the coil mass is to rebalance the plate by adding nodal ring masses, but they do not remove all the modes completely and they reduce efficiency by adding to the total moving mass [15].

Construction of an induction loudspeaker

What if we were to drive the plate without attaching a coil to it at all, but instead could drive it from a stationary voice coil? One option might be to look to the past by reintroducing the reluctance transducer as used in telephone receivers for much of the 20th century.

The scheme shown in Fig. 14.14 has like magnetic pole pieces facing each other. In other words, north faces north and south faces south so that the steady-state flux in the gap is forced to flow radially through the plate between the inner and outer pole pieces rather than across the gap between opposite pole pieces. In Fig. 14.14, the voice coil is wound in two halves, one on each side of the plate, where the + signs denote current flowing into the page while the - signs denote current flowing out of it. Of course, the signal current is alternating, so this just indicates the relative directions of the instantaneous currents in the windings, which are arranged for an induction loudspeaker. For a reluctance loudspeaker, the winding on one side would be reversed and the plate would be made from a ferromagnetic material. Hence, during one half of a cycle, the magnetic flux in one core would increase while in the other it would decrease and thus cause the plate to be attracted towards the one with the greater flux. In this way, we would have a push-pull reluctance transducer. The plate of the single-sided version used in telephones had to be clamped at the perimeter, rather than elastically supported, to prevent it from being pulled toward the magnetic pole pieces. The push-pull arrangement shown balances out the quiescent force of attraction so that a compliant surround may be used.

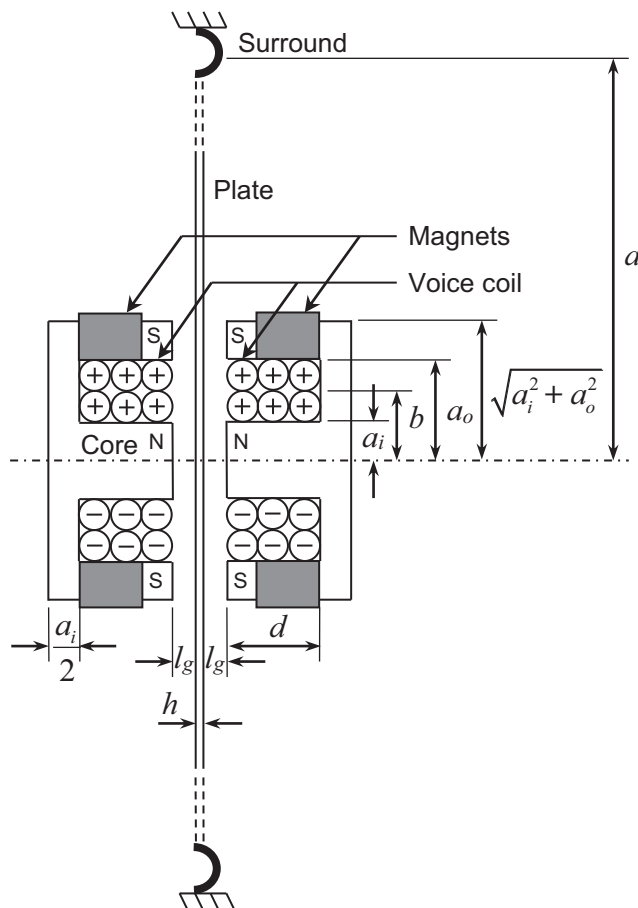


Figure 14.14 Cross-sectional sketch of an induction loudspeaker, which is assumed to be mounted in an infinite baffle. Not shown is a rigid, but acoustically transparent, basket structure to support the magnets on each side. To minimize its effect on the radiation of sound, the radius of the magnet is much smaller than that of the plate.

However, thin steel plates saturate at relatively low flux levels and therefore the reluctance loudspeaker would have very limited acoustic output, which is why early loudspeakers using this principle were essentially telephone receivers with horns attached to boost the inevitably weak sound output.

Instead, we shall induce a current in a nonferromagnetic plate using the configuration shown in Fig. 14.14. The quiescent field still flows radially through the plate, but the signal field flows across it in two loops around the upper and lower halves of the windings. Hence, the voice coil can be considered as the primary winding of a transformer that induces a circular eddy current in the plate, so that the plate behaves as a shorted secondary winding if it is blocked. However, if it is free to move, a back emf \tilde{e} is produced, which is proportional to its velocity \tilde{u}_C according to

$$\tilde{e} = Bl\tilde{u}_C, \quad (14.230)$$

where B is the flux density in the gap and l is the path length of the induced eddy current loop.

The eddy current \tilde{i} produces a magnetic field that in turn produces a force \tilde{f}_C , which acts on the plate to make it move according to

$$\tilde{f}_C = Bl\tilde{i}. \quad (14.231)$$

In our analysis, we shall ignore the fact that both faces of the plate shown in Fig. 14.14 are partially covered by the magnet structure. In our worked example, the magnet structure will cover less than 15% of the surface area, so the error should be small.

Analogous circuit

The complete electro-mechano-acoustical analogous circuit is shown in Fig. 14.15 using the impedance analogy throughout.

This is an approximate circuit that represents the plate as a lumped mass M_{MD} and ignores its vibrational behavior. Therefore, it is only valid for frequencies below the first plate mode. We shall replace everything beyond the terminals 4 and 5 with an analytical model later in this section, while incorporating everything before them in the driving force and boundary conditions (after some simplifications). For simplicity, we assume all the flux produced by the coil couples the “shorted turn” of the plate; and therefore the inductance L_{EC} is mutual to both the primary and secondary windings of the virtual transformer of turns ratio N . Otherwise, we would have to add two leakage inductances: one in series with coil resistance R_{EC} and the other in series with the resistance R_{ED} of the “shorted turn.” Although the coil inductance is a series impedance in a dynamic loudspeaker, which limits the high-frequency output, here it is a shunt impedance that shorts the input at low frequencies and should therefore be made as large as possible. In fact, there is a trade-off between greater low-frequency displacement when the gap distance l_g is increased and larger inductance when it is reduced. The blocking capacitor C_E , together with L_{EC} , forms a second-order high-pass filter that reduces the low-frequency displacement, avoids shorting of the input, and prevents saturation of the iron core.

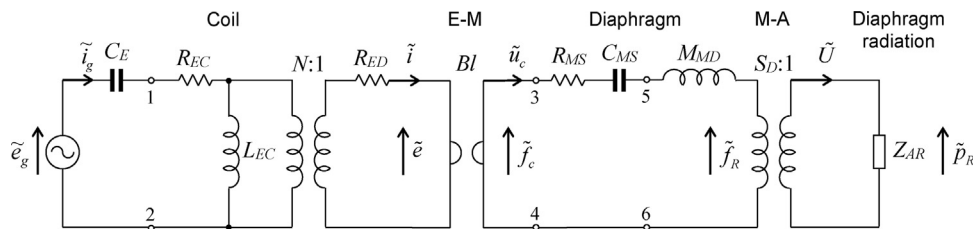


Figure 14.15 Electro-mechano-acoustical analogous circuit of the induction loudspeaker using the impedance analogy throughout.

The symbols have the following meanings:

\tilde{e}_g is voltage of the generator or amplifier (assuming negligible output impedance) in volts (V).

R_{EC} is resistance of voice coil in ohms (Ω).

L_{EC} is inductance of voice coil in henrys (H).

N is number of turns of voice coil.

R_{ED} is loop resistance seen by induced plate eddy current in ohms (Ω).

B is steady state air gap magnetic field or flux density in Tesla (T).

l is length in meters (m) of eddy current loop induced in plate.

\tilde{i} is plate eddy current in amperes (A).

\tilde{f}_C is force acting on the plate according to Eq. (14.231).

\tilde{u}_C is plate velocity in m/s according to Eq. (14.230).

R_{MS} is mechanical resistance of the surround in N·s/m.

C_{MS} is mechanical compliance of the surround in m/N.

M_{MD} is mechanical mass of the plate in Kg.

$S_D = \pi a^2$ is area of the plate (ignoring the surround) in m^2 .

Z_{AR} is acoustical radiation impedance in $N \cdot s/m^5$.

\tilde{p} is pressure on the plate in Pa due to the radiation load.

\tilde{U} is volume velocity in m^3/s produced by the plate.

We will use the following definitions:

$$R_{EC} = \frac{\sigma_c l_c}{\pi a_w^2}, \quad (14.232)$$

where σ_c is the resistivity of the coil wire, a_w is the wire radius given by

$$a_w = \frac{1}{2} \sqrt{\frac{A_w}{N}}, \quad (14.233)$$

A_w is the winding window area, assuming only $2/3$ of the area is available after allowing for the bobbin, insulation, etc., so that

$$A_w = \frac{4}{3} d(a_o - a_i), \quad (14.234)$$

l_c is the length of the voice coil given by

$$l_c = 2N\pi b, \quad (14.235)$$

and $b = (a_i + a_o)/2$ is the average radius of the voice coil windings as well as that of the induced eddy current. Whereas the flux density B in a dynamic loudspeaker is normally set to the saturation density B_{SAT} , here we will set it to around 1 T m where the relative permeability μ_r is maximum (around 35,000 for silicon steel). This ensures that the

inductance is dominated by the air gap, which in turn gives maximum linearity, according to

$$L_{EC} = \frac{N^2 \mu_0 A_g}{4l_g + l_c/\mu_r} \approx \frac{N^2 \mu_0 A_g}{4l_g}, \quad \mu_r \gg l_c/(4l_g), \quad (14.236)$$

where A_g is the cross-sectional area of the core given by

$$A_g = \pi a_i^2. \quad (14.237)$$

The resistance of the eddy current loop, or “shorted turn,” is

$$R_{ED} = \frac{\sigma_d l}{A_d}, \quad (14.238)$$

where σ_d is the resistivity of the plate, l is the length of the eddy current loop given by

$$l = 2\pi b, \quad (14.239)$$

and A_d is the cross-sectional area of the eddy current loop given by

$$A_d = (a_o - a_i)h. \quad (14.240)$$

Because the shorted turn, which comprises the secondary winding of the transformer, occupies only a small part of the winding window, the total electrical resistance R_E (referred to the primary) is dominated by the resistance of the shorted turn R_{ED} , such that

$$R_E = R_{EC} + N^2 R_{ED} \approx N^2 R_{ED}, \quad (14.241)$$

Hence, the number of turns required for a given coil resistance is

$$N = \sqrt{\frac{h(a_o - a_i)R_E}{\pi(a_o + a_i)\sigma_d}}. \quad (14.242)$$

Before we develop the analytical model of the mechanical and acoustical parts of Fig. 14.15, we shall simplify the electrical part as shown in Fig. 14.16, where the electrical impedance Z_E is given by

$$Z_E = R_{ED} + \left(\frac{N^2}{j\omega L_{EC}} + \frac{N^2}{R_{EC} + \frac{1}{j\omega C_E}} \right)^{-1} \quad (14.243)$$

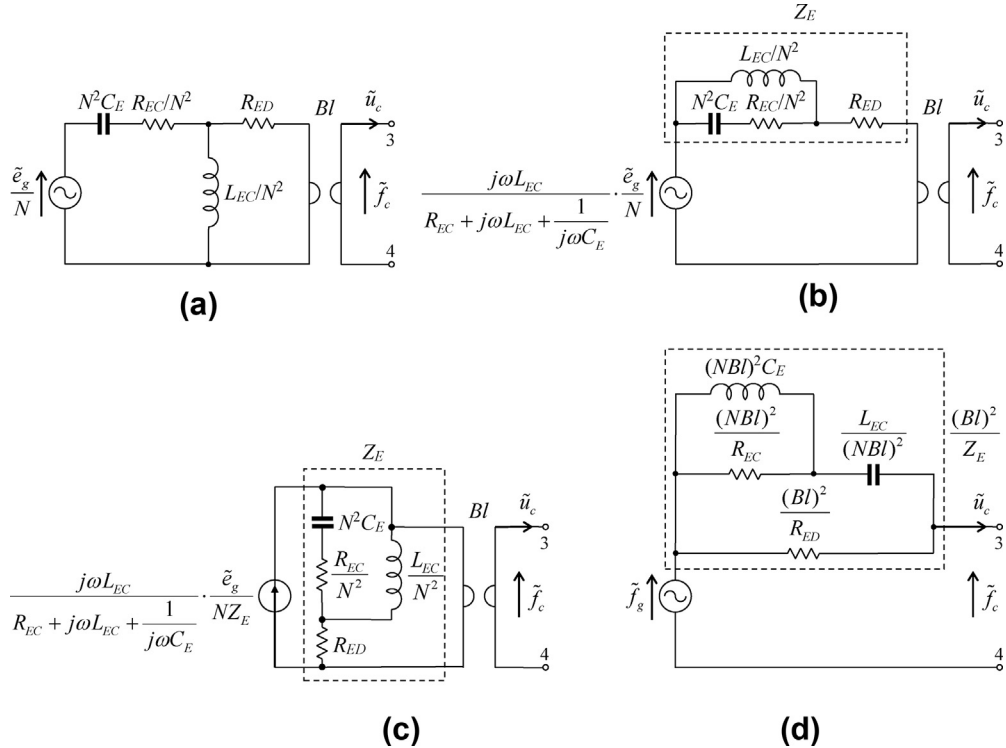


Figure 14.16 (a) The electrical part of Fig. 14.15 referred to the secondary side of the induction transformer. (b) The Thévenin equivalent of the generator voltage source, together with R_{EC} and L_{EC} . (c) The equivalent of (b) according to Norton's theorem. (d) The admittance analogy of the electrical part from (c) referred to the mechanical side.

and the force \tilde{f}_g , which we shall apply to the plate as a ring force due to the eddy current, is given by

$$\tilde{f}_g = \frac{j\omega L_{EC}}{R_{EC} + j\omega L_{EC} + \frac{1}{j\omega C_E}} \cdot \frac{Bl}{NZ_E} \tilde{e}_g \quad (14.244)$$

$$\approx \frac{\omega^2}{\omega^2 - j\omega \frac{\omega_C}{Q_C} - \omega_C^2} \cdot \frac{Bl}{NR_{ED}} \tilde{e}_g, \quad N^2 R_{ED} \gg R_{EC}$$

where ω_C is the lower cut-off frequency due to the induction coil winding inductance

$$\omega_C = \frac{1}{\sqrt{L_{EC} C_E}} \quad (14.245)$$

and

$$Q_C = N^2 R_{ED} \sqrt{\frac{C_E}{L_{EC}}}. \quad (14.246)$$

The cut-off frequency ω_C should be well above the frequency below which saturation occurs

$$\omega_{SAT} = \frac{\sqrt{2}e_g}{(B_{SAT} - B)A_g N}. \quad (14.247)$$

In the boundary conditions at the perimeter of the plate, we will add the mechanical resistance R_{MS} to the stiffness reactance of the surround so that the mechanical Q is defined by

$$Q_{MS} = \frac{1}{R_{MS}} \sqrt{\frac{M_{MD}}{C_{MS}}}. \quad (14.248)$$

Although the coil produces a ring force of radius b , for the electrical damping due to the resistance of the “shorted turn” we will simplify the boundary conditions by assuming that this damping produces an equivalent mechanical resistance of $(Bl)^2/R_{ED}$ at the center, which is a reasonable approximation provided that $b \leq 0.26 a$. We will assume that this resistance dominates Z_E (see Fig. 14.16(d)) so that

$$Q_{ES} = \frac{R_{ED}}{B^2 l^2} \sqrt{\frac{M_{MD}}{C_{MS}}}. \quad (14.249)$$

However, because the Bessel functions Y_0 and K_0 are singular when their arguments are zero, we shall apply a small offset δ from the center to begin with and then derive the equation for the eigenvalues as $\delta \rightarrow 0$.

Boundary conditions

Although we will reuse the derivation for the shell in an infinite baffle to analyze the behavior of the plate diaphragm, there are two important differences here. Firstly, because the plate is flat, we set

$$H = 0, \quad (14.250)$$

which leads to

$$\xi = \tilde{C}_{5n} = C_n = 0 \text{ and } R = \infty, \quad (14.251)$$

so that after setting $k_D a = \beta_n$, the eigenfunctions of Eq. (14.156) become

$$\tilde{\eta}_n(w) = \tilde{C}_{1n} J_0(\beta_n w/a) + \tilde{C}_{2n} Y_0(\beta_n w/a) + \tilde{C}_{3n} I_0(\beta_n w/a) + \tilde{C}_{4n} K_0(\beta_n w/a). \quad (14.252)$$

Secondly, because there is no coil former joined to the perimeter, we replace the boundary condition of zero bending at the perimeter with one of *zero bending moment*, so that as the stiffness of the surround is reduced to zero, we have a truly free edge. Hence, we replace Eq. (14.164) with an axisymmetric version of Eq. (14.111)

$$\begin{aligned}
& \left(\frac{\partial^2}{\partial w^2} + \frac{\nu}{w} \cdot \frac{\partial}{\partial w} \right) \tilde{\eta}_n(w) \Big|_{w=a} \\
&= -D \frac{\beta_n}{a^2} \left\{ \tilde{C}_{1n}((1-\nu)J_1(\beta_n) - \beta_n J_0(\beta_n)) + \tilde{C}_{2n}((1-\nu)Y_1(\beta_n) - \beta_n Y_0(\beta_n)) \right. \\
&\quad \left. - \tilde{C}_{3n}((1-\nu)I_1(\beta_n) - \beta_n I_0(\beta_n)) + \tilde{C}_{4n}((1-\nu)K_1(\beta_n) + \beta_n K_0(\beta_n)) \right\} = 0,
\end{aligned} \tag{14.253}$$

At the perimeter, we have a shear force due to the surround

$$\begin{aligned}
\tilde{Q}_n(w) \Big|_{w=a} &= -D \frac{\partial}{\partial w} \nabla^2 \tilde{\eta}_n(w) \Big|_{w=a} \\
&= -\frac{\beta_n^3}{a^3} D (\tilde{C}_{1n} J_1(\beta_n) + \tilde{C}_{2n} Y_1(\beta_n) + \tilde{C}_{3n} I_1(\beta_n) - \tilde{C}_{4n} K_1(\beta_n)) \\
&= -\left(\frac{1}{C_{MS}} + j\omega_n R_{MS} \right) \frac{\tilde{\eta}_n(a)}{2\pi a},
\end{aligned} \tag{14.254}$$

where C_{MS} and R_{MS} are the mechanical compliance and resistance of the surround respectively, as given by Eqs. (14.175) and (14.248). Near the center, we have a shear force due to the electrical damping resistance of the “shorted turn”

$$\begin{aligned}
\tilde{Q}_n(w) \Big|_{w=\delta} &= -D \frac{\partial}{\partial w} \nabla^2 \tilde{\eta}_n(w) \Big|_{w=\delta} \\
&= -\frac{\beta_n^3}{a^3} D (\tilde{C}_{1n} J_1(\beta_n \delta/a) + \tilde{C}_{2n} Y_1(\beta_n \delta/a) + \tilde{C}_{3n} I_1(\beta_n \delta/a) - \tilde{C}_{4n} K_1(\beta_n \nu/a)) \\
&= -j\omega_n \frac{B^2 l^2}{R_{ED}} \frac{\tilde{\eta}_n(\delta)}{2\pi \delta},
\end{aligned} \tag{14.255}$$

We also use the angular eigenfrequency ω_n from Eq. (14.167), and total mass M_{MD} from Eqs. (14.173) and (14.174) with the coil mass $M_{MC} = 0$ and mass loading factor $\zeta = 1$. Substituting these into Eqs. (14.254) and (14.255), while rearranging, leads to

$$\begin{aligned} & \tilde{C}_{1n}(\gamma_n J_0(\beta_n) - \beta_n^3 J_1(\beta_n)) + \tilde{C}_{2n}(\gamma_n Y_0(\beta_n) - \beta_n^3 Y_1(\beta_n)) \\ & + \tilde{C}_{3n}(\gamma_n I_0(\beta_n) - \beta_n^3 I_1(\beta_n)) + \tilde{C}_{4n}(\gamma_n K_0(\beta_n) + \beta_n^3 K_1(\beta_n)) = 0 \end{aligned} \quad (14.256)$$

$$\begin{aligned} & \tilde{C}_{1n} \left(\tau_n J_0 \left(\beta_n \frac{\delta}{a} \right) - \beta_n^3 J_1 \left(\beta_n \frac{\delta}{a} \right) \right) + \tilde{C}_{2n} \left(\tau_n Y_0 \left(\beta_n \frac{\delta}{a} \right) - \beta_n^3 Y_1 \left(\beta_n \frac{\delta}{a} \right) \right) \\ & + \tilde{C}_{3n} \left(\tau_n I_0 \left(\beta_n \frac{\delta}{a} \right) - \beta_n^3 I_1 \left(\beta_n \frac{\delta}{a} \right) \right) + \tilde{C}_{4n} \left(\tau_n K_0 \left(\beta_n \frac{\delta}{a} \right) + \beta_n^3 K_1 \left(\beta_n \frac{\delta}{a} \right) \right) = 0 \end{aligned} \quad (14.257)$$

where

$$\gamma_n = \frac{\beta_0^2}{2} \left(\beta_0^2 + j \frac{\beta_n^2}{Q_{MS}} \right) \quad (14.258)$$

$$\tau_n = \frac{a}{\delta} j \frac{\beta_0^2 \beta_n^2}{2Q_{ES}} \quad (14.259)$$

and the notional zeroth eigenvalue β_0 is defined by

$$\beta_0^4 = \frac{a^2 M_{MD}}{\pi D} \omega_0^2. \quad (14.260)$$

For continuity at the center, there is zero slope

$$\begin{aligned} \left. \frac{\partial}{\partial w} \tilde{\eta}_n(w) \right|_{w=\delta} &= -\frac{\beta_n}{a} \left(\tilde{C}_{1n} J_1 \left(\beta_n \frac{\delta}{a} \right) + \tilde{C}_{2n} Y_1 \left(\beta_n \frac{\delta}{a} \right) \right. \\ & \left. - \tilde{C}_{3n} I_1 \left(\beta_n \frac{\delta}{a} \right) + \tilde{C}_{4n} K_1 \left(\beta_n \frac{\delta}{a} \right) \right) = 0 \end{aligned} \quad (14.261)$$

From Eqs. (14.253), (14.256), (14.257), and (14.261) we obtain the following equation for the eigenvalues β_n

$$\begin{vmatrix} (1-\nu)J_1(\beta_n) - \beta_n J_0(\beta_n) & (1-\nu)Y_1(\beta_n) - \beta_n Y_0(\beta_n) & -(1-\nu)I_1(\beta_n) + \beta_n I_0(\beta_n) & (1-\nu)K_1(\beta_n) + \beta_n K_0(\beta_n) \\ J_1\left(\beta_n \frac{\delta}{a}\right) & Y_1\left(\beta_n \frac{\delta}{a}\right) & -I_1\left(\beta_n \frac{\delta}{a}\right) & K_1\left(\beta_n \frac{\delta}{a}\right) \\ \gamma_n J_0(\beta_n) - \beta_n^3 J_1(\beta_n) & \gamma_n Y_0(\beta_n) - \beta_n^3 Y_1(\beta_n) & \gamma_n I_0(\beta_n) - \beta_n^3 I_1(\beta_n) & \gamma_n K_0(\beta_n) + \beta_n^3 K_1(\beta_n) \\ \tau_n J_0\left(\beta_n \frac{\delta}{a}\right) - \beta_n^3 J_1\left(\beta_n \frac{\delta}{a}\right) & \tau_n Y_0\left(\beta_n \frac{\delta}{a}\right) - \beta_n^3 Y_1\left(\beta_n \frac{\delta}{a}\right) & \tau_n I_0\left(\beta_n \frac{\delta}{a}\right) - \beta_n^3 I_1\left(\beta_n \frac{\delta}{a}\right) & \tau_n K_0\left(\beta_n \frac{\delta}{a}\right) + \beta_n^3 K_1\left(\beta_n \frac{\delta}{a}\right) \end{vmatrix} = 0 \quad (14.262)$$

In the limit, as $\delta/a \rightarrow 0$, we obtain the equation for the eigenvalues where the electrical damping resistance is represented by a concentrated shear force at the center

$$\begin{aligned}
& I_1(\beta_n) \{ 4\beta_n^2 (2\beta_n^3(1-\nu)J_1(\beta_n) - \varepsilon_n J_0(\beta_n)) \\
& \quad - \chi_n (\pi (2\beta_n^3(1-\nu)Y_1(\beta_n) - \varepsilon_n Y_0(\beta_n)) - 2\beta_n^4 K_0(\beta_n)) \} \\
& + I_0(\beta_n) \{ 4\beta_n^2 (2\beta_n \gamma_n J_0(\beta_n) - \varepsilon_n J_1(\beta_n)) \\
& \quad - \chi_n (\pi (2\beta_n \gamma_n Y_0(\beta_n) - \varepsilon_n Y_1(\beta_n)) + 4\beta_n \gamma_n K_0(\beta_n) + 2\beta_n^4 K_1(\beta_n)) \} \\
& + 2\chi_n \{ J_1(\beta_n) (2\beta_n^3(1-\nu)K_1(\beta_n) - (\beta_n^4 - \gamma_n(1-\nu))K_0(\beta_n)) \\
& \quad - \varepsilon_n J_0(\beta_n) K_1(\beta_n) - \beta_n^3 + 2\gamma_n(1-\nu)/\beta_n \} = 0,
\end{aligned} \tag{14.263}$$

where

$$\chi_n = j \frac{\beta_0^2 \beta_n^2}{2Q_{ES}}, \tag{14.264}$$

$$\varepsilon_n = \beta_n^4 + (1-\nu) \frac{\beta_0^2}{2} \left(\beta_0^2 + j \frac{\beta_n^2}{Q_{MS}} \right). \tag{14.265}$$

If there is no damping, such that $Q_{MS} = Q_{ES} = \infty$, the eigenvalue equation simplifies to

$$\begin{vmatrix}
\frac{\beta_0^4}{2} J_0(\beta_n) - \beta_n^3 J_1(\beta_n) & \frac{\beta_0^4}{2} I_0(\beta_n) - \beta_n^3 I_1(\beta_n) \\
\beta_n J_0(\beta_n) - (1-\nu) J_1(\beta_n) & -\beta_n I_0(\beta_n) + (1-\nu) I_1(\beta_n)
\end{vmatrix} = 0 \tag{14.266}$$

These eigenvalues are plotted in [Fig. 14.17](#) against β_0 .

The eigenfrequencies are given by

$$f_n = \frac{\beta_n^2}{2\pi a^2} \sqrt{\frac{D}{\rho_D h}}. \tag{14.267}$$

Because the plate is continuous at the center, we now set

$$\tilde{C}_{2n} = \tilde{C}_{4n} = 0, \tag{14.268}$$

so that the eigenfunctions are given by

$$\tilde{\eta}_n(w) = J_0(\beta_n w/a) - B_n I_0(\beta_n w/a), \tag{14.269}$$

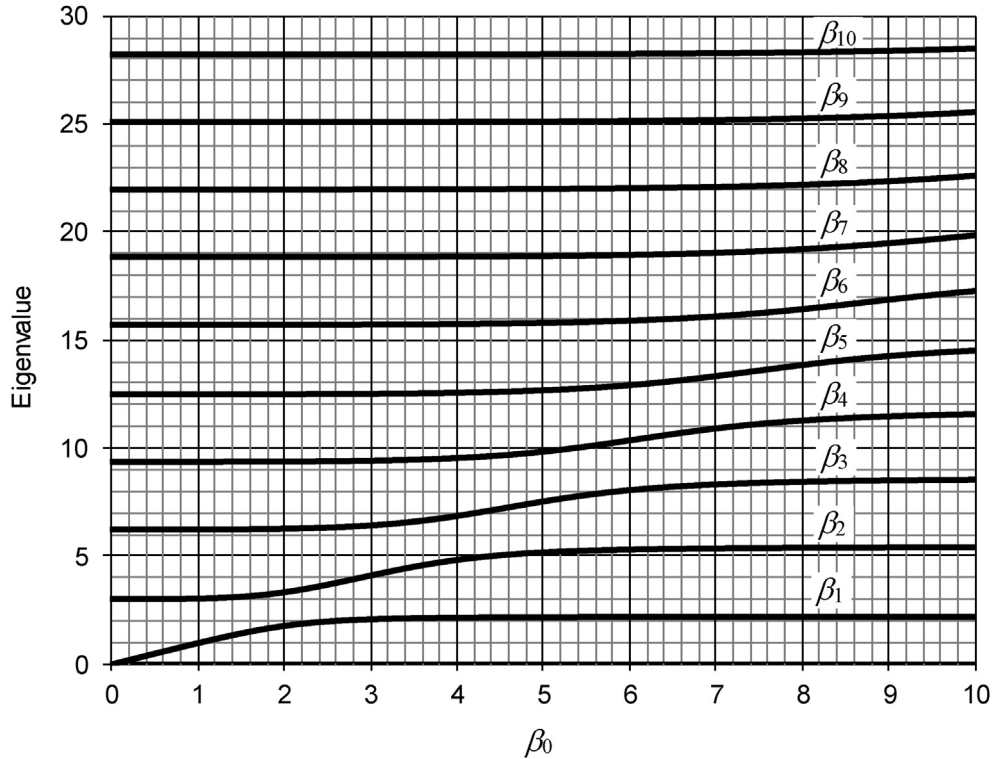


Figure 14.17 Eigenvalues of an elastically supported circular plate calculated from Eq. (14.263) with a Poisson's ratio $\nu = 0.3$ and zero damping so that $Q_{ES} = Q_{MS} = \infty$. As we vary β_0 from 0 to ∞ , the stiffness of the surround increases such that when $\beta_0 = 0$ we have a free plate and when $\beta_0 = \infty$ it is simply supported because, although it cannot be deflected vertically at the perimeter, it can still bend.

where from Eq. (14.253) we obtain

$$B_n = -\frac{\tilde{C}_{3n}}{\tilde{C}_{1n}} = -\frac{(1-\nu)J_0(\beta_n) - \beta_n J_1(\beta_n)}{(1-\nu)I_0(\beta_n) - \beta_n I_1(\beta_n)}. \quad (14.270)$$

Far-field pressure of a free plate with an evenly distributed radiation load

To begin with, we shall assume that the radiation impedance of a rigid piston is evenly distributed over the surface of the plate. For this purpose, we shall use the complex wavenumber of Eqs. (14.198) and (14.199) with $\zeta = 1$, $\xi = 0$, and

$$z_S = \rho_0 c \left(1 - \frac{J_1(2ka)}{ka} + j \frac{\mathbf{H}_1(2ka)}{ka} \right). \quad (14.271)$$

Inserting the Green's function of Eq. (14.201), together with Eq. (14.269) for the eigenfunctions, into Eq. (14.197), while ignoring the surface pressure term, and integrating over the surface of the plate yields

$$\tilde{\eta}(w) = -\frac{a^2 \tilde{f}_g}{\pi D} \sum_{n=1}^{\infty} \frac{(J_0(\beta_n w/a) - B_n I_0(\beta_n w/a))(J_0(\beta_n^* b/a) - B_n^* I_0(\beta_n^* b/a))}{\Delta_n(\beta_n^4 - k_D^4 a^4)}. \quad (14.272)$$

The surface velocity is simply the first time-derivative of the displacement, which in the steady state gives

$$\tilde{u}_0(w) = j\omega \tilde{\eta}(w) = jkc \tilde{\eta}(w). \quad (14.273)$$

The far-field pressure is derived by inserting the far-field Green's function in spherical-cylindrical coordinates from Eq. (13.70), together with Eqs. (14.273) and Eq. (13.158), into Eq. (13.177) and integrating over the surface of the plate using Eqs. (76) and (95) from Appendix II (with $z = kw_0 \sin \theta$, $b = k \sin \theta$, and letting $\phi = \pi/2$ so that $\cos(\phi - \phi_0) = \sin \phi_0$) together with the integrals of Eqs. (14.217) and (14.218) to give

$$\tilde{p}(r, \theta) = -j \frac{a \tilde{F}_g}{4r S_D} e^{-jkr} D(\theta), \quad (14.274)$$

where the directivity function is given by

$$\begin{aligned} D(\theta) &= 2\alpha^2 (ka) \sum_{n=1}^{\infty} \frac{J_0(\beta_n^* b/a) - B_n^* I_0(\beta_n^* b/a)}{j\Delta_n(\beta_n^4 - k_D^4 a^4)} \\ &\times \left(\frac{\beta_m J_1(\beta_m) J_0(ka \sin \theta) - (ka \sin \theta) J_1(ka \sin \theta) J_0(\beta_m)}{\beta_m^2 - (ka \sin \theta)^2} \right. \\ &\left. - B_n \frac{\beta_m I_1(\beta_m) J_0(ka \sin \theta) + (ka \sin \theta) J_1(ka \sin \theta) I_0(\beta_m)}{\beta_m^2 + (ka \sin \theta)^2} \right), \end{aligned} \quad (14.275)$$

and α is the fluid-loading factor given by Eq. (14.215). For the on-axis response we have

$$D(0) = 2\alpha^2 (ka) \sum_{m=1}^M \frac{J_0(\beta_m^* b/a) - B_m^* I_0(\beta_m^* b/a)}{j\Delta_m(\beta_m^4 - k_D^4 a^4)} \left(\frac{J_1(\beta_m)}{\beta_m} - B_m \frac{I_1(\beta_m)}{\beta_m} \right). \quad (14.276)$$

If there are no losses so that $Q_{ES} = Q_{MS} = \infty$ and the surround is perfectly flexible so that $\beta_0 = 0$, Eq. (14.266) for the eigenvalues reduces to that of a free circular plate

$$((1 - \nu)J_1(\beta_n) - \beta_n J_0(\beta_n))I_1(\beta_n) + ((1 - \nu)I_1(\beta_n) - \beta_n I_0(\beta_n))J_1(\beta_n) = 0 \quad (14.277)$$

from which

$$B_m = -\frac{(1-\nu)J_0(\beta_m) - \beta_m J_1(\beta_m)}{(1-\nu)I_0(\beta_m) - \beta_m I_1(\beta_m)} = \frac{J_1(\beta_m)}{I_1(\beta_m)}, \quad m > 1. \quad (14.278)$$

Hence, if we insert $B_m = J_1(\beta_m)/I_1(\beta_m)$ into Eq. (14.276), we see that all the terms for $m > 1$ vanish. However, for $m = 1$ or $\beta_0 = 0+$, we need to take more care because, according to Eq. (14.270), $B_1 = -1$, not $+1$. Also, $J_1(\beta_1)/\beta_1 = I_1(\beta_1)/\beta_1 = 0.5$. From Eq. (14.145) (with $m = 0$ for axisymmetry), we have $\Delta_1 = 4$. Then, the on-axis response reduces to

$$D(0) = j \frac{\alpha^2(ka)}{k_D^4 a^4} = j \frac{2a\rho_0}{\left(\rho_D h + \frac{z_S}{j\omega}\right)}, \quad (14.279)$$

which contains no modes whatsoever! If we insert this into Eq. (14.274), while noting that at low frequencies $z_S \approx j\omega M_{MR}/S_D$, where the radiation mass M_{MR} is given by Eq. (14.225), we obtain

$$\tilde{p}(r, 0)|_{ka < 0.1} = \frac{\tilde{e}_g B l}{R_E} \frac{S_D \rho_0}{M_{MD} + M_{MR}} \frac{e^{-ikr}}{2\pi r}, \quad (14.280)$$

which is simply Eq. (6.32) for the on-axis pressure of a dynamic loudspeaker in an infinite baffle. The evenly distributed on-axis response of a free magnesium plate is plotted in Fig. 14.18 using Eq. (14.274) and the quantities given in Table 14.8. We see that the response is perfectly smooth with just a small lift at higher frequencies as the radiation load transitions from mass reactance to resistance. However, we do see a model response 45 degrees off-axis. Interestingly, the directivity pattern is much broader when the plate is driven by a concentrated point force at the center ($b = 0$) than when it is driven by a ring force of the same magnitude at the perimeter ($b = a$), as can also be seen in the directivity patterns of Fig. 14.19.

Far-field response of the induction loudspeaker

We will now calculate the far-field pressure response of a fully coupled magnesium alloy plate configured as an induction loudspeaker according to Fig. 14.14 using the quantities given in Tables 14.8 and 14.9. Magnesium alloy is an excellent choice of material for the plate because it has both good electrical and mechanical properties. According to Table 6.1, it is one of the highest-ranking materials for a voice coil, having a high ratio of conductivity to density. It also has a high ratio of Young's modulus to density. The far-field pressure is derived by inserting the far-field Green's function in spherical-cylindrical coordinates from Eq. (13.70), together with Eq. (14.203) and (13.158), into Eq. (13.177) and integrating over the surface of the plate using Eqs. (76) and (95) from Appendix II (with $z = kw_0 \sin \theta$, $b = k \sin \theta$, and letting $\phi = \pi/2$ so that $\cos(\phi - \phi_0) = \sin \phi_0$) together with the integrals of Eqs. (14.217) and (14.218) to give

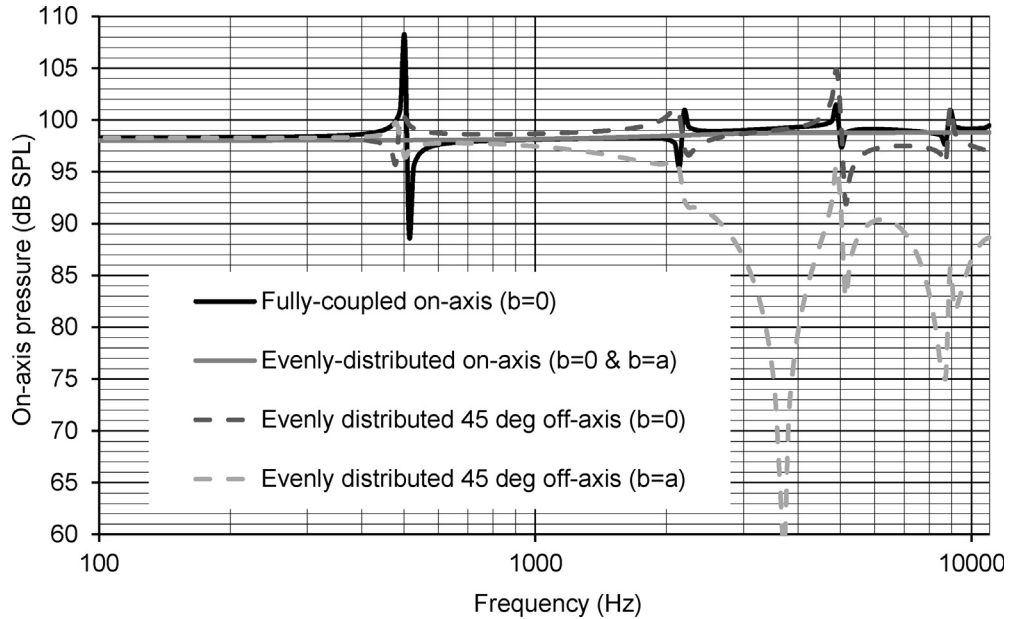


Figure 14.18 Far-field on-axis pressure response of the 100 mm dia. free circular plate in an infinite baffle with an evenly distributed radiation load (gray) and fully coupled to the surrounding air (black). In both cases, the plate is driven with a concentrated point force of $f_g = 10$ N at the center ($b = 0$), although the evenly distributed response is identical to that with a ring force of any radius b , including $b = a$. Also shown is the off-axis response at 45 degrees with a concentrated force of $f_g = 10$ N at the center ($b = 0$) (dark gray dashed) and a ring force of the same magnitude at the perimeter ($b = a$) (light gray dashed). In both cases, the radiation load is evenly distributed. The parameters are given in Table 14.8.

Table 14.8 Magnesium plate quantities for the 100 mm dia. induction loudspeaker

Radius	$a = 50$ mm
Thickness	$h = 600$ μ m
Resistivity	$\sigma_D = 46$ n Ω ·m
Young's modulus	$Y = 42$ GN/m ²
Poisson's ratio	$\nu = 0.3$
Density of plate	$\rho_D = 1740$ kg/m ³
Plate mass	$M_{MD} = 8.2$ g
Density of air	$\rho_0 = 1.18$ kg/m ³
Speed of sound in air	$c = 345$ m/s
Observation distance	$r = 1$ m

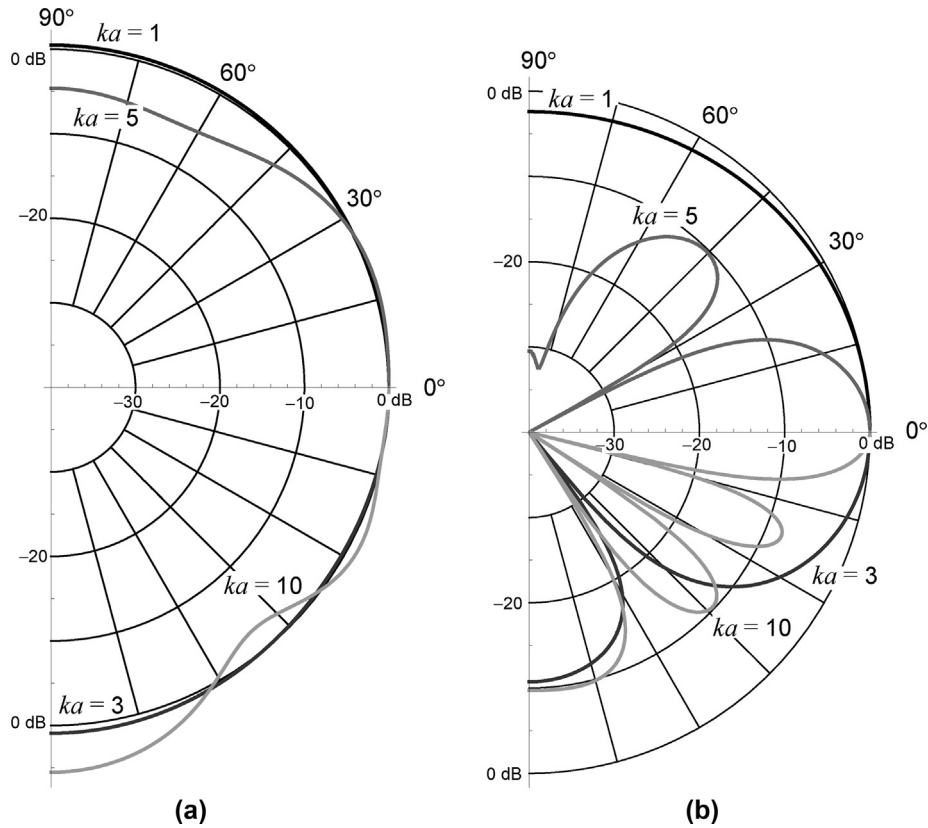


Figure 14.19 Directivity pattern of the 100 mm dia. free circular plate in an infinite baffle with an evenly distributed radiation load at $ka = 1$ ($f = 1.1$ kHz, black), $ka = 3$ (3.3 kHz, dark gray), $ka = 5$ ($f = 5.5$ kHz, medium gray), and $ka = 10$ ($f = 11$ kHz, light gray). (a) Driven by a concentrated point force of $f_g = 10$ N at the center ($b = 0$) (b) Driven by a ring force of the same magnitude at the perimeter ($b = a$).

$$\tilde{p}(r, \theta) = -j \frac{a \tilde{f}_g}{4rS_D} e^{-jkr} D(\theta), \quad (14.281)$$

where the directivity function is given by

$$D(\theta) = 2ka \sum_{n=1}^{\infty} A_n \left(\frac{\beta_n J_1(\beta_n) J_0(ka \sin \theta) - (ka \sin \theta) J_1(ka \sin \theta) J_0(\beta_n)}{\beta_n^2 - (ka \sin \theta)^2} \right. \\ \left. - B_n \frac{\beta_n I_1(\beta_n) J_0(ka \sin \theta) + (ka \sin \theta) J_1(ka \sin \theta) I_0(\beta_n)}{\beta_n^2 + (ka \sin \theta)^2} \right), \quad (14.282)$$

Table 14.9 Coil and suspension quantities for the 100 mm dia. induction loudspeaker

Electrical cut-off frequency	$f_C = 676$ Hz
Electrical cut-off Q	$Q_C = 0.747$
Capacitor value	$C_E = 22$ μ F
Coil electrical resistance	$R_E = 8$ Ω
Coil electrical inductance	$L_{EC} = 2.5$ mH
Coil average radius	$b = 13$ mm
Coil wire diameter	$t = 0.95$ mm
Coil window half-width	$d = 10$ mm
Coil window height	$a_O - a_i = 6$ mm
Coil wire resistivity	$\sigma_C = 17.2$ n $\Omega \cdot$ m
Coil wire total length	$l_C = 7.15$ m
Coil wire length per turn	$l = 81.7$ mm
Coil number of turns	$N = 88$
Magnetic flux density	$B = 1$ T
Saturation flux density	$B_{SAT} = 1.4$ T
Flux coil-length product	$Bl = B \times l = 98$ mT \cdot m
Magnetic gap width	$l_g = 0.3$ mm
Saturation frequency	$f_{SAT} = 183$ Hz
Suspension frequency	$f_0 = 150$ Hz
Mechanical Q	$Q_{MS} = 7.73$
Electrical Q	$Q_{ES} = 1.21$
Total suspension Q	$Q_{TS} = 1.05$
Suspension resistance	$R_{MS} = 1$ N \cdot s/m
Input voltage for 10 W	$e_{g(\text{rms})} = R_E W _{W=10 \text{ W}_{\text{rms}}} = 8.94$ V

and the coefficients A_m are found by solving the set of simultaneous equations in Eq. (14.213). The on-axis response is by

$$D(0) = 2ka \sum_{m=1}^M A_m \left(\frac{J_1(\beta_m)}{\beta_m} - B_m \frac{I_1(\beta_m)}{\beta_m} \right). \quad (14.283)$$

In the case of a free plate, this reduces to

$$D(0) = 2kaA_1. \quad (14.284)$$

The on-axis response of the fully coupled free plate is shown in Fig. 14.18 using the quantities given in Table 14.8. We see that even though the plate is thick enough for the fluid–structure coupling to be relatively weak ($\alpha(ka)$ is seven times lower than that of the membrane of Section 14.10), the variation in acoustic load across the surface is enough

to produce modal features in the on-axis response compared to the evenly distributed response. The displacement at the center is obtained by setting $w = 0$ and $C_m = 0$ in Eq. (14.203) for the velocity and then dividing by $j\omega$ to obtain

$$\tilde{\eta}(0) = \frac{\tilde{f}_g}{2j\omega\rho_0cS_D} \sum_{m=1}^M A_m(1 - B_m). \quad (14.285)$$

The peak displacement of an equivalent piston giving the same sound pressure is

$$\eta_{pk} = \frac{\sqrt{2}r10^{\left(\frac{\text{SPL}}{20}-5\right)}}{\pi f^2\rho_0S_D}. \quad (14.286)$$

where $\text{SPL} = 20 \log_{10}(|p_{\text{rms}}|/20 \times 10^{-6})$. The far-field on-axis response of a 100 mm dia. magnesium induction loudspeaker is plotted in Fig. 14.20 (black), together with the 45-degree off-axis (dark gray dashed). Apart from the small dip at 3–4 kHz, the modes are largely smoothed out both on and off-axis because of the mechanical and electrical resistances in the boundary conditions. However, these resistances also have the effect of

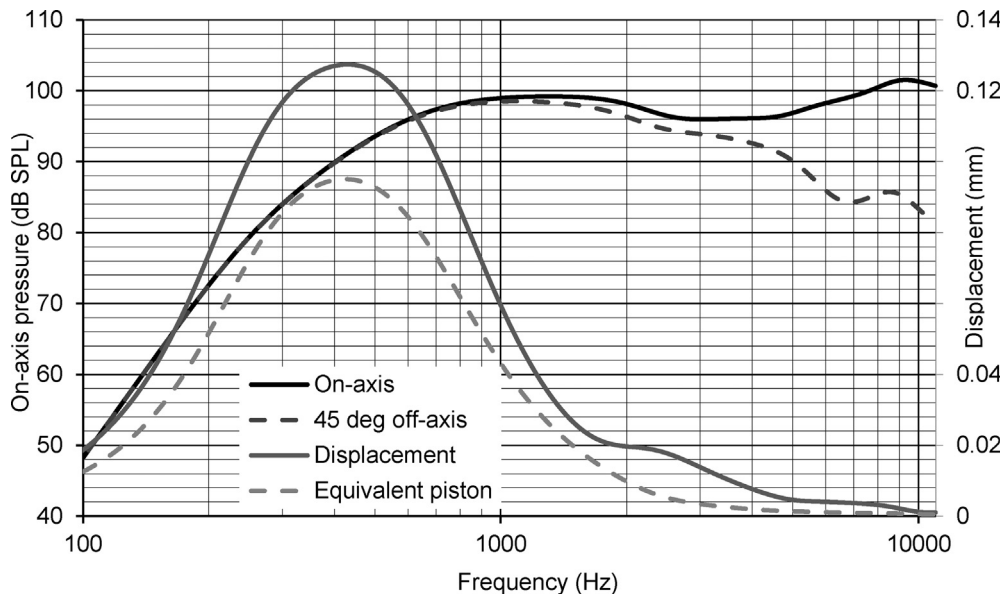


Figure 14.20 Far-field pressure response of the fully coupled 100 mm dia. magnesium alloy induction loudspeaker in an infinite baffle with 10 W input on-axis (black) and 45 degrees off-axis (dark gray dashed). Also shown are the displacement at a distance b from the center (dark gray) and the displacement of an equivalent rigid piston (light gray dashed). The quantities and in vacuo eigenfrequencies are given in Tables 14.8–14.10.

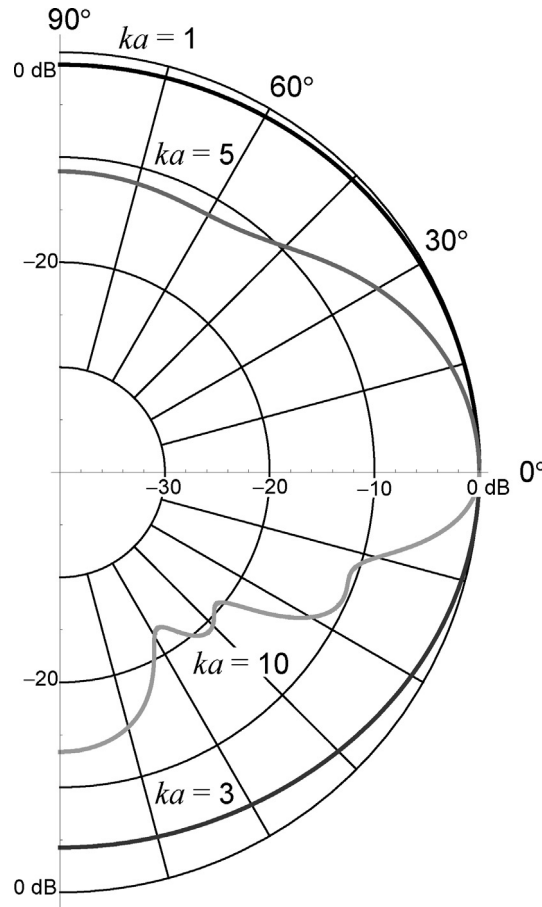


Figure 14.21 Directivity pattern of the 100-mm induction loudspeaker at $ka = 1$ (1.1 kHz, black), $ka = 3$ (3.3 kHz, dark gray), $ka = 5$ (5.5 kHz, medium gray), and $ka = 10$ (11 kHz, light gray).

removing some of the energy from the plate at higher frequencies, which leads to a moderate narrowing of the directivity pattern compared to the free plate, as we see from Fig. 14.21. However, the directivity is still much broader than that of a rigid piston shown in Fig. 13.5. Also shown in Fig. 14.20 are the peak displacement at the center (dark gray) and the displacement of an equivalent rigid piston (light gray dashed). This demonstrates how much more volume velocity is produced by a plate, especially at higher frequencies, than by a rigid piston with the same on-axis response. The in vacuo eigenfrequencies are given in Table 14.10.

Problem 14.1. Show that the Green's function for a rectangular membrane, given by Eq. (14.23), is a solution to the inhomogeneous wave equation of Eq. (14.24).

Table 14.10 Eigenfrequencies for the 100-mm magnesium plate

$n = 1$	$n = 2$	$n = 3$	$n = 4$	$n = 5$	$n = 6$	$n = 7$	$n = 8$
264 Hz	507 Hz	2.28 kHz	5.08 kHz	9.00 kHz	14.0 kHz	20.2 kHz	27.5 kHz

Hint: Let the Green's function be of the form $G(x, y|x_0, y_0) = \sum_{m=1}^{\infty} \sum_{n=1}^{\infty} A_{mn} \sin(m\pi x/l_x) \sin(n\pi y/l_y)$ and solve for A_{mn} by inserting this into Eq. (14.24), using the identity of Eq. (14.16) for the Laplace operator, multiplying both sides by $\sin(p\pi x/l_x) \sin(q\pi y/l_y)$, and integrating over the surface of the membrane using the integral of Eq. (14.18) together with the property of the Dirac delta function of Eq. (A2.154) from Appendix II.

Problem 14.2. Using the recursion formulas of Eqs. (A2.83) and (A2.84) from Appendix II, show that $\nabla^2 G(w, \phi|w_0, \phi_0) = -\frac{\alpha_{mn}^2}{a^2} G(w, \phi|w_0, \phi_0)$ is valid, where $G(w, \phi|w_0, \phi_0)$ is the Green's function for a circular membrane given by Eq. (14.43). Show that this Green's function is a solution to the inhomogeneous wave equation of Eq. (14.44).

Hint: Let the Green's function be of the form $G(w, \phi|w_0, \phi_0) = \sum_{m=0}^{\infty} \sum_{n=1}^{\infty} A_{mn} \cos(m\phi) J_m(\alpha_{mn} w/a)$ and solve for A_{mn} by inserting this into Eq. (14.44), multiplying both sides by $\cos(p\phi) J_p(\alpha_{pq} w/a)$, and integrating over the surface of the membrane using the integrals of Eqs. (14.38) and (14.39) together with the property of the Dirac delta function of Eq. (A2.154) from Appendix II.

Problem 14.3. Calculate the first three axisymmetric eigenfrequencies f_{01} , f_{02} , and f_{03} of a simply supported circular aluminum plate with a radius of 12.5 mm and thickness of 0.2 mm, where $\rho_D = 2700 \text{ kg/m}^3$, $Y = 69 \times 10^{-9} \text{ N/m}^2$, and $\nu = 0.3$.

Hint: Use Eq. (14.108) with eigenvalues from Table 14.3.

Problem 14.4. Show that the Green's function for a shallow spherical shell, given by Eq. (14.148), is a solution to the inhomogeneous wave equation of Eq. (14.149).

Hint: Let the Green's function be of the form $G(w, \varphi|w_0, \varphi_0) = \sum_{m=0}^{\infty} \sum_{n=1}^{\infty} A_{mn} \eta_{mn}(w, \varphi)$, where $\eta_{mn}(w, \varphi) = \cos(m\varphi) (J_m(\alpha_{mn} w/a) - B_{mn} I_m(\alpha_{mn} w/a) + C_{mn})$ and solve for A_{mn} by inserting this into Eq. (14.149), using the identity of Eq. (14.138) for the Laplace operator, multiplying both sides by $\eta_{pq}^*(w, \varphi)$ from Eq. (14.140) and integrating over the surface of the shell using the integrals of Eq. (14.142) together with the property of the Dirac delta function of Eq. (A2.154) from Appendix II.

Problem 14.5. Calculate the first four axisymmetric eigenfrequencies f_{01} , f_{02} , and f_{03} of a clamped aluminum spherical shell with a radius of 12.5 mm, thickness of 40 μm , and height of 2 mm, where $\rho_D = 2700 \text{ kg/m}^3$, $Y = 69 \times 10^{-9} \text{ N/m}^2$, and $\nu = 0.3$.

Hint: Use Eq. (14.184). The first four eigenvalues from Eq. (14.187) are: $\beta_1 = 12.854 + j12.854$, $\beta_2 = 5.9034$, $\beta_3 = 9.1898$, and $\beta_4 = 12.386$. Note that $\beta_1^4 = -109.2 \times 10^3$.

REFERENCES

- [1] Morse PM, Ingard KU. Theoretical acoustics. New York: McGraw-Hill, Inc.; 1968. p. 191–5. 643.
- [2] Chiang HY, Huang YH. Vibration and sound radiation of an electrostatic speaker based on circular diaphragm. *J Acoust Soc Am* 2015;137(4):1714–21.
- [3] Mellow TJ, Kärkkäinen LM. On the sound field of a membrane in free space and an infinite baffle. *J Acoust Soc Am* 2006;120(5):2460–77.
- [4] Streng JH. Calculation of the surface pressure on a vibrating circular stretched membrane in free space. *J Acoust Soc Am* 1987;82(2):679–86.
- [5] Streng JH. Sound radiation from a circular stretched membrane in free space. *J Audio Eng Soc* 1989;37(3):107–18.
- [6] Bouwkamp CJ. Theoretical and numerical treatment of diffraction through a circular aperture. *IEEE Trans Antennas Propag* 1970;AP18(2):152–76.
- [7] Walker PJ. New developments in electrostatic loudspeakers. *J Audio Eng Soc* 1980;28(11):795–9.
- [8] Timoshenko S, Woinowsky-Krieger S. Theory of plates and shells. New York: McGraw-Hill; 1959. p. 36–41. 79–82, 429–435, 533–559.
- [9] Reissner E. On axi-symmetrical vibrations of shallow spherical shells. *Q Appl Math* 1955;13(3):279–90.
- [10] Gradowczyk MH. Some remarks on the theory of shallow spherical shells. *Ing Arch* 1963;32:297–303.
- [11] Gradshteyn IS, Ryzhik IM. In: Jeffrey A, editor. Table of integrals, series, and products. 6th ed. New York: Academic Press; 2000.
- [12] Mellow TJ, Kärkkäinen LM. On the sound field of a shallow spherical shell in an infinite baffle. *J Acoust Soc Am* 2007;121(6):3527–41.
- [13] Suzuki H, Tichy J. Sound radiation from an elastically supported circular plate. *J Acoust Soc Am* 1979;65(1):106–11.
- [14] Rdzanek W. Sound radiation of a vibrating elastically supported circular plate. *J Sound Vib* 2018;434:92–125.
- [15] Harris N, Bank G. Available from: In: A balanced modal radiator. On the CD ROM: audio engineering society convention papers, 119th convention paper 6595, New York, 7–10 October 2005. Audio Engineering Society Inc.; 2005. 60 East 42nd Street, Room 2520, New York, NY 10165–2520.

Electrostatic loudspeakers

PART XXXXII: FUNDAMENTALS OF ELECTROSTATIC LOUDSPEAKERS

15.1 INTRODUCTION TO ELECTROSTATIC LOUDSPEAKERS

Although the number of electrostatic loudspeaker manufacturers in the world can be counted on two hands, this type of loudspeaker has been regarded as a benchmark for sound quality for more than 60 years because of its low distortion, low coloration, and outstanding transient response. The main drawback is that it is difficult to produce high sound pressure levels, especially at lower frequencies, unless the diaphragm is very large. This can then lead to beaming at high frequencies, although we shall examine a method to counter this.

Instead of passing a current through a coil within a magnetic field to drive a rigid cone or dome radiator, an electrostatic loudspeaker simply consists of a perfectly flexible charged membrane held under the tension between two perforated electrodes or “stators.” The signal across the stators creates an electric field that pulls the charged membrane back and forth to produce sound waves, which exit through the perforations in the stators. It is the same force that makes your hair stand on end when you rub a balloon on your clothes and then hold it close to your head. The membrane is thinner than a human hair, which makes this the closest thing to moving air particles directly without any mechanical structure.

Compared to a dynamic loudspeaker, this simple transduction method turns the whole design paradigm on its head. Whereas the radiation load of a dynamic loudspeaker only accounts for a small portion of the total moving mass, including the voice coil and diaphragm, the mass of the gossamer-thin membrane of an electrostatic loudspeaker is tiny compared to that of the air which it is moving. Therefore, the stiffness of the air in an enclosure would raise the fundamental resonance frequency so high that all the bass would be lost. Indeed, the fundamental resonance frequency would occur when the enclosure depth is roughly one quarter of the wavelength. To prevent this, electrostatic loudspeakers mostly operate in free space. Hence, a large diaphragm is needed to prevent the antiphase rear waves from canceling those from the front at the lower frequencies.

Because the membrane is so light and there is no enclosure, an electrostatic loudspeaker is acoustically transparent over its working frequency range, which starts at the

fundamental resonance, as determined by the tension and radiation mass, and ends where the inertia of the membrane starts to have an effect.

Another major difference from dynamic loudspeakers is that, to avoid problems with vibration modes or cone “breakup,” the diaphragm of a dynamic loudspeaker must be made as rigid as possible, which means that there is a lower limit to how thin it can be made. To reduce the moving mass and thus improve efficiency and transient response, the thickness can only be reduced further by employing expensive exotic materials. Even then, the inevitable “breakup” cannot be eradicated altogether—only moved up to frequencies above those to be reproduced by the driver. Higher frequencies must be reproduced by another smaller driver with the added complexity of a crossover. Another approach is to use highly damped materials, but these reduce the high-frequency radiation efficiency due to a shrinking effective area and, in the case of domes, narrow the directivity pattern because the dome effectively becomes a ring source.

By contrast, the membrane of an electrostatic loudspeaker may be perfectly flexible with the restoring force provided purely through tensioning. Although the driving force is uniform over the whole membrane, this does not make it immune to vibration modes, unless the membrane were somehow freely suspended (such as the resilient disk in Chapter 13). As we saw in the Chapter 14, the clamped perimeter does result in modes, but these can be effectively damped out by the acoustic flow resistance of a fine mesh cover material, which also serves to exclude dust and moisture. In any case, at higher frequencies, where the radiation load becomes more resistive than massive, the modes are effectively damped by the radiation resistance.

Various methods have been used to prevent high-frequency beaming. One of the most common is to use separate “wide” and “narrow” electrostatic drive units for the lower and higher frequency ranges, respectively, with a crossover network to separate the frequency ranges feeding each one of them. Another method is to curve the membrane, but this adds distortion to an otherwise linear transduction mechanism and curtails the lower frequencies due to increased stiffness. If you curve a piece of paper, you can support small objects on it, which is why such designs typically use shallow curves that only spread the sound out over relatively narrow angles. In this chapter, we shall focus on the use of delay lines to control the directivity pattern.



15.2 CONSTRUCTION

A typical electrostatic loudspeaker configuration is shown in [Fig. 15.1](#).

In the middle is a light flexible membrane, which is held under tension and clamped at its perimeter between insulating ring spacers. The spacers separate the membrane from the rigid stators or ring electrodes located on either side of it at a distance d . The membrane is circular with a radius a and has a conductive coating that is charged by a polarizing supply with a dc voltage E_p . The polarizing supply is connected via a high-value resistor

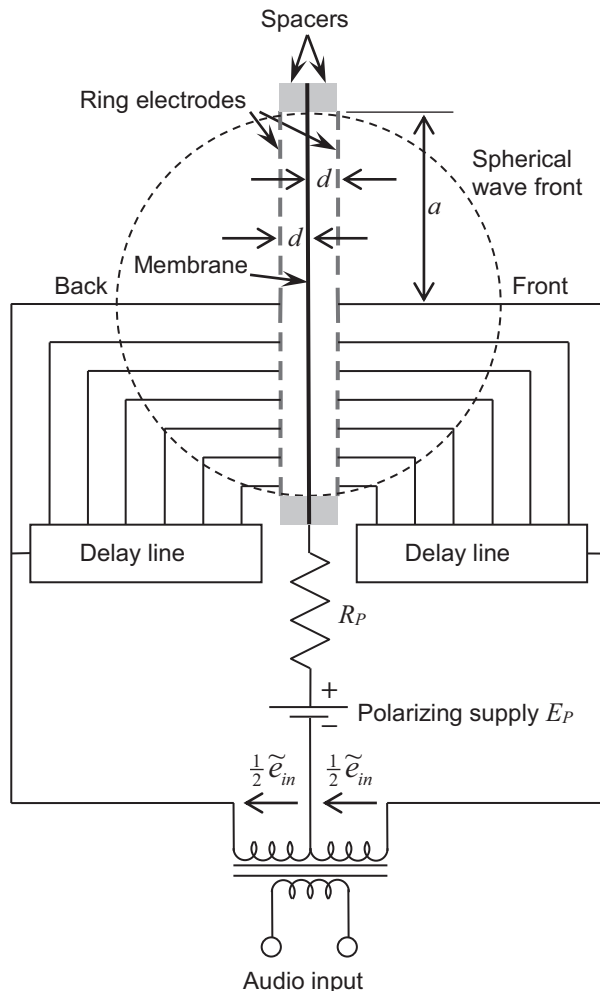


Figure 15.1 Construction of push–pull electrostatic loudspeaker with delay lines.

R_P to prevent the charge on the membrane from varying significantly when the alternating signal voltage \tilde{e}_{in} is applied to deflect the membrane to either side of its central position. This keeps the force acting on the membrane linear, and the constant-charge principle was an important step forward in making commercial electrostatic loudspeakers viable [1,2]. We take the input voltage \tilde{e}_{in} to be that across the entire secondary of the push-pull step up transformer in Fig. 15.1, which is still the most common way to develop the large signal voltage required to drive an electrostatic loudspeaker. As the membrane moves, it produces sound that passes through the perforations in the stators. The most common membrane material is polyester (PET or Mylar), but

polyimide (Kapton) has also been used. If the loudspeaker is required to produce low frequencies and therefore large membrane excursions, the conductive coating on the membrane is likely to have a high resistance to prevent the charge migrating to the central part, which will be closest to the stator at maximum excursion. Such coatings are usually in the form of graphite, Elvamide, or indium-tin-oxide (ITO).

PART XXXXIII: DIRECTIVITY CONTROL

15.3 DIRECTIVITY CONTROL

Although there will probably always be a heated debate on exactly what directivity pattern is most desirable for sound reproduction through loudspeakers in an average listening room, one thing there does at least seem to be a consensus on is that the pattern should be as consistent as possible over the entire audio frequency range [3–5]. In the normal listening position, most of what we hear is reflected sound coming from the off-axis directions. Hence, if the reflected sound does not have the correct tonal balance, it cannot possibly sound natural.

In addition to having low coloration and low distortion, electrostatic loudspeakers enable us to control the directivity pattern produced by a single diaphragm in a way that is not possible with dynamic loudspeakers, by partitioning the stators into concentric annular rings, which are connected to tappings along the delay line shown in Fig. 15.1.

Because the membrane is flexible, each part can move more-or-less independently from the rest according to the signal on the nearest ring. Because of the delay line, the sound first emanates from the center, followed by the first ring, and then each successive ring in turn until it is radiated from the outermost ring by which time the sound from the center is already some distance away from the membrane. We just need to determine how to configure the delay to produce the optimum wavefront shape.

The traditional approach has been to arrange the delay to reproduce the wavefront of a virtual point source located behind the membrane [6]. Because of the finite size of the membrane, Walker [7] correctly pointed out that the delay line needs to be attenuated to prevent irregularities in the frequency response of the radiated sound. Because the far-field pressure response is the Fourier transform of the sound source, the attenuation may be regarded as a windowing function. It is essentially a shaded array.

Now imagine a massless sphere oscillating back and forth with constant velocity at all frequencies, thus radiating sound into free space. Such a sound source would have a constant figure-of-eight directivity pattern and at higher frequencies, where the wavelength is smaller than the sphere, constant power would be radiated because of the mainly resistive radiation impedance. Unfortunately, such a sound source is impractical to construct. Even if it were possible to make a large perfectly rigid hemispherical dynamic

driver, it would need a lot of signal boosting at high frequencies to make it move with constant velocity, rather than constant acceleration, and thus radiate constant power.

Instead, we shall describe how to imitate an oscillating sphere using a planar circular electrostatic loudspeaker with stators partitioned into concentric annular rings that are connected to a delay line [8]. These rings reproduce the sound that would emanate from an oscillating sphere placed immediately behind the membrane (and in contact at the center) as it arrives at the membrane. It turns out that using a geometric approximation that assumes a plane wave traveling axially from the face of the imaginary sphere gives far superior results to reproducing the true magnitude and phase of the waves produced by the sphere using a finite membrane. We shall compare the effect of partitioning them into a finite number of rings with equal area, equal delay sections, and equal widths, using a continuously varying radial delay as an ideal reference. A significant benefit of using an analog delay line is that it converts the capacitive load of the electrostatic loudspeaker into an almost purely resistive one that is much easier for amplifiers to drive.

To begin with, we shall ignore secondary effects, such as the membrane mass and stiffness, the stator perforations, and stray capacitances, which are all considered later in the chapter. This will enable us to concentrate fully on how to control the directivity. In other words, we shall treat the membrane as a pure pressure source with zero mass and stiffness, aka a resilient disk as described in Section 13.8.



15.4 CONTINUOUS DELAY

Let us now consider the ideal situation whereby we increase the number of rings while reducing their widths until the delay becomes continuously variable along the radius of the membrane. Then we can isolate the effect of the delay profile from the discretization of the rings. If we treat the membrane as a pure pressure source with zero mass and stiffness, the far-field radiated sound pressure at a distance r and angle θ from its center is obtained by inserting Eqs. (13.70) and (13.121) into Eq. (13.124) to yield

$$\tilde{p}(r, \theta) = jk \cos \theta \frac{e^{-jkr}}{r} \int_0^a \tilde{p}_+(w) J_0(kw \sin \theta) w dw, \quad (15.1)$$

where J_0 is the zero-order Bessel function, $k = \omega/c$ is the wave number, $\omega = 2\pi f$ is the angular frequency, and $\tilde{p}_+(w)$ is the radial distribution of the electrostatic driving pressure. The tilde denotes a harmonically varying quantity where the term $e^{j\omega t}$ has been suppressed.

No Delay. If there is no delay, then the pressure everywhere on the surface of each side is just half the driving pressure

$$\tilde{p}_+(w) = \frac{\tilde{p}_0}{2}, \quad (15.2)$$

where

$$\tilde{p}_0 = \frac{\varepsilon_0 E_P \tilde{e}_{\text{in}}}{d^2} \quad (15.3)$$

and ε_0 is the permittivity of air. The far-field pressure response then becomes that of Eq. (13.125)

$$\tilde{p}(r, \theta) = jka^2 \varepsilon_0 \frac{E_P}{d} \cdot \frac{\tilde{e}_{\text{in}}}{2d} \cdot \frac{e^{-jkr}}{2r} D(\theta), \quad (15.4)$$

where the directivity function is given by

$$D(\theta) = \frac{2J_1(ka \sin \theta)}{ka \sin \theta} \cos \theta. \quad (15.5)$$

The normalized directivity pattern $20 \log_{10}|D(\theta)| - 20 \log_{10}|D(0)|$ is plotted in Fig. 15.2.

Noting that $D(0) = 1$, let the normalized on-axis response be

$$p_{\text{norm}} = \frac{\tilde{p}(r, 0)}{\tilde{a}\tilde{p}_0 e^{-jkr}/(4r)} = jkaD(0) = jka, \quad (15.6)$$

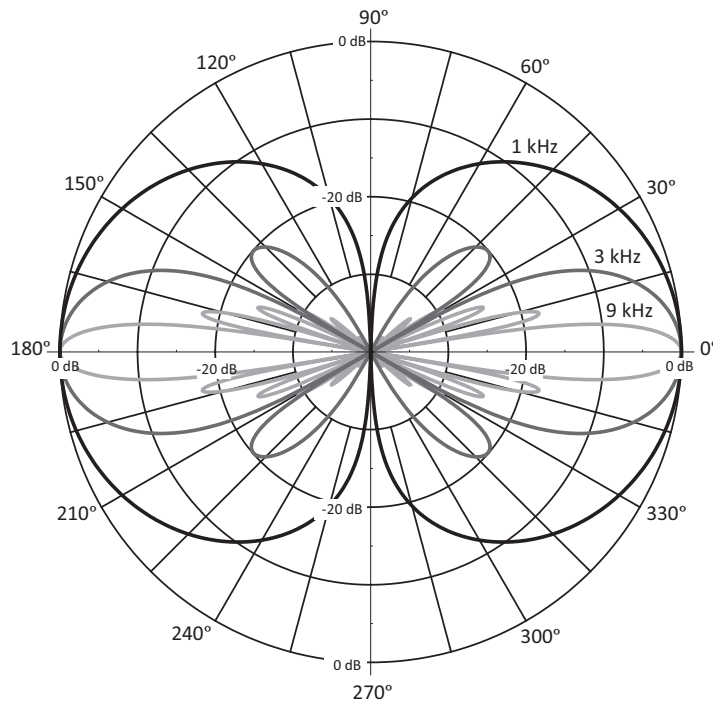


Figure 15.2 Directivity patterns at various frequencies of 280 mm diameter membrane with no delay. Naturally, the high frequencies are extremely directive.

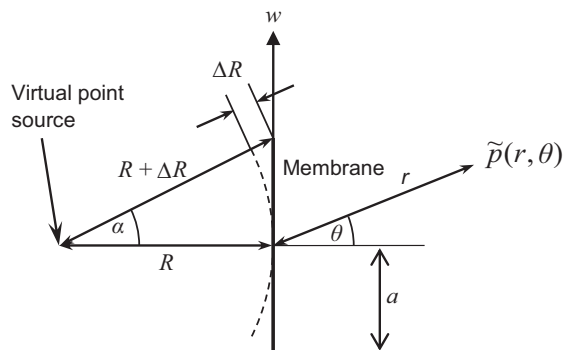


Figure 15.3 Geometry of virtual point source, which behaves like two back-to-back spherical caps with a discontinuity where they join, unlike a smooth oscillating sphere.

which is plotted in Fig. 15.7 (black dashed). The input current $\tilde{I}_{\text{in}} \approx j\omega C_E \tilde{e}_{\text{in}}$ is almost entirely due to the static capacitance $C_E = \epsilon_0 \pi a^2 / (2d)$ so that the on-axis pressure simply becomes Walker's equation [7]

$$\tilde{p}(r, 0) = \frac{E_P}{d} \cdot \frac{e^{-jkr}}{2\pi r} \cdot \frac{\tilde{I}_{\text{in}}}{c}. \quad (15.7)$$

Virtual point source. The geometry of a traditional “virtual point source” is shown in Fig. 15.3.

Because of its finite radius a , the membrane can only reproduce the part of the wavefront emanating from the source, which forms a spherical cap with half angle α and radius of curvature R , where

$$R = a \cot \alpha. \quad (15.8)$$

To reproduce this, the delay must account for the time taken for the wave to travel the distance ΔR at each point w along the radius according to

$$\Delta R = \sqrt{R^2 + w^2} - R. \quad (15.9)$$

Hence, the surface pressure distribution is given by

$$\tilde{p}_+(w) = \frac{\tilde{P}_0}{2} e^{jk\Delta R} = \frac{\tilde{P}_0}{2} e^{-jk(\sqrt{a^2 \cot^2 \alpha + w^2} - a \cot \alpha)}, \quad (15.10)$$

which leads to the directivity pattern

$$D(\theta) = 2 \cos \theta \int_0^1 e^{-jka(\sqrt{\cot^2 \alpha + s^2} - \cot \alpha)} J_0(kas \sin \theta) ds, \quad (15.11)$$

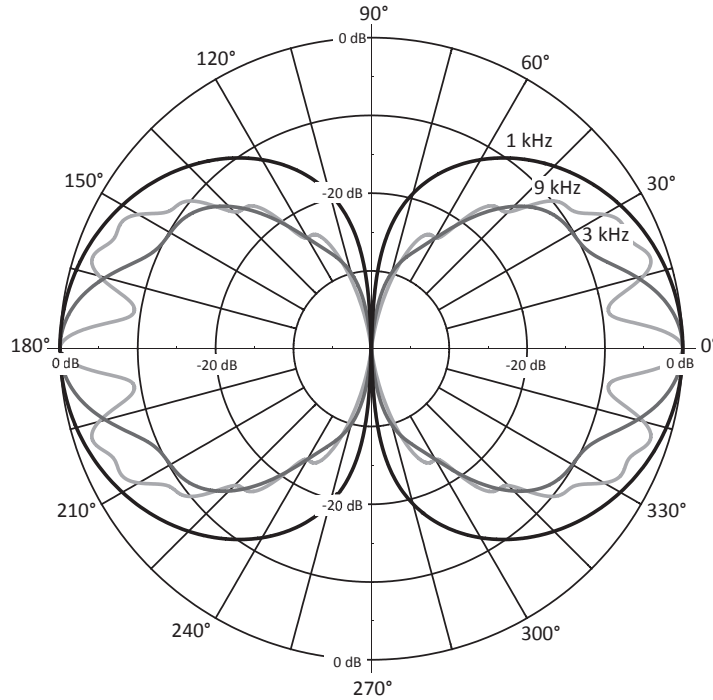


Figure 15.4 Directivity patterns at various frequencies of a virtual point source (unshaded) using a 280 mm diameter membrane, where the half angle $\alpha = 40$ degrees is close to that of the Quad ESL63 [6].

where we have substituted $s = w/a$. The directivity pattern $20 \log_{10}|D(\theta)| - 20 \log_{10}|D(0)|$ is plotted in Fig. 15.4. The on-axis response is

$$p_{\text{norm}} = jkaD(0) = \frac{2j}{ka} \left(\left(1 + \frac{jka}{\sin \alpha} \right) e^{\frac{-jka}{\sin \alpha}} - \left(1 + \frac{jka}{\tan \alpha} \right) e^{\frac{-jka}{\tan \alpha}} \right), \quad (15.12)$$

which is plotted in Fig. 15.7 (dark gray).

Virtual oscillating sphere. Naively, we might insert the pressure produced by an oscillating sphere, given by Eq. (4.129), into Eq. (15.1), while setting $\tilde{P}_0 = \rho_0 c \tilde{U}_0 / (\pi a^2)$, to yield

$$p_{\text{norm}} = \frac{-2k^2 a^2}{2 - k^2 a^2 + j2ka} \left(e^{-jka} - \frac{e^{-j\sqrt{2}ka}}{\sqrt{2}} \right), \quad (15.13)$$

where we have substituted $r^2 = w^2 + a^2$ and $\cos \theta = a/r$. The first term in parentheses gives the true response of an oscillating sphere that would be obtained if the membrane were infinitely large. However, the second term, which is a “diffraction” term because of

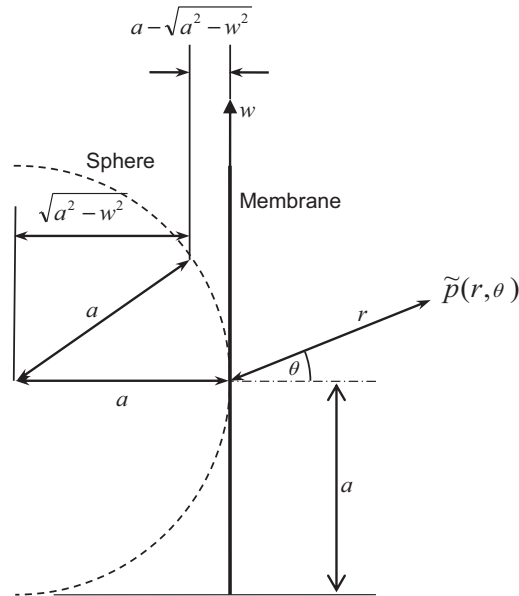


Figure 15.5 Geometry of virtual oscillating sphere.

the membrane's finite size, interferes with the first term to produce an irregular response as shown in Fig. 15.7 (light gray dashed). Hence, for our virtual oscillating sphere, we shall adopt the geometry shown in Fig. 15.5, where the axial distance between each point on the front surface of the virtual sphere and the membrane is $a - \sqrt{a^2 - w^2}$.

The amount of delay required at each point along the radius of the membrane is the time taken for sound to travel this distance axially as a plane wave. Hence,

$$\tilde{p}_+(w) = \frac{\tilde{p}_0}{2} e^{-jk(a - \sqrt{a^2 - w^2})}, \quad (15.14)$$

which leads to the directivity pattern

$$D(\theta) = 2 \cos \theta \int_0^1 e^{-jka(1 - \sqrt{1 - s^2})} J_0(kas \sin \theta) ds, \quad (15.15)$$

where we have substituted $s = w/a$. The directivity pattern $20 \log_{10}|D(\theta)| - 20 \log_{10}|D(0)|$ is plotted in Fig. 15.6.

The on-axis response is

$$p_{\text{norm}} = kaD(0) = \frac{2j}{ka} (1 - e^{-jka} - jka), \quad (15.16)$$

which is plotted in Fig. 15.7 (black) along with the following first-order high-pass filter approximation (light gray)

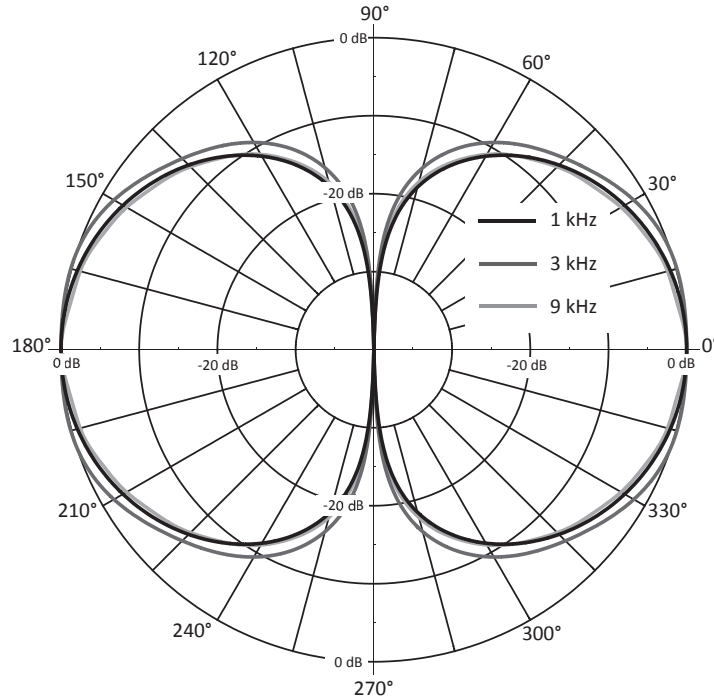


Figure 15.6 Directivity patterns at various frequencies of a virtual oscillating sphere using a 280 mm diameter membrane. The broad figure-of-eight pattern is almost constant at all frequencies.

$$p_{\text{norm}} \approx \frac{2jka}{2 + jka}. \quad (15.17)$$

This approximation can be included as part of a crossover filter response, for example. The cut-off frequency is given by $f_C = c/(\pi a)$. Above f_C , we have

$$p_{\text{norm}} \approx 2, \quad f > \frac{c}{\pi a}. \quad (15.18)$$

Then from Eqs. (15.4), (15.6), and (15.18), the voltage sensitivity is

$$\tilde{p}(r, 0) = \epsilon_0 a \frac{E_P}{d} \cdot \frac{\tilde{e}_{\text{in}}}{2d} \cdot \frac{e^{-jkr}}{r}, \quad f > \frac{c}{\pi a} \quad (15.19)$$

and at lower frequencies we have

$$\tilde{p}(r, 0) = j\epsilon_0 k a^2 \frac{E_P}{d} \cdot \frac{\tilde{e}_{\text{in}}}{2d} \cdot \frac{e^{-jkr}}{2r}, \quad f < \frac{c}{\pi a}, \quad (15.20)$$

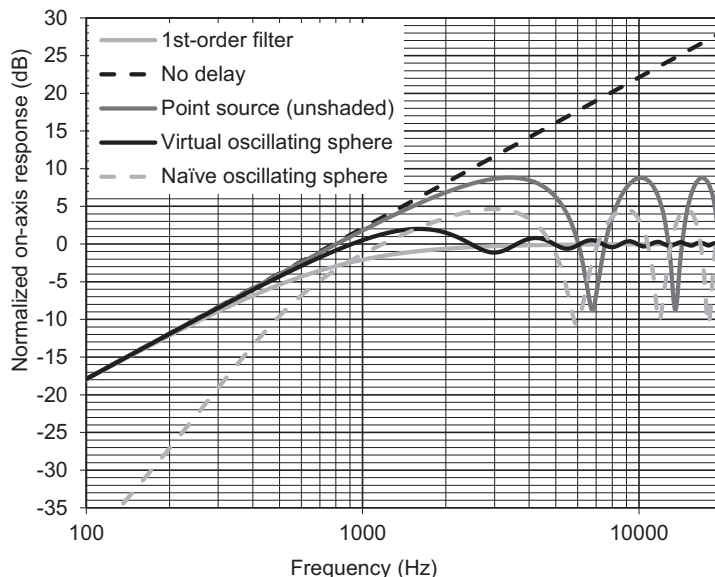


Figure 15.7 On-axis responses $20 \log_{10}|p_{norm}/2|$ of a 280 mm diameter membrane with a continuous and unattenuated delay line configured to simulate a virtual oscillating sphere (black), a naïve oscillating sphere (dark gray dashed), and a point source (dark gray) where the half angle of the arc is 40 degrees. Also shown is a first-order filter response that approximates the oscillating sphere (light gray with $f_c = 784$ Hz) and the on-axis response of the membrane with no delay (black dashed), which keeps rising as the energy is focused on-axis. The -3 dB frequency of the virtual oscillating sphere is $0.75 f_c = 588$ Hz.

which is the same as Eq. (15.4) (with $D(0) = 1$) for the voltage sensitivity of a massless flexible membrane at all frequencies. It is equivalent to Walker's Eq. (15.7) but given in terms of input voltage instead of current, so we shall call it Walker's voltage equation. The maximum field strength that we can realistically expect without breakdown is $E_p/d = 2000$ V/mm. Similarly, the input voltage should not exceed 4000 V peak across 2 mm. If the radius a is 14 cm and the permittivity of free space ϵ_0 is 8.85 pF/m, the maximum RMS sound pressure from Eq. (15.19) is 105 dB SPL at 1 m re 20 μ Pa. This pressure increases by 6 dB for every doubling of the diameter.

The on-axis plot of a virtual oscillating sphere shown in Fig. 15.7 tells us that, in theory, a continuously increasing delay in the driving pressure along the radius of the membrane produces a very smooth response, with just some very small ripples, and an almost constant figure-of-eight directivity pattern at all frequencies, as shown in Fig. 15.6. Although perfectly constant directivity is not achieved, the result is remarkably good considering the finite size of the membrane. Next, we will look at the discretization of the delay into rings of various widths.



15.5 EFFECT OF DISCRETIZATION INTO RINGS OF FINITE WIDTH

Rings of Equal Delay. One option might be to vary the widths of the rings so that there are equal delay sections between them, in which case the on-axis pressure is

$$p_{\text{norm}} = kaD(0) = ka \sum_{n=0}^N e^{-jka \frac{n+1/2}{N+1}} \left(\frac{a_n^2 - a_{n-1}^2}{a^2} \right) \quad (15.21)$$

where the radius of the n th ring is

$$a_n = a \sqrt{1 - \left(1 - \frac{n+1}{N+1}\right)^2}, \quad (15.22)$$

a_0 is the radius of the center disk and $a_{-1} = 0$. In Eq. (15.21), the term in parentheses is proportional to the area of the n th ring while the exponent term represents the delay applied to that ring. The cross section of a stator with rings of equal delay is shown in Fig. 15.8.

Rings of Equal Area. Another option might be to vary the widths of the rings so that they all have the same area and capacitance, in which case the on-axis pressure is

$$p_{\text{norm}} = kaD(0) = ka \sum_{n=0}^N e^{-jka \left(1 - \sqrt{1 - \frac{a_n^2}{a^2}}\right)} \left(\frac{a_n^2 - a_{n-1}^2}{a^2} \right), \quad (15.23)$$

where the radius of the n th ring is

$$a_n = a \sqrt{\frac{n+1}{N+1}}. \quad (15.24)$$

The cross section of a stator with rings of equal delay is shown in Fig. 15.9.

Rings of Equal Width. The last option we shall consider is one in which the rings are of equal width, in which case the on-axis pressure is again given by Eq. (15.23), but with the radius of the n th ring given by

$$a_n = a \frac{n+1}{N+1}. \quad (15.25)$$

The cross section of a stator with rings of equal delay is shown in Fig. 15.10, while the on-axis responses with equal delay, equal area, and equal width are plotted in Fig. 15.11. The ring widths are listed in Table 15.1. Arguably, the rings of equal delay produce the smoothest response at higher frequencies because of their finer resolution of the rapid increase in delay near the rim, as shown in Fig. 15.8.

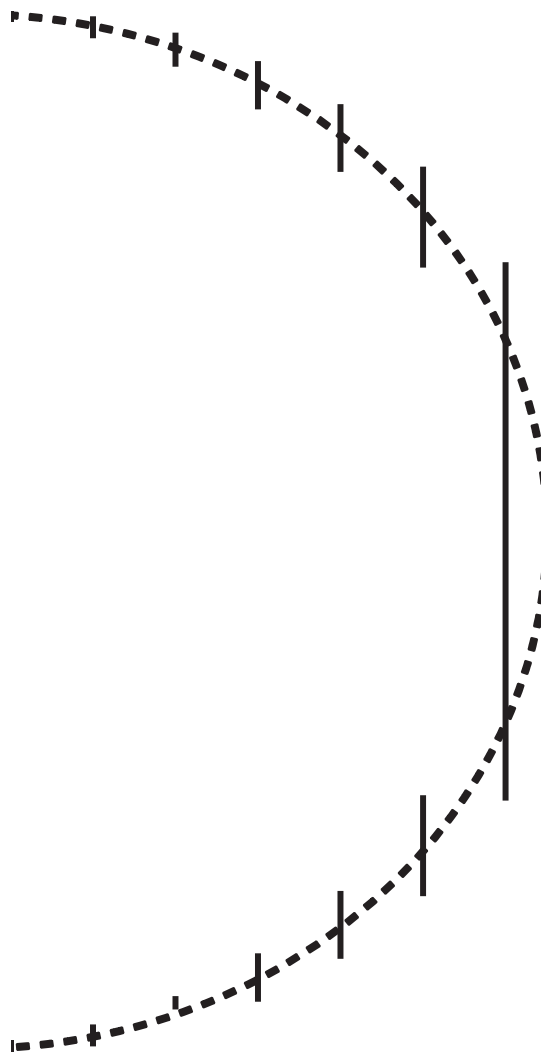


Figure 15.8 Cross section of a stator divided into concentric rings of *equal delay*, where purely for illustration each ring has been shifted to the left by the distance that a wave would have traveled during the time delay applied to that ring.

However, the outer rings are so thin that stray capacitances will dominate the ring capacitances, whereas a stator with rings of equal width largely avoids this problem. Also, the wide center disk (144 mm diameter) will produce high-frequency beaming. If the rings have equal width, they can all be narrow compared to the wavelength over most of the audio spectrum.

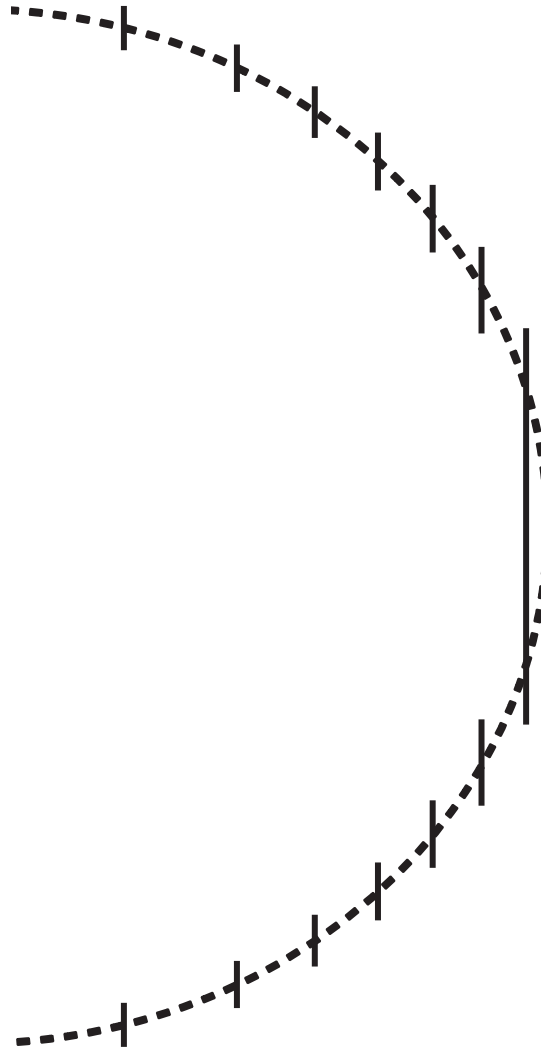


Figure 15.9 Cross section of a stator divided into concentric rings of *equal area*, where purely for illustration each ring has been shifted to the left by the distance that a wave would have traveled during the time delay applied to that ring.



15.6 A PRACTICAL DELAY LINE

Delay Path Length. We saw in the last section that discretization of the delay into rings of finite width produces irregularities in the response at higher frequencies. However, the delay was an ideal delay like that produced by a DSP, whereas in practice, the delay is more likely to take the form of an analog delay line on the high-voltage side

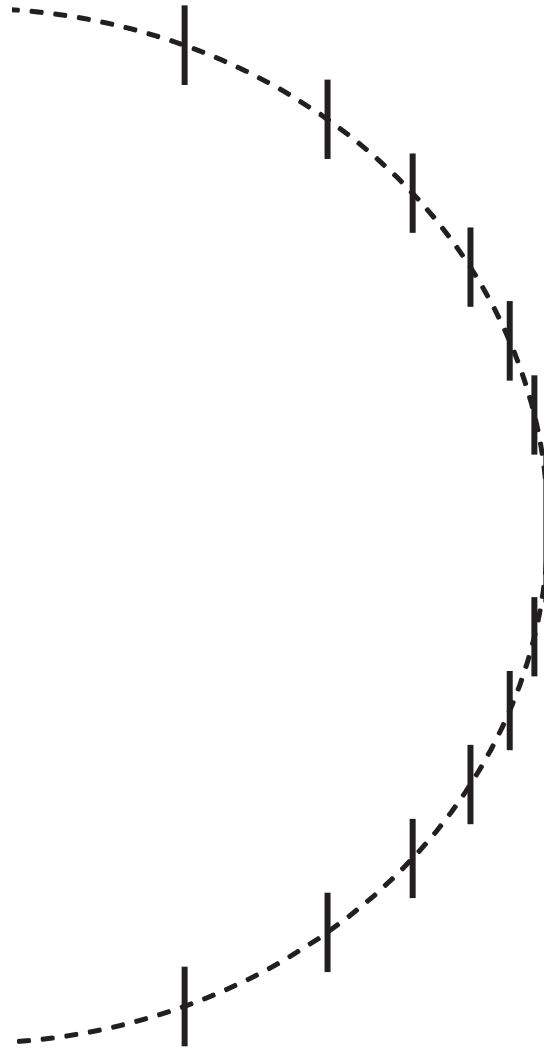


Figure 15.10 Cross section of a stator divided into concentric rings of *equal width*, where purely for illustration each ring has been shifted to the left by the distance that a wave would have traveled during the time delay applied to that ring.

of the transformer, such as that shown in [Fig. 15.12](#). Otherwise, a separate stepping up transformer would be needed to feed each ring. Unless complicated inductors with center taps or a very large number of inductors are used, analog delay lines tend to introduce a degree of attenuation at the higher frequencies. In this case, this turns out to have a smoothing effect on the response.

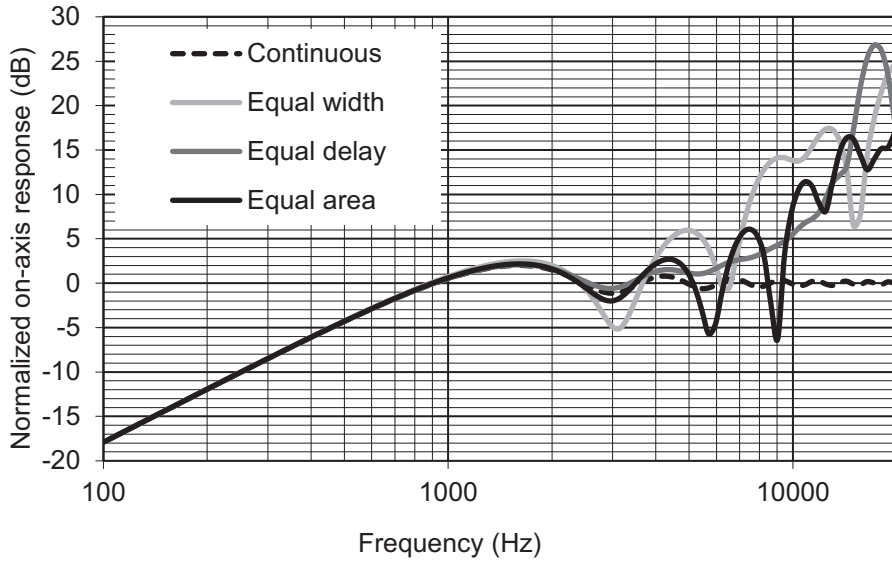


Figure 15.11 Effects of discretization on a 280 mm diameter membrane where the stator is divided into six rings and a center disk of various widths with the delay configured to simulate an oscillating sphere.

Table 15.1 Dimensions of rings.

Ring	Equal delay (mm)	Equal area (mm)	Equal width (mm)
a_0	72	53	20
$a_1 - a_0$	26	22	20
$a_2 - a_1$	17	17	20
$a_3 - a_2$	12	14	20
$a_4 - a_3$	7.7	12	20
$a_5 - a_4$	4.4	11	20
$a_6 - a_5$	1.4	10	20

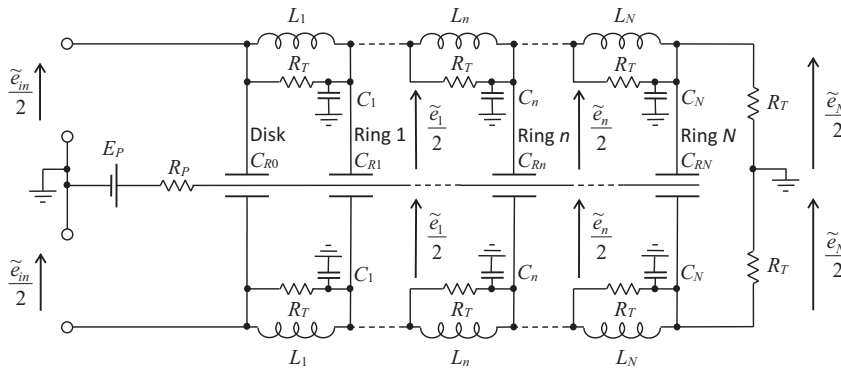


Figure 15.12 Constant impedance delay line ignoring stray capacitance.

From Fig. 15.5, we see that the *total* delay path length z_T at each point along the radial ordinate w is given by

$$z_T = a - \sqrt{a^2 - w^2} = a \left(1 - \sqrt{1 - \frac{w^2}{a^2}} \right). \quad (15.26)$$

For discretized rings, the delay section z_n required for the n th ring is the difference between the total delay z_{Tn} at that ring and the sum of all the previous delay sections

$$z_n = z_{Tn} - \sum_{m=1}^{n-1} z_m, \quad (15.27)$$

where

$$z_{Tn} = a \left(1 - \sqrt{1 - \left(\frac{a_{n-1} + a_n}{2a} \right)^2} \right). \quad (15.28)$$

Notice that we have taken the delay path to the mid-point $(a_{n-1} + a_n)/2$ of each ring. The n th path length z_n is related to the time delay T_n of the n th section by

$$z_n = cT_n, \quad (15.29)$$

where c is the speed of sound.

Delay Line ignoring Stray Capacitance. In Fig. 15.12, C_{Rn} are the ring capacitances that are given by

$$C_{Rn} = \frac{\epsilon_0 \pi (a_n^2 - a_{n-1}^2)}{2d} \quad (15.30)$$

$$C_{R0} = \epsilon_0 \pi a_0^2 / (2d) \quad (15.31)$$

while C_n are shunt capacitors used to make up the required capacitance for the correct delay and impedance. The delay line comprises inductors L_n together with the total capacitances of each section

$$C_{Tn} = C_{Rn} + C_n/2 \quad (15.32)$$

where R_T is the termination resistance on the far right-hand side of Fig. 15.12. The same resistance R_T is also connected across each inductor to create a series of Zobel networks such that the impedance presented to the preceding section is always $2R_T$. The voltage transfer function of each delay section is given by

$$\frac{\tilde{e}_n}{\tilde{e}_{n-1}} = \frac{\omega_n}{s + \omega_n} \quad (15.33)$$

provided that the inductor values are set to

$$L_n = 2R_T^2 C_{Tn}, \quad (15.34)$$

where $s = j\omega$ and the angular turnover frequency is given by

$$\omega_n = \frac{1}{2R_T C_{Tn}}. \quad (15.35)$$

The time delay T_n per section is defined by

$$T_n = \frac{z_n}{c} = \frac{1}{\omega_n} = 2R_T C_{Tn} = \frac{L_n}{R_T}. \quad (15.36)$$

so that the total capacitance per section is given by

$$C_{Tn} = \frac{z_n}{2cR_T}. \quad (15.37)$$

We can now furnish each section of the delay with its respective component values

$$C_n = 2(C_{Tn} - C_{Rn}) \quad (15.38)$$

where C_{Tn} is given by Eq. (15.37) and C_{Rn} by Eq. (15.30). From Eq. (15.36) we have

$$L_n = \frac{z_n R_T}{c}. \quad (15.39)$$

We wish to minimize the capacitor values so that most of the signal current flows through the rings. If we set $C_1 = 0$ so that $C_{T1} = C_{R1}$, then

$$R_T = \frac{z_1}{2cC_{R1}}. \quad (15.40)$$

Each delay section is represented by the transmission matrix

$$\begin{bmatrix} \tilde{e}_{n-1} \\ \tilde{i}_{n-1} \end{bmatrix} = \mathbf{A}_n \cdot \begin{bmatrix} \tilde{e}_n \\ \tilde{i}_n \end{bmatrix} \quad (15.41)$$

where each element of \mathbf{A}_n is given by

$$a_{11}(n) = \left. \frac{\tilde{e}_{n-1}}{\tilde{e}_n} \right|_{\tilde{i}_n=0} = 1 + 2 \frac{sL_n R_T}{sL_n + R_T} sC_{Tn}, \quad (15.42)$$

$$a_{12}(n) = \left. \frac{\tilde{e}_{n-1}}{\tilde{i}_n} \right|_{\tilde{e}_n=0} = 2 \frac{sL_n R_T}{sL_n + R_T}, \quad (15.43)$$

$$a_{21}(n) = \left. \frac{\tilde{i}_{n-1}}{\tilde{e}_n} \right|_{\tilde{i}_n=0} = sC_T n, \quad (15.44)$$

$$a_{22}(n) = \left. \frac{\tilde{i}_{n-1}}{\tilde{i}_n} \right|_{\tilde{e}_n=0} = 1. \quad (15.45)$$

However, the first section contains no inductor, only the capacitance of the center disk

$$\mathbf{A}_0 = \begin{bmatrix} 1 & 0 \\ sC_{R0} & 1 \end{bmatrix}. \quad (15.46)$$

Hence, we can describe the whole delay line of Fig. 15.12 by multiplying together the chain matrices for all the sections

$$\begin{aligned} \begin{bmatrix} \tilde{e}_{in} \\ \tilde{i}_{in} \end{bmatrix} &= \mathbf{A}_0 \cdot \mathbf{A}_1 \cdots \mathbf{A}_N \cdot \begin{bmatrix} 1 & 0 \\ (2R_T)^{-1} & 1 \end{bmatrix} \cdot \begin{bmatrix} \tilde{e}_N \\ 0 \end{bmatrix} \\ &= \mathbf{A} \cdot \begin{bmatrix} \tilde{e}_N \\ 0 \end{bmatrix} = \begin{bmatrix} a_{11} & a_{12} \\ a_{21} & a_{22} \end{bmatrix} \cdot \begin{bmatrix} \tilde{e}_N \\ 0 \end{bmatrix} \end{aligned} \quad (15.47)$$

where \tilde{e}_{in} and \tilde{i}_{in} are the input voltage and current, respectively, and \tilde{e}_N is the voltage across the termination impedance $2R_T$. We evaluate \tilde{e}_N from

$$\tilde{e}_N = \tilde{e}_{in} / a_{11}. \quad (15.48)$$

The then voltage and current at the junction of each section may be calculated by working back from the termination resistor R_T as follows

$$\begin{bmatrix} \tilde{e}_n \\ \tilde{i}_n \end{bmatrix} = \mathbf{A}_{n+1} \cdot \mathbf{A}_{n+2} \cdots \mathbf{A}_N \cdot \begin{bmatrix} 1 & 0 \\ 1/(2R_T) & 1 \end{bmatrix} \cdot \begin{bmatrix} \tilde{e}_N \\ 0 \end{bmatrix}. \quad (15.49)$$

Hence the driving pressure produced by each ring is

$$\tilde{p}_n = \frac{\varepsilon_0 E p_{\sim}}{d^2} \varepsilon_n \quad (15.50)$$

$$\tilde{p}_0 = \frac{\varepsilon_0 E p_{\sim}}{d^2} \varepsilon_{in} \quad (15.51)$$

15.7 FAR-FIELD SOUND PRESSURE

The far-field pressure is derived in the same way as that for a resilient disk in free space in Section 13.8 and is the sum of the pressures radiated from each individual ring

$$\tilde{p}(r, \theta) = -j a \tilde{p}_0 \frac{e^{-jkr}}{4r} D(\theta) \quad (15.52)$$

where $D(\theta)$ is the directivity function given by

$$D(\theta) = \frac{2}{a} \cot \theta \left(a_0 J_1(ka_0 \sin \theta) + \sum_{n=1}^N \frac{\tilde{p}_n}{\tilde{p}_0} (a_n J_1(ka_n \sin \theta) - a_{n-1} J_1(ka_{n-1} \sin \theta)) \right). \quad (15.53)$$

The normalized directivity pattern $20 \log_{10}|D(\theta)| - 20 \log_{10}|D(0)|$ is plotted in Fig. 15.13. The on-axis response is given by

$$p_{\text{norm}} = kaD(0) = \frac{ka_0^2}{a} + \sum_{n=1}^N \frac{\tilde{p}_n k (a_n^2 - a_{n-1}^2)}{\tilde{p}_0 a}, \quad (15.54)$$

which is plotted in Fig. 15.14 using the quantities shown in Table 15.2, where the total delay is 255 μs and the width of each ring is 2 cm.

15.8 NEUTRALIZATION OF STRAY CAPACITANCES

Inevitably, in the real world, we encounter stray capacitances between adjacent rings. This may be in the form of capacitance between the stator rings themselves (anything up to 10% of the capacitance of the air gap), in the wiring and most significantly within the windings of the inductors, which need many turns of wire to produce the high inductance values needed. The capacitances between adjacent rings and within the wiring can be measured directly, but the winding capacitances of the inductors are best found indirectly by measuring their self-resonance frequencies. The effect of the stray capacitance is to bypass the inductors at high frequencies and thus reduce the amount of delay in the delay line. This in turn narrows the directivity pattern and thus

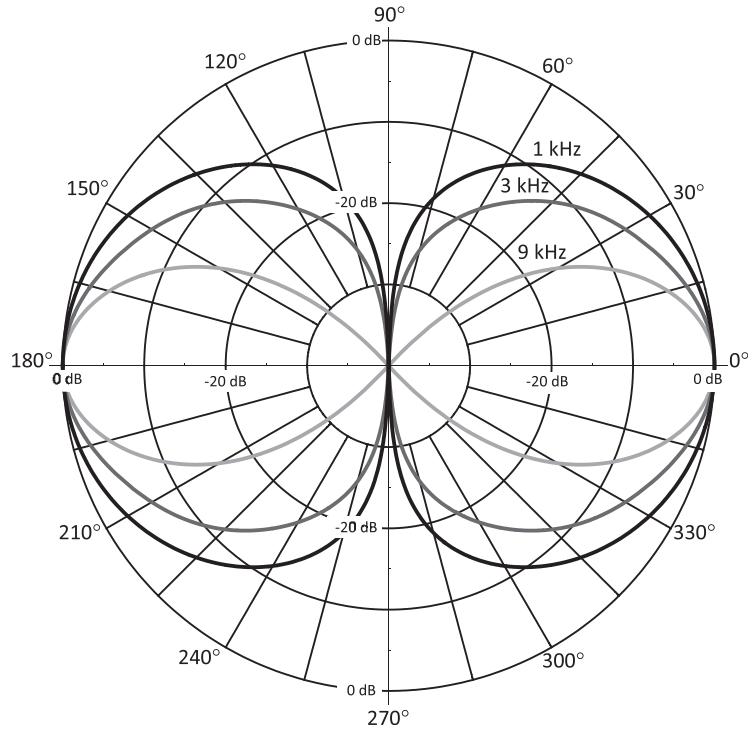


Figure 15.13 Directivity patterns at various frequencies of a 280 mm diameter membrane discretized into six equal rings, each having a width of 20 mm, and a center disk with a radius of 20 mm, using the delay line of Fig. 15.12 with six sections.

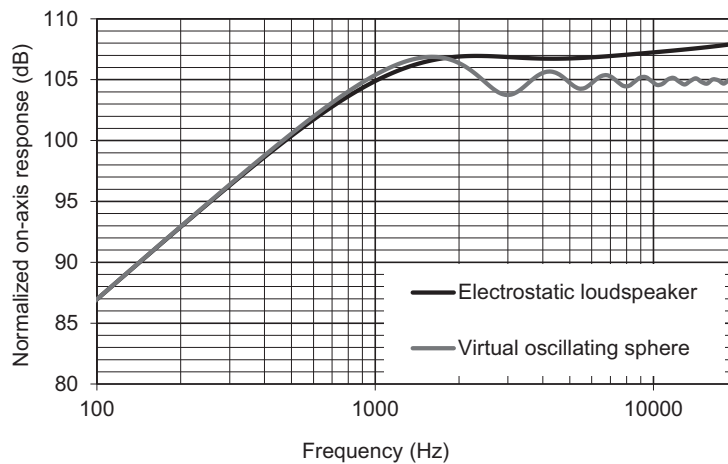


Figure 15.14 On-axis responses of a 280 mm diameter membrane with the delay configured to simulate an oscillating sphere where the delay is continuous (*gray*) and discretized into six equal rings and center disk (*black*) using the delay line of Fig. 15.12.

Table 15.2 Quantities for idealized electrostatic loudspeaker and delay line.

Parameters	Resistor and constants	Inductors (H)	Capacitors (pF)	Turnover frequencies (kHz)
$a = 14$ cm	$R_T = 282$ k Ω	$L_1 = 2.66$	$C_1 = 0$	$f_1 = 16.9$
$d = 1$ mm	$\rho_0 = 1.18$ kg/m ³	$L_2 = 4.90$	$C_2 = 5.75$	$f_2 = 9.18$
$r = 1$ m	$c = 345$ m/s	$L_3 = 7.80$	$C_3 = 20.0$	$f_3 = 5.77$
$e_{in} = 2\sqrt{2}$ kV _{rms}	$\epsilon_0 = 8.85$ pF/m	$L_4 = 11.5$	$C_4 = 43.6$	$f_4 = 3.92$
$E_P = 2$ kV		$L_5 = 16.9$	$C_5 = 89.4$	$f_5 = 2.66$
$N = 6$		$L_6 = 28.4$	$C_6 = 211$	$f_6 = 1.59$

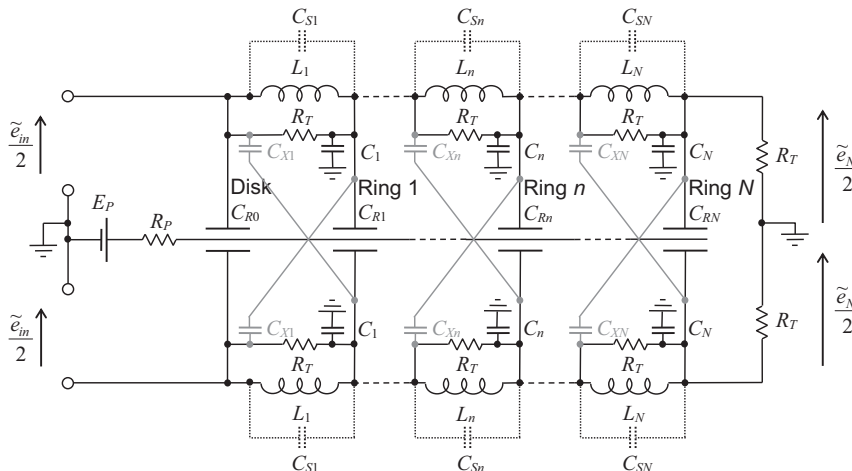
lifts the on-axis response. Although we will describe a method for neutralizing the stray capacitances, it is best not to neutralize all of them in practice because some lift in the on-axis response is usually needed to compensate for the high-frequency roll-off due to the inertia of the membrane.

A scheme for neutralizing the stray capacitances C_{Sn} is shown in Fig. 15.15 in the form of the cross-coupled capacitors C_{Xn} . For effective neutralization, we set

$$C_{Xn} = C_{Sn}. \quad (15.55)$$

Although the effect of these neutralizing capacitors is to make the stray capacitances between adjacent rings vanish, the capacitances between opposite rings are effectively increased to include C_{Sn} . Hence, we modify Eq. (15.34) for the inductors to

$$L_n = 2R_T^2(C_{Tn} + C_{Sn}), \quad (15.56)$$

**Figure 15.15** Constant impedance delay line with compensation for stray capacitance C_{Sn} in the form of C_{Xn} .

and Eq. (15.35) for the turnover frequency to

$$\omega_n = \frac{1}{2R_T(C_{Tn} + C_{Sn})}, \quad (15.57)$$

where the voltage transfer function of each delay section is still given by Eq. (15.33). The time delay T_n per section is defined by

$$T_n = \frac{z_n}{c} = \frac{1}{\omega_n} = 2R_T(C_{Tn} + C_{Sn}) = \frac{L_n}{R_T}. \quad (15.58)$$

so that the total capacitance per section is given by

$$C_{Tn} = \frac{z_n}{2cR_T} - C_{Sn}. \quad (15.59)$$

We can now furnish each section of the delay with its respective component values

$$C_n = 2(C_{Tn} - C_{Rn}) \quad (15.60)$$

where C_{Tn} is given by Eq. (15.59) and C_{Rn} by Eq. (15.30). From Eq. (15.58) we have

$$L_n = \frac{z_n R_T}{c}. \quad (15.61)$$

Each delay section is defined by the transmission matrix

$$\begin{bmatrix} \tilde{e}_{n-1} \\ \tilde{i}_{n-1} \end{bmatrix} = \mathbf{A}_n \cdot \begin{bmatrix} \tilde{e}_n \\ \tilde{i}_n \end{bmatrix} \quad (15.62)$$

where each element of \mathbf{A}_n is given by

$$a_{11}(n) = \frac{R_T L_n (2C_{Tn} + C_{Sn} + C_{Xn})s^2 + L_n s + R_T}{R_T L_n (C_{Sn} - C_{Xn})s^2 + L_n s + R_T}, \quad (15.63)$$

$$a_{12}(n) = \frac{2R_T L_n s}{R_T L_n (C_{Sn} - C_{Xn})s^2 + L_n s + R_T}, \quad (15.64)$$

$$a_{21}(n) = \frac{(C_{Tn} + 2C_{Xn})s \left(R_T L_n \left(C_{Sn} + \frac{C_{Tn} C_{Xn}}{C_{Tn} + 2C_{Xn}} \right) s^2 + L_n s + R_T \right)}{R_T L_n (C_{Sn} - C_{Xn})s^2 + L_n s + R_T}, \quad (15.65)$$

$$a_{22}(n) = \frac{R_T L_n (C_{Sn} + C_{Xn})s^2 + L_n s + R_T}{R_T L_n (C_{Sn} - C_{Xn})s^2 + L_n s + R_T}, \quad (15.66)$$

The remaining calculations proceed as per the previous section from Eq. (15.46) onwards.

15.9 SUMMARY OF DIRECTIVITY CONTROL

We see that when the delay line of an electrostatic loudspeaker is configured so that it imitates an oscillating sphere, it is not the delay line but the discretization of the stator into rings of finite width that produces irregularities in the pressure response of Fig. 15.11. However, a very smooth response may be obtained using an analog delay line, as shown in Fig. 15.14. Although this does not produce a constant directivity pattern up to the very highest frequencies, broad directivity is maintained throughout the vital midrange and lower treble, as shown in Fig. 15.13. Eq. (15.19) is a useful formula for the voltage sensitivity when such a delay line is used, although Walker's voltage equation of Eq. (15.20) still applies for $f < c/(\pi a)$.

PART XXXIV: LUMPED-ELEMENT MODEL OF AN ELECTROSTATIC LOUSPEAKER

15.10 ELECTRO-MECHANO-ACOUSTICAL CIRCUIT

In Section 14.10 we developed an analytical (distributed-element) model of a circular electrostatic loudspeaker. Here we will develop a simpler lumped-element model which is valid when there is sufficient resistance (usually in the form of a dust screen) to suppress the membrane modes. Using an analogous circuit, we will then develop useful design formulas.

The analogous circuit of the electrostatic loudspeaker shown in Fig. 15.1 is given by Fig. 15.16. Although this is a general circuit, we shall assume for this analysis that the loudspeaker is circular with radius a and has no enclosure whatsoever.

The symbols have the following meanings:

\tilde{e}_{in} is the voltage of the generator (audio amplifier) in volts (V).

\tilde{i}_{in} is the total input current in amperes (A).

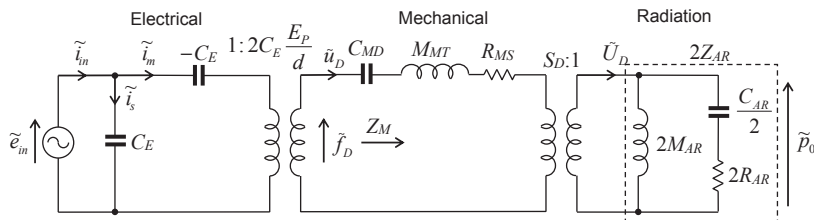


Figure 15.16 Electro-mechano-acoustical analogous circuit of the electrostatic loudspeaker shown in Fig. 15.1.

\tilde{i}_s is the static part of the input current in amperes (A).

\tilde{i}_m is the motional part of the input current in amperes (A).

C_E is the static capacitance between the electrodes in Farads (F).

$-C_E$ represents the negative capacitance due to electrostatic attraction in Farads (F).

E_P is the polarization supply voltage in volts (V).

d is the separation distance between the membrane and each electrode in meters (m).

\tilde{f}_D is the mechanical force driving the membrane in Newtons (N).

\tilde{u}_D is the average velocity of the membrane in m/s.

$Z_M = \tilde{f}_D / \tilde{u}_D$ is the total mechanical impedance in N·s/m.

C_{MD} is the mechanical compliance of the membrane in m/N due to its tension.

M_{MT} is the total moving mass of the membrane and stator perforations in kg.

R_{MS} is the mechanical resistance due to viscous flow losses through the stator electrode perforations and dust screen.

$S_D = \pi a^2$ is the surface area of the membrane in m², where a is the radius in m.

$\tilde{U}_D = S_D \tilde{u}_D$ is the total volume velocity in m³/s.

\tilde{p}_0 is the pressure in N/m² driving the radiation load $2Z_{AR}$ on *both* sides of the membrane.

M_{AR} is the acoustic radiation mass on one side of the membrane in kg/m⁴.

C_{AR} is the acoustic radiation compliance on one side of the membrane in m⁵/N.

R_{AR} is the acoustic radiation resistance on one side of the membrane in N·s/m⁵.

For simplicity, we assume that the output impedance of the amplifier and resistance of the cables are negligible, and we also ignore any stray capacitance in the cables. There are two transformers: the first acts as an interface between the electrical domain and the mechanical one converting voltage to force \tilde{f}_D and current \tilde{i}_m to velocity \tilde{u}_D , while the second acts as an interface between the mechanical and acoustical domains, converting force to pressure \tilde{p}_0 and velocity \tilde{u}_D to volume velocity \tilde{U}_D .

Notice how the input current \tilde{i}_m divides into two: one is the static current \tilde{i}_s while the other is the motional current \tilde{i}_m . The static current still flows when the membrane is blocked (or the polarization voltage E_P is turned off), but the motional current is dependent on the membrane velocity \tilde{u}_D . Unfortunately, in most practical electrostatic loudspeakers $\tilde{i}_s \gg \tilde{i}_m$, so that the electrical input impedance is defined almost entirely by C_E , although it is possible to measure the motional current by “balancing out” the static current with a capacitor [7]. The stator resistance R_{MS} is technically an acoustic flow resistance, but it is included on the mechanical side of Fig. 15.16 for convenience.



15.11 NEGATIVE COMPLIANCE AND STABILITY

The negative capacitance $-C_E$ represents the electrostatic force of attraction. When referred to the mechanical side, it forms a negative compliance and must always exceed C_{MD} in value to prevent the membrane from being attracted to whichever stator is closest. Hence,

if there were insufficient tension to counteract this, we would have an unstable equilibrium in the central position, like that of a marble balanced on top of a dome. Therefore

$$C_{MD} < \frac{d^2}{4C_E E_P^2} \quad (15.67)$$

Although the force acting on the membrane is linear under dynamic conditions, because of the constant-charge principle mentioned at the beginning of the chapter, the resistance R_P in Fig. 15.1 (together with any resistive coating) will not prevent charge from migrating to the closest stator during very slow or static displacements. Hence, the electrostatic force of attraction will increase as the membrane approaches the stator, causing it to stick. Hence, a reasonably thick layer of insulation is needed on the insides of the stators to limit the minimum distance between the membrane and the conducting parts of the stators. This is equivalent to driving the stators with series capacitors in which the insulating material forms the dielectric, but, for simplicity, we shall omit these capacitors in this analysis.



15.12 STATIC MEMBRANE COMPLIANCE

At very low frequencies, all inertial and resistive elements have very little effect and can therefore be removed from the analogous circuit of Fig. 15.16 to obtain that shown in Fig. 15.17.

To obtain the static membrane and negative compliances C_{MD0} and $-C_{ME0}$ respectively, we solve the static (in vacuo) membrane wave equation for the displacement $\eta(w)$ versus the radial ordinate w

$$\left(\frac{\partial^2}{\partial w^2} + \frac{1}{w} \frac{\partial}{\partial w} + \frac{1}{C_{ME} S_D T} \right) \eta(w) = -\frac{f_{D0}}{S_D T}, \quad \eta(a) = 0 \quad (15.68)$$

where f_{D0} is the static membrane driving force, which is given by

$$f_{D0} = \beta e_{in}, \quad (15.69)$$

and β is the electromechanical conversion factor, which is given by

$$\beta = 2C_E \frac{E_P}{d}, \quad (15.70)$$

where $C_E = \epsilon_0 S_D / (2d)$.

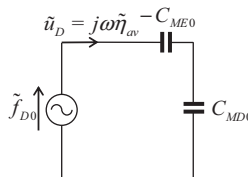


Figure 15.17 Simplified analogous circuit for very low frequencies referred to the mechanical side.

We have referred the negative capacitance $-C_E$ to the mechanical side in Eq. (15.68) so that it becomes a negative mechanical compliance

$$-C_{ME} = \frac{C_E}{\beta^2} = -\frac{d^2}{4C_E E_p^2}. \quad (15.71)$$

We solve Eq. (15.68) to obtain

$$\eta(w) = \frac{2f_{D0}J_0(\alpha_0 w/a)}{\pi T \alpha_0 \left(\alpha_0^2 - (C_{ME} S_D T)^{-1} a^2 \right) J_1(\alpha_0)} \quad (15.72)$$

where α_0 is the first zero of the Bessel function J_0 . From this we see that the displacement becomes indeterminate when

$$\alpha_0^2 = (C_{ME} S_D T)^{-1} a^2. \quad (15.73)$$

Hence for stability,

$$T > \frac{2\varepsilon_0 a^2}{\alpha_0^2 d} \left(\frac{E_p}{d} \right)^2. \quad (15.74)$$

The average displacement is given by

$$\begin{aligned} \eta_{av} &= \frac{1}{\pi a^2} \int_0^{2\pi} \int_0^a \eta(w) w dw d\varphi = \frac{4f_{D0}}{\pi T \alpha_0^2 \left(\alpha_0^2 - (C_{ME} S_D T)^{-1} a^2 \right)} \\ &= \frac{2J_1(\alpha_0)\eta(0)}{\alpha_0} = \frac{\eta(0)}{2.316} \end{aligned} \quad (15.75)$$

Hence, the displacement at the center is about 2.3 times the average, and the total combined static compliance is given by

$$C_{MT0} = \frac{\eta_{av}}{f_{D0}} = \frac{4}{\pi T \alpha_0^2 \left(\alpha_0^2 - (C_{ME} S_D T)^{-1} a^2 \right)} = \left(\frac{1}{C_{MD0}} - \frac{1}{C_{ME0}} \right)^{-1}, \quad (15.76)$$

so that

$$C_{MD0} = \frac{4}{\pi \alpha_0^4 T}, \quad (15.77)$$

$$C_{ME0} = \frac{4}{\alpha_0^2} C_{ME} = \frac{C_{E0}}{\beta^2}, \quad (15.78)$$

Hence, from Eqs. (15.71) and (15.78), the static negative capacitance is related to the dynamic negative capacitance by

$$-C_{E0} = -\frac{4}{\alpha_0^2} C_E. \quad (15.79)$$



15.13 DYNAMIC MEMBRANE COMPLIANCE AND DYNAMIC RESISTANCE

By similar argument, we find that the dynamic mechanical compliance is given by

$$C_{MD} = \frac{\alpha_0^2}{4} C_{MD0} = \frac{1}{\pi \alpha_0^2 T} \quad (15.80)$$

and the dynamic resistance is given by

$$R_{MS} = \frac{\alpha_0^2}{4} S_D R_S. \quad (15.81)$$

However, it is inconvenient to have different circuit element values for static and dynamic conditions. Hence, we use the following bilinear approximations for hybrid static–dynamic compliances, which transition from static to dynamic at around half the resonance frequency f_0

$$C'_{MD} = \frac{1 + 2\frac{f}{f_0}}{\frac{\alpha_0^2}{4} + 2\frac{f}{f_0}} C_{MD} \quad (15.82)$$

$$-C'_E = \frac{1 + 2\frac{f}{f_0}}{\frac{\alpha_0^2}{4} + 2\frac{f}{f_0}} (-C_E). \quad (15.83)$$

We will derive an expression for the membrane resonance frequency f_0 further on. Note that we only apply this transformation to the negative electrical capacitance associated with the motional current, not the positive one associated with the static current. By applying the same bilinear approximation to both the negative and positive mechanical compliances, we are not changing the condition for stability of Eq. (15.74).



15.14 SETTING TENSION TO LIMIT DISPLACEMENT AND MAINTAIN STABILITY

The stress must not exceed the maximum value σ_{\max} for the membrane material, which for polyester is 55–75 MPa, yet for stability it must be greater than the minimum value given by Eq. (15.74). Hence the tension should lie within the range

$$\frac{2\varepsilon_0 a^2}{\alpha_0^2 d} \left(\frac{E_P}{d} \right)^2 < T < \sigma_{\max} h, \quad (15.84)$$

where h is the thickness of the membrane. However, the tension is usually set to at least three times the minimum value for stability to allow for varying environmental conditions and aging. Now that we have established the safe limits for the tension, we wish to set it so that the displacement at low frequencies stays within the gap width d . By applying ohms law to the total impedance of the two compliant elements, C_{MD0} and $-C_{ME0}$, given by Eqs. (15.77) and (15.78) respectively and shown in Fig. 15.17, then rearranging we obtain

$$T = \frac{4C_E E_P}{\pi \alpha_0^2 d} \left(\frac{2\tilde{e}_{\text{in}}}{\alpha_0^2 \tilde{\eta}_{\text{av}}} + \frac{E_P}{d} \right). \quad (15.85)$$

The most efficient way to operate the loudspeaker is to arrange for the maximum peak input voltage to be equal to twice the polarization voltage. Also, let us set the peak average displacement to one-third of the gap width so that $\tilde{e}_{\text{in}}/\tilde{\eta}_{\text{av}} = 6E_P/d$ in Eq. (15.85). Hence

$$T = \frac{\varepsilon_0 a^2}{d} \left(\frac{E_P}{d} \right)^2, \quad (15.86)$$

which is nearly three times the minimum value in Eq. (15.74). If we use this tension value in Eqs. (15.71 and (15.80), then

$$C'_{ME} = \frac{\alpha_0^2}{2} C'_{MD} = 2.89 C'_{MD}. \quad (15.87)$$



15.15 RADIATION IMPEDANCE

To derive the radiation impedance Z_{AR} , we modify Eq. (13.212) from Section 13.10 for the uniform velocity distribution of a rigid piston to obtain that for one with a parabolic velocity distribution

$$\Phi(w) = 2 \left(1 - \frac{w^2}{a^2} \right) = 2 \sum_{m=0}^{\infty} (\delta_{m0} - \delta_{m1}) \left(\frac{w}{a} \right)^{2m}, \quad 0 \leq w \leq a \quad (15.88)$$

and replace Eq. (13.215) with $\mathbf{b}(m+1) = 2(-\delta_{m0} + \delta_{m1})$. By analyzing the low frequency asymptotic behavior, we obtain the radiation impedance elements

$$M_{AR} = \frac{8\rho_0}{5\pi^2 a}, \quad (15.89)$$

$$C_{AR} = \frac{\sqrt{5}\pi a^3}{6\rho_0 c^2}, \quad (15.90)$$

$$R_{AR} = \frac{\rho_0 c}{\pi a^2}. \quad (15.91)$$

From Eq. (13.125), the far-field on-axis pressure with no delay is given by

$$\tilde{p}(r) = jka^2 \tilde{p}_0 \frac{e^{-jkr}}{4r} \quad (15.92)$$

Notice that the far-field pressure is the first-order derivative of the driving pressure. At high frequencies, where the wavelength is small compared to the membrane; this rising response is caused by the decreasing beam width that concentrates the radiated energy on axis. At low frequencies, the antiphase rear radiation partially cancels that from the front. Only the phase shift due to the path difference prevents the cancellation from being complete. However, as the frequency decreases, the cancellation becomes more complete as the path difference is equal to an ever-smaller portion of the wavelength.



15.16 FREQUENCY RESPONSE

A simplified on-axis frequency response of the electrostatic loudspeaker using linear approximations is shown in Fig. 15.18, although the full response from the analogous circuit of Fig. 15.16 together with Eq. (15.92) is given by

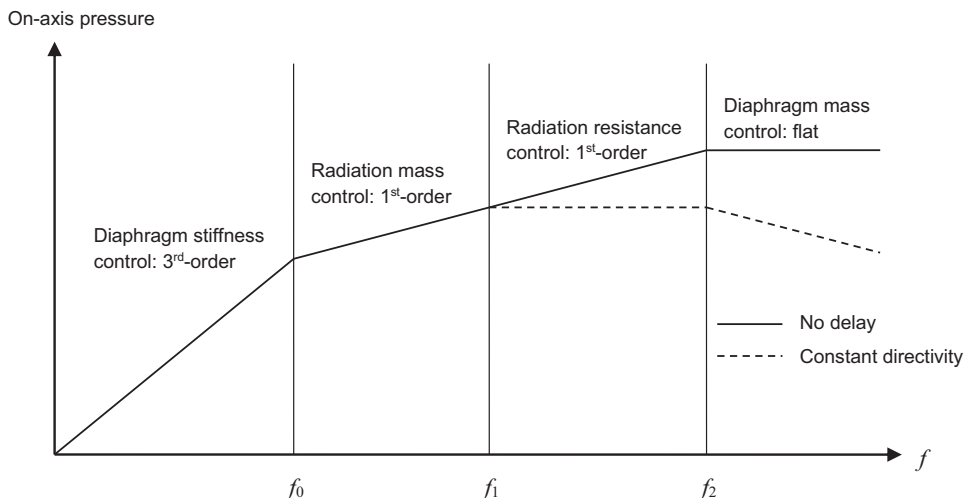


Figure 15.18 Frequency response using linear approximations. Solid curve is for no delay and dashed curve is for constant directivity (virtual oscillating sphere), which is achieved using concentric ring electrodes fed from tappings along a delay line, as described in Sections 15.4–15.6.

$$\tilde{p}(r) = j\epsilon_0 k a^2 \zeta \cdot \frac{E_P}{d} \cdot \frac{\tilde{e}_{in}}{2d} \cdot \frac{e^{-jkr}}{2r}, \quad (15.93)$$

where ζ is the *force factor*, which is given by

$$\zeta = \frac{S_D \tilde{p}_0}{\tilde{f}_D} = \frac{2S_D^2 Z_{AR}}{2S_D^2 Z_{AR} + Z_{MD}}. \quad (15.94)$$

The acoustic radiation impedance is given by

$$Z_{AR} = \left(\frac{1}{j\omega M_{AR}} + \frac{1}{R_{AR} + \frac{1}{j\omega C_{AR}}} \right)^{-1}, \quad (15.95)$$

and the mechanical membrane impedance by

$$Z_{MD} = j\omega M_{MT} + R_{MS} + \frac{1}{j\omega} \left(\frac{1}{C'_{MD}} - \frac{\beta^2}{C'_E} \right). \quad (15.96)$$

To ensure the displacement does not exceed the gap width d , it is useful to calculate the peak displacement, which from Eq. (15.75) is given by

$$\eta_{\text{peak}} = \frac{\alpha_0}{2J_1(\alpha_0)} \sqrt{2} \tilde{\eta}_{av} = 2.316 \sqrt{2} \tilde{\eta}_{av}, \quad (15.97)$$

where the average displacement is given by

$$\tilde{\eta}_{av} = \frac{\tilde{u}_D}{j\omega(Z_{MD} + 2S_D^2 Z_{AR})}. \quad (15.98)$$

Now let us simplify the circuit of Fig. 15.16 over specific frequency ranges to gain a better understanding of how the frequency response is determined.

The mechanical impedance is plotted in Fig. 15.19, also using linear approximations, which can be divided into five regions as follows:

1. **Membrane stiffness control, $f \ll f_0$.** In the region $f \ll f_0$, the membrane mass M_{MD} and stator resistance R_{MS} have negligible effect and the radiation load is almost a pure mass. Hence, after omitting the electrical part and referring the negative capacitance and acoustical elements to the mechanical side, the circuit of Fig. 15.16 simplifies to that of Fig. 15.20. This is a simple second-order high-pass filter, but when combined with the increasing amount of cancellation between the rear and front radiation with decreasing frequency, it gives rise to the third-order slope shown in Fig. 15.18.
2. **Stator resistance control, $f \approx f_0$.** At the fundamental membrane resonance frequency f_0 , the reactance of the combined positive and negative compliances in Fig. 15.20

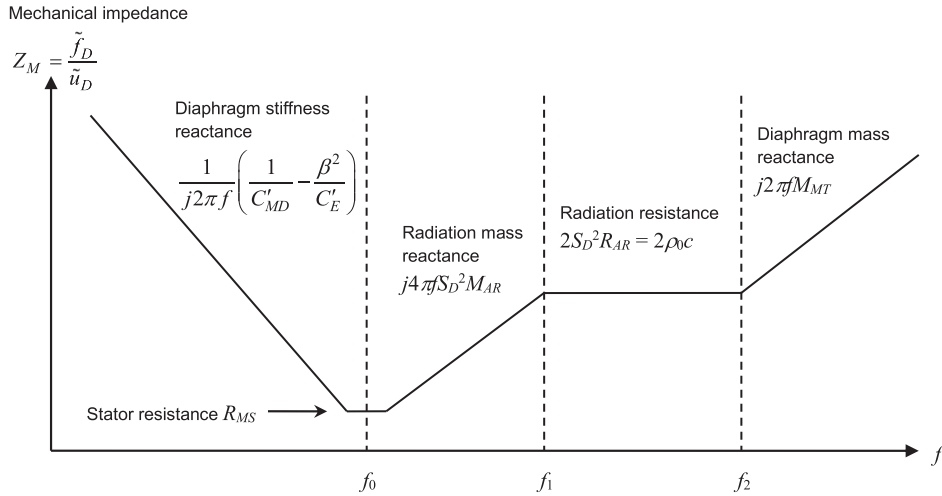


Figure 15.19 Plot of mechanical impedance Z_M versus frequency f for the analogous circuit shown in Fig. 15.16 using linear approximations.

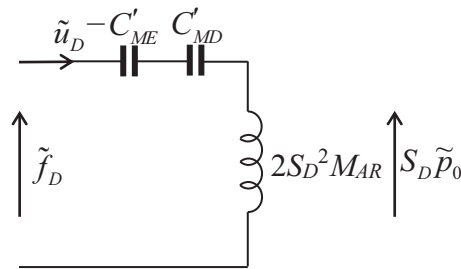


Figure 15.20 Simplified analogous circuit for mechanical impedance when $f < f_0$.

cancels that of the radiation mass, so that in Fig. 15.16 we are left with just the stator resistance R_{MS} , as shown in Fig. 15.21.

Ignoring the mass of the membrane, the resonance frequency is given by

$$f_0 = \frac{1}{2\pi S_D} \sqrt{\frac{1}{2M_{AR}} \left(\frac{1}{C_{MD}} - \frac{1}{C_{ME}} \right)} \quad (15.99)$$

with a Q factor of

$$Q = \frac{2\pi f_0 S_D^2 2M_{AR}}{R_{MS}} = \frac{S_D}{R_{MS}} \sqrt{2M_{AR} \left(\frac{1}{C_{MD}} - \frac{1}{C_{ME}} \right)} \quad (15.100)$$

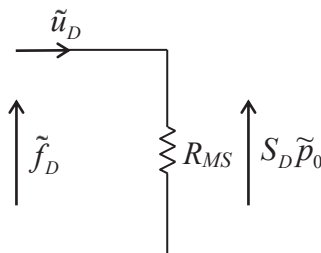


Figure 15.21 Simplified analogous circuit for mechanical impedance when $f \approx f_0$.

where M_{AR} , C_{ME} , and C_{MD} are given by Eqs. (15.89), (15.71), and (15.80), respectively. If we set the tension according to Eq. (15.86) so that $-C_{ME} = -1/(2\pi T)$, then

$$f_0 = \frac{1}{8a} \sqrt{\frac{5(\alpha_0^2 - 2)T}{\pi a \rho_0}} = \frac{1}{3.26a} \sqrt{\frac{T}{a \rho_0}} \quad (15.101)$$

$$Q = \frac{4a}{R_{MS}} \sqrt{\frac{\pi(\alpha_0^2 - 2)a \rho_0 T}{5}} = \frac{6.17a \sqrt{a \rho_0 T}}{R_{MS}} \quad (15.102)$$

To prevent excessive membrane excursion at the resonance frequency yet maintain an optimum bass response, the ideal value of Q is in the range 0.7–1.0. Hence, we choose the dust screen to have a specific acoustic resistance of

$$R_S = \frac{R_{MS}}{S_D} = \frac{1}{Q} \sqrt{\frac{2M_{AR}(C_{ME} - C_{MD})}{C_{ME}C_{MD}}} = \frac{2}{Q} \sqrt{\frac{\rho_0 T}{a}} \quad (15.103)$$

Note that when we turn off the polarizing voltage, both f_0 and Q increase by 24% because $C_{ME} = 2.89C_{MD}$.

3. Radiation mass control, $f_0 < f < f_1$. In the region $f_0 < f < f_1$, the membrane impedance is small compared to the radiation load, which is still mainly mass, although the radiation resistance is increasing with frequency. Note that the radiation mass is much greater than the mechanical mass of the membrane. Hence, the circuit of Fig. 15.16 simplifies to that of Fig. 15.22.

Here the driving pressure \tilde{p}_0 is constant, but the wavelength is still larger than the half-circumference of the membrane, so that the directivity pattern is a reasonably constant figure-of-eight; and we still have an increasing amount of cancellation between the rear and front waves with decreasing frequency. Hence, we have a first-order slope in Fig. 15.18 and Eq. (15.20) for the on-axis pressure is valid in this region. Notice that the effect of C_{AR} in Fig. 15.16 is to make the net radiation

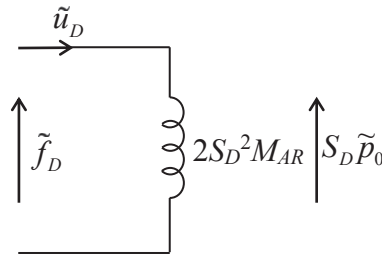


Figure 15.22 Simplified analogous circuit for mechanical impedance when $f_0 < f < f_1$.

resistance proportional to f^4 in this region. Combined with the predominantly massive radiation impedance (due to M_{AR}), this causes the velocity \tilde{u}_D to be inversely proportional to f . Hence the radiated power is proportional to f^2 , i.e., 6 dB/octave. The radiated power could only be leveled by mounting the membrane in an infinite baffle or an extremely large enclosure, in which case C_{AR} would vanish from Fig. 15.16.

4. **Radiation resistance control, $f_1 < f < f_2$.** In the region $f_1 < f < f_2$, the wavelength is smaller than the half-circumference, but membrane impedance is still small compared to the radiation load; and the radiation load has now become resistive so that the radiated power is constant. However, the on-axis pressure in Fig. 15.18 continues to rise at a rate of 6 dB/octave because of the narrowing directivity pattern without a delay, according to Eq. (15.20). However, if a delay line is used to imitate an oscillating sphere, the on-axis pressure is constant as given by Eq. (15.19). The simplified circuit is shown in Fig. 15.23.

Only in this region, where the membrane velocity is constant and the radiation load resistive, is the total radiated power constant. The frequency f_1 is given by

$$f_1 = \frac{c}{\pi a} \quad (15.104)$$

The radiation resistance effectively damps the diaphragm modes, whereas below f_1 , we rely on the viscous flow resistance of a dust screen.

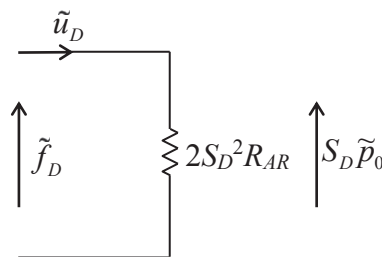


Figure 15.23 Simplified analogous circuit for mechanical impedance when $f_1 < f < f_2$.

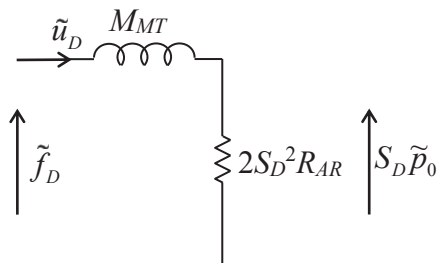


Figure 15.24 Simplified analog circuit for mechanical impedance when $f > f_2$.

5. **Membrane and stator mass control, $f > f_2$.** In the region $f > f_2$, the combined mass reactance of the membrane and stator perforations is greater than the radiation resistance so that we have the circuit shown in Fig. 15.24. Here, the radiated power decreases with increasing frequency. Hence, without a delay, the on-axis pressure response flattens off. As the directivity pattern continues to shrink, the radiated power becomes increasingly on-axis concentrated. Otherwise, if a delay line is used to keep the pattern constant, the on-axis pressure falls at a rate of 6 dB/octave with increasing frequency.

The frequency f_2 is given by

$$f_2 = S_D^2 R_{AR} / (\pi M_{MT}) \quad (15.105)$$

where M_{MT} is the total moving mass of the membrane and stator perforations

$$M_{MT} = M_{MD} + 2M_{MS} \quad (15.106)$$

and R_{AR} is the acoustic radiation resistance given by Eq. (15.91). At high frequencies, the membrane moves almost uniformly as a piston, unlike at very low frequencies where the displacement is almost parabolic. Hence, the effective mass of the membrane is

$$M_{MD} = S_D \rho_D h, \quad (15.107)$$

where ρ_D and h are the density and thickness of the membrane respectively. From Eq. (4.26), the mass of the air in the stator perforations is

$$M_{MS} = S_D \rho_0 \left(t + 0.85 a_h \left(1 - 1.28 \sqrt{\phi_h} \right) \right) / \phi_h, \quad (15.108)$$

where t is the thickness of the stator, a_h is the radius of the holes, and ϕ_h is the porosity, that is, ratio of open area to total area. The end correction factor of 0.85 is for the outside of the stator only. On the inside, the distance d between the stator and membrane is usually so small that there will be little in the way of extra mass extending beyond the hole entrance. Notice that the end correction factor depends on the square root of the

porosity. For a triangular array of holes of radius a_h and hole pitch b_h , the porosity is given by

$$\phi_h = \frac{2\pi a_h^2}{\sqrt{3}b_h^2}. \quad (15.109)$$

Hence,

$$f_2 = \frac{\rho_0 c}{\pi(\rho_D h + 2\rho_0(t + 0.85a_h(1 - 1.2\sqrt{\phi_h}))/\phi_h)}. \quad (15.110)$$

Notice how this cut-off frequency is independent of the membrane area. This is a fairly simple stator model and a more comprehensive one can be found in Ref. [9].



15.17 SUMMARY OF ELECTROSTATIC LOUDSPEAKER DESIGN

We can see from Eqs. (15.19) and (15.20) that to maximize the radiated sound pressure, the field strength E_p/d should be as close to its maximum allowable value as possible, which is around 2 kV/mm. Similarly, we generally set the maximum peak signal voltage $^{1/2}\tilde{e}_{in}$ to the same value as the polarizing voltage E_p because the maximum sound pressure is proportional to the product of the two, but their sum should not exceed 4 kV/mm.

If the gap distance d is reduced, we can reduce both E_p and \tilde{e}_{in} while keeping the sound pressure constant. Hence the sensitivity is increased. Although the capacitance is increased proportionately, the input current does not change because of the reduced voltage. Hence the reactive power is reduced, while the efficiency is increased. With a smaller gap, some very low bass is sacrificed, but this is usually in a region where there is little output anyway because of rear-wave cancellation.

A good place to start the design process is with the highest frequency of interest because we can use this to define the membrane thickness h independently of its radius a . From this we can work out the maximum tension T that it can withstand. Maximizing the tension enables a smaller gap d to be employed without the membrane touching the electrodes at the maximum input voltage at low frequencies, where the displacement is highest. We have shown (see Eqs. 15.84 and 15.86) that making the tension large enough to avoid contact automatically meets the condition for stability under the electrostatic force of attraction.

Knowing the tension, we can then define the fundamental resonance frequency f_0 for any given radius a or choose a fundamental resonance frequency to find the required radius. Having found the radius, we can define the gap d , the polarizing voltage E_p , the specific resistance of the dust screen R_s (for the desired Q factor), and the sound pressure level.

1. Referring to Fig. 15.18, choose the highest frequency of interest f_2 . By rearranging Eq. (15.110), calculate the membrane thickness h using

$$h = \frac{\rho_0}{\rho_D} \left(\frac{c}{\pi f_2} - 2 \frac{t + 0.85a_h(1 - 1.28\sqrt{\phi_h})}{\phi_h} \right) \quad (15.111)$$

or we can calculate the cut-off frequency for a given thickness

$$f_2 = \frac{\rho_0 c}{\pi(\rho_D h + 2\rho_0(t + 0.85a_h(1 - 1.28\sqrt{\phi_h}))/\phi_h)}. \quad (15.112)$$

2. Let the tension be 60% of the maximum value, so that

$$T = 0.6\sigma_{\max}h. \quad (15.113)$$

3. Using this tension, choose the lowest frequency of interest (or fundamental resonance frequency) f_0 , which is given by Eq. (15.101) and repeated here for convenience

$$f_0 = \frac{1}{3.26a} \sqrt{\frac{T}{a\rho_0}} \quad (15.114)$$

From this we obtain the membrane radius a in terms of the fundamental resonance frequency f_0

$$a = \frac{1}{2.2} \sqrt[3]{\frac{T}{f_0^2 \rho_0}}. \quad (15.115)$$

When building an electrostatic loudspeaker, it is easier to adjust the tension by measuring the resonance frequency, like tuning a drum skin, rather than by measuring the tension directly, as Eq. (15.114) gives a direct relationship between the two.

4. Assuming the maximum peak input signal is equal to the polarizing voltage such that $1/2\tilde{e}_{\text{in}} = E_p$, we obtain from Eq. (15.93) the maximum rms sound pressure at f_0 assuming $Q = 1$ so that $\zeta \approx 1$

$$\text{SPL}_0 = 94 + 20 \log_{10} \left(\frac{\epsilon_0 \pi a^2 f_0}{\sqrt{2}rc} \cdot \frac{E_p^2}{d^2} \right) \text{ dB at } f_0. \quad (15.116)$$

If this is not loud enough, then it is necessary to lower f_0 by increasing a . Note that this equation ignores the attenuation due to the resistance R_S of a dust screen.

5. Choose a suitable Q value of 0.7–1.0. Again, using $T = 0.6 \cdot \sigma_{\max} \cdot h$, we obtain the optimum specific acoustic resistance of the covering cloth from Eq. (15.103) as follows

$$R_S = \frac{2}{Q} \sqrt{\frac{\rho_0 T}{a}}. \quad (15.117)$$

6. Assuming $E_P/d = 2000$ V/mm and $T = 0.6 \cdot \sigma_{\max} \cdot h$, we obtain from Eq. (15.86) the gap distance between the membrane and each stator

$$d = \frac{\epsilon_0 a^2}{T} \left(\frac{E_P}{d} \right)^2. \quad (15.118)$$

7. Then we obtain the polarizing voltage using simply

$$E_P = \left(\frac{E_P}{d} \right) d. \quad (15.119)$$

8. If a delay line is used, this may be designed using the formulas given in Sections 15.6 and 15.8. Some experimentation will be needed to find the maximum value of the termination resistance R_T that does not result in negative capacitor values yet guarantees optimum efficiency. If the push–pull transformer shown in Fig. 15.1 has a turns ratio of $1:\tau + \tau$, and the nominal input impedance is Z_{nom} , then the turns ratio is given by

$$\tau = \sqrt{\frac{R_T}{2Z_{\text{nom}}}}. \quad (15.120)$$

Once the design has been arrived at, the frequency response with normal directivity may be calculated using Eq. (15.93). Constant directivity may be modeled by including the factor $\omega_1/(j\omega + \omega_1)$, where $\omega_1 = 2c/a$.

Example 15.1. We now use the equations of Section 15.17, to derive the tension, resistance, gap width, and polarizing voltage required for the 280 mm diameter membrane for which we derived the on-axis pressure and directivity pattern in the previous sections while assuming an ideal membrane with no mass or tension. If we use a stator with a thickness of $t = 1$ mm perforated with holes of radius $a_h = 1.5$ mm and pitch $b_h = 5$ mm in a triangular array, the porosity is given by

$$\phi_h = \frac{2\pi a_h^2}{\sqrt{3} b_h^2} = \frac{2 \times 3.14 \times 1.5^2}{\sqrt{3} \times 5^2} = 0.33.$$

Then if we use a membrane with a thickness of $h = 12 \mu\text{m}$ and density of $\rho_D = 1400 \text{ kg/m}^3$, the upper cut-off frequency is given by

$$\begin{aligned}
 f_2 &= \frac{\rho_0 c}{\pi(\rho_D h + 2\rho_0(t + 0.85a_h(1 - 1.28\sqrt{\phi_h}))) / \phi_h} \\
 &= \frac{1.18 \times 344.8}{3.14 \times \left(1400 \times 12 \times 10^{-6} + 2 \times 1.18 \times \frac{10^{-3} + 0.85 \times 1.5 \times 10^{-3} \times (1 - 1.28 \times \sqrt{0.33})}{0.33} \right)} \\
 &= 4.9 \text{ kHz.}
 \end{aligned}$$

Assuming the tensile strength of polyester is $\sigma_{\text{max}} = 60 \text{ MPa}$ and the stress is 60% of the maximum, we obtain the tension from

$$T = 0.6\sigma_{\text{max}}h = 0.6 \times 60 \times 10^6 \times 12 \times 10^{-6} = 432 \text{ N.}$$

Then, for a membrane radius of 140 mm, the resonance frequency is

$$f_0 = \frac{1}{3.26a} \sqrt{\frac{T}{a\rho_0}} = \frac{1}{3.26 \times 0.14} \sqrt{\frac{432}{0.14 \times 1.18}} = 112 \text{ Hz}$$

and the maximum output at f_0 is given by

$$\begin{aligned}
 \text{SPL}_0 &= 20\log_{10} \left(\frac{\epsilon_0 \pi a^2 f_0}{20 \times 10^{-6} \times \sqrt{2}rc} \cdot \frac{E_P^2}{d^2} \right) \\
 &= 20\log_{10} \left(\frac{8.85 \times 10^{-12} \times 3.14 \times 0.14^2 \times 112}{20 \times 10^{-6} \times 1.414 \times 1 \times 344.8} \left(\frac{2000}{10^{-3}} \right)^2 \right) = 88 \text{ dB}
 \end{aligned}$$

We let $Q = 1$ so that we can obtain the optimum specific acoustic resistance of the dust screen

$$R_S = \frac{2}{Q} \sqrt{\frac{\rho_0 T}{a}} = \frac{2}{1} \sqrt{\frac{1.18 \times 432}{0.14}} = 121 \text{ rayls.}$$

Referring to Table 4.1 on p. 126, this value may be made up from using a 75 rayls dust screen on the front and a 47 rayls screen on the back, for example. The gap between the membrane and each stator is given by

$$d = \frac{\epsilon_0 a^2}{T} \left(\frac{E_P}{d} \right)^2 = \frac{8.85 \times 10^{-12} \times 0.14^2}{432} \left(\frac{2000}{10^{-3}} \right)^2 = 1.6 \text{ mm}$$

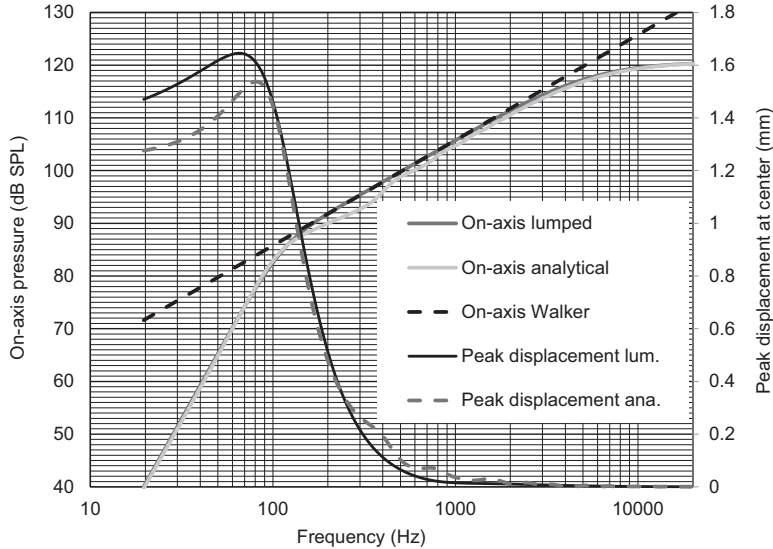


Figure 15.25 Comparison of the on-axis response of an electrostatic loudspeaker without a delay line calculated using the lumped-element Eq. (15.93), based on the quantities given in Example 15.1, with an analytical calculation using distributed-element equations from Section 14.10. Also shown is a plot of the Walker's voltage equation from Eq. (15.121).

and the polarizing voltage by

$$E_P = \left(\frac{E_P}{d} \right) d = \frac{2000}{10^{-3}} \times 1.6 \times 10^{-3} = 3200 \text{ V.}$$

These values are used in Eq. (15.93) to calculate the on-axis response shown in Fig. 15.25 for an electrostatic loudspeaker without a delay line. Also shown is the on-axis response of the same loudspeaker calculated from rigorous equations [10] from Section 14.10 based on an analytical model. This reveals an excellent correlation between the lumped-element model and the analytical one, except that the latter shows a 2.7 dB dip at 330 Hz, which is smoothed out by the simpler lumped-element model. Because the simple model cannot reproduce any harmonics above the fundamental resonance, this correlation is dependent on the membrane being well damped through the use of a dust screen. The simple model appears to overestimate the peak displacement by around 10% at the lowest frequencies, whereas the rigorous model keeps it just within the gap width of 1.6 mm.

Note that the plot of Walker's voltage equation shown in Fig. 15.25 uses the following version of Eq. (15.20) which is modified to include the resistance R_S of the dust screen

$$\tilde{p}(r, 0) = j\epsilon_0 k a^2 \frac{2\rho_0 c}{2\rho_0 c + R_S} \cdot \frac{E_P}{d} \cdot \frac{\tilde{e}_{in}}{2d} \cdot \frac{e^{-jkr}}{2r}, \quad f_0 < f < f_2. \quad (15.121)$$

Next, we combine the on-axis response of a real membrane, based on the lumped-element model, from Eq. (15.93) with Eq. (15.52) for the far-field pressure of an ideal electrostatic loudspeaker with a delay line to yield that of a real membrane with a delay line

$$\tilde{p}(r, \theta) = -jka^2 \tilde{p}_0 \frac{2S_D^2 Z_{AR}}{2S_D^2 Z_{AR} + Z_{MD}} \cdot \frac{e^{-jkr}}{4r} D(\theta), \quad (15.122)$$

where $D(\theta)$ is given by Eq. (15.53). This is plotted in Fig. 15.26 for $\theta = 0$ (on-axis). Also, the reference sensitivity is given by Eq. (15.19), modified to include the resistance of the dust screen

$$\tilde{p}(r, 0) = j\epsilon_0 a \frac{2\rho_0 c}{2\rho_0 c + R_S} \cdot \frac{E_P}{d} \cdot \frac{\tilde{e}_{in}}{2d} \cdot \frac{e^{-jkr}}{r}, \quad f_1 < f < f_2. \quad (15.123)$$

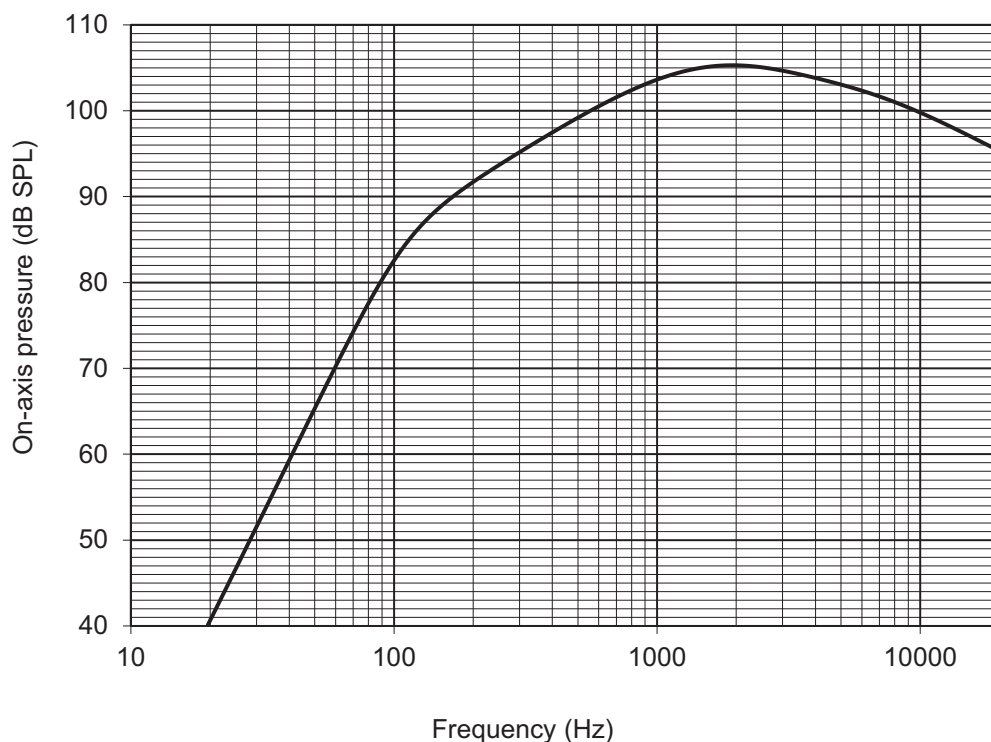


Figure 15.26 The on-axis response of the electrostatic loudspeaker with a delay line as previously shown in Fig. 15.14 but modified to include the response of a real membrane as given by Eqs. (15.122) and (15.53) using the quantities derived in Example 15.1. The fundamental resonance frequency is $f_0 = 112$ Hz and the “flat” region lies between $f_1 = 784$ Hz and $f_2 = 4.9$ kHz.

Assuming $1/2\tilde{e}_{\text{in}} = E_P = 3200 \text{ V}$, $d = 1.6 \text{ mm}$, $a = 160 \text{ mm}$, and $R_S = 121 \text{ rayls}$, this gives a pressure of 4.31 Pa rms or 106.7 dB SPL with an input voltage of $2 \times 3200 \text{ V rms}$.

Although the high-frequency response appears to roll-off prematurely, in practice this can be compensated for by omitting some of the stray neutralizing capacitors.

Problem 15.1. A simple electrostatic loudspeaker with no delay or any kind of directivity control whatsoever has a diameter of 10 cm (i.e., radius of 5 cm). Assuming a maximum field strength of 2000 V/mm , calculate the maximum rms sound pressure in Pa and dB SPL re $20 \mu\text{Pa}$ at 1 m on-axis at 1 kHz . Assume that $1/2\tilde{e}_{\text{in}} = E_P$.

Hint: From Eq. (15.20), $p_{\text{rms}}(r, 0) = 2\pi f \epsilon_0 a^2 (E_P/d)^2 / (2\sqrt{2}rc)$ and use Eq. (1.18) to calculate the sound pressure level in dB SPL.

Problem 15.2. Suppose that the loudspeaker has a gap width of $d = 0.224 \text{ mm}$. Calculate the polarization voltage E_P minimum tension T needed for stability (from Eq. 15.86), resonance frequency f_0 , and specific resistance R_S needed for unity Q . Assuming the maximum membrane stress before breaking is 55 MPa , calculate the maximum allowable tension according to Eq. (15.113).

REFERENCES

- [1] Hunt FV. Electroacoustics. Chichester: John Wiley; 1954.
- [2] Walker PJ. Wide range electrostatic loudspeakers. Wireless World 1955;61(5,6,8):208–11. 265–269, 381–384.
- [3] Toole FE. Music, rooms and listeners: science in the creation and delivery of audio art. Acoust Today 2013;9(2):36–44. <http://acousticstoday.org/issues/2013AT/Apr2013/#?page=36>.
- [4] Linkwitz S. The Magic in 2-channel sound reproduction — why is it so rarely heard? Int J Archit Eng Technol 2015;2:113–26. <http://www.linkwitzlab.com/IJAETv2n2a2-Linkwitz-1.pdf>.
- [5] Watkinson J. We need to talk about speakers: sorry, ‘audiophiles’, only IT will break the sound barrier. The Register 07/02/2014. http://www.theregister.co.uk/2014/07/02/feature_the_future_loudspeaker_design/?page=1.
- [6] Borwick J. Loudspeaker and headphone handbook. 3rd ed. Oxford: Focal; 2001. p. 108–95.
- [7] Walker PJ. New developments in electrostatic loudspeakers. J Audio Eng Soc 1980;28(11):795–9.
- [8] Mellow TJ, Kärkkäinen LM. A dipole loudspeaker with a balanced directivity pattern. J Acoust Soc Am 2010;128(5):2749–57.
- [9] White DR, Bolser ST. Acoustic transparency of electrostatic loudspeaker assemblies. J Audio Eng Soc 2017;65(6):497–506.
- [10] Mellow TJ, Kärkkäinen LM. On the sound field of a circular membrane in free space and an infinite baffle. J Acoust Soc Am 2006;120(5):2460–77.



Frequency response shapes for loudspeakers [1]

In the following high-pass filter functions $G(s)$, the order of the function is denoted by N and the frequency at which the magnitude of the response is $1/\sqrt{2}$ (that is, 3 dB below the pass band level) is denoted by $\omega_{3\text{dB}}$.

Synchronous

$$G(s) = \left(\frac{s}{s + \omega_0} \right)^N$$

where

$$\omega_0 = \omega_{3\text{dB}} \sqrt{2^{1/N} - 1}$$

Bessel

The Bessel polynomials are generated from the following power series in s :

$$B_n(s) = \sum_{k=0}^n a_k s^k$$

where $s = j\omega$ and

$$a_k = \frac{(2n - k)!}{2^{n-k} k! (n - k)!}$$

Also, we define a frequency scaling factor γ such that

$$|B_n(j\gamma)| = a_0 \sqrt{2} = \frac{2n!}{2^{n-1/2} n!}$$

Bessel polynomials

First order: $B_1(s) = s + 1$

Second order: $B_2(s) = s^2 + 3s + 3$

Third order: $B_3(s) = s^3 + 6s^2 + 15s + 15$

Fourth order: $B_4(s) = s^4 + 10s^3 + 45s^2 + 105s + 105$

Fifth order: $B_5(s) = s^5 + 15s^4 + 105s^3 + 420s^2 + 945s + 945$

Sixth order: $B_6(s) = s^6 + 21s^5 + 210s^4 + 1260s^3 + 4725s^2 + 10,395s + 10,395$

If the real parts of the roots or poles are $\alpha_1, \alpha_2, \dots, \alpha_N$ and the imaginary parts of the roots or poles are $\beta_1, \beta_2, \dots, \beta_N$, then

$$\omega_n = \frac{\gamma}{\sqrt{\alpha_n^2 + \beta_n^2}}$$

$$Q_n = \frac{\sqrt{\alpha_n^2 + \beta_n^2}}{2\alpha_n}$$

Odd order

$$G(s) = \frac{s^N}{\left(s^2 + \frac{\omega_1}{Q_1}s + \omega_1^2\right)\left(s^2 + \frac{\omega_2}{Q_2}s + \omega_2^2\right)\cdots\left(s^2 + \frac{\omega_{(N-1)/2}}{Q_{(N-1)/2}}s + \omega_{(N-1)/2}^2\right)(s + \omega_{(N+1)/2})}$$

Even order

$$G(s) = \frac{s^N}{\left(s^2 + \frac{\omega_1}{Q_1}s + \omega_1^2\right)\left(s^2 + \frac{\omega_2}{Q_2}s + \omega_2^2\right)\cdots\left(s^2 + \frac{\omega_{N/2}}{Q_{N/2}}s + \omega_{N/2}^2\right)}$$

Butterworth

Odd order

$$G(s) = \frac{s^N}{\left(s^2 + \frac{\omega_{3dB}}{Q_1}s + \omega_{3dB}^2\right)\left(s^2 + \frac{\omega_{3dB}}{Q_2}s + \omega_{3dB}^2\right)\cdots\left(s^2 + \frac{\omega_{3dB}}{Q_{(N-1)/2}}s + \omega_{3dB}^2\right)(s + \omega_{3dB})}$$

The poles lie on a circle of radius ω_{3dB} , each at an angle of θ_n to the real axis, where

$$Q_n = \frac{1}{2 \cos \theta_n}$$

and

$$\theta_n = \pm \frac{n}{N} \pi, \quad n = 1, 2, \dots, (N-1)/2$$

Even order

$$G(s) = \frac{s^N}{\left(s^2 + \frac{\omega_{3dB}}{Q_1}s + \omega_{3dB}^2\right) \left(s^2 + \frac{\omega_{3dB}}{Q_2}s + \omega_{3dB}^2\right) \cdots \left(s^2 + \frac{\omega_{3dB}}{Q_{N/2}}s + \omega_{3dB}^2\right)}$$

where

$$\theta_n = \pm \frac{n-1}{2N} \pi, \quad n = 1, 2, \dots, N/2$$

Chebyshev

Chebyshev polynomials

First order: $C_1(\Omega) = \Omega$

Second order: $C_2(\Omega) = 2\Omega^2 - 1$

Third order: $C_3(\Omega) = 4\Omega^3 - 3\Omega$

Fourth order: $C_4(\Omega) = 8\Omega^4 - 8\Omega^2 + 1$

Fifth order: $C_5(\Omega) = 16\Omega^5 - 20\Omega^3 + 5\Omega$

Sixth order: $C_6(\Omega) = 32\Omega^6 - 48\Omega^4 + 18\Omega^2 - 1$

where

$$\Omega = \frac{\omega}{\omega_p}$$

and ω_p is the pass-band limit, which is defined as the frequency at which the final 0 dB crossing occurs before roll-off. Let R be the maximum permitted magnitude of the pass-band ripples in dB. Thus we define a ripple factor by

$$\varepsilon = \sqrt{10^{0.1R} - 1}$$

Also, we define a frequency scaling factor γ by

$$\gamma = \frac{\omega_{3dB}}{\omega_p} = \cosh\left(\frac{1}{N} \operatorname{arccosh}\left(\frac{1}{\epsilon}\right)\right)$$

and then find the roots of the polynomial

$$1 + \epsilon^2 C_N^2$$

so that the imaginary parts of the roots $\alpha_1, \alpha_2, \dots, \alpha_N$ give the real parts of the poles and the real parts of the roots $\beta_1, \beta_2, \dots, \beta_N$ give the imaginary parts of the poles. Then

$$\omega_n = \frac{\gamma}{\sqrt{\alpha_n^2 + \beta_n^2}}$$

$$Q_n = \frac{\sqrt{\alpha_n^2 + \beta_n^2}}{2\alpha_n}$$

Odd order

$$G(s) = \frac{s^N}{\left(s^2 + \frac{\omega_1}{Q_1}s + \omega_1^2\right)\left(s^2 + \frac{\omega_2}{Q_2}s + \omega_2^2\right)\cdots\left(s^2 + \frac{\omega_{(N-1)/2}}{Q_{(N-1)/2}}s + \omega_{(N-1)/2}^2\right)\left(s + \omega_{(N-1)/2}\right)}$$

Even order

$$G(s) = \frac{s^N}{\left(s^2 + \frac{\omega_1}{Q_1}s + \omega_1^2\right)\left(s^2 + \frac{\omega_2}{Q_2}s + \omega_2^2\right)\cdots\left(s^2 + \frac{\omega_{N/2}}{Q_{N/2}}s + \omega_{N/2}^2\right)}$$

REFERENCE

- [1] Zverev AI. Handbook of filter synthesis. New Jersey: Wiley; 1967.



Mathematical formulas [1,2]

In the following formulas, m and n are integers, and μ and ν can have any value.

Binomial theorem

$$(1 \pm x)^n = \sum_{m=0}^n (\pm 1)^m \binom{n}{m} x^m = \sum_{m=0}^n \frac{(\pm 1)^m n!}{m!(n-m)!} x^m, \text{ any } x, n \text{ positive integer} \quad (\text{A2.1})$$

$$(1 \pm x)^\nu = \sum_{m=0}^{\infty} \frac{(\pm 1)^m \Gamma(\nu + 1)}{m! \Gamma(\nu - m + 1)} x^m, 0 \leq |x| < 1, \nu \neq -1, -2, -3, \dots \quad (\text{A2.2})$$

$$(1 \pm x)^{-1} = \sum_{m=0}^{\infty} (\mp 1)^m x^m, 0 \leq |x| < 1 \quad (\text{A2.3})$$

$$(1 \pm x)^{-2} = \sum_{m=0}^{\infty} (\mp 1)^m (m+1) x^m, 0 \leq |x| < 1 \quad (\text{A2.4})$$

$$\frac{1}{\sqrt{1-x^2}} = \sum_{m=0}^{\infty} \frac{(2m)!}{(m!)^2} \left(\frac{x}{2}\right)^{2m}, 0 \leq |x| < 1 \quad (\text{A2.5})$$

Gamma function

$$\Gamma(n) = n!/n = (n-1)! \quad (\text{A2.6})$$

$$\Gamma(n+1) = n\Gamma(n) = n! \quad (\text{A2.7})$$

$$\Gamma(\nu+1) = \int_0^{\infty} x^\nu e^{-x} dx \quad (\text{A2.8})$$

$$\Gamma(1/2) = \sqrt{\pi} \quad (\text{A2.9})$$

$$\Gamma(n + 1/2) = \frac{\sqrt{\pi}\Gamma(2n)}{2^{2n-1}\Gamma(n)} = \frac{\sqrt{\pi}(2n)!}{2^{2n}n!} \quad (\text{A2.10})$$

$$\Gamma(-n + 1/2) = \frac{(-1)^n \pi}{\Gamma(n + 1/2)} = \frac{(-1)^n \sqrt{\pi} 2^{2n-1} \Gamma(n)}{\Gamma(2n)} = \frac{(-1)^n \sqrt{\pi} 2^{2n} n!}{(2n)!} \quad (\text{A2.11})$$

$$\frac{\Gamma(m - \nu)}{\Gamma(-\nu)} = \frac{(-1)^m \Gamma(\nu + 1)}{\Gamma(\nu - m + 1)} \quad (\text{A2.11a})$$

$$\frac{\Gamma(-\nu)}{\Gamma(-\nu - m)} = \frac{(-1)^m \Gamma(\nu + m + 1)}{\Gamma(\nu + 1)} \quad (\text{A2.11b})$$

Pochhammer symbol

$$(\mu)_\nu = \frac{\Gamma(\mu + \nu)}{\Gamma(\mu)} \quad (\text{A2.12})$$

Hyperbolic formulas

$$e^x = \sum_{k=0}^{\infty} \frac{x^k}{k!} \quad (\text{A2.13})$$

$$e^{-x} = \sum_{k=0}^{\infty} \frac{(-1)^k x^k}{k!} \quad (\text{A2.14})$$

$$e^x = \cosh x + \sinh x \quad (\text{A2.15})$$

$$e^{-x} = \cosh x - \sinh x \quad (\text{A2.16})$$

$$\cosh x = \frac{e^x + e^{-x}}{2} \quad (\text{A2.17})$$

$$\sinh x = \frac{e^x - e^{-x}}{2} \quad (\text{A2.18})$$

$$\cosh jx = \cos x \quad (\text{A2.19})$$

$$\sinh jx = j \sin x \quad (\text{A2.20})$$

$$\operatorname{sech} x = \frac{1}{\cosh x} \quad (\text{A2.21})$$

$$\operatorname{cosech} x = \frac{1}{\sinh x} \quad (\text{A2.22})$$

$$\tanh x = \frac{\sinh x}{\cosh x} \quad (\text{A2.23})$$

$$\coth x = \frac{\cosh x}{\sinh x} \quad (\text{A2.24})$$

$$\cosh^2 x - \sinh^2 x = 1 \quad (\text{A2.25})$$

$$\cosh^2 x + \sinh^2 y = \cosh(x + y) \cosh(x - y) \quad (\text{A2.26})$$

$$\cosh(x \pm jy) = \cosh x \cosh jy \pm \sinh x \sinh jy = \cosh x \cos y \pm j \sinh x \sin y \quad (\text{A2.27})$$

$$\sinh(x \pm jy) = \sinh x \cosh jy \pm \cosh x \sinh jy = \sinh x \cos y \pm j \cosh x \sin y \quad (\text{A2.28})$$

$$\cosh^2 x = \frac{1 + \cosh 2x}{2} \quad (\text{A2.29})$$

$$\sinh^2 x = \frac{\cosh 2x - 1}{2} \quad (\text{A2.30})$$

$$\frac{d}{dx} \cosh x = \sinh x \quad (\text{A2.31})$$

$$\frac{d}{dx} \sinh x = \cosh x \quad (\text{A2.32})$$

Trigonometric formulas

Definitions

$$e^{\pm jx} = \sum_{k=0}^{\infty} \frac{(\pm jx)^k}{k!} \quad (\text{A2.33})$$

$$e^{jx} = \cos x + j \sin x \quad (\text{A2.34})$$

$$e^{-jx} = \cos x - j \sin x \quad (\text{A2.35})$$

$$\cos x = \frac{e^{jx} + e^{-jx}}{2} \quad (\text{A2.36})$$

$$\sin x = \frac{e^{jx} - e^{-jx}}{2} \quad (\text{A2.37})$$

$$\cos jx = \cosh x \quad (\text{A2.38})$$

$$\sin jx = j \sinh x \quad (\text{A2.39})$$

$$\sec x = \frac{1}{\cos x} \quad (\text{A2.40})$$

$$\operatorname{cosec} x = \frac{1}{\sin x} \quad (\text{A2.41})$$

$$\tan x = \frac{\sin x}{\cos x} = \sum_{k=0}^{\infty} \frac{2x}{\left(k + \frac{1}{2}\right)^2 \pi^2 - x^2} \quad (\text{A2.42})$$

$$\cot x = \frac{\cos x}{\sin x} = \sum_{k=0}^{\infty} \frac{(2 - \delta_{0k})x}{x^2 - k^2 \pi^2} \quad (\text{A2.43})$$

$$\operatorname{csc} x = \frac{1}{\sin x} = \sum_{n=0}^{\infty} \frac{(2 - \delta_{0n})(-1)^n x}{x^2 - n^2 \pi^2} \quad (\text{A2.43a})$$

Formulas

$$\cos^2 x + \sin^2 x = 1 \quad (\text{A2.44})$$

$$\cos^2 x - \sin^2 y = \cos(x + y) \cos(x - y) \quad (\text{A2.45})$$

$$\cos(x \pm y) = \cos x \cos y \mp \sin x \sin y \quad (\text{A2.46})$$

$$\sin(x \pm y) = \sin x \cos y \pm \cos x \sin y \quad (\text{A2.47})$$

$$\tan(x \pm y) = \frac{\tan x \pm \tan y}{1 \mp \tan x \tan y} \quad (\text{A2.48})$$

$$\cos^2 x = \frac{1 + \cos 2x}{2} \quad (\text{A2.49})$$

$$\sin^2 x = \frac{1 - \cos 2x}{2} \quad (\text{A2.50})$$

$$\sin nx = \sin x \sum_{k=\frac{1-n}{2}}^{\frac{n-1}{2}} \cos(2kx) \quad (\text{A2.51})$$

$$\arctan x - \arctan y = \arctan\left(\frac{x - y}{1 + xy}\right) \quad (\text{A2.52})$$

$$\arctan x + \arctan y = \arctan\left(\frac{x + y}{1 - xy}\right) \quad (\text{A2.53})$$

Derivatives

$$\frac{d}{dx} \cos x = -\sin x \quad (\text{A2.54})$$

$$\frac{d}{dx} \sin x = \cos x \quad (\text{A2.55})$$

Integrals

$$\int_0^{2\pi} \cos(m\phi) \cos(n\phi) d\phi = \begin{cases} 0, & m \neq n \\ (1 + \delta_{n0})\pi, & m = n \end{cases} \quad (\text{A2.56})$$

$$\int_0^{2\pi} \sin(m\phi) \sin(n\phi) d\phi = \begin{cases} 0, & m \neq n \\ (1 - \delta_{n0})\pi, & m = n, \end{cases} \quad (\text{A2.57})$$

Oblique-angled triangle (Fig. AII.1)

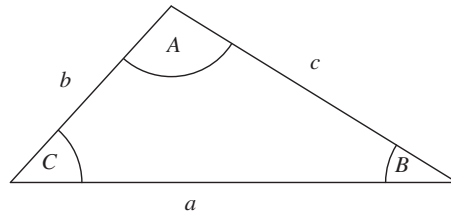


FIG. AII.1 Oblique-angled triangle.

$$a^2 = b^2 + c^2 - 2bc \cos A \quad (\text{A2.58})$$

$$b^2 = a^2 + c^2 - 2ac \cos B \quad (\text{A2.59})$$

$$c^2 = a^2 + b^2 - 2ab \cos C \quad (\text{A2.60})$$

Legendre functions

Definitions

$$P_n(z) = \frac{(-1)^n}{2^n n!} \frac{d^n}{dz^n} (1 - z^2)^n \quad \text{Rodrigues' formula} \quad (\text{A2.61})$$

$$P_n(z) = \frac{1}{2^n} \sum_{k=0}^{\lfloor \frac{n}{2} \rfloor} \frac{(-1)^k (2n - 2k)!}{k! (n - k)! (n - 2k)!} z^{n-2k} \quad (\text{A2.62})$$

$$P_\nu^m(z) = (-1)^m (1 - z^2)^{m/2} \frac{d^m}{dz^m} P_\nu(z) \quad (\text{A2.63})$$

Recursion formulas

$$(n+1)P_{n+1}(z) + nP_{n-1}(z) = (2n+1)zP_n(z) \quad (\text{A2.64})$$

$$n(n+1)(P_{n+1}(z) - P_{n-1}(z)) = (2n+1)(z^2 - 1) \frac{d}{dz} P_n(z) \quad (\text{A2.65})$$

Integrals

$$\int_0^\pi P_m(\cos \theta) P_n(\cos \theta) \sin \theta \, d\theta = \frac{2\delta_{mn}}{2n+1} \quad (\text{A2.66})$$

$$\int_0^\delta P_m(\cos \theta) \sin \theta \, d\theta = \frac{\delta^2}{2}, \delta \rightarrow 0 \quad (\text{A2.67})$$

$$\int_0^\alpha P_n(\cos \theta) \cos \theta \sin \theta \, d\theta = \begin{cases} (\sin^2 \alpha)/2, & n = 0 \\ (1 - \cos^3 \alpha)/3, & n = 1 \\ -\sin^2 \alpha \frac{P_n(\cos \alpha) + \cot \alpha P_n^1(\cos \alpha)}{(n-1)(n+2)}, & n \geq 2 \end{cases} \quad (\text{A2.68})$$

$$\int_0^\alpha P_n(\cos \theta) \sin \theta \, d\theta = \sin \alpha P_n^{-1}(\cos \alpha) \quad (\text{A2.69})$$

$$\int_\alpha^\alpha P_n(\cos \theta) P_m(\cos \theta) \sin \theta \, d\theta = \begin{cases} \frac{\sin \alpha (P_m(\cos \alpha) P_n'(\cos \alpha) - P_n(\cos \alpha) P_m'(\cos \alpha))}{m(m+1) - n(n+1)}, & m \neq n \\ \frac{1 + (P_m(\cos \alpha))^2 \cos \alpha + 2 \sum_{j=1}^{m-1} P_j(\cos \alpha) (P_j(\cos \alpha) \cos \alpha - P_{j+1}(\cos \alpha))}{2m+1}, & m = n \end{cases} \quad (\text{A2.70})$$

Bessel functions

Definitions

$$J_\nu(z) = \left(\frac{z}{2}\right)^\nu \sum_{m=0}^{\infty} \frac{(-1)^m}{m!(m+\nu)!} \left(\frac{z}{2}\right)^{2m}, \text{ Bessel function} \quad (\text{A2.71})$$

$$Y_\nu(z) = \frac{\cos \nu\pi J_\nu(z) - J_{-\nu}(z)}{\sin \nu\pi}, \text{ Neumann function} \quad (\text{A2.72})$$

$$Y_n(z) = \frac{2}{\pi} \ln\left(\frac{z}{2}\right) J_n(z) - \frac{1}{\pi} \sum_{k=0}^{n-1} \frac{(m-k-1)!}{k!} \left(\frac{z}{2}\right)^{2k-n} \quad (\text{A2.73})$$

$$\frac{-1}{\pi} \sum_{k=0}^{\infty} \frac{(-1)^k (\psi(k+1) + \psi(k+n+1))}{k!(k+n)!} \left(\frac{z}{2}\right)^{2k+n}$$

$$H_\nu^{(1)}(z) = J_\nu(z) + jY_\nu(z), \text{ Hankel function} \quad (\text{A2.74})$$

$$H_\nu^{(2)}(z) = J_\nu(z) - jY_\nu(z), \text{ Hankel function} \quad (\text{A2.75})$$

Integral representations

$$J_n(z) = \frac{1}{2\pi} \int_0^{2\pi} e^{j(z \sin \phi - n\phi)} d\phi \quad (\text{A2.76})$$

$$J_n(z) = \frac{1}{2\pi} \int_0^{2\pi} \cos(z \sin \phi - n\phi) d\phi \quad (\text{A2.77})$$

$$J_\nu(z) = \frac{2}{\Gamma\left(\nu + \frac{1}{2}\right)\Gamma\left(\frac{1}{2}\right)} \left(\frac{z}{2}\right)^\nu \int_0^{\pi/2} (\sin \phi)^{2\nu} \cos(z \cos \phi) d\phi \quad (\text{A2.78})$$

Relations

$$J_{-n}(z) = (-1)^n J_n(z) \quad (\text{A2.79})$$

$$Y_{-n}(z) = (-1)^n Y_n(z) \quad (\text{A2.80})$$

$$Y_{-n-\frac{1}{2}}(z) = (-1)^n J_{n+\frac{1}{2}}(z) \quad (\text{A2.81})$$

$$Y_{n+\frac{1}{2}}(z) = (-1)^{n-1} J_{-n-\frac{1}{2}}(z) \quad (\text{A2.82})$$

Recursion formulas

$$Z_{\nu-1}(az) + Z_{\nu+1}(az) = \frac{2\nu}{az} Z_\nu(az) \quad (\text{A2.83})$$

$$Z_{\nu-1}(az) - Z_{\nu+1}(az) = \frac{2}{a} \cdot \frac{d}{dz} Z_\nu(az) \quad (\text{A2.84})$$

where Z can represent J , Y , $H^{(1)}$, or $H^{(2)}$.

Limiting forms for small arguments

$$J_\nu(z)|_{z \rightarrow 0} = \frac{1}{\Gamma(\nu+1)} \left(\frac{z}{2}\right)^\nu, \quad \nu \neq -1, -2, -3, \dots \quad (\text{A2.85})$$

$$Y_0(z)|_{z \rightarrow 0} = \frac{2}{\pi} \ln z \quad (\text{A2.86})$$

$$Y_\nu(z)|_{z \rightarrow 0} = \frac{\Gamma(\nu)}{\pi} \left(\frac{z}{2}\right)^\nu, \quad \nu \neq 0 \quad (\text{A2.87})$$

Forms for large arguments

$$J_\nu(z) = \sqrt{\frac{2}{\pi z}} \left[\cos\left(z - \nu\frac{\pi}{2} - \frac{\pi}{4}\right) \sum_{k=0}^{\infty} \frac{(-1)^{k+\nu} \Gamma\left(2k - \nu + \frac{1}{2}\right) \Gamma\left(2k + \nu + \frac{1}{2}\right)}{\pi(2k)!(2z)^{2k}} \right. \\ \left. - \sin\left(z - \nu\frac{\pi}{2} - \frac{\pi}{4}\right) \sum_{k=1}^{\infty} \frac{(-1)^{k+\nu} \Gamma\left(2k - \nu - \frac{1}{2}\right) \Gamma\left(2k + \nu - \frac{1}{2}\right)}{\pi(2k-1)!(2z)^{2k-1}} \right] \quad (\text{A2.88})$$

$$Y_\nu(z) = \sqrt{\frac{2}{\pi z}} \left[\sin\left(z - \nu\frac{\pi}{2} - \frac{\pi}{4}\right) \sum_{k=0}^{\infty} \frac{(-1)^{k+\nu} \Gamma\left(2k - \nu + \frac{1}{2}\right) \Gamma\left(2k + \nu + \frac{1}{2}\right)}{\pi(2k)!(2z)^{2k}} \right. \\ \left. + \cos\left(z - \nu\frac{\pi}{2} - \frac{\pi}{4}\right) \sum_{k=1}^{\infty} \frac{(-1)^{k+\nu} \Gamma\left(2k - \nu - \frac{1}{2}\right) \Gamma\left(2k + \nu - \frac{1}{2}\right)}{\pi(2k-1)!(2z)^{2k-1}} \right] \quad (\text{A2.89})$$

Asymptotic forms for very large arguments

$$J_\nu(z)|_{z \rightarrow \infty} = \sqrt{\frac{2}{\pi z}} \cos\left(z - \nu\frac{\pi}{2} - \frac{\pi}{4}\right) \quad (\text{A2.90})$$

$$Y_\nu(z)|_{z \rightarrow \infty} = \sqrt{\frac{2}{\pi z}} \sin\left(z - \nu\frac{\pi}{2} - \frac{\pi}{4}\right) \quad (\text{A2.91})$$

$$H_\nu^{(1)}(z)|_{z \rightarrow \infty} = \sqrt{\frac{2}{\pi z}} e^{j\left(z - \nu\frac{\pi}{2} - \frac{\pi}{4}\right)} \quad (\text{A2.92})$$

$$H_\nu^{(2)}(z)|_{z \rightarrow \infty} = \sqrt{\frac{2}{\pi z}} e^{-j\left(z - \nu\frac{\pi}{2} - \frac{\pi}{4}\right)} \quad (\text{A2.93})$$

Integrals

$$\int_0^a J_0(bx) dx = a \left\{ J_0(ab) + \frac{\pi}{2} (J_1(ab) \mathbf{H}_0(ab) - J_0(ab) \mathbf{H}_1(ab)) \right\} \quad (\text{A2.94})$$

$$\int_0^a J_0(bx) x dx = \frac{a}{b} J_1(ab) \quad (\text{A2.95})$$

$$\int_0^a \left(1 - \frac{x^2}{a^2}\right)^{\mu + \frac{1}{2}} J_0(bx) x dx = \frac{a^2}{2} \Gamma\left(\mu + \frac{3}{2}\right) \left(\frac{2}{ab}\right)^{\mu + \frac{3}{2}} J_{\mu + \frac{3}{2}}(ab), \text{ Sonine's Integral} \quad (\text{A2.96})$$

$$\int_0^\infty \left(\frac{x^2}{a^2} - 1\right)^{m + \frac{1}{2}} J_0(bx) x dx = \frac{a^2}{2} \Gamma\left(m + \frac{3}{2}\right) \left(\frac{2}{ab}\right)^{m + \frac{3}{2}} J_{-m - \frac{3}{2}}(ab), \text{ Pritchard's Integral} \quad (\text{A2.97})$$

$$\int_0^\infty \left(1 - \frac{x^2}{a^2}\right)^{m + \frac{1}{2}} J_0(bx) x dx = \frac{a^2}{2} \Gamma\left(m + \frac{3}{2}\right) \left(\frac{2}{ab}\right)^{m + \frac{3}{2}} H_{m + \frac{3}{2}}^{(2)}(ab) \quad (\text{A2.98})$$

$$\int_0^a \left(1 - \frac{x^2}{a^2}\right)^{\mu + \frac{1}{2}} J_\nu(bx) x dx = \sqrt{\pi} \frac{a^2}{2} \left(\frac{ab}{4}\right)^\nu \frac{\Gamma\left(\mu + \frac{3}{2}\right)}{\Gamma\left(\frac{\nu}{2} + \frac{1}{2}\right) \Gamma\left(\frac{\nu}{2} + \mu + \frac{5}{2}\right)} \quad (\text{A2.99})$$

$$\times {}_1F_2\left(\frac{\nu}{2} + 1; \frac{\nu}{2} + \mu + \frac{5}{2}, \nu + 1; -\frac{a^2 b^2}{4}\right)$$

$$\int_0^a \left(\frac{x}{a}\right)^\mu J_\nu(bx) x dx = \frac{a^2}{\nu + \mu + 2} \left(\frac{ab}{2}\right)^\nu \frac{1}{\Gamma(\nu + 1)} \times {}_1F_2\left(\frac{\nu}{2} + \frac{\mu}{2} + 1; \frac{\nu}{2} + \frac{\mu}{2} + 2, \nu + 1; -\frac{a^2 b^2}{4}\right) \quad (\text{A2.100})$$

$$\int_0^a J_k(\alpha_{km}x/a) J_k(\alpha_{kn}x/a) x dx = \begin{cases} 0, & \alpha_{km} \neq \alpha_{kn} \\ a^2 J_{k+1}^2(\alpha_{kn})/2 & \alpha_{km} = \alpha_{kn} \end{cases}, \quad J_k(\alpha_{kn}) \neq 0 \quad (\text{A2.101})$$

where

$$\alpha_{kn} \approx \left(\frac{k}{2} + n - \frac{1}{4}\right)\pi, \quad n \rightarrow \infty.$$

$$\int_0^a J_k(\beta_{km}x/a) J_k(\beta_{kn}x/a) x dx = \begin{cases} 0, & \beta_{km} \neq \beta_{kn} \\ a^2 \left(1 - \frac{k^2}{\beta_{kn}^2}\right) \frac{J_k^2(\beta_{kn})}{2}, & \beta_{km} = \beta_{kn} \end{cases}, \quad J'_k(\beta_{kn}) = 0 \quad (\text{A2.101a})$$

where

$$\beta_{kn} \approx \left(\frac{k}{2} + n + \frac{1}{4}\right)\pi, \quad n \rightarrow \infty.$$

$$\int_0^a J_k(\alpha_{km}x/a) J_k(\alpha_{kn}x/a) x dx = \begin{cases} a^2 \frac{\alpha_{km} J_k(\alpha_{kn}) J_{k+1}(\alpha_{km}) - \alpha_{kn} J_k(\alpha_{km}) J_{k+1}(\alpha_{kn})}{\alpha_{km}^2 - \alpha_{kn}^2}, & \alpha_{km} \neq \alpha_{kn} \\ a^2 \frac{J_k^2(\alpha_{kn}) - J_{k-1}(\alpha_{kn}) J_{k+1}(\alpha_{kn})}{2}, & \alpha_{km} = \alpha_{kn} \end{cases}, \quad J_k(\alpha_{kn}) \neq 0 \quad (\text{A2.102})$$

$$2 \int_0^1 \frac{J_1^2(zx)}{x\sqrt{1-x^2}} dx = 1 - \frac{J_1(2z)}{z} \quad (\text{A2.103})$$

$$2 \int_1^\infty \frac{J_1^2(zx)}{x\sqrt{1-x^2}} dx = \frac{\mathbf{H}_1(2z)}{z} \quad (\text{A2.104})$$

$$2 \int_0^1 \frac{J_1^2(zx)}{x} \sqrt{1-x^2} dx = {}_1F_2\left(\frac{1}{2}; \frac{3}{2}, 2; -z^2\right) \quad (\text{A2.105})$$

$$2 \int_1^\infty \frac{J_1^2(zx)}{x} \sqrt{1-x^2} dx = \frac{4}{\pi} \left\{ \frac{1}{z} + \frac{z}{3} {}_2F_3\left(1, 1; \frac{3}{2}, 2, \frac{5}{2}; -z^2\right) \right\} \quad (\text{A2.106})$$

$$\int_0^\infty J_m(ax)J_n(bx) \frac{x^\gamma}{\sqrt{k^2-x^2}} dx = \frac{j\sqrt{\pi}(-jk)^\gamma(-1)^{(p+1)/2}}{2n!} \left(\frac{b}{a}\right)^n \sum_{r=0}^\infty \left(\frac{-jka}{2}\right)^{r-\gamma} \\ \times \frac{\Gamma\left(\frac{r+1}{2}\right) {}_2F_1\left(\frac{p-r}{2}, \frac{q-r}{2}; n+1; \frac{b^2}{a^2}\right)}{\Gamma\left(\frac{r}{2}+1\right)\Gamma\left(\frac{r-p}{2}+1\right)\Gamma\left(\frac{r-q}{2}+1\right)}, \quad (\text{A2.106a})$$

for $-1 \leq \gamma \leq 3$, where $p = m + n + \gamma$ is a positive odd integer and $q = n - m + \gamma$.

$$\int_0^\infty J_m(ax)J_n(bx) \sqrt{k^2-x^2} x^\gamma dx = \frac{j\sqrt{\pi}(-jk)^\gamma(-1)^{(p+1)/2}}{a^2 n!} \left(\frac{b}{a}\right)^n \sum_{r=0}^\infty \left(\frac{-jka}{2}\right)^{r-\gamma} \\ \times \frac{\Gamma\left(\frac{r-1}{2} + \delta_{r,1}\right) {}_2F_1\left(\frac{p-r}{2} + 1, \frac{q-r}{2} + 1; n+1; \frac{b^2}{a^2}\right)}{\Gamma\left(\frac{r}{2}+1\right)\Gamma\left(\frac{r-p}{2}\right)\Gamma\left(\frac{r-q}{2}\right)} \quad (\text{A2.106b})$$

for $-1 \leq \gamma \leq 1$, where $p = m + n + \gamma$ is a positive odd integer and $q = n - m + \gamma$.

Expansions

$$J_0\left(z\sqrt{1+t^2}\right) = 2 \sum_{n=0}^{\infty} \frac{(-1)^n}{1+\delta_{n0}} J_{2n}(z) J_{2n}(zt), \text{ Gegenbauer summation theorem} \quad (\text{A2.107})$$

$$J_0\left(z\sqrt{1-t^2}\right) 2 \sum_{n=0}^{\infty} \frac{J_n(z)}{n!} \left(\frac{z}{2}\right)^n t^{2n}, \text{ Lommel addition theorem} \quad (\text{A2.108})$$

$$J_\nu(az) J_\mu(bz) = \frac{\left(\frac{1}{2}az\right)^\nu \left(\frac{1}{2}bz\right)^\mu}{\Gamma(\mu+1)} \sum_{n=0}^{\infty} \frac{(-1)^n \left(\frac{1}{2}az\right)^{2n}}{n! \Gamma(n+\nu+1)} {}_2F_1\left(-n, -n-\nu; \mu+1; \frac{b^2}{a^2}\right) \quad (\text{A2.109})$$

$$e^{\pm jx \cos \theta} = J_0(x) + \sum_{k=1}^{\infty} j^{\pm k} \cos(k\theta) J_k(x) \quad (\text{A2.110})$$

Wronskian

$$J_\nu(z) Y_{\nu+1}(z) - J_{\nu+1}(z) Y_\nu(z) = -\frac{2}{\pi z} \quad (\text{A2.111})$$

Hyperbolic Bessel functions

Definitions

$$I_\nu(z) = j^{-\nu} J_\nu(jz), \text{ Hyperbolic Bessel function} \quad (\text{A2.112})$$

$$I_\nu(z) = \left(\frac{z}{2}\right)^\nu \sum_{m=0}^{\infty} \frac{1}{m!(m+\nu)!} \left(\frac{z}{2}\right)^{2m} \quad (\text{A2.113})$$

$$K_\nu(z) = \frac{\pi}{2} j^{\nu+1} H_\nu^{(1)}(jz), \text{ Hyperbolic Neumann function} \quad (\text{A2.114})$$

$$K_\nu(z) = \frac{\pi}{2}(-j)^{\nu+1} H_\nu^{(2)}(-jz) \quad (\text{A2.115})$$

$$K_n(z) = (-1)^{n+1} \ln\left(\frac{z}{2}\right) I_n(z) + \frac{1}{2} \sum_{k=0}^{n-1} \frac{(-1)^k (n-k-1)!}{k!} \left(\frac{z}{2}\right)^{2k-n} \\ + \frac{(-1)^n}{2} \sum_{k=0}^{\infty} \frac{\psi(k+1) + \psi(k+n+1)}{k!(k+n)!} \left(\frac{z}{2}\right)^{2k+n} \quad (\text{A2.116})$$

Recursion formulas

$$I_{\nu-1}(z) - I_{\nu+1}(z) = \frac{2\nu}{z} I_\nu(z) \quad (\text{A2.117})$$

$$I_{\nu-1}(z) + I_{\nu+1}(z) = 2 \frac{d}{dz} I_\nu(z) \quad (\text{A2.118})$$

$$K_{\nu-1}(z) - K_{\nu+1}(z) = -\frac{2\nu}{z} K_\nu(z) \quad (\text{A2.119})$$

$$K_{\nu-1}(z) + K_{\nu+1}(z) = -2 \frac{d}{dz} K_\nu(z) \quad (\text{A2.120})$$

Limiting forms for small arguments

$$I_\nu(z)|_{z \rightarrow 0} = \frac{1}{\Gamma(\nu+1)} \left(\frac{z}{2}\right)^\nu, \quad \nu \neq -1, -2, -3, \dots \quad (\text{A2.121})$$

$$K_0(z)|_{z \rightarrow 0} = -\ln z \quad (\text{A2.122})$$

$$K_\nu(z)|_{z \rightarrow 0} = \frac{\Gamma(\nu)}{2} \left(\frac{2}{z}\right)^\nu \quad (\text{A2.123})$$

Wronskian

$$I_\nu(z)K_{\nu+1}(z) + I_{\nu+1}(z)K_\nu(z) = \frac{1}{z} \quad (\text{A2.124})$$

Struve function**Definitions**

$$\mathbf{H}_\nu(z) = \left(\frac{z}{2}\right)^{\nu+1} \sum_{m=0}^{\infty} \frac{(-1)^m}{\Gamma\left(m + \frac{3}{2}\right)\Gamma\left(m + \nu + \frac{3}{2}\right)} \left(\frac{z}{2}\right)^{2m}, \text{ Struve function} \quad (\text{A2.125})$$

Integral representation

$$\mathbf{H}_\nu(z) = \frac{2}{\Gamma\left(\nu + \frac{1}{2}\right)\Gamma\left(\frac{1}{2}\right)} \left(\frac{z}{2}\right)^\nu \int_0^{\frac{\pi}{2}} (\sin \phi)^{2\nu} \sin(z \cos \phi) d\phi \quad (\text{A2.126})$$

Recursion formulas

$$\mathbf{H}_{\nu-1}(z) + \mathbf{H}_{\nu+1}(z) = \frac{2\nu}{z} \mathbf{H}_\nu(z) + \frac{\left(\frac{1}{2}z\right)^\nu}{\sqrt{\pi}\Gamma\left(\nu + \frac{3}{2}\right)} \quad (\text{A2.127})$$

$$\mathbf{H}_{\nu-1}(z) - \mathbf{H}_{\nu+1}(z) = 2 \frac{d}{dz} \mathbf{H}_\nu(z) - \frac{\left(\frac{1}{2}z\right)^\nu}{\sqrt{\pi}\Gamma\left(\nu + \frac{3}{2}\right)} \quad (\text{A2.128})$$

Integrals

$$\int_0^a \mathbf{H}_0(bx) dx = a^2 \frac{b}{\pi} {}_2F_3\left(1, 1; \frac{3}{2}, \frac{3}{2}, 2; -\frac{a^2 b^2}{4}\right) \quad (\text{A2.129})$$

Spherical bessel functions

Definitions

$$j_n(z) = \frac{\sqrt{\pi}}{2z} J_{n+\frac{1}{2}}(z), \text{ Spherical Bessel function} \quad (\text{A2.130})$$

$$y_n(z) = \frac{\sqrt{\pi}}{2z} Y_{n+\frac{1}{2}}(z), \text{ Spherical Neumann function} \quad (\text{A2.131})$$

$$h_n^{(1)}(z) = j_n(z) + jy_n(z), \text{ Spherical Hankel function} \quad (\text{A2.132})$$

$$h_n^{(2)}(z) = j_n(z) - jy_n(z), \text{ Spherical Hankel function} \quad (\text{A2.133})$$

$$j_n(z) = (-1)^n z^n \left(\frac{1}{z} \frac{d}{dz}\right)^n \frac{\sin z}{z}, \text{ Rayleigh's formula} \quad (\text{A2.134})$$

$$y_n(z) = -(-1)^n z^n \left(\frac{1}{z} \frac{d}{dz}\right)^n \frac{\cos z}{z}, \text{ Rayleigh's formula} \quad (\text{A2.135})$$

$$j_0(z) = \frac{\sin z}{z} \quad (\text{A2.136})$$

$$j_1(z) = -z \frac{1}{z} \frac{d}{dz} \frac{\sin z}{z} = \frac{\sin z}{z^2} - \frac{\cos z}{z} \quad (\text{A2.137})$$

$$j_2(z) = z^2 \frac{1}{z} \frac{d}{dz} \left(\frac{1}{z} \frac{d}{dz} \frac{\sin z}{z}\right) = \left(\frac{3}{z^3} - \frac{1}{z}\right) \sin z - \frac{2}{z^2} \cos z \quad (\text{A2.138})$$

$$y_0(z) = -\frac{\cos z}{z} \quad (\text{A2.139})$$

$$y_1(z) = z \frac{1}{z} \frac{d}{dz} \frac{\cos z}{z} = -\frac{\cos z}{z^2} - \frac{\sin z}{z} \quad (\text{A2.140})$$

$$y_2(z) = -z^2 \frac{1}{z} \frac{d}{dz} \left(\frac{1}{z} \frac{d}{dz} \frac{\cos z}{z} \right) = \left(-\frac{3}{z^3} + \frac{1}{z} \right) \cos z - \frac{3}{z^2} \sin z \quad (\text{A2.141})$$

Recursion formulas

$$f_{n-1}(z) + f_{n+1}(z) = \frac{2n+1}{z} f_n(z) \quad (\text{A2.142})$$

$$n f_{n-1}(z) - (n+1) f_{n+1}(z) = (2n+1) \frac{d}{dz} f_n(z) \quad (\text{A2.143})$$

where f can represent j , y , $h^{(1)}$, or $h^{(2)}$.

Limiting forms for small arguments

$$j_\nu(z)|_{z \rightarrow 0} = \frac{\sqrt{\pi}}{2\Gamma\left(\nu + \frac{3}{2}\right)} \left(\frac{z}{2}\right)^\nu, \quad \nu \neq -1, -2, -3, \dots \quad (\text{A2.144})$$

$$y_\nu(z)|_{z \rightarrow 0} = -\frac{\Gamma\left(\nu + \frac{1}{2}\right)}{2\sqrt{\pi}} \left(\frac{2}{z}\right)^{\nu+1} \quad (\text{A2.145})$$

Asymptotic forms for large arguments

$$j_\nu(z)|_{z \rightarrow \infty} = \frac{\sin\left(z - \nu \frac{\pi}{2}\right)}{z} \quad (\text{A2.146})$$

$$y_\nu(z)|_{z \rightarrow \infty} = \frac{\cos\left(z - \nu \frac{\pi}{2}\right)}{z} \quad (\text{A2.147})$$

$$h_v^{(1)}(z)|_{z \rightarrow \infty} = -j \frac{e^{j\left(z - v\frac{\pi}{2}\right)}}{z} \quad (\text{A2.148})$$

$$h_v^{(2)}(z)|_{z \rightarrow \infty} = j \frac{e^{-j\left(z - v\frac{\pi}{2}\right)}}{z} \quad (\text{A2.149})$$

Hypergeometric function

$$\begin{aligned} {}_pF_q(a_1, a_2, \dots, a_p; b_1, b_2, \dots, b_q; z) &= \frac{\Gamma(b_1)\Gamma(b_2)\cdots(b_q)}{\Gamma(a_1)\Gamma(a_2)\cdots(a_p)} \\ &\times \sum_{n=0}^{\infty} \frac{\Gamma(n+a_1)\Gamma(n+a_2)\cdots(n+a_p)}{\Gamma(n+b_1)\Gamma(n+b_2)\cdots(n+b_q)} \frac{z^n}{n!} \end{aligned} \quad (\text{A2.150})$$

Dirac delta function

$$\delta(z-a) = \begin{cases} 0, & z \neq a \\ \text{Indeterminate,} & z = a \end{cases} \quad (\text{A2.151})$$

$$\delta(z) = \left. \frac{e^{-z^2/a^2}}{a\sqrt{\pi}} \right|_{a \rightarrow 0} \quad (\text{A2.152})$$

$$\int_{-\infty}^{\infty} \delta(z) dz = 1 \quad (\text{A2.153})$$

$$\int_{-\infty}^{\infty} F(z)\delta(z-a) dz = F(a) \quad (\text{A2.154})$$

Miscellaneous functions

$$\delta_{mn} \begin{cases} 0, & m \neq n \\ 1, & m = n \end{cases}, \text{ Kronecker delta function} \quad (\text{A2.155})$$

$$(\mu)_\nu = \frac{\Gamma(\mu + \nu)}{\Gamma(\mu)}, \text{ Pochhammer symbol} \quad (\text{A2.156})$$

REFERENCES

- [1] Gradshteyn IS, Ryzhik IM. In: Jeffrey A, editor. Table of integrals, series, and products. 6th ed. New York: Academic; 2000.
- [2] Watson GN. A treatise on the theory of bessel functions. 2nd ed. London: Cambridge University Press; 1944.



Answers to problems

Problem 2.1.

From Eq. (2.112), we see that the eigenfrequencies of the pan flute are in multiples of $2n + 1$. In other words, they are in *odd* multiples, and the even ones are missing. The fundamental resonance frequency is given by $f = c/(4l) = 345/(4 \times 0.294) = 293$ Hz.

From Eq. (2.94), we see that the eigenfrequencies of the pan flute are in multiples of n . In other words, they are in *odd* and *even* multiples. The fundamental resonance frequency is given by $f = c/(2l) = 345/(2 \times 0.294) = 587$ Hz.

Problem 2.2.

In the steady state, the *homogenous* wave equation in cylindrical coordinates from Eq. (2.23) becomes

$$\left(\frac{\partial^2}{\partial w^2} + \frac{1}{w} \cdot \frac{\partial}{\partial w} + k^2 \right) \tilde{p}(w) = 0.$$

Although a solution is given by Eqs. (2.125) and (2.126), we omit the Y_0 function because of continuity at the center so that the solution becomes

$$\tilde{p}(w) = \tilde{p}_- J_0(kw),$$

where the J_0 function is analogous to the cosine function in the case of a closed tube and satisfies the boundary condition at the center

$$\frac{\partial}{\partial w} \tilde{p}(w) \Big|_{w=0} = 0.$$

At the cylinder wall, where $w = a$, we have

$$\frac{1}{-jk\rho_0 c} \cdot \frac{\partial}{\partial w} \tilde{p}(w) \Big|_{w=a} = -\tilde{u}_0,$$

which leads to

$$\tilde{p}_- = \frac{j\rho_0 c \tilde{u}_0}{J_1(ka)}.$$

Hence,

$$\tilde{p}(w) = j\rho_0 c \tilde{u}_0 \frac{J_0(kw)}{J_1(ka)}. \quad (\text{A3.1})$$

Next, we shall rewrite the *inhomogeneous* Eqs. (2.80) and (2.81) in cylindrical coordinates using the Laplace operator of Eq. (2.23)

$$\begin{aligned} \left(\frac{\partial^2}{\partial w^2} + \frac{1}{w} \frac{\partial}{\partial w} + k^2 \right) \tilde{p}(w) &= -\delta(w-a) \frac{\partial}{\partial w} \tilde{p}(w) \Big|_{x=a} \\ &= jk\rho_0 c \delta(w-a) \tilde{u}_0, \end{aligned} \quad (\text{A3.2})$$

which includes the sound source at $w = a$ on the right-hand side, where δ is the Dirac delta function. Let the solution be in the form of an *eigenfunction* expansion

$$\tilde{p}(w) = \sum_{n=0}^{\infty} \tilde{A}_n J_0(\beta_n w/a), \quad (\text{A3.3})$$

where β_n is the solution to

$$J_1(\beta_n) = 0.$$

When the wall is stationary, this satisfies the boundary conditions

$$\frac{\partial}{\partial w} \tilde{p}(w) \Big|_{w=0} = 0, \quad \frac{\partial}{\partial w} \tilde{p}(w) \Big|_{w=a} = 0.$$

Inserting Eq. (A3.3) into Eq. (A3.2) and multiplying both sides by $J_0(\beta_m w/a)$ while integrating over the radius of the cylinder gives

$$\begin{aligned} \sum_{n=0}^{\infty} \tilde{A}_n \left(k^2 - \frac{\beta_n^2}{a^2} \right) \int_0^a J_0(\beta_m w/a) J_0(\beta_n w/a) w dw \\ = jk\rho_0 c \tilde{u}_0 \int_0^a J_0(\beta_m w/a) \delta(w-a) w dw. \end{aligned}$$

The two integrals have the following identities:

$$\int_0^a J_0(\beta_m w/a) J_0(\beta_n w/a) w dw = \begin{cases} 0, & m \neq n \\ a^2 J_0^2(\beta_n)/2, & m = n \end{cases}$$

$$\int_0^a J_0(\beta_m w/a) \delta(w-a) w dw = a J_0(\beta_m).$$

The first is the property of *orthogonality* from Eq. (A2.101a) of Appendix II, and the second is a property of the Dirac delta function from Eq. (A2.154) of Appendix II. Hence, $J_0(\beta_m w/a)$ in this case is the *orthogonal* (or *normalizing*) function and we can eliminate the summation to yield

$$\tilde{A}_n = \frac{2jk a \rho_0 c \tilde{u}_0}{(k^2 a^2 - \beta_n^2) J_0(\beta_n)}$$

so that the solution of Eq. (2), given by Eq. (3), becomes

$$\tilde{p}(w) = 2jka\rho_0\tilde{c}u_0 \sum_{n=0}^{\infty} \frac{J_0(\beta_n w/a)}{(k^2 a^2 - \beta_n^2)J_0(\beta_n)}. \quad (\text{A3.4})$$

By comparing the pressures given by Eqs. (A3.1) and (A3.4) at $w = a$, we obtain

$$\frac{J_0(ka)}{J_1(ka)} = \sum_{n=0}^{\infty} \frac{2ka}{k^2 a^2 - \beta_n^2}.$$

Hence,

$$Q(x) = \frac{2J_1(x)}{xJ_0(x)} = \left(\sum_{n=0}^{\infty} \frac{x^2}{x^2 - \beta_n^2} \right)^{-1}.$$

For large n , we can substitute $\beta_n \approx (n + 1/4)\pi$, $n \rightarrow \infty$.

Problem 7.1.

From Eq. (6.10), we obtain $Q_{TS} = 0.46 \times 7.58 / (0.46 + 7.58) = 0.43$. This is within 7% of the Q_{TS} value in Table 7.4 required for a 0.01 dB Chebyshev alignment. Multiplying the V_{AB}/V_{AS} figure from the table by V_{AS} of the drive unit gives the box volume $V_{AB} = 1.5511 \times 19.5 = 30.3$ L. Also, from the table, we see that the required port resonance frequency is $f_B = f_B/f_S \times f_S = 0.8838 \times 50 = 44.2$ Hz. From the ‘‘Summary of bass-reflex design’’ on p. 334, we obtain the maximum peak pressure

$$p_{\max} = 2\sqrt{2} \times 10^{\left(\frac{\text{SPL}_{\max}}{20} - 5\right)} = 2.83 \text{ Pa}$$

and the maximum volume displacement require to produce that pressure

$$V_{\max} = \frac{rp_{\max}}{2\pi f_B^2 \rho_0} = \frac{1 \times 2.83}{2 \times 3.14 \times 44.2^2 \times 1.18} = 195 \text{ cm}^3.$$

We let the port volume be $V_P = 10V_{\max} = 1.95$ L. The approximate tube length t is given by Eq. (7.97)

$$t \approx \frac{c}{\omega_B} \sqrt{\frac{V_P}{V_{AB}}} = \frac{345}{2 \times 3.14 \times 44.2} \sqrt{\frac{1.95}{30.3}} = 31.5 \text{ cm}$$

where the cross-sectional area of the tube from Eq. (7.96) is $S_P = V_P/t = 1.96 \times 10^{-3} / 0.315 = 62.2 \text{ cm}^2$ and the diameter is $d_P = 2\sqrt{S_P/\pi} = 8.9 \text{ cm}$. If we use a 9 cm diameter tube with a cross-sectional area $S_P = \frac{1}{4}\pi \times 9^2 = 63.6 \text{ cm}^2$, the exact length is given by Eq. (7.98)

$$\begin{aligned} t &= \frac{S_P c^2}{V_{AB} \omega_B^2} - 0.84\sqrt{S_P} = \frac{63.6 \times 10^{-4} \times 345^2}{30.3 \times 10^{-3} \times (2 \times 3.14 \times 44.2)^2} - 0.84\sqrt{63.6 \times 10^{-4}} \\ &= 25.7 \text{ cm.} \end{aligned}$$

Also, from Table 7.4, we see that the cutoff frequency is $f_{3dB} = f_{3dB}/f_S \times f_S = 0.8143 \times 50 = 40.7$ Hz.

Problem 10.1.

The total volume is simply $V = 12.5 \times 10 \times 8 = 1000$ m³ and, from the table, the total absorptive area is $S_{tot} = 100 + 125 + 32 = 257$ m². The average Sabine absorption coefficient α_{tot} is given by Eq. (10.52)

$$\alpha_{tot} = \frac{\sum \alpha_{s,i} S_i}{S_{tot}} = \frac{0.7 \times 100 + 0.6 \times 125 + 0.5 \times 32}{257} = \frac{161}{257} = 0.626.$$

The reverberation time T is given by Eq. (10.50)

$$T = \frac{0.161V}{S_{tot}\alpha_{tot}} = \frac{0.161V}{\sum \alpha_{s,i} S_i} = \frac{0.161 \times 1000}{257 \times 0.626} = 1s,$$

which according to Fig. 10.13 is fairly optimum for the size of auditorium. The sound strength G is given by Eq. (10.65)

$$\begin{aligned} G &= 10 \log_{10} \left(\frac{100}{r^2} + \frac{1600\pi(1 - \alpha_{tot})}{S_{tot}\alpha_{tot}} \right) \\ &= 10 \log_{10} \left(\frac{100}{10^2} + \frac{1600 \times 3.14 \times (1 - 0.626)}{257 \times 0.626} \right) = 11 \text{ dB}. \end{aligned}$$

The distance r_{rev} from a source to equal direct and reverberant fields is given by Eq. (10.68)

$$r_{ev} = \frac{1}{4} \sqrt{\frac{QS_{tot}\alpha_{tot}}{\pi(1 - \alpha_{tot})}} = \frac{1}{4} \sqrt{\frac{1 \times 257 \times 0.626}{3.14 \times (1 - 0.626)}} = 2.93 \text{ m}.$$

The average Eyring absorption coefficient α_{ey} is given by Eq. (10.70)

$$\alpha_{ey} = 1 - e^{-0.161V/(S_{tot}T)} = 1 - 2.72^{-0.161 \times 1000 / (257 \times 1)} = 0.466.$$

The required acoustic power is given by Eq. (10.71) using the maximum peak SPL of a large orchestra from column three of Table 10.2

$$\begin{aligned} W &= \frac{4 \times 10^{(SPL/10)-10}}{\rho_0 c} \left(\frac{Q}{4\pi r_{ref}^2} + \frac{4(1 - \alpha_{ey})}{S_{tot}\alpha_{ey}} \right)^{-1} \\ &= \frac{4 \times 10^{(102.5/10)-10}}{1.18 \times 345} \left(\frac{1}{4\pi \times 10^2} + \frac{4 \times (1 - 0.466)}{257 \times 0.466} \right)^{-1} = 0.938 \text{ W}. \end{aligned}$$

If the loudspeakers have an efficiency of 0.5%, the required amplifier power is $0.938 \times 100/0.5 = 188 \text{ W}$.

Problem 12.1.

The specific radiation impedance is given by

$$Z_s = \frac{\tilde{p}(a)}{\tilde{u}_0} = j\rho_0 c \frac{H_0^{(2)}(ka)}{H_1^{(2)}(ka)},$$

which is separated into real and imaginary parts as follows:

$$\begin{aligned} Z_s &= j\rho_0 c \frac{H_0^{(2)}(ka)H_1^{(1)}(ka)}{H_1^{(2)}(ka)H_1^{(1)}(ka)} \\ &= \rho_0 c \frac{Y_0(ka)J_1(ka) - J_0(ka)Y_1(ka) + j(J_0(ka)J_1(ka) + Y_0(ka)Y_1(ka))}{J_1^2(ka) + Y_1^2(ka)}. \end{aligned}$$

Applying the Wronskian yields,

$$Z_s = \rho_0 c \left(\frac{2}{\pi ka(J_1^2(ka) + Y_1^2(ka))} + j \frac{J_0(ka)J_1(ka) + Y_0(ka)Y_1(ka)}{J_1^2(ka) + Y_1^2(ka)} \right).$$

Problem 12.2.

The spherical cap is set in a rigid sphere of radius R and moves with a radial velocity \tilde{u}_0 such that the velocity distribution is described by

$$\tilde{u}(R, \theta) = \begin{cases} \tilde{u}_0, & 0 \leq \theta \leq \alpha \\ 0, & \alpha < \theta \leq \pi \end{cases}, \quad (\text{A3.1})$$

where α is the half angle of the arc formed by the cap. The total volume velocity is given by

$$\tilde{U}_0 = \tilde{u}_0 R^2 \int_0^{2\pi} \int_0^\alpha \sin \theta \, d\theta \, d\varphi = S \tilde{u}_0, \quad (\text{A3.2})$$

where S is the *effective* surface area of the cap given by

$$S = 2\pi R^2 (1 - \cos \alpha) = 4\pi R^2 \sin^2(\alpha/2). \quad (\text{A3.3})$$

Near-field Pressure. Again, assuming that the pressure field generated is a general axisymmetric solution to Eq. (2.180), the Helmholtz wave equation in spherical coordinates is

$$\tilde{p}(r, \theta) = \rho_0 c \tilde{u}_0 \sum_{n=0}^{\infty} A_n h_n^{(2)}(kr) P_n(\cos \theta). \quad (\text{A3.4})$$

Applying the velocity boundary condition gives

$$\begin{aligned}\tilde{u}(R, \theta) &= \frac{1}{-jk\rho_0 c} \frac{\partial}{\partial r} p(r, \theta)|_{r=R} \\ &= \frac{\tilde{u}_0}{-jk} \sum_{n=0}^{\infty} A_n h_n^{(2)}(kR) P_n(\cos \theta) = \begin{cases} \tilde{u}_0, & 0 \leq \theta \leq \alpha \\ 0, & \alpha < \theta \leq \pi, \end{cases}\end{aligned}\quad (\text{A3.5})$$

where the derivative of the spherical Hankel function $h_n^{(2)}(kR)$ is given by Eq. (12.32). We now multiply both sides of Eq. (A3.5) with the orthogonal function $P_m(\cos \theta)$ and integrate over the surface of the sphere, where the area of each surface element is given by $\delta S = 2\pi R^2 \sin \theta \delta \theta$, so that

$$\frac{1}{-jk} \sum_{n=0}^{\infty} A_n h_n^{(2)}(kR) \int_0^\pi P_n(\cos \theta) P_m(\cos \theta) \sin \theta d\theta = \int_0^\alpha P_m(\cos \theta) \sin \theta d\theta, \quad (\text{A3.6})$$

from which we obtain the coefficients as follows:

$$A_n = -jk(2n+1) \frac{\sin \alpha P_n^{-1}(\cos \alpha)}{2h_n^{(2)}(kR)}, \quad (\text{A3.7})$$

where we have used the integral identities from Eqs. (A2.66) and (A2.69) in Appendix II. Finally, by inserting Eq. (A3.7) in Eq. (A3.4), we can write the near-field pressure as

$$\tilde{p}(r, \theta) = -jk\rho_0 c \tilde{u}_0 \sum_{n=0}^{\infty} (n+1/2) \sin \alpha P_n^{-1}(\cos \alpha) P_n(\cos \theta) \frac{h_n^{(2)}(kr)}{h_n^{(2)}(kR)}. \quad (\text{A3.8})$$

Far-field Pressure. In the far field, we can use the asymptotic expression for the spherical Hankel function from Eq. (12.18), which when inserted into Eq. (A3.8) gives

$$\tilde{p}(r, \theta)|_{r \rightarrow \infty} = \tilde{p}(r, \theta) = -jk\rho_0 c S \tilde{u}_0 \frac{e^{-jkr}}{4\pi r} D(\theta), \quad (\text{A3.9})$$

where S is the dome effective area given by Eq. (A3.3) and

$$D(\theta) = \frac{\sin \alpha}{2k^2 R^2 \sin^2(\alpha/2)} \sum_{n=0}^{\infty} \frac{j^{n+1} (2n+1)^2 P_n^{-1}(\cos \alpha) P_n(\cos \theta)}{nh_{n-1}^{(2)}(kR) - (n-1)h_{n+1}^{(2)}(kR)}. \quad (\text{A3.10})$$

The far field on axis response is given by

$$D(0) = \frac{\sin \alpha}{2k^2 R^2 \sin^2(\alpha/2)} \sum_{n=0}^{\infty} \frac{j^{n+1} (2n+1)^2 P_n^{-1}(\cos \alpha)}{nh_{n-1}^{(2)}(kR) - (n-1)h_{n+1}^{(2)}(kR)}. \quad (\text{A3.11})$$

Radiation Impedance. The total radiation force \tilde{F} is given by

$$\begin{aligned}\tilde{F} &= R^2 \int_0^{2\pi} \int_0^\alpha \tilde{p}(R, \theta) \sin \theta \, d\theta \, d\varphi \\ &= -4\pi R^2 j\rho_0 c\tilde{u}_0 \sum_{n=0}^{\infty} \frac{\left(n + \frac{1}{2}\right)^2 \left(\sin \alpha P_n^{-1}(\cos \alpha)\right)^2 h_n^{(2)}(kR)}{nh_{n-1}^{(2)}(kR) - (n-1)h_{n+1}^{(2)}(kR)}\end{aligned}\quad (\text{A3.12})$$

using the identity of Eq. (A2.69). The specific impedance Z_s is then given by

$$Z_s = \frac{\tilde{F}}{\tilde{U}_0} = -j\rho_0 c \frac{\sin^2 \alpha}{\sin^2(\alpha/2)} \sum_{n=0}^{\infty} \frac{\left(n + \frac{1}{2}\right)^2 \left(P_n^{-1}(\cos \alpha)\right)^2 h_n^{(2)}(kR)}{nh_{n-1}^{(2)}(kR) - (n-1)h_{n+1}^{(2)}(kR)}, \quad (\text{A3.13})$$

where we have used the expression for \tilde{U}_0 from Eq. (A3.2).

Problem 13.1.

The far-field pressure is given by Eq. (13.6)

$$\tilde{p}(x, y, z) = 2jk\rho_0 c\tilde{u}_0 \int_{-l_y/2}^{l_y/2} \int_{-l_x/2}^{l_x/2} g(x, y, x|x_0, y_0, z_0)|_{z_0=0} dx_0 dy_0,$$

where the Green's function is given by Eqs. (13.33) and (13.34)

$$g(x, y, x|x_0, y_0, z_0) = \frac{e^{-jk(x(x-x_0)+y(y-y_0)+z(z-z_0))/R}}{4\pi R},$$

$$R = \sqrt{x^2 + y^2 + z^2}.$$

By combining the above equations, we get

$$\begin{aligned}\tilde{p}(x, y, z) &= 2jk\rho_0 c\tilde{u}_0 \frac{e^{-jkR}}{4\pi R} \int_{-l_x/2}^{l_x/2} e^{jkxx_0/R} dx_0 \int_{-l_y/2}^{l_y/2} e^{jky_0/R} dy_0 \\ &= jkl_x l_y \rho_0 c\tilde{u}_0 \frac{e^{-jkR}}{2\pi R} \cdot \frac{\sin(kl_x x/2R)}{kl_x x/2R} \cdot \frac{\sin(kl_y y/2R)}{kl_y y/2R}.\end{aligned}$$

We note that $\sin \theta_x = x/R$ and $\sin \theta_y = y/R$ which yields

$$\tilde{p}(x, y, z) = jkl_x l_y \rho_0 c\tilde{u}_0 \frac{e^{-jkR}}{2\pi R} D(\theta_x, \theta_y),$$

where

$$D(\theta_x, \theta_y) = \frac{\sin\left(\frac{1}{2}kl_x \sin \theta_x\right) \sin\left(\frac{1}{2}kl_y \sin \theta_y\right)}{\frac{1}{2}kl_x \sin \theta_x \frac{1}{2}kl_y \sin \theta_y}.$$

Problem 13.2.

The near-field pressure is given by Eq. (13.6)

$$\tilde{p}(x, y, z) = 2jk\rho_0\tilde{u}_0 \int_{-l_y/2}^{l_y/2} \int_{-l_x/2}^{l_x/2} g(x, y, x|x_0, y_0, z_0)|_{z_0=0} dx_0 dy_0,$$

where the Green's function is given by Eqs. (13.33) and (13.34)

$$g(x, y, x|x_0, y_0, z_0) = \frac{-j}{8\pi^2} \int_{-\infty}^{\infty} \int_{-\infty}^{\infty} \frac{e^{-j(k_x(x-x_0)+k_y(y-y_0)+k_z|z-z_0|)}}{k_z} dk_x dk_y$$

$$k_z = \begin{cases} \sqrt{k^2 - k_x^2 - k_y^2}, & k_x^2 + k_y^2 \leq k^2 \\ -j\sqrt{k_x^2 + k_y^2 - k^2}, & k_x^2 + k_y^2 > k^2. \end{cases}$$

By combining the above equations, we get

$$\tilde{p}(x, y, z) = \frac{k\rho_0 c \tilde{u}_0}{4\pi^2} \int_{-\infty}^{\infty} \int_{-\infty}^{\infty} \frac{e^{-j(k_x x + k_y y + k_z |z|)}}{k_z} \int_{-l_x/2}^{l_x/2} e^{jk_x x_0} dx_0 \int_{-l_y/2}^{l_y/2} e^{jk_y y_0} dy_0 dk_x dk_y.$$

The total radiation force is then given by

$$\tilde{f} = \int_{-l_y/2}^{l_y/2} \int_{-l_x/2}^{l_x/2} \tilde{p}(x, y, z)|_{z=0} dx dy.$$

The imaginary parts of the complex exponents cancel over the negative and positive values of k_x and k_y so that this simplifies to

$$\tilde{f} = \frac{k\rho_0 c \tilde{u}_0}{4\pi^2} \int_{-\infty}^{\infty} \int_{-\infty}^{\infty} \int_{-l_x/2}^{l_x/2} \cos(k_x x) dx \int_{-l_y/2}^{l_y/2} \cos(k_y y) dy$$

$$\times \int_{-l_x/2}^{l_x/2} \cos(k_x x_0) dx_0 \int_{-l_y/2}^{l_y/2} \cos(k_y y_0) dy_0 \frac{1}{k_z} dk_x dk_y.$$

The specific radiation impedance is the ratio of the total radiation force to the total volume velocity. Hence, after integrating over the surface of the piston, we have

$$Z_s = \frac{\tilde{f}}{\tilde{U}_0} = \frac{\tilde{f}}{l_x l_y \tilde{u}_0} = \frac{k l_x l_y \rho_0 c}{4\pi^2} \int_{-\infty}^{\infty} \int_{-\infty}^{\infty} \text{sinc}^2(k_x l_x / 2) \text{sinc}^2(k_y l_y / 2) \frac{1}{k_z} dk_x dk_y,$$

where $\text{sinc}(z) = \sin(z)/z$. By using polar coordinates, where $k_x = kt \cos \phi$, $k_y = kt \sin \phi$, and $dk_x dk_y = k^2 t dt d\phi$, we reduce the double infinite integral to a single infinite one over t and a single finite one over ϕ . Also, the infinite integral is split to produce the real resistance \mathbf{R}_s and the imaginary reactance X_s so that

$$Z_s = \mathbf{R}_s - jX_s,$$

where

$$\mathbf{R}_s = \frac{k l_x l_y \rho_0 c}{4\pi^2} \int_0^{\pi/2} \int_0^1 \text{sinc}^2\left(\frac{k l_x}{2} t \cos \phi\right) \text{sinc}^2\left(\frac{k l_y}{2} t \sin \phi\right) \frac{t dt d\phi}{\sqrt{1-t^2}},$$

$$X_s = \frac{k l_x l_y \rho_0 c}{4\pi^2} \int_0^{\pi/2} \int_1^{\infty} \text{sinc}^2\left(\frac{k l_x}{2} t \cos \phi\right) \text{sinc}^2\left(\frac{k l_y}{2} t \sin \phi\right) \frac{t dt d\phi}{\sqrt{t^2-1}}.$$

Substituting $t = \sin \theta$ in the above equation yields

$$\mathbf{R}_s = \frac{k l_x l_y \rho_0 c}{4\pi^2} \int_0^{\pi/2} \int_0^{\pi/2} \text{sinc}^2\left(\frac{k l_x}{2} \sin \theta \cos \phi\right) \text{sinc}^2\left(\frac{k l_y}{2} \sin \theta \sin \phi\right) \sin \theta d\theta d\phi,$$

$$X_s = \frac{k l_x l_y \rho_0 c}{4\pi^2} \int_0^{\pi/2} \int_{\pi/2+j0}^{\pi/2+j\infty} \text{sinc}^2\left(\frac{k l_x}{2} \sin \theta \cos \phi\right) \text{sinc}^2\left(\frac{k l_y}{2} \sin \theta \sin \phi\right) \sin \theta d\theta d\phi,$$

where we note that $\sin(\pi/2 + j\infty) = \cos j\infty = \cosh \infty = \infty$.

Problem 13.3.

$$D(\theta, \phi) = \frac{2J_1(ka \sin \theta)}{ka \sin \theta} \cdot \frac{\sin(2kd \sin \theta \sin \phi)}{4 \sin\left(\frac{1}{2}kd \sin \theta \sin \phi\right)}$$

$$= \frac{2J_1(ka \sin \theta)}{ka \sin \theta} \cdot \cos\left(\frac{1}{2}kd \sin \theta \sin \phi\right) \cos(kd \sin \theta \sin \phi)$$

Problem 14.1.

Let the Green's function be of the form

$$G(x, y|x_0, y_0) = \sum_{m=1}^{\infty} \sum_{n=1}^{\infty} A_{mn} \sin(m\pi x/l_x) \sin(n\pi y/l_y).$$

Inserting this into Eq. (14.24), multiplying both sides by $\sin(p\pi x/l_x) \sin(q\pi y/l_y)$, and integrating over the surface of the membrane gives

$$\begin{aligned} & \sum_{m=1}^{\infty} \sum_{n=1}^{\infty} A_{mn} \left(k_D^2 - \frac{m^2 \pi^2}{l_x^2} - \frac{n^2 \pi^2}{l_y^2} \right) \int_0^{l_x} \sin\left(\frac{m\pi x}{l_x}\right) \sin\left(\frac{p\pi x}{l_x}\right) dx \int_0^{l_y} \sin\left(\frac{n\pi y}{l_y}\right) \sin\left(\frac{q\pi y}{l_y}\right) dy \\ &= - \int_0^{l_x} \delta(x - x_0) \sin\left(\frac{p\pi x}{l_x}\right) dx \int_0^{l_y} \delta(y - y_0) \sin\left(\frac{q\pi y}{l_y}\right) dy. \end{aligned}$$

Applying the integral of Eq. (14.18) together with the property of the Dirac delta function of Eq. (A2.154) from Appendix II yields

$$A_{mn} = \frac{4}{l_x l_y \left(\frac{m^2 \pi^2}{l_x^2} + \frac{n^2 \pi^2}{l_y^2} - k_D^2 \right)} \sin\left(\frac{m\pi x_0}{l_x}\right) \sin\left(\frac{n\pi y_0}{l_y}\right).$$

Hence,

$$G(x, y | x_0, y_0) = 4 \sum_{m=1}^{\infty} \sum_{n=1}^{\infty} \frac{\sin(m\pi x/l_x) \sin(n\pi y/l_y) \sin(m\pi x_0/l_x) \sin(n\pi y_0/l_y)}{(k_{mn}^2 - k_D^2) l_x l_y},$$

where

$$k_{mn} = \pi \sqrt{\frac{m^2}{l_x^2} + \frac{n^2}{l_y^2}}.$$

Problem 14.2.

Let the Green's function be of the form

$$G(w, \phi | w_0, \phi_0) = \sum_{m=0}^{\infty} \sum_{n=1}^{\infty} A_{mn} \cos(m\phi) J_m(\alpha_{mn} w/a).$$

Inserting this into Eq. (14.44), multiplying both sides by $\cos(p\phi) J_p(\alpha_{pq} w/a)$, and integrating over the surface of the membrane gives

$$\begin{aligned} & \sum_{m=0}^{\infty} \sum_{n=1}^{\infty} A_{mn} \left(k_D^2 - \frac{\alpha_{mn}^2}{a^2} \right) \int_0^{2\pi} \cos(m\phi) \cos(p\phi) d\phi \int_0^a J_m(\alpha_{mn} w/a) J_p(\alpha_{pq} w/a) w dw \\ &= - \int_0^{2\pi} \delta(\phi - \phi_0) \cos(p\phi) d\phi \int_0^a \delta(w - w_0) J_p(\alpha_{pq} w/a) dw. \end{aligned}$$

Applying the integrals of Eqs. (14.38) and (14.39) together with the property of the Dirac delta function of Eq. (A2.154) from Appendix II yields

$$A_{mn} = \frac{2 \cos(m\phi_0) J_m(\alpha_{mn} w_0/a)}{\pi(1 + \delta_{m0})(\alpha_{mn}^2 - k_D^2 a^2) J_{m+1}^2(\alpha_{mn})}.$$

Hence,

$$G(w, \phi | w_0, \phi_0) = \frac{2}{\pi} \sum_{m=0}^{\infty} \sum_{n=1}^{\infty} \frac{\cos(m\phi) J_m(\alpha_{mn} w/a) \cos(m\phi_0) J_m(\alpha_{mn} w_0/a)}{(1 + \delta_{m0})(\alpha_{mn}^2 - k_D^2 a^2) J_{m+1}^2(\alpha_{mn})}.$$

Problem 14.3.

$$\begin{aligned} f_{01} &= \frac{\alpha_{01}^2 h}{4\pi a^2} \sqrt{\frac{Y}{3(1 - \nu^2)\rho_D}} = \frac{2.2215^2 \times 0.2 \times 10^{-3}}{4\pi \times (12.5 \times 10^{-3})^2} \sqrt{\frac{69 \times 10^9}{3 \times (1 - 0.3^2) \times 2700}} \\ &= 1.54 \text{ kHz}, \end{aligned}$$

$$f_{02} = \left(\frac{\alpha_{02}}{\alpha_{01}}\right)^2 f_{01} = \left(\frac{5.4516}{2.2215}\right)^2 668 = 9.26 \text{ kHz},$$

$$f_{03} = \left(\frac{\alpha_{03}}{\alpha_{01}}\right)^2 f_{01} = \left(\frac{8.6114}{2.2215}\right)^2 668 = 23.1 \text{ kHz},$$

Problem 14.4.

Let the Green's function be of the form

$$G(w, \phi | w_0, \phi_0) = \sum_{m=0}^{\infty} \sum_{n=1}^{\infty} A_{mn} \eta_{mn}(w, \phi),$$

where $\eta_{mn}(w, \phi) = \cos(m\phi) (J_m(\alpha_{mn} w/a) - B_{mn} I_m(\alpha_{mn} w/a) + C_{mn})$. Inserting this into Eq. (14.149), multiplying both sides by $\eta_{pq}^*(w, \phi)$, and integrating over the surface of the shell gives

$$\begin{aligned} &\sum_{m=0}^{\infty} \sum_{n=1}^{\infty} A_{mn} \left(\frac{\alpha_{mn}^4}{a^4} - k_D^4\right) \int_0^{2\pi} \int_0^a \eta_{mn}(w, \phi) \eta_{pq}^*(w, \phi) w dw d\phi \\ &= - \int_0^{2\pi} \int_0^a \delta(w - w_0) \delta(\phi - \phi_0) \eta_{pq}^*(w, \phi) w dw d\phi. \end{aligned}$$

Applying the integrals of Eq. (14.142) together with the property of the Dirac delta function of Eq. (A2.154) from Appendix II yields

$$A_{mn} = \frac{a^2 \eta_{mn}^*(w_0, \varphi_0)}{\pi \Delta_{mn} (k_D^4 a^4 - \alpha_{mn}^4)}.$$

Hence,

$$G(w, \varphi | w_0, \varphi_0) = \frac{a^2}{\pi} \sum_{m=0}^{\infty} \sum_{n=1}^{\infty} \frac{\eta_{mn}(w, \varphi) \eta_{mn}^*(w_0, \varphi_0)}{\Delta_{mn} (k_D^4 a^4 - \alpha_{mn}^4)}.$$

Problem 14.5.

$$\begin{aligned} f_{01} &= \frac{h}{4\pi a^2} \sqrt{\frac{Y}{3\rho_D} \left(\frac{\beta_1^4}{1-\nu^2} + 48 \frac{H^2}{h^2} \right)} \\ &= \frac{40 \times 10^{-6}}{4\pi \times (12.5 \times 10^{-3})^2} \sqrt{\frac{69 \times 10^9}{3 \times 2700} \left(\frac{-109.2 \times 10^3}{1-0.3^2} + 48 \times \left(\frac{2 \times 10^{-3}}{40 \times 10^{-6}} \right)^2 \right)} = 0 \text{ Hz}, \end{aligned}$$

$$f_{02} = \frac{40 \times 10^{-6}}{4\pi \times (12.5 \times 10^{-3})^2} \sqrt{\frac{69 \times 10^9}{3 \times 2700} \left(\frac{5.9034^4}{1-0.3^2} + 48 \times \left(\frac{2 \times 10^{-3}}{40 \times 10^{-6}} \right)^2 \right)} = 20.7 \text{ kHz},$$

$$f_{03} = \frac{40 \times 10^{-6}}{4\pi \times (12.5 \times 10^{-3})^2} \sqrt{\frac{69 \times 10^9}{3 \times 2700} \left(\frac{9.1898^4}{1-0.3^2} + 48 \times \left(\frac{2 \times 10^{-3}}{40 \times 10^{-6}} \right)^2 \right)} = 21.3 \text{ kHz},$$

$$f_{04} = \frac{0.2 \times 10^{-3}}{4\pi \times (12.5 \times 10^{-3})^2} \sqrt{\frac{69 \times 10^9}{3 \times 2700} \left(\frac{12.386^4}{1-0.3^2} + 48 \times \left(\frac{2 \times 10^{-3}}{40 \times 10^{-6}} \right)^2 \right)} = 22.7 \text{ kHz}.$$

Problem 15.1.

$$\begin{aligned} p_{rms}(r, 0) &= 2\pi f \epsilon_0 a^2 \left(\frac{E_p}{d} \right)^2 \frac{1}{2\sqrt{2}rc} \\ &= \frac{2 \times 3.14 \times 10^3 \times 8.85 \times 10^{-12} \times 0.05^2 \times (2000/10^{-3})^2}{2 \times \sqrt{2} \times 1 \times 345} = 0.570 \text{ Pa} \end{aligned}$$

Hence, the sound pressure level is $20 \log_{10}(0.57/(20 \times 10^{-6})) = 89.1 \text{ dB SPL}$.

Problem 15.2.

From Eq. (15.119), the polarization voltage is

$$E_p = \left(\frac{E_p}{d}\right)d = \frac{2000}{10^{-3}} \times 0.224 \times 10^{-3} = 448 \text{ V.}$$

From Eq. (15.86), the minimum tension is

$$T = \frac{\epsilon_0 a^2}{d} \left(\frac{E_p}{d}\right)^2 = \frac{8.85 \times 10^{-12} \times 0.05^2}{0.224 \times 10^{-3}} \left(\frac{2000}{10^{-3}}\right)^2 = 395 \text{ N/m.}$$

From Eq. (15.114), the resonance frequency is

$$f_0 = \frac{1}{3.26a} \sqrt{\frac{T}{a\rho_0}} = \frac{1}{3.26 \times 0.05} \sqrt{\frac{395}{0.05 \times 1.18}} = 502 \text{ Hz.}$$

From Eq. (15.117), the resistance is

$$R_S = \frac{2}{Q} \sqrt{\frac{\rho_0 T}{a}} = \frac{2}{1} \sqrt{\frac{1.18 \times 395}{0.05}} = 193 \text{ rayls.}$$

From Eq. (15.113), the maximum tension is

$$T = 0.6\sigma_{\max}h = 0.6 \times 55 \times 10^6 \times 12 \times 10^{-6} = 396 \text{ N/m.}$$

Index

'Note: Page numbers followed by "f" indicate figures; "t" indicate tables and "b" indicate boxes.'

A

Absorption coefficients (room)

Eyring, 535–536

Sabine, 535–536

Absorption in air, 536

Acoustic, definition, 11

Acoustic compliance, 54, 105–106, 145–149

Acoustic components, 143–229

Acoustic conductance, 106–107, 471

Acoustic generators, 107–112

Acoustic impedance, 16

Acoustic inertance. *See* Mass

Acoustic mass, 104–105, 144

Acoustic materials, 2, 149, 347–348, 535

Acoustic radiation impedance, 821

Acoustic resistance, 106–107, 149–152

Acoustic transformers, 155–161

Acoustical, definition, 12

Acoustical circuits, 102–112

Acoustical elements, 102–104

Acoustical holography, 713–715

Acoustical standards, 16

Acoustics

in concert halls, 547

in living rooms, 549–552

Adiabatic, definition, 7

Adiabatic alternations, 7–8

Admittances

analogies, 85, 93

conversion to impedance analogies,
124–125

definitions, 85

mechanical, 81–82

Air, basics, 6, 8–10

Air attenuation constant, 537t

Air density, 14–15

Air losses, 500–501

Air speed, 15–16

Air-suspension loudspeakers, 332

Airy

diffraction pattern, 628

disk, 637–639

stress function, 747–748

Alignment tables for loudspeaker in

bass-reflex enclosure, 374–376

closed-box enclosure, 339–340, 370f, 382

Alternating signal voltage, 792–794

American Standards Assoc., 16

Analogies, 81–82

admittance type, 85

conversion of, 124–125

impedance type, 85

rotational, 112

transformation, 84

Anechoic chamber, 164, 183–184, 282, 297,
496–497, 539

Angular eigenfrequency, 778

Arbitrary specific acoustic impedance,
732–734

Area, effective, of diaphragm, 234, 282, 447

Attenuation of sound in air, 536

Auditoriums

mean free path, 534

reverberation time, 535–536

sound absorption coefficients, 534

sound decay rate, 531–532

sound energy density, 17–18

sound pressure levels, 15

Average room absorption coefficient, 535

Axisymmetric solutions to shell wave equations,
754–755

B

Babinet-Bouwkamp principle, 655, 683–690

Baffle

bass-reflex, 333, 374–376

closed-box, 333f, 337–366

finite, 336–337

infinite, 336

open back, 337

unbaffled, 334–336

Barometric pressure (atmospheric), 14

Bass quality

explanation, 259

pressure-gradient microphone, 265

ribbon microphone, 263

Beam width, 162, 820

Beam-forming, 4–5, 173–179

- Bending-wave velocity
 in plate, 740
 in shell, 749
- Bends in horns, 496–498
- Bessel functions, 62, 71, 75, 727, 728t, 776
- Boundary conditions, 39, 44, 55, 211, 403–404, 475–476, 626–628, 731–732, 752–754, 777–781
 of continuity at center, 755
 Dirichlet, 637, 659–660
 Neumann, 626–628, 648, 659–660, 727
 slip, 207
 of zero bending at perimeter, 755
 of zero radial strain at perimeter, 755–756
- Boundary integral method, 553–603
 case study, 567–570
- Boundary layer thickness, 213
- Boundary value method, 553–603
- Bouwkamp impedance theorem, 192, 690–691, 694–695, 702
- Box
 bass-reflex, 333, 374–376
 closed, 314, 337–366
 open-back, 337
 transmission-line, 333–334, 409–425
- C**
- Capacitor microphones
 construction and properties, 249
 humidity effects, 249
 temperature effects, 248
- Cardioid pattern, 239
 hypercardioid, 263
 supercardioid, 263
- Cellphone acoustics, 445–462
 call loudspeaker, 445
 diaphragm, 445
 dust screen, 150, 449
 electret microphone, 452–455
 low-pass filter, 448–449
 magnetic fields, 450
 MEMS microphone, 455–457
 sidetone, 460–461
 testing, 451, 457–461
 turbulence, 450–451
 wind noise, 451
- Characteristic impedance, 17, 46–47, 62
- Charles-Boyle gas law, 28
- Circular membrane. *See also* Rectangular membrane
 Eigenfunctions, 729f
 Green's function for, 728–730
 membrane wave equation solution for, 727–728
 modes, 728
 radiation from circular membrane without baffle, 731–739
 boundary conditions, 731–732
 far-field pressure, 738–739
 radiation impedance, 737–738
 simultaneous equations for power-series coefficients, 736–737
 solution of free-space wave equation, 735–736
 solution of membrane wave equation, 734–735
 wave equation for membrane in free space, 732–734
- Circular plate
 modes of simply supported, 743–745
 solution of plate wave equation for, 741–742
- Clamped circular plate
 eigenfunctions, 744f
 eigenvalues for, 743t
 modes of, 742–743
- Closed tube, 55–58. *See also* Tubes
- Closed-box baffle, 333f, 337–366
- Coefficients
 absorption, 535–536
 reflection, 45, 559–560
 transmission, 497, 559–560, 565–566, 647
- Coil, voice, 307–310
- Coil driving force, 753–754
- Coil impedance at perimeter, 756–757
- Coil inductance, 772–773
- Combination microphones, 262–265
- Complex wavenumber of shell, 762
- Compliance, 757
 acoustic, 105–106, 145–149, 153
 closed box, 337–366
 closed tube, 207
 drive unit, 278–279
 jug, 148
 mechanical, 89–91
 series, acoustic, 146–149

- Components, acoustic, 143–229
- Compressibility dynamic, 207, 214–215, 217
- Condenser microphones. *See* Capacitor microphones
- Cone. *See* Diaphragm
- Conical horn, 474–477
- Connector, exponential, 158–161
- Constants
 - barometric pressure, 14
 - characteristic impedance, 17, 47, 60–62
 - decay, room, 527
 - density-of-air, 15
 - drive unit, 279–280
 - flare, 483–484
 - reference quantities, 18–19
 - speed of sound, 15–16
 - Thiele-Small, 440
- Continuity equation, 29–31
- Conversion tables, impedance-to-admittance analogies, 85, 124–125
- Coordinates
 - cylindrical, 70–73
 - oblate spheroidal, 647–648, 659
 - rectangular, 68–69
 - spherical, 73–78
- Coupled shell formulation, 764
- Coupler. *See* Connector
- Cross-section shapes, horns, 498–499
- Crossover networks, 436–440
- Curvature of membrane, 722–723
- Cut-off frequency, 776, 800
- Cut-off frequency of horn, 440–441
- Cylindrical wave, 62–64

- D**
- Decay curves, for sound in rooms, 531
- Delay line ignoring stray capacitance, 807–808
- Delay path length, 804–805
- Density, air
 - definition, 15
 - dynamic, 207, 214, 218
 - formula, 15
 - normal, 15
 - variational, 15
- Diameter, effective, of diaphragms, 310
- Diaphragms
 - behavior, 310–314
 - diameter, effective, 310
- Diffraction of plane wave
 - through resilient screen, 688–690
 - through rigid screen, 687–688
- Diffuse sound field, 533
- Dimensionless parameter, 764–765
- Dipole source. *See* Doublet
- Dipole strength, 181
- Dirac delta functions, 726, 858–859, 866
- Direct sound, 547–548
- Directivity, 189
- Directivity characteristics
 - of loudspeakers, 162, 550
 - of microphones, 161, 236f, 240
- Directivity control of electrostatic loudspeakers, 794–795, 814
 - continuous delay, 795–801
 - discretization effects into rings of finite width, 802–803
 - far-field sound pressure, 810
 - neutralization of stray capacitances, 810–814
 - practical delay line, 804–810
- Directivity factor, 189
- Directivity function, 738–739, 765–767, 781–782
- Directivity index (DI)
 - calculation, 190–194
 - definition, 189
 - of sources, 192
- Directivity patterns, 170, 179, 314
 - dipole point source (doublet), 179–183
 - sphere (pulsating & oscillating), 164–167
- Dirichlet boundary condition, 731
- Discretization effects into rings of finite width, 802–803, 803f–805f
- Dispersive medium, 741
- Displacement, 747–748
 - of shell, 754
- Distortion
 - horn, 472–474
 - large-amplitude waves, 478
 - loudspeakers, 322–325
 - phase delay of crossover, 435–436
 - transient, 322–323
- Doublet
 - microphone, 179–183
 - piston without baffle, 184–185
 - simple, 182
- Driving pressure, 732–734
- Dual diaphragm microphones, 265–275

- Dynamic compressibility, 207, 214–215, 217
- Dynamic density, 207, 214, 217
- Dynamic loudspeaker. *See* Direct-radiator Loudspeakers
- Dynamic membrane compliance, 818
- Dynamic microphone, 241–248
- Dynamic resistance, 818
- Dynamic shell wave equations, 747–748
- E**
- Early sound, 539–540
- Eddy current, 772
- Effective area of diaphragm, 234, 282, 447
- Effective diameter of diaphragm, 310
- Effective length of tube, 145
- Effective particle velocity, 16
- Effective sound pressure, 15
- Effective volume velocity, 16
- Efficiency
 - horn, 466–468
 - loudspeakers, 295–296
- Eigen-frequencies, 724, 728, 743, 758–759
 - for 100-mm magnesium plate, 788t
 - for 25 mm aluminum shell, 768t
 - of shallow spherical shell with infinite load at perimeter, 761f
 - of shallow spherical shell with zero load at perimeter, 759f
- Eigenfunction, 724, 761–762
 - of circular membrane, 729f
 - of clamped circular plate, 744f
 - of free circular plate, 747f
 - of rectangular membrane, 725f
 - of simply supported circular plate, 745f
- Eigenvalues
 - calculation, 757–758
 - for clamped circular plate, 743t
 - with finite load at perimeter, 760
 - for free circular plate, 746t
 - with infinite load at perimeter, 760
 - for simply supported circular plate, 745t
 - with zero load at perimeter, 758–759
- Electret microphone, 452–455
- Electrical damping resistance, 779
- Electrical impedance, 775–776
- Electro-mechano-acoustical circuit, 814–815
- Electrodynamic loudspeakers, 277–330
 - advantages, 277–278
 - baffle
 - finite, 279–280, 289
 - infinite, 279–280, 289
 - bass-reflex, 300, 374–376
 - closed-box, 298–299, 337–366
 - constants, 247
 - construction, 278–280
 - design factors, 302–306
 - diaphragm, 310–314
 - directivity, 314–316
 - dual concentric, 440–441
 - efficiency, 295–296
 - element values, 289
 - impedance, input, 294
 - metals, 308t
 - non-linearity, 323–330
 - power output, 287–288
 - response, 292–293
 - Thiele–Small parameters, 288–289, 297–300
 - transfer function, 316–318
 - transient, 318–323
 - transmission-line enclosures, 333–334, 409–425
 - unbaffled, 334–336
 - voice-coil velocity, 283–284
- Electromagnetic microphones, 241–248
- Electromagnetic transducers, 113–115, 128–130
- Electromechanical conversion factor, 732–734
- Electrostatic loudspeakers, 732–734, 733f, 791–792
 - construction, 792–794, 793f
 - design, 826–832, 830f–831f
 - directivity control, 794–795
 - lumped-element model of, 814–815
- Electrostatic microphones. *See* Capacitor Microphones
- Electrostatic transducers, 115–120, 133–134
- Elements of circuits
 - acoustical, 102–112
 - compliance, acoustic, 105–106
 - compliance, mechanical, 89–91
 - general, 81–82
 - generator, acoustic, 107–112
 - generator, mechanical, 92–93
 - mass, acoustic, 104–105, 144
 - mass, mechanical, 294
 - mechanical, 81–82

- resistance, acoustic, 106–107
- resistance, mechanical, 91–92
- transformers, acoustic, 155–161
- transformers, mechanical, 94
- Elvamide, 792–794
- Enclosures
 - bass-reflex, 317–318, 374–376
 - closed-box, 337–366
 - transmission-line, 333–334, 409–425
- End corrections, tubes, 144–145
- Energy density, definition, 17–18
- Energy flux. *See* Intensity
- Equivalent suspension volume, 288–289, 299, 355
- Exponential, horn, 481–484, 487, 490
- Exponential connector, 158–161
- Eyring, equation, 535–536
- F**
- Far-field
 - pressure, 738–739, 765–769, 766f, 862
 - of free plate with evenly distributed radiation load, 781–784
 - response of induction loudspeaker, 784–789
 - sound pressure, 810
 - directivity patterns at various frequencies, 811f
 - parameters for idealized electrostatic loudspeaker and delay line, 812t
- Ferrofluid, 326
- Field, sound
 - near, 183–184
 - diffuse, 533
 - direct, 536
 - far, 183–184
 - free, 357, 512
 - reverberant, 164, 534, 539–541
- Field matching, 588–589, 594–597
- Figure-of-eight directivity pattern, 794–795
- Filters, electrical, 320, 382–383, 428–430, 432–433
- Finite element modal (FEM), 738–739
- Flare constant, 483–484
- Flexural rigidity, 740, 748–749
- Flow resistance, 347–348, 415, 418
- Fluctuations of sound, in room, 533
- Fluid-loading factor, 736–737, 764–765, 781–782
- Fluid–structure coupling, 731
- Fluid–structure interaction, 721
- Flux density
 - definition, 485–486
 - typical, for loudspeakers, 303, 325–326
- Force equation, 25
- Force transmission coefficient, 737
- Forward traveling wave, 73, 478, 482, 485–486, 516
- Fourier series, 15, 37–38
- Fourier transform, 179, 319–320, 613–614, 695–701, 713–714
- Fourier's law, 149
- Fraunhofer
 - diffraction pattern, 628
 - diffraction zone, 631–633
- Free circular plate
 - Eigenfunctions of, 747f
 - Eigenvalues for, 746t
 - modes of, 746–747
- Free-space wave equation
 - membrane in, 732–734
 - solution of, 735–736, 763–764
- Frequency response, 820–826, 820f
- Fresnel region, 631–633
- Friction, in air, 145
- Fundamental in vacuo resonance frequency, 738–739
- Fundamental resonance, 757
 - frequency, 791, 826–828, 857
- G**
- Gas
 - adiabatic, 7
 - isothermal, 7
 - law, 25, 28–29
- Generators
 - acoustic, 107–112
 - constant force, 93, 93f–94f, 111, 111f
 - constant pressure, 108–109, 108f
 - constant velocity, 92, 92f–93f
 - loudspeakers. *See* Direct radiator Loudspeakers
 - mechanical, 92–93
- Graphite, 792–794
- Green's function, 863, 865–868
 - for circular membrane, 728–730
 - for rectangular membrane, 724–726
 - for shallow spherical shell, 749–752

H

Handsfree loudspeaker, 445–446
 Hankel functions, 727
 Harmonic function, 748–749
 Helmholtz form, 748–749
 Helmholtz resonator, 111, 111f, 448–449
 Helmholtz wave equation, 38, 55, 861–862

- cylindrical coordinates, 70–73
- infinite lossy tube, 213–214
- inhomogeneous, 609
- plane wave, 37
- rectangular coordinates, 68–69
- for sound pressure waves, 723
- spherical coordinates, 73–78

 History, 1–5
 Homogeneous membrane wave equation, 724–725
 Homogeneous wave equation in coordinate system, 740
 Homogenous wave equation, 857
 Horn drive units, 463–464

- circuit for, 464–465
- efficiency, 466–468
- response, 468–472

 Horn loudspeakers, 463–510
 Horns

- advantages, 463
- bends, 496–498
- circuit for, 464–465
- conductance, 466
- conical, 479–481, 489–490
- cross-section shapes, 498–499
- cutoff frequency, 484, 486–487
- disadvantages, 463
- distortion
 - drive unit, 463–464
 - non-linear, 493–496
- exponential, 481–484, 490, 498–499
- finite, 487–496
- flare constant, 483–484
- folded, 496, 502
- frequency response, 468–472
- high frequencies, 471–472
- hyperbolic, 485–487, 490–491
- impedance, 463, 478–479, 481, 483–484, 486, 488
- Klipsch, 502
- low-frequency, 469–471
- materials, 499–509

- midfrequency, 469
- mouth, 477
 - parabolic, 477–479, 483, 486
- Humidity, effects, 241
 Huygens-Fresnel principle, 605–606
 Hyperbolic Bessel function, 741–742

I

Impedances

- acoustic, 16
- analogies, 29, 31, 124–125
- characteristic, 17, 60–62
- closed box, 337–366
- definitions, 16–17
- horn. *See* Horns
- infinite, 48–49
- loudspeaker, 309–310
- measurement, 47–48
- mechanical, 17, 88
- perforated sheet, 154–155
- screens, 149
- specific, 15–17, 61–64
- transducer, 127–140
- tubes, 43–60

 Indium-tin-oxide (ITO), 792–794
 Induction loudspeakers, 770–789, 771f

- analogous circuit, 772–776
- boundary conditions, 777–781
- coil and suspension parameters, 785t
- construction, 770–772
- electro-mechano-acoustical analogous circuit, 772f
- far-field pressure of free plate with evenly distributed radiation load, 781–784
- far-field response, 784–789
- radiation from circular plate in infinite baffle, 770

 Inertance. *See* Mass
 Infinite baffle, 145, 198–201, 336, 588–602, 625–635, 647–657, 691–692, 701–713
 Inhomogeneous membrane equation, 724–725
 Inhomogeneous steady-state wave equation for displacement, 732–734, 762
 Inhomogeneous wave equation, 858
 Intensity

- definition, 17
- level, 19–20

 Isothermal, definition, 7

J

Jug, 147

K

Kelvin function. *See* Thomson function
 King integral, 634, 643, 649, 661
 Kirchhoff-Helmholtz boundary integral, 609–611
 Klipsch horn, 502
 Knudsen number, 151

L

Laplace operator, 732–734, 741, 747–748
 cylindrical coordinates, 70–73
 Green's theorem, 609–610
 rectangular coordinates, 68–69
 spherical coordinates, 73–78
 Laplace transform, 316–318, 527
 Large amplitude waves, 478
 Least-mean-squares method, 663–664
 Legendre function, 76
 Levels, 17–22
 Levers, 94–102
 Linings, baffle box, 338b–339b, 344–347
 Loudness
 concert hall, 547
 listening room, 549–552
 Loudspeakers
 bass-reflex enclosed, 374–376
 box enclosed, 337–366
 direct radiator. *See* Electrodynamic loudspeakers
 dual concentric, 440–441
 electrodynamic, 277–278
 magnet size, 303–306
 transmission line enclosures, 333–334, 409–425
 wave, 357–360
 Lumped-element model of electrostatic
 loudspeaker
 dynamic membrane compliance and dynamic
 resistance, 818
 electro-mechano-acoustical circuit, 814–815
 frequency response, 820–826
 negative compliance and stability, 815–816
 radiation impedance, 819–820
 setting tension to limiting displacement and
 maintaining stability, 818–819
 static membrane compliance, 816–818

M

Magnesium alloy, 784–786
 Magnet size, 303–306
 Magnetic fields, 450
 Mass
 acoustic, 144
 diaphragm, 310–314
 mechanical, 81–82
 voice-coil, 307–310
 Mass loading factor, 757
 Materials, sound absorbent, 347–349
 Matrices
 transmission parameter, 127–128, 216–217
 z-parameter, 117, 131–132, 135, 252, 397–398
 Mean free path
 of air molecules, 6, 151, 210–211, 217
 of waves, 534
 Mechanical circuits, 81–82
 Mechanical compliance, 89–91
 Mechanical elements, 85–102
 Mechanical generators, 92–93
 Mechanical impedance, 17, 88
 Mechanical resistance, 91–92
 Mechano-acoustic transducers, 120–121
 Membrane(s), 721
 Green's function for circular membrane,
 728–730
 Green's function for rectangular membrane,
 724–726
 modes of circular membrane, 728
 modes of rectangular membrane, 724
 radiation from circular membrane without baffle,
 731–739
 and stator mass control, 825–826
 stiffness control, 821
 vibroacoustics, 721
 wave equation
 in polar coordinates, 727
 in rectangular coordinates, 721–723
 solution, 734–735
 solution for circular membrane, 727–728
 solution for rectangular coordinates, 723–724
 MEMS microphone, 455–457
 Metals
 density, 308t
 resistivity, 308t

- Microphones, 231–275
 bass quality, 236–237, 243–244
 capacitor. *See* Capacitor microphones
 cardioid, 239, 262–265
 combination, 237–239, 262–265
 directivity, 236, 239, 262–265
 dual diaphragm, 265–275
 electret, 452–455
 electrostatic. *See* Capacitor microphones
 gradient, 233–237, 259–262
 MEMS, 455–457
 moving coil, 241–248
 piezoelectric, 115
 pressure, 232–233, 240
 pressure gradient, 233–237, 259–262
 ribbon. *See* Ribbon microphones
 summary, 231t
- Modified Walker's equation, 738–739
- Mutual impedance of
 bend in horn, 496–498
 pistons in closed box with or without lining, 349–352
 pistons in infinite baffle, 403, 690–691
- N**
- Navier—Stokes equation, 207, 209
- Near field, 164, 183–184, 631–633
 pressure, 861–862, 864
- Negative impedance, 732–734
- Networks, 124, 253–254
- Neumann functions, 727
- Neutral layer, 740
- Neutralization of stray capacitances, 810–814
 constant impedance delay line, 812f
- Non-linear distortion
 in horns, 474
 in loudspeakers, 474
- Normal frequencies, 512–518, 527, 530
- Normal frequency diagram, 532f
- Normal modes of vibration, 351, 513, 517, 530
- Norton's theorem, 282–283, 282f, 775f
- Notional zeroth eigenvalue, 757–758, 778
- O**
- On-axis pressure, 738–739
- Optimum reverberation time, 538, 543f, 548
- Orchestra power levels, 544
- Orthogonality, 55–56, 59, 567, 750
- Oscillating sphere, 196–197
- P**
- Parabolic horn, 411–412, 420f, 475–478
- Perforated sheet, 154–155, 154f
- Piezoelectric transducer, 118f–119f, 164
- Pipes, junctions, 158–161
- Piston
 without baffle, 676
 directivity, 705–706
 eigenfrequency, 759
 in infinite baffle, 170, 198–201, 625–635
 one-sided (closed-back), 193, 204–206, 357, 676f, 679
- Plane waves
 impedance terminated tube, 43–44
 reflection from plane, 162–164
- Plate(s), 721, 740–741
 modes
 of clamped circular plate, 742–743
 of free circular plate, 746–747
 of simply supported circular plate, 743–745
 solution of plate wave equation for circular plate, 741–742
 wave equation in polar coordinates, 740–741
- Point source
 dipole (doublet), 179–183
 monopole (simple), 168
- Poiseuille flow, 224
- Poisson's ratio, 740
- Polar coordinates
 membrane wave equation in, 727
 plate wave equation in, 740–741
 shell wave equation in, 747–749
- Polar diagram. *See* Directivity patterns
- Polyester, 792–794
- Polyimide, 792–794
- Port
 definition, 374–376
 performance, 390
- Power
 level, band, spectrum, 20, 22
 power-series coefficients, simultaneous equations for, 736–737, 764–765
- Prandtl number, 209–210
- Pressure
 ambient (atmosphere), 10–11
 gradient, 183–184, 556–557
 microphones, 232–233, 237–240
 reference, 19

- Pressure level, 310–311
- Pressure spectrum level, 22
- Product theorem, 700f
- Propagation
 - through gas, 8–10
 - general, 11–13
 - in porous materials, 347–348
 - speed in air, 10
- Pulsating sphere, 196

- Q**
 - of loudspeakers, 278–279
 - of perforated sheet, 155

- R**
- Radial membrane force, 756–757
- Radiation
 - from concave dome in infinite baffle, 594–602
 - from convex dome in infinite baffle, 588–594
 - from dipole point source (doublet), 179–183
 - impedance, 737–738, 819–820, 863
 - of pistons, 673–674
 - between pistons in infinite baffle, 703–713
 - from infinite cylinder or line source, 554–555
 - from infinite strip in infinite baffle, 691–695
 - from linear array (beam-forming), 171–173
 - from loudspeaker, 636
 - mass control, 823–824
 - from monopole point source (simple), 168
 - from one-sided piston (closed-back), 204–206, 356–357
 - from oscillating sphere, 184–188, 196–197
 - from piston in a sphere, 582–588
 - from piston in finite circular closed baffle, 676–683
 - from piston in finite circular open baffle, 659–674
 - from piston in infinite baffle, 198–201
 - from point source on sphere, 567–570
 - from pulsating sphere, 164–167, 196
 - from rectangular cap in a sphere, 577–582
 - from rectangular piston in infinite baffle, 701–703
 - from resilient disk in infinite baffle, 647–657
 - from resilient disk without baffle, 636–647
 - resistance control, 824
 - from spherical cap in a sphere, 570–577
- Rate of sound decay, 527
- Rayl, 16
- Rayleigh distance, 633
- Rayleigh integrals, 606–608
- Reactance. *See* Impedance
- Receiver, 446–448
- Reciprocity, 567, 609–610
- Rectangular coordinates, membrane wave
 - equation in, 721–723
- Rectangular membrane. *See also* Circular membrane
 - Eigenfunctions of, 725f
 - Green's function for, 724–726
 - modes, 724
- Reference
 - intensity, 19–20
 - power, 22
- Reflection
 - diffuse, 162–163, 527
 - plane wave from plane, 162–164
 - plane wave from plane resilient object, 686–687
 - plane wave from plane rigid object, 684–686
 - point source from plane, 623–625
 - specular, 162–163, 527
- Relative humidity. *See* Humidity
- Resistance
 - acoustic, 106–107, 149–152
 - flow, 60, 338–339
 - frictional, 91
 - lossy tube, 220
 - mechanical, 91–92
 - radiation, oscillating sphere, 192
 - radiation, pistons, 625–635
 - radiation, pulsating sphere, 167
 - screens, 150
 - viscous, 91
 - voice-coil, 341–342
- Resistivity
 - metals, 308t
 - wire, 768
- Resonance curve, 526–527
- Resonance frequency, 469, 821–823
- Resonator, Helmholtz, 111, 448–449
- Response of loudspeaker
 - in bass-reflex enclosure, 374–376
 - in closed-box enclosure, 337–366
 - in infinite baffle, 336
- Response of microphone, 236, 241, 245, 246f, 247–248, 256f

- Reverberant sound, 539–541
 definition, 539
 enclosures, 533–535
 equations, 535–536
 Eyring, 535–536, 538
 Sabine, 535–536
 living rooms, 549
 optimum, 538
 Reynolds number, 450
 Ribbon microphones, 259
- S**
- Sabine, 1, 535–536
 Sabine absorption coefficient, 860
 Scattering
 plane wave from sphere, 555
 point source from sphere, 560–566
 Shallow spherical shell
 green's function for, 749–752
 radiation in infinite baffle, 752–769, 753f
 Shear force, 756–757
 Sheets, perforated, 154–155
 Shell(s), 747–749
 aluminum shell parameters, 767t
 coil and suspension parameters, 768t
 eigenfrequencies for aluminum shell, 768t
 green's function for shallow spherical shell,
 749–752
 mass, 768–769
 radiation from circular shallow spherical shell,
 752–769
 solution of wave equation for shell, 762
 wave equation in polar coordinates, 747–749
 Shorted turn, 772–774, 776
 Side lobe, 173, 179
 Simple source, 168
 Single steady-state homogeneous wave equation,
 748–749
 Slip (boundary), 151, 207–208, 210, 213,
 270–271
 Slit, impedance, 151
 Sound
 definition, 5–8
 diffuse field, 461, 527, 533
 direct, 540–541
 energy density, 17–18
 intensity, 17
 pressure, 18–19, 51–53
 reverberant, 540–541
 speed, 6
 velocity, 6, 61, 63
 weighting curves, 21f
 Sound absorption, in air, 534
 Sound energy, density, 17–18
 Sound levels, 21
 for music, 542–544
 for speech, 542–544
 Sound strength, G, 539
 Sources
 dipole point source (doublet), 179–183
 free piston without baffle, 636–647, 731–739
 linear array (beam-forming), 171–173
 monopole point source (simple), 168
 one-sided piston (closed-back), 676–683, 676f
 piston in infinite baffle, 198–201, 625–635
 pulsating sphere, 164–167, 196
 rooms, inside, 548
 spherical. *See* Spherical sources
 two (simple) point sources in phase, 168–170
 Specific acoustic impedance
 cylindrical wave, 61–62
 definition, 16–17
 plane wave, 53–54
 spherical wave, 63–64
 Specific diaphragm impedance, 737–738
 Specific heat, of air, 7
 Specific radiation impedance, 171–172, 237, 674,
 737, 861, 865
 Spherical shell, 721, 752
 Spherical wave, 65–67
 Squawker, 425
 Standing wave, 48, 60, 313, 498–499, 511–513,
 601, 616, 721
 Standing wave ratio, 45, 46t
 Static membrane compliance, 816–818
 Stationary wave, 48, 512
 Stator resistance control, 821–823
 Stiffness (reciprocal of compliance). *See*
 Compliance
 Stray capacitances
 delay line ignoring, 807–808
 neutralization of, 810–814
 Superposition, 95–96
 of fields, 403, 556, 562, 574–575, 624, 676, 676f
 of waves, 533
 Suspension resonance frequency, 284, 297–298,
 415
 Symbols, meaning of, 82, 83t

T

Terminology, 11
Thermal and viscous losses, 207
Thermal conductivity, 209
Thermal diffusion wave, 28
Thévenin's theorem, 125–127
Thiele-Small
 measurement, 297–300
 parameters, 3–4, 288–289, 338
Thomson function, 749
Time reversal, 715–717
Total mechanical damping resistance (R_{MT}),
 753–754
Transducers, 113
Transformers, acoustic, 155–161
Transient behavior
 loudspeakers, 318–323
 rooms, 527–530
Transmission
 line loudspeaker enclosure, 60, 353, 413f, 414
 matrix, 813–814
Tubes
 closed, 55–58
 filled with absorbent material, 60–61
 intermediate diameter, 153–154
 lossy, 207–229
 piston in end of, 109
 rigidly closed, 511, 513–514
 small diameter, 144, 151
 specific acoustic impedance, 66–67
 termination impedances, 46t, 496–497
Turbulence, 450–451
Tweeter, 352, 425–427, 428f, 430f, 431, 432f,
 433–436

U

Units, mks, SI, 305–306

V

Velocity distribution, 762–763
Vibroacoustics, 721

induction loudspeakers, 770–789
 membranes, 721
 plates, 740–741
 shells, 747–749
Virtual oscillating sphere, 798–799, 799f
Virtual point source, 797, 797f
Viscosity of air, 153–154, 209, 270–271, 398
Viscous and thermal losses, 207
Voice-coil
 design, 307–310
 velocity, 283–286
Volume velocity, 16

W

Walker's voltage equation, 800–801, 830–831
Wave equation for membrane in free space,
 732–734. *See also* Helmholtz wave
 equation
Wave number, 215, 740, 748–749
Wavelength, 10
Waves
 backward traveling, 514–516
 cylindrical, 62–64
 evanescent, 73, 714
 forward traveling, 514–516
 free progressive, 17
 plane, 555
 spherical, 65–67
 standing, stationary, 511–512
Webster's equation, 34, 475–476
Weighting curves, 21f
Wind noise, 451
Wire mass, 768–769
Woofer, 425–426, 438

Y

Young's modulus, cone, 327

Z

Zero bending moment, 743–744, 746, 777
Zero shear force, 746

ACOUSTICS

Sound Fields, Transducers and Vibration

Leo Beranek and Tim Mellow

Serving both as a text for students in engineering departments and as a reference for practicing engineers, *Acoustics: Sound Fields, Transducers and Vibration, 2nd Edition* focuses on electroacoustics, analyzing the behavior of transducers with the aid of electromechanoacoustical circuits.

Assuming knowledge of electrical circuit theory, it starts by guiding readers through the basics of sound fields, the laws governing sound generation, radiation, and propagation, and general terminology. It then moves on to examine the following:

- Microphones (electromagnetic, electrostatic, and ribbon), loudspeakers (electrodynamic and electrostatic), earphones, and horns
- Loudspeaker enclosures, baffles, transmission lines, and horns
- Miniature applications (e.g. MEMS microphones and microspeakers in tablets and smartphones)
- Sound in enclosures of all sizes, such as school rooms, offices, auditoriums, and living rooms
- Vibrating surfaces (membranes, plates, and shells) and fluid–structure interaction

Numerical examples and summary charts are given throughout the text to make the material easily applicable to practical design. It is a valuable resource for experimenters, acoustical consultants, and to those who anticipate being engineering designers of audio equipment.

Educated at Harvard and Cornell, **Dr. Leo Beranek** (deceased) was an acoustical design consultant. Recent work includes several concert halls in Japan. In 1948, he cofounded Bolt, Beranek and Newman (now BBN Technologies) to provide consultation for major auditoriums. BBN also reduced jet noise, developed the ARPANET (Internet forerunner), and founded Channel 5 among other achievements.

Tim Mellow was educated at Lancing College before obtaining a BSc in Electrical Engineering and Electronics from the University of Dundee, Scotland. A career as a design engineer at BICC, Marconi, Thorn EMI, Racal, VTech, and Nokia followed. In 2011, he founded Mellow Acoustics Ltd to provide acoustical consultancy and develop high-end audio products.



ACADEMIC PRESS

An imprint of Elsevier
elsevier.com/books-and-journals

ISBN 978-0-12-815227-0



9 780128 152270